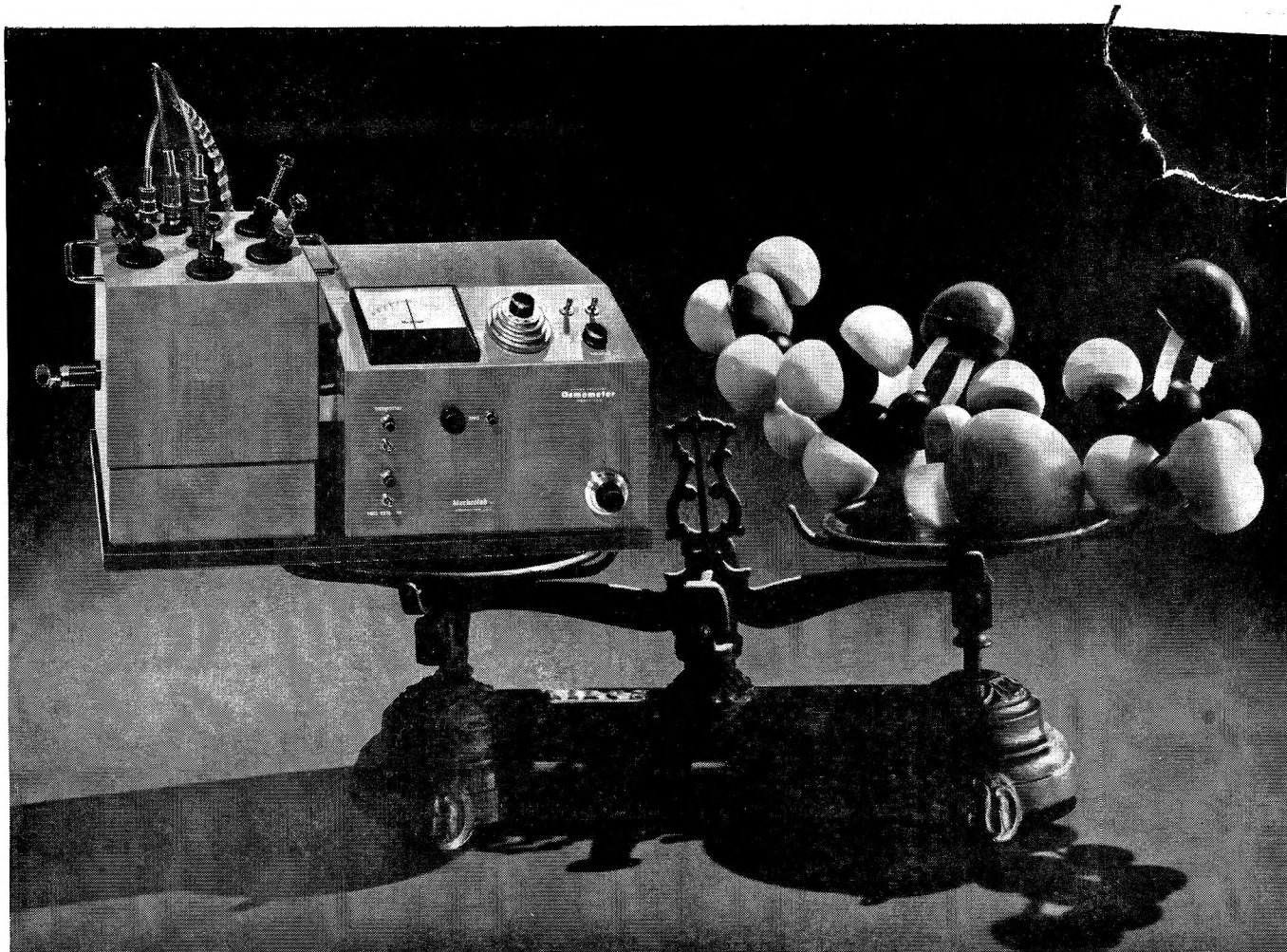


THE JOURNAL OF
PHYSICAL CHEMISTRY

Volume 69, Number 3 March 1965

International Conference on Photosensitization in Solids,
Illinois Institute of Technology, Chicago, Illinois, June 22-24, 1964

Spectral Sensitization of Chemical Effects in Solids	Jean Bourdon	705
Minority Carrier Trapping and Dye Sensitization	R. C. Nelson	714
Sensitization of Electrical Effects in Solids	H. Meier	719
Some Experiments on the Photosensitization Mechanism of Semiconductors by Dyes	A. Terenin and I. Akimov	730
Photoluminescence of Adsorbed Dyes	Edmond Lendvay	738
The Relationship between Exciton Absorption and the Photoelectric Effect	S. Nikitine, A. Coret, J. P. Zielinger, C. Jeanclaude, C. Boehm, and M. Zouaghi	745
Luminescence of Doped Aromatic Crystals	A. Schmillen	751
On Photoelectric Effects in Polymers and Their Sensitization by Dopants	Helmut Hoegl	755
Hypersensitization of Photoconduction in Microcrystalline Zinc Oxide	Eiichi Inoue, Hiroshi Kokado, and Takashi Yamaguchi	767
Color Sensitization of Zinc Oxide with Cyanine Dyes	Susumu Namba and Yasushi Hishiki	774
Effect of Gases on the Conductivity of Organic Solids. III. Sensitization of Bulk Photoconductivity in <i>p</i> -Chloranil Crystals	P. J. Reucroft, O. N. Rudyj, R. E. Salomon, and M. M. Labes	779
Exciton States in Polymers	John S. Avery and Ronald Mason	784
An Electron-Hole Picture of Photosynthesis	William Arnold	788
<hr/>		
Exchange of Substituents on Nitrogen in Molten Ammonium Salts and Amines	Heinz K. Hofmeister and John R. Van Wazer	791
Rate of Exchange of Chlorine between Dimethylchloramine and Succinimide	Takeru Higuchi and Jun Hasegawa	796
Chemical Synthesis with Ion Beams	Stanley Singer, N. G. Kim, A. W. Merkl, and M. Farber	799
Evidence of Structure and Dissociation Equilibrium in Liquid Iron Oxide from Iron Oxide Activity Data	Oliver N. Salmon and Roger D. Hilde	804
γ -Radiolysis of Liquid Cyclopentanone	W. W. Bristowe, M. Katayama, and C. N. Trumbore	807
Radiolysis of Ethylene. I. Yield of Hydrogen Atoms and Formation of Saturated Hydrocarbons	G. G. Meisels and T. J. Sworski	815
Photoreduction of Methyl Red Sensitized by Ethyl Chlorophyllide <i>a</i>	G. R. Seely	821
A Comparison of Fast Neutron and γ -Irradiation of Polystyrene. I. Cross-Linking Rates	W. W. Parkinson, C. D. Bopp, D. Binder, and J. E. White	828
Shock Waves in Chemical Kinetics. The Dissociation of Molecular Chlorine	Mathias van Thiel, Daniel J. Seery, and Doyle Britton	834
Kinetics of the γ -Ray-Induced Decomposition of Chloroform	Horst R. Werner and Richard F. Firestone	840
The Chemiluminescent Reaction of Oxygen Atoms with Sulfur Monoxide at Low Pressures	Thomas R. Rolfes, Robert R. Reeves, Jr., and Paul Harteck	849



The Only Way to Weigh a Molecule

For osmolalities and molecular weight determinations from 100 to 25,000 (number average), Mechrolab's Vapor Pressure Osmometer has proved to be the most satisfactory — if not the only — way of doing the job.

Operating on the principle of vapor pressure lowering, more than 700 VPOs are now in use, replacing other techniques such as ebulliometry and cryoscopy. Why? Because the VPO is: *rapid* (you can make 60 to 80 individual measurements each 8-hour day); *precise* (1% accuracy for low molecular weight polymers, useful data for molecular weights to 25,000); *convenient* (it's compact and is designed for routine operation); *versatile* (wide choice of sol-

vents [aqueous or organic], operating temperatures, broad range of molecular weights and samples, with sample size requirements as low as 10 microliters).

Mechrolab's standard Model 301A VPO, maximum operating temperature 65°C, costs \$2,390. High temperature Model 302 operates to 130°C, price \$2,900. Direct sales and service by Mechrolab technical field personnel.

Call or write for further details on 300 series VPO's and/or a demonstration by a factory representative. Also, be sure to ask for your free subscription to our news letter, "The Molecule." Write to 1062 Linda Vista, Mountain View 43, California.

Typical Applications

Bio-Medical Osmolalities • Osmotic Coefficients
Proteins • Sugars.

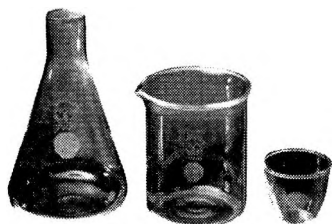
Chemical Monomers • Hydrocarbons • Prepolymers
Polyolefins • Polyamides • Cellulosics • Elastomers
Petrochemicals • Silicones.

HEWLETT
PACKARD  MECHROLAB
DIVISION

"Advanced Instrumentation for Increasing Laboratory Productivity"
High Speed Membrane Osmometers, Light-Scattering Photometers, Automanometers

Halogen Displacement Reactions of Chloro- and Bromoacetic Acids in Water and Dioxane-Water Solutions	J. F. Hinton and F. J. Johnston	854
The Kinetics of Thermal Decomposition of Diacetylene in a Flow System	K. C. Hou and H. B. Palmer	858
The Kinetics of Thermal Decomposition of Benzene in a Flow System	K. C. Hou and H. B. Palmer	863
Transport Properties of a Dense Fluid of Molecules Interacting with a Square-Well Potential	H. Ted Davis and K. D. Luks	869
Dislocations as Active Centers of Catalysis and Chemical Action in Silver	Ituro Uhara, Shozo Kishimoto, Yasuko Yoshida, and Tadashi Hikino	880
Cation Interchange across Ion-Exchange Membranes	M. Worsely, A. S. Tombalakian, and W. F. Graydon	883
The Radiolysis of Propane at Extremely Low Conversions	L. W. Sieck, N. K. Blocker, and J. H. Futrell	888
Rare Gas Sensitized Radiolysis of Acetylene	J. H. Futrell and L. W. Sieck	892
Electrochemical Characterization of the Surface Composition of Heterogeneous Platinum-Gold Alloys	M. W. Breiter	901
Hydrogen Atom Addition to Olefins: Relative Rates at the Two Carbon Positions and Derived Heats of Formation of Several Alkyl Radicals	Richard D. Kelley, Ralph Klein, and Milton D. Scheer	905
Mechanism of Homogeneous Gas-Phase Partial Oxidation of <i>o</i> -Xylene	Jordan Loftus and Charles N. Satterfield	909
Carbon Isotope Effects in the Pyrolytic Decomposition of Magnesium Oxalate	Peter E. Yankwich and Petros D. Zavitsanos	918
Rydberg Potential Energy Function for Diatomic Molecules as Extended to Polyatomic Species and Activated Complex	William F. Sheehan	923
Acidity and Autocatalysis of Esterification of Acetylenic and Fluoro Acids	Jack Radell, B. W. Brodman, Amiram Hirshfeld, and E. D. Bergmann	928
Solvent Vapor Pressures in Dilute Solutions of Gallium in Cadmium	Guy R. B. Elliott, Joe Fred Lemons, and Harold S. Swofford, Jr.	933
Two Phosphorescences and Electron Transfer in Dye-Disulfhydryl Compound Complex	Eiji Fujimori	940
The Photochemistry of Methyl Isopropyl Ketone	A. Zahra and W. Albert Noyes, Jr.	943
Nuclear Quadrupole Resonance of Bi ²⁰⁹ in BiBr ₃	Elizabeth D. Swiger, Paul J. Green, Gary L. McKown, and Jack D. Graybeal	949
Electron Spin Resonance Line Shape of Triplet Triphenylene in Rigid Solution	J. B. Farmer, C. L. Gardner, and C. A. McDowell	953
The Nucleation of Long-Chain Molecules in Monomolecular Layers	L. Mandelkern, J. G. Fatou, and C. Howard	956
Equilibrium Ultracentrifugation of Hydrolyzed Lead(II) Perchlorate Solutions	O. E. Esval and James S. Johnson, Jr.	959
Entropy and Volume Changes on Ionization of Aqueous Acids	Loren G. Hepler	965
Micelle Formation in Concentrated Sulfuric Acid as Solvent	Joseph Steigman and Norman Shane	968
The Reactivity of Metal Ions and Some Oxy Anions toward Hydrated Electrons	M. Anbar and Edwin J. Hart	973
The $n-\pi^*$ Cotton Effect of the Peptide Linkage	Burton J. Litman and John A. Schellman	978
Investigation of Fatty Acid Monolayers on Metals by Contact Potential Measurements	C. O. Timmons and W. A. Zisman	984
The Heats of Formation of Anhydrous Europium(II) Chloride and of the Aqueous Europium(II) Ion	C. T. Stubblefield, J. L. Rutledge, and R. Phillips	991
Ethanol Hydrate	A. D. Potts and D. W. Davidson	996
Photochemistry of the Fluoroketenes. Heptafluoropropyl Ethyl Ketone	G. O. Pritchard and R. L. Thommarson	1001
Microwave Absorption and Molecular Structure in Liquids. LXI. The Dielectric Relaxation Mechanism for Molecules Similar in Structure to Diphenyl Ether	Ralph D. Nelson, Jr., and Charles P. Smyth	1006

what you
should know
about VYCOR[®]
BRAND
96%
silica labware



Our octagon design trademark means it is VYCOR brand ware. Nearly pure silica, it is capable of continuous service at 900°C. It can be quenched safely and repeatedly in ice water from that temperature. It may be safely used in place of fused silica or quartz.

You can do that with VYCOR brand ware because its coefficient of expansion is only 0.000008/°C, the lowest of any commercial glass except fused silica.

Chemically, VYCOR brand ware is superior to borosilicate glasses in its resistance to acids and to alkalis even at high temperatures.

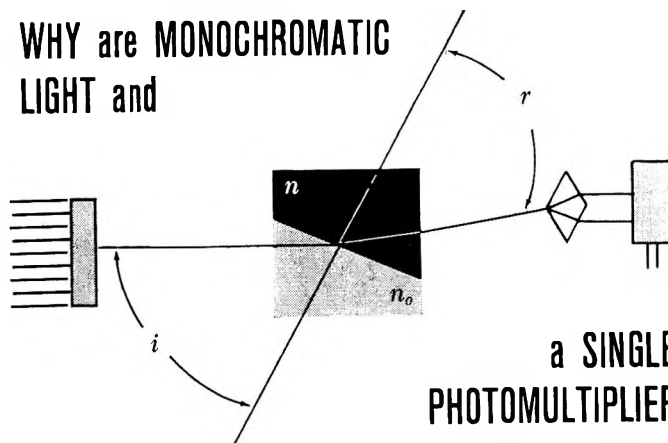
VYCOR brand ware is available nationwide. Your local labware supplier stocks beakers, flasks, crucibles, ground joints, and tubing. Choose from 132 types and sizes of this unique ware. It is in our PYREX[®] brand Labware Catalog LG-3.

Item for item, VYCOR brand ware generally costs you less than transparent fused quartz, performs just as well, and is more readily available. You can bring its price down even lower by combining VYCOR brand items with your PYREX brand labware order to save as much as 28 cents on the dollar with quantity discounts.

Laboratory Glassware Dept., Corning Glass Works, 7803 Crystal St., Corning, N. Y.

CORNING
THE MAKERS OF PYREX[®] LABWARE

WHY are MONOCHROMATIC LIGHT and



a SINGLE PHOTOMULTIPLIER

VITAL to
AUTOMATIC DIFFERENTIAL REFRACTOMETRY?

MONOCHROMATIC LIGHT?

The use of monochromatic light eliminates the dispersion effect found in instruments employing polychromatic light. Only the use of monochromatic light permits differential refractometers to be calibrated in terms of absolute refractive index difference.

A SINGLE PHOTOMULTIPLIER?

Drift due to temperature changes, spectral shifts, and fatigue are eliminated with the use of a single photomultiplier tube. This also permits measurement of highly absorbing and turbid samples, a capability not provided by other photo-detectors.

The end result is an instrument with greater accuracy, more sensitivity, extended range and increased stability . . . the Phoenix Differential Refractometer. Want more reasons? Write for Bulletin R-2000.



PHOENIX PRECISION INSTRUMENT COMPANY
A Subsidiary of CENCO INSTRUMENTS CORP.
3803-05 N. 5th Street, Phila., Penna. 19140, U.S.A.

No. 35 in the ADVANCES IN CHEMISTRY SERIES

AZEOTROPIC DATA-II

For those chemists and chemical engineers who make or plan separations of multi-component mixtures by fractional distillation, AZEOTROPIC DATA-II is now available.

This volume consists of 92 pages of tables plus a short introduction. The data are grouped under: I. Binary Systems (1674); II. Ternary Systems (251); and III. Quaternary Systems (12). Included are an empirical formula index and a bibliography.

Most of the data are taken from the original literature, and from handbooks, review articles, etc. However, a number of companies supplied unpublished data. They are Commercial Solvents, Dow Chemical, Eastman Chemical Products, Farbenwerke Hoechst, Imperial Chemical Industries, Minnesota Mining and Union Carbide.

If you are a petroleum chemist or chemical engineer, or an organic or physical chemist, you will find this book invaluable, as will workers in other fields of chemistry.

100 pages.

Paper bound.

Price: \$4.50

Order from:

Special Issues Sales/American Chemical Society
1155 Sixteenth Street, N.W./Washington 6, D.C.

Heats of Reaction of Boron Trifluoride with HF·3.75H ₂ O and of Diborane with Trimethylamine. Correlation of Thermochemical Data for Some Boron Compounds	Stuart R. Gunn	1010
Thermal Diffusion Measurements by Wave-Front-Shearing Interferometry	Silas E. Gustafsson, Julius G. Becsey, and James A. Bierlein	1016
The Formation and Decomposition Reactions of the Acetyl Radical and the Heat of Formation of the Acetyl Radical	J. Alistair Kerr and Jack G. Calvert	1022
C ¹³ Magnetic Resonance Study of the Protonation of Acetic and Benzoic Acids and Their Ethyl Esters in Concentrated Sulfuric Acid	Gary E. Maciel and Daniel D. Traficante	1030
Electronic Commutator Determination of <i>E</i> ^o of Formation and Related Thermodynamic Quantities for Molten Lead Chloride.	Theodore B. Warner and Ralph L. Seifert	1034
Reaction of Tritium Atoms with Films of Solid Ethylene. Disproportionation and Combination of Ethyl Radicals at 63°K.	K. W. Watkins and H. C. Moser	1040
Effect of Density on the Radiolysis of Ethane	Catherine M. Wodetzki, P. A. McCusker, and D. B. Peterson	1045
Sedimentation Equilibria in Polydisperse Pseudo-Ideal Solutions and at Low Centrifugal Fields	H. W. Osterhoudt and J. W. Williams	1050

NOTES

Effect of Additives in Radiolysis of Ethane at High Densities	Catherine M. Wodetzki, P. A. McCusker, and D. B. Peterson	1056
Disproportionation and Combination of Tritium-Labeled Isopropyl Radicals	Han Bo Yun and H. C. Moser	1059
Remarks on Förster's Theory of Transfer of Excitation Energy	Mira Leibowitz	1061
The Temperature Dependence of the <i>cis-trans</i> Photoisomerization of Azo Compounds: Theoretical Considerations	David R. Kearns	1062
Note on the Thermodynamics of the Formation of Dolomite	F. Halla	1065
Relation of Ring Size to Ultraviolet Extinction Coefficient in Cyclosiloxanes Containing Phenyl Substituents on Silicon	C. R. Sporck and A. E. Coleman	1066
Electrooxidation of the Tetraphenylborate Ion in Aqueous Solution at the Platinum Disk Electrode	W. Richard Turner and Philip J. Elving	1067
The Thermodynamic and Physical Properties of Beryllium Compounds. VII. Enthalpy and Entropy of Sublimation of Beryllium Fluoride	Jay A. Blauer, Michael A. Greenbaum, and Milton Farber	1069
Reactivities of Perfluoroalkylnitriles toward Butadiene	Alan R. Monahan and George J. Janz	1070
The Thermal Isomerization of Cyclobutene	Robert W. Carr, Jr., and W. D. Walters	1073
The C-C Bond Dissociation Energy in C ₂ F ₆	E. Tschuikow-Roux	1075
Radiation Yields of Carbon Monoxide and Dioxide for Some Aromatic Carbonyl Compounds	A. A. Miller	1077
Molar Extinction Coefficients of O ₂ F ₂ in the Visible Range and a Comparison with Other Oxygen Fluorides	A. G. Streng and L. V. Streng	1079
Radiolysis of Frozen Solutions. II. Sodium Nitrite Ices	Larry Kevan	1080
On Electron Trapping in Polycrystalline and in Glassy Alkaline Ices	Larry Kevan	1081
The Effect of Oxygen on the Electron Spin Resonance Spectra of Anthracene and Perylene Adsorbed on Silica-Alumina	Haruo Imai, Yoshio Ono, and Tominaga Keii	1082

COMMUNICATIONS TO THE EDITOR

Surface Free Energy of Polymers	Harold Schonhorn	1084
An Anomaly in the Interaction of CF ₃ H Radicals	G. O. Pritchard and J. T. Bryant	1085
Note on Molecular Diffusion and Heat Conductivity in Liquids	Marcel J. E. Golay	1086

AUTHOR INDEX

- Akimov, I., 730
 Anbar, M., 973
 Arnold, W., 788
 Avery, J. S., 784

 Becsey, J. G., 1016
 Bergmann, E. D., 928
 Bierlein, J. A., 1016
 Binder, D., 828
 Blauer, J. A., 1069
 Blocker, N. K., 888
 Boehm, C., 745
 Bopp, C. D., 828
 Bourdon, J., 705
 Breiter, M. W., 901
 Bristowe, W. W., 807
 Britton, D., 834
 Brodman, B. W., 928
 Bryant, J. T., 1085

 Calvert, J. G., 1022
 Carr, R. W., Jr., 1073
 Coleman, A. E., 1066
 Coret, A., 745

 Davidson, D. W., 996
 Davis, H. T., 869

 Elliott, G. R. B., 933
 Elving, P. J., 1067
 Esval, O. E., 959

 Farber, M., 799, 1069
 Farmer, J. B., 953
 Fatou, J. G., 956
 Firestone, R. F., 840
 Fujimori, E., 940
 Futrell, J. H., 888, 892

 Gardner, C. L., 953
 Golay, M. J. E., 1086
 Graybeal, J. D., 949
 Graydon, W. F., 883
 Green, P. J., 949
 Greenbaum, M. A., 1069
 Gunn, S. R., 1010
 Gustafsson, S. E., 1016

 Halla, F., 1065
 Hart, E. J., 973
 Harteck, P., 849
 Hasegawa, J., 796
 Hepler, L. G., 965
 Higuchi, T., 796
 Hikino, T., 880
 Hilde, R. D., 804
 Hinton, J. F., 854
 Hirshfeld, A., 928
 Hishiki, Y., 774
 Hoegl, H., 755
 Hofmeister, H. K., 791
 Hou, K. C., 858, 863
 Howard, C., 956

 Imai, H., 1082
 Inoue, E., 767

 Janz, G. J., 1070
 Jeanclaude, C., 745
 Johnson, J. S., Jr., 959
 Johnston, F. J., 854

 Katayama, M., 807
 Kearns, D. R., 1062
 Keii, T., 1082
 Kelley, R. D., 905

 Kerr, J. A., 1022
 Kevan, L., 1080, 1081
 Kim, N. G., 799
 Kishimoto, S., 880
 Klein, R., 905
 Kokado, H., 767

 Labes, M. M., 779
 Leibowitz, M., 1061
 Lemons, J. F., 933
 Lendvay, E., 738
 Litman, B. J., 978
 Loftus, J., 909
 Luks, K. D., 869

 Maciel, G. E., 1030
 Mandelkern, L., 956
 Mason, R., 784
 McCusker, P. A., 1045, 1056
 McDowell, C. A., 953
 McKown, G. L., 949
 Meier, H., 719
 Meisels, G. G., 815
 Merkl, A. W., 799
 Miller, A. A., 1077
 Monahan, A. R., 1070
 Moser, H. C., 1040, 1059

 Namba, S., 774
 Nelson, R. C., 714
 Nelson, R. D., Jr., 1006
 Nikitine, S., 745
 Noyes, W. A., Jr., 943

 Ono, Y., 1082
 Osterhoudt, H. W., 1050

 Palmer, H. B., 858, 863
 Parkinson, W. W., 828
 Peterson, D. B., 1045, 1056
 Phillips, R., 991
 Potts, A. D., 996
 Pritchard, G. O., 1001, 1085

 Radell, J., 928
 Reeves, R. R., Jr., 849
 Reucroft, P. J., 779
 Rolfes, T. R., 849
 Rudyj, O. N., 779
 Rutledge, J. L., 991

 Salmon, O. N., 804
 Salomon, R. E., 779
 Satterfield, C. N., 909
 Scheer, M. D., 905
 Schellman, J. A., 978
 Schmillen, A., 751
 Schonhorn, H., 1084
 Seely, G. R., 821
 Seery, D. J., 834
 Seifert, R. L., 1034
 Shane, N., 968
 Sheehan, W. F., 923
 Sieck, L. W., 888, 892
 Singer, S., 799
 Smyth, C. P., 1006
 Sporck, C. R., 1066
 Steigman, J., 968
 Streng, A. G., 1079
 Streng, L. V., 1079
 Stubblefield, C. T., 991
 Swiger, E. D., 949
 Swofford, H. S., Jr., 933

 Sworski, T. J., 815

 Terenin, A., 730
 Thommarson, R. L., 1001
 Timmons, C. O., 984
 Tombalakian, A. S., 883
 Traficante, D. D., 1030
 Trumbore, C. N., 807
 Tschuikow-Roux, E., 1075
 Turner, W. R., 1067

 Uhara, I., 880

 van Thiel, M., 834
 Van Wazer, J. R., 791

 Walters, W. D., 1073
 Warner, T. B., 1034
 Watkins, K. W., 1040
 Werner, H. R., 840
 White, J. E., 828
 Williams, J. W., 1050
 Wodetzki, C. M., 1045, 1056
 Worsely, M., 883

 Yamaguchi, T., 767
 Yankwich, P. E., 918
 Yoshida, Y., 880
 Yun, H. B., 1059

 Zahra, A., 943
 Zavitsanos, P. D., 918
 Zielinger, J. P., 745
 Zisman, W. A., 984
 Zouaghi, M., 745

Spectral Sensitization of Chemical Effects in Solids¹

by Jean Bourdon

Centre de Recherches Kodak-Pathé, Vincennes, Seine, France (Received October 5, 1964)

The processes of spectral sensitization of the chemical effects in silver bromide and zinc oxide are described and discussed along the following lines. In what respect is the intrinsic photochemical effect modified when sensitized by a dye? In what respect does the photochemical effect modify or perturb the spectral sensitization process? In the case of silver bromide, photoholes generated intrinsically are mobile into the crystal. This behavior can be altered considerably when they are generated by light absorbed by the dye. On the other hand, surface bromide ions seem to play an important role in the spectral sensitization process. In the case of zinc oxide, the present available data render it difficult to reach a definite conclusion on the reciprocal influence of oxygen photodesorption and the spectral sensitization process.

Many solids exhibit a chemical modification when illuminated by ultraviolet or visible light. Among these photosensitive solids are silver halides, mercury salts, many salts of heavy metallic ions^{2a} (organic salts in particular), zinc oxide, and many organic solids^{2b} such as photochromic compounds or photosensitive high polymers (fabrics and textiles being a practical example of the latter).

The chemical modifications which are observed can be very different, varying from the photolysis of silver halides³ to the photodesorption of oxygen from zinc oxide, the photo cross linking of certain high polymers,⁴ the photochromism in some organic solids, and the photoionization of organic molecules in a solid matrix. (See in the second part of this paper the reasons for including ZnO in photochemically sensitive solids.)

Some of the photosensitive systems can be spectrally sensitized by dyes and this is particularly the case for silver halides, mercurous oxalate,⁵ zinc oxide, and some organic materials.⁶

The purpose of this review is not to give a comprehensive description of the various photosensitive systems described above, which is beyond the scope of this paper, but to present the main aspects of the mechanism of the only two systems which have been the subject of thorough studies: silver halides and zinc oxide. We

(1) Presented to the International Conference on Photosensitization in Solids, Chicago, Ill., June 22-24, 1964.

(2) (a) P. Glafkides, "Chimie Photographique," P. Montel, Paris, 1957, p. 350; (b) H. S. Gilmour, "Physics and Chemistry of the Organic Solid State," Vol. I, Interscience Publishers, Inc., New York, N. Y., 1963, p. 330.

(3) C. E. K. Mees, "The Theory of the Photographic Process," Macmillan and Co., Ltd., London, 1954 (see also the new edition by T. H. James, in preparation).

(4) L. M. Minsk, J. G. Smith, W. P. Van Deusen, and J. F. Wright, *J. Appl. Polymer Sci.*, **2**, 302 (1959).

(5) P. A. Van der Meulen and R. H. Brill, *Phot. Sci. Eng.*, **2**, 121 (1958).

(6) E. M. Robertson, W. P. Van Deusen, and L. M. Minsk, *J. Appl. Polymer Sci.*, **2**, 308 (1959).

intend in particular to discuss the problem along the following lines.

The process of spectral sensitization of inorganic photosensitive solids such as silver halides or zinc oxide goes through an electronic step, as in the case of any dye-sensitized photoelectric effect in a semiconductor. This electronic step is followed by the chemical step itself, which is, for silver bromide, the formation of a latent image (Ag_0) and evolution of bromine, and for zinc oxide, the desorption of oxygen.⁷

No differences should therefore be found between the mechanism of spectral sensitization of these two systems (chemical transformation or electronic effect) and as a matter of fact, they have been, for the most part, the object of the same studies and the same discussions.⁸⁻¹⁰

In spite of this consideration, it should be of interest to try to answer the following questions.

(1) In what respect is the chemical effect which is produced by irradiation in the intrinsic absorption band of the solid modified when the irradiation is given in the absorption band of the sensitizer?

(2) In what respect does the chemical effect modify or perturb the spectral sensitization process? The influence of photolytic silver on the spectral sensitization process is not considered.

(3) In relation to the second question, what is the part taken by the photochemical transformation in the regeneration of electron donor levels, which appear to be essential to this process?

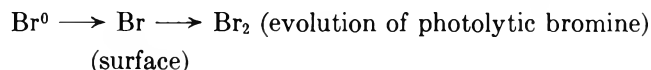
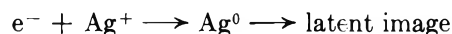
(4) Is there energy transfer or electron transfer? Though here somewhat outside the subject, a discussion on spectral sensitization mechanism would not be complete without a few comments on this highly controversial subject.

In spite of the many points of similarity between spectral sensitization of silver halides and of zinc oxide, for reason of convenience, these two topics will be discussed separately.

The following report will deal mostly with cases of spectral sensitization by dyes in a molecular state of adsorption, excluding therefore, unless specifically mentioned, cases of spectral sensitization by dye films.

A. Silver Bromide

I. Intrinsic Process. The chemical effect initiated by light in silver bromide is a photolysis resulting in the formation of metallic silver and evolution of bromine. For very weak illuminations, the metallic silver will be described as a latent image: for stronger illuminations, very large amounts of silver and bromine are released; this is called print-out. In both cases, the photochemical reactions are written



The mechanism of formation of the latent image has been the object of many studies and very good review papers have been given on the subject.¹¹

We will accept, for the present discussion, the mechanism as described by Gurney and Mott, one of the best pieces of evidence, among others, being the experiments of Haynes and Shockley,¹² later repeated and very thoroughly developed by Webb¹³ and Hamilton, *et al.*¹⁴ These experiments consist of the displacement, in the silver halide sample, of electrons and holes by a pulsed applied field synchronized with the excitation flash. They showed without ambiguity that the absorbed photon creates a mobile hole and a mobile electron, the latter resulting finally in the formation of the latent image.

II. Spectral Sensitization of Silver Bromide.^{3,15} West and Carroll recently have written a very good review on the subject¹⁶ and hence only a few points will be developed here to recall the main aspects of the problem.

A. Conditions of Spectral Sensitization (Figure 1). A dye molecule will be a good sensitizer for the photolysis and the photoconduction of silver bromide if several requirements, arising from the following considerations, are met.

The energy of the photon absorbed by the dye has to be transferred (as energy or as an electron) to the silver bromide crystal, the efficiency of the transfer being decreased by any competing factors which will interfere with it and increased if the dye possesses the corresponding required qualities.

(7) D. B. Medved, *J. Chem. Phys.*, **28**, 870 (1958).

(8) R. C. Nelson, *J. Opt. Soc. Am.*, **46**, 13, 1016 (1956); **51**, 1182, 1186 (1961).

(9) J. Meier, "Die Photochemie der organischen Farbstoffe," Springer-Verlag, Berlin, 1963: (a) p. 273; (b) p. 288.

(10) (a) A. Terenin, E. Putzeiko, and I. Akimov, *J. chim. phys.*, 716 (1957); (b) A. Terenin and I. Akimov, *Z. physik. Chem. (Leipzig)*, **217**, 307 (1961).

(11) W. F. Berg, "Photographic Science Symposium, Zürich, 1961," Focal Press, London, 1963, p. 27; T. H. James, "The Theory of the Photographic Process," new edition in preparation.

(12) J. R. Haynes and W. Shockley, *Phys. Rev.*, **82**, 935 (1951).

(13) J. H. Webb, *J. Appl. Phys.*, **26**, 1309 (1955).

(14) J. F. Hamilton, F. A. Hamm, and L. E. Brady, *ibid.*, **27**, 874 (1956); J. F. Hamilton and L. E. Brady, *ibid.*, **30**, 1902 (1959).

(15) B. H. Carroll, *Phot. Sci. Eng.*, **5**, 65 (1961).

(16) W. West and B. H. Carroll, "The Theory of the Photographic Process," new edition by T. H. James, in preparation.

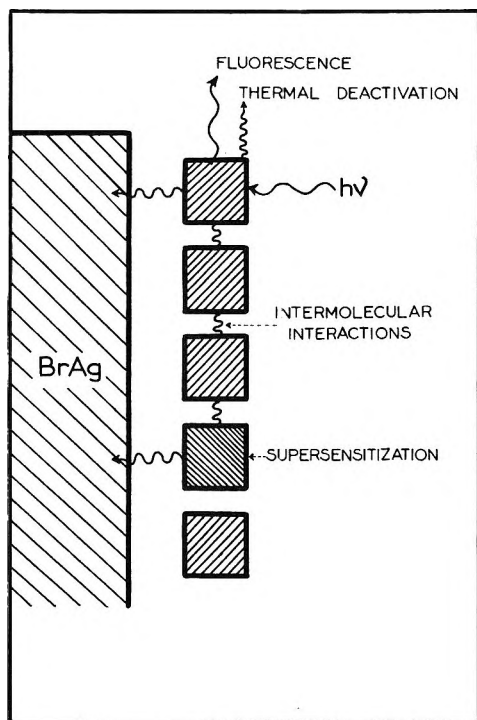


Figure 1. Fate of the absorbed energy in the spectral sensitization.

(a) *Coplanarity*. Any substituent perturbing the planarity of the dye molecule inhibits the existing fluorescence, if any, by favoring thermal energy degradation processes and therefore the sensitizing efficiency. To be a good sensitizer, a dye molecule has to present a coplanar structure resulting eventually in fluorescent properties and better sensitizing ability.

(b) *Adsorption*. Poor adsorption prevents good transfer. A strong adsorption of the dye is shown by measurements of heat of adsorption and by the observation of the ultraviolet and visible absorption spectrum of the adsorbed dye. The latter usually shows a strong modification, compared to the unadsorbed dye, indicating a dye-crystal interaction.¹⁷

Another competing process which decreases the efficiency of transfer from the dye to the substrate can come from the strong interaction between dye molecules when present in a state of aggregation (*J*-aggregate).

Adding a supersensitizer¹⁸ allows the energy "stored" in the dye layer to be transferred to the crystal. Recent experiments at low temperature¹⁹ demonstrate very well the poor interaction between *J*-aggregate and crystal.

(c) *Respective Energy Levels of the Dye and the Crystal*.²⁰ This requirement is to be considered only in the case of a mechanism of electron transfer and is discussed later.

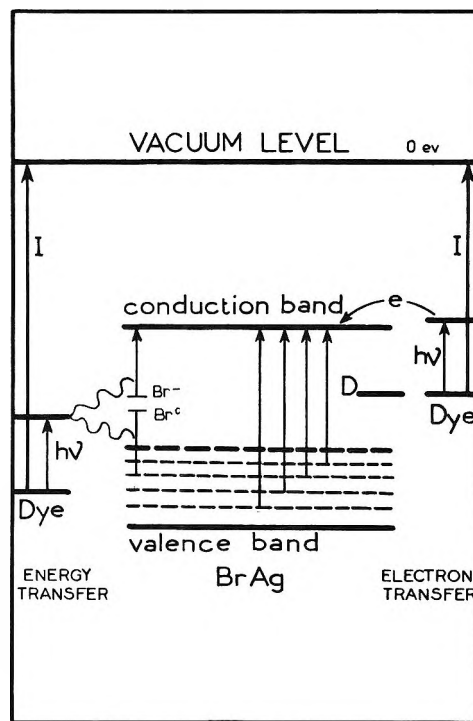


Figure 2. Energy level diagram of the dye-silver bromide system.

B. Mechanism of Spectral Sensitization of Silver Bromide (Figure 2). (a) *Role and Behavior of the Positive Hole*. Since the dye sensitizer is adsorbed at the surface of the silver bromide, the absorption of photons by the dye results in the formation of a latent image in a fashion similar to the one resulting from absorption of photons in the intrinsic absorption band of the silver bromide (one can observe, in particular, internal and surface latent images equally well in both cases).

This observation shows that after absorption of a photon by the dye, an electron has been excited into the conduction band of the halide and ultimately combined with a silver ion to give a silver atom.

However, the energy of the photon absorbed by the dye (1 to 2.5 e.v.) is inferior to that corresponding to the absorption edge of the silver bromide (2.5 e.v.). The donor level from which the electron is excited has therefore to be located in the forbidden gap, 1 to 2.5 e.v. below the bottom of the conduction band; conse-

(17) S. Boyer, *J. chim. phys.*, **381** (1960); W. West and L. A. Geddes, *J. Phys. Chem.*, **68**, 837 (1964).

(18) R. Brünner, A. Oberth, and G. Scheibe, *Z. Wiss. Phot.*, **50**, 283 (1955).

(19) H. Frieser, A. Graf, and D. Eschrich, *Z. Elektrochem.*, **65**, 870 (1961).

(20) W. West, ref. 11, p. 71.

quently, a positive hole cannot be created by the primary absorption act of the photon in the valence band of the silver bromide, unless by a two-quantum mechanism. In fact, after the sensitization act, a positive hole should be left at the intermediate level in the forbidden gap, being trapped either at the dye site as a dye positive radical ion (electron transfer), or at the surface of the AgBr crystal as an empty donor level (energy transfer).

The fact that the positive hole, whatever its nature may be, is directly "formed" on a trap at an energy level located in the forbidden gap probably explains the impossibility of exciting the fluorescence of dye-sensitized silver bromide by illumination in the dye absorption band, as was noted by West.²⁰

A similar observation was made by Akimov²¹ with dye-sensitized AgX, TlX, PbO, and ZnO.

This intrinsic trapping of the positive hole should result in its inability to move through the crystal. This has been demonstrated recently by Saunders, Tyler, and West^{22,23} by experiments on dyed sheet crystals of silver bromide. The authors showed that photoelectrons, formed by illumination either in the absorption band of silver bromide or in the absorption band of the dye, could be moved deep into the crystal by a pulsed electric field. Positive holes showed a very different behavior; with the proper reversed electric field and irradiation with ultraviolet or blue light, mobile holes were observed inside the crystal, but with visible light, no sign of hole mobility could be observed and as was pointed out by the authors, the process of spectral sensitization in these crystals is not accompanied by the formation of mobile holes.

These experiments seem almost conclusive in spite of some halogen acceptance properties of the dye when illuminating the AgBr crystal with the 254-m μ mercury line (a nonpenetrating radiation). They are also in agreement with the observation of e.p.r. signals²⁴ arising in dyed silver bromide powders illuminated at liquid nitrogen temperature, if one accepts the hypothesis that trapped holes would be responsible for such e.p.r. signals.

However, these observations seem to be in contradiction with those made by Terenin and co-workers¹⁰ in their studies on the Demer effect of dye-sensitized silver bromide powders. These authors claim, indeed, that only a positive charge-carrier internal photoelectric effect can be observed with such samples.

In fact, it appears that these two experiments are not in contradiction but they represent two different aspects of the same phenomenon. In West's experiments,²² the samples used are highly purified monocrystals of silver bromide melted into thin sheets.

Such crystals have, without any doubt, very few physical or chemical defects able to trap electrons, allowing the authors to observe their displacement.

In Terenin's experiments, the samples are microcrystalline powders of silver bromide characterized by a high specific surface and probably by many physical defects, all factors being favorable to electron trapping. In confirmation of this view, Hamilton²⁵ has shown in particular that photoelectron lifetimes are shorter in small crystals than in large crystals, this effect being due to their trapping by superficial silver ions.

On the other hand, such high specific area samples would be very sensitive to the presence of adsorbed bromine, which creates surface acceptor levels, as suggested by Terenin and co-workers.²⁶⁻²⁸

All of these factors are therefore very unfavorable to the appearance of an electronic photocurrent but very favorable to that of a hole photocurrent.

Two hypotheses can be brought forward to explain the observation of a dye-sensitized hole migration.

(1) *Surface Migration.* Photoholes resulting from the light absorption by the dye, intrinsically trapped at the dye site as suggested by West,²² could have some mobility at the surface of the silver bromide itself in the quasi-conduction band which exists as a consequence of the high specific surface of these microcrystals and of the presence of bromine.

(2) *Internal Migration.* Photoholes initiated in the valence band by excitation of electrons from that band to surface acceptor levels (bromine), as suggested by Terenin, would be able to migrate inside the crystal.

This latter hypothesis suggests the possibility of a two-quantum mechanism in spectral sensitization of silver bromide and introduces the question of regeneration of electron donor levels in this process.

(b) *Regeneration of Electron Donor Levels.* The problem has been raised by the observation of Leszinski,²⁹ who found that by irradiation of dye-sensitized AgBr, many silver atoms can be formed for each dye

(21) I. A. Akimov, *Zh. Nauchn. i Prikl. Fotogr. i Kinematogr.*, **4**, 64 (1959).

(22) V. Saunders, R. W. Tyler, and W. West, Turin Photography Conference, 1963.

(23) W. West, *J. Phys. Chem.*, **66**, 2398 (1962).

(24) W. C. Needler, R. L. Griffith, and W. West, *Nature*, **191**, 902 (1961).

(25) J. F. Hamilton and L. E. Brady, *J. Phys. Chem.*, **66**, 2384 (1962).

(26) I. A. Akimov, *Dokl. Akad. Nauk SSSR*, **121**, 311 (1958).

(27) A. Terenin and I. A. Akimov, "Scientific Photography," Photographic Science Symposium, Liège, 1959, Pergamon Press, London, 1962, p. 532.

(28) A. Akimov, *Fiz. Tverd. Tela*, **4**, 1138 (1962).

(29) W. Leszinski, *Z. Wiss. Phot.*, **24**, 261 (1926).

molecule adsorbed on the silver bromide surface. The particularly high value of 160 silver atoms formed per dye molecule was found later by Eggert³⁰ with some infrared sensitizers.

From the latter facts arises the evidence that, in some cases at least, electron donor levels, belonging either to the dye molecule or to the crystal surface, should be regenerated and that the photochemical transformation taking place in the silver bromide should have an influence on such a process.

Some data permit the following statement of the problem. The area of an average silver bromide grain in a highly sensitive emulsion is $1 \mu^2$. At the optimum dye coverage (30 to 80% of its surface), it will adsorb about 5×10^5 to 10^6 dye molecules each 74 \AA^2 in area, (3-3'-diethylthiacarbocyanine bromide in the *J*-aggregate).

On the other hand, several authors have measured the number of quanta necessary to render a silver bromide grain developable: the most sensitive grains of a highly sensitive emulsion: 4 quanta/grain³¹; half of the grains of a similar emulsion: 10 to 25 quanta/grain³²; average grain of a moderately sensitive emulsion: up to 500 quanta/grain.³³

These numbers are very low compared to the number of adsorbed dye molecules just mentioned, and show without any doubt that the regeneration of electron donors is not necessary for the formation of the latent image in practical photography, but there still remains the question of whether or not, in the individual sensitizing act, the mechanism is such that the dye is destroyed.

Anyhow, this regeneration process seems to be necessary, in the practical sense, in two cases: (a) the photolysis of silver bromide with the formation of visible metallic silver (print-out), if an efficient halogen acceptor has been added to prevent a rapid dye destruction (no serious consideration of possible spectral sensitization by photolytic silver has been given in these experiments); (b) studies of spectrally sensitized photoelectric effects in silver bromide.

Mechanism of Electron Donor Regeneration. As West has written,²³ "The donor levels are at present little more than a concept which secures conservation of energy in spectral sensitization." However, the work of Carroll and co-workers,³⁴ showing that the efficiency of spectral sensitization is not influenced by chemical sensitization, suggests that the donor levels are not modified by chemical impurities and that they may belong, in an intrinsic way, to the silver bromide surface itself. It has been proposed³⁵ that the donor sites could be superficial bromide ions, having an energy content somewhat higher than those of the regular lattice.

Such ions would provide a large supply of electrons and in fact a carbocyanine dye molecule adsorbed flat covers 155 \AA^2 , that is to say, is in possible interaction with 14 bromide ions and when adsorbed on the edge (*J*-aggregate), it covers 74 \AA^2 ³⁶ and is therefore in interaction with seven bromide ions.

These figures are, of course, an upper limit, the dye-crystal interaction taking place only between specific parts of the dye and energy-rich bromide ions.

Several hypotheses have been made to explain the occurrence of energy-rich bromide ions, the most often cited being the location of bromide ions at dislocations and the effect of adsorption of the dye on the energy levels of the bromide ions.

Accepting the hypothesis of energy-rich superficial bromide ions as electron donors, it has to be recalled that the regeneration process has to take place only in cases of heavy or long exposures, conditions which result in a photolysis of the crystal. The surface of such a crystal should therefore present a continuous modification by elimination of the bromine by "bromine acceptors" and of silver ions to metallic silver. Such a process contributes in a very efficient way to the renewal of the surface and therefore to the regeneration of the electron donor sites.

In such a discussion, one should not neglect bromine acceptors which have to be present to protect the dye and which certainly can be efficient electron donors.

These various considerations lessen the problem of the electron donor regeneration and at the same time render the "two-quantum mechanism" mentioned above less probable, if not less useful.

As has been said, the possibility of this mechanism comes from Terenin's work^{10b} which emphasizes the role of adsorbed bromine as an electron acceptor level or as an electron donor level (as adsorbed bromide ions).

In such a mechanism, a first quantum absorbed by the dye would raise an electron from the valence band to the bromine acceptor level, a second quantum raising it to the conduction band. However, it is difficult to imagine that such a process would operate in practical cases at low exposure levels and it is more probable that, according to the population of the donor-acceptor

(30) J. Eggert, W. Meidinger, and H. Arens, *Helv. Chim. Acta*, **31**, 1163 (1948).

(31) A. Marriage, *J. Phot. Sci.*, **9**, 93 (1961).

(32) G. Farnell and J. Chanter, *ibid.*, **9**, 81 (1961).

(33) C. E. K. Mees, "The Theory of the Photographic Process," Macmillan and Co., Ltd., London, 1954, p. 122.

(34) B. H. Carroll, E. A. MacWilliams, and R. B. Henrickson, ref. 11, p. 68.

(35) N. F. Mott and R. W. Gurney, "Electronic Processes in Ionic Crystals," 2nd Ed., Oxford University Press, London, 1948, p. 242.

(36) E. Klein and F. Moll, *Phot. Sci. Eng.*, **3**, 232 (1959).

levels, one would observe either electron photoconduction or hole photoconduction (*cf.* above discussion of West's and Terenin's experiments).

One should remember also that examples of spectral sensitization³⁷ with a quantum yield close to unity excludes such a process, at least for those examples.

Finally, the fact that the reciprocity failure in the region of dye absorption is the same as that in the region of halide absorption for the dyed emulsion imposed an almost insuperable difficulty against a two-quantum process.

(c) *Electron or Energy Transfer (Figure 3).* This subject has been the topic of many discussions and still remains the most controversial point of the spectral sensitization process. For a good coverage of the problem, one should refer to Meier,⁹ Terenin,^{10b} Nelson,⁸ or to the recent and comprehensive review given by West and Carroll.¹⁶ Some comments will be made here on some recent developments. The problem is essentially a question of the origin of electron donor sites.

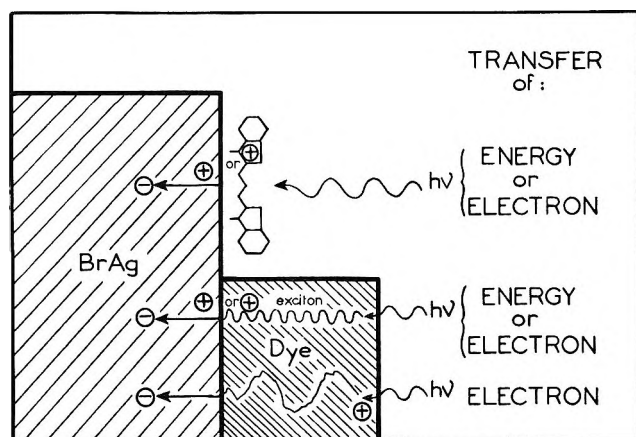


Figure 3. Schematic representation: energy or electron transfer?

In the context of the preceding discussion, if the electron is provided by the dye, one has an electron transfer; if the electron is provided by a donor level at the crystal surface, one has an energy transfer (Figure 3).

Studies made on systems of silver halide (or other inorganic photoconductors) sensitized with dye films seem to give support to an electron transfer mechanism.^{8,9}

In particular, all data on photoconductivity, photovoltaic effect, ionization potential of dye films, and the relative energy levels of the dye film and the silver bromide are consistent with the possibility of such a mechanism.

Considerations from studies made on systems sensitized by adsorbed dye molecules in the molecular state would be in favor of an energy transfer mechanism,^{10b} one of the strong arguments being that the sign of the charge carrier of the sensitized semiconductor does not depend upon the sign of the charge carrier of the dye^{10b}; another argument for energy transfer arises from the value of the ionization potential of the dye measured in the vapor phase, a value which makes an electron transfer impossible.

However, a new observation gives support to the possibility of electron transfer even in the case of a dye molecule in a molecular state of adsorption. Several authors^{38,39} have shown recently that organic molecules (carbocyanines in particular) exhibit, in rigid media, a delayed fluorescence when excited in the long wave length absorption band, this fluorescence being interpreted as a photoionization of the molecule. Such a photoionization results in a positive radical ion and in a trapped electron, which recombine later with the emission of fluorescence. Kern³⁸ points out that such a process could occur at the surface of the silver bromide, corresponding to the transfer of electrons from the dye to the crystal.

In conclusion, it seems likely, therefore, that in the present state of our knowledge, all possibilities exist for an electron transfer mechanism both in cases of dye film, and in cases of isolated molecules, though no argument can definitely exclude the energy transfer mechanism.

B. Mechanism of Spectral Sensitization of Zinc Oxide

Zinc oxide possesses a light sensitivity which appears as an internal photoelectric effect, and as photoconductive properties, these effects are accompanied by a photodesorption of the oxygen adsorbed at the surface.

The oxygen photodesorption from the zinc oxide surface can be considered as a chemical phenomenon since it results from the transformation of chemisorbed oxygen, O_2^- , to physisorbed oxygen, O_2 , followed by the oxygen desorption by thermal activation.

When zinc oxide is sensitized by a dye, photoelectric effects and photoconductivity are observed by illumination in the absorption band of the dye as well as in the

(37) W. West, *J. chim. phys.*, 672 (1958); W. West and B. H. Carroll, *J. Chem. Phys.*, 15, 529 (1947).

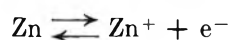
(38) J. Kern, F. Dörr, and G. Scheibe, *Z. Elektrochem.*, 66, 462 (1962).

(39) (a) A. H. Kalantar and A. C. Albrecht, *J. Phys. Chem.*, 66, 2279 (1962); E. C. Lim and G. W. Swenson, *J. Chem. Phys.*, 36, 118 (1962); E. C. Lim and W.-Y. Wen, *ibid.*, 39, 847 (1963); (b) W. West, personal communication.

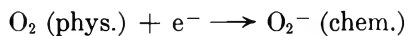
intrinsic absorption band of the zinc oxide. The spectral sensitization process and the oxygen photodesorption process both being surface phenomena, a discussion on the relationship between the two problems is therefore relevant to the present review, the purpose being to see under what conditions the two processes interact or if oxygen photodesorption is only a secondary factor. As a preliminary to the discussion of the subject itself, the main characteristics of zinc oxide will be recalled briefly along with the views generally accepted on the mechanism of its intrinsic photoelectric properties.

Zinc oxide is an n-type semiconductor.⁴⁰ Its semi- and photoconductive properties are considered to originate from excess zinc, ionized at room temperature as interstitial zinc ions or as oxygen ion vacancies.⁴¹

This situation can be described by the equations

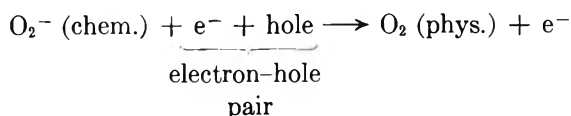


and



It appears from the second equation that the semi-conductive properties of zinc oxide are strongly dependent upon the presence of adsorbed oxygen at its surface; the electrons coming from excess zinc thermally ionized are captured by physisorbed oxygen which, as a consequence, becomes chemisorbed with creation of a potential barrier layer.

The light excitation in the intrinsic absorption band ($\lambda < 385 \text{ m}\mu$) of zinc oxide produces an electron-hole pair; a mobile electron appears in the conduction band, and the corresponding hole, apparently of very low mobility,⁴² is readily trapped by chemisorbed oxygen



the latter reaction being the cause of the oxygen photodesorption. Hauffe⁴⁰ concludes that in cases of very strong illuminations, even oxygen ions belonging to the crystal lattice could be desorbed, resulting in a real photolysis of zinc oxide. This point deserves verification.

On the other hand, Medved⁴³ remarks that the weak photoconduction of zinc oxide excited by irradiation between 400 and 600 $\text{m}\mu$ could be due to a direct photoionization of O^- and O_2^- ions adsorbed at the surface and occupying energy levels in the forbidden gap of ZnO.

Spectral Sensitization of Zinc Oxide. Recent work has shown that several aspects of spectral sensitization are

similar for zinc oxide and silver bromide and in particular, in the following instances.

Dye Adsorption and Desensitization. Markevich and Putzeiko⁴⁴ have shown indeed that the adsorption isotherms from alcoholic solutions of erythrosin are represented by the Langmuir equation and those of trypanflavine by the Freundlich equation. The maximum photoelectric effect sensitized by the dye is reached when 30 to 40% of the zinc oxide surface is covered by the dye. A higher coverage value results in a desensitizing action of the dye.

*Supersensitization.*⁴⁵ When mixtures of two sensitizing dyes were used (1,1'-diethyl-2,2'-quinocyanine iodide and 3-ethyl-2-(*p*-dimethylaminostyryl)benzothiazolium iodide, for example), an increased sensitization of the photoconductivity was observed compared to the process sensitized by one of the two dyes only.

Fluorescence Quenching of the Dye Sensitizer by Adsorption. As a general rule, effective sensitization of photolysis or of an internal photoelectric effect results in fluorescence quenching of the sensitizer, whereas no such quenching is observed when the sensitizer is adsorbed on photoinsensitive substrates such as SiO_2 and BaO. Akimov⁴⁶ has reported such experiments on the following dyes: fluorescein derivatives, rhodamine B, methylene blue, chlorophyll, and three carbocyanines. This observation confirms the effective transfer of light energy (as energy or as a charge) to the photosensitive substrate.

The heavy atom effect does not seem to be the reason for fluorescence quenching of the dyes by a singlet-triplet conversion process. These experiments therefore favor the participation of the excited singlet state of the sensitizer in the sensitization process. Similar conclusions had been reached previously by West with silver bromide.⁴⁷

Ability of a Dye Molecule to Perform the Sensitization Act Many Times. Matejec has shown that up to 250 photoelectrons can be formed for each dye molecule.⁴⁸

*Photoinduced E.p.r. Signals in Dye-Sensitized Zinc Oxide.*⁴⁹ According to Baranov, *et al.*,⁴⁹ the observed

(40) K. Hauffe, *J. Phot. Sci.*, **10**, 321 (1962).

(41) E. Mollwo and F. Stöckmann, *Ann. Phys.*, (6) **3**, 240 (1948).

(42) D. B. Medved, *J. Chem. Phys.*, **28**, 870 (1958).

(43) D. B. Medved, *J. Phys. Chem. Solids*, **20**, 255 (1961).

(44) N. N. Markevich and E. K. Putzeiko, *Russ. J. Phys. Chem.*, **36**, 1297 (1962).

(45) S. Namba and Y. Hishiki, *Rept. Inst. Phys. Chem. Res. Tokyo*, **39**, 27 (1963).

(46) I. A. Akimov, *Zh. Nauchn. i Prikl. Fotogr. i Kinematogr.*, **4**, 64 (1959).

(47) W. West, "Scientific Photography," Pergamon Press, London, 1962, p. 557.

(48) R. Matejec, ref. 11, p. 289; *Z. Elektrochem.*, **65**, 783 (1961).

signals are indicative of a possibility of photosensitization of the oxygen desorption process.

Discussion

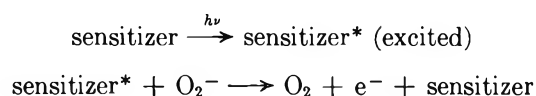
Several mechanisms of spectral sensitization are actually proposed; all of them agree on the liberation of electrons in the conduction band, following the sensitization act, but they differ on the origin of the electron and on the role played by oxygen in the process.

Classical Theory. This consists of the sensitized photoexcitation of an electron from a donor level in the forbidden gap to the conduction band of zinc oxide. The donor level is provided either by the ZnO surface (energy transfer) or by the dye (electron transfer). This theory is supported by various authors,^{48,50} each proposing a different mechanism for the regeneration of donor levels.

Terenin, Putzeiko, and Akimov¹⁰ gave much attention to the role of adsorbed oxygen as an electron acceptor and an electron donor level. They studied, in particular, the Dember effect by the condenser method on dyed ZnO powders.

They report that the presence of oxygen at the surface of zinc oxide was necessary to observe a sensitized internal photoelectric effect under intermittent illumination.

The proposed mechanism consists of a sensitized photoionization of the chemisorbed oxygen (as O_2^- or $O_2^{\cdot-}$)



The reverse dark reaction causes a regeneration of electron donor levels and therefore allows the observation of the sensitized photoelectric effect.

*Theory of Grossweiner and Dudkowski.*⁵¹ The merit of the present theory is that it is a completely new approach to the problem. It is based on photoconductivity and photovoltaic measurements of zinc oxide films sensitized by eosin films, both having a thickness of about 100 Å.

The studies were made after the samples were carefully freed from oxygen. Various photoconductivity measurements, including light intensity, temperature, and wave length dependence have been performed and it was observed in particular that the dye-sensitized photoresponse was proportional to the zinc oxide dark current. The following mechanism, consistent with these data, was proposed by the authors.

Eosin is a positive charge carrier photoconductor. Excitation by red or green light produces holes in the dye layer which are injected in the zinc oxide layer and

trapped at the interstitial Zn^+ ions, thus forming Zn^{+2} ions. Assuming, by analogy with the F-center in potassium chloride⁵² that the capture cross section of the Zn^{+2} ions is smaller than that of Zn^+ ,⁵³ the reduction in the concentration of Zn^+ should result in an increase of the lifetime of the electrons present in the zinc oxide.

This mechanism can be applied to ZnO if conduction electrons are provided only from excess zinc, and are therefore limited in number. Of course, such a model is valid only for a p-type sensitizer and cannot be extended, *a priori*, to n-type sensitizers.

Conclusion

Striking differences exist between the Terenin and the Grossweiner spectral sensitization theories and these differences deserve some discussion. As Grossweiner has pointed out, a usable conductivity of zinc oxide can be obtained only by thorough elimination of oxygen to release conduction electrons. This oxygen removal is achieved by heating at 350° under vacuum or by ultraviolet irradiation. On the other hand, Terenin, *et al.*,¹⁰ working with dyed zinc oxide powders, noted that adsorbed oxygen is indispensable to the observation of a photoelectric response by the condenser method.

The discrepancy probably arises from the different methods and the different samples used and, as a matter of fact, one has to bear in mind that the condenser method allows one to observe only the instantaneous change of photovoltage produced by each flash of light but does not give any measure of the total photovoltage created in the sample by a succession of flashes when the recombination time is slow compared to the dark period as is the case here. With due consideration of these facts, several hypotheses can be proposed for the possible role of oxygen.

(1) The oxygen acts as an electron donor as chemisorbed O_2^- and as an electron acceptor as physisorbed O_2 , the observation of the photoelectric effect depending upon the electronic population of the donors as suggested by Terenin. In such a case, one can suppose that Terenin's mechanism would be operative in the presence of oxygen and Grossweiner's or another one, in its absence. The possibility then arises as two different

(49) E. V. Baranov, V. E. Kholmogorov, and A. N. Terenin, *Dokl. Akad. Nauk SSSR*, **146**, 125 (1962).

(50) J. W. Weigl, ref. 11, p. 345.

(51) S. J. Dudkowski and L. I. Grossweiner, *J. Opt. Soc. Am.*, **54**, 486 (1964).

(52) H. Fedders, M. Hunger, and F. Luty, *J. Phys. Chem. Solids* **22**, 299 (1961).

(53) R. H. Bube, "Photoconductivity of Solids," John Wiley and Sons, Inc., New York, N. Y., 1960, p. 195.

processes of ZnO spectral sensitization according to the state of the surface.

In relation to this point, it is interesting to note that the presence of electron-acceptor molecules⁵⁴ other than oxygen produces a strong enhancement of the sensitized photocurrent. Are these effective because they compete with oxygen for adsorption sites and thus decrease the electron trap efficiency, assuming that adsorbed oxygen had the highest electron trapping ability, or do they provide a more efficient donor-acceptor system for spectral sensitization?

(2) The oxygen acts only as an electron trap, as physisorbed O₂, decreasing the over-all photoresponse, but permitting observation of the Dember effect in intermittent light by trapping photoelectrons during the dark period. In that case, oxygen would not be operative in the sensitized process itself. As a conse-

quence, other sensitization processes would be required for the excitation of electrons. Either a process in which electron donor levels would be, for example, the oxygen ions belonging to the ZnO lattice surface, or Grossweiner's process, if such a process, related more to a solid-state effect between two semiconductors, could be applied to the case of sensitization by dye molecules.

Acknowledgments. The author wishes to thank Professor L. I. Grossweiner and the Organization Committee of the Photosensitization Conference (Chicago, Ill., June 1964) for their invitation and financial support, and Dr. W. West and Dr. M. Van Horn of The Eastman Kodak Co. for their helpful suggestions and criticism.

(54) E. Inoue, T. Yamaguchi, and I. Maki, *Kogyo Kagaku Zasshi*, **66**, 428 (1963).

Minority Carrier Trapping and Dye Sensitization^{1a,b}

by R. C. Nelson

Department of Physics, The Ohio State University, Columbus 10, Ohio (Received October 5, 1964)

The customary criteria for judging the plausibility of the electron-transfer mechanism of dye sensitization in a given case are the production of charge carriers by the sensitizer when illuminated and the sign of the contact potential difference between sensitizer and substrate. These data do not distinguish adequately between sensitizers and nonsensitizers in certain experimental situations, in which there is substantial evidence for electron-transfer sensitization on other grounds. A search for an additional criterion suggests an adverse effect of hole-trapping in the dye phase when cationic sensitizers are used. The evidence for hole-trapping is discussed, as well as its significance for both photochemical and photoconductive dye-sensitized solid state processes. It is suggested that the effect in the former case may be on the energy of a hole-electron pair in the dye phase, whereas, in the latter, it is involved primarily in the slowing of the relaxation process tending to restore the original conditions after the observation of a sensitized response. This dual expression of its influence would account for the similarities observed between photographic sensitization and sensitization of photoconductivity in cadmium sulfide, in spite of the essential differences between the two experimental situations.

Introduction

For more than 25 years, there have been two principal types of mechanisms contesting the field of dye-sensitized, solid state processes. During most of this time, the resonant energy-transfer type of process has had fairly general acceptance while the electron-transfer type was in eclipse. The latter type of mechanism appeals to experiment since its plausibility depends on measurable effects and relationships, and in recent years it has been shown that, for certain sensitizer-substrate combinations, the requirements imposed by these relationships are fulfilled. It is known that, in general, sensitizing dyes in the solid form produce hole-electron pairs on illumination and that, in many cases, the contact potential difference between sensitizer and substrate is of a sign and magnitude such as to permit spontaneous transfer of electrons from the dye phase to the substrate.

There are two experimental results which strongly suggest the validity of the electron-transfer mechanism for the cases with which they deal. One is the fact that a dye-cadmium sulfide interface shows a photovoltaic effect, and, when this junction is made part of an electrical circuit, a continuous current will flow across it,

driven by light absorbed by the dye.^{2a} The second is the fact that a sort of "sensitized photoconductivity" can be observed in glass in contact with a layer of sensitizing dye, in spite of the fact that there is no intrinsic process to which energy could be transferred by resonance.^{2b}

However, a difficulty remains; both of these experiments discriminate strongly between good and poor sensitizers, but it is not known upon what basis the discrimination rests since the result cannot be predicted solely upon grounds of being able to produce charge carriers on illumination or upon the sign of the contact potential difference. Clearly, if the electron-transfer mechanism is valid, some criterion must exist according to which the results of these experiments can be anticipated. Thus, a search for such a criterion imposes a test on the electron-transfer mechanism.

It is characteristic of this mechanism that it attempts

(1) (a) This investigation was supported in part by a Public Health Service research career program award No. GF-560-64 from the Institute of General Medical Sciences and in part by the C. F. Kettering Foundation; (b) presented to the International Conference on Photosensitization in Solids, Chicago, Ill., June 22-24, 1964.

(2) (a) R. C. Nelson, *J. Opt. Soc. Am.*, **46**, 13 (1956); (b) **50**, 1029 (1960).

to explain the peculiarities of sensitized systems, not only by consideration of transport phenomena at the interface but also by application of our knowledge of the processes of charge carrier separation and diffusion in the dye phase. Thus, a possible and hopeful criterion for predicting the efficacy of a sensitizer may be found in considering the energy carried by a hole-electron pair in the dye solid since there are evidently cases of sensitization in which this must assume importance. This paper deals with the applicability of such a criterion to sensitized processes in general and, in particular, with its relevance to the two special cases just mentioned.

The Energy Requirement of a Dye-Sensitized Process

The resonance mechanism foresees no difficulty with energy; it is an assertion that the energy of the excited state of the molecule is sufficient to do what needs to be done. The form given by Franck and Teller³ is basically an application of the Franck-Condon principle; they note that the lifetime of the excited state of the sensitizer is of the order of 10^4 lattice vibration periods of the substrate, so that one can hope to carry out the creation of a hole-electron pair with the energy available by transferring it to a favorable lattice configuration. This is assumed to be likely to occur at least once during the lifetime of the excited state.

Although the electron-transfer type of mechanism rests on a knowledge of the energy level structure of the system, which can often be worked out, it still is not a simple matter to say how much energy must be carried across the interface by the hole-electron pair. The primary photographic process is of interest because one can set a lower limit to the energy requirement from the free energy of the products. If these are silver metal and gaseous bromine, then we must transfer at least 0.8 e.v. of energy to the silver bromide crystal.⁴ However, the actual energy required will be determined by the pathway over which the system moves in energy-configuration space and will, thus, depend on rates and mechanisms. If we suppose that only the transfer of an electron from sensitizer to substrate need take place promptly, that is, within the lifetime of the excited state of the dye molecule, and that all other processes may proceed slowly enough so that thermal energy may be used to overcome activation barriers, then the total energy requirement need not be much greater than that stored in the products.

In photosynthesis, the luxuriance of hypotheses is such that, even for the restricted case of electron-transfer mechanisms, the energy of a hole-electron pair may appear in different roles. Calvin and Androes have sug-

gested an energy-doubling process which will work only if the energy of a hole-electron pair in the chlorophyll phase is small.⁵ More traditional types of mechanisms resemble those of Katz, in requiring that the pair carry a large fraction of the energy of the photon.⁶

While the significance of the energy of the pair is obvious in a system in which chemical work is done, it is difficult to see why it should be of importance in one in which the only effect expected is an enhancement of photoconductivity because in this case it should suffice that charge carriers of either sign are donated to the substrate under illumination. However, there is a marked parallelism of behavior of sensitizers for the two systems, photographic sensitization and sensitization of photoconductivity in cadmium sulfide, and it is of interest to attempt to uncover the reasons for this, in hope of coming upon a unifying idea.

The Energy of a Hole-Electron Pair

We define the energy of a hole-electron pair to be the separation on an energy level diagram of the final levels occupied by hole and electron when a pair is created. This is the difference in energy between ground and conductive excited states diminished by any losses due to trapping of either carrier. The energy difference between ground and conductive states can be determined by a two-step process. First, we measure, by means of the external photoelectric effect, the energy of an electron in the ground state. We measure the energy of an electron in the conductive state by the electron-beam-retardation method. If the difference of these two be compared with the energy of a photon at the photoconductive threshold, the two will be found to be equal, within experimental error, for good sensitizers. For certain other dyes, more complicated relationships are found, but in all cases it is possible to construct an over-determined, consistent energy level diagram in which the energy of the threshold photon appears as a difference between two levels, the positions of which can be determined without reference to it.⁷

In view of the fact that the threshold energy for photoconduction is somewhat less than that corresponding to the lowest allowed electronic transition of the molecule in solution, we must recognize this to be a remarkable result which we do not yet understand. Its

(3) J. Franck and E. Teller, *J. Chem. Phys.*, **6**, 861 (1938).

(4) W. F. Berg and J. H. Webb in "The Theory of the Photographic Process," C. E. K. Mees, Ed., The Macmillan Co., New York, N. Y., 1954, p. 145.

(5) M. Calvin and G. M. Androes, *Science*, **138**, 867 (1962).

(6) E. Katz in "Photosynthesis in Plants," W. E. Loomis and J. Franck, Ed., Iowa State College Press, Ames, Iowa, 1949, p. 291.

(7) R. C. Nelson, *J. Opt. Soc. Am.*, **51**, 1186 (1961); *J. Mol. Spectry.*, **7**, 439 (1961).

importance for the electron-transfer hypothesis of sensitization is obvious; it also suggests at least as a possibility that even single dye molecules on the surface of a substrate possessing a photoconductivity of its own might be able to participate in an electron-transfer process.

Thus, in the absence of trapping, the energy of a hole-electron pair is nearly that of the least energetic photon which will produce it. We now consider the problem of trapping, confining ourselves to the discussion of cationic dyes, since our knowledge of energy levels in these is rather more extensive than in anionic or nonionic dyes.

Many cationic dyes have large densities of electron traps, which lie within a rather narrow range of energy levels, so that they can be considered to be monoenergetic for many purposes. Usually, these traps are about 0.35 to 0.40 e.v. deep so that they represent only about a 25% diminution of the energy of the pair. However, they may affect sensitization by electron transfer by bringing the effective energy of an electron in the dye phase very near the Fermi level in the substrate. These trapping levels are easily accessible to study either by kinetic methods or by an external photoelectric effect arising from electrons occupying them.⁸

The question of hole traps is a much more difficult one. The writer has suggested that since cationic dyes are usually n-type conductors, the anion may act as a hole trap.⁹ In the case of the halide ions, their energies as hole traps may be estimated from the electron affinities of the corresponding halogen atoms. Since these lie in the neighborhood of 3.5 e.v., to be compared with energies of the ground states of photoconductive dyes in the range 4.3 to 5.5 e.v., they would act as rather deep hole traps, deep enough so that the energy of the pair would be greatly reduced. Where the hole is a minority carrier, it is very difficult to find out anything about hole traps by ordinary methods. We shall, instead, go at the question indirectly by considering a classical paradox of the field of organic photoconductors concerned with the so-called "intrinsic semiconductivity" of these substances.

Many measurements attest to the fact that, if one plots the log of dark conductivity of a dye against the reciprocal of the absolute temperature, the data fall on a straight line, the slope of which is taken to be a measure of the intrinsic forbidden gap between ground and conductive excited states, so that $\sigma = \sigma_0 \exp(-E/kT)$, where E is the energy of a hole-electron pair. E is usually ~ 1 e.v. and ordinarily not greatly different from one-half the energy of a photon at the photoconductive threshold. If we now estimate the density of

electrons in the ground state, using the number of molecules, the number of π -electrons, or a density of states in k-space and multiply this by the Boltzmann factor, usually the product is rather a small number, often less than unity. If we attempt to account for the current using this density of charge carriers, we are forced to attribute a very large mobility to the carriers, often $\sim 10^4$ to 10^6 cm.²/v. sec. On the other hand, values of the mobility arrived at in more direct ways are invariably ~ 1 cm.²/v. sec. or less. Since the number of carriers corresponding to the large mobility is such that shot noise effects should be prominent and these are not seen, it seems more satisfactory to accept the lower range of values. By the same token, we must give up the idea that E can be the energy of a hole-electron pair since, if we take the mobility to be low, we must have a density of carriers several orders of magnitude greater than is consistent with the measured value of E . Because of this state of affairs, we shall refer to this dark conduction as anomalous.

This paradox seems to be proof against resolution in any simple way. It cannot be resolved using donor states or any reasonable density of states in the lower level. It does not seem to be due to electrode effects, and there is evidence that it is not ascribable to the presence of the applied field used to measure the conductivity. The writer has investigated the dark conductivities of a number of triphenylmethane dye halides having known energy level structures and has proposed a scheme in which the halide ions appear as deep hole traps. E now has something of the character of the height of an activation barrier over which the distribution of electrons between hole traps and the conductive level is changed as a function of temperature, and the dark conductivity data can be accounted for reasonably well in terms of small mobilities.¹⁰ It is not necessary to accept this scheme in order to pursue the argument; it is sufficient to say that, if we take the best values for the mobility, for an anomalous dark conductor, E cannot be the energy of a hole-electron pair, and this energy must indeed be considerably less than E .

We now note that there is a strong negative correlation between anomalous dark conductivity and ability to sensitize photoconductivity in cadmium sulfide when the sensitizer is in the form of a "thick" film. The same correlation applies to the ability to sensitize photoconductivity in glass and to the photovoltaic

(8) B.-Y. Cho, R. C. Nelson, and L. C. Brown, *J. Chem. Phys.*, **39**, 499 (1963).

(9) R. C. Nelson, *ibid.*, **22**, 890 (1954).

(10) R. C. Nelson, *ibid.*, **39**, 859 (1963).

effect at a dye-cadmium sulfide interface, the character of which is markedly different for a dye with anomalous dark conductivity. We thus find in the anomalous dark conductivity a characteristic which has diagnostic value for effectiveness of sensitizers in interesting situations. There appears to be a connection between it and the energy of a hole-electron pair. If this should be so, it might be a link between the performance of sensitizers in systems in which chemical work is done and the less interesting, but more accessible, situations in which only the enhancement of photoconductivity is found.

Sensitization by Thick Dye Films

A "thick" dye film in the context of sensitization is one which is much thicker than a monolayer and comparable to the films used to study the photoconductivity of the dye itself. Such systems represent an extreme of the sensitization effect. The simplest sensitized system is one in which the sensitizer is so sparsely adsorbed on the substrate that each molecule can be considered to be isolated. A great many dyes produce an observable effect in this regime. The most useful state, for most purposes, is that in which the dye is adsorbed as a close-packed monolayer, and, for this regime, the number of effective sensitizers is notably less than in the first. In passing to multilayers, there is a further diminution of the number of effective sensitizers, and such systems are highly specific and discriminatory. Within the range of sensitizers with which the writer has worked, those which perform well in multilayers are also the most satisfactory in monolayers, so that the phenomena are probably fundamentally similar. Multilayers are also of interest as being closely related to the dye-substrate junction cells in which the photovoltaic effect is observed.¹¹

We now list the most prominent differences in behavior between films which show anomalous dark conduction (HDC) and films which do not (LDC).

(1) For HDC films the mobility inferred from the intrinsic semiconduction model is high; for LDC films it is low. (2) LDC films sensitize photoconductivity in cadmium sulfide; HDC films do not. (3) The same is true of the "sensitized photoconductivity" of glass. (4) The photovoltaic effect at the LDC-cadmium sulfide junction saturates at low illuminance at a value numerically equal to the measured contact potential difference; that for the HDC junction is proportional to the log of illuminance over a wide range and tends toward the contact potential difference as a limit. (5) LDC films show a fast decay of photoconductivity in the dark ($\tau \sim 10^{-3}$ sec.); HDC films always have a slow component in the decay curve ($\tau \sim 10^2$ sec.). (6) If a cadmium sulfide cell is sensitized with a thick layer

of LDC film and both are illuminated, the decay of photoconductivity in this system is faster than in the cadmium sulfide cell by itself and is, conversely, slower if the film is HDC. (7) Although the photoconductivity of the HDC film persists in the dark, the photovoltaic effect disappears very quickly from both types when illumination is discontinued. (8) For the HDC film, the photovoltaic effect is very small for a very thick film and can approach the magnitude of the contact potential difference only for a thin film; for a thick film the photo-e.m.f. is of the order of a few millivolts. This effect is not seen with LDC films. (9) HDC films have electron traps 0.3 to 0.4 e.v. below the conductive level; these are inconspicuous or absent in LDC films.

Since both dye and cadmium sulfide films may be n-type conductors, we do not consider n-p junction effects. A fairly straightforward account of the phenomena in HDC-cadmium sulfide junction cells can be given on the basis of the observations listed above. The Fermi level in the cadmium sulfide film, as measured by the electron-beam-retardation method, lies in the neighborhood of -3.5 e.v., measured from the vacuum level. The conductive state in many dyes, measured in the same way, is found from -3.0 to -3.2 e.v., so that trapped electrons lie near or a little above the Fermi level of the substrate. We suppose that, before the measurement is made, the Fermi level in the cadmium sulfide has been raised almost to the electron trap energy of the dye phase, possibly by carriers present in the dark or, more likely, excited by a small amount of illumination incidental to the preparation of the cell and pumping it down for measurement.

We now illuminate. In a thick dye film, only a small fraction of the dye molecules is illuminated, whereas the excited electrons are trapped throughout the film so that the photovoltage is very small. For thin films and very bright light, we are able to drive the effective energy of excited electrons upward so that the photovoltage may approach the energy difference between the conductive state of the dye and the Fermi level in the cadmium sulfide. Since this effect is due to electrons which are not in thermal equilibrium with traps, it disappears immediately upon cessation of illumination because there is no longer an energy gradient at the interface. According to this point of view the sensitization effect is not entirely absent but is very small; it could escape observation by the techniques used to detect it. Since the conductivity of HDC films is persistent and the decay is especially slow in the sensitizer-substrate system, only after some time and with great

(11) R. C. Nelson, *J. Opt. Soc. Am.*, 51, 1182 (1961).

care, would it be possible to observe an energy gradient at the interface.

The absence of electron traps in the LDC films increases the magnitude of the photo-e.m.f., but the most important factor in establishing the characteristic differences is the fast recovery time of the LDC-cadmium sulfide system. When the system is illuminated, there is a short transient peak in the photo-e.m.f. which apparently is due to the rise in the Fermi level in the cadmium sulfide due to the electrons donated by the dye. The system very quickly comes to a steady state, and the current remains constant. When the photo-e.m.f. is measured, by applying a countervoltage just sufficient to make the current across the junction zero, the recovery is so fast that the Fermi level in the cadmium sulfide is almost independent of the illuminance under the conditions of measurement. In the case of pinacyanole, a particularly effective sensitizer in thick films, the photo-e.m.f. is substantially independent of the illuminance over a range of 100 to 1. For HDC films, not only is the photo-e.m.f. strongly dependent on illuminance, but there are also long-term drifts and fatigue phenomena which are probably to be associated with changes in the Fermi level in the cadmium sulfide due to the process of electron transfer and the slow recovery from it.

Presumably, considerations of a similar sort apply to the sensitization of photoconductivity in glass. Although glass is hardly a semiconductor in any ordinary sense, there appears to be a limited number of surface states through which electrons can enter the glass. If one assumes these to be distributed over a range of energies and to be accessible only to electrons more energetic than the highest filled state, they might play a role which simulates that of the Fermi level in cadmium sulfide, leading to a small sensitization effect in the case of HDC films and a large one for LDC material.¹²

Hole-Trapping and Sensitization

We have attempted to account for the difference in behavior between the two kinds of film as sensitizers in terms of three characteristics, electron-trapping, presence of carriers in the dark, and relaxation time for photoconductivity. The principal effect is concerned with the last two since the effect of electron-trapping is on the magnitude of the photovoltage. We have already suggested that the anomalous dark conductivity is associated with the presence of deep traps for holes. We now wish to suggest further that the long relaxation time is also ascribable to hole-trapping.

In the cationic dyes of which we are speaking, there seems to be no explicit role for the anion in the processes

of charge carrier separation and transport. The energy levels connected with these processes are determined by the colored cation and are nearly independent of the nature of the associated anion. The effect of the anion shows in only two ways, being associated with the dark conductivity and with the relaxation time for photoconductivity. For crystal violet, an HDC type material, one can decrease the dark conductivity and the relaxation time for photoconductivity, each by two orders of magnitude, by substituting iodide for chloride as the anion, without greatly changing the electron trap depth, the work function, the electron affinity, or the photoconductive threshold.

Considerations of this sort, which emphasize the difference in the roles played by anion and cation, lead to a point of view which encourages one to speak of the domain of anions and that of cations and to visualize them as interacting only weakly insofar as the phenomena of photoconductivity are concerned. Similarly, one is led to associate the role of the anion with the minority carrier since the processes involving transport of electrons can be associated explicitly with the cation. Bearing in mind the negative charge of the anion, its identification as a hole trap is a short step, and the association of the slow decay of photoconductivity with the weak interaction between the two domains is natural.

There is also fairly direct evidence of deep trapping of holes in some triphenylmethane dyes, where Petruzzella and Nelson found a rather small p-type photoconductivity in the presence of oxygen, which quenches the n-type conduction seen *in vacuo*. Since the p-type photoconductivity was very much smaller than the n-type, deep trapping can be inferred.¹³

If we then suppose that the difference in activity as sensitizers of photoconductivity between the HDC and LDC films is ascribable to trapping of holes in the domain of the anions in the former whereas in the latter they remain untrapped in the domain of the cations, we see that these conditions are also vitally involved in the question of the energy of the hole-electron pair although this energy does not enter directly into sensitized photoconductivity. Thus it seems likely that there will be a good correlation between ability to convey energy to a solid state photochemical system by charge-carrier transfer and the ability to sensitize photoconductivity of cadmium sulfide. Although the immediately operating causes differ, the basic cause, hole-trapping, is the same in both cases.

(12) R. C. Nelson, *J. Appl. Phys.*, **34**, 629 (1963).

(13) N. Petruzzella and R. C. Nelson, *J. Chem. Phys.*, **37**, 3010 (1962).

Sensitization of Electrical Effects in Solids¹

by H. Meier

Staatliches Forschungsinstitut für Geochemie, Bamberg, Germany (Received October 5, 1964)

Photoelectrical effects in solids can be optically sensitized by dyes. In this paper the experimental facts on this phenomenon are reviewed, and, furthermore, a discussion of the different theories for the sensitization mechanism—energy and electron transfer hypothesis—is given. On account of discrepancies between the experiments and the theories it seems to be necessary to correct the mechanisms discussed hitherto. Measurements of the photovoltaic effects of semiconductor-dye arrangements (CdS-dye, AgBr-dye, etc.), which are models of sensitized systems, suggests that the sensitization of p- and n-conducting solids can be explained by an electronic p-n mechanism. Experimental results obtained with different photovoltaic couples are reported, and the possible connection between the photovoltaic effect of these systems and the optical sensitization of the photoconductivity—which supports the p-n mechanism—is discussed.

In the process of spectral sensitization the energy absorbed by a dye in contact with a solid is transferred to the solid causing it to show photoelectrical effects. The problem is that the sensitized electrical effects brought about by adsorbed dyes are induced by quanta of energy less than those required by the semiconductors for the intrinsic process.

This paper is an attempt to summarize the experimental facts on this phenomenon, which was first observed about 100 years ago by Moser and Rigolot,^{2a,b} and to give a review on the possible interpretations of the process.

There is a series of electrical effects that can be optically sensitized by dyes at wavelengths longer than those in the proper sensitivity range of the solid: the photovoltaic Becquerel effect,^{2,3} the photoeffect of silver-silver bromide-silver photoelements,⁴⁻⁶ the condenser or Dember effect in intermittent light,⁷⁻¹¹ the change of the photocontact potential,¹² the photoconductivity in electrophotographic arrangements,^{13,14} and the photoconductivity in surface and sandwich cells.¹⁵⁻²² For instance, Figure 1 shows the photoconductive response for a cadmium sulfide surface cell before and after sensitization with a layer of a merocyanine dye. The data have been normalized to equal energies at all wave lengths.

The various measurements, made by Sheppard, Eggert, Putzeiko, Terenin, West, Carroll, Nelson, Rose,

and others,⁴⁻²⁵ showed that a large variety of dyes can serve as sensitizers; see Table I.²⁶⁻²⁹

- (1) Presented to the International Conference on Photosensitization in Solids, Chicago, Ill., June 22-24, 1964.
- (2) (a) J. Moser, *Monatsh. Chem.*, **8**, 373 (1887); (b) H. Rigolot, *Compt. rend. acad. sci. Paris*, **116**, 873 (1893).
- (3) S. E. Sheppard, W. Vanselow, and G. J. Happ, *J. Phys. Chem.*, **44**, 411 (1940); **53**, 331, 1403 (1949).
- (4) J. Eggert and H. Amsler, *Z. Elektrochem.*, **56**, 733 (1952).
- (5) H. Amsler, *ibid.*, **57**, 801 (1953).
- (6) J. Eggert, *Angew. Chem.*, **73**, 417 (1961).
- (7) E. K. Putzeiko and A. Terenin, *Zh. Fiz. Khim.*, **23**, 676 (1949).
- (8) I. A. Akimov and E. K. Putzeiko, *Dokl. Akad. Nauk SSSR*, **102**, 481 (1955).
- (9) A. Terenin, "Electrical Conductivity in Organic Solids," Interscience Publishers, Inc., New York, N. Y., 1961, pp. 39-59.
- (10) A. Terenin and I. A. Akimov, *Z. physik. Chem.*, **217**, 307 (1951).
- (11) A. Terenin, E. Putzeiko, and I. Akimov, "Ergebnisse der Internationalen Konferenz für wissenschaftliche Photographie Köln 1956," Verlag O. Helwich, Darmstadt, 1958, pp. 117-122.
- (12) A. Terenin and E. Putzeiko, "Proceedings of the International Colloquium Liège 1959," Pergamon Press, Oxford, 1962, pp. 532-543.
- (13) H. J. Gerritsen, W. Ruppel, and A. Rose, *Helv. Phys. Acta*, **30**, 504 (1957).
- (14) K. Hauße, *Angew. Chem.*, **72**, 730 (1960).
- (15) N. Kameyama and T. Fukimoto, *J. Soc. Chem. Ind. Japan*, **42**, 244, 426 (1939).
- (16) W. West and B. H. Carroll, *J. Chem. Phys.*, **15**, 529 (1947); **19**, 17 (1951); *J. Phys. Chem.*, **57**, 797 (1953).
- (17) A. G. Goldman and I. A. Akimov, *Zh. Fiz. Khim.*, **27**, 355 (1953).
- (18) I. A. Akimov, *ibid.*, **30**, 1007 (1956); *Phot. Sci. Eng.*, **3**, 197 (1959); *Dokl. Akad. Nauk SSSR*, **137**, 624 (1961).

Table I: Dye Sensitizers for Photoelectrical Effects

Dye	Charge	Type	Substrate	Photographic behavior	References
Kryptocyanine	Cationic	p	AgBr, CdS	Sensitizer	15, 19
Malachite green	Cationic	n	ZnO, AgBr, AgI	Desensitizer	11, 14, 16, 26
Erythrosin	Anionic	p	ZnO	Sensitizer	11, 27
Fluorescein	Anionic	p	ZnO	Sensitizer	13
Merocyanine	Nonionic	p	CdS	Sensitizer	21
Rhodamine B	Cationic	n	TlI, CdS	Desensitizer	11 ^a
Phthalocyanine	Nonionic	p	ZnO, HgO		27, 28
Chlorophyll	Nonionic	p	ZnO, HgO		25, 28, 29

^a Unpublished results, also.

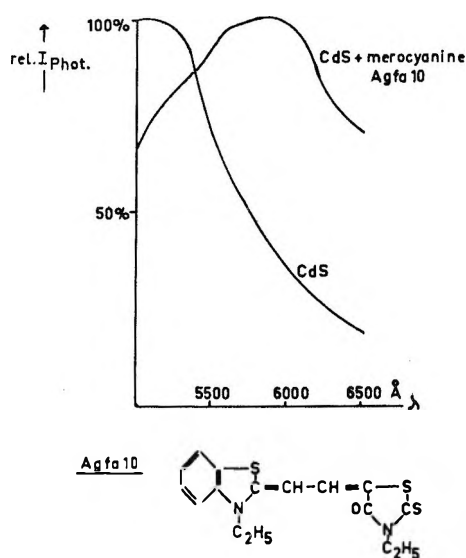


Figure 1. Action spectrum for sensitized CdS photoconductivity.

The table, summarizing some of the dye sensitizers, illustrates that anionic, cationic, and uncharged dyes of different classes have the ability of sensitizing electrical effects. There also seems to be no correlation between the sensitizing ability and the sign of the charge carriers of the dye itself.

Furthermore, it must be remarked that not only photographic sensitizers but also photographic desensitizers produce optical sensitization of the photoeffects in solids. For instance, the photoeffect of AgI and TlI can efficiently be sensitized by typical photographic sensitizers such as eosine, erythrosin, and pinacyanol, as well as by typical desensitizers as phenosafranin, malachite green, and other dyes.¹¹ Furthermore, a sensitization of the photoconductivity by desensitizers has been observed in AgBr emulsions.¹⁶ These observations show that there must be an important difference between the sensitization of the pho-

toconductivity and the optical sensitization in photography. There is no doubt that the explanation of this difference can be of great importance for the mechanism of the photographic sensitization.

The sensitized photoeffects amount, in the best cases, to 80% of the proper photoeffect of the semiconductor, and the dye can act as sensitizer both in an adsorbed monomolecular state and in the aggregated form.^{7,10,25} The spectral sensitivity curves contain either the maxima of the monomolecularly adsorbed dye or the *H*- and *J*-spectral maxima,³⁰ owing to its aggregated form.

It must be noted that adsorbed electronegative gases produce an enhancement of the sensitization by dyes. For instance, in the case of thallos bromide, dyed with malachite green, bromine gives rise to a considerable sensitization.¹² These results show that the presence of electronegative gases at the surface of halides is of great influence. In our opinion, however, the presence of electronegative molecules is not essential for the sensitization of all photoconductors because we could observe sensitized cadmium sulfide photoconductivity without gases.

There is a variety of inorganic solids that can be

- (19) R. C. Nelson, *J. Opt. Soc. Am.*, **46**, 13 (1956).
- (20) R. C. Nelson, *ibid.*, **51**, 1182 (1961).
- (21) H. Meier and W. Albrecht, *Ber. Bunsenges. physik. Chem.*, **67**, 838 (1963).
- (22) S. Dudkowski and L. I. Grossweiner, *J. Opt. Soc. Am.*, **54**, 486 (1964).
- (23) I. Akimov and A. Terenin, *Dokl. Akad. Nauk SSSR*, **135**, 109 (1960).
- (24) A. G. Goldman and I. Akimov, *Zh. Fiz. Khim.*, **27**, 355 (1953).
- (25) A. Terenin and E. Putzeiko, *J. chim. phys.*, **55**, 681 (1958).
- (26) J. W. Weigl, "Photographic Science Symposium: Zürich 1961," The Focal Press, London and New York, N. Y., 1963, p. 354.
- (27) E. Putzeiko, *Dokl. Akad. Nauk SSSR*, **129**, 303 (1959).
- (28) E. Putzeiko, *Radiotekhn. i Elektron.*, **1**, 1127 (1956).
- (29) A. Terenin and E. Putzeiko, *Angew. Chem.*, **70**, 508 (1958).
- (30) G. Scheibe, *Z. Elektrochem.*, **52**, 283 (1948).

Table II: Solids Which Can Be Sensitized

Substrate sensitized by dyes	Photoeffect ^a	References
Silver halide emulsions	I	16
AgBr	B	3
	C	7, 8, 11, 18
	P	4-6
	I	15
AgI	C	11, 18
	I	17
	CP	12
TlCl	C	31
TlBr	C	12, 18, 33
TlI	C	10, 11, 33, 34
NaCl	I	35
HgI ₂	C	18
CdS	I	19-21
ZnO	C	25, 27, 33, 36
	I	22, 37-41
	E	13, 14, 42-45
PbO	C	18
Cu ₂ O	B	2a, b
HgO	C	29
SnO	C	29
CdO	C	33
Organic substrate	E	46
Anthracene	I	47-49

^a B, Becquerel effect; C, condenser or Dember effect; P, photovoltaic effect; CP, change of contact potential; I, photoconductivity in sandwich and surface cells; E, electrophotographic method.

sensitized. In Table II a compilation of these semiconductors is given³¹⁻⁴⁹; see also ref. 31.

Table II shows that photoelectrical effects in semiconducting halides, oxides, and sulfides, and in organic photoconductive materials can be optically sensitized by dyes.

It must be noted that the sign of the charge carriers in the sensitized photoeffect is, in the most cases, the same as that of the intrinsic photoeffect of the semiconducting solid. This rule was obtained by Terenin, Putzeiko, and Akimov^{12, 38, 50-52} by the help of the Dember effect (determination of the polarity of the diffusion photo-e.m.f.) and the vibrating condenser method (determination of the change in the contact potential).

For instance, they found that in layers of zinc oxide, which is a typical electronic semiconductor of the n-type, the photocarriers are negative, either in their own spectral sensitivity range or in the sensitized one.^{10, 11} The charge carriers of the sensitized photocurrent, therefore, are electrons as for the proper photoeffect of zinc oxide.

In silver halides and thallos halides, which normally

are semiconductors of the p-type, the sign of the charge carriers is positive in the range of the absorption of the sensitizer and in that of the proper photoeffect. The photoelectric current in these solids is due to holes.

However, there are some exceptions. For example, after the sensitization with photographic sensitizers, such as 3,3'-diethylthiatricarboyanine and others, electron majority photocarriers could be observed by Terenin and colleagues¹¹ in AgI and TlI of the p-type. Whereas, in n-conducting materials the charge carriers always are negative, there exists the possibility of changing the sign of the photocarriers in p-conducting silver and thallos halides. This observation and, above all, the fact that the majority carriers of the sensitized photocurrent of a hole conducting p-type silver halide can also be electrons seem to be of great interest for the photographic sensitization.

With regard to the mechanism of the spectral sensitization, the following observations, besides the results discussed above, are of great importance.

(1) The dye molecules in the adsorbed layer seem to act several times on the average because the photocurrents in sensitized semiconductors remain stable

(31) H. Meier, "Die Photochemie der organischen Farbstoffe," Springer-Verlag, Berlin, 1963.

(32) L. G. Gross, *Zh. Nauchn. i Prikl. Fotogr. i Kinematogr.*, **5**, 54 (1960).

(33) E. Putzeiko and A. Terenin, *Dokl. Akad. Nauk SSSR*, **70**, 401 (1950); **90**, 1005 (1953).

(34) I. Akimov, *ibid.*, **151**, 310 (1963).

(35) H. Yagi, *Mem. Coll. Sci., Univ. Kyoto*, **A26**, 75 (1950).

(36) E. Putzeiko, *Dokl. Akad. Nauk SSSR*, **91**, 1070 (1953).

(37) G. A. Korssunowski, *ibid.*, **134**, 1394 (1960).

(38) A. Terenin, E. Putzeiko, and I. Akimov, *J. Chim. Phys.*, **54**, 716 (1957).

(39) R. Matejec, *Z. Elektrochem.*, **65**, 183 (1961).

(40) Y. Hishiki, H. Tamura, S. Namba, and K. Taki, *Rika Gaku Kenkyusho Hokoku*, **36**, 386 (1960).

(41) S. Namba and Y. Hishiki, *ibid.*, **39**, 27 (1963).

(42) I. Zelevic, B. Kalinauskienė, L. Nyunko, I. Plavina, and E. Suveizdis, *Elektrofotogr. i Magnitogor.*, **17** (1959).

(43) S. G. Grenishin and A. Cherkasov, *Zh. Nauchn. i Prikl. Fotogr. i Kinematogr.*, **5**, 433 (1960).

(44) J. T. Bickmore, R. E. Hayford, and H. Clark, *Phot. Sci. Eng.*, **3**, 210 (1959).

(45) H. G. Greig, U. S. Patent 3,052,540 (April 20, 1959 and April 9, 1962).

(46) Kalle Akt. Ges., Belgian Patent 588,660 (March 18, 1959); Austrian Patent 220,949 (June 7, 1960).

(47) B. J. Mulder and J. De Jonge, *Koninkl. Ned. Akad. Wetensch. Proc. Ser. B*, **66**, 320 (1963).

(48) B. J. Mulder, *Philips tech. Rdsch.*, **25**, 195 (1963-1964).

(49) J. W. Steketeer and J. De Jonge, *Koninkl. Ned. Akad. Wetensch. Proc., Ser. B*, **66**, 76 (1963).

(50) E. Putzeiko, *Dokl. Akad. Nauk SSSR*, **67**, 1009 (1949).

(51) I. Akimov, *ibid.*, **128**, 691 (1959).

(52) A. Terenin, E. Putzeiko, and I. Akimov, *Discussions Faraday Soc.*, **27**, 83 (1959).

during a long illumination period. Measurements showed that in the case of sensitized ZnO about 250 electrons can be formed for each dye molecule.³⁹ From this observation that no essential destruction of the dye occurs in the process we come to the conclusion that the mechanism of the spectral sensitization must be an electronic one.

(2) It is necessary for a good sensitizing activity that the dye be strongly adsorbed at the surface of the semiconductor.⁵³⁻⁵⁶ Besides this requirement, the coplanarity of the dye molecule increases the efficiency of the sensitization.^{56,57} This fact speaks in favor of an electron-transfer mechanism because according to this requirement, a good contact between dye and semiconductor seems to be necessary for the sensitization of the photoconductivity. In the case of an energy-transfer mechanism, there must be an energy transfer, also, in systems in which there exists a small distance between dye and semiconductor; the experiments of Kuhn, *et al.*,^{58,59} may give further information about this problem.

(3) Furthermore, it must be stated that the fluorescence of a series of dyes (fluorescein, chlorophyll, and others) is quenched by the adsorption to substrates in which they can sensitize photoconductivity, but they exhibit fluorescence when adsorbed to insulators which cannot be optically sensitized by these dyes.^{18,60}

For the discussion of the different theories of spectral sensitization, it is necessary to consider the disposition of the dye molecule energy levels in relation to those of the semiconductors. For that purpose we will use the band model both for inorganic semiconductors and for organic dye layers.

The various electronic levels, which are necessary for the discussion, are diagrammed in the Figure 2. The values are given in e.v. in relation to the zero reference energy level at infinity. In order to take into consideration the effect of macroscopic space charges, it is desirable to introduce the macropotential V_M . Every change of this potential brought about by any kind of charges—for example, those charges produced by adsorption, and so on—brings about analogous changes of all levels. For the purpose of simplification this macropotential shall be zero in our scheme. The scheme exhibits the following energy levels.

(1) The Fermi level E_F is below the zero level or exactly below the electrostatic macropotential. In intrinsic semiconductors and insulators this level lies between the valence band and the conduction band. For p-type semiconductors, the position is near the valence band, and for n-type semiconductors, it is below the conduction band. In n-type semiconductors the Fermi level is raised by light (quasi-Fermi level),

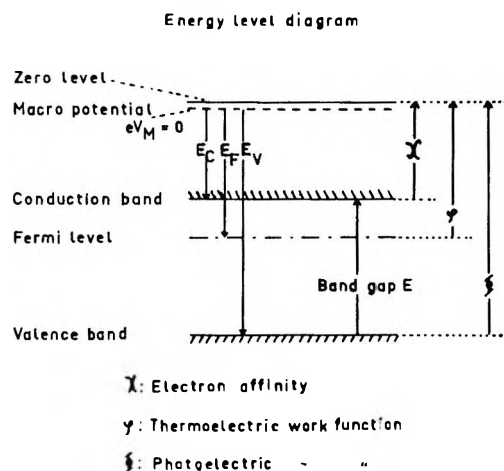


Figure 2. Energy level diagram.

and in p-type semiconductors we observe a decrease of the Fermi level under illumination. The depths of the Fermi levels are obtained from measurements of the thermoelectric work function ϕ *in vacuo* because the work function measures the energy that is involved in the process of raising an electron from the Fermi level to the top of any potential barrier that may exist at the surface. The thermoelectric work function of a solid itself can be obtained by the measurement of the contact potential difference between the solid and any metal. This is possible because the contact potential is equal to the difference in the work functions of the metal and the solid.

The methods of determining the contact potential difference are the Thomson vibrating-condensor method and the electron-beam-retardation method.⁶¹⁻⁶⁴ With the retardation method, Nelson⁶⁴ determined the work

(53) R. Brünner, A. Oberth, and G. Scheibe, *Z. wiss. Phot. Photochem. Photochem.*, **50**, 283 (1955).

(54) B. H. Carroll, *Phot. Sci. Eng.*, **5**, 65 (1961).

(55) N. N. Markevitch and E. Putzeiko, *Zh. Fiz. Khim.*, **36**, 1297 (1962).

(56) S. E. Sheppard, R. H. Lambert, and R. D. Walker, *J. Chem. Phys.*, **9**, 107 (1941).

(57) L. G. S. Brooker, F. L. White, R. H. Sprague, S. G. Dentje, and G. van Zandt, *Chem. Rev.*, **41**, 325 (1947).

(58) M. M. Zwick and H. Kuhn, *Z. Naturforsch.*, **17a**, 411 (1962).

(59) K. H. Drexhage, M. M. Zwick, and H. Kuhn, *Ber. Bunsenges. physik. Chem.*, **67**, 62 (1963).

(60) I. Akimov, *Zh. Nauchn. i Prikl. Fotogr. i Kinematogr.*, **4**, 64 (1959).

(61) D. Fox, M. Labes, and A. Weissberger, "Physics and Chemistry of Organic Solid State," Vol. I, Interscience Publishers, Inc., New York, N. Y., 1963.

(62) E. Spenke, "Elektronische Halbleiter," Springer-Verlag, Berlin, 1955.

(63) J. T. Law, in "Semiconductors," Reinhold Publishing Corp., New York, N. Y., 1959, p. 707.

(64) R. C. Nelson, *J. Opt. Soc. Am.*, **46**, 1016 (1956).

functions of dyes and the contact potential difference between cadmium sulfide and solid dye films. It must be stressed that the surrounding atmosphere and space charge layers at the surface can influence the value of the contact potential and the work function. Therefore, the location of the Fermi level is not exactly known in many solids, and further measurements—above all, in dyes—would be of great interest.

The Fermi level or, in other words, the electrochemical potential of electrons is a very important value of a solid. In general, the relative heights of the Fermi levels are significant for the electron exchange between semiconductors. In cases in which the position of a semiconductor Fermi level is higher relative to the Fermi level of another solid, there must be flow of electrons across a boundary from the first level to the second until the Fermi levels are equal in height on both sides of the boundary.

(2) Another energy value is the photoelectric work function, Φ , which can be obtained from the threshold wave length for the external photoelectric effect. This function is identical with the ionization potential or the position of the ground level of a solid. Values are obtained by Vilesov, Nelson, and others⁶⁴⁻⁷⁰ in inorganic p- and n-conductors and in dyes. It should be mentioned that further information on this energy level in dyes can also be obtained from the polarographic anodic half-wave potentials because the anodic potential is a measure of the energy required to make an electron to pass from the ground level of the dye to the electrode.

(3) The magnitude of the energy gap, E , between the valence band and the conduction band can be obtained from the onset of the absorption spectrum of the semiconductor or from the measurement of the optical threshold energy for photoconductivity.

(4) The energy of the bottom of the conduction band is identical with the electron affinity, χ , of a semiconductor because the electron affinity is defined as the negative work done in moving an electron into the conductive state from outside. From the measurements of the work function, φ , Nelson^{64,71} deduced the values of the electron affinity of some dyes. This is possible when the Fermi level is near the bottom of the conduction band as, for example, in excess n-conductors. Terenin and Akimov¹⁰ computed values of the electron affinity from the difference between the photoelectric work function, Φ , and the energy gap, E : $\chi = \Phi - E$. Further information on dyes may be obtained from their oxidation-reduction potentials⁷² or polarographic cathodic half-wave potentials,⁷³ which are a measure of the energy that is required to make an

electron pass from the electrode to the lowest unoccupied level of the dye molecule.

It may be noted that, according to Scheibe and co-workers,⁷⁴ the first excited electronic state of many organic molecules is situated 3.4 e.v. below the vacuum level. This universal rule has been derived from the hydrogen-like absorption band procession of dyes in solution. The fact that the measured values of the electron affinity in solid dye films are similar to the universal value of Scheibe confirms the identity of the position of the excited level of a single dye molecule with the conduction band of aggregated dye molecules.

Table III shows the values of the energy levels of semiconductors and dyes as defined above.

Table III

Solid	Type	φ , e.v.	Φ , e.v.	χ , e.v.	E , e.v.	Contact potential, mv.	References	
AgBr	p	5.33	6.0	3.5	2.5	Pd, -380	10, 12	
				3.5		W, -290	64	
TlI	p	5.4	5.6	3.0	2.5	Pd, -450	10, 12	
CdS	n			3.5			64	
ZnO	n	4.84	7.3	4.3	3.0	Pd, +110	10, 12	
			6.3			65		
Rhodamine B	n	4.45	5.2	3.2	2.0	Pd, +500	10, 12	
			4.6	5.1			68	
Erythrosin	p	4.64	5.5	3.3	2.2	Pd, +310	10	
			5.5	3.4	2.0		68	
Malachite green	n	4.86	5.2		2.0	Pd, +90	10	
			4.6				68	
Pinacyanol	(n)	4.55	5.2	3.2	1.6		70	
			4.9	3.1	1.8	Pd, +400	10	
Merocyanine	p	3.1	7.28	5.1			10	
			4.3	3.0	1.6	CdS, +320	64, 70	
Crystal violet	n	3.32	5.3	3.5	2.3		10	
			7.35	4.8			10	
Phthalocyanine	p	5.0	5.3	3.3	2.3		68	
			3.32	5.1	3.0	1.7	CdS, +180	64, 70
Phenosafranine	p	5.2	4.5	5.0			68	
			6.0	4.3	1.7		10	
Methylene blue	p	5.2	5.0	5.4	3.3	2.1		68
			5.4	3.6	1.8		68	
Dye				3.4			Rule of Scheibe, 74	

(65) F. I. Vilesov and A. Terenin, *Dokl. Akad. Nauk SSSR*, **125**, 55 (1959); **133**, 1060 (1960); **134**, 71 (1960); *Naturwissenschaften*, **46**, 167 (1959).

(66) E. A. Taft, H. R. Philip, and L. Apker, *Phys. Rev.*, **110**, 876 (1958).

(67) F. I. Vilesov, *Dokl. Akad. Nauk SSSR*, **132**, 632 (1960).

(68) B. L. Kurbatov and F. I. Vilesov, *ibid.*, **141**, 1343 (1961).

(69) R. Fleischmann, *Ann. Physik*, **5**, 73 (1930).

(70) R. C. Nelson, *J. Opt. Soc. Am.*, **51**, 1186 (1961); *J. Mol. Spectry.*, **7**, 439 (1961).

(71) R. C. Nelson, *J. Chem. Phys.*, **27**, 864 (1957).

(72) S. E. Sheppard, R. H. Lambert, and R. D. Walker, *J. Phys. Chem.*, **50**, 201 (1946).

(73) S. Umamo, *Nippon Kagaku Zasshi*, **77**, 796 (1956).

(74) G. Scheibe, D. Brück, and F. Dörr, *Chem. Ber.*, **85**, 867 (1952).

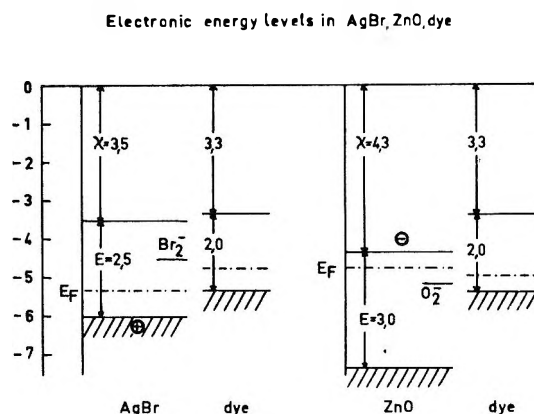


Figure 3. Electronic energy levels in AgBr-dye and ZnO-dye.

From the data of this table we can obtain the relative position of the electronic levels of the semiconductors and solid dyes. The diagram in Figure 3 exhibits this relative position of the electronic energy levels in zinc oxide, silver bromide, and dye molecules.

One can see that the excited singlet level (or the conduction band) of dye molecules must be situated above the conduction band of semiconductors if we postulate that the values given by Nelson and Scheibe are the correct ones. However, there is no completely satisfactory knowledge of its magnitude; corresponding to measurements of the photoionization potential of the gaseous dye molecules by Terenin and Akimov,¹⁰ the excited dye level is situated below the conduction band.

In the discussion of this problem we must remember that not the relative position of conduction bands, but the relative heights of the Fermi levels are significant for the electron exchange between semiconductors. The discussion of the relative position of energy levels is connected with the different types of sensitizing mechanism. Before discussing these mechanisms, it should be said that no single mechanism can apply in all cases; however, there is no evidence that optical sensitization can be divided into two or more types of different characteristics. Furthermore, it must be noted that no theory of spectral sensitization has been generally supported hitherto. At present, there exist two main types of mechanisms which are of interest for the solution of the problem—the energy-transfer or resonance mechanism and the electron-transfer mechanism. See the scheme of Figure 4.

According to the resonant mechanism, supported, above all, by Putzeiko,³⁶ Terenin, and Akimov,¹⁰ the excitation energy of the sensitizing dye molecule is transferred to the intermediate and surface levels

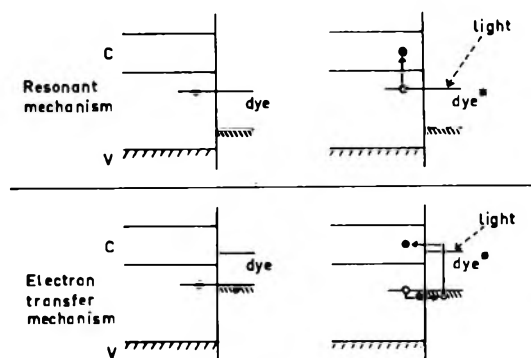


Figure 4. Scheme of the sensitization mechanisms.

of the semiconductor that are occupied by electrons. In the case of an n-type semiconductor these electrons can be raised to the conduction band of the semiconductor and bring about n-type sensitized photoconductivity.

The resonant mechanism seems to be supported by the fact that such intermediate levels, from which electron transitions are possible, exist on surfaces, on edges, and at defects and that electronegative gases, such as oxygen and bromine, produce an enhancement of the sensitized photoconductivity in silver halides.^{10,12,36} However, the effect is also produced in primitive, chemically unsensitized silver halide emulsions,⁷⁵ and furthermore, a sensitization of photoconductivity by dyes also takes place in pure organic photoconductors and in cadmium sulfide under vacuum.

An important reason for the discussion of the resonant mechanism is based on the calculations and measurements of Coulson, Akimov, and others (see Table III) according to which the excited level of the dye lay too low to permit electron transfers from the dye to the semiconductor.

Because of theoretical estimations of Coulson which, from the value of the dye ionization potential of 7 to 8 e.v., resulted in a deep position of the excited level of dyes, Mitchell⁷⁶ discussed the two-electron process. In Mitchell's opinion, the excited dye molecule receives in silver halide an electron from the surface halide ion (Br^-) into its vacated ground level. After raising the energy levels of the negatively charged dye molecule, there exists the possibility of an electron transfer to acceptor levels from which an additional thermal energy can raise the electron into the conduction band.

In our opinion there is no necessity for the resonant

(75) B. H. Carroll, "Proceedings of the International Colloquium Liège 1959," Pergamon Press, Oxford, 1962, p. 435.

(76) J. W. Mitchell, *J. Phot. Sci.*, **6**, 57 (1958).

transfer mechanism or for the two-electron process because the ground and the excited levels of the dye lay near the levels of the semiconductor. Furthermore, it is remarkable that the resonant transfer mechanism is not able to explain the sensitization by thick dye films, layers hundreds of molecules in thickness, because the excitation energy can only be transferred to electrons that are trapped within an area of 50-Å radius.^{77,78} The observation of a considerable sensitization of photoconductivity in cadmium sulfide by thick dye films, observed by Nelson²⁰ and by us,²¹ therefore, disagrees with the resonant process.

According to the electron-transfer mechanism the excited dye molecule gives up its electron to the semiconductor. This mechanism, first proposed by Gurney and Mott⁷⁹ and later discarded by Mott,⁸⁰ has been confirmed by Nelson,^{19,64,81} Eggert,⁸² Scheibe, Dörr,⁸³ and other authors. We have discussed this mechanism since 1951; see Noddack, *et al.*^{31,84-86}

Mott⁸⁰ discarded this hypothesis because of calculations of Coulson according to which the excited level of the dye should lie too low to permit electron transfer to the silver halide. However, the measured values of the energy levels in dyes, as described above, indicate that electron transfer from the dye to the semiconductor is energetically possible.

It is evident that the electron-transfer mechanism requires the restoration of the electron lost by the dye because a single molecule can act many times. According to Scheibe⁸⁷ and Eggert,⁸² the emptied ground level of the dye can be replenished by an electron from donor levels in the semiconductor; see also ref. 31 and 88.

The electron-transfer mechanism can be divided into two acts: (1) the appearance of a free electron in the excited level of the dye which may be able to travel through a close-packed layer of dye molecules and the transition of the excited electron, the energy of which must be greater than that in the conductive state of the solid, to the semiconductor, and (2) the replenishing of the hole in the emptied ground level of the dye from the semiconductor.

It is necessary to point out that this picture does not explain the possibility of the sensitization of p-conducting semiconductors by dyes because in this case the effect is characterized by an increase of holes—and not of electrons—in the semiconductor. Furthermore, this mechanism cannot explain the fact that photographic desensitizing dyes have the ability of sensitizing electrical effects. Therefore, it is necessary to correct the electron-transfer mechanism, which will be discussed subsequently.

Photoconductivity of Dyes. The fact that organic

sensitizing dyes can show electronic photoelectric effects is an important experimental proof that speaks in favor of the electron mechanism. Certainly, the existence of an electron and hole transfer in dye deposits is, in itself, not a proof of any intertransport between dye and semiconductor, but without this fact there cannot be a positive discussion of the electron-transfer mechanism. Besides, only the possibility of a migration of electrons and holes in dyes can explain the sensitization effects observed with thick dye films.

In 1952, our experiments on the photoconductivity of sensitizing dyes (see Noddack and others^{31,84-86,88-92}) led us to postulate an electronic mechanism for the photoconductivity of organic dyes, a mechanism with which the measurements of Nelson, Eggert, Weigl, Terenin, Wartanjan, and other authors^{4,9,33,93-96} are in good agreement. The following facts are important for the discussion.

(1) Cationic, anionic, and nonionic dyes show the same photoelectrical effects which are characteristic for photoconductive inorganic semiconductors: the Becquerel effect,^{61,84,90} the Dember effect,⁹ the barrier-layer photoeffect,^{89,91} the change in the photocontact potential,⁵¹ and the typical photoconductivity measured by means of surface cells and sandwich cells.^{84,85,92,93,97}

(77) T. Förster, "Fluoreszenz organischer Verbindungen," Vandenhoeck and Ruprecht, Göttingen, 1951.

(78) T. Förster, *Ann. Physik.* (6) 2, 55 (1948).

(79) R. W. Gurney and N. F. Mott, *Proc. Roy. Soc. (London)*, **A164**, 151 (1938).

(80) N. F. Mott, *Phot. J.*, **88**, 119 (1948).

(81) R. C. Nelson, *J. Opt. Soc. Am.*, **48**, 948 (1958); *J. Chem. Phys.*, **27**, 864 (1957).

(82) J. Eggert, *Ann. Physik.* (7) **4**, 140 (1959).

(83) G. Scheibe and F. Dörr, "Proceedings of the International Colloquium Liège 1959," Pergamon Press, Oxford, 1962, pp. 511-513.

(84) W. Noddack, G. Eckert, and H. Meier, *Z. Elektrochem.*, **56**, 735 (1952).

(85) H. Meier, *Z. wiss. Phot. Photophysik. Photochem.*, **50**, 20 (1955).

(86) W. Noddack and H. Meier, *Z. Elektrochem.*, **63**, 971 (1959).

(87) G. Scheibe, *ibid.*, **63**, 117 (1959).

(88) W. Noddack and H. Meier, "Proceedings of the International Colloquium Liège 1959," Pergamon Press, Oxford, 1962, pp. 515-531.

(89) H. Meier, *Z. Elektrochem.*, **59**, 1029 (1955).

(90) G. Eckert, *Z. wiss. Phot. Photophysik. Photochem.*, **49**, 220 (1953).

(91) W. Noddack and H. Meier, *Z. Elektrochem.*, **57**, 691 (1953).

(92) H. Meier, *Phot. Sci. Eng.*, **6**, 235 (1962).

(93) R. C. Nelson, *J. Chem. Phys.*, **22**, 885 (1956); **30**, 406 (1959); *J. Opt. Soc. Am.*, **46**, 10 (1956).

(94) J. W. Weigl, *J. Mol. Spectry.*, **1**, 216 (1957).

(95) I. A. Karpovitch and A. T. Wartanjan, *Dokl. Akad. Nauk SSSR*, **117**, 57 (1957).

(96) B. Rosenberg, *J. Opt. Soc. Am.*, **48**, 581 (1958); **51**, 238 (1961); *J. Chem. Phys.*, **34**, 63 (1961).

(2) The action spectra of the various photoeffects correspond with the absorption spectrum of the dye; see, for instance, Weigl.⁹⁸

(3) The quantum yield of the photocurrent is between 0.2 and 0.5 for pinacyanol, merocyanine dyes, and others.⁹⁹ This result contradicts the exciton theory which says that an energy transfer takes place without any formation of charge carriers.

(4) Solvents, humidity, or impurities are not responsible for the photoeffect. This fact and, especially, the reversibility and stability of photoconductivity refute the often-discussed hypothesis saying that the photoconductivity is a consequence of a photoelectrolytic decomposition of the dyes.

(5) The order of the mean mobility of electrons and holes is about 0.1 to 1 cm.²/v. sec. This value could also be estimated by Nelson and others¹⁰⁰ with electron spin resonance studies of some dye photoconductors; see ref. 31.

(6) By addition of various electron acceptors, such as *o*-chloranil, iodine, and others, the photoconductivity of p-type dyes can be enhanced by a factor of 5 to 10⁴ over that of the pure dye. This doping effect, observed by Kearns, Tollin, and Calvin¹⁰¹ on phthalocyanine and by us¹⁰² on merocyanine surface cells was first described by Hoegl^{103,104} in highly conjugated resins.

It is remarkable that the coadsorption of both sensitizing dye and electron affinitive molecules on the surface of a photoconductor (zinc oxide) enhanced the photoconductivity strongly, compared to the photoconductor with dye or electron acceptor only. This supersensitization, observed by Inoue and others,¹⁰⁵ seems to be in relation to the doping effects of the dye photoconductivity.

(7) As in inorganic semiconductors, one type of charge carriers—electrons or holes—is generally more mobile than the other. A series of experiments—measurements of the Hall effect,^{106–108} of the thermoelectric effect,^{109–112} of the influence of gases,¹¹³ and of other effects⁵² proves that the dyes can be divided into n-conductors and p-conductors.

Organic-Inorganic p-n Junctions. The fact that dyes can be divided into n-conductors and p-conductors points to a remarkable similarity between the electrical properties of organic and inorganic solids. In our opinion, this similarity seems to be important in connection with the discussion of the electron-transfer mechanism of sensitization. We supposed that the arrangement consisting of a p-type dye or semiconductor and a n-type dye or semiconductor would produce p-n photovoltaic effects, and we postulated that these photovoltaic effects would be connected with the

photosensitization of electrical effects. Indeed, there is a series of experiments which seems to indicate the validity of this postulation.

Firstly, we could prove^{31,92,114,115} that a system, composed of dyes of the p- and n-type, is a photoelement which produces photocurrents up to 10⁻⁸ amp. and photovoltages up to 100 mv. when exposed to visible light. In conformity with inorganic p-n photoelements, the current is directed from the p- to the n-conducting dye; see, for instance, Figure 5.

Secondly, an analogous system, composed of an organic dye conductor of the p- or n-type and an n- or p-type inorganic semiconductor, is a photoelement which produces photocurrent and photovoltage when exposed to light absorbed in the semiconductor or in the dye. This effect was first observed by Nelson,¹⁹ who prepared cells having platinum, dye film, cadmium sulfide, and platinum in series connection. We could confirm this observation.^{21,116} Moreover, we could observe similar photoeffects in cells in which dyes of the p- or n-type made a series contact with n-type cadmium selenide, p-type silver bromide, or p-type silver iodide.¹¹⁷ From these experiments we

(97) H. Meier, *Z. Elektrochem.*, **58**, 859 (1954).

(98) J. W. Weigl, *J. Chem. Phys.*, **24**, 883 (1956).

(99) W. Noddack, H. Meier, and A. Haus, *Z. physik. Chem.*, **212**, 55 (1959).

(100) B. Y. Cho, R. C. Nelson, and L. C. Brown, *J. Chem. Phys.*, **39**, 499 (1963).

(101) D. M. Kearns, G. M. Tollin, and M. Calvin, *ibid.*, **32**, 1020 (1960); *J. Am. Chem. Soc.*, **83**, 2110 (1961).

(102) H. Meier and W. Albrecht, *Z. physik. Chem. (Frankfurt)*, **39**, 249 (1963).

(103) H. Hoegl, Kalle Akt. Ges. Belgian Patent 591,164 (1960).

(104) R. P. Kohin, K. A. Müller, and H. Hoegl, *Helv. Chim. Acta*, **35**, 255 (1962).

(105) E. Inoue and T. Yamaguchi, *Bull. Chem. Soc. Japan*, **36**, 1573 (1963).

(106) A. Epstein and B. Wildi, "Electrical Conductivity in Organic Solids," Interscience Publishers, Inc., New York, N. Y., 1961, pp. 337–357.

(107) G. Delacote and M. Schott, *Phys. Status Solidi*, **2**, 1460 (1962).

(108) G. H. Heilmeyer, G. Warfield, and E. Harrison, *Phys. Rev.*, **8**, 309 (1962).

(109) N. Petruzella and R. C. Nelson, *J. Chem. Phys.*, **37**, 3010 (1962).

(110) P. E. Fielding and F. Gutman, *ibid.*, **26**, 411 (1957).

(111) C. Haman and I. Storbeck, *Naturwissenschaften*, **50**, 327 (1963).

(112) F. H. Moser and A. L. Thomas, "Phthalocyanine Compounds," Reinhold Publishing Corp., New York, N. Y., 1963, p. 75.

(113) H. Meier, *Z. wiss. Phot. Photophysik. Photochem.*, **53**, 1 (1958).

(114) H. Meier and A. Haus, *Z. Elektrochem.*, **64**, 1105 (1960); *Angew. Chem.*, **72**, 631 (1960).

(115) W. Noddack, H. Meier, and A. Haus, *Z. wiss. Phot. Photophysik. Photochem.*, **55**, 7 (1961).

(116) H. Meier and W. Albrecht, *Ber. Bunsenges. physik. Chem.*, **68**, 64 (1964).

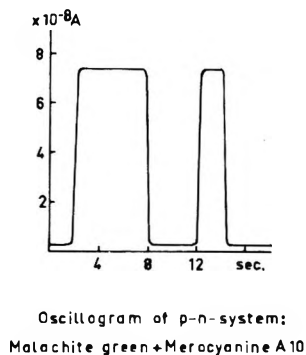


Figure 5. Oscillogram of the p-n system: malachite green-merocyanine A 10 (for formula see Figure 1).

could deduce the following rules about charge polarity in the described arrangement upon illumination: (1) p-type dyes become positively charged with respect to n-type semiconductors; (2) n-type dyes become negatively charged with respect to p-type semiconductors; (3) in cells with an n-type semiconductor and an n-type dye the substance with the greater density of free electrons in the dark becomes negatively charged with respect to the other one; (4) in p-type dyes and semiconductors connected with one another, the difference of the hole density produces an analogous charge direction.

The experiments clearly prove that in systems consisting, for instance, of a p-type semiconductor and an n-type dye, the density of holes in the p-type semiconductor must be increased upon illumination of the dye. Similarly, upon illumination the density of free electrons of an n-type semiconductor must be increased when connected with a p-type dye. It must be stressed that this observation is identical with the spectral sensitization of photoconductivity in solids by dye films, as previously described. The scheme of Figure 6 illustrates this fact.

It is remarkable that the effects observed by the help of the simple model photocell of sensitization systems are not changed when we alter the arrangement. See the schemes of Figure 7. Upon illumination, photocurrents and photovoltages could also be observed in sandwich-type cells in which a cadmium sulfide or a silver halide deposit and a sublimed dye film, 0.1-1 μ in thickness, were placed between a back and a transparent front electrode.^{21,116,117}

Principally, this arrangement is identical with any sensitized system in which the semiconductor—for instance, CdS—is sensitized by a thick dye film. Therefore, the photoelectrical effects of model photocells of this kind give us a direct insight into the electrical behavior of sensitized solids. Figures 8, 9, and

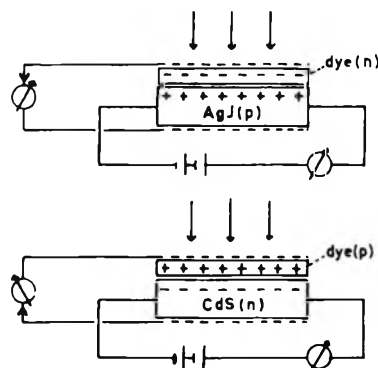


Figure 6. Scheme for p-n sensitization mechanism.

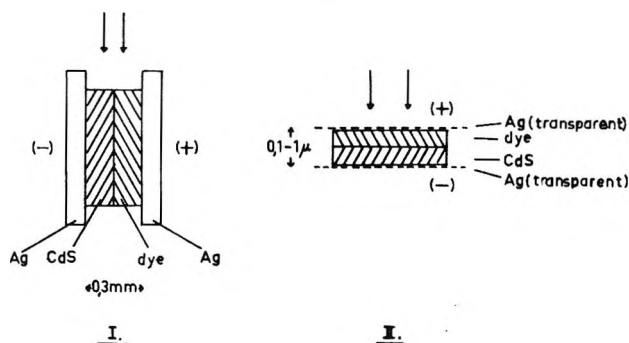


Figure 7. Arrangement for the measurement of the p-n photovoltaic effect (CdS-dye, AgI-dye, and other systems).

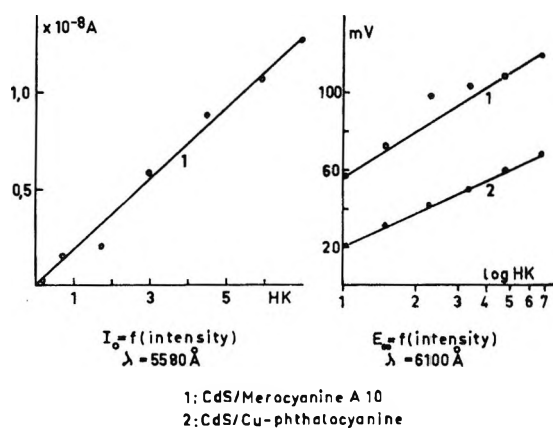


Figure 8. Dependence of photocurrent and photovoltage in a CdS-dye system on intensity of light.

10 illustrate some experimental properties of these photoelements.

(1) The photovoltage and the photocurrent increase logarithmically and linearly, respectively, with the increase of light intensity. (2) The photoeffect is

(117) H. Meier and W. Albrecht, *Ber. Bunsenges. physik. Chem.*, to be published.

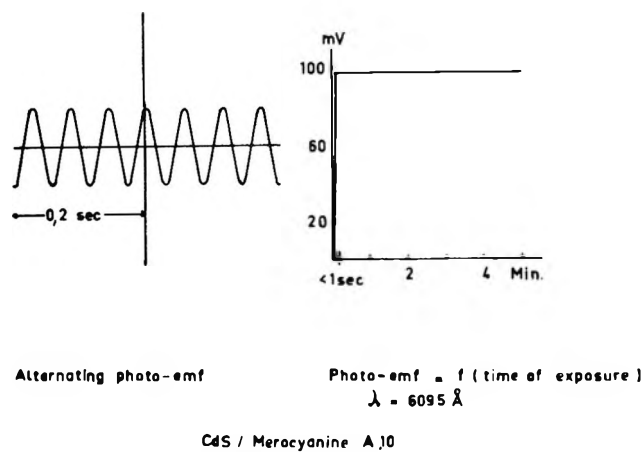


Figure 9. Buildup and decay of the photovoltage in a CdS-dye photovoltaic cell.

reversible. The oscillogram of Figure 9 shows that photovoltages and photocurrents are generated in times shorter than 10^{-2} sec. (3) The stability of photovoltages and photocurrents proves that there exists steady exchange of electronic charge carriers between the inorganic semiconductor and the organic dye film; see Figure 9. (4) The rules about the charge polarity, as previously mentioned, could also be observed in the sandwich-type photoelements. (5) From Figure 10 we see that the action spectra for both the sensitized photoconductivity of CdS and the photovoltage of a CdS-dye photovoltaic cell are nearly identical.

The p-n Mechanism of Sensitization. From the fact that, upon absorption of light quanta in the dye, photo-

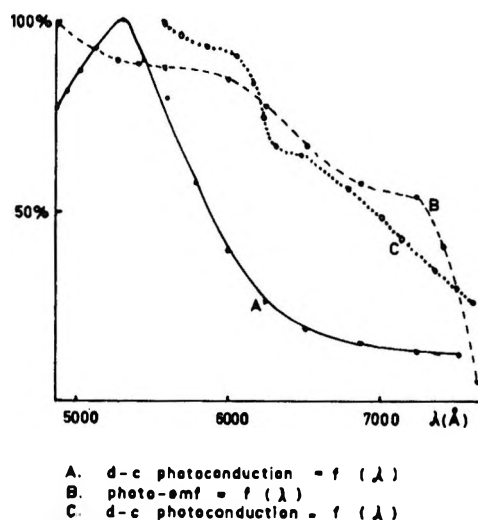


Figure 10. Action spectra: A, CdS surface cell; B, CdS-merocyanine A 10 photovoltaic effect; C, CdS-merocyanine A 10 sandwich cell (photoconductivity).

effects are generated both in the semiconductor-dye arrangement and in the sensitized semiconductor, we can draw the conclusion that the photoeffects of the different arrangements are correlated with one another. Therefore, we suppose that any mechanism which can explain the photovoltaic effect of the dye-semiconductor arrangement must also be able to explain the sensitization of electrical effects in solids. We postulate that the photovoltaic effects of semiconductor-dye systems are the result of a p-n photoeffect between the p- or n-type semiconductor and the n- or p-type dye. Furthermore, we suppose that the sensitization of electrical effects in solids can be explained, especially in the case of thick dye layers, by the help of an analogous hypothesis.

This hypothesis says that in the case of a p-n junction (see, for instance, ref. 118) there exists an electrostatic field between the p- and the n-region, which is the result of the tendency of the holes or electrons to diffuse in the dark to the n- or to the p-region. This effect is, in other words, the consequence of the requirement that the Fermi level must be constant throughout the system.

It is remarkable that any potential difference can be expected in all those cases in which there exists a difference of electron or hole densities between contacted materials, for instance, between two n-conductors with various electron concentrations (zinc oxide-rhodamine B). The electrostatic potential is always more positive in the n-type material or in the region with the greater electron concentration and more negative in the p-type material or in the region with the greater hole concentration; see Figure 11.

For our problem it is important that the electrostatic field can separate electron-hole pairs which are optically generated. As a consequence, electrons flow into the more positive n-region and holes flow into the more negative p-region upon illumination of the specimen. It must be stressed that the direction of photocurrents and the polarity of photovoltages of the semiconductor-dye arrangement, which are summarized in the rules discussed above, can be explained exactly by help of this mechanism. Because of the parallelism between the photoelectrical behavior of the semiconductor-dye photoelements and the electrical behavior of solids sensitized with thick dye layers, we conclude that the p-n mechanism may be extended beyond its usual range of application and give the key for the explanation of the photosensitization of electrical effects in solids. This mechanism can explain the various ex-

(118) W. Shockley, "Electrons and Holes in Semiconductors," D. van Nostrand Co., Inc., London, 1956.

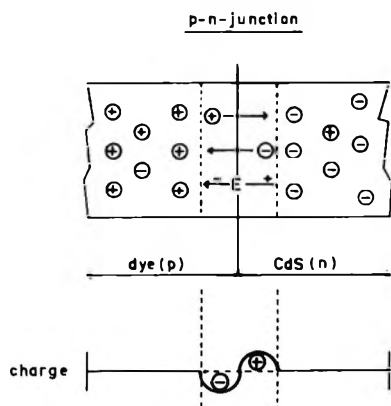


Figure 11. Scheme of the p-n junction.

perimental facts: (1) the sensitization of n-type semiconductors by p-type dyes and also by n-type dyes—for instance, by photographic desensitizing dyes—the latter having, however, a smaller efficiency; (2) the sensitization of p-type conductors, which can be the result of an increase of the hole or electron concentration, corresponding to the type of the sensitizing dye; (3) the sensitization of electrical effects in organic semiconductors by organic dyes because the arrange-

ment consisting of a p-type dye and an n-type dye exhibits the same photoelectrical effects as inorganic p-n junctions or inorganic-organic p-n junctions; (4) the supersensitization of photoconductivity—we could observe that the photovoltaic effect of the semiconductor-dye arrangement can be enhanced by the adsorption of electron-acceptor molecules on the dye component.

We do not know if the electronic p-n mechanism, as discussed above, is really the correct one, but we hope that through this hypothesis, which is an improvement of the electron-transfer mechanism, a solution of the spectral sensitization is reasonably possible. It is necessary to get further theoretical and experimental information on energy levels in dye layers and inorganic solids, on the electronic conductivity of dyes, on the p-n photoeffects of dye layers and inorganic materials, on the temperature dependences of the sensitized photoconductivity and of the inorganic-organic p-n photoeffect, on the electron paramagnetic resonance of sensitized systems, and other facts.

Acknowledgment. The author is grateful to Diplom-Chemiker W. Albrecht for helping with the measurements. The financial support of the Fonds der chemischen Industrie, Düsseldorf, is acknowledged.

Some Experiments on the Photosensitization Mechanism of Semiconductors by Dyes^{1a}

by A. Terenin and I. Akimov

Physics Department, Leningrad University, U. S. S. R. (Received October 5, 1964)

The thermal activation energy for photoconductivity of TII at its long wave length tail remains practically unchanged when the sensitizer is adsorbed and photoexcited in the same spectral range. The necessity of surface electron traps for AgI sensitization is demonstrated by the gradual increase of its efficiency upon the semiconductor photolysis, leading to the formation of iodine on the surface. The reduced dye (hematoporphyrin) proved to be a far less efficient photosensitizer of ZnO than the initial form of the dye. Dyes protonized or deprotonized on the surface of ZnO and TII *in situ* exhibit remarkable changes in the efficiency and spectral distribution of photosensitization. These and other experiments are discussed from the viewpoint of the two alternatives: electron or energy transfer from the sensitizer.

Introduction

In a previous paper,^{1b} we presented arguments to substantiate the viewpoint that an excitation energy, but *not* a direct electron transfer from the dye molecule, takes place in the photosensitized conductivity of ZnO, TlX, AgX, HgI₂, etc., studied by us. In short, these arguments were:

(a) The first singlet excited level for several sensitizers is situated definitely below the bottom of the conduction band of the semiconductor.

(b) The photosensitization process is achieved during a time less than 10⁻⁹ sec. after photon absorption. A greater time lag should be expected in an electron exchange, the more so at low temperatures.

(c) No marked difference is observed between dyes of different types (oxidants and reductants), in particular between typical photographic sensitizers and desensitizers, for the same semiconductor.

(d) The sensitizing efficiency does not depend on the presence of photoconductivity in the solid sensitizer itself, nor on the sign of its photocarriers. The optimum photosensitization is observed at a coverage less than monomolecular of the semiconductor surface.

(e) The sign of the photocurrent carriers in the sensitization spectral range always coincides with that of the proper photoconductivity of the semiconductor.

(f) The photosensitization efficiency is increased

when gases and vapors with high electron affinity (O₂, X₂, *p*-benzoquinone) are additionally adsorbed on the surface, thus creating local electron trapping levels in the forbidden band of the semiconductor.

In the meantime, additional experiments described below have been carried out.

1. *Thermal Activation Energies.* The temperature dependence of the dark conductivity of sublimed TII has been measured as well as that of the photoconductivity in its *proper* spectral range at two wave lengths, *viz.*, at 436 mμ in the region of strong absorption of the semiconductor and at 578 mμ, where its absorption is low, but that of the sensitizer has its maximum. These measurements were carried out before and after the sensitizer adsorption with the same sample.^{2a} A typical plot of the results is shown in Figure 1.^{2b} The temperature range was from 20 to -170°.

(1) The presence of the adsorbed dye does not significantly change either the dark or the proper photoconductance at 436 mμ.

(1) (a) Presented to the International Conference on Photosensitization in Solids, Chicago, Ill., June 22-24, 1964; (b) A. Terenin and I. Akimov, *Z. physik. Chem. (Leipzig)*, **217**, 307 (1961).

(2) (a) The sensitizers in these experiments were: rhodamine B, erythrosin, and the photographic sensitizers 1,1'-diethyl-3,3,3',3'-tetramethylcarbocyanine iodide and 3,3'-diethyl-5,5'-dinitrothiacarbocyanine-*n*-toluene sulfonate; (b) I. Akimov, *Dokl. Akad. Nauk SSSR*, **151**, 310 (1963).

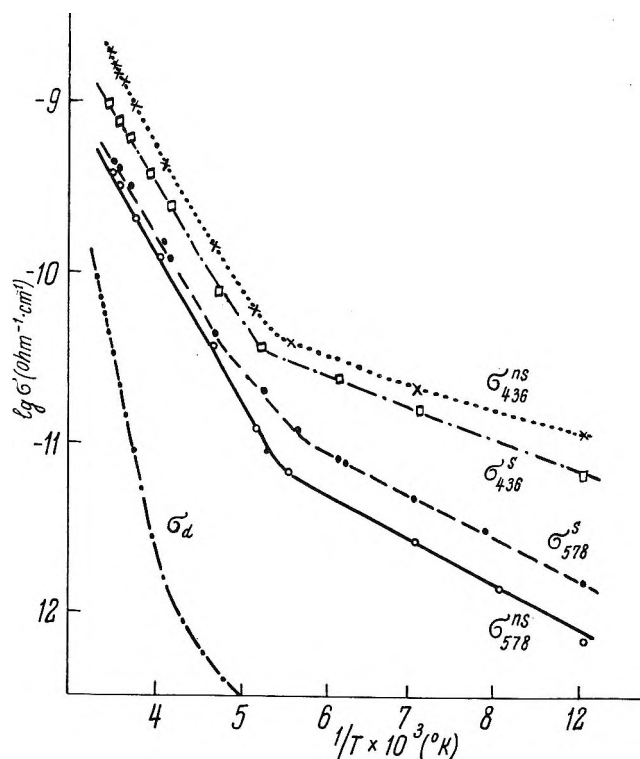


Figure 1. Temperature dependence of the dark conductivity (σ_d) and of the photoconductivity (σ_λ) of TII layers (in air) before sensitization, σ^{ns} , by rhodamine B and after it, σ^s . The acting wave lengths, λ , are in the proper range (436 $m\mu$), or in the sensitizing range (578 $m\mu$).^{2b}

(2) At the longer wave length (578 $m\mu$) the activation energy E_{ph} of the proper photoconductivity of the undyed semiconductor is larger than the values observed at 436 $m\mu$. On lowering the temperature from 20 to -170° this causes a decrease of the proper photoconductivity at the longer wave length by three orders of magnitude, which is 10 times the change at the shorter wave length (436 $m\mu$).

(3) Upon dye adsorption, the photoconductivity in the long wave length range at the sensitization maximum is markedly increased. However, the main point is that the temperature dependence and the activation energies E_{ph} in this range remain practically the same as before dye adsorption.

This result is striking in that the temperature effect on the photoconductivity in the sensitized range was usually found to be more considerable than that in the proper range at the shorter wave lengths. This discrepancy can be explained by the suggestion that in reality it is the low proper photosensitivity at the longer wave lengths which is sharply enhanced with temperature, but not the sensitized one.

2. *Origin of the Electron Traps.* The important

role for photosensitization of the presence of electron acceptors on the semiconductor surface has been demonstrated with the help of a scanning monochromator³ (cf. Experimental). The spectral curve of the response (photoconductivity, or photo-e.m.f.) is recorded during a 0.5-sec. exposure time on an oscilloscope. Measurements with this apparatus have been performed with samples of microcrystalline AgI and AgBr powders, synthesized and dyed in the dark.

In Figure 2A, the gradual appearance of the photoconductivity in the sensitized spectral range is shown after subsequent exposures. The spectral sensitization is significantly enhanced on repeated exposures, whereas the proper sensitivity increases only slightly. After the fiftieth exposure, no further change in the spectral distribution could be found.

This behavior can readily be explained by the formation at the surface of AgI of an excess of I_2 . In fact, if the initially unexposed sample of AgI is brought into contact in the dark with iodine vapor (ca. 0.1 mm.), a strong photosensitivity maximum in the range of the dye absorption spectrum is observed at the first short exposure (Figure 2B). Evacuation decreases both the proper and, more markedly, the sensitized photosensitivity, evidently owing to the removal of adsorbed iodine.

3. *Sign of Charge Carriers.* The sign of the dominant photocarriers in the semiconductor usually has been obtained by us, either (1) from the polarity of the diffusion photo-e.m.f. in the static condenser, determined by means of a phase-sensitive detector,⁴⁻⁶ or (2) from the change in the contact potential of the semiconductor surface under illumination, measured with the dynamic condenser.^{6,7} The results of both methods were concordant. Lately, the signs of the dark current carriers have been obtained with the thermo-e.m.f. method, which agreed with those of the previous two methods. The Hall photoeffect helped to settle ambiguities found before (cf. Experimental).

It could be shown on sublimed TII layers dyed with photographic desensitizers, viz., phenosafranine, pinacryptol green, methylene blue, naphthol green, etc., that these dyes have a twofold function. First, they act as photosensitizers like the other dyes, and secondly, they function in their ground state as electron traps. As a result of the latter a double electric layer is formed

(3) I. Akimov, *Fiz. Tverd. Tela*, **4**, 1549 (1962).

(4) E. Putzeiko, *Dokl. Akad. Nauk SSSR*, **67**, 1009 (1949).

(5) A. Terenin, E. Putzeiko, and I. Akimov, *J. chim. phys.*, **54**, 717 (1957).

(6) A. Terenin, E. Putzeiko, and I. Akimov, *Discussions Faraday Soc.*, **27**, 83 (1959).

(7) I. Akimov, *Dokl. Akad. Nauk SSSR*, **128**, 691 (1959).

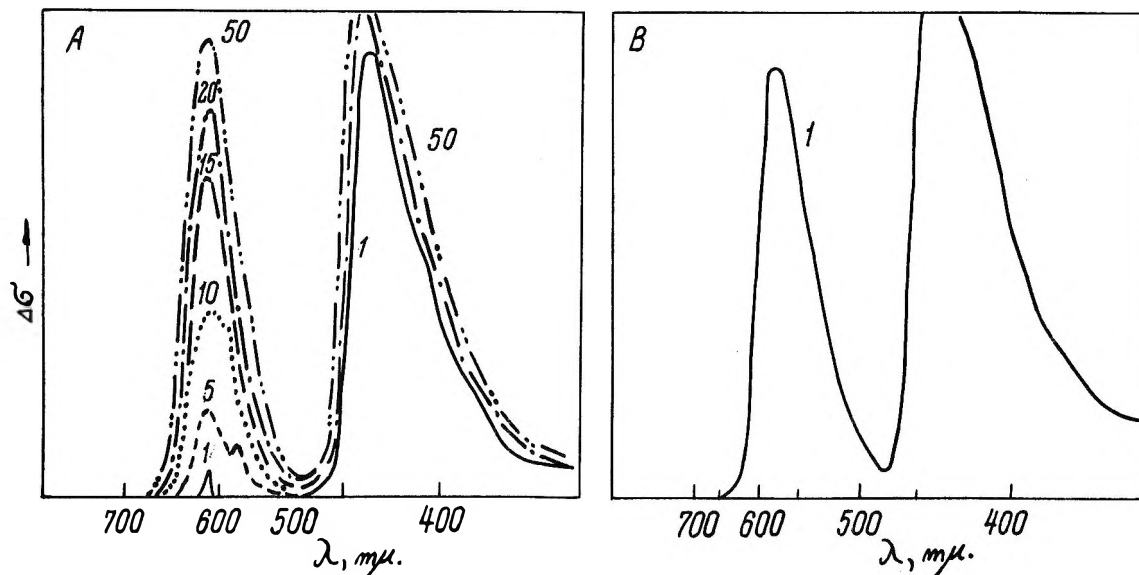


Figure 2. Photoconductivity spectrum of an AgI layer, sensitized by a carbocyanine dye. A: 1, the first measurement with 0.5-sec. exposure; 5, the fifth one; and so on. B: 1, the first measurement after iodine vapor adsorption in the dark.³

on the surface with an excess of negative charges on the adsorbed dye molecules and compensating positive charges in the semiconductor. This produces at the surface of the semiconductor an antiblocking band curvature.

4. *Spectral Sensitization by the Reduced Form of the Sensitizer.* From the viewpoint of the electron transfer mechanism of sensitization, it could be expected that reduced forms of the sensitizing dye, which are known to possess a stronger electron-donating power, should have a higher photosensitization efficiency than the initial form of the dye. Experiment showed the reverse behavior. For that purpose ZnO, an n-type photosemiconductor, was sensitized by hematoporphyrin, which possesses characteristic narrow spectral bands in the normal and reduced form⁹ (cf. the experimental procedure below). In Figure 3, curve 1, the photoconductivity spectrum of ZnO, sensitized *in vacuo* by reduced hematoporphyrin can be seen. The photoconductivity spectral curve 2 has been obtained after admitting oxygen to the sample, under the action of which the reduced sensitizer reverts to the original form. It will be seen that the spectral maxima (at 720, 640, 540, 500, and 460 m μ) for the reduced sensitizer are replaced by the maxima (630, 575, 540, 510, and 410 m μ) of the normal dye, previously observed in this laboratory.¹⁰ However, as shown by the respective scales of the ordinates for the two curves, the photosensitization efficiency by the reduced dye is *two orders* of magnitude lower than that of the normal molecule.

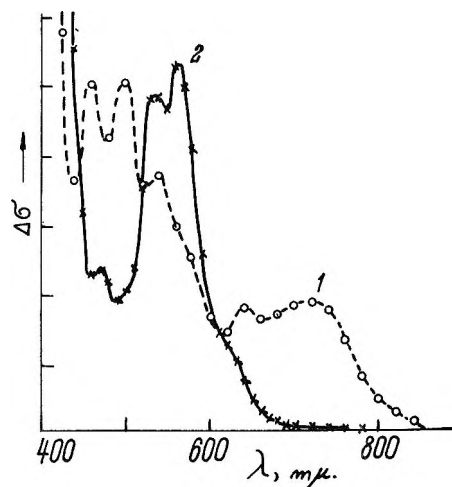


Figure 3. Photoconductivity spectra of ZnO sensitized by the reduced form of hematoporphyrin *in vacuo* (curve 1) and the initial one (curve 2). The ordinate scale of curve 2 is 1:100 of that of curve 1.

5. *Spectral Sensitization by Acid Indicators.* We investigated the behavior of the same sensitizing dye after it has been transformed into a negative ion by the loss of a proton, or, on the contrary, has added one.

(8) A. Terenin and I. Akimov, "Proceedings of the International Colloquium, Liège, 1959," Pergamon Press, Oxford, 1962; *Sci. Phot.*, 532 (1962).

(9) A. Krassnovsky and K. Voynovskaya, *Dokl. Akad. Nauk SSSR*, 96, 1209 (1954).

(10) E. Putzeiko and A. Terenin, *ibid.*, 90, 1005 (1953); *J. chim. phys.*, 55, 681 (1958).

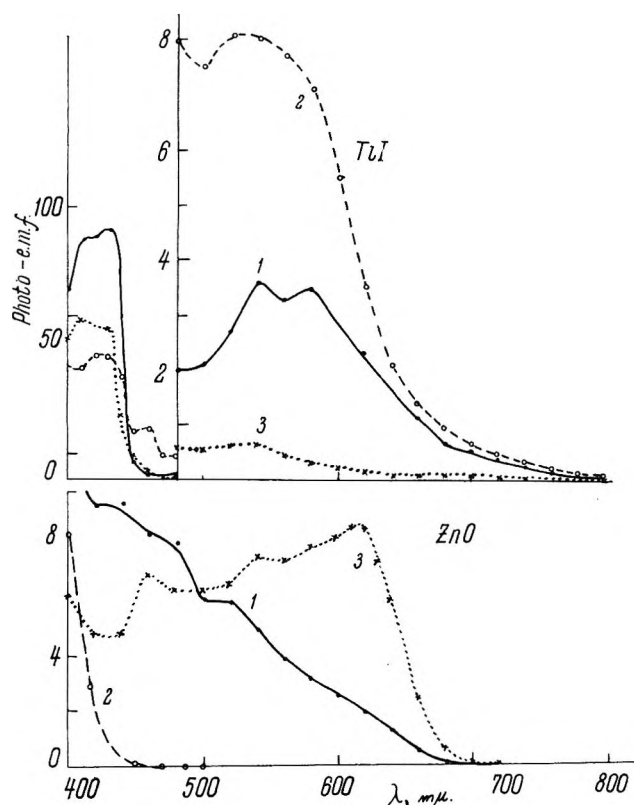


Figure 4. Condenser photo-e.m.f. spectra for TlI and ZnO sensitized with brom thymol blue: 1, neutral form of the dye; 2, after HCl vapor adsorption; 3, after NH₃ vapor adsorption.

For this purpose, several acid dye indicators have been adsorbed on the two photoconductors, ZnO (n) and TlI (p) and their protonization changed by additionally adsorbing on them the dried vapors of NH₃ or HCl, respectively.¹¹ (Cf. Experimental section.)

As an example, neutral yellow-brown brom thymol, which becomes blue when deprotonized by adsorbed NH₃ vapor thus acquiring a negative charge, exhibits a photosensitization spectral maximum at 620 mμ on ZnO (Figure 4, curve 3). The dye in the neutral form gives a maximum of a comparable magnitude at 450 mμ declining gradually to 700 mμ (Figure 4, curve 1). The same neutral dye adsorbed on TlI shows a double peak at 540 and 580 mμ which reveals the presence of a protonated form (Figure 4, curve 1), its sensitization efficiency being enhanced when HCl is adsorbed (Figure 4, curve 2). The addition of NH₃ to the initially adsorbed form depresses the sensitization, and likewise the proper sensitivity of TlI (curve 3). A similar behavior is shown by thymolphthalein.

This fact could be interpreted as a confirmation of the electron-transfer mechanism. Indeed, a negative charge on the anion of the deprotonized dye

seems to be favorable for the sensitization of a n-semiconductor (ZnO), and unfavorable for that of a p-type (TlI). However, such a correlation is not general. Thus, safranine T, or Nile blue, which are normally cations, are excellent sensitizers for both ZnO and TlI.¹¹ For further details see the Experimental part.

6. *Volume Photoconductivity of Sensitized Materials.* A contactless photoconductivity method has been devised by measurements of energy losses in a microwave field of 10¹⁰ c.p.s.¹² instead of the usual d.c. method.^{13,14} The method has been used by these authors in order to obtain the photoconductivity spectra for various materials sensitized by dyes, viz., AgBr and ZnO powders, photographic silver halide emulsions, and electrophotographic ZnO paper in polyvinylbutyral (Electrofax type). In all cases spectral bands in the sensitization range have been obtained closely corresponding to absorption bands of the adsorbed sensitizer, together with the proper photosensitivity range of the semiconductors mentioned (Figures 5, 6).

Two important conclusions emerge from the results. (a) The microwave method measures mainly the volume conductivity of the AgBr and ZnO microcrystals and the photographic emulsion grains.¹² Therefore, the experiments with the photosensitized systems prove that the charge carriers are liberated in the bulk of the semiconductor, although the sensitizer is localized on its surface. (b) The sensitized photoconductivity has been observed not only at 20°, but for the first time at -196°. At low temperature, the photosensitization efficiency for the silver halide emulsions drops by a factor of 10-20. The sensitization spectra of the emulsion photoconductivity coincide entirely with the absorption spectrum of the dye even at this low temperature.

Discussion

It is obvious that a fast electron interchange cannot in principle be distinguished from an excitation energy transfer. However, the experimentally determined upper limit of the time interval during which the sensitization process takes place, 10⁻⁹ sec.,^{15,16} does impose

(11) I. Akimov and A. Terenin, *Dokl. Akad. Nauk SSSR*, **135**, 109 (1960).

(12) E. Baranov and I. Akimov, *ibid.*, **154**, 184 (1964).

(13) W. West and B. H. Carroll, *J. Chem. Phys.*, **15**, 529 (1947); **19**, 417 (1951).

(14) L. Gross, *Zh. Nauchn. i Prikl. Fotogr. i Kinematogr.*, **4**, 411 (1959); **5**, 54, 219 (1960).

(15) H. Heerlin, *Proc. Intern. Congr. High Speed Phot.*, **3rd**, London, 227 (1957).

(16) I. Sazepin, *Zh. Nauchn. i Prikl. Fotogr. i Kinematogr.*, **5**, 60 (1960).

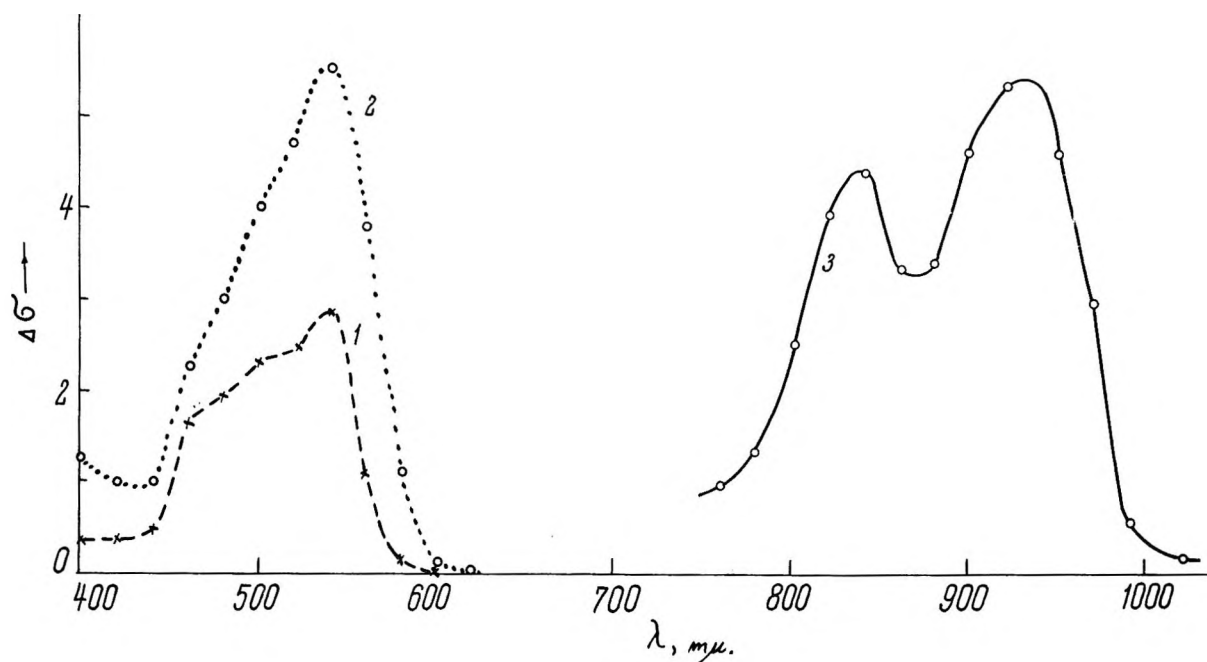


Figure 5. Spectrum of the volume microwave photoconductivity of sensitized ZnO: 1, xerographic paper, sensitized by eosine at -196° ; 2, the same at 20° ; 3, ZnO powder sensitized with xenocyanine at 20° .

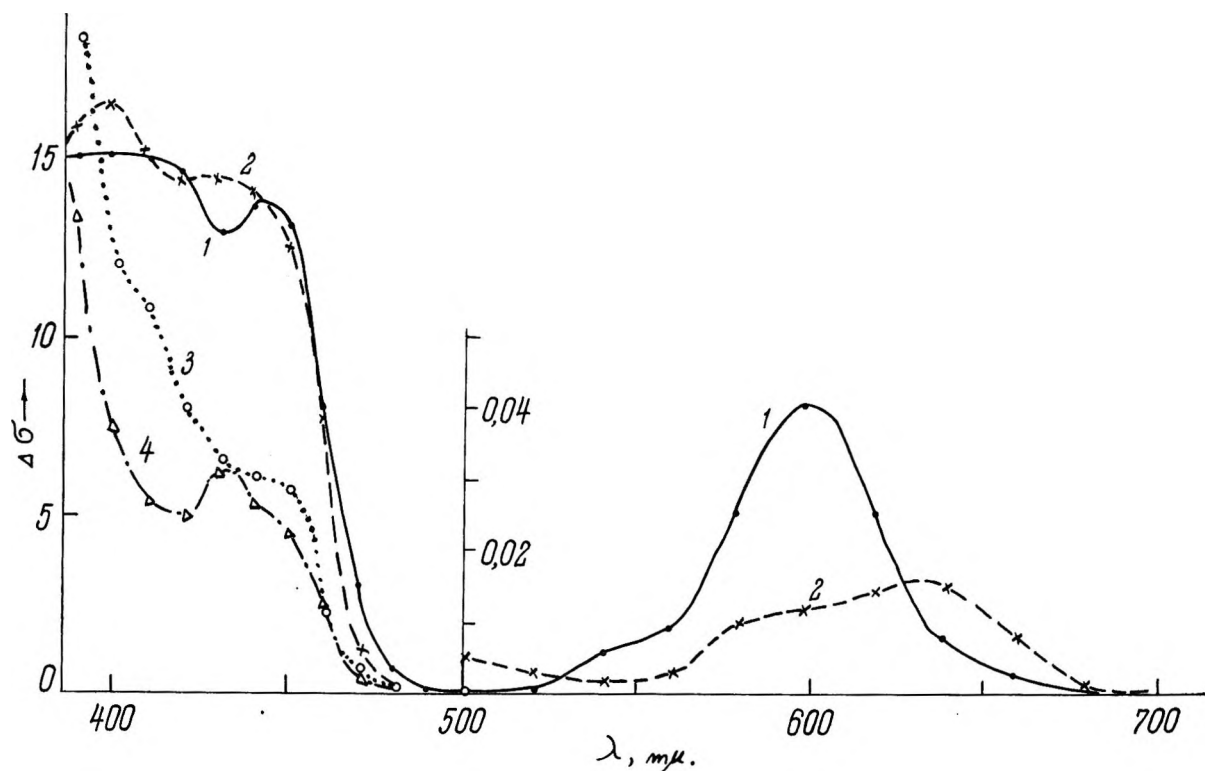


Figure 6. Spectra of the volume microwave photoconductivity of silver halide emulsions at -196° : 1, a negative film (type A); 2, Isopanochrom film; 3, X-ray film; 4, photopaper Unibrom No. 4.

severe requirements on an electron transport mechanism.

The fact that no conspicuous widening of the narrow

spectral bands of such sensitizers as chlorophyll, magnesium phthalocyanine, and hematoporphyrin is noticed on ZnO^{6,10} indicates the absence of a coupling

between the excited singlet level of the sensitizer and the vacant continuum of the semiconductor conduction band. Thus we have to imagine an electron tunneling through high potential barriers, or that the electron abstracted from the excited dye does not directly enter into the conduction band, but is first trapped at a local level of the semiconductor surface, from which it is raised thermally to the conduction state.

The close similarity of the values for the thermal activation energy for the proper photoconductivity of TII in the long wave length range before sensitization and in the same range after dye adsorption (section 1) means that electrons are at the outset thermally distributed among the local levels (imperfections, internal and external surfaces) of the semiconductor. The thermal activation of the sensitized photoconductivity, like that of the proper one, consists in the replenishing of these traps.

There is no necessity to assume either that the trapped electrons originate from the excited dye, or that its electron loss is restored by thermal activation of the semiconductor, which should require about 1.0–1.2 e.v., depending specifically on the dye. No such specificity on the dye has been established in the activation energies measured in these experiments and the additional activation energy eventually required for the excited dye to achieve the sensitization process does not exceed several hundredths of 1 e.v.

Furthermore, on both separate stages of the assumed electron passage between the dye and the semiconductor, the transferred electrons should have to overcome potential barriers at the semiconductor surface (section 3). This should require additional activation energy, specific for the presence of a dye and its properties.

In the alternative sensitization mechanism, the excited molecule gives up its excitation energy to electrons already trapped on surface levels (section 2) raising them to the conduction band. This mechanism is in some respect similar to the classical collisions of the "second kind" between excited atoms and electrons.

The anomalously slow delayed fluorescence established for many molecules, including the sensitizing dyes,¹⁷ which is observed in frozen rigid solvents, actually proves the fact that an electron can be abstracted with low efficiency directly from the excited singlet level, then kept in a trap, before recombining with the molecular ion left. Similarly, as was said before, the electron detached from the sensitizer should be kept in a trap on the surface of the semiconductor. The electron should more probably recombine with the parent sensitizer at ordinary temperature rather than

enter into the semiconductor, which requires activation energy. Moreover, it has been demonstrated in the rigid media mentioned that for detrapping and electron transport a second photon is necessary.¹⁸ Therefore, we do not consider the electron detachment from an excited dye molecule, observed under special conditions, as a decisive argument for the electron transfer mechanism in photosensitization. The quantum yield of the latter reaches unity and is not dependent on the square of the light intensity.

It is significant that the spectral sensitization has been found in this laboratory for acetylenic polymers and copper phenylacetylenide, which are p-photo-semiconductors, upon adsorption of a series of dyes (methylene blue, rhodamine 6G, pinacyanol, magnesium phthalocyanine, chlorophyll, etc.).¹⁹ The proper photoconductivity of these polymers is enhanced by preliminary ultraviolet irradiation, which presumably creates electron traps. The function of the optically excited sensitizer is evidently to provide electron transitions between the filled valence band and these traps.

As mentioned in the Appendix, the electron paramagnetic resonance (e.p.r.) signal appearing on photosensitized AgBr powder is not the product of an electron interchange with the semiconductor, but that of a reaction with photolytically evolved bromine. We also mentioned^{1b} our unsuccessful attempts to detect by flash spectrophotometry a change in the absorption spectrum of the sensitizing dye, adsorbed on a AgI sol.

The experiments and comments given above do not give sufficient support for an unreserved acceptance of the electron detachment mechanism from the excited sensitizer with its transfer to the conduction band of an n-type semiconductor. For the p-type semiconductors this mechanism is not at all applicable. To explain the sensitization of these latter semiconductors, we have to assume that the excess of the electronegative component (halide, oxygen) function as electron traps on the surface already in the dark (section 2). The excited sensitizer depopulates these traps by raising the trapped electrons to higher situated traps, thus increasing the hole concentration in the valence band.

(17) I. Kern, F. Dörr, and G. Scheibe, *Z. Elektrochem.*, **66**, 462 (1962).

(18) A. C. Albrecht and G. E. Johnson, paper presented at the International Conference on Photosensitization in Solids, Chicago, Ill., June 1964.

(19) V. Mylnikov and A. Terenin, *Dokl. Akad. Nauk SSSR*, **155**, 1167 (1964); *Mol. Phys.*, in press.

Experimental Methods

Section 1. Thallous iodide layers 5–8 μ thick were obtained by sublimation *in vacuo* onto quartz plates with sputtered platinum electrodes in the form of a gap (3×10 mm.), or a "comb" pattern (with a gap 0.1 mm. wide and 80 mm. long). The adsorption of the sensitizers on these layers was carried out from alcohol solutions (10^{-4} M) with subsequent elution of the dye excess.

The layer was kept at definite temperatures (in the range -170 to 20°) in a cell of the dewar type. The photoconductivity was measured under either constant or intermittent (600 c.p.s.) illumination by a mercury lamp through monochromatic filters, the light flux being of the order of 10^{15} photons cm.^{-2} sec.^{-1} . The following facts have been ascertained.

(1) In the plots of $\log \sigma$ vs. $1/T$ (cf. Figure 1) two linear parts are observed, the transition point being at -50° for the dark conductivity, and at -80 to -100° for the photoconductivity.

(2) The activation energy E_d , in the dark, deduced from the relationship $\sigma_T = \sigma_0 \exp(-E_d/2kT)$, is equal to 0.15–0.25 e.v. below -50° and 1.0–1.2 e.v. above -50° .

(3) The activation energy E_{ph} of the photoconductivity in the proper range at 436 $m\mu$, deduced from the expression $\sigma_{ph} = \sigma_{ph}^0 \exp(-E_{ph}/kT)$, is equal to 0.02–0.03 e.v. below -80° and to 0.12–0.14 e.v. above -80° .

Section 2. The modulated (600 c.p.s.) continuous spectrum of a xenon high pressure lamp is scanned at the exit slit of the monochromator, a synchronized shutter being opened for 0.5 sec. to allow a single exposure only of the photoconductor sample to wave lengths from 1000 to 350 $m\mu$. The total incident light flux during this exposure was very small (10^{-6} w. cm.^{-2}) and the absorbed energy was surely less by one or two orders of magnitude. By repeating the exposure several times a family of curves was recorded showing the gradual changes in a photoconductor, which is photochemically unstable.

Section 3. In the Hall effect setup, the semiconductor layer was illuminated through a quartz monochromator by modulated (600 c.p.s.) light of a xenon lamp. A constant potential of 100 v. was applied to the electrodes generating the current. The magnetic field was 12,000 oersteds in a 25-mm. gap. The alternating Hall (600 c.p.s.) photopotential was measured by a tuned amplifier with a sensitivity of 1 $\mu\text{v.}$, the effective input resistance being 10^9 ohms. As one amplifier, we used a cathode follower of the cascade type,²⁰ the output signal being rectified by a photoelectric synchronous phase-sensitive detector. This

setup has permitted measurement of the Hall photoeffect in AgBr monocrystalline layers with an internal resistance of 10^{10} ohms. This sensitivity was insufficient for the measurements on sublimed or powdered samples which are used in sensitization experiments.

For ZnO, the photo-e.m.f. was invariably of the same sign in the entire spectral ranges (proper and sensitized), indicating a diffusion current due to electrons. In some samples of the thallium and silver halides, the photo-e.m.f. measured as a function of spectral distribution revealed at the long wave length onset of the semiconductor absorption an additional low maximum with charge carriers of opposite sign to those of the main absorption^{1–8,21,22} (Figure 7).

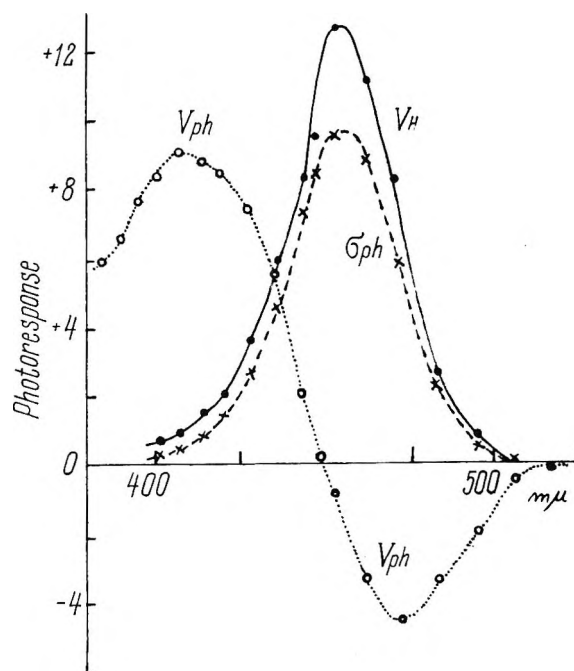


Figure 7. Spectra of the photoconductivity, σ_{ph} , the condenser photo-e.m.f., V_{ph} , and the Hall photoeffect, V_H , for an AgBr layer.

It was noticed that the spectrum of the photoconductivity did not reveal a similar splitting into two bands, and moreover its maximum was situated just between them. The anomalous behavior of the photo-e.m.f. could be explained either by a hole photocurrent at the onset of the absorption band^{3,8,21,22} or by the formation of an antiblocking curvature of the semiconductor bands at the illuminated surface.^{3,23} These alterna-

(20) J. R. McDonald, *Rev. Sci. Instr.*, **25**, 144 (1954).

(21) E. Putzeiko, *Dokl. Akad. Nauk SSSR*, **78**, 453 (1951).

(22) P. Meyklar and E. Putzeiko, *ibid.*, **73**, 63 (1950).

(23) A. M. Goodman and G. Warfield, *Phys. Rev.*, **120**, 1142 (1960).

tives have been experimentally resolved in favor of the second explanation by measurement of the Hall photoeffect.

In Figure 7, spectra of the condenser photo-e.m.f. (V_{ph}), the photoconductivity (σ_{ph}), and the Hall photoeffect (V_H) are plotted for the same monocrystalline AgBr layer, subjected to a preliminary illumination. This exposure produced an additional maximum at 450–490 $m\mu$ in the spectrum of only the photo-e.m.f. This leads to the important conclusion that this additional maximum is due not to a positive diffusion current from the illuminated surface inward, but to the presence of an antiblocking transition layer on it. In the spectral range of feeble absorption (450–490 $m\mu$), the photogenerated electrons are nearly uniformly distributed through the layer. In the antiblocking surface field, the electrons are drifting toward the illuminated surface simulating an inward hole current. In the strongly absorbed spectral range a large concentration gradient of the photocarriers does appear and the inward diffusion will dominate over the trend toward the surface. The sign of the photocarriers obtained in the Hall set was negative over the entire spectral range, the spectral curve coinciding with that of the photoconductivity as shown in Figure 7.²⁴

During modulated photo-e.m.f. measurements by the condenser method for sublimed or powdered TII layers, it has been previously observed that under an additional constant illumination in the proper spectral range of the semiconductor or in a constant electric field, a new narrow spectral maximum appeared at the threshold of the proper sensitivity, its maximum being reduced.²¹ For dyed TII the additional constant illumination in the proper range increased the sensitivity in the sensitized spectral range.²⁵ On the contrary, an additional constant illumination in this latter case sharply decreased the sensitization effect. These peculiar results recently have been revised and explained by the interplay of the diffusion current and the photocarrier drift in the antiblocking field.²⁶

Section 4. The photoresistivity cell consisted of ZnO as a dried paste covering a gap (3 mm. wide) between two platinum sputtered electrodes on the silica plate. The cell was mounted in a side arm of a vacuum vessel; the other side arm contained an ethanolic solution of hematoporphyrin ($10^{-3} M$) with 10 vol. % of pyridine and $10^{-2} M$ of ascorbic acid as the reductant. After degassing, the solution in the side arm was illuminated by a 100-w. incandescent lamp for 3–5 min. until the photoreduction was complete, as judged from the color change.⁹ By tilting the evacuated vessel, the solution was brought into contact with the

ZnO photoresistivity cell for 3–5 min. and then poured back.

Only a fully reduced form of the dye was obtained, not the negatively charged semiquinone which must possess a still higher electron donating power. Experiments along this line, which are more difficult, are in progress.

Section 5. When dye cations are additionally protonized by HCl, the sensitization of ZnO disappears, but that of TII remains with a changed spectrum. Ammonia gas has no influence on the photosensitization of ZnO by the safranin cation, but practically eliminates that of TII.

A similar opposite action of NH_3 and HCl on the sensitization of TII also has been observed for erythrosin (anionic), methylene blue, and malachite green (cationic). The adsorption of HCl enhanced both the proper and the sensitized photo-e.m.f. On the contrary, NH_3 adsorption lowered the proper photosensitivity and strongly depressed the sensitized one.

Appendix

Nature of the E.p.r. Signal in Sensitized AgBr.

An e.p.r. narrow signal has been observed when samples of AgBr powder, dyed with quino- and thiacyanines have been illuminated in the spectral range of the dyes.²⁷ This signal could be assigned to a dye radical, formed by an electron loss either to AgBr in the photosensitization process, or to bromine released from the crystal during a photolytic reaction (*cf.* section 2). As this signal does not disappear immediately when the illumination ceases, it cannot be regarded as evidence for the first alternative. Moreover, the signal rises monotonously with concentration increase of the dye, which is at variance with the known concentration optimum for sensitization. Holmogorov and Akimov²⁸ have extended the experiments cited and have given confirmation of the second alternative. The arguments were (a) a similar singlet e.p.r. line ($g = 2.005$, $\Delta H = 12$ oersteds) appears when the dyed AgBr powder is illuminated in the proper absorption spectral range, instead of the sensitized one; (b) in the dark the same signal appears when the dyed AgBr has been

(24) On the basis of the results thus obtained, it has been found (in accordance with the previous results) that in TII the dominant photocarriers are positive in the whole spectral range (proper and sensitized), whereas in AgBr (at variance with the former conclusion^{1b}) the dominant carriers are electrons.

(25) E. Putzeiko and A. Terenin, *Dokl. Akad. Nauk SSSR*, **70**, 401 (1950).

(26) I. Akimov and A. Mesakov, *ibid.*, in press.

(27) W. C. Needler, K. L. Griffith, and W. West, *Nature*, **191**, 902 (1961).

(28) V. Holmogorov and I. Akimov, *Dokl. Akad. Nauk SSSR*, **144**, 402 (1962).

brought in contact with bromine vapor; (c) a similar e.p.r. signal appears in dye solutions on bromine admixture; (d) no e.p.r. signal is observed for dyed TII which is more stable photochemically.

Comments. For the case of solid pinacyanole films on CdS, Nelson²⁹ arrives at the conclusion that the best ones for sensitization are those with a greater mobility of charge carriers. However, the sensitization efficiency of dyes in the solid state is generally low, whereas the optimum sensitization is observed at about 30% of monomolecular coverage; *i.e.*, the single dye molecules are the most active. This is confirmed by the concentration dependence of the effect.²⁹

The same argument concerns Meier,³⁰ who restricts his presentation to solid dye sensitizers, stressing their n-, or p-type. For single sensitizing dye molecules such assignment loses its significance. Moreover, as was shown in our recent paper,³¹ the conductivity type

changes abruptly when the same solid dye film experiences a modification in the state of aggregation (amorphous-crystalline).

We have to correct a misinterpretation of our viewpoint in the survey of the field by Bourdon.³² We have never proposed a two-quantum process in the photosensitization of semiconductors. We considered in the paper referred to the two alternatives: either an electron transition from the valence band to an acceptor level, or an electron transition from a trap to the conduction band. In the former case, a p-conduction, in the latter case an n-conduction should be produced.

(29) R. C. Nelson, *J. Opt. Soc. Am.*, **48**, 948 (1958).

(30) H. Meier, *J. Phys. Chem.*, **69**, 719 (1965).

(31) A. Terenin, E. Putzeiko, I. Akimov, and A. Meshkov, *Dokl. Akad. Nauk SSSR*, **155**, 900 (1954).

(32) J. Bourdon, *J. Phys. Chem.*, **69**, 705 (1965).

Photoluminescence of Adsorbed Dyes¹

by Edmond Lendvay

Research Institute for Technical Physics of the Hungarian Academy of Sciences, Budapest, Hungary
(Received November 27, 1964)

The character of the adsorbent strongly influences the photoluminescence of adsorbed dyes. Inorganic adsorbents form all known types of chemisorption bonds. Interesting interactions occur on the surface of semiconductors: *e.g.*, inorganic luminophors and solids containing hydroxyl groups. The adsorption of dyes on inorganic phosphors can result in the quenching of the fluorescence of the dye accompanied by a marked change in the intensity but no change in the spectra of the luminescence of the phosphor. Striking changes in the luminescence of dyes occur when they are hydrogen-bonded to the solid.

Introduction

The study of the luminescence of adsorbed dyes can give valuable information about the adsorption and the physical state of the molecules on the surface. However, few results of such studies have been published.

The majority of the dyes studied contain a large number of atoms and a conjugated bond system. The simple physical model of such a molecule is a system of

energy levels where different transitions are possible between the ground and excited states. As all of the experimental data show that radiative transitions never occur from the second or higher excited level of the dye molecule, it is sufficient physically to take into consideration the ground state and the first excited state

(1) Presented at the International Conference on Photosensitization in Solids, Chicago, Ill., June 22-24, 1964.

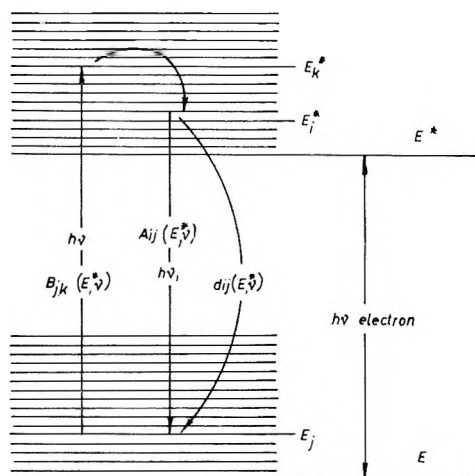


Figure 1. The simplified physical model of the luminescent dye molecule. E and E^* correspond, respectively, to the ground and excited states. $h\nu_{el}$ is the difference between the electron levels. $B_{jk}(E^*, \nu)$ and $A_{ij}(E_i^*, \nu)$ are the spontaneous transition probabilities for the absorption of $h\nu_1$ photon and for the radiation of $h\nu_1$ photon. $d_{ij}(E_i^*, \nu)$ is the probability of radiationless transitions. The curved arrow in the system E^* denotes the radiationless transitions before thermal equilibrium.

(see Figure 1). (As the metastable state of molecules of adsorbed dyes at room temperature has no decisive role, we can neglect the discussion of it.)

In the case of photoluminescence, transition of electrons into the excited state takes place with a spontaneous transition probability $B_{jk}(E^*, \nu)$. Since the time required to attain thermal equilibrium is much shorter than the mean lifetime of the excited state, the molecules in this state are chiefly in thermal equilibrium with their surroundings.

There are certain possibilities for the molecule to return to its ground state. First of all, radiationless transitions must be taken into consideration with a probability of $d_{ij}(E_i^*, \nu)$. If, according to the theory developed by Stepanov,² we denote the integrated value of the radiationless transitions with $d_i(E^*)$ and

$$d_i(E^*) \ll \int_0^{E^* + h\nu_i} d\nu \sum_j A_{ij}(E_i^* \nu) = A_i(E^*) \quad (1)$$

a visible fluorescence of the organic molecule is produced by irradiation of $h\nu$. Conversely, in the opposite case of (1) a total or partial quenching of the molecular luminescence can take place.

In case of adsorbed organic dyes both cases can occur with the same dye. The following sections of this paper will briefly describe both cases in systems where the optical properties of the inorganic adsorbents make possible the luminescence experiments.

Molecular Luminescence in the Adsorbed State

From the theory of molecular luminescence it follows that the physical state of the organic molecule strongly influences its optical qualities (absorption and luminescence spectra). The same molecule under different physical circumstances may emit different emission bands. If the inequality (1) in the original form is valid, the interaction between the adsorbed molecule and the adsorbent is localized. Although the position, intensity, etc. (generally the energy distribution) of the emission changes, the inequality (1) is still valid, and the radiation is emitted by the molecule itself. This is the consequence of the short-range interaction of the excited molecule with the inorganic adsorbent. In solutions and in some cases of adsorbed dyes this type of interaction is realized. Frequently, this type of the interaction is a resonance process or the formation or decomposition of H bonds. As the adsorbed dye molecule is joined to the surface through H bonds, we will discuss this type of interaction in detail.

The shape and position of the emission band are determined by the energy difference between the electron levels, the structure of the vibration system of the first excited state and the distribution function in it, and the transition probabilities. All of these parameters change during the formation of H bridges. These al-

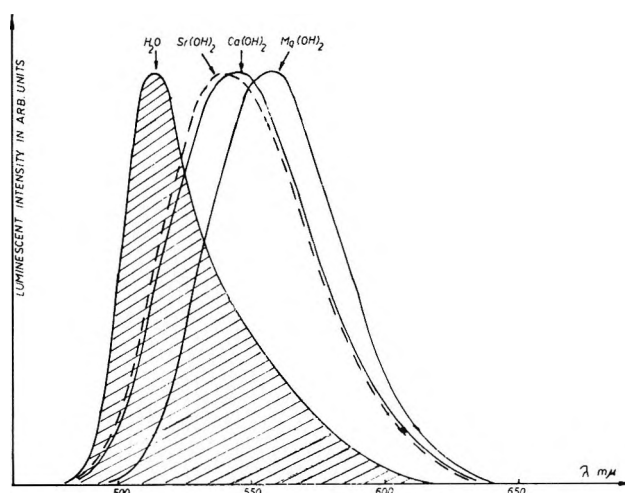


Figure 2. The luminescence spectra of fluorescein adsorbed on hydroxides of metals belonging to the second main group of the periodic system. The shaded band represents the emission of fluorescein in water at a concentration of 5×10^{-6} mole/l. The intensity maxima of the individual bands are normalized to the same value. The concentration of dye on the adsorbent is 5×10^{-6} mole/g. of adsorbent.

(2) (a) B. I. Stepanov, *Izv. Akad. Nauk SSSR*, 22, 1367 (1958);
(b) B. I. Stepanov, *Dokl. Akad. Nauk SSSR*, 112, 839 (1957).

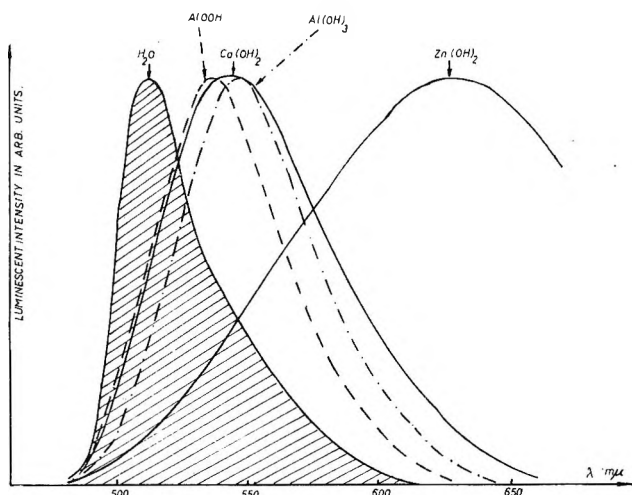


Figure 3. The luminescence of fluorescein adsorbed on AlOOH , $\text{Al}(\text{OH})_3$, and the hydroxides of metals of the second sub-group. The shaded band is the luminescent band of the fluorescein in water at a concentration of 5×10^{-6} mole/l. All bands are normalized to the same intensity maximum. The concentration of the dye on the adsorbent is 5×10^{-6} mole/g. of adsorbent.

terations depend on the donor-acceptor character of the surface and the dye (symmetrical or asymmetrical character of the H bond) and the energy of this bond. In Figures 2 and 3 the fluorescent spectra are shown for fluorescein adsorbed on hydroxides of the metals of the second group of the periodic system, as well as on the AlOOH and $\text{Al}(\text{OH})_3$. For comparison, the luminescent band of the fluorescein in water is also shown. The emission in the adsorbed state shows a strong red shift and the half-widths of the bands are also changed. The luminescence of the dye changes very sensitively with the quality of the hydroxides. This can be explained by the assumption that the electron distribution in the OH groups of the several hydroxides is different. If the characteristic luminescence of the adsorbed molecules is due to H bonds with certain electron distributions, the observed shift and broadening must, of course, depend on the polarizability and electronegativity of metal ions. Some characteristic examples can be seen in Figure 2 where the emission of the metals belonging to the second main group of the periodic system (Mg, Ca, Sr) are shown. From the comparison of the spectra it is clear that the emission of fluorescein adsorbed on $\text{Ca}(\text{OH})_2$ or $\text{Sr}(\text{OH})_2$ are nearly the same. The emission on $\text{Mg}(\text{OH})_2$ differs from the previous two. It is well known that in their compounds the Ca and Sr are very similar to each other although the Mg differs from them. The ionic character of the Me-OH bond (corresponding to the electronegativities) of $\text{Ca}(\text{OH})_2$ and $\text{Sr}(\text{OH})_2$ is nearly the same,

but is different in the case of $\text{Mg}(\text{OH})_2$. This change of charge distribution causes a difference in the energy and symmetry of the H bonds and as a result a marked change in the luminescence spectra.

The charge distribution of the -OH group in Al compounds has the same importance. The -OH group is more acidic in AlOOH than in $\text{Al}(\text{OH})_3$. The difference can easily be seen in the luminescence of the adsorbed dye (see Figure 3). The luminescence spectrum is very markedly influenced by the chemical and physical properties of the adsorbent; therefore, it is easy to investigate composite surfaces and the processes on these surfaces by studying luminescence.

$\text{Al}_2\text{O}_3 \cdot x\text{H}_2\text{O}$ is a composite system where on the surface there are OH groups with boehmite and gibbsite character. The emission belonging to a certain adsorption bond can be represented as a function of the type

$$W^L(\nu) = n^* h \nu \int \rho^*(E^*) A_{ij}(E^*, \nu) dE^* \quad (2)$$

The n^* in eq. 2 is the number of the excited molecules and $\rho^*(E^*)$ is the distribution function in the vibrational level system of the excited state. Since the $\rho^*(E^*)$ and $A_{ij}(E^*, \nu)$ are the same for molecules in similar states, $W^L(\nu)$ is proportional with n^* . It follows that from the change of the luminescence spectra with time, some kinetic data of adsorption can be determined. For a given type of excitation, the change of n^* is a linear function of the change of N , the number of surface groups which react with the dye molecules. As the rates of the adsorption on the different kinds of surface groups are different, the luminescence of dye adsorbed on a heterogeneous surface changes as a function of the adsorption time. (Naturally, this is valid only in cases when the dye reacts with all types of surface groups or with the majority of them.) As

$$\frac{W^L_{t_1}(\nu)}{W^L_{t_2}(\nu)} = \frac{n^*_{t_1}}{n^*_{t_2}} \approx \frac{N_{t_1}}{N_{t_2}} \quad (3)$$

where t_1 and t_2 are two different adsorption times and N_{t_1} and N_{t_2} the number of groups of the same band which have reacted with the dye.

$$\left(\frac{\partial N^A}{\partial t} \right) \neq \left(\frac{\partial N^B}{\partial t} \right) \quad (4)$$

where N^A and N^B are the number of groups A and B_1 reacted with the dye.³⁻⁵ Information concerning the adsorption kinetics can be gained from luminescence experiments.

(3) E. Lendvay, *Acta Phys. Acad. Sci. Hung.*, **13**, 289 (1961).

(4) E. Lendvay, *ibid.*, **13**, 249 (1961).

(5) E. Lendvay, *ibid.*, **13**, 333 (1961).

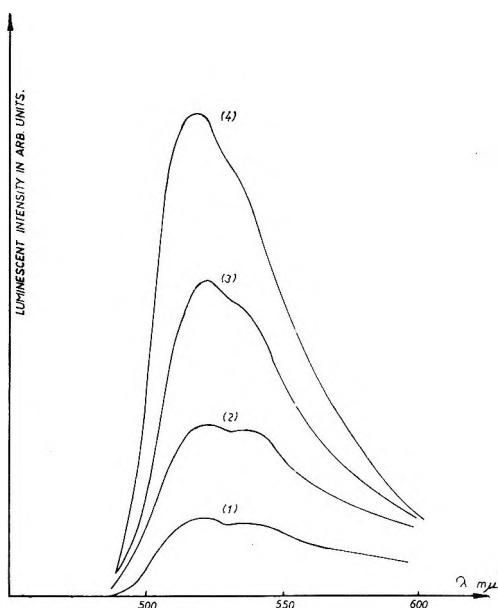


Figure 4. The change of the spectrum of fluorescein adsorbed on $\text{Al}_2\text{O}_3 \cdot x\text{H}_2\text{O}$ as a function of the adsorption time. Curve 1, 2 hr.; curve 2, 3 hr.; curve 3, 6 hr.; and curve 4, 24 hr. The starting concentration of dye solution was 5×10^{-5} mole/l.

In Figure 4, the change of the luminescence of adsorbed fluorescein on $\text{Al}_2\text{O}_3 \cdot x\text{H}_2\text{O}$ is shown as a function of adsorption time. It has been suggested that the whole emission band in each phase of the adsorption can be represented by the superposition of the elementary emission bands belonging to the different groups. The complexity of spectra is caused by the heterogeneity of the surface. The shape of the spectrum in every stage of adsorption can be approximated by theoretical calculations if we know the elementary bands.⁶⁻¹⁰

Until now we have investigated only the shift of the emission bands. The broadening of the emission band differs on the different hydroxides. On $\text{Ca}(\text{OH})_2$, $\text{Sr}(\text{OH})_2$, $\text{Mg}(\text{OH})_2$, and $\text{Al}(\text{OH})_3$ and on AlOOH , the emission band of the adsorbed fluorescein has nearly the same half-width. For other types of hydroxides (second sub group of the periodic system) particularly on $\text{Cd}(\text{OH})_2$ and $\text{Zn}(\text{OH})_2$, the broadening of the bands can be much larger. In case of $\text{Zn}(\text{OH})_2$ this broadening results in a band of which the half-width exceeds the normal half-width of the classical crystal phosphors. The intensity distribution within the luminescent band is simple; therefore, it is probable that it consists of a simple band. Such a behavior can be explained by the assumption that the polarizability of Zn and Cd ions has a very important role in the phenomena. It is well known that the polarizability of the ions of the second sub-group is much higher than that of ions in

the second main group of the periodic system. It is probable that the strong broadening of the luminescent bands and the red shift is caused by dipole effects in the excited state. This is supported by the fact that in halogenated fluorescein derivatives the half-width of the emission band increases with the number of the halogen atoms. For an exact investigation, the change of the half-width of $\rho^*(E^*)$, the distribution function must be taken into account. The halogen substitution within the molecule strongly influences the vibrational systems; therefore the effects are complex. In Figure 5 the luminescent spectra of four halogenated fluorescein derivatives on $\text{Zn}(\text{OH})_2$ can be seen. For comparison, the luminescence of these dyes in water is shown. It appears from this figure as from Figure 3 that the luminescence of the adsorbed dyes shows a remarkable red shift and the broadening of the bands increases with the halogen content.

Dyes Adsorbed on Inorganic Luminescent Materials

In addition to localized interactions, very interesting phenomena can be observed in the case of dyes adsorbed on semiconductors. The photoconductivity of such systems has been investigated by several authors.⁸⁻¹²

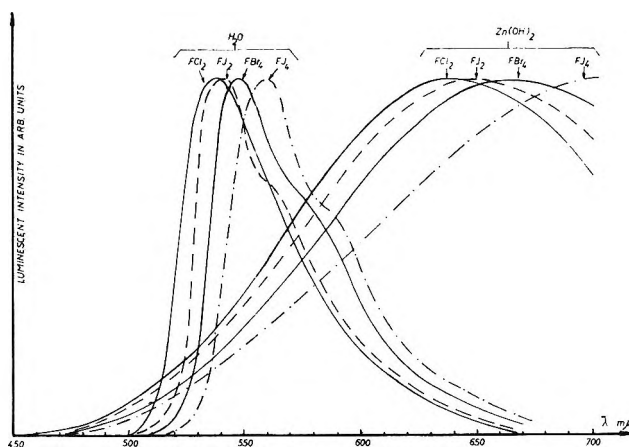


Figure 5. Luminescence spectra of the fluorescein derivatives in water and on the surface of $\text{Zn}(\text{OH})_2$. The bands are normalized to the same maximum. The concentrations of the solutions are 1.0×10^{-5} mole/l. on $\text{Zn}(\text{OH})_2$, 5.0×10^{-6} mole/g. of adsorbent. F, fluorescein; FCl_2 , dichlorofluorescein; FJ_2 , diiodofluorescein; FBr_4 , tetrabromofluorescein; and FJ_4 , tetraiodofluorescein.

- (6) E. Lendvay, *Acta. Phys. Acad. Sci. Hung.*, **14**, 187 (1962).
- (7) E. Lendvay, Materials of the Conference of Hungarian Chemists, Veszprem, 1962.
- (8) W. West and B. H. Carroll, *J. Chem. Phys.*, **19**, 417 (1951).
- (9) E. K. Putseiko and A. N. Terenin, *Russ. J. Phys. Chem.*, **30**, 1019 (1956).
- (10) I. A. Akimov, *ibid.*, **30**, 1007 (1956).

A rather limited amount of work has been done on the sensitization of the photoluminescence by certain dyes.¹³ No work has been published dealing with an exact investigation of the photoluminescence of phosphor-dye systems excited by ultraviolet radiation.

It is characteristic for adsorbed dyes on inorganic luminophors that inequality (1) turns. At such concentrations where the adsorbed dyes in the case of localized interactions show intense luminescence, they are generally not luminescent when adsorbed on semiconductors. The probability of the radiationless transitions exceeds that of the radiative transitions. In the adsorbed state, the strong absorption of dye molecules remains in the visible part of spectrum. Energy migration from the excited molecule to the solid phase is highly probable.

The absorption of the adsorbed dye can easily be observed even at low concentrations. In Figure 6 some characteristic reflection curves of adsorbed fluorescein and its halogenated derivatives are shown on self-activated ZnS. The measurements were relative to the reflectivity of the adsorbent without dye, which was taken as 100% for all wave lengths. The curves in

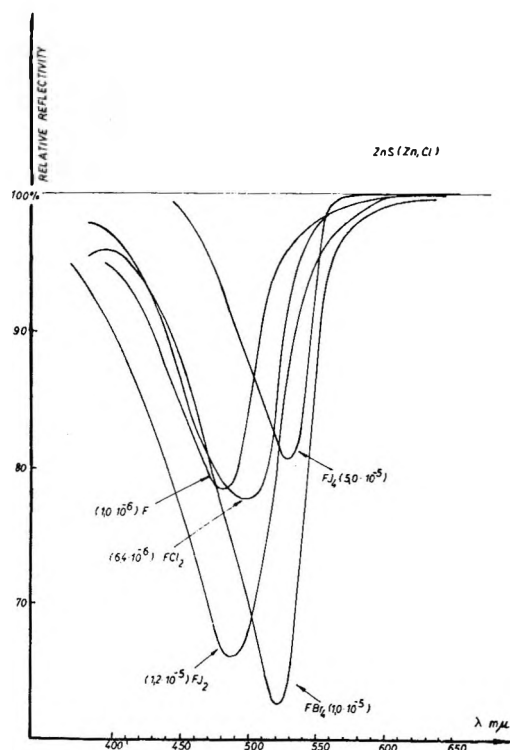


Figure 6. Relative reflection spectra of fluorescein derivatives adsorbed on ZnS(Zn, Cl). The numbers at the bands are the concentrations of the dye on the surface in moles/g. The symbols in this figure are the same as in Figure 5.

the figure represent the difference between the reflectivity of the dyed and original adsorbent. The absorption bands of the adsorbed dyes (see Figure 6) are similar to the absorption bands in solution. Since the relatively narrow absorption bands are characteristic of the corresponding electronic transitions, one can say that in the ground state the physical state of adsorbed and dissolved molecules are similar. The absorption bands on other materials (*e.g.*, on ZnO(Zn)) have nearly the same shape and position.

If such a system is excited with ultraviolet light (*e.g.*, with the 365-m μ line of mercury (Mc.)) generally only the luminescent emission of the crystal phosphor appears. Only at very high concentrations of the adsorbed dye is a trace of the molecular luminescence observed. In Figure 7 are shown the luminescence spectra of three inorganic luminophors: self-activated ZnS, activated ZnO, and ZnO produced from Zn(OH)₂ at low temperature (800°). If these materials adsorb fluorescein or its derivatives, only at concentrations higher than 10⁻⁵ mole of dye/g. of adsorbent can a deformation, at the long wave length tail, of the lumines-

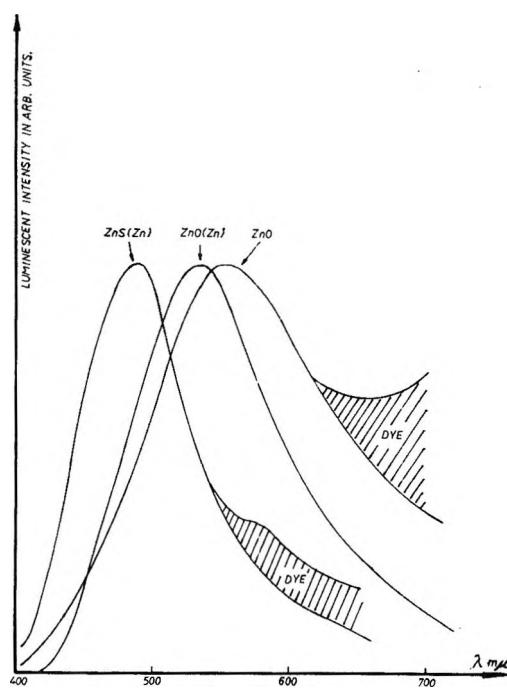


Figure 7. Emission spectra of the different crystal phosphors with and without dye. The bands are normalized. The shaded parts in the figure correspond to the deformation in the spectral shape at high concentration of dyes.

- (11) G. O. Schenck, *Naturwiss.*, **35**, 28 (1948).
- (12) G. Oster and A. H. Adelman, *J. Am. Chem. Soc.*, **78**, 913 (1956).
- (13) I. A. Akimov, *Zh. Nauchn. i Prikl. Fotogr. i Kinematogr.*, **4**, 64 (1959).

cence spectra be observed. (In the following, we will use this type of concentration unit. The mole/g. concentration is approximate only for the same adsorbent with similar specific surface. The exact comparison of the experiments needs specific surface measurements for the determination of mole/surface concentrations.) The shape of the original emission of the crystal phosphor remains unchanged. This concentration limit depends on the nature of the adsorbent and luminescent dye. The strongest deformation appears in case of ZnO prepared at 800° (see Figure 7), but generally this does not disturb the luminescent energy distribution of the crystal phosphors.

In practice this effect does not have a decisive role because, generally, at equilibrium the surface concentration of the dye is lower than the mentioned limit. The phenomenon seems much more important in controlling the intensity of the emission belonging to the inorganic adsorbent. This change in intensity occurs below the mentioned concentration limit. The experiments show that certain organic dyes (*e.g.*, the fluorescein derivatives) at very low concentrations (10^{-7} mole of dye/g. of adsorbent) can increase or decrease the intensity of the emission without changing the shape of the original luminescent band. In Figure 8 the luminescent emission of ZnO(Zn) crystal phosphor can be seen at different surface concentrations of diiodofluorescein. The system was excited by an HP mercury lamp with Zeiss UG 11 and BG 12 filters. The intensity of the emission band strongly depends on the surface concentration of dye, and at the lowest concentration the emission intensity exceeds the original by 55%. In the case of self-activated ZnS, under the same experimental circumstances, intensity growth and quenching appear, depending on the dye concentration. (The concentration values in the figures correspond in both cases to the equilibrium concentrations. As under the same experimental conditions the adsorption capacity of our ZnS(Zn, Cl) was higher than the ZnO(Zn), the concentrations in the figures are slightly different.) For the type of excitation used, the intensity change does not reach the value measured for the ZnO(Zn)-diiodofluorescein system. In this case there also appears a $\pm 15\%$ change of the original intensity. Similar effects are caused by the dyes mentioned in the foregoing part of the paper. Using these dyes, quenching and intensity growth, depending on the nature and quantity of the dye, can be observed. It is interesting that the influence of the halogenated compounds is stronger than that of the others. This is valid for the ZnO(Zn) phosphors, too. It must be remarked that in addition to the intensity growth (Figure 8) in the case of ZnO(Zn), the quenching effect of certain dyes and at

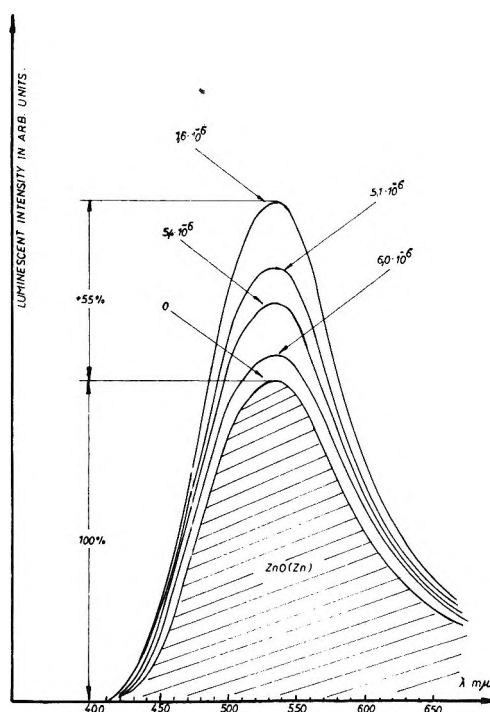


Figure 8. The influence of diiodofluorescein on intensity of luminescence of the ZnO(Zn) phosphor. The shaded band is the original emission curve, without dye. The numbers on curves represent the dye concentrations on ZnO(Zn) in moles/g. of adsorbent.

certain concentrations is also observable. (See Figure 9.)

Similar effects can be observed on ZnO prepared from $\text{Zn}(\text{OH})_2$ at 800° . In this case the strong influence of the adsorbed dye is also observable on the weak emission of the ZnO. It is remarkable that on this type of adsorbent, beside the original yellowish green emission, a strong red radiation appears. Both emissions are influenced by the dye concentration. This band distortion appears at low concentrations, unlike the aforementioned crystal phosphors (see Figure 7).

The problem is complicated by the uncertainty of the surface concentrations mentioned earlier. During the preparation of crystal phosphors by firing at high temperatures, the average size of the crystallites reaches $10\text{--}50 \mu$. With a diminution of the specific surface, the inorganic materials adsorb less and less of the dye. Powders prepared at relatively low temperatures have higher specific surfaces; therefore, the equilibrium concentration of the adsorbed dye is higher. In the case of unfired ZnS, for instance, the equilibrium concentration is generally one order of magnitude higher than in the previous case. The dye on the surface emits its own band. This emission can be detected on

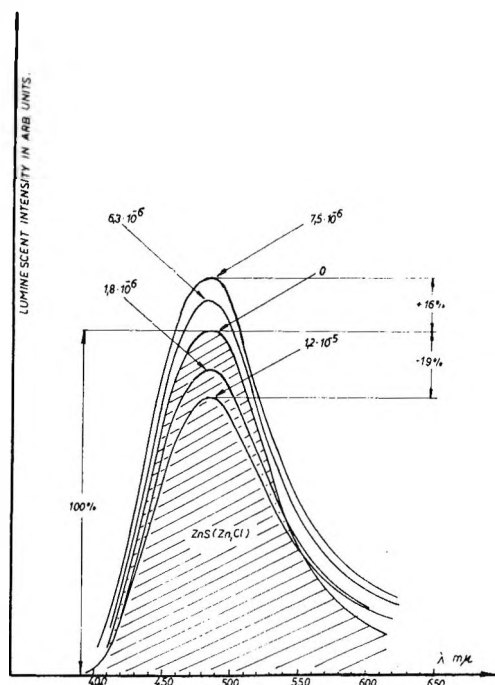


Figure 9. The influence of the adsorbed diiodofluorescein on intensity of luminescence of the self-activated ZnS. All of the symbols correspond to Figure 8.

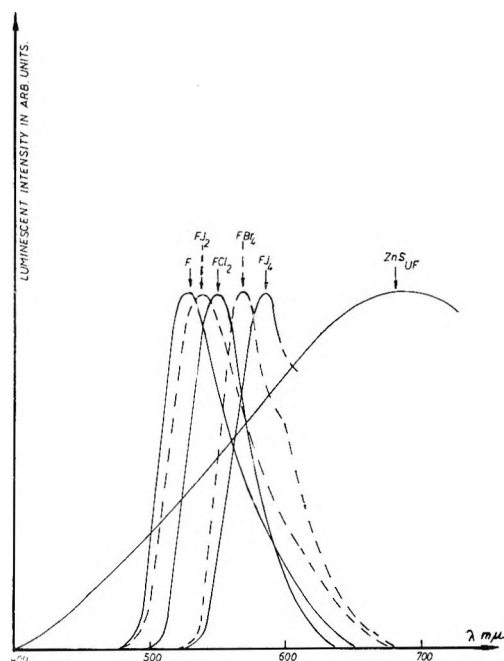


Figure 10. The emission spectra of fluorescein and its derivatives on unfired ZnS phosphor. The bands are normalized to the same intensity maximum. For comparison, the emission of unfired ZnS without dye is also shown.

fired ZnS(Zn, Cl) only at the highest concentrations. Since the unfired ZnS itself is luminescent,¹⁴ a composite spectrum is obtained containing the bands of the dye and the adsorbent. The two bands may be separated by graphical methods, subtracting the ZnS emission from the spectra normalized to the emission maximum of the unfired ZnS's spectrum. The luminescence of these dyes is presented in Figure 10. For the sake of comparison, the emission band of the unfired ZnS is also plotted in the figure. The measured spectra can be represented as the sum of the corresponding bands of dye and ground material. The emission bands in the figure are similar to emissions in solution, both in regard to their shape and half-width. The red shift is considerable only in case of tetraiodo and tetrabromo derivatives. These facts indicate that the molecule has in its excited state an interaction of a different type from the phosphors. For the molecular luminescence, contrary to the above, inequality (1) remains valid, but a strong quenching of the luminescence of the inorganic substrate can be observed. All of

these examples show that different interactions can exist for different luminescent adsorbents.

The effects on the classical phosphors, ZnO(Zn) and ZnS(Zn, Cl), seem the most interesting. The investigation of these types of effects is simpler, as the spectra at low concentration of dye contain only one band and only the intensity of the luminescence of the inorganic substrate is detectably changed. The strong alteration in intensity shows that the bulk properties of the crystal phosphors can be influenced by the state of the surface. Preliminary examinations show that in the case of ZnO(Zn) and ZnS(Zn, Cl), a sensitization may be caused by the change of the excitation spectra by the alteration in the recombination processes. Further experimental work dealing with the temperature dependence, the excitation spectra, and measurement of other parameters is necessary for an exact interpretation of the phenomena.

(14) E. Lendvay, *et al.*, *Czech. J. Phys.*, B13, 142 (1963).

The Relationship between Exciton Absorption and the Photoelectric Effect¹

by S. Nikitine, A. Coret, J. P. Zielinger, C. Jeanclaude,
C. Boehm, and M. Zouaghi

*Laboratoire de Spectroscopie et d'Optique de Corps Solide, Institut de Physique, Université de Strasbourg, France
(Received October 5, 1964)*

The photoconductivity spectra of HgI₂, PbI₂, GaSe, and Cu₂O crystals, at low temperatures, show an important edge which is shifted toward the longer wave lengths in comparison with the absorption edge and a number of maxima and minima which correspond with the absorption lines attributed to excitons. Different mechanisms can explain these phenomena, and for each crystal a model is proposed. The photoelectromagnetic effect is also studied for Cu₂O crystals.

Introduction

The absorption spectra of many semiconductors consist of a number of absorption lines on the low energy side of an edge of continuous absorption. The lines are interpreted as transitions to exciton states and the continuous absorption is interpreted as band-to-band transitions.² It is obvious that the latter type of transition corresponds to the formation of a free hole in the valence band and a free electron in the conduction band. Both can carry a current. Hence, the absorption of light in the continuum is expected to correspond to photoconductivity, *i.e.*, the internal photoelectric effect.

As will be seen later, it is not obvious whether a photoeffect is to be observed on irradiation of the photoconductor by light within the exciton lines. This relation between the exciton part of the absorption spectrum and the photoconductivity has been studied recently in different laboratories. Though the interpretation is still rather complicated, an attempt is made in this communication to summarize and discuss the results obtained by the Strasbourg group for some substances; crystals of HgI₂, PbI₂, GaSe, and Cu₂O have been studied in some detail.

Theoretical Background. Frenkel and Peierls have suggested that electrons and holes could be created in a bound state in which a rather small Coulomb interaction exists between them. This bound pair corresponds to an excited state of the crystal and is called an exciton. The excitons can diffuse through the crystal; however, no current is carried by excitons as they consist of a bound pair of charges of both signs.

In an exciton, the binding energy is quantized as

in a hydrogen atom, and therefore, a series of energy states of the exciton is possible. Transitions to these states correspond to a series of sharp absorption lines converging to a limit.

The theory of exciton spectra has been developed by Elliott,^{3a} Haken,^{3b} and Dresselhaus⁴ and is well known now; therefore, we intend to omit these developments here. A very simple model, however, shows that the interaction between the electron and the hole is an electrostatic Coulomb interaction in a dielectric medium of dielectric constant ϵ . The problem is then similar to a hydrogen-like atom, and the exciton states are quantized. The binding energy of the exciton is then given by

$$E_b = E - E_c = -\frac{e^4 \mu_c}{2\hbar^2 n^2 \epsilon^2}$$

E_b is the binding energy, E_c the energy of the lowest state of the conduction band, $\mu_c = m_h m_e / (m_h + m_e)$, e is the charge of the electron, \hbar is Planck's constant divided by 2π , and n is a quantum number.

It has to be emphasized that, in an exciton transition, the ground state is an unperturbed crystal, and the excited state consists of an exciton in an otherwise un-

(1) Presented to the International Conference on Photosensitization in Solids, Chicago, Ill., June 22-24, 1964.

(2) S. Nikitine, *Progr. Semicond.*, **6**, 235 (1962).

(3)(a) R. J. Elliott, *Phys. Rev.*, **108**, 1402 (1957); R. J. Elliott and R. Loudon, *J. Phys. Chem. Solids*, **8**, 382 (1959); (b) H. Haken, *Fortschr. Physik*, **38**, 271 (1958); "Halbleiterprobleme," Vol. II, W. Schottky, Ed., Vieweg, Berlin, 1955; *J. Phys. Chem. Solids*, **8**, 166 (1959); *Z. Physik*, **155**, 223 (1959).

(4) G. Dresselhaus, *J. Phys. Chem. Solids*, **1**, 14 (1955).

perturbed crystal. The oscillator strengths of exciton lines have been calculated by Haken,^{3b} Elliott,^{3a} and Dresselhaus.⁴ It can be shown that different exciton spectra can be observed. The transition matrix element can be expanded as a function of \vec{k} , the wave vector, the value of which has to be very close to zero ($\vec{k} \simeq 0$).

The First Class of Spectra. A spectrum of the first class corresponds to the case when the first term of the expansion differs from zero. It can be shown that, in this case, the second term is usually zero, and excitons in spectroscopic S states are formed. The intensity of the lines decreases as $1/n^3$, and in the visible region, the absorption coefficient is expected to be about 2 to $4 \times 10^5 \text{ cm.}^{-1}$.

Second Class of Transition. In some transitions the first term of the expansion of the matrix element for the transition moment may be zero. In this case, the second term of the expansion may differ from zero, and excitons in spectroscopic P states are formed. The oscillator strength can be written $f_a = [(n^2 - 1)/n^5 \epsilon^5] C_2$, where C_2 is a constant. The absorption in this kind of transitions is expected to be roughly 10^3 times weaker than that in transitions of the first class.

*Photoconductivity in the Exciton Lines.*⁵ The theory of photoconductivity in connection with excitons has not been worked out. It is clear that the excitation of an electron into the conduction band by absorption of a suitable photon $\hbar\omega > E_g$ should correspond to the creation of a free electron and a free hole, both of which can carry a current.

When excitons are created by optical absorption, an electron and a hole are created in a bound state, and excitons cannot carry a current. However, different cases have to be examined regarding the fate of the excitons. (a) Once created, the exciton can be annihilated by a radiation or a radiationless process, and therefore, no free carriers will be created. (b) The exciton can, however, dissociate on an impurity or defect, and the majority carrier can be trapped. The minority carrier is likely to recombine rapidly with a majority carrier. (c) The exciton may dissociate with the liberation of a majority and a minority carrier which do not recombine immediately. (d) The exciton may dissociate, and the minority carrier may be trapped.

In both cases a and b, no photoeffect is expected when light is absorbed in an exciton line. In case c and particularly in case d, a photocurrent is expected when the crystal is irradiated in the line.⁶

Usually the exciton lines are superposed on a background absorption, the origin of which is not clear but is certainly connected with defects, impurities, etc.,

though part of this absorption may also be due to a tail of the band-to-band transitions. The threshold frequency of this edge is usually not well defined, and the absorption ends gradually. This continuous background usually gives a contribution to the photocurrent. Furthermore, active impurities or defects can give a strong photocurrent even beyond the intrinsic absorption. These effects may be complicated, but usually, in cases a and b the exciton absorption line is observed as a minimum in the photoconduction response curve. In cases c and d, the exciton line is observed as a maximum on the photoconduction response curve. Some other complications in the interpretation of photoconduction curves will be discussed later.

It is interesting to note that Frenkel suggested the existence of excitons in order to explain an absorption which does not give use to photoconductivity. He had obviously in mind one of the cases a or b considered above. But in some cases (c and d), the exciton line corresponds to a maximum of the photocurrent, in contradiction with Frenkel's expectation.

Experimental Results

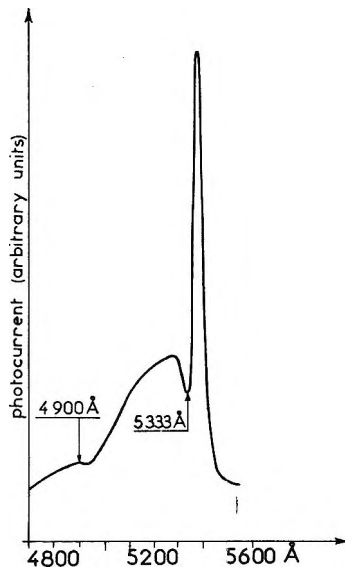
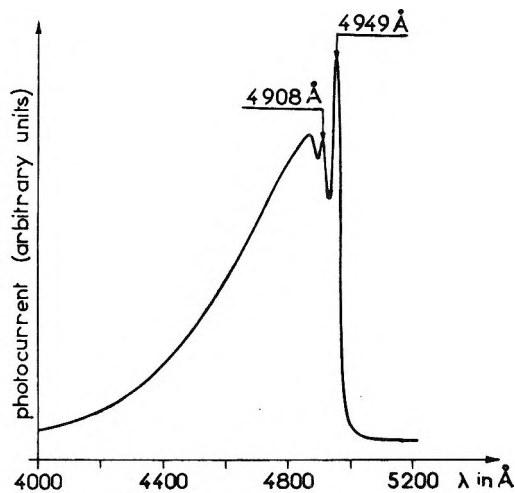
Mercuric Iodide Crystals (Red Variety). The crystals were prepared by Professor Sieskind in this laboratory by evaporation of a solution of HgI_2 in acetone. HgI_2 has a tetragonal structure and at 20 and 4°K. is dichroic. When the electric vector of the light vibrates parallel to the axis ($E \parallel c$) and when the vibration is perpendicular to the axis ($E \perp c$), the absorption spectrum is not the same. In the first case, the spectrum is called the extraordinary spectrum; in the second, the ordinary. So far, we have investigated the photoconductivity spectrum of the crystals at 77°K., and the "ordinary photoconductivity spectrum" is the same as the "extraordinary photoconductivity spectrum." Gross and Novikov⁷ have found, however, different photoconductivity spectra for the two orientations of E . In Figure 1, we have represented the photoconductivity spectrum. We observe, after the rise of the photoconductivity on the low energy side of the absorption edge, an important drop and two minima at $\lambda = 5330$ and 4900 \AA . The absorption spectrum shows two lines for these two wave lengths which are due to exciton transitions of the first class.

Furthermore, for crystals a few millimeters thick, a strong photoeffect is observed on the low energy side of

(5) A. Coret and S. Nikitine, *J. Phys. Radium*, **24**, 587 (1963).

(6) We are thankful to Professor Stöckmann of Karlsruhe for stimulating discussions on this subject.

(7) E. F. Gross and B. V. Novikov, *J. Phys. Chem. Solids*, **22**, 87 (1961).

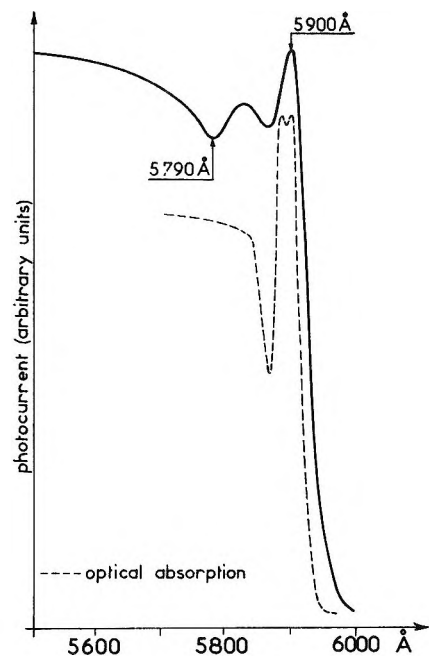
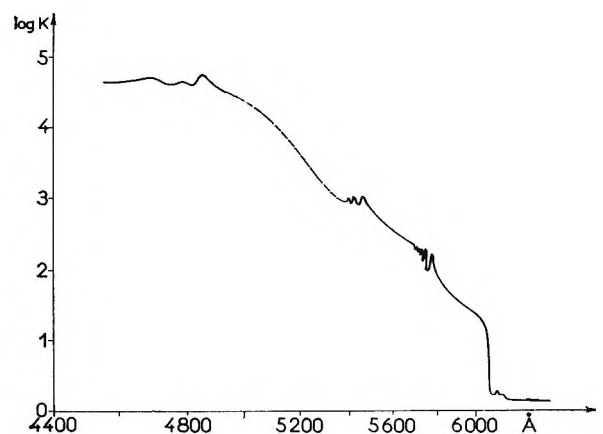
Figure 1. Photoconductivity spectrum of HgI_2 at 77°K .Figure 2. Photoconductivity spectrum of PbI_2 at 20°K .

the absorption lines. This effect, due probably to impurities, can cover the band-to-band transitions.

Lead Iodide Crystals. The crystals were prepared by Mrs. Schmitt-Burckel in this laboratory by evaporation of an aqueous solution of PbI_2 which crystallizes in the hexagonal structure. All of the crystals studied have been perpendicular to the axis. The photoconductivity spectrum at 20°K . shows a maximum at $\lambda = 4949 \text{ \AA}$. which corresponds to the first absorption line (Figure 2). However, the second maximum at $\lambda = 4908 \text{ \AA}$. does not correspond to the second exciton absorption line at 4898 \AA .

Gallium Selenide Crystals. The crystals were prepared at the RCA Laboratory of Zurich by Professor

Nitsche⁸ by a method of chemical transport. They are thin slices about 200μ thick; their illuminated surfaces are perpendicular to the optical axis. The photoconductivity spectrum at 77°K . (Figure 3) shows a maximum at $\lambda = 5900 \text{ \AA}$. which corresponds to the absorption doublet observed in this laboratory⁹ and a minimum at 5790 \AA . which corresponds to a weak band observed by Gross.¹⁰

Figure 3. Photoconductivity spectrum of GaSe at 77°K .Figure 4. Optical absorption spectrum of Cu_2O at 4.2°K .(8) R. Nitsche, *J. Phys. Chem. Solids*, **17**, 163 (1960).(9) S. Nikitine, R. Nitsche, M. Sieskind, and J. Vogt, *J. chim. phys.*, **60**, 667 (1963).(10) E. F. Gross, B. S. Razbirin, and G. Suslina, *Opt. i Spektroskopiya*, **6**, 569 (1959).

Cuprous Oxide. The photoconductivity of cuprous oxide samples has been studied more in detail than that of other crystals for several reasons. In the first place, the absorption spectrum shows many absorption edges and many exciton series (Figure 4) which are now well known.¹¹ (1) Two edges in the red correspond to indirect transitions to an exciton state with emission or absorption of a phonon. (2) There is a first series of lines in the yellow preceding an edge. Figure 5 shows the band scheme of Cu_2O given by Elliott¹²; there are two valence bands and two conduction bands (owing to the spin-orbit splitting). Transition 1 is the yellow edge. (3) A second series of lines and a second edge are in the green (transition 2). (4) There is a maximum of absorption at 4800 Å. (transition 3). (5) There is also a maximum of absorption at 4585 Å. (transition 4).

The calculated oscillator strength of the lines and the values of the absorption coefficient show that the yellow and the green series are due to the second class of exciton spectra. The two maxima in the blue are due to the first class of exciton spectra.

A second reason is that thick samples can be used. They are prepared in this laboratory by Dr. Grosmann from plates of copper which are oxidized at 1000° in oxygen at low pressure. Aquadag is applied to the two broad faces of the electrodes.

However, the study of the spectrum has shown that the photoconductivity properties of Cu_2O depend greatly on the state of the optical surface. Indeed, two kinds of spectra are observed, as we have already mentioned in a preceding paper.⁵

(a) For a natural surface or for a surface etched with dilute nitric acid, the response of the photoeffect is rapid and corresponds to an increase of the conductivity of the sample. The absorption lines appear either as maxima or as minima in the photoeffect. The relaxation time is $\tau < 10^{-4}$ sec.

(b) For a sample which has been left a few days in the open air the photoeffect is quite different. The response is much slower (about a few minutes), and in a limited domain of wave lengths ($6200 \text{ \AA} < \lambda < 5000 \text{ \AA}$), a negative photoeffect has been observed; that is to say, the conductivity decreases under illumination. This last effect depends also on the applied potential (the greater the potential, the greater the effect) and on the dimensions of the domains.

We shall study only the first case in detail. Figure 6 shows the photoconductivity spectrum of the Cu_2O sample at 4°K. We can compare it with the absorption spectrum at the same temperature (Figure 4). The dispersion of the monochromator used does not allow the observation of the lines of high quantum number. However, we can see the lines $n = 2$ of the

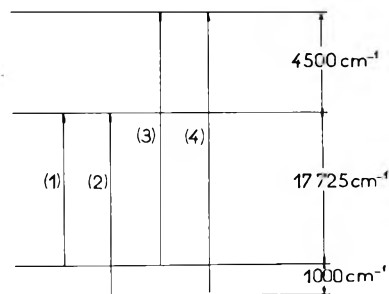


Figure 5. Band scheme of Cu_2O . Transitions (1) and (2), green and yellow series; transitions (3) and (4), blue and violet series.

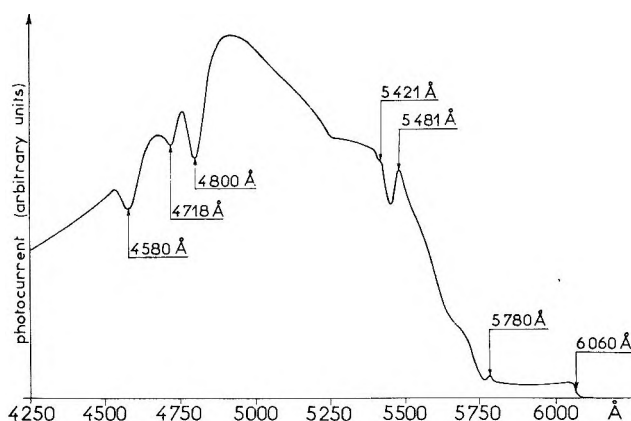


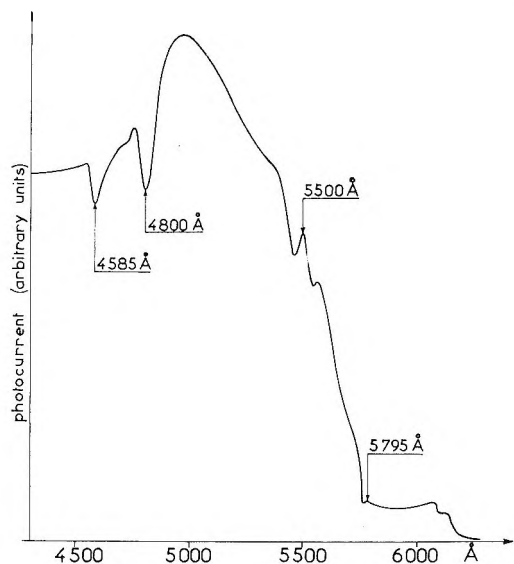
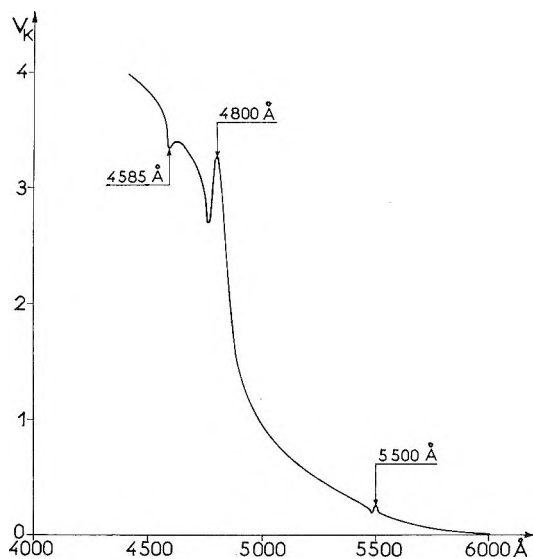
Figure 6. Photoconductivity spectrum of Cu_2O at 4.2°K.

yellow and green series as maxima in the photoeffect. On the contrary, the lines at 4800 and 4585 Å. appear as minima in the photoeffect. A third line appears at 4718 Å. and can be attributed to the line $n = 2$ of the series corresponding to transition 3 in Figure 5. The photoconductivity is greatest in the green and blue parts of this spectrum. The photoconductivity curve can be used to observe the absorption lines of a crystal without consideration of its thickness. On account of the high value of the absorption coefficient, thin samples have to be used for the measurement of the absorption coefficient, and it is not easy to obtain samples of a thickness of a fraction of a micron (we have seen that for the first class spectra, absorption coefficients of 10^5 to 10^6 are frequent). For the high energy part of the spectrum, the photoconductivity spectrum can give information of great importance on the absorption.

Recently, we have studied a different experimental method which allows us to investigate the absorption of a sample—the photoelectromagnetic effect (PEM

(11) J. B. Grun, *Rev. d'Optique* (Thèse), **41**, 439 (1962).

(12) J. B. Grun, M. Sieskind, and S. Nikitine, *J. Phys. Chem. Solids*, **21**, 119 (1961).

Figure 7a. Photoconductivity spectrum of Cu_2O at 77°K .Figure 7b. Spectrum of the PEM effect of Cu_2O (same sample as in Figure 7a) at 77°K .

effect). Here we detect the potential difference created by the deviation of the diffusion current of photocarriers by a magnetic field. This effect is proportional to the gradient of the concentration of photocarriers and, thus, directly related to the absorption coefficient. In Figure 7 we can compare the photoelectric effect and PEM effect, both at 77°K . The latter is very important in the blue where we can detect potentials of several volts. The $4800\text{-}\text{\AA}$. line appears as a maximum, and the $4585\text{-}\text{\AA}$. line, as a minimum.

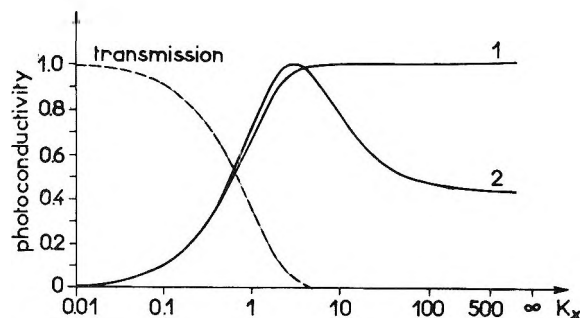


Figure 8. Photoconductivity (normalized to 1.0 at peak) absorption curve.

Discussion

The results described can be discussed, at least qualitatively, on the basis of the different cases of exciton annihilation or dissociation examined above. However some complications may prevent a unique interpretation.

The de Vore Effect. It has been shown¹³ that the photoconductivity can vary with the optical density of the sample in a rather complicated way.

If only one kind of recombination is considered, the photocurrent should increase with Kx (K , absorption coefficient; x , thickness of the sample) and reach a saturation for high values of Kx when all the light penetrating the sample is absorbed (curve 1, Figure 8). However, this is never the case, and it has been shown that the photocurrent passes through a maximum for a given value of Kx and then decreases asymptotically to a constant value (curve 2, Figure 8). This effect has been explained by de Vore in assuming that the recombination is not the same in the bulk and on the surface of the crystal. This assumption is quite plausible, and it can be foreseen that the recombination will probably be faster on the surface, on account of the numerous defects and adsorption layers. It can be shown that, for plausible values of the ratio ξ of surface to volume recombination, the photocurrent passes through a maximum but tends, for greater values of Kx , to an asymptotic value. From this value, by comparison with values calculated by de Vore, ξ can be determined. This theory considers the variation of the photoconductivity with Kx . Usually, however, the photoconductivity is studied as a function of the wave length. As the absorption varies also with the wave length, the theory can be applied, at least in a semiquantitative way, to the photoconduction response curves.

The Wing of the Absorption Edge. It has been mentioned that the exciton lines are usually observed on top

(13) H. B. de Vore, *Phys. Rev.*, **102**, 86 (1956).

of a background absorption. This absorption can be due to the edge absorption or to some absorption centers active regarding photoconductivity. Indirect transitions from the Brillouin zone center may also be possible. It appears that, in some cases, the photoconductivity in this part of the spectrum may be considerable. It has to be noted that this part of the spectrum is not well understood theoretically.

The results obtained will be discussed in the light of these considerations and of the mechanisms of exciton decay mentioned previously.

HgI₂ at 77°K. As seen from the curve in Figure 1, the photoconductivity of HgI₂ at 77°K. shows a strong maximum on the low energy side of the exciton line, and the exciton lines are observed as minima on the photoconductivity curve. As this substance is rather strongly luminescent, it is plausible to interpret the minima in the photoconductivity curve according the process discussed under (a). A confirmation of this interpretation is obtained from a study of an HgI₂ crystal submitted to a thermal treatment (a few hours at 100°). In this case the exciton line appears as a maximum on the photoconductivity curve. It seems plausible to assume that the treatment has produced defects on which the excitons can now decompose.

It is to be noted that, in these cases, the study of the photoconductivity shows a pronounced maximum on the low energy side of the exciton line which is an obvious indication in favor of strongly active centers. One is tempted to admit that these centers emit only carrier whereas the band-to-band transition produces carriers of both signs which recombine rapidly.

GaSe at 77°K. and PbI₂ at 20°K. The mechanism of this photoconductivity corresponds to case c or d. Hall photomeasurements which are now being carried out may decide between the two processes. It has to be mentioned that the de Vore effect explains the low value of the photoconductivity for the band-to-band transitions.

Cu₂O at 77 and 4.2°K. The photoeffect in crystals with only a "natural" or an etched surface will be discussed. A tentative interpretation only is suggested. The negative photoeffect of crystals with a surface modified by exposure to open air or after thermal treatment has been discussed in a previous paper.⁵ The photoconductivity spectrum shows a positive effect in the exciton lines of the yellow and green series, as well as in the indirect transition red continuum. This gives an indication in favor of the decomposition of excitons giving electrons and holes (the last are the majority carriers). The photoeffect passes through a maximum, as predicted by de Vore's theory, at about 4950 Å. However, with the samples used, the absorption of

light is total for the yellow part of the spectrum. Therefore, the maximum should be expected at much lower energies than observed. This may be explained by the suggestion that excitons partly dissociate on a defect and partly recombine through a radiationless process by emission of a great number of phonons. In the continuum the process may be similar; the electron and hole recombine rapidly, or one or both (the electron probably) are trapped by defects. This effect is likely to shift the maximum of the photoconductivity curve to higher energies as suggested by the experiment. The blue and violet lines are observed as minima, probably essentially on account of the de Vore effect. A different process is not quite excluded though it might be difficult to interpret on the basis of the energy level diagram of Elliott. From the values of the photoconductivity in the high energy part of the spectrum, it is possible to conclude that the ratio $\xi = 3$. This value must be considered, rather, as an order of magnitude. Unfortunately, only qualitative data are known regarding the lifetime of the photoconductivity. We have been able to show that $\tau < 10^{-4}$ sec. Further investigations are necessary.

Conclusions

The data obtained are still not sufficient to support a final interpretation of our photoconductivity measurements. However, some important, though provisional, conclusions can be attempted.

In HgI₂ the threshold energy of the photons in the photoconductivity curves is *lower* than that of the exciton lines. This suggests a strongly active wing of the absorption spectrum on the low energy side, possibly owing to defects. The excitons decay probably essentially by a radiative process which is observed in exciton luminescence. The de Vore effect is responsible for the small value of the photoconductivity in the high energy part of the spectrum.

In GaSe and PbI₂ the excitons formed can dissociate to give free carriers which make an important contribution to the photocurrent.

In Cu₂O two processes probably take place. (a) The excitons and carriers in the conduction and the valence bands recombine in a radiationless process; (b) excitons decay giving probably majority carriers (holes). The electrons may be captured, so the efficiency of the photoconductivity is diminished by (a).

The de Vore effect explains, at least partly, the behavior of the photoconductivity in the high energy part of the spectrum. Some parameters of the photoeffect have been roughly evaluated.

Further experiments are necessary, but it can be con-

cluded that the general lines of the photoconductivity and its relations with the decay of excitons are not far

from being understood. No experimental data are yet available for or against a diffusion of excitons.

Luminescence of Doped Aromatic Crystals¹

by A. Schmillen

Physikalisches Institut der Universität Giessen, Germany (Received October 5, 1964)

The transfer constant, a , for the radiationless transfer of excitation energy from a photo-excited host crystal to foreign molecules in the lattice with a lower excitation level is given by the equation $\tau_0/\tau(c) = 1 + ac$, where τ_0 and τ are the fluorescence decay times of the host without and with the impurity, and c is the concentration of the impurity, which has been determined for several systems. A phase fluorometer was used to determine decay times from the phase angles of the directly excited fluorescence of the host and of the impurity in the lattice and of the fluorescence of the impurity excited by transfer. For 2,3-dimethylnaphthalene as host and anthracene as solute, τ_0 is 69.7×10^{-9} sec. and a is 1.05×10^5 . This value of a is similar to the value 0.87×10^5 for 2,3-dimethylnaphthalene-perylene, although the lowest excitation levels of perylene are considerably below those of anthracene, suggesting perhaps that overlap of host emission with the foreign molecule absorption may not be a dominating factor in transfer. For fluorene-anthracene, τ_0 is 7.3×10^{-9} sec. and a is 8.5×10^3 , although these values may be subject to some systematic experimental error. In fluorene-pyrene, two anomalies prevent the determination of a . At low concentrations of pyrene, only the fluorescence of anthracene appeared, although the anthracene concentration was less than 10^{-6} . It is suggested that a pyrene-anthracene complex, with strong mutual coupling, would account for the observations. Also, at high concentrations of pyrene, the excited dimer or "excimer" fluorescence appeared.

One of the main problems on the luminescence of molecular crystals is the transfer of excitation energy from the host lattice to foreign molecules having a lower-lying excitation level. To the numerous experimental and theoretical investigations treating this problem, this paper adds a further modest contribution.

Without restriction to a defined energy transfer model, let us suppose that the radiationless transition of excitation energy from the host lattice to the foreign molecules is a process competing with the luminescence emission of the host material. Further, we may assume that the transfer probability is proportional to the concentration of foreign molecules.

Then the following relation should hold between the decay times τ and τ_0 of the host luminescence (with and without foreign molecules) and the concentration C of foreign molecules

$$\frac{\tau_0}{\tau(c)} = 1 + ac \quad (1)$$

where a is a characteristic constant of the transfer.

If we use for the decay time measurements a phase fluorometer with a periodically varying excitation intensity, the three measurable phase angles ϕ_k (the

(1) Presented to the International Conference on Photosensitization in Solids, Chicago, Ill., June 22-24, 1964.

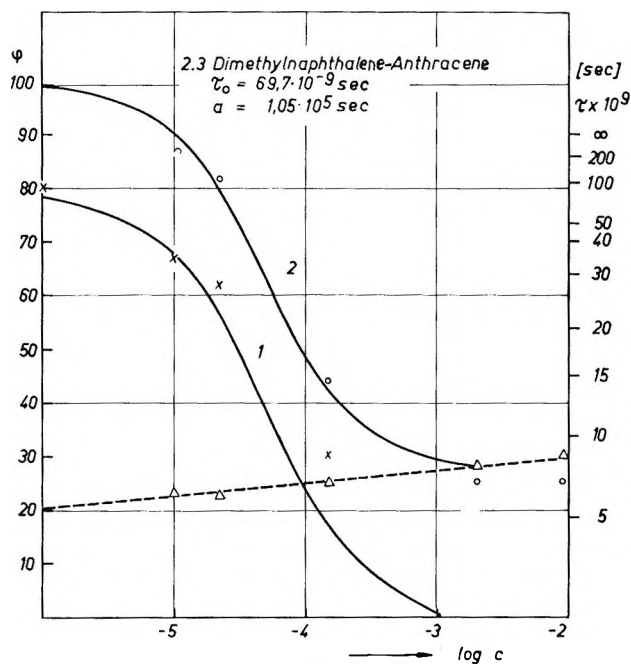


Figure 1. Phase angles of the system 2,3-dimethylnaphthalene-anthracene: curve 1, $\lambda_{\text{ex}} = 3130\text{-}\text{\AA}$, 2,3-dimethylnaphthalene fluorescence; curve 2, $\lambda_{\text{ex}} = 3130\text{-}\text{\AA}$, anthracene fluorescence; Δ , $\lambda_{\text{ex}} = 3660\text{-}\text{\AA}$, anthracene fluorescence.

phase angle of the host lattice fluorescence), ϕ_a (the phase angle of the foreign molecule fluorescence directly excited by longer wave length), and ϕ_a^* (the phase angle of the foreign molecule fluorescence excited by transfer from the host lattice) should be related by

$$\phi_a^* = \phi_g + \phi_a \quad (2)$$

Thus, if we measure the three phase angles, we are able to prove the validity of eq. 1 and to determine the transfer constant a .

Recently, we carried out such measurements on doped single crystals of aromatic hydrocarbons having well-defined concentrations of foreign molecules. In addition to the already published results on 2,3-dimethylnaphthalene-perylene and dibenzyl-tetracene, Figure 1 shows data for the system 2,3-dimethylnaphthalene-anthracene.² The solid curve 1 is calculated by using eq. 1 with the values $\tau_0 = 69.7 \times 10^{-9}$ sec. and $a = 1.05 \times 10^5$. Curve 2 is derived from curve 1 by addition of the dashed line for the phase angles of the directly excited anthracene molecules ($\lambda_{\text{ex}} = 3660 \text{ \AA}$). The circles and crosses are the measured values of ϕ_a^* or ϕ_a , respectively. The measured points fit the solid curves calculated according to the initial suppositions satisfactorily, considering the dif-

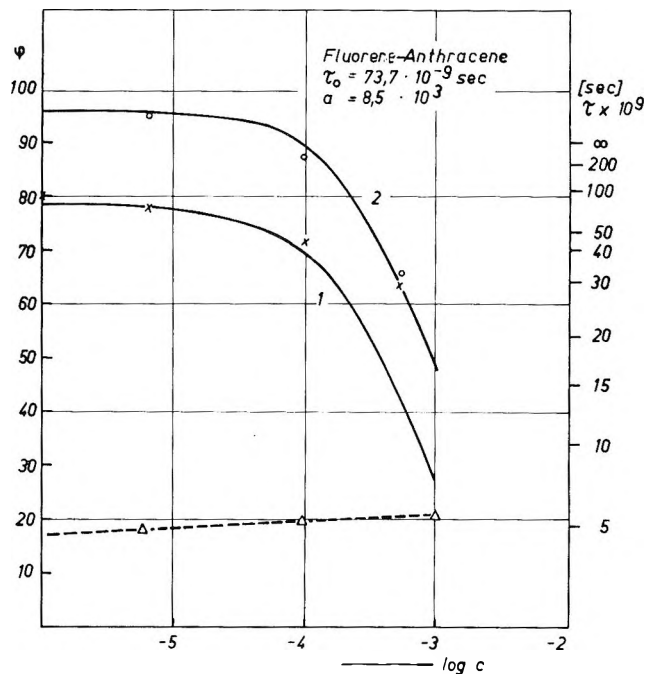


Figure 2. Phase angles of the system fluorene-anthracene; curve 1, $\lambda_{\text{ex}} = 3130\text{-}\text{\AA}$, fluorene fluorescence; curve 2, $\lambda_{\text{ex}} = 3130\text{-}\text{\AA}$, anthracene fluorescence; Δ , $\lambda_{\text{ex}} = 3660\text{-}\text{\AA}$, anthracene fluorescence.

ferences in separating the two fluorescence components from each other and from the exciting radiation.

If we compare the value of the transfer constant a of the system 2,3-dimethylnaphthalene-anthracene with that of the system 2,3-dimethylnaphthalene-perylene ($a = 87,000$) we find them to be very similar although anthracene and perylene have lowest excitation levels which differ in energy. (The emission of perylene lies in the spectral range $22,000\text{--}18,000 \text{ cm.}^{-1}$ and that of anthracene in the range $26,000\text{--}22,000 \text{ cm.}^{-1}$.) This result may indicate that the overlapping of the host lattice emission and the foreign molecule absorption is not the dominating factor of the energy transfer.

In the same representation, the results for the system fluorene-anthracene are plotted in Figure 2. The agreement between measured points and the curve calculated by using the parameters $\tau_0 = 73.7 \times 10^{-9}$ sec. and $a = 8.5 \times 10^3$ is not as convincing as in the first example. The constant a is fitted to the measured points of the indirectly excited anthracene fluorescence (curve 2). However, at the highest concentration the phase angle of the host lattice fluorescence gives too high a value, which may be caused by superposition of

(2) A. Schmillen and J. Kohlmannsperger, *Z. Naturforsch.*, **18a**, 627 (1963).

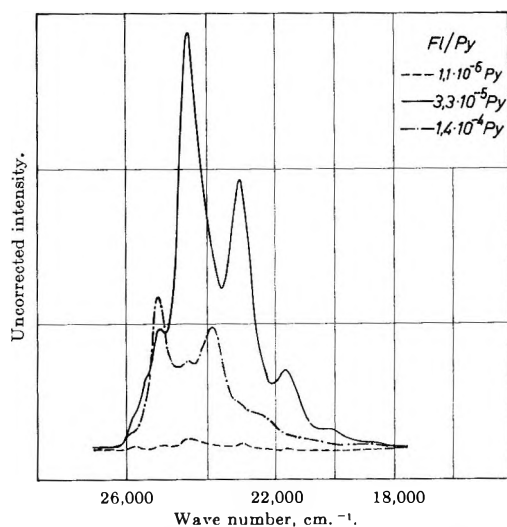


Figure 3. Luminescence of the system fluorene-pyrene by excitation with $\lambda = 3660 \text{ \AA}$. for different pyrene concentrations.

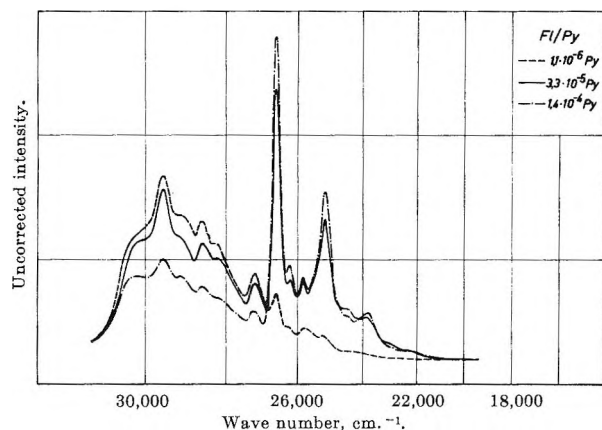


Figure 4.

the not fully separated anthracene fluorescence. However, the adaption of the transfer constant to the ϕ_a^* values of indirectly excited anthracene (curve 2) may not be correct in this case, because eventually a direct excitation of anthracene at the highest concentration contributes much shorter values to the measured phase angles. In every case a should not be greater than 8.5×10^3 .

A third investigated system, fluorene-pyrene, does not allow an interpretation in that manner, because two remarkable effects hinder the determination of the phase angle of the directly excited pyrene fluorescence. In the spectra of the directly excited foreign molecule fluorescence (excitation with 3660 \AA), Figure 3, at the two lowest concentrations used the expected pyrene fluorescence does not appear. In-

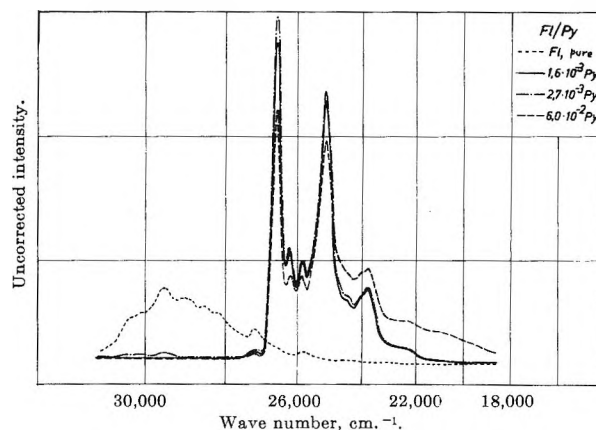


Figure 5. Luminescence of the system fluorene-pyrene by excitation with $\lambda = 3130 \text{ \AA}$. for different pyrene concentrations.

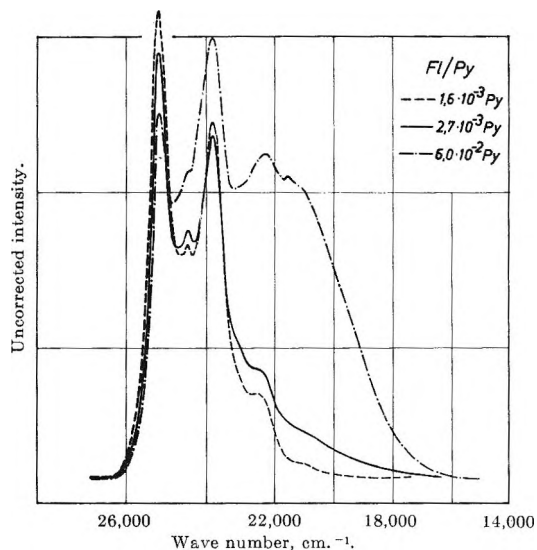


Figure 6. Luminescence of the system fluorene-pyrene by excitation with $\lambda = 3660 \text{ \AA}$. for different pyrene concentrations.

stead, an anthracene fluorescence shows up, the intensity of which increases by addition of pyrene. Only at higher pyrene concentrations does the pyrene emission arise and the anthracene fluorescence disappear. Anthracene is an impurity in the technical fluorene product, but we reduced its concentration by purification to values smaller than 10^{-6} . The increase of the anthracene fluorescence by addition of small amounts of pyrene could be caused by an energetical coupling between these two foreign molecules. Perhaps the molecules are located at neighboring sites in the lattice. (anthracene-pyrene complex centers). Then one could understand the disappearance of the anthracene fluorescence at higher pyrene concentrations, since

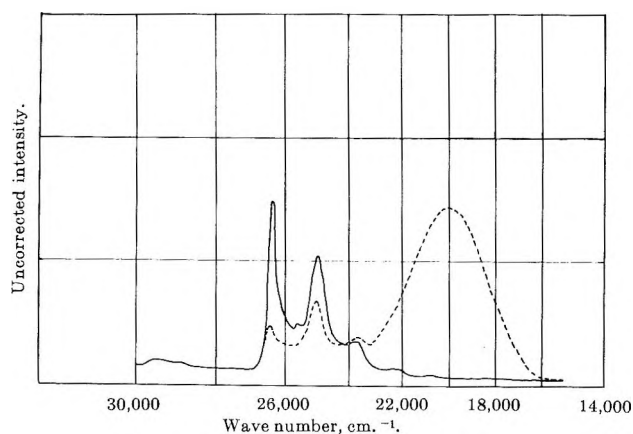


Figure 7. Luminescence of a single crystal of 2-methylnaphthalene- 10^{-3} pyrene: —, $\lambda_{\text{ex}} = 3130 \text{ \AA.}$; ·····, $\lambda_{\text{ex}} = 3660 \text{ \AA.}$

after the occupation of all anthracene neighboring sites with pyrene molecules, the absorption and emission would result more and more from pyrene centers without anthracene. This explanation is supported by the fact that the anthracene fluorescence in the same crystals does not appear by exciting with short wave lengths ($\lambda_{\text{ex}} = 3130 \text{ \AA.}$) absorbed from the host lattice. In this case the energy is absorbed in a very thin layer, Figures 4 and 5. The hypothetical anthracene-pyrene complex centers do not seem to participate in the energy transfer. However, this interesting question needs further investigation.

In Figure 6, at the highest concentrations, the excimer fluorescence of pyrene arises as indicated by an increase of the fluorescence intensity at $20,000 \text{ cm.}^{-1}$.

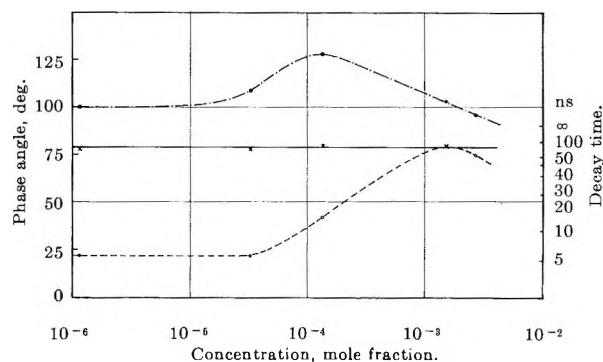


Figure 8. Phase angles of the system fluorene-pyrene: \times , fluorene fluorescence ($\lambda_{\text{ex}} = 3130 \text{ \AA.}$); \bullet , pyrene fluorescence ($\lambda_{\text{ex}} = 3130 \text{ \AA.}$); \circ , pyrene fluorescence ($\lambda_{\text{ex}} = 3660 \text{ \AA.}$).

This emission arises preferably by direct excitation. The effect is especially impressive for the system 2-methylnaphthalene-pyrene (10^{-3}), Figure 7. The intensity and decay time of the excimer fluorescence increase reversibly with cooling to liquid nitrogen temperature. In accordance with earlier measurements on polycrystalline powders, the maximum of the excimer fluorescence in the single crystal 2-methylnaphthalene-pyrene lies at $20,000 \text{ cm.}^{-1}$, whereas that of pure pyrene crystals lies at $21,500 \text{ cm.}^{-1}$. Therefore, we can definitely conclude that this emission is not due to precipitated pyrene. The decay time diagram (Figure 8) shows immediately the difficulties caused by the gradual change from the anthracene fluorescence over the monomer pyrene fluorescence to the excimer emission with increasing concentration.

On Photoelectric Effects in Polymers and Their Sensitization by Dopants¹

by Helmut Hoegl

Battelle Memorial Institute, Carouge-Geneva, Switzerland (Received December 3, 1964)

Electrostatic imaging techniques have been applied to the study of the chemical aspects of photoconductance in organic compounds. The materials were studied in the form of thin films coated on conductive substrates. It was found that poly-N-vinylcarbazole and a variety of other polymers with aromatic or heterocyclic chain units exhibit photo-induced discharge. The photoresponse may be strongly improved by doping with a wide variety of electron acceptors. The same effects may be observed with aromatic or heterocyclic electron donor-type photoconductors when dispersed in nonphotoconductive resin binder and doped with electron acceptors. The reverse case is given when aromatic or heterocyclic electron acceptors are doped with small amounts (0.1–2 mole %) of electron donors and dispersed in a resin binder. These and other findings show that donor (D)–acceptor (A) interactions according to $DA \xrightleftharpoons{\text{light}} D^+A^-$ play a decisive role for the photo-induced generation of charge carriers. p-Type conduction may be postulated when D-hosts are doped with A-impurities, which act as electron traps, and if an exchange of positive charges (holes) between excess D molecules takes place. In the reverse case, n-type conduction with trapping of holes and migration of electrons may be postulated.

Introduction

The purpose of this work is to show that the methods used for electrostatic imaging processes ("electrostatography")^{2–4} also may be used for the study of phenomenological aspects related to photoconduction in organic compounds. The relevant chemical problems are the relationships between chemical structure and photoconductive properties, and the mechanisms of charge carrier formation and transport in a bulk of originally neutral molecules. An objective of more practical importance is to explore whether organic materials can attain at all the photosensitivity of inorganic photoconductors, *e.g.*, zinc oxide and selenium. Another problem was to find better means of controlling the photosensitivity of organic photoconductor films. The results presented in this paper have so far appeared only in patents.^{5–12}

Experimental Techniques

The materials investigated were photoconducting polymers and low molecular weight compounds embedded in nonphotoconducting polymers. Low molecular weight starting materials were purified by recrystallization or distillation. The polymers were

applied in the form of thin films, cast mainly on aluminum sheets. For comparisons of results, they were also coated on paper. The film thickness was varied between 2 and 20 μ ; however, for measurements it was kept mainly at about 6 μ .

The physical principles involved in electrostatog-

- (1) Presented at the International Conference on Photosensitization in Solids, Chicago, Ill., June 22–24, 1964.
- (2) (a) J. Dessauer in "Photographic Science, Symposium, Zurich 1961," The Focal Press, London, 1963, p. 263; (b) C. J. Claus, *Phot. Sci. Eng.*, **7**, 5 (1963); (c) J. W. Weigl in "Photographic Science, Symposium, Zurich 1961," p. 345; (d) H. Meier, "Die Photochemie der organischen Farbstoffe," Springer-Verlag, Berlin, 1963, p. 158.
- (3) P. M. Cassiers, *Ind. Chim. Belge*, **25**, 127 (1960).
- (4) C. J. Young and H. G. Greig, *R C A Rev.*, **40**, 469 (1954).
- (5) H. Hoegl, O. Süss, and W. Neugebauer, German Patent 1,068,115 (1957).
- (6) H. Hoegl, O. Süss, and W. Neugebauer, German Patent 1,111,935 (1958).
- (7) H. Hoegl and W. Neugebauer, Belgian Patent 592,291 (1959).
- (8) H. Hoegl, E. Lind, and H. Schlesinger, Belgian Patent 592,557 (1959).
- (9) H. Hoegl, German Patent 1,133,976 (1959).
- (10) H. Hoegl and H. Schlesinger, German Patent 1,131,988 (1959).
- (11) H. Hoegl, German Patent 1,127,218 (1959); see also Belgian Patent 591,164 (1960).
- (12) H. Hoegl, Belgian Patent 606,574 (1960).

raphy are photoconductivity and electrostatics. Typically, a photoconductor plate is grounded at one surface and the other surface is corona-charged to a voltage V_0 . The positive or negative charges imparted to the samples in the dark by passing them under corona wires held at a potential of a few thousand volts are very probably due to ionized gas molecules (N_2^+ or O_2^-). After corona-charging, the connection to the ground is switched off. Now, the electrostatically charged plate may be used either for measuring dark and photo-induced discharge characteristics with an electrostatic voltmeter or for electrostatographic imaging processes. Both techniques have been used in this investigation.

1. *Electrostatic Voltmeter Method.* The electrostatically charged plates (*positive* in all cases reported) were placed under a wire netting serving as a probe for the electrostatic voltmeter (Type R 1019, Rothschild, Zurich, Switzerland). For comparison, the dark and light decay characteristics were measured. Usually, a 125-w. mercury high pressure lamp was used as a light source. Since these measurements could be made only rather qualitatively at this time, they were intended mainly to check results obtained with the imaging methods.

2. *Imaging Methods.* In these cases, a latent electrostatic image on the insulating photoconductive surface is obtained by exposure of the uniformly charged layer to light. The light causes neutralization of the charges on the surface. The nonexposed areas remain charged. The latent electrostatic charge patterns are made visible by application of electrically charged particles (toners). The toner particles adhere selectively either to the charged or to the uncharged areas of the photoconductor depending on the polarity of their charge. In all cases presented below, only a "direct" toner was used. Thus all images are direct ("positive") prints of the originals. These toner images were then fixed by melting, *i.e.*, they were not transferred to paper sheets as in xerography with selenium plates. Two variations of the same imaging technique have been used.

(a) *Density Strip Method.* The electrostatically charged plates (*negative* in all cases reported below) were exposed to light under a photographic density strip (Kodak No. 2 photographic step tablet with the color patches blue, green, and red, seen from the right end of the strip; 21 steps, uncalibrated; density range from 0 to 3.0, with the transmittance increasing from step to step by the ratio of $\sqrt{2}$). The light source for all cases of density strip copies shown was a mercury high-pressure lamp (Philips HPR 125 watts, Deutsche Philips GmbH). Comparison experiments with other commercially available light sources were also made.

The higher the photosensitivities of the plates, the fewer the dark steps that may be seen on the copies.

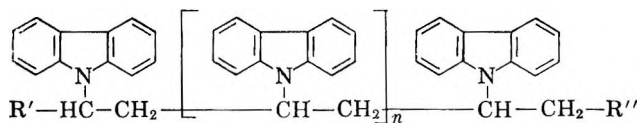
(b) *Exposure Time Method.* In this case (simply a variation of the density strip method 2a) the charged plates were exposed to light under any given original (*e.g.*, a drawing or a density strip). The exposure time necessary to obtain background-free copies of the originals after development was estimated. Therefore, the higher the photosensitivity of the plates, the shorter time of exposure was necessary. For the above methods *photosensitivity* is defined as the speed of light-induced discharge of electrostatically charged, photoconductive polymer layers by a given light intensity. The methods described gave principally the same qualitative results which were highly reproducible.

3. *Optical Measurements.* In some cases the optical absorption spectra of the photoconductors were measured, *e.g.*, poly-N-vinylcarbazole. They were found to correspond qualitatively with the xerographic action spectra. A rough indication of the spectral sensitivities of the plates is given by the color patches on the density strips (see 2a).

Experimental Results

Photoconductive Electron Donor Type Materials.

1. *Polymers.* (a) *Poly(-N-vinyl-carbazole) [PVK].* Using the aforementioned methods, it was found in 1957 that PVK behaves like a photoconductor,⁵ which was the first example of a polymer with photoconductive properties to be described in the literature. PVK



layers can be sensitized (in the bulk) with the same dyes as those which can be used for zinc oxide-silicone layers (*e.g.*, rhodamine B, methyl violet, rose bengal, etc.).

Since it is polymeric itself, PVK represents a valuable model for photoconductivity studies with the electrostatic imaging methods because it can be cast on conductive substrates without addition of a resin binder. In working with PVK layers, it turned out that all commercially available samples (Luvican[®] samples from the Badische Anilin & Soda Fabrik, Ludwigshafen a. Rh., Germany) behaved quite differently in their light response. Therefore, the polymer was prepared directly from the monomeric N-vinylcarbazole according to literature specifications.¹³ However, the purest samples obtained by thermal polymerization of purified

(13) W. Reppe, *et al.*, *Justus Liebigs Ann. Chem.*, **601**, 132 (1956); German Patent 664,231 (1934); see also J. Remond, *Rev. Prod. Chim.*, **66**, 515, 582 (1963).

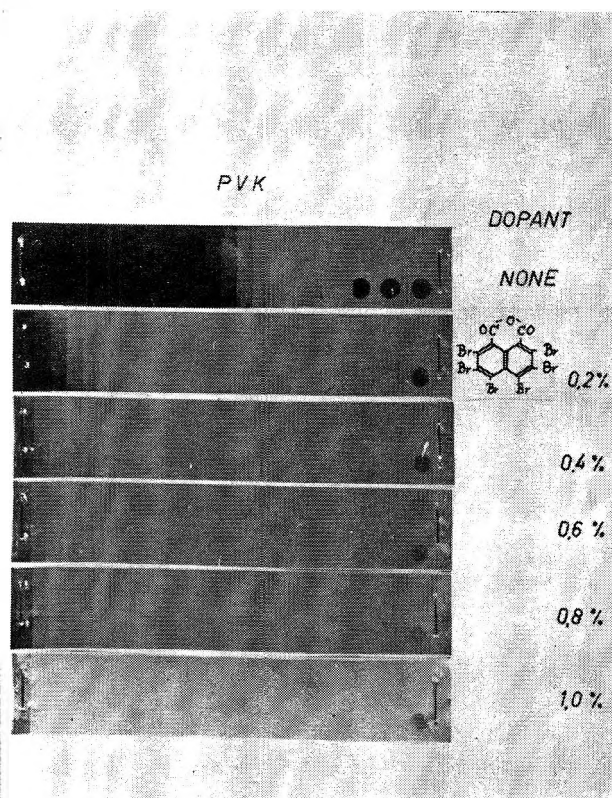


Figure 1. Density strip copies: PVK photoconductor with increasing amounts of hexabromophthalic anhydride.

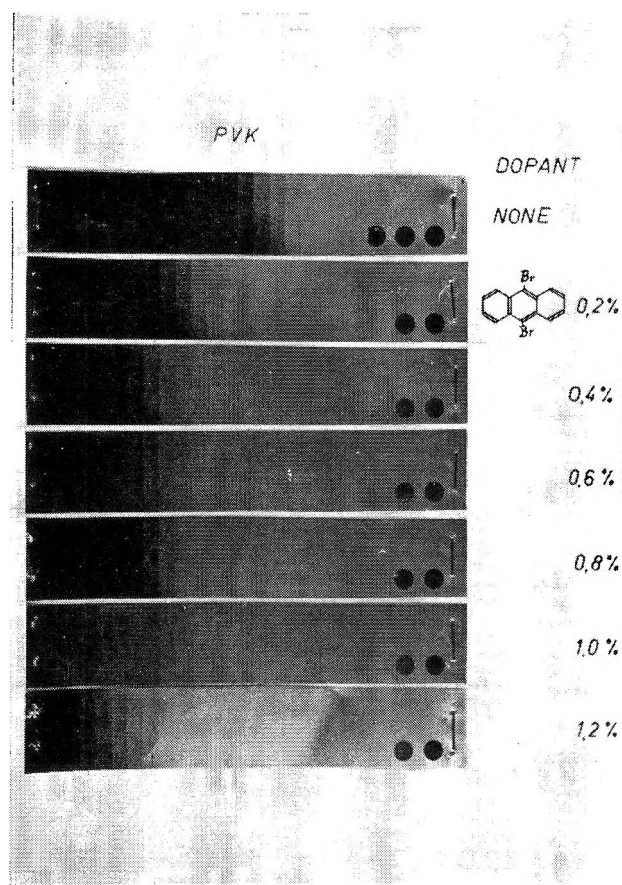


Figure 2. Density strip copies: PVK photoconductor with increasing amounts of 9,10-dibromoanthracene.

monomer gave the poorest results with regard to photosensitivity. The degree of polymerization seemed to exhibit no great influence. Polymer samples obtained by using Lewis acids as initiators (BF_3 , AlCl_3 , ZnCl_2 , H_2SO_4 , tetranitromethane, etc.) were much more sensitive. Thus, Lewis acids were added directly to the standard PVK samples (commercial Luvican®; thermally polymerized samples, or polymers prepared by initiation with α, α' -azodiisobutyronitrile).

It was found that the photosensitivity of the PVK layers increases with increasing Lewis acid concentration; *i.e.*, there is a relationship between the Lewis acid "dopant" concentration and the light response of the electrostatically charged PVK films. The Lewis acids were added in increasing molar concentrations based on N-vinylcarbazole chain units. The strongest effects on photosensitivity were observed in the range of about 0.1 to 2 mole % dopant. In the case of very strong acids such as H_2SO_4 , at higher concentrations the dark conductivity is increased rather strongly. Furthermore, it was found that doping with *electron acceptors* quite generally increases the photosensitivity

of PVK films.⁶ Systematic doping experiments were made with a wide variety of organic compounds in order to correlate the chemical structure of the dopants with their capability for influencing the photoelectric behavior of the PVK host (matrix). The following list of compounds and those listed on the density strip copies (Figures 1–8) are selected as typical examples: *nitro compounds*, *e.g.*, 1,3,5-trinitrobenzene; picric acid; 3,5-dinitrosalicylic acid; 9-nitroanthracene; 2,7-dinitroanthraquinone; 3,6-dinitrocarbazole; 5-nitrobarbituric acid; *ciano compounds*, *e.g.*, cyanoacetic acid; phenyl-*p*-bis(methylene malonic dinitrile); 2-cyanocinnamic acid; 9-cyanoanthracene; *acids*, *e.g.*, HCl; acetone dicarboxylic acid; fumaric acid; maleic acid; dibromomaleic acid; malonic acid; muconic acid; phthalic acid; cinnamic acid; benzenephosphonic acid; anthracene-9-carboxylic acid; *carboxylic acid anhydrides*, *e.g.*, phthalic anhydride; tetrahalogenated phthalic anhydrides; chrysene-2,3; 8,9-tetracarboxylic acid anhydride; *esters*, *e.g.*, ethylene tetracarboxylic acid tetraethyl ester; terephthalic dimethyl ester; nitroterephthalic dimethyl ester; phthalic acid diesters;

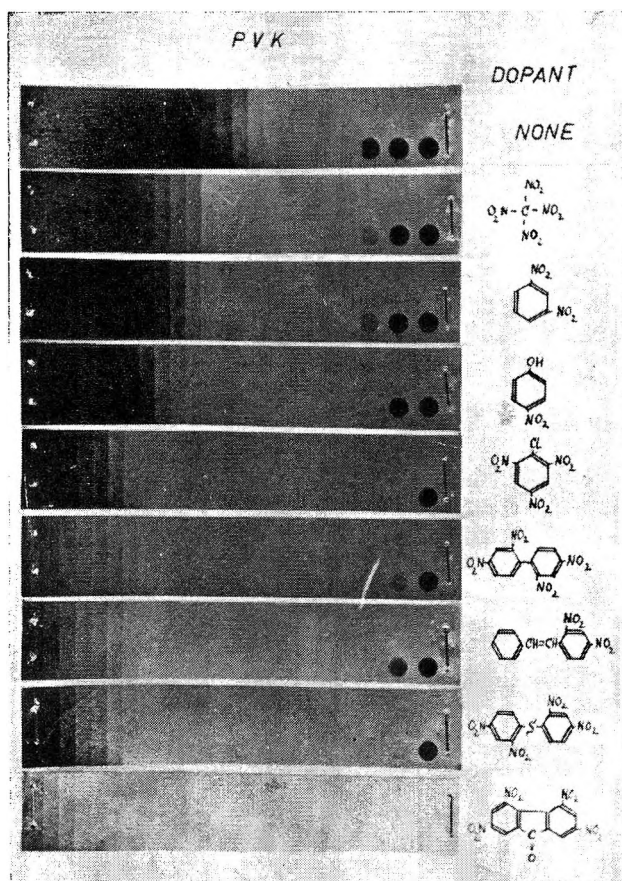


Figure 3. Density strip copies: PVK doped with nitro compounds (1 mole % with reference to vinylcarbazole monomer unit).

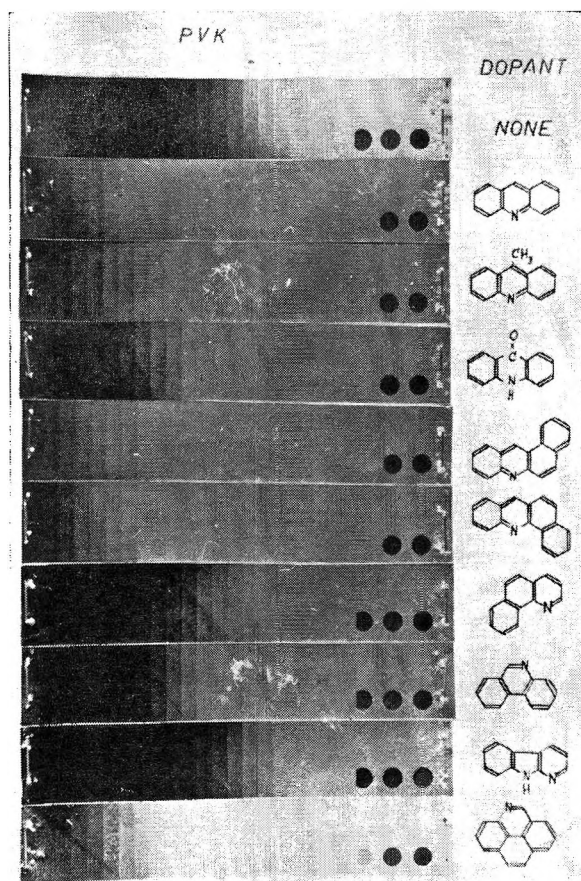


Figure 4. Density strip copies: PVK doped with aza compounds (1 mole %).

anthracene-9-carboxylic acid methyl ester; *halogen compounds*, e.g., tetrabromo-*p*-xylene; triphenylchloromethane; octachloronaphthalene; 9-bromoanthracene; 9,10-dichloroanthracene; *quinones*, e.g., chloranil; bromanil; acenaphthenequinone; phenanthrenequinone; chrysenequinone-(1,2); *keto compounds*, e.g., pyrene-3-aldehyde; benzil; benzoin; 2-nitroindandione-(1,3); 9-propionylantracene; xanthone; 2,2'-pyridil; *aza compounds* (see Figure 4).

With combinations of some dopants and dye sensitizers, PVK layers could be obtained which were as sensitive as ZnO-silicone layers (sensitized with rhodamine B), according to electrophotographic imaging methods.

The copies show effects of increasing dopant concentrations (Figures 1 and 2), of different dopants in equal concentrations with the same substituents (Figures 3-5), and with different substituents on one aromatic ring system (Figures 6-8).

It is important to note that *desensitization* of PVK was observed on adding stronger *electron donors* (e.g., 4,4'-diaminobiphenyl; 2,2'-dinaphthylamine; etc.); see Figure 9.

(b) *Other Polymeric Photoconductors*. The experiments made with PVK were extended to other polymers containing aromatic or heterocyclic chain units. The objective was twofold: to test whether polymers with π -bonded systems generally exhibit photoconductive properties when in the form of thin films, and whether dopant effects as in PVK may be observed generally. Both expectations were confirmed. The polymer films prepared and some of the dopants exhibiting increase of photosensitivities are listed in Table I. Structural formulas of the compounds are given in Figures 10 and 15.

Density strip copies of polystyrene and polyacenaphthylene are shown in Figures 11, 12, and 13. A series of patents has been issued on xerographic utilization of polyvinylaromatic compounds,⁷ polyvinylheterocyclics,⁸ polyindene and polyacenaphthylene,⁹ and derivatives of polyacrylate and polymethacrylate.¹⁰ It is interesting to note that significant photocurrents were reported also for glow discharge-formed polystyrene films by Spokas.¹⁴

Table I: Some Further Photoconductive Polymers

No.	Polymers	Sensitizing dopants
1. I	Polystyrene ^a	See Figure 11
1. II	Polyvinylxylene ^b	Tetracyanoethylene (TCNE); dibromomaleic anhydride (DBMA); 3. XI; 3. IX; 1,3,5-trinitrobenzene (TNB); 2-nitroindandione-(1,3) (NID); 3. III; 3. X; 3. V
1. III	Poly- <i>l</i> -vinylanthracene ^c	TCNE; DBMA; 3. XI; 3. IX; TNB; NID; 3. III; 3. X; 3. IV; 9,10-dichloroanthracene (DCA); and 3. XII
1. IV	Poly-2-vinylanthracene ^d	3. XI; 3. IX; 3. I; anthraquinone (AQ); 2,4,7-trinitrofluorenone (TNF)
1. V	Poly-4-vinylbiphenyl ^e	No doping experiments made
1. VI	Poly-9-vinylanthracene ^e	No doping experiments made
1. VII	Poly-3-vinylpyrene ^e	No doping experiments made
1. VIII	Poly-2-vinylquinoline ^f	All dopants listed above; sensitization was also observed with strong electron donors such as 2,2'-dinaphthylamine
1. IX	Polyindene ^g	TCNE; 3. XI; DCA; 3. I
1. X	Polyacenaphthylene ^h	See Figures 17 and 18
1. XI	Poly(3,3'-dimethyldiphenylene-4,4') ⁱ	TCNE DBMA; 3. XI; 3. IX; 3. X
1. XII	Various aromatic and heteroaromatic derivatives of polyacrylamide and polymethacrylamide ^j	3. XI

^a Mostly Polystyrol III (glasklar) from Badische Anilin & Soda Fabrik (BASF), Germany. ^b Monomer from L. Light and Co. GmbH, Hamburg, Germany; purified, and polymerized with 0.1% benzoyl peroxide in a tube (48 hr., 110°). ^c Monomer from L. Light and Co.; polymerized as under b. ^d Synthesized from α -hydroxyethyl naphthalene and polymerized as under b. ^e Monomers prepared according to methods described in the literature; polymerization as under b. ^f Monomer polymerized as under b. ^g Polymerized with BF₃-etherate in methylene chloride. ^h Thermally polymerized (110°, 1 to 2 hr.). ⁱ Prepared from 4,4'-diiodo-3,3'-dimethyldiphenyl by heating with copper powder according to W. Kern and O. Wirth, *Kunststoffe-Plastics*, **6**, 12 (1959). ^j For preparation, see German Patent 1,131,988 (1962).

Table II: Low Molecular Weight Electron Donor Type Photoconductors

No.	Donor type photoconductors	Photosensitizing dopants
2. I	Naphthalene	3. IV; 3. XI
2. II	Biphenyl	3. IX; 3. XI; picryl chloride (PC); 3. IV; 3. XII
2. III	Fluorene	3. XI; PC; 3. IX; 3. X; 3. IV; 3. XII ¹
2. IV	Anthracene	Dibromomaleic anhydride (DBMA); 3,5-dinitrosalicylic anhydride (DNSA); 3. X; 3. XII
2. V	Phenanthrene	TCNE; DBMA; 3. IX; 1,3,5-trinitrobenzene (TNB); PC; 3. X; 3. XII; 3. IV
2. VI	Acenaphthene	DBMA; 3. XI; PC; 3. X; 3. V; 3. XII
2. VII	Acenaphthylene	3. XI; 3. X; 3. IV
2. VIII	Chrysene	3. IX; DNSA; 3. IX; PC; 3. X; 3. IV; 3. XII
2. IX	Pyrene	TNB; 3. XII
2. X	1,4-Dimethoxybenzene	3. XI; 3. X; 3. IV
2. XI	Diphenylamine	3. XI; 3. IV
2. XII	2,2'-Dinaphthylamine	DBMA; 3. XI; DNSA; PC; 3. IX; 3. X; 3. IV; 3. XII
2. XIII	1,5-Diethoxynaphthalene	DBMA; 3. IX; PC; DNSA; 3. XI; 3. X; 3. IV; 3. XII
2. XIV	2-Phenylindole	DBMA; 3. XI; PC; 3. IX; 3. X; 3. IV; 3. XII
2. XV	Carbazole	DBMA; 3. XI; PC; 3. IX; DNSA; 3. X; 3. IV
2. XVI	Phenothiazine	3. XII
2. XVII	2,4-Bis(4'-diethylaminophenyl)-1,3,4-oxadiazole	See Figure 17; 3. IX; 3. XI; TNB; 3. X; 3. IV
2. XVIII	2,4-Bis(4'-diethylaminophenyl)-1,3,4-triazole	DBMA; 3. IX; DNSA; PC; 3. X; 3. IV; 3. XII

2. *Low Molecular Weight Donor Type Photoconductors.* Doping experiments were performed also with a variety of aromatic and heterocyclic donor compounds. The electrostaticographic methods can be ap-

plied only to uniform, continuous films. Therefore, since low molecular weight compounds of the types

(14) J. J. Spokas in *Proc. Princeton Univ. Conf. Semicond. Mol. Solids*, Princeton, N. J., 69 (1960).

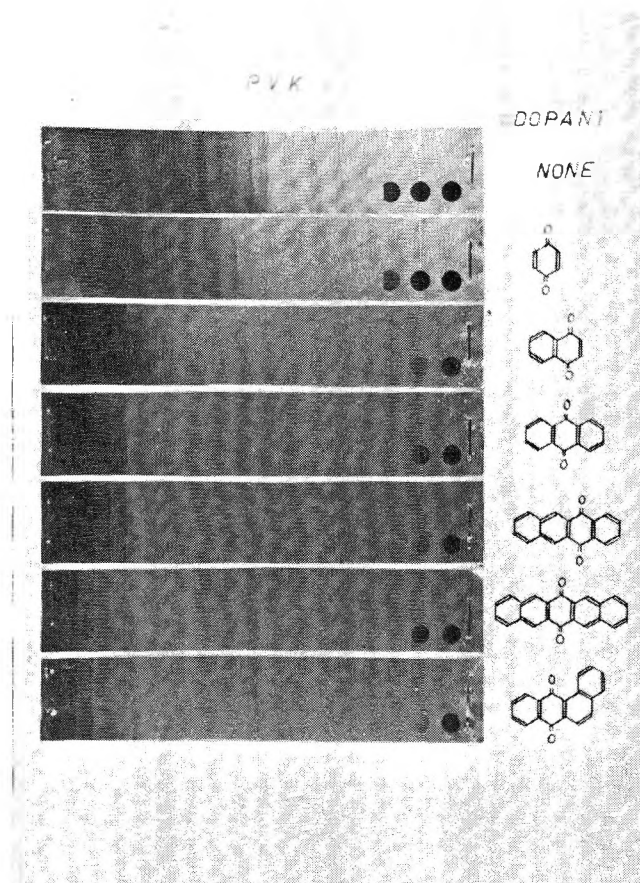


Figure 5. Density strip copies: PVK doped with *p*-quinones (1 mole %).

listed in Table II and shown in Figure 14 are unable to form continuous films, they must be embedded into a resin binder. The binder must be highly insulating, nonphotoconducting, and should not interact appreciably with the photoconductor dispersed or dissolved in it.

During the course of the work described here, various binders have been used in order to determine their influence: e.g., polyvinyl acetate [Mowilith[®] 50 usually, but sometimes also the lower polymeric types Mowilith[®] 40 and 30 of Farbwerke Hoechst AG, Frankfurt a.M./Höchst, Germany]; chlorinated polyvinyl chloride [Rhenoflex[®] of DAG-Werk, Rheinfelden, Germany]. For control, also, the following plastic binders were used: chlorinated rubber [“Pergut S 40[®]” of Farbenfabriken Bayer, Leverkusen, Germany; and “Parlon[®] S 5 cps” of Hercules Powder Co., U.S.A.]; butadiene-styrene copolymer [“Pliolite[®] S-5D” of Goodyear, U.S.A.], etc.

For the photosensitivity tests, the donor compounds listed in Table II were dissolved in equal parts (by weight) as the binders. Electron acceptors were added

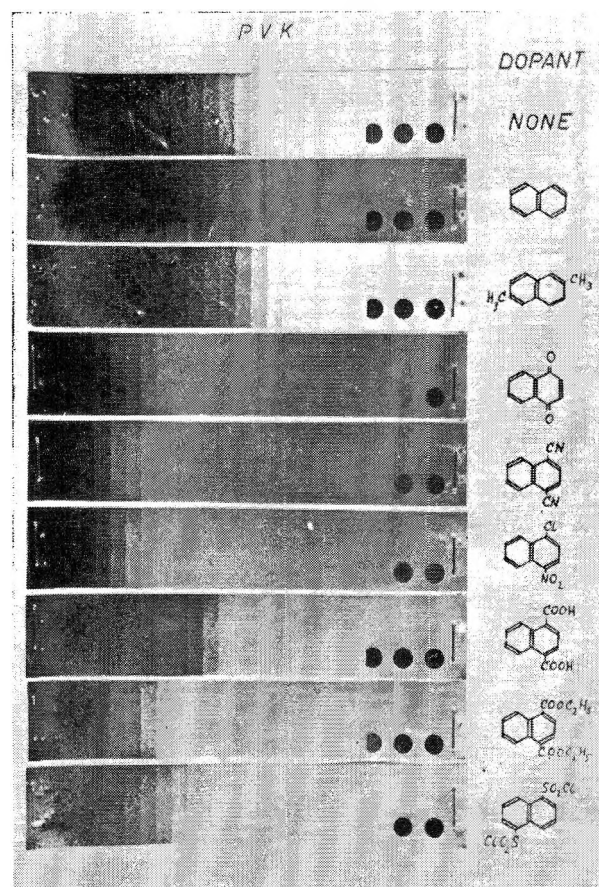


Figure 6. Density strip copies: PVK doped with derivatives of naphthalene, mainly 1,4-substituted (1 mole %).

in small concentrations to the solution (about 0.1 to 2 mole %) and the films were cast as usual. The effects of dopants were investigated by the methods described above. In all cases tested an increase of photosensitivities induced by doping was observed.¹¹ Table II lists some of the compounds tested. The structural formulas of the compounds are given in Figures 14 and 15. The effects of dopants are illustrated in Figures 16 and 17.

3. Electron Acceptor Type Photoconductors. When the importance of donor-acceptor interactions was established in donor host systems, the reverse case was studied. Typical acceptor compounds were doped in small amounts with donor compounds chosen from those listed in Table II. The mixture was embedded in a resin binder as described under section 2. An increase of photosensitivity by doping was found¹² to take place with a number of host compounds (Table III; Figures 14 and 15).

Figure 18 illustrates the effects of donor type dopants upon photosensitivity of an acceptor host.

Table III: Low Molecular Weight Electron Acceptor Type Photoconductors

No.	Acceptor type photoconductors	Photosensitizing additives
3. I	1,5-Dinitronaphthalene	2. XIII
3. II	1,8-Dinitronaphthalene	2. XII; 2. XVII
3. III	1,4,5-Trinitronaphthalene	2. IV; NEC
3. IV	2,4,5,7-Tetrafluorenone	See Figure 18 and HMB; 2. X; DBF; NEC; PVK
3. V	1,5-Dichloronaphthalene	2. XII
3. VI	1,4-Dibromonaphthalene	PVK; 2. XII; 2. XVII
3. VII	9,10-Dibromoanthracene	2. XII; 2. XVII
3. VIII	Phthalic anhydride	2. IV; 2. IX; 2. VIII; 2. XII; 2,3,5-triphenylpyrole (TPP); N-ethylcarbazole (NEC); 2. IV; 2. IX; 2. VIII; 2. XII; TPP; NEC
3. IX	Tetrachlorophthalic anhydride ^a	Hexamethylbenzene (HMB); 2. X; 2. I; 2. VIII; 2. XII; 2. XIV; dibenzofuran (DBF); 2. XI; PVK
3. X	Hexabromonaphthalic anhydride	NEC
3. XI	p-Chloranil	HMB; 2. X; 2. I; 2. IV; 2. VIII; 2. XII; NEC; TPP
3. XII	1,2-Benzoanthraquinone	2. IV; 2. XII; 2. XVII; PVK
3. XIII	Benzil	PVK; 2. XII
3. XIV	Pyrene-3-aldehyde	2. X; HMB; 2. I; 2. IV; 2. VIII; 2. XII; NEC; TPP
3. XV	9-Acetylanthracene	2. X; HMB; 2. IV; NEC

^a In the case of tetrachlorophthalic anhydride, *desensitization* was observed when another acceptor had been added, e.g., 4-bromonitrobenzene or 4-cyanopyridine.

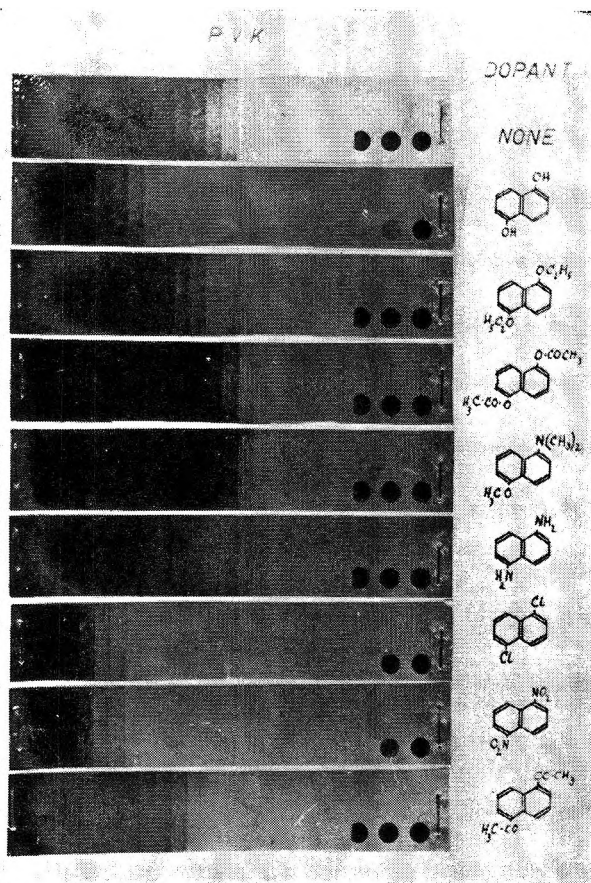


Figure 7. Density strip copies: PVK doped with derivatives of naphthalene, mainly 1,5-substituted (1 mole %).

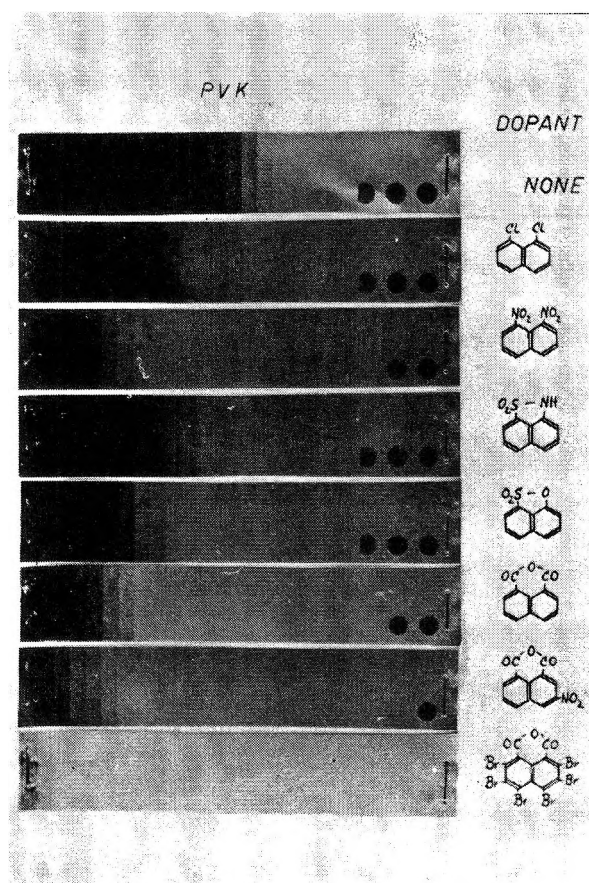


Figure 8. Density strip copies: PVK doped with derivatives of naphthalene, mainly 1,8-substituted (1 mole %).

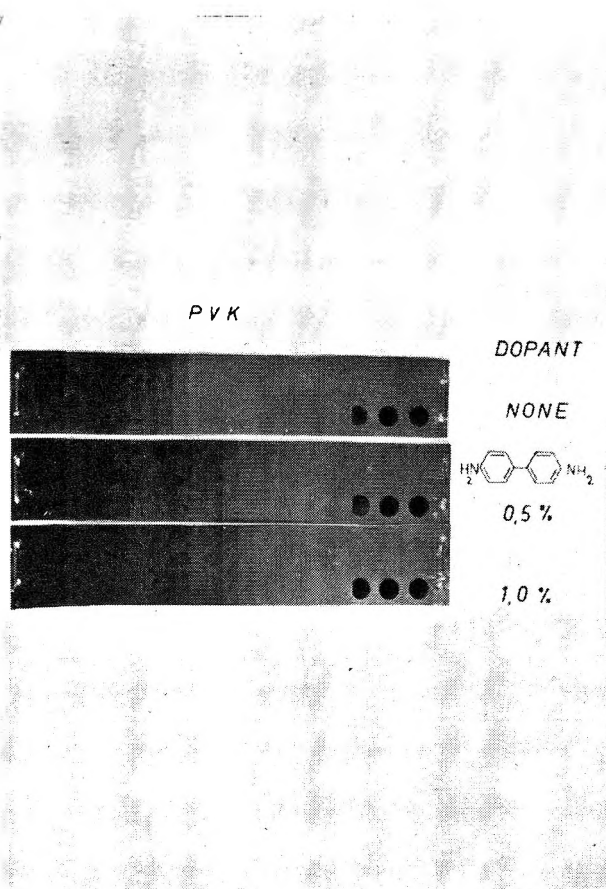


Figure 9. Density strip copies: PVK doped with increasing amounts of 4,4'-diaminobiphenyl.

Discussion of Results

The most significant observations made in the course of this study are given in this section. (1) Electrostatic imaging techniques provide a simple and rapid means for the investigation of phenomena associated with photoconductivity in organic compounds. They are especially useful for the screening of dopant effects, which would take much more time with the usual conductivity measurements.

(2) Photoconductivity is a common feature of organic systems containing conjugated double bonds (aromatic and heteroaromatic, monomeric and high polymeric).

(3) One may distinguish clearly between two different types of organic compounds: (a) *electron donors* (D), π -electronic systems (aromatic, heteroaromatic), especially with electron-repelling groups, such as amino, alkylamino, alkoxy, acetoxy, alkyl groups, etc.; (b) *electron acceptors* (A), π -electronic systems with electron-attracting groups, such as nitro, cyano, carbalkoxy, acetyl, carboxylic acid anhydride, halogen groups, etc., and quinones. It should be noted that the dopants

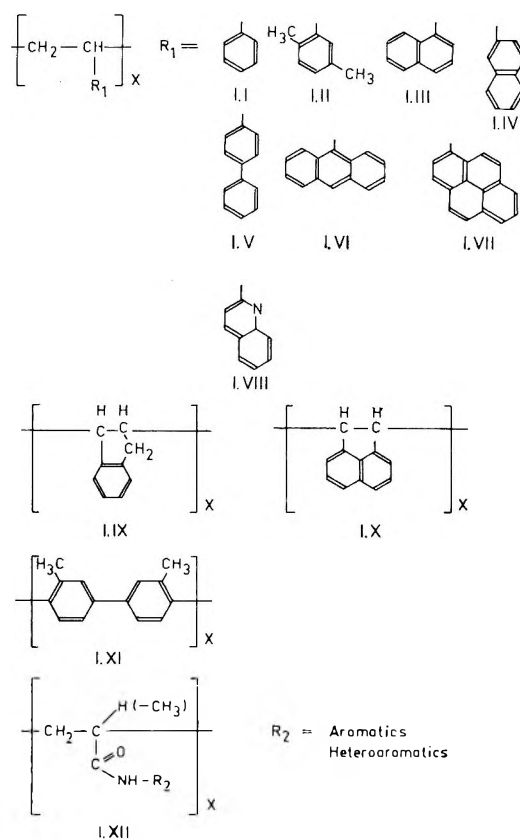


Figure 10. Structure formulas of polymeric photoconductors.

must not be photoconductive themselves (e.g., BF_3 or H_2SO_4 , in the case of PVK).

(4) The effects of additives upon the photosensitivity of the host compounds are due to charge-transfer (CT) type interactions between host and dopant. This is indicated (a) by structural features, (b) by the appearance of CT bands in the absorption spectra, (c) by the formation of stable CT complexes between the D and A components in many cases, and (d) by electron spin resonance (e.s.r.) measurements.¹⁵

(5) There exist mainly the following possibilities for the combination of different D and A compounds, of which the following observations have been made with regard to photosensitivities (see Table IV). However, this classification is useful only for compounds with very pronounced donor or acceptor character. It has been observed also that a host compound may act either as donor or as acceptor, with respect to different dopants, and that it is sensitized by both of them (e.g., anthracene, poly-2-vinylquinoline).

(6) If the same host material is doped with equal molar amounts of different dopants (e.g., PVK with

(15) R. P. Kohin, K. A. Müller, and H. Hoegl, *Helv. Phys. Acta*, **35**, 255 (1962).

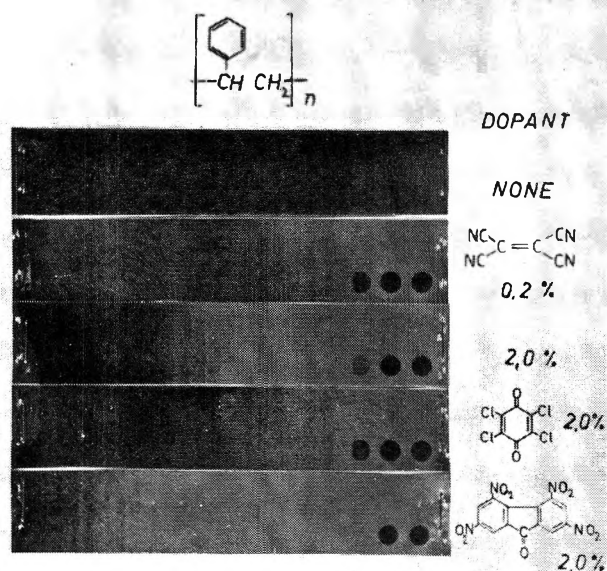


Figure 11. Density strip copies: polystyrene doped with electron acceptors.

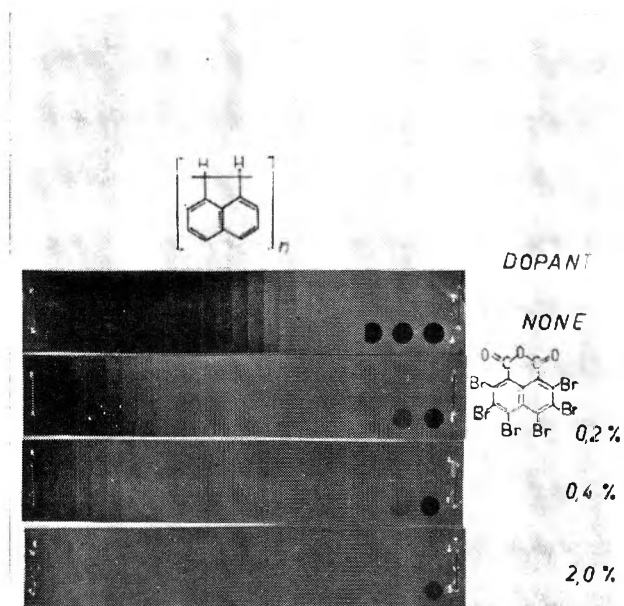


Figure 12. Density strip copies: polyacenaphthylene doped with increasing amounts of hexabromonaphthalic anhydride.

Table IV: Host-Dopant Combinations

Photoconductive matrix	Dopant	Effect upon photoconductivity
D	A	Sensitization
A	D	Sensitization
D	D'	Desensitization
A	A'	Desensitization

nitro and aza compounds and with naphthalene derivatives; Figures 3-8), significant relationships between dopant activity and chemical structure may be observed. This method provides a means of classifying materials according to their relative donor-acceptor strength.

Interpretation of Results

To explain the most significant results, one has to introduce several well-founded concepts.

(1) *Charge Carrier Formation.* According to Weiss,¹⁶ Brackman,¹⁷ Mulliken,¹⁸ Briegleb,¹⁹ and others,²⁰⁻²³

the interaction between an electron donor and an electron acceptor is characterized by the equilibrium



This equilibrium is influenced also by other forms of energy, such as thermal and mechanical energy (pressure). In the "normal state" (e.g., room temperature, normal pressure, absence of light), the system already may contain significant concentrations of the ionized structures depending on the components D and A. Furthermore, the electron transfer between adjacent

(16) J. Weiss, *J. Chem. Soc.*, 245 (1942).
 (17) W. Brackman, *Rec. trav. chim.*, 68, 147 (1949).
 (18) R. S. Mulliken, *J. Am. Chem. Soc.*, 74, 811 (1952); *J. Phys. Chem.*, 56, 801 (1952).
 (19) G. Briegleb, "Elektronen-Donator-Acceptor Komplexe," Springer-Verlag, Berlin, 1961.
 (20) L. J. Andrews, *Chem. Rev.*, 54, 713 (1954).
 (21) S. P. McGlynn, *ibid.*, 58, 1113 (1958).
 (22) J. N. Murrell, *Quart. Rev. (London)*, 15, 191 (1961).
 (23) H. A. Staab, "Einführung in die theoretische organische Chemie," Verlag Chemie, Weinheim, Germany, 1959, p. 694.

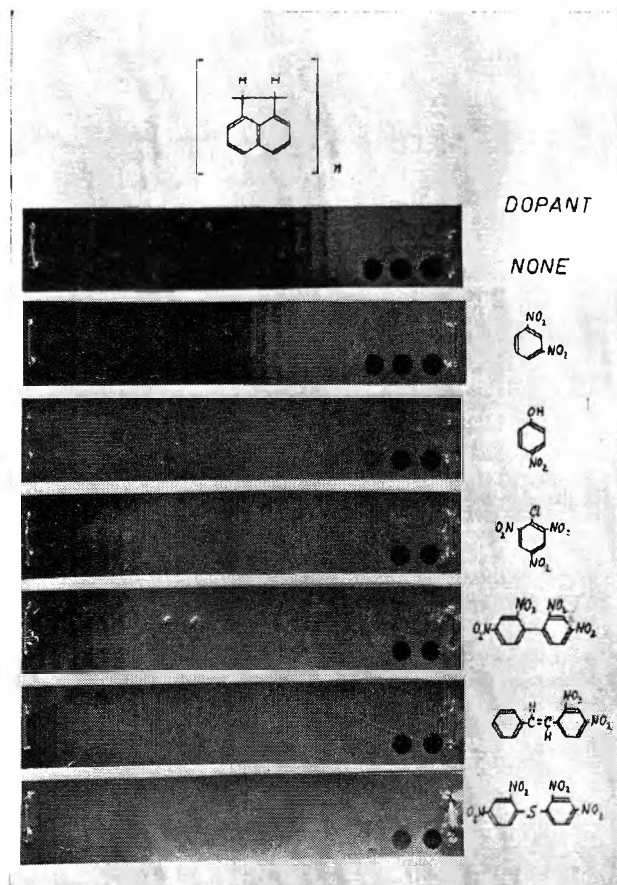


Figure 13. Density strip copies: polyacenaphthylene doped with various nitro compounds (2 mole %).

D and A molecules may be more or less complete, so that one speaks of intermolecular mesomerism.¹⁹

Of importance here is that charged molecules may be formed from originally neutral molecules by CT in the dark or with light. In the cases of an excess of either D or A molecules (or D and A side groups in polymers) important new consequences arise as discussed below. There is general agreement that the charge carriers formed by the interaction of photons with a photoconductor are electron and hole pairs; see, *e.g.*, Rube²⁴ and Rose.²⁵ If one assumes that CT is essentially electron-hole pair formation, one may deduce models for photo-induced discharge.

According to the electron-hole pair picture, either one of the charge carriers or both of them may contribute to the photocurrent, *i.e.*, to the discharge of the electrostatically charged plates. The following cases can be distinguished.

(a) *D Host Doped with A Impurity.* Migration of positive charges, *p-type conduction*, by exchange between the D-molecules may be postulated from this scheme. Electrons are trapped in the form of A⁻.

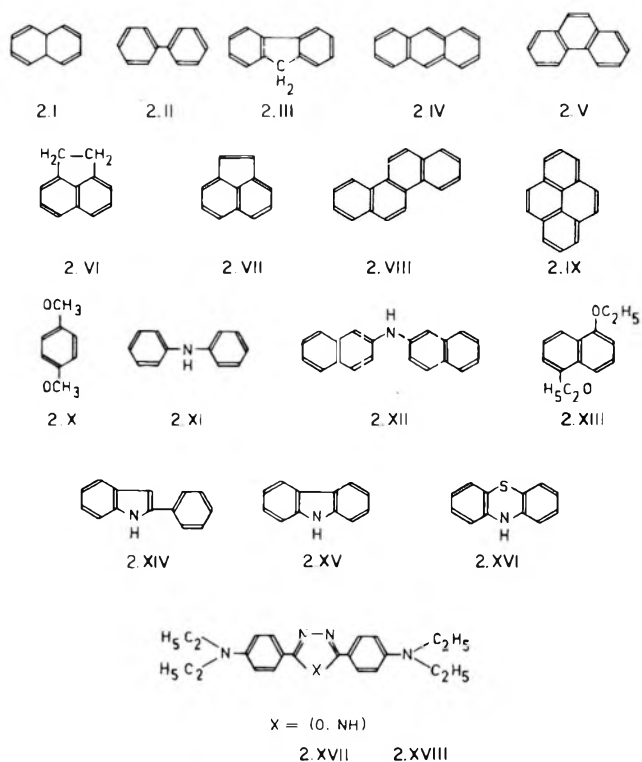


Figure 14. Structure formulas of electron-donor type photoconductors.

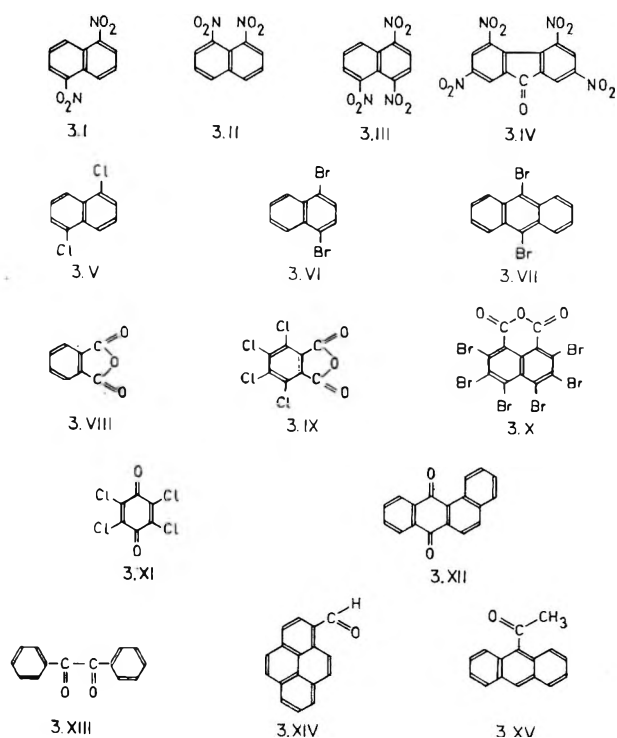


Figure 15. Structure formulas of electron-acceptor type photoconductors.

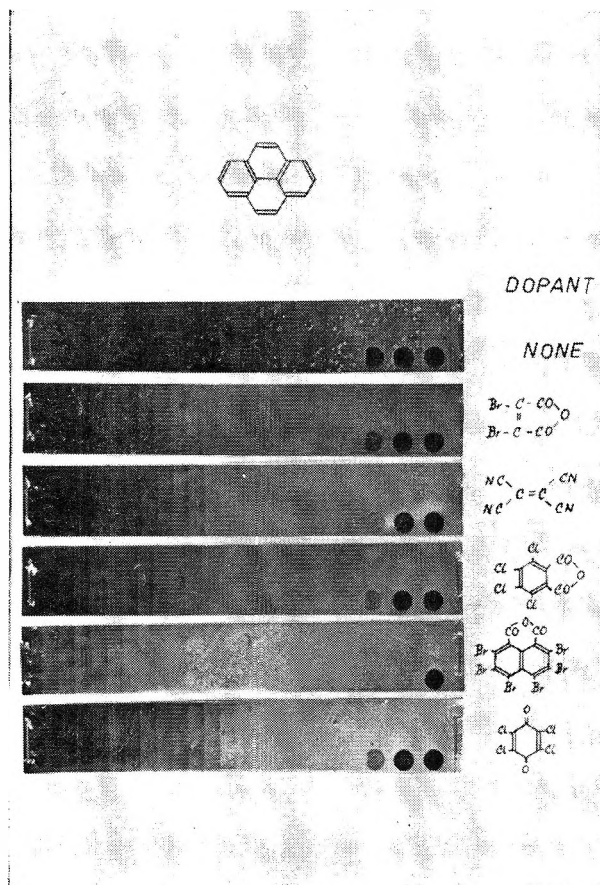


Figure 16. Density strip copies: pyrene doped with various electron acceptors (2 mole %).

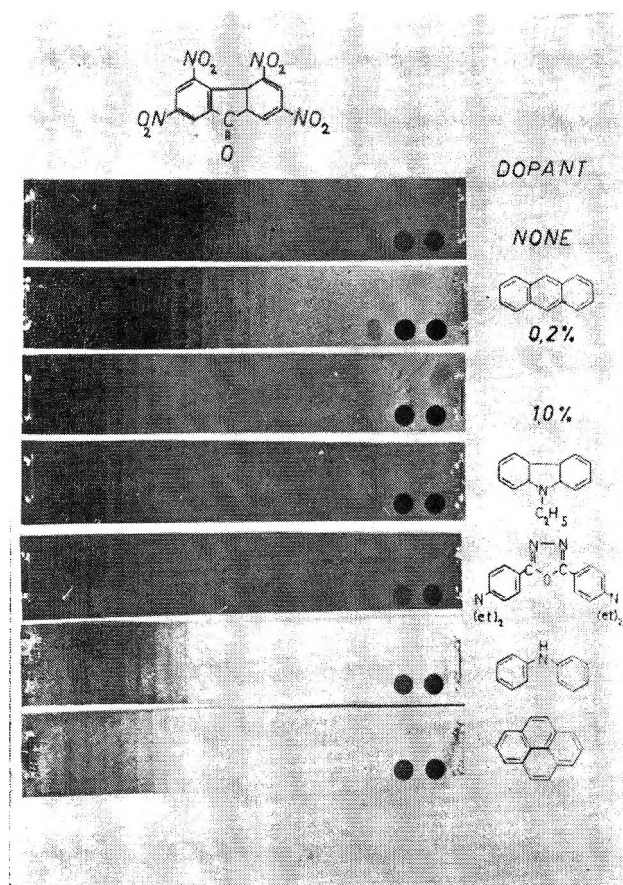


Figure 18. Density strip copies: 2,4,5,7-tetranitrofluorenone doped with various electron donors.

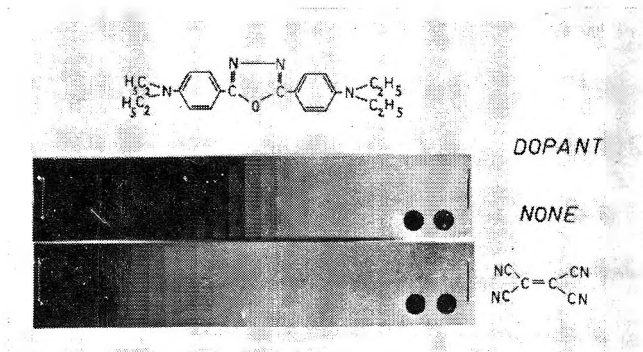


Figure 17. Density strip copies: 2,4-bis-(*p,p'*-diethylaminophenyl)-1,3,4-oxadiazole doped with tetracyanoethylene (2 mole %).

Exchange between A^- and D to form D^- is very unlikely. In the energy-band model the A dopant is represented by discrete levels in the forbidden band, from which holes are injected into (or electrons "extracted" from) the valence band.

If the charged plates are illuminated with very strongly absorbed light, which creates charge carriers

effectively only near the surface, polarity effects should be observed. Discharge rates should be significantly higher in a *p*-type photoconductor when it is positively charged than when it is negatively charged. Such polarity effects have in fact been observed with PVK films indicating holes as majority carriers.

(b) *A Host Doped with D Impurity.* In this case migration of negative charge carriers, *n*-type conduction, may be postulated. The positively charged D^+ molecules constitute the traps for the holes. In the band picture, the D dopant represents discrete energy levels near the empty conduction band, into which it injects electrons. It is worthwhile to note that e.s.r. measurements have shown that electrons may be exchanged rapidly between negatively charged and neutral molecules even in solutions.²⁶

(24) R. H. Bube, "Photoconductivity of Solids," John Wiley and Sons, New York, N. Y., 1960.

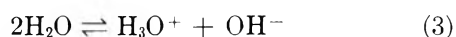
(25) A. Rose, "Concepts in Photoconductivity and Allied Problems," Interscience Publishers, Inc., New York, N. Y., 1963.

(26) R. L. Ward and S. I. Weissman, *J. Am. Chem. Soc.*, **76**, 3612 (1954); **79**, 2086 (1957).

(c) *Pure Compounds without Dopants.* There is little question that all cases of photoconductivity reported above are due to the activity of small amounts of impurities either in the bulk or on the surface. One may extend the principles discussed above for optical generation of charge carriers to pure materials, *i.e.*, to intrinsic effects. Any organic material capable both of accepting and of donating electrons will be represented by I (for intrinsic). There is some evidence that electron transfer can occur also between two I molecules according to



in analogy to the proton transfer in water



For example, formation of dimers is very often observed with aromatics and heteroaromatics, and one may theorize that it occurs *via* intermediate CT complexes. According to this, one may assume that intrinsic conduction in extremely pure materials occurs as shown in the scheme



In the band picture, this would imply that an electron is transferred from the filled valence band to the empty conduction band if the photon energy exceeds the band gap. In that case, a hole is left in the valence band and both carriers can contribute to the photocurrent.

(2) *Desensitization Effects.* As described above, a D host may be desensitized if doped with a stronger donor D' impurity. The same result holds for an A host when doped with a stronger A' impurity. One can postulate that D' traps holes in a D bulk



or A' electrons in an A bulk



It seems evident that in these cases the intermolecular exchange of charge carriers is much less probable than in cases a and b above. It is certainly easier for holes to flow through a D crystal than it is for electrons. The same holds for the reverse case.

(3) *General Remarks.* The conductivity of any material is proportional both to the concentration of charge carriers in the material and to the mobility of those carriers. Therefore, it seems that the effects of dopants are due to the increase of the number of charge carriers. Recombination of electron-hole pairs may occur at the D or A impurities or through other more complex mechanisms. Conclusions may not be drawn concerning this point from the experiments made.

The effects of dopants described here are in agreement with results of photoconductivity measurements reported by Kearns, Tollin, and Calvin,²⁷ and Meier.²⁸

Acknowledgments. The author is indebted to Kalle Aktiengesellschaft, Wiesbaden, Federal Republic of Germany, in whose Research Laboratories this work originated and wishes to acknowledge the assistance provided by Kurt Heylmann, Eddy-Fred Helmrich, Günther Berghäuser, and Miss Uta Hütter in performing the experimental work.

(27) (a) D. Kearns and M. Calvin, *J. Chem. Phys.*, **29**, 950 (1959); (b) G. Tollin, D. R. Kearns, and M. Calvin, *ibid.*, **32**, 1013-1020 (1960).

(28) H. Meier, *Z. physik. Chem. (Frankfurt)*, **39**, 249 (1963).

Hypersensitization of Photoconduction in Microcrystalline Zinc Oxide¹

by Eiichi Inoue, Hiroshi Kokado, and Takashi Yamaguchi

Graphic Engineering Laboratory, Tokyo Institute of Technology, Tokyo, Japan (Received November 4, 1964)

A discussion is given of two types of sensitization for photoconduction in microcrystalline zinc oxide. Sensitization by organic acid or acid anhydride is supposed to take place similarly to that by oxygen: the electron transfer between a positively charged interstitial zinc ion and a negatively charged organic acid radical ion is suggested. Optical sensitization, the other type of sensitization, also is studied with various dyestuffs and photodesorption of oxygen is observed during that process. Between the efficiencies for photodesorption and for sensitized photoconduction, a parallel relation is found. When acid anhydride or other electron-affinitive substances and dyestuff coexist on zinc oxide surface, an anomalous sensitizing effect is observed. This "hypersensitization" is considered to be caused by an interaction between the dye and the electron-affinitive molecule. Weigl's mechanism for optical sensitization is favored on the basis of the experimental results.

Introduction

Microcrystalline zinc oxide exhibits remarkable photoconduction as long as its surface is covered with chemisorbed oxygen, but it turns out to be a quite poor photoconductor as the oxygen is removed from the surface.² For this reason, chemisorbed oxygen may, in a sense, be regarded as a chemical sensitizer for zinc oxide photoconduction. Several other electron-affinitive molecules (EAM) such as nitrogen oxide, nitrogen peroxide, and quinones have been proved to be effective for this kind of sensitization.^{3,4} The mechanism of sensitization by these substances has been well understood since the work of Ruppel and co-workers²: EAM adsorbed on a zinc oxide surface produces an acceptor level for conduction electrons. A depletion layer formed there lowers the dark conductivity. Destruction of the depletion layer takes place during the illumination of zinc oxide with light shorter than 4000 Å., increasing the electron density.

It will be of interest to see the sensitizing effect when two or more different kinds of EAM coexist on the surface of zinc oxide. It has been reported that further sensitization is possible if an adequate second electron-affinitive adsorbate is given to the surface which already has chemisorbed oxygen.⁵

A quite different type of sensitization is the optical sensitization by dyestuffs or the dye sensitization. The mechanism for this phenomenon has been widely

discussed for zinc oxide by several investigators,⁶⁻⁸ though it is not yet fully understood. A distinct point is, however, that the dye sensitization can be observed only with light absorbed by the dye molecules.

An interacting sensitization of EAM and dyestuff has been found to improve further the photoconduction performance of zinc oxide.^{5a,b} We shall call such a cooperative sensitization "hypersensitization of photoconduction."

In the first section of the present paper, work done concerning the sensitization by benzoic acid, phthalic anhydride, and other electron-affinity substances will be described. In the second section, the optical sensitization by various dyestuffs will be discussed in relation to photodesorption of oxygen from dyed zinc

(1) Presented to the International Conference on Photosensitization in Solids, Chicago, Ill., June 22-24, 1964.

(2) W. Ruppel, H. J. Gerritsen, and A. Rose, *Helv. Phys. Acta*, **30**, 495 (1957).

(3) H. Kokado, E. Inoue, T. Yamaguchi, and K. Takahashi, *Bull. Chem. Soc. Japan*, **34**, 705 (1961).

(4) A. Terenin, E. Putzeiko, and I. Akimov, *J. chim. phys.*, **54**, 716 (1957).

(5) (a) E. Inoue, I. Maki, and T. Yamaguchi, *Kogyo Kagaku Zasshi*, **66**, 428 (1963); (b) E. Inoue and T. Yamaguchi, *Bull. Chem. Soc. Japan*, **36**, 1573 (1963).

(6) J. W. Weigl, Internationales Kolloquium über Wissenschaftliche Photographie, Zurich, September 1961.

(7) R. Matejec, *Z. Elektrochem.*, **65**, 783 (1961).

(8) S. J. Drudkowski and L. I. Grossweiner, *J. Opt. Soc. Am.*, **54**, 486 (1964).

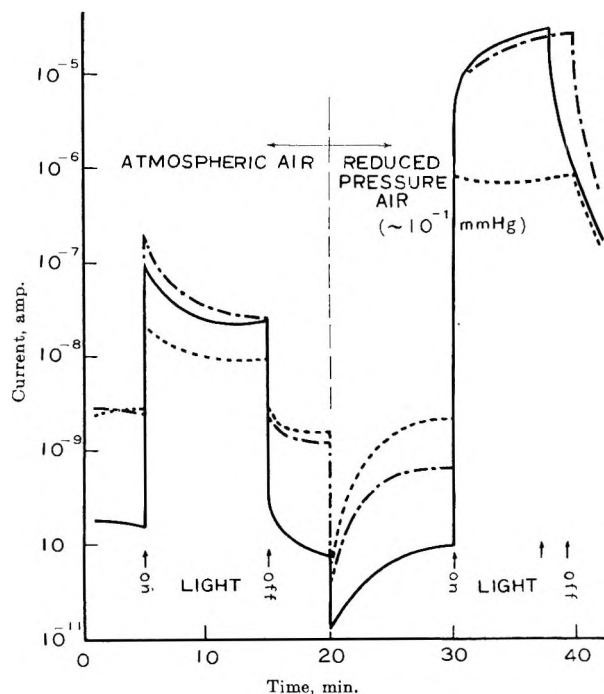


Figure 1. Typical response curves for photoconduction: - - - -, basic system (ZnO with chemisorbed oxygen); - · - · -, basic system + 0.01 mole % benzoic acid; — · — · —, basic system + 0.01 mole % phthalic anhydride; excitation: $365 \text{ m}\mu$, $1 \times 10^{-4} \text{ w./cm.}^2$.

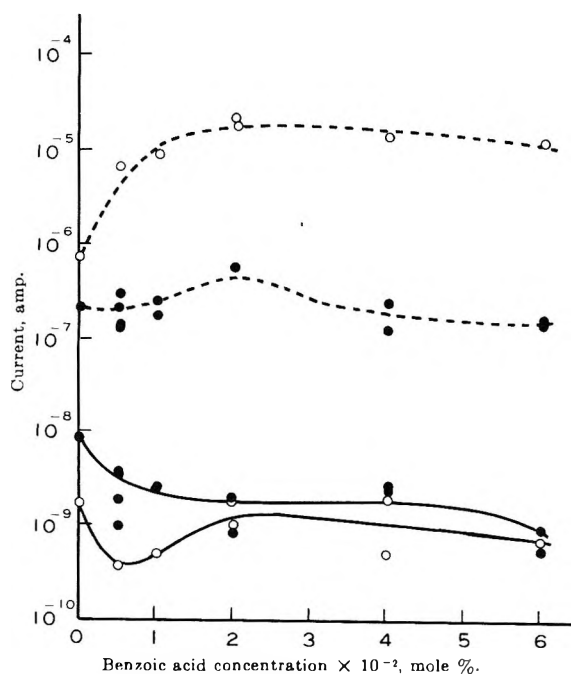


Figure 2. Dark and photocurrents in ZnO vs. concentration of benzoic acid added: — · — · —, dark current; - - - -, photocurrent; ●, in atmospheric air; ○, in reduced-pressure air ($\sim 10^{-1} \text{ mm.}$); excitation: $365 \text{ m}\mu$, $1 \times 10^{-4} \text{ w./cm.}^2$; ZnO used: no. 2.

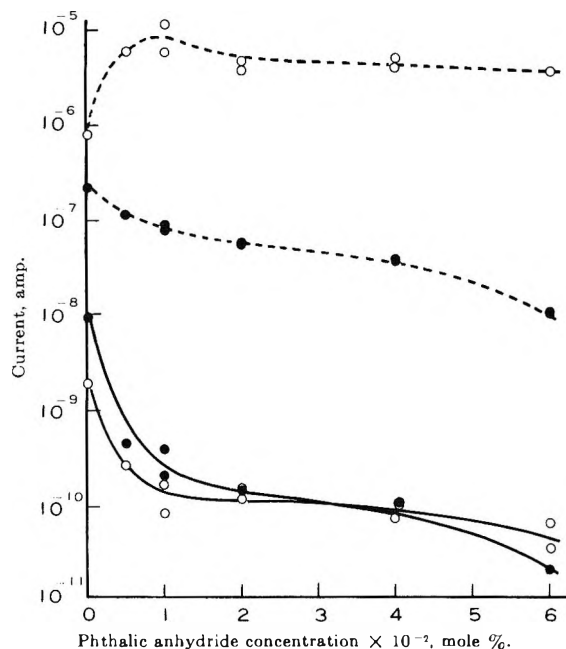


Figure 3. Dark and photocurrents in ZnO vs. concentration of phthalic anhydride added: — · — · —, dark current; - - - -, photocurrent; ●, in atmospheric air; ○, in reduced-pressure air ($\sim 10^{-1} \text{ mm.}$); excitation: $365 \text{ m}\mu$, $1 \times 10^{-4} \text{ w./cm.}^2$; ZnO used: no. 2.

oxide, and in the last section the hypersensitization will be discussed.

I. Effect of Organic Acid and Acid Anhydride on Photoconduction of Zinc Oxide Having Chemisorbed Oxygen

It has been reported that phthalic anhydride, iodine, and *p*-chloroanil have a sensitizing effect for the photoconduction of zinc oxide in the intrinsic region of light absorption, as coadsorbed with oxygen.^{5a,b} The thermal activation energy of EAM adsorbed zinc oxide was, in most cases, found to be a little lower compared to that of the basic system (zinc oxide with chemisorbed oxygen), indicating that the adsorption had changed the surface barrier height of zinc oxide.^{5b} A further experiment was carried out to investigate the mechanism of sensitization by phthalic anhydride which has been found to be most efficient in the previous work. Attention was paid especially to comparison of phthalic anhydride with benzoic acid.

The microcrystalline zinc oxide used was Merck's reagent, $\sim 0.1\text{--}0.3 \mu$ in particle size. The adsorption of phthalic anhydride or benzoic acid was carried out in the dark from an alcoholic solution. During this procedure, no attempt was made deliberately to remove chemisorbed oxygen already present on the surface of zinc oxide; therefore most of the oxygen was considered

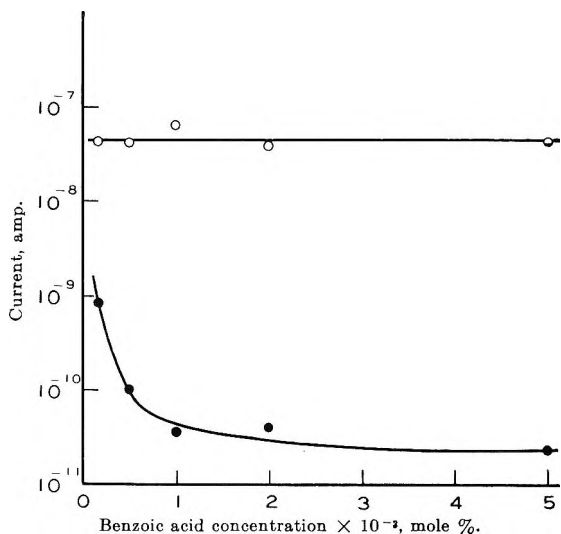


Figure 4. Dark and photocurrents in ZnO vs. concentration of benzoic acid added (in atmospheric air): ●, dark current; ○, photocurrent; excitation: 365 mμ, 1 × 10⁻⁴ w./cm.²; ZnO used: no. 1.

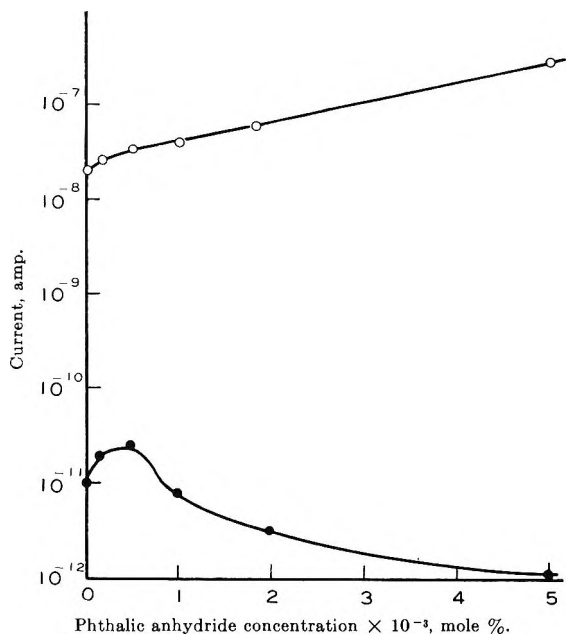


Figure 5. Dark and photocurrents in ZnO vs. concentration of phthalic anhydride added (in atmospheric air): ●, dark current; ○, photocurrent; excitation: 365 mμ, 1 × 10⁻⁴ w./cm.²; ZnO used: no. 3.

to remain chemisorbed. The samples prepared were coated in the dark on glass plates to a thickness of ~30-50 μ. Two aluminum strips used as electrodes were placed 0.5 cm. apart on each of the specimens to accomplish a surface-type arrangement. In order to eliminate any past irradiation history of the samples, every specimen was kept in the dark for 3 weeks or more

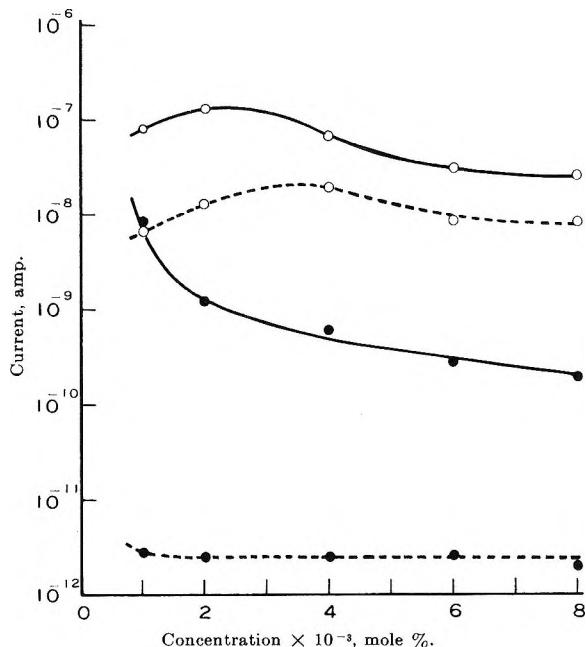


Figure 6. Dark and photocurrents in ZnO vs. concentration of phthalic acid or benzoyl peroxide added (in atmospheric air): —○—, phthalic acid; - - -○- - -, benzoyl peroxide; ●, dark current; ○, photocurrent; excitation: 365 mμ, 1 × 10⁻⁴ w./cm.²; ZnO used: no. 2.

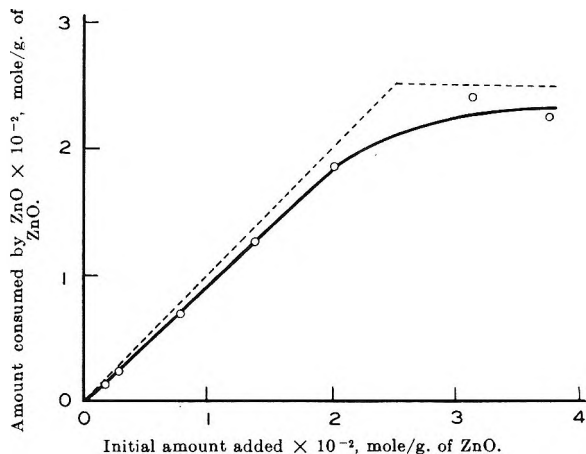


Figure 7. Consumption of benzoic acid by ZnO. The broken line shows the expected relation for 2:1 consumption.

before its electric current was measured with a vibrating reed electrometer. A high pressure mercury lamp coupled with an ultraviolet filter was used as the light source for photoconduction measurements.

Figure 1 illustrates typical photoresponse curves of the two kinds of zinc oxide, together with the basic system. Zinc oxide samples employed for these measurements (no. 2) seem to have an inversion layer with surface p-type characteristics as noticed by Cimino and co-

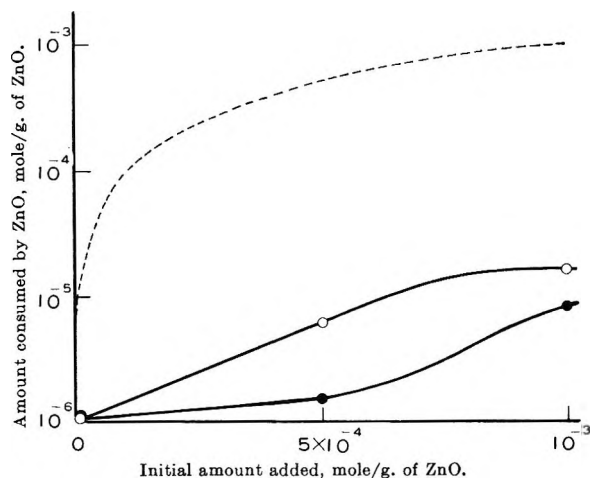


Figure 8. Adsorption of phthalic anhydride by ZnO: ●, in the dark; O, under illumination with a mercury lamp. The broken line shows the expected relation for 1:1 consumption.

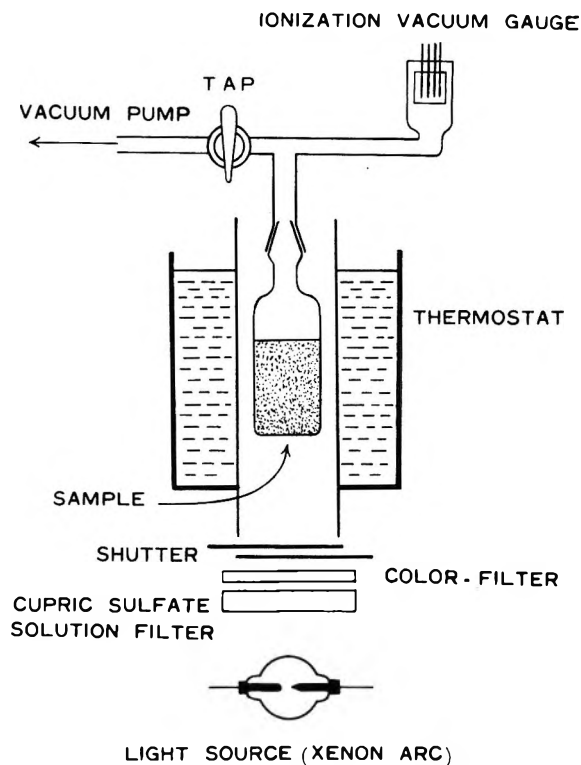


Figure 9. Experimental setup for photodesorption measurement.

workers.⁹ The dramatic decrease of photocurrent with time in atmospheric air and the sharp decrease of current immediately after rapid evacuation of the specimen container, followed by the slow increase, indicate the presence of an inversion layer. Figures 2 and

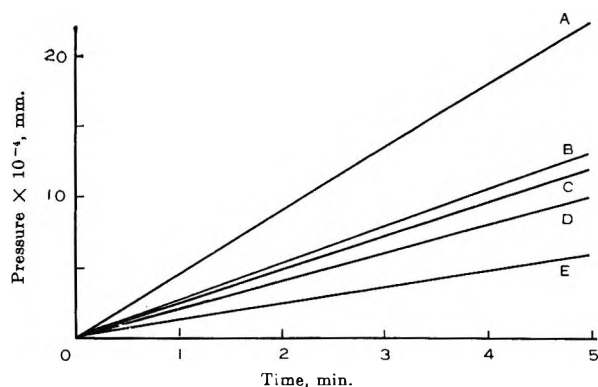


Figure 10. Photodesorption of oxygen from dyed ZnO with rose bengal: A, 0.002 mole %; B, 0.001 mole %; C, 0.0005 mole %; D, 0.01 mole %; E, 0.005 mole % of rose bengal added; excitation: $\sim 510\text{--}700\text{ m}\mu$; $1.5 \times 10^{-3}\text{ w./cm.}^2$.

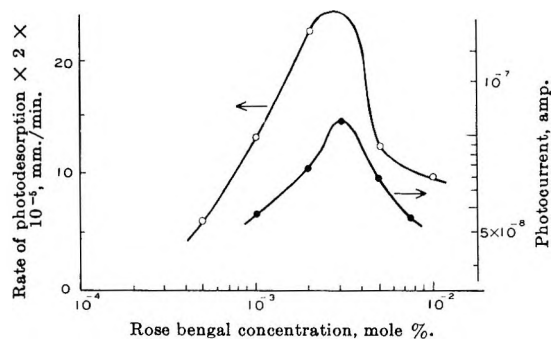


Figure 11. Correspondence of oxygen photodesorption and photosensitivity of dyed ZnO with rose bengal; excitation: $\sim 510\text{--}700\text{ m}\mu$, $1.5 \times 10^{-3}\text{ w./cm.}^2$.

3 show the dependence of dark and photocurrents upon the amount added of the two adsorbates. When only a small amount is added (less than 0.005 mole %), organic acid and acid anhydride affect the conductivity of zinc oxide essentially in the same manner, while a little difference appears as the amount is increased. The difference may be attributed to a difference in the adsorption processes of the two substances which will be described later. A more detailed relation between the current and the amount of addition in the region up to 0.005 mole % was studied in atmospheric air (Figures 4 and 5). It should be noted that the curves in Figure 4 which were consistent with those measured in atmospheric air in Figure 2 were obtained with zinc oxide no. 1 that had a less pronounced inversion layer than no. 2, while the curves in Figure 5 which reproduced those in reduced-pressure air in Figure 3 were obtained with zinc oxide no. 3 that had a normal de-

(9) A. Cimino, E. Molinari, and F. Cramarossa, *J. Catalysis*, **2**, 315 (1963).

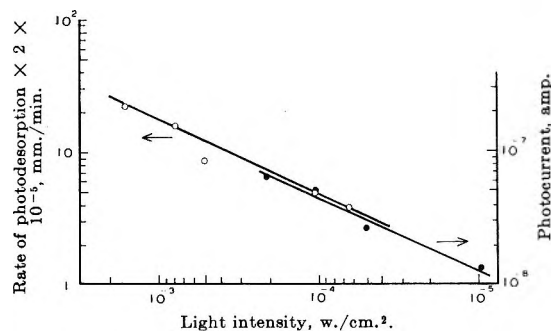
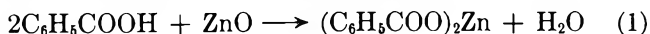


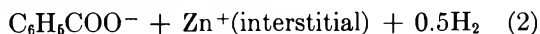
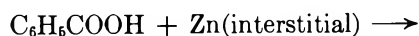
Figure 12. Light intensity dependence of the oxygen photodesorption rate; ZnO used: dyed with 0.002 mole % rose bengal; wave length of light: $\sim 510\text{--}700\text{ m}\mu$.

pletion layer. This is understandable by assuming that the inversion layer of zinc oxide no. 2 was destroyed by illuminating and outgassing. Curves similar to Figure 4 were obtained for phthalic acid-adsorbed and benzoyl peroxide-adsorbed zinc oxides (Figure 6).

An attempt was made to find any difference in adsorption behavior between benzoic acid and phthalic anhydride. A weighed amount of zinc oxide was thrown into toluene or alcoholic solutions of different concentration of benzoic acid or phthalic anhydride and the change in solute concentration after stirring for 1 hr. was plotted against the initial concentration. The concentration was determined spectroscopically at the wave length of $295\text{ m}\mu$ in the case of benzoic acid and of $290\text{ m}\mu$ in the case of phthalic anhydride. A stirring time of 1 hr. was experimentally confirmed to be enough to establish the adsorption equilibrium for both adsorbates. From the results shown in Figures 7 and 8, it is obvious that most of the added benzoic acid was consumed by zinc oxide up to the molar ratio of 2:1 to zinc oxide. On the other hand, only a few per cent of phthalic anhydride was adsorbed. The intensification of adsorption by light from the mercury lamp is considered to be an indication of chemisorption. No effect of light was observed on the adsorption of benzoic acid. These results strongly suggest that benzoic acid reacts with zinc oxide in toluene.



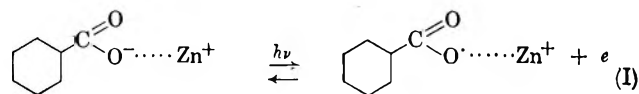
When the amount of benzoic acid is small, however, interstitial zinc atoms will be attacked first by the acid.



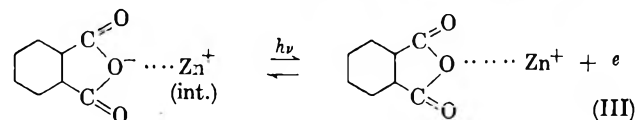
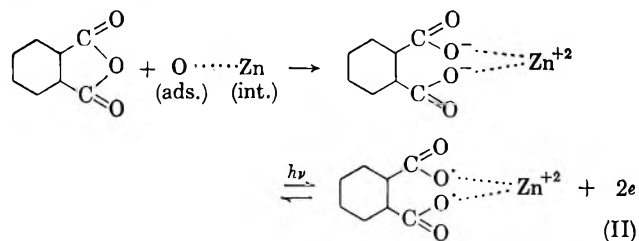
Evidence for the first reaction was given by the fact that benzoic acid-treated zinc oxide (in toluene) completely dissolved in diluted aqueous ammonium hy-

droxide solution, whereas untreated zinc oxide did not. The difference in adsorption behavior between acid and acid anhydride is possibly responsible for the difference in the sensitizing behavior at the higher concentrations in Figures 2 and 3.

Possible mechanisms of the sensitization of zinc oxide by organic acid and acid anhydride are listed below. For benzoic acid



For phthalic anhydride



The second possibility assumes catalytic oxidation of acid anhydride and after that sensitization takes place just as well as in the first one. This mechanism is plausible to interpret the similarity of acid and acid anhydride in sensitizing behavior at the lower concentrations. The mechanism, however, can be decided only from additional experimental information. In a recent publication, Markevich and Putseiko¹⁰ concluded that chemisorbed oxygen served as the adsorption center for acidic dyes. This also provides a quite interesting suggestion for the present case. There is nothing to disprove the reasoning that the adsorption of phthalic anhydride takes place similarly to that of acidic dyes.

II. Desorption of Oxygen during Optical Sensitization

Photodesorption of oxygen from zinc oxide has been reported by several workers.¹¹⁻¹³ The same phenomenon was observed for the first time in the course of the optical sensitization with various dyestuffs. The experimental apparatus used is illustrated in Figure 9.

(10) N. N. Markevich and E. K. Putseiko, *Kinetika i Kataliz*, **4**, 307 (1963).

(11) D. B. Medved, *J. Chem. Phys.*, **28**, 870 (1958).

(12) Y. Fujita and T. Kwan, *Bull. Chem. Soc. Japan*, **31**, 379 (1958).

(13) A. Terenin and Y. Solonitzin, *Discussions Faraday Soc.*, **28**, 28 (1959).

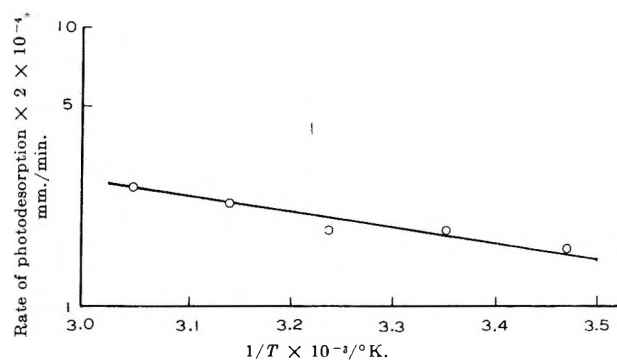


Figure 13. Temperature dependence of the oxygen photodesorption rate; ZnO used: dyed with 0.002 mole % rose bengal; excitation: 510–700 $m\mu$, 1.5×10^{-3} w./cm.².

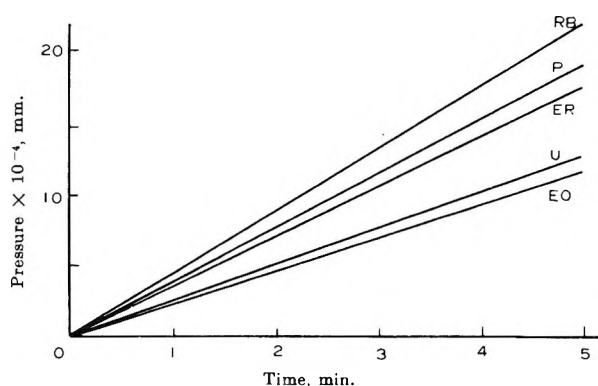


Figure 14. Photodesorption of oxygen from ZnO dyed with p-type dyestuffs; RB, rose bengal; P, phloxine; ER, erythrosine B; U, uranine; EO, eosine; concentration: 0.002 mole %; excitation: ~ 510 –700 $m\mu$, 1.5×10^{-3} w./cm.².

The amount of oxygen photodesorbed was measured *via* the pressure increase in the sample container and plotted against the illumination time. Figure 10 shows the results obtained with various concentrations of rose bengal. The satisfactory correspondence between the rate of photodesorption and the sensitized photocurrent in Figure 11 strongly indicates that the two processes are common in origin. Additional evidence for that is given by the same light intensity dependence of the two processes (Figure 12). A value of 0.04 e.v. was obtained for the thermal activation energy of photodesorption in the temperature range in Figure 13. The photodesorbed gas was examined with a mass spectrometer and also with a gas chromatograph. Within the experimental accuracy of 1%, no decomposition fragments from the dye molecules were found. The amount of photodesorbed oxygen was compared for various kinds of n-type and p-type dyestuffs. As is observed in Figures 14 and 15, the amount increased in the order:

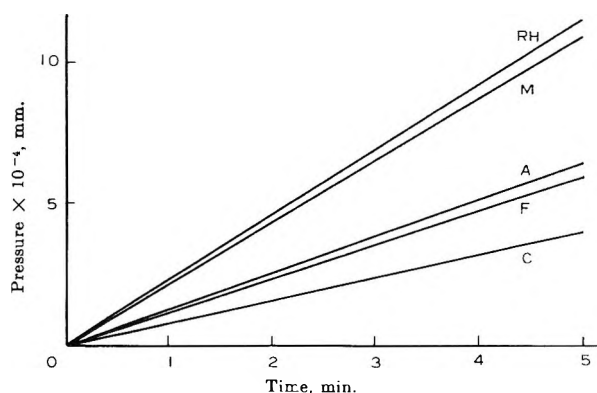


Figure 15. Photodesorption of oxygen from ZnO dyed with n-type dyestuffs; RH, rhodamine B; M, methylene blue; A, acridine orange; F, fuchsine; C, crystal violet; concentration: 0.002 mole %; excitation: ~ 510 –700 $m\mu$, 1.5×10^{-3} w./cm.².

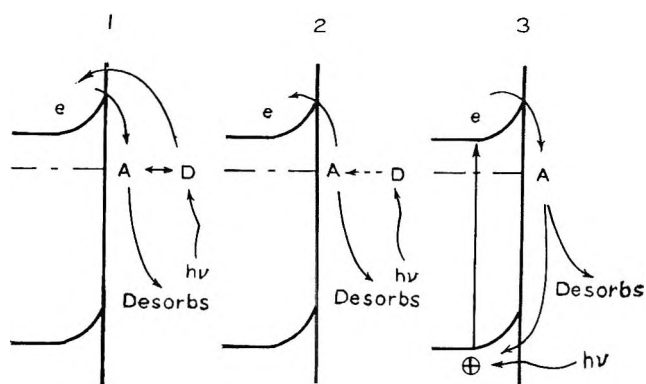


Figure 16. Mechanisms for the optical sensitization: (1) Weigl's mechanism: $A + e \rightarrow A^-$ (in the dark); $D + h\nu \rightarrow D^+ + e$ (into the conduction band); $D^+ + A^- \rightarrow D + A$. (2) Terenin's mechanism: $D + h\nu \rightarrow D^*$; $D^* + A^-$ (or T^-) $\rightarrow D + A$ (or T) + e ; A (or T) + $e \rightarrow A^-$ (or T^-) (in the dark). (3) When the dye is absent: $A + e \rightarrow A^-$ (in the dark); $h\nu \rightarrow \oplus + e$; $A^- + \oplus \rightarrow A$. D, dye molecule; A, electron-affinitive molecule (oxygen, phthalic anhydride, or others); T, electron trap other than A; \oplus , hole.

eosin, uranine, erythrosine B, phloxine, rose bengal for p-type dyestuffs, and crystal violet, fuchsine, acridine orange, methylene blue, rhodamine B for n-type dyestuffs, in accord with the order of increasing sensitizing efficiency for photoconduction.

At the present stage, it is still too difficult to determine the mechanism of optical sensitization. In light of the present experiment, however, two of several proposed mechanisms seem to survive: one proposed by Weigl⁶ (Figure 16 (1)) which involves the electron transfer from dye molecules to zinc oxide and the other proposed by Terenin and co-workers⁴ (Figure 16 (2))

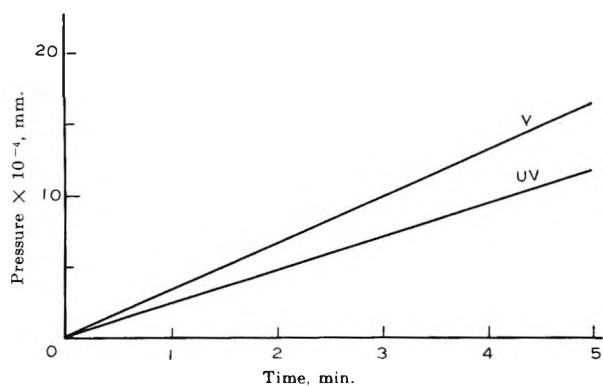


Figure 17. Photodesorption of oxygen from ZnO dyed with rose bengal: V, $\sim 510\text{--}700\text{ m}\mu$ excited; UV, $\sim 360\text{--}370\text{ m}\mu$ excited; rose bengal concentration: 0.002 mole %; light intensity: $7.5 \times 10^{-4}\text{ w./cm.}^2$.

which involves the energy transfer. Another mechanism suggested by Drudkowski and Grossweiner,⁸ who applied the concept of a compensated acceptor, is of interest but only for chemisorbed oxygen-free zinc oxide.

III. Interacting Sensitization of EAM and Dyestuff—Hypersensitization

It has been established that the desorption of oxygen from the zinc oxide surface occurs during the dye sensitization of photoconduction. On the other hand, the photodesorption of oxygen from zinc oxide under ultraviolet light illumination is well known to increase the electron density (Figure 16 (3)). The rate of oxygen release by ultraviolet light was compared with that by visible light of the same intensity (Figure 17). The fact that oxygen can be desorbed by either ultraviolet or visible light provides a possibility of interacting sensitization when dyed zinc oxide is exposed to light which includes both regions of wave length. If the rate-determining step for photoconduction is the bimolecular recombination of oxygen atoms discharged at the surface of zinc oxide, the coirradiation would greatly increase its opportunity because of higher atomic concentration and, consequently, the photocurrent would be higher than the sum of those under separate irradiation. Figure 18 shows that this is actually the case. This superposing effect¹⁴ should be distinguished from the hypersensitization effect described below.

The term "hypersensitization" is given to the phenomenon that coaddition of EAM and dyestuff yields an enormous increase of photocurrent in zinc oxide in the visible region. This was observed with most of the electron-affinitive substances examined. The spectral response of hypersensitization is reproduced in Figure 19. Here, supposedly, the electron-

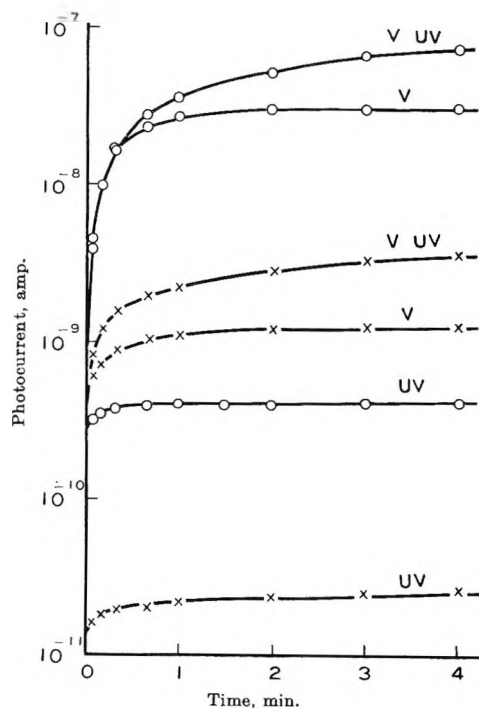


Figure 18. Superposing effect of photoconduction: O, ZnO with chemisorbed oxygen + 0.002 mole % rose bengal; X, ZnO with chemisorbed oxygen + 0.002 mole % rose bengal + 0.03 mole % *p*-chloranil; V, 577 $\text{m}\mu$ excited; UV, 365 $\text{m}\mu$ excited.

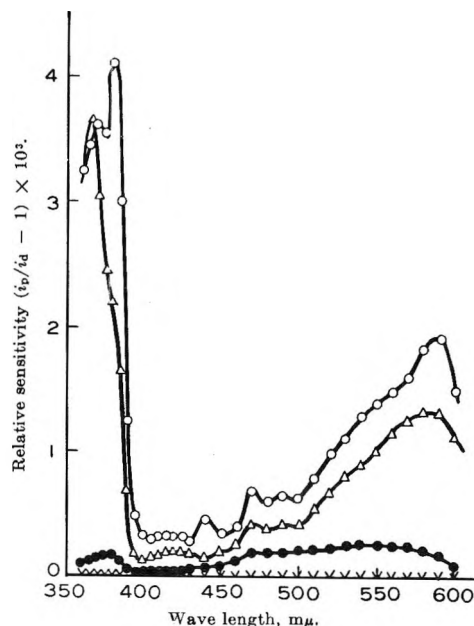


Figure 19. Hypersensitization of zinc oxide photoconduction: ●, basic system (dyed ZnO with 0.002 mole % rose bengal); ○, basic system + phthalic anhydride (0.02 mole %); Δ, basic system + iodine (0.03 mole %); X, basic system + *p*-chloranil (0.03 mole %); light intensity: $4 \times 10^{-4}\text{ w./cm.}^2$.

affinitive molecule cooperates with the dye molecule in the optical sensitization process; in other words, the optical sensitization is intensified by the electron-affinitive molecule. This appears to favor Weigl's mechanism for optical sensitization, in which a direct interaction between a positively charged dye ion and a negatively charged electron-affinitive molecule ion is postulated. This mechanism would allow one to interpret the photosensitivity in terms of the nature and the surface density of both the dye and the electron-affinitive molecule. It is surprising that the wave length of effective light was so widely extended that the photore-

sponse curves cover a new region where only negligible sensitivity had been observed before the coaddition of EAM. The reason for that is not yet clear. The negligible photosensitivity might be emphasized by the interaction between the two adsorbates, or a new absorption due to the interaction might arise there.

Acknowledgment. The authors wish to thank Mr. Isamu Maki for his earnest assistance with the experimental details.

(14) Terenin and his co-workers,⁴ who also observed this superposing effect, ascribed it to an accumulation of trapped carriers caused by the simultaneous exposure to ultraviolet light.

Color Sensitization of Zinc Oxide with Cyanine Dyes¹

by Susumu Namba and Yasushi Hishiki

The Institute of Physical and Chemical Research, Bunkyo-ku, Tokyo, Japan (Received October 5, 1964)

The photoconductivity of zinc oxide can be supersensitized by dyeing the surface with concentrated solutions of cyanine dyes or combinations of two cyanine dyes which have been used in the field of photographic sensitization. The time response of the photoconductivity of zinc oxide can be modified over the range of two decades by the effect of the adsorbed dyes.

Introduction

The photoconductivity of zinc oxide can be sensitized for wave lengths longer than the fundamental absorption wave length of the host crystal by the effect of adsorbed dyes on the surface.^{2,3} It also can be supersensitized by dyeing the surface with a concentrated solution of a cyanine dye or combinations of two cyanine dyes.^{4,5}

Although many kinds of cyanine dyes were used to sensitize the photoconductivity of zinc oxide, the following special features of interest are pointed out. (1) Some dyes show the supersensitizing character in the presence of *J*-band aggregation on the surface of zinc oxide which is similar to the case of silver halides. (2) Some dyes show the supersensitizing character under the existence of other special dyes (which is similar to

the case of silver halide). (3) The time response of photoconductivity of zinc oxide is fast when ZnO is sensitized by some particular group of dyes, and is slow when ZnO is sensitized by other groups of dyes.

Experimental

(1) *Zinc Oxide Powder Cell.* As shown in Figure 1(a), ZnO powder cells were prepared by applying ZnO paste on a glass substrate on which aluminum electrodes

(1) Presented to the International Conference on Photosensitization in Solids, Chicago, Ill., June 22-24, 1964.

(2) J. A. Amick, *RCA Rev.*, **20**, 770 (1959).

(3) S. J. Dudkowski and L. I. Grossweiner, *J. Opt. Soc. Am.*, **54**, 486 (1964).

(4) Y. Hishiki, *et al.*, *Rept. Inst. Phys. Chem. Res. (Tokyo)*, **36**, 386 (1960).

(5) S. Namba and Y. Hishiki, *ibid.*, **39**, 27 (1963).

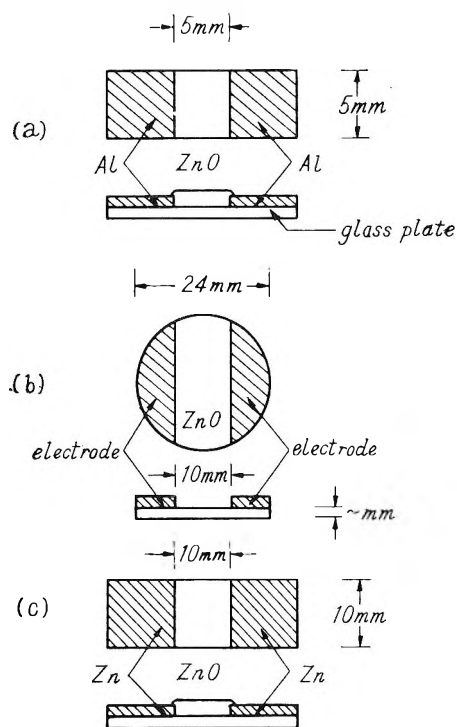


Figure 1. Experimental arrangement of the ZnO powder cell (a), sintered cell (b), and thin film cell (c).

were predeposited, and drying in a desiccator in a dark room. The thickness of ZnO was about 20μ . ZnO powder was dyed with various cyanine dyes.

(2) *ZnO Sintered Cell.* The chemically pure ZnO powder was compressed with pressures of the order of 1 ton/cm.² into a cylinder of 24-mm. diameter and heated in a crucible in air to a high temperature.

Electrodes were prepared by the evaporated metal film or silver paint as shown in Figure 1(b). Dark conductivity and photoresponse of the ZnO sintered cell were changed over a wide range by the temperature and the time of the sintering. Specimens were prepared by sintering at 750° for 3 hr. and dyeing with various cyanine dyes.

(3) *ZnO Thin Film Cell.* As shown in Figure 1 (c), ZnO thin films were prepared on glass or quartz substrates by oxidizing vacuum-deposited zinc films in air at 350° , and its dark conductivity was changed over a range of $\sim 10^4$ by the oxidizing time. The film thickness was measured by an interferometer to be about 1000 \AA . Curves I' and I of Figure 2 (c) show the transmission of the zinc film and the ZnO film.

Observation by electron diffraction showed that these films were zinc oxide with weak orientation of the C-axis perpendicular to the glass substrate. To avoid erratic contact between electrodes and ZnO films, zinc films of 1-cm. width were oxidized to a length of 1 cm. so that

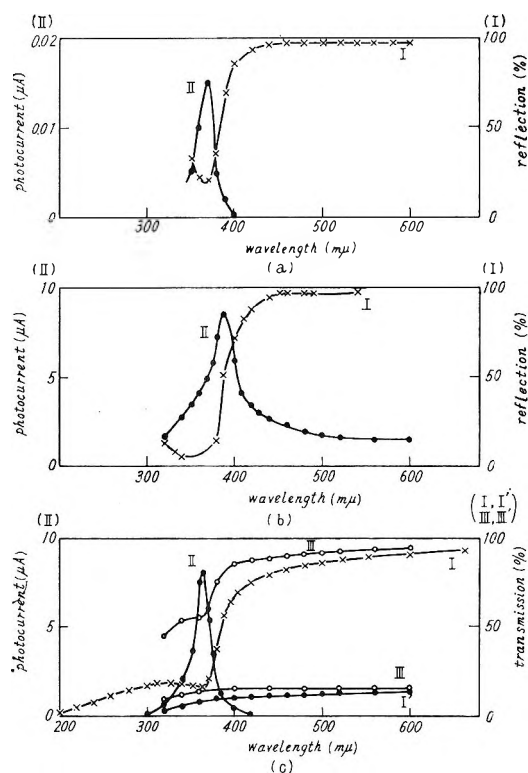


Figure 2. Absorption spectrum (I) and spectral response of photoconductivity (II) of ZnO: (a) powder cell; (b) sintered cell; (c) thin film cell.

the oxidized area was 1 cm.², and the unoxidized zinc films of both sides were used as electrodes.

(4) *Dyes.* For some representative cyanine dyes, the adsorption on zinc oxide was found to conform to the Langmuir isotherm from their aqueous or alcoholic aqueous solutions.

As cyanine dyes are less well adsorbed (about one-tenth) on zinc oxide compared with silver halides, concentrated dye solutions must be used. Typical dyes listed in Table I were used.

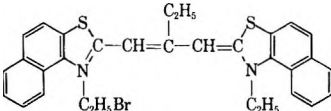
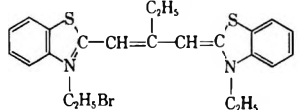
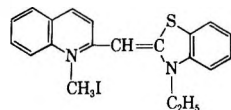
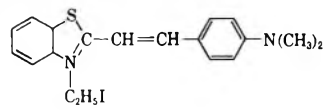
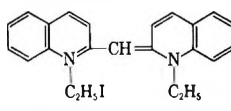
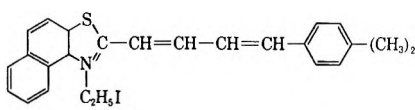
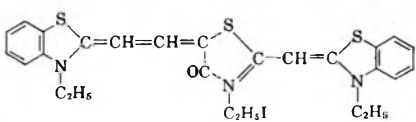
Supersensitization was obtained by using a *J*-aggregation of cyanine dye (for example, dye L) or a combination of two dyes (for example, dye M + dye K or dye H + dye Q).

Results

(1) *Color Sensitization.* The photoconductivity of ZnO is sensitized for the absorption band of many dyes which are adsorbed on the surface of ZnO, but supersensitization constitutes a problem of special interest of this report.

In this report, the light at fundamental absorption in ZnO is called ZnO-light, and the light at absorption in dye is called dye-light.

Table I: Names and Structures of Typical Dyes

Dye	Name and structure	Remarks
L	3,3'-Diethyl-9-ethyl-4,5,4',5'-naphthothiacarbocyanine bromide 	Supersensitization by <i>J</i> -band
H	3,3'-Diethyl-9-methylthiacarbocyanine bromide 	
Q	1-Methyl-3-ethyl-2,2'-monomethinequinothiacyanine iodide 	Supersensitization by combination of dye H + Q
K	3-Ethyl-2-(<i>p</i> -dimethylaminostyryl)benzothiazolinium iodide 	
M	1,1'-Diethyl-2,2'-quinocyanine iodide 	Supersensitization by combination of dye K + M
S	3-Ethyl-2-(<i>p</i> -dimethylaminophenyltetramethine)-4,5-naphthothiazolinium iodide 	Characteristic "slow time response"
T	3-Ethyl-5-[(3-ethyl-2(3H)-benzothiazolylidene)-ethylidene]-2-[(2-benzothiazolylidene)methylene]-4-thiazolidone iodide 	Characteristic "fast time response"

(i) *Photoresponse in ZnO Cells.* Figure 2 shows examples of the spectral response of the photocurrent in ZnO powder, sintered, and thin film cells. In these cells the wave length of maximum absorption is about 365–370 μ , which coincides with the wave length of maximum photocurrent.

The large photoconductivity of ZnO thin film cells can only be observed by the specially prepared films described previously. ZnO films can also be obtained by oxidizing the evaporated ZnO film in which the

evaporation material is ZnO powder, but these films do not have any measurable photoconductivity. Curves III' and III of Figure 2 (c) show the transmission of the zinc film and the ZnO film prepared by using ZnO powder as the evaporation material. The film obtained by vacuum evaporation of ZnO is the metallic zinc film.

(ii) *Supersensitization with Dye L.* Figure 3 gives a typical example of the spectral response of photocurrent in ZnO powder cells which were sensitized with dye L at two different concentrations. Curve III

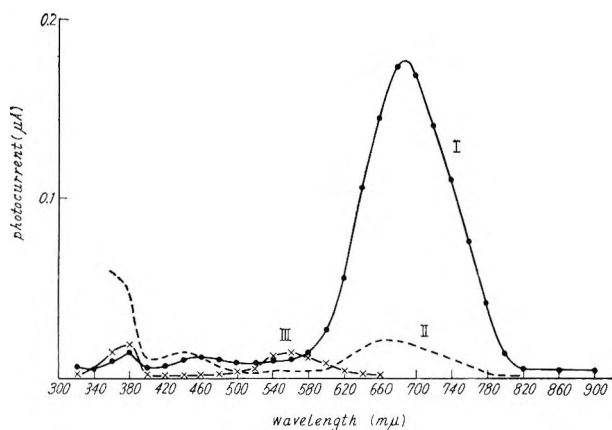


Figure 3. Spectral response of photoconductivity of ZnO powder cells sensitized with dye L: I, sensitized photoconductivity by *J*-band (slit width: constant); II, calculated curve from curve I (light energy: 125 $\mu\text{w.}/\text{cm.}^2$ constant); III, sensitized photoconductivity by molecular band (slit width: constant).

shows a peak of photocurrent at a wave length of 560 $m\mu$ corresponding to the molecular band of the dye, which is confirmed by the absorption measurement of a dilute solution of the dye. Curve I shows a large peak of photocurrent at a wave length of 670 $m\mu$ which seems to be caused by the *J*-aggregation of the dye.

(iii) *Supersensitization with the Combination of Dye K + Dye M.* Figures 4a, 4b, and 4c are presented as typical examples of the spectral response of photocurrent in ZnO thin film cells which were sensitized with dyes K, M, and K + M, respectively. Curves I and II of these figures show transparency of films before and after sensitization with dyes, and the difference between curves I and II corresponds to the net photon absorption by the dyes. A strong absorption over a wide spectral range of Figure 4c is caused by the enhanced absorption of dye M on the surface of ZnO, which is effected by the additional dye K acting as the supersensitizer. The *H*-band and *J*-band of dye M are located at 510 and 580 $m\mu$, respectively. Absorption bands of the solution of dye M are observed at 575 $m\mu$ (*J*-band), 525 $m\mu$ (*M*-band), and 490 $m\mu$ (*H*-band).

Curve III of Figure 4c gives the spectral response of a photocurrent whose peak coincides with that of absorption.

Curve IV of Figures 4a, 4b, and 4c is the photoreponse at the constant light illumination of 125 $\mu\text{w.}/\text{cm.}^2$, which is calculated from curve III.

(iv) *Supersensitization with the Combination of Dye Q + Dye H.* Table II is presented as a typical example of the spectral response of photocurrent in ZnO powder cells which were sensitized with dyes Q, H, and Q + H,

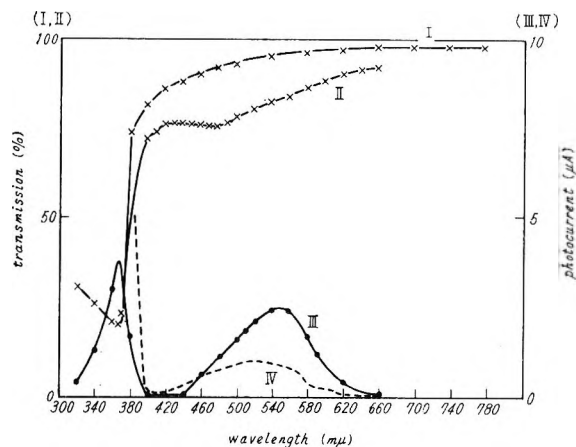


Figure 4a. Spectral response of the photoconductivity of ZnO thin film cells sensitized with dye K: I, transmission spectrum of ZnO thin films before dyeing; II, transmission spectrum of ZnO thin films after dyeing; III, spectral response of sensitized ZnO thin films (slit width: constant); IV, calculated curve from curve III (light energy: 125 $\mu\text{w.}/\text{cm.}^2$ constant).

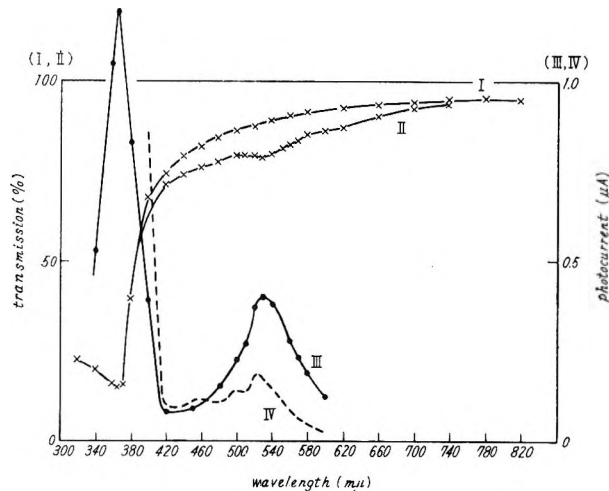


Figure 4b. Spectral response of photoconductivity of ZnO thin film cells sensitized with dye M: I, transmission spectrum of ZnO thin films before dyeing; II, transmission spectrum of ZnO thin films after dyeing; III, spectral response of sensitized ZnO thin films (slit width: constant); IV, calculated curve from curve III (light energy: 125 $\mu\text{w.}/\text{cm.}^2$ constant).

respectively. The photoconductivity of the sensitized cells is changed remarkably by the various concentrations of dye Q with constant concentration of dye H, but is unaffected by the various concentrations of dye H. Although the *J*-aggregation of dye Q has never been recognized, the sensitization effect may be caused by the enhanced adsorption of dye Q effected by dye H.

Figure 5 is a typical example of the spectral response of photocurrent in a ZnO sintered cell which was

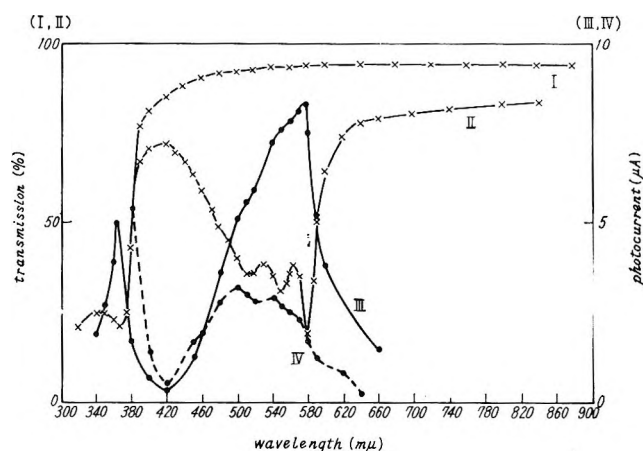


Figure 4c. Spectral response of the photoconductivity of ZnO thin film cells sensitized with dye K + M: I, transmission spectrum of ZnO thin films before dyeing; II, transmission spectrum of ZnO thin films after dyeing; III, spectral response of sensitized ZnO thin films (slit width: constant); IV, calculated curve from curve III (light energy: $125 \mu\text{w./cm.}^2$ constant).

Table II: Sensitization of ZnO Powder by Dye Q, Dye H, and a Combination of Dyes Q and H

Dye	Concn., wt. %	Max. photoconductivity	
		Wave length, mμ	Photocurrent, μA.
Q	0.10	490	0.0028
	0.05	490	0.0048
	0.03	500	0.0023
	0.02	500	0.0026
H	0.02	545	0.073
	0.01	560	0.038
Q	0.02	550	0.445
H	0.01		
Q	0.05	550	0.170
H	0.01		
Q	0.01	535	0.055
H	0.03		

sensitized with dye Q + H. Curves I and II are spectral responses before and after sensitization with dyes, respectively.

For all samples of ZnO film, dark current and photocurrent by the ZnO-light after dye sensitization are always decreased compared with that before the sensitization. This result shows that photocurrent by the ZnO-light is competitive with that by the dye-light. Current carriers excited in dyes by absorption in the wave length of dye-light will be transferred in the ZnO base and will contribute to the photocurrent, but in contrast to this, a part of the current carriers excited in the ZnO

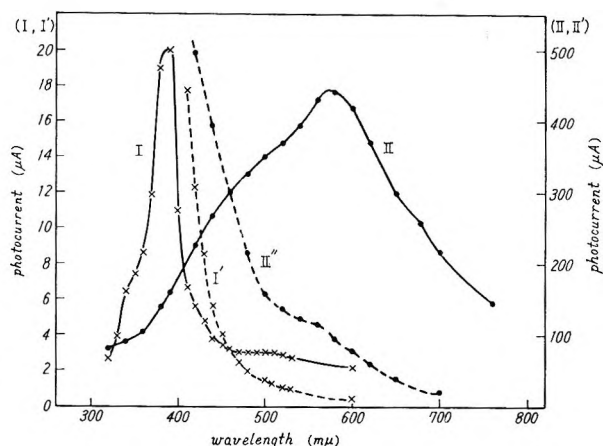


Figure 5. Spectral response of photocurrent in ZnO sintered cells sensitized with dye Q + H: I, spectral response before sensitization (slit width: constant); II, spectral response after sensitization (slit width: constant); I', II', calculated curves from curves I and II (light energy: $125 \mu\text{w./cm.}^2$ constant).

base by photoabsorption in the wave length of ZnO-light will be trapped by the adsorbed dyes and will not contribute to the photocurrent.

(2) *Time Response.* It is well known that the photoconductivity of ZnO shows two kinds of the time response, *i.e.*, the slow process and the fast process. The slow process is associated with a sluggish rise and fall of the photoconductivity and with an irreversible response under vacuum. In contrast to this, the fast process corresponds to a rapid rise and fall of the photoconductivity.

The photoconductivity of the thin film or sintered cells seems to be mainly a slow process with buildup and decay times of approximately several tens of minutes, in which chemisorbed oxygen on the surface of ZnO plays the leading role. The decay of photoconductivity can be explained by the Elovich equation which is given for the rate of chemical adsorption of oxygen.

The photoconductivity of the ZnO powder seems to be mainly a fast process, having buildup and decay times of approximately several seconds. The time response of the photoconductivity of ZnO can be modified by the effect of the adsorbed dyes.

Many kinds of dyes were examined to measure the effect of the sensitization to the time response. ZnO dyed with styryl dyes such as dye S has a slow photoresponse, the buildup and decay times being about 20 and 80 sec., respectively. ZnO dyed with some kinds of rhodacyanine, however, has a fast photoresponse, the buildup and decay times being shorter than 1 sec. Among the rhodacyanines, the most effective dyes to give shorter response time are characterized by the

benzothiazole nucleus at the 2-position of thiazolidone. One of the effective dyes is dye T, which gives a very fast response of about 0.2 sec.

Summary

The photoconductivity of ZnO, as well as silver halides, was sensitized with cyanine dyes. The experimental results are listed in this summary.

(1) In the dyed ZnO, the wave length of the maximum photocurrent coincides with the absorption maximum caused by the adsorbed dye.

(2) After dye sensitization, the photocurrent at the wave length of the fundamental absorption in ZnO is always decreased compared with that before the sensitization.

(3) In the ZnO dyed by dye L, the wave lengths of maximum photocurrent vary with the degree of aggregation of the adsorbed dye, and a supersensitization at the absorption wave length caused by *J*-aggregation of the dye is observed.

(4) In the ZnO dyed by the combination of special dyes, the adsorption of one dye is enhanced by the effect of the other dye, and a supersensitization at the absorption wave length of the dye showing enhanced adsorption is observed.

(5) The time response of photocurrent in the ZnO powder varies from 0.2 to 20 sec., according to the nature of the adsorbed dyes; rhodacyanine dyes make the time response fast, and styryl cyanine dyes make it slow.

Effect of Gases on the Conductivity of Organic Solids. III. Sensitization of Bulk Photoconductivity in *p*-Chloranil Crystals^{1a,b}

by P. J. Reucroft, O. N. Rudyj, R. E. Salomon,^{1c} and M. M. Labes

The Franklin Institute Laboratories, Chemistry Division, and Department of Chemistry, Temple University, Philadelphia, Pennsylvania (Received October 5, 1964)

Enhancement of bulk photoconductivity has been obtained on exposing *p*-chloranil, an electron-acceptor crystal, to electron-donor vapors such as ammonia and aliphatic amines. The sensitization occurs mainly in the most photosensitive regions of the unexposed crystal photocurrent spectrum. Ambient gas-induced photosensitization in the charge-transfer absorption bands of the respective donor-acceptor systems is not markedly different from other spectral regions. An unusually photoconductive region is found at wave lengths longer than 450 m μ in the photocurrent spectrum of the unexposed crystal. A possible origin for the photocurrent in this spectral region is discussed.

Introduction

Investigations on the effect of donor-acceptor interaction on the conductivity of organic crystals have shown that, in general, conductivity increases are produced in systems where these interactions are operative. Many studies have found, for instance, that the bulk dark resistivity of charge-transfer com-

plex crystals, such as perylene-iodine or diamino-durene-chloranil, is usually much lower than the re-

(1) (a) Presented at the International Conference on Photosensitization in Solids, Chicago, Ill., June 22-24, 1964; (b) supported by the U. S. Air Force Cambridge Research Laboratories, Office of Aerospace Research, under Contract No. AF19(628)-1660; (c) Temple University; all other authors, Franklin Institute Laboratories.

sistivity of the parent components. It has also been shown that bulk dark conductivity increases occur when electron-donor organic crystals are exposed to electron-acceptor vapors^{2a} and *vice versa*.^{2b} Anthracene crystals exposed to iodine vapor were investigated as a donor crystal-acceptor vapor system, and *p*-chloranil (tetrachloro-*p*-benzoquinone) crystals exposed to aliphatic amine vapors were considered as typical acceptor crystal-donor vapor systems. In these cases common gases such as nitrogen, water vapor, sulfur dioxide, oxygen, and hydrogen chloride produce no discernible effects on the bulk dark conductivity. The effect was, therefore, discussed in terms of a bulk charge-carrier injection process, involving in some way the formation of a loosely bound donor-acceptor complex at the surface of the crystal. In these crystal-ambient vapor systems the conductivity effects were reversible upon evacuating the conductivity cell.

In order to elucidate further the role of donor-acceptor interactions in these ambient gas-induced phenomena, a study of photoeffects was initiated, a prime objective being to assess the effect of illumination in the charge-transfer absorption bands of various amine-chloranil systems. The amine-chloranil systems were chosen in spite of the low photoconductivity in *p*-chloranil crystals because (a) amines are generally less corrosive and easier to work with than iodine vapor, (b) different acceptor crystal-donor vapor systems can be studied easily by simply evacuating the crystal and exposing to a new amine, and (c) simple aliphatic amines do not appreciably absorb light of wave length longer than 240 $m\mu$ so that possible effects due to sensitization *via* the vapor phase can be eliminated.

Experimental

The crystal was arranged sandwich fashion between a semitransparent conducting electrode and a silver paint electrode. A grounded, silver paint guard ring was arranged on the crystal surface between the two electrodes in order to eliminate surface conductivity effects. Semitransparent electrodes were prepared by evaporating thin films of metallic silver or gold on to a quartz slide. Illumination occurred through the semitransparent electrode on to the crystal. These electrodes gave, in general, 10–50% transmission of the incident light.

Illumination with polychromatic light was accomplished with a Hanovia high pressure mercury lamp, mercury lines in the 340–580- $m\mu$ range being selected by means of a filter. A Bausch and Lomb grating monochromator No. 33-86-25 with either a SP-200 super pressure mercury lamp or a tungsten-iodine

light source was used for experiments with monochromatic light (exit slit dimensions 11.2×0.75 mm., entrance slit dimension 20×1.34 mm.). When light of wave length longer than 400 $m\mu$ was used, particular attention was given to the elimination of short wave length overtones accompanying the fundamental wave length. Corning filter No. 0-54 cleared the region between 400 and 600 $m\mu$, and filter No. 3-74 cleared the region up to 800 $m\mu$. The intensity of the monochromatic light was measured by means of a bismuth-silver thermopile in order to correct the photoconductivity to the same intensity throughout the wave length region considered.

Photo- and dark currents were measured by means of a Cary vibrating reed electrometer, Model 31-31V, and a Keithley d.c. power supply, Model 240. The conductivity cell could be evacuated to 10^{-4} to 10^{-5} mm. and the ambient vapor was allowed in to any desired pressure.

Results

Preliminary measurements with polychromatic light showed that the bulk photoconductivity of *p*-chloranil in the presence of ammonia, trimethylamine, or triethylamine vapor was enhanced compared to the value under vacuum or in an inert gas like N_2 . The enhancement was, in general, greater than a simple addition of the vapor-induced, bulk dark conductivity to the bulk photoconductivity of the unexposed crystal. Figure 1 shows typical current-voltage data which illustrates the effect of illumination and ambient trimethylamine at 20 mm. on the bulk conductivity of a chloranil crystal. Similar enhancement effects were observed with the semitransparent electrode at positive and negative potential.

Measurements with monochromatic light revealed that certain regions were more effective in promoting ambient gas-induced photocurrent enhancement. The bulk photocurrent-wave length spectrum for a chloranil crystal is first shown in Figure 2 (200–800 $m\mu$) corrected to an incident light intensity of 21 $\mu w./cm.^2$. The extinction coefficient is also shown demonstrating that, although a small photocurrent can be obtained in the region where the crystal strongly absorbs light (250–400 $m\mu$), an unusual photosensitivity exists between 450 and 600 $m\mu$, tailing off to longer wave lengths. This latter region is where the crystal absorbs light weakly.

Figure 3 shows the effect of three amine vapors on the photocurrent spectrum. The ratio of the photo-

(2) (a) M. M. Labes and O. N. Rudyj, *J. Am. Chem. Soc.*, **85**, 2055 (1963); (b) P. J. Reucroft, O. N. Rudyj, and M. M. Labes, *ibid.*, **85**, 2059 (1963).

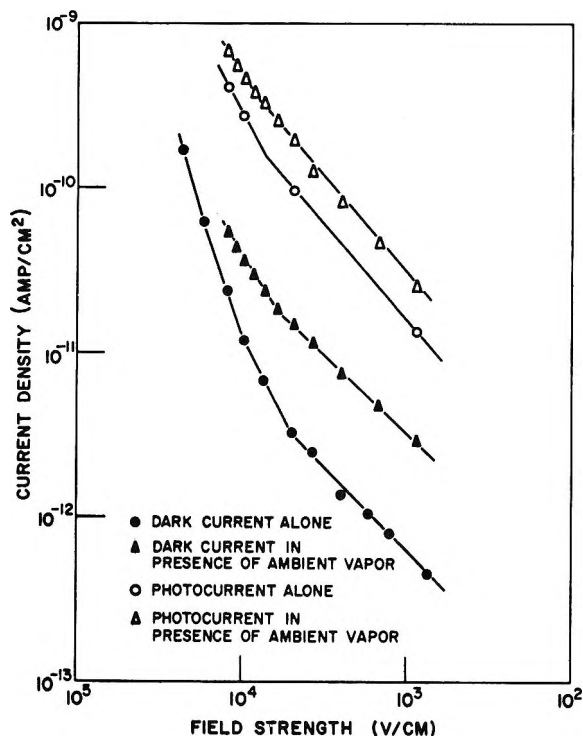


Figure 1. Bulk current-voltage plots for a *p*-chloranil crystal exposed to trimethylamine vapor at 20 mm.

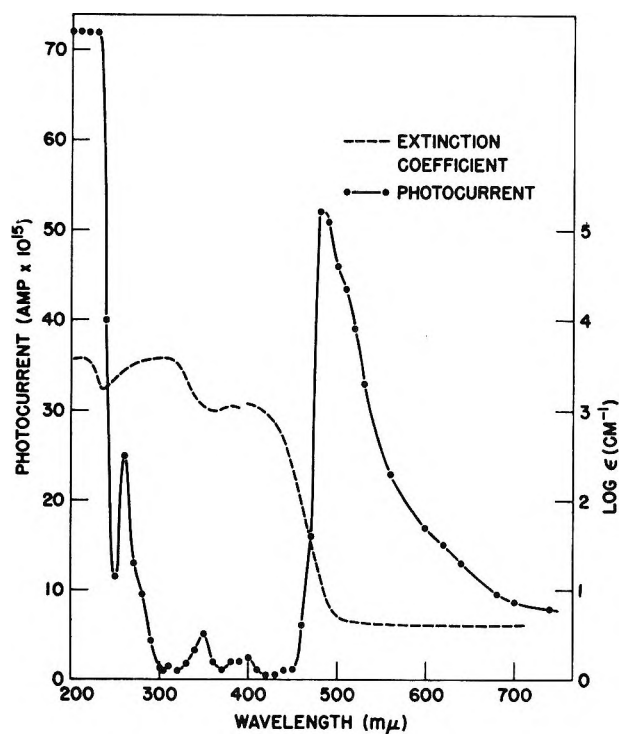


Figure 2. Extinction coefficient and bulk photocurrent spectrum for *p*-chloranil. (Photocurrent corrected to incident illumination intensity of $21 \mu\text{w./cm.}^2$.)

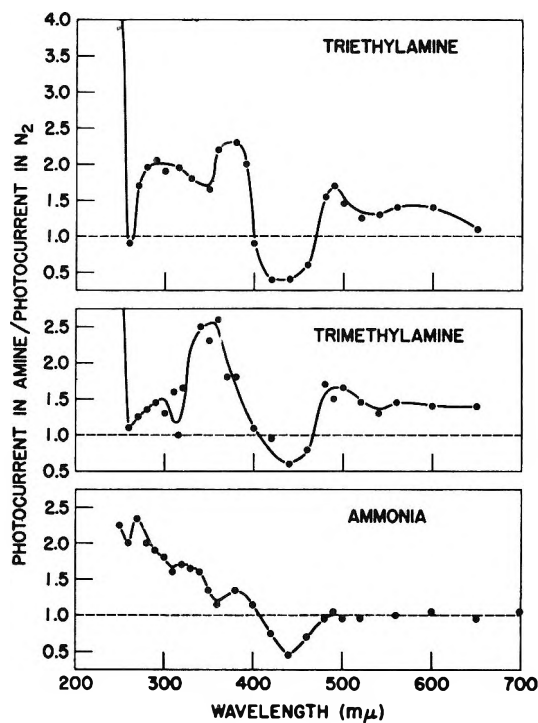


Figure 3. Bulk photocurrent enhancements produced in *p*-chloranil by amine vapors. (Ambient pressure, 20 mm.; incident intensity, $21 \mu\text{w./cm.}^2$.)

current in 20 mm. of amine vapor to the photocurrent in 20 mm. of dry nitrogen is plotted against wavelength of exciting light. The results are corrected to an incident light intensity of $21 \mu\text{w./cm.}^2$. Four features can be discerned. (1) The photocurrent-enhancement regions occur generally where the crystal is already strongly photosensitive before exposure to amine vapor. (2) The enhancement region between 250 and $400 \text{ m}\mu$ shows some resemblance to the absorption spectra of the chloranil crystal. (3) The enhancement between 260 and $280 \text{ m}\mu$ in ammonia is more pronounced than in either trimethylamine or triethylamine. (4) Both trimethylamine and triethylamine give a broad enhancement region between 460 and $650 \text{ m}\mu$ whereas no effect is found with ammonia. Earlier work indicated that ammonia was also capable of producing low enhancements in this spectral region, but later, more reliable data showed that the effect was negligibly small compared to that of the two amines.

Table I gives estimates of the charge-transfer absorption bands for the three amine-chloranil systems considered. The observed values were obtained from new absorption regions in the solution spectra of chloranil when amine vapor was bubbled through the solution. The calculated values were obtained from literature data on the charge-transfer absorption of the triethyl-

amine-chloranil system³ and data on the ionization potential of the three amines.⁴

Table I: Charge-Transfer Absorption in *p*-Chloranil-Amine Systems

System	Charge-transfer absorption region, m μ (obsd.) ^a	Charge-transfer absorption region, m μ (calcd.) ^b
Ammonia	...	275
Trimethylamine	390-490	550
Triethylamine	650	640, 655

^a Estimated from solution spectra. ^b Estimated from literature data on the triethylamine-chloranil system³ and ionization potential data,⁴ assuming

$$\nu_2 = \nu_1 + \frac{I_2 - I_1}{h}$$

where ν_1 = charge-transfer frequency for triethylamine-chloranil, ν_2 = estimated frequency, I_1 = ionization potential of triethylamine, and I_2 = ionization potential of trimethylamine or ammonia.

Discussion

The main conclusions can be summarized as follows. (1) Ambient-induced, photosensitized conductivity occurs primarily in the region of strong crystal light absorption. (2) A generally higher effect in ammonia vapor at 260-280 m μ may possibly be attributed to absorption in the ammonia-chloranil charge-transfer absorption band. (3) While both trimethylamine and triethylamine give enhancements in the general region of their respective charge-transfer absorption bands, the similarity in the two enhancements suggests that this excitation is not the dominant cause of photosensitization for these systems in this spectral region.

It can, therefore, be concluded that, although electron-donor vapors influence the bulk photoconductivity of electron-acceptor crystals by a process which probably involves surface donor-acceptor interaction, no especially marked effects are produced in the charge-transfer absorption regions of the respective donor-acceptor systems. The general effect is to increase the sensitivity of the most photosensitive regions in the unexposed crystal.

The mechanism of ambient-induced photosensitization is not readily explained. One possibility that might be considered is that the charge-transfer complex at the surface increases the efficiency of dissociation of excitons into charge carriers. This is a reasonable explanation for the photosensitization in the region where the crystal strongly absorbs light. Photo-carrier production in organic crystals in these regions

is usually attributed to exciton dissociation at the crystal surface since most of the incident illumination is absorbed in the first few molecular layers of the crystal. The photosensitization where the crystal weakly absorbs light, however, probably involves another process since photocarrier generation will take place uniformly through the bulk of the crystal. In this case a surface-induced detrapping of charge carriers may be involved.

The absence of special effects in the charge-transfer absorption regions suggests that the donor-acceptor ground state is mainly responsible for the conductivity enhancements rather than the excited state. In the case of aliphatic amine-quinone systems it is not known with certainty whether the ground state is dominated by the dative form of the complex or the "no-bond" form. It is, thus, not possible to say unambiguously which form of the complex is responsible for the enhancement effects.

Adsorption studies currently being initiated are expected to contribute to an understanding of these phenomena, but, at the present time, a complete description of the ambient-induced photosensitization is not possible.

Figure 2 demonstrates the unusual photosensitivity in the chloranil crystal at wave lengths longer than 450 m μ . The origin of the photosensitivity in this spectral region is not clear at the present time and represents an interesting feature in the photoconductivity of chloranil. Although the absorption of light by the crystal is weak in this region, an absorption tail can be measured extending up to wave lengths as long as 700 m μ with an extinction coefficient on the order of 4 cm.⁻¹. Measurements of the absorption spectrum of *p*-chloranil dissolved in methyl iodide show an increased absorption at 500-700 m μ compared to the spectrum in chloroform. These observations suggest the presence of a singlet-triplet absorption, enhanced in the methyl iodide solvent by external heavy-atom spin-orbital coupling⁵ and just discernible in the crystal spectra because of the high concentration of absorbing species. Singlet-triplet absorption spectra have not been reported in *p*-chloranil, but Sidman has tentatively assigned a weak absorption at 500-600 m μ in the spectrum of benzoquinone, to an $n \rightarrow \pi^*$ singlet-triplet transition.⁶

(3) (a) S. K. Chakrabarty and A. K. Chandra, *Naturwiss.*, **49**, 206 (1962); (b) J. B. Birks and M. A. Slifkin, *Nature*, **197**, 42 (1963).

(4) K. Watanabe, *J. Chem. Phys.*, **26**, 542 (1957).

(5) (a) S. P. McGlynn, R. Sunseri, and N. Christodouleas, *J. Chem. Phys.*, **37**, 1818 (1962); (b) S. P. McGlynn, T. Azumi, and M. Kasha, *ibid.*, **40**, 507 (1964); (c) M. Kasha, *ibid.*, **20**, 71 (1952).

(6) J. W. Sidman, *J. Am. Chem. Soc.*, **78**, 2363 (1956).

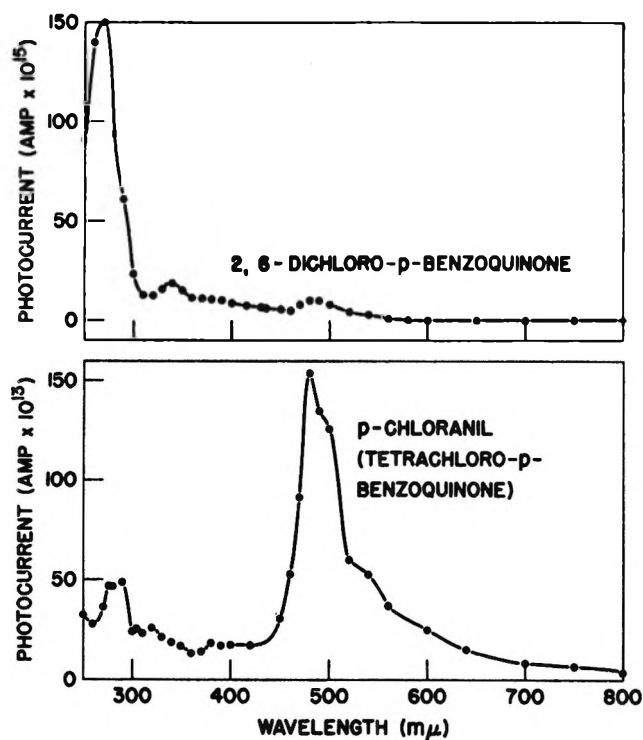


Figure 4. Photocurrent spectra of substituted benzoquinones. (Ambient pressure, 760 mm. of dry N_2 ; incident intensity, $21 \mu w./cm.^2$.)

It is, therefore, a possibility that the anomalous, long wave length photocurrent is in some way connected with a weak $n \rightarrow \pi^*$ triplet absorption in the crystal. Such transitions are expected to be more marked in the case of chloranil than in benzoquinone because of the spin-orbital coupling effect of the substituted chlorine atoms. If the triplet is involved in the photoconductivity it may be expected that this photocurrent would be increased in the series *p*-benzoquinone < dichloro-*p*-benzoquinone < tetrachloro-*p*-benzoquinone. Measurements on 2,6-dichloro-*p*-benzoquinone and *p*-benzoquinone show that the photoconductivity in the long wave length region is, indeed, much smaller in dichloro-*p*-benzoquinone in comparison to the photoeffect in the short wave length region, and no photoeffect at all could be

observed in benzoquinone in any region of the spectrum. Figure 4 shows the photocurrent spectrum of chloranil compared with that of 2,6-dichloro-*p*-benzoquinone. Grounded guard ring circuitry was dispensed with in these measurements in order to detect the weak photocurrent in 2,6-dichloro-*p*-benzoquinone.

The possible intermediacy of the first excited triplet state in the photocarrier generation process in organic crystals has been considered before.^{7,8} Kleinerman and co-workers⁸ have concluded that the production of photocarriers proceeds more probably from the lowest excited singlet state than from the lowest excited triplet state. The latter conclusion was formed after an examination of the photoconduction characteristics of several sets of molecular crystals, *e.g.*, anthracene, acridine, and phenazine, where the relative singlet-triplet populations are known from fluorescence-phosphorescence data. In the case of chloranil, however, the long wave length photosensitivity may arise from a process where trapped charge carriers are detrapped by triplet excitons. This mechanism has been suggested to explain weak photocurrents observed in the triplet absorption region of anthracene⁹ and is likely to be more marked in the case of chloranil in view of the generally higher density of carrier traps in these crystals.¹¹

Impurity photosensitization cannot be entirely ruled out but would seem unlikely in view of the care taken in purifying the chloranil, *i.e.*, by recrystallization and sublimation, and in view of the similar results obtained for crystals grown in different media. Further work is proceeding on other substituted benzoquinone crystals, *e.g.*, bromanil and fluoranil, to ascertain whether the photoconduction characteristics found in chloranil are general in this class of crystals and to elucidate further the mechanism of photocarrier generation.

(7) B. Rosenberg, *J. Chem. Phys.*, **29**, 1108 (1958); **31**, 238 (1959).

(8) M. Kleinerman, L. Azarraga, and S. P. McGlynn, *ibid.*, **37**, 1825 (1962).

(9) J. Adolphe, E. Baldinger, and I. Granacher, *Physics Letters*, **8**, 224 (1964).

(10) P. J. Reucroft, O. N. Rudyj, and M. M. Labes, *J. Chem. Phys.*, **39**, 1136 (1963).

Exciton States in Polymers¹

by John S. Avery and Ronald Mason

*Departments of Chemistry, Imperial College, London, England, and University of Sheffield, Sheffield, England
(Received November 6, 1964)*

Calculations relevant to exciton states and exciton energy migration in polymers are summarized. In particular the effects of departures from strict periodicity are discussed.

Introduction

Since the original work of Frenkel² and Peierls³ on excitons in crystals of the alkali halides, considerable progress has been made in the application of exciton theory to such varied topics as the spectroscopy of molecular crystals⁴⁻¹⁰ and to the optical rotatory dispersion and hypochromism of proteins.¹¹⁻²² In these theories, it is implicitly assumed that the polymer has translational symmetry; it is also assumed that there are no significant impurities which may act as traps for excitation energy or, more generally, perturb the structure of the exciton band. Recently, spectra of mixed crystals,²³ such as anthracene-tetracene, have required the development of methods for dealing with the effects of impurities. The work presented here was prompted by the current interest in the properties of biopolymers which often lack strict periodicity, at least over distances greater than 50 Å. or so.

The Effect of a Sharp Change in the Lattice

In another paper²⁴ we have discussed the wave-like manner in which an initially localized excitation propagates along a polymer. In order to determine the effect of irregularities on such a traveling wave, it may be helpful to consider the following rather idealized example: suppose that we have a long chain, divided into two parts, in the first of which the exciton energy is related to its momentum by the function $E_1(k)$, and in the second by $E_2(k)$. If a monoenergetic exciton wave with amplitude α_1 is incident on the boundary, it will be reflected with a certain amplitude, call it β_1 , and transmitted with amplitude α_2 . Thus in region 1

$$\psi = \{\alpha_1 e^{ik_1z} + \beta_1 e^{-ik_1z}\} e^{-iEt/\hbar}$$

and in region 2

$$\psi = \alpha_2 e^{ik_2z - iEt/\hbar}$$

The traveling wave will be reflected at the discontinuity with a coefficient of reflection

$$R = \left| \frac{\beta_1}{\alpha_1} \right|^2$$

The constants α_1 and β_1 are determined by the requirements that the wave function, ψ , and the probability

- (1) Presented to the International Conference on Photosensitization in Solids, Chicago, Ill., June 22-24, 1964.
- (2) (a) J. Frenkel, *Phys. Rev.*, **37**, 17, 1276 (1931); (b) *Physik. Z. Sowjetunion*, **9**, 158 (1936).
- (3) R. E. Peierls, *Ann. Physik.*, **13**, 905 (1932).
- (4) G. H. Wannier, *Phys. Rev.*, **84**, 809 (1951).
- (5) W. R. Heller and A. Marcus, *ibid.*, **84**, 809 (1951).
- (6) A. S. Davydov, *Zh. Eksperim. i Teor. Fiz.*, **18**, 210 (1948).
- (7) D. P. Craig and P. C. Hobbins, *J. Chem. Soc.*, 539 (1955).
- (8) W. T. Simpson and D. L. Peterson, *J. Chem. Phys.*, **26**, 588 (1957).
- (9) M. Kasha, *Rev. Mod. Phys.*, **31**, 162 (1959).
- (10) A. S. Davydov, "Theory of Molecular Excitations," McGraw-Hill Book Co., Inc., New York, N. Y., 1962.
- (11) C. A. Coulson, *Proc. Roy. Soc. (London)*, **A164**, 383 (1938).
- (12) W. Moffitt, *J. Chem. Phys.*, **25**, 467 (1956).
- (13) W. Moffitt, D. D. Fitts, and J. G. Kirkwood, *Proc. Natl. Acad. Sci. U. S.*, **43**, 723 (1957).
- (14) W. Moffitt, *ibid.*, **42**, 736 (1956).
- (15) G. S. Levinson, W. T. Simpson, and W. Curtis, *J. Am. Chem. Soc.*, **79**, 4314 (1957).
- (16) D. L. Peterson and W. T. Simpson, *ibid.*, **79**, 2375 (1957).
- (17) I. Tinoco, Jr., *ibid.*, **82**, 4785 (1960).
- (18) I. Tinoco, Jr., *J. Chem. Phys.*, **33**, 1332 (1960).
- (19) W. Rhodes, *J. Am. Chem. Soc.*, **83**, 3609 (1961).
- (20) A. Rich and M. Kasha, *ibid.*, **82**, 6197 (1960).
- (21) I. Tinoco, Jr., R. W. Woody, and D. F. Bradley, *J. Chem. Phys.*, **38**, 1317 (1963).
- (22) D. F. Bradley, S. Lifson, and B. Honig in "Electronic Aspects of Biochemistry," B. Pullman, Ed., Academic Press, New York, N. Y., 1964, p. 77.
- (23) D. P. Craig, Proceedings of the Organic Crystal Symposium, National Research Council, Ottawa, Canada, 1962, p. 7.

current, S , be continuous across the boundary.²⁵ (We note that the gradient of ψ is not necessarily continuous, unless E is a quadratic function of k .) Solving for α_1 and β_1 we obtain

$$R = \left(\frac{\left. \frac{\partial E}{\partial k} \right|_{k=k_1} - \left. \frac{\partial E}{\partial k} \right|_{k=k_2}}{\left. \frac{\partial E}{\partial k} \right|_{k=k_1} + \left. \frac{\partial E}{\partial k} \right|_{k=k_2}} \right)^2$$

k_1 and k_2 are determined by the requirement that

$$E_1(k_1) = E_2(k_2) = E$$

Figures 1-3 show, for illustration, an idealized example where

$$E_1(k) = A \cos(kd)$$

and

$$E_2(k) = B \cos(kd) + C$$

In Figure 1, $A = 1$, $B = 1$, and $C = 0.6$, while Figure 2 shows the reflection coefficient R , again in the case where $A = 1$ and $B = 1$, for various values of C . Figure 3 shows R when $B = 1$ and $C = 0$ for values of A .

The Effect of Gradual Changes in the Lattice—A W.K.B. Approximation for Excitons

We can continue by considering an example in which $E(k)$ changes gradually as one moves along the lattice. For a simple monoenergetic wave of constant amplitude α propagating in a perfectly periodic chain, the probability current is just the square of the wave amplitude times the group velocity²⁵

$$S = \alpha^2 v_g$$

where

$$v_g = - \frac{1}{\hbar} \frac{\partial E}{\partial k}$$

If $E(k)$ varies slowly as a function of position, this expression for S will only be approximately valid, but if we nevertheless make use of it in expressing the requirement that S be continuous, we obtain

$$\alpha^2 \sim \frac{1}{\frac{\partial E}{\partial k}}$$

and

$$\psi(x) \sim \frac{1}{\sqrt{\frac{\partial E}{\partial k}}} e^{*i \int k dx} \tag{1}$$

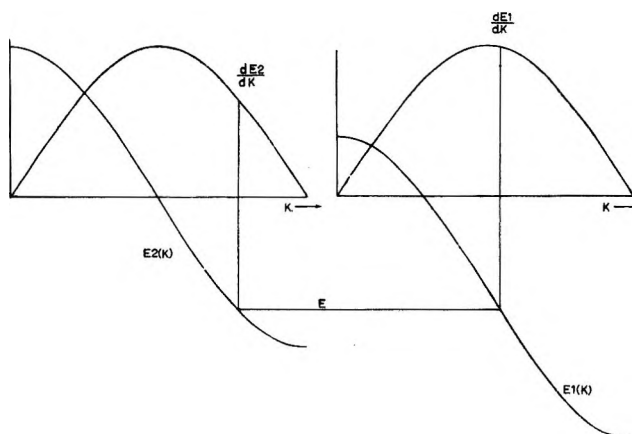


Figure 1. Energy, E , as a function of momentum, k , in two parts of an idealized chain. k_1 and k_2 , the momenta in the two sections, are found by requiring that $E_1(k_1) = E_2(k_2) = E$.

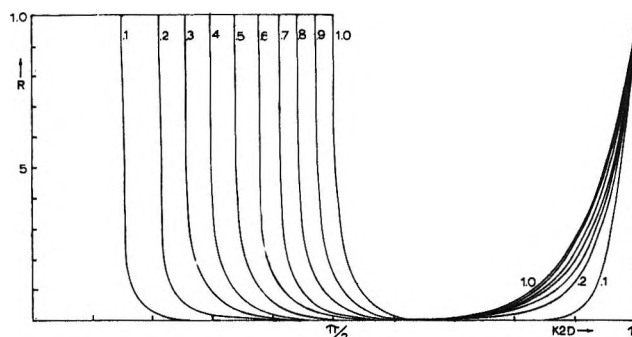


Figure 2. The reflection coefficient R in the idealized chain of Figure 1 in the case where $E_1(k) = \cos(kd)$ and $E_2(k) = \cos(kd) + C$. The various curves correspond to various values of C . The energies are expressed in units of the nearest neighbor coupling energy, and d is the length of the unit cell.

This expression for ψ reduces to the usual W.K.B. approximation in cases where E is a quadratic function of k . Figure 4 shows an example where the bias of $E(k)$ changes gradually as one moves along the polymer. The energy levels of the first few states in the exciton band are denoted by horizontal lines, and the corresponding wave functions are shown in Figure 5. The exciton wave functions, calculated from the expression 1, are represented by dashed curves, and may

(24) J. S. Avery, R. Mason, and L. G. Augenstein in "Quantum Aspects of Polypeptides and Polynucleotides," M. Weissbluth, Ed., Biopolymers, Symposia No. 1, Interscience Publishers, Inc., New York, N. Y., 1964, p. 259.

(25) J. S. Avery in "Electronic Aspects of Biochemistry," B. Pullman, Ed., Academic Press, New York, N. Y., 1964, p. 29.

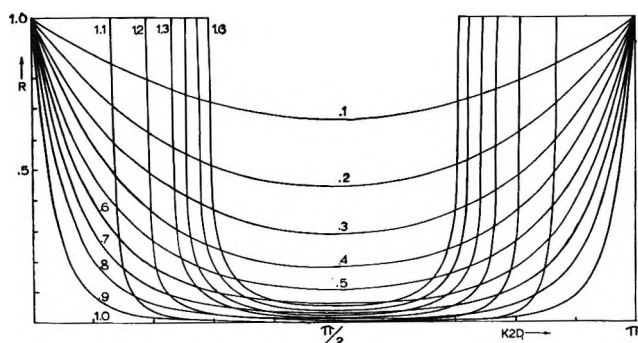


Figure 3. The reflection coefficient when $E_1(k) = A \cos(k_1 d)$ and $E_2(k) = \cos(k_2 d)$ for various values of A .

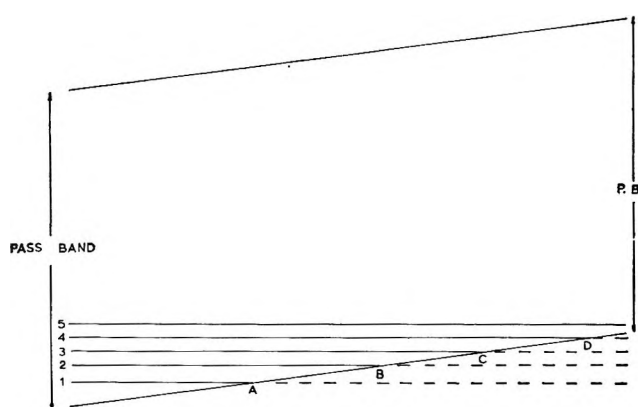


Figure 4. An idealized example where $E(k)$ is a gradually changing function of position $E(k) = \cos(kd) + 0.05x/d$.

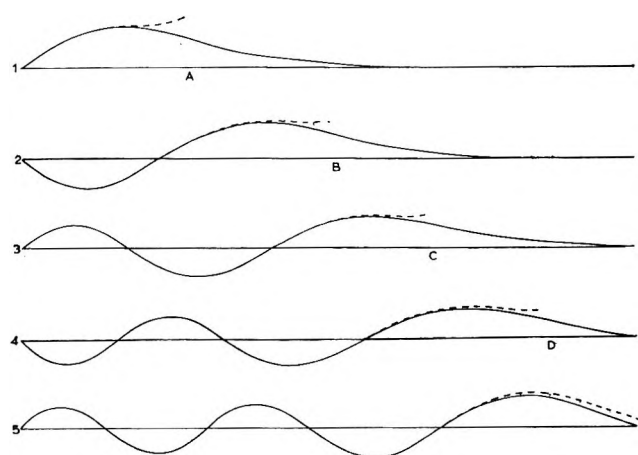


Figure 5. The first few exciton states in the band for $E(k)$ as shown in Figure 4 for a chain 20 residues long. The quasiparticle W.K.B. approximation (indicated by the dashed lines) is seen to agree very well with the exact solutions (solid lines) except, of course, in the neighborhood of the turning points.

be compared with the solid curves obtain by exact solution of the secular equations²⁶

$$\begin{aligned} (E_\xi \pm E_k)a_{k_1} + H'_{12}a_{k_2} + \dots + H'_{1N}a_{k_N} &= 0 \\ H'_{21}a_{k_1} + (E_\xi \pm E_k)a_{k_2} + \dots + H'_{2N}a_{k_N} &= 0 \\ \vdots & \\ H'_{N1}a_{k_1} + H'_{N2}a_{k_2} + \dots + (E_\xi \pm E_k)a_{k_N} &= 0 \end{aligned}$$

Agreement between the two sets of curves (except, of course, near the classical turning point), is indicative of the validity of approximation 1. It is interesting to notice that at the points A, B, C, and D, shown in Figures 4 and 5, where the energy of the exciton states becomes negative, the wave function has a point of inflection, that is, it changes from a sinusoidal form to an exponentially decaying form at the point where the value of k , obtained by solving $E(k, x) = E$, changes from real to imaginary. Thus, the exciton state tunnels to some extent into regions where it is energetically forbidden. An impurity (Figure 6) or the point at which a side chain is joined to a polymer (Figure 7) may be treated as small regions where $E(k)$ is a different function than in the remainder of the chain. Figures 6 and 7 show examples where exciton states are permitted only at such points, but tunnel into the remainder of the chain.

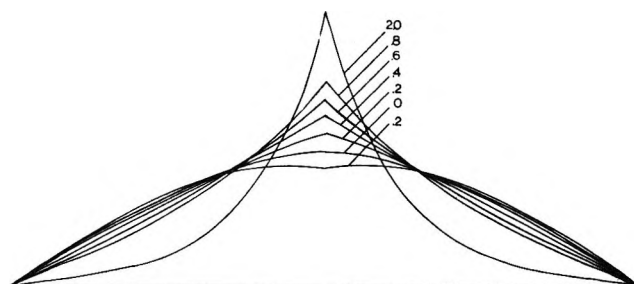


Figure 6. The first exciton state in the band (computed in the nearest neighbor approximation) for a chain 10 residues long with an impurity at the center. The numbers labeling the various curves correspond to various differences between the resonance energy of the normal residues and that of the impurity in units of the inter-residue coupling energy.

Irreversible Trapping and Directionality of Energy Transfer

In a situation such as that shown in Figures 3 and 4, the exciton states of highest energy are localized at one end of the chain, whereas those of lowest energy are localized at the other end. If a residue at the high end of the chain is initially excited, the energy will be transferred irreversibly to the low end by a two-step mechanism. First of all, the initially localized ex-

(26) J. S. Avery and R. Mason in "Physical Processes in Radiation Biology," L. G. Augenstein, R. Mason, and B. Rosenberg, Ed., Academic Press, New York, N. Y., 1964, p. 197.

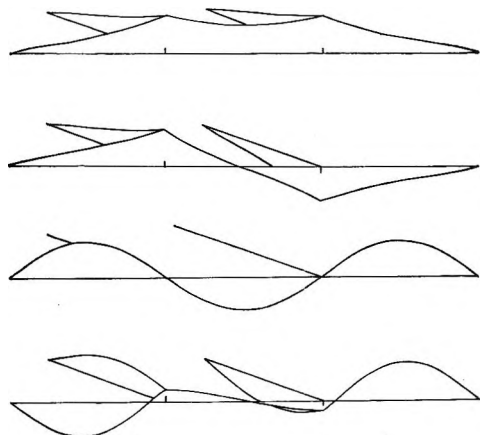


Figure 7. The first few exciton states for a chain having two branches. In this example, the first two states are energetically allowed only at the points of juncture but tunnel into the rest of the chain.

citation must be represented as a linear superposition of exciton eigenstates. As time progresses, the phase relationships between the eigenstates in the superposition change, and they no longer add together to form a localized state.²⁴ In this way, the excitation will spread rapidly along the chain with a wave-like motion. The velocity of the crest of the wave is given approximately by²⁴

$$v = \frac{H'_{12}d}{\hbar}$$

For typical polymers, v is of an order of magnitude between 10^6 and 10^7 cm./sec., so that the wave takes only 10^{-14} sec. to travel some 10^3 Å. The next step in this hypothetical process is the transfer of energy to vibrational modes of the polymer, with the result that the lowest exciton states will eventually predominate in the superposition. This will cause the delocalized

exciton to become relocalized and trapped at the low end of the chain. Such an energy-transfer mechanism could be important in biological systems, since it could provide a directionality and irreversibility to energy migration which would otherwise be random.²⁶⁻³¹

Discussion

It can be seen from the idealized examples given here that the exact forms of the exciton states, particularly those which are the highest and lowest in the band, are very sensitive to irregularities and aperiodicity. If we remember that even a protein like myoglobin, containing a high degree of helicity ($\sim 75\%$), lacks translational symmetry for distances greater than 35 Å. (the polypeptide chain consists of eight segments, each of them 7-24 residues long), it becomes clear that one ought to be cautious about applying an oversimplified exciton model to a study of the optical properties of such polymers. Hypochromism and, to an even greater extent, optical rotatory dispersion, will undoubtedly be sensitive to coupling with side chains and general lack of periodicity and in a way which will perhaps not be clear until the configurations are known in detail from crystallographic studies.

The particular question of desensitization and supersensitization of photographic emulsions by organic dyes can be treated, within the framework of an exciton model, by a formalism similar to that summarized here and will be discussed elsewhere.

(27) J. S. Avery, Z. Bay, and A. Szent-Gyorgyi, *Proc. Natl. Acad. Sci. U. S.*, **47**, 1742 (1961).

(28) L. G. Augenstein and R. Mason in "Electronic Aspects of Biochemistry," B. Pullman, Ed., Academic Press, New York, N. Y., 1964.

(29) A. Szent-Gyorgyi, "Bioenergetics," Academic Press, New York, N. Y., 1957.

(30) A. Szent-Gyorgyi, "Introduction to a Submolecular Biology," Academic Press, New York, N. Y., 1960.

(31) R. Mason, *Radiation Res. Suppl.*, **2**, 452 (1960).

An Electron-Hole Picture of Photosynthesis^{1a,b}

by William Arnold

Biology Division, Oak Ridge National Laboratory, Oak Ridge, Tennessee (Received October 5, 1964)

The present picture of the light reaction in photosynthesis consists of two (0.8-v.) electron transfers separated by an electron-transport chain. The arguments for this scheme make use of the information from spectral changes shown by plants upon illumination and by the oxidation or reduction of dyes added to illuminated chloroplasts. No use is made of the information from the fluorescence or the delayed light emitted by the plants. If we emphasize the information given by the two light emissions and neglect the chemical information, we are led to a picture of the light reaction in photosynthesis in which free electrons and holes play an essential part.

Introduction

Photosynthesis is the process by which green plants reduce CO₂ to carbohydrates and oxidize water to O₂. This act stores in the carbohydrate about 5.1 e.v. of free energy/atom of carbon. The energy comes from sunlight absorbed by chlorophyll. Since the process can go in red light, we know that the energy per quantum is about 1.8 e.v. Respiration of plants and animals and combustion of coal and oil reverse the process. The yearly turnover² of some 2×10^{11} tons of carbon in this cycle furnishes the energy for living things.

Research with radioactive carbon, largely by Calvin and associates,³ has shown that CO₂ does not take part in any photochemical reaction. Carbon reduction is a series of enzyme reactions that can take place in the dark. This Calvin cycle is driven by electrons at -0.4 v. and by ATP. The problem in photosynthesis is to show how chlorophyll and light can lift an electron from the level of water (+0.8 v.) to that of the reductant (-0.4 v.) and make ATP.

The most popular scheme *at present* is shown in Figure 1. There are two light reactions, each of which lifts an electron 0.8 v. Between them there is a 0.4-v. electron-transport system making ATP. A number of the papers in the Warrenton Symposium⁴ gives the evidence on which the idea stands. Essentially what is done is to emphasize the absorption changes seen in green plants on illumination and to make use of the information as to the oxidation and reduction of dyes by illuminated chloroplasts. No use is made of the information furnished by the fluorescent and delayed light emitted by the plant.

Emphasizing the information on light emission and neglecting that on the light absorption and dye reduction, we come to a picture of photosynthesis in which electrons and holes play an important part. The idea that photosynthesis is an electronic process has been suggested several times.⁵⁻⁸

Experiments Considered

We use four kinds of experiments.

I. Quantum Yield. There is now general agreement that green plants absorb 8 quanta of light to reduce one CO₂. The measurement of this number has been the subject of a long and bitter controversy that we will not explore. If 8 quanta (1.8 e.v.) are used to store 5.1 e.v., then the efficiency of the whole process of photosynthesis is 35%. This high efficiency tells us that the point at which reducing power is generated

(1) (a) Research sponsored by the U. S. Atomic Energy Commission under contract with the Union Carbide Corp.; (b) presented to the International Conference on Photosensitization in Solids, Chicago, Ill., June 22-24, 1964.

(2) E. I. Rabinowitch, "Photosynthesis and Related Processes," Interscience Publishers, Inc., New York, N. Y., 1945.

(3) J. A. Bassham and M. Calvin, "Path of Carbon in Photosynthesis," Prentice-Hall, Inc., Englewood Cliffs, N. J., 1952.

(4) "Photosynthetic Mechanisms of Green Plants," National Academy of Sciences, National Research Council, Washington, D. C., 1963.

(5) A. Szent-Gyorgyi, *Science*, **93**, 609 (1941).

(6) E. Katz, "Photosynthesis in Plants," Iowa State College Press, Ames, Iowa, 1949, Chapter XV, p. 291.

(7) J. A. Bassham and M. Calvin, USAEC Unclassified Report UCRL-2853, 1955.

(8) W. Arnold and E. S. Meek, *Arch. Biochem. Biophys.*, **60**, 809 (1956).

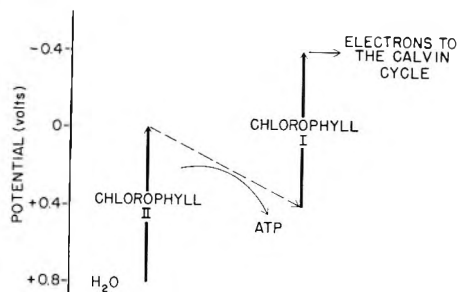


Figure 1. Present scheme for the electron transfer in photosynthesis.

is separated from the point at which oxidizing power is generated. We will refer to these points as A and B. The separation can be by distance or by a membrane, but, in either case, there must be an electronic conductor between points A and B.

II. *Photosynthetic Unit*. Experiments⁹ made long ago with Robert Emerson showed that in green plant photosynthesis 2000–2500 chlorophyll molecules are involved in the reduction of one CO_2 molecule. Since this reduction needs four electrons, we see that 500–600 chlorophyll molecules cooperate in the transfer of an electron from water to the Calvin cycle.

III. *Fluorescence*. Although it has been known since the time of Stokes that green plants fluoresce, it is only recently that we have had good measurements. Latimer, *et al.*,¹⁰ showed that fluorescence amounts to 2–3% of the light absorbed in the region where the rate of photosynthesis is a linear function of light intensity. We will use 2.5% in our argument.

A number of people have studied fluorescence as a function of the exciting light intensity. Figure 2 is a schematic representation of the results of Franck and collaborators.¹¹

At low light intensities the rate of photosynthesis is proportional to the intensity of the exciting light. At higher light intensities, the rate becomes independent of the exciting light, and we say that it is saturated. From the curve it can be seen that, as the rate of photosynthesis becomes saturated, the slope of the curve for fluorescence doubles.

IV. *Delayed Light*. In addition, we know that green plants emit a delayed light. This emission, which has the same spectral composition as fluorescence, has been studied from 5×10^{-5} to 6×10^3 sec. Figure 3 shows the intensity of the delayed light as a function of time in the dark. The data are for *Chlorella* at three different temperatures. The points for -165° were taken from a paper by Tollin, *et al.*¹² As can be seen, the decay is not exponential; it is very roughly proportional to the reciprocal of the time.

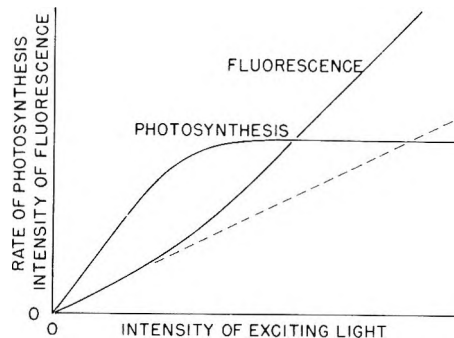


Figure 2. Photosynthesis and fluorescence as a function of exciting light intensity.

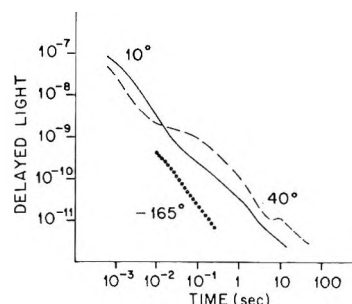


Figure 3. Decay of delayed light at three temperatures for *Chlorella*.

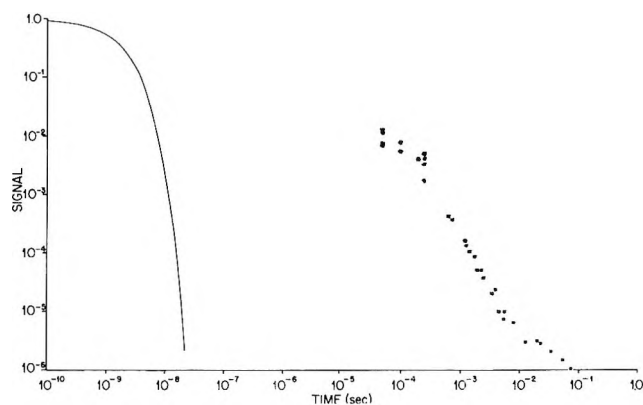


Figure 4. Decay of delayed light at short times. The solid line is an exponential with a time constant of 1.7×10^{-9} sec.

The long times involved, as well as the small temperature effect, argue that the delayed light comes from the

- (9) R. Emerson and W. Arnold, *J. Gen. Physiol.*, 16, 191 (1932).
 (10) P. Latimer, T. T. Bannister, and E. Rabinowitch, *Science*, 124, 585 (1956).
 (11) J. Franck, "Photosynthesis in Plants." Iowa State College Press, Ames, Iowa, 1949, Chapter XVI, p. 293.
 (12) G. Tollin, E. Fujimori, and M. Calvin, *Proc. Natl. Acad. Sci. U. S.*, 44, 1035 (1958).

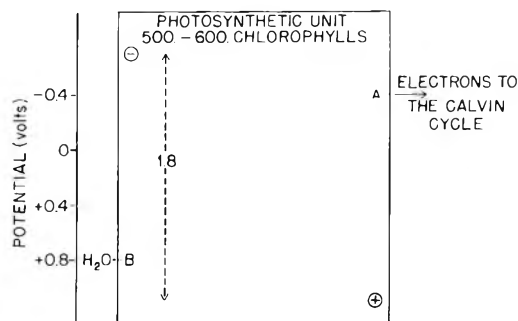


Figure 5. The electron-hole scheme for the electron transfer in photosynthesis.

recombination of electrons and holes as was suggested by Tollin.

Figure 4, taken from the Warrenton Symposium (Arnold and Davidson),⁴ is a decay curve for the delayed light from *Chlorella*. The delayed light signals are plotted as a fraction of the steady-state fluorescence (taken to be unity). The solid curve is an exponential having a time constant of 1.7×10^{-9} sec., which is the lifetime of fluorescence from *Chlorella* given by Tomita, *et al.*¹³ It must be remembered that, in determining the lifetime, the assumption was made that the decay was exponential.

Extrapolation of the decay to shorter times suggests that a large fraction of the *in vivo* fluorescence of green plants is delayed light. In the electron-hole picture of photosynthesis that we now present we make that assumption.

The Electron-Hole Picture

In Figure 5, the rectangle represents a photosynthetic unit made from 500-600 chlorophyll molecules. A and B are the two reaction centers. The absorption of a light quantum by any one of the 500 chlorophyll molecules forms an exciton that can run over the whole unit.

An exciton that hits the reaction center A is broken up to form a free hole in the chlorophyll and an electron bound to A. This electron, at -0.4 v., can go to the Calvin cycle or to an electron-transport chain that makes ATP. A second exciton cannot react with A until the electron has moved out of A. Similarly, an exciton can react at B to form a bound hole and a free electron in the chlorophyll. Again, a second exciton cannot react with B until the hole has been used in the oxidation of water. The free electron and hole can move about in the chlorophyll until they recombine and form an exciton. This movement constitutes the electronic conductor that we need between A and B and determines the nonexponential decay of the delayed light.

An approximate estimation of the lifetimes involved can be made from the fluorescence experiments. At high light intensities an exciton will generally find the two reaction centers filled. If the quantum yield of fluorescence is to be 5% at high intensities, then the lifetime of the exciton must be one-twentieth as large as the 1.5×10^{-8} sec.¹⁴ that is believed to be the natural lifetime of chlorophyll. Thus, the lifetime of an exciton, when the traps are filled, is 7×10^{-10} sec. At low intensities of exciting light, the traps A and B will be empty. Since we know that the process of photosynthesis is very efficient at low intensities, the lifetime of the exciton must be about one-tenth as large as, say, 7×10^{-11} sec. This agrees with the calculations of Bay and Pearlstein¹⁵ for the time for an exciton to react with the reaction center in a photosynthetic unit. The lifetimes and yields are shown in Table I.

Table I: Lifetime and Fate of Excitation

Lifetime, sec.	% of excitations resulting in			
	Fluorescence	Heat	Electron transfer	
Natural lifetime of chlorophyll ¹⁴	1.5×10^{-8}	100.0	0	0
Exciton when traps are filled (high intensity)	7×10^{-10}	5.0	95.0	0
Exciton when traps are empty (low intensity)	7×10^{-11}	0.5	9.5	90.0
Exciton when traps are empty (calcd. ¹⁵)	3.6×10^{-11}
	8.6×10^{-11}

The main points in favor of the electron-hole model are now given. (1) At low light intensities, where we know that the process of photosynthesis is very efficient, the model gives a probability of 0.9 that an absorbed quantum will be used. (2) At high light intensities, above the saturation of photosynthesis, the model gives a mechanism for the plant to dispose of the excess energy absorbed. When both traps are filled, the probability that an exciton will be converted to heat is 0.95. (3) At low light intensities the experimentally observed fluorescence yield consists of 0.5% true fluorescence and somewhat less than 2.5% delayed light. This agrees with the measurements of Latimer, *et al.*¹⁰ (4) At high light intensities the differential yield of

(13) G. Tomita and E. Rabinowitch, *Biophys. J.*, **2**, 483 (1962).

(14) S. Brody and E. Rabinowitch, *Science*, **125**, 555 (1957).

(15) Z. Bay and R. Pearlstein, *Proc. Natl. Acad. Sci. U. S. A.*, **50**, 1071 (1963).

fluorescence will be 5%. This agrees with the findings of Franck.¹¹ (5) The model provides the electronic conductor that is needed to prevent back-reactions between the reducing and the oxidizing power. (6) The model provides a mechanism for the production of delayed light.

Two problems in solid state physics must be solved before the electron-hole picture of photosynthesis has to be taken seriously. (1) Can an exciton break up to give a bound electron and a free hole? (2) How do free electrons and holes move in an aggregate of a few hundred pigment molecules?

Exchange of Substituents on Nitrogen in Molten Ammonium Salts and Amines

by Heinz K. Hofmeister and John R. Van Wazer

Monsanto Company, Central Research Department, St. Louis, Missouri (Received February 13, 1964)

At 200–300° in sealed tubes, methyl groups and hydrogen atoms exchange places on the nitrogen atoms of ammonium ions in melts of tetramethylammonium chloride with ammonium chloride. Likewise, the three pure mixed methylammonium cations— CH_3NH_3^+ , $(\text{CH}_3)_2\text{NH}_2^+$, and $(\text{CH}_3)_3\text{NH}^+$ —undergo such rearrangements. In all cases, there is an equilibrium between the various ammonium ions which is not much different from that expected for random sorting of the hydrogens and methyl groups. The kinetics of the thermal equilibration of methyl-, dimethyl-, and trimethylammonium ions at 300° are presented. Mixtures of aniline and dimethylaniline in the same temperature range also exchange hydrogens and methyl groups to give a near-random equilibrium in the presence of appreciable amounts of HCl. Shifting of phenyl groups between nitrogen atoms is immeasurably slow under the conditions studied.

As pointed out by Skinner,¹ the enthalpy of redistribution reactions gives a direct measure of the departure of bond-energy-term values from constancy. This information may also be obtained indirectly² by measuring the deviations from statistically random sorting in the scrambling of substituents in such reactions. As part of a broad quantitative study of new families of inorganic compounds, ranging from small molecules to macromolecular species, it has been deemed desirable to establish certain generalities concerning deviations from the statistically random sorting of substituents in scrambling reactions. The information presented below represents a specific experimental example studied for this purpose, since we could find no quantitative chemical data or any thermochemical information concerning the scrambling of substituents on quadruply connected nitrogen. Simultaneously,

data were also obtained for another general treatment we are attempting which deals with the kinetics of scrambling reactions.³

Experimental Details

The N,N-dimethylaniline, aniline, methylamine hydrogen chloride, and ammonium chloride were reagent

(1) H. A. Skinner, *Rec. trav. chim.*, **73**, 991 (1954).

(2) The values of ΔH may be estimated, rather closely in many cases, by calculating (in terms of free energy) the deviations from randomness of the measured equilibrium constants of the appropriate scrambling reactions. This assumes cancellation of the partition functions for translation, rotation, and vibration. See A. G. Evans and E. Warhurst, *Trans. Faraday Soc.*, **44**, 189 (1948); J. R. Van Wazer and L. Maier, *J. Am. Chem. Soc.*, **86**, 811 (1964); K. Moedritzer and J. R. Van Wazer, *Inorg. Chem.*, **3**, 139 (1964).

(3) Manuscripts concerned with (a) regularities in the deviations of scrambling reactions from randomness and (b) a theory of the variations to be found in the kinetics of such reactions are now in preparation.

grade chemicals from the Fisher Scientific Co. Di- and trimethylamine hydrogen chlorides, as well as aniline hydrogen chloride and tetramethylammonium chloride, were Eastman White Label chemicals. The N-methylaniline was redistilled Eastman practical grade (Yellow Label). The ammonium chloride and tetramethylammonium chloride were recrystallized from water and alcohol, respectively, and then dried in a desiccator over phosphorus pentoxide at room temperature.

It was found that mixtures of tetramethylammonium chloride and ammonium chloride in sealed Pyrex glass tubes melted over a period of several hours when heated to about 300°. Even after heating at this temperature for 4 days, no residual gas pressure was noted after cooling to room temperature and opening those tubes which contained more than 50 mole % ammonium chloride. Even when there were large amounts of tetramethylammonium chloride, decomposition was inappreciable during the period needed to achieve equilibrium. Four or five replicate determinations were made at mole fractions of tetramethylammonium chloride equal to 0.25, 0.50, and 0.75, and a few scattered determinations were carried out for other compositions. Proof that equilibrium was achieved in these studies was based on the fact that the same final compositions were obtained when the monomethylammonium, dimethylammonium, and trimethylammonium chlorides were subjected to the same thermal treatment. The majority of the equilibrium measurements were carried out at 300°, but some runs were also made on melts at 200°. In order to avoid shifting of the equilibrium with lowering temperature and upon crystallization, quick quenching was employed. This consisted of dropping the sealed Pyrex tubes into a well-stirred mixture of ice and water. After the samples were quenched, the tubes were opened and the contents were dissolved in 20% hydrochloric acid for the nuclear magnetic resonance (n.m.r.) measurements.

Equilibrium between aniline and N,N-dimethylaniline was also achieved in sealed Pyrex tubes in the temperature range of 200–300°. In this case, the desired ratios of the two end-member compounds were combined with various proportions of hydrochloric acid, in the range of 0 to 0.5 mole of HCl/g.-atom of N. Achievement of equilibrium was checked by heating N-methylaniline under the same conditions. For this system at 200°, preliminary experiments indicated that equilibrium was reached within 2 days with 0.5 mole HCl/g.-atom of N as accelerator. Again rapid quenching was employed, following which the contents of the tubes were shaken with an aqueous

alkaline solution in a separatory funnel so that, after drying, the pure liquid amines could be used for the n.m.r. measurements.

A Varian A-60 analytical spectrometer running at a frequency of 60 Mc./sec. was employed for the H¹ n.m.r. determinations, generally using the smallest available sweep width (50 c.p.s. for the entire scale). A typical spectrum of the reaction products obtained from a molten mixture of tetramethylammonium chloride and ammonium chloride is shown in Figure 1, from which it can be seen that there were four resonance

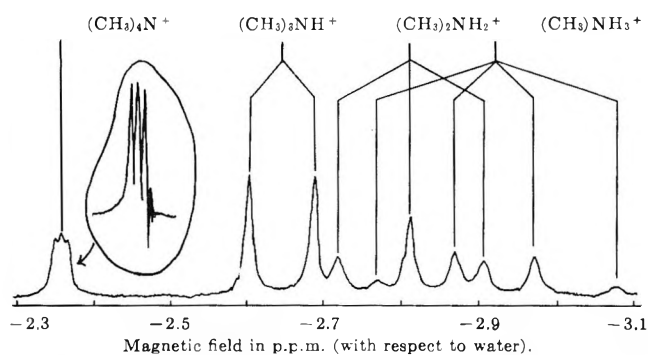


Figure 1. Typical H¹ n.m.r. spectrum at 60 Mc. for an equilibrated mixture of 0.75 mole of tetramethylammonium chloride with 1.25 moles of ammonium chloride. Water is generally taken to have a shift of -5.3 p.p.m. with respect to tetramethylsilane.

peaks used for determination of the methylammonium ion as compared to one peak for the tetramethylammonium ion. The unsubstituted ammonium ion was measured by subtracting the proper equivalence of hydrogen for the substituted ammonium ions from the single resonance peak corresponding to all of the hydrogens directly attached to the nitrogen atom. The N-hydrogens corresponding to the various ammonium ions were not resolvable but appeared as a single resonance. The full spectrum of Figure 1 demonstrates the type of resolution generally obtained in this study. However, on the few occasions when optimum conditions were achieved, the multiplet corresponding to the spin-spin coupling between the hydrogen and nitrogen of the tetramethylammonium ion gave a well-separated triplet, as shown in the insert of Figure 1. The coupling constant for this H-C-N configuration, as obtained from these measurements, is found to be $J_{HN} = 0.55$ c.p.s. As expected, the unsymmetrical methylamines and methylammonium ions do not show splitting due to this coupling. The H-N-C-H coupling constant between the hydrogens on the nitrogen and on the ammonium ion was found to be 5.20 ± 0.06

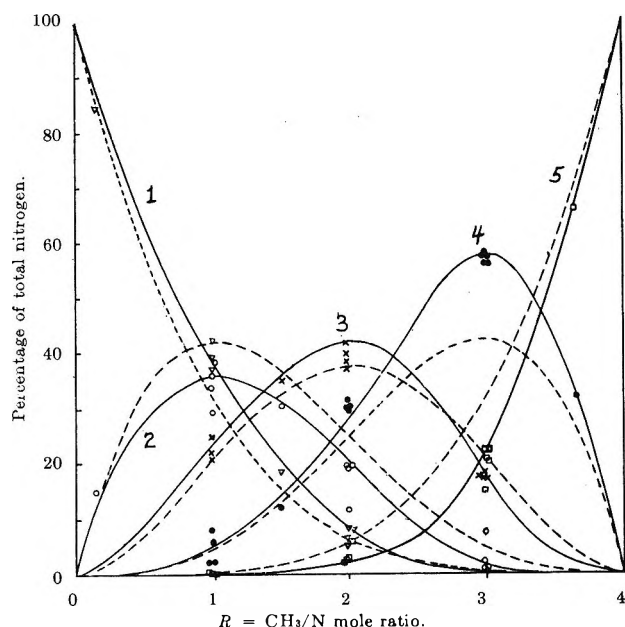


Figure 2. Equilibrium between tetramethylammonium chloride and ammonium chloride at 300°. The dotted lines correspond to an ideal random system and the solid lines to $K_1 = 0.68$, $K_2 = 0.33$, and $K_3 = 0.115$; 1, NH_4^+ ; 2, CH_3NH_3^+ ; 3, $(\text{CH}_3)_2\text{NH}_2^+$; 4, $(\text{CH}_3)_3\text{NH}^+$; 5, $(\text{CH}_3)_4\text{N}^+$.

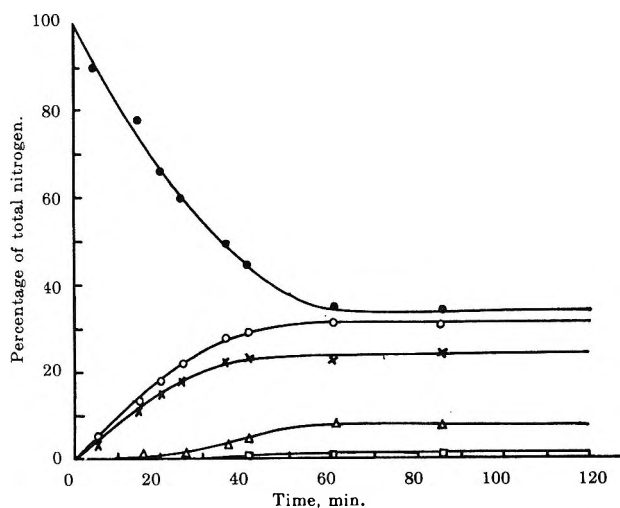


Figure 3. Reorganization of the methylammonium ion at 300° in molten $\text{CH}_3\text{NH}_3\text{Cl}$: ●, CH_3NH_3^+ ; ○, NH_4^+ ; ×, $(\text{CH}_3)_2\text{NH}_2^+$; Δ, $(\text{CH}_3)_3\text{NH}^+$; □, $(\text{CH}_3)_4\text{N}^+$.

c.p.s. for the $(\text{CH}_3)_3\text{NH}^+$ ion, 5.78 ± 0.07 for the $(\text{CH}_3)_2\text{NH}^+$, and 6.20 ± 0.05 for the CH_3NH_3^+ ion.

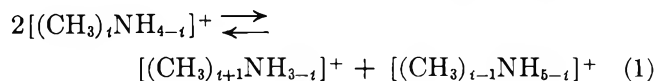
Analysis of the aniline system was carried out by measuring the integral of the individual methyl group n.m.r. peaks as well as that of the total phenyl. Thus, the N,N-dimethylaniline and the N-methylaniline were determined directly, and the amount of unsubstituted aniline was obtained by subtracting the proper hydro-

gen equivalent of the substituted anilines from the total phenyl group resonance.

A statistical study⁴ of the data showed that the overall standard error in the n.m.r. determination of the various ammonium ions with respect to the weighed amounts of reactants in the system $\text{N}(\text{CH}_3)_4^+ - \text{NH}_4^+$ was 1.54% of the total nitrogen. The error was greatest (3.0%) for NH_4^+ ion and least (0.5%) for the $\text{N}(\text{CH}_3)_4^+$ ion, as calculated from measurements on known mixtures. For the $\text{C}_6\text{H}_5\text{NH}_2 - \text{C}_6\text{H}_5\text{N}(\text{CH}_3)_2$ system, the over-all standard error was rather high, being 10.0% of the total nitrogen. Since the standard deviation of the equilibrium constant for the aniline system (see eq. 2 below) was found to be only 3% of its value, this 10% standard error in the material balance is probably due in considerable part to inconsequential side reactions.

Results and Conclusions

The Molten Ammonium Chloride System. The experimental data on the system ammonium chloride vs. tetramethylammonium chloride is compared with the smooth curves for the observed averaged equilibrium constants in Figure 2. There are three such constants, corresponding to values of $i = 1, 2, \text{ or } 3$ in eq. 1. Based on the 16 separate preparations, the



equilibrium constants are calculated⁴ to be 0.115 with a standard deviation, s , of 0.008 for $i = 1$; 0.33 with $s = 0.02$ for $i = 2$; and 0.68 with $s = 0.05$ for $i = 3$. Were the system ideally random,⁵ the constant for $i = 1$ and 3 would be 0.375, whereas the constant for $i = 2$ would be 0.444. The greatest deviation from randomness is thus seen to be found for the reaction having $i = 1$ in eq. 1 and the least for $i = 2$. However, in all cases, the deviations are small.

The kinetics of reorganization of originally pure samples of $(\text{CH}_3)\text{NH}_3^+$, $(\text{CH}_3)_2\text{NH}_2^+$, and $(\text{CH}_3)_3\text{NH}_3^+$ were studied at 300°. The resulting data are presented in Figures 3, 4, and 5, from which it can be seen that, for all practical purposes, equilibrium is reached within 20 min. for the trimethylammonium ion, 70 min. for the dimethylammonium ion, and 60 min. for the monomethylammonium ion. Although the kinetics are quite involved, they may be fitted to first-order rate equations. When this is done, the

(4) L. C. D. Groenweghe and J. R. Van Wazer, *Anal. Chem.*, **36**, 303 (1964).

(5) G. Calingaert and H. A. Beatty, *J. Am. Chem. Soc.*, **61**, 2748 (1939).

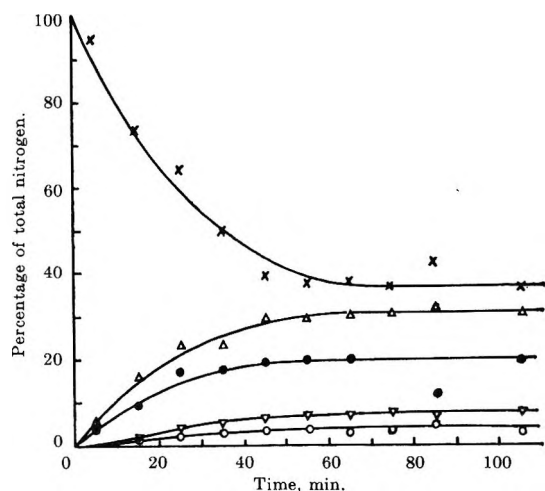


Figure 4. Reorganization of the dimethylammonium ion at 300° in molten $(\text{CH}_3)_2\text{NH}_2\text{Cl}$: \times , $(\text{CH}_3)_2\text{NH}_2^+$; Δ , $(\text{CH}_3)_3\text{NH}^+$; \bullet , CH_3NH_3^+ ; ∇ , NH_4^+ ; \circ , $(\text{CH}_3)_4\text{N}^+$.

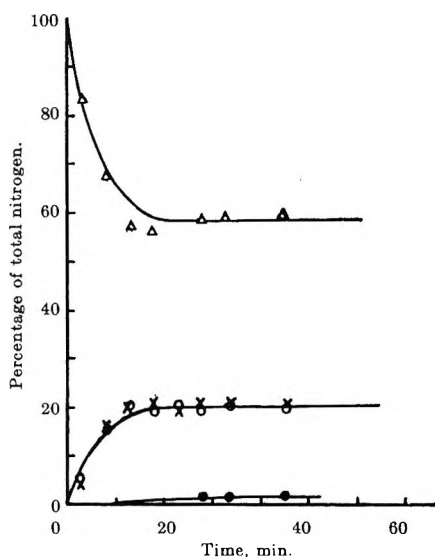


Figure 5. Reorganization of the trimethylammonium cation at 300° in molten $(\text{CH}_3)_3\text{NHCl}$: Δ , $(\text{CH}_3)_3\text{NH}^+$; \circ , $(\text{CH}_3)_4\text{N}^+$; \times , $(\text{CH}_3)_2\text{NH}_2^+$; \bullet , CH_3NH_3^+ .

pseudo-first-order rate constants for the diminution of the original species and the growth of the species formed are found to be equal within experimental error. At 300°, the half-life for reorganization of the trimethylammonium cation is 0.8 min., for the dimethylammonium cation it is 7.2 min., and for the monomethylammonium cation it is 17.5 min. From comparison with measurements made at 200°, an activation energy of 38 kcal. was found for the reorganization of the dimethylammonium cation.

The Aniline System. The experimental data were obtained on the system aniline *vs.* dimethylaniline with 0.5 mole of HCl/g.-atom of N being used as a rate

accelerator. The equilibrium constant was found to be 0.30 with $s = 0.09$, for the reaction



Since for ideal randomness, the equilibrium constant is 0.250, we see that—within experimental error—the exchange of methyl groups and hydrogens on aniline is indistinguishable from random behavior.

It is interesting to note that methyl and hydrogen substituents on ammonia readily exchange places under conditions where the phenyl groups do not. In one preliminary experiment, a mixture of aniline and dimethylaniline with 0.5 mole of HCl/g.-atom of N was heated for a week at 200° with no evidence of exchange of the phenyl group with either hydrogen or the methyl group. With no added HCl, decomposition rather than exchange was observed.

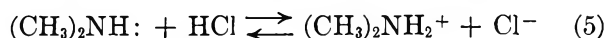
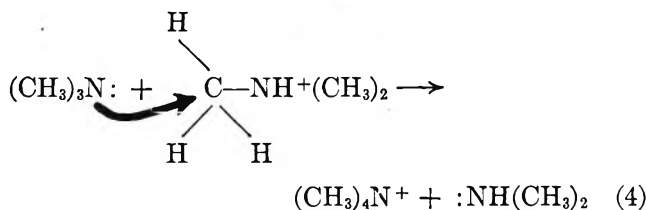
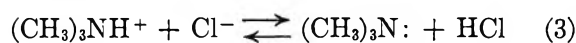
Miscellaneous Studies. The poor exchangeability of phenyl groups on nitrogen was also evidenced by an experiment in which 1 mole of diphenylamine with 0.5 mole of HCl was heated for two days at 300°. No exchange was found, although as little as 1% of substituent interchange could have been detected. Likewise, a mixture of triphenylamine and tetramethylammonium chloride was heated at 300° for 1 week. Again no exchange was detectable although the n.m.r. spectrum showed some small peaks due to side reactions. These findings, using modern C.p. reagents, probably mean that the old commercial process⁶ for the synthesis of diphenylamine from aniline by redistribution of the phenyl groups was accelerated by impurities in the HCl catalyst or the aniline or by the autoclave walls.

Upon heating monobutylammonium chloride at 300° for 2 days, considerable gas pressure built up in the sealed tube. Although an analysis was not carried out, this gas was probably butylene. Proton n.m.r. study of a solution of the solid resulting from quenching showed a number of small unidentified resonance peaks. A similar situation, with many small n.m.r. peaks being found in both the $\text{CH}_2\text{—CH}_3$ region and in the phenyl region of the proton n.m.r. spectrum, was observed when benzylammonium chloride was heated at 300° for 2 days. In this case, however, gas pressure was not noted.

Reaction Mechanism. It is quite apparent that the reorganization mechanism must involve the ammonium ion, since the pure amines were always found to undergo decomposition before any substituent inter-

(6) P. H. Groggins, "Aniline and Its Derivatives," D. Van Nostrand and Co., New York, N. Y., 1924, p. 164. Alternatively, see K. Winnacker, Ed., "Chemische Technologie, Organ. Tech. II," Carl Hanser, München, 1954, p. 56.

change could be detected. Likewise, it seems reasonable to conclude that because permanent gases did not form over most of the range of interest in either the substituted ammonium chloride melts or the substituted aniline mixtures, the redistribution reactions probably follow ionic and not free-radical mechanisms. A reasonable mechanism⁷ for this process is given below, as exemplified by the exchange between two trimethylammonium ions

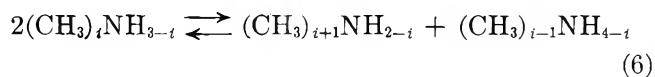


This mechanism indicates that the reactions should go the fastest for mixtures of amine and ammonium salt, and several experiments have shown this to be the case. Mechanisms involving reaction between methyl chloride and the free amines or the ammonium ions are not ruled out by these experiments. However, it is difficult to picture a transition state for the reaction between methyl chloride and the ions.

Discussion

From available thermodynamic data⁸ on amines, one can compare the methyl *vs.* hydrogen exchange on

triply connected nitrogen (in the amines) with the same exchange on quadruply connected nitrogen (in the ammonium ions). Thus, the reaction of eq. 6 may be compared with that of eq. 1



For $i = 1$, the equilibrium at 300° is calculated to be 8×10^{-2} for the gaseous and 6×10^{-2} for the liquid amines as compared to our measured value of 11.5×10^{-2} for the ammonium chloride melts. Also, estimation² of ΔH from the equilibrium constants given in this paper consistently leads to somewhat smaller numerical values for these exchange reactions on the quadruply as compared to the triply connected nitrogen. One is tempted to ascribe these apparently somewhat greater deviations from random scrambling on the amines to the ready ability of triply connected nitrogen to undergo changes in rehybridization by formation of an abortive bond involving its unshared pair of electrons.⁹

Acknowledgment. We wish to thank Dr. Harold Weingarten for helpful discussions concerning the reaction mechanism.

(7) For related work see H. R. Snyder, R. E. Carnahan, and E. R. Lovejoy, *J. Am. Chem. Soc.*, **76**, 1301 (1954).

(8) F. D. Rossini, D. D. Wagman, W. H. Evans, S. Levine, and I. Jaffe, "Selected Values of Chemical Thermodynamic Properties," National Bureau of Standards Circular 500, U. S. Government Printing Office, Washington, D. C., 1952.

(9) C. A. Coulson, "Valence," Oxford University Press, Oxford, 1952, p. 210.

Rate of Exchange of Chlorine between Dimethylchloramine and Succinimide¹

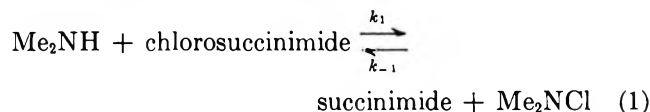
by Takeru Higuchi and Jun Hasegawa

School of Pharmacy, University of Wisconsin, Madison, Wisconsin (Received February 18, 1964)

Data are presented to show that the exchange of chlorine for hydrogen between succinimide and dimethylchloramine occurs directly and not through intermediate formation of hypochlorous acid. The pH profiles of the reaction rates in both directions have been determined.

Introduction

Formation of dialkylchloramine in mixed aqueous solutions of dialkylamine and a halogenating agent may result either from a direct exchange of chlorine or through an intermediate formation of hypochlorous acid. Thus, for example, production of dimethylchloramine from dimethylamine and N-chlorosuccinimide (NCSI) may be written



or



Results of experimental measurement of these reactions suggest that (1) is normally the primary route. Values of k_1 and k_{-1} are reported as functions of pH.

I. Formation of Dimethylchloramine from N-Chlorosuccinimide and Dimethylamine. The reaction can be readily followed spectrophotometrically since the end product absorbs strongly at 263 m μ . Figure 1 shows the approximate changes in the absorption spectrum of a mixture of the organohalogenating agent and the amine in water at pH 2.9 and 25°. The curve shown for zero time is that corresponding to the sum of individual spectra of the reactants. The equilibrium values shown are based on the molar absorptivity, essentially, as given by Weil and Morris² and as confirmed by our own work.

In Figure 2 the initial rates of appearance of dimethylchloramine in these systems are shown for several molar ratios of dimethylamine to chlorosuc-

cinimide at a constant initial chlorosuccinimide concentration. The linear plot clearly indicates that the rate is directly dependent on the amine. The usual $x/x(a-x)$ plots against time, however, showed substantial departure from linearity for equiconcentration of the reacting species. This is ascribed to the reverse reaction corresponding to k_{-1} .

All evidence available clearly rules out the possibility of the exchange reaction taking place through hypochlorous acid mediation as set forth in reactions 2 and 3. The formation of dimethylchloramine in freshly prepared solution of chlorosuccinimide and the amine exhibits no lag time. There is no spectral evidence of intermediate production of hypochlorous acid. The kinetic dependency on the amine as described above would not, moreover, be compatible with reaction 2 being rate determining. A recent separate study in these laboratories³ has indicated, in addition, that the forward reaction³ is apparently extremely slow in the pH range covered in the present study. These facts, taken together with the observation that the k_1/k_{-1} values calculated from the initial phases of the corresponding reactions agree with the observed equilibrium constant, are only consistent with the first mechanism.⁴

The second-order constant, k_1 , for the system calculated from initial rate of concentration change is shown in Figure 3 plotted against the pH of the buf-

(1) This study was supported in part by the U. S. Army Research and Development Laboratories under Grant No. DA-CML-18-108-61-G22 and DA-CML-18-108-G-53.

(2) I. Weil and J. C. Morris, *J. Am. Chem. Soc.*, **71**, 3123 (1949).

(3) T. Higuchi, A. Hussain, and A. Hurwitz, private communication.

(4) At the request of one of the referees, this conclusion was further substantiated by showing that addition of succinimide had no significant effect on the forward reaction rate.

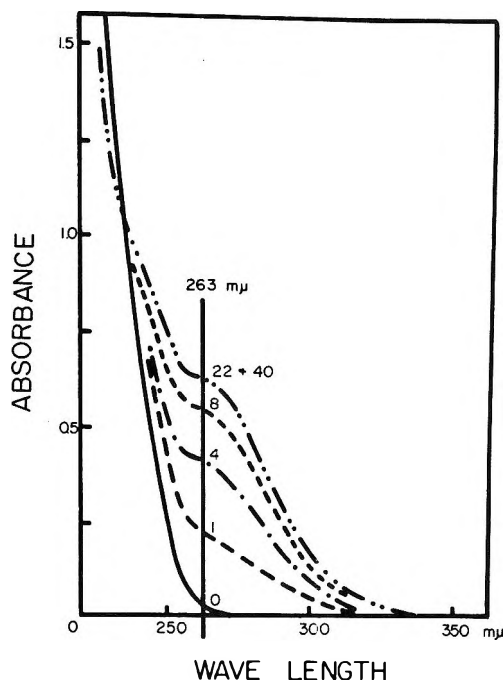


Figure 1. Spectral changes during reaction of dimethylamine with N-chlorosuccinimide in 0.05 M phosphate buffer at pH 2.9 and 25°. $[\text{Me}_2\text{NH}]_{\text{initial}} = [\text{C}_4\text{H}_4\text{O}_2\text{NCl}]_{\text{initial}} = 5.0 \times 10^{-3} M$. 0, before mixing; 1, 4, 8, 22, and 40, after mixing of Me_2NH , in min. $\text{Yield}_{\text{eq}} = 35\%$.

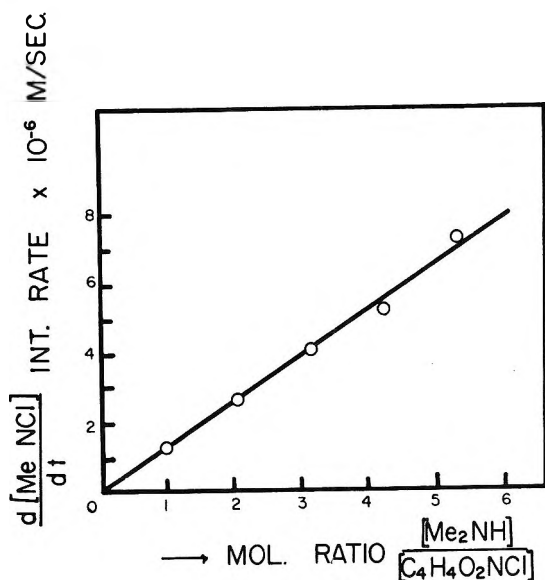


Figure 2. Initial rate vs. molar ratio for the reaction, $\text{Me}_2\text{NH} + \text{C}_4\text{H}_4\text{O}_2\text{NCl} \rightarrow \text{Me}_2\text{NCl} + \text{C}_4\text{H}_4\text{O}_2\text{NH}$, at pH 2.9 (0.05 M phosphate buffer solution) and 25°. The concentration of chlorosuccinimide was $2.29 \times 10^{-3} M$ in every instance.

ferred systems. The pH dependency suggests that the reaction probably involves only the free form of the amine. The second-order rate constants for the re-

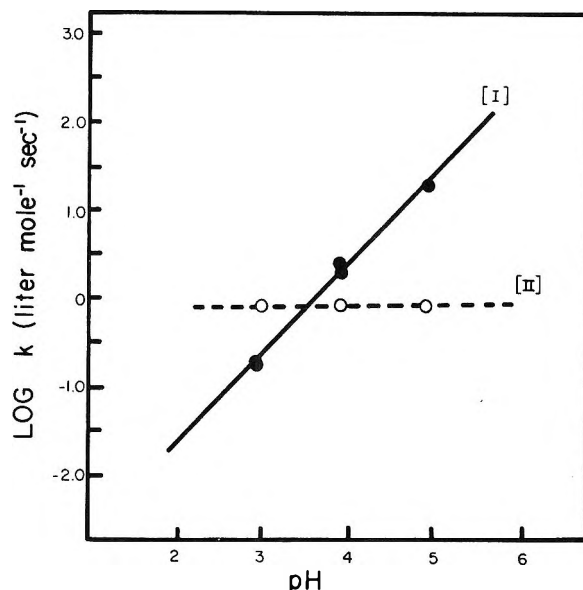


Figure 3. pH rate profiles of $\text{C}_4\text{H}_4\text{O}_2\text{NCl} + \text{Me}_2\text{NH}_2^+ \xrightarrow{k_1} \text{Me}_2\text{NCl} + \text{C}_4\text{H}_4\text{O}_2\text{NH}$ [I] and $\text{Me}_2\text{NCl} + \text{C}_4\text{H}_4\text{O}_2\text{NH} \xrightarrow{k_{-1}} \text{Me}_2\text{NH} + \text{C}_4\text{H}_4\text{O}_2\text{NCl}$ [II].

action, chlorosuccinimide + free dimethylamine \rightarrow succinimide + $(\text{CH}_3)_2\text{NCl}$, calculated for several pH values at 25° and based on a pK_b value of 3.22 for dimethylamine⁵ are given in Table I.

Table I: Second-Order Rate Constant for Reaction of N-Chlorosuccinimide with Free Dimethylamine

pH	Rate constant $\times 10^{-2}$, l. mole ⁻¹ sec. ⁻¹
4.90	1.5
3.90	1.9
2.90	1.3
Mean 1.6×10^2 l. mole ⁻¹ sec. ⁻¹	

II. Formation of N-Chlorosuccinimide from Dimethylchloramine and Succinimide. Spectral changes following mixing of equiconcentration solutions of dimethylchloramine and succinimide at pH 3.01 and 25° are shown in Figure 4. The second-order rate constant obtained directly on this system from initial changes was $0.86 \text{ l. mole}^{-1} \text{ sec.}^{-1}$. The value is shown as a solid square in Figure 3. The remaining two points for the reverse reaction were calculated from the equilibrium concentration of the halogenating species

(5) D. H. Everett and W. F. K. Wynne-Jones, *Proc. Roy. Soc. (London)*, A177, 499 (1941).

$$k_{-1} = \frac{k_1}{K_1} = \frac{k_1}{\frac{(\text{Me}_2\text{NCl})_{\text{eq}}(\text{C}_4\text{H}_4\text{O}_2\text{NH})_{\text{eq}}}{(\text{C}_4\text{H}_4\text{O}_2\text{NCl})_{\text{eq}}(\text{Me}_2\text{NH}_2^+)_{\text{eq}}}}$$

It is evident that this reaction is largely pH independent, as would be expected from the nature of the reactants. The second-order rate constants calculated as above from the equilibrium constants at pH 3.90 and 4.90 were 0.88 and 0.92 l. mole⁻¹ sec.⁻¹, respectively, in good agreement with those determined directly.

The corresponding K_1 values based on total remaining amine concentration (essentially Me_2NH_2^+) as given previously are shown in Table II. The value at pH 3.01 was determined from k_1 and k_{-1} obtained from initial rates, and the remaining two values were obtained from equilibrium concentrations. The constant decreases inversely with hydrogen ion as expected. Other studies over pH range 2–6 are consistent with this relationship.

Experimental

Reagents. All reagents used were of the highest grade commonly available and were normally subjected to further purification before use. *N*-Chlorosuccinimide was recrystallized twice from benzene and stored in a blackened desiccator. Succinimide was recrystallized from acetone. Dimethylamine solution was prepared from the hydrochloride salt (Eastman Kodak, A.R. grade). The reagents used for preparation of the buffer solutions were recrystallized from solutions treated with hypochlorous acid to remove oxidizable material. Water used in the studies was prepared by redistilling tap distilled water from an acid permanganate solution. This procedure was found to reduce oxidizable residue to a negligible level.

The hypochlorous acid solutions were prepared by dilution of distillate obtained from sodium hypochlorite solution under reduced pressure. Fifteen grams of boric acid, 250 ml. of sodium hypochlorite (Fisher Scientific, 5–6% available chlorine), and 500 ml. of water were distilled together. The first 50 ml. of the distillate was discarded, and the following 500 ml. was collected to yield a solution containing 0.04–0.08 mole of hypochlorous acid/l.

Table II: Equilibrium Constant for the Exchange

Reaction at 25°, $\text{C}_4\text{H}_4\text{O}_2\text{NCl} + \text{Me}_2\text{NH}_2^+ \xrightleftharpoons{K_1} \text{C}_4\text{H}_4\text{O}_2\text{NH} + \text{Me}_2\text{NCl}$	
pH	K_1
3.01	0.32
3.90	2.5
4.90	23.0

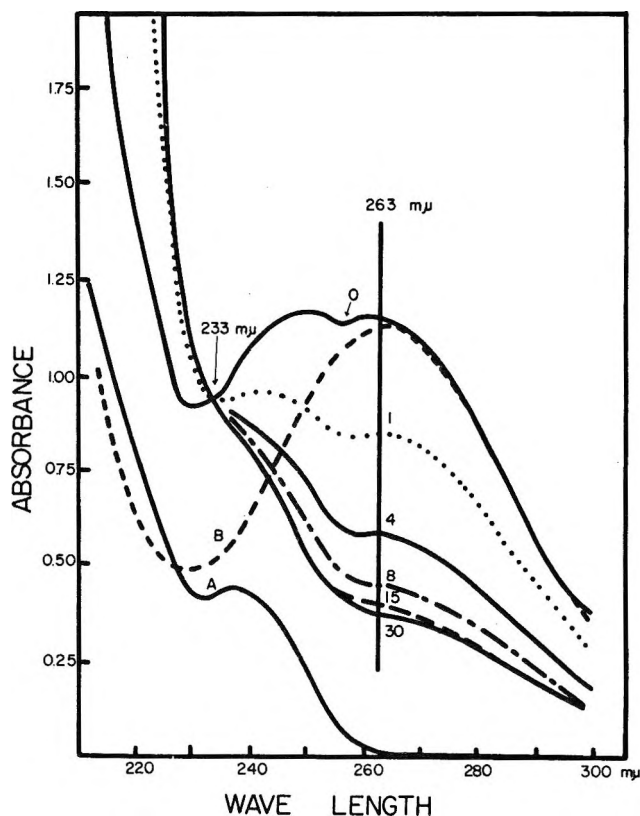


Figure 4. Changes in ultraviolet absorption during the reaction, $\text{C}_4\text{H}_4\text{O}_2\text{NH} + \text{Me}_2\text{NCl} \xrightarrow{k_{-1}} \text{C}_4\text{H}_4\text{O}_2\text{NCl} + \text{Me}_2\text{NH}$, in 0.05 *M* phosphate buffer solution at pH 3.24 and 25°. Curve B corresponds to 5.0×10^{-3} *M* Me_2NCl by itself, and curve A corresponds to 5.0×10^{-3} *M* succinimide only. That marked 0 corresponds to the arithmetic sum of A and B. Others correspond to spectra obtained 1, 4, 8, 15, and 30 min. after mixing the reactants to yield individual concentrations of 5.0×10^{-3} *M*.

Determination of the Forward Rate. Fresh 5.00×10^{-4} *M* *N*-chlorosuccinimide solution was prepared by mixing 50 ml. of 0.2 *M* acetate buffer and 5.0 ml. of 0.01 *M* *N*-chlorosuccinimide (0.1336 g. in 100 ml.) just before use in a 100-cc. volumetric flask. A second solution consisting of 50 ml. of 0.2 *M* acetate buffer solution and 5.49 ml. of 0.00910 *M* dimethylamine solution was prepared and diluted to 100 ml. Both solutions were then brought to $25.0 \pm 0.1^\circ$. An equivolume mixture of these was prepared as rapidly as possible in a 10-cm. light path silica cell, and the change in absorbance at 263 mμ was followed in a Cary Model 11 spectrophotometer. After the run was completed, the pH of the reaction mixture was determined.

Determination of the Reverse Rate. A 5.00×10^{-3} *M* dimethylchloramine solution was prepared by mixing 50 ml. of 0.1 *M* phosphate buffer, 11.0 ml. of 0.0901

M dimethylamine, and 15.3 ml. of 0.0654 *M* hypochlorous acid and water to the mark in a 100-ml. volumetric flask. A second solution consisting of 5.0 ml. of 0.01 *M* succinimide solution and 50 ml. of 0.1 *M* phosphate buffer solution was diluted to 100 ml. with water. Mixtures of the two solutions were prepared and allowed to react in a 10-cm. cell as above, and the decrease in absorbancy at 263 $m\mu$ was determined as described before.

Determination of Equilibrium Constant. Appropriate amounts of 5.00×10^{-4} *M* N-chlorosuccinimide and dimethylamine solutions were mixed, and the change in absorbance at 263 $m\mu$ was followed in appropriate buffer solutions. An equilibrium state was usually reached in 30–60 min. The equilibrium constant was arrived at from the independently determined molar absorptivity of dimethylchloramine and the absorbancy at equilibrium.

Chemical Synthesis with Ion Beams

by Stanley Singer,* N. G. Kim,* A. W. Merkl, and M. Farber

Maremont Corporation, Research Division, Pasadena, California (Received March 2, 1964)

A method of chemical synthesis by gas phase ion-molecule reactions analogous to known liquid phase reactions is described. The synthesis of nitrobenzene by the reaction of NO_2^+ and benzene is reported. The interaction of a beam of NO_2^+ ions with maximum energies of 1 e.v. with gaseous benzene gave nitrobenzene in high yield. A 1-ma. ion current consisting of 99% NO_2^+ was formed by electron impact with nitrogen dioxide in a concentric dual-anode magnetron.

This paper describes the use of low kinetic energy ion beams for chemical synthesis. Gas phase ion-molecule reactions have been the subject of numerous investigations.¹ In the usual method of study the ionic products are determined in a mass spectrometer over the range of conditions available. Neutralization of the ionic species can lead to compounds produced in the usual gas or liquid phase reactions.

Many different ions have been formed in electron bombardment of chemical compounds.² The ability to produce high currents of selected ions at controlled energies would make possible study of interesting gas phase reactions. For example, reactions which proceed through ionic intermediates in the liquid phase could be investigated in the gas phase as ion-molecule reactions. Three ion beams containing as major species NO_2^+ , NF_2^+ , and OF^+ have been reported.³

A molecular beam method in which the ion beam is directed into a reaction zone containing the neutral

target molecules can be used to study such reactions. In the apparatus shown in Figure 1, for example, a plasma is generated in the ion source. The ion beam is extracted by an electrostatic potential on the control grid. Ions passing through this grid enter the reaction zone where they encounter the neutral molecules flowing into the zone. The apparatus thus consists of three major parts: (1) the ion source for forming the ions from a suitable gas, (2) the electrostatic grid for ex-

* Correspondence may be addressed to these authors at Dynamic Science Corp., South Pasadena, Calif.

(1) F. W. Lampe, J. L. Franklin, and F. H. Field, *Progr. Reaction Kinetics*, **1**, 67 (1961).

(2) F. H. Field and J. L. Franklin, "Electron Impact Phenomena," Academic Press, Inc., New York, N. Y., 1957.

(3) S. Singer, N. G. Kim, A. W. Merkl, L. B. Marantz, and C. Bodai, "The Formation of Plasma Beams Containing Ionic Species," presented before the Division of Fuel Chemistry, 147th National Meeting of the American Chemical Society, Philadelphia, Pa., April 1964; *Division of Fuel Chemistry Preprints of Papers*, Vol. 8, No. 2, 1964, pp. 1–5.

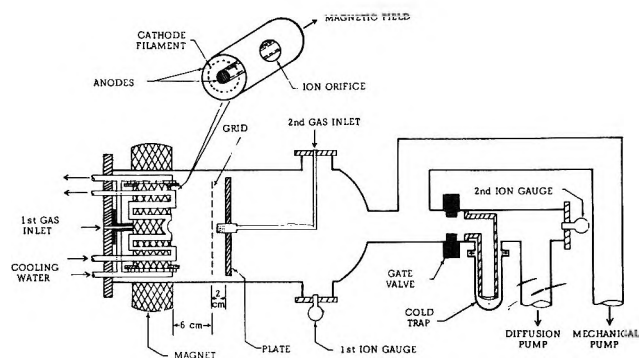


Figure 1. Ion reaction apparatus with dual-anode magnetron.

tracting the ion beam and controlling the ion energy, and (3) the reaction zone containing the target molecules. The ionic products can be detected mass spectrometrically as usual in ion-molecule reactions or the stable products formed on neutralization can be trapped from the reaction zone and identified by conventional chemical methods. Sufficient quantities to permit isolation of the product involve on the order of 1 ma. of ion current reacting with target molecules for several hours.

An ion beam consisting of a single ionic species in a well-defined energy level is desirable. A mass separation prior to the reaction zone is required if a mixture of ions is formed in the source. A narrow distribution in kinetic energy of the ions is also advantageous because of the variation in reaction cross section with ion velocity. Ionization by electron impact using low energy electrons near the appearance potential of the desired ion minimizes fragmentation of polyatomic molecules and excitation to higher energy levels. Large beam currents, however, generally involve broad kinetic energy distribution.

The magnetron ion source is an effective device for production of strong ion currents by electron impact with low energy electrons.^{4,5} The current available at 1 e.v. from known ion sources, including the magnetron, estimated from the current reported at the usual kv. extraction potentials would be inadequate for synthesis of the desired quantities. Measurements made with the usual magnetron configuration during this study support this conclusion. The concentric dual-anode magnetron ion source shown in Figure 1 proved capable of providing the desired 1-ma. currents at 1-e.v. extraction potentials.

In synthesis by means of the ion beam reaction, the possibility of alternate reactions resulting from charge transfer must be considered. In place of the desired reaction of the ions with the target molecules the ions may transfer charge either to the initial unionized gas

or to the target reagent. Some charge-transfer reactions, which would introduce possible alternate reaction paths, may be minimized by appropriate selection of the reaction parameters. Charge transfer of the ion with its gas can be minimized by ionizing the entering gas completely, thus avoiding appreciable concentrations of this particular neutral molecule; the pressure can be reduced to minimize close encounters of the ion with its gas. Charge transfer with the target molecules is in general not amenable to such control. The relative cross section of the desired ion-molecule reaction thus determines the product.

The diffusion of target molecules toward the ion source from the reaction zone is also undesirable because the ion energies are well-controlled only in the reaction zone. In addition, ionization of the target molecules can readily take place in the ion source if electron energies are sufficient. In these studies the pressure was adjusted so that the length of the reaction zone was approximately 1-3 mean free paths, ignoring possible specific gas or ion-gas interactions which would increase the number of ion-molecule encounters in the reaction zone.⁶

The nitration of benzene with NO_2^+ , a reaction which has been studied extensively in the liquid phase,⁷ was selected for the initial investigation.

Experimental

The ion beam reaction with the neutral target reagent is carried out in the apparatus shown in Figure 1. Ions formed in the source are extracted by appropriate grid potentials into the reaction zone, where they react with the neutral target molecules flowing into the zone. The gas from which the ions are prepared by electron bombardment enters the back of the ion source. Electrons emitted from the heated filament are accelerated to the concentric anodes by a potential only slightly above the appearance potential of the desired ion. The resulting ions are extracted through the circular orifice in the source by a 1-v. potential drop to the external grid. The reaction zone, one boundary of which is marked by this grid, is a short cylindrical volume 2 cm. in length and 15 cm. in diameter. A solid plate maintained at the same potential as the grid forms the rear boundary of the zone. The target gas, benzene in this study, enters the center of the reaction zone through a hollow

(4) B. G. Perovic, *Proceedings of the 3rd International Congress on Ionization Phenomena in Gases*, Venice, 1957, p. 813.

(5) H. R. Kaufman, NASA, Tech. Note D-585 (1961).

(6) S. Dushman, "Vacuum Technique," John Wiley and Sons, Inc., New York, N. Y., 1960, pp. 24-44.

(7) C. K. Ingold, "Structure and Mechanism in Organic Chemistry," Cornell University Press, Ithaca, N. Y., 1953, pp. 269-283.

tube perforated with 30 small radial holes 0.127 cm. in diameter, but closed at its end. This inlet provides high velocity radial gas flow. The gases flow out of the reaction zone through a circumferential gap of 0.125 cm. between the back potential plate and the large glass tube which is the vacuum chamber.

Ion Source. Ion currents of the order of 1 ma. were obtained with the magnetron ion source shown in Figure 1. The heated filament which serves as the cathode was drawn back and forth in a roughly cylindrical surface concentric with the anodes with its strands running generally along the axis of the cylinder. The two anodes were placed at the same potential. An axial magnetic field of approximately 500 gauss was applied which served to extend the paths of the electrons and thus increase the efficiency of ionization.

The outer cylindrical anode of the ion source was a copper tube 7.5 cm. in diameter and 10 cm. in length. The orifice for the ion current was a circular hole 1.9 cm. in diameter in this cylinder. Cooling water circulated in copper coils wrapped around this anode. The central anode was a steel rod 0.5 cm. in diameter. The tungsten filament of the cathode was 0.76-mm. (0.030-in.) tungsten wire 66 cm. in length. The magnetic field was provided by a 70-lb. magnet from a radar magnetron; the field varied from 700 gauss near the pole faces to 450 gauss in the center of the source. The magnet was placed outside the 6-in. diameter Pyrex "Double tough" glass tubing which served as the vacuum chamber, and pole pieces closely fitting the glass were attached. The cathode was heated with approximately 30 amp. of 60-v. a.c. current (at d.c. ground).

The ion current obtained was a very sensitive function of the filament temperature. A particularly critical threshold was observed, often accompanied by marked effects on the anode potentials and the gas pressure. The exact adjustment of the temperature varies with (1) the gas to be ionized, (2) the pressure, and (3) the anode potential. The tungsten filament was degassed before use by heating for several hours under vacuum. The filament lasted 10-15 hr. in use with nitrogen dioxide before burning out.

Formation of Ion Current. The following procedure was used to generate the ions for the reaction. The flow of nitrogen dioxide into the source was adjusted to give a pressure of 2×10^{-4} to 2×10^{-3} torr in the system. The anodes were placed at 12.5 e.v.; for other gases a potential a few volts above the reported ionization potential would be applied. The ionization potential of nitrogen dioxide has been reported from 9.78 to 18.87 e.v.⁸⁻¹⁴ The higher values have been attributed to the formation of the ion at electronic states above the lowest level.^{8,13,14}

The filament temperature was gradually increased until a strong current was obtained at a grounded collector placed 6 cm. from the orifice of the ion source. With the filament temperature and the gas pressure thus set, the anode potentials were reduced until no ion current was emitted. The anode potentials were then gradually increased to measure the variation of ion current with anode potential. Potentials should be sufficient to give 1 ma. yet as close as possible to the desired ionization process; with nitrogen dioxide 11 or 12.5 e.v. were used. When electron energies are close to the appearance potential of the ion desired, the cross section for ionization is low. This difficulty in producing a high ion current was overcome by using a large electron flow and a strong magnetic field perpendicular to the electric field. Under typical operating conditions an electron current of 1.5 to 5 amp. was observed to the anodes. The ion current emitted was analyzed with an r.f. quadrupole mass spectrometer.¹⁵

The kinetic energy of the ions was controlled by the potential placed on the control grid marking the formal boundary of the reaction zone. The grid was a mesh made of 1-mm. wire with square openings 3 mm. on a side. The effectiveness of this grid in controlling ion potentials was checked in each experiment by observing that no current was collected either at the grid or the plate at the rear of the reaction zone when they were placed at the same potential as the anode of the ion source. The presence of a small current was corrected, usually by a slight increase in pressure just sufficient to reduce the current observed to zero. In order to limit the ions entering the reaction zone to 1 e.v. the control grid and back plate marking the boundaries of the reaction zone were placed at a potential 1 e.v. below the anode potentials.

During the course of the reaction the source was adjusted to give complete ionization of the entering gas as determined by the current observed at the control grid and back plate. In the experiments reported here the flow of nitrogen dioxide was ca. 1 μ l./hr. of liquid at 25°, corresponding to a current of 844 μ a. With the added pressure of the target gas and the low extrac-

- (8) T. Nakayama, M. Y. Kitamura, and K. Watanabe, *J. Chem. Phys.*, **30**, 1180 (1959).
- (9) D. C. Frost, D. Mak, and C. A. McDowell, *Can. J. Chem.*, **40**, 1064 (1962).
- (10) R. J. Kandel, *J. Chem. Phys.*, **23**, 84 (1955).
- (11) K. Watanabe, *ibid.*, **26**, 542 (1957).
- (12) W. C. Price and D. M. Simpson, *Trans. Faraday Soc.*, **37**, 106 (1941).
- (13) J. Collin and F. P. Lossing, *J. Chem. Phys.*, **28**, 900 (1958).
- (14) Y. Tanaka and A. S. Jursa, *ibid.*, **36**, 2493 (1962).
- (15) W. Paul, H. P. Reinhard, and H. von Zahn, *Z. Physik*, **152**, 143 (1958).

tion potential during the synthesis the current of NO_2^+ actually reaching the reaction zone was reduced below that corresponding to the nitrogen dioxide flow. Readjustment of the ion source can increase the current, and under favorable conditions up to 80% of the expected current was observed.

NO_2^+ -Benzene Reaction. Liquid nitrogen tetroxide (Matheson, 99.5%) and benzene (Mallinckrodt, thiophene-free analytic reagent) were placed in pipets graduated in $\mu\text{l.}$ and sealed at the delivery tip. Each pipet was connected to the vacuum system through a micrometer needle valve.¹⁶ The volume of each liquid utilized in the reaction was thus measured directly.

The flow of nitrogen dioxide was started, and the ion source was adjusted to form the NO_2^+ current as described above. The flow of benzene was then initiated, followed by readjustment of the ion source for improved ion current if necessitated by the increase in pressure.

The total pressure in the reaction zone was approximately $1-5 \times 10^{-3}$ torr. The linear function relating the actual quantity of each reagent injected to the pressure observed at different positions in the apparatus was determined. The ratio of benzene to NO_2^+ in the reaction zone is conveniently given by the ratio of the reagent quantities reported.

A liquid nitrogen trap was used to collect the condensable products. The system was pumped from the rear of the reaction zone, maintaining gas flow from the ion source to the reaction zone and to the trap. The contents of the trap were taken up in an accurately measured benzene wash (1-2 ml.). The benzene solution was analyzed with an Apiezon-coated firebrick column at 170° in the Loe Model 15B gas chromatograph.¹⁷ Quantitative analyses were obtained by comparison with chromatograms of nitrobenzene-benzene solutions which were close in concentration to that obtained from the reaction. The product was isolated by condensation of the chromatographic gases. Its infrared absorption in the 2-15 μ region was the same as that of an authentic sample of nitrobenzene.

The quantities of reagents involved and product formed in a reaction are as follows: 0.0019 ml. of $\text{N}_2\text{O}_4(\text{l})$ at 31° (0.00270 g., 2.93×10^{-5} mole), 0.006 ml. of $\text{C}_6\text{H}_6(\text{l})$ at 31° (0.00520 g., 6.66×10^{-5} mole), and NO_2^+ current at 1 e.v.: 2.88 coulombs gave 2.87 mg. of nitrobenzene (78% based on NO_2^+ ; 40%, on N_2O_4).

When the molar ratio of benzene to nitrogen dioxide was increased the yield of nitrobenzene was higher. For example, 0.00285 g. of nitrogen dioxide (6.20×10^{-5} mole NO_2) in reaction with 0.564 g. of benzene (7.22×10^{-3} mole), a ratio greater than 100, formed 7.5 mg. of nitrobenzene (99%).

The reaction is very sensitive to proper adjustment of the pressure in the system. At high nitrogen dioxide pressures many electrons were apparently emitted from the source accompanying the positive ions. Under these conditions a low yield of mixed organic products was obtained, but nitrobenzene was absent. At appreciably lower pressures no NO_2^+ formed and no products were obtained, even though all other conditions were correct. When the reagent pressures were properly adjusted, however, the only condensable product obtained was nitrobenzene.

Discussion

NO_2^+ Ion Beam. Preparation of a beam containing only NO_2^+ avoids competing reactions by other ions. In previous studies^{18,19} NO^+ was obtained as the predominant ion from ionization of nitrogen dioxide by electron impact when electron energies of 40-70 e.v. were employed. These energies are typical of ion sources used in mass spectrometers. In the mixture of ions formed, NO_2^+ varied from less than 10% to perhaps 20% of the total. Monatomic and diatomic positive ions of both nitrogen and oxygen were also present.

In this work a beam consisting of 99% NO_2^+ with less than 1% NO^+ was formed from nitrogen dioxide by using electrons with maximum energies carefully limited to 11.0 to 12.5 e.v. With increasing anode potential the amount of NO^+ increased. With 15 v. on the anodes the beam contained ca. 5% NO^+ ; at 30 v. the concentration of NO^+ had arisen to 25%.

The formation of the NO_2^+ beam with 1-e.v. ion energies at 1-ma. current level is indicated by current measurements and mass spectrometric study, which are in agreement with the results of the ion-molecule reaction. Since the 1-e.v. extraction potential apparently provides a gradient less than that of the potentials applied inside the ion source itself, unlike previous sources, the formation of the beam is of interest. Direct comparison of the dual-anode magnetron with the usual magnetron configuration showed that the field provided by the central anode markedly increases positive ion current through the orifice at low potentials. The formation of a large ion density assists in emission of the ion current from the source. The concentric poten-

(16) Edwards High Vacuum, Inc., Niagara Falls, N. Y., Speedivac LB2A stainless steel needle valve was used for nitrogen dioxide; Nuclear Products Co., Cleveland, Ohio, fine metering valve SS4M was used for benzene.

(17) Loe Engineering Co., Altadena, Calif.

(18) E. G. C. Stueckelberg and H. D. Smyth. *Phys. Rev.*, **36**, 478 (1930).

(19) R. A. Friedel, A. G. Sharkey, Jr., J. L. Schultz, and C. R. Humbert, *Anal. Chem.*, **25**, 1314 (1953).

tial field tends to focus the ions in a cylindrical surface between the two anodes. At the ion orifice the potential gradient from the central anode combined with a slight potential well in the outer anode, the ion charge density, and the potential drop to the control grid provides sufficient force for the desired ion flow. The higher plasma density inside the magnetron can affect the potential gradients by shielding.

The energy distribution in the ion beam was determined by the variation of the current with the electrostatic potential of a collector. The ions in the beam extracted by a 1-e.v. potential drop to the control grid were uniformly distributed from 0 to 1 e.v. in energy.

Charge Transfer. Several experiments were made to study possible reaction which neutral nitrogen dioxide with the energies available in this reaction system as a result of charge transfer could undergo with benzene.

When the reagents were mixed under the conditions of the ion beam reaction but with the ion source off, no nitrobenzene was formed. If the reagent mixture in the product trap was allowed to stand at room temperature, traces of nitrobenzene were formed. A reaction run with all conditions as in the synthesis producing nitrobenzene, including heating of the filament to the usual temperature, but with the anodes of the ion source at zero potential yielded no nitrobenzene. This indicates that the radiation from the hot filament was not responsible for the reaction of neutral reagents. The only organic material trapped under these conditions was benzene itself.

Under conditions more closely resembling the actual reaction, the anode potentials were applied and nitrogen dioxide was admitted as in the usual generation of the ion current. The potential on the control grid at the boundary of the reaction zone was increased, however, to the lowest value required to prevent any current from reaching the grid. Again no nitrobenzene was obtained, indicating the nitrobenzene is not formed in the ion source.

A further experiment was made with an additional grid interposed between the ion source and the usual control grid to ensure the extraction of ions from the source. The second grid was placed approximately 1 cm. toward the ion source from the control grid. The normal NO_2^+ current was extracted with a 1-e.v. potential drop to the interposed grid, but the ions were prevented from reaching the reaction zone containing the benzene target molecules by a potential on the control grid equal to that on the anode. Again no nitrobenzene

was obtained. In this experiment only neutral nitrogen dioxide molecules, especially those provided with increased kinetic energy by charge transfer, could enter the reaction zone. The result indicates that nitrobenzene was produced only by an ionic reaction in the investigation reported here. Combined with the previous experiments, it also appears that the formation of nitrobenzene occurred in the specified reaction zone. Concentrations of benzene effective in producing nitrobenzene are evidently largely limited to the region directly in or near the reaction zone.

If under these conditions benzene is restricted to the reaction region, the experimental facts point strongly to the occurrence of reaction 1 with great efficiency. On the other hand this restriction has not been proved, and until it is other explanations for nitrobenzene formation cannot be excluded.

The formation of the benzene ion C_6H_6^+ is an additional possibility from charge transfer of NO_2^+ with the target gas. To determine the effect of this process a preliminary study was made in which a beam of benzene ions was directed into nitrogen dioxide. No nitrobenzene was formed.

Benzene- NO_2^+ Reaction. High yields of nitrobenzene were obtained in the reaction of NO_2^+ with high ratios of benzene.

The absorption of the neat product in the infrared was the same as that of an authentic sample of nitrobenzene. Chromatography of the product with a small additional quantity of nitrobenzene gave a single peak with no indication of fractionation. No other condensable products could be detected when the reaction was run under suitable conditions.

The over-all reaction observed can be summarized as shown in eq. 1. The present study did not include



the question of the reaction path which will be reported in future investigations.

Acknowledgment. The authors are grateful to Dr. L. B. Marantz for valuable suggestions and assistance and to Dr. Conrad Bodai for suggesting the design of the ion source and assisting in its construction. B. J. Chai provided essential experimental aid. The encouragement of Dr. J. F. Masi and the support of this work by the Air Force Office of Scientific Research are deeply appreciated.

Evidence of Structure and Dissociation Equilibrium in Liquid

Iron Oxide from Iron Oxide Activity Data

by Oliver N. Salmon and Roger D. Hilde

*Minnesota Mining and Manufacturing Company, Central Research Laboratories, St. Paul, Minnesota
(Received April 20, 1964)*

Thermodynamic activities for FeO have been calculated for the liquid iron oxide system based on a quasi-magnetite structure and compared with the experimental values from the scientific literature at three temperatures for compositions ranging from FeO to Fe₃O₄. Using the experimental values for FeO and derived activity expressions for FeO, Fe₃O₄, and Fe₂O₃, an equilibrium constant has been calculated for the dissociation reaction $\text{Fe}_3\text{O}_4 \rightleftharpoons \text{FeO} + \text{Fe}_2\text{O}_3$, in the liquid state.

Introduction

Flood and Hagermark¹ have suggested that a quasi-crystalline structure similar to the spinel structure of magnetite [Fe₃O₄(γ)] exists in liquid iron oxide in the composition range between FeO and Fe₃O₄. Since a spinel-like structure is assumed, this infers that liquid iron oxide containing an oxygen to iron atom ratio of less than $\frac{4}{3}$ contains defects. Flood and Hagermark have assumed that these defects are oxygen vacancies.

From what is known of the structures of wüstite [FeO(w)] and magnetite, the assumption of a quasi-magnetite structure for the liquid iron oxide is reasonable. However, rather than the defects being oxygen vacancies, it is more reasonable to assume that they are iron atoms in interstitial positions which are octahedrally surrounded by oxygen ions. This is in accordance with the neutron-diffraction study of the wüstite structure by Roth² in which he found that excess oxygen appeared to be present as magnetite molecular islands in solid solution. On the basis of Roth's findings, Salmon³ assumed that wüstite itself had a magnetite-like structure in which one-half of the iron atoms in FeO(w) were present as zero-valent iron atoms in interstitial octahedral positions in the magnetite-like lattice. Thermodynamic activities of FeO calculated³ on the basis of this model gave good agreement with the experimental values of Darken and Gurry.⁴ The model arrived at by Salmon is equivalent to assuming that wüstite has a magnetite-like lattice in which FeO in solid solution in Fe₃O₄ introduces

defects consisting of 0.5 interstitial iron atom in octahedral sites per molecule of FeO. Accordingly, in the following treatment of thermodynamic activities in liquid iron oxide, we have assumed a magnetite-like structure and the presence of interstitial iron atoms in octahedral sites when the atom ratio of oxygen to iron is less than $\frac{4}{3}$.

Results and Discussion

The following expression was derived by Salmon³ for calculating the activities of FeO in the wüstite phase.

$$a_1 = \left(\frac{0.5X_1}{0.5X_1 + 2X_2} \right)^{0.5} \quad (1)$$

where a_1 = activity of FeO; X_1 = mole fraction of FeO; X_2 = mole fraction of Fe₃O₄. We have used the same expression to calculate the activities of FeO in liquid iron oxide in the composition region between FeO and Fe₃O₄. The results at 1400, 1500, and 1600° are compared in Table I with the corresponding experimental values of Darken and Gurry.⁵ The compositions are expressed in mole fractions of Fe₃O₄, the other component being FeO unless otherwise specified.

(1) H. Flood and K. Hagermark, *Acta Chem. Scand.*, **15**, 1624 (1961).

(2) W. L. Roth, *J. Appl. Phys., Suppl.*, **30**, No. 4, 303S (1959).

(3) O. N. Salmon, *J. Phys. Chem.*, **65**, 550 (1961).

(4) L. S. Darken and R. W. Gurry, *J. Am. Chem. Soc.*, **67**, 1407 (1945).

(5) L. S. Darken and R. W. Gurry, *ibid.*, **68**, 798 (1946).

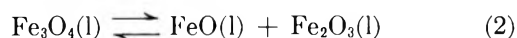
In Table I each of the experimental values of Darken and Gurry have been multiplied by the same constant factor which was selected so as to cause the calculated and experimental values of a_1 to be equal at a composition of 0.081 mole fraction of Fe_3O_4 . This is equivalent to selecting a new standard state composed of stoichiometric FeO rather than the nonstoichiometric standard state used in arriving at the experimental activities.

Table I: Activity of FeO in Liquid Iron Oxide

Atom ratio oxygen/iron	Mole fraction of Fe_3O_4	Activity of FeO					
		1400°		1500°		1600°	
		Darken and Gurry	Calcd.	Darken and Gurry	Calcd.	Darken and Gurry	Calcd.
1.012	0.012					0.92	0.98
1.023	0.024			0.92	0.95		
1.034	0.036	0.91	0.93				
1.04	0.043	0.90	0.92	0.90	0.92	0.90	0.92
1.07	0.081	0.86	0.86	0.86	0.86	0.86	0.86
1.10	0.125	0.81	0.80	0.81	0.80	0.81	0.80
1.12	0.153	0.77	0.76				
1.15	0.214	0.69	0.69	0.69	0.69	0.70	0.69
1.20	0.333	0.54	0.58	0.56	0.58	0.57	0.58
1.22	0.380			0.51	0.48		
1.25	0.500					0.44	0.45
1.30	0.750					0.31	0.28
1.33	1.000					0.23	0.00
1.34	0.941 ^a					0.22	
1.37	0.703 ^a					0.16	

^a These compositions are on the oxygen-rich side of Fe_3O_4 , and, hence, the composition is expressed as mole fraction of Fe_3O_4 , the other component being Fe_2O_3 rather than FeO.

The agreement between the calculated and experimental activities is quite good at 1400, 1500, and 1600°, with the exception of the compositions approaching Fe_3O_4 . Experimental activities for these near-stoichiometric Fe_3O_4 compositions were reported by Darken and Gurry only for the 1600° case. The high experimental values for the FeO activities for compositions having an oxygen to iron ratio near $4/3$ suggested that some FeO molecules were being produced by the dissociation of Fe_3O_4 at 1600° according to the reaction



We next proceeded with an attempt to determine the equilibrium constant for this reaction by use of the values for the experimental activities of FeO and the activities expressions which we derived for FeO, Fe_3O_4 , and Fe_2O_3 in liquid iron oxide. The expressions are derived below.

It will be assumed that liquid iron oxide has a quasi-magnetite structure over its entire composition range. For compositions having an oxygen to iron ratio less than $4/3$, the initial composition will be considered as being made up of N_1' molecules of FeO and N_2' molecules of Fe_3O_4 . At equilibrium, the dissociation of Fe_3O_4 , according to eq. 2, contributes N additional molecules of FeO and N molecules of Fe_2O_3 giving a total of $N_1 = N_1' + N$ molecules of FeO; $N_2 = N_2' - N$ molecules of Fe_3O_4 ; $N_3 = N$ molecules of Fe_2O_3 .

For compositions having an oxygen to iron ratio greater than $4/3$, the initial composition will be considered as being made up of N_2' molecules of Fe_3O_4 and N_3' molecules of Fe_2O_3 . At equilibrium in the dissociation reaction the liquid contains a total of $N_1 = N$ molecules of FeO; $N_2 = N_2' - N$ molecules of Fe_3O_4 ; $N_3 = N_3' + N$ molecules of Fe_2O_3 .

The next step involves the derivation of activity expressions for FeO, Fe_3O_4 , and Fe_2O_3 in liquid iron oxide containing a total of N_1 molecules of FeO, N_2 molecules of Fe_3O_4 , and N_3 molecules of Fe_2O_3 . Following the treatment used by Salmon³ for the solid iron-oxygen system, it will be assumed that N_1 molecules of FeO contribute $0.5N_1$ neutral Fe^0 atoms in interstitial octahedral sites which are randomly mixed with $(2N_2 + 1.5N_3)$ neutral octahedral vacancies contributed by the N_2 molecules of Fe_3O_4 and N_3 molecules of Fe_2O_3 . In addition, it will be assumed that the N_3 molecules of Fe_2O_3 contribute $0.25N_3$ $2+$ vacancies in octahedral sites which are randomly mixed with $(0.25N_1 + N_2)$ Fe^{2+} ions in octahedral sites. The number of distinguishable configurations, Ω , in the liquid state by the above random mixing is given by

$$\Omega = \frac{(0.5N_1 + 2N_2 + 1.5N_3)!}{(0.5N_1)! (2N_2 + 1.5N_3)!} \times \frac{(0.25N_1 + N_2 + 0.25N_3)!}{(0.25N_1 + N_2)! (0.25N_3)!} \quad (3)$$

The standard state for FeO, Fe_3O_4 , and Fe_2O_3 has been chosen to be the liquid state having a quasi-magnetite structure. It is assumed that the interstitial and vacancy defects mentioned above for FeO and Fe_2O_3 , respectively, do not appreciably change the configurational entropies of the FeO and Fe_2O_3 standard states from that of Fe_3O_4 . Also, it is assumed that the thermal entropies of the three species do not change on mixing. From this, it follows that the entropy of mixing ΔS_m is given by $\Delta S_m = k \ln \Omega$, where k is Boltzmann's constant. The activity a_i of component i can be defined by $RT \ln a_i = (\bar{H}_i - H_i^\circ) - T(\bar{S}_i - S_i^\circ)$, where subscript $i = 1, 2$, and 3 , and refers to components FeO, Fe_3O_4 , and Fe_2O_3 , respec-

tively. T = absolute temperature; $\bar{H}_i - H_i^\circ$ = partial molal heat of mixing of component i ; $\bar{S}_i - S_i^\circ = (\delta\Delta S_M/\delta n_i)_{T,P, \text{ other } n\text{'s}}$ the partial molal entropy of mixing of component i ; n_i = number of moles of component i ; $R = kN_0$ the gas constant; N_0 = Avogadro's number. The standard states have been selected such that $(\bar{H}_i - H_i^\circ)$ is small and to a good approximation will be assumed to be zero. Then, it follows that

$$R \ln a_i = -(\bar{S}_i - S_i^\circ) = -\left(\frac{\delta\Delta S_M}{\delta n_i}\right)_{T,P, \text{ other } n\text{'s}}$$

or

$$R \ln a_i = -k \left(\frac{\delta \ln \Omega}{\delta n_i}\right)_{T,P, \text{ other } n\text{'s}} \quad (4)$$

By applying Stirling's approximation to $\ln \Omega$ obtained from eq. 3 to eliminate the factorials, replacing the N_i 's by n_i 's in the appropriate manner, substituting the resulting expression for $\ln \Omega$ into eq. 4, and differentiating with respect to n_i , as indicated, we arrived at the following expressions for the activities

$$a_1 = \left(\frac{0.5X_1}{0.5X_1 + 2X_2 + 1.5X_3}\right)^{0.5} \times \left(\frac{0.25X_1 + X_2}{0.25X_1 + X_2 + 0.25X_3}\right)^{0.25} \quad (5)$$

$$a_2 = \left(\frac{2X_2 + 1.5X_3}{0.5X_1 + 2X_2 + 1.5X_3}\right)^2 \times \left(\frac{0.25X_1 + X_2}{0.25X_1 + X_2 + 0.25X_3}\right) \quad (6)$$

$$a_3 = \left(\frac{2X_2 + 1.5X_3}{0.5X_1 + 2X_2 + 1.5X_3}\right)^{1.5} \times \left(\frac{0.25X_3}{0.25X_1 + X_2 + 0.25X_3}\right)^{0.25} \quad (7)$$

where X_1 , X_2 , and X_3 are the equilibrium mole fractions of FeO, Fe₃O₄, and Fe₂O₃, respectively, in liquid iron oxide.

For compositions having an oxygen to iron atom ratio less than $4/3$

$$X_1 = \frac{X_1' + X}{1 + X} \quad (8)$$

$$X_2 = \frac{X_2' - X}{1 + X} \quad (9)$$

$$X_3 = \frac{X}{1 + X} \quad (10)$$

where X_1' and X_2' are the initial mole fractions of FeO and Fe₃O₄, respectively, and X is the mole fraction

of Fe₃O₄ which dissociates according to eq. 2. For compositions having an oxygen to iron atom ratio greater than $4/3$

$$X_1 = \frac{X}{1 + X} \quad (11)$$

$$X_2 = \frac{X_2' - X}{1 + X} \quad (12)$$

$$X_3 = \frac{X_3' + X}{1 + X} \quad (13)$$

where X_2' and X_3' are the initial mole fractions of Fe₃O₄ and Fe₂O₃, respectively.

X can be calculated by substituting for X_1 , X_2 , and X_3 in eq. 5 from eq. 8–10 or eq. 11–13, whichever are appropriate, and using the experimental values of Darken and Gurry for X_1' , X_2' , X_3' , and a_1 . Activities of Fe₃O₄ and Fe₂O₃ were obtained by substituting the calculated value of X into the activity expressions (6) and (7). Knowing the activities, a_1 , a_2 , and a_3 , the dissociation constant K for reaction 2 can be calculated from the expression $K = a_1 a_3 / a_2$. The results of these calculations are shown in Table II.

Table II: Dissociation of Fe₃O₄ in Liquid Iron Oxide at 1600°

Atom ratio oxy- gen/ iron	Initial mole fraction			Mole fraction of Fe ₃ O ₄ dissociated	Activities at equilibrium			Dissociation constant
	FeO	Fe ₃ O ₄	Fe ₂ O ₃		FeO	Fe ₃ O ₄	Fe ₂ O ₃	
1.30	0.250	0.750	0.000	0.0657	0.31	0.798	0.327	0.127
1.33	0.000	1.000	0.000	0.2185	0.23	0.839	0.457	0.125
1.34	0.000	0.941	0.059	0.1983	0.22	0.834	0.484	0.128
1.37	0.000	0.703	0.297	0.1021	0.16	0.816	0.584	0.115

These results give considerable support to the belief that the lack of agreement between calculated and experimental values of the FeO activity for compositions of liquid iron oxide near Fe₃O₄ is due to the dissociation of some Fe₃O₄ into FeO and Fe₂O₃. A reasonable value of the equilibrium constant for this dissociation appears to be 0.124 ± 0.004 at 1600°.

The relative influence of this dissociation of Fe₃O₄ on the experimental activities should decrease rapidly as the liquid composition departs farther from an oxygen to iron atom ratio of $4/3$. To check this, the activity of a composition having an oxygen to iron atom ratio of 1.25 was calculated to be 0.45 at 1600° when the effect of the Fe₃O₄ dissociation was included. This compares well with the experimental value of 0.44

and with the calculated value of 0.45 in Table I where the influence of the dissociation was neglected.

Conclusions

The good agreement found between experimental and calculated thermodynamic activities supports the view that liquid iron oxide has a quasi-magnetite structure. It also supports the belief that interstitial iron defects are present on the oxygen-deficient side of liquid Fe_3O_4 and iron vacancy defects are present on the oxygen-excess side.

The deviation of the calculated and experimental

activities of FeO for liquid iron oxide compositions in the neighborhood of stoichiometric Fe_3O_4 at 1600° is explained by the dissociation of Fe_3O_4 into FeO and Fe_2O_3 . By use of the experimental FeO activity data and derived expressions for FeO, Fe_3O_4 , and Fe_2O_3 activities in liquid iron oxide, the equilibrium constant for the Fe_3O_4 dissociation was found to be 0.124 ± 0.004 at 1600° . The method used here for determining the equilibrium constant in the liquid state should work equally as well for studying equilibria in one phase, solid state systems, provided the appropriate activities can be accurately determined over composition ranges of appreciable magnitude.

γ -Radiolysis of Liquid Cyclopentanone^{1a,b}

by W. W. Bristowe, M. Katayama, and C. N. Trumbore^{1c}

Department of Chemistry, University of Delaware, Newark, Delaware (Received May 16, 1964)

The major primary products of the γ -radiolysis of liquid cyclopentanone and their initial G values are as follows: H_2 , 0.68 ± 0.02 ; CO, 0.8 ± 0.1 ; ethylene, 0.85 ± 0.04 ; cyclobutane, 0.11 ± 0.01 ; 4-pentenal, 0.74 ± 0.05 ; cyclopentanol, 0.81 ± 0.05 ; 2-cyclopentanone, 0.21 ± 0.02 ; dimer, 0.23 ± 0.02 ; and total polymer, 4.4 ± 0.5 (based on cyclopentanone). Minor primary products are 1-butene, *n*-butane, and propylene (all with G values < 0.1). The effects of added oxygen, iodine, and DPPH are reported. The isotopic hydrogen and ethylene yields from irradiated 2,2,5,5-cyclopentanone- d_4 are discussed. Possible mechanisms for the formation of the products are also discussed.

Introduction

In view of the ability of ionizing radiation not only to ionize but also to excite molecules electronically, it is of interest to compare in detail the radiolysis and photolysis of a suitable chemical system. The somewhat unique photolytic behavior of cyclopentanone²⁻⁴ described in a series of papers by Srinivasan led us to initiate an investigation of the possible relationships between the photochemistry and radiation chemistry of cyclopentanone.⁵

Katayama, Whitmer, and Trumbore⁵ noted, in a preliminary report, qualitative comparisons between

the products of the radiolysis and photolysis of cyclopentanone. Singh and Freeman⁶ have more recently

(1) (a) This research was supported by the U. S. Atomic Energy Commission; (b) taken in part from the Ph.D. Thesis of M. Katayama, University of Delaware, 1963; (c) to whom communications should be addressed.

(2) The mechanism proposed by Srinivasan³ for this system is one in which the final products of the vapor phase photolysis are governed by the degree of collisional deactivation of the vibrationally excited upper singlet state cyclopentanone molecule. Both the studies by Srinivasan and Blacet and Miller⁴ pointed toward a wave length dependence.

(3) R. Srinivasan in "Advances in Photochemistry," Vol. I, W. A. Noyes, G. S. Hammond, and J. N. Pitts, Ed., Interscience Publishers, Inc., New York, N. Y., 1963.

reported on the radiolysis of liquid cyclohexanone and mixtures containing cyclohexanone.

In this paper the results of a detailed study of the cobalt-60 γ -radiolysis of liquid cyclopentanone are reported.

Experimental

Cyclopentanone (Eastman Kodak reagent grade) was fractionally distilled through a Whitmore distillation column, and the middle third was collected. The purity of the cyclopentanone was monitored gas chromatographically with a flame ionization gas chromatograph. Among other very small amounts ($<0.05\%$) of impurities shown by the flame ionization detector, an impurity was found at the same retention time as 4-pentenal. It was not possible to remove this impurity with various purification procedures.

A flask containing this center cut was attached to a conventional vacuum line. A freeze-pump-thaw technique was used for degassing the sample. The cyclopentanone was then distilled to the irradiation cells.

2,2,5,5-Cyclopentanone- d_4 was prepared through successive exchange reactions of cyclopentanone and 99.5% heavy water by the manner of Streitwieser, *et al.*⁷ The yield was about 10%. The infrared spectrum showed no peak at 1407 cm.^{-1} , which is attributed to deformation of a methylene group next to a carbonyl group. Chromatographic analysis showed over 99% purity. The deuteriocyclopentanone was degassed and used in the above manner.

4-Pentenal was prepared by the high-pressure, mercury arc photolysis of pure liquid cyclopentanone.⁸ Separation of the 4-pentenal from the cyclopentanone was obtained by a combination of fractional distillation and preparative gas chromatography on a Carbowax 400 preparative column. The resulting product was analyzed to be 98% pure by further mass spectrographic and chromatographic analysis. The mass spectral cracking pattern agreed quantitatively with that reported by Srinivasan.⁸

2-Cyclopentanone was obtained from the Aldrich Chemical Co. and after purification was found to be 99% pure.

Ethylene, 1-butene, *n*-butane, carbon monoxide, oxygen, and hydrogen were obtained in gas cylinders of highest purity and were used without purification.

A sample of pure cyclobutane was obtained through the generosity of Dr. W. D. Walters of the University of Rochester.

Cyclopentanol, iodine, and diphenylpicrylhydrazil (DPPH) were obtained from the Eastman Kodak Co. and were used without further purification.

Irradiation Procedure and Analysis

Hydrogen and carbon monoxide were determined by two different methods. In one method a cell which was equipped with a break-seal was filled with degassed cyclopentanone and irradiated. After irradiation, the cell was attached to a standard analytical vacuum line. The reaction mixture was fractionated through a series of traps. Volatile products (not condensable in liquid nitrogen) were then transferred by means of a Toepler pump to a McLeod gauge where they were either measured quantitatively with the use of a CuO furnace or collected for mass spectral analysis.

The other method was a modification of the syringe technique described by Hart.⁹ In this technique the solution is deoxygenated in a vessel through a glass frit with 99.995% pure argon. The solution is transferred to a syringe and irradiated. The gases are extracted by a Van Slyke apparatus and analyzed by gas chromatography using a molecular sieve (13x) column.

The gaseous hydrocarbons and the liquid products were analyzed differently. Cylindrical irradiation cells were constructed from 10-mm. o.d. Pyrex tubing and were attached to a vacuum line through a single capillary (0.5-mm. i.d.). The degassed cyclopentanone was distilled into the cell so as to fill the entire cell, including part of the capillary. The cell was sealed off in the capillary region, thus allowing an average of 0.5% gas volume. The small capillary was used so that the diffusion of volatile products out of the bulk of the irradiated liquid during radiolysis was reduced to a minimum.

Immediately following the irradiation, the cell capillary was cracked open and a known volume (3–10 $\mu\text{l.}$) of the solution was injected directly into the gas chromatograph. For analysis of dissolved gases a 4.57-m. β,β -oxydipropionitrile column maintained at 0° was used. For the analysis of liquid products a 2-m. Carbowax 20 M column was used with linear programming from 85 to 150° at $1.1^\circ/\text{min.}$, and for the dimer species a 0.6-m. silicone gum rubber column at 130° was employed. Peak areas were measured, and G values were calculated from standardizations using solutions containing known amounts of product. Identifications of irradiation products were made through comparisons of their gas chromatographic

(4) F. Blacet and A. Miller, *J. Am. Chem. Soc.*, **79**, 4327 (1957).

(5) M. Katayama, J. C. Whitmer, and C. N. Trumbore, *ibid.*, **84**, 4025 (1962).

(6) A. Singh and G. R. Freeman, *Can. J. Chem.*, **42**, 1869 (1964).

(7) A. Streitwieser, *et al.*, *J. Am. Chem. Soc.*, **80**, 2326 (1958).

(8) R. Srinivasan, *ibid.*, **81**, 1546 (1959).

(9) E. Hart, S. Gordon, and D. Hutchison, *ibid.*, **75**, 6165 (1953).

retention times and of their mass spectral cracking patterns with those of known compounds.

In the studies carried out in the presence of added oxygen, iodine, and DPPH the above analytical procedures were employed.

In this paper "polymer" is defined as the viscous oil left after thorough evacuation of the irradiation vessel of all volatile material. To determine the initial yield of total polymer, a cell was irradiated, and the volatile products were removed. The irradiation cell was washed thoroughly with acetone in which the polymer was completely soluble. The washings were transferred to a previously weighed vessel, and the acetone was removed in a vacuum desiccator. The vessel and polymer were weighed until constant weight was established. Blanks were also run for acetone and for unirradiated cyclopentanone. Acetone solutions of the resulting polymer were found by gas chromatography to be completely free of cyclopentanone.

The irradiation source was a Gammacell 220 manufactured by Atomic Energy of Canada, Ltd., with a dose rate of approximately 5×10^{18} e.v./g. hr. as measured with the Fricke dosimeter.

Results

The primary products found in the γ-radiolysis of cyclopentanone and their corresponding G values are listed in Table I. The G values are based on linear concentration-dose plots or on initial slopes estimated from nonlinear plots of the product in question.

Table I: Products and G Values of Irradiated Cyclopentanone

Product	G, molecules/100 e.v.
H ₂	0.68 ± 0.02
CO	0.8 ± 0.1
C ₂ H ₄	0.85 ± 0.04
4-Pentenal	0.74 ± 0.05
Cyclopentanol	0.81 ± 0.05
2-Cyclopentanone	0.21 ± 0.02
Polymer (-C ₅ H ₈ O)	4.4 ± 0.5
Dimer	0.23 ± 0.02
Cyclobutane	0.11 ± 0.01
1-Butene	0.07 ± 0.01
n-Butane	0.05 ± 0.01
Propylene	~0.02

The dependence of the product yields on the dose, which was received by either degassed or oxygen-saturated liquid cyclopentanone, is presented in Figures 1-8.

Hydrogen and Carbon Monoxide. G(H₂) was found to be 0.68 ± 0.02 and independent of dose by two dif-

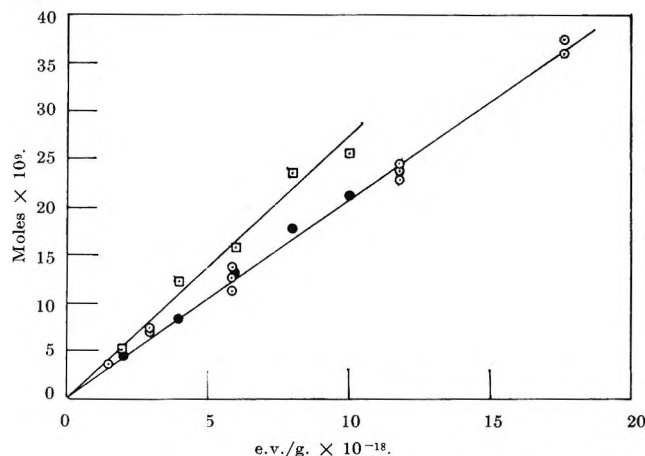


Figure 1. Yields of CO and H₂ from the Co⁶⁰ radiolysis of pure liquid cyclopentanone: ○, H₂ from break-seal; ●, H₂ from syringe technique; □, CO from syringe.

ferent analytical techniques. The results of these studies are found in Figure 1.

In a study of the effects of added DPPH on the amount of hydrogen produced for a constant dose (1.6×10^{19} e.v./5 ml. of cyclopentanone) the amount of hydrogen was reduced from a value of $9.0 \pm 0.5 \times 10^{-7}$ mole for pure cyclopentanone to $8.1 \pm 0.4 \times 10^{-7}$ mole at 1.6×10^{-3} M DPPH and $7.1 \pm 0.4 \times 10^{-7}$ mole at 3.2×10^{-3} M DPPH.

G(CO) was found to be 0.8 ± 0.1 by the syringe technique. Results of this study are also shown in Figure 1. Corrections (owing to incomplete separation of ethylene from the H₂ and CO fraction) were applied to the CO data reported earlier,⁵ and G(CO) was found to be within experimental error of the above value. Contrary to our previous report, the CO yield is a linear function of dose to 1.0×10^{19} e.v./g.

2,2,5,5-Cyclopentanone-d₄. Since the amount of 2,2,5,5-cyclopentanone-d₄ available was not large and it was necessary to obtain a large amount of gaseous product for isotopic analysis with reasonable accuracy, a rather small amount of this ketone (1 ml.) was irradiated to a relatively large total dose. It can be seen from Table II that the ratio of H₂:HD:D₂ is reasonably constant with respect to the time of irradiation and temperature.

Other Primary Products. Ethylene dose dependence data are shown in Figure 2. Both oxygenated and degassed solutions not only give linear concentration-dose plots but also show the same yield of G(C₂H₄) = 0.85 ± 0.04. The cyclobutane yield was also unaffected in oxygen-saturated solutions as compared with the pure liquid.

The mass spectrum of the ethylene fraction from

Table II: Ratio of H₂:HD:D₂ from Radiolysis of 1 ml. of 2,2,5,5-Cyclopentanone-*d*₄

E.v./g. × 10 ⁻²⁰	Temp., °C.	Additive	Concn., <i>M</i>	Moles × 10 ⁷ (CO + H ₂)	H ₂ :HD:D ₂
42.25	23	1:1.26:0.37
3.24	23	62.0	1:1.26:0.33
4.19	-78	30.7	1:1.25:0.37
3.03	23	Cyclohexene	9.9 × 10 ⁻¹	55.0	1:0.78:0.15
3.24	23	DPPH	3.8 × 10 ⁻³	60.0	1:0.78:0.34

2,2,5,5-cyclopentanone-*d*₄ was examined and characterized as 90% CH₂=CD₂ and 10% CH₂=CHD.¹⁰

The yield-dose plots of 1-butene and *n*-butane are presented in Figure 3 where it is seen that the addition of oxygen has a marked effect on both products. It appears that the limiting slope of the oxygen curve for *n*-butane at zero dose is zero while that for 1-butene is finite. At higher doses the slopes of the oxygenated solution curves appeared to approach those of the degassed solution curves. Independent experimental evidence showed that oxygen was rapidly consumed in these solutions. In the pure liquid the *G* values of both these compounds are independent of dose, over the dose range studied (up to 3 × 10²⁰ e.v./g.).

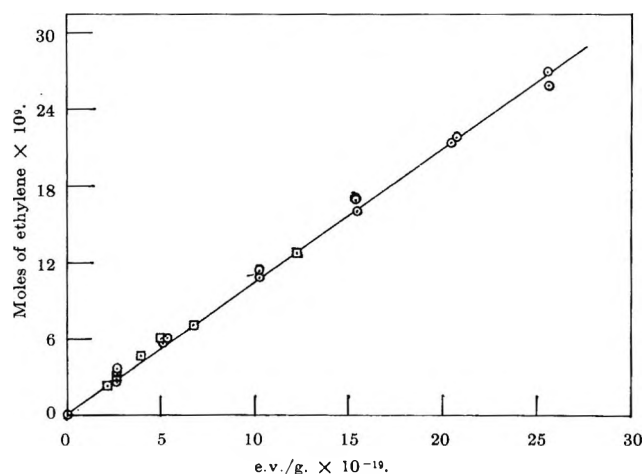


Figure 2. Ethylene yields from γ -irradiated liquid cyclopentanone (8- λ sample) in the presence and absence of oxygen: \circ , degassed; \square , oxygen-saturated.

Figure 4 shows 4-pentenal concentration-dose curves with and without oxygen in irradiated cyclopentanone solutions. In both solutions the zero dose values (blank values) are rather high compared to the change in concentration of the product during radiolysis. Despite this, in the pure liquid the yield of 4-pentenal

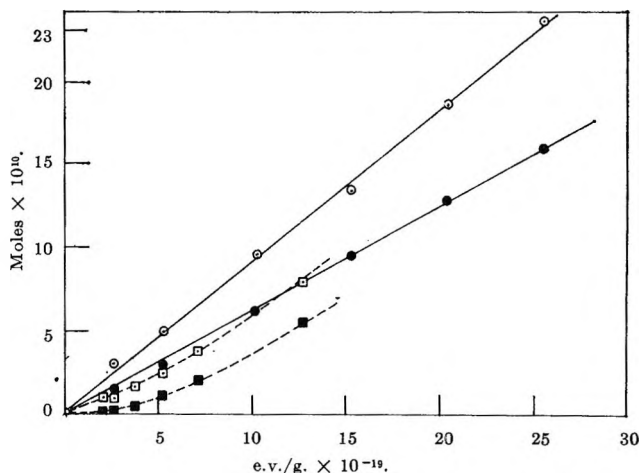


Figure 3. *n*-Butane and 1-butene yields in the γ -radiolysis of liquid cyclopentanone: \circ , degassed; \square , oxygen-saturated; open figures, 1-butene; shaded figures, *n*-butane.

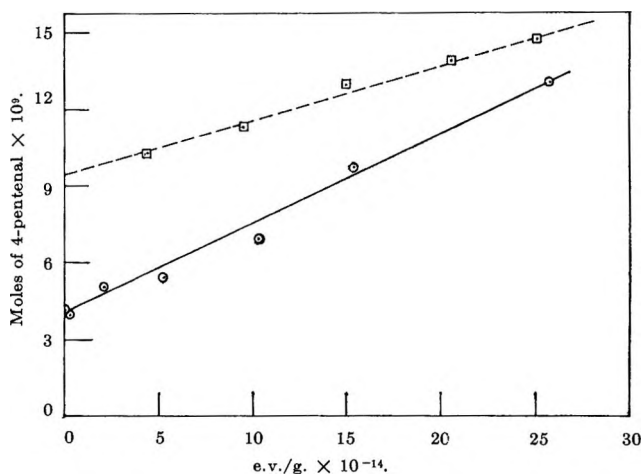


Figure 4. 4-Pentenal yields in the γ -radiolysis of liquid cyclopentanone. High blank values are due to the very high sensitivity of the flame ionization detector used: \circ , degassed; \square , oxygen-saturated.

was constant with dose. In oxygen-saturated solutions there appears to be a definite lowering of the yield of 4-pentenal.

Figure 5 illustrates that cyclopentanol is a primary product with no secondary reactions occurring before a dose of 2.5 × 10²⁰ e.v./g. In the presence of oxygen the initial yield of cyclopentanol is eliminated completely.

2-Cyclopentenone may also be a minor impurity if the chromatographic retention time is used as an identifying characteristic. This is illustrated by zero dose

(10) V. Dibeler, F. Mohler, and M. de Hemptine, *J. Res. Natl. Bur. Std.*, **53**, 107 (1954).

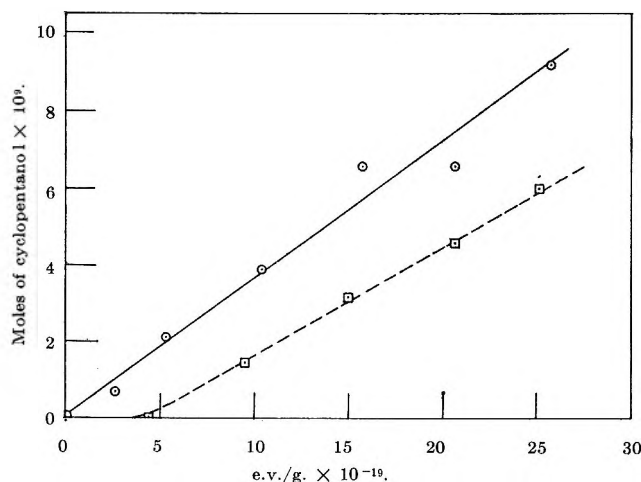


Figure 5. Cyclopentanol yields in the γ -radiolysis of liquid cyclopentane: \circ , degassed; \square , oxygen-saturated.

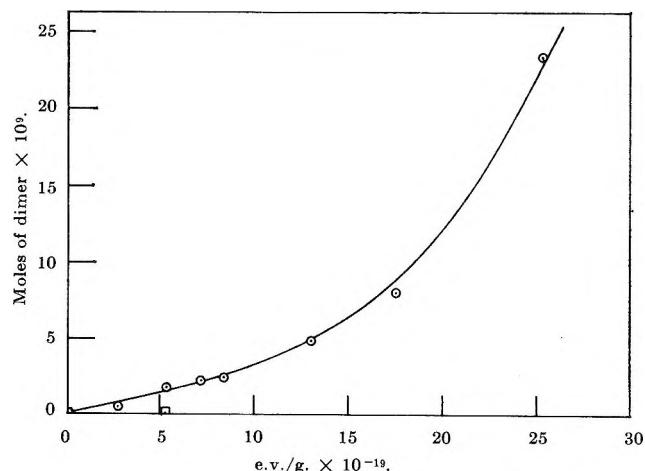


Figure 7. The yield of dimeric material from the γ -radiolysis of cyclopentane: \square , degassed cyclopentane.

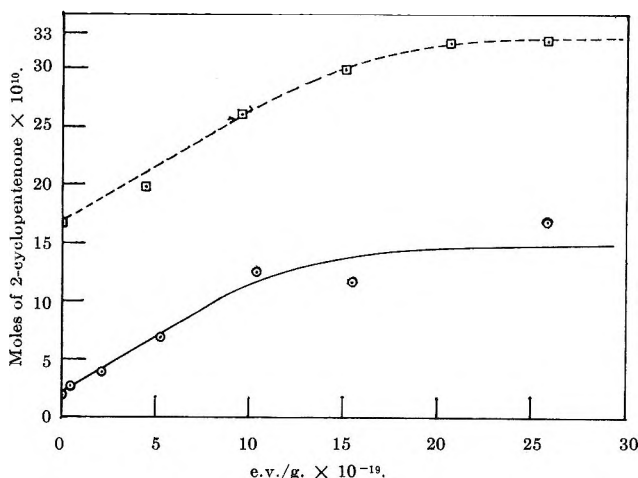


Figure 6. The effect of oxygen on the yield of 2-cyclopentenone in the γ -radiolysis of cyclopentane: \circ , degassed; \square , oxygen-saturated.

values in Figure 6. In both the pure liquid and the oxygen-saturated solutions, the curves are roughly linear and parallel up to about 10^{20} e.v./g. and then appear to be of lower slope owing to secondary reactions. An additional experiment (not shown in Figure 6) was performed on a degassed cyclopentane solution in which the zero-dose blank was even higher than that for the oxygen-saturated solution in Figure 6. This resulted in another curve similar to that for the degassed curve in Figure 6 with an equal initial slope.

The cyclopentane dimer was characterized mainly by its mass spectral cracking peaks at m/e 166, 84, and 83. The yield of this compound *vs.* dose is seen in Figure 7. The slope of the yield-dose curve increases with increasing dose. Added oxygen has the effect of eliminating this product completely. The

infrared spectrum of the dimer fraction was quite similar to that of cyclopentane and closely resembled that of the total polymer.

The results of the addition of iodine and DPPH to irradiated liquid cyclopentane are given in Table III. It is concluded from these studies that the initial yields of ethylene, 1-butene, and cyclopentenone are unaffected by the addition of DPPH and—with the possible exception of 2-cyclopentenone—iodine. The initial yield of cyclobutane may actually be increased by the addition of these same substances. The initial yields of *n*-butane, cyclopentanol, and the dimeric material were all reduced to zero by DPPH. The results with 4-pentenal appear to be anomalous. Iodine is known to react slowly with cyclopentane and does appear in certain cases to give anomalous results.

In the investigation of the initial yield of total polymer in degassed cyclopentane shown in Figure 8 the weight-dose relationship is apparently linear within experimental error.

The infrared spectrum of the polymer has many of the characteristic features of the parent cyclopentane including a strong carbonyl band at 1745 cm^{-1} , a $-\text{CH}_2-$ stretching band, and several $-\text{CH}_2-$ deformation bands. Elemental analyses of the polymer from several different runs are reported in Table IV. The polymer formed yellow solutions when dissolved in acetone even at very low doses (1×10^{19} e.v./g.).

Discussion

The relative insensitivity of $G(\text{H}_2)$ to free-radical scavengers points to one or more of the following commonly invoked mechanistic interpretations: (1) a "hot atom" process in which hot hydrogen atoms abstract

Table III: Effects of Iodine and DPPH on Products

Additive	Concn., <i>M</i>	Dose, e.v./g.	Products of irradiation, moles $\times 10^8$							Dimeric species
			C ₂ H ₄	Cyclobutane	1-Butene	<i>n</i> -Butane	4-Pentenal ^a	Cyclopentanone ^a	Cyclopentanol ^a	
Iodine	9.3×10^{-4}	2.6×10^{19}	2.8	0.71	0.31	0.00	0.86	1.09	0.84	0.00
Iodine	9.3×10^{-4}	12.8×10^{19}	15.8	1.70	0.77	0.08	1.09	2.39	1.20	0.00
DPPH	1.8×10^{-3}	2.7×10^{19}	3.2	0.72	0.26	0.00	7.14	0.40	0.00	0.00
DPPH	7.5×10^{-4}	5.4×10^{19}	6.0	0.82	0.43	0.05	10.7	1.69	0.00	0.00
DPPH	3.10×10^{-3}	13.0×10^{19}	16.3	1.87	1.11	0.22	0.87	0.00
None	0	5.4×10^{19}	5.7	0.77	0.49	0.34	1.90	0.50	2.1	1.5

^a Corrected for blank values.

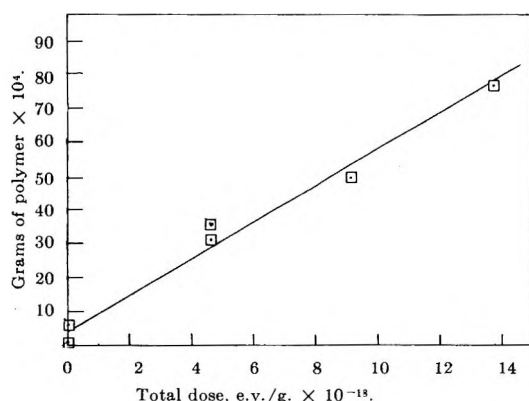


Figure 8. Yield of total polymer (oil) from the radiolysis of liquid degassed cyclopentanone

hydrogen from cyclopentanone molecules; (2) formation of molecular hydrogen in a concerted process; (3) an ion-molecule reaction which liberates hydrogen. The evidence presented does not allow a distinction between these processes. There are several features of the results with the partially deuterated compound which reflect the nature of the hydrogen-forming process and are worth examining.

Table IV: Mass Analysis of the Polymer

Dose, e.v./g.	%C	%H	%O
5.44×10^{20}	71.56	9.30	19.15
1.4×10^{19}	71.57	7.86	20.57 ^a

^a Obtained by difference.

First the isotopic ratio in the pure compound is independent of dose, of physical state, and of temperature. The run at -78° , during which the irradiated cyclopentanone was in the solid state, shows a remarkable similarity in isotopic ratio to that of the liquid at

room temperature, despite the lower hydrogen yield in the solid state.

Added cyclohexene and DPPH both altered the isotopic ratios. With added DPPH the ratio of H₂ to D₂ remained unaltered whereas the HD was lowered relative to the other two isotopic species. This would be consistent with a mechanism in which DPPH scavenges a fraction of the thermal free radicals, H or D, which would otherwise abstract H or D from cyclopentanone. The addition of DPPH would then have to reduce both H₂ and D₂ by the same amount and reduce the HD yield by an even greater factor. There are two different isotope effects possible here: (1) that associated with the C-H or C-D bond-breaking step to form the hydrogen radical and (2) that which may be attributed to the abstraction of the H or D from the partially deuterated cyclopentanone.

The addition of cyclohexene gives the same H₂:HD ratio as the DPPH experiment, but the H₂:D₂ ratio is higher than that in any of the other experiments.

The presence of 2-cyclopentanone is an indication that some of the hydrogen is formed by a molecular elimination process. The constancy of the H₂:D₂ yields in the tetradeuteriocyclopentanone experiments (in all but the cyclopentanone-cyclohexene case, where energy transfer may play an important role¹¹) could be explained by a loss of two hydrogen atoms from the same carbon atom, a process which has been postulated in the vacuum ultraviolet photolysis of hydrocarbons.^{12,13} On the other hand, H₂ and D₂ may be the result of "hot atom" abstraction by H or D of like atoms.

Ethylene appears to arise from a concerted decomposition of the cyclopentanone molecule to give either one molecule of ethylene and a diradical ($\cdot\text{CH}_2$ -

(11) W. Bristowe, M. Katayama, and C. Trumbore, unpublished research.

(12) H. Okabe and J. McNesby, *J. Chem. Phys.*, **34**, 668 (1961).

(13) M. Sauer and L. Dorfman, *ibid.*, **35**, 497 (1961).

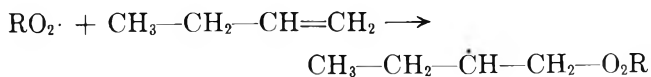
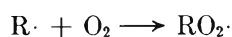
CH₂CO·) or two molecules of ethylene and one of CO. This is based on the decomposition of the tetradeuterated cyclopentanone which gives primarily the CD₂CH₂ ethylene species. The insensitivity of ethylene yields to 10⁻³ M quantities of radical scavengers indicates either a nonradical precursor or possibly a diradical precursor which decomposes before being scavenged at these scavenger concentrations.

The initial yields of 2-cyclopentenone are relatively insensitive to the addition of iodine, DPPH, and oxygen. The origin of the cyclopentenone in the radiolytic process may therefore be postulated as the result of a loss of molecular hydrogen in a concerted process or from a stepwise loss of two hydrogen atoms, the latter process being so rapid that the scavengers do not interfere with either reaction step.

The secondary reactions which reduce the yield of cyclopentenone could involve the scavenging of either hydrogen atoms or of other free radicals by cyclopentenone as its concentration increases. The presence of nonscavengable HD in the radiolysis of the partially deuterated cyclopentanone may be due to a concerted loss of HD from the 2-3 carbon atoms in an electronically excited cyclopentanone molecule.

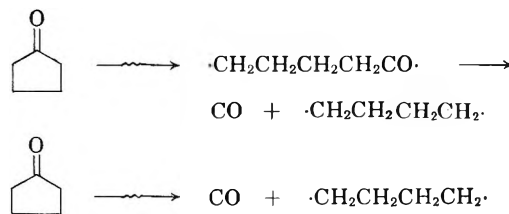
It is noted that the yield of dimer in the cyclopentanone radiolysis increases with increasing dose. It is probable that the character of the dimer and/or the polymer changes with dose and that secondary dimerization reactions owing to cyclopentenone may be responsible for at least part of these changes.

Data on the influence of additives on *G*(1-butene) are not clear. In the case of added oxygen the 1-butene *G* value is reduced by at least a factor of 2 and, as oxygen is consumed, builds up quickly to the same value found in the absence of oxygen. On the other hand, the same decrease is not observed with iodine and DPPH. It is possible that 1-butene is formed from either a concerted primary process or from a diradical that undergoes rapid rearrangement before scavengers have a chance to act with it. The oxygen effect could be explained by an attack on the primary yield of 1-butene by oxygenated radicals RO₂·, formed from the reaction



The radiolytic formation of *n*-butane is eliminated by the addition of all three additives. Only after the concentration of the additives is reduced drastically does *n*-butane again appear among the radiolysis products. This is the strongest evidence for the

presence of a diradical species, which might be formed in the following reactions



Cyclobutane yields were relatively unaffected by all the additives. This result would point to the formation of cyclobutane in a concerted process, perhaps with the elimination of CO, or at least in a process involving a short-lived intermediate which is not easily scavenged. The presence of *n*-butane as a primary product of the radiolysis strongly implies the presence of a four-carbon diradical species, and the insensitivity of the cyclobutane yield to added scavengers tends to eliminate the diradical species as the precursor of cyclobutane.

Both DPPH and oxygen reduced the initial yield of cyclopentanol to zero. After consumption of most of the oxygen and DPPH, the cyclopentanol again appeared as a measurable product. It is postulated that cyclopentanol is formed from the stepwise addition of hydrogen atoms to the parent cyclopentanone molecule. Singh and Freeman⁶ have discussed the probable nature of the cyclohexanone free-radical intermediate after the addition of one hydrogen atom. It is probable that the same type of species is involved in the case of cyclopentanone.

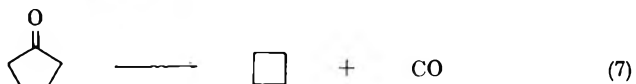
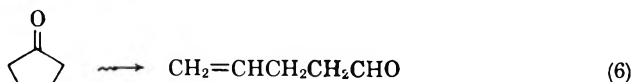
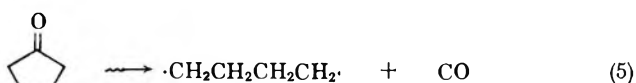
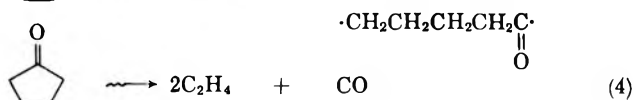
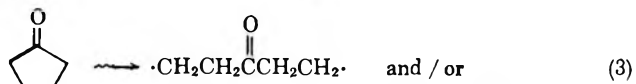
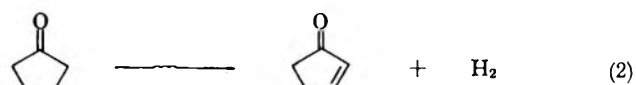
As is observed in Figure 5, the *G* value of cyclopentanol may be reduced to below its original value beginning at a dose of about 1.5 × 10²⁰ e.v./g. A secondary reaction could be due to a competition of products such as cyclopentenone for hydrogen atoms which would otherwise produce cyclopentanol.

The disappearance of the dimeric product upon addition of scavengers indicates probable free-radical precursors. Since the dimeric species was identified by mass spectral analysis, the location of the points of attachment of the two rings is uncertain. It is also possible that at higher total doses the dimer changes character in view of the increasing yield of the dimer as seen in Figure 7. The dose at which the dimer yield starts to increase is approximately the same as that at which the yield of 2-cyclopentenone begins to decrease.

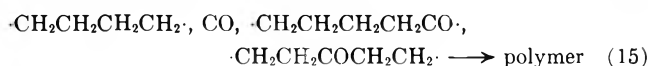
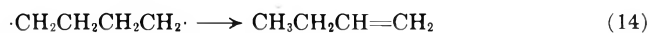
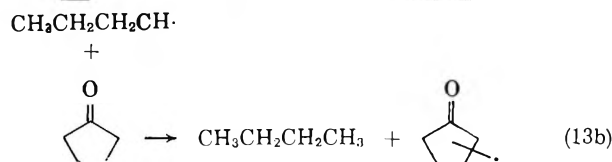
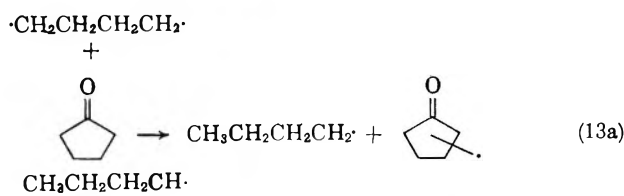
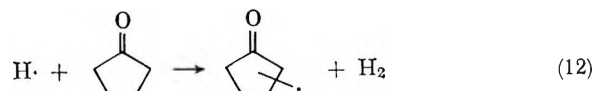
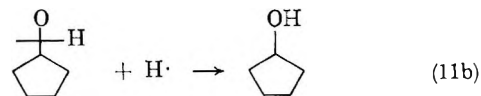
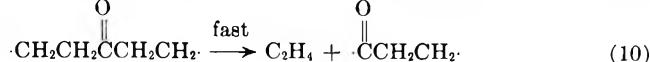
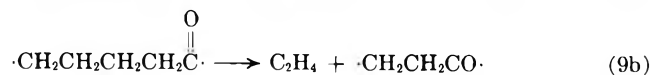
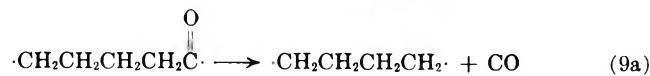
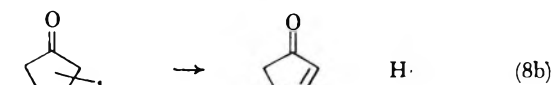
The infrared spectrum of the total polymer at several different total doses indicates little change from the dominant character of the infrared spectrum of the parent compound. A polymer incorporating cyclopentanone units appears to be present on the basis of

the infrared spectrum. Elemental analysis varies slightly with dose and is not inconsistent with these cyclopentanone units.

The following reactions may be postulated as one possible set which might explain the radiolysis products and the dependence of their yields on added oxygen, DPPH, and iodine. This is not meant to be an exhaustive list of reactions but, rather, offers a plausible mechanism for the main products in terms of a free-radical mechanism. Postulated primary reactions are



Secondary reactions of primary products are



As with many other radiolytic mechanisms, the postulation of a free-radical mechanism in the present system does not rule out the possibility of ion-molecule and electron-attachment reactions. The role of solvated electrons in liquid ketones has not been reported, but has been reported for nonpolar hydrocarbons¹⁴ and for polar media such as ammonia,¹⁵ water,^{16a} and ethanol.^{16b} In this connection it is interesting to note that if solvated electrons were important in the radiolysis of liquid cyclopentanone their $G(e^-_{\text{solv}})$ would be expected to be between 0.2 and 2.8, the values obtained for hydrocarbons¹⁴ and water,¹⁷ respectively. It is interesting to note that the $G(e^-_{\text{solv}})$ for ethanol is reported as 1.0.^{16b} Five of the major products in the radiolysis of cyclopentanone (H_2 , CO , C_2H_4 , 4-pentenal, and cyclopentanol) have G values between 0.7 and 0.9, values which would not be unreasonable for solvated electron yields in cyclopentanone.

4-Pentenal has been found as a radiolysis product. It is also reported¹⁸ as the major product in the 3130-Å photolysis of liquid cyclopentanone.¹⁹ The further

(14) (a) G. R. Freeman, *J. Chem. Phys.*, **38**, 1022 (1963); (b) G. R. Freeman, *ibid.*, **39**, 988 (1963).

(15) D. Cleaver, E. Collinson, and F. S. Dainton, *Trans. Faraday Soc.*, **56**, 164 (1960).

(16) (a) J. Thomas, S. Gordon, and E. J. Hart, *J. Phys. Chem.*, **68**, 1524 (1964); (b) I. Taub, D. Harter, M. Sauer, and L. Dorfman, *J. Chem. Phys.*, **41**, 979 (1964).

(17) J. Rabani, private communication.

(18) P. Dunion, *et al.*, Third Annual Metropolitan Regional Meeting, New York and New Jersey sections of the American Chemical Society, Jan. 1964.

(19) P. Dunion and C. N. Trumbore, unpublished work.

comparisons of the photochemistry and radiation chemistry of cyclopentanone awaits the results of studies being performed at shorter wave lengths. Such studies are now in progress in our laboratory.

The comparisons of the radiolytic behavior of cyclopentanone with cyclohexanone³ are numerous. It is highly probable that the primary physical and chemical

processes and intermediate species are quite similar in their states of excitation and ionization.

Acknowledgments. The authors wish to thank Dr. G. R. Freeman for prepublication copies of his manuscripts on the radiolysis of cyclohexanone and to acknowledge stimulating discussions with Dr. R. Srinivasan.

Radiolysis of Ethylene. I. Yield of Hydrogen Atoms and Formation of Saturated Hydrocarbons¹

by G. G. Meisels and T. J. Sworski

Union Carbide Corporation, Nuclear Division, Research Center, Tuxedo, New York (Received June 4, 1964)

The yield of ethyl radicals in the radiolysis of ethylene was estimated as 6.7 ± 0.4 radicals/100 e.v. by attributing the formation of ethane, propane, and *n*-butane solely to reactions of methyl and ethyl radicals. A yield of 6.8 ± 1.9 hydrogen atoms/100 e.v. was determined by use of the hydrogen atom exchange reaction with deuterium. It appears that all ethyl radicals have hydrogen atoms as precursors and that deuterium does not affect hydrogen atom formation from ethylene. A marked enhancement of alkane yields by addition of deuterium to ethylene is attributed to a yield of 15.8 ± 0.5 deuterium atoms/100 e.v. absorbed in deuterium. The occurrence of either deutron or charge transfer suggests that the yield of deuterium atoms in pure deuterium may be as high as 25 atoms/100 e.v.

Reactions of ethyl radicals, formed by addition of hydrogen atoms to ethylene, provide a unique mechanism for the formation of ethane and *n*-butane in the photolysis of ethylene.^{2,3} There is uncertainty, however, about the mechanism for the formation of these products in the radiolysis of ethylene. Yang and Manno⁴ report that *n*-butane does not result from reactions involving free radicals while Sauer⁵ proposes that ethane, propane, and *n*-butane result from reactions of ethyl radicals probably formed by the addition of hydrogen atoms to ethylene. A detailed study of ethylene-deuterium mixtures was therefore undertaken to evaluate the importance of hydrogen atoms as intermediates in the radiolysis of ethylene.

Experimental

Materials. Phillips research grade ethylene was purified by repeated distillations in a high vacuum system, the middle third being retained. It contained traces of an unidentified component having the same re-

(1) This paper was presented at the 141st National Meeting of the American Chemical Society, Washington, D. C., April 1962, Abstracts, p. 18R, Paper No. 43.

(2) M. C. Sauer, Jr., and L. M. Dorfman, *J. Chem. Phys.*, **35**, 497 (1961).

(3) H. Okabe and J. R. McNesby, *ibid.*, **36**, 601 (1962).

(4) K. Yang and P. J. Manno, *J. Phys. Chem.*, **63**, 752 (1959).

(5) M. C. Sauer, Jr., Abstracts, 140th National Meeting of the American Chemical Society, Chicago, Ill., Sept. 1961, p. 44R.

tention volume on a silica gel-diethyl hexylsebacate column as either carbon monoxide, air, argon, or krypton. Deuterium from Stuart Oxygen Co., containing $0.86 \pm 0.02\%$ hydrogen deuteride, was passed through a liquid nitrogen trap before use.

Analysis. Acetylene and saturated hydrocarbon concentrations were determined with a Perkin-Elmer Model 154-B vapor fractometer using columns J and B (silica gel and diethyl hexylsebacate, 2 m. each) at 100° with a flow rate of 80 ml./min. Eluted components were identified by retention volumes and by mass spectrometric analysis of trapped effluents. The mass spectrometric identification and the determination of C_2H_4/D_2 and HD/D_2 ratios were made with an Atlas-Werke Model CH-4 mass spectrometer. The effect of instrumental variation was reduced by analyses of HD/D_2 ratios in standard and irradiated samples in rapid succession using a dual-inlet system. Ethylene and condensable reaction products were removed by a liquid nitrogen trap before analysis for these ratios. The changes in relative peak heights at masses 2 and 3 produced by irradiation usually amounted to only a small fraction of their initial values. Yields of HD were therefore not as accurate as one would desire and yields of H_2 proved unreliable. Larger changes were avoided since excessive decomposition of ethylene would have been required.

The yields of decomposition of ethylene were obtained from C_2H_4/D_2 ratios corrected for the decrease in deuterium pressure due to enhanced production of saturated hydrocarbons in the presence of deuterium. This correction becomes small at higher partial pressures of deuterium.

Irradiations. Irradiation cells were similar in design to gas phase infrared spectrometry cells. They were Pyrex cylinders approximately 1.9 cm. in height and 5.1 cm. in diameter with 0.013-cm. aluminum windows at each end. Vacuum-tight seals were obtained by amalgamated lead gaskets between cell and window with stainless steel pressure rings on the outside. These cells were also used as ionization chambers with the aluminum windows also serving as electrodes. Micarta insulators were inserted between the amalgamated lead gaskets and pressure rings. Cells were fitted with a 2-mm. stopcock and standard taper joint for attachment to a high vacuum sampling system. Cell volume was about 28 ml.

Source of radiation was a 1-Mev. Van de Graaff accelerator. Irradiations were usually with beam currents of 5 or 10 μ a. with current and total charge monitored on an Elcor Model A309A current indicator and integrator. Charge was collected on an aluminum block behind the cell. Positioning was made repro-

ducible by a special fitting between beam tube and irradiation cell. Irradiation cells, initially at room temperature, were quickly heated to about 40° during irradiation. A 10- μ a. beam current with 50 torr of ethylene in the cell corresponded to a dose rate of 3.0×10^{15} e.v. cc.⁻¹ sec.⁻¹. The linearity of product yields with dose was established at one composition; subsequent experiments were carried out at a single dose.

Dosimetry. Determination of energy absorbed by samples of pure ethylene was based on measurements of saturation ionization currents when an electric field was applied to the aluminum windows. A *W*-value of 25.9 e.v./ion-pair was used for ethylene.^{6,7} Energy absorbed by ethylene-deuterium mixtures relative to samples of pure ethylene was assumed to be in the ratio of their total stopping powers for 1-Mev. electrons. The validity of such an assumption for pure gases has been established previously for these experimental procedures.⁷

Saturation ionization currents were not measured during irradiation of those samples in which the products were to be determined since the necessary electric fields markedly enhance rates of product formation.⁸ A number of cells were calibrated for energy absorption characteristics relative to each other; saturation currents were determined in one and product formation was followed in the others.

Results

Yields of observed products, in molecules/100 e.v. absorbed, are denoted by parenthetical notations such as $G(HD)$. The subscript notation is used for assumed intermediates such as G_H . Superscript notation is used for $C_2H_4-D_2$ mixtures: G^E and G^D values for yields of products and intermediates formed as a result of energy absorbed by ethylene and deuterium, respectively; S^E and S^D for 1-Mev. stopping powers/electron for ethylene and deuterium, respectively, relative to air; and N^E and N^D for the number of electrons for ethylene and deuterium molecules, respectively; σ^E and σ^D for stopping power fractions of ethylene and deuterium, respectively, where, for example, $\sigma^E = S^E N^E [C_2H_4] / (S^E N^E [C_2H_4] + S^D N^D [D_2])$.

Production of C_2H_2 and HD. The addition of deuterium has little or no effect on the production of acetylene from ethylene. As shown in Figure 1, $G(C_2H_2) / \sigma^E$ is essentially independent of variations in $[D_2] / [C_2H_4]$ from 0 to 15. There is apparently no energy

(6) G. N. Whyte, *Radiation Res.*, **18**, 265 (1963).

(7) G. G. Meisels, *J. Chem. Phys.*, **41**, 51 (1964).

(8) G. G. Meisels and T. J. Sworski, Abstracts, 141st National Meeting of the American Chemical Society, Washington, D. C., April 1962, p. 18R, Paper No. 44.

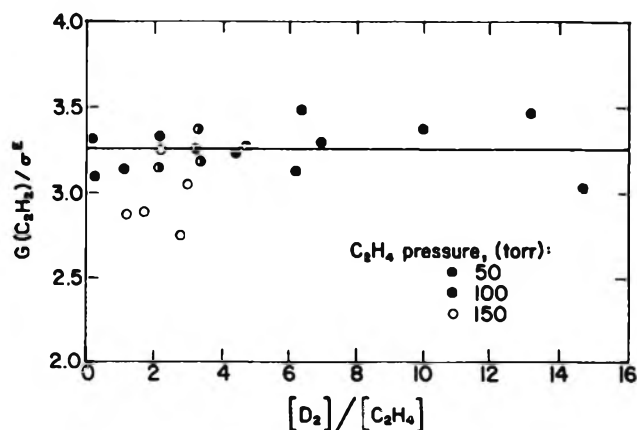


Figure 1. Dependence of $G(\text{C}_2\text{H}_2)/\sigma^E$ on $[\text{D}_2]/[\text{C}_2\text{H}_4]$.

transfer between ethylene and deuterium involving those ionized or electronically excited species of ethylene which are precursors of acetylene and $G(\text{C}_2\text{H}_2)/\sigma^E$ is assumed to equal $G^E(\text{C}_2\text{H}_2)$. The average of all values plotted in Figure 1 is 3.25 ± 0.25 . An effect of pressure on yields has been observed previously^{3,7} and is apparent here also.

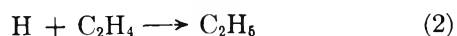
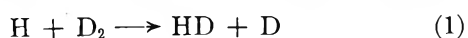
This constancy is an important point since it is the basis for kinetic analysis of product G -values: the energy absorbed by the mixture is divided between the two components in the ratio of their stopping power fraction using 1-Mev. stopping powers. This is fortunate since stopping powers for degradation spectrum electrons are not known. Let M , E , and E^E denote molecules of product, total energy absorbed by the mixture, and energy absorbed by ethylene at the same pressure as its partial pressure in the mixture, respectively. M and E^E are experimentally determinable, the latter by measurements of saturation ionization currents. $G(\text{product})/\sigma^E$, therefore, is an experimentally measurable quantity which we employ. This can be seen from the relationships I and IIa or IIb.

$$E = E^E/\sigma^E \quad (\text{I})$$

$$G(\text{product}) = 100M/E = 100M\sigma^E/E^E \quad (\text{IIa})$$

$$G(\text{product})/\sigma^E = 100M/E^E \quad (\text{IIb})$$

If we assume that hydrogen atom exchange with deuterium is in competition only with hydrogen atom addition to ethylene as shown by reactions 1 and 2,



the kinetic relationship given in eq. III can be derived

$$\frac{\sigma^E}{G(\text{HD})} = \frac{\sigma^E}{G_{\text{H}}} + \frac{\sigma^E k_2 [\text{C}_2\text{H}_4]}{G_{\text{H}} k_1 [\text{D}_2]} \quad (\text{III})$$

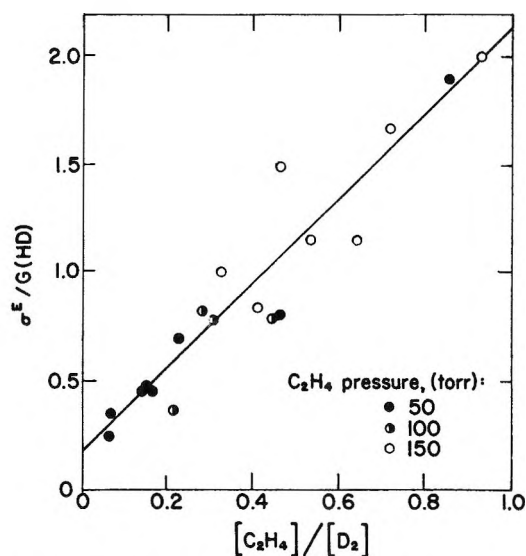


Figure 2. Dependence of $\sigma^E/G(\text{HD})$ on $[\text{C}_2\text{H}_4]/[\text{D}_2]$.

without the necessity of a steady-state approximation.⁹ As shown in Figure 2, $\sigma^E/G(\text{HD})$ is a linear function of $[\text{C}_2\text{H}_4]/[\text{D}_2]$ with intercept and slope yielding $G_{\text{H}}^E = 6.8 \pm 1.9$ and $k_2/k_1 = 14 \pm 5$, respectively. The rate constant ratio is in excellent agreement with the value $k_2/k_1 \approx 16$ calculated from the data of Darwent and Roberts¹⁰ by neglecting isotope effects. The hydrogen atom abstraction reactions of hydrogen and deuterium atoms with ethylene are assumed to occur to a negligible extent only.^{3,10}

Production of Saturated Hydrocarbons. Addition of deuterium to ethylene markedly increases the production of saturated hydrocarbons (isotopic distribution of hydrogen was not determined for hydrocarbon mixtures). Let us assume that G_{H}^E and G_{D}^D are constant for ethylene-deuterium mixtures, independent of variations in $[\text{D}_2]/[\text{C}_2\text{H}_4]$. Then the relationship shown in eq. IV can be derived for the production of both ethane

$$G(\text{product})/\sigma^E = G^E(\text{product}) + \frac{S^{\text{D}}N^{\text{D}}[\text{D}_2]}{S^{\text{E}}N^{\text{E}}[\text{C}_2\text{H}_4]} G^{\text{D}}(\text{product}) \quad (\text{IV})$$

and n -butane. Figure 3 shows that both $G(\text{C}_2\text{H}_6)/\sigma^E$ and $G(n\text{-C}_4\text{H}_{10})/\sigma^E$ increase linearly with $[\text{D}_2]/[\text{C}_2\text{H}_4]$ as required by eq. IV. Intercept values for $G^E(\text{C}_2\text{H}_6)$ and $G^E(n\text{-C}_4\text{H}_{10})$ are 0.66 ± 0.03 and 2.14 ± 0.10 , respectively. Values of $G^{\text{D}}(\text{C}_2\text{H}_6)$ and $G^{\text{D}}(n\text{-C}_4\text{H}_{10})$,

(9) H. A. Schwarz and A. O. Allen, *J. Am. Chem. Soc.*, **77**, 1324 (1955).

(10) D. deB. Darwent and R. Roberts, *Discussions Faraday Soc.*, **14**, 55 (1953).

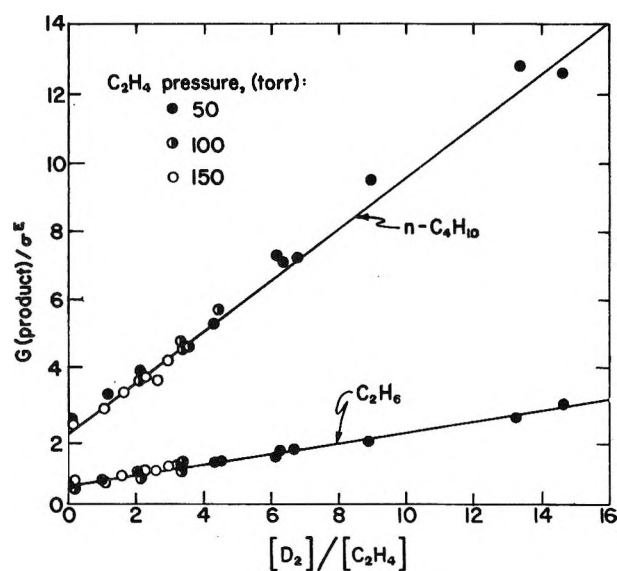


Figure 3. Dependence of $G(\text{C}_2\text{H}_6)/\sigma^E$ and $G(n\text{-C}_4\text{H}_{10})/\sigma^E$ on $[\text{D}_2]/[\text{C}_2\text{H}_4]$.

evaluated from the slopes of the lines in Figure 3, are 1.28 ± 0.07 and 5.83 ± 0.16 , respectively.

Figure 4 shows that $G(\text{C}_3\text{H}_8)/\sigma^E$ is markedly dependent on the partial pressure of ethylene, although reasonable linearity with $[\text{D}_2]/[\text{C}_2\text{H}_4]$ is observed at 50 torr of ethylene. An investigation of this pressure dependence has been undertaken and results will be reported elsewhere.¹¹ Figure 5 shows that $G(-\text{C}_2\text{H}_4)/\sigma^E$ also increases linearly with $[\text{D}_2]/[\text{C}_2\text{H}_4]$. G^E -Values from intercepts and G^D -values from slopes are summarized in Table I.

Table I: Product Yields in the Radiolysis of Ethylene and Ethylene-Deuterium Mixtures

Product	G^E -value	G^D -value
Acetylene	3.25 ± 0.25	< 0.3
Ethane	0.66 ± 0.03	1.28 ± 0.07
Propane ^a	0.84 ± 0.05	0.58 ± 0.04
<i>n</i> -Butane	2.14 ± 0.10	5.83 ± 0.16
Ethylene	-20.5 ± 2.0	-20 ± 3

^a Pressure dependent; values for 50 torr of ethylene.

G^E -Values summarized above are independent of any assumptions concerning the absorption of energy by the mixture. G^D -Values, however, will vary if relative stopping powers are calculated by different methods. For example, if the common assumption is made that energy absorption is a linear function of electron density, instead of stopping powers, eq. V, where e^E de-

$$G(\text{product})/e^E = G^E(\text{product}) + \frac{N^D[\text{D}_2]}{N^E[\text{C}_2\text{H}_4]} G^D(\text{product}) \quad (\text{V})$$

notes electron fraction ethylene, would result instead of eq. IV. Furthermore, $G(\text{product})/e^E$ would be equal to the experimentally determinable quantity $100M/E^E$; identical G^E -values would be obtained but values of G^D would differ by the factor $S^D/S^E = 1.11$.⁷ Thus, the demonstration of the linear dependence of energy absorption on total stopping power for our experimental conditions⁷ provides a firm basis for avoiding the errors

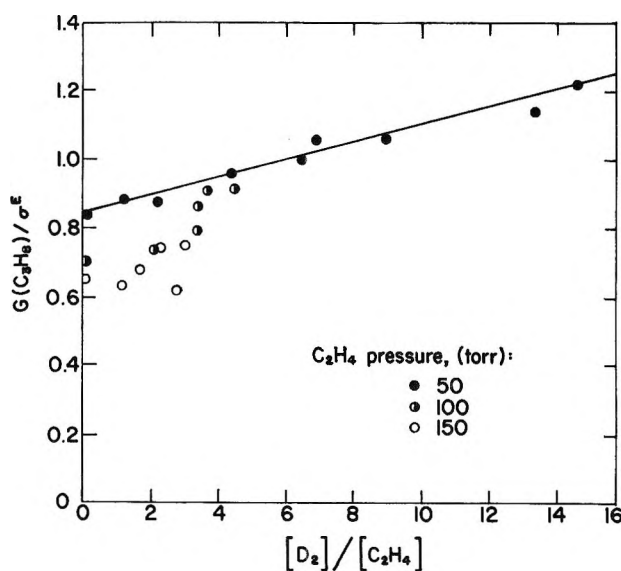


Figure 4. Dependence of $G(\text{C}_3\text{H}_8)/\sigma^E$ on $[\text{D}_2]/[\text{C}_2\text{H}_4]$.

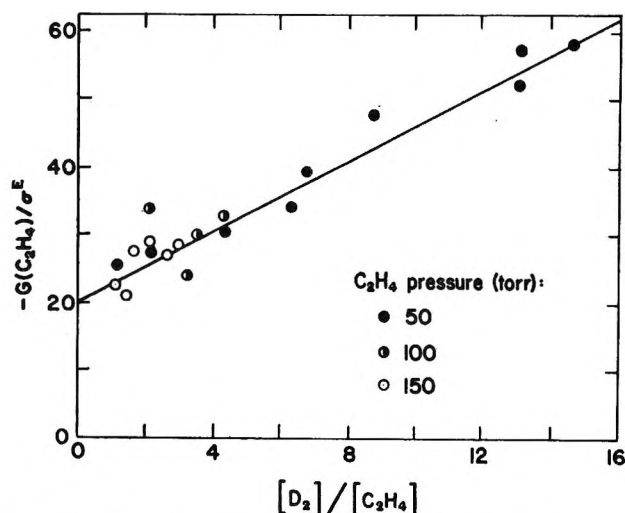


Figure 5. Dependence of $-G(\text{C}_2\text{H}_4)/\sigma^E$ on $[\text{D}_2]/[\text{C}_2\text{H}_4]$.

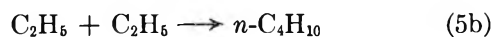
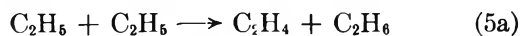
(11) G. G. Meisels, Abstracts, 148th National Meeting of the American Chemical Society, Chicago, Ill., Sept. 1964, p. 1R.

inherent in the use of electron density as an approximation.

In a number of experiments, 10% nitric oxide was added to ethylene before irradiation. Ethane, propane, and *n*-butane production was completely inhibited; this is further evidence for their formation by free radical precursors. Acetylene production, however, was unaffected.

Discussion

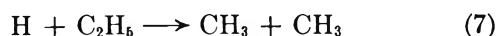
Ethane, propane, and *n*-butane are formed predominantly by combination and disproportionation reactions of methyl and ethyl radicals (eq. 3-5). Ethyl radi-



cals result from addition of hydrogen atoms to ethylene while methyl radicals result from reactions of ionic precursors⁸ such as by the ion-molecule reaction

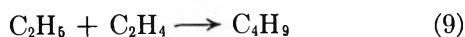
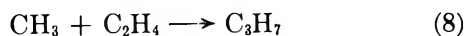


which accounts for 90% of the ion-molecule reactions of ethylene ion.¹² Under our experimental conditions, less than 1% of the hydrogen atoms yield methyl radicals by the reaction (7) considered by Lampe.¹³ This

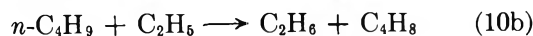
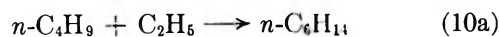


conclusion is based on a kinetic analysis using known rate constants¹⁴ for reactions 2, 4, and 5 and collision frequency for reaction 7.

Methyl and ethyl radicals may also add to ethylene^{8,11} followed by the reactions of the resultant *n*-



propyl and *n*-butyl radicals with ethyl radicals. For example, *n*-butyl radicals disappear primarily by the reactions 10a-c. Under our conditions, $r_{10a}/(r_{5b} +$



$r_{10c}) \simeq 0.08^{8,11}$ and $r_8/(r_{4a} + r_{4b}) \simeq 0.07^{11}$

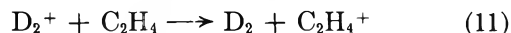
Determination of G_D^D . If it is assumed that the increase in $G(\text{C}_2\text{H}_4)/\sigma^E$, $G(\text{C}_2\text{H}_6)/\sigma^E$, and $G(n\text{-C}_4\text{H}_{10})/\sigma^E$ upon addition of deuterium to ethylene results solely

from production of deuterium atoms and their addition to ethylene, one can evaluate G_D^D by determining the $G_{\text{C}_2\text{H}_6}^D$ necessary to cause these increased values, listed in Table I. The ratio $G^D(\text{C}_2\text{H}_6)/G^D(n\text{-C}_4\text{H}_{10}) = 0.22$ is markedly larger than the accepted value of 0.15 for k_{5a}/k_{5b} . This excess ethane probably results principally from reaction 10b since the increase of 0.07 in $G^D(\text{C}_2\text{H}_6)/G^D(n\text{-C}_4\text{H}_{10})$ is in excellent agreement with $r_{10a}/(r_{5b} + r_{10c}) = 0.08$. The above considerations lead to the estimate of the ethyl radical yield given by eq. VI, where the factors 1.06 and 1.07 correct for (a) the $G_{\text{C}_2\text{H}_6}^D \simeq 2G^D(\text{C}_2\text{H}_6) + (1.06)(1.07)G^D(\text{C}_3\text{H}_8) +$

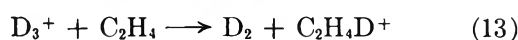
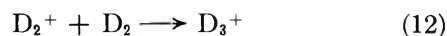
$$2.16G^D(n\text{-C}_4\text{H}_{10}) \simeq 15.8 \pm 0.5 \quad (\text{VI})$$

disproportionation reaction of methyl and ethyl radicals¹⁴ and (b) the conclusion that *n*-propyl radicals formed by reaction 8 disappear primarily by reaction with ethyl radicals, respectively. The occurrence of the reaction sequence suggested above has been established for the mercury-photosensitized hydrogenation of ethylene.¹⁵

The kinetic treatment implies that ethylene has no effect on deuterium atom production from deuterium. Charge transfer^{16,17} (reaction 11) and/or deutron



transfer¹⁸ (reactions 12 and 13) may occur but appar-



ently are not manifested kinetically. In fact, the validity of our estimate of G_{H}^E from eq. III requires that the ionic chain process¹⁹ for the exchange reaction between H_2 and D_2 be inhibited by ethylene. If ethyl ions produced in reaction 13 ultimately lead to ethyl radicals, $G_D^D = 21.3$ would result for pure deuterium since neutralization of D_3^+ should yield three atoms.²⁰ The occurrence of charge exchange would lead to a

(12) F. H. Field, J. L. Franklin, and F. W. Lampe, *J. Am. Chem. Soc.*, **79**, 2419 (1957).

(13) F. W. Lampe, *ibid.*, **82**, 1551 (1960).

(14) J. A. Kerr and A. F. Trotman-Dickenson, "Reaction Kinetics," Vol. I, G. Porter, Ed., Pergamon Press, Inc., New York, N. Y., 1961, p. 107.

(15) A. B. Callear and W. P. D. Pereira, *Trans. Faraday Soc.*, **59**, 2758 (1963).

(16) C. F. Smith, B. G. Gorman, and F. W. Lampe, *J. Am. Chem. Soc.*, **83**, 3559 (1961).

(17) J. H. Futrell and T. O. Tiernan, *J. Chem. Phys.*, **38**, 150 (1963).

(18) P. Ausloos and S. G. Lias, *ibid.*, **40**, 3599 (1964).

(19) O. A. Schaeffer and S. O. Thompson, *Radiation Res.*, **10**, 671 (1959).

(20) H. Eyring, J. O. Hirschfelder, and H. S. Taylor, *J. Chem. Phys.*, **4**, 479 (1936).

maximum estimate of $G_D^D = 25.8$ in the absence of ethylene. These large values are not unreasonable in view of the theoretical estimate²⁰ of 13.8 to 16.6 hydrogen atoms/100 e.v. from hydrogen, and the observed yield of 23.4 radicals/100 e.v. absorbed in water vapor.²¹

Correlation of $G_{C_2H_6}^E$ with G_H^E . The ratio $G^E(C_2H_6)/G^E(n-C_4H_{10}) = 0.30$ is larger than the value of 0.22 for $G^D(C_2H_6)/G^D(n-C_4H_{10})$ probably due at least in part to formation of ethane by reaction 3. The relative rates of reactions 3, 4, and 5 are known to be in agreement with simple collision theory.^{14,22} Using $k_4^2/k_3k_5 = 4.0$ and the values for $G^E(C_3H_8)$ and $G^E(n-C_4H_{10})$ yields a G^E -value of 0.08 for ethane formation by reaction 3. Correction of eq. VI for reaction 3 and substitution of G^E for G^D leads to an estimate of 6.7 ± 0.4 for $G_{C_2H_6}^E$ in excellent agreement with $G_H^E = 6.8 \pm 1.9$.

No correction is made for the formation of propane and ethane by disproportionation of propyl and ethyl radicals. However, the effect of such a reaction should not exceed more than 20% of the propyl radical yield by analogy with homodisproportionation¹⁴ or 4% of the calculated methyl radical yield. Also neglected is the contribution of other primary radicals produced by irradiation¹¹ such as propyl and butyl radicals whose yield is less than 0.1 radicals/100 e.v.

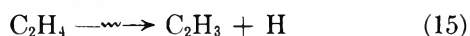
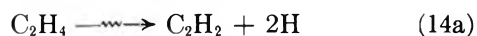
$G_{CH_3}^E$ at 50 Torr of Ethylene. The above considerations lead to the estimate of the methyl radical yield given by eq. VII. This methyl radical yield may be

$$G_{CH_3}^E \simeq 0.16 + (1.06)(1.07)G^E(C_3H_8) \simeq 1.01 \quad (\text{VII})$$

compared with a yield of 1.50 $C_2H_4^+$ ions/100 e.v. calculated from mass spectral data²³ corresponding to a value $G_{CH_3}^E = 1.37$ predicted by reaction 6a.

$G_{CH_3}^D \simeq 0.6$ can be estimated from $(1.06)(1.07)G^D(C_3H_8)$ at 50 torr. A number of factors may contribute to this apparent methyl radical yield, such as charge transfer from deuterium to ethylene, collisional stabilization of excited ethylene ion at higher pressures, reduction of radical addition to ethylene at effectively higher dose rates, the occurrence of reaction 7, and an increase in the rate of ethyl radical formation decreasing the importance of reaction 3. In this respect it may be noted that the observed $G(\text{propane})/\sigma^E$ never exceeds the value 1.37 predicted by reaction 6a. The significance of $G^D(\text{methyl})$ is therefore uncertain, and the apparent linearity at 50 torr may result from an accidental superposition of these factors.

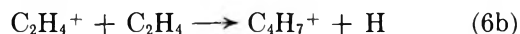
Mechanism of H Atom Formation. The formation of hydrogen atoms from ethylene may be ascribed to primary excitation processes 14a and 15, to the formation



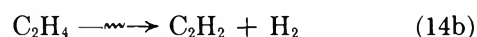
of fragment ions by reactions 16a and 17, and to ion-



molecule reactions such as 6b. The yield of hydrogen



atoms from these steps can be estimated since recent evidence has confirmed the applicability of mass spectral fragmentation patterns to ethylene radiolysis near atmospheric pressure²⁴ and the absence of simple ion-molecule reactions leading to acetylene formation.^{24,25} Correction for the contribution from the reactions 14b and 16b can be made on the basis of $G(H_2) = 1.3$ at 50



torr.^{7,26} $G(C_2H_3)$ is probably less than 0.1⁸ while the yield of ionic intermediates can be calculated to be $G_{C_2H_2^+} = 0.94$ and $G_{C_2H_3^+} = 0.96$.²⁴ Simple material balance considerations yield

$$G_H = 2[G(C_2H_2) + G_{C_2H_2^+} - G(H_2)] + G_{C_2H_3^+} +$$

$$G_{C_2H_3^+} + (G_{C_2H_3^+} + k_{6b})/(k_{6a} + k_{6b}) = 6.9$$

The calculated value, is, of course, uncertain because H, H_2 , and C_2H_2 may also be produced by higher-order ion-molecule reactions.^{25,27}

The effect of deuterium on hydrogen atom formation following energy absorption in ethylene and on subsequent ion-molecule reactions should be minor. Excitation transfer and simple charge exchange (reaction 11) should also be unimportant because the acetylene yield is constant and the methyl radical yield varies only little. However, ethylene ion produced in reaction 11 may dissociate into vinyl ion and hydrogen atoms. If dissociation follows each charge exchange step, then the contribution of this process is $G_H^E \simeq 0.6$ when $[D_2]/[C_2H_4] = 15$, decreasing with decreasing values of this ratio. This is well within experimental error. The excellent agreement of the calculated and the ex-

(21) R. F. Firestone, *J. Am. Chem. Soc.*, **79**, 5593 (1957).

(22) J. A. Kerr and A. F. Trotman-Dickenson, *Chem. Ind.* (London), 125 (1959).

(23) "Catalogue of Mass Spectral Data," American Petroleum Institute, Research Project 44, Carnegie Institute of Technology, Pittsburgh, Pa., 1947-1962, No. 23.

(24) G. G. Meisels, *Trans. Am. Nucl. Soc.*, **7**, 308 (1964).

(25) F. H. Field, *J. Am. Chem. Soc.*, **83**, 1523 (1961).

(26) M. C. Sauer, Jr., and L. M. Dorfman, *J. Phys. Chem.*, **66**, 322 (1962).

(27) S. Wexler and R. Marshall, *J. Am. Chem. Soc.*, **86**, 781 (1964).

perimental values for G_H^E , obtained from the use of eq. III and the estimate of $G_{C_2H_6^E}$, supports the applicability of the reaction mechanism employed.

Acknowledgment. The authors wish to express their gratitude to R. B. Wilkin for his diligent assistance in the collection of experimental data.

Photoreduction of Methyl Red Sensitized by Ethyl Chlorophyllide *a*¹

by G. R. Seely

Charles F. Kettering Research Laboratory, Yellow Springs, Ohio (Received July 15, 1964)

The chlorophyllide-photosensitized reduction of methyl red by ascorbic acid, hydrazobenzene, and mercaptosuccinic acid in ethanol has been studied over a wide range of reducing agent concentration. Evidence is presented that the primary photochemical reaction of photoexcited chlorophyllide is with methyl red. Even with a deficiency of reducing agent, reduction is practically complete to the four-electron stage, at least in weakly acidic or neutral solution. As the reaction progresses, the quantum yield changes in a complex way peculiar to the reducing agent; the reaction products responsible for this have thus far eluded identification. Empirical expressions are obtained for the initial quantum yield as a function of reagent concentrations, and a rather general expression is derived for the high reducing agent concentration region, based on the postulate that the reducing agent may react either with an initially produced ion pair Chl^+MR^- or with the separated radical ions.

Introduction

In their quantitative study of the chlorophyll-sensitized reduction of methyl red by phenylhydrazine² Livingston and Pariser suggested a mechanism whereby photoexcited chlorophyll reacts first with methyl red to form a complex which then reacts with the reducing agent. On the basis of later results³ they rejected this mechanism in favor of ones in which photoexcited chlorophyll reacts first with the reducing agent. A similar order of events was favored by Evstigneev and Gavrilova.⁴

Our present interest in the reaction arose in connection with our investigation of the photoreduction of ethyl chlorophyllide,⁵ through the hope that methyl red might intercept the primary product of the reaction between chlorophyllide and ascorbic acid. Although on investigation the sensitized reduction of methyl red by ascorbic acid showed superficial simi-

larities to the reduction of chlorophyllide itself, as for example the apparent inactivity of ascorbate ion and retardation by malic acid or $MgCl_2$, there were important differences, the chief being that the reduction of methyl red proceeded most rapidly in ethanol without the addition of any base, whereas chlorophyllide is very slowly, if at all, reduced under these conditions.

Re-examination of the reduction of methyl red therefore seemed justified, and in the present paper results with ascorbic acid, hydrazobenzene, and mercapto-

(1) Contribution No. 158 from the Charles F. Kettering Research Laboratory.

(2) R. Livingston and R. Pariser, *J. Am. Chem. Soc.*, **70**, 1510 (1948).

(3) R. Livingston and R. Pariser, *ibid.*, **78**, 2948 (1956).

(4) V. B. Evstigneev and V. A. Gavrilova, *Dokl. Akad. Nauk SSSR*, **98**, 1017 (1954).

(5) G. R. Seely and A. Folkmanis, *J. Am. Chem. Soc.*, **86**, 2763 (1964).

succinic acid are presented. As before,⁵ ethyl chlorophyllide *a* was used in place of chlorophyll. In ethanol none of the reducing agents which are effective reducing agents for methyl red have any comparable ability to reduce chlorophyllide in the absence of methyl red; in the absence of a reducing agent there is no visible reaction between chlorophyllide and methyl red.

Experimental

Ethyl chlorophyllide *a* (Chl) was prepared from the leaves of *Datura stramonium* and purified chromatographically.⁶

Methyl red (MR) was recrystallized from ethanol. The extinction coefficient was 3.19×10^4 l./mole-cm. for the 494-m μ band of the neutral form in ethanol. In the presence of ascorbic acid (Asc) or mercaptosuccinic acid (Msa) methyl red was entirely in the neutral form in ethanol; with hydrazobenzene (Hzb) it was necessary to add a small amount of benzoic acid to put the methyl red entirely in the neutral form, which, according to previous work, is the only reducible form.²

The reducing agents were recrystallized from ethanol or water, and their stock solutions were stored cold under nitrogen. Anthranilic acid and azobenzene were recrystallized, but β -carotene (Nutritional Biochemicals) and the other reagents were used as received. Ethanol was distilled from magnesium ethoxide. The contents of the reaction tubes were flushed with nitrogen, purified by bubbling through a solution of sodium benzophenone ketyl in anisole.

The reaction was sensitized by light from a 750-w. projector lamp passed through a Baird-Atomic 6600- \AA . interference filter of band pass 90 \AA . This light is absorbed only by chlorophyllide; there is no reaction when only methyl red absorbs light. The rate of light absorption was generally around 4×10^{-6} einstein/l. sec. Light intensity was measured with an Eppley thermopile, and the rate of fall of the methyl red band at 494 m μ was followed with a Beckman DU spectrophotometer. Quantum yields were determined as averages over intervals of usually 10 sec. until the methyl red was exhausted.

Results

Carotene Retardation. We had previously found⁵ that at an ascorbic acid concentration of 1.84×10^{-3} M and a β -carotene concentration of 3×10^{-6} M the quantum yield for reduction of chlorophyllide was reduced to about one-fifth of the value obtained in the absence of carotene. The quantum yield for photo-reduction of methyl red at the same ascorbic acid concentration is reduced only by half at a carotene con-

centration of 3×10^{-5} M. If the function of the carotene is to quench triplet state chlorophyllide by energy transfer,⁷ it is most unlikely that the primary photochemical reaction is with ascorbic acid, and the most obvious alternative, primary reaction with methyl red, is to be preferred. A similar conclusion has recently been reached by Evstigneev, Gavrilova, and Savkina on other grounds.⁸

If carotene (Q) competes with methyl red for photoexcited chlorophyllide (Chl*) and the spontaneous rate of decay of Chl* is comparatively small, the rate constant k_1 for the reaction between Chl* and methyl red can be calculated from the equation

$$k_1/k_Q = \Phi_Q[Q]/(\Phi - \Phi_Q)[MR] \quad (1)$$

in which Φ_Q and Φ are the quantum yields in the presence and absence of the quencher carotene. With the known⁹ value $k_Q = 1.3 \times 10^9$, the third carotene run of Table I gave $k_1 = 1.4 \times 10^9$. According to this, methyl red ranks among the best quenchers of triplet state chlorophyllide.⁹

The conclusion that photoexcited chlorophyllide reacts first with methyl red is supported by the ascorbic acid concentration dependence of the quantum yield—efficient reduction of methyl red persists at ascorbic acid concentrations 0.01 times those required for efficient photoreduction of chlorophyllide.⁵

Ascorbic Acid. The variation of quantum yield during runs at different ascorbic acid levels is shown in Figure 1. At the lower ascorbic acid concentrations the yield decreases gradually with extent of reaction, but at higher concentrations it increases almost to the end of the run. The drop-off in the yield in the neighborhood of 10^{-6} M methyl red remaining is consistent with $K_1 \approx 10^{-9}$ l./mole sec. and a Chl* lifetime of about 10^{-3} sec.

The initial quantum yield creeps upward with ascorbic acid concentration (Figure 2). Points below 2×10^{-5} M ascorbic acid were calculated from the two lowest curves of Figure 1, on the assumption that reaction stopped when ascorbic acid was exhausted and consumption of ascorbic acid was proportional to consumption of methyl red.

Above $[\text{Asc}] = 10^{-4}$ M the initial quantum yield increases with $[\text{Asc}]$ according to

$$\Phi_0 = 0.055 + 0.86[\text{Asc}]^{1/2} \quad (2)$$

(6) A. S. Holt and E. E. Jacobs, *Am. J. Botany*, **41**, 710 (1954).

(7) H. Claes, *Z. Naturforsch.*, **16b**, 445 (1961).

(8) V. B. Evstigneev, V. A. Gavrilova, and I. G. Savkina, *Bio-khimiya*, **151**, 227 (1963).

(9) E. Fujimori and R. Livingston, *Nature*, **180**, 1036 (1957).

Table I: Effect of Various Substances and Conditions on the Initial Quantum Yield for Sensitized Photoreduction of Methyl Red. Ethanol Solution at 25° (light absorption rate $\sim 4 \times 10^{-6}$ einstein/l. sec., except as noted. [Chl] $\sim 5 \times 10^{-6}$ M)

Reducing agent and concn., $10^{-3}M$	[MR] ₀ , $10^{-5}M$	Other conditions; concn. in mole/l.	$10^2\Phi_0$	Reducing agent and concn., $10^{-3}M$	[MR] ₀ , $10^{-5}M$	Other conditions; concn. in mole/l.	$10^2\Phi_0$
Ascorbic acid				0	1.73	Dehydroascorbic acid, 1.9×10^{-3}	0
1.57	3.08	...	9.2				
1.89	3.13	β -Carotene, 0.30×10^{-5}	8.1	Hydrazobenzene			
1.84	3.05	β -Carotene, 1.17×10^{-6}	7.8	0.36	1.73	...	10.7
1.86	3.09	β -Carotene, 3.55×10^{-6}	4.4	0.47	1.61	...	11.4
1.59	0.27	...	4.9	0.37	1.61	$I_a = 0.27 \times 10^{-6}$	7.3
1.58	0.66	...	6.0	0.36	1.59	$I_a = 1.6 \times 10^{-6}$	7.4
1.58	7.73	...	11.5	0.35	1.52	Tetrabutylammonium hydroxide, 1.03×10^{-3}	0.2 ^A
4.61	7.50	...	11.3 ^a	0.36	1.59	Antitransilic acid, 5.9×10^{-3}	7.4
1.55	22.8	...	11.5 ^b	0.37	1.69	Azobenzene, 1.73×10^{-4}	10.9
1.86	3.06	$I_a = 0.22 \times 10^{-6}$	5.0 ^c	0.36	1.71	DMPD, 1.37×10^{-3}	3.6
1.61	3.10	$I_a = 1.8 \times 10^{-6}$	9.4	0.36	1.67	Benzoic acid, 9.75×10^{-3}	13.5
1.55	2.65	$I_a = 7.5 \times 10^{-6}$	8.5				
0.26	0.24	$I_a = 0.88 \times 10^{-6}$	5.1	Cysteine			
1.57	3.08	Pyridine, $x_{py} = 0.108^d$	5.8	0.70	3.30	...	0.26
0	3.11	Sodium ascorbate, 0.70×10^{-3}					
		Water, 1.4% (vol.)	1.7 ^e	Mercaptosuccinic acid			
1.61	3.03	Benzoic acid, 1.74×10^{-2}	9.4 ^f	1.47	1.75	...	0.115
0.16	3.14	Malic acid, 1.13×10^{-2}	1.2	1.47	1.79	Cyclohexene, 0.136	0.175
1.86	3.05	MgCl ₂ ·6H ₂ O, 7.4×10^{-3}	4.1	1.48	1.76	Cyclohexene, 0.272	0.18
1.86	3.05	KI, 4.6×10^{-3}	14.8	1.82	0.31	Cyclohexene, 0.264	0.45 ^g
0.21	1.60	...	6.0	1.44	7.07	Cyclohexene, 0.265	0.22 ^h
0.21	1.58	DMPD, 1.37×10^{-3}	6.4	9.18	1.44	Cyclohexene, 0.27; reducing agent 10% oxidized/ I_2	6.6 ⁱ
2.08	1.58	Dehydroascorbic acid, 1.3×10^{-3}	14.5				

^a Quantum yield rose to 0.18 and remained there for most of run. ^b For first interval; quantum yield rose to 0.15 then gradually declined through remainder of run. ^c Quantum yield rose steadily during reaction until equal to yield at higher light intensities. ^d At this mole fraction, methyl red is not entirely in the anionic form.^{2,5} ^e Initially methyl red was not entirely in the anionic form, perhaps, because of an ascorbic acid impurity in the sodium ascorbate. The quantum yield quickly fell to zero from this value for the initial period as the solution became more basic, and methyl red was converted entirely to the anionic form. The inactivity of ascorbate is only apparent and arises from conversion of methyl red to the anionic form in its presence. ^f Yield rose to 0.125 by the middle of the run. ^g All hydrazobenzene runs contain 3.9×10^{-4} M benzoic acid, except where noted. ^h Benzoic acid absent. Reaction apparently reversible and self-retarding. In 40 min. only 10% of the methyl red had been reduced (?), and on standing in the dark most of this was regenerated, judging by the absorption increase at 406 m μ . There have been other indications that the anionic form of methyl red is reducible but that the reduction is shallow and reversible. ⁱ For second light interval. ^j Methyl red was reduced during intervals of darkness but more slowly than during intervals of light. The dark reduction probably did not begin before some photoreduction had occurred.

At lower ascorbic acid concentrations the yield can be represented by

$$\Phi_0 = 0.055[\text{Asc}]/(1.15 \times 10^{-5} + [\text{Asc}]) \quad (3)$$

Curves for eq. 3, $0.86[\text{Asc}]^{1/2}$, and their sum are plotted in Figure 2.

The effects of other reagents are summarized in Table I. Between $[\text{MR}]_0 = 10^{-6}$ and 10^{-4} M the yield increases approximately as $[\text{MR}]_0^{1/2}$. The yield is almost independent of light intensity over a 30-fold range. The accelerating effect of dehydroascorbic acid is surprising and may be the basis of the rise in

quantum yield with conversion at high ascorbic acid concentrations. Dimethyl-*p*-phenylenediamine (DMPD) does not affect the quantum yield when present together with ascorbic acid, nor does it support reduction of methyl red in the absence of ascorbic acid.

Hydrazobenzene. In contrast with ascorbic acid, the quantum yield declines immediately and rather steeply with extent of reduction (Figures 3 and 4). The rate of decline is smaller at higher hydrazobenzene concentrations. Again the initial quantum yield creeps upward with increasing hydrazobenzene and initial methyl red concentrations (Figures 4 and 5).

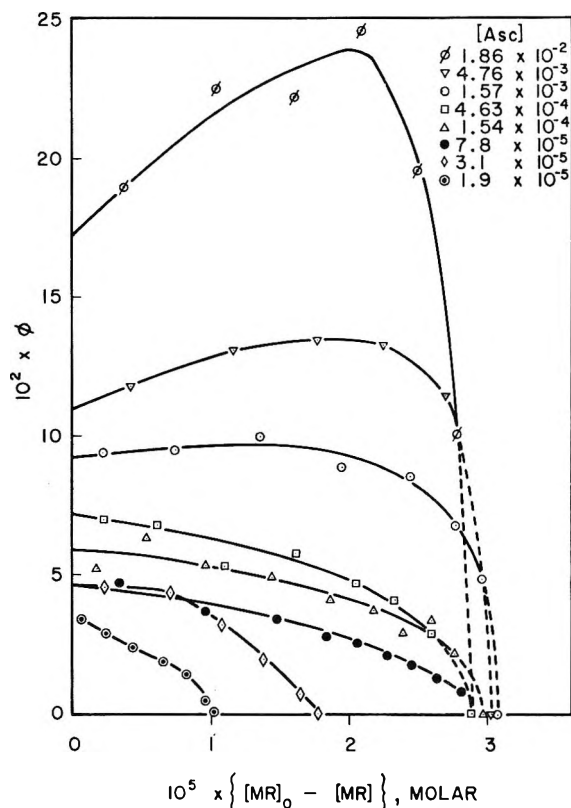


Figure 1. Variation of quantum yield for reduction of methyl red with extent of reduction and ascorbic acid concentration. $[MR]_0 \sim 3 \times 10^{-5} M$.

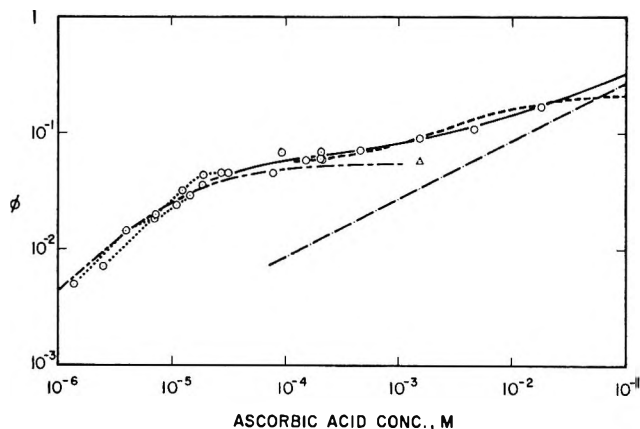


Figure 2. Variation of initial quantum yield with ascorbic acid concentration. Curves plotted according to equations of text: $-\cdot-\cdot-$, eq. 2; $-\cdot-\cdot-$, eq. 3; $---$, sum of (2) and (3); $-\cdot-\cdot-$, eq. 27; $\circ-\cdot-\cdot-\circ$, unites points of the same run at low ascorbic acid concentration; Δ : contained pyridine, $x_{py} = 0.108$.

DMPD reduces both yield and slope but leaves their ratio about the same (Figure 3). Azobenzene, anthranilic acid, and light intensity have no effect. The

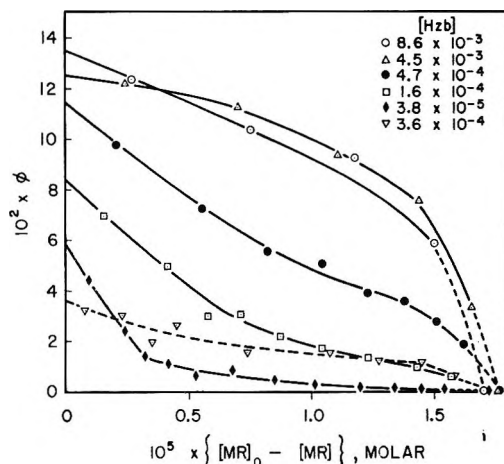


Figure 3. Variation of quantum yield for reduction of methyl red with extent of reduction and hydrazobenzene concentration. $[MR]_0 \sim 1.8 \times 10^{-6} M$. ∇ : contained DMPD, $1.37 \times 10^{-3} M$.

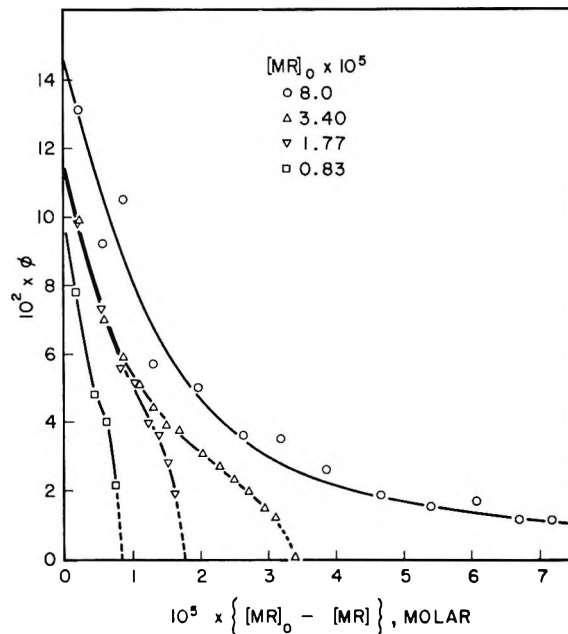


Figure 4. Variation of quantum yield for methyl red reduction with extent of reduction and initial methyl red concentration. $[Hzb] = 4.7 \times 10^{-4} M$. Curve through uppermost set of points is the hyperbola of eq. 4, with constants cited in text.

presence of 25 times the usual amount of benzoic acid increased the yield by 30% but did not affect the rate of decline of yield with conversion.

The simplest curve fitting points for the run of Figure 4 made at highest $[MR]_0$ is a hyperbola of the form

$$B\Phi\Delta + C\Phi^2 + E\Phi = 1 \quad (4)$$

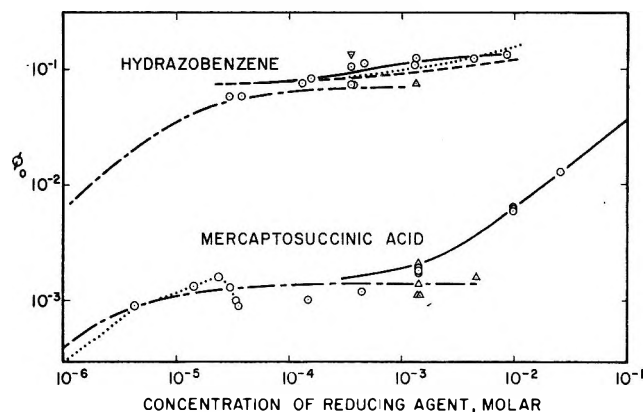


Figure 5. Variation of initial quantum yield with hydrazobenzene and mercaptosuccinic acid concentration. Curves plotted according to equations of text. For hydrazobenzene: - - - - , eq. 11; - - - - - , eq. 12; - - - , eq. 13; ———, eq. 27 with parameters cited in text; runs designated by \circ contained $3.9 \times 10^{-4} M$ benzoic acid; Δ contained no benzoic acid; ∇ contained $9.8 \times 10^{-3} M$ benzoic acid. For mercaptosuccinic acid: ———, eq. 15; ———, eq. 27 with parameters cited in text; \circ - - - \circ connects points of a run deficient in mercaptosuccinic acid; runs designated by \circ contained cyclohexene; Δ did not.

($\Delta = [\text{MR}]_0 - [\text{MR}]$), having asymptotes on the Δ -axis and at an angle $\tan^{-1}(-B/C)$ to the Δ -axis, with $B = 1.45 \times 10^6$, $C = 140$, and $E = -13.7$.

In search of clues to the reason for the behavior of the quantum yield in the hydrazobenzene runs, hyperbolas of the same form have been assumed for other runs. Values of B , C , and E were calculated when sufficient data were available from the extrapolated values of Φ_0 , $(d\Phi/d\Delta)_0$, and the quantum yield at a point near the end of the run with the aid of (4), (5), and (6).

$$\Phi_0 = (-E + \sqrt{E^2 + 4C})/2C \quad (5)$$

$$(d\Phi/d\Delta)_0 = -B\Phi_0/(E + 2C\Phi_0) \quad (6)$$

Over the range 0.4 to $5 \times 10^{-4} M$ for $[\text{Hzb}]$ and 1.6 to $8 \times 10^{-5} M$ for $[\text{MR}]$, the constants in (4) were related to each other and the concentrations by

$$B = 2.64/[\text{MR}]_0[\text{Hzb}]^{1/2} \quad (7)$$

$$C = 0.98 \times 10^{-4}B \quad (8)$$

$$E = -0.071C \quad (9)$$

with an average deviation of about 20%. The greatest deviation occurred at the lowest hydrazobenzene concentration, where the effect of depletion of hydrazobenzene was felt.

Inserting (7), (8), and (9) into (4) and rewriting it in

a somewhat more conventional form for the quantum yield gives

$$\Phi = \frac{[\text{MR}]_0[\text{Hzb}]^{1/2}}{2.64\Delta + 2.6 \times 10^{-4}\Phi - 1.85 \times 10^{-5}} \quad (10)$$

This is, no doubt, only an approximation to the true and probably rather complicated form, but it suggests that there are at least two retarding agents—one having a concentration proportional to Δ , the other a transient with concentration proportional to Φ . The numerator in (10) would probably also contain a term in acid concentration had this been taken into account.

Solving (10) for Φ_0 gives

$$\Phi_0 = 0.0355 (1 + \sqrt{1 + 3.04 \times 10^6[\text{MR}]_0[\text{Hzb}]^{1/2}}) \quad (11)$$

For small values of $[\text{Hzb}]$ and $[\text{MR}]_0 = 1.6 \times 10^{-5} M$, (11) may be approximated by

$$\Phi_0 = 0.071 + 0.87[\text{Hzb}]^{1/2} \quad (12)$$

Equations 11 and 12 are plotted through the points for hydrazobenzene in Figure 5; (12) represents the initial yields somewhat better at high hydrazobenzene concentration, where direct evaluation of B , C , and E was impossible. Equation 12 is remarkably like eq. 2 for ascorbic acid though it was arrived at in a much more roundabout way.

Because of the self-retardation it proved impossible to determine the form of the Φ vs. $[\text{Hzb}]$ curve at very low $[\text{Hzb}]$ from runs deficient in hydrazobenzene. From the two lowest initial quantum yields and with consideration of (11) or (12), the relationship

$$\Phi_0 = 0.071[\text{Hzb}]/(1.0 \times 10^{-5} + [\text{Hzb}]) \quad (13)$$

is estimated for this region.

Mercaptosuccinic Acid. In these runs radicals produced by oxidation of mercaptosuccinic acid attacked chlorophyllide. The extent of the chlorophyllide loss was reduced but not entirely eliminated by incorporation of olefins such as allyl alcohol, cyclohexene, camphene, and anethole. All were effective, and purified cyclohexene was included in most reaction mixtures. Quantum yields were sometimes increased by inclusion of an olefin but by no more than a factor of $3/2$.

Quantum yields with mercaptosuccinic acid were much lower than those with ascorbic acid or hydrazobenzene. At low $[\text{Msa}]$ the yield increases linearly as the reaction progresses; at high $[\text{Msa}]$ the yield is initially high and decreases as the reaction progresses (Figure 6).

Initial yields show a linear increase with $[\text{Msa}]$ above $10^{-3} M$ according to eq. 14.

$$\Phi_0 = 0.0014 + 0.48[\text{Msa}] \quad (14)$$

From the mercaptosuccinic acid-deficient run, as a very rough estimate at low [Msa]

$$\Phi_0 = 0.0014[\text{Msa}]/(2.5 \times 10^{-6} + [\text{Msa}]) \quad (15)$$

Equation 15 is plotted in the lower part of Figure 5.

A run in which the mercaptosuccinic acid had been partially oxidized (by I_2 , the HI being neutralized with PbCO_3) showed a comparatively large quantum yield, and a dark reaction ensued.

Cysteine reduced methyl red with about the same quantum yield as mercaptosuccinic acid; the yield dropped slowly during the reaction.

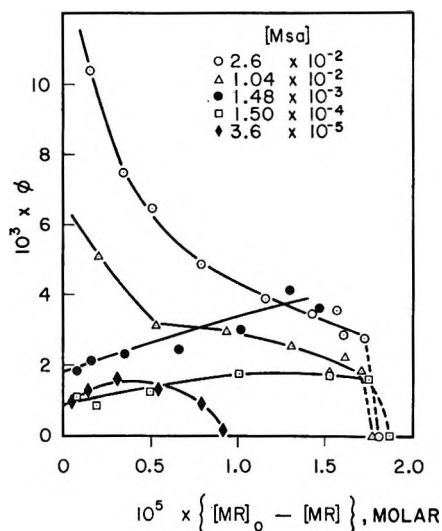


Figure 6. Variation of quantum yield for reduction of methyl red with extent of reduction and mercaptosuccinic acid concentration. $[\text{MR}]_0 \sim 1.8 \times 10^{-5} M$; [cyclohexene] = 0.27 M.

Discussion

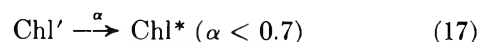
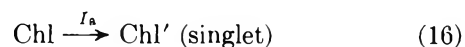
In two runs with ascorbic acid—one with hydrazobenzene and one with mercaptosuccinic acid in which insufficient reducing agent was present to reduce all the methyl red—the ratios of reducing agent initially present to methyl red consumed were 1.52, 1.82, 1.91, and 3.90, respectively. Even when the reducing agent is deficient, methyl red is apparently reduced beyond the hydrazo stage to products at the oxidation level of anthranilic acid and DMPD. No methyl red is regenerated on exposure to air or benzoquinone, even when the reducing agent is exhausted. The variation of quantum yield during the runs, which depends so much upon the nature of the reducing agent, shows that it is difficult to separate the early steps in the reduction from the follow-up steps that complete the four-electron

reduction of methyl red. For example, the comparatively low quantum yield with mercaptosuccinic acid may be a consequence of the inability of its thyl radical to act as a reducing agent under the conditions of the reaction.

The products of the chemical reduction of methyl red have been identified as anthranilic acid and DMPD.¹⁰⁻¹² Presumably, these are the products of the four-electron photochemical reduction also, but the evident complexity of the follow-up reactions and relative inertness of added anthranilic acid and DMPD give rise to the suspicion that other products may also be formed. In one run ($[\text{Asc}] = 2.0 \times 10^{-4}$, $[\text{MR}]_0 = 3.2 \times 10^{-5}$) changes in the near-ultraviolet were followed in hopes of detecting products of the reaction. The bands of methyl red were replaced by a band with ϵ 12,500 l./mole-cm. at 320 m μ , 10,200 at 330, 8300 at 340, and 5100 at 350. Anthranilic acid and DMPD both absorb in this region, but their combined extinction coefficient is only about half that observed. Unfortunately, attempts to prepare larger amounts of the reduced products failed because of self-retardation.¹³

The evident complexity of the reaction makes it impossible to account for the rate once reaction products have accumulated, but if attention is confined to initial rates it appears from Figures 2 and 5 or eq. 2, 12, and 14 that reactions with the three reducing agents have one feature in common—an increase in the quantum yield with reducing agent concentration in the neighborhood of $10^{-3} M$. Although these increases could be the result of unrelated reactions between the reducing agents and later products of reaction, it is also likely that a common step, early in the reaction, is involved.

The following mechanism is proposed as being able to account in a general way for the variation of initial quantum yields with concentration. It is based on the assumption that the initial reaction between triplet excited chlorophyllide and methyl red produces a radical-ion pair.



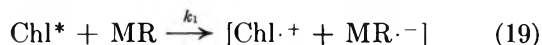
(10) K. Fukui, Y. Inamoto, H. Kitano, and C. Nagatu, *J. Org. Chem.*, **26**, 1394 (1961).

(11) S. Kubota, T. Akita, and T. Yokoshima, *Yakugaku Zasshi*, **78**, 1194 (1958); *Chem. Abstr.*, **53**, 5162 (1959).

(12) W. C. J. Ross and G. P. Warwick, *J. Chem. Soc.*, 1724 (1956).

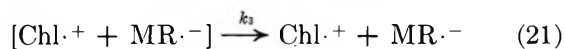
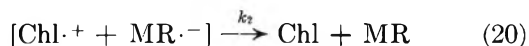
(13) Attempts to generate Würster's red from DMPD after reduction by exposure to air or quinone have never succeeded, but failure may be due to interference by some other product and need not imply absence of DMPD.

I_a is the rate of light absorption in einstein/l. sec. The fraction α of singlet excited chlorophyll that crosses over to triplet is less than $(1 - \text{fluorescence yield})$ about 0.7.

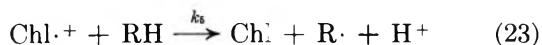


Recent measurements¹⁴ suggest a value of about $1.5 \times 10^3 \text{ sec.}^{-1}$ for k_d in ethanol; from carotene retardation, $k_1 = 1.4 \times 10^9 \text{ l./mole sec.}$

The pair of ions may or may not separate, but, in the absence of a reducing agent, there is no net reaction.¹⁵



At low concentration, a reducing agent RH competes with $\text{MR}\cdot^-$ for $\text{Chl}\cdot^+$.



The reduction is completed by any of a variety of possible reactions of radicals with each other or with the reducing agent.

The above sequence of reactions leads to a quantum yield expression of the following form, in which γ is the probability that (23) will ultimately lead to reduction of a molecule of methyl red.

$$\Phi = \frac{\alpha[\text{MR}]}{(k_d/k_1) + [\text{MR}]K_A + [\text{RH}]} \gamma[\text{RH}] \quad (24)$$

The interpretation of K_A , which is 1.15×10^{-5} for ascorbic acid, 1.0×10^{-5} for hydrazobenzene, and perhaps 2.5×10^{-6} for mercaptosuccinic acid, depends on assumptions about the rates of the various radical disproportionation reactions and is too involved to warrant further discussion without more information.

Equation 24 is applicable up to reducing agent concentrations around $10^{-4} M$. The continued increase of quantum yield at higher RH concentration needs to be accounted for.

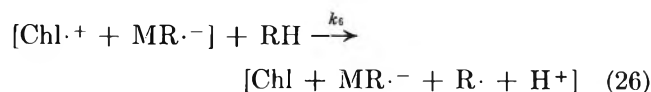
It is possible that the reducing agent reacts with $\text{MR}\cdot^-$ or rather $\text{MRH}\cdot$ directly.



Against this is the lack of any distinct increase of quantum yield with decreased light intensity, as would

be predicted if (25) competes with radical recombination reactions.

If the product of (19) is an ion pair with a long enough life, reaction with reducing agent may compete with (20) and (21) as well as with (22).



If the probability of net reduction of methyl red after (26) is γ' , the quantum yield at high reducing agent concentration can be approximated by

$$\Phi = \frac{\alpha\gamma k_3}{k_2 + k_3} \left[\frac{1 + (\gamma'k_6/\gamma k_3)[\text{RH}]}{1 + [k_6/(k_2 + k_3)][\text{RH}]} \right] \quad (27)$$

Curves of (27) have been fitted to the experimental points of Figures 2 and 5. Taking $\alpha = 0.7$ the curves have the parameters $\gamma' = 0.32, 0.20,$ and $0.20,$ and $k_6/(k_2 + k_3) = 780, 2900,$ and 360 for ascorbic acid, hydrazobenzene, and mercaptosuccinic acid.¹⁶ The curves, plotted in Figures 2 and 5, fit the data fairly well for hydrazobenzene and mercaptosuccinic acid, but data for ascorbic acid are better represented by (2).

Equation 27 is versatile enough to account for power law expressions like (2), (12), and (14). In passing, it may be noted that, for the yield to be greater at high reducing agent concentration, it is not necessary that γ' be greater than γ , but only that it be greater than $\gamma k_3/(k_2 + k_3)$.

The data of references 2 and 3 were obtained at high reducing agent concentrations, where the sequence of reactions 16, 17, 19, and 26 dominates, and the meaning of the constants in their rate expressions should be reinterpreted in that light.

Acknowledgments. The assistance of Messrs. J. Miller, A. Folkmanis, and D. Stoltz is appreciated.

(14) R. Livingston and P. J. McCartin, *J. Phys. Chem.*, **67**, 2511 (1963).

(15) In the absence of reducing agent, methyl red does, however, suppress a very slow degradation of chlorophyllide by ethanol or an impurity in the ethanol, which presumably goes via the triplet state of chlorophyllide [R. Livingston and D. Stockman, *ibid.*, **66**, 2533 (1962)].

(16) The bracketted expression of (27) is a family of curves of the form $(1 + px)/(1 + x)$, where $x = k_6[\text{RH}]/(k_2 + k_3)$ and $p = \gamma'(k_2 + k_3)/\gamma k_3$. If the curves are plotted logarithmically for several values of the parameter p and comparison is made with experimental quantum yield curves, ordinate and abscissa give values of $\alpha\gamma k_3/(k_2 + k_3)$ and $k_6/(k_2 + k_3)$. Values of $\alpha\gamma k_3/(k_2 + k_3)$ are the first term on the right in (2), (12), and (14); combining with the values of p for the curve which seems best to fit the experimental points gives values for γ' , but γ by itself cannot be obtained.

A Comparison of Fast Neutron and γ -Irradiation of Polystyrene.

I. Cross-Linking Rates¹

by W. W. Parkinson, C. D. Bopp, D. Binder,

Reactor Chemistry Division, Oak Ridge National Laboratory, Oak Ridge, Tennessee

and J. E. White

Science and Technology Division, Southern Illinois University, Edwardsville, Illinois (Received July 15, 1964)

Linear energy transfer (LET) effects in polymers provide an indication of the reaction mechanisms involved, as well as a basis for the prediction of property changes in a radiation field. Polystyrene specimens irradiated in γ -sources and in a nuclear reactor have been compared by solution viscosity, gel content, and solvent-swelling measurements. The cross-linking rate was two- to threefold higher for the reactor by all three methods. For fast neutrons (LET ~ 3 e.v./ \AA .), $G(\text{cl}) = 0.096 \pm 0.015$; for ^{60}Co γ -radiation (LET ~ 0.02 e.v./ \AA .), $G(\text{cl}) = 0.034 \pm 0.002$. The ratio of scission to formation of cross-linked units was 0.14 for both cases. The increased yields of cross links at high LET can be accounted for by enhancement of second-order processes in overlapping spurs at the expense of competing first-order reactions. Several reaction mechanisms can meet these general requirements.

Introduction

Radiation effects will be dependent on the linear energy transfer rate (LET) of the incident radiation or particles if the radiation products result from competing reactions of different kinetic order.² Therefore, the existence of LET effects provides indications of the nature of radiation-induced processes. Furthermore, in the cross linking of commercial polymers, LET effects are also of technical importance since certain mechanical properties are altered by cross linking.

Previous work on aliphatic hydrocarbons³ and high polymers⁴⁻⁶ had revealed only small LET effects although Charlesby and co-workers⁷ noted a strong dependence on LET for the steady-state concentration of unsaturation in polyethylene. In contrast, aromatic liquids have shown a marked dependence of radiation yields on LET,^{8,9} and recent investigations¹⁰ of aliphatics indicate that LET effects are more general than suspected.

The increased yields of coupling reactions in molten biphenyl and terphenyl at high LET suggest that cross linking in polystyrene should be enhanced similarly. Earlier work on polystyrene gave about the same yield of cross links from low LET irradiations¹¹ as from a

nuclear reactor.^{4,5,12} (Charged particles having high LET are produced in a reactor through scattering collisions of fast neutrons.) The reactor dose determinations, however, were performed with a relative dosimeter, polymethyl methacrylate, which shows uncer-

(1) Research sponsored by the U. S. Atomic Energy Commission under contract with the Union Carbide Corp. A part of this paper was presented at the Conference on Nuclear Reactor Chemistry, Gatlinburg, Tenn., Oct. 12, 1961.

(2) W. G. Burns and R. Barker, "Progress in Reaction Kinetics," Vol. III, G. Porter, Ed., Pergamon Press, Ltd., London, in press. Presently available as AERE-R4240, Atomic Energy Research Establishment, Harwell, Berkshire, England, 1963.

(3) H. A. Dewhurst and R. H. Schuler, *J. Am. Chem. Soc.*, **81**, 3210 (1959).

(4) A. Charlesby, "Atomic Radiation and Polymers," Pergamon Press, Inc., New York, N. Y., 1960, pp. 47, 288.

(5) A. Chapiro, "Radiation Chemistry of Polymeric Systems," Interscience Publishers, Inc., New York, N. Y., 1962, pp. 342, 448.

(6) R. F. Itzhaki and P. Alexander, *Radiation Res.*, **15**, 553 (1961).

(7) A. Charlesby, A. R. Gould, and K. J. Ledbury, *Proc. Roy. Soc. (London)*, **A277**, 348 (1964).

(8) T. Gäumann and R. H. Schuler, *J. Phys. Chem.*, **65**, 703 (1961).

(9) W. G. Burns and C. R. V. Reed, *Trans. Faraday Soc.*, **59**, 101 (1963).

(10) W. G. Burns and J. R. Parry, *Nature*, **201**, 814 (1964).

(11) L. A. Wall and D. W. Brown, *J. Phys. Chem.*, **61**, 129 (1957).

(12) A. Charlesby, *J. Polymer Sci.*, **11**, 521 (1953).

tainties in the influence of temperature,^{13,14,15} and the possibilities of an LET effect itself.^{6,16}

This paper describes measurements of cross linking in polystyrene irradiated with γ -radiation and with the mixed γ -neutron field of a reactor, in which the dose rate had been determined by an absolute method. A succeeding paper, part II,¹⁷ discusses the analysis of radiolysis products and long-lived free radicals.

Experimental

Materials. Commercial polystyrene pellets (2–3 mm. on edge), free of additives and having low monomer content (<1%), were used without further purification for most of the measurements.¹⁸ The weight-average molecular weight, by conventional light-scattering techniques, was $2.72 (\pm 0.05) \times 10^5$ with light of 436 $m\mu$ and 2.85×10^5 with light of 546 $m\mu$ after applying dissymmetry and polarization corrections. A second type of sample material was also used for some of the solution viscosity measurements to reduce the possibility that undetected impurities in a single material would vitiate the reactor dose determinations. This second material was commercial, clear, extruded, and oriented polystyrene sheet, 0.25 mm. thick.¹⁹ Both sample stocks were analyzed for traces of elements of high neutron cross section by activation analysis, spectrographic, or chemical methods.

All samples were encapsulated for irradiation in 10–14-mm. quartz or borosilicate glass (Pyrex brand) tubes after evacuation for 24 hr. or longer at 2- μ pressure and room temperature. Only quartz tubes were used for the reactor irradiations while glass tubes were used for most of the γ -irradiations. A few γ -irradiated specimens were contained in quartz to determine whether wall effects were occurring, but no differences were noted.

Irradiation Procedures. The γ -irradiations were carried out in water-cooled, cylindrical ⁶⁰Co sources. The source used for most of the irradiations imparted a dose of 2.2×10^{18} e.v./g.-min. A few preliminary irradiations were performed in a source imparting a dose of 9.3×10^{18} e.v./g.-min. No effect of dose rate was noted. Irradiation temperatures were 20–25°.

The reactor irradiations were performed in a water-cooled hole in the Oak Ridge graphite reactor. Irradiation temperatures were 18–25°. The thermal neutron flux was 6.2×10^{11} neutrons/cm.²-sec., and the flux of fast neutrons in the energy range of the "fission spectrum" (average energy ~ 2 Mev.) was about 0.6×10^{11} neutrons/cm.²-sec. The dose rate to polystyrene was 1.1×10^{18} e.v./g.-min. for most of the irradiations.

Measurement of Radiation Dose. The dose rate of

the two γ -sources was measured by the ceric sulfate method.²⁰ The cerous yield was normalized with the ferrous sulfate dosimeter, $G(\text{Fe}^{+3}) = 15.6$ ions/100 e.v.²¹ Dose rates in the dosimeter solution were converted to doses in polystyrene by multiplying by the ratio of the electron densities, 0.970. The accuracy of the γ -doses was approximately $\pm 5\%$.

Doses in the reactor were calculated from parameters for the energy imparted to hydrogen and to carbon, determined by calorimeters of nylon and of graphite.²² The parameters were related to the thermal neutron flux and to the apparent dose rate in dilute H₂SO₄ by the irradiation of cobalt foil monitors and Ce(SO₄)₂ dosimeters at convenient intervals. The Ce(SO₄)₂ dosimeter shows a sufficiently low LET dependence to indicate in this manner the changes in the relation between total dose rate and thermal neutron flux.²³ The doses to individual specimens were calculated from the thermal neutron flux as measured by cobalt monitors using

$$D = \phi t \frac{C_1}{C_0} [f_C(N_C + G_C) + f_H(N_H + G_H)] \quad (1)$$

where ϕ = thermal neutron flux, t = time duration, C_1 = cerous yield per thermal neutron per cm.², C_0 = the yield at the time of calorimetry, f_i = weight fraction of element i , N_i = energy from fast neutrons per gram of element i per thermal neutron per cm.², and G_i = energy from γ -radiation on the same basis.²⁴

This method of determining doses in the reactor did not account for energy imparted through neutron reactions with impurities in the polystyrene. The

(13) P. Alexander, *et al.*, *Proc. Roy. Soc. (London)*, **A223**, 392 (1954).

(14) P. Alexander, *et al.*, *Radiation Res.*, **9**, 509 (1958).

(15) R. M. Black, *Nature*, **178**, 305 (1956).

(16) D. Binder, *et al.*, Solid State Division Annual Progress Report, Aug. 31, 1959, U. S. Atomic Energy Commission Report, ORNL-2829, p. 185.

(17) R. M. Keyser, R. A. Weeks, and W. W. Parkinson, in press.

(18) Union Carbide Plastics Division Grade SGD-3002 polystyrene was kindly supplied by Drs. F. M. Rugg and J. E. Potts.

(19) "Polyflex 100" was kindly supplied by Dr. Jules Pinsky, of Plax Corp., Hartford, Conn.

(20) T. J. Hardwick, *Can. J. Chem.*, **30**, 39 (1952).

(21) C. J. Hochanadel and J. A. Ghormley, *J. Chem. Phys.*, **21**, 880 (1953).

(22) D. Binder, C. D. Bopp, and R. L. Towns, *Am. Soc. Testing Mater., Spec. Tech. Publ.*, **286**, 105 (1960).

(23) A. O. Allen, "The Radiation Chemistry of Water and Aqueous Solutions," D. Van Nostrand Co., Inc., Princeton, N. J., 1961, p. 54.

(24) The viscosity specimens were irradiated to low doses requiring short exposures during which only minimal changes occurred in the operating conditions of the reactor. Consequently, doses were calculated for these specimens from the dose rate established by calorimetry, corrected for minor changes indicated by Ce(SO₄)₂ dosimeters exposed at intervals.

nuclear properties of the trace elements determined as described above were used to calculate contributions to the total reactor dose from nuclear reactions. These contributions had an upper limit of 2.5% of the reactor dose and were neglected since the accuracy of the calorimetric measurements was about $\pm 15\%$.

Measurements of Irradiated Polystyrene. For a convenient comparison of cross-linking rates in the two types of sample material and in the two radiation sources, intrinsic viscosities were determined by the usual methods. In all cases, the intrinsic viscosity was obtained by extrapolation from the viscosities of at least four dilute solutions.

Solvent-swelling measurements were performed by infusion of toluene (ACS reagent grade) into irradiated specimens in a Soxhlet extractor over a 12-hr. period at temperatures near the boiling point of toluene. The volume-swelling ratio was calculated from the original weight and density of the specimen and from the weight of the swollen specimen and the solvent density, assuming that the swollen specimen had the density of the solvent.

The sol fraction of specimens irradiated in excess of the gel dose was determined by extraction with toluene in a Soxhlet extractor for three periods of 6 hr. each. After each period, the specimens were dried in a vacuum oven and weighed. By the third extraction, the fraction dissolving had reached a negligible value for all specimens except those with the highest and lowest doses.

Results

Solution Viscosity Measurements. The apparent change in the number of molecules per gram was used to compare the two sample stocks rather than the solution viscosities directly, since the initial viscosities and molecular weights were not the same. The molecular weights were calculated from the empirical equation²⁵

$$[\eta] = 1.70 \times 10^{-4} M_v^{0.69} \quad (2)$$

in which $[\eta]$ = intrinsic viscosity and M_v = viscosity-average molecular weight. The actual change in the number of molecules per unit mass represents the cross-link production, but the apparent change, ΔN of eq. 3, is not equivalent to cross links because the equations relating viscosity to molecular weight are not valid for varying degrees of molecular branching. In this equation

$$\Delta N = \frac{A}{0.54} \left(\frac{1}{M_{v0}} - \frac{1}{M_v} \right) \quad (3)$$

M_{v0} is the initial viscosity-average molecular weight,

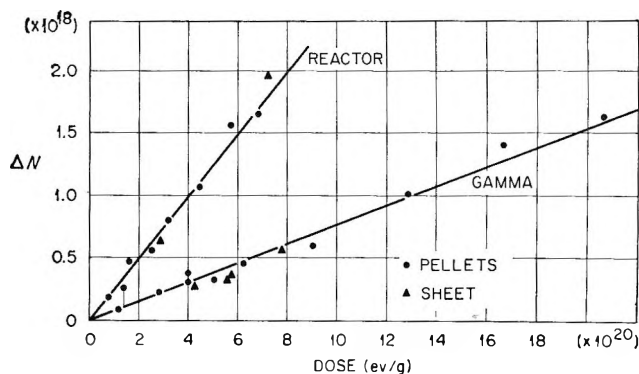


Figure 1. Apparent change in number of molecules/g.

A is Avogadro's number, and 0.54 is the ratio of the number-average molecular weight to the viscosity average (assuming a random distribution). The apparent change in number per gram, ΔN , is plotted as a function of dose in Figure 1.

The initial viscosity-average molecular weight can be compared to the weight average from light scattering to indicate the conformity to a random molecular weight distribution. The viscosity measurements gave $M_{v0} = 2.40 \times 10^5$ while, for a random distribution

$$2M_{v0} = M_w [(1+a)\Gamma(1+a)]^{1/a} \quad (4)$$

where M_w = weight average and $\Gamma(1+a)$ is the Γ -function of a , 0.69, from the viscosity equation (2). Inserting 2.78×10^5 , the mean of the light-scattering determinations, yields $M_{v0} = 2.58 \times 10^5$. This value is sufficiently near the measured value above to permit the use of equations based on a random distribution, *i.e.*, eq. 6.

Solvent-Swelling Ratios. The Flory-Rehner equation relating volume-swelling ratio, V , to density of cross links has been simplified by Charlesby¹² to the form

$$V^{5/3} = \frac{(0.5 - \mu)M_c}{d_0 v} \quad (5)$$

in which μ = thermodynamic constant of interaction between solvent and polymer, M_c = molecular weight between cross links, d_0 = density of polystyrene, and v = molar volume of toluene. Since M_c is proportional to the reciprocal of dose, a log-log plot of V vs. dose should have a slope of -0.6 . The data are presented in this manner in Figure 2 with the lines constrained to a slope of -0.6 . The agreement of points and line is good except in the low dose range where the effects of chain ends and soluble material become appreciable.

(25) P. Outer, C. I. Carr, and B. H. Zimm, *J. Chem. Phys.*, **18**, 830 (1950).

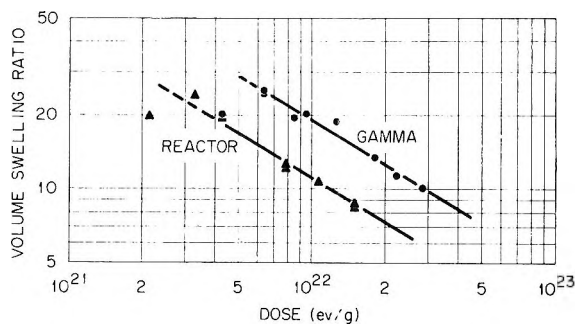


Figure 2. Solvent swelling of irradiated polystyrene.

Soluble Fraction. At the first appearance of insoluble polymer (gel point) there is one cross-linked repeating unit (0.5 cross link) per weight-average molecule, regardless of molecular weight distribution. For extrapolation to the gel point, the soluble fractions have been plotted *vs.* dose on a log-log plot in Figure 3, assuming that the degree of cross linking is proportional to dose. The doses at the gel points are $1.5 (\pm 0.2) \times 10^{21}$ e.v./g. for the reactor and $3.5 (\pm 0.2) \times 10^{21}$ e.v./g. for the γ -irradiations. The indicated error limits are the estimated uncertainty of the dose determination.

To permit the calculation of cross-link yields, a determination of scission concurrent with cross linking is necessary. Charlesby²⁶ has derived the expression below for a random molecular weight distribution

$$s + \sqrt{s} = \frac{p_0}{q_0} + \frac{1}{q_0 u_1 r} \quad (6)$$

where s = sol fraction, p_0 = fraction of repeating units "scissioned" per unit dose, q_0 = fraction of repeating units cross linked per unit dose, u_1 = number-average degree of polymerization, and r = radiation dose. In Figure 4, $s + \sqrt{s}$ is plotted against $1/r$ for specimens irradiated in a γ -source and in the reactor. Extrapolation to $1/r = 0$ gives values for p_0/q_0 , the scission to cross-linking ratio, of 0.14 ± 0.01 and 0.13 ± 0.01 for the two groups of specimens. Certainly, within the experimental errors involved in the sol fraction measurements, the ratio of scission to cross linking is the same for γ - and reactor-irradiated specimens. Extrapolation to complete solubility ($s + \sqrt{s} = 2$) permits an estimate of the gel points. Values of 3.6×10^{21} e.v./g. for γ -radiation and 1.4×10^{21} e.v./g. for the mixed reactor field corroborate the more precise gel points from the log-log plot, Figure 3.

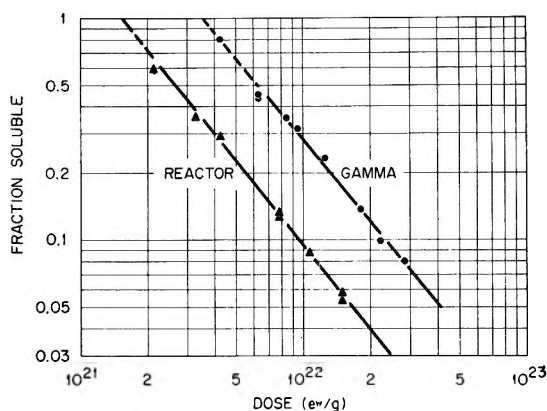


Figure 3. Soluble fraction of irradiated polystyrene.

lation to $1/r = 0$ gives values for p_0/q_0 , the scission to cross-linking ratio, of 0.14 ± 0.01 and 0.13 ± 0.01 for the two groups of specimens. Certainly, within the experimental errors involved in the sol fraction measurements, the ratio of scission to cross linking is the same for γ - and reactor-irradiated specimens. Extrapolation to complete solubility ($s + \sqrt{s} = 2$) permits an estimate of the gel points. Values of 3.6×10^{21} e.v./g. for γ -radiation and 1.4×10^{21} e.v./g. for the mixed reactor field corroborate the more precise gel points from the log-log plot, Figure 3.

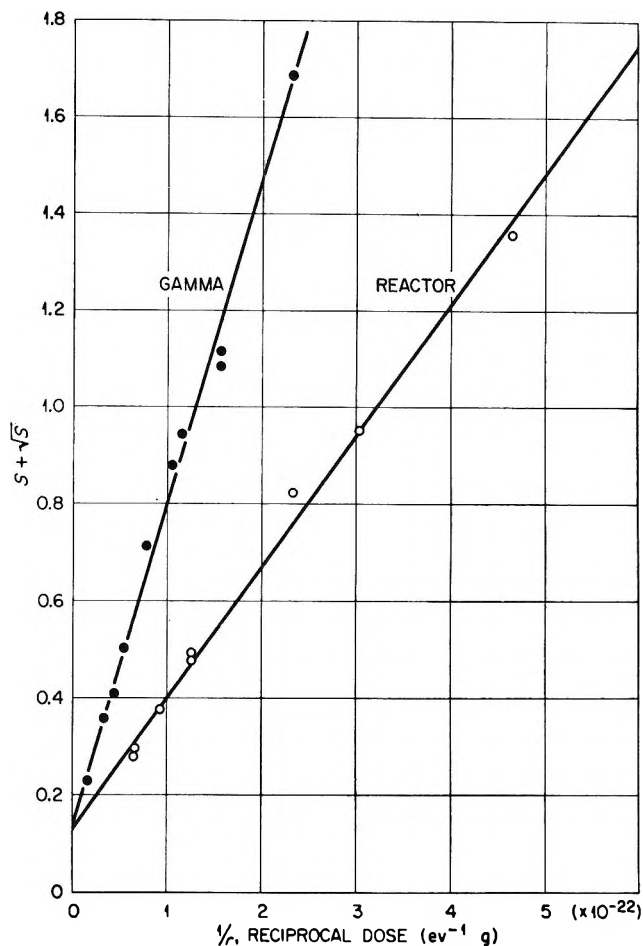


Figure 4. Solubility as a function of the reciprocal of dose.

For a calculation of both cross-linking and scission yields, the gel point doses, r_g , and the scission to cross-linking ratios may be substituted into eq. 7²⁶

$$\frac{w}{M_w} = r_g \left(q_0 - \frac{p_0}{2} \right) \quad (7)$$

in which w = molecular weight of a repeating unit. Substituting $p_0/q_0 = 0.14$ gives $w/M_w = r_g(0.93q_0)$,

(26) See ref. 4, p. 172.

and converting q_0 to the yield of cross-linked units/100 e.v., $G(\text{clu})$

$$G(\text{clu}) = \frac{100A}{0.93M_w r_g} \quad (8)$$

For γ -radiation, $r_g = 3.5 (\pm 0.2) \times 10^{21}$ e.v./g. and $G(\text{clu}) = 0.067 \pm 0.003$. Since there are two cross-linked units in each cross link, the yield of cross links is $G(\text{cl}) = 0.034 \pm 0.002$. Alternatively, the yield can be expressed as 2900 ± 100 e.v. of γ -energy absorbed for each cross link. The scission yield is $G(\text{s}) = 0.14(0.067) = 0.0094 \pm 0.0005$.

For the mixed neutron- γ radiation field of the reactor, $r_g = 1.5 (\pm 0.2) \times 10^{21}$ e.v./g., and $G(\text{clu}) = 0.15 \pm 0.02$. For cross links, $G(\text{cl}) = 0.077 \pm 0.010$ or 1300 ± 200 e.v./cross link. The scission yield is $G(\text{s}) = 0.022 \pm 0.003$.

Discussion

Viscosity Measurements. The viscosity data plotted in Figure 1 show that both sample stocks behave similarly in the reactor and indicate that neutron reactions with impurities are not producing an undetected augmentation of the reactor radiation dose. While branching effects preclude the calculation of cross-linking rates from these curves, it is significant that the slope for the reactor specimens is about three times that for the γ -irradiated material.

Swelling Ratio Measurements. The solvent-swelling determinations are useful for comparative purposes since they are independent of the initial molecular weight distribution, while the solution viscosities depend on branching and the sol fraction curves are influenced by the initial distribution. Calculations of radiation yields of cross links from changes in M_w , eq. 5, are not accurate because of the large uncertainty in the term $(0.5 - \mu)$ when the experimental value of 0.44 for μ is used.¹² However, for a given degree of swelling, 2.4 times as much dose is required from a γ -source as from the mixed field of the reactor.

Sol Fraction Determinations. The cross-link yields calculated from gel doses are $G(\text{cl}) = 0.034$ for γ -radiation and 0.077 for the reactor. The ratio of the reactor yield to the γ -yield is 2.3, about the same as the ratio of efficacies in the swelling measurements, while the ratio of the slopes of the viscosity plots (Figure 1) is even larger, exceeding 3. Since these three methods of comparing cross-linking rates depend in a different manner on molecular branching and molecular weight distribution, it is clear that energetic neutrons produce higher yields of cross links than does γ -radiation, rather than producing only a different spatial distribution

of links or a different molecular weight distribution.

Our cross-link yields observed for γ -radiation, 2900 e.v./cross link, may be compared to those reported in the literature. Wall and Brown,¹¹ using γ -radiation under vacuum, reported 1360 e.v./cross link for freshly prepared samples and 2200 for older sample material. Burlant, *et al.*,²⁷ for similar irradiation conditions, determined 2000 e.v./cross link for freshly polymerized material.

The lower γ -yield which we found could have been caused by small quantities of oxygen either within the polymer or in the capsule (sealed at a pressure of 2μ). Oxidative degradation of the gel during extraction also could produce an appreciably lower cross-linking rate, but such a process should have been accounted for by inclusion of the scission to cross-linking ratio in the yield calculation. Another possible cause of our lower yields is a lower content of styrene monomer in our aged samples compared with the freshly polymerized samples used by others. Lyons²⁸ has observed that unsaturated compounds accelerate radiation-induced gel formation in polystyrene and other polymers.

LET Effects. The calorimetric measurements of the dose parameters of eq. 1 permit the division of the reactor dose into portions from neutron scattering and from γ -photon absorption. For polystyrene (C_8H_8)_n, 0.70 of the energy was imparted by fast neutrons and 0.30 by γ -radiation. By use of the cross-link yield measured in the γ -source, the yield from reactor neutrons alone can be calculated. Letting $G_n(\text{cl})$ be the neutron G value and $G_\gamma(\text{cl})$ the γ G value, $0.70G_n(\text{cl}) + 0.30G_\gamma(\text{cl}) = 0.077$, the over-all reactor yield. Substituting our measured $G_\gamma(\text{cl}) = 0.034$ gives $G_n(\text{cl}) = 0.096 \pm 0.015$ for neutrons alone. The scission yield for neutrons alone is 0.14 times the yield for cross-linked units: $G_n(\text{s}) = 0.14(2 \times 0.096) = 0.027 \pm 0.004$.

These neutron G values are 2.8 ± 0.4 times the yields for ^{60}Co γ -photons. The LET for the H^+ recoils scattered by neutrons averages about 3 e.v./ \AA , while the value for ^{60}Co γ -radiation is 0.02 e.v./ \AA .^{2,29} The LET dependence of cross linking is very similar to that of the coupling reactions of molten biphenyl and terphenyl. Molten biphenyl gave coupling yields of $G = 0.69$ in a reactor with a dose distribution similar to our facility. This yield is 2.7 times that from

(27) W. Burlant, J. Neerman, and V. Serment, *J. Polymer Sci.*, **58**, 491 (1962).

(28) B. J. Lyons, *Nature*, **185**, 604 (1960).

(29) C. J. Hochanadel in "Comparative Effects of Radiation," M. Burton, *et al.*, Ed., John Wiley and Sons, Inc., New York, N. Y., 1960, pp. 159, 174.

electron bombardment⁹ ($LET = 0.02 \text{ e.v./\AA}$). This ratio does not greatly exceed that which we observed, 2.4, between cross-link yields in the reactor and in the γ -source. The coupling reaction in molten terphenyl shows a somewhat greater dependence on LET,⁹ but it was observed that enhancement of yields did not occur until the LET exceeded 2 to 3 e.v./ \AA .³⁰ Such a threshold effect has been suggested in benzene² also and could be explained as the LET value at which spurs begin to overlap if the energy per spur (60 e.v.) and the radius (10 \AA .) calculated for water³¹ are applicable.

Possible Mechanisms for the LET Effect. Microscopic melting in the densely ionized particle track might be proposed to explain the increase of cross linking with LET. Such melting within the spurs has been suggested to account for the isotopic yields from mixtures of deuterated and normal biphenyl³² although calculations indicate that such effects should not be appreciable. In the case of polystyrene, the low temperature coefficient observed^{11,27} for cross linking, even above the glass transition temperature, rules out such an explanation.

The increased cross-link yield in polystyrene at high LET appears to result from competing reactions of different kinetic order as in the case of aromatic liquids. Second-order reactions of excited molecules competing with first-order collisional deactivation have been proposed^{8,9} as a reaction scheme for the

aromatic liquids, and such a scheme could account for the LET effect in polystyrene.

On the other hand, under the condition of overlapping spurs, all second-order processes would be accelerated, and any first-order back-reaction or competing process would suffice to produce the observed LET effect. Either the ionic processes advanced for solid alkanes³³ or the many proposed radical reactions can be conceived to involve such competing mechanisms. Consequently, any of several general reaction schemes could produce increased cross linking at high LET. Therefore, an analysis of radiolysis products in addition to cross links is required for a more specific delineation of the nature of radiation-induced processes in polystyrene.

Acknowledgments. We express our appreciation to Oscar Sisman for his continued interest and support of the work and to W. K. Kirkland for performance of the solubility and solvent-swelling measurements. We wish to thank also R. M. Keyser for discussions regarding treatment of the solubility data.

(30) J. Y. Yang, F. C. Goodspeed, and J. G. Burr, *Chem. Ind.* (London), 1018 (1962); J. Y. Yang, J. D. Strong, and J. G. Burr, Division of Physical Chemistry, Paper No. 97, 144th National Meeting of the American Chemical Society, Los Angeles, Calif., April 1, 1963.

(31) A. K. Ganguly and J. L. Magee, *J. Chem. Phys.*, **25**, 129 (1956).

(32) J. M. Scarborough and J. G. Burr, *ibid.*, **37**, 1890 (1962).

(33) L. Kevan and W. F. Libby, *ibid.*, **39**, 1288 (1963).

Shock Waves in Chemical Kinetics.

The Dissociation of Molecular Chlorine¹

by Mathias van Thiel, Daniel J. Seery, and Doyle Britton

Department of Chemistry, University of Minnesota, Minneapolis, Minnesota 55455 (Received July 27, 1964)

From spectrophotometric observations on shock waves in chlorine-argon mixtures the rate of dissociation of molecular chlorine in the presence of argon has been measured at temperatures between 1600 and 2600°K. In mixtures of 5% Cl₂ and 95% Ar the results may be summarized by $\log k_D$ (mole⁻¹ l. sec.⁻¹) = 10.66 - 9930/T. This corresponds to an apparent activation energy of 45 ± 2 kcal./mole. Emission of light due to radiative recombination of chlorine atoms complicated the study of the dissociation process and had to be corrected for. From the change in the rate of emission with temperature, activation energies for the emission as a function of the wave length could be determined.

Introduction

As part of a series of investigations of the rates of dissociation of molecular halogens²⁻⁵ we report here the rate of dissociation of Cl₂ in the presence of an excess of argon. Other workers⁶⁻⁸ have studied this system, but their results do not agree.

The rate constants are indicated by $X_2 + M \xrightleftharpoons[k_R]{k_D} X + X + M$ and $d(X_2)/dt = -k_D(M)(X_2) + k_R(M)(X)^2$. All concentrations will be given in moles/l. and all times in the rate expressions in sec.

It was observed in studies on the dissociation of bromine^{4,9,10} that light was emitted as soon as atoms were present. This was attributed to radiative recombination, $X + X \rightarrow X_2 + h\nu$, and at the higher temperatures it was sufficiently large that it had to be corrected for in measuring the dissociation rate. It was of considerable interest, however, as a separate process, and Palmer¹⁰ was able to deduce information about the upper states involved from the temperature and wave length dependence of the emission. The emission in the presence of Cl atoms is even greater than that in the presence Br atoms, and we have studied this emission in a similar fashion, both to be able to correct the absorption results and to determine which excited states are involved.

Experimental

Apparatus. The shock tube, photometric arrangement, and vacuum system have been described pre-

viously.^{4,5,11} The shock tube had a 10-cm. i.d., a 240-cm. drive section, and a 480-cm. downstream section. In some of the experiments the observation section was Pyrex pipe, and the light beam passed three times through the tube.⁴ In other experiments the observation section was aluminum tubing with sapphire windows, and the light beam passed once through the tube.⁵ The results were the same regardless of the arrangement. The rate measurements were made at 385 and 365 mμ, respectively, in the two arrangements; the emission measurements were made at 385, 410, 460, and 510 mμ; and a few extinction measurements were made at 350 mμ. At each wave length except 350 mμ approximately monochromatic light was obtained by using a Bausch and Lomb second-order interference filter in combination with a Corning sharp-cut filter to cut out the shorter wave length light.

(1) Presented at the 18th International Congress of Pure and Applied Chemistry, Montreal, Aug. 1961.

(2) (a) D. Britton, N. Davidson, and G. Schott, *Discussions Faraday Soc.*, **17**, 58 (1954); (b) D. Britton, N. Davidson, W. Gehman, and G. Schott, *J. Chem. Phys.*, **25**, 804 (1956).

(3) D. Britton and N. Davidson, *ibid.*, **25**, 810 (1956).

(4) D. Britton, *J. Phys. Chem.*, **64**, 742 (1960).

(5) C. D. Johnson and D. Britton, *ibid.*, **68**, 3032 (1964).

(6) H. Hiraoka and R. Hardwick, *J. Chem. Phys.*, **36**, 1715 (1962).

(7) T. A. Jacobs and R. R. Giedt, *ibid.*, **39**, 749 (1963).

(8) R. W. Diesen and W. J. Felmlee, *ibid.*, **39**, 2115 (1963).

(9) H. B. Palmer and D. F. Hornig, *ibid.*, **26**, 98 (1957).

(10) H. B. Palmer, *ibid.*, **26**, 648 (1957).

(11) C. D. Johnson and D. Britton, *ibid.*, **38**, 1455 (1963).

At 350 $m\mu$ the third order of a 500- $m\mu$ second-order filter was used in combination with an ultraviolet-transmitting, wide-band pass filter.

Chemicals. The Cl_2 used was from Matheson Co., Inc., who stated it to be 99.5% pure. However, when a sample was transferred to a 10-cm. infrared cell (by passing it through a trap at Dry Ice temperature into a collecting bulb at liquid nitrogen temperature, allowing the solid to melt, and then allowing some of the liquid to evaporate and expand into the cell), the sample showed as much as 10% CO_2 as judged by the pressure and intensity of the infrared band at 2350 cm^{-1} . This was essentially the procedure we used to transfer the Cl_2 to the mixture storage bulbs, so it was clear that purification was necessary. The following method of purification finally proved satisfactory. A small amount of vapor was expanded out of a bulb containing condensed liquid and was discarded; 1 or 2 min. was allowed to re-establish equilibrium between the vapor and liquid, and then another small amount of vapor was discarded; this process was repeated 20 to 30 times after which test samples were considerably purer, only about 1% CO_2 . Matheson argon was used without further purification. The CO_2 was prepared from commercial Dry Ice. A sample of Dry Ice was placed in the vacuum line, and about half was sublimed and thrown away. The next portion to sublime was used in the experiments. Mixtures were made up in the usual way.⁴

Calculations. The calculations used to obtain the various results have been outlined previously. The necessary thermodynamic data were taken from the NBS tables.¹² The Cl_2 was assumed to be vibrationally relaxed in all of the calculations. This is a reasonable assumption in view of the measured vibrational relaxation times for Cl_2 , pure and in the presence of He.¹³

Results

Extinction Coefficients. The intensity of the absorption spectrum of Cl_2 changes considerably with temperature as the higher vibrational states become populated. The values of the decadic extinction coefficients as a function of temperature and wave length have been measured in static experiments up to 1038°K.,¹⁴ and agree well with a theoretical expression developed by Sulzer and Wieland.¹⁵ The room temperature extinction coefficient at 385 $m\mu$ was determined from the drop in photocurrent on filling the tube. The high temperature extinction coefficients were determined from the initial decrease in photocurrent after the passage of the shock wave. At room temperature 96 measurements gave $\epsilon = 11.4$ with an

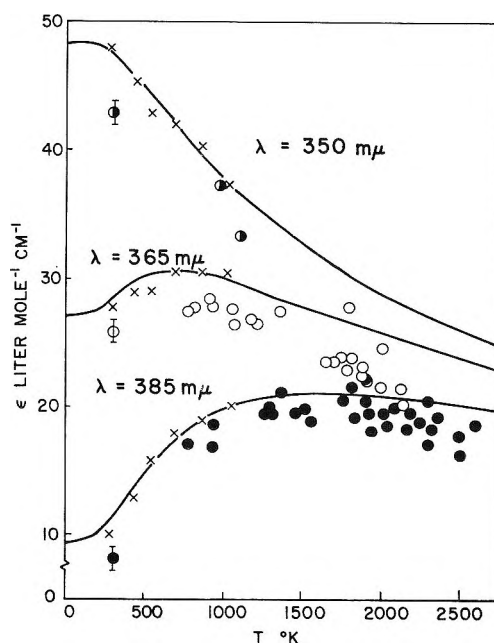


Figure 1. Extinction coefficients of Cl_2 . The crosses are the static experimental results of Gibson and Bayliss. The lines are the theoretical results of Sulzer and Wieland (based on the data of Gibson and Bayliss). The circles are the shock wave results. At 385 $m\mu$ only a representative set of points is shown.

average deviation of 0.9. This can be compared with the experimental values, 10.2, of Gibson and Bayliss,¹⁴ and 10.8, of Seery and Britton,¹⁶ and the calculated value, 11.2, of Sulzer and Wieland.¹⁵ At high temperatures our results, shown in Figure 1, are clearly lower than the calculated curve by about 10%. This may be due to a small background of longer wave length light which is not removed by the interference filter. At these temperatures the assumptions made in the theoretical calculation are no longer as valid, and it is possible that the calculated curve is unreliable here. Also shown in Figure 1 are the results of some preliminary experiments at 350 $m\mu$ which were made while deciding which wave length to use for the experiments and the results at 365 $m\mu$ using the sapphire windows in the aluminum tube.

Recombination Rate Constants. Dissociation rate constants were calculated from the initial slopes of the oscilloscope traces in the usual way.⁴ In those cases where emission was large, the pictures were enlarged,

(12) "Selected Values of Chemical Thermodynamic Properties," Series III, National Bureau of Standards, Washington, D. C., 1954.

(13) E. F. Smiley and E. H. Winkler, *J. Chem. Phys.*, **22**, 2018 (1954).

(14) G. E. Gibson and N. S. Bayliss, *Phys. Rev.*, **44**, 188 (1933).

(15) P. Sulzer and K. Wieland, *Helv. Phys. Acta*, **25**, 653 (1952).

(16) D. J. Seery and D. Britton, *J. Phys. Chem.*, **68**, 2263 (1964).

and the emission trace was subtracted graphically from the absorption trace before the slope was measured. Measurements were made in several 5% Cl₂-95% Ar and 10% Cl₂-90% Ar mixtures. In each case there were small discrepancies which might have been experimental error but which seemed to correlate with the small CO₂ impurity present (0.01-0.06 mole % CO₂ in the 5%, and 0.1-0.3 mole % CO₂ in the 10% Cl₂ mixtures). To check whether traces of CO₂ would cause misleading results, a series of measurements was made in a 1% CO₂-5% Cl₂-94% Ar mixture. The results for the 5 and 10% Cl₂ experiments are shown in Figures 2 and 3, respectively.

It is clear from Figure 2 that the small CO₂ impurities would have negligible effects on the observed rate constants. Therefore, we assume that the apparent dependence of the various mixtures on the amount of CO₂ impurity was accidental and that this represented experimental scatter. We also added a small amount of water vapor in a few experiments but observed no detectable changes. The parameters for smooth curves, fitted through the data points by the method of least squares, are given in Table I together with similar parameters for the earlier work. The curves are compared in Figure 4.

Table I: Dissociation Rate Constants for the Reaction
Cl₂ + Ar → Cl + Cl + Ar

Ref.	% Cl ₂	No. of points	A ^a	B ^a	H ^b
6	4	8	12.39 ± 1.27	11,210 ± 2550	51.3 ± 11.7
	20	7	11.75 ± 0.49	10,020 ± 910	45.8 ± 4.2
	25	6	12.14 ± 0.25	10,770 ± 440	49.3 ± 2.0
7	2	18	10.94 ± 0.08	10,570 ± 180	48.4 ± 0.8
	4	12	10.93 ± 0.13	10,640 ± 280	48.7 ± 1.3
8	0.5	23	10.85 ± 0.12	8,840 ± 270	40.4 ± 1.2
This work	5	38	10.66 ± 0.20	9,930 ± 400	45.4 ± 1.8
	10	28	9.90 ± 0.44	7,810 ± 960	35.8 ± 4.4

^a log k_D = A - B/T (mole⁻¹ l. sec.⁻¹). ^b k_D = P exp(-H/RT).

The large uncertainties in the 5 and 10% data make it impossible to calculate any good estimate of the separate rate constants for Ar and Cl₂ as the third bodies. Taking the values from the smoothed curves at 2000°K. leads to k_{Ar} = 0.40 × 10⁸ and k_{Cl₂} = 22.8 × 10⁸. A similar estimate at 2200°K. gives k_{Ar} = 0.63 × 10⁸ and k_{Cl₂} = 12.2 × 10⁸. The units of k are mole⁻¹ l. sec.⁻¹. That the value of k_{Ar} increases with temperature is surely wrong. In addition, the extra efficiency of Cl₂ over Ar is greater than the extra efficiency of Br₂ or I₂ at these temperatures; this also seems wrong. The most that can be said is that Cl₂

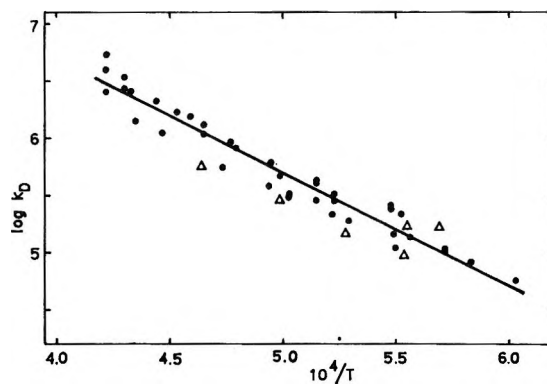


Figure 2. Dissociation rate constants in the 5% Cl₂ mixtures: circles, 5% Cl₂-95% Ar; triangles, 5% Cl₂-1% CO₂-94% Ar.

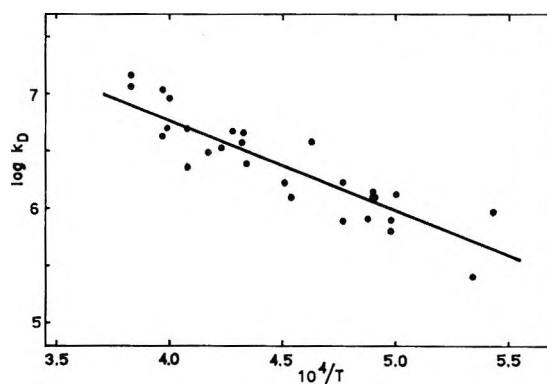


Figure 3. Dissociation rate constants in the 10% Cl₂-90% Ar mixtures.

is more efficient than Ar as a third body for the recombination of Cl atoms.

Emission. At the high temperatures in the shock waves, emission occurs in the same wave length region used for the absorption studies. Similar emission occurs in bromine at high temperatures^{4,10}; this has been shown to be due to two-body radiative recombinations of Br atoms. Presumably, the same process is occurring in chlorine, and the rate of emission is given by $d(h\nu)/dt = \text{intensity} = k_E(\text{Cl})^2$. This recombination process may involve atoms in the ground state, ²P_{1/2}, or in the first excited state, ²P_{1/2}, or both. The separation between these two states is much smaller (881 cm.⁻¹) for chlorine than it is for bromine (3685 cm.⁻¹). This means that at equilibrium a large fraction of the atoms is in the excited state; in the range of these experiments 20.4% are excited at 1900°K., and 23.5% are excited at 2600°K. Palmer¹⁰ found that for bromine the emission could be accounted for in terms of the previously known excited states, ³π_{0+u} which dissociates into one ground state and one excited atom, and ¹π_u and ³π_u which dissociate into two

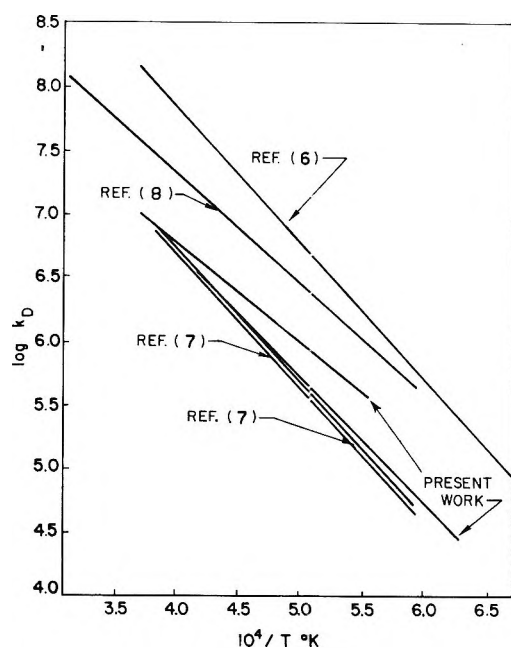


Figure 4. Comparison of the various shock wave measurements of the rate of dissociation of Cl_2 in Ar. The curve for ref. 6 is a composite of 4, 20, and 25% Cl_2 , which are virtually indistinguishable. The upper and lower curves for ref. 7 are for 2 and 4% Cl_2 , respectively. Reference 8 is for 0.5% Cl_2 . The data points from ref. 8 show a pronounced curve, but they have been summarized here by a straight line. Our lower and upper curves are for 5 and 10% Cl_2 , respectively.

ground-state atoms. Chlorine data are available for only the $^3\pi_{0+u}$ and $^1\pi_u$ states, and we shall discuss our results in terms of these.¹⁷ Figure 5 shows the ground state and the two known upper states. The $^1\Sigma_0^+$ ground state and the $^3\pi_{0+u}$ state were calculated from the data given by Herzberg¹⁸ using a Hulbert-Hirschfelder potential.¹⁹ The $^1\pi_u$ state is generally believed to be the upper state for the continuous absorption around 3300 Å. The slope of this potential was determined as suggested by Sulzer and Wieland.¹⁵ The three lowest vibrational wave functions of the ground state were used in this calculation. A potential of the form $V = V_\infty \exp[-a/(r - r_0)]$ was then fitted through this upper curve at the points of half maximum intensity in order to extrapolate to lower energies.

Emission from heated chlorine, consisting of both continuous and banded emission, has been previously observed.²⁰ The banded region was later shown to be due to recombination at the walls.²¹ The continuous emission consisted of visible and ultraviolet radiation and stopped in the red. It is not clear why the radiation should stop in the red if the $^1\pi_u$ state were responsible, but it seems reasonable if the $^3\pi_{0+u}$ state were involved since emission might only be significant from the

repulsive region. However, it would be expected that emission should involve the same states as absorption in the region where absorption occurs since the emission and absorption coefficients are proportional to one another. Other banded emission has been observed,²² but this was attributed to Cl_2^+ and can be ignored here.

In our experiments observations of the emitted light were made at two stations, one at 385 m μ for comparison, and the other variously at 385, 410, 460, and 510 m μ . The measured equilibrium intensities, which were only relative, were divided by the square of the $^2P_{3/2}$ Cl atom concentration to obtain a set of relative rate constants at each wave length. The activation energy for this emission process was calculated assuming¹⁰ $k_E \sim T^{-1/2} \exp(-E_{\text{ACT}}/kT)$.

The results described here were complicated, compared to the results with Br, by the fact that the emission did not reach a steady value but continued to rise slowly after the initial, relatively rapid dissociation reaction. This is shown for a typical emission in Figure 6 where equilibrium emission should have been reached at about 200 $\mu\text{sec.}$, but where the emission continues to rise slowly till the cold front arrives at the observation station. In order to try to correct for this slow increase in emission, which is probably due to some sort of nonideal shock wave behavior, the equilibrium emission was estimated once by taking the value at 200 $\mu\text{sec.}$ after the shock front and once by extrapolating the slow rise back to the shock front. In each case the emission was divided by the square of the calculated equilibrium concentration of $^2P_{3/2}$ atoms in order to obtain relative rate constants.

The data, which are summarized in Table II, were treated in two ways. First, each station in each wave length series was treated as independent, and activation energies were calculated from the observed intensities. Second, the intensity of the emission at the second station was compared to the 385-m μ emission at the first station, and the difference in activation energies was determined from the ratio. This difference was combined with the value of the activation energy

(17) For discussions of the possible electronic states of the halogen molecules see R. K. Asundi and P. Venkateswarlu, *Indian J. Phys.*, **21**, 101 (1947), or P. Venkateswarlu, *Proc. Indian Acad. Sci.*, **26A**, 22 (1947), or R. S. Mulliken, *Phys. Rev.*, **46**, 563 (1934).

(18) G. Herzberg, "Spectra of Diatomic Molecules," D. Van Nostrand Co., Inc., New York N. Y., 1950, p. 519.

(19) H. M. Hulbert and J. O. Hirschfelder, *J. Chem. Phys.*, **9**, 61 (1941). See also J. O. Hirschfelder, *ibid.*, **35**, 1901 (1961).

(20) U. Konratjew and A. Leipunsky, *Z. Physik*, **50**, 366 (1928).

(21) Y. Uchida, *Sci. Papers Inst. Phys. Chem. Res. (Tokyo)*, **30**, 71 (1936).

(22) W. H. B. Cameron and A. Eliot, *Proc. Roy. Soc. (London)*, **A158**, 681 (1937); **A164**, 53 (1938); **A169**, 463 (1939).

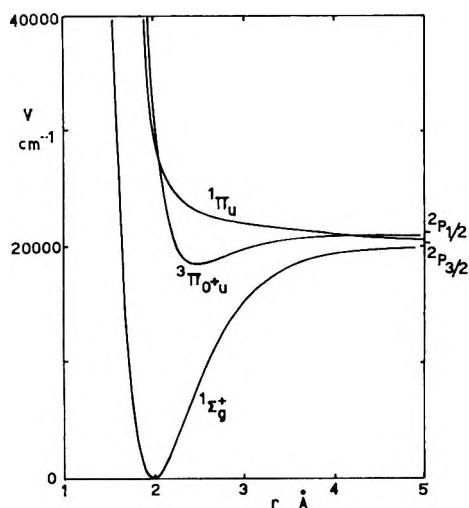


Figure 5. Potential diagram of known states of Cl_2 arising from $^2P_{3/2}$ and $^2P_{1/2}$ atoms.

Table II: Activation Energies (cm^{-1}) for Radiative Recombination^a

Series	Station 1		Station 2		
	385 μm	385 μm	410 μm	460 μm	510 μm
From extrapolated emission at 0 μsec .					
1	8900	9500			
2	8600		5800		
3	6300			4000	
4	9800				3000
From actual emission at 200 μsec .					
1	5500	6800			
2	6400		3700		
3	6900			3600	
4	8200				1700

^a All figures are uncertain by about 2000 cm^{-1} .

at 385 μm determined from all of the data. The first method is more straightforward; the second is probably more reliable since the comparison allows for partial cancellation of random errors in the individual shocks. The average of the two methods of calculation is given in Table II. The scatter in the data for any given wave length plus the difference in the energies calculated by the two methods, which should be equivalent, gives an uncertainty of about 2000 cm^{-1} in the values given.

Whatever the cause of the slow rise in light emission, it would be reasonable that it had a temperature dependence. The data show that this temperature dependence is not negligible. The extrapolated emission at zero time generally has an activation energy about 1500 cm^{-1} greater than at 200 μsec . In Figure

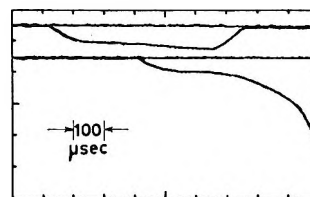


Figure 6. Typical emission record in 5% Cl_2 -95% Ar shock wave. Temperature at the shock front, 1990°K; at equilibrium, 1770°K. Calculated equilibrium, 43% dissociation. The two horizontal lines are base lines. Emission increases downward in the trace, and time increases from left to right. Upper trace, $\lambda = 460 \mu\text{m}$; lower trace $\lambda = 385 \mu\text{m}$. Only the first 600 μsec . is of interest (the decrease in emission in the upper trace at $\sim 700 \mu\text{sec}$. is due to the passage of the cold front; the increase in emission between 700 and 1000 μsec . in the lower trace is due to the reflected shock wave). In the upper trace notice the slow rise between 250 and 600 μsec ., which is probably due to some sort of nonideal shock behavior.

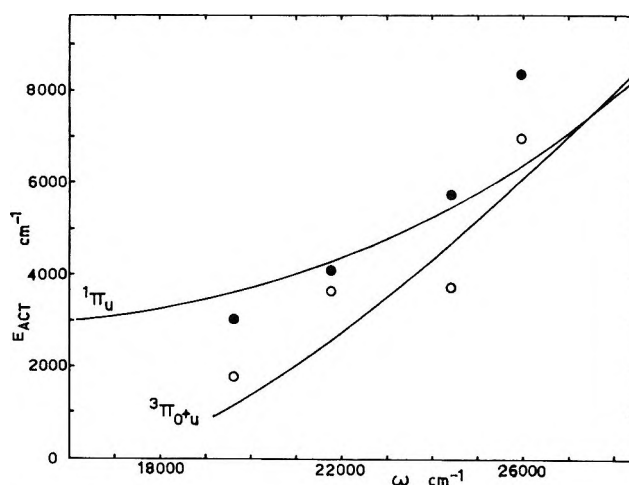


Figure 7. Observed *vs.* predicted activation energies of emission: lines, predicted values from Figure 5. Note that $^3\Pi_{0^+u}$ starts around 19,000 cm^{-1} ; this follows since only transition from the repulsive part of the potential can arise from two-body recombination. Solid circle, E_{ACT} calculated from extrapolated emission at 0 μsec ., open circle, E_{ACT} calculated from actual emission at 200 μsec .

7 the results are compared with the activation energies estimated from the potential curves. The predicted curves in Figure 7 were estimated from a large scale drawing of Figure 5, assuming that transitions occur from the highest point reached on the upper curve in a particular collision to the point directly below on the lower curve. For each activation energy the shape of the wave functions in the lower vibrational states should have been taken into account. This makes the curve uncertain by a few hundred cm^{-1} . In addition, the curves would be slightly shifted to shorter wave lengths since the maxima of the wave functions lie to

the left of the lower curve and to the right of the upper curve in Figure 5. The predicted curve for ${}^3\pi_{0+u}$ has been measured relative to ground-state atoms since the activation energies were calculated on this basis.

If all of the calculated activation energies are given equal weight, there is no basis of choice between the curves. If the 0- μ sec. values are used, they favor slightly ${}^1\pi_u$, which is the normal and reasonable state to be involved in the emission if it is responsible for the absorption. The 200- μ sec. value favors ${}^3\pi_{0+u}$ although, as stated before, the slow rise in emission may be due to some nonideal shock wave behavior, in which case the 200- μ sec. points have little meaning. However, it is a possibility that the transition $\text{Cl}({}^2P_{1/2}) \rightarrow \text{Cl}({}^2P_{3/2})$ is a slow reaction and that excited atoms are only produced slowly and are giving rise to another emission spectrum. The data reported here are insufficient to test this suggestion, but the lower activation energies at longer times are consistent with it.

Discussion

We have measured the dissociation rate constants in 5 and 10% Cl_2 in Ar. Ideally, we should be able to calculate the rate constants for pure Ar and pure Cl_2 as third bodies from the results. The 10% values are higher than the 5%, suggesting that Cl_2 is a more efficient third body for the dissociation and recombination of chlorine than argon is. However, the scatter of the experimental points is sufficiently great that we do not regard any calculated values for Cl_2 third bodies as meaningful. In the 10% experiments the initial slopes, from which the rate constants are measured, are very small since the density increase about balances the fractional decrease in the number of molecules. For this reason, we regard the 5% results as the best measurement of the rate constant for the reaction $\text{Ar} + \text{Cl}_2 \rightarrow \text{Ar} + 2\text{Cl}$. These results were compared in Figure 4 with the results from other laboratories. Our results, where emission was observed and corrected

for, and those of Jacobs and Giedt,⁷ where the geometry of the detection system made emission negligibly small relative to absorption, agree completely but are lower than the results of Hiraoka and Hardwick⁶ and Diesen and Felmlee.⁸ It is possible that in Hiraoka and Hardwick's arrangement emission was significant. If so, this might contribute to their higher values, but it is difficult to see how this could account for an order of magnitude difference and also to see how it would leave the activation energy unchanged. Diesen and Felmlee used a mass spectrometric method, which takes samples from a boundary layer, to measure concentrations. We prefer further information about the reliability of this method of sampling before giving it high weight.

For comparison of these results with theoretical calculations see Jacobs and Giedt.⁷ For comparison with the other halogens see Johnson and Britton.⁵

The emission that occurs in this system is consistent with the known excited states of Cl_2 , but the data are uncertain to the extent that they do not allow a choice to be made between the possibilities. To settle the question as to whether the ${}^2P_{1/2}$ state is readily excited in the atoms would require more experimental work; it might be decided by looking at the apparent equilibrium concentrations of Cl_2 after dissociation over a wide range of conditions since the effective equilibrium constant would change if the atomic products were not completely at equilibrium.

Acknowledgments. The authors wish to thank Mr. William Streib for running some preliminary experiments. We are grateful for support received from the Research Corp., the U. S. Army Research Office (Durham), the Graduate School of the University of Minnesota, and the Du Pont Corp. The Univac Scientific 1103 and Control Data 1604 computers of the Numerical Analysis Center of the University of Minnesota were used for many of the calculations.

Kinetics of the γ -Ray-Induced Decomposition of Chloroform¹

by Horst R. Werner and Richard F. Firestone²

Departments of Chemistry of Western Reserve University, Cleveland, Ohio, and The Ohio State University, Columbus, Ohio (Received July 31, 1964)

Some effects of temperature, dose rate, and scavenger additives in the radiolysis of air-free liquid CHCl_3 are interpreted by means of a free-radical mechanism. The primary free radicals are shown to be $\text{CHCl}_2\cdot$ ($G = 5.6$ radicals/100 e.v.), Cl atoms ($G = 5.4$ atoms/100 e.v.), CCl_2 ($G = 0.4$ radical/100 e.v.), $\text{CCl}_3\cdot$ ($G = 0.25$ radical/100 e.v.), and H atoms ($G = 0.2$ atom/100 e.v.). Additional CCl_3 radicals are formed by reactions of CHCl_2 radicals, Cl atoms, and H atoms with CHCl_3 , and the total yield of CCl_3 radicals exceeds $G(\text{CHCl}_2\cdot)$ above -30° . A relatively broad and diffuse spatial distribution of primary radicals is proposed for consistency with the onset of dose rate effects at low dose rates, a low spur radical yield, and the high probability that the fate of virtually all electrons is dissociative electron attachment in irradiated CHCl_3 . Effects of temperature in the radiolysis of solid CHCl_3 are also reported and discussed briefly.

Introduction

The first reported reasonably complete characterization of the organic products of the radiolysis of air-free CHCl_3 is that of Cooper and Stafford in 1958.³ Some effects of variations in dose rate were reported by Gardner and Harper in 1960,⁴ and Ottolenghi and Stein have observed a dependence of the yields of several products upon both dosage and dosage rate at room temperature.⁵ This article comprises a report and interpretation of the results of a systematic and detailed investigation of the effects of temperature, dosage, and several scavenger additives in the Co^{60} γ -ray-induced decomposition of liquid and solid CHCl_3 .

Experimental

Liter quantities of Baker reagent grade CHCl_3 were purified by stirring for 30 min. with successive volumes of the following reagents as indicated: two times with fresh 500-ml. volumes of fuming sulfuric acid, of distilled water, of NaHCO_3 solution, and two additional times with 500-ml. volumes of distilled water. Nitrogen was bubbled through the mixtures during stirring. The CHCl_3 was dried over Drierite for 24 hr., filtered, and fractionally distilled at atmospheric pressure in a five-plate column. A countercurrent of dry nitrogen was slowly passed through the still head to remove last traces of phosgene from the distillate. The middle third was collected over anhydrous BaO and immedi-

ately outgassed on a vacuum system and sealed off under vacuum in batches of 30 to 40 ml. The resulting material contained only CCl_4 as a detectable impurity (mole fraction <0.0001). Other materials, when commercially available, were the purest obtainable and were used without purification. Some compounds needed as quantitative gas chromatography standards were prepared and purified in the laboratory. These were unsymmetrical heptachloropropane,⁶ hexachloropropylene,⁷ octachloropropane,⁷ and symmetrical pentachloropropane.⁸ Compounds prepared as qualitative standards were $\text{CHCl}_3\text{CCl}_2\text{Br}$, $\text{CHClBrCCl}_2\text{Br}$, $\text{C}_2\text{Cl}_5\text{Br}$, $1,2\text{-C}_2\text{Cl}_4\text{Br}_2$, *sym*- C_3HCl_7 , and $1,1,2,3,3$ -pentachloropropylene.

All irradiated samples were carefully outgassed

(1) Based upon a dissertation submitted in partial fulfillment of requirements for the Ph.D. degree at Western Reserve University by H. R. W., 1963.

(2) To whom communications should be directed at The Ohio State University, Columbus, Ohio.

(3) W. Cooper and W. H. Stafford, *Proc. 2nd Intern. Conf. Peaceful Uses At. Energy*, 29, 118 (1958).

(4) J. B. Gardner and B. G. Harper, Paper No. 53, 8th Annual Meeting of the Radiation Research Society, San Francisco, Calif., May 9-11, 1960.

(5) M. Ottolenghi and G. Stein, *Radiation Res.*, 14, 281 (1961).

(6) M. W. Farlow, *Org. Syn.*, 17, 58 (1937).

(7) A. L. Henne and E. C. Ladd, *J. Am. Chem. Soc.*, 60, 2494 (1938).

(8) H. J. Prins and F. J. W. Engelhard, *Rec. trav. chim.*, 54, 309 (1935).

and distilled over anhydrous BaO on a vacuum line into either 8-ml. annular Pyrex vessels⁹ or 8-ml. test tube vessels immersed in liquid nitrogen and were then sealed off. All samples were of 5-ml. volume at 25°. Each irradiation vessel was provided with a side arm in which a few drops of CHCl₃ was sealed off as a blank control sample for later reference. Optical cells fabricated from 1-cm. square precision bore Pyrex tubing and break-seal tubes were also attached to some vessels to facilitate optical analysis and removal of gaseous products.

Irradiations were performed with a 100-curie Co⁶⁰ γ -ray source essentially similar to one described previously.⁹ A hot-air bath provided constant temperatures ($\pm 1^\circ$) for irradiations above room temperature. Irradiation temperatures in the range -30 to -125° were attained by immersing the sample vessel in a dewar vessel containing an appropriate liquid (acetone to -90° , petroleum ether at -90 to -125°) and a copper coil through which liquid nitrogen was forced with compressed air. Temperature control ($\pm 5^\circ$) was effected by means of a solenoid valve in the compressed air line which was controlled by a Wheelco Amplitrol 151 thermocouple-actuated bridge circuit.

Analyses for organic products were performed by isothermal gas-liquid partition chromatography, using thermal conductivity and hydrogen flame ionization detectors. Columns were packed in 0.6-cm. o.d. stainless steel tubing of 2-m. length. Diisodecylphthalate on Celite and DC 200 silicone oil on Celite were used for analyses at 40° for lower boiling products and at 140° for two-carbon and three-carbon products.

Inorganic gases, excepting HCl, were determined by mass spectrometry and by gas-solid partition chromatography with a 2-m. 0.6-cm. silica gel column at 48°. HCl was determined by opening the irradiation vessels beneath the surface of KI-KIO₃ solutions and titrating for I₂ with standard 0.1 N thiosulfate solution.

Free halogens were determined spectrophotometrically with a Beckman DU spectrophotometer. Molar absorptivities for Cl₂, BrCl, Br₂, and I₂ in CHCl₃ were determined between 320 and 580 m μ by the method of Popov and Manion.¹⁰

Ferrous sulfate dosimetry was used to determine dosage rates, assuming $G(\text{Fe}^{+3}) = 15.6$ in air-saturated 0.01 M FeSO₄, 0.8 N H₂SO₄ solutions, a molar absorptivity of 2166 for Fe⁺³ at 304 m μ and 25°. Corrections for electron density provide the expression, (e.v./ml.-min. in CHCl₃) = (e.v./ml.-min. in water at 25°) \times (0.857) \times (density of CHCl₃ at the irradiation temperature). Corrections for photoelectric and pair production absorption are considered negligible for

Co⁶⁰ γ -rays in CHCl₃ and water within experimental error.

Results

Although there are differences in numerical values assigned by various investigators to the 100-e.v. yields of the major products of the radiolysis of CHCl₃ at 25°, there is agreement that HCl, CH₂Cl₂, C₂C₆, C₂HCl₅, and *sym*-C₂H₂Cl₄ are among the five or six most abundant initial products at dosage rates from 10¹⁸ e.v./g.-hr. to 10²¹ e.v./g.-hr. (cf. Table I). The major products found in this investigation at 25° and at dosage rates from 10¹⁸ e.v./g.-hr. to 10¹⁹ e.v./g.-hr. are, in decreasing order of their 100-e.v. yields, HCl (5.3), C₂Cl₆ (2.4), CH₂Cl₂ (2.4), C₂HCl₅ (0.91), CCl₄ (0.80), and *sym*-C₂H₂Cl₄ (0.58). Yields of minor

Table I: 100-E.v. Yields of Major Products at 25°

Investigators	HCl	CH ₂ Cl ₂	C ₂ H ₂ Cl ₄	C ₂ HCl ₅	C ₂ Cl ₆	CCl ₄
Gardner and Harper ^a	...	2.9	0.6	1.0	2.5	0.23
Ottolenghi and Stein ^b	5.0-6.3	0.9-0.4	1.1	1.3	3.1-3.4	0.0
Cooper and Stafford ^c	4.3	1.3	0.6	0.9	2.5	0.1
This work	5.3	2.4	0.58	0.91	2.4	0.8

^a Cf. ref. 4, dosage rate = 2.0×10^{18} e.v./g.-hr. ^b Cf. ref. 5, dosage rate = 3.7×10^{18} e.v./g.-hr. ^c Cf. ref. 3, dosage rate unknown.

products clearly identified as radiolysis products at 25° are also presented in Table II. At these dosage rates chloroform is converted into stable products with an efficiency of 12 molecules/100 e.v. No systematic variations of rates of formation of the major products with respect to dosage were observed between 1.0×10^{20} e.v./g. and 2.6×10^{21} e.v./g. at 25° or at other temperatures and dosages indicated in Tables II and III. All products reported in Tables II and III, as well as HCl, appear to be initial products which are formed at constant rates at constant temperature and dosage rate.

Apparent 100-e.v. yields of HCl obtained by titration of nine samples irradiated at 25° ranged from 5.21 to 5.64 molecules/100 e.v. The average value of 5.5 ± 0.1 molecules/100 e.v. must be corrected for HCl formed by the hydrolysis of phosgene during titration. Phosgene was observed as a product in all irradiated samples and appears to have been formed at a constant rate. All chloroform samples and irradiation vessels

(9) R. F. Firestone and J. E. Willard, *Rev. Sci. Instr.*, **24**, 904 (1953).

(10) A. I. Popov and J. J. Manion, *J. Am. Chem. Soc.*, **74**, 222 (1952).

Table II: 100-E.v. Yields in Liquid CHCl_3

	Temp., °C.					
	-62	-30	0	20	25	63
Dosage rate (e.v./g.-hr. $\times 10^{-19}$)	1.74	1.73	1.72	1.65	<i>a</i>	2.01
Dosage (e.v./g. $\times 10^{-20}$)	4.13	4.16	4.14	0.99	<i>a</i>	4.79
COCl_2	0.11	0.09	0.17	...	0.15	0.11
CH_2Cl_2	0.23	0.66	1.5	2.2	2.4	3.4
CCl_4	0.59	0.68	0.76	0.79	0.80	0.9
C_2Cl_4	0.01	0.02	0.05	0.08	0.08	0.2
$\text{C}_2\text{H}_2\text{Cl}_4$	0.97	0.92	0.82	0.60	0.58	0.50
C_2HCl_5	1.6	1.8	1.8	1.3	0.91	0.60
C_2Cl_6	0.58	1.0	1.9	2.2	2.4	2.8
$\text{CHCl}_2\text{CCl}_2\text{CHCl}_2$	0.15	0.13	0.10	0.05	0.04	...
$\text{CHCl}_2\text{CCl}_2\text{CCl}_3$	0.17	0.20	0.20	0.08	0.1	...
C_3Cl_8	0.03	0.06	0.04
$-\text{CHCl}_3$	8.3	10	13	12	12	12
HCl^b	4.0	4.6	5.4	5.3	5.3	5.0
H_2^c	0.02	0.03	...
N_2	0.1	1.9	...
O_2	0.001	0.06	...
CO	0.3	0.39	...

^a Selected best values at 25° at dosages up to 2.6×10^{21} e.v./g. and dosage rates in the range 0.28×10^{19} e.v./g.-hr. to 2.2×10^{19} e.v./g.-hr. ^b Computed from material balance for all products observed. ^c Permanent gas yields were measured at dosages in the range 1 to 3×10^{20} e.v./g. delivered at 1.6×10^{19} e.v./g.-hr.

Table III: 100-E.v. Yields in Solid CHCl_3

	Temp., °C.				
	-196	-125	-90	-78	-67
Dosage rate (e.v./g.-hr. $\times 10^{-19}$)	1.63	1.63	1.73	2.04	1.73
Dosage (e.v./g. $\times 10^{-20}$)	1.30	1.01	4.15	17.5	3.60
COCl_2	0.014	0.013
CH_2Cl_2	0.80	0.90	1.05	0.86	0.79
CCl_4	0.61	0.80	0.87	0.81	0.88
C_2Cl_4	0.01	0.04	0.07	0.06	0.06
$\text{C}_2\text{H}_2\text{Cl}_4$	0.04	0.07	0.08	0.09	0.12
C_2HCl_5	0.38	1.2	1.6	1.6	2.4
C_2Cl_6	0.20	0.36	0.54	0.43	0.33
$\text{CHCl}_2\text{CCl}_2\text{CHCl}_2$	0.01	0.01	0.02	...	0.05
$\text{CHCl}_2\text{CCl}_2\text{CCl}_3$	0.04	0.07	0.08	...	0.08
$\text{CHCl}_2\text{CHClCCl}_3$	0.01	...	0.01
$\text{CCl}_3\text{CHClCCl}_3$	0.03	...	0.02
C_3Cl_8	0.01	0.02	0.04	...	0.04
$-\text{CHCl}_3$	2.8	5.3	7.1	...	8.1
HCl^a	0.71	1.9	2.2	...	3.4
H_2^b	0.004
N_2	0.013
O_2	0.007
CO	0.0025

^a Computed from material balance for all products observed. ^b Cf. footnote c, Table II.

were outgassed by the usual procedures. The surface-volume ratio in our annular irradiation vessels is, however, relatively great, and it is apparent that glass serves as a reservoir of chemisorbed oxygen and other gases which migrate into the vessel's contents during irradiation. Radiolytic decomposition of silica must also be considered an available source of oxygen. Corrections for contributions of phosgene provide an average $G(\text{HCl})$ of 5.2 to 5.3 molecules/100 e.v., in agreement with an average of 5.3 to 5.4 molecules/100 e.v. computed by means of a material balance among five samples irradiated at 25°.

The 100-e.v. yields of permanent gases formed during irradiation of chloroform in glass annular vessels are reported in Tables II and III. Hydrogen is a genuine radiolysis product, but mass spectrometric and gas chromatographic analyses indicate that the bulk of gases noncondensable at -196° consisted of N_2 and CO . The reported $G(\text{H}_2)$ at 25° has recently been verified by F. P. Abramson of Ohio State University as 0.030 ± 0.002 using a D_2 dilution technique for determining the H_2 content of product gases on an isotope ratio mass spectrometer.

Formation of Cl_2 was observed spectrophotometrically in several samples irradiated at 25° at 2.1×10^{19} e.v./g.-hr. It was formed at an estimated initial rate of the order 0.1 to 1 molecule/100 e.v., attained a maximum concentration of $2 \pm 0.2 \times 10^{-4} M$ at 4×10^{20} e.v./g., and decreased slowly but steadily at larger dosages up to 2×10^{21} e.v./g. If a steady-state Cl_2 concentration is ultimately attained under these conditions, it must be of the order of 0.0001 M or less. The initial $G(\text{Cl}_2)$ in the presence of 0.04 M Br_2 was approximately 0.4, and the Cl_2 concentration attained a maximum approximately 25-fold greater than that attained in initially pure chloroform. The maximum BrCl concentration attained was of the order of $10^{-3} M$. Addition of Cl_2 prior to irradiation at 25° greatly accelerated the decomposition of CHCl_3 and the formation of CCl_4 (cf. Table IV). The 100-e.v. yield of $\text{C}_2\text{-Cl}_6$ increased significantly, whereas those of *sym*- $\text{C}_2\text{H}_2\text{Cl}_4$ and C_2HCl_6 were essentially unaffected by the presence of chlorine. C_2Cl_4 was essentially removed as a product, and the yield of CH_2Cl_2 was also diminished.

Addition of Br_2 prior to irradiation leads to formation of a variety of alkyl bromides, as reported in Table IV, but appears to have little effect on $G(-\text{CHCl}_3)$. The yields of CH_2Cl_2 , C_2Cl_6 , and the propyl halides are reduced to nearly zero. The yields of C_2HCl_6 and *sym*- $\text{C}_2\text{H}_2\text{Cl}_4$ are reduced by approximately 80% and 40%, respectively, but these products and CCl_4 emerge as the most abundant nonbrominated

Table IV: 100-E.v. Yields in 0.045 M CHCl_3 - Br_2 and CHCl_3 - Cl_2 Solutions at 25°

Dosage (e.v./g. $\times 10^{-20}$)	0.71	1.42	2.84	4.23	5.28	Pure CHCl_3	0.400
Fraction of Br_2 consumed	$1/8$	$1/4$	$1/2$	$3/4$	$1/1$...	a
CH_2Cl_2	...	0.04	0.06	0.06	0.10	2.4	1.3
CCl_4	0.64	0.82	0.60	0.72	0.79	0.80	58
C_2Cl_4	...	0.07	0.09	0.04	0.06	0.08	0.005
$\text{C}_2\text{H}_2\text{Cl}_4$	0.36	0.36	0.34	0.28	0.33	0.58	0.55
C_2HCl_5	0.20	0.16	0.19	0.91	1.0
C_2Cl_6	0.02	0.02	0.02	2.4	3.7
CHCl_2Br	5.4	5.3	5.3	4.8	4.9
CCl_3Br	6.0	4.0	4.4	3.0	3.3
CHClBr_2	0.02
CCl_2Br_2	0.58	0.44	0.43	0.29	0.22
$\text{C}_2\text{HCl}_4\text{Br}$	0.05	0.07	0.07
$\text{C}_2\text{HCl}_3\text{Br}_2$	0.04	0.05
$\text{C}_2\text{Cl}_5\text{Br}$	0.04	0.05
$\text{C}_2\text{Cl}_4\text{Br}_2$	0.01
$\text{CHCl}_2\text{CCl}_2\text{CHCl}_2$	0.01	0.04	...
$\text{CHCl}_2\text{CCl}_2\text{CCl}_4$	0.01	0.15	...
$-\text{CHCl}_3$	13	12	12	11	11	12	70

^a 0.045 M CHCl_3 - Cl_2 solution: 1.84×10^{19} e.v./g.-hr.

organic products in the presence of Br_2 . The predominance of CHCl_2Br and CCl_3Br among the brominated products indicates that the predominant free-radical intermediates at room temperature are CCl_3 radicals and CHCl_2 radicals. Iodine was also employed as a free-radical scavenger in several experiments. Effects on the alkyl chloride yields were similar to those of Br_2 . Iodine showed distinct disadvantages as a scavenger in comparison with bromine, however, because of the limited thermal stabilities of CCl_3I and CHCl_2I and consequent difficulties in gas chromatographic analysis for these and higher molecular weight iodides.

Some effects of temperature and phase are presented graphically in Figures 1 and 2, which are constructed with data from Tables II and III. $G(-\text{CHCl}_3)$, computed by material balance, increases steadily from -196 to 0° and appears to remain nearly constant up to 63° . No temperature independent effects of phase upon $G(-\text{CHCl}_3)$ are apparent. $G(\text{HCl})$, also computed by material balance at temperatures other than 25° , parallels $G(-\text{CHCl}_3)$ as a function of temperature. Phase and temperature exhibit more dramatic effects on the 100-e.v. yields of the organic products, and it is clear that the relative abundances of these products can be altered significantly by changes in phase and/or temperature at constant dosage rate. At 63° , CH_2Cl_2 and C_2Cl_6 predominate, but $G(\text{CH}_2\text{Cl}_2)$ and $G(\text{C}_2\text{Cl}_6)$ decrease rapidly with decreasing temperature in the liquid phase, leaving C_2HCl_5 and *sym*- $\text{C}_2\text{H}_2\text{Cl}_4$ as the two most abundant products near the freezing point

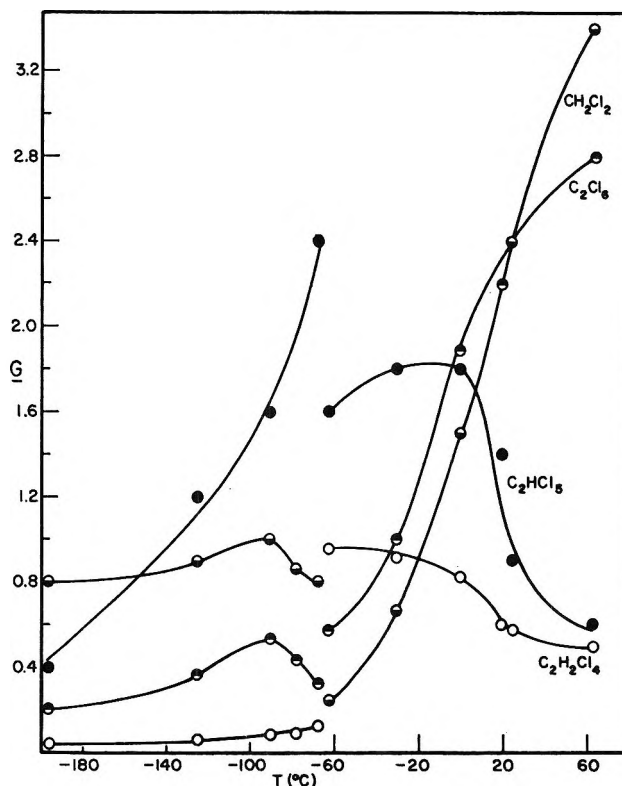


Figure 1. 100-E.v. yields of major organic products.

at -62° . In the liquid phase, the rates of formation of four major products (CH_2Cl_2 , C_2Cl_6 , C_2Cl_4 , and CCl_4) exhibit consistently positive temperature coefficients. The plot of $\ln G(\text{CH}_2\text{Cl}_2)$ vs. $1/T$ conforms nicely to

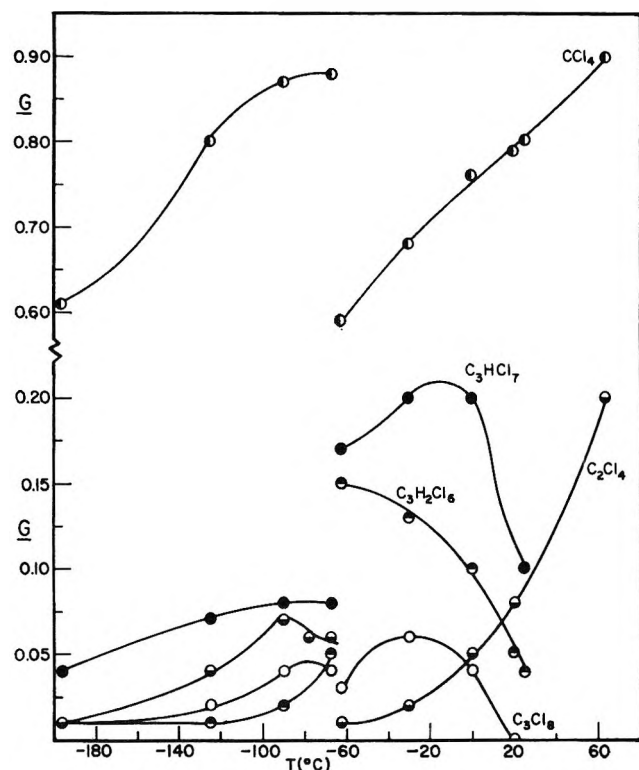


Figure 2. 100-E.v. yields of minor products and CCl_4 .

a straight line up to 25° with a slope corresponding to an apparent over-all activation energy of 4 kcal./mole, but falls off rapidly at 63° . Similar form is exhibited by $\ln G(\text{C}_2\text{Cl}_6)$ vs. $1/T$, and an apparent over-all activation energy of 2 kcal./mole is indicated. There is marked similarity in the forms of members of two pairs of G vs. T curves—those of C_2HCl_5 and C_3HCl_7 on the one hand, and those of *sym*- $\text{C}_2\text{H}_2\text{Cl}_4$ and $\text{C}_3\text{H}_2\text{Cl}_6$ on the other. It is also interesting to observe that C_3Cl_8 is a stable product of samples irradiated at 0° and lower temperatures, but is not observed in chloroform irradiated at room temperature.

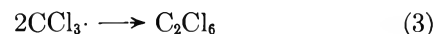
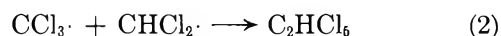
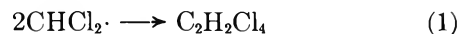
Comparison of the data of Gardner and Harper⁴ with those of Figures 1 and 2 permits the important observation that those products whose G values exhibit consistently positive temperature coefficients in the liquid phase are most sensitive to variations in the dosage rate. The converse is also apparently true; the G values of *sym*- $\text{C}_2\text{H}_2\text{Cl}_4$ and C_2HCl_6 decrease with increasing temperature at constant dosage rate and are affected only slightly by a millionfold variation in dosage rate at 25° .

Discussion

Pronounced sensitivity of the 100-e.v. yields of several major products to dosage rate indicates that there is a significant abundance of relatively stable interme-

diates, *i.e.*, sufficiently long-lived to diffuse from track to track, in irradiated chloroform at 25° . This indication is consistent with the observation that the yields of these products are also most sensitive to irradiation temperature and to the presence of bromine. The extent of the effects of dosage rate, temperature, and bromine scavenger suggests that thermal free radicals are the predominant immediate precursors of the major organic products. The identities of these products suggest that CHCl_2 radicals, CCl_3 radicals, and Cl atoms are the most abundant thermal free radicals. There is no compelling reason to invoke ionic or excited intermediates as immediate precursors of the stable products observed in the liquid phase.

Product yields in the presence of Br_2 provide a basis for estimating the relative numbers of CHCl_2 and CCl_3 radicals formed in the track spurs at 25° , *i.e.*, in regions competitively inaccessible to Br_2 molecules during the radical lifetimes. $G(\text{C}_2\text{H}_2\text{Cl}_4)$, $G(\text{C}_2\text{HCl}_6)$, and $G(\text{C}_2\text{Cl}_6)$ are tentatively assumed to represent the respective contributions of reactions 1, 2, and 3 in the presence of Br_2 .



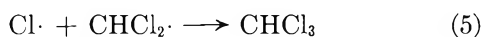
Relative spur concentrations are then proportional to $(\text{CHCl}_2 \cdot) = [G(\text{C}_2\text{H}_2\text{Cl}_4)/k_1]^{1/2}$ and $(\text{CCl}_3 \cdot) = G(\text{C}_2\text{HCl}_6)/k_2[G(\text{C}_2\text{H}_2\text{Cl}_4)/k_1]^{1/2}$, each representing an effective local relative radical density averaged over the mean lifetime of the track spurs at 0.045 M Br_2 concentration. Using $G(\text{C}_2\text{H}_2\text{Cl}_4) = 0.34$ and $G(\text{C}_2\text{HCl}_6) = 0.18$, and assuming $2k_1 = k_2 = 2k_3$, $(\text{CHCl}_2 \cdot)_{\text{spur}}/(\text{CCl}_3 \cdot)_{\text{spur}} = 3.8$. $G(\text{C}_2\text{Cl}_6)$ is, consistently, equal to $k_1 k_3 G(\text{C}_2\text{HCl}_6)^2 / k_2^2 G(\text{C}_2\text{H}_2\text{Cl}_4)$, or 0.024, which agrees acceptably with the measured value (0.02). A recent investigation of the direct photolysis of CHCl_3 vapor at 1849 Å. and 25° ¹¹ demonstrates that the primary photolytic process is C-Cl fracture and that Cl atoms react rapidly *via* reaction 4, thereby forming



CHCl_2 and CCl_3 radicals in equal numbers in that system. Ratios of the observed rates of formation of $\text{C}_2\text{H}_2\text{Cl}_4$, C_2HCl_6 , and C_2Cl_6 may, consequently, be equated to $k_1/k_2/k_3 = 1.00/2.08/0.744$. These values provide a slightly modified ratio, $(\text{CHCl}_2 \cdot)_{\text{spur}}/(\text{CCl}_3 \cdot)_{\text{spur}}$, of 3.9 and a corresponding calculated 100-e.v. yield for C_2Cl_6 of 0.016, again in acceptable agreement with the measured value.

(11) G. P. Semeluk and I. Unger, *Nature*, 198, 853 (1963).

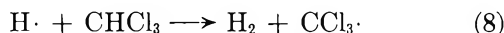
Examination of the effects of temperature indicates that Cl atoms also react readily with liquid CHCl_3 at 25° and that few, if any, undergo reactions with free radicals *via* reactions 5 and 6 at room temperature



If, to the contrary, reactions 5 and 6 were important to the over-all mechanism at 25° , $G(-\text{CHCl}_3)$ should decrease and $G(\text{CCl}_4)$ should increase with decreasing temperature. In fact, $G(-\text{CHCl}_3)$ appears to be essentially constant between 25 and 0° , and $G(\text{CCl}_4)$ decreases with decreasing temperature. An estimate of the absolute contribution of primary C-H bond fracture to $G(\text{CCl}_3\cdot)_{\text{spur}}$ is provided by $G(\text{H}_2)$ and Hardwick's carefully measured ratio¹² $k_7/k_8 = 7.3$ at 23° , for the reactions



and



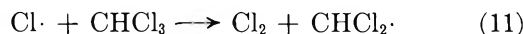
Using $G(\text{H}_2) = 0.03$ at room temperature (*cf.* Table II) and the assumption that all H_2 is formed by reaction 8, we estimate that 0.25 CCl_3 radical/100 e.v. is formed by spur reactions other than atomic or free-radical reactions. These radicals are precisely accounted for by the sum of $G(\text{C}_2\text{HCl}_6)$ and $2G(\text{C}_2\text{Cl}_6)$ in the presence of Br_2 (*cf.* Table IV), indicating that essentially none of these primary CCl_3 radicals are scavenged by Br_2 at 25° . The absolute primary yield of CHCl_2 radicals formed in the spurs is, then, 3.8 times $G(\text{CCl}_3\cdot)_{\text{spur}}$, or approximately 1.0 radical/100 e.v. The appropriate sum of product yields, $G(\text{C}_2\text{HCl}_6) + 2G(\text{C}_2\text{H}_2\text{Cl}_4)$, is 0.86 radical/100 e.v., indicating that essentially all of the CHCl_2 radicals formed in the spurs also appear as stable radical-radical products at 25° . These estimates tend to confirm the assumption that radical-radical reactions are responsible for essentially all of the chloroethanes formed in the presence of scavenger bromine. They also indicate that the spurs are a relatively insignificant source of either radicals or final products at 25° . $G(-\text{CHCl}_3)$ in the spurs (1.1 molecules/100 e.v.) is approximately the same as $G(-\text{CCl}_4)$ at 25° (1.6 molecules/100 e.v.) for pure air-free CCl_4 ,¹³ a substance which, unlike CHCl_3 , is inert to free-radical attack at 25° and in which, as in CHCl_3 , roughly $1/12$ of the detectable free radicals react inside the spurs. In CHCl_3 , and perhaps in CCl_4 as well, it appears that essentially all radicals which react outside of the spurs are also formed outside of the spurs, and that the effects of

temperature at 0° and above in CHCl_3 cannot be attributed to the influence of temperature on the rate of spur expansion or to cage effects.

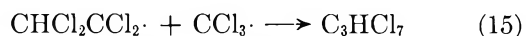
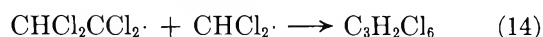
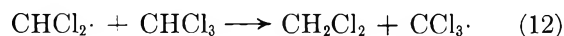
It is clear upon examination of the dependence of $G(\text{CCl}_3\text{Br})$ and $G(\text{CHCl}_2\text{Br})$ on dosage that neither product is radiolytically stable in CHCl_3 and that neither yield can be simply equated to the corresponding radical yield. At 25° , reaction 9 cannot be ruled out as a source of CCl_3 radicals.¹⁴



As a first approximation, reactions 10 and 11 may be ignored on energetic grounds ($\Delta H_{10} \simeq 21$ kcal./mole; $\Delta H_{11} \simeq 16$ kcal./mole)¹⁶ if only thermal halogen atoms are considered.



Linear extrapolation of $G(\text{CHCl}_2\text{Br})$ to zero dosage provides an estimate of 5.5 radicals/100 e.v. for a total of 6.4 radicals/100 e.v., including those formed in the spurs. The CHCl_2 radical appears to be a precursor of CH_2Cl_2 , $\text{C}_3\text{H}_2\text{Cl}_6$, and C_3HCl_7 in initially pure CHCl_3 through reactions 12, 13, 14, and 15.



All three of these products are absent in the presence of Br_2 , indicating that they are probably formed by reactions of thermal radicals. The positive temperature coefficient of $G(\text{CH}_2\text{Cl}_2)$ suggests a radical-solvent step with an apparent activation energy of about 4 kcal./mole, and the very similar variations of $G(\text{C}_2\text{H}_2\text{Cl}_4)$ and $G(\text{C}_3\text{H}_2\text{Cl}_6)$ on the one hand and of $G(\text{C}_2\text{HCl}_6)$ and $G(\text{C}_3\text{HCl}_7)$ on the other with respect to temperature indicate that the members of each pair have one or more precursors in common. Assuming that all products are accounted for and that back-reaction of the CHCl_2 radical can be neglected, $G(\text{CHCl}_2\cdot)$ in initially pure CHCl_3 equals $2G(\text{C}_2\text{H}_2\text{Cl}_4) + G(\text{C}_2\text{HCl}_6) + G(\text{CH}_2\text{Cl}_2) + 2G(\text{C}_3\text{H}_2\text{Cl}_6) + G(\text{C}_3\text{HCl}_7) =$

(12) T. J. Hardwick, *J. Phys. Chem.*, **66**, 2246 (1962).

(13) F. P. Abramson, B. M. Buckhold, and R. F. Firestone, *J. Am. Chem. Soc.*, **84**, 2285 (1962).

(14) J. H. Sullivan and N. Davidson, *J. Chem. Phys.*, **19**, 143 (1951).

(15) T. L. Cottrell, "The Strengths of Chemical Bonds," Butterworth and Co., Ltd., London, 1954.

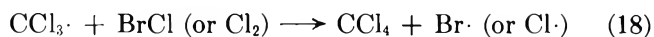
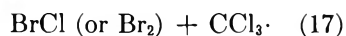
5.0 ± 0.2 radicals/100 e.v. at 0, 20, 25, and 63° , and is, therefore, essentially independent of temperature above 0° . The additional 1.2 radicals/100 e.v. apparently detectable in the presence of Br_2 may be interpreted either as evidence for one or more back-reactions in initially pure CHCl_3 or as an artifact of the use of Br_2 as a scavenger. The latter appears more likely, and additional work is being done to determine the effects of concentration, dosage rate, dosage, and temperature in irradiated CHCl_3 - Br_2 solutions.

The effects of added Cl_2 indicate that CHCl_2 radicals do not react appreciably with either Cl atoms or Cl_2 relative to the frequency of reaction 12 in initially pure CHCl_3 at 25° . We observe a decrease of 1.6 CHCl_2 radicals/100 e.v. in the net CHCl_2 radical yield in the presence of added Cl_2 (average concentration of the order $10^{-2} M$). Approximately 70% of the decrease corresponds to the observed lowering of the CH_2Cl_2 yield. It appears, then, that in initially pure CHCl_3 roughly 50% of the CHCl_2 radicals react with the solvent, and that about 25% do so even in the presence of $10^{-2} M$ Cl_2 . Thus, at 25° none live sufficiently long to react with either Cl atoms or Cl_2 molecules in the absence of added Cl_2 . Suppression of Cl_2 [$G(\text{Cl}_2)$ initial $\simeq 0.1$ to 1] must be attributed primarily to the other abundant species, the CCl_3 radical, *via* reactions 6 and 16 below 0° and *via* reaction 16 alone above 0°



At the lower temperatures, reactions 4 and 12 should decrease markedly in efficiency. This in turn decreases the abundance of CCl_3 radicals, and both effects favor back-reaction 5 and promote reaction 6 as a major contributor of CCl_4 below 0° .

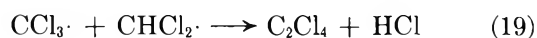
The observed insensitivity of $G(\text{CCl}_4)$ to the presence of Br_2 need not preclude serious consideration of reactions 6 and 16 as possibly the only sources of CCl_4 in view of the radiolytic instability of CCl_3Br in CHCl_3 . The rapid decrease in $G(\text{CCl}_3\text{Br})$ with respect to dosage is accompanied at low dosages by slower decreases in $G(\text{CHCl}_2\text{Br})$ and $G(\text{CCl}_2\text{Br}_2)$, and it is clear that free halogen atoms abstract bromine easily from these molecules at 25° . It is very likely that CCl_3Br is preferentially converted to CCl_4 *via* reactions 17 and 18



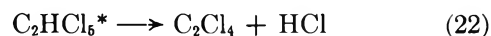
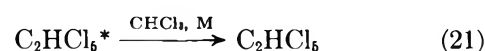
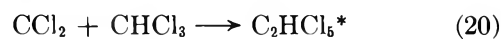
in view of the observed high efficiency of exchange of Br^{82} atoms in γ -irradiated CCl_3Br - BrBr^{82} solutions at 25° ¹⁶ and the virtual absence of Cl_2 and BrCl among

the free-halogen products of irradiated CCl_3Br .¹⁷ Similarly, a portion of the CCl_2Br_2 yield may be attributed to H atom abstraction from CHCl_2Br by halogen atoms followed by Br atom addition in bromine rich solutions. Attempts to measure brominated product yields at essentially zero dosage are in progress, and it is hoped that effects of these secondary reactions may be eliminated.

The observation that $G(\text{C}_2\text{Cl}_4)$ is essentially unaffected by the presence of Br_2 appears to indicate that it is not formed by radical-radical reaction 19, as previously suggested.³



Similarly, the suggestion³ that C_2Cl_4 and other olefinic products may be important precursors of C_3 and C_4 products cannot be supported by our findings. $G(\text{C}_2\text{Cl}_4)$ exhibits a steadily increasing positive temperature coefficient (Figure 1) at -30° and above, whereas the 100-e.v. yields of the C_3 products decrease in this range. The latter decrease is entirely consistent with the expectation that an increasingly larger fraction of CHCl_2 radicals attack the solvent as temperature increases (reaction 12) thereby forming CH_2Cl_2 at the expense of the C_3 products. C_2Cl_4 appears not to be a product of radical-radical reactions, but rather to be formed by attack of an intermediate on CHCl_3 . The effects of Br_2 indicate that its reactivity toward CHCl_3 is somewhat greater than that of $\text{CHCl}_2\cdot$ and roughly equal to that of the Cl atom at room temperature. It is suggested that this intermediate may be dichloromethylene (CCl_2) formed in a sequence of events similar to that which establishes the decomposition of CHCl_3 into CCl_2 and HCl as the predominant primary sequence in the pyrolysis of CHCl_3 vapor.¹⁸ The proposed sequence¹⁸



must proceed almost entirely *via* (22) in the vapor pyrolysis, since C_2HCl_5 is a minor product relative to C_2Cl_4 . It is entirely a matter for conjecture whether CCl_2 is formed as the diradical or the carbene in the radiolysis of liquid CHCl_3 , and whether it is more likely to abstract from or insert into CHCl_3 . These reactions have not to our knowledge been investigated

(16) A. H. Young and J. E. Willard, *J. Phys. Chem.*, **66**, 271 (1962).

(17) R. F. Firestone and J. E. Willard, *J. Am. Chem. Soc.*, **83**, 3551 (1961).

(18) A. I. Shilov and R. P. Sabirova, *Russ. J. Phys. Chem.*, **34**, 408 (1960).

experimentally. The sequence proposed by Shilov and Sabirova appears, however, to be necessary for understanding the vapor pyrolysis in which abstraction steps are patently ruled out. Simons and Yarwood¹⁹ have demonstrated that "hot" CHCl_2 radicals are precursors of CCl in the photolysis of CHCl_3 vapor, but their mean lifetime is much too long (*ca.* 10^{-10} sec.) to suggest that CCl may serve as a precursor of either CCl_2 or C_2Cl_4 in liquid CHCl_3 . An alternative to reaction 20 which may be presumed to predominate at lower temperatures is addition to the CHCl_2 radical (reaction 13) leading to C_3 product formation. Thus, at 63° the virtual absence of C_3 products may be attributed to the high reactivity of both CHCl_2 radicals and dichloromethylene toward CHCl_3 . The fraction of the C_2HCl_5 yield assignable to reaction 20 followed by stabilization of the excited product is unknown, but a sum over CCl_2 units at lower temperatures in the liquid phase suggests that $G(\text{CCl}_2)$ is approximately 0.4/100 e.v. and that roughly 50% of them lead to C_2Cl_4 at 63° . The plot of $\ln G(\text{C}_2\text{Cl}_4)$ vs. $1/T$ is linear with a slope corresponding to an apparent activation energy of approximately 5 kcal./mole between -30 and 63° .

A quantitative test for consistency of the proposed set of reactions with the experimental data can be made with the following relationships based in part on several apparently reasonable assumptions. (i) All CCl_3 radicals, excepting those few which have been classified as spur-produced radicals, are formed by reactions of primary radicals with the solvent, *i.e.*, by reactions 4, 8, and 12. (ii) Only one back-reaction, reaction 5, occurs. (iii) All Cl atoms either back-react or appear as HCl or CCl_4 , *i.e.*, $G(\text{Cl}_2)$ is negligibly small at all temperatures. It follows that (I): $G(\text{Cl}\cdot)_{\text{net, calcd}} = G(\text{HCl}) - G(\text{H}\cdot) + G(\text{H}_2) - G(\text{CCl}_2) - G(\text{C}_2\text{Cl}_4) + G(\text{CCl}_4)$; (IIA) $G(\text{CHCl}_2\cdot)_{\text{net, calcd}} = G(\text{Cl}\cdot)_{\text{net}} + G(\text{H}\cdot) - G(\text{H}_2)$; (IIB): $G(\text{CHCl}_2\cdot)_{\text{net, obsd}} = 2G(\text{C}_2\text{H}_2\text{Cl}_4) + G(\text{C}_2\text{HCl}_6) - Z + G(\text{CH}_2\text{Cl}_2) + 2G(\text{C}_3\text{H}_2\text{Cl}_6) + G(\text{C}_3\text{HCl}_7)$; (IIIA): $G(\text{CCl}_3\cdot)_{\text{calcd}} = 2G(\text{H}_2) + G(\text{CH}_2\text{Cl}_2) + G(\text{HCl}) - G(\text{CCl}_2) - G(\text{C}_2\text{Cl}_4)$; (IIIB): $G(\text{CCl}_3\cdot)_{\text{obsd}} = 2G(\text{C}_2\text{Cl}_6) + G(\text{CCl}_4) + G(\text{C}_2\text{HCl}_6) - Z + G(\text{C}_3\text{HCl}_7) + 2G(\text{C}_3\text{Cl}_8)$; (IV): $G(\text{CCl}_2) = G(\text{C}_2\text{Cl}_4) + G(\text{C}_3\text{H}_2\text{Cl}_6) + G(\text{C}_3\text{HCl}_7) + G(\text{C}_3\text{Cl}_8) + Z$, where Z is the 100-e.v. yield of C_2HCl_5 attributable to CCl_2 ; (V): $G(-\text{CHCl}_3)_{\text{calcd}} = G(\text{CCl}_3\cdot) + G(\text{CHCl}_2\cdot)_{\text{net}} + 2G(\text{CCl}_2) - G(\text{chloropropanes})$. Since Z will have a positive temperature coefficient, and since we find that $G(\text{C}_2\text{Cl}_4)$ is nearly negligible relative to the second, third, and fourth terms on the right of (IV) at -62 , -30 , and 0° , we conclude that constancy of the sum of these three terms indicates that

$Z = 0.0$ at these temperatures. Thus, $G(\text{CCl}_2) = 0.4$, and Z is roughly equal to 0.2 at room temperature and 63° . $G(\text{H}\cdot)$ is equal to $G(\text{CCl}_3\cdot)_{\text{spur}} + G(\text{H}_2)$, and $G(\text{HCl})$ is assumed constant at 5.3 at 20, 25, and 63° and to the tabulated values (Table II) at -62 and -30° . Calculated and observed values of $G(\text{CHCl}_2\cdot)_{\text{net}}$, $G(\text{CCl}_3\cdot)$, and $G(-\text{CHCl}_3)$ are presented in Table V. Agreement between members of each of the several pairs of calculated and observed values is excellent at -62 , -30 , and 0° . There appears, however, to be a shortage of both CHCl_2 radicals and CCl_3 radicals at room temperature and 63° . Recent measurements by F. P. Abramson in this laboratory (Ohio State University) have yielded consistently higher values for $G(\text{C}_2\text{Cl}_6)$ and $G(\text{C}_2\text{HCl}_5)$ at room temperature and 63° and values for the 100-e.v. yields of other major products which are very similar to those reported in Table II. It is, as one might anticipate, more difficult to reproduce G -values at the higher temperatures, and the discrepancies are not too large to be attributed to normal experimental errors.

Table V

	-62°	-30°	0°	20–25°	63°
$G(\text{Cl}\cdot)_{\text{net, calcd}}$	4.0	4.6	5.4	5.4	5.4
$G(\text{CHCl}_2\cdot)_{\text{net, calcd}}$	4.2	4.8	5.6	5.6	5.6
$G(\text{CHCl}_2\cdot)_{\text{net, obsd}}$	4.2	4.8	5.3	4.8	4.8
$G(\text{CCl}_3\cdot)_{\text{calcd}}$	3.9	4.9	6.4	7.0	8.1
$G(\text{CCl}_3\cdot)_{\text{obsd}}$	3.6	4.8	6.6	6.6	7.1
$G(-\text{CHCl}_3)_{\text{calcd}}$	8.5	10	13	13	14
$G(-\text{CHCl}_3)_{\text{obsd}}$	8.3	10	13	12	12

The effects of temperature in the radiolysis of solid CHCl_3 indicate that Cl atoms abstract H atoms from CHCl_3 at an appreciable rate in the range -67° to approximately -90° . The Arrhenius plots of both $G(\text{HCl})$ and $G(\text{Cl}\cdot)_{\text{net}}$ are linear above -90° and continue without a break through the melting point and into the liquidus range to 0° , but the values at -125 and -196° lie well above the line. The apparent activation energy (0.8 kcal./mole) agrees with that recently calculated for reaction 4,²⁰ but is about 3 kcal./mole lower than the experimental value for the gas phase reaction.²¹ There seems to be little doubt, however, that reaction 4 is a major source of HCl and CCl_3 radicals in both solid and liquid phases.

(19) J. P. Simons and A. J. Yarwood, *Trans. Faraday Soc.*, **59**, 90 (1963); **57**, 2167 (1961).

(20) H. S. Johnston and P. Goldfinger, *J. Chem. Phys.*, **37**, 700 (1962).

(21) J. H. Knox, *Trans. Faraday Soc.*, **58**, 275 (1962).

The fraction of CCl_3 radicals appearing as C_2HCl_5 increases steadily with increasing temperature in the solid, attains a maximum of about $1/2$ near the melting point, and falls off rapidly at higher temperatures in liquid CHCl_3 . This effect is consistent with the observed positive temperature coefficient for reaction 4 and only slight reactivity of CHCl_2 radicals toward CHCl_3 below -62° and suggests that reaction 4 occurs on the average in close proximity to a CHCl_2 radical in the solid phase. The very low yields of $\text{C}_2\text{H}_2\text{Cl}_4$ in the solid phase also suggest that the spatial distribution of radicals favors reactions 2 and 5 relative to reaction 1 in the solid, and that, as in the liquid, the distribution of CHCl_2 radicals is quite broad and diffuse. The relatively high 100-e.v. yields of CH_2Cl_2 and CCl_4 in the solid probably cannot be accounted for by a free-radical mechanism. Their average values in the solid are 0.9 ± 0.1 and 0.8 ± 0.1 , respectively, and the sum of their 100-e.v. yields is essentially constant at 1.7 ± 0.1 , suggesting that they may be formed simultaneously in a disproportionation step involving an excited CHCl_3 molecule. Several possible ion-molecule steps, including hydride ion transfer to the collisionally stabilized parent molecule ion or the CHCl_2^+ ion followed by reaction 6 or, possibly, electron transfer from a negative to a positive molecule ion would also be formally acceptable, but our data shed no light on such possibilities.

Recent measurements of the electron attachment coefficient of dilute CHCl_3 vapor as a function of average electron energy demonstrate that the mean distance travelled by a 0.1 to 1-e.v. electron before dissociative capture is of the order 1 to 10 cm. at 1 p.p.m. of CHCl_3 in N_2 at 1 atm.²² Direct extrapolation to pure liquid CHCl_3 is clearly not possible, but it appears likely that dissociative capture must be the fate of substantially all electrons as their energies fall below the ionization potential (11.4 e.v.) and that there is probably a relatively broad and diffuse distribution of CHCl_2 radicals and Cl^- ions about each of the higher energy electron tracks. It follows that the neutralization of positive ions must then proceed *via* resonance charge transfer to the Cl^- sites and/or slow diffusion of Cl^- ions and positive ions. The anticipated result of the capture and neutralization processes is a very high proportion of scavengable CHCl_2 radicals and a very low yield of so-called spur products in the presence of scavenger. The observed spur-radical yields may correspond to numbers of closely spaced radical pairs formed along the track axes by very rapid events, such as dissociation following excitation without ionization or positive ion-molecule reactions.

The effects of dose rate variations on the major

product yields at room temperature are generally consistent with the proposed mechanism, if one assumes that the predominant effect of the greater number of tracks per unit volume associated with higher dose rates is to increase the probability of radical-radical reactions at the expense of radical-solvent reactions. Consistently, it is anticipated that the point of onset and the extent of the dose rate effect upon a given radical-solvent product will depend upon the average lifetime of its free-radical precursor at low dose rates. Thus, among those products characterized above as radical-solvent products, $G(\text{CH}_2\text{Cl}_2)$ should exhibit sensitivity to dose rate variations at lower dose rates than $G(\text{CCl}_3\cdot)$ and $G(\text{C}_2\text{Cl}_4)$, and the proportional decrease in $G(\text{CH}_2\text{Cl}_2)$ should be markedly greater because of the lesser reactivity of the CHCl_2 radical relative to that of the Cl atom and CCl_2 at 25° . Gardner and Harper's data are in accord with this expectation. In the range 0.06 to 0.25 megarad/hr., CH_2Cl_2 alone exhibits an experimentally significant dose rate dependence, and between 0.25 and 18,000 megarads/hr., $G(\text{CH}_2\text{Cl}_2)$ decreases by a factor of 100 while $G(\text{CCl}_3\cdot)$ and $G(\text{C}_2\text{Cl}_4)$ each decrease only 3-fold. Preliminary results of a study of the effects of dose rate at 62° by Abramson demonstrate further that at moderate dose rates the dose-rate dependence of radical-solvent reactions tends to vanish under conditions which enhance the reactivity of the radicals, and that increasing temperature diminishes the dose-rate dependence of $G(\text{CH}_2\text{Cl}_2)$ to a greater extent than that of $G(\text{C}_2\text{Cl}_6)$. Gardner and Harper's data fail to exhibit the anticipated increase in the yields of radical-radical products, suggesting; perhaps, that track overlap favors the back-reaction to a markedly greater extent than reactions 1, 2, and 3. Abramson's recent data, however, exhibit a strong positive dose rate dependence for $G(\text{C}_2\text{HCl}_5)$ at 23 and 62° and a small positive dependence for $G(\text{C}_2\text{H}_2\text{Cl}_4)$ at 23° .

In summary, it can be concluded for the present that the effects of temperature, dose rate, and scavenger additives are consistent with a mechanism based upon reactions of two primary free radicals ($\text{CHCl}_2\cdot$ and $\text{Cl}\cdot$) and a third ($\text{CCl}_3\cdot$) which is, except for a small spur yield, produced entirely by thermally activated reactions of the former two with CHCl_3 . Further, chemical evidence indicates that the spatial distribution of the primary radicals is unusually broad and diffuse and suggests that dissociative electron capture can be a process of major importance as a source of free radicals in irradiated halocarbons. Investigations

(22) T. G. Lee, *J. Phys. Chem.*, **67**, 360 (1963).

directed toward a more complete understanding of the combined effects of phase, dose rate, temperature, and scavenger additives are in progress.

Acknowledgments. The authors are grateful for

support of this work by the U. S. Atomic Energy Commission (Contracts At(11-1)-685 and At(11-1)-1116) and for fellowship support provided for H. R. W. by the Diamond Alkali Co.

The Chemiluminescent Reaction of Oxygen Atoms with Sulfur Monoxide at Low Pressures

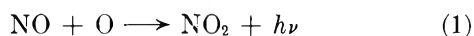
by Thomas R. Rolfes, Robert R. Reeves, Jr., and Paul Harteck

Rensselaer Polytechnic Institute, Troy, New York (Received August 8, 1964)

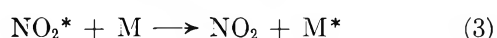
The reaction of oxygen atoms with sulfur monoxide results in a visible blue emission, extending into the ultraviolet. The reaction was studied in the low pressure region up to a total pressure of 20 μ where the emission was found to be due to the simple two-body reaction, $\text{SO} + \text{O} \rightarrow \text{SO}_2 + h\nu$, analogous to the two-body reaction of nitric oxide and oxygen atoms. The rate coefficient for this reaction was estimated as 7×10^{-16} cm.³/molecule sec. The SO was produced by reaction with O atoms *via* $\text{COS} + \text{O} \rightarrow \text{CO} + \text{SO}$. This reaction could also be used under certain conditions to titrate the oxygen atoms to obtain a quantitative measure of the oxygen atom concentration.

Introduction

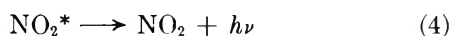
In a previous publication¹ a study was made of the light emission from the reaction of nitric oxide with oxygen atoms at low pressure. The light emission was shown to be due to a direct two-body combination



An alternate mechanism for light emission was possible involving a preliminary three-body reaction followed by alternate paths of deactivation or emission



or



At high pressures, substantially above 1 mm., this complex mechanism (reactions 2-4) or a similar mech-

anism may become important: Originally some investigators believed that reaction 1 was not likely and favored the three-body mechanism. The observation of diffuse bands in the observed emission at higher pressures, as well as some dependence on a third body for the intensity of emission, supported this view.²

However, the experimental results at low pressures are in agreement with those obtained recently by Johnathan and Doherty,³ and there can be no doubt that reaction 1 does occur and predominates at least at total pressures substantially below 1 mm.

Light emission also occurs from the reaction of sulfur monoxide with O atoms

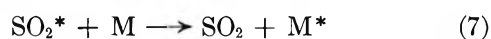
(1) R. R. Reeves, P. Harteck, and W. H. Chace, *J. Chem. Phys.*, **41**, 764 (1964).

(2) H. P. Broida, H. I. Schiff, and T. M. Sugden, *Trans. Faraday Soc.*, **57**, 259 (1961).

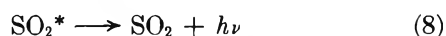
(3) G. Doherty and N. Johnathan, *Discussions Faraday Soc.*, to be published.



This reaction is 127 kcal. exothermic, equivalent to a wave length limit of approximately 2300 Å., which corresponds to the observed wave length limit of the emission. The emission visually appears as a strong blue compared to the greenish white NO-O atom emissions. Again an alternate mechanism may be postulated



or



As discussed in the previous work, the light emission at very low total pressures, *i.e.*, in the micron region, must be dependent on the third body (M) owing to the primary reaction (6). If no dependence on pressure (or M) is observed under these conditions, then a simple combination *via* reaction 5 must occur and dominate in this region.

The purpose of the present work was to study the reaction of sulfur monoxide and oxygen atoms in order to determine if the light emission was due to the simple combination described by reaction 5 or to a more complex mechanism of the type described by reactions 6-8.

Experimental

The experimental method and equipment used in this work was essentially the same as that used in the previously reported work on the chemiluminescent reaction of nitric oxide and O atoms.¹ In this case, however, a 50-l. spherical reaction vessel was used as shown in Figure 1. A pumping speed of 75-100 l./sec. was easily attained at 5 μ. As in the previous work, there was a negligible consumption of the reactants on the vessel walls or in the gas phase.

The SO was generated by adding carbonyl sulfide to the O atom stream in the reaction tube at a point upstream of the side tube to the 50-l. vessel. The resultant SO-O atom gas mixture was pumped under steady-state conditions with only a small fraction being pumped into the 50-l. system. Conditions were held constant in the reaction tube to assure a constant percentage of reactants being fed into the 50-l. system where no further appreciable consumption of reactants occurred. Variations of pressure in the 50-l. vessel while conditions were held constant in the reaction tube permitted reaction studies at constant percentage of reactants but at different pressures.

A photomultiplier tube placed on the high-pressure input reaction tube (see Figure 1) was used with appropriate filters to monitor the SO-O atom emission at

300-500 μ. In this way, changes in the constituents could be detected as the pressure-intensity values were obtained. This was important because the curves of intensity *vs.* pressure would be altered significantly if the input quantities changed during a run. The relative intensity of light emission from the 50-l. flask was followed using an EMI/US 6256B photomultiplier tube which has a quartz window giving response extending into the ultraviolet. To avoid extraneous light, the emission was generally monitored using a CS7-37 Corning filter. This filter transmitted the light emission only in the 3200- to 3900-Å. region which is also transmitted by the wall of the Pyrex reaction vessel.

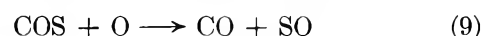
Since the phototubes measure the emission intensity of the reaction, it was possible to measure the concentrations of the constituents at any point in the reaction vessel using the following titration method. Experimental conditions were maintained constant such that a steady flow of O atoms was produced. The COS input was then allowed to increase steadily which caused a corresponding increase in the relative intensity of the emission. When enough COS was added, the intensity passed through a maximum, then decreased steadily until ultimately enough COS was added to consume all the O atoms, and no emission could be observed downstream.

In Figure 1 is also shown a side tube attached to the 50-l. vessel. The diameter of this was equal to the reaction tube used at high pressure. Measurements of the emission intensity in the two tubes could be directly compared to obtain the relative light intensity at the different pressures.

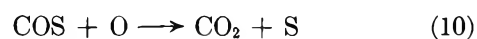
The 15-cm. cold trap was cooled with liquid nitrogen to avoid contaminating the diffusion pump. The gas flow was sufficient to avoid any interference between the cold trap and the reaction vessel.

Results and Discussion

COS can react with oxygen atoms in two ways⁴



and



At room temperature with a total pressure in the millimeter range no CO₂ could be detected by a mass spectrometer located downstream of the reaction zone.⁵

(4) A. L. Myerson, F. R. Taylor, and P. L. Hanst, *J. Chem. Phys.*, **26**, 1309 (1957).

(5) The ratio k_9/k_{10} has been found to be $>10^3$; therefore, any interference by reaction 10 is negligible: S. Dondes and D. Safrany, private communication.

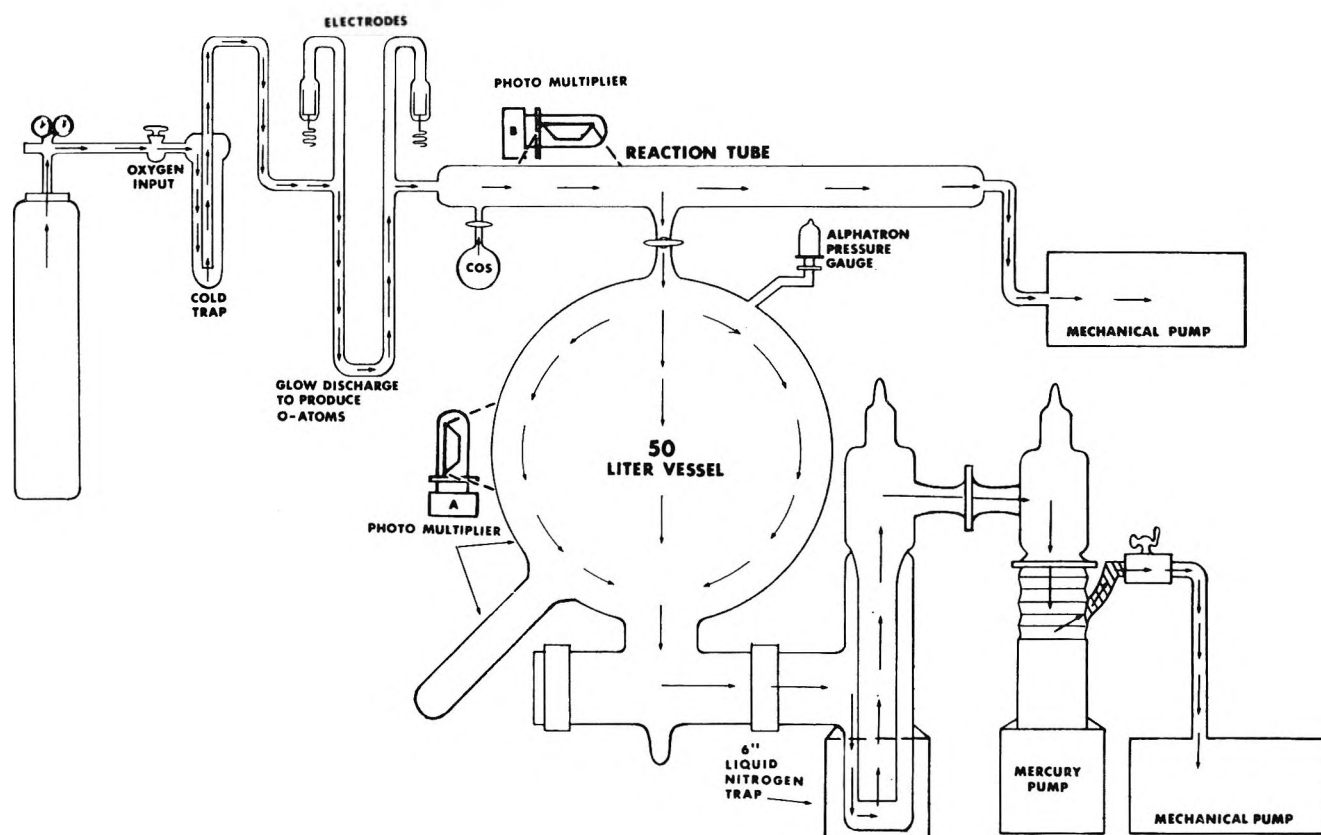


Figure 1. Schematic of apparatus.

Reaction 9 is, therefore, predominating, and it was estimated that the rate coefficient was of the order of 10^{-14} cm.³/molecule/sec. This reaction rate was important to the titration described above. The maximum intensity was attained when the quantity of COS equaled half the O atom concentration, and no emission was observed when the concentrations were equal. Essentially, an O atom was immediately consumed to produce each sulfur monoxide molecule from the COS by reaction 9, and then the light-emitting reaction (5) followed. The emission was readily observed, but no further significant consumption of O atoms occurred since reaction 5 is relatively slow.

The rate of the three-body collision reaction, $\text{SO} + \text{O} + \text{M} \rightarrow \text{SO}_2 + \text{M}$, was negligible under these conditions. It should be noted that the reactions of CO are sufficiently slow that the CO produced in reaction 9 acted essentially as an inert gas and did not interfere with the measurements reported here. The heats of reaction for a number of the reactions of interest in this study are listed in Table II as derived from the heats of formation given in Table I.

Reactions 9 and 5 are completely analogous to the O atom titration method using the reaction of NO_2 with O atoms.² In this case NO is formed, an O atom is

Table I: Heats of Formation for the Constituents Involved

Molecule	ΔH_f from atoms, kcal./mole
S_2	-83 ^a
SO	-127 ^b
S_2O	-189 ^c
SO_2	-254 ^d
COS	-340 ^e
CO_2	-381
CO	-256
O_2	-118

^a S. W. Benson, "Foundation of Chemical Kinetics," McGraw-Hill Book Co., Inc., New York, N. Y., 1960, p. 663. ^b W. D. McGrath and J. J. McGarvey, *J. Chem. Phys.*, **37**, 1574 (1962). ^c A recent article by R. Hagemann (*Compt. rend.*, **255**, 899 (1962)) gives the heat of formation of S_2O from rhombic sulfur and molecular oxygen as -17 kcal. With this information and an assortment of dissociation energies for S_2 , the value $\Delta H_f(\text{S}_2\text{O}) = -189$ seems reasonable. ^d Calculated from ΔH_f for SO and from reaction 5. ^e Calculated using the value given by Myerson (ref. 4) for reaction 9.

consumed (as in (9)), and the unreactive constituent is the O_2 formed instead of CO

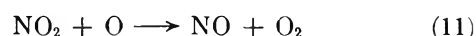
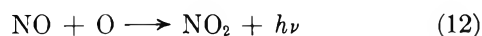


Table II: Heats of Reaction

Reaction	ΔH (exothermic), kcal./mole ^a
(1) $\text{NO} + \text{O} \rightarrow \text{NO}_2 + h\nu$	-72
(5) $\text{SO} + \text{O} \rightarrow \text{SO}_2 + h\nu$	-127
(9) $\text{COS} + \text{O} \rightarrow \text{CO} + \text{SO}$	-43 ^b
(10) $\text{COS} + \text{O} \rightarrow \text{CO}_2 + \text{S}$	-51 ^b
(13) $\text{SO} + \text{O}_2 \rightarrow \text{SO}_2 + \text{O}$	-9
(14) $\text{SO} + \text{SO} \rightarrow \text{SO}_2 + \text{S}$	0
(15) $\text{S} + \text{O}_2 \rightarrow \text{SO} + \text{O}$	-9
(16a) $\text{S}_2\text{O} + \text{O} \rightarrow \text{SO} + \text{SO}$	-65 ^c
(18) $\text{S}_2\text{O} + \text{S} \rightarrow \text{SO} + \text{S}_2$	-21 ^c

^a In some cases values of ΔH are uncertain, but all the reactions are expected to remain exothermic as written. ^b Myerson (ref. 4). ^c These representative exothermic values were estimated from the heats of formation in Table I. The importance lies not in the exact values, but in that the reactions are exothermic as written.

A second O atom is consumed when the NO formed in the fast reaction (11) reacts to give NO_2 plus light emission



Comparison of the two methods gave identical results. A two-step method was used for titration with NO_2 where a maximum light intensity was determined in the first step, and NO was added separately until the corresponding value of intensity was reached in order to obtain the actual rate of flow.⁶ This avoided the complications due to $2\text{NO}_2 \rightleftharpoons \text{N}_2\text{O}_4$. It should be noted that, in the case of COS, no such dimer is formed, and, in addition, COS is a less corrosive or reactive gas than NO_2 and, therefore, somewhat easier to handle and measure. The titration could be readily made directly in a single step using the disappearance of the blue emission as indicative of the end point with increasing COS flow or using the maximum light intensity as indicative of half the O atoms present, as with NO_2 .

The emission was observed as the COS flow rate was varied, which changed the SO concentration directly since reaction 9 was very fast under these conditions. The O atoms remained essentially constant with only slight change due to consumption *via* reaction 9 because the COS was always a small fraction of the O atoms. The resultant emission intensity in the low-pressure reaction vessel was plotted *vs.* the emission intensity in the high-pressure side, and a linear dependency was observed.

The O atom concentration could be varied by varying the power to the glow discharge. A linear dependency also resulted.

With the fraction of reactants constant, the pres-

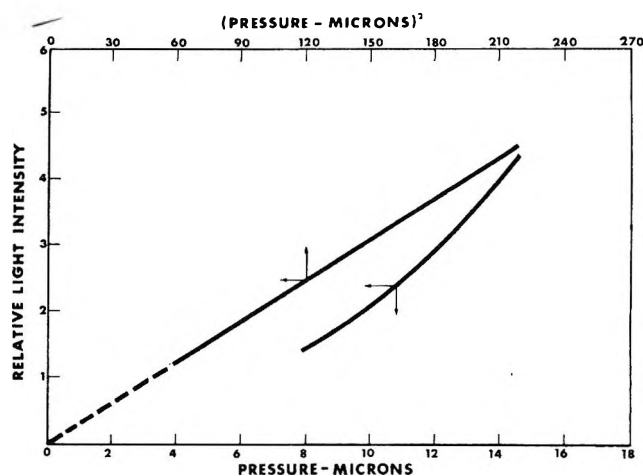


Figure 2. Typical oscillograph plot of intensity *vs.* pressure.

sure in the 50-l. vessel was permitted to increase by turning off the diffusion pump as described in the previous publication. The emission intensity in the vessel increased with the square of the pressure, or, more specifically, $I = kp^{1.98 \pm 0.02}$, for a series of nine runs made under different conditions of starting pressure and reactant concentrations. A typical oscillograph plot of intensity *vs.* pressure is given in Figure 2. The data were then plotted as I *vs.* p^2 as also shown in Figure 2. The resulting straight line, typical of many runs, confirms a two-body mechanism.

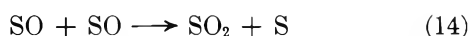
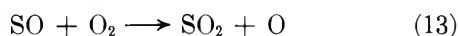
This variation of intensity with the square of the pressure at constant mole fraction was also found when the intensity of emission in the high-pressure reaction tube and in the low-pressure, 50-l. reaction vessel were compared. This comparison was made by simultaneously observing the emission intensities in the high-pressure reaction tube and in a 45-mm. diameter side arm attached to the 50-l. vessel. The intensities varied by more than a factor of 1000 and were found to be proportional to the square of the pressure even over this wide range within 10% or less, or within the experimental error of the measurements. This result adds additional support to the conclusion that the two-body emission reaction (5) occurred.

An estimate was made of the rate of reaction 5 by comparing the maximum light intensity of emission of the NO-O atom reaction observed by adding NO_2 with the maximum obtainable under identical conditions using COS. Except for the complications of photomultiplier sensitivities and transmission of the emission through glass envelopes and filters, the ratio of the rate coefficients would be proportional to the ratio of these

(6) P. Harteck, R. R. Reeves, and G. G. Mannella, *J. Chem. Phys.*, **32**, 632 (1960).

maximum light intensities. Allowing for these factors, a ratio of the rate coefficients of k_5/k_1 was found equal to 25 within a factor 2. Assuming $k_1 = 3 \times 10^{-17}$ cm.³/molecule sec.,⁷ then $k_5 = 7 \times 10^{-16 \pm 0.3}$.

As previously noted, linear dependence on O atom concentration was observed with fixed concentration of COS. However, under the conditions where the SO formed was greater than the remaining O atoms, a displacement of the linear response from the coordinate origin was observed. This was attributed to the reactions of the SO molecules producing additional O atoms by the alternate mechanisms below. Under the experimental conditions normally used, however, no appreciable consumption (or production) of reactants could be observed. The various reactions which may occur under alternate conditions are

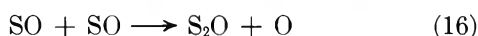


followed by



Some sulfur is found in the reaction vessel after long operation lending support to reaction 14. Obviously reaction 15 cannot be very fast, or no sulfur deposit would have been observed.

An alternate path for reaction 14 is not possible



since it is a strongly endothermic reaction as can be seen in Table II.

When the system had been operating for some time the 50-l. flask became contaminated in certain areas, and it was observed that an enhanced blue emission occurred in these general areas. This corresponded to a surface-catalyzed excitation of the SO₂ molecule, SO + O surface SO₂* → SO₂ + hν. A similar excitation had been observed earlier with NO and O atoms which resulted in a catalyzed emission of the NO₂ molecule. Visually, the NO₂-excited emission was reddish in appearance. The areas which catalyzed the excitation and resultant blue emission of SO₂ were also found to be

effective in catalyzing the excitation of the NO₂ with the resultant reddish emission. Under these conditions, with only oxygen and O atoms in the system, the emission in the ultraviolet was also observed, which could be attributed to the oxygen Herzberg bands, owing to surface-catalyzed recombination of O atoms to form the excited O₂A³Σ_u⁺. These catalysis effects yielded spurious results when studying the homogeneous gas-phase reactions, and thorough cleaning of the system was periodically necessary to ensure that such effects were avoided.

The simple two-body reaction mechanism found for the light emission from the nitric oxide-oxygen atom reaction was in contrast to the proposed complex mechanism initiated by a three-body reaction which was more generally expected to be the source of the emission even at low pressures.¹ The present work shows a similar two-body mechanism for the sulfur monoxide-oxygen atom reaction. It certainly appears reasonable to expect this mechanism to occur, not as an exception, but as a relatively common source of light emission in many systems.

Conclusions

The experimental results show a second-order dependence of the emission intensity of the chemiluminescent reaction of sulfur monoxide with O atoms corresponding to reaction 5.

The COS reaction with O atoms can also be used under certain conditions for titration and determination of the oxygen atoms present in a gas stream analogous to the NO₂ titration method.

Acknowledgment. The authors wish to acknowledge the support of the Air Force Cambridge Research Laboratories under Contract No. AF 19(628)-4069 and the Air Force Office of Scientific Research AF-AFOSR-174-63. We wish to thank Mr. William Chace for his experimental assistance.

(7) A. Fontijn and H. I. Schiff in "Chemical Reactions in the Lower and Upper Atmosphere," Interscience Publishers, Inc., New York, N. Y., 1961, p. 239.

Halogen Displacement Reactions of Chloro- and Bromoacetic Acids in Water and Dioxane–Water Solutions¹

by J. F. Hinton and F. J. Johnston

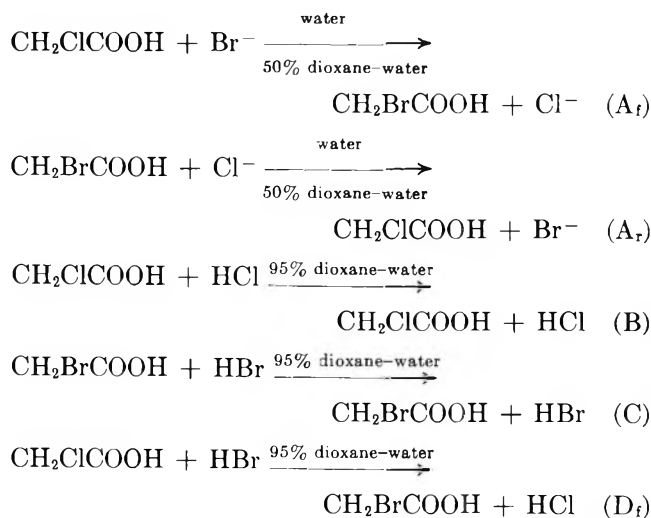
Department of Chemistry, University of Georgia, Athens, Georgia (Received August 24, 1964)

The reactions involving halogen displacement in chloroacetic acid by bromide and in bromoacetic acid by chloride have been studied in aqueous and in 50% dioxane solutions. The corresponding reactions involving chloro- and bromoacetic acids with both hydrogen chloride and hydrogen bromide were studied in a 95% dioxane solvent. In each case, rates were first order with respect to the haloacetic acid and to the total halide or halogen acid concentrations. Activation enthalpies and entropies were determined. For the reactions involving different halogen atoms, equilibrium constants and reaction enthalpies and entropies were evaluated from the kinetic parameters. In the 95% dioxane system, equilibrium constants measured directly were in good agreement with those determined from the rate constant ratio. Activation parameters in the 95% dioxane system were markedly different from those in aqueous solution and are best explained in terms of a protonation equilibrium involving the haloacetic acid and the halogen acid.

Introduction

Several halogen-exchange and replacement reactions involving halide ions and α -halogen acids in aqueous solutions have been previously described. Wagner² studied the reactions between chloroacetic acid and iodide and between iodoacetic acid and chloride. Olson^{3,4} and co-workers have measured exchange and replacement reaction rates in systems consisting of chloro- and bromosuccinic acids and the corresponding halide ions and in systems consisting of phenylchloro- and bromoacetic acids and halide ions. The latter reactions involved substitution on an asymmetric carbon and were followed by optical activity measurements. We have^{5,6} used radioactive tracers to follow the exchange reactions between chloro-, bromo-, and iodoacetic acids and the corresponding halide ions. In every case, these reactions were second order and evidently involved a direct nucleophilic displacement process. When replacement of one halogen by another was involved, enthalpy and entropy changes evaluated from the activation parameters were consistent with available thermochemical data.

We have studied the kinetics of the following reactions in the indicated solvent systems



(1) (a) This paper was abstracted from the Ph.D. dissertation of James F. Hinton, University of Georgia, Aug. 1964; (b) this work has been performed under A.E.C. Contract AT(40-1)2826.

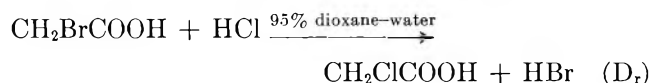
(2) C. Wagner, *Z. physik. Chem.*, **115**, 121 (1925).

(3) A. R. Olson and F. A. Long, *J. Am. Chem. Soc.*, **58**, 393 (1936).

(4) A. R. Olson and M. J. Young, *ibid.*, **58**, 1157 (1936).

(5) R. A. Kenney and F. J. Johnston, *J. Phys. Chem.*, **63**, 1426 (1959).

(6) J. F. Hinton and F. J. Johnston, *ibid.*, **67**, 2557 (1963).



Radioactive tracers were used to follow both the exchange reactions and the replacement reactions. Formation of molecular iodine under the conditions of these reactions prevented our obtaining meaningful data on the corresponding systems in which iodide or hydrogen iodide were involved.

From the rate expressions and activation parameters for the forward and reverse replacement processes, enthalpies and entropies for the over-all reaction were evaluated. This report summarizes our rate studies and presents thermochemical data for replacement reactions in water and dioxane-water solutions.

Experimental

Reagents. Baker Analyzed chloroacetic acid was used after fractional recrystallization from benzene. Eastman White Label bromoacetic acid was used without further purification. Eastman White Label *p*-dioxane was refluxed over potassium hydroxide for approximately 24 hr. and distilled. The final fraction used in the solvent mixture had a refractive index of 1.4198 at 25°. Solvent compositions are expressed as per cent by volume.

Chlorine-36 labeled hydrochloric acid as obtained from Oak Ridge was diluted with reagent hydrochloric acid. Sodium bromide or hydrobromic acid solutions were spiked with potassium bromide-82 obtained from Oak Ridge.

Procedure. The experimental procedures are similar to those described previously. In general, reactant aliquots were quenched in ice-water, and halide separation was accomplished through silver nitrate titration. The HCl-CH₂ClCOOH system in 95% dioxane was studied at higher temperatures, and individual, sealed cells were used. In every case, background and separation-induced reactions were negligible. Chlorine-36 activities were measured by Geiger-Mueller counting of liquid samples, and bromine-82 samples were counted in a scintillation system. Comparisons of reacted samples containing the bromine activity were made with a standard stock sample within time intervals such that decay corrections were unnecessary. Stock samples of the unseparated reaction mixture were adjusted to the same solvent conditions as the reacted samples so that counting rates were compared under similar density conditions. Standard deviations for the net counting rates were always within 2%.

In the aqueous systems hydrolysis of the chloro- and bromoacetic acids was evident upon prolonged exposure at the temperatures used in these experiments.

This prevented our studying the replacement rates under conditions close to equilibrium. In general, at the concentrations used, hydrolysis was not detectable, and the reverse reaction was negligible to at least 10% and as high as 30% replacement. Under these conditions, second-order rate constants were obtained using the expression

$$k = \frac{1}{(a-b)t} \ln \frac{b(a-x)}{a(b-x)} \quad (1)$$

For the replacement reactions, radioactivity was used as a direct measure of concentration.

Rates for the exchange reactions which were studied in the 95% dioxane systems obeyed the familiar exchange rate law

$$\text{Rate} = -\frac{ab}{(a+b)} \ln \frac{(1-F)}{t} \quad (2)$$

For a process first order in each of the exchanging species, this expression becomes

$$k = -\frac{\ln(1-F)}{(a+b)t} \quad (3)$$

In these equations *a* and *b* have their usual significance as initial reactant concentrations, and *F* is given by the ratio

$$F = \frac{(\text{specific activity, haloacetic acid})_t}{(\text{specific activity, haloacetic acid})_{t=\infty}}$$

In the 95% dioxane systems hydrolysis of the haloacetic acids was not detectable in any of the experiments.

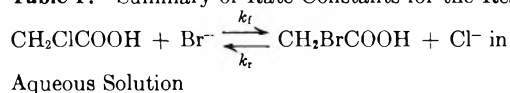
Equilibrium constants were evaluated from the ratios of the rate constants for the forward and reverse reactions, $K = k_f/k_r$. Enthalpies and entropies for the reactions were obtained as $\Delta H = \Delta H_f^* - \Delta H_r^*$ and $\Delta S = \Delta S_f^* - \Delta S_r^*$.

Results and Discussion

Rates of reactions A_r through D_r were first order with respect to the total concentration of each of the exchanging species under all conditions studied. Our experiments were performed over reactant concentration ranges of from 0.03 to 0.48 *M* in haloacetic acid and from 0.02 to 0.09 *M* in the halogen acid. The widest range covered at a given temperature in the aqueous and 50% dioxane systems was from 0.0755 to 0.364 *M* for the haloacetic acid and from 0.0200 to 0.0947 *M* for the halide. In the 95% dioxane system, the widest range covered at a given temperature was from 0.0911 to 0.2109 *M* for the haloacetic acid and from 0.0197 to 0.0420 *M* for the halogen acid. Standard deviations

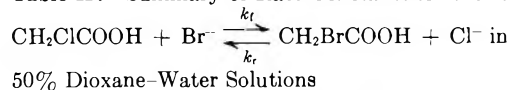
for the second-order rate constants corresponded with few exceptions to variations within 2%. The maximum deviation corresponded to a variation of slightly over 6%. The aqueous systems were 0.006 to 0.6 *M* in nitric acid in order to ensure the presence of the haloacetic acid in the molecular form. No effect on the rate constants resulted from variation of the nitric acid concentration over this range. In the 50 and 95% dioxane systems the rate constants were the same in the presence or absence of nitric acid. The rate constants for the several systems studied are summarized in Tables I through V.

Table I: Summary of Rate Constants for the Reactions



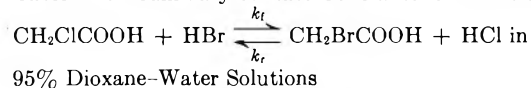
Temp., °K.	k_f , l. mole ⁻¹ sec. ⁻¹	k_r , l. mole ⁻¹ sec. ⁻¹
304.1	2.14×10^{-6}	1.25×10^{-6}
311.9	5.56×10^{-6}	3.17×10^{-5}
323.7	2.10×10^{-5}	1.20×10^{-4}
333.7	5.86×10^{-5}	3.36×10^{-4}

Table II: Summary of Rate Constants for the Reactions



Temp., °K.	k_f , l. mole ⁻¹ sec. ⁻¹	k_r , l. mole ⁻¹ sec. ⁻¹
323.6	4.39×10^{-5}	3.49×10^{-4}
333.7	1.15×10^{-4}	8.90×10^{-4}
343.4	2.75×10^{-4}	2.14×10^{-3}

Table III: Summary of Rate Constants for the Reactions



Temp., °K.	k_f , l. mole ⁻¹ sec. ⁻¹	k_r , l. mole ⁻¹ sec. ⁻¹
313.7	2.36×10^{-5}	1.50×10^{-4}
323.6	6.50×10^{-5}	3.12×10^{-4}
333.7	1.79×10^{-4}	6.55×10^{-4}
343.4	4.14×10^{-4}	1.29×10^{-4}

Conductance measurements by Owen and Waters⁷ on hydrochloric acid solutions which are 45% by weight dioxane indicate little ion association. Conductance measurements on hydrobromic acid in the 50% by volume dioxane solvent show a similar result. We have assumed, therefore, that the rate constants in

Table IV: Summary of Rate Constants for the Reaction
 $\text{CH}_2\text{ClCOOH} + \text{HCl}^* \rightleftharpoons \text{CH}_2\text{Cl}^*\text{COOH} + \text{HCl}$ in
95% Dioxane-Water Solutions

Temp., °K.	k , l. mole ⁻¹ sec. ⁻¹
333.7	1.05×10^{-5}
343.6	1.83×10^{-5}
355.1	3.67×10^{-5}
371.2	8.72×10^{-5}

Table V: Summary of Rate Constants for the Reactions
 $\text{CH}_2\text{BrCOOH} + \text{HBr}^* \rightleftharpoons \text{CH}_2\text{Br}^*\text{COOH} + \text{HBr}$ in
95% Dioxane-Water Solutions

Temp., °K.	k , l. mole ⁻¹ sec. ⁻¹
305.9	1.85×10^{-3}
315.0	4.23×10^{-3}
323.6	8.37×10^{-3}

these systems are characteristic of a process involving the haloacetic acid molecule and halide ion.

Activation parameters were obtained by a least-squares fitting of the rate constants to the expression

$$k_r = \frac{kT}{h} \exp[\Delta S^*/R] \exp[-\Delta H^*/RT] \quad (4)$$

Standard deviations for the activation enthalpies were within ± 0.15 kcal. mole⁻¹ in the aqueous and 50% dioxane systems and within ± 0.20 kcal. mole⁻¹ in the 95% dioxane systems. For the entropies of activation the corresponding deviations were within ± 0.4 and ± 0.5 e.u.

The activation parameters for the replacement reactions in aqueous solutions are summarized in Table VI and compared with those for the exchange reactions which we have previously reported. The results parallel very closely those obtained by Olson with the halosuccinic acids and phenylhaloacetic acid.

Table VI: Activation Parameters for the Reactions
 $\text{CH}_2\text{XCOOH} + \text{Y}^- \rightarrow \text{CH}_2\text{YCOOH} + \text{X}^-$ in
Aqueous Solution

X	Y	ΔH^* , kcal. mole ⁻¹	ΔS^* , e.u.
Cl	Cl ^a	23.85	-10.5
Cl	Br	22.06	-11.5
Br	Cl	21.97	-8.8
Br	Br ^b	18.98	-13.4

^a See ref. 5. ^b See ref. 6.

(7) B. Owen and B. Waters, *J. Am. Chem. Soc.*, **60**, 2371 (1938).

In the 50% dioxane solutions the enthalpy of activation for reaction A_f is 19.70 kcal. mole⁻¹, and the entropy of activation is -17.8 e.u. The corresponding values for reaction A_r are 19.39 kcal. mole⁻¹ and -14.7 e.u. The exchange reactions were not studied in the 50% system.

The equilibrium constant for the reaction with chloroacetic acid and bromide ions as reactants may be obtained from the ratio of forward to reverse reaction rate constants. In water this value is 0.174, and in 50% dioxane it is 0.129. These quantities were essentially constant over the temperature range studied. In water ΔH for the reaction is approximately zero, and in 50% dioxane it is endothermic by 0.3 ± 0.2 kcal. mole⁻¹. The entropy changes in the two solvents are -2.7 and -3.1 e.u. Standard enthalpies of chloride and bromide ions in water are -40.0 and -28.9 kcal. mole⁻¹, respectively.⁸ The corresponding entropies are 13.2 and 19.3 e.u. Neglecting concentration effects, the over-all zero enthalpy change for the reaction leads to an enthalpy difference in aqueous solution between chloroacetic and bromoacetic acids of 11.1 kcal. mole⁻¹. From the entropy change for the reaction in water, one obtains for the corresponding entropy difference between the two haloacetic acids -3.4 e.u. Thermochemical data for the dioxane systems were not available, and similar comparisons were not made.

Activation parameters for reactions B through D in the 95% dioxane systems are summarized in Table VII. The values are markedly different from those in

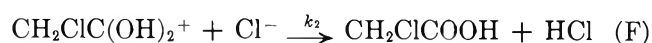
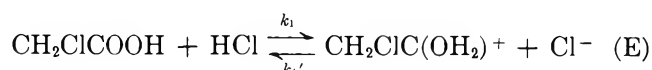
Table VII: Activation Parameters for the Reactions $\text{CH}_2\text{XCOOH} + \text{HY} \rightarrow \text{CH}_2\text{YCOOH} + \text{HX}$ in 95% Dioxane Solutions

X	Y	ΔH^* , kcal. mole ⁻¹	ΔS^* , e.u.
Cl	Cl	13.22	-42.0
Cl	Br	20.11	-16.0
Br	Cl	14.89	-28.7
Br	Br	16.40	-17.4

aqueous systems. The most striking feature involves the very low activation enthalpies and large negative entropy terms associated with the HCl systems. Owen and Waters⁷ give a value of 2×10^{-4} as the dissociation constant at 25° for HCl in 82% by weight dioxane. Conductivities of HCl and HBr solutions in 95% dioxane were not measurable with the type of apparatus available to us. It must be assumed that in this system both halogen acids exist essentially in the molecular form. A reaction mechanism involving

the haloacetic acid molecule and a halide ion, the latter concentration depending upon a dissociation of the halogen acid, is not consistent with the second-order character of the rate expression. A mechanism involving a direct exchange reaction between a haloacetic acid molecule and a halogen acid molecule cannot be discounted and would result in a rate expression consistent with our data.

An energetically more satisfying mechanism, however, is one which involves a protonation equilibrium between the haloacetic acid and halogen acid. Using the chlorine exchange reaction as an example



The exchange rate is $k_2K[\text{CH}_2\text{ClCOOH}][\text{HCl}]$ where K is the equilibrium constant for reaction E. According to this picture the observed second-order rate constants are given by k_2K . The apparent enthalpy of activation is then $\Delta H^*_{\text{obsd}} = \Delta H_2^* + \Delta H_E$ where ΔH_2^* is the activation enthalpy for reaction F, and ΔH_E is the enthalpy change for reaction E. The more highly exothermic the protonation or dissociation reaction, the smaller will be the measured activation enthalpy. A reliable estimate of ΔH_E for either HCl or HBr is difficult to make. The corresponding reaction in water, $\text{H}_2\text{O} + \text{HCl} \rightarrow \text{H}_3\text{O}^+(\text{aq}) + \text{Cl}^-(\text{aq})$, is estimated⁹ to be exothermic by approximately 25 kcal. mole⁻¹. For HBr, the dissociation is estimated by the same process to be exothermic by approximately 14 kcal. mole⁻¹. While both enthalpy changes will be numerically smaller in 95% dioxane, it is quite reasonable that the process involving HCl will be more exothermic than that with HBr. The activation enthalpies for reactions involving HCl will then be lowered to a greater extent than those with HBr, a result consistent with our observations.

Entropies of activation for the reactions will be of the form $\Delta S^*_{\text{obsd}} = \Delta S_2^* + \Delta S_E$. In water, dissociation entropies for acids are of the order of -20 e.u. with values for larger ions being less negative. Again, the values in 95% dioxane are not easily estimated. Our observed activation entropies are consistent, at least in direction, with these considerations.

The independence of the rate constants from the concentration of added acid in aqueous and 50% di-

(8) G. N. Lewis and M. Randall, "Thermodynamics," 2nd Ed., McGraw-Hill Book Co., Inc., New York, N. Y., 1961, p. 400.

(9) A. A. Frost and R. G. Pearson, "Kinetics and Mechanism," 2nd Ed., John Wiley and Sons, Inc., New York, N. Y., 1961, p. 132.

oxane solutions precludes the possibility that such a protonation mechanism occurs in these solvents.

The equilibrium constant for the reaction with chloroacetic acid and HBr as reactants in 95% dioxane may be obtained from the rate constant ratio. The values for the temperatures studied are listed in Table VIII.

Table VIII: The Equilibrium Constant for the Reaction $\text{CH}_2\text{ClCOOH} + \text{HBr} \longrightarrow \text{CH}_2\text{BrCOOH} + \text{HCl}$ in 95% Dioxane Solution

Temp., °K.	$K = k_t/k_r$	K (measd.)
313.7	0.157	...
323.6	0.209	0.213
333.7	0.272	0.272
343.4	0.318	...

Since no hydrolysis of the haloacetic acids was detected in this solvent system upon prolonged exposure to the temperatures at which the replacement reactions were studied, it was possible to obtain a direct measurement of the equilibrium constant. The results of two such experiments are listed in column 3 of Table VIII. The agreement with the results obtained from the kinetic data is quite satisfactory.

The enthalpy change for the reaction in 95% dioxane is 5.22 kcal. mole⁻¹, and the entropy change is 12.7 e.u. Thermochemical data are not available in this solvent to allow comparison with that obtained from kinetics.

Acknowledgment. We appreciate helpful discussions with Dr. R. C. Lamb concerning this work.

The Kinetics of Thermal Decomposition of Diacetylene in a Flow System¹

by K. C. Hou and H. B. Palmer

Department of Fuel Technology, College of Mineral Industries, The Pennsylvania State University, University Park, Pennsylvania (Received August 27, 1964)

Diacetylene decomposes in a manner very similar to acetylene. Between 973 and 1223°K., the decomposition is second order in the diacetylene concentration. The rate constant behaves with increasing temperature in a way that implies a transition from long-chain toward nonchain decomposition. The long-chain rate constant is approximately $k = 10^{16} \exp(-40 \text{ kcal.}/RT)$ cc./mole sec. It is suggested that 40 kcal. may represent the approximate energy of a low-lying triplet state of diacetylene.

Diacetylene C_4H_2 , has been reported to be a significant product of the pyrolysis of acetylene in shock waves^{2a} and in a flow system.^{2b,c} It also is found as a product of the thermal decomposition of benzene^{3,4}; in fact, Kinney and Slysh³ concluded that it is a primary product (with hydrogen and acetylene) of benzene pyrolysis. Although our own more recent work⁴ indicates that this conclusion was not quite correct, diacetylene is, nevertheless, a significant product and may be an important intermediate in the processes

leading to carbon formation. Therefore, a study of its thermal decomposition seems worthwhile.

(1) This work has been supported by a grant from the J. M. Huber Corp.

(2) (a) C. F. Aten and E. F. Greene, *Combust. Flame*, **5**, 55 (1961); (b) H. B. Palmer and F. L. Dormish, *J. Phys. Chem.*, **68**, 1553 (1964); (c) F. L. Dormish, M.S. Thesis, Department of Fuel Technology, Pennsylvania State University, 1962.

(3) C. R. Kinney and R. S. Slysh, *Proc. Conf. Carbon, 4th, Buffalo, 1967*, 301 (1960).

(4) K. C. Hou and H. B. Palmer, *J. Phys. Chem.*, **69**, 863 (1965).

Only two such studies have been reported previously—those carried out by Kinney and Slysh³ and those by Hou and Anderson,⁵ both being studies in flow systems. The study of Kinney and Slysh was restricted to one temperature, 1200°, and to a fixed concentration of 0.1% C₄H₂ in helium carrier gas, at a total pressure of approximately 1 atm. It appears to have suffered from difficulties in regulating the concentration of C₄H₂ and from a poor temperature profile in the reactor. Hou and Anderson examined the pyrolysis over a range of temperatures at and below 800°, at a high concentration (25 mole %), and a long contact time (9 sec.). They did not obtain kinetic data but concentrated on product analysis. The main products were found to be ethylene and acetylene.

Kinney and Slysh examined a plot of C₄H₂ concentration against time and concluded that the decomposition was first order with rate constant 22.4 sec.⁻¹ at 1200°. Their contact times were of the order of tens of milliseconds, and the main products reported were H₂, CH₄, and C₂H₂. Owing to their difficulties with concentration and temperature, their kinetic result must be regarded as preliminary.

The present work is an effort to carry out a comprehensive kinetic study of the decomposition of C₄H₂, using a high-temperature flow system. The main features of the experiments include (a) variation of the temperature from 973 to 1223°K. in 50° intervals, (b) variation of the C₄H₂ concentration from 0.3 to 1.4% in helium carrier gas, (c) variation of the residence time from 30 to 250 msec., (d) examination of heterogeneity by varying the reactor diameter by a factor of 2, (e) introduction of NO to assess the free-radical contributions to the rate, and (f) measurements of product distributions and carbon formation. The total pressure has been 735 ± 5 torr in all experiments.

Experimental Details

The basic features of the apparatus and method were identical with those in our study of benzene.⁴ As before, the principal reactor (A) was a cylindrical mullite tube of 5-mm. i.d. A second reactor (B) was used for varying the surface-to-volume ratio, having four holes of 0.24-cm. i.d. The uniform hot zone in the reactor was 25.4 cm. long, including a small allowance for end effects.

Diacetylene was prepared from 1,4-dichloro-2-butyne by dehydrohalogenation as described by Armitage, *et al.*⁶ Starting material was obtained from Columbia Organic Chemicals Co. The product C₄H₂ was purified by distillation and its final purity assessed at 98% by gas chromatography and mass spectrometry.

Introduction of C₄H₂ into the helium carrier gas stream was controlled by maintaining liquid C₄H₂ in a saturator at -24°. Fluctuations in the liquid temperature were less than ±0.1°.

The concentration of C₄H₂ in the input to and effluent from the reactor was determined using a vapor fractometer (Perkin-Elmer Model 154-C) with a 1-m. dinonyl phthalate column. Retention time was 20 mm. from the air peak. Light hydrocarbons were determined in the product gas using a silica gel column. Carbon deposition was determined by burn-off and trapping of CO₂ according to the procedure described by Dormish.^{2c}

Nitric oxide (Matheson) was introduced through a precision bore flowmeter that was calibrated against a soap bubble flowmeter. Helium (Matheson) was the 99.99% minimum grade.

Results and Discussion

In Table I are presented the pertinent data for treatment of the kinetics of decomposition. The results

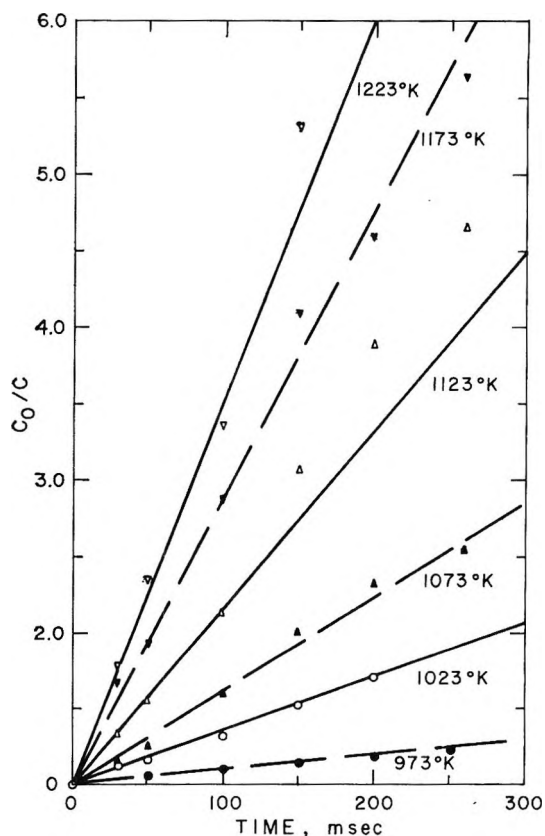


Figure 1. Second-order kinetic plot of data for starting concentrations near 10^{-7} mole/cc. for all temperatures covered.

(5) K. C. Hou and R. C. Anderson, *J. Phys. Chem.*, **67**, 1579 (1963).

(6) J. B. Armitage, E. R. H. Jones, and M. C. Whiting, *J. Chem. Soc.*, 46 (1951).

are found to be described adequately by second-order kinetics. First-order kinetics are unsatisfactory. Figure 1 contains second-order plots for experiments in which the starting concentrations all were close to 10^{-7} mole/cc. The 1123°K. results are not entirely satisfying. The line for this case was drawn through the points at the shorter residence times because concentrations at short times could be measured most accurately. However, discrepancies of this sort require that an uncertainty of about $\pm 10\%$ be assigned to the rate constants derived from such plots.

Table I: Summary of Decomposition Data: Concentration of C_4H_2 as a Function of Time (all concentrations are in mole/cc. $\times 10^7$)

Temp., °K.	Time, msec.						
	0	30	50	100	150	200	250
973	1.45	...	1.335	1.2	1.19	1.15	1.075
	1.02	...	0.954	0.924	0.89	0.858	0.836
	0.582	0.566	0.55	0.505	0.485

1023	1.43	1.27	1.19	0.99	0.81	0.71	0.61
	1.12	0.995	0.96	0.85	0.735	0.66	0.588
	0.686	...	0.625	0.585	0.55	0.506	0.496
	0.575	...	0.52	0.506	0.46	0.425	0.405
1073	0.96	0.812	0.764	0.60	0.477	0.41	0.376
	0.80	0.67	0.626	0.49	0.373	0.316	...
	0.505	0.45	0.404	0.384	0.333	0.31	0.263

1123	0.545	0.464	0.441	0.405	0.346	0.306	...
	1.30	0.875	0.71	0.51	0.35	0.254	0.21
	1.025	0.755	0.668	0.48	0.332	0.263	0.22
	0.263	0.232	0.218	0.197	0.168	0.139	0.131
1173	0.694	0.58	0.546	0.464	0.382	0.304	0.26
	1.38	0.70	0.51	0.342	0.248	0.183	0.149
	1.15	0.692	0.595	0.40	0.282	0.251	0.205
	0.311	0.242	0.230	0.210	0.167	0.143	0.121
1223	0.532	0.454	0.420	0.364	0.298	0.267	0.237
	0.770	0.625	0.574	0.46	0.382	0.335	0.322
	1.13	0.635	0.48	0.336	0.212	0.135	0.096
	1.02	0.628	0.505	0.259	0.201	0.144	0.130
1223	0.923	0.55	0.46	0.32	0.238	0.177	0.138
	0.55	0.356	0.32	0.295	0.212	0.164	0.138
	0.29	0.224	0.204	0.170	0.123	0.096	0.086
	0.714	0.560	0.490	0.384	0.270	0.226	0.180

Table II contains a summary of the second-order rate constants. The number in parentheses was rejected on statistical grounds. We believe the four numbers in brackets to be erroneously low but have not rejected them because there is no valid argument for doing so (one of them is a result obtained a month before any of the others, and two of them represent the first data taken on a particular day, when the furnace

interior may not have been up to the temperature indicated by the recorder-controller). The self-consistency among most of the runs is quite good, indicating that temperature equilibrium in the reactor was attained with, perhaps, two or three exceptions. Thus, at 973, 1023, 1073, and 1223°K., we believe temperatures to have been constant to within about $\pm 5^\circ$ K. so that the spread in rate constants is a reflection of the precision in determining concentrations. Flow rates or residence times were known to about $\pm 1\%$.

Table II: Second-Order Rate Constants for C_4H_2 Decomposition

	Temp., °K.					
	973	1023	1073	1123	1173	1223
Log k	7.00	7.544	7.820	8.076	8.34	8.344
k , cc./mole sec.	6.987	7.505	7.898	8.054	8.220	8.332
	7.054	7.439	7.833	8.130	8.283	8.318
		7.380		[7.880]	[7.978]	8.387
				[7.858]	[7.945]	8.318
						(8.185)
Log k_{av}	7.026	7.471	7.852	8.012	8.185	8.347

Figure 2 is an Arrhenius plot of the second-order rate constants. The curve has been drawn by eye. It should be apparent why we believe the bracketed numbers in Table II to be erroneously low. The vertical line through each point represents the average deviation of the k values at that temperature.

The Arrhenius plot shows curvature very similar to that exhibited by acetylene,^{2b,c} which suggests that C_4H_2 may also exhibit long chains at low temperatures and undergo a transition to nonchain behavior at high temperatures. The conclusion is much less firm than in the case of C_2H_2 because the present data are not supplemented by studies at lower and higher temperatures.

Nevertheless, there is supporting evidence from the present work. On the Arrhenius plot in Figure 3 we have dashed in an extension of the lowest temperature portion on the basis that the curvature seems to have disappeared, with falling temperature, by about 1050°K. Thus, the two lowest points may define a limiting rate constant at low temperature reasonably well. The equation of the straight line is $k = 10^{16.08} \exp(-40.3 \text{ kcal.}/RT)$ cc./mole sec. It seems unlikely that the slope could be much less than that indicated in the figure, which implies that the pre-exponential factor is at least 10^{16} cc./mole sec. Such a high frequency factor in a second-order reaction implies a

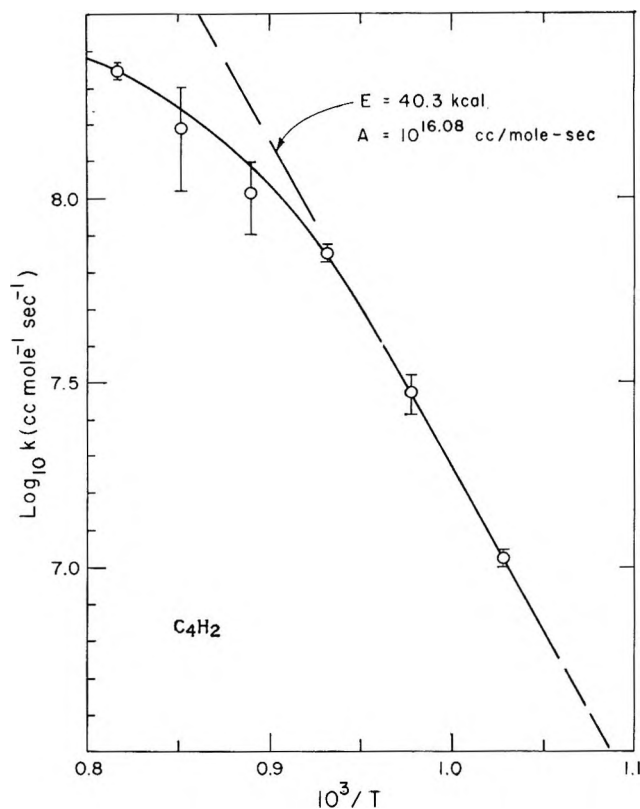


Figure 2. Arrhenius plot of second-order rate constants.

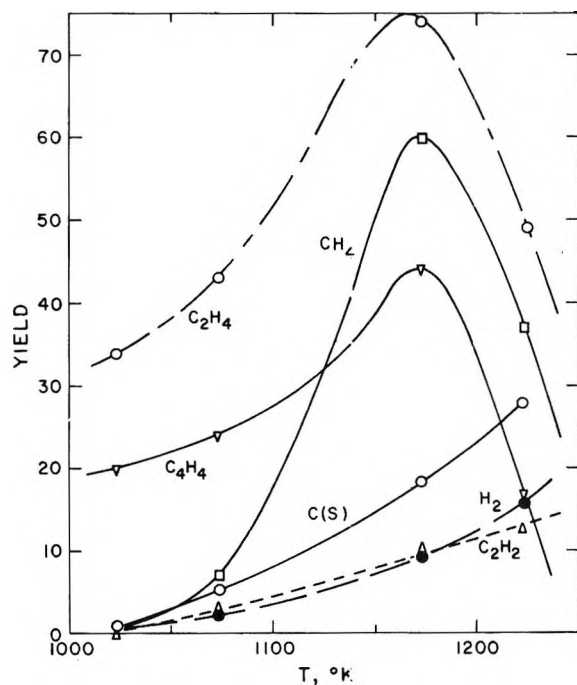


Figure 3. Product distribution as a function of temperature. The yield is in moles/mole of C_4H_2 decomposed, times 100. For convenience, $C(s)$ has been divided by 10, C_2H_4 has been multiplied by 10, and C_4H_4 has been multiplied by 40.

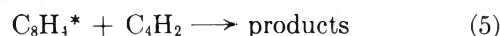
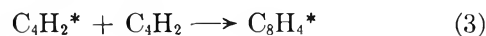
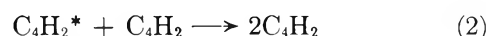
chain rather strongly. It may be compared to the value of C_2H_2 , $10^{16.57}$ cc./mole sec., at low temperature.⁷

It is difficult to assign an uncertainty to the activation energy or to the pre-exponential factor, other than by inspection of the Arrhenius plot. From it, we would suggest that the limits on k fall between about $10^{15.6} \exp(-38 \text{ kcal./RT})$ and $10^{17.8} \exp(-48 \text{ kcal./RT})$ cc./mole sec.

Further support for a chain mechanism appears in the effect of NO addition. However, NO does not inhibit the reaction strongly, though it affects it abruptly. The rate at 1123°K. is reduced by approximately 50% when 0.5% or more NO is added. This may indicate that NO is behaving in a manner similar to that which Laidler has postulated for inhibited pyrolyses of paraffin hydrocarbons⁸; *i.e.*, it may fully inhibit one or more of the original chain-propagating steps but may replace them with one or more steps in which NO is a participant.

By carrying out experiments with reactor B, we have increased the surface-to-volume ratio by a factor of 2. A study of the rate was made at 1023°K. that revealed no effect of the S/V ratio. Variation of S/V by a factor of 2 is only a weak test for surface effects, but, if the reaction were controlled entirely by the surface, an effect surely would have been found. Problems with carbon formation and measurement of reactor volume prevented the performing of packed reactor experiments. Probably, stronger evidence against heterogeneous rate control is the observation of second-order kinetics.

The activation energy (*ca.* 40 kcal.) for C_4H_2 at low temperature may be compared with the figure for C_2H_2 (50 kcal.) under chain decomposition at low temperature.⁷ Having found similarities in the reaction order and chain character for decompositions of these two species, we propose that the reaction mechanisms may be analogous. If so, 40 kcal. probably represents an approximate figure for the energy of a low-lying triplet state of C_4H_2 ; *i.e.*, the essentials of the mechanism may be



(7) C. G. Silcocks, *Proc. Roy. Soc. (London)*, A242, 411 (1957).

(8) B. W. Wojciechowski and K. J. Laidler, *Trans. Faraday Soc.*, 59, 369 (1963).

by analogy to C_2H_2 .^{2b,c} Nitric oxide might have a weak effect in such a mechanism, in that it would be expected to remove $C_4H_2^*$ by an addition reaction, but the addition product would be a free radical. Furthermore, NO might catalyze the singlet-triplet transition in C_4H_2 .

It is difficult to draw upon product analyses for evidence regarding the mechanism. The result of a study, mainly by chromatography, of the product distributions at various temperatures is shown in Figure 3. Virtually no sooty carbon is formed in the pyrolysis of C_4H_2 under the conditions of our experiments. Only at the highest temperatures and larger concentrations ($>1\%$) was there any hint of sooting. It is of some interest to observe that over much of the temperature range covered, CH_4 is the dominant gaseous product. A parallelism is noted among the yields of CH_4 , C_2H_4 , and C_4H_4 , while another parallelism exists among $C(s)$, H_2 , and C_2H_2 . Not plotted in the figure are small quantities of methylacetylene and what seems to be methyldiacetylene, $CH_3C\equiv$

$C-C\equiv CH$. A polymer that was obtained in small yields has also been omitted. It is an intriguing substance in that it is extremely inert, chemically, and is insoluble in a wide variety of organic solvents. Its infrared absorption spectrum shows it to be essentially identical with the polymer obtained in the solution polymerization of C_4H_2 .⁹

Conclusions

The thermal decomposition kinetics of C_4H_2 exhibit a strong similarity to those of C_2H_2 . The decomposition is second order and homogeneous, exhibiting long chains at low temperature and a transition at higher temperatures that may lead eventually to nonchain behavior. The effect of NO is ambiguous. The mechanism may well be similar to that for C_2H_2 , in which case a triplet state of C_4H_2 appears to be located at about 40 kcal. above the ground state.

(9) N. L. Desai and P. H. Given, private communication, Department of Fuel Technology, Pennsylvania State University.

The Kinetics of Thermal Decomposition of Benzene in a Flow System

by K. C. Hou and H. B. Palmer

Department of Fuel Technology, College of Mineral Industries, The Pennsylvania State University, University Park, Pennsylvania (Received August 27, 1964)

Benzene in helium carrier gas has been decomposed at temperatures from 1173 to 1523°K. and at residence times from 20 to 250 msec., using a tubular flow reactor with a well-defined temperature plateau. The kinetics are complex, demonstrating mixed-order behavior with back reactions and wall effects. Sooting also causes enhancement of the rate. In the early stages of reaction, the decomposition kinetics are compatible with a treatment based upon mixed first- and second-order reactions. The first-order contribution appears to be an unusual chain that involves the wall in one chain-carrying step, while the second-order reaction is probably the homogeneous, bimolecular formation of biphenyl and hydrogen. The rate constant for the former is $k_I = 10^{9.15} \exp(-52 \text{ kcal./RT}) \text{ sec.}^{-1}$ while the latter is estimated to be $k_{II} = 10^{14} \exp(-40 \text{ kcal./RT}) \text{ cc./mole sec.}$

Introduction

As the simplest aromatic hydrocarbon, benzene has provided the point of departure for innumerable studies, theoretical and experimental, of molecular properties and reactions. It should likewise provide the starting point in a systematic understanding of thermal decompositions involving aromatics, and, indeed, it has been studied from time to time, *e.g.*, in connection with formation of surface carbon deposits¹⁻³ or with soot formation in diffusion flames.^{4,5} Kinetic studies have been carried out by Mead and Burk,⁶ Kinney and DelBel,⁷ Kinney and Slysh,⁸ and most recently by Bauer and Aten.⁹ Attempts to obtain rate constants were made mainly by the first and last of these. Slysh⁸ did obtain a rate constant, but only at one temperature (1473°K.). Mead and Burk studied the decomposition in a flow system over temperatures from 1023 to 1125°K. They treated the kinetics by means of the differential equation, $dx/dt = k(a - x)^2/x$, where a is the starting concentration and x/a is the fraction decomposed at time t . They used this equation because it suited the data and because they felt it made sense in terms of a bimolecular surface reaction that was strongly inhibited by products. The equation suffers from the severe defect that it predicts an infinite rate at the start of reaction, and we therefore do not believe that their rate constants are meaningful.

The work of Bauer and Aten was done with a shock

tube in connection with a study of the optical (2537-Å.) absorption coefficient of C₆H₆ at high temperatures. They measured the initial rate of reaction, and this fact, plus the use of a shock tube, guarantees that they measured a homogeneous reaction rate. Because they did not have information on the extinction coefficients of products, their rate information was confined to *relative* values. However, these covered a wide temperature range and provided, on a first-order treatment, a good estimate of the activation energy, putting it at about 40 kcal.

The present work stems not only from the intrinsic challenge of the problem but also from an interest in the rate of carbon formation and its relationship to the rates of decomposition of starting materials. A study by Murphy, Palmer, and Kinney¹⁰ provided

- (1) R. Iley and H. L. Riley, *J. Chem. Soc.*, 1362 (1948).
- (2) A. R. G. Brown and W. Watt, *Ind. Carbon Graphite, Papers Conf. London*, 86 (1958).
- (3) J. S. Conroy, R. S. Slysh, D. B. Murphy, and C. R. Kinney, *Proc. Conf. Carbon, 3rd., Buffalo, 1957*, 395 (1959).
- (4) N. Thorp, R. Long, and F. H. Garner, *Fuel*, **30**, 266 (1951).
- (5) W. G. Parker and H. G. Wolfhard, *J. Chem. Soc.*, 2038 (1950).
- (6) F. C. Mead and R. E. Burk, *Ind. Eng. Chem.*, **27**, 299 (1935).
- (7) C. R. Kinney and E. DelBel, *ibid.*, **46**, 548 (1954).
- (8) C. R. Kinney and R. S. Slysh, *Proc. Conf. Carbon, 4th, Buffalo, 1957*, 301 (1960).
- (9) S. H. Bauer and C. F. Aten, *J. Chem. Phys.*, **39**, 1253 (1963).
- (10) D. B. Murphy, H. B. Palmer, and C. R. Kinney, *Ind. Carbon Graphite, Papers Conf. London*, 77 (1958).

precise information on the rate of carbon film deposition from benzene and could be reasonably interpreted in terms of the rate of decomposition of benzene; however, reliable independent information on this rate was not available and was clearly needed, not only for this purpose but also because of a wish to understand the ease with which benzene forms carbon black.

Experimental

Apparatus and Procedure. The pyrolysis chamber for the flow system used in most of the work (reactor A) was a mullite combustion tube of 5-mm. i.d. The furnace had an over-all length of 66 cm. with a 25.4-cm., essentially uniform hot zone. The current input to the furnace was first led through a rheostat into the control circuit consisting of an on-off switch, pilot light, ammeter, and a mercury relay. This was actuated by a Leeds and Northrup Speedomax indicating controller operating from the thermocouple situated in the center of the heating chamber. The temperature so controlled was maintained within $\pm 1^\circ$. The apparatus was operated at atmospheric pressure, using helium as a diluent and carrier gas. Its rate of flow was controlled by Sho-Rate flowmeters equipped with differential relays. The purity of helium was ensured by passing the gas first through a copper furnace at 500° to remove oxygen and then through absorption towers filled with Anhydrone and Ascarite to remove water and carbon dioxide.

A spectroscopic grade of benzene was evaporated into the furnace by bubbling a portion of helium through a sample flask, the temperature of which was maintained at $14.0 \pm 0.1^\circ$ by circulating water from a constant temperature bath through the outer jacket. The benzene vapor was then routed into the main helium stream. After combining the two gases, the mixture was passed through a multiple loop packed with glass wool to ensure homogeneous mixing. The rate of evaporation was controlled by the bath temperature and the helium flow rate. By adjusting the flow rate of the two helium streams, the desired contact time and the concentration of benzene in the reaction zone was obtained. The total pressure in all runs was 735 ± 5 torr. Normally, the temperature profile for each experimental condition was determined by inserting a platinum-platinum-10% rhodium thermocouple into the pyrolysis tube from the downstream side. The thermocouple used in these measurements was calibrated against a certified platinum-platinum-10% rhodium thermocouple purchased from The Thermoelectric Co.

To test the heterogeneity of the reaction, a four-hole reactor (B) with 0.24-cm. i.d. per hole was used to

replace the 0.5-cm. tube. This increased the surface-to-volume ratio by a factor of about 2.

Analysis. A Perkin-Elmer Model 154-C vapor fractometer was used for identification of products and measurement of the rate of benzene decomposition. The input or effluent gas streams could be directly flushed through a gas-sampling valve. A comparison of the benzene content of two such gas samples provided a direct measure of the extent of decomposition. The exhaust gas was first quenched by cooling water and was passed through a multiple loop installed downstream of the furnace to ensure that it reached room temperature before the sample was taken. Dinonyl phthalate, obtained from Eastman Organic Chemicals, was used as adsorbant in the separating column. A 1-m. column was used for the analysis of benzene at 45° column temperature and 50-cc./min. helium flow. The retention distance of benzene from sample injection was 3 cm.

Results and Discussion

Typical temperature profiles of the two reactors for the same temperature setting are illustrated in Figure 1. These are measured gas temperatures under flow conditions (with He) comparable to those in the kinetic runs. The complete profiles were determined for most of the temperature settings used in kinetic runs. They possessed well-defined plateaus in all cases and were found to be essentially independent of flow velocity, from which it is inferred that the thermocouple was reading the gas temperature. The plateaus

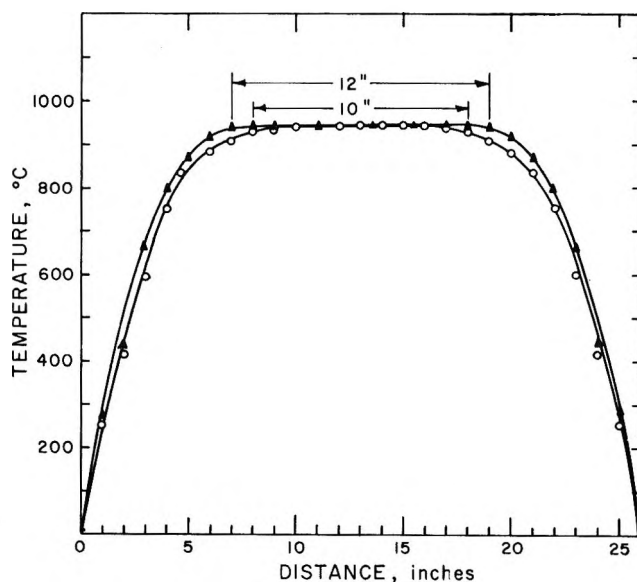


Figure 1. Temperature profiles for a controller setting of 946° : open circles, reactor A (5-mm. i.d.); black triangles, reactor B (4 holes, 2.4-mm. i.d. each).

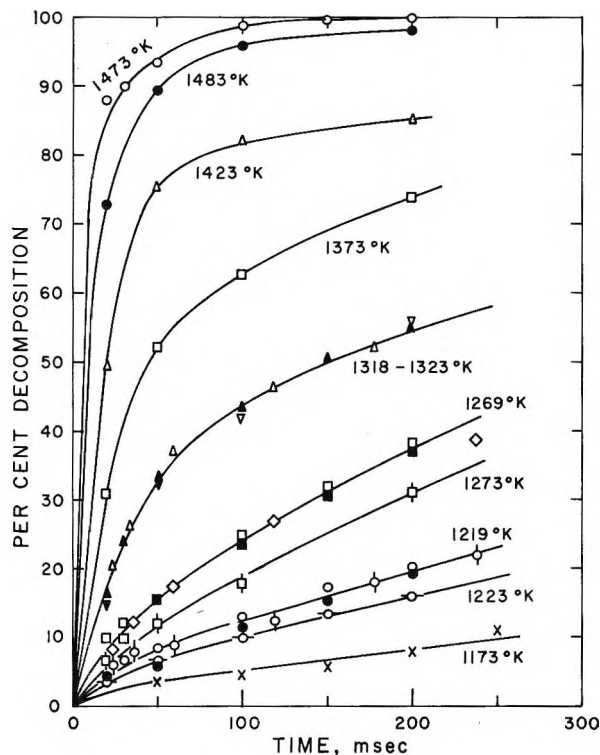


Figure 2. Per cent decomposition as a function of time, at ten temperatures, for a starting concentration of 1 mole % of C_6H_6 . Different symbols are used to distinguish duplicate runs made at the same temperature (1219, 1269, and 1318-1323°K.).

were long enough that the end effect was very small; nevertheless, an allowance was made for this by extending the effective hot zone 2.54 cm. beyond the plateau on both the input end and the output end of the reactor.

Plug flow was assumed; *i.e.*, the reaction time was taken to equal the average residence time of an element of gas in the reactor. Although the flow was laminar, the plug flow assumption was adequate. This can be shown by considering the average diffusion time for a molecule in the tube to reach the wall. With a helium carrier, this time was of the order of 4×10^{-3} sec. for reactor A and 10^{-3} sec. for reactor B. The shortest residence time studied was 20×10^{-3} sec., for which there may have been a moderate nonuniformity of composition in the radial direction for reactor A. However, the agreement in results between reactors A and B supports the conclusion that the nonuniformity was slight.

Plots of the % decomposition as a function of time are shown in Figure 2, for a starting concentration of 1% C_6H_6 in He. Some inconsistency in temperatures is noted. This is probably attributable to placing too much reliance upon the calibration of the temperature

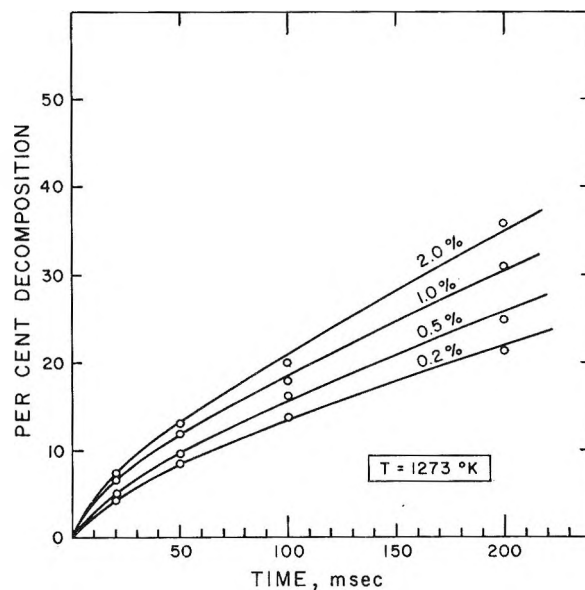


Figure 3. Per cent decomposition as a function of time at 1273°K., showing the effect of variations in the starting concentration.

controller in several of the earlier experiments. In the absence of information on this point, all experiments are included, and an uncertainty of about $\pm 10^\circ K.$ is assigned to the reported temperatures.

At each temperature, several concentrations were studied. A plot showing the concentration effect at one temperature appears in Figure 3. A somewhat more convenient way of showing concentration effects is to plot the % decomposition at fixed residence time *vs.* the mole % of C_6H_6 at a series of temperatures. Such a plot is given for two temperatures in Figure 4.

Some qualitative conclusions may be drawn from the several plots: (a) the finite intercepts in Figure 4 show that there is a first-order contribution to the rate; (b) the finite slopes in the same figure show that there are higher order reactions occurring; (c) however, the shapes of these plots and also of the plots in Figure 2 show that the order is not simple; (d) in particular, one sees shoulders on the plots in Figure 2 that imply significant contributions from back reactions, but equilibrium is not attained; this suggests that, although there is a *tendency* toward equilibration, decomposition of reaction products prevents it; (e) heterogeneous contributions to the decomposition rate appear to be small; this is implied by the plots for $T = 1219, 1269,$ and $1318-1323^\circ K.$, which include points for both reactors A and B.

Because of the complications presented by back-reactions and decomposition of products, quantitative information on rate constants can be obtained most

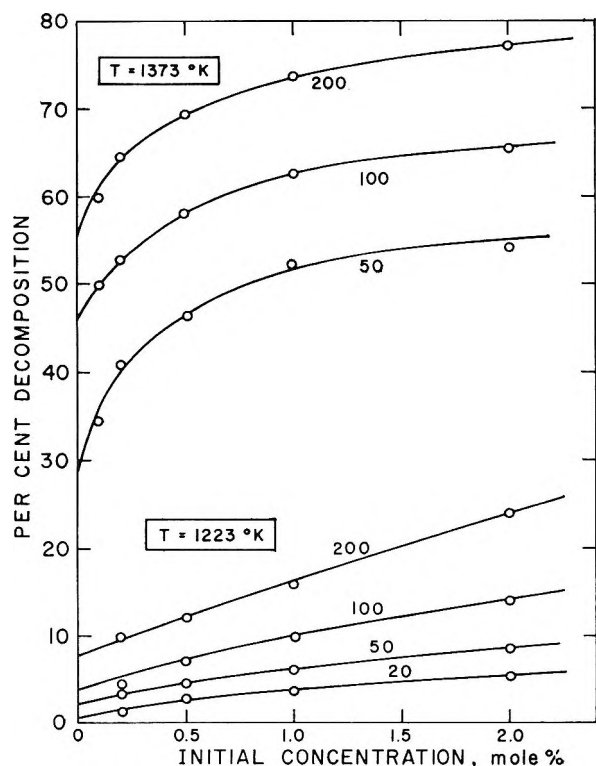


Figure 4. Cross plots of data at 1223 and 1373°K., showing the per cent decomposition as a function of initial concentration, at fixed residence times. The times (in msec.) are indicated on the curves.

readily by using data at short times. Initial slopes could be employed, but better accuracy is available by observing the extent of reaction over short times and comparing this with an integrated expression for a mixed-order reaction. For the latter, we have used an assumed mixture of first- and second-order kinetics. There clearly is a first-order contribution. As for the higher order contribution(s), the data are not sufficiently detailed or sufficiently accurate to permit one to write $-dC/dt = k_1C + k_nC^n$ and determine n by curve-fitting. Instead, one hopes to choose the correct n and justify the choice later by examining the consequences.

Actually, there are some grounds for choice: (a) among homogeneous gaseous reactions of higher order, $n = 2$ is very frequent, $n = 3/2$ is fairly common, and other values are rare; (b) dating clear back to the work of Bertholet (as discussed by Mead and Burk⁶), it has been known that the main products of benzene pyrolysis at low temperatures are biphenyl and hydrogen. The first thought that occurs to one is the suitability of the reaction $2C_6H_6 \rightarrow C_{12}H_{10} + H_2$ as a means of producing biphenyl. If, as seems possible, this is a

straightforward, four-center reaction, it should be second order.

With $n = 2$, we have

$$-dC/dt = k_1C \text{ and } k_{II}C^2 \quad (1)$$

as the rate equation. This can be integrated to give

$$-\ln(C/C_0) = k_1t + \ln[(1 + qC_0)/(1 + qC)] \quad (2)$$

where $q = k_{II}/k_1$. For convenience, this can be written as

$$-\ln(C/C_0) = k_1t + \ln W \quad (3)$$

where $W = (1 + qC_0)/(1 + qC)$. One can now use experimental determinations of (C/C_0) corresponding to two values of C_0 , at fixed time, and determine both k_1 and the ratio of the W values. From the latter, one can determine q and then k_{II} .

The results of this treatment at $t = 0.020$ sec. are tabulated in Table I, and an Arrhenius plot of the rate constants appears in Figure 5. The figure includes some additional data from other sources which will be discussed later. The short time, 0.020 sec., was chosen for the calculations in the hope of minimizing the

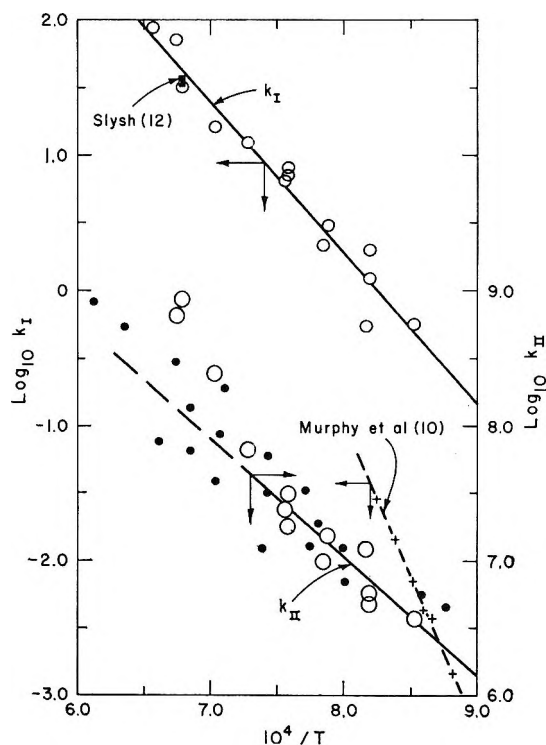


Figure 5. Arrhenius plot of k_I and k_{II} , in units of sec.^{-1} and cc./mole-sec. , respectively. Arrows on the lines indicate the scale to be used: open circles, present results; black circles, normalized data of Bauer and Aten.⁹ Results of Murphy, *et al.*,¹⁰ from carbon deposition kinetics are also included, for comparison.

effects of back-reactions. In the absence of knowledge concerning their rates, the success of the treatment can be judged only by the self-consistency of the resulting rate constants. The first-order values, which are the more reliable of the two, seem to behave well. The k_{II} values at higher temperatures lie above the line that best satisfies the lower temperature results. This divergence is almost certainly due to sooty carbon formation in the gas phase, which was severe at higher temperatures when the concentration exceeded about 0.1%. Because the sooting tendency was a function of concentration, it rendered determination of k_{II} very unreliable; k_I , on the other hand, could be calculated quite well under these conditions because it involved essentially the modest correction from 0.1% to infinite dilution.

Table I: Rate Constants Computed from the Data at $t = 0.020$ Sec. by Means of Eq. 3

$T, ^\circ\text{K.}$	$10^4/T$	$k_I, \text{sec.}^{-1a}$	$k_{II}, \text{cc./mole sec.}^a$
1173	8.53	0.56	3.6×10^6
1219	8.20	1.23 (A)	4.8×10^6 (A)
		2.01 (B)	5.5×10^6 (B)
1223	8.17	0.55	1.2×10^7
1269	7.88	3.05	1.5×10^7
1273	7.85	2.13	0.98×10^7
1318	7.59	7.2 (B)	2.1×10^7 (B)
		7.4 (A)	1.8×10^7 (A)
1323	7.56	6.6	2.4×10^7
1373	7.28	12.3	6.6×10^7
1423	7.03	16.3	2.46×10^8
1473	6.79	32.5	8.7×10^8
		35 ^b	
1483	6.74	70.5	6.45×10^8
1523	6.56	88.5 ± 20	...

^a (A) and (B) refer to the two reactors. ^b Corrected to initial rate; from R. S. Slysh, Ph.D. Dissertation, Department of Fuel Technology, The Pennsylvania State University, 1960.

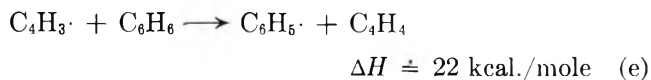
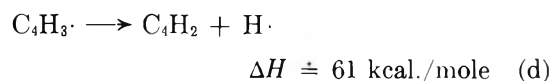
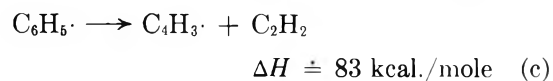
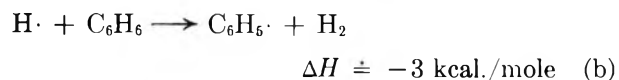
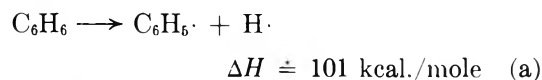
It should be remarked that a mixed first-order-three-halves-order treatment of the data yielded a negative k_I at 1173°K. and erratic values at higher temperatures [e.g., k_I (1373°K.) \neq k_I (1483°K.)] without appreciably improving (i.e., straightening) the Arrhenius plot for the higher order contribution.

The Arrhenius expressions for the lines (drawn by eye) in Figure 5 are $k_I = 10^{9.16} \exp(-51.9 \text{ kcal./RT}) \text{ sec.}^{-1}$ and $k_{II} = 10^{14.0} \exp(-40.0 \text{ kcal./RT}) \text{ cc./mole sec.}$

The slope of the line for k_{II} was not determined statistically from the data, but was chosen as a convenient value that was compatible with the lower

temperature results. Its choice was influenced by three considerations: (a) the recent shock tube work by Bauer and Aten⁹ yields an activation energy of the order of 40 kcal.; (b) the A-factor that results is typical of four-center reactions, which is the class to which we believe reaction II belongs; (c) the straight line that is most compatible with *all* results for k_{II} has a slope corresponding to $E \approx 60$ kcal. and an A factor of about 10^{17} cc./mole sec. This activation energy can be rationalized, but the A factor is impossibly large for a bimolecular reaction. We have not been able to construct a second-order chain reaction that will give an unusually large A factor.

The activation energy of the first-order reaction, 52 kcal., is too low to be reconciled with simple unimolecular decomposition, or even with decomposition in which rate control rests in excitation to the triplet state at 83 kcal. The first-order reaction is almost certainly a chain. Bauer and Aten,⁹ reporting first-order decomposition kinetics for benzene in shock waves, have postulated a chain mechanism consisting essentially of the following steps

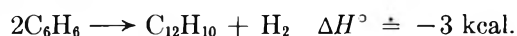


plus terminating radical recombinations. The steps involved all appear quite reasonable. However, while a steady-state treatment of this chain shows that one can obtain first-order kinetics by choosing the terminations properly, one cannot obtain a low activation energy. The main problem is that phenyl radicals are too stable in the gas phase.

The answer to this problem may be that phenyl radicals decompose on the reactor wall. This raises the immediate objection that Bauer and Aten used a shock tube in their study, and, hence, a heterogeneous step involving the wall is ruled out. However, re-examination of their data¹¹ reveals that the scatter in their rate

(11) We are indebted to Dr. Carl Aten for supplying further information on shock conditions that permitted these calculations to be performed.

constants is appreciably reduced when they are treated as second order rather than first. These second-order values are the black circles in Figure 5, normalized (they reported only *relative* rate constants, not absolute values) so as to provide values comparable to our own values for k_{11} . Their data seem to support the 40-kcal. Arrhenius slope, with perhaps some tendency to drift above it at higher temperatures. The difference in techniques (they looked at initial reaction rates) lends support to our attribution of high k_{11} values at high temperatures to sooting in the gas stream. Further support for interpreting their results as simple second order is provided by their failure to observe an induction period. We therefore suggest that k_{11} is the rate constant for



Biphenyl is, as mentioned earlier, the dominant product of low-temperature pyrolysis, which is consistent with this interpretation.

Now, in the first-order chain, modification of step c in the Bauer and Aten mechanism to provide heterogeneous decomposition of phenyl on the wall can yield an over-all activation energy of the order of 55 kcal., which is well within the uncertainty of our experimental results. The new step c might well be diffusion

controlled and exhibit an effective activation energy of only a few kcal. The products of the heterogeneous decomposition are not known; however, it is only necessary to assume that some radical is returned to the gas phase and participates in further steps of the type represented by reaction e.

There are some difficulties with this scheme: for example, heterogeneity of step c requires that there be an effect of tube diameter upon the rate. Our experimental data concerning this point (Table I) are ambiguous. A second difficulty is that the first-order rate constants do not agree with the first-order results of Murphy, *et al.*,¹⁰ obtained from studies of carbon film deposition. These are included in Figure 5. The discrepancy probably means that the kinetics of carbon deposition are not related in a simple way to the rate of the first step in the pyrolysis. Further shock tube studies of benzene by Aten¹² may help to clear up some of these questions.

Acknowledgments. We are very much indebted to the J. M. Huber Corp. for its generous support of this work.

(12) C. F. Aten, private communication, Department of Chemistry, Hobart College, Geneva, N. Y.

Transport Properties of a Dense Fluid of Molecules Interacting with a Square-Well Potential

by H. Ted Davis and K. D. Luks

*Department of Chemical Engineering, University of Minnesota, Minneapolis, Minnesota
(Received August 28, 1964)*

The theory developed by Davis, Rice, and Sengers¹ for the transport properties of a model fluid whose molecules interact according to a square-well potential is outlined herein and numerical computations based on the theory are presented. A perturbation technique is given for obtaining the equilibrium pair correlation function using the correlation function of hard spheres as the unperturbed term. Numerical calculations are performed for liquid argon leading to the conclusion that the square-well model furnishes a good first approximation to simple liquids. Also examined is a modified hard-sphere theory whereby the basic mechanism of transport is assumed to arise from hard-core collisions while the attractive interactions increase the effective collision cross section by increasing the magnitude of the pair correlation function. This modified hard-sphere theory is much better than the unmodified hard-sphere theory.

I. Introduction and Remarks

In recent years many investigators have attempted to develop a kinetic theory of liquids and dense gases which would have the same simplicity and degree of rigor enjoyed by the kinetic theory of dilute gases. The general approach to this problem has been to try to obtain, from the Liouville equation for the N -body distribution function, kinetic equations or equations of change for the singlet distribution function $f(\mathbf{R}_1, \mathbf{p}_1; t)$ and the doublet distribution function $f_2(\mathbf{R}_1, \mathbf{R}_2, \mathbf{p}_1, \mathbf{p}_2; t)$, where \mathbf{R}_i and \mathbf{p}_i are, respectively, the position and momentum of the i th particle in an N -particle system. The singlet distribution function for particle i denotes the probability of finding at time t the i th particle at position \mathbf{R}_i with momentum \mathbf{p}_i regardless of the state of the other particles in the system, while the doublet distribution function denotes the probability of finding at time t two particles i and j at positions \mathbf{R}_i and \mathbf{R}_j with momenta \mathbf{p}_i and \mathbf{p}_j regardless of the state of the other particles in the system.

The most general kinetic theory of dense fluids to date based on the Liouville equation is the theory begun by Kirkwood² and later extended by his co-workers. Kirkwood took the Liouville equation as a starting point and derived a Fokker-Planck type trans-

port equation for liquids. He introduced a dissipative mechanism (which in the case of a dilute gas is the binary collision) by time-smoothing reduced distribution functions (*e.g.*, the singlet and doublet distribution functions) over an interval of time τ , where τ is macroscopically short but microscopically long. That is, τ must be long relative to the interval during which there is appreciable correlation between the total intermolecular force acting upon a specified molecule at the beginning and end of that interval. Using analogies to the theory of Brownian motion, Kirkwood was able to derive a Fokker-Planck equation in which a friction constant ζ is to be identified with the phenomenological friction coefficient appearing in the Langevin equation. The friction constant is defined in terms of the intermolecular interactions averaged in time over τ and over an equilibrium ensemble in phase space. Using the Fokker-Planck equation (for both the singlet and doublet distribution functions) all the transport properties of a system of molecules can be found in terms of ζ and the local thermodynamic variables of the system. Thus, in principle, the transport proper-

(1) H. T. Davis, S. A. Rice, and J. V. Sengers, *J. Chem. Phys.*, **35**, 2210 (1961).

(2) J. G. Kirkwood, *ibid.*, **14**, 180 (1946).

ties of a fluid are determined simply by evaluating ζ , a task not at all easy for liquids, however.

The biggest criticism to be levied against Kirkwood's theory is that he had to assume that the momentum exchange between particles is small during the time interval τ ; that is, it was assumed that molecules moved through the fluid experiencing small random deflections. Clearly, this assumption excludes the possibility of core collisions (strong short-range repulsive interactions) between molecules resulting in strong deflections of the interacting molecules. Rice and Allnatt^{3,4} have developed a theory which avoids the difficulty encountered by Kirkwood's theory. They have assumed that a molecule moving through a dense fluid will undergo a motion in which it experiences a rigid-core collision followed by a "Brownian motion" during which it undergoes small random deflections due to the soft attractive interactions with its neighbors. Thus the motion is determined by rigid-core collisions between which "Brownian motion" occurs. Rice and Allnatt subsequently obtained a modified Boltzmann equation in which the hard-core collisions were treated as in the theory of the dense rigid-sphere fluid while the soft attractive interactions were handled in the Fokker-Planck approximation.

Several numerical comparisons of theory and experiment^{5,6} indicate that the Rice-Allnatt theory gives indeed a quantitative description of transport in simple liquids. However, in order to calculate the transport coefficients from the Rice-Allnatt theory, one must have accurate values for the intermolecular potential and, more importantly, one must know quantitatively the equilibrium correlation function as a function of the intermolecular distance at various temperatures and pressures. This latter demand is rather hard to meet since the pair correlation function has not been determined very accurately experimentally and the theoretical methods are still approximate and difficult.

The practical difficulties involved in utilizing the more rigorous Rice-Allnatt theory seem to justify the exploitation of models which are cruder representations of reality but which can be treated more easily and exactly mathematically. Rigid spheres are the simplest molecules, but having no attractive interaction, they are missing one of the major features of a real liquid. Thus the next simplest choice is the "square-well" model fluid composed of particles which interact as rigid spheres at an intermolecular distance of say σ_1 , have a constant attractive potential energy ϵ for intermolecular distances between σ_1 and σ_2 , and do not interact for intermolecular distances greater than σ_2 .

Recently, Davis, Rice, and Sengers¹ derived a modi-

fied Boltzmann equation for a "square-well" fluid, from which they were able to formulate in analytic form the coefficient of viscosity and thermal conductivity. In sections II and III we outline briefly their work, giving also the self-diffusion coefficient for a "square-well" fluid which was obtained by Longuet-Higgins and Valleau.⁷ In the remaining sections are presented numerical computations of the transport coefficients for liquid argon for a rather wide range of temperature and pressure (87–150°K. and 1–500 atm.). The results are encouraging, indicating that the "square-well" fluid furnishes an adequate first approximation to a real liquid.

In section V we made the interesting observation that in the case of the square-well model the major function of the attractive potential is to increase the magnitude of the pair correlation function while the transport of energy and momentum proceeds chiefly *via* rigid-sphere collisions.

In section VI it was demonstrated that a very simple perturbation theory allows for theoretical determination of the pair correlation function for the square-well model. The analysis makes use of the exact solution, for the case of hard spheres, to the Percus-Yevick integral equation for equilibrium pair correlation function.^{8,9} Thusly predicted values for the correlation function lead to quite accurate estimates of the transport properties of argon based on the square-well model.

In view of the calculations herein, we feel that the formulas given in section II for the transport coefficients (at least for viscosity and thermal conductivity) plus the technique employed in section VI for obtaining the pair correlation function constitute reliable formulas for the calculation of the transport properties of simple dense fluids and liquids. The potential parameters σ_1 , σ_2 , and ϵ must of course be obtained by measurement. The parameters used for this work were determined from virial coefficient data on gaseous argon. We have carefully examined argon and obtained promising results, but it goes without saying that other systems may not behave so conveniently. We hope to investigate several other liquids in the future.

- (3) S. A. Rice and A. R. Alnatt, *J. Chem. Phys.*, **34**, 2144 (1961).
- (4) A. R. Alnatt and S. A. Rice, *ibid.*, **34**, 2156 (1961).
- (5) L. D. Ikenberry and S. A. Rice, *ibid.*, **39**, 1561 (1963).
- (6) J. Naghizadeh and S. A. Rice, *ibid.*, **36**, 2710 (1962).
- (7) H. C. Longuet-Higgins and J. P. Valleau, *Mol. Phys.*, **1**, 284 (1956).
- (8) M. S. Wertheim, *Phys. Rev. Letters*, **10**, 321 (1963).
- (9) E. Thiele, *J. Chem. Phys.*, **39**, 474 (1963).

II. Transport Equation for a Dense Fluid of Molecules Interacting with a Square-Well Potential

A “square-well” fluid is defined as one composed of N particles which interact according to the pair potential

$$\begin{aligned} V(R_{ij}) &= 0 & R_{ij} > \sigma_2 \\ V(R_{ij}) &= -\epsilon & \sigma_1 < R_{ij} \leq \sigma_2 \\ V(R_{ij}) &= +\infty & R_{ij} \leq \sigma_1 \end{aligned} \tag{2-1}$$

where R_{ij} is the distance of separation of particles i and j . By definition, the force between square-well molecules is impulsive, *i.e.*, any collision occurs instantaneously. This is in fact the simplifying feature of the square-well interaction. In real liquids or dense fluids, a molecule is in continuous interaction with many molecules in the surrounding medium. Consequently, the concept of transport by binary collision, which has proved so useful in the analysis of transport properties of dilute gases, is not obviously relevant to the theory of transport in dense fluids. However, since collisions occur instantaneously in a “square-well” fluid, one may anticipate that energy and momentum exchange in these fluids, even at high densities, proceeds *via* binary collisions. In support of this thesis, one argues that in order for a molecule to experience a ternary collision, two other molecules must be at *exactly* the right points in space (either at $R_{ij} = \sigma_1$ or σ_2) at *exactly* the same instant. The likelihood of this simultaneous occurrence is very small compared to that of a binary event which requires only that a second molecule move within a distance σ_1 or σ_2 of the first molecule. The possibility of a higher order collision than ternary would presumably be even more remote on the basis of the preceding argument.

Thus, although the square-well potential is a crude representation of reality, it does have the features necessary to describe a real fluid, namely an attractive part plus a repulsive part. Furthermore, due to the singular nature of the square-well potential, calculations can be extended quite far by relatively simple means so that it should prove quite useful to study the transport properties of dense fluids for this model.

In a recent work, Davis, Rice, and Sengers¹ (DRS) have derived a modified Maxwell-Boltzmann integro-differential equation for the case of a dense “square-well” fluid. We shall follow more or less their work herein. Noting that, due to the discontinuous nature of the square-well potential, momentum and energy exchanges occur only at $R_{12} = \sigma_1$ and $R_{12} = \sigma_2$, they divided the collision integral into four parts representing the four types of binary encounter possible for the square-well potential.

Type 1. When two particles collide at a distance equal to the repulsive diameter σ_1 , they will exchange energy and momentum in the same manner as rigid spheres.

Type 2. When two particles approach each other from a distance greater than the attractive diameter σ_2 , they will experience a sudden increase in velocity and kinetic energy due to an amount of potential energy ϵ being converted into kinetic energy.

Type 3. When two particles, initially moving apart with relative kinetic energy greater than ϵ , reach the separation σ_2 , relative kinetic energy of amount ϵ will instantaneously be converted to potential energy.

Type 4. When two particles moving apart have a relative kinetic energy less than ϵ , the relative velocity is simply reversed with the conservation of kinetic energy and momentum.

Longuet-Higgins and Valleau⁷ have calculated a zeroth approximation to the transport coefficients using the same division of collisions for a square-well model. Their results will be mentioned later.

Of course, momentum and total energy are conserved for each of the partial collisions (1) through (4). In terms of the above four types of collision, DRS obtained, for a one-component system, the following modified Maxwell-Boltzmann equation for the singlet distribution function

$$\frac{\partial f}{\partial t}(\mathbf{R}_1, \mathbf{p}_1; t) + \frac{\mathbf{p}_1}{m} \cdot \nabla_{\mathbf{R}_1} f(\mathbf{R}_1, \mathbf{p}_1; t) = J(f) \tag{2-2}$$

where the collision integral $J(f)$ is defined as

$$\begin{aligned} J(f) &= \sigma_1^2 \iint_{\mathbf{g} \cdot \mathbf{k} > 0} [g(\mathbf{R}_1, \mathbf{R}_1 + \sigma_1 \mathbf{k})f(\mathbf{R}_1, \mathbf{p}_1 - \Delta \mathbf{p}_1^{(1)}; t)f(\mathbf{R}_1 + \\ &\sigma_1 \mathbf{k}, \mathbf{p}_2 - \Delta \mathbf{p}_2^{(1)}; t) - g(\mathbf{R}_1, \mathbf{R}_1 - \sigma_1 \mathbf{k})f(\mathbf{R}_1, \mathbf{p}_1; t)f(\mathbf{R}_1 - \\ &\sigma_1 \mathbf{k}, \mathbf{p}_2; t)] \mathbf{g} \cdot \mathbf{k} d\mathbf{k} d\mathbf{p}_2 + \sigma_2^2 \iint_{\mathbf{g} \cdot \mathbf{k} > 0} [g^*(\mathbf{R}_1, \mathbf{R}_1 + \sigma_2 \mathbf{k})f(\mathbf{R}_1, \mathbf{p}_1 - \\ &\Delta \mathbf{p}_1^{(2)}; t)f(\mathbf{R}_1 + \sigma_2 \mathbf{k}, \mathbf{p}_2 - \Delta \mathbf{p}_2^{(2)}; t) - \\ &g(\mathbf{R}_1, \mathbf{R}_1 - \sigma_2 \mathbf{k})f(\mathbf{R}_1, \mathbf{p}_1; t)f(\mathbf{R}_1 - \sigma_2 \mathbf{k}, \mathbf{p}_2; t)] \mathbf{g} \cdot \mathbf{k} d\mathbf{k} d\mathbf{p}_2 + \\ &\sigma_2^2 \iint_{\mathbf{g} \cdot \mathbf{k} < -\left(\frac{4\epsilon}{m}\right)^{1/2}} [g(\mathbf{R}_1, \mathbf{R}_1 + \sigma_2 \mathbf{k})f(\mathbf{R}_1, \mathbf{p}_1 - \Delta \mathbf{p}_1^{(3)}; t)f(\mathbf{R}_1 + \\ &\sigma_2 \mathbf{k}, \mathbf{p}_2 - \Delta \mathbf{p}_2^{(3)}; t) - g^*(\mathbf{R}_1, \mathbf{R}_1 - \sigma_2 \mathbf{k})f(\mathbf{R}_1, \mathbf{p}_1; t)f(\mathbf{R}_1 - \\ &\sigma_2 \mathbf{k}, \mathbf{p}_2; t)] \mathbf{g} \cdot \mathbf{k} d\mathbf{k} d\mathbf{p}_2 + \sigma_2^2 \iint_{-\left(\frac{4\epsilon}{m}\right)^{1/2} < \mathbf{g} \cdot \mathbf{k} < 0} [g^*(\mathbf{R}_1, \mathbf{R}_1 + \\ &\sigma_2 \mathbf{k})f(\mathbf{R}_1, \mathbf{p}_1 - \Delta \mathbf{p}_1^{(4)}; t)f(\mathbf{R}_1 + \sigma_2 \mathbf{k}, \mathbf{p}_2 - \\ &\Delta \mathbf{p}_2^{(4)}; t) - g^*(\mathbf{R}_1, \mathbf{R}_1 - \sigma_2 \mathbf{k})f(\mathbf{R}_1, \mathbf{p}_1; t)f(\mathbf{R}_1 - \\ &\sigma_2 \mathbf{k}, \mathbf{p}_2; t)] \mathbf{g} \cdot \mathbf{k} d\mathbf{k} d\mathbf{p}_2 \end{aligned} \tag{2-3a}$$

The quantities \mathbf{R}_i , \mathbf{p}_i , and m appearing in eq. 2-2 and 2-3a are, respectively, the position, momentum, and mass of the i th particle. $\mathbf{g} = [(\mathbf{p}_1/m) - (\mathbf{p}_2/m)]$

is the relative velocity of particles 1 and 2, \mathbf{k} is a unit vector in the direction of their line of centers at the instant of collision, and $d\mathbf{k}$ is the differential solid angle. In eq. 2-3a, the pair correlation function $g(\mathbf{R}_1, \mathbf{R}_2, \mathbf{p}_1, \mathbf{p}_2; t)$ has been approximated by the local equilibrium pair correlation function $g(\mathbf{R}_1, \mathbf{R}_2)$. Throughout eq. 2-3a, the position vector \mathbf{R}_2 is evaluated at the contact position for the particular partial collision considered, e.g., $g(\mathbf{R}_1, \mathbf{R}_1 + \sigma_1 \mathbf{k})$ denotes the pair correlation function for particles 1 and 2 when particle 2 is found at position $\sigma_1 \mathbf{k}$ relative to the position of particle 1. $g(\mathbf{R}_1, \mathbf{R}_1 + \sigma_2 \mathbf{k})$ is the pair correlation function at $\sigma_2 + \delta$ and $g^*(\mathbf{R}_1, \mathbf{R}_1 + \sigma_2 \mathbf{k})$ is the pair correlation function at $\sigma_2 - \delta$ with $\delta \rightarrow 0+$. Under the assumption that $g(\mathbf{R}_1, \mathbf{R}_2)$ is the local equilibrium pair correlation function, we have the relation $g(\mathbf{R}_1, \mathbf{R}_1 + \sigma_2 \mathbf{k})/g^*(\mathbf{R}_1, \mathbf{R}_1 + \sigma_2 \mathbf{k}) = \exp(-\epsilon/kT)$.

For each of the four collision integrals of eq. 2-3a, one can calculate the momentum change from the binary dynamics of the four different types of collision.

Type 1. $\mathbf{g} \cdot \mathbf{k} > 0$

$$\Delta \mathbf{p}_1^{(1)} = \mathbf{p}_1 - \mathbf{p}_1' = -m(\mathbf{g} \cdot \mathbf{k})\mathbf{k} \quad (2-3b)$$

Type 2. $\mathbf{g} \cdot \mathbf{k} > 0$

$$\Delta \mathbf{p}_1^{(2)} = \frac{m}{2} \left\{ -\mathbf{g} \cdot \mathbf{k} + \sqrt{(\mathbf{g} \cdot \mathbf{k})^2 + \frac{4\epsilon}{m}} \right\} \mathbf{k} \quad (2-3c)$$

Type 3. $\mathbf{g} \cdot \mathbf{k} < -(4\epsilon/m)^{1/2}$

$$\Delta \mathbf{p}_1^{(3)} = -\frac{m}{2} \left\{ \mathbf{g} \cdot \mathbf{k} + \sqrt{(\mathbf{g} \cdot \mathbf{k})^2 - \frac{4\epsilon}{m}} \right\} \mathbf{k} \quad (2-3d)$$

Type 4. $-(4\epsilon/m)^{1/2} < \mathbf{g} \cdot \mathbf{k} < 0$

$$\Delta \mathbf{p}_1^{(4)} = -m(\mathbf{g} \cdot \mathbf{k})\mathbf{k} \quad (2-3e)$$

The constraint $\mathbf{g} \cdot \mathbf{k} > 0$ for types 1 and 2 indicate that the particles are initially approaching each other. The constraint $\mathbf{g} \cdot \mathbf{k} < -(4\epsilon/m)^{1/2}$ indicates that for a type 3 collision the particles are initially moving apart with a relative kinetic energy greater than ϵ , while for a type 4 collision, $-(4\epsilon/m)^{1/2} < \mathbf{g} \cdot \mathbf{k} < 0$ indicates that the particles are moving apart and have a relative kinetic energy less than ϵ . Finally, one should recall that $\Delta \mathbf{p}_1^{(i)} = -\Delta \mathbf{p}_2^{(i)}$ because of the conservation of momentum.

Equation 2-2 was linearized by a procedure following the Chapman-Enskog¹⁰ solution of the Maxwell-Boltzmann equation. The singlet distribution function was written as

$$f = f_0(1 + \phi) \quad (2-4)$$

where f_0 is the local equilibrium singlet distribution function defined by the relation

$$f_0 = \rho(2\pi mkT)^{-3/2} \exp \left[-\frac{(\mathbf{p}_1 - m\mathbf{u})^2}{2mkT} \right] \quad (2-5)$$

In this expression ρ , T , and \mathbf{u} represent, respectively, the local values of the number density, temperature, and hydrodynamic velocity. These quantities are defined in the usual manner by

$$\rho(\mathbf{R}_1; t) = \int f_0(\mathbf{R}_1, \mathbf{p}_1; t) d\mathbf{p}_1$$

$$\rho(\mathbf{R}_1; t)\mathbf{u}(\mathbf{R}_1; t) = \int \frac{\mathbf{p}_1}{m} f_0(\mathbf{R}_1, \mathbf{p}_1; t) d\mathbf{p}_1$$

$${}^{3/2}\rho(\mathbf{R}_1; t)kT(\mathbf{R}_1; t) =$$

$$\int {}^{1/2} \left[\frac{\mathbf{p}_1}{m} - \mathbf{u} \right]^2 f_0(\mathbf{R}_1, \mathbf{p}_1; t) d\mathbf{p}_1 \quad (2-6)$$

The scalar k appearing always in the combination kT is the Boltzmann constant. ϕ is the perturbation which in the linear approximation was shown to have the form

$$\phi = \mathbf{A} \cdot \nabla_{\mathbf{R}_1} \ln T + \mathbf{B} \cdot \nabla_{\mathbf{R}_1} \mathbf{u} \quad (2-7)$$

\mathbf{A} and \mathbf{B} were evaluated in terms of Sonine polynomials according to a variational method introduced by Hirschfelder, *et al.*¹¹ To the first approximation \mathbf{A} and \mathbf{B} were found to be

$$\mathbf{A} = a^{(1)(5/2} - W^2)\mathbf{W}$$

$$\mathbf{B} = b_0^{(1)}(\mathbf{W}\mathbf{W} - {}^{1/3}W^2\mathbf{1}) \quad (2-8)$$

where

$$a^{(1)} = \frac{15}{16\sqrt{2\pi\rho\sigma_1^2}} \times \left\{ \frac{1 + {}^{3/6}b\rho(g(\sigma_1) + R^3g(\sigma_2)\Psi)}{g(\sigma_1) + R^2g(\sigma_2)[\Xi + {}^{11/16}(\epsilon/kT)^2]} \right\} \quad (2-9)$$

$$b_0^{(1)} = -\frac{5}{8\rho\sigma_1^2} \left(\frac{m}{\pi kT} \right)^{1/2} \times \left\{ \frac{1 + {}^{2/6}b\rho(g(\sigma_1) + R^3g(\sigma_2)\Psi)}{g(\sigma_1) + R^2g(\sigma_2)[\Xi + {}^{1/6}(\epsilon/kT)^2]} \right\} \quad (2-10)$$

with the abbreviations

$$\Psi = 1 - e^{\epsilon/kT} + \frac{\epsilon}{2kT} \times \left[1 + \frac{4}{\sqrt{\pi}} e^{\epsilon/kT} \int_{\sqrt{\epsilon/kT}}^{\infty} e^{-x^2} x^2 dx \right] \quad (2-11)$$

(10) S. Chapman and T. G. Cowling, "The Mathematical Theory of Non-Uniform Gases," Cambridge University Press, New York, N. Y., 1953.

(11) J. O. Hirschfelder, C. F. Curtiss, and R. B. Bird, "Molecular Theory of Gases and Liquids," John Wiley and Sons, Inc., New York, N. Y., 1954.

$$\bar{\epsilon} = e^{\epsilon/kT} - \frac{\epsilon}{2kT} - 2 \int_0^\infty x^2(x^2 + \epsilon/kT)^{1/2} e^{-x^2} dx \quad (2-12)$$

$$b = \frac{2\pi\sigma_1^3}{3} \quad (2-13)$$

$$R = \sigma_2/\sigma_1 \quad (2-14)$$

\mathbf{W} is the reduced peculiar velocity and is given by

$$\mathbf{W} = \left(\frac{m}{2kT}\right)^{1/2} \left[\frac{\mathbf{p}}{m} - \mathbf{u}\right] \quad (2-15)$$

$g(\sigma_1)$ and $g(\sigma_2)$ are the equilibrium radial distribution functions for $R_{12} = \sigma_1 + 0$ and $\sigma_2 + 0$, respectively.

III. Transport Coefficients of a Dense "Square-Well" Fluid

Energy and momentum transfer can be accomplished by two molecular mechanisms in a fluid. In the one case, kinetic energy and momentum may be transported by a single molecule from one point to another in a fluid simply by the molecular motion of the molecule. This mechanism gives rise to the so-called kinetic contribution to the heat flux and pressure tensor. In the other case, transport arises from collisional transfer whereby energy and momentum may be passed across an arbitrary surface by binary collisions involving no net transfer of molecules across the surface. This type of mechanism gives rise to the so-called intermolecular force contribution to the fluxes.

Let us discuss first the kinetic contributions to the heat flux and pressure tensor denoted respectively as \mathbf{q}_k and \mathbf{p}_k . These quantities are simply the mean values of the molecular energy flux $^{1/2}m(\mathbf{p}_1/m - \mathbf{u})^2 \cdot (\mathbf{p}_1/m - \mathbf{u})$ and the molecular momentum flux $(\mathbf{p}_1 - m\mathbf{u})(\mathbf{p}_1/m - \mathbf{u})$, where $\mathbf{p}_1/m - \mathbf{u}$ is the velocity of particle 1 with respect to the hydrodynamic velocity \mathbf{u} . In terms of the singlet distribution function the mean values of these fluxes are

$$\mathbf{q}_k = \frac{m}{2} \iint f(\mathbf{R}_1, \mathbf{p}_1; t) \left| \frac{\mathbf{p}_1}{m} - \mathbf{u} \right|^2 \left(\frac{\mathbf{p}_1}{m} - \mathbf{u} \right) d\mathbf{p}_1 \quad (3-1)$$

$$\mathbf{p}_k = - \iint f(\mathbf{R}_1, \mathbf{p}_1; t) (\mathbf{p}_1 - m\mathbf{u}) \left(\frac{\mathbf{p}_1}{m} - \mathbf{u} \right) d\mathbf{p}_1 \quad (3-2)$$

The perturbation solution for $f(\mathbf{R}_1, \mathbf{p}_1; t)$ given in section II is substituted into eq. 3-1 and 3-2 and the integrations are carried out leading to the expressions

$$\mathbf{q}_k = -^{5/4}\rho \left(\frac{2k^3T}{m}\right)^{1/2} a^{(1)} \nabla_{\mathbf{R}_1} T \quad (3-3)$$

$$\mathbf{p}_k = -\rho kT b_0^{(1)} [^{1/2}(\nabla_{\mathbf{R}_1} \mathbf{u} + \nabla_{\mathbf{R}_1} \mathbf{u}^+) - ^{1/3} \nabla_{\mathbf{R}_1} \cdot \mathbf{u} \mathbf{1}] - \rho kT \mathbf{1} \quad (3-4)$$

where $\nabla_{\mathbf{R}_1} \mathbf{u}^+$ is the transpose of $\nabla_{\mathbf{R}_1} \mathbf{u}$. Comparison of the phenomenological equations

$$\mathbf{q} = -(\kappa_K + \kappa_V) \nabla_{\mathbf{R}_1} T \quad (3-5)$$

$$\mathbf{p} = -[P + (^{2/3}\eta_K + ^{2/3}\eta_V - \Phi) \nabla_{\mathbf{R}_1} \cdot \mathbf{u}] \mathbf{1} + 2(\eta_K + \eta_V) (\nabla_{\mathbf{R}_1} \mathbf{u} + \nabla_{\mathbf{R}_1} \mathbf{u}^+) \quad (3-6)$$

leads to the results

$$\kappa_K = ^{5/4}\rho \left(\frac{2k^3T}{m}\right)^{1/2} a^{(1)} \quad (3-7)$$

$$\eta_K = -\rho \frac{kT}{2} b_0^{(1)} \quad (3-8)$$

where κ_K and κ_V are, respectively, the kinetic and intermolecular contributions to the heat conductivity, η_K and η_V are the kinetic and intermolecular contributions to the shear viscosity, Φ is the bulk viscosity, and P is the hydrostatic pressure. There is no kinetic contribution to the bulk viscosity Φ .

Let us turn next to the intermolecular contributions to the fluxes. Chapman and Cowling¹⁰ show that for rigid spheres the rate of transfer of momentum or energy due to the intermolecular forces is equal to

$$^{1/2}\sigma^3 g(\sigma) \iiint (\Psi' - \Psi) f(\mathbf{R}_1 + ^{1/2}\sigma \mathbf{k}, \mathbf{p}_1; t) f(\mathbf{R}_1 - ^{1/2}\sigma \mathbf{k}, \mathbf{p}_2; t) \times \mathbf{k} g \cdot \mathbf{k} d\mathbf{k} d\mathbf{p}_1 d\mathbf{p}_2 \quad (3-9)$$

where Ψ is the molecular property transferred. In the case of momentum transfer $\Psi' - \Psi = -\Delta \mathbf{p}$. The singlet distribution functions in eq. 3-9 are expanded in a Taylor's series about the point \mathbf{R}_1 and to the linear approximation eq. 3-9 becomes

$$^{1/2}\sigma^3 g(\sigma) \iiint (\Psi' - \Psi) f(1) f(2) \mathbf{k} (g \cdot \mathbf{k}) d\mathbf{k} d\mathbf{p}_1 d\mathbf{p}_2 + ^{1/4}\sigma^4 g(\sigma) \iiint (\Psi' - \Psi) f_0(1) f_0(2) \mathbf{k} \cdot \nabla_{\mathbf{R}_1} \times \ln \left[\frac{f_0(1)}{f_0(2)} \right] \mathbf{k} (g \cdot \mathbf{k}) d\mathbf{k} d\mathbf{p}_1 d\mathbf{p}_2 \quad (3-10)$$

In eq. 3-10, terms of order $\nabla_{\mathbf{R}_1} \phi$ have been neglected and the abbreviation $f(\mathbf{R}_1, \mathbf{p}_j; t) = f(j)$ has been introduced.

In the case of molecules interacting according to the square-well potential, the expression for the rate of transfer of momentum or energy has the same form as that of eq. 3-9 except that there are four types of collisions giving rise to four terms like the one in eq. 3-9. Thus the intermolecular force contribution to the pressure tensor is

$$\begin{aligned}
\mathbf{p}_v = & \frac{1}{2}\sigma_1^3 g(\sigma_1) \iiint_{\mathbf{g}\cdot\mathbf{k} > 0} \Delta\mathbf{p}_1^{(1)} f(\mathbf{R}_1 + \frac{1}{2}\sigma_1\mathbf{k}, \mathbf{p}_1; t) f(\mathbf{R}_1 - \\
& \frac{1}{2}\sigma_1\mathbf{k}, \mathbf{p}_2; t) \mathbf{k}(\mathbf{g}\cdot\mathbf{k}) d\mathbf{k} d\mathbf{p}_1 d\mathbf{p}_2 + \\
& \frac{1}{2}\sigma_2^3 g(\sigma_2) \iiint_{\mathbf{g}\cdot\mathbf{k} > 0} \Delta\mathbf{p}_1^{(2)} f(\mathbf{R}_1 + \frac{1}{2}\sigma_2\mathbf{k}, \mathbf{p}_1; t) f(\mathbf{R}_1 - \\
& \frac{1}{2}\sigma_2\mathbf{k}, \mathbf{p}_2; t) \mathbf{k}(\mathbf{g}\cdot\mathbf{k}) d\mathbf{k} d\mathbf{p}_1 d\mathbf{p}_2 + \\
& \frac{1}{2}\sigma_2^3 g^*(\sigma_2) \iiint_{\mathbf{g}\cdot\mathbf{k} < -\left(\frac{4\epsilon}{m}\right)^{1/2}} \Delta\mathbf{p}_1^{(3)} f(\mathbf{R}_1 + \frac{1}{2}\sigma_2\mathbf{k}, \mathbf{p}_1; t) f(\mathbf{R}_1 - \\
& \frac{1}{2}\sigma_2\mathbf{k}, \mathbf{p}_2; t) \mathbf{k}|\mathbf{g}\cdot\mathbf{k}| d\mathbf{k} d\mathbf{p}_1 d\mathbf{p}_2 + \\
& \frac{1}{2}\sigma_2^3 g^*(\sigma_2) \iiint_{-\left(\frac{4\epsilon}{m}\right)^{1/2} < \mathbf{g}\cdot\mathbf{k} < 0} \Delta\mathbf{p}_1^{(4)} f(\mathbf{R}_1 + \frac{1}{2}\sigma_2\mathbf{k}, \mathbf{p}_1; t) f(\mathbf{R}_1 - \\
& \frac{1}{2}\sigma_2\mathbf{k}, \mathbf{p}_2; t) \mathbf{k}|\mathbf{g}\cdot\mathbf{k}| d\mathbf{k} d\mathbf{p}_1 d\mathbf{p}_2 \quad (3-11)
\end{aligned}$$

where the momentum changes $\Delta\mathbf{p}_1^{(i)}$ for each type of collision are given in eq. 2-3b-2-3e.

Expanding the singlet distribution functions in eq. 3-11, keeping the linear approximation as indicated by eq. 3-10, and finally performing the indicated integrations leads to

$$\begin{aligned}
\mathbf{p}_v = & -\rho kT(b\rho)[g(\sigma_1) + R^3g(\sigma_2)(1 - e^{\epsilon/kT})]\mathbf{1} - \\
& \frac{2}{5}b_0^{(1)}\rho kT(b\rho)[g(\sigma_1) + R^3g(\sigma_2)\Psi](\epsilon - \frac{1}{3}\nabla_{\mathbf{R}_1}\cdot\mathbf{u}\mathbf{1}) + \\
& \frac{8}{15}(\pi mkT)^{1/2}\rho^2\sigma_1^4[g(\sigma_1) + R^4g(\sigma_2)\Xi] \times \\
& (\epsilon + \frac{1}{2}\nabla_{\mathbf{R}_1}\cdot\mathbf{u}\mathbf{1}) \quad (3-12)
\end{aligned}$$

where we have denoted by ϵ the rate of strain tensor, *i.e.*, $\epsilon = \nabla_{\mathbf{R}_1}\mathbf{u} + \nabla_{\mathbf{R}_2}\mathbf{u}^+$. If eq. 3-12 is combined with eq. 3-4 and the result is compared with the phenomenological equation, eq. 3-6, it is easily seen that

$$P = \rho kT\{1 + b\rho[g(\sigma_1) + R^3g(\sigma_2)(1 - e^{\epsilon/kT})]\} \quad (3-13)$$

$$\begin{aligned}
\eta = \eta^* \left\{ \frac{[1 + \frac{2}{5}b\rho(g(\sigma_1) + R^3g(\sigma_2)\Psi)]^2}{g(\sigma_1) + R^2g(\sigma_2)[\Xi + \frac{1}{6}(\epsilon/kT)^2]} + \right. \\
\left. \frac{48}{25\pi} (b\rho)^2(g(\sigma_1) + R^4g(\sigma_2)\Xi) \right\} \quad (3-14)
\end{aligned}$$

$$\Phi = \frac{16}{5\pi} \eta^*(b\rho)^2(g(\sigma_1) + R^4g(\sigma_2)\Xi) \quad (3-15)$$

with

$$\eta^* = \frac{5}{16\sigma_1^2} \left(\frac{mkT}{\pi} \right)^{1/2} \quad (3-16)$$

where we have inserted into eq. 3-14 the explicit value of $b_0^{(1)}$ as given by eq. 2-10. The quantities b , R , Ξ and ψ were defined in section II (eq. 2-11 to 2-14).

Proceeding with an equation for the intermolecular heat flux similar to eq. 3-11, it is found after some manipulation that the thermal conductivity is

$$\begin{aligned}
\kappa = \kappa^* \left\{ \frac{[1 + \frac{3}{5}b\rho(g(\sigma_1) + R^3g(\sigma_2)\Psi)]^2}{g(\sigma_1) + R^2g(\sigma_2)[\Xi + \frac{11}{16}(\epsilon/kT)^2]} + \right. \\
\left. \frac{32}{25\pi} (b\rho)^2(g(\sigma_1) + R^4g(\sigma_2)\Xi) \right\} \quad (3-17)
\end{aligned}$$

with¹²

$$\kappa^* = \frac{75}{64\sigma_1^2} \left(\frac{k^3T}{\pi m} \right)^{1/2} \quad (3-18)$$

In eq. 3-14 and 3-17, the second term inside the braces is the same result obtained by Longuet-Higgins and Valleau for the zeroth approximation to the transport coefficients. The zeroth approximation is that for which the perturbation to the singlet distribution function is zero, *i.e.*, $a^{(1)} = b_0^{(1)} = 0$. The other contributions to η and κ arise from sums of the kinetic terms η_K and κ_K and the intermolecular contribution due to the perturbation to the singlet distribution function (the quantity multiplying the factor $\epsilon - \frac{1}{3}\nabla_{\mathbf{R}_1}\cdot\mathbf{u}\mathbf{1}$ in eq. 3-12 is this sort of contribution).

We shall not give herein a derivation of the self-diffusion coefficient for a "square-well" theory, but rather we shall simply take the results of Longuet-Higgins and Valleau,⁷ namely

$$D = \frac{3}{8\rho\sigma_1^2} \left(\frac{kT}{\pi m} \right)^{1/2} [g(\sigma_1) + R^2g(\sigma_2)\Xi]^{-1} \quad (3-19)$$

Equation 3-19 was obtained by assuming that the velocity correlation dies out exponentially with time. In the limit of a zero attractive potential ($\epsilon = 0$), eq. 3-19 reduces to the first approximation for dense hard spheres.

IV. Some Numerical Computations

In order to calculate one of the transport properties from the above equations, one must know the values of the parameters σ_1 , σ_2 , ϵ , $g(\sigma_1)$, and $g(\sigma_2)$ in addition to equation of state data. Values of σ_1 , σ_2 , and ϵ can be determined empirically from gaseous data. In principle, $g(\sigma_1)$ and $g(\sigma_2)$ can be calculated from equilibrium statistical mechanics if one is given σ_1 , σ_2 , and ϵ . However, to the author's knowledge, there have been no theoretical calculations of the correlation function for a dense "square-well" fluid. Furthermore, there is to date no way of performing the calculations exactly. On the other hand, if one of the transport coefficients is known experimentally, then the predicted equation of state (eq. 3-13) and the predicted

(12) In their publication, Davis, Rice, and Sengers¹ submitted the expressions for κ and η in much less transparent forms than presented in eq. 3-14 and 3-17. The simpler and more symmetrical versions presented herein are due to Dr. J. Sengers, who rearranged the original results.

equation for the known transport coefficient can be solved simultaneously for $g(\sigma_1)$ and $g(\sigma_2)$, presuming, of course, that σ_1 , σ_2 , ϵ , and the *PVT* data are known for the fluid in question. This semiempirical procedure is the one we have followed in this section. In section VI we shall present an approximation scheme for calculating directly the pair correlation function.

Ikenberry and Rice⁵ and Sengers¹³ have recently made rather extensive measurements of the thermal conductivity of several simple fluids. We have used the former's measurements to compute the correlation functions and from these we predicted the viscosity coefficient and diffusion coefficient for liquid argon over temperatures and pressures ranging from 87 to 150°K. and 1 to 500 atm. Values for σ_1 , σ_2 , and ϵ/k were taken from virial coefficient data¹¹ to be, respectively, 3.16 Å., 5.86 Å., and 69.4°K. Equation of state data were taken from tables compiled by Cook^{14a} for the liquid along the saturated vapor pressure curve, while the generalized charts of Hougen, Watson, and Ragatz^{14b} were used in computing the remainder of the *PVT* data used.

The predicted values for the viscosity and self-diffusion coefficients are presented in Table I. The observed viscosity coefficients were taken from a table compiled by Cook.^{14a} The observed diffusion co-

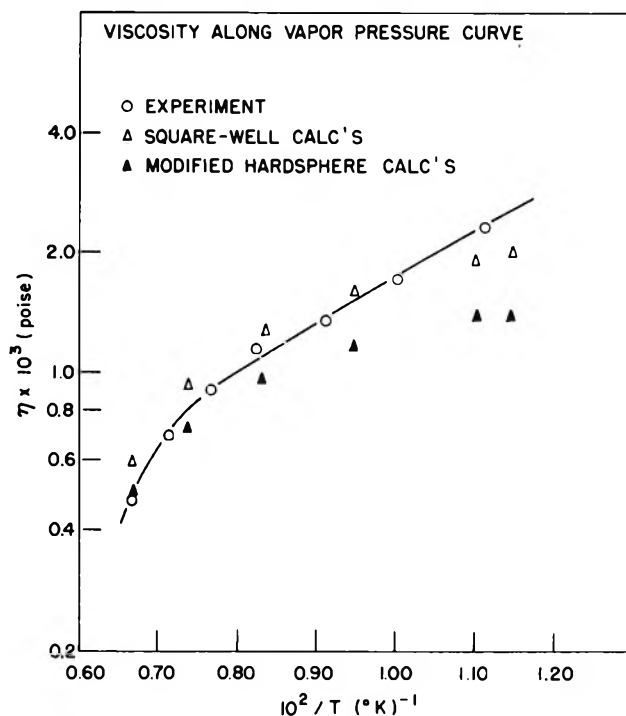


Figure 1. Observed viscosity coefficients, viscosity coefficients calculated for square-well model from empirically determined pair correlation functions, and those calculated according to the "modified hard-sphere" approximation vs. the inverse of the absolute temperature.

Table I: Calculated and Observed Values of the Viscosity Coefficient η and the Self-Diffusion Coefficient D for Liquid Argon at Various Temperatures T and Pressures P . Experimental Values for the Thermal Conductivity Were Used to Determine the Pair Correlation Functions

T , °K.	P , atm.	$\eta \times 10^2$ (calcd.), poise	$\eta \times 10^2$ (obsd.), poise	$D \times 10^4$ (calcd.), cm. ² /sec.	$D \times 10^4$ (obsd.), cm. ² /sec.
87.5	1.0	0.199	0.246	1.70	2.27
91.0	1.5	0.194	0.220	1.81	2.50
105.6	5.0	0.159	0.148	2.54	4.20
120.3	12.3	0.113	0.113	3.46	6.03
136.3	26.8	0.0927	0.077	4.96	8.26
149.4	45.5	0.0599	0.051	6.57	10.00
91.04	23.9	0.196		1.80	2.32
91.27	100.0	0.203		1.76	1.72
91.06	498.8	0.356		0.955	
105.57	25.0	0.163		2.45	4.13
105.47	100.3	0.173		2.36	3.07
105.35	498.1	0.217		1.76	
120.25	24.7	0.127		3.33	5.96
120.46	100.1	0.142		3.15	4.96
120.48	500.8	0.203		2.32	
136.26	27.9	0.0942		5.09	8.35
135.78	100.0	0.122		4.01	6.37
135.87	500.5	0.176		3.00	
149.63	100.0	0.109		4.33	8.16
149.60	500.8	0.143		3.68	

efficients were taken from a recent publication of Naghizadeh and Rice.⁶

As is illustrated in Figure 1, the agreement between the predicted and observed viscosities is quite good where we have data for comparison (the data presented in Figure 1 are for the liquid along the saturated vapor pressure curve).

The agreement between observed and calculated self-diffusion coefficients is less satisfying than that for viscosities. The predicted values are too small by a factor of about 1.6 in most cases. However, as is shown in Figure 2, the correct temperature and pressure dependence is predicted. The data presented in Figure 2 are for values along the saturated vapor pressure curve. The dashed curve was calculated by Naghizadeh and Rice⁶ using experimental viscosity data to determine $g(\sigma_1)$ and $g(\sigma_2)$ while the open triangular points were taken from Table I.

The lack of agreement of the magnitude of the calculated diffusion coefficients perhaps reflects the in-

(13) J. V. Sengers, Thesis, University of Amsterdam, Amsterdam, Holland.

(14) (a) G. A. Cook, "Argon, Helium and the Rare Gases," Interscience Publishers, New York, N. Y., 1961; (b) O. A. Hougen, K. M. Watson, and R. A. Ragatz, "Chemical Process Principles," Vol. 2, John Wiley and Sons, Inc., New York, N. Y., 1962.

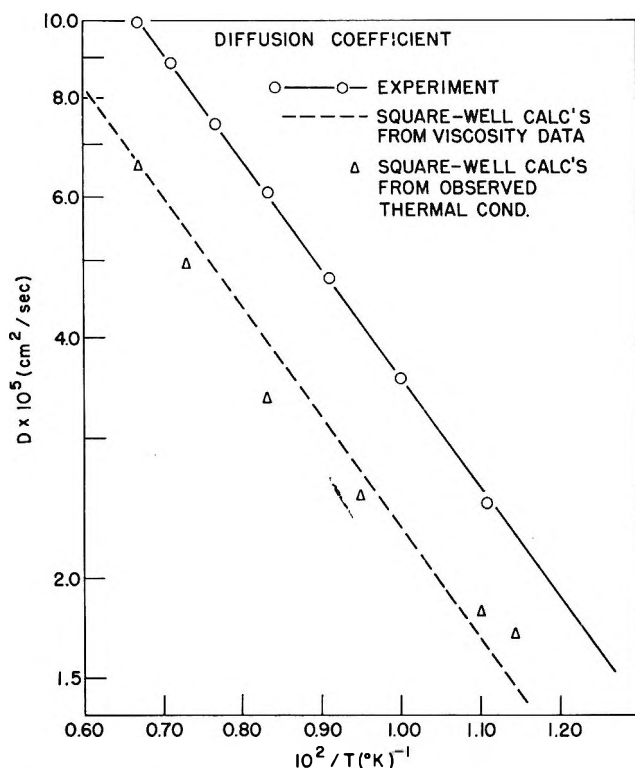


Figure 2. Observed self-diffusion coefficients and those calculated for the square-well model from empirically determined pair correlation functions vs. the inverse of the absolute temperature.

adequacies of the model or perhaps arises from the assumption that the autocorrelation function of momentum decays exponentially in time. It would be interesting to calculate D à la Chapman-Enskog from the transport equation (eq. 2-2). Actually, DRS estimated the diffusion coefficient by expanding the collision integral into a Fokker-Planck type differential equation thus obtaining a diffusion coefficient. They improved on the Longuet-Higgins and Valleeau D by about 3%. However, there is no reason to make the approximations leading to a Fokker-Planck equation since D may be found by the same procedure employed to obtain η and κ .

In view of the agreement of the predicted and experimental viscosities as indicated by Figure 1, one may conclude that the square-well model is a good first approximation to simple fluids.

V. Modified Rigid-Sphere Theory

In addition to obtaining numerical estimates of the transport coefficients, there is another point of interest in our theory. In order to develop a general theory of transport for liquids, one is faced with the problem of determining the mechanism of transport, that is,

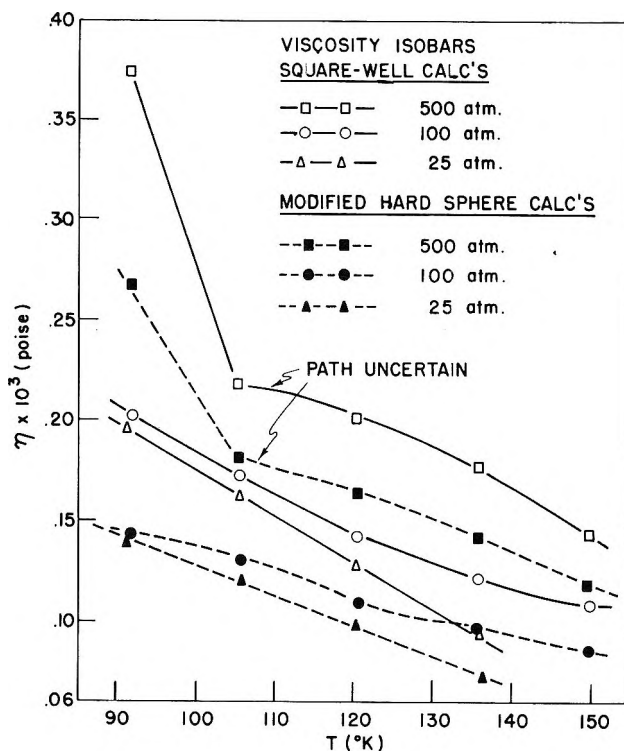


Figure 3. Viscosity coefficients calculated for the square-well model from empirically determined pair correlation functions and "modified hard-sphere" viscosities vs. the absolute temperature.

are the interactions giving rise to energy and momentum transport the hard core (short-range repulsive forces), or soft attractive dispersion forces, or a combination of the two? If the combination contributes, then which is more important? It is generally accepted that a strictly hard-core model does not adequately account for either the transport properties or the thermodynamic properties of a liquid. However, we are suggesting in this section that the role of dispersion forces is to contribute to the structure of the fluid while the major mechanism of transport is the hard-sphere type collision (in other words, one might say that the very short-range repulsive interactions contribute most in the collisional transport).

In order to lend credence to the above notion, we have estimated η and κ from the following "hard-sphere" formulas obtained by setting $\epsilon = 0$ in eq. 3-14 and 3-17

$$\eta_{\text{HC}} = \eta^* \left[\frac{\{1 + {}^2/{}_6 b \rho g(\sigma_1)\}^2}{g(\sigma_1)} + \frac{48}{25\pi} (b\rho)^2 g(\sigma_1) \right] \quad (5-1)$$

$$\kappa_{\text{HC}} = \kappa^* \left[\frac{\{1 + {}^3/{}_6 b \rho g(\sigma_1)\}^2}{g(\sigma_1)} + \frac{32}{25\pi} (b\rho)^2 g(\sigma_1) \right] \quad (5-2)$$

Instead of taking $g(\sigma_1)$ to be the pair correlation function for rigid spheres, we took the values estab-

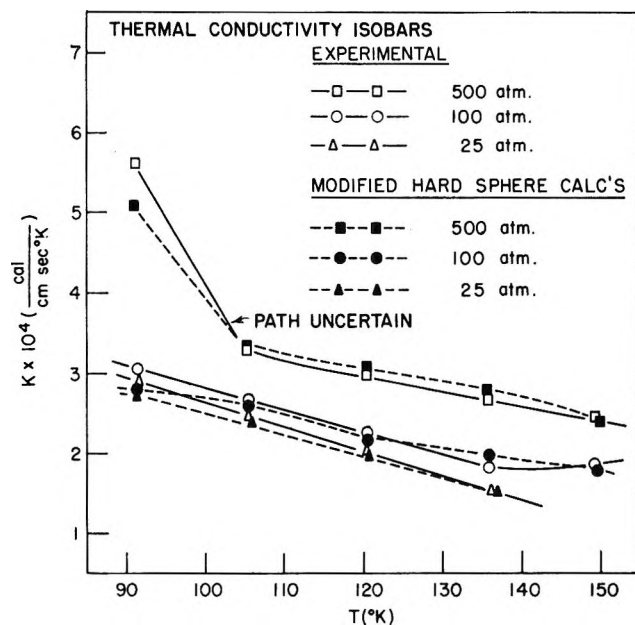


Figure 4. Observed thermal conductivities and "modified hard-sphere" thermal conductivities vs. the absolute temperature.

lished empirically in making the computations of η and D in Table I. In this manner, we estimated η and κ by assuming that momentum and energy are transferred *via* hard-core collisions while the pair correlation function $g(\sigma_1)$ (that is to say the local structure) was determined by including both the attractive and repulsive interactions. We call this method the *modified rigid-sphere* approximation.

Comparisons of the modified rigid-sphere (or hard-core) estimates of viscosity η_{HC} with values for η calculated in the previous section are presented in Figure 3. Also, the filled triangles in Figure 1 represent modified hard-core estimates. In Figure 4 are experimental values of κ compared with κ_{HC} . We display experimental κ -values since they were used in determining values for $g(\sigma_1)$ and $g(\sigma_2)$ from which we calculated η . As is illustrated by Figures 1 and 3, the modified hard-core contributions represent at least 70% of the total viscosity. This contribution is even greater for thermal conductivities; in fact, from Figure 4 we conclude that the modified hard-core thermal conductivity is in quantitative agreement with experiment.

On the basis of the preceding results, one is encouraged that perhaps an adequate approximate fluid model for describing transport in a liquid is one for which the molecular collisions are primarily of the hard-core type while the molecular structure of the fluid is determined by both the attractive forces and the repulsive forces. The problem of finding transport

coefficients is then reduced to the equilibrium problem of calculating the pair correlation function for a liquid, the collisional transport mechanism for hard spheres being well understood. In the naive hope that life could be so simple, this modified rigid-sphere notion warrants further investigation for fluids other than argon.

It should be noted that the method pursued herein is similar to the procedure employed by Enskog (see ref. 10, p. 288), by Michels and Gibson,¹⁵ and recently by Michels, Sengers, *et al.*,¹⁶ for predicting the transport coefficients of several dense gases. They note that the equation of state of a gas of attracting rigid spheres may be taken to be of the form

$$P + a\rho^2 = \rho kT(1 + b\rho g(\sigma_1)) \quad (5-3)$$

where the parameter a arises from the attractive forces and is essentially one of the constants appearing in the van der Waals equation of state. The investigators then assume that a is temperature-independent and that $b\rho g(\sigma_1)$ is a function only of density to obtain the relation

$$b\rho g(\sigma_1) = (\rho k)^{-1} \left(\frac{\partial P}{\partial T} \right)_\rho - 1 \quad (5-4)$$

which allows for deduction of $b\rho g(\sigma_1)$ from equation of state data. Taking the rigid-sphere results, eq. 5-1 and 5-2, and utilizing eq. 5-4 to determine $b\rho g(\sigma_1)$, the investigators have demonstrated remarkable agreement between experiment and theory for several dense gases (*e.g.*, N_2 , CO_2 , Ne , and Ar gases). In the case of liquids, the assumptions leading to eq. 5-4 seem unfounded; they are clearly invalid for the square-well model (see eq. 3-13). Hence, we feel that our method is superior for the liquid state, especially in view of the following section where we suggest an *a priori* method for estimating the pair correlation function $g(\sigma_1)$.

VI. Numerical Computations with Theoretically Determined Pair Correlation Functions

On the basis of the calculations in section IV, it was concluded that the square-well model was quite good for the purpose of computing transport coefficients. However, at least one transport coefficient must be known experimentally in order to compute the other two coefficients. Hence, in this section we shall use an approximation method for obtaining $g(\sigma_1)$ and $g(\sigma_2)$

(15) A. Michels and E. O. Gibson, *Proc. Roy. Soc. (London)*, **A134**, 288 (1931).

(16) A. Michels, J. V. Sengers, and van der Gulik, *Physica*, **28**, 1216 (1962); A. Michels, J. V. Sengers, and van de Klundert, *ibid.*, **29**, 149 (1963); J. V. Sengers, W. T. Bolk, and C. J. Stigter, *ibid.*, **30**, 1018 (1964).

theoretically so that the transport coefficients can be predicted without prior empirical knowledge of one of the coefficients.

Recently, Lowry, Davis, and Rice¹⁷ developed a perturbation technique for calculating the equilibrium pair correlation function. The theory proceeds under two assumptions: (1) the pair potential energy can be separated into two contributions, $V(R_{12}) = V^{(0)} + V^{(1)}$, where $V^{(0)}$ is the unperturbed potential energy and $V^{(1)}$ is the perturbation potential energy; (2) the perturbation energy is less than kT . They then showed that the pair correlation function for particles 1 and 2 was given by

$$g(R_{12}) = g^0(R_{12})e^{-\beta V^{(1)}(R_{12})}[1 + \Theta(R_{12})] \quad (6-1)$$

where $g^0(R_{12})$ is the pair correlation function for particles interacting according to the unperturbed potential energy, $e^{-\beta V^{(1)}}$ is the Boltzmann factor arising from the perturbation pair interaction between particles 1 and 2, and $\Theta(R_{12})$ is an effect due to the presence of many interacting molecules in the vicinity of particles 1 and 2. We shall not give the detailed structure of $\Theta(R_{12})$ herein since we intend to use the lowest-order approximation to eq. 6-1, that is, we shall set $\Theta = 0$. This is not expected to be too unreasonable as a first approximation to $g(R)$; LDR found that for a perturbation interaction strength of the order $\beta\epsilon \sim 0.5$ and at liquid argon densities, the contribution arising from $e^{-\beta V^{(1)}}$ was very much greater than that arising from the quantity Θ . They used as an unperturbed correlation function those calculated by Kirkwood and co-workers¹⁸ for the Lennard-Jones 6-12 potential.

For the square-well model, we choose the unperturbed part of the potential energy to be the hard-core part

$$\begin{aligned} V^{(0)}(R_{12}) &= 0 & R_{12} > \sigma_1 \\ &= +\infty & R_{12} \leq \sigma_1 \end{aligned} \quad (6-2)$$

while the attractive well constitutes the perturbation

$$\begin{aligned} V^{(1)}(R_{12}) &= 0 & R_{12} > \sigma_2 \\ &= -\epsilon & \sigma_1 < R_{12} \leq \sigma_2 \\ &= 0 & R_{12} \leq \sigma_1 \end{aligned} \quad (6-3)$$

In terms of this model, the first approximation to eq. 6-1 becomes

$$g(R_{12}) \simeq g^0(R_{12})e^{-\beta V^{(1)}} \quad (6-4)$$

where $g^0(R_{12})$ is the pair correlation function for a fluid composed of rigid spheres and $V^{(1)}$ is given by eq. 6-3.

Now if $g^0(R_{12})$ can be found, we can calculate $g(\sigma_1)$ and $g(\sigma_2)$ on the basis of eq. 6-4 and thereby compute

the transport coefficients from the equations given in section III. There are various approximate integral equations for the equilibrium pair correlation function. Of these, the integral equation due to Percus and Yevick¹⁹ seems the most promising for hard-sphere fluids since the equation of state predicted on the basis of the Percus-Yevick equation not only yields good agreement with known values of virial coefficients, but also quantitatively reproduces the Monte Carlo results for the dense fluid equation of state.²⁰ Furthermore, Wertheim⁸ and, at about the same time, Thiele⁹ have recently solved the PY equation for the hard-sphere case to obtain the pair correlation function explicitly. For the range $\sigma_1 < R_{12} < 2\sigma_1$ Wertheim obtained

$$xg^0(x) = (1-y)^{-2} \sum_{l=0}^2 A_l \exp[l_i(x-1)] \quad (6-5)$$

where

$$A_l = 1/3 \sum_{m=0}^2 H_m j^{ml} \quad (6-6)$$

and

$$\begin{aligned} H_0 &= 1 + 1/2y \\ H_1 &= -(4y)^{-1}(f^2 + 1/8)^{-1/2} [x_-^2(1 - 3y - 4y^2) + x_+(1 - 5/2y^2)] \\ H_2 &= (4y)^{-1}(f^2 + 1/8)^{-1/2} [x_+^2(1 - 3y - 4y^2) + x_-(1 - 5/2y^2)] \end{aligned} \quad (6-7)$$

with the further definitions

$$f = (3 + 3y - y^2)/4y^2 \quad (6-8)$$

$$t_l = 2y(1-y)^{-1}[-1 + x_+ j^l + x_- j^{-l}] \quad (6-9)$$

$$j = \exp[2/3\pi i] \quad (6-10)$$

$$r_{\pm} = [f \pm (f^2 + 1/8)^{1/2}]^{1/3} \quad (6-11)$$

$$y = \frac{\pi}{6} \sigma_1^3 \rho \quad (6-12)$$

Finally, the argument of g^0 has been written as a reduced variable defined by

$$x = R_{12}/\sigma_1 \quad (6-13)$$

The form of $g^0(x)$ becomes more complicated for $x > 2$, but we shall not worry about that here since for argon

(17) B. A. Lowry, H. T. Davis, and S. A. Rice, *Phys. Fluids*, **7**, 402 (1964).

(18) J. G. Kirkwood, V. A. Lewinson, and B. J. Alder, *J. Chem. Phys.*, **20**, 929 (1952).

(19) J. K. Percus and G. J. Yevick, *Phys. Rev.*, **110**, 1 (1957).

(20) W. W. Wood and J. D. Jacobsen, *J. Chem. Phys.*, **27**, 1207 (1957).

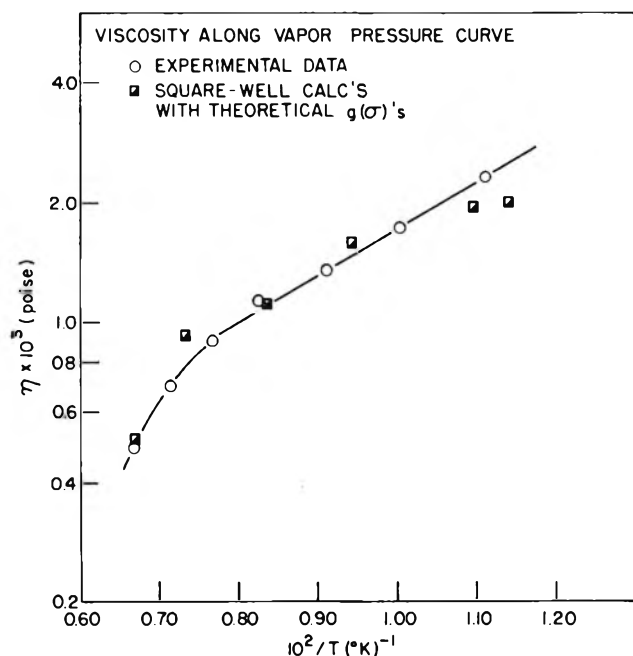


Figure 5. Observed viscosity coefficients and viscosity coefficients calculated for the square-well model from theoretically determined pair correlation functions vs. the inverse of the absolute temperature.

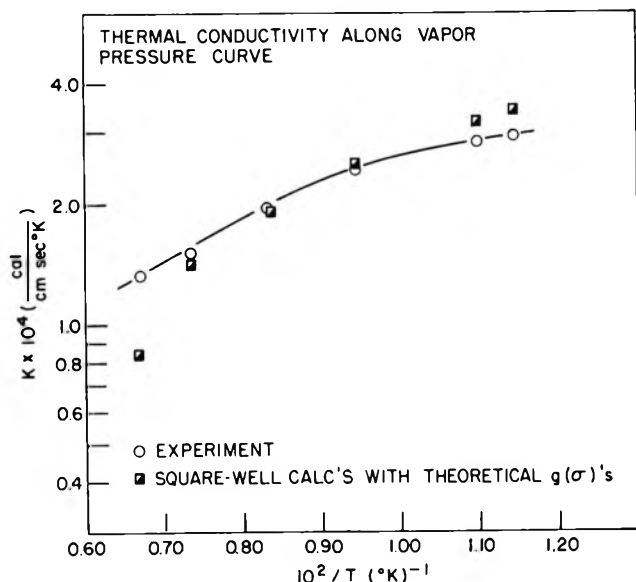


Figure 6. Observed thermal conductivities and those calculated for the square-well model from theoretically determined pair correlation functions vs. the inverse of the absolute temperature.

$x = 1.85$ at $R_{12} = \sigma_2$. Thus, the desired $g^0(R_{12})$ has a rather simple form and is a function only of simple polynomials of the parameter $y = \pi/\sigma_1^3 \rho$.

Viscosities and thermal conductivities are now computed from eq. 3-14 and 3-17 on the basis of $g(\sigma_1)$ and $g(\sigma_2)$ values obtained from $g(R_{12})$ given in eq. 6-4 where $g^0(R_{12})$ is given by eq. 6-5. These computations are presented in Table II along with the observed thermal conductivities⁵ (the observed thermal conductivities along the saturated vapor pressure curve were obtained by extrapolating Ikenberry and Rice's results). In Figures 5 and 6 are plotted predicted and observed viscosities and thermal conductivities along the saturated vapor pressure curve.

Table II: Calculated Values of the Viscosity η and Calculated and Observed Values of the Thermal Conductivity κ for Liquid Argon at Various Temperatures T and Pressures P . $g(\sigma_1)$ and $g(\sigma_2)$ Were Obtained Theoretically According to the Perturbation Method Presented in Section VI

T , °K.	P , atm.	$\eta \times 10^2$ (calcd.), poise	$\kappa \times 10^4$ (calcd.), cal./cm. sec. °K.	$\kappa \times 10^4$ (obsd.), cal./cm. sec. °K.
87.5	1.0	0.241	3.43	2.92
91.0	1.5	0.223	3.21	2.85
105.6	5.0	0.171	2.54	2.43
120.3	12.3	0.113	1.96	1.99
136.3	26.8	0.090	1.42	1.51
149.4	45.5	0.0515	0.832	1.32
91.04	23.9	0.224	3.21	2.90
91.27	100.0	0.231	3.31	3.02
91.06	498.8	0.252	3.64	5.61
105.57	25.0	0.170	2.56	2.49
105.47	100.3	0.183	2.72	2.65
105.35	498.1	0.186	2.82	3.28
120.25	24.7	0.127	1.95	2.03
120.46	100.1	0.138	2.12	2.23
120.48	500.8	0.173	2.68	2.97
136.26	27.9	0.091	1.43	1.50
135.78	100.0	0.108	1.70	1.82
135.87	500.5	0.140	2.26	2.65
149.63	100.0	0.080	1.29	1.78
149.60	500.8	0.124	2.03	2.40

As is clearly illustrated in Figures 5 and 6, the agreement between predicted and measured results is remarkably good, differing only by a few per cent (0–15%) except for the thermal conductivity at 45.5 atm. and 149.4°K., where the predicted value is only about 63% of the observed value; at these conditions argon is near its critical point. Also, at 91.06°K. and 498.1 atm., where argon is solidified, the predicted κ is only 65% of the measured κ . Otherwise, Figures 5 and 6 and Table II indicate very good quantitative agreement between experiment and theory.

On the basis of the calculations presented in this

section it is concluded that the square-well model using the above-described perturbation technique for obtaining the pair correlation function provides a good

first-order theory of the transport properties of simple liquids. In the future we hope to apply this model to several simple liquids.

Dislocations as Active Centers of Catalysis and Chemical Action in Silver

by Ituro Uhara, Shozo Kishimoto, Yasuko Yoshida, and Tadashi Hikino

Chemistry Department, Faculty of Science, Kobe University, Rokkodai, Nada-ku, Kobe, Japan
(Received September 1, 1964)

On annealing cold-worked Ag, decrease in hardness and in thermoelectric force with increase in temperature is observed in the temperature range 200–350° (T_D), where dislocations disappear. Parallel studies on catalytic activities for (A) decomposition of H_2O_2 , (B) oxidation of ethanol, and (C) decomposition of HCO_2H showed that activities decrease on annealing at nearly the same temperature range (T_A). Chemical activity was demonstrated autoradiographically to anneal out in a similar way. It was concluded that active centers of both catalysis and chemical action in Ag are the surface terminations of dislocations.

Introduction

On annealing cold-worked metals, vacancies and dislocations disappear at two temperature ranges, T_V and T_D , respectively. These ranges can be observed separately if the degree of cold-working is slight, as shown in the case of Ni.^{1,2} These phenomena are traced by measuring the changes in various physical properties on annealing.

Uhara and his co-workers found that the thermal deactivation temperature (T_A) of Cu catalyst (in fact, cold-worked pieces of wire) is approximately the same as T_D ³ and that catalytic activities of slightly cold-worked Ni for many reactions decrease in two steps at temperature ranges corresponding to T_V and T_D , respectively, on annealing and estimated that the active centers in Cu catalyst are the terminations of dislocations at the metallic surface and those in Ni catalyst are both point defects and dislocations at the surface. In order to determine the structure of active centers in metallic catalysts by means of this method,³ the use of slightly cold-worked specimens is necessary to avoid overlapping of T_V and T_D and

theoretical complexity due to the interaction of lattice defects of high concentration. Ordinary catalysts as reduced metals are not appropriate for the same reason.⁴ Since the value of T_D varies considerably with the degree of cold-working (or the degree of distortion of the crystal lattice) and the purity of the specimen, we must employ an identical specimen or at least a specimen of identical material cold-worked equally for the comparison of T_A and T_D . T_V and T_D can be most conveniently determined by measuring hardness (H), thermoelectric force (E),⁵ and electric resistivity (ρ) of ribbon or wire with a small quantity of the specimen. Clarebrough, *et al.*,⁶ observed heat

(1) L. M. Clarebrough, M. E. Hargreaves, and G. W. West, *Proc. Roy. Soc. (London)*, **A232**, 252 (1955); *Phil. Mag.*, **1**, 528 (1956).

(2) I. Uhara, S. Yanagimoto, K. Tani, and G. Adachi, *Nature*, **192**, 867 (1961); I. Uhara, S. Yanagimoto, K. Tani, G. Adachi, and S. Teratani, *J. Phys. Chem.*, **66**, 2691 (1962).

(3) I. Uhara, S. Kishimoto, T. Hikino, Y. Kageyama, H. Hamada, and Y. Numata, *ibid.*, **67**, 996 (1963).

(4) Besides, determination of T_V and T_D of powder specimens is very difficult.

(5) S. Kishimoto, *ibid.*, **66**, 2694 (1962); **67**, 1161 (1963).

evolution and changes in ρ , in density, and in H at 110–210° on annealing a 75% compressed Ag specimen of 99.98% purity and attributed them to the disappearance of dislocations. Since point defects generated in Ag by slight cold-working disappear at around –150 and –40°,⁷ they are out of the question as far as catalysis at a higher temperature is concerned. Decrease in H with increase in temperature of a specimen quenched from 600° was reported to occur at 250°.⁸ These data indicate a remarkable difference in values of T_D existing among individual specimens.

Experimental

Ag (99.95% pure) was rolled to a constant degree (90% compression) to plate or ribbon at room temperature and annealed in N_2 for 1 hr. at various temperatures. H was measured with a micro-Vickers hardness tester and E was measured potentiometrically against well-annealed wire (Figure 1).

The thermal deactivation temperature (T_A) was measured for the following three catalytic reactions and one chemical reaction of Ag.

(A) *Decomposition of H_2O_2* . A 0.10% solution was decomposed by rolled plate of apparent area 2.1 cm.² in a Warburg apparatus at 20° (Figure 2A).

(B) *Oxidation of Ethanol*. Rolled plate of apparent area 2.0 cm.² was used as catalyst after being washed with dilute HNO_3 and NH_3 . Ethanol was purified by adding 2,4-dinitrophenylhydrazine to remove carbonyl compounds. Air (1 l.) was bubbled through ethanol at a constant temperature and over the catalyst kept at $280 \pm 2^\circ$ in 40 min. The acetaldehyde formed was caught in cold water, then was analyzed colorimetrically at 470 $m\mu$ after being treated with an alkaline solution of 2,4-dinitrophenylhydrazine (Figure 2B). It was ascertained that dehydrogenation does not take place under this experimental condition.

(C) *Decomposition of HCO_2H ($\rightarrow H_2 + CO_2$)*. A ribbon of 100 cm.² area was employed after annealing in H_2 for 1 hr. at various temperatures. HCO_2H was purified by means of repeated vacuum distillation after standing over B_2O_3 . The reaction rate at 220° was determined statically by measuring the pressure increase (the initial pressure being 20–30 mm.). It is reproducible and of zero order, the initial value being used for the comparison of activities (Figure 2C).

(D) *Combination of Ag with S Vapor*. Thin plates are exposed to saturated S vapor (at 50° for 30 min.) containing radioactive ³⁵S (ca. 1 mc./mg. of S) and studied autoradiographically (3-month exposure).

Results and Discussion

As seen in Figures 1 and 2, changes in H and in E of the specimens employed are remarkable at 200–350°

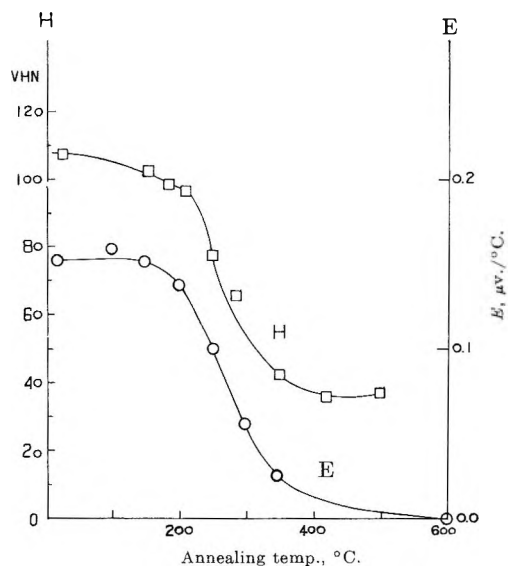


Figure 1. Hardness (H) and thermoelectric force (E) of cold-worked Ag as functions of annealing temperatures.

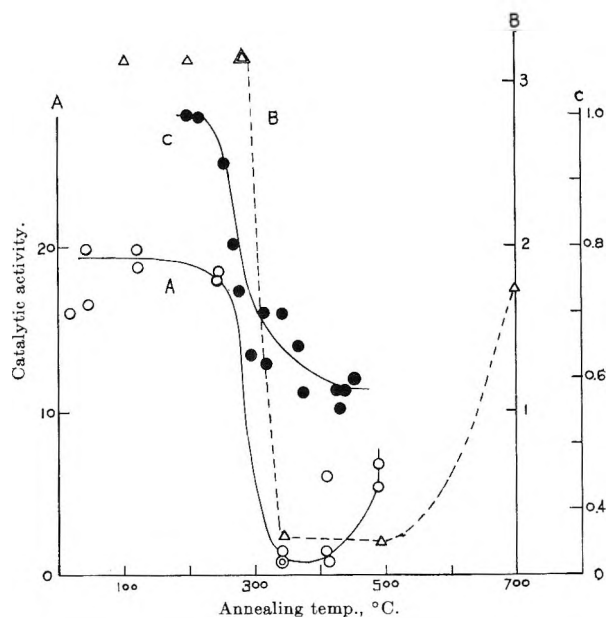


Figure 2. Catalytic activities of cold-worked Ag as functions of annealing temperatures: A, decomposition of H_2O_2 (O); volume (μ l. at STP) of O_2 evolved in 1 hr.; B, oxidation of ethanol (Δ); fraction of CH_3CHO formed (%); C, decomposition of HCO_2H (\bullet); relative activity.

(T_D) and the catalytic activities for reactions A, B,⁹ and C decrease on annealing mainly at 260–340°,

(6) L. M. Clarebrough, M. E. Hargreaves, and M. H. Loretto, *Phil. Mag.*, 7, 115 (1962).

(7) J. A. Manintveld, *Nature*, 169, 623 (1952).

(8) International Critical Tables, Vol. 2, National Research Council, New York, N. Y., 1927, p. 478.

ca. 300°, and 260–370° (T_A), respectively. The change of surface area of plates used as catalysts on annealing is considered to be negligible, because Uhara² found that Cu powder has almost the same adsorption capacity for methylene blue even after it is annealed at a temperature higher than T_D and loses most of the catalytic activity, and the behavior of Ag is very similar to that of Cu in both annealing and catalysis. We may be able to conclude in the same way as for Cu that T_A is approximately the same as T_D and that the active centers of Ag catalysts are the surface terminations of dislocations. According to Sosnousky,¹⁰ a single crystal of Ag which was bombarded with argon ion can decompose HCO_2H catalytically and its activity is of the same order as a cold-worked one. Since the activity remains even after 18 hr. annealing at 250°, he concluded that the active centers are not point defects but dislocations, in accordance with our results (C).

In A and B most of the activities are lost with the disappearance of dislocations, therefore the normal surface is proved to be practically inactive. In C, on the other hand, ca. 60% of the activity remains even when dislocations are annealed out (decomposition on glass surface or in the gaseous phase is negligible). This means that the normal surface is fairly active for this reaction. In the case of industrial oxidation of methanol the temperature of metallic catalysts is much higher (500–900°), and contribution of active centers may be negligible and the reaction may take place rather uniformly at the surface of catalysts.

New Active Center Generated at Higher Temperatures than T_D . On annealing metals at T_D or at higher temperatures most of the dislocations disappear. Although a small fraction of them survives their catalytic activities do not seem to be significant. In Figure 2, however, we see enhanced activity of specimens which were heated at temperatures much higher than T_D . This tendency is frequently observed in some metals such as Pt, Pd, and Ni, too, for certain catalytic reactions. Since there is no indication of concurrent change in physical properties of bulk metal as shown for E in Figure 1 (density and ρ do not change either

as are well known), this might be attributed to some surface phenomena. Researches on this line are now in progress.

Active Centers of Chemical Reaction. Chemical activities of the surface termination of dislocations are well known from the formation of etch pits. In our case (D), Ag plates with and without dislocations were exposed to S vapor containing ³⁵S. Whether dislocations are chemically more active than the normal plane or not can be decided by comparing the blackness (B) of the autoradiograph as follows: (α) rolled plate (dense gray autoradiograph), (β) plate rolled and annealed for 1 hr. at 250° (almost transparent), and (γ) plate rolled and annealed for 1 hr. at 350° (transparent). B may be originated from (X) van der Waals adsorption of S on Ag, (Y) chemisorption of S on Ag, and (Z) surface compound formation. The negligibly small values of B for specimens β and γ indicate that none of X, Y, and Z took place appreciably in these annealed specimens. Besides, the decrease in the surface area of the plates is probably negligible as described previously and so X cannot be responsible for the large difference in B between α and β or γ . Consequently, the large B value of α that contains dislocations may be concluded to have been caused by Y or Z. At any rate, the combination of Ag and S is chemical, being probably the initial stage of the chemical reaction, and the existence of dislocation is indispensable to it at least at 50°. It may be concluded, therefore, that chemical action takes place preferentially at the surface terminations of dislocations.

Acknowledgment. The authors express their hearty thanks to Professor T. Iida for her kind advice and to Mr. S. Taniguchi for his assistance.

(9) As for the data of B at 100 and 200°, the specimens must have undergone annealing corresponding to 280° to some extent during the catalytic reaction since the rate was measured at this temperature. But the perfect coincidence of the data with that at 280° demonstrates the nonexistence of any change in the catalyst at 100–280°, as long as the disappearance of dislocations is not too fast.

(10) H. M. C. Sosnousky, *J. Phys. Chem. Solids*, **10**, 304 (1959).

Cation Interchange across Ion-Exchange Membranes

by M. Worsely, A. S. Tombalakian,¹ and W. F. Graydon

Department of Chemical Engineering and Applied Chemistry, University of Toronto, Toronto, Canada
(Received September 2, 1964)

The possibility of preparing polystyrenesulfonic acid ion-exchange membranes having various degrees of porosity by changing the alcohol group in the ester monomer was investigated. Polystyrenesulfonic acid ion-exchange membranes were formed using the methyl, ethyl, *n*-propyl, *n*-hexyl, and *n*-octyl esters of *p*-styrenesulfonic acid. The membranes were found to exhibit an increase in permeability with increase in the size of the alcohol group of the ester monomer. No preferential ion screening or sieve effect was observed as successively larger univalent inorganic and organic cations were used to interchange with hydrogen ion. The dependence of the membrane interdiffusion coefficient on the single ion diffusion coefficients of the interchanging ion species in the membrane for various conditions of the membrane diffusion was determined. Good agreement was found between the observed interdiffusion coefficients and values calculated using single ion diffusion coefficients of hydrogen in the membrane and limiting ionic mobility ratios in water.

Introduction

The swelling and transfer behavior of polystyrenesulfonic acid ion-exchange membranes formed by the bulk copolymerization of the *n*-propyl ester of *p*-styrenesulfonic acid with styrene and divinylbenzene have been investigated.²⁻⁷ The effects of membrane exchange capacity and cross linking, solution concentration, temperature, counterion valence, and size on mass-transfer rates have been recently reported.⁷

The results of measurements of membrane moisture contents in various ionic forms and rates of ion transfer during the interchange of hydrogen with univalent inorganic and organic cations across membranes formed from the methyl, ethyl, *n*-propyl, *n*-hexyl, and *n*-octyl esters of *p*-styrenesulfonic acid are given in this report. The effects of variation of the alcohol group in the ester monomer on the structure and permeability of the membranes formed have been determined.

Experimental

(A) *Preparation of Monomers.* The methyl, ethyl, *n*-propyl, *n*-hexyl, and *n*-octyl esters of *p*-styrenesulfonic acid were prepared from β -phenyl ethyl bromide by a sequence of sulfochlorination, esterification, and dehydrobromination reactions.⁸

(B) *Membranes.* The membranes used in this work were prepared by the bulk copolymerization of

the esters of *p*-styrenesulfonic acid with styrene, divinylbenzene, and benzoyl peroxide as catalyst and subsequent hydrolysis in 5% caustic soda solution to produce polystyrenesulfonic acid.^{2,8,9}

The membranes were formed at 110–120° in 2 hr. A mass balance on a membrane formed from the *n*-propyl ester of *p*-styrenesulfonic acid showed a loss in weight of about 4% during polymerization and of a further 3% during the hydrolysis.

The methods used for the determination of membrane moisture content, exchange capacity, and thickness have been described previously.² In Table I are given the characteristics of the membranes used in this work and the membrane moisture contents in various ionic forms in contact with pure water at 25°.

(1) Department of Chemistry and Engineering, Laurentian University of Sudbury, Sudbury, Ontario, Canada.

(2) W. F. Graydon and R. J. Stewart, *J. Phys. Chem.*, **59**, 86 (1955).

(3) R. J. Stewart and W. F. Graydon, *ibid.*, **60**, 750 (1956).

(4) R. J. Stewart and W. F. Graydon, *ibid.*, **61**, 164 (1957).

(5) A. S. Tombalakian, H. J. Barton, and W. F. Graydon, *ibid.*, **66**, 1006 (1962).

(6) J. Ciric and W. F. Graydon, *ibid.*, **66**, 1549 (1962).

(7) A. S. Tombalakian, C. Y. Yeh, and W. F. Graydon, *Can. J. Chem. Eng.*, **42**, 61 (1964).

(8) I. H. Spinner, J. Ciric, and W. F. Graydon, *Can. J. Chem.*, **32**, 143 (1954).

(9) W. F. Graydon, U. S. Patent 2,877,191 (March 10, 1959).

Table I: Membrane Characteristics

Membrane no.	Mole % DVB	Capacity, mequiv./g. of dry resin, H form	Ester form	Moisture content, moles of H ₂ O/equivalent						Thickness, cm. (± 0.0002)
				K ⁺	Na ⁺	H ⁺	Li ⁺	(CH ₃) ₄ N ⁺	(C ₂ H ₅) ₄ N ⁺	
1	6	1.93	Methyl	18.9	20.0	20.3	20.5	17.5	18.6	0.1392
2	6	2.56	Ethyl	19.7	21.4	22.6	22.8	20.5	21.0	0.1612
3	6	2.49	<i>n</i> -Propyl	22.2	23.9	24.3	25.0	22.4	23.3	0.1573
4	6	2.29	<i>n</i> -Hexyl	25.9	28.3	29.1	30.1	25.3	23.8	0.1460
5	6	2.24	<i>n</i> -Octyl	27.3	30.5	31.0	32.2	26.4	26.9	0.1040
6	4	1.79	Methyl	23.1	24.3	24.7	25.0	21.3	24.3	0.1335
7	4	2.54	Ethyl	25.1	30.1	30.4	30.9	27.5	29.0	0.1402
8	4	2.47	<i>n</i> -Propyl	28.5	30.4	31.2	31.6	28.4	29.3	0.1440
9	2	1.97	Ethyl		33.7					0.0762
10	6	1.60	<i>n</i> -Propyl	10.4	10.8	11.3	11.7	9.2		0.0712
11	6	2.31	<i>n</i> -Propyl		23.1					0.0688

Table II: Cation Interchange, Various Ion-Pair Exchange Systems at 25.0°

System	Membranes		Initial exchange flux, g. equiv./cm. ² hr. $\times 10^4$					Over-all ion-interchange coefficient, cm./sec. $\times 10^6$					Inter-diff. coeff., cm. ² /sec. $\times 10^6$
	No.	Ester form	0.1 N	0.5 N	1.0 N	2.0 N	3.0 N	0.1 N	0.5 N	1.0 N	2.0 N	3.0 N	
KCl-HCl	1	Methyl	18.9	29.3	32.9	41.9	45.3	27.2	7.82	4.65	2.84	2.13	1.32
	2	Ethyl	20.9					56.6					3.41
	3	<i>n</i> -Propyl	23.5					66.9					4.38
	4	<i>n</i> -Hexyl	25.4					74.2					4.93
	5	<i>n</i> -Octyl	30.7					98.5					5.10
NaCl-HCl	1	Methyl	15.0					19.1					0.97
	2	Ethyl	16.4					40.7					2.56
	3	<i>n</i> -Propyl	18.8					48.2					3.29
	4	<i>n</i> -Hexyl	19.2					49.0					3.57
	5	<i>n</i> -Octyl	24.1					69.8					3.82
LiCl-HCl	1	Methyl	10.6	14.1	15.7	19.4	24.5	13.2	4.05	2.42	1.43	1.08	0.67
	2	Ethyl	12.4					28.0					1.87
	3	<i>n</i> -Propyl	14.7					33.7					2.34
	4	<i>n</i> -Hexyl	15.0					33.9					2.50
	5	<i>n</i> -Octyl	17.9					45.9					2.62
(CH ₃) ₄ NCl-HCl	1	Methyl	7.80	10.5	13.9	18.4	25.2	9.62	2.81	1.62	0.96	0.72	0.45
	2	Ethyl	9.70					22.2					1.35
	3	<i>n</i> -Propyl	11.4					25.5					1.67
	4	<i>n</i> -Hexyl	11.7					25.8					1.74
	5	<i>n</i> -Octyl	13.7					35.8					1.83
(C ₂ H ₅) ₄ NCl-HCl	1	Methyl	2.56	4.31	6.31	8.52	10.2	3.43	1.04	0.62	0.36	0.26	0.17
	2	Ethyl	4.30					8.83					0.55
	3	<i>n</i> -Propyl	4.97					10.5					0.66
	4	<i>n</i> -Hexyl	5.85					11.6					0.71
	5	<i>n</i> -Octyl	6.54					14.9					0.77

(C) *Flux Measurements.* A two-compartment Lucite cell, previously described,³ was used to measure the rates of ion transfer. At zero time each compartment, separated from the other by the ion-exchange membrane, contained 10-ml. solutions of equal normal-

ity. The cell agitator was set at 300 oscillations/min. and the two ionic species were allowed to interchange across the membrane for several 5-min. periods until a constant flux was obtained. The interchange was then allowed to proceed for various time intervals.

At the end of each interval the contents of the compartments were analyzed by titration.

Results and Discussion

Examples of the results of cation-interchange fluxes, over-all ion-interchange coefficients, and membrane interdiffusion coefficients, which have been obtained across five typical polystyrenesulfonic acid ion-exchange membranes formed from the various esters of *p*-styrenesulfonic acid, are given in Table II. Membranes 1, 2, 3, 4, and 5 had the same nominal exchange capacity and cross linking but were formed from the methyl, ethyl, *n*-propyl, *n*-hexyl, and *n*-octyl esters of *p*-styrenesulfonic acid, respectively. The results were calculated from the experimental data using the relationship described previously.⁷ The over-all ion-interchange coefficient (K_i) is given by expression 1. This quantity is determined entirely by changes in the external solutions.

$$K_i = \frac{V}{2At} \ln \frac{\Delta C_0}{\Delta C_t} \quad (1)$$

K_i is the over-all ion-interchange mass-transfer coefficient, cm./sec.; V is the volume in the cell compartment (10 ml.); A is the membrane surface area exposed to the solutions (3.14 cm.²); ΔC_0 is the difference in concentration of the interchanging species between half-cells at zero time, equiv./ml.; and ΔC_t is the difference in concentration of the interchanging species between half-cells at time t , equiv./ml. The interdiffusion coefficient (D_m) is given by expression 2 and is quite independent of solution concentration.

$$D_m = K_i L \frac{C_0}{C_i} \quad (2)$$

Where D_m is the membrane interdiffusion coefficient, cm.²/sec.; L is the membrane thickness, cm.; C_0 is the initial concentration of external solutions, equiv./ml.; and C_i is the membrane internal ion concentration, equiv./ml.

It is to be expected that the ester of *p*-styrenesulfonic acid with the larger alcohol group would produce membranes of a larger pore size. Indeed, the membrane moisture contents in various ionic forms presented in Table I and the rates of ion interchange given in Table II indicate this effect.

The data in Table II show that for a given ion pair the diffusivities of the ions through the membranes increase with increasing alcohol size of the ester monomer in the order membrane 1, 2, 3, 4, and 5. In all cases membrane porosity increased markedly with increasing alcohol size. The removal of successively larger alcohol groups from the membranes during hy-

drolysis produced membranes of a successively larger pore size.

It may be seen from Table II that the fluxes, over-all ion-interchange coefficients, and interdiffusion coefficients for the exchange between hydrogen and the various univalent cations decrease in the order potassium, sodium, lithium, tetramethylammonium, and tetraethylammonium; whereas the effective radii of these ions in their hydrated forms decrease in the sequence potassium, sodium, tetramethylammonium, lithium, and tetraethylammonium.¹⁰ This indicates that the ion-membrane interaction experienced by organic cations in the membranes is greater than that for inorganic cations of the same valence and size. For the membranes prepared from the methyl ester of *p*-styrenesulfonic acid, the observed dependence of the over-all ion-interchange coefficient on solution concentration for the univalent inorganic and organic cations is similar to that reported previously⁷ for other univalent inorganic cations interchanging with hydrogen across membranes formed from the *n*-propyl ester.

It might be expected that as the pore size of a membrane becomes smaller, the diffusion of the larger counterions would be relatively more hampered than that of the smaller ions. In Table III are given the values of the ratio of the observed membrane interdiffusion coefficient of one ion-pair exchange system to the membrane interdiffusion coefficient of a reference ion-pair exchange system (K^+-H^+) for eight different membranes. It can be seen that the ratios of membrane interdiffusion coefficients for any two exchange systems are quite constant regardless of differences in membrane porosity. There is very little sieve effect resulting from membrane network interference. The pore widths of these polystyrenesulfonic acid ion-exchange membranes appear to be much larger than the diameter of even a hydrated tetraethylammonium ion, reported¹⁰ to be 8 Å.

In order to determine the extent to which the interchanging ions were hindered in the membrane pores, the ratios of interdiffusion coefficients listed in Table III were divided by similar ratios of interdiffusion coefficients calculated using relationship 3¹¹ and limiting

$$D_{12} = \frac{2D_1D_2}{D_1 + D_2} \quad (3)$$

ionic mobilities in water.¹² The results, given in Table IV, show that the interdiffusion coefficients for univalent

(10) R. A. Robinson and R. H. Stokes, "Electrolyte Solutions," Butterworths, London, 1955.

(11) K. S. Spiegler and C. D. Coryell, *J. Phys. Chem.* **57**, 687 (1953).

Table III: Ratio of Membrane Interdiffusion Coefficients

Membrane no.	Ester form	Na^+-H^+	Li^+-H^+	$(\text{CH}_3)_4\text{N}^+-\text{H}^+$	$(\text{C}_2\text{H}_5)_4\text{N}^+-\text{H}^+$
		K^+-H^+	K^+-H^+	K^+-H^+	K^+-H^+
1	Methyl	0.74	0.51	0.34	0.13
2	Ethyl	0.75	0.55	0.39	0.16
3	<i>n</i> -Propyl	0.75	0.53	0.38	0.15
4	<i>n</i> -Hexyl	0.73	0.52	0.35	0.14
5	<i>n</i> -Octyl	0.75	0.51	0.36	0.15
6	Methyl	0.75	0.52	0.35	0.14
7	Ethyl	0.79	0.58	0.41	0.18
8	<i>n</i> -Propyl	0.76	0.54	0.39	0.16

inorganic cation-exchange systems in the membrane are nearly in the same ratio as in aqueous solution, whereas the interdiffusion of univalent organic cations with hydrogen is considerably slower in the membrane solution than in water relative to the K^+-H^+ interchange. Although the inorganic and organic cations exhibit an increase in ion-membrane interactions with increasing ionic size, this effect is much greater for organic than inorganic cations (Figure 1). This interaction is quite independent of the pore size. The large counterion exerts the major control over the rate of ion interchange.

Since solutions of equal volume and concentration were used in these counterdiffusion experiments, the two cation species interchanged across the membrane in equivalent quantities under the influence of equal

Table IV: Ratio of Interdiffusion Coefficient in Membrane to Water

Membrane no.	$\left(\frac{\text{Na}-\text{H}}{\text{K}-\text{H}}\right)_m$	$\left(\frac{\text{Li}-\text{H}}{\text{K}-\text{H}}\right)_m$	$\left(\frac{\text{TMA}^a-\text{H}}{\text{K}-\text{H}}\right)_m$	$\left(\frac{\text{TEA}^b-\text{H}}{\text{K}-\text{H}}\right)_m$
	$\left(\frac{\text{Na}-\text{H}}{\text{K}-\text{H}}\right)_w$	$\left(\frac{\text{Li}-\text{H}}{\text{H}-\text{K}}\right)_w$	$\left(\frac{\text{TMA}-\text{H}}{\text{K}-\text{H}}\right)_w$	$\left(\frac{\text{TEA}-\text{H}}{\text{K}-\text{H}}\right)_w$
1	1.03	0.90	0.52	0.27
2	1.04	0.96	0.60	0.33
3	1.04	0.93	0.58	0.31
4	1.02	0.91	0.54	0.29
5	1.04	0.90	0.55	0.31
6	1.04	0.91	0.54	0.29
7	1.10	1.01	0.62	0.37
8	1.05	0.94	0.60	0.33

^a TMA = tetramethylammonium ion. ^b TEA = tetraethylammonium ion.

and opposite concentration gradients and the resulting electrical cation diffusion potential. Application of the Nernst-Planck equation¹³ to the interchange of

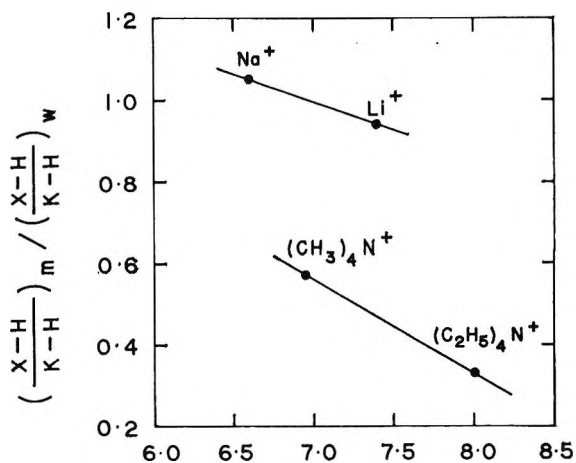


Figure 1. Dependence of ratio of interdiffusion coefficient in membrane to water on inorganic and organic counterion (X) diameter. The plots are based on mean values of results (Table IV) for eight different membranes.

univalent cations across an ion-exchange membrane leads to the relationship

$$J_i = \frac{D_1 D_2 C_i A}{D_1 - D_2} \ln \frac{C_1'(D_1 - D_2) + C_0 D_2}{C_1''(D_1 - D_2) + C_0 D_2} \quad (4)$$

where J_i is the interchange flux, equiv./sec.; D_1 , D_2 are the single ion diffusion coefficients of ion species 1 and 2 in the membrane, cm.²/sec.; and C_1' , C_1'' are the concentration of ion species 1 in the two half-cells, equiv./ml.

The cation-interchange fluxes obtained in the counterdiffusion experiments were used in a graphical integration of eq. 4 together with the assumption that limiting inorganic ionic mobility ratios in water apply in the membrane solution to estimate the single ion diffusion coefficients for hydrogen (D_{H^+}). Examples of D_{H^+} obtained by this method for two membranes formed from the ethyl and methyl esters of polystyrenesulfonic acid are given in Table V. These results are lower than the values of D_{H^+} obtained previously⁶ by counterdiffusion and electrical resistance measurements across membranes of higher porosity formed from the *n*-propyl ester of *p*-styrenesulfonic acid. It may be seen from Table V that the diffusivity of hydrogen ion in membrane 9 of low cross linking and relatively larger pore size is greater than that observed for a tighter membrane 1 of a higher cross linking and smaller pore size.

(12) H. S. Harned and B. B. Owen, "The Physical Chemistry of Electrolytic Solutions," Reinhold Publishing Corp., New York, N. Y., 1958.

(13) F. Helfferich, *Discussions Faraday Soc.*, 21, 83 (1956).

Table V: Single Ion Diffusion Coefficients of Hydrogen at 25.0°

Membrane no.	Ester form	System	Extr. soln. concn., moles/l.	D_{H^+} , cm. ² /sec. $\times 10^6$
9	Ethyl	KCl-HCl	0.1	1.09
		NaCl-HCl	0.1	1.06
		LiCl-HCl	0.1	0.94
		Av.	1.03	
1	Methyl	KCl-HCl	0.1	0.61
		NaCl-HCl	0.1	0.60
		Av.	0.61	

It is of interest to compare the values of membrane interdiffusion coefficients obtained for our experimental conditions by eq. 2 with interdiffusion coefficients which may be estimated from single ion diffusion coefficients of the interchanging ions in the membrane using eq. 5 and 3, which are limiting evaluations of D_{12} from eq. 4 for initial and final diffusion conditions, respectively.¹³

$$D_{12} = \frac{D_1 D_2}{D_1 - D_2} \ln \frac{D_1}{D_2} \quad (5)$$

In order to test the validity of eq. 3 and 5, "differential" interdiffusion coefficients were determined using 10-min. periods. Solutions of varied composition (0.1 *N* total solution concentration) corresponding to various time intervals during a normal integral interchange process were used. In Table VI are given the observed "differential" interdiffusion coefficients as defined by eq. 2 for various ion-pair exchange systems. The values of interdiffusion coefficients calculated by eq. 3 and 5 using single ion diffusion coefficients of hydrogen obtained by graphical integration of eq. 4 and limiting ionic mobility ratios in water are also given.

It can be seen from Table VI that the values of the experimental "differential" interdiffusion coefficients obtained for the initial boundary condition of the membrane decrease by about 50% as the interchange nears equilibrium. The interdiffusion coefficients calculated by eq. 3 and 5 are in fair agreement with mem-

Table VI: Membrane Interdiffusion Coefficients at 25°

Membrane no.	System	Initial counter-ion concn., equiv./l.		D_{12} , cm. ² /sec. $\times 10^6$		Integral exptl eq. 2	
		Half-cell 1	Half-cell 2	"Differential" exptl eq. 2	Calcd.		
10	KCl-HCl	0.10	0	0.607	0.541 eq. 5	0.488	
		0.09	0.01	0.575			
		0.08	0.02	0.521			
		0.07	0.03	0.422			
		0.06	0.04	0.345			0.452 eq. 3
		0.06	0.04	0.345			0.452 eq. 3
	LiCl-HCl	0.10	0	0.266	0.232 eq. 5	0.204	
		0.09	0.01	0.238			
		0.08	0.02	0.219			
		0.07	0.03	0.181			
		0.06	0.04	0.146			0.169 eq. 3
		0.06	0.04	0.146			0.169 eq. 3
(CH ₃) ₄ NCl-HCl	0.10	0	0.128	0.098 eq. 5	0.080		
	0.09	0.01	0.095				
	0.08	0.02	0.085				
	0.07	0.03	0.073				
	0.06	0.04	0.063			0.074 eq. 3	
	0.06	0.04	0.063			0.074 eq. 3	
11	NaCl-HCl	0.10	0	1.42	1.37 eq. 5	1.12	
		0.095	0.005	1.24			
		0.090	0.011	1.16			
		0.082	0.019	1.08			
		0.071	0.035	0.99			1.06 eq. 3
		0.071	0.035	0.99			1.06 eq. 3

brane interdiffusion coefficients obtained for our experimental conditions by eq. 2.

The interdiffusion coefficients previously reported^{3, 6, 7} are integral values over ranges up to 60–80% of equilibrium. Samples of such values are listed in Table VI. These coefficients are of course of intermediate value. As shown previously,⁶ eq. 3 may be used to obtain a self-consistent set of single ion diffusion coefficients which serve to correlate integral diffusion behavior for various ion pairs. Such single coefficients are to some degree fictitious. Neither eq. 3 nor 5 may be used to calculate single diffusivities from such integral interdiffusion coefficients. Indeed, the experimental range of short chord, "differential" ion interdiffusion coefficients is much larger than the range predicted by the Nernst-Planck equation (4).

Acknowledgment. The authors are indebted to the National Research Council, Ottawa, Canada, the Ontario Research Foundation, and the President's Advisory Committee on Scientific Research, University of Toronto, for financial support.

The Radiolysis of Propane at Extremely Low Conversions^{1a}

by L. W. Sieck, N. K. Blocker,^{1b} and J. H. Futrell

Aerospace Research Laboratories, Office of Aerospace Research, Wright-Patterson Air Force Base, Ohio
(Received September 5, 1964)

The gas phase radiolysis of propane has been investigated at extremely low conversions in order to determine initial G values. Yields of unsaturated products are found to be significantly higher than those obtained in the presence of added scavengers, and the differences can be correlated with radical-disproportionation reactions. Dose dependence is discussed in some detail and possible explanations for the variations in yield are offered. Although no detailed mechanism is advanced, the quantitative yield data upon which the mechanism must rest are presented.

Introduction

Although the gas phase radiolysis of propane has been extensively investigated in various laboratories,²⁻⁷ no attempt has been made to determine initial yields of hydrocarbon products obtained in the absence of added scavengers. Because of the possibility of free radical and ionic attack involving unsaturated products, the yields of C₄-C₆ products obtained at higher conversions may well be distorted relative to their primary values obtained at conversions low enough to prevent complicating secondary reactions.⁸ In addition, it might be expected that initial unsaturate yields may differ from those obtained in the presence of scavengers as a result of contributions from disproportionation reactions of free radical intermediates. The present study was initiated with the expectation that the establishment of low conversion values and the concurrent knowledge of the dose dependence of the various yields would give an insight into the magnitude of certain primary processes about which insufficient information exists.

Experimental

Phillips research grade propane was extensively purified by gas chromatography and bulb-to-bulb distillation *in vacuo*. The total hydrocarbon impurity was less than 10⁻⁵% in all experiments, as indicated by analysis on a modified Perkin-Elmer Model 800 dual-flame ionization gas chromatograph. Volatile radiolysis products (excluding hydrogen, which was not measured) were analyzed on the same instrument, as follows: ethane, ethylene, acetylene, and propylene, 2.5-m.

25% squalane column at -14°; ethane and butanes, 2.5-m. 10% squalane column at room temperature; and methane, ethane, pentanes, and hexanes, 1.5-m. 40-60 mesh silica gel, programmed from room temperature to 90°. Yields were determined relative to the amount of ethane produced in each experiment, and the reproducibility for identical samples was always within ±2%.

The radiolysis vessel was a brass cylinder equipped with O-ring-sealed 0.0127-cm. aluminum foil windows through which the electron beam passed along an axis perpendicular to the longitudinal axis of the cell. It was felt that such a design would allow lateral thermal diffusion of products away from the primary reaction zone defined by the passage of the electron beam through the center of the system, thus reducing the probability of secondary reactions. Filling and evacuation was achieved through Whitey Teflon-seated needle valves fitted with metal tapered joints

(1) (a) Presented at the 12th Annual Meeting of the Radiation Research Society, Miami Beach, Fla., May 17-20, 1964; (b) abstracted in part from the Master's thesis of N. K. Blocker, Air Force Institute of Technology, Air University, 1964.

(2) (a) B. F. Birdwell and G. W. Crawford, *J. Chem. Phys.*, **33**, 928 (1960); (b) K. Yang and P. J. Manno, *J. Am. Chem. Soc.*, **81**, 3507 (1959).

(3) P. Ausloos and S. Lias, *J. Chem. Phys.*, **36**, 3163 (1962).

(4) J. H. Futrell and T. O. Tiernan, *ibid.*, **37**, 1694 (1962).

(5) S. G. Lias and P. Ausloos, *ibid.*, **37**, 877 (1962).

(6) I. B. Sandoval and P. Ausloos, *ibid.*, **38**, 2454 (1963).

(7) P. Ausloos, S. G. Lias, and I. B. Sandoval, *Discussions Faraday Soc.*, **36**, 66 (1963).

(8) R. A. Back, *J. Phys. Chem.*, **64**, 124 (1960).

for connection to a vacuum and gas-handling apparatus. The vessel contained a volume of 4720 cc. and could be evacuated to 10^{-6} mm. with no detectable leakage or outgassing after a 24-hr. period.

The radiation source was a 1.0-Mev. High Voltage Engineering Corp. Van de Graaff electron accelerator. All irradiations were carried out at room temperature with an integrated beam current of 5.0 μ a. delivered at 0.55 Mev. The propane pressure employed in all experiments was 40.0 mm., and the dose rate calculated according to the method described in the following section was 2.0×10^{17} e.v./sec.

Results

The conversion dependence of the various yields is shown in Figures 1 and 2. The values are normalized to that of the major product, C_2H_6 , which was found to have an invariant energy yield (constant G) within experimental error throughout the range of conversions studied. Although no chemical dosimetry was attempted, the magnitude of $G(C_2H_6)$ was estimated to be 1.95 ± 0.10 . This value is based on absorbed doses calculated from electrical measurements and the measured path length for electrons traversing the vessel, using tabulated values of $(dE/dX)_E$ for the energy range of interest. The % conversion was defined as $4.6 \times 10^2 \times [C_2H_6]/[C_3H_8]$, which is stoichiometrically correct at lower conversions assuming all carbon-containing products were analyzed. Although such a relationship is only approximate at higher conversions ($>0.05\%$), other values serve only to shift the points along the abscissa of the two figures and do not modify the relative G values in any way.

The initial and high conversion yields obtained in the present study are compared in Table I with the values obtained by Yang and Manno^{2b} after normalization of their data to the C_2H_6 yield. The agreement is quite satisfactory between our high conversion yields and their values in spite of the difference in radiolysis pressures between the two investigations. Comparison with the results of other workers is difficult because nitric oxide has been employed as an additive in many other recent studies³⁻⁷ in order to simplify the interpretation of results. In addition to the products cited in Table I, 1-butene, *n*-pentane, 2-methyl pentane, and *n*-hexane were also detected in more concentrated samples. The yield of any of these products was always ≤ 0.04 relative to C_2H_6 .

Two experiments in which nitric oxide was admitted (partial pressure = 3.1 mm.) gave a relative $G(C_2H_6)$ scavenged of 0.70, in excellent agreement with the value reported by Yang and Manno. No other prod-

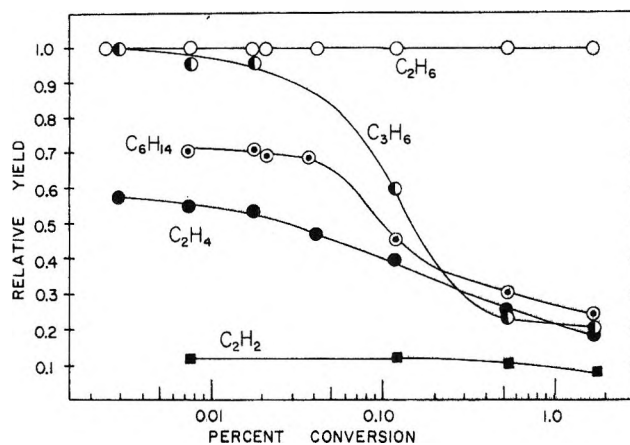


Figure 1.

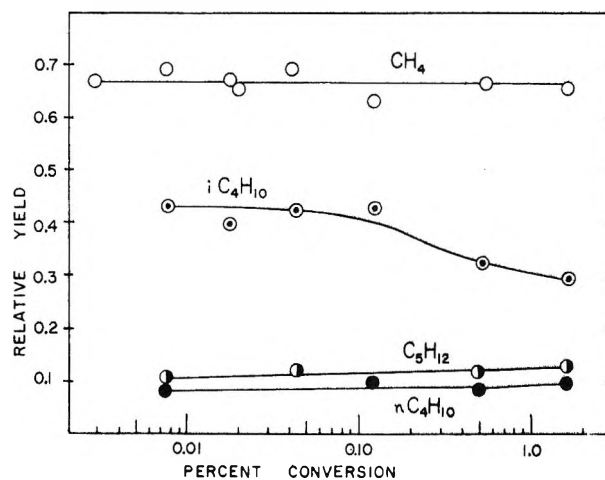


Figure 2.

ucts were analyzed during the present study in the scavenged system.

The yields of all low molecular weight products calculated on the basic mechanism proposed previously⁹ involving initial ionic fragmentation, ion-molecule reaction of the hydride ion transfer type, neutralization of propyl ions, and ensuing free radical disproportionation and combination reactions are in good quantitative agreement with the observed G values. Better agreement is obtained using a distribution of ion fragments extrapolated by means of the quasi-equilibrium theory to the shorter time scale appropriate to radiolysis¹⁰ than using the mass spectral pattern directly. The zero-dose G values of C_3 - C_6 products are not con-

(9) J. H. Futrell, *J. Am. Chem. Soc.*, **81**, 5921 (1959).

(10) M. Vestal, A. L. Wahrhaftig, and W. H. Johnston, ARL 62-426, Sept. 1962, available from Office of Technical Services, U. S. Dept. of Commerce, Washington 25, D. C.; M. Vestal and J. H. Futrell, to be published.

Table I: Comparison of Product Yields from the Radiolysis of $C_3H_8^a$

	CH_4	C_2H_6	$n-C_4$	$i-C_4$	$i-C_5$	C_2H_4	C_3H_6	C_2H_2	C_6^b
Yang and Manno ^c (unscavenged)	0.735	1.00	0.12	0.32	0.20	0.12	0.12	0.09	<i>d</i>
Yang and Manno ^c (added NO)	0.47	0.68	0.03	0.03	0.00	0.35	0.65	0.17	<i>d</i>
Present work (high conversion)	0.68	1.00	0.10	0.28	0.13	0.18	0.20	0.08	0.24
Present work (initial yields)	0.68	1.00	0.08	0.42	0.11	0.58	1.00	0.12	0.70

^a Yields normalized to principal hydrocarbon product, ethane, yield of unity. *G* values obtained in the present work may be derived by multiplying above values by 1.95. ^b 2,3-Dimethylbutane. ^c See ref. 2. ^d Not determined.

sistent with this mechanism if only the simple neutralization step, $C_3H_7^+ + e \rightarrow C_3H_6 + H$, proposed earlier for an analogous system⁹ maintains. However, the modified scheme proposed by Tiernan and Futrell⁴ for neutralization, plus the appropriate free-radical reactions, provide a self-consistent explanation for the observed yields. Sufficient uncertainties in the relative rates of the various reactions now exist, however, that the detailed mechanism cannot be considered as more than plausible. It is therefore felt that further discussion at this time is unwarranted.¹¹

Comparison of the high dose yields obtained in a 1.8% conversion with those of Yang and Manno (reported degree of conversion <1%) indicates that the cell geometry and high dose rate used in the present study result in a higher unsaturate yield owing to diffusion of products away from the primary reaction zone. This effect has been demonstrated previously for other hydrocarbon systems.¹²

Although the yield of propylene obtained in the presence of added scavengers relative to the unscavenged ethane yield has not been determined in the present study, treatment of the data of Ausloos and co-workers^{3,5} affords results in excellent agreement with those of Yang and Manno listed in Table I (relative yield = 0.65). Since 0.65 must define a "molecular" yield resulting from elimination processes, ion-molecule reactions, or charge neutralization, the difference between this value and the initial value of 1.00 obtained in the present work probably results from radical disproportionation ($\Delta[C_3H_6] = 0.35$). At lower conversions, the relative *G* of 2,3-dimethylbutane is 0.70, reflecting a high yield of isopropyl radicals produced *via* hydrogen atom abstraction processes which dimerize in the absence of scavengers. No ion-molecule reactions or excited state mechanisms leading to hexane analogs have been detected in propane, suggesting that the observed yield is entirely free radical in nature. Additional evidence for a free radical scheme is the fact that the C_4 - C_5 yield is reduced to trace amounts in the presence of nitric oxide as shown in Table I. If we assume that $\Delta[C_3H_6]$ over the scavenged value

results from disproportionation reactions of isopropyl radicals, we calculate $K_{disp}/K_{comb} = \Delta[C_3H_6]/[C_6] = 0.35/0.70 = 0.50$, in excellent agreement with literature values of 0.54¹³ and 0.50¹⁴ determined from photolysis studies. Cross disproportionation reactions of other radical intermediates with $i-C_3H_7\cdot$ would serve to lower the calculated value in our system although there is presently no way to assess their relative importance.

It is not appropriate in this discussion, however, to attempt to interpret the increase in C_2H_4 over the scavenged value ($\Delta = 0.22$) in a quantitative manner because of the complexity of the free radical distribution and the various cross-disproportionation reactions which are possible. The general observation that unsaturate yields are significantly higher at extremely low conversions than the values obtained with added free-radical inhibitors is consistent with the predictions of Back made several years ago.⁸

The decrease in the unsaturate yields with increasing conversion is indicative of secondary processes involving reactive intermediates, as has been suggested previously. In addition to the unsaturate decrease, the yields of isobutane and 2,3-dimethylbutane exhibit a concurrent trend which seems to be related while very slight increases are indicated by *n*-butane and isopentane. If the decrease in unsaturates is treated numerically as a relative *G* of carbon content using the initial and high conversion yields listed in Table I (*i.e.*, the decrease in relative G_{carbon} for C_3H_6 is $3 \times (1.00 - 0.20) = 2.40$, $2 \times (0.58 - 0.18) = 0.80$ for C_2H_4 , etc.), the total depletion in G_{carbon} for C_3H_6 , C_2H_4 , and C_2H_2 becomes 3.28. Treating the decrease in $i-C_4$ and C_6 in a corresponding manner, the resultant depletion for these products is 3.32. This equivalence

(11) An internal ARL report, L. W. Sieck and J. H. Futrell, available on request from the authors, provides a detailed discussion of the possible mechanism and constraints which the present data provide.

(12) J. H. Futrell, *J. Phys. Chem.*, **65**, 565 (1961).

(13) R. A. Back, *Can. J. Chem.*, **37**, 1834 (1959).

(14) P. J. Boddy and J. C. Robb, *Proc. Roy. Soc. (London)*, **A214**, 518 (1959).

suggests that related processes are involved in the variations observed, and this fact is worthy of some discussion.

If the premise is made that the decrease in unsaturates at higher doses is due to hydrogen atom addition reactions, then the slight increases in the *n*-C₄ and *i*-C₅ yields can be attributed to an enhanced C₂H₅ yield (resulting from H· attack of C₂H₄) occurring simultaneously with a decreasing yield of isopropyl radicals (the *i*-C₃H₇ steady-state concentration should be depleted at higher conversions owing to a decrease in the relative importance of H· abstraction reactions involving propane, which occurs almost exclusively from the secondary position). The dilemma in such an interpretation is that competition for H· by C₃H₆, the major unsaturate present in the system, should lead principally to *i*-C₃H₇ even though abstraction would be inhibited. Thus, the major internal scavenging reaction should not seriously effect the steady-state concentration of the expected precursors for *i*-C₄ and C₆, which exhibit the strongest dependence upon the degree of conversion. A possible explanation for the effect, consistent with the mechanism, is that the *sec*-propyl radical produced in the scavenging reaction is vibrationally excited and exhibits an abnormally high disproportionation-combination ratio. Such an interpretation is not unreasonable based on the results of Back¹⁵ from a study of the mercury-sensitized photolyses of propane and of propane with added propylene scavenger. He finds ratios of k_d/k_c for propyl radicals in this system of 0.5 and 0.8 at 600 and 300 mm., respectively. Hence, for propane at 40 mm. pressure in the present research, it is plausible to postulate that a much larger value of k_d/k_c pertains, and the sharp falloff in the dimer product may be explained in this fashion. Indeed, the rather similar results of Yang and Gant¹⁶ on the radiolysis of ethane at low conversion have been interpreted using such a mechanism.

We feel, however, that an equally plausible explanation for these effects is the interception by propylene of the major precursor of H atoms in the system. Back⁸ has reported that the addition of trace amounts of C₃H₆ to propane greatly reduces the yield of hydrogen. Futrell and Tiernan⁴ have proposed that a major reaction producing C₃H₆ and H atoms in the radiolysis of propane is neutralization of C₃H₇⁺ ions previously generated *via* hydride-transfer reactions. The occurrence of hydride transfer has also been extensively investigated by Ausloos and co-workers, and reasonable estimates from various isotopic studies indicate that such reactions dominate the ionic radiolysis mechanism. Since neutralization of C₃H₇⁺ ions should result in

unscavengable propylene and an equivalent yield of hydrogen following abstraction by H·, interfering reactions would significantly reduce the yields of these products. For reasons given below, this observation of Back may be explained as the reaction of C₃H₇⁺ ions (which cannot react further with propane except for the resonance hydride-transfer reaction) with the propylene additive (or accumulated C₃H₆ in the high dose experiments), such that molecular hydrogen and hydrogen atoms are not generated at some later stage.

Preliminary, high-pressure, mass spectrometric investigations in this laboratory involving mixtures of isopropyl ions (from isobutane) and propylene indicate that the adduct ion C₆H₁₃⁺ is obtained at lower repeller voltages, *viz.*, C₃H₇⁺ + C₃H₆ → C₆H₁₃⁺. This ion occurs without the appearance of adjacent masses corresponding to H· or H₂ loss from the complex, as would be expected from the endothermicity of the overall reaction¹⁷ in the latter cases. The observed cross section is rather low ($<1 \times 10^{-16}$ cm.²) for an ion-molecule reaction but is still large enough to be important at propylene concentrations of the order of 10⁻³%. Since propylene is obtained in high yields in the nitric oxide-scavenged system, this mechanism requires that this scavenger interferes with ionic attack of accumulated C₃H₆. Ausloos, Gorden, and Lias,¹⁸ as a result of some radiolysis investigations involving mixtures of methane and various additives, concluded that alkyl radical ions which cannot react with the hydrocarbon parent react readily with radical scavengers even though these compounds constitute less than 0.02% of the total reaction mixture.

Whether or not this observation can be attributed to greatly enhanced neutralization rates owing to electron capture by electronegative scavengers or to interfering ion-molecule reactions cannot be evaluated quantitatively. Both types of processes are possible, and one or the other seems to be operating in the propane-nitric oxide system. A further possibility in the unscavenged system which should be considered is attack of C₄ and C₆ by *i*-C₃H₇⁺ after accumulation of these products at higher conversions. In this instance, hydride transfer and other reactions are exothermic, but no prediction can be made as to the nature of the resultant species. On the basis of the

(15) R. A. Back, *Can. J. Chem.*, **37**, 1834 (1959). Note an apparent typographical error in K_5/K_4 at 300 mm. on p. 1840.

(16) K. Yang and P. Gant, *J. Phys. Chem.*, **65**, 1861 (1961).

(17) F. H. Field and J. L. Franklin, "Electron Impact Phenomena," Academic Press, New York, N. Y., 1957.

(18) P. Ausloos, R. Gorden, and S. G. Lias, *J. Chem. Phys.*, **39**, 3341 (1963).

present evidence, we are unable to suggest which of these plausible mechanisms is the more likely explana-

tion for the conversion effects observed in the present work.

Rare Gas Sensitized Radiolysis of Acetylene¹

by J. H. Futrell and L. W. Sieck

*Aerospace Research Laboratories, Office of Aerospace Research, Wright-Patterson Air Force Base, Ohio
(Received September 5, 1964)*

The gas phase radiolysis of acetylene has been investigated in the presence and absence of various sensitizers at various dose rates. The polymerization reactions have been correlated with high-pressure, mass spectrometric studies of mixtures with rare gases, with the conclusion that the precursors for polymer propagation do not depend upon charge exchange (ionization of acetylene). A quantitative investigation of benzene production and sensitization indicates that neon is unique among the noble gases in that it alone enhances the formation. The initial interaction, $\text{Ne}^+ + \text{C}_2\text{H}_2 \rightarrow \text{C}_2\text{H}^+ + \text{H} + \text{Ne}$, observed mass spectrometrically is responsible. Various photolysis and radiolysis experiments involving argon-deuterium-acetylene and deuterium-acetylene mixtures have defined the mechanism for the increase in $G(\text{C}_6\text{H}_6)$ observed in this work and in previous studies at lower dose rates.

Introduction

The radiation-induced polymerization of acetylene and the sensitized radiolysis of acetylene early attracted the attention of workers in the field of radiation chemistry.² The simplicity of the over-all reaction, which produces only benzene and an insoluble polymer, cuprene, in significant quantities, has, no doubt, been partly responsible for the sustained interest in this subject. Recent investigations³ have quantitatively established the radiolytic yields of benzene and cuprene and have shown them to be invariant with dose, dose rate, radiation type, and pressure over a substantial range at pressures above 20 torr and at dose rates above 2×10^{13} e.v. cm.⁻³ sec.⁻¹. Dorfman and Wahl studied the effect of rare gases as sensitizers in an attempt to assess the importance of ionic processes in the over-all reaction.^{3b} Mains, Niki, and Wijnen⁴ and Field⁵ have recently conducted an extensive study of acetylene radiolysis, including isotopic studies and the influence of added scavengers and sensitizing agents. Despite the

long history of careful investigation, however, the mechanisms for formation of benzene and polymer cannot be considered as established.

Recently Lindholm, Szabo, and Wilmenius have studied charge-exchange reactions of a great many ions with acetylene,⁶ and it is now possible to discuss the sensitized radiolysis in a more definitive manner. Accordingly, the radiolysis of acetylene and the efficiency

(1) Presented at the 12th Annual Meeting of the Radiation Research Society, Miami Beach, Fla., May 17-20, 1964.

(2) See S. C. Lind, "Radiation Chemistry of Gases," Reinhold Publishing Corp., New York, N. Y., 1961, Chapter 9, for summary of early work and for references.

(3) (a) L. M. Dorfman and F. J. Shipko, *J. Am. Chem. Soc.*, **77**, 4723 (1955); (b) L. M. Dorfman and A. C. Wahl, *Radiation Res.*, **10**, 680 (1959).

(4) G. J. Mains, H. Niki, and M. H. J. Wijnen, *J. Phys. Chem.*, **67**, 11 (1963).

(5) F. H. Field, *ibid.*, **68**, 1039 (1964).

(6) E. Lindholm, I. Szabo, and P. Wilmenius, *Arkiv Fysik*, **25**, 417 (1964).

of the rare gases xenon, krypton, argon, neon, and helium as sensitizers has been reinvestigated. Since it has been demonstrated that benzene can serve as an inhibitor of acetylene polymerization,⁷ particular attention has been given to working at low conversion and to using pure compounds.

Experimental

Irradiations were performed using 0.95-Mev. electrons produced by a nominal 1-Mev. Van de Graaff accelerator using general procedures described previously.^{8,9} Pyrex flasks of ca. 1-l. volume containing thin "bubble" entrance windows were used in most experiments while similar 200-ml. targets were used in the experiments in which only cuprene formation by rare gases was measured. The beam current during irradiation was monitored by a Varian recorder using an appropriate voltage divider network to give approximately half to full-scale pen deflection for the desired current. The total dose was determined by graphical integration, and G values (molecules produced or consumed/100 e.v. absorbed) were calculated as previously described.⁸

Acetylene was obtained from the Matheson Co. and was purified by the following procedure. The vacuum manifold, including a Wallace and Tiernan differential pressure gauge, the targets to be filled, an \sim 1-l. reservoir volume with trap, and the gas cylinder line were evacuated to a pressure less than 0.01 μ , isolated from the pump system, and filled to a slightly greater pressure of acetylene than was required for the experiment. This sample was condensed into the reservoir-trap system and frozen out with liquid nitrogen, after which the system was re-evacuated. This sample was then re-expanded into the system, refrozen, and the cycle was repeated until degassing was complete. The acetylene was permitted to expand into the system to the desired pressure (35 mm. in most experiments) at which time the reservoir containing the excess acetylene and heavier contaminants was quickly isolated from the system. Careful mass spectrometric analysis demonstrated that this procedure effectively removed carbon monoxide, acetone, and benzene initially present as trace impurities.

Matheson research grade rare gases were analyzed mass spectrometrically and found to contain no detectable impurities except for small quantities of other rare gases. Matheson deuterium contained ca. 0.4% HD as the only impurity, and no contaminants were detected in Matheson hydrogen. Accordingly, these gases were used without purification.

Product yields were determined by mass spectrometry. Low conversion studies were possible through

use of an electron multiplier detector on a modified Consolidated Model 21-103C described earlier.^{10,11} The multiplier gain characteristics relative to an electrometer detector were determined experimentally over the mass range of interest. The relative signal intensity of the benzene parent ion to that of the C_2^+ ion from acetylene was determined empirically for particular settings of the multiplier and Wien bridge parameters. Adherence to a strict time schedule for analysis after admitting the sample and careful attention to the previous history of the source to minimize adsorption-desorption problems were necessary for acceptable precision of analysis at low conversion levels.

No attempt was made to measure quantitatively other radiolysis products after it was determined that they are formed only in very small amounts. Gas chromatography indicated the probable formation of vinylacetylene and diacetylene and possibly butadiene, but only in amounts of less than 5% of the benzene yield. These results are in general accord with earlier studies, and it is clear that benzene and cuprene are the only products formed in significant quantities.

In the mercury-sensitized experiments a quartz cell of \sim 200-ml. volume enclosed in an insulated aluminum block wrapped with heating wires was used as the photolysis vessel. It was charged with 25 mm. of acetylene, approximately 3 ml. of liquid mercury, and various amounts of deuterium. It was then heated to $260 \pm 1^\circ$ (at which the vapor pressure of mercury is approximately 96 mm.) and exposed to radiation from a Hanovia Type 30600 mercury-resonance lamp. The intensity was adjusted by changing the lamp-to-cell distance to approximate the rate of benzene formation observed in the medium dose rate radiolysis study. Monodeuteriobenzene, HD, and CHCD were the only deuterated products formed in significant quantities, and the deuteriobenzene-benzene ratios were determined from the reported cracking pattern for deuteriobenzene¹² and calibration standards for ordinary benzene.

The polymer formation was determined by assuming that the partial pressure of rare gas additive was unchanged during radiolysis. The ratios of acetylene to rare gas were then measured mass spectrometrically before and after radiolysis. A correction for the con-

(7) S. C. Lind and P. S. Rudolph, *J. Chem. Phys.*, **26**, 1768 (1957).

(8) J. H. Futrell and T. O. Tiernan, *ibid.*, **37**, 1694 (1962).

(9) J. H. Futrell and T. O. Tiernan, *ibid.*, **38**, 150 (1963).

(10) J. H. Futrell and T. O. Tiernan, *ibid.*, **39**, 2539 (1963).

(11) K. R. Ryan, L. W. Sieck, and J. H. Futrell, *ibid.*, **41**, 111 (1964).

(12) F. D. Rossini, Ed., "Catalog of Mass Spectral Data," American Petroleum Institute Project 44, Carnegie Institute of Technology, Serial 538, contributed by the National Bureau of Standards.

version of acetylene to benzene by direct radiolysis was applied, and it was assumed that the remaining decrease in partial pressure of acetylene led to cuprene formation. A detailed study of polymer formation from pure acetylene was not made, but a crude manometric study of the pressure decrease gave results in agreement with earlier workers [$G(-C_2H_2) = 71.9^{3a}$ and the fraction of that amount converted to benzene is approximately 0.20].

The charge-exchange reactions of rare gas ions with acetylene were studied using the technique introduced by Cermak and Herman.¹³

Results and Discussion

Polymer Formation. The charge-exchange studies of Lindholm, Szabo, and Wilmenius have established that acetylene exhibits several remarkable characteristics⁶ such that it seems to resemble a diatomic molecule more than a typical hydrocarbon. The molecule ion is formed in two isolated electronic states, the first extending from the ionization potential, 11.4 e.v., to 12.5 e.v. and the second, rather broader state extending from ca. 15.5 to 22 e.v. In the region from 12.5 to 15 e.v. the cross section of acetylene for ionization by charge exchange is essentially zero, and low kinetic energy ions with recombination energies in this "window" region do not produce acetylene ions. Thus, the elementary condition that the initially ionized species have the higher ionization potential is insufficient to assure that the reaction takes place for acetylene and probably for all systems with limited internal degrees of freedom.

The rare gases have appropriate recombination energies (Xe^+ , 12.13 and 13.44 e.v.; Kr^+ , 14.0 and 14.7 e.v.; Ar^+ , 15.7 and 15.9 e.v.; Ne^+ , 21.6 and 21.7 e.v.; He^+ , 24.6 e.v.) to permit verification of Lindholm's findings by the modified operation of a conventional mass spectrometer as described previously.¹⁰ The results of such a study are summarized in Table I and are in complete accord with their conclusions. The acetylene molecule ion signal observed for mixture A establishes the level expected for self-charge exchange. Mixtures B and D exhibit a substantial increase in ion signal from charge exchange of xenon and argon ions. Mixture C with krypton, by contrast, shows no increase over that produced by acetylene itself. Thus, it seems clearly established that there are at least two states of the acetylene ion separated by an energy gap. The recombination energies of both the $^2P_{3/2}$ and $^2P_{1/2}$ states of krypton ion fall in this region.

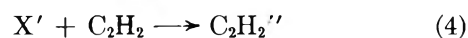
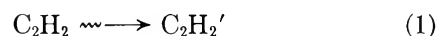
This peculiarity of acetylene made a reinvestigation of the radiolysis of acetylene sensitized by a large excess of these rare gases pertinent to assessing the rele-

Table I

Mixture	Reservoir pressures	$C_2H_2^+$ intensity, arbitrary units
A	12.0 μ of C_2H_2	210 \pm 3
B	12.0 μ of C_2H_2 520 μ of Xe	1680 \pm 20
C	12.0 μ of C_2H_2 498 μ of Kr	208 \pm 5
D	12.0 μ of C_2H_2 570 μ of Ar	1610 \pm 30

vance of ionic processes in the over-all mechanism. In the case of xenon, only the lower $^2P_{3/2}$ state can produce the molecule ion of acetylene by charge exchange. Furthermore the metastable levels of xenon lie below the ionization potential. Krypton ions, as we have seen, do not charge-exchange with acetylene, and the metastable levels of krypton at 9.9 and 10.6 e.v. are also below the ionization potential of acetylene. Argon, on the other hand, produces acetylene ions in the upper electronic state by charge exchange from both the $^2P_{3/2}$ and $^2P_{1/2}$ states of the argon ion, while the argon metastables at 11.5 and 11.7 e.v. produce lower state acetylene ions on collision.¹⁴

The sensitized formation of cuprene may be discussed in terms of a generalized mechanism without expressing the nature of the precursors as



where X represents a rare gas or other sensitizing agent. From this

$$\frac{d(\text{polymer})}{dt} = \frac{Q_{C_2H_2}[C_2H_2]G(C_2H_2')}{100} + \frac{Q_X[X]G(X')}{100}$$

where Q_i = rate of energy absorption per unit pressure per unit time (e.v. cm.⁻³ sec.⁻¹) and $G(Y)$ = yield of Y in molecules/100 e.v. of absorbed energy. Representing the first and second energy absorption terms by α and β , respectively, the rate of polymerization is given by $R = \alpha G(C_2H_2') + \beta G(X')$, and the relative efficiency of energy utilization to produce polymer by the sensitizer compared to acetylene is $G(X')/G(C_2H_2') = 1/\beta G(C_2H_2') [R - \alpha G(C_2H_2')]$.

(13) V. L. Cermak and Z. Herman, *Nucleonics*, **19**, 106 (1961).

(14) V. L. Cermak and Z. Herman, private communication.

Typical experimental results are given in Table II. They are in agreement with the early results of Lind and Bardwell that the rare gases are efficient sensitizers of acetylene polymerization.¹⁵ These workers assert that, in our terminology, $G(X')/G(C_2H_2')$ is unity for low concentrations of sensitizer but that the efficiency falls with increasing ratio of rare gas to acetylene. Their Table IV also indicates that krypton is a more efficient sensitizer than xenon or argon.

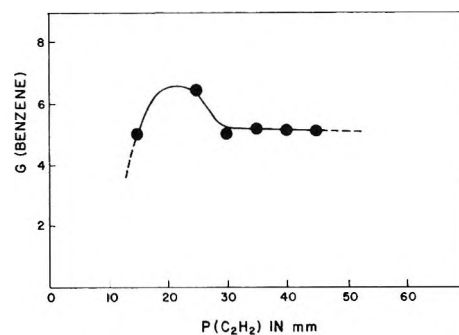
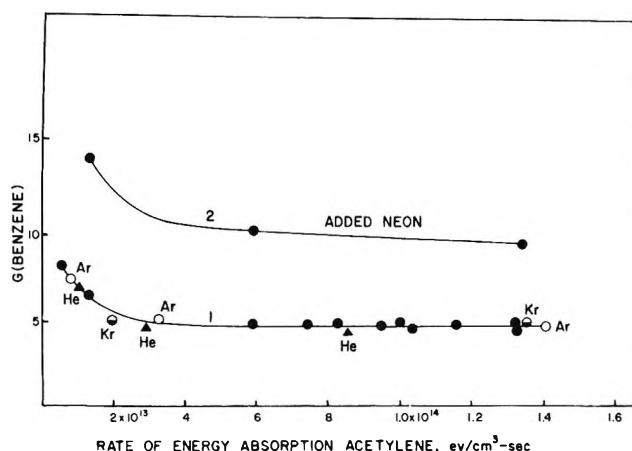
Table II

Mixture	Relative polymerization efficiency $G(X')/G(C_2H_2')$
24 mm. of C_2H_2	0.44
145 mm. of Xe	
24 mm. of C_2H_2	0.51
199 mm. of Kr	
24 mm. of C_2H_2	0.44
413 mm. of Ar	
35 mm. of C_2H_2	0.35
400 mm. of He	
35 mm. of C_2H_2	0.39
450 mm. of Ne	

From the preceding discussion we would expect the concentration of acetylene ions from the heavier rare gases to be $Ar > Xe \gg Kr$. Since there is no correlation of rate of sensitization of polymerization with this inequality, the precursor in reaction 4 cannot be identified as the acetylene molecule ion. It also seems unlikely that this ion is of such major importance in pure acetylene that it can be identified as the precursor in reaction 1 although some contribution of acetylene ions to polymer formation as proposed by Rudolph and Melton¹⁶ cannot be ruled out. A similar conclusion that the major polymer formation mechanism is not ionic in character has been reached by Field on the basis of the observed temperature coefficient of the reaction.⁵

Benzene Formation. It was noted in these experiments that no substantial increase in the benzene yield over that expected from direct radiolysis occurred, confirming the previous results of Dorfman and Wahl.^{3b} However, both of the two most recent publications^{4,5} on acetylene radiolysis cite evidence that energy transfer from the rare gases to acetylene leading ultimately to benzene does occur. Accordingly, we have made a quantitative kinetic study of benzene formation in the presence and absence of rare gases. We have restricted ourselves to the low conversion region since it has been shown that the presence of moderate amounts of benzene alters the kinetics of acetylene decomposition.⁷

It was first necessary to establish the pressure effect and the intensity effect on this reaction.¹⁷ The pressure effect was investigated for a constant incident current of 0.95-Mev. electrons corresponding to a dose rate of $2.4 \times 10^{12} P$ e.v. $cm^{-3} sec^{-1}$, for P expressed in torr, and is shown in Figure 1. The shape of this curve is qualitatively similar to the corresponding Figure 2 in Field's paper. The area of the maximum is, however, somewhat narrower in our experiments, and the constant yield region is achieved at a much lower pressure. These differences may possibly be attributed to the different geometry of our radiolysis vessel. Dorfman and Wahl^{3b} have demonstrated the importance of cell geometry and have suggested diffusion to the walls by a benzene precursor as an explanation for the falloff in benzene yield. Although it was not observed in their

Figure 1. Effect of pressure on $G(C_6H_6)$.Figure 2. Effect of dose rate on $G(C_6H_6)$ in the rare gas sensitized radiolysis.

(15) S. C. Lind and D. G. Bardwell, *J. Am. Chem. Soc.*, **48**, 1575 (1926).

(16) P. S. Rudolph and C. E. Melton, *J. Phys. Chem.*, **63**, 916 (1959).

(17) The unsuspected presence of these effects slightly modifies the results presented at the 12th Meeting of the Radiation Research Society, Miami, Fla., May 1964.

work, it may be noted that Mains, Niki, and Wijnen predict such a maximum in $G(\text{benzene})$ at low pressure.⁴

The effect of intensity at constant pressure is given in curve 1 of Figure 2 for a constant acetylene pressure of 35 mm. Field has observed a similar intensity effect⁵ while Mains, *et al.*, observe a drastic change in $G(\text{C}_6\text{H}_6)$ from Co^{60} γ -irradiation compared with X-rays,⁴ which may be, in part, an intensity effect. The present results differ from the work cited in that a constant $G(\text{C}_6\text{H}_6)$ is observed over a wide range of radiation intensity. Dorfman and Shipko^{3a} also found a broad range of pressure and radiation intensity where $G(\text{C}_6\text{H}_6)$ is invariant, and it seems that variations are found only at rather low pressure and/or low radiation intensity.

Figure 2 also summarizes the results of our investigation of the sensitized radiolysis of acetylene. In these experiments the acetylene pressure was 35 mm., as in the intensity study, and 450 mm. of the rare gases was added. Argon, neon, and helium were studied at different intensities while krypton was studied only in the dose rate-independent region. Xenon was not reinvestigated quantitatively, but preliminary experiments gave no evidence for sensitization. Since the points for argon, helium, and krypton fall on the curve for pure acetylene, it is clear that no sensitization occurs for these gases. The same conclusion was reached by Dorfman and Wahl,^{3b} who studied all the common noble bases except neon.

In contradiction of these results, Mains, Niki, and Wijnen have reported that krypton sensitizes *both* benzene and polymer formation. We think a possible explanation may have been the presence of trace impurities in their experiment, as this has proven a significant factor in our own study. In preliminary experiments we used acetylene which had not been purified carefully and which contained, therefore, trace quantities of acetone detectable mass spectrometrically using the electron multiplier-amplifier system. For all systems, except krypton-acetylene, results in reasonably good agreement with those plotted in Figure 2 were obtained. Krypton, however, gave indications of sensitization and very nonreproducible results. It was further observed that the acetone impurity was greatly depleted in radiolysis. Since methyl radicals are known to produce benzene from acetylene,¹⁸ we may reasonably attribute these results to dissociative charge exchange of krypton ions with the acetone impurity to generate free-radical precursors of benzene. The krypton system is especially susceptible to this artifact because, as previously discussed, krypton ions do not undergo charge exchange with acetylene.

Although he does not discuss his results in terms of

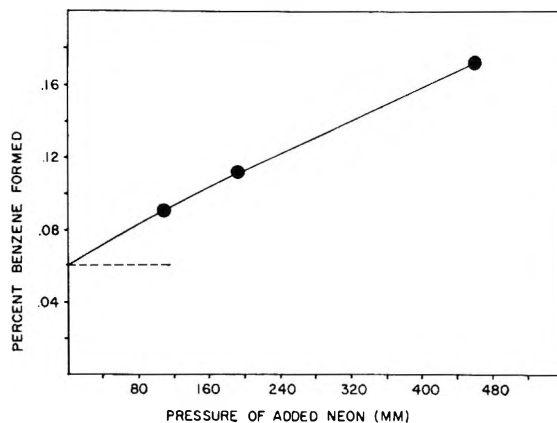


Figure 3. Yield of C_6H_6 in the neon-sensitized radiolysis as a function of added neon in the high dose rate region.

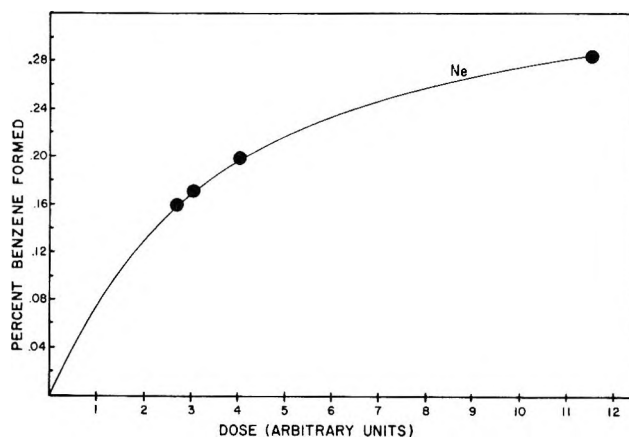


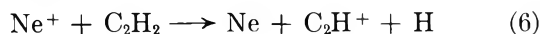
Figure 4. Effect of % conversion in $G(\text{C}_6\text{H}_6)$ in the neon-sensitized radiolysis at high dose rate.

sensitization, Field reports data which may be taken as evidence for sensitization by both krypton and argon.⁵ It is difficult to estimate the magnitude of this effect as he reports his data in terms of benzene produced per unit of energy absorbed by the system (rare gas plus acetylene). Indeed, this paper asserts that argon at low partial pressures enhances the reaction and at high pressure inhibits it. The demonstrated effects of pressure, intensity, and geometry on the reaction may possibly be responsible for the discrepancy in our results. Nevertheless, we feel that curve 1 of Figure 2 clearly establishes that argon does not have any detectable effect, either inhibition or sensitization, on the radiolytic formation of benzene by acetylene.

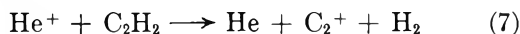
Since neon, alone, of the rare gases serves as a sensitizer, this system was studied further. Figure 3 shows that the sensitization is linear with pressure at low conversion while Figure 4 shows that the effect falls off at

(18) C. M. Drew and A. S. Gordon, *J. Chem. Phys.*, **31**, 1417 (1959).

higher conversion. The falloff occurs at much higher conversions than the kinetic runs presently reported. In interpreting these results, it is of interest to examine the information on dissociative charge exchange.⁶ As discussed previously, xenon and krypton ions produce $C_2H_2^+$ by charge exchange. Helium ions produce mostly C_2^+ while the major acetylene ion from neon charge exchange is C_2H^+ , *viz.*



Since H atoms are known to initiate polymerization of acetylene to benzene,¹⁹ we may reasonably attribute the sensitization by neon to reaction 6. By the same token, since helium does not sensitize benzene formation, the charge-exchange reaction must not produce hydrogen atoms. Hence, the charge-exchange reaction observed by Lindholm must be



rather than the corresponding reaction producing H atoms.

Although the H atom hypothesis is attractive, a logical alternative to explain the neon results is the proton-transfer reaction

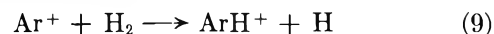


which cannot be ruled out on energetic grounds. Accordingly, we have searched for evidence for this reaction mass spectrometrically and have reinvestigated some of the previously reported ion-molecule reactions of acetylene. In Table III we report the reactions observed previously. We have established the pre-

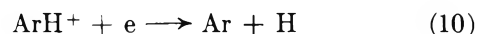
produce $C_4H_3^+$ ions. The latter is in agreement with Field, Franklin, and Lampe²⁰ and Barker, Hamill, and Williams,²¹ who identified $C_2H_2^+$ as the reactant ion from appearance potential measurements. We also find evidence for proton transfer from the upper state $C_2H_2^{+*}$ ion as in reaction 2 of Table III, but the principal proton-transfer reactant ion is CH^+ in reaction 4 of Table III. The reaction of greatest importance for C_2H^+ is eq. 3 of Table III, which may result simply in doubling the number of H atoms to be expected in the radiolysis system from charge exchange of acetylene with Ne^+ .

It cannot be stated with certainty that this doubling of H atom production will occur in the radiolysis system at much higher pressure. In fact, Rudolph, Lind, and Melton²² have shown that the probability of decomposition of certain ion-molecule complexes decreases with increasing pressure. The nonsensitization of benzene formation by Xe^+ may be taken as further evidence that reaction 1a of Table III does not go to completion at higher pressure, *i.e.*, that $C_4H_4^+$ is formed without dissociation to the $C_4H_3^+$ product observed in the mass spectrometer.

In an attempt to explore further the H atom mechanism, hydrogen was added in a series of experiments to the argon-acetylene system. The hydrogen may be expected to complete with acetylene for argon ions according to the well-known reaction



In the absence of competing reactions, neutralization would give a second hydrogen atom



A pronounced sensitization of benzene formation was indeed found to occur in the argon-acetylene-hydrogen system. An equivalent series of reactions occurs when deuterium is substituted for hydrogen, and the results from the latter study are summarized in Figures 5, 6, and 7.

With added deuterium, the benzene formed is a mixture of benzene and monodeuteriobenzene. The increase in benzene C_6H_6 is shown in Figure 5 for two different dose rates. Curve 1 represents the yield obtained at high dose rate (beam current $5.0 \mu a.$, corresponding to a dose rate in pure C_2H_2 of 8.0×10^{13} e.v.

Table III: Ion-Molecule Reactions in Acetylene

- | | |
|------|---|
| (1a) | $C_2H_2^+ + C_2H_2 \rightarrow C_4H_3^+ + H$ |
| (1b) | $C_2H_2^+ + C_2H_2 \rightarrow C_4H_2^+ + H_2$ (or 2H) |
| (1c) | $C_2H_2^{+*} + C_2H_2 \rightarrow C_4H_2^+ + H_2$ (or 2H) |
| (2) | $C_2H_2^{+*} + C_2H_2 \rightarrow C_2H_3^+ + C_2H$ |
| (3) | $C_2H^+ + C_2H_2 \rightarrow C_4H_2^+ + H$ |
| (4) | $CH^+ + C_2H_2 \rightarrow C_2H_3^+ + C$ |

cursor ion(s) by means of the technique of comparing normalized ionization efficiency curves of primary and secondary ions.¹¹ No evidence for proton transfer from C_2H^+ was obtained, as only the addition reaction was observed. Lindholm, Szabo, and Wilmenius⁶ suggest that the lower state $C_2H_2^+$ ion reacts with acetylene to produce only $C_4H_3^+$, as in reaction 1a in Table III, while the upper state $C_2H_2^{+*}$ reacts as eq. 1c in Table III. Our results confirm this but indicate that the ground-state ion also reacts as in eq. 1b to

(19) D. J. LeRoy and E. W. R. Steacie, *J. Chem. Phys.*, **12**, 369 (1944).

(20) F. H. Field, J. L. Franklin, and F. W. Lampe, *J. Am. Chem. Soc.*, **79**, 2665 (1957).

(21) R. Barker, W. H. Hamill, and R. R. Williams, *J. Phys. Chem.*, **63**, 825 (1959).

(22) P. S. Rudolph, S. C. Lind, and C. E. Melton, *J. Chem. Phys.*, **36**, 1031 (1962).

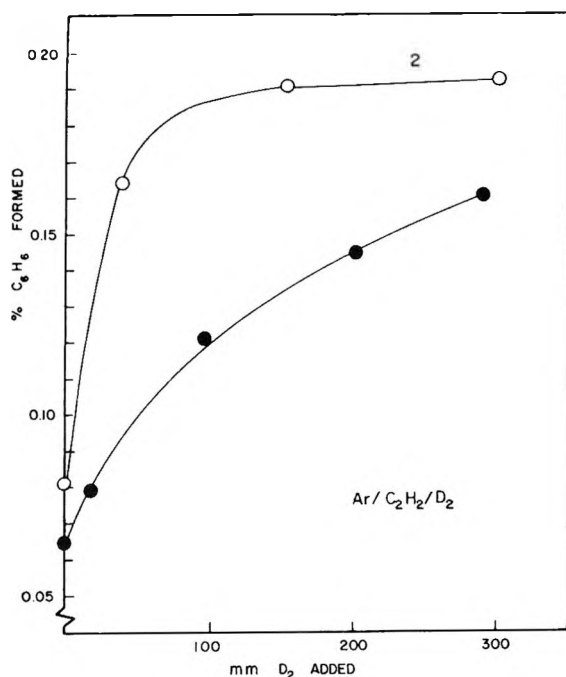


Figure 5. Yield of C_6H_6 in the $Ar-D_2-C_2H_2$ system as a function of added D_2 : curve 1, high dose rate; curve 2, low dose rate.

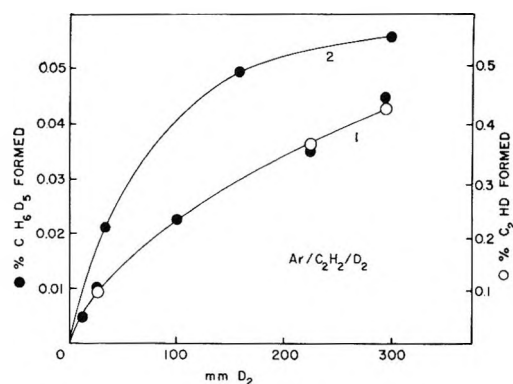


Figure 6. Yield of C_6H_5D and C_2HD in the $Ar-D_2-C_2H_2$ system as a function of added D_2 : curve 1, high dose rate; curve 2, low dose rate.

$cm^{-3} sec^{-1}$) whereas curve 2 resulted from experiments carried out at $0.9 \mu a.$ ($1.44 \times 10^{13} e.v. cm^{-3} sec^{-1}$). The intercept of curve 1 corresponds to $G(C_6H_6) = 5.2$ for acetylene alone or acetylene plus argon while the lower current experiments are extrapolated to $G(C_6H_6) = 6.5$ as obtained from Figure 2. The yield of benzene C_6H_5D is shown in Figure 6 as a function of added D_2 , with curves 1 and 2 again representing the high and low dose rate cases, respectively. Also shown in Figure 6 as the right-hand ordinate is the amount of C_2HD produced in the radiolysis for the higher dose rate experiments. Coincidentally, the rate of exchange to

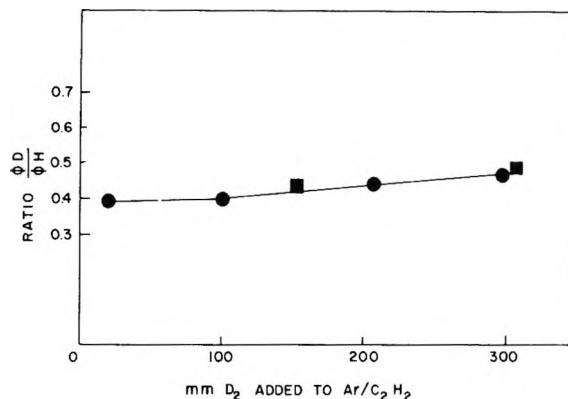
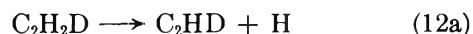
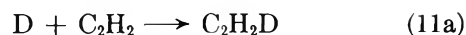


Figure 7. Ratio of C_6H_5D produced to $\Delta[C_6H_6]$ in the $Ar-D_2-C_2H_2$ system as a function of added D_2 : ■, low dose rate; ●, high dose rate.

C_2HD is very nearly ten times the rate of formation of C_6H_5D . The exchange reaction presumably goes *via*

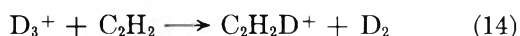
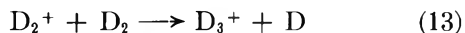


as indicated both by the extensive H-D exchange which occurs and by the fact that the $Ar-C_2H_2-D_2$ -sensitized radiolysis produces more C_6H_6 than C_6H_5D benzene. Figures 5 and 6 clearly demonstrate a significant dose rate effect in both C_6H_6 and C_6H_5D production initiated by D atoms. The plateau region in curve 2 (Figure 5) indicates that all argon ions are intercepted when approximately 100 mm. of D_2 is added, and any slight increase observed in the plateau portion of the plot can be attributed to direct absorption of energy by D_2 as its partial pressure is increased. The observed enhancement of the resultant benzene yields at lower dose rates is qualitatively similar to the effect observed in the radiolysis of pure acetylene and in the rare gas-sensitized systems (Figure 2). The further implications of this data will be discussed in another section.

The ratio $[C_6H_5D]/\Delta[C_6H_6]$, where $\Delta[C_6H_6]$ refers to the increase in C_6H_6 benzene as a result of the sensitization reaction, is plotted for both dose rates in Figure 7. This parameter is of interest as it may be a characteristic of D atom-initiated polymerization of acetylene. For comparison, the mercury-sensitized photolysis of the system $Hg-D_2-C_2H_2$ was studied. Since the lamp used emitted a small amount of 1849-Å. light, a minor correction for direct photolysis was necessary. This was accomplished by extrapolating the benzene yield to zero deuterium and subtracting this intercept from each point. The resulting value for the ratio $[C_6H_5D]/[C_6H_6]$ for deuterium atom initiation from a series of

five experiments was 0.35 ± 0.05 . This may be compared with the dose rate-independent value, 0.42 ± 0.03 , for the Ar-D₂-C₂H₂ system. The agreement is therefore satisfactory with the postulate that D atoms are the initiators of the sensitized formation of benzene in this system.

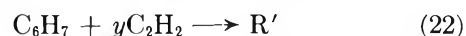
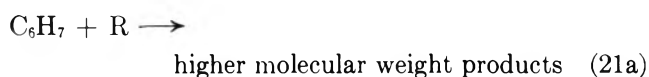
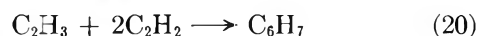
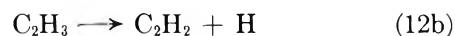
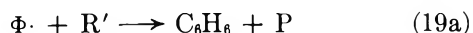
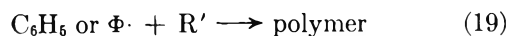
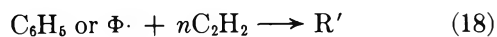
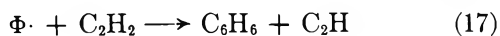
A similar preliminary radiolytic investigation of the D₂-C₂H₂ system was carried out. In this case the ratio $[C_6H_6D]/\Delta[C_6H_6]$ cannot be determined as accurately because the stopping power of deuterium is so much less than that of argon, and the amount of sensitization is correspondingly less. However, the approximate value for the ratio is 1.1 ± 0.2 , which is substantially larger than the deuterium atom value. It therefore seems necessary to postulate an additional precursor for benzene in this system. One possibility is proton transfer according to the sequence



Mains, Niki, and Wijnen supported the H atom hypothesis with a study of various free-radical scavengers in which they have shown that moderate amounts of isobutylene, oxygen, or iodine suppress benzene formation.⁴ We confirmed this observation by adding 8 mm. of purified air to 35 mm. of C₂H₂ before radiolysis. Mass spectrometric analysis after irradiation showed that this amount of oxygen was sufficient to prevent benzene production, that oxygen was consumed in the reaction, and that cuprene formation (from the C₂H₂/N₂ ratio, assuming [N₂] remained constant) was substantially enhanced by the presence of air.

Conclusions

Although the present results and previous data are far from sufficient to establish a unique mechanism for either benzene or cuprene formation, the nature of some of the reactions involved can be discussed in some detail. For benzene, an oversimplified mechanism which seems to be consistent with the experimental facts is



We feel that the effect of added scavengers, isotopic experiments,⁴ and other pertinent data clearly demonstrates the participation of H atoms, and, thus, the chain-initiating step must be C-H cleavage. Reaction 16 leads to the production of 1,3-hexadien-5-ynyl radicals (C₆H₆) while (20) results in the formation of 1,3,5-hexatrienyl (C₆H₇). Both of these intermediates are noncyclic, and both are presumably primarily in the *trans* configuration from simple minimum energy considerations. Of these, cyclization to an aromatic structure would proceed at a faster rate for C₆H₆ owing to greater delocalization and orbital overlap within the π -system. Following cyclization, reaction 17 is favored (although abstraction by C₆H₆ is endothermic by approximately 21 kcal./mole²³ for normal phenyl radicals) because the formation of the aromatic form by the route indicated is exothermic by some 163 kcal./mole. Chain reaction is therefore possible.

As mentioned above, cyclization of *trans*-1,3,5-hexatrienyl radicals would be a comparatively slow process and perhaps could not occur at all without prior loss of one of the two H atoms from the terminal methylene position. Aromatic formation by this sequence will be greatly affected by interfering radical combination reactions, as has been confirmed by the observed dose rate dependence for the D atom-sensitized system. Reaction 21b or cyclization can only compete favorably at reduced dose rates, and reactions of type 19, 21a, and 22 could account for the observation that aromatic groups are incorporated in the polymer.²⁴ Although the H atom-sensitized sequence is clearly dose rate dependent, it would be expected that cyclization of trimer intermediates having C₂H precursors followed by hydrogen abstraction (reactions 16 and 17) would not be seriously affected by increased radical concentrations. This assumes, however, that the cyclization step is very rapid compared with the chain propagation sequence represented by (18) and (19). Once cyclization occurs, abstraction to produce benzene should

(23) T. L. Cottrell, "The Strengths of Chemical Bonds," Academic Press, Inc., New York, N. Y., 1954.

(24) Dr. L. A. Harrah, personal communication.

occur at the first collision because of the excess energy available. The increase in the $[C_6H_5D]/\Delta C_6H_6$ ratio at higher D_2 concentration suggests that some excited C_6H_5 intermediates (produced by direct absorption of incident energy by acetylene) abstract D from D_2 , which is allowed energetically. Other details notwithstanding, benzene formation initiated by C_2H precursors is proposed to account for the dose-independent G value for benzene production in the acetylene system. The marked dose dependence for the series of reactions initiated by vinyl radical precursors can account for the enhancement of benzene formation at lower dose rates. This mechanism suggests that yields will fall off at lower pressures owing to diffusion of long-lived C_6 intermediates to the wall prior to cyclization.

The cuprene-forming reactions are still very much in doubt, and one difficulty with acetylene is the ease with which polymerization can be initiated by many agents. Free radicals and ions in independent studies produce polymer, and possibly also nondissociative, excited molecules.²⁵ The present sensitization studies are consistent with the "ion cluster hypothesis" of Lind and Bardwell,¹⁵ which is, however, untenable on theoretical ground.^{26,27} A possible alternative explanation for the nearly equal efficiency of the rare gases as sensitizers is anionic polymerization initiated by electron attachment. Although there is no experi-

mental evidence for such a process, it seems plausible for such a readily polymerizable substance. It is evident that no unique mechanism can be suggested, and the relatively constant rate of cuprene formation, as a number of experimental parameters is varied, remains a puzzle to those who have investigated this system.

Independent of mechanistic details, this research seems to establish a duality of precursors for benzene and cuprene as suggested by Dorfman and Wahl.^{3b} Ionic processes do not seem to contribute at all to benzene formation in the dose rate independent region where most of our studies were carried out, and they do not appear to be determinative in the polymerization to cuprene.

Acknowledgments. The authors wish to acknowledge helpful discussions with Dr. Leonard Spialter of this laboratory, Professor G. J. Mains of Carnegie Institute of Technology, and Professor Leon Dorfman of Ohio State University concerning the complex chemistry of this simple molecule.

(25) M. Zelikoff and L. M. Aschenbrand, *J. Chem. Phys.*, **24**, 1034 (1956).

(26) H. Eyring, J. O. Hirschfelder, and H. S. Taylor, *ibid.*, **4**, 479 (1936).

(27) J. L. Magee and K. Funabashi, *Radiation Res.*, **10**, 622 (1959).

Electrochemical Characterization of the Surface Composition of Heterogeneous Platinum-Gold Alloys

by M. W. Breiter

General Electric Research Laboratory, Schenectady, New York (Received September 8, 1964)

The electrochemical formation and reduction of oxygen layers on heterogeneous platinum-gold alloys which are a mixture of two phases, α_1 and α_2 , were studied. Periodic voltammetric current-potential curves on the alloys in 1 *N* H₂SO₄ at 30° can be composed additively of the respective curves of the pure metals in a satisfactory approximation. Phase α_1 which is rich in platinum exhibits the electrochemical behavior of platinum, while phase α_2 which is rich in gold has the electrochemical properties of gold. Thus the surface composition can be characterized by two parameters which are determined by a least-squares fit from the experimental data.

Introduction

The alloying characteristics of gold and platinum were reviewed in two recent communications.^{1,2} Heterogeneous alloys consist of a phase α_1 which is rich in platinum and a phase α_2 which is rich in gold. The extent to which each of these two phases is formed depends² strongly upon the preparation of the alloy, and the surface composition need² not be equal to that of the bulk. The platinum-gold alloys appeared attractive to an electrochemical study. It was conceivable that the α_1 -phase might have electrochemical properties similar to those of pure platinum and that the α_2 -phase might have those of pure gold. Since platinum and gold differ considerably in the formation and reduction of surfacial oxygen layers,³ the development of an electrochemical method of distinguishing between the α_1 -phase and the α_2 -phase on the surface was considered possible. The described approach will allow the characterization of the surface composition of platinum-gold alloys in studies where the reactivity with respect to certain catalytic or electrochemical reactions is decreased gradually by increasing the α_2 -phase at the expense of the α_1 -phase. The interpretation of the preferential formation of the one or the other phase at the surface under certain conditions, especially after different heat treatments, should be simplified. It is suggested that the surface composition of heterogeneous platinum-gold alloys be characterized by two parameters *a* and *b* whose values are determined from electrochemical

measurements of periodic current-potential curves (*I-U* curves). The parameter *a* is representative for the α_1 -phase, the parameter *b* for the α_2 -phase. The electrochemical properties of the α_1 -phase are approximated by those of pure platinum, the properties of the α_2 -phase by pure gold. An attempt is made to compose the *I-U* curves of the alloys additively of the respective curves of the pure metals

$$I(U) = aI_{\text{Pt}}(U)/Q_{\text{Pt}}(1.5) + bI_{\text{Au}}(U)/Q_{\text{Au}}(1.5) \quad (1)$$

Here *I*(*U*), *I*_{Pt}(*U*), and *I*_{Au}(*U*) designate the current density on the alloy, on smooth platinum, and on smooth gold at the potential *U* during the anodic or cathodic sweep of voltammetric *I-U* curves. *Q*_{Pt}(1.5) is the charge equivalent in mcoulombs/cm.² of the oxygen layer on platinum at 1.5 v. under the chosen voltammetric conditions; *Q*_{Au}(1.5) is that of gold. The definition of the parameters *a* and *b* which have the same units as *Q*_{Pt}(1.5) and *Q*_{Au}(1.5) makes them independent of the roughness of the particular platinum or gold electrodes which were used as standards. They represent the charge equivalent of the oxygen layer on the α_1 -phase or the α_2 -phase at 1.5 v. and depend upon the roughness factors of the two phases. These roughness

(1) A. S. Darling, *Platinum Metals Rev.*, **6**, 60 (1962).

(2) A. S. Darling, *ibid.*, **6**, 106 (1962).

(3) See, for instance, K. J. Vetter, "Elektrochemische Kinetik," Springer-Verlag, Berlin, 1961, pp. 500-506.

factors may differ considerably. If eq. 1 is applicable, it can be expected to hold in the potential range $U \leq 1.5$ v. in which thick oxide layers are not yet formed under voltammetric conditions on the pure metals⁴⁻⁷ and in which the evolution of molecular oxygen is still negligible. It was already demonstrated⁸ that voltammetric $I-U$ curves of alloys with gold contents from 5 to 70 atomic % exhibit a characteristic shape with two reduction waves during the cathodic sweep.

The following procedure was used to check the applicability of eq. 1. The current densities $I_{Pt}(U)$ and $I_{Au}(U)$ were measured under the same conditions as $I(U)$. A periodic voltage of triangular shape was applied potentiostatically to the test electrode between 0.5 and 1.5 v. at 0.03 v./sec. The constants a and b were determined from a least-squares fit of $I(U)$ during the cathodic sweep according to eq. 1. Values of I , I_{Pt} , and I_{Au} at 50 different potentials were employed. $Q_{Pt}(1.5)$ and $Q_{Au}(1.5)$ were determined by integration of the cathodic $I-U$ curves. The least-squares fit was carried out with suitable programs by the G.E. 225 computer. Finally, the degree of the approximation was checked by comparing the measured values of $I(U)$ with those which were computed with the constants a and b according to eq. 1. The comparison was made for both the cathodic and the anodic sweep.

Experimental

The experiments were made in a Pyrex vessel of conventional design at $30 \pm 0.5^\circ$ in 1 N H_2SO_4 . The solution was prepared from double-distilled water and analytical reagent grade sulfuric acid and purified as described⁹ previously. The measurements were taken in quiescent solutions saturated with purified helium. The potential is referred to a hydrogen electrode in the same electrolyte and at the same temperature as the test electrodes. The initial $I-U$ curves changed their shape with the number of consecutive sweeps on the alloys⁸ and also on smooth platinum¹⁰⁻¹² and gold electrodes. This is a well-known phenomenon; therefore, the I values were taken during the twentieth sweep when the subsequent change of the shape of the $I-U$ curves became negligible. The initial behavior can be attributed as on smooth platinum¹² to the removal of impurities from the surface by the repeated surface oxidation.

Platinum-gold alloys with the bulk composition 5, 10, 20, to 70 atomic % gold were supplied as wires of 0.3-mm. diameter by the Sigmund Cohn Corporation, New York, N. Y. The alloys were made ductile by the manufacturer in the described way² so that wires could be drawn. The subsequent results were obtained on wires in the cold-worked state as received from the

manufacturer. The wires were sealed into one end of a short piece of polyethylene tubing by melting it locally with a hot platinum wire. The other end of the polyethylene tubing fitted the glass tubing of a glass joint tightly. Sealing of the alloys in glass was avoided because a glowing in the gas flame was not considered desirable.

Each electrode was cleaned in chromic acid solution at room temperature and thoroughly washed with distilled water. After insertion in the vessel, the electrode stayed for 5 min. at open circuit under vigorous stirring with purified helium. Subsequently, the stirring was stopped and the solution became quiescent in 2 min. Then the electrode was connected to the potentiostatic circuit. The $I-U$ curves were registered by the Varian F 80 X-Y recorder.

Results and Discussion

Resistivity measurements can determine¹³ in a simple way whether the alloy is homogeneous or heterogeneous. Curve a in Figure 1 represents the resistivity of the alloys at room temperature as a function of the gold content while curve b corresponds¹³ to the resistivity of homogeneous alloys. Curve a has a shape

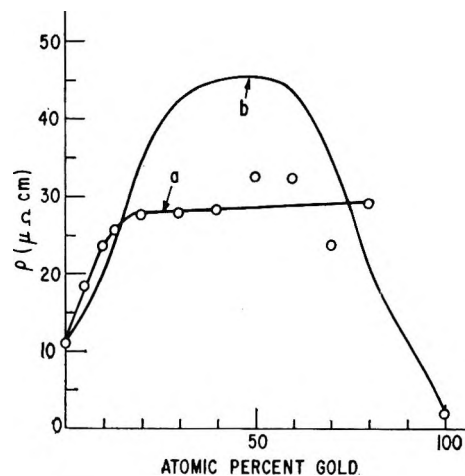


Figure 1. Resistivity of platinum-gold alloys at room temperature as a function of gold content: curve a, heterogeneous alloys; curve b, homogeneous alloys.

- (4) F. Will and C. A. Knorr, *Z. Elektrochem.*, **64**, 258 (1960).
- (5) W. Böld and M. Breiter, *Electrochim. Acta*, **5**, 145 (1961).
- (6) F. Will and C. A. Knorr, *Z. Elektrochem.*, **64**, 270 (1960).
- (7) M. W. Breiter, *Electrochim. Acta*, **8**, 973 (1963).
- (8) M. W. Breiter, *ibid.*, submitted for publication.
- (9) M. W. Breiter, *J. Phys. Chem.*, **68**, 2249 (1964).
- (10) M. Breiter and K. Kennel, *Z. Elektrochem.*, **68**, 1279 (1964).
- (11) W. G. French and T. Kuwana, *J. Phys. Chem.*, **68**, 1279 (1964).
- (12) M. W. Breiter, *J. Electroanal. Chem.*, **8**, 230 (1964).
- (13) G. H. Johansson and I. O. Linde, *Ann. Phys.*, **5**, 762 (1930).

which is characteristic^{2,13} for heterogeneous alloys. The resistivity of the alloys studied is nearly equal to that of the homogeneous alloys at gold contents below 15% and increases in a nearly linear manner with the composition above 15%. The latter behavior is to be expected^{2,13} for duplex alloys which are a mechanical mixture of two phases. The considerable scattering of the points above 50% is attributed to the heat treatment by which the alloys were made ductile.

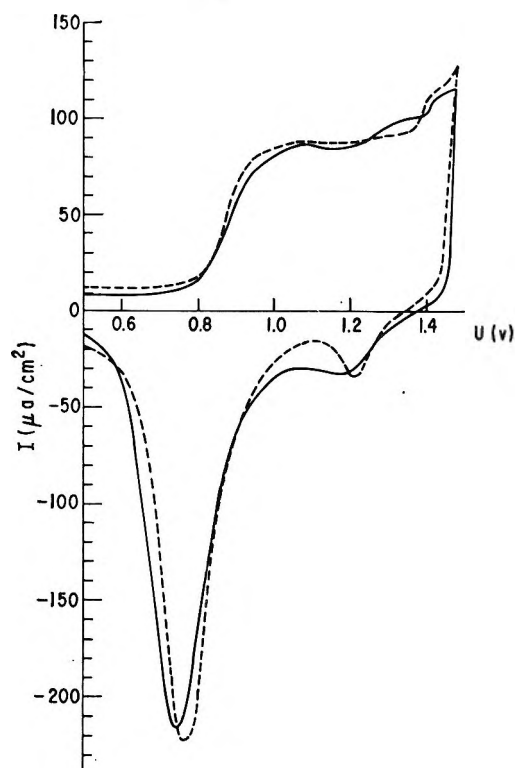


Figure 2. Current-potential curves on a platinum-gold alloy with 20% gold: —, experimental curve; ---, computed curve.

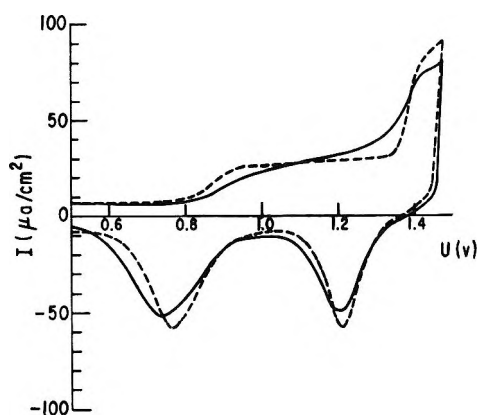


Figure 3. Current-potential curves on an alloy with 40% gold: —, experimental curve; ---, computed curve.

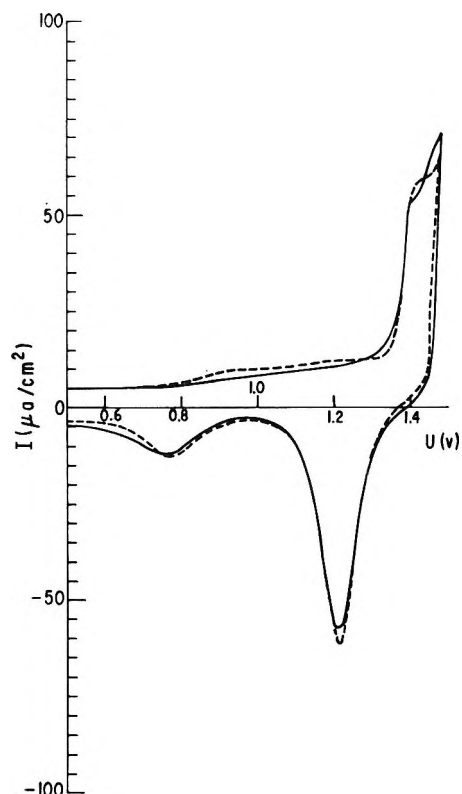


Figure 4. Current-potential curves on an alloy with 60% gold: —, experimental curve; ---, computed curve.

Periodic voltammetric $I-U$ curves have been reported and discussed extensively for smooth platinum^{4,5} and smooth gold^{6,7} in acid solution. Since the $I-U$ curves which were measured here on platinum and gold had the same shape as the published⁴⁻⁷ curves, the reader is referred to the previous work.

Experimental $I-U$ curves on three alloys (20, 40, and 60% Au) are represented by solid lines in Figures 2 to 4, while the respective computed curves are dashed. The curves in Figure 2 are an example for an alloy rich in platinum; the curves in Figure 4 are for an alloy rich in gold. Finally, the curves in Figure 3 correspond to an intermediate state. The height of the wave which is due to the reduction of the oxygen layer of the α_2 -phase between 1.4 and 1.0 v. during the cathodic sweep increases with the gold content while the height of the wave due to the reduction of the oxygen layer on the α_1 -phase between 1.0 and 0.6 v. decreases. This behavior is paralleled by a more rapid rise of the current with potential between 1.3 and 1.5 v. during the anodic sweep with increasing gold content. The rapid rise can be attributed to the formation of the oxygen layer on the α_2 -phase which starts as on gold^{6,7} at about 1.2 v. under the given conditions.

The agreement between the experimental and the

computed $I-U$ curves in Figures 2 to 4 is considered fair. It demonstrates that eq. 1 is a first approximation. The parameters a and b can be used to characterize the surface composition. There is a systematic deviation between the experimental and the computed curves. The peaks of each of the two reduction waves appear at slightly less anodic potentials on the alloys than on the respective pure metals. This indicates that the reduction of the oxygen layer on the two phases occurs with a slightly larger hindrance than on the pure metals.

The parameters a and b are plotted as a function of the gold content in Figure 5 which is representative for the particular set of platinum-gold alloys which were used here. The parameter b as a function of composition exhibits a shape similar to an adsorption isotherm. It increases initially and tends toward a limiting value of about 0.3 mcoulomb/cm.² at gold contents above 50% where a approaches zero. This means that the α_2 -phase replaces the α_1 -phase gradually and that the α_2 -phase is present to nearly the same extent on the surface of the studied alloys at gold contents above 50%. The oxygen layer on the alloys above 50% corresponds to 0.3 mcoulomb/cm.² at 1.5 v. It is slightly smaller than that on smooth gold (0.34 mcoulomb/cm.²). The parameter a increases with small additions of gold, passes through a maximum at about 20%, and then decreases. Since the amount of the α_2 -phase increases continually on the surface between 0 and 30% gold, the initial increase of a has to be attributed to an increase of the roughness factor of the α_1 -phase. This effect overcompensates the simultaneous decrease which results from the replacement of the α_1 -phase by the α_2 -phase up to gold contents of 20%. Then the latter ef-

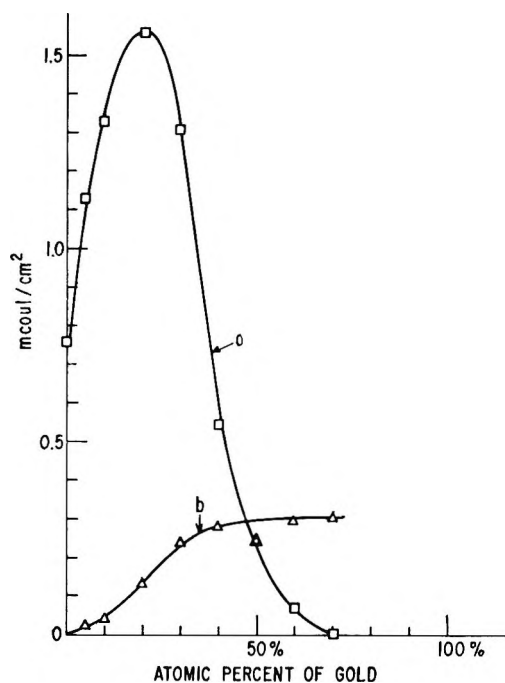


Figure 5. Parameters a and b of eq. 1 as a function of gold content.

fect is stronger. An analogous increase of the roughness factor of heterogeneous platinum-gold alloys was observed¹⁴ earlier in an electrochemical study of hydrogen adsorption.

Acknowledgments. The author gratefully acknowledges the helpful discussions with Dr. D. Vermilyea, General Electric Research Laboratory.

(14) K. A. Lapteva, T. I. Borissova, and M. G. Slinko, *Zh. Fiz. Khim.*, 30, 61 (1956).

Hydrogen Atom Addition to Olefins: Relative Rates at the Two Carbon Positions and Derived Heats of Formation of Several Alkyl Radicals

By Richard D. Kelley, Ralph Klein, and Milton D. Scheer

National Bureau of Standards, Washington, D. C. 20234 (Received September 9, 1964)

The relative rates of H atom addition at 90°K. to the two positions of several unsymmetric alkyl-substituted ethylenes have been measured. Relative rates of addition to the terminal and nonterminal carbon atoms of a number of 1-olefins were derived. Using Evans' rule relating activation energy differences to changes in reaction exothermicity, and the value of 40 kcal./mole for the exothermic terminal H addition, a set of values for the heats of formation and R-H bond energies for several radicals, R, were calculated. These quantities extend previous compilations obtained by electron impact methods.

I. Introduction

Provided an olefin is not symmetric about the double bond, addition of an H atom may occur on either carbon to give two distinct radical species. Relative rates can be determined by product analysis, certain of the products being uniquely associated with one or the other of the radicals. After the initial formation of an alkyl radical by H atom addition to an olefin at 90°K., reaction proceeds by combination and disproportionation of the radicals. It has been shown previously^{1,2} that in a "nonrigid" matrix where diffusional processes are rapid, the H atom-radical reactions are negligible. Consequently, the ratio of rate constants for addition to the two positions can be determined either from analysis of the dimer or the disproportionation products. It is possible to estimate the heats of formation of the pertinent alkyl radicals by empirical rules relating activation energy to enthalpy changes. The number of alkyl radicals for which data can be obtained is greatly extended by this method.

A recent tabulation of the heats of formation of organic radicals has been made by Bernecker and Long.³ Of the alkyl radicals with more than two carbons, only the values of *n*- and isopropyl and *n*- and *t*-butyl are available. The values were obtained from electron impact data. Further estimates of the heats of formation of the R's are of considerable interest, and these may be obtained from the relative rates of H atom addition to the olefin. The semi-empirical relationship between the energy of activation and heat of reaction,

as proposed by Evans,^{4,5} has been used by Walling⁶ for methyl radical reactions. It seems reasonable to apply Evans' rule to the H atom-olefin reaction. The requirement that the entropy changes associated with the reaction be approximately the same for the entire set of reactions is probably fulfilled in the H atom-olefin reaction series.

II. Experimental Details and Results

H atoms, generated in the gas phase, reacted with a condensed olefin at 90°K. The experimental methods used were similar to those described previously.¹ To achieve better control of rates, and to attain the condition of a "nonrigid" matrix,² the olefin was diluted with propane. Reaction products were analyzed with gas chromatography after warm-up. A flame ionization detector was used and the columns were calibrated with appropriate standard samples. Since the rates are determined from either dimer ratios or olefinic disproportionation products, it is desirable to maintain as low a conversion as possible consistent with analytical accuracy. Otherwise, the further

(1) R. Klein, M. D. Scheer, and R. Kelley, *J. Phys. Chem.*, **68**, 598 (1964).

(2) R. Klein and M. D. Scheer, *ibid.*, **66**, 2677 (1962).

(3) R. R. Bernecker and F. A. Long, *ibid.*, **65**, 1565 (1961).

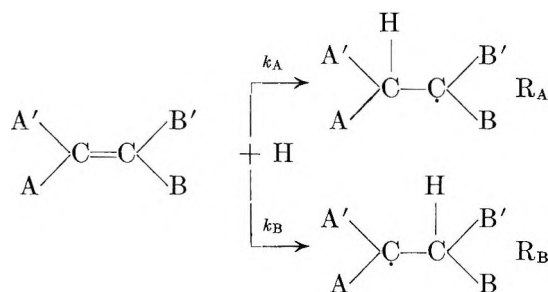
(4) M. G. Evans, *Discussions Faraday Soc.*, **2**, 271 (1947).

(5) M. G. Evans, J. Gergly, and E. C. Seaman, *J. Polymer Sci.*, **3**, 866 (1948).

(6) C. Walling, *J. Phys. Chem.*, **64**, 166 (1960).

hydrogenation of the olefinic products could lead to uncertainties. The conversion did not exceed 5% of the total initial olefin in all cases considered. The results for several olefins are shown in Tables I and II.

The relative rates of H atom addition were determined from the analytical data in the following way. If the olefin molecule is represented by $\begin{matrix} A' \\ \diagup \\ C=C \\ \diagdown \\ B \end{matrix}$ where A, A', B and B' are alkyl groups or hydrogen, the reactions may be presented as



the radical formed with specific rate constant k_A designated as R_A , and similarly for R_B . Once formed, the radicals R_A and R_B combine and disproportionate, leading to products R_A-R_A , R_A-R_B , R_B-R_B , R_A-H (R_B-H is equivalent) and olefins formed by the abstraction of H from R_A and R_B . The abstraction of H from R_A , for example, leads to one of three possible olefins if R_A is not symmetrical and does not have the free spin on a terminal carbon. One of these olefins is identical with the original olefin except in those cases involving *cis-trans* isomers.¹ The product analysis can provide data for determining the ratio of rate constants k_A/k_B . Each product is associated with R_A , R_B , or a combination of the two. The dimer product R_A-R_A , for example, is equivalent to $2R_A$. The ratio $\Sigma R_A/\Sigma R_B$ determined from the products would equal k_A/k_B . This follows since

$$\frac{d(\Sigma R_A)}{dt} = k_A(H)(\text{olefin})$$

$$\frac{d(\Sigma R_B)}{dt} = k_B(H)(\text{olefin})$$

ΣR_A is the total of all products that have arisen from R_A through its combination with another radical, or its addition or loss of H through disproportionation. Considering propylene, terminal and nonterminal additions result in the products propane, propylene, 2,3-dimethylbutane, 2-methylpentane, and *n*-hexane. Therefore

$$\frac{k_A}{k_B} = \frac{2(2,3\text{-DMB}) + 2\text{-MP} + N_1}{2(n\text{-H}) + 2\text{-MP} + N_2} \quad (1)$$

The quantities N_1 and N_2 are propylene plus propane yields from the disproportionation reaction associated with R_A and R_B , respectively. The dimers 2,3-dimethylbutane, 2-methylpentane, and *n*-hexane are represented by 2,3-DMB, 2-MP, and *n*-H, respectively. The disproportionation-combination ratio for isopropyl radicals has been found to be a constant (K) under the conditions of these experiments.^{7,8} It follows that

$$N_1 = 2K(2,3\text{-DMB}) + K'(2\text{-MP}) \quad (2)$$

$$N_2 = 2K''(n\text{-H}) + K'(2\text{-MP})$$

The expression for k_A/k_B becomes

$$\frac{k_A}{k_B} = \frac{2(1 + K)(2,3\text{-DMB}) + (1 + K')(2\text{-MP})}{2(1 + K'')(n\text{-H}) + (1 + K')(2\text{-MP})} \quad (3)$$

To the approximation that $K = K' = K''$ below 100°K.

$$\frac{k_A}{k_B} = \frac{2(2,3\text{-DMB}) + (2\text{-MP})}{2(n\text{-H}) + (2\text{-MP})} \quad (4)$$

Table II gives the results for H + propylene at 90°K. This method was not extended to larger terminal olefins because of analytical difficulties in the determination of dimer ratios.

Table I: Analysis for Product Olefins of H + 40:1 Propane-Olefin Reaction Mixtures at 90°K.^a

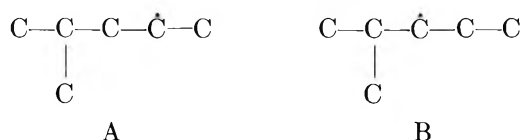
Reactants	Olefin products	Yield, nanomoles
<i>cis</i> -2-Pentene	<i>trans</i> -2-Pentene	210.0
	1-Pentene	63.0
<i>cis</i> -2-Hexene	3-Hexene	133.2
	1-Hexene	85.2
	<i>trans</i> -2-Hexene	186.6
4-Methyl-2-pentene	2-Methyl-2-pentene	58.9
	4-Methyl-1-pentene	16.5
2-Heptene	3-Heptene	36.6
	1-Heptene	26.2

^a All olefins used in this study were A.P.I. standard samples.

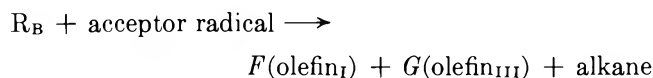
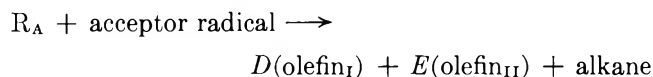
Unsymmetrical olefins give olefinic products in disproportionation of the radicals from the H atom addition that are in part uniquely associated with the precursor radical. For example, 4-methyl-2-pentene gives two radicals, A and B.

(7) M. D. Scheer and R. Klein, *J. Phys. Chem.*, **65**, 375 (1961).

(8) R. Klein, M. D. Scheer, and J. G. Waller, *ibid.*, **64**, 1247 (1960).



The olefin 2-methyl-2-pentene can arise only from B, and 4-methyl-1-pentene from A. Thus



The approximate rate ratio would be

$$\frac{k_A}{k_B} = \frac{\text{olefin}_{\text{II}} \left(1 + \frac{D}{E}\right)}{\text{olefin}_{\text{II}} \left(1 + \frac{F}{G}\right)} \quad (5)$$

Dimer products may be neglected, since they are negligibly small for large radicals at low temperatures. The ratios D/E and G/F are calculable since the various olefins are obtained in ratios proportional to the number of abstractable hydrogens leading to their

Table II: Dimer Yields for H + Propylene at 90°K.

Product yields, nanomoles ^a			k_A/k_B
<i>n</i> -Hexane ^b	2,3-DMB ^c	2-MP ^d	
0.7	2760	86	64
0.3	1037	34	62
0.1	524	17	63

^a The analysis was performed with g.l.c. using 40% isoquinoline on Chromosorb-P at 20°. ^b Obtained from $(2\text{-MP})^2/(2,3\text{-DMB})(n\text{-hexane}) = 4$. ^c 2,3-Dimethylbutane. ^d Methylpentane.

formation (Table II of ref. 1). The olefinic products are reactive to H atoms so that the correct ratio of rate constants is obtained by extrapolation to zero conversion. The validity of this was checked using *cis*-2-hexene. Here 3-hexyl and 2-hexyl radicals are produced. Their disproportionation reactions give hexene-3 and hexene-1, respectively, as well as hexene-2.

The *trans/cis* hexene-2 ratio is about 30 when equilibrated at 90°K,⁹ and since the *cis-trans* isomers are produced in equilibrium quantities,¹ the product olefins are effectively separate from the reactant. It was found that 3-hexene plus two-thirds of 1-hexene equaled *trans*-2-hexene when extrapolated to zero conversion. Table III gives the rate constant ratios

for several olefins derived from the experimental data of Table I.

III. Some Derived Thermochemical Quantities

The experimental data on the relative rates of addition of H to the two positions of the double bond are useful for estimating certain thermochemical quantities such as heats of formation of the alkyl radicals and radical-hydrogen bond energies. The values were compiled for radicals resulting from H atom addition to terminal olefins. This was done to make all calculations relative to the propyl radicals for which acceptable thermodynamic data are available.¹⁰⁻¹²

Substituent alkyl groups are assumed to act independently in their effect on the rate constant ratios. From Table III and the value for propylene in Table II, the rate ratios k_T/k_{NT} of Table IV may be derived. For example, the ratio of 63 for propylene combined with 1.6 for 2-pentene gives a value of 101 for 1-butene. Equal pre-exponential factors for H atom addition to either carbon of the terminal double bond permit calculation of the activation energy differences.

Stevenson¹⁰ and Benson and Nangia¹² obtained values of 17 and 17.6 kcal./mole, respectively, for the heat of formation of *i*-C₃H₇, while Szwarc¹¹ reported 22 kcal./mole for *n*-C₃H₇. From these values the exothermicity of terminal (ΔH_T) and nonterminal (ΔH_{NT}) H atom additions to the olefin can be calculated as 40 and 35 kcal./mole, respectively. With equal pre-exponential factors in the Arrhenius expressions for the rate constants k_T and k_{NT} , a value of $E_{NT} - E_T = 740$ cal./mole is obtained for propylene. Evans,^{4,5} using semi-empirical considerations of potential energy surfaces, has proposed that such an increase in activation energy is proportional to a corresponding decrease in the exothermicity of the addition reaction. Walling⁶ has demonstrated that the addition of methyl radicals to a series of 1-olefins exhibits just such a behavior. He obtained a value of 0.16 for the constant $\alpha_{Me} = \Delta E/\Delta H$. For the addition of H atoms to propylene we find $\alpha_H = (E_{NT} - E_T)/(\Delta H_T - \Delta H_{NT}) = 0.15$. Values of $(\Delta H_T - \Delta H_{NT})$ in Table IV were calculated using this value of α_H . These quantities are equal to the difference in the heats of formation of the *n*- and *sec*-alkyl radicals as well as the bond energy differences

(9) F. D. Rossini, K. S. Pitzer, W. J. Taylor, J. P. Ebert, J. E. Kilpatrick, C. W. Beckett, M. G. Williams, and H. G. Werner, "Selected Values of Properties of Hydrocarbons," National Bureau of Standards Circular C461, U. S. Government Printing Office, Washington, D. C., 1947.

(10) D. P. Stevenson, *Discussions Faraday Soc.*, **10**, 35 (1957).

(11) M. Szwarc, *ibid.*, **10**, 336 (1957).

(12) P. S. Nangia and S. W. Benson, *J. Am. Chem. Soc.*, **86**, 2773 (1964).

Table III: Relative Positional Rate Constants for H + Olefins at 90°K.

Olefin	R _A	R _B	k _A /k _B
(CH ₃) ₂ CHCH=CHCH ₃	(CH ₃) ₂ CHCHCH ₂ CH ₃	(CH ₃) ₂ CHCH ₂ CHCH ₃	6.4
CH ₃ CH ₂ CH=CHCH ₃	CH ₃ CH ₂ CHCH ₂ CH ₃	CH ₃ CH ₂ CH ₂ CHCH ₃	1.6
CH ₃ CH ₂ CH ₂ CH=CHCH ₃	CH ₃ CH ₂ CN ₂ CHCH ₂ CH ₃	CH ₃ CH ₂ CH ₂ CH ₂ CHCH ₃	1.9
CH ₃ CH ₂ CH ₂ CH ₂ CH=CHCH ₃	CH ₃ CH ₂ CH ₂ CH ₂ CHCH ₂ CH ₃	CH ₃ CH ₂ CH ₂ CH ₂ CH ₂ CHCH ₃	1.7

between the corresponding primary and secondary R-H bonds.

Table IV: Derived Rate Constant Ratios, Activation Energy Differences, and Enthalpy Differences between the Terminal and Nonterminal Addition of H Atoms to Several 1-Olefins at 90°K.

Olefin	k _T /k _{NT}	log k _T /k _{NT}	E _{NT} - E _T cal./mole	ΔH _T - ΔH _{NT} kcal./mole
Propylene	63	1.80	740	5.0 ^a
1-Butene	101	2.01	830	5.5
1-Pentene	120	2.08	860	5.7
1-Hexene	107	2.03	840	5.6
3-Methyl-1-butene	403	2.61	1080	7.2

^a References 9, 10, and 15.

The addition of an H atom to ethylene is exothermic by 39.3 kcal./mole.¹³ ΔH_T obtained for propylene is little different, and it is unlikely that ΔH_T for any aliphatic 1-olefin will differ very much from 40 kcal./mole. Within the limits of such an approximation, a set of alkyl radical heats of formation and bond energies [D(R-H)] can be obtained from column 5 of Table IV. These quantities are given in Table V. The values for CH₃, CH₃CH₂, CH₃CH₂CH₂, and CH₃-CHCH₃, listed in previous compilations,^{3,8,10,11} are included for comparison.

The addition of radicals to π-electron systems has been the subject of considerable theoretical study using the molecular orbital approximation. Pullman¹⁴ has suggested that the relative rates of radical addition should correlate with the difference in free valence at the two positions of the double bond. Burkitt, Coulson, and Longuet-Higgins,¹⁵ on the other hand, show that predictions of radical reactivity toward simple aliphatic olefins based on free valence calculations are unreliable. In either case, the approximate

Table V: Heats of Formation and D(R-H) for Some Alkyl Radicals

R	ΔH _f ²⁹⁸ kcal./mole	D(R-H)
·CH ₃	32	102
·CH ₂ CH ₃	25	98
·CH ₂ CH ₂ CH ₃	22	99
·CH ₂ CHCH ₃	17	94
·CH ₂ CH ₂ CH ₂ CH ₃	18	101
·CH ₂ CH ₂ CHCH ₃	12	95
·CH ₂ CH ₂ CH ₂ CH ₂ CH ₃	13	100
·CH ₂ CH ₂ CH ₂ CHCH ₃	7	94
·CH ₂ CH(CH ₃)CH ₂ CH ₃	12	100
·CH ₂ CH(CH ₃)CHCH ₃	5	93
·CH ₂ CH ₂ CH ₂ CH ₂ CH ₂ CH ₃	8	100
·CH ₂ CH ₂ CH ₂ CH ₂ CHCH ₃	2	94

nature of all such theoretical estimates casts considerable doubt on the significance of the derived conclusions. The correlation of relative rates of addition to differences in activation energy, and hence by the Evans' rule to the differences in exothermicity, has been shown by Walling to be applicable to methyl radical additions. The use of this approach to the data obtained here resulted in a set of thermochemical data which is internally consistent. The independence of groups in their effect on addition makes possible the prediction of relative reactivities of H atoms toward the two carbon atoms of the double bond for a number of aliphatic olefins. Relative to a primary C-H bond energy of about 100 kcal./mole, a secondary C-H bond energy of about 94 kcal./mole is obtained with only minor differences due to variations in substituent alkyl groups.

(13) M. Szwarc, *Chem. Rev.*, **47**, 75 (1950).

(14) B. Pullman, *J. chim. phys.*, **55**, 790 (1958).

(15) F. H. Burkitt, C. A. Coulson, and H. C. Longuet-Higgins *Trans. Faraday Soc.*, **47**, 553 (1951).

Mechanism of Homogeneous Gas-Phase Partial Oxidation of *o*-Xylene

by Jordan Loftus and Charles N. Satterfield

Department of Chemical Engineering, Massachusetts Institute of Technology, Cambridge, Massachusetts
(Received September 14, 1964)

The homogeneous partial oxidation of 1 mole % of *o*-xylene in air was studied at 1 atm. in a flow reactor in the temperature range of 455 to 525°. The products were identified by gas chromatography, infrared spectroscopy, and nuclear magnetic resonance spectroscopy. A major product was *o*-xylene oxide, previously not reported in partial oxidation studies of *o*-xylene. A postulated mechanism for the reaction is presented.

One of the commercial processes for the manufacture of phthalic anhydride is based on the partial oxidation of 1 to 1.4 mole % of *o*-xylene in air in the temperature range of 480 to 620° over a vanadium pentoxide catalyst. Yields are about 50 to 60% of the theoretical maximum. The present study was aimed at determining the nature of the products formed by homogeneous reaction under conditions approaching those of a commercial unit and elucidating the mechanism of the initial stages of the reaction.

Little information has been published concerning the homogeneous reaction. Wright¹ studied the non-catalytic partial oxidation of 14 to 67 mole % of *o*-xylene in air at 650°. The major products were, in order of decreasing yields, methylvinylbenzene, toluene, benzene, and *o*-tolualdehyde. Earlier studies^{2,3} were hampered by the lack of adequate analytical methods to resolve the products formed—in particular, homologs—into their individual components. The rate of reaction is first order with respect to *o*-xylene and has an activation energy of 20,000 cal./mole.⁴

Experimental

The reaction was studied in a flow reactor at 1 atm., at temperatures of 455 to 525° and a residence time of 6 to 7 sec. The experimental apparatus was the same as that described previously and is described in more detail elsewhere.⁴ Liquid *o*-xylene (Phillips Petroleum Co., research grade, 99.89% minimum purity) was vaporized, mixed with air, and rapidly preheated to reaction temperature before entering the reactor itself.

The borosilicate glass reactor, 2.6 cm. in diameter and 20.1 cm. long, was enclosed in an aluminum pipe

to reduce axial temperature gradients. This, in turn, was wrapped with heating wire and insulation. The reactor was positioned vertically with the inlet at the top. Three thermocouples were placed on the outside wall of the reactor—one at the inlet, the second at the horizontal midplane of the reactor, and the third at the outlet. During experimental runs, the first (top) thermocouple indicated a temperature 12–13° lower than the second one, while the bottom thermocouple indicated a temperature 2° lower than that at the middle. The temperature indicated by the midplane thermocouple was taken as the reaction temperature. The outlet of the reactor led to a Vycor tube, 15 mm. in o.d. and 27.5 cm. long, which was held at 150° by a heating rope. Tarry materials formed by the reaction were collected here.

Condensable products in the exit from the Vycor tube were recovered in an electrostatic precipitator-condenser. This consisted of a 0.175-cm. o.d., high-voltage electrode centered within a soda glass tube, 22 mm. in o.d. and 25.4 cm. long. An electrical ground was provided by closely wrapping 20-gauge copper wire around the outside of the glass tube. A 7.62-o.d. aluminum tube was placed around the soda glass tubing to provide a container for coolant and was filled with carbon tetrachloride (f.p. –22.6°) chilled by solid carbon dioxide. Liquid products, principally oxygenated aromatics plus unreacted *o*-xylene, were

(1) F. J. Wright, *J. Phys. Chem.*, **66**, 2023 (1962).

(2) J. H. Burgoyne, *Proc. Roy. Soc. (London)*, **A175**, 539 (1940).

(3) J. H. Burgoyne, T. L. Tang, and D. M. Newitt, *ibid.*, **A174**, 379 (1940).

(4) C. N. Satterfield and J. Loftus, *Ind. Eng. Chem., Proc. Design Develop.*, **4**, 102 (1965).

drained from the precipitator-condenser into a 10-ml. buret. The effluent gas left the top of the precipitator and then flowed through a water bubbler and wet test meter to the exhaust system.

The *o*-xylene concentration in the reactor inlet gas was 1.0 mole %. At this concentration the amount of air present is twice that corresponding to complete conversion of *o*-xylene to carbon dioxide and water, and seven times that corresponding to complete conversion to phthalic anhydride and water. Runs extended over periods of 4 to 10 hr.

One cannot tell from this study whether the borosilicate glass wall made any contribution to the reaction. However, its participation, if any, did not change with time. There was no detectable shift in rate of reaction attributable to the sequence of runs, and the walls of the reactor were not visibly blackened or otherwise altered to the eye at the end of the studies, except for a short deposit at the end of the outlet tube of the reactor.

Analytical Procedures

The products were identified by gas chromatography, infrared spectroscopy, and n.m.r. spectroscopy. The aromatic products, as well as almost all of the unreacted *o*-xylene, were collected in the electrostatic precipitator-condenser. Gas chromatography analysis of this liquid showed the presence of 13 areas (12 products plus unreacted *o*-xylene).

Nine of the twelve aromatic products formed were identified by comparing their gas chromatography (g.c.) retention times to known compounds and their chemical behavior to acidic 2,4-dinitrophenylhydrazine solution and to 1 *N* sodium hydroxide. Where these results were inconclusive, milligram quantities of pure samples (for two additional compounds) were separated by g.c. procedures, and the elemental analysis, infrared spectrum, and nuclear magnetic resonance (n.m.r.) spectrum were obtained.

The analytical apparatus used were as follows: (a) Burrell Corp. Kromatog K-1 isothermal gas chromatography unit equipped with a thermal conductivity detection cell; (b) Baird-Atomic Inc. Model KM-1 infrared spectrophotometer equipped with rock salt optics; (c) Perkin-Elmer Model 21 infrared spectrophotometer equipped with rock salt optics; (d) Varian A-60 nuclear magnetic resonance spectroscope.

Gas Chromatography. Twenty per cent Dow-Corning silicone vacuum grease on 30-60 mesh Chromosorb-P firebrick support—dried at 300° and 14 mm. for 5 days—was used as the partitioning agent in a g.c. column 7 mm. in i.d. and 213.4 cm. long, having an average H.E.T.P. of 0.19 cm. Three passes, each at

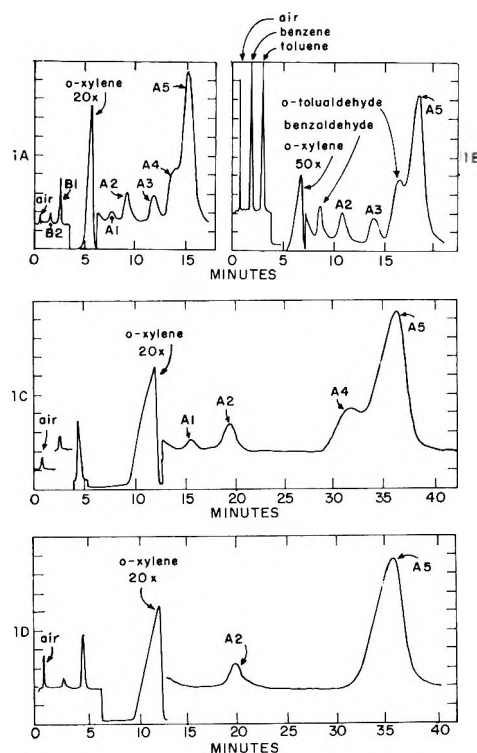


Figure 1. Chromatograms of liquid from run 9. (A) 10 μ l. of untreated liquid; 99 ml. of He/min. at 4 p.s.i.g. (B) 10 μ l. of untreated liquid plus 5 μ l. of mixture of benzene, toluene, and *o*-tolualdehyde in *o*-xylene; 85 ml. of He/min. at 3.2 p.s.i.g. (C) 20 μ l. of liquid after extraction with 1 *N* NaOH; 88 ml. of He/min. at 3 p.s.i.g. (D) 20 μ l. of liquid after extraction with acidic solution of 2,4-dinitrophenylhydrazine; 88 ml. of He/min. at 3 p.s.i.g.

a different column temperature, were required to obtain a complete analysis because of the wide boiling range of the products. Figure 1A shows a typical chromatogram for untreated product liquid, from run 9, at a g.c. column temperature of 100°.

Initial identification was made by superimposing a chromatogram of known mixture over the chromatogram of the unknown mixture. The procedure was to load a hypodermic microsyringe with a small quantity of the known mixture, followed by an air gap and then a small quantity of the unknown. The liquids were injected into the g.c. column simultaneously. Figure 1B shows the chromatogram obtained when a known mixture of benzene, toluene, benzaldehyde, and *o*-tolualdehyde in *o*-xylene was injected with untreated liquid from run 9. By visual inspection it is easily discernible that the chromatograms of air, and species B2, B1, A1, and A4 have increased with respect to A2, A3, and A5. The principle of superposition is superior to measuring retention time alone since retention time is strongly dependent upon column

temperature and carrier gas flow rate. Also, some compounds tail; *i.e.*, show a trailing rear boundary, more than others. Irregularities in superimposed chromatograms usually indicate the presence of another compound. Nine of the eleven products were tentatively identified by superposition. Using this method there was no difficulty in distinguishing between benzaldehyde (b.p. 179°), *o*-ethyltoluene (b.p. 165.2°), and benzofuran (b.p. 173–174°).

For further identification a portion of the liquid product was extracted with two volumes of 1 *N* NaOH to remove acid and esters. One of the chromatograms of the extracted product, shown on Figure 1C, shows that only A3 of the group shown in Figures 1A and 1B was extracted. A3 had been tentatively identified as phenylacetaldehyde by superposition. Since it has an α -hydrogen, it would be expected to undergo aldol condensation in the presence of a dilute base and be removed. Another portion of liquid product was extracted with an acidic solution of 2,4-dinitrophenylhydrazine (DNPH). One of the chromatograms for the extracted liquid from run 9 is shown in Figure 1D. This confirms that peaks A1, A3, and A4 were carbonyl compounds and, together with the results of the sodium hydroxide extraction and identification by superposition, identifies them as benzaldehyde, phenylacetaldehyde, and *o*-tolualdehyde, respectively. (In all four chromatograms in Figure 1 the recorder sensitivity was reduced by a factor of 20 or 50 during the appearance of the *o*-xylene, and this was accompanied by a shift in the base line. The chromatograms in Figures 1C and 1D were made at a slightly lower column temperature than those in Figures 1A and 1B.)

Phthaldialdehyde, phthalic anhydride, and phthalide were also identified in this way. In Table I a summary of the identifications made by these gas chromatographic methods is given. In addition to showing that the compounds listed were present, the superposition method was used to eliminate 1-methyl-2-ethylbenzene, 1-methyl-2-vinylbenzene, acetophenone, benzoic acid, and *o*-toluic acid as possible products.

Infrared and Nuclear Magnetic Resonance Spectroscopy. The substances corresponding to two of the three remaining peaks in the g.c. analysis were identified by interpretation of their elemental analysis, infrared spectrum, and nuclear magnetic (n.m.r.) spectrum. The milligram quantities of material needed—30 to 40 mg. for the three assays—were separated using the silicone grease-on-firebrick column mentioned above.

For separation and analysis of the lower boiling

Table I: Products Identified by Gas Chromatography

Symbol	Compound	Formula	Subtractive method removed by	
			2,4-DNPH	1 <i>N</i> NaOH
B2	Benzene	C ₆ H ₆	No ^a	No
B1	Toluene	C ₆ H ₅ CH ₃	No	No
A1	Benzaldehyde	C ₆ H ₅ CHO	Yes	No
A2	Benzofuran	C ₆ H ₅ CHCHO	No	No
A3	Phenylacetaldehyde	C ₆ H ₅ CH ₂ CHO	Yes	Yes
A4	<i>o</i> -Tolualdehyde	CH ₃ C ₆ H ₄ CHO	Yes	No
A7	Phthaldialdehyde	C ₆ H ₄ (CHO) ₂	Yes	Yes
A8	Phthalic anhydride	C ₆ H ₄ (CO) ₂ O	No	Yes
A9	Phthalide	C ₆ H ₄ COOCH ₂	No	Yes

^a "No" includes those compounds whose concentrations were reduced. "Yes" indicates substantially quantitative removal.

unknown (peak A5 in Figure 1A) the liquid collected in the precipitator-condenser was first extracted with DNPH to remove interfering carbonyls (phenylacetaldehyde and *o*-tolualdehyde). A portion of the organic layer was then injected into the g.c. column. A stainless steel tube, 10.16 cm. long and 0.16 cm. in o.d., was inserted in the discharge port of the thermal conductivity cell when the rise of the recorder pen indicated that the desired compound was leaving the cell. The liquid was collected in a small vial. Ten μ l. of the sample was transferred by a microsyringe onto the face of a 1-cm. diameter sodium chloride disk which was then mounted in the infrared spectrophotometer.

The thin-film infrared spectrum for pure A5 is shown in Figure 2A. Absence of peaks in the range of 1640 to 1800 cm.⁻¹ demonstrates the effectiveness of the DNPH extraction method for removal of carbonyls. The main peaks occurred at 9.6, 11.1, and 13.45 μ . Aliphatic ethers (—CH₂—O—CH₂—) absorb strongly at 8.7 to 9.4 μ and the phthalan radical absorbs at 10.9 to 11.2 μ .⁵ The n.m.r. spectrum is shown in Figure 2B. Two sharp peaks occurred at 5.05 and 7.2 p.p.m.—protons in tetramethylsilane being assigned a value of 0 p.p.m. These may be compared with tabulated values⁶ as shown in Table II, where *H* is the proton indicated, *R* is a proton or hydrocarbon, and *Ar* is a benzene ring.

(5) A. D. Cross, "Introduction to Practical Infra-Red Spectroscopy," Butterworth and Co. Ltd., London, 1960, pp. 51–78.

(6) Massachusetts Institute of Technology, Department of Chemistry, seminar in organic chemistry, notes on nuclear magnetic resonance, Cambridge, Mass., 1961.

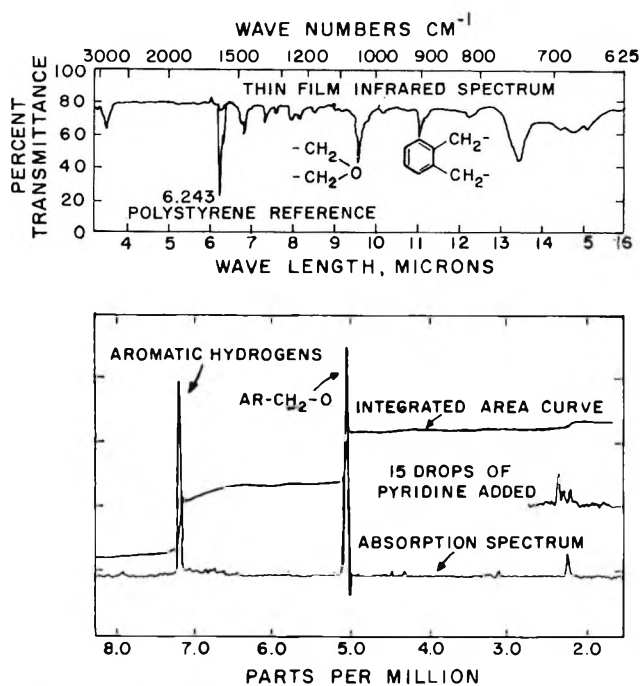


Figure 2. Identification of unknown A5 as *o*-xylene oxide. (A) Thin-film infrared spectrum. (B) Nuclear magnetic resonance spectrum; 20% A5 in CCl_4 .

Table II; Some N.m.r. Spectral Peaks, for Comparison with Those of Product A5

Grouping	Peak position, p.p.m.	No. of compds. studied
Ar-CH ₂ -OR Ar-CH-OR	4.36-4.49	3
Ar-CH ₂ -O-CO-R Ar-CH-O-CO-R	5.36	1
C ₆ H ₅ -R	7.09-7.32	15

The elemental analysis indicated the empirical formula of $\text{C}_{7.94}\text{H}_{7.99}\text{O}$ after correcting for 1.5 weight % of water. The presence of a small amount of water was also indicated in the n.m.r. spectrum. From this evidence the unknown was concluded to be *o*-xylene oxide, ($\text{C}_6\text{H}_4\text{-CH}_2\text{-O-CH}_2$).

The unknown of highest boiling point (A10) eluted from the g.c. column at about 300° and appeared to be somewhat impure and to contain some phthalide. However, it was not possible to obtain separation into two clearly separate phases in attempting to extract it with either DNPH solution or 1 N NaOH although a similar procedure on the A5 unknown was successful. The sample containing the mixture was subjected to infrared, n.m.r., and elemental analyses as described

below. A portion of the sample used for the n.m.r. study was then rerun through the g.c. column, and this time two separate peaks resulted. One of these, identified as phthalide, constituted approximately 25% of the total.

The thin-film infrared spectrum of A10 is shown in Figure 3A. The peak at 1765 cm^{-1} is coincident with the phthalide C=O stretching peak while that at 1700 cm^{-1} is indicative of another C=O stretching peak. The other peaks were coincident with those for dibenzyl (Stadler Reference No. 3203).⁷

The peak position, integral displacement, and indicated groupings taken from the n.m.r. spectrum (Figure 3B) are shown in Table III. The peak at 5.33 was coincident with one for Eastman Co. Pure grade phthalide analyzed separately. The peak at 5.18 was considered to be a carbonyl impurity in addition to the 25% phthalide present.

Table III: Some N.m.r. Spectral Peaks and Relative Integral Displacements, Compared to Those for Product A10

Position, p.p.m.	Relative integral displacement		Grouping ^a
	2,2-Dimethyl-dibenzyl	Unknown	
7.24	2.0	2.20	C ₆ H ₅ -R
5.33	0.0	0.18	Ar-CH ₂ -O-CO-R
5.18	0.0	0.14	Probably a carbonyl
2.88	1.0	1.00	Ar-CH ₂ -
2.32	1.5	1.55	Ar-CH ₃

^a See ref. 6.

The ultimate analysis was $\text{C}_{19.4}\text{H}_{20.2}\text{O}$. A mixture of 1 part by weight of phthalide and 3 parts 2,2'-dimethyldibenzyl agrees with this empirical formula. Based on all the above evidence the unknown compound was concluded to be 2,2'-dimethyldibenzyl ($\text{CH}_3\text{C}_6\text{H}_4\text{CH}_2\text{CH}_2\text{C}_6\text{H}_4\text{CH}_3$).

One g.c. peak, which appeared close to that for phthalaldehyde, remained unknown. However, its amount was so small that it had no significant effect on the over-all material balance.

Differential Infrared Analysis. A differential infrared analysis was made of untreated liquid from the electrostatic precipitator-condenser from one run (no. 11) in which only 12.9% of the *o*-xylene reacted. Pure *o*-xylene was used as the reference liquid. By using a slightly wider spaced cell in the reference position, all unbalanced peaks due to the *o*-xylene are displayed

(7) "Stadler's Infrared Spectra Collection," Stadler Research Laboratories, Philadelphia, Pa.

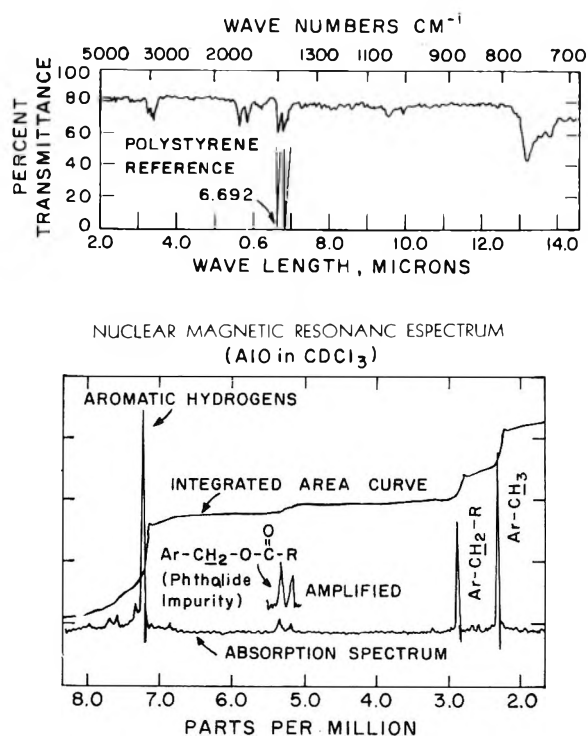


Figure 3. Identification of unknown A10 as 2,2'-dimethyldibenzyl. (A) Thin-film infrared spectrum. (B) Nuclear magnetic resonance spectrum, A10 in CDCl_3 .

above the base line whereas unbalanced peaks due to the products are displayed below the base line. The infrared spectrum for *o*-xylene with air as reference is shown in Figure 4A while the differential infrared spectrum is shown in Figure 4B. The peaks for $\text{C}=\text{O}$ stretching for phthalide (5.7μ), *o*-tolualdehyde (5.9μ), and the characteristic peaks for *o*-xylene oxide (9.6 and 11.1μ) are clearly discernible. Water, a known product, absorbs strongly in the region of 2.6 to 3.1μ and 5.9 to 6.2μ .⁷ The broad, shallow band at 2.8 to 3.2μ is more characteristic of water than an aromatic alcohol, but, in either case, the amount present in the condenser sample was quite small (concentrations are proportional to the logarithm of the absorbance).

Quantitative Analysis

Reaction products appeared in one or more of three different locations in the apparatus depending upon their volatility. The three product groups were quantitatively analyzed as follows: (a) liquid collected in the electrostatic precipitator-condenser, for unreacted *o*-xylene and condensable products; (b) effluent gas from the electrostatic precipitator-condenser, for CO , CO_2 , and remaining aromatics; (c) tarry products condensed in the Vycor tube preceding the precipitator-condenser, for total carbon.

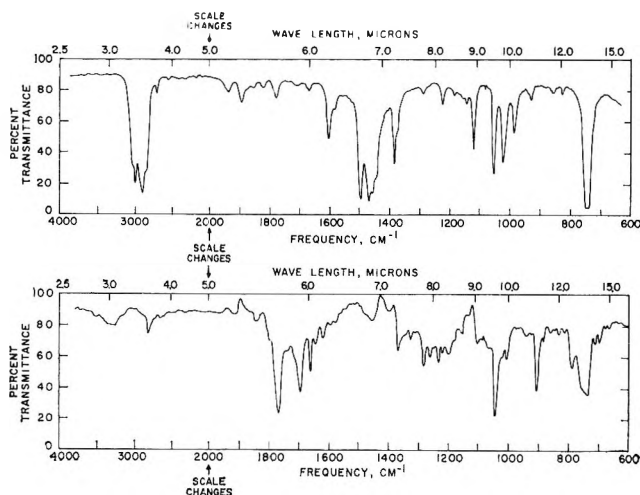


Figure 4. Differential infrared spectrum of untreated liquid from run 11. (A) Spectrum for *o*-xylene with air as reference. (B) Differential spectrum.

Liquid Products. The same g.c. partitioning column used in the identification procedure was used for quantitative analysis. Equal volumes of sample and of *o*-xylene were injected into the g.c. column in successive runs under identical conditions. The amount of *o*-xylene present in the unknown was calculated from the ratio of the *o*-xylene chromatogram area in the unknown to the chromatogram area of an equal volume amount of pure *o*-xylene. The $50\text{-}\mu\text{l}$. injection syringe was equipped with a Chaney adapter to improve reproducibility in volume delivery. A calibrated, 2-ml . Gay-Lussac weighing bottle was used to determine the density of the liquid unknown.

Three passes, each at a different g.c. column temperature, were required to obtain a complete analysis of the products. The chromatograms for *o*-tolualdehyde and *o*-xylene oxide overlapped, so a fourth pass was made after extraction with 2,4-dinitrophenylhydrazine solution. The amount of each product present was taken as the ratio of product chromatogram area to that of *o*-xylene, multiplied by the quantity of *o*-xylene represented by that area, as determined above. In the normal g.c. procedure, *o*-tolualdehyde was determined by subtracting the amount of *o*-xylene oxide present from the amount of *o*-xylene oxide plus *o*-tolualdehyde. In run no. 11, however, the amount of *o*-tolualdehyde present was determined from the differential infrared spectrum at 1767 cm^{-1} wave number, using a Beer's law plot. The concentration of *o*-xylene oxide was then determined by subtracting the concentration of *o*-tolualdehyde present in the sample (by infrared analysis) from the total concentration of *o*-tolualdehyde plus *o*-xylene oxide (by g.c. analysis).

Electrostatic Precipitator Gas Effluent. A number of investigators^{8,9} have reported on condensing systems for concentrating trace amounts of compounds in gas streams. The procedure is to adsorb the trace compounds at low temperature and then to desorb the compounds very rapidly by helium elutriation at an elevated temperature. The basic problem is to select a g.c. sorbent agent that allows the diluting gas to pass through the "trapping" tube at low temperatures while retaining the trace compounds. Further, the trace compounds must be rapidly and completely desorbed at the elevated temperature.

In order to reduce the concentration of oxygenated products in the effluent gas from the electrostatic precipitator-condenser (e.p.), it was operated at the lowest practical operating temperature, *i.e.*, slightly above the freezing point of *o*-xylene. Even at these low temperatures, a significant portion of low-boiling aromatics—benzene, toluene, and *o*-xylene—was present in the e.p. effluent.

The sorbent agent used for the aromatics (benzene, toluene, and *o*-xylene) was the 20 wt. % silicone grease on Chromosorb-P packing which was also used in the g.c. column. Silica gel (28–60 mesh Davison Chemical Co., grade H) was used for adsorbing CO and CO₂. The trap was an elongated U-tube, 10 mm. in i.d. and 63.5 cm. long. During the adsorption step the trap was placed in a dewar flask containing a trichloroethylene–solid carbon dioxide slurry. Silica gel was used as partitioning agent for separating carbon dioxide from air and CO while Linde 5A Molecular Sieve adsorbent was used for separating carbon monoxide from air and CO₂.

Carbon in Tar. The total amount of carbon present in the tar collected in the Vycor tube was determined in a modified ultimate analysis apparatus. Oxygen was passed through the Vycor tube at a rate of 30 ml./min. while the flame of a gas-blowing torch was played on the outside. The effluent gases from the Vycor collection tube then flowed through a 14.6-cm. long Vycor tube filled with 7 g. of oxidized, 24-gauge copper wire at 800°. The carbon dioxide formed was determined gravimetrically using ascarite as the absorbing agent.

From the sum of the over-all analyses, a carbon material balance was calculated.

Results

Results are reported in Table IV in the order of decreasing *o*-xylene conversion. The temperature is that reported for the center thermocouple on the reactor wall.

The products are reported as g.-atoms of carbon in

the products per 12.5 moles of *o*-xylene reacted (*i.e.*, per 100 g.-atoms of carbon in the form of *o*-xylene). Had all the *o*-xylene that reacted been converted to benzene and carbon dioxide, the values listed for these compounds would have been 75 and 25, respectively. Carbon balances on reacted material (calculated as total carbon in all products compared to carbon in the *o*-xylene that reacted, the latter obtained by difference) varied from 91.6 to 102.5%, except for one run. Total carbon balances were also made, in which the carbon in the form of all products plus unreacted *o*-xylene was compared to that in the *o*-xylene fed. These over-all carbon balances were between 96.5 and 100.3%.

The product distributions are shown in Figures 5A and 5B, as a function of the degree of reaction. Note that all runs were made with 1 mole % of *o*-xylene in air and at the same residence time, so that the degree of reaction was increased by increasing the temperature. The variation of product composition with degree of reaction, thus, might be somewhat different than if studies were made at constant temperature but with varying residence times.

Additional Observations. Upon completion of this run series, the reactor was removed from the furnace for inspection. There was no discoloration of the wall or of the inlet or outlet tubes except that a heavy deposit, approximately 1 cm. long, existed at the end of the outlet tube.

Two additional runs were made to verify the absence of chemical reaction in the electrostatic field of the precipitator. In one run *o*-xylene was vaporized in the mixer, and the reactor was bypassed. A differential infrared spectrum of the liquid collected *vs.* the *o*-xylene fed showed that no reaction products were formed. In the second run, a 10% solution of *o*-tolualdehyde in *o*-xylene was vaporized, bypassing the reactor, and condensed in the precipitator. A differential infrared spectrum of the liquid collected *vs.* the feed showed that no products were formed.

Discussion

From the results shown in Table IV and Figure 5, the following facts are noted.

(a) Compounds formed by rupture of the benzene ring or of the C–C bond attaching the methyl group to the ring accounted for about 46% of the *o*-xylene reacted at 510° and 34% conversion of *o*-xylene, but only 17% of that reacted at 455° and 13% conversion. (These consist of all products isolated except for *o*-tolu-

(8) N. Brenner and L. S. Ettre, *Anal. Chem.*, **31**, 1815 (1959).

(9) H. A. Stewart, Linde Co., Tonawanda, N. Y., personal communication, Oct. 9, 1961.

Table IV: Summary of Results

	Run no.							
	6	4	5	7	9	10	12	11
Temp., °C.	525	517	510	510	505	490	477	455
Pressure, mm.	766	764	773	757	765	750	753	763
Frac. of inlet <i>o</i> -xylene reacted	0.435	0.350	0.344	0.341	0.300	0.251	0.215	0.129
Mole % <i>o</i> -xylene in inlet	1.01	0.96	0.97	0.98	0.94	0.99	0.98	0.93
Residence time, sec.	6.8	6.3	6.6	6.5	6.3	6.7	6.7	6.7
Over-all carbon balance, %			98.3	97.7	100.3	96.5	97.0	98.7

	Formula	Mol. wt.	B.p., °C.	G-atoms of carbon in product per 12.5 moles of <i>o</i> -xylene reacted							
Benzene	C ₆ H ₆	78.1	80.1		3.3 ^a	1.4 ^a	0.2	0.8	3.7	7.3	
Toluene	C ₆ H ₅ CH ₃	92.1	110.6		3.3 ^a	1.7	3.3	1.1	1.5	1.2	
Benzaldehyde	C ₆ H ₅ CHO	106.1	179.1		1.0	0.8	0.7	0.6	0.8	0.6	
Benzofuran	C ₆ H ₄ CHCHO	118.1	173-174		4.7	4.7	3.5	1.7	2.1	1.3	
Phenylacetaldehyde	C ₆ H ₅ CH ₂ CHO	120.1	193-194		4.1	4.6	3.4	3.6	3.1	4.7	
<i>o</i> -Tolualdehyde	CH ₃ C ₆ H ₄ CHO	120.1	196-199		14.0	16.6	11.2	11.6	8.7	11.3 ^b	
<i>o</i> -Xylene oxide	C ₆ H ₄ CH ₂ OCH ₂	120.1	192		24.7	24.7	30.3	37.5	47.1	52.8	
Unknown					2.5	2.7	2.5	1.9	2.6	2.7	
Phthalialdehyde	C ₆ H ₄ (CHO) ₂	134.1	284.5		0.6	0.3	0.2	0.3	0.6	0.9	
Phthalic anhydride	C ₆ H ₄ (CO) ₂ O	148.1									
Phthalide	C ₆ H ₄ COOCH ₂	134.1	290		5.8	7.1	6.6	6.9	7.1	9.1	
2,2'-Dimethyldibenzyl	[CH ₂ C ₆ H ₄ CH ₂] ₂	210.3	177-178 ^c		4.3	6.0	5.3	4.6	7.0	8.2	
Carbon dioxide	CO ₂	44.0		7.2	(3.4) ^d	3.2	2.3	(1.8) ^d	1.6	1.4	
Carbon monoxide	CO	28.0		28.5	14.4	(14.0) ^d	13.8	11.7	6.1	5.9	
Tar					17.9	(13.0) ^d	9.9	10.4	5.4	4.8	
Carbon balance on reacted material, %					98.7	97.5	91.6	83.9	96.5	102.5	

^a Includes products other than benzene and toluene. ^b 7.8 by infrared analysis. ^c At 20 mm. ^d Numbers in parentheses were obtained by graphical interpolation.

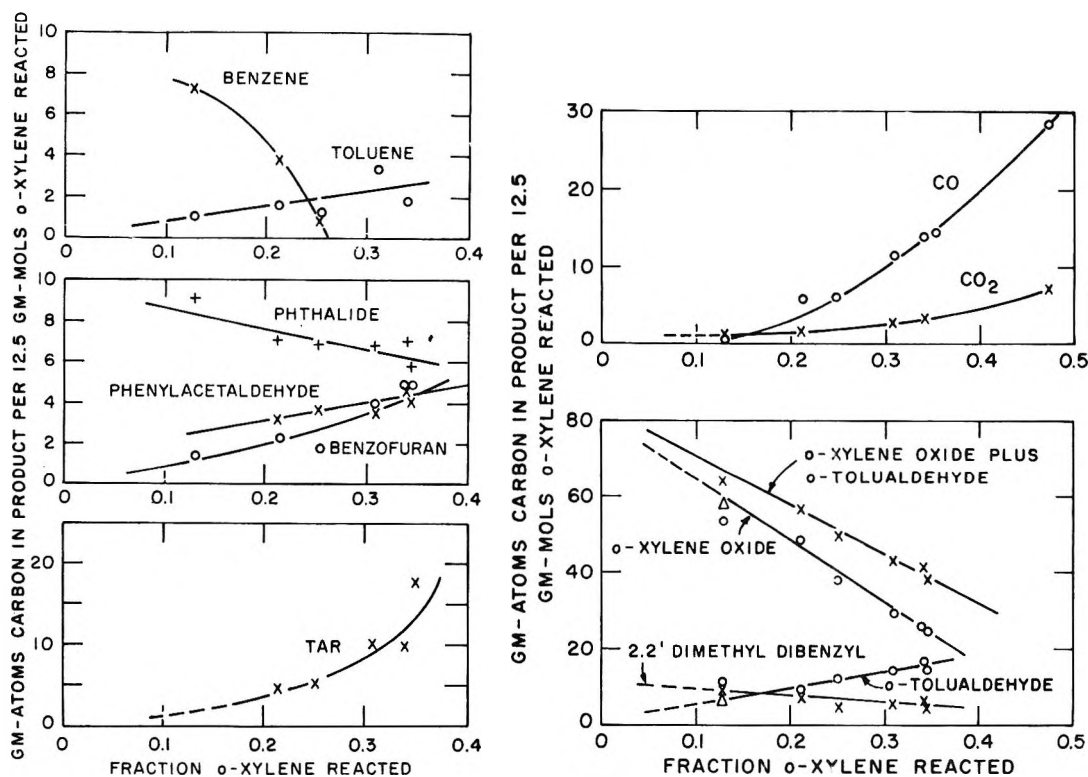


Figure 5. Variation of product composition with degree of reaction. All data were obtained by gas chromatography except for two values, designated by Δ, obtained by infrared analysis.

aldehyde, *o*-xylene oxide, phthaldialdehyde, phthalic anhydride, phthalide, and 2,2'-dimethyldibenzyl.)

(b) The aromatic products formed were almost all oxygenated; *i.e.*, little oxygen-sensitized cracking occurs under these oxygen-rich conditions. The major product formed was *o*-xylene oxide.

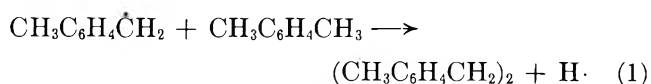
(c) Judging from the variation of product composition with degree of reaction, *o*-xylene oxide is the major stable molecular product formed initially. 2,2'-Dimethyldibenzyl is also probably formed as an initial product, with *o*-tolualdehyde formed by subsequent reactions.

With substituted benzene ring compounds, in general, oxidation of the side chain predominates at low temperatures, and ring rupture becomes relatively more important at higher temperatures. For example,¹⁰ Kroger and Bigorajski reported that for the homogeneous gas-phase oxidation of ethylbenzene in a batch system, at 380° with a conversion of 70% of the ethylbenzene, products formed by rupture of the benzene ring accounted for only 10% of the ethylbenzene reacted and at 410°, at a conversion of 75%, accounted for 21%. Wright¹ reported studies of the homogeneous oxidation of *o*-xylene at 650° and 1 atm. At this much higher temperature a relatively greater degree of attack on the ring occurs. In a run in which 72% of the *o*-xylene reacted, one-third of the *o*-xylene that disappeared went to form CO and CO₂; about one-third formed nonoxygenated aromatic products; about one-tenth formed oxygenated aromatic products, and the rest formed fragmentary products.

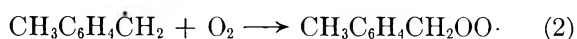
In the present study *o*-xylene oxide was the major product. This compound has never been reported previously as the product of gas-phase *o*-xylene oxidation either by homogeneous or by catalytic reaction.^{1,11-16} The inert behavior of ethers may well be the reason for its having eluded discovery up to this time. However, the mechanism of the homogeneous reaction is quite different from that for the catalytic reaction, and it is only in the recent studies at 650° by Wright that a detailed analysis of reaction products from the homogeneous reaction has been published. *o*-Xylene oxide may be an insignificant product at the much higher temperatures he studied.

Proposed Mechanism. The homogeneous gas-phase oxidation of hydrocarbons proceeds by free-radical reactions involving the formation and disappearance of a variety of transitory and reactive free-radical intermediates. Most of the studies on mechanisms have been on paraffins, and only a relatively minor amount of work has been done on aromatic hydrocarbons, particularly substituted aromatics. The first step in the present reaction is presumably the formation of

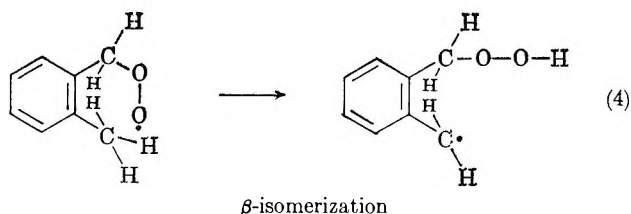
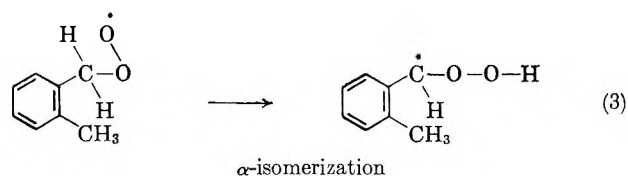
the xylyl radical which may readily occur by hydrogen abstraction from *o*-xylene by the oxygen molecule, hydroxide radical, or the peroxide radical. 2,2'-Dimethyldibenzyl presumably results from the collision of two xylyl radicals or a xylyl radical with *o*-xylene



To account for the formation of large amounts of *o*-xylene oxide, we may proceed by analogy with the mechanism of other hydrocarbon oxidation reactions. The initial oxygenation reaction is presumably predominantly the formation of the xylyl peroxide radical



A hydroperoxide can then readily be formed by hydrogen abstraction. In view of the products formed, this must occur usually as an internal transfer of a hydrogen atom, *i.e.*, an isomerization. Considering the spatial proximity of the two methyl groups on *o*-xylene, two isomerization reactions of the xylyl peroxide radical are possible.



The reaction of the peroxide radical with a hydrogen on the second methyl group is referred to here as β -isomerization while the reaction with a hydrogen on its own carbon atom is referred to as α -isomerization. Subsequent cleavage of the weak O-O bond would lead to the formation of *o*-xylene oxide if preceded by

(10) C. Kroger and G. Bigorajski, *Erdoel Kohle*, **15**, 109 (1962).

(11) S. K. Bhattacharyya and I. B. Gulati, *Ind. Eng. Chem.*, **50**, 1719 (1958).

(12) S. K. Bhattacharyya and R. Krishnamurthy, *Current Sci. (India)*, **28**, 363 (1959).

(13) P. H. Emmett, Ed., "Catalysis," Vol. VII, Reinhold Publishing Corp., New York, N. Y., 1960, p. 212.

(14) V. E. Leibnitz, H. G. Konnecke, and H. Knopel, *J. prakt. Chem.*, [4] **4**, 298 (1957).

(15) W. G. Parks and C. E. Allard, *Ind. Eng. Chem.*, **31**, 1162 (1939).

(16) F. J. Wright, *J. Phys. Chem.*, **64**, 1944 (1960).

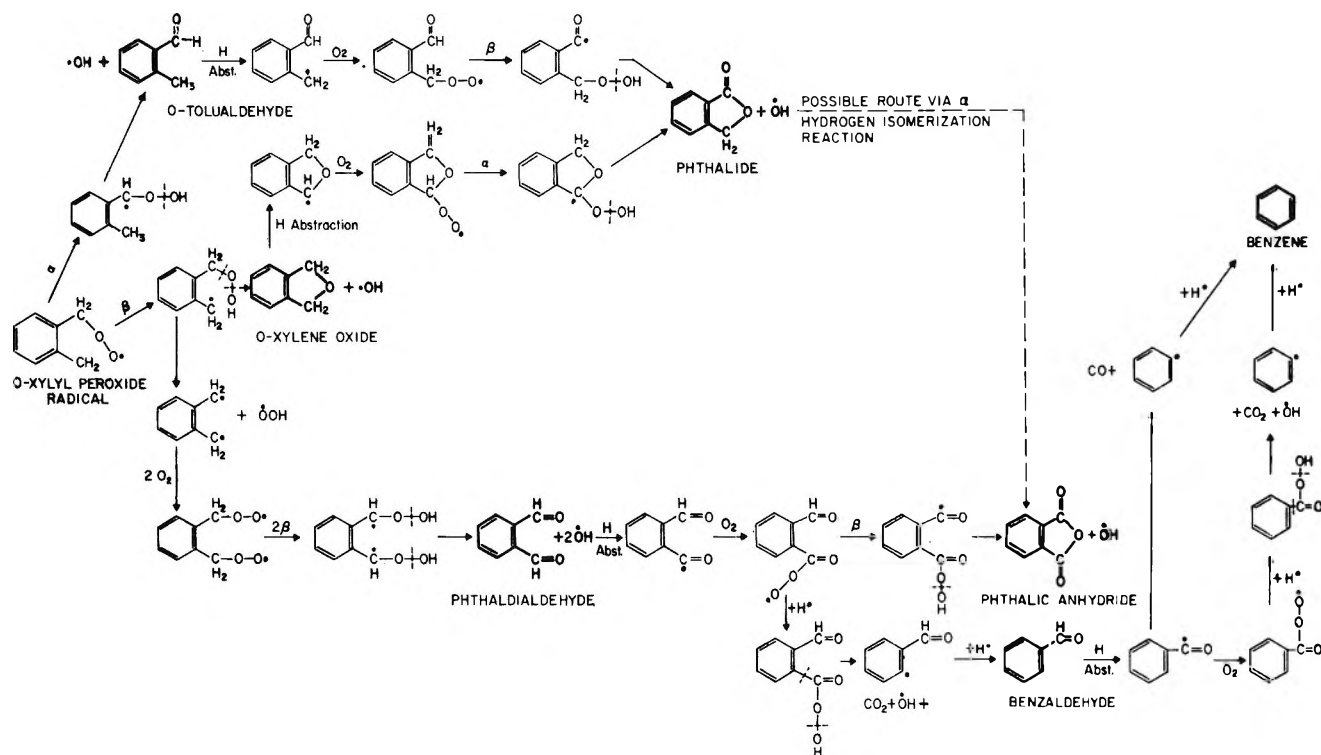
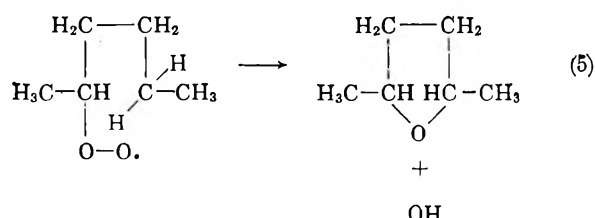
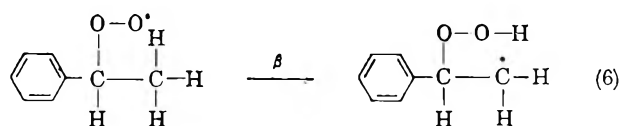


Figure 6. Suggested reaction mechanism for initial stages of the homogeneous oxidation of *o*-xylene: α , hydrogen isomerization by α -route; β , hydrogen isomerization by β -route; $+H\cdot$, transfer of hydrogen atom to specified radical by abstraction from an unspecified species; H (abst.), removal of hydrogen atom from specified molecule by abstraction to an unspecified radical.

reaction 4 and to the formation of *o*-tolualdehyde if preceded by reaction 3. β -Isomerization would appear more probable than α -isomerization on the basis of structural considerations, and this is also consistent with the observed predominance of *o*-xylene oxide over *o*-tolualdehyde in the initial stages of the reaction. There have been but few studies in which cyclic ethers have been formed in homogeneous gas-phase oxidations, and little information is available to suggest the mechanism of their formation. A recent patent¹⁷ describes conditions for the formation of propylene oxide by noncatalytic gas phase oxidation of propane with oxygen. Substantial amounts of cyclic ethers were reported in the homogeneous oxidation of *n*-hexane.¹⁸ The principal cyclic ether was 2,5-dimethyltetrahydrofuran, which implies a substantial degree of β -type isomerization.



In the homogeneous oxidation of ethylbenzene,¹¹ styrene is formed in preference to acetophenone, which implies that β -isomerization, as in reaction 6, is preferred to α -isomerization.



Subsequent cleavage of the C-O bond leads to the formation of styrene.

Figure 6 shows a possible reaction mechanism for the initial stages of the homogeneous air oxidation of *o*-xylene. Steps labeled ($+H\cdot$) indicate transfer of a hydrogen atom to the radical specified from some other species. Steps labeled (H abstraction) indicate removal of a hydrogen atom from the molecule specified. Many of the steps are speculative, but the broad outline is in accord with the facts observed here. Phthalic anhydride, benzene, and phthalide decrease

(17) R. C. Lemon, P. C. Johnson, and J. M. Berty, U. S. Patent 3,132,156 (May 5, 1964).

(18) H. C. Bailey and R. G. W. Norrish, *Proc. Roy. Soc. (London)*, **A212**, 311 (1952).

in yield with increasing conversion, which indicates that they probably appear as intermediates and then disappear, following the initial formation of *o*-xylene oxide and 2,2-dimethyldibenzyl.

Acknowledgment. This work was done in conjunction with a study of the reaction kinetics of *o*-xylene oxidation in vanadium pentoxide melts, supported by the National Science Foundation under Grant G-23480.

Carbon Isotope Effects in the Pyrolytic Decomposition of Magnesium Oxalate

by Peter E. Yankwich and Petros D. Zavitsanos

Noyes Laboratory of Chemistry, University of Illinois, Urbana, Illinois (Received September 14, 1964)

The C^{13} isotope fractionation in the pyrolytic decomposition of anhydrous magnesium oxalate (prepared from the dihydrate upon admixture of solutions of magnesium chloride and sodium oxalate) has been studied as a function of temperature. Between 350 and 600° the intramolecular isotope effect observed at complete decomposition falls from 0.87 to 0.62‰, exhibiting thus normal magnitude and temperature dependence (the zinc and manganous oxalate systems serving for comparison). The temperature-independent factor in the intramolecular isotopic rate constant ratio is significantly different from unity; the reaction coordinate motion makes a sizable contribution to the observed isotope fractionation—a difference from the zinc and manganous oxalate pyrolyses. *Ab initio* calculations of the intramolecular isotope effect *via* the Wilson-Johnston method, employing a three-particle model Mg-O-C, replicate the experimental results well; further, it is shown that calculations of this type account correctly for the effect of metal atom mass on the temperature-independent factor referred to above. The partial decomposition (0–2% and 2–4%) isotope effects were measured in experiments at 350 and 373°. Generally, the pattern of the results is similar to that observed with manganous oxalate (slight temperature dependence, large influence of degree of reaction). Unlike results obtained for zinc and manganous oxalate similarly prepared, the intramolecular isotope effects observed for sodium oxalate-precipitated magnesium oxalate *are* dependent upon the degree of reaction.

Introduction

This paper reports experiments designed to establish the magnitude and temperature dependence of C^{13} isotope effects in the pyrolysis of anhydrous magnesium oxalate. The kinetics and stoichiometry of the decomposition were subjects of an earlier report from this laboratory.¹ The current study is the fourth in a series^{2–4} on isotope effects in thermal decompositions of metal oxalates.

Experimental

Preparation of Magnesium Oxalate Dihydrate. Aque-

- (1) P. E. Yankwich and P. D. Zavitsanos, *J. Phys. Chem.*, **68**, 442 (1965).
- (2) P. E. Yankwich and J. L. Copeland, *J. Am. Chem. Soc.*, **79**, 2081 (1957).
- (3) P. E. Yankwich and P. D. Zavitsanos, *Pure Appl. Chem.*, **8**, 287 (1964).
- (4) P. E. Yankwich and P. D. Zavitsanos, *J. Phys. Chem.*, **68**, 1275 (1964).

ous solutions of equal volume of 0.50 *M* magnesium chloride and of 0.55 *M* sodium oxalate⁵ (reagent grade chemicals in de-ionized water) were brought to their boiling points and the former added rapidly to the latter; the mixture was stirred occasionally as it cooled to room temperature. The crystals of the dihydrate formed in this way are fine (particle size 12–16 μ) and rather uniform in appearance. The precipitate was washed several times with distilled water, air-dried for 2–3 hr. at 110°, and stored over magnesium perchlorate in a desiccator.

Apparatus and Procedure. The apparatus and the procedures employed in this study have been described in detail in an earlier publications from this laboratory.^{4,6}

Isotope Analyses. The carbon isotope analytical procedures and methods for correcting the raw output data have been described in earlier publications from this laboratory.^{2,7}

Notation and Calculations. The notation of Lindsay, McElcheran, and Thode⁸ is adopted for the isotopic specific rate constants. Where α is the mole fraction of C¹³ in carbon dioxide obtained from combustion of the original magnesium oxalate, $(X_d)_t$ that in the carbon dioxide collected up to time *t*, and $(X_m)_t$ that of carbon dioxide obtained by combustion of carbon monoxide produced up to time *t*, the intramolecular isotope effect in the deviation from unity of

$$\frac{k_2}{k_3} = \frac{(X_d)_t}{(X_m)_t} \quad (1)$$

while intermolecular isotope effects are related similarly to

$$\frac{k_1}{2k_2} = \frac{\alpha}{(X_d)_0} \quad (2)$$

and

$$\frac{k_1}{2k_3} = \frac{\alpha}{(X_m)_0} \quad (3)$$

where the subscript zero denotes, rigorously, the limit of zero time or infinitesimal degree of pyrolysis, but, practically, collection up to about 5% reaction.^{9,10} Use will be made later of two additional quantities: α' is the calculated mean of X_m and X_d for the increment 0–2% decomposition, and α'' is the calculated mean for the increment 2–4%; one would expect $\alpha' = \alpha''$.

Results

Complete decomposition isotope effects measurements were obtained at seven temperatures between 350 and 600°; values of $(k_2/k_3)_{\text{obsd}}$ for each experiment

Table I: Observed Intramolecular Isotope Effects in the Pyrolysis of Magnesium Oxalate: $(\alpha)_C \times 10^6 = 10,695 \pm 5$

Temp., °C.	$(X_d) \times 10^6$	$(X_m) \times 10^6$	$(k_2/k_3)_{\text{obsd}}$	Av. $(k_2/k_3)_{\text{obsd}}$
350	10,736	10,646	1.0085	1.0087 \pm 0.0007
	10,738	10,654	1.0079	
	10,740	10,637	1.0097	
373	10,734	10,644	1.0085	1.0085 \pm 0.0004
	10,740	10,648	1.0086	
	10,735	10,652	1.0086	
	10,740	10,641	1.0070	
	10,730	10,643	1.0092	
400	10,728	10,637	1.0086	1.0084 \pm 0.0005
	10,725	10,635	1.0085	
	10,735	10,643	1.0086	
	10,717	10,642	1.0070	
	10,738	10,640	1.0090	
450	10,719	10,641	1.0073	1.0072 \pm 0.0004
	10,718	10,636	1.0077	
	10,729	10,659	1.0066	
	10,719	10,638	1.0076	
	10,711	10,638	1.0069	
500	10,728	10,656	1.0068	1.0072 \pm 0.0003
	10,725	10,645	1.0075	
	10,718	10,636	1.0077	
	10,729	10,653	1.0071	
	10,735	10,661	1.0069	
550	10,714	10,661	1.0050	1.0059 \pm 0.0007
	10,747	10,677	1.0066	
	10,741	10,667	1.0069	
	10,709	10,656	1.0050	
	10,710	10,642	1.0064	
	10,704	10,643	1.0057	
	10,722	10,664	1.0054	
600	10,710	10,653	1.0054	1.0062 \pm 0.0004
	10,710	10,638	1.0068	
	10,714	10,643	1.0067	
	10,713	10,649	1.0060	
	10,729	10,664	1.0061	
	10,718	10,652	1.0062	

(5) Preparations of magnesium oxalate are designated A when precipitated by oxalic acid, C when precipitated by sodium oxalate. The two types of solids may exhibit different kinetic and isotope effect behavior.³

(6) P. E. Yankwich and P. D. Zavitsanos, *J. Phys. Chem.*, **68**, 457 (1964).

(7) P. E. Yankwich and R. L. Belford, *J. Am. Chem. Soc.*, **75**, 4178 (1953); *ibid.*, **76**, 3067 (1954).

(8) J. G. Lindsay, D. E. McElcheran, and H. G. Thode, *J. Chem. Phys.*, **17**, 589 (1949).

(9) J. Bigeleisen, *Science*, **110**, 14 (1949).

(10) J. Y.-P. Tong and P. E. Yankwich, *J. Phys. Chem.*, **61**, 540 (1957).

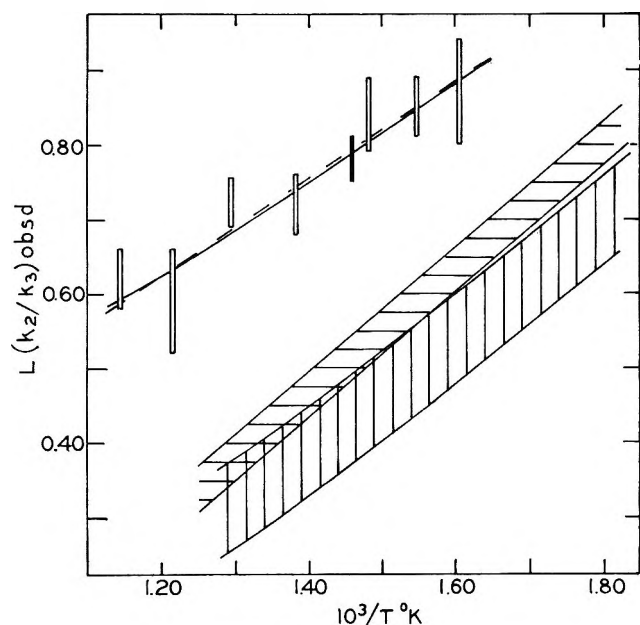


Figure 1. Influence of temperature on intramolecular carbon isotope effects: — — —, eq. 4, MgC_2O_4 ; — — —, eq. 5, MgC_2O_4 ; band with horizontal shading, MnC_2O_4 ; band with vertical shading, ZnC_2O_4 .⁴

are listed in Table I. The calculated average value of this rate constant ratio at each temperature is shown in the last column of the table, the appended errors being average deviations from the mean; the mean precision of individual $(k_2/k_3)_{\text{obsd}}$ values is estimated to be ± 0.0003 . Values of $L(k_2/k_3) = 100 \ln(k_2/k_3)$ calculated from the last column of Table I are plotted vs. $\theta = (1000/T)$ in Figure 1; the open rectangles encompass the average deviations. The dashed and solid lines, respectively, are obtained from least-squares fitting of the data to equations of the form

$$L(k_2/k_3)_{\text{obsd}} = M_1\theta + B_1 \quad (4)$$

and

$$L(k_2/k_3)_{\text{obsd}} = M_2\theta^2 + B_2 \quad (5)$$

The mean deviations of the experimental points from the least-squares obtained eq. 4 and 5 are ± 0.05 in L , or approximately 7% of the average isotope effect observed.

With a single exception, all of the results compared in Figure 1 were obtained with metal oxalates of type C⁵; the black vertical rectangle (which has a length equal to the estimated mean precision of a single datum) represents a single experiment carried out at 410° with magnesium oxalate precipitated by oxalic acid (type A oxalate). The shaded bands in Figure 1 represent intramolecular isotope effect results obtained through complete decomposition of manganese and

zinc oxalates; the vertical span of the bands is equal to twice the mean precision of the data.

Partial decomposition experiments were carried out at 350 and 373°, for 0–2% and 2–4% decomposition at the lower temperature, but only for 2–4% decomposition at the higher. In Table II are collected the various average C¹³ mole fractions observed and the derived isotopic rate constant ratios. For comparison, results are shown for 0–2% decomposition of manganese oxalate at 352°.

Table II: Comparison of Isotope Effects Observed in Partial Decompositions of Magnesium and Manganese¹ Oxalates

	MgC_2O_4	MnC_2O_4
$(\alpha)_C \times 10^6$	10,695 \pm 4	10,692 \pm 3
A. Experiments at 350°		
i. First 2% reaction		
$(X_d) \times 10^6$	10,708 (1) ^a	10,684 \pm 23 (4) ^b
$(X_m) \times 10^6$	10,545	10,620 \pm 31
$(\alpha') \times 10^6$	10,627	10,652 \pm 27
$(k_2/k_3)_{\text{obsd}}$	1.0155	1.0060 \pm 0.0009
$(k_1/2k_3)_{\text{obsd}}$	1.0142	1.0067 \pm 0.0029
$(k_1/2k_2)_{\text{obsd}}$	0.9988	1.0007 \pm 0.0022
ii. Second 2% reaction		
$(X_d) \times 10^6$	10,724 \pm 16 (3)	
$(X_m) \times 10^6$	10,609 \pm 13	
$(\alpha'') \times 10^6$	10,667 \pm 14	
$(k_2/k_3)_{\text{obsd}}$	1.0108 \pm 0.0004	
$(k_1/2k_3)_{\text{obsd}}$	1.0081 \pm 0.0012	
$(k_1/2k_2)_{\text{obsd}}$	0.9971 \pm 0.0014	
B. Experiments at 373°		
Second 2% reaction ^c		
$(X_d) \times 10^6$	10,720 \pm 1 (3)	
$(X_m) \times 10^6$	10,622 \pm 13	
$(\alpha'') \times 10^6$	10,667 \pm 2	
$(k_2/k_3)_{\text{obsd}}$	1.0100 \pm 0.0002	
$(k_1/2k_3)_{\text{obsd}}$	1.0069 \pm 0.0009	
$(k_1/2k_2)_{\text{obsd}}$	0.9977 \pm 0.0001	

^a Number of experiments. ^b Temperature was 352°. ^c No isotope ratios taken on samples from first 2% reaction.

The average value of the ratio CO_2/CO for the product gases from the pyrolysis of anhydrous magnesium oxalate was found to be 1.01 ± 0.01 in experiments carried out between 350 and 500°; there was no sensible temperature dependence of this ratio. By contrast, the stoichiometries of the manganese³ and zinc⁶ oxalate pyrolyses are as great as 7%. There does not seem to be any reflection of this situation in the isotope contents of the product gases collected during complete decompositions, as reference to the

last two lines of Table III will show. The remainder of Table III is a collection of the parameters of eq. 4 and 5 for the three reactions.

Table III: Comparison of Isotope Effects Observed in Complete Decompositions of Several Metal Oxalates

Temp. range, °C.	MgC ₂ O ₄ 350-600	MnC ₂ O ₄ 280-510	ZnC ₂ O ₄ 282-500
<i>M</i> ₁	0.647 ± 0.069	0.844 ± 0.076	0.722 ± 0.091
<i>B</i> ₁	-0.152 ± 0.094	-0.717 ± 0.117	-0.612 ± 0.141
<i>M</i> ₂	0.237 ± 0.025	0.263 ± 0.026	0.240 ± 0.029
<i>B</i> ₂	0.285 ± 0.048	-0.061 ± 0.062	-0.076 ± 0.070
(α_0) _C × 10 ⁶	10,695 ± 5	10,691 ± 3	10,692 ± 4
(<i>X</i> _d + <i>X</i> _m)/2(<i>n</i>) ^a	10,687 ± 7 (36)	10,685 ± 4 (6)	10,687 ± 5 (34)

^a Number of experiments.

Discussion

The results shown in Table I indicate a carbon isotope effect of small magnitude and normal temperature dependence for the thermal decomposition of C-type samples of magnesium oxalate. Figure 1 shows that $L(k_2/k_3)_{\text{obsd}}$ for the magnesium compound is 0.30-0.35 higher than for zinc and manganous oxalates, and the data collected in Table III show that this difference resides more in *B* than in *M*. Also, the result at 410° for A-type magnesium oxalate is not deviant in comparison with the results on C-type material.

The data shown in Table II illustrate the sensitivity of all the isotope effects to degree of reaction. (k_2/k_3)_{obsd} measured for zinc and manganous C-oxalates did not depend upon degree of reaction, whereas it did for A-type samples. The data in Table II indicate also that the several isotope effects are not strongly dependent upon temperature; further α' is definitely smaller than α'' , and α is larger than either. An interpretation is suggested in ref. 4.

These considerations lead us to the conclusion that only complete decomposition can be treated even approximately by current isotope effect theory.

Ab Initio Calculation of the Intramolecular Isotope Effect. In general, we can write

$$(k_2/k_3) = (\text{TIF})(\text{TDF}) \quad (6)$$

TIF is the ratio (ν_{2v}/ν_{3v}) of the imaginary vibration frequencies associated with the reaction coordinate; TDF, the temperature-dependent factor, arises in the mass dependence of the genuine vibrations of the normal molecules and activated complexes. The size of the magnesium oxalate intramolecular isotope effect and the similarity of its temperature dependence to that found for the decompositions of the salts of the heavier metals indicate that TIF is slightly larger than

unity; *i.e.*, that the contribution of the reaction coordinate to the observed isotope fractionation is of the order of one-third to one-half that of the remaining coordinates.

Since the dependence of $L(k_2/k_3)$, or $L(\text{TDF})$, on temperature is expected to be as $1/T$ at "low" temperatures and as $1/T^2$ at "high" temperatures, *B*₁ likely is a minimum estimate of $L(\text{TIF})$. If we adopt the criterion that a vibration occurs at "high" temperature when $u = (hc\omega/kT) \leq 3$,¹¹ 500° is of that nature for vibrations of the order of 1500-1600 cm.⁻¹, a region containing or higher than the frequencies of the stretching vibrations of systems like Mg-O-C, O-C-C, etc.; so, *B*₂ should be a good approximation to $L(\text{TIF})$.

The earlier results for zinc⁴ and manganous³ oxalates suggest that a good approximation to the reaction coordinate is the asymmetric stretching vibration of the system Mg-O-C. Vibration frequencies were calculated by matrix methods¹²; the frequency associated with the reaction coordinate being driven to zero in the manner suggested by Johnston, Bonner, and Wilson.¹³ The input parameters for the "best-fit" calculation and the results are shown in Table IV.

Table IV: C-O-Mg: Isotope Effect Calculated by Wilson-Johnston Method

	$m_1 = 12$; $m_2 = 16$; $m_3 = 24.3$	
	$m_1' = 13$; $m_2' = 16$; $m_3' = 24.3$	
	(i) Normal molecules	
$r_{12} = 1.38 \text{ \AA.}$; $r_{23} = 1.78 \text{ \AA.}$; $\phi = 180^\circ$		
$f_{12} = 6.0 \text{ mdyne/\AA.}$; $f_{23} = 3.0 \text{ mdyne/\AA.}$; $f_{\phi}/r_{12}r_{23} = 1.0 \text{ mdyne/\AA.}$		
	(ii) Activated complexes	
$r_{12} = 1.47 \text{ \AA.}$; $r_{23} = 1.78 \text{ \AA.}$; $\phi = 180^\circ$		
$f_{12} = f_{23} = f_{\phi} = 4.0 \text{ mdyne/\AA.}$; $f_{\phi}/r_{12}r_{23} = 0.25 \text{ mdyne/\AA.}$		
reaction coordinate: $Q = (q_{12}/\sqrt{2}) - (q_{23}/\sqrt{2})$		
	(iii) Results	
	Calcd.	Obsd. (eq. 5)
$L(\text{TIF}), B_2$	0.418	0.285 ± 0.048
$L(\text{TDF})$ at 350°	0.660	0.610 ± 0.049
at 600°	0.350	0.311 ± 0.025
Slope, <i>M</i> ₂	0.245	0.237 ± 0.025

The agreement between calculated and observed isotope effects compared in Table IV is satisfactory. $L(\text{TDF})$ is 0.04-0.05 higher than observed, a situation

- (11) J. Bigeleisen and M. G. Mayer, *J. Chem. Phys.*, **15**, 261 (1947).
 (12) E. B. Wilson, Jr., J. C. Decius, and P. C. Cross, "Molecular Vibrations," McGraw-Hill Book Co., Inc., New York, N. Y., 1955.
 (13) H. S. Johnston, W. A. Bonner, and D. J. Wilson, *J. Chem. Phys.*, **26**, 1002 (1957).

which could be remedied by using slightly larger force constants in the activated complexes, but at the expense of the agreement between calculated and observed values of M_2 . The discrepancy, 0.13, between $B_2(\text{calcd.})$ and $B_2(\text{obsd.})$ is not so easily reduced, for $L(\text{TDF})$ is quite sensitive to parameter variations which yield small changes in $L(\text{TIF})$.

More fundamental difficulties associated with the Mg-O-C model are that it requires $(k_1/2k_2) \equiv 1$, and that a valence potential is assumed for the Mg^{2+} -O interaction. $(k_1/2k_2)$ differs from unity by much less than either of the other rate constant ratios, so the first difficulty is perhaps not a large one. The dependence of all the isotope effects on degree of reaction suggests that major features of the molecular mechanism are ignored by this simple model.

Bigeleisen and Wolfsberg¹⁴ and Yankwich and Ikeda¹⁵ have given formulas for the calculation of TIF for three- and four-center models, respectively, based on a notion of Slater¹⁶; the three-center formula, in particular, has been helpful in the interpretation of kinetic isotope effects observed in several reactions. These formulas employ atomic masses, bond angles, and measures of degrees of bond rupture and bond formation in the activated complexes. For systems like M-O-C, these formulas predict that TIF should increase with increasing atomic mass of M, the reaction coordinate assumed being an asymmetric stretch. Metal atom mass increasing, the values of $L(\text{TIF})$ observed are:

0.29, -0.06, and -0.08; calculations using the Wilson-Johnston approach yield, for the same quantity: 0.42, 0.14, and 0.11. Even though the present situation is beclouded by the complexity of solid-state reaction, the relative success of the Wilson-Johnston approach in accounting for the influence of metal atom mass on the temperature-independent factor lends weight to the recent criticism of some approximation methods by Stern and Wolfsberg.¹⁷

The dependence of several isotope effects on degree of decomposition and other factors may provide a useful probe for study of these pyrolyses. Experiments to elucidate the effects of mode of preparation, particle size, degree of reaction, etc., are in progress in this laboratory.

Acknowledgments. We are indebted to Dr. Geneva Belford for generous assistance in programming certain of the theoretical calculations, and to Mrs. Eula Ihnen for all mass spectrometric analyses. This research was supported by the United States Atomic Energy Commission.

(14) J. Bigeleisen and M. Wolfsberg, *J. Chem. Phys.*, **21**, 1927 (1953); **22**, 1264 (1954).

(15) P. E. Yankwich and R. M. Ikeda, *J. Am. Chem. Soc.*, **81**, 1532 (1959).

(16) N. B. Slater, *Proc. Leeds Philosophical Soc.*, **8**, 75 (1949).

(17) M. J. Stern and M. Wolfsberg, *J. Chem. Phys.*, **39**, 2776 (1963).

Rydberg Potential Energy Function for Diatomic Molecules as Extended to Polyatomic Species and Activated Complex

by William F. Sheehan

Chemistry Department, University of Santa Clara, Santa Clara, California 95053
(Received September 24, 1964)

The diatomic Rydberg potential energy function $U_0(q) = -D_e(1 + q)e^{-q}$ is extended to triatomic (and polyatomic) species when bonds are essentially independent, as in stable molecules, and when bonds are interdependent, as in activated complexes. For reactions that are only slightly exothermic or endothermic, the interatomic distances and the energy of the activated complex are related to each other (Table I) and a rule that activation energies are less than about one-fourth a bond energy is suggested. A simple graphical method of constructing an approximate potential energy function for bimolecular reactions is applied to the reactions $H_2 + Br \rightarrow H + HBr$ and $H_2 + I \rightarrow H + HI$.

Introduction

Perhaps the simplest of the reasonably accurate diatomic potential energy functions is the Rydberg function¹

$$U_0(q) = -D_e(1 + q)e^{-q} \quad (1)$$

The parameter q depends on internuclear distance r (r_e at equilibrium) and a scale factor b according to the definition $q = b(r - r_e)$. If the dissociation energy D_e of a diatom MX can be factored by Errede's rule² in the form

$$D_e = \lambda_M \lambda_X \epsilon_M \epsilon_X \quad (2)$$

then $U_0(q)$ for MX is the real part of

$$W_{MX} = -u_M^* u_X = -u_X^* u_M \quad (3)$$

The complex atomic amplitude factors u_j in (3) are given by

$$u_j = \lambda_j \epsilon_j (1 + i\sqrt{q_j}) \exp(-q_j/2) \quad (4)$$

The parameter q_j for MX is chosen as

$$q_M = q_X = b_{MX}(r_{MX} - r_{eMX}) \quad (5)$$

to facilitate correlation of (3) and (1), but for a homonuclear diatom M_2 it is $q_{MM} = b_{MM}(r_{MM} - r_{eMM})$, which differs from q_{XX} for another homonuclear diatom X_2 . The special choice (5) places the burden of the correlation of U_0 and W on b_{MX} . Within the accuracy of

the Rydberg function, b_{MX} depends only on the atomic numbers of M and X .

This paper extends the Rydberg function to the realm of triatomic species having two strong bonds (e.g., CO_2 , N_2O , SO_2 , H_2O) and to species having an unstable equilibrium like that in the activated complex ABC^\ddagger for the reaction $AB + C \rightarrow A + BC$. The nature of the Rydberg function allows distances between atoms to be discussed, but not angles between bonds. Various expressions for $U(q)$ in factored form can be generalized readily for species containing more than three atoms.

Two Strong Bonds

Polyatomic molecules are described conventionally in terms of atoms joined by bonds each of which has a kind of individuality because nuclei generally remain fixed relative to each other. If (1) is used to describe the electronic energy or vibrational potential energy of such an arrangement of atoms, the values of the scale parameters b are set, at least approximately and as in diatoms, by the atomic numbers of the bonded atoms and not by bond type or even by local electronic structure. Only D_e and r_e remain as (potentially observable) parameters that might characterize a particu-

(1) Y. P. Varshni, *Rev. Mod. Phys.*, **29**, 664 (1957).

(2) L. A. Errede, *J. Phys. Chem.*, **64**, 1031 (1960); *ibid.*, **65**, 2262 (1961); *J. Org. Chem.*, **27**, 3425 (1962).

lar bond as unusual or different from a typical or isolated bond between M and X. Moreover, since (1) originates with diatoms, it is possible in the same vein to ignore angles and angular effects of orbital hybridization.

This very simple approach to a triatom ABC thus requires just two independent coordinates, $q_{AB} = b_{AB}(r_{AB} - r_{eAB})$ and $q_{BC} = b_{BC}(r_{BC} - r_{eBC})$. Without any interaction between A and C, the potential energy of ABC in this approximation is the potential energies of two bonds

$$U_{ABC} = -D_{eAB}(1 + q_{AB})e^{-q_{AB}} - D_{eBC}(1 + q_{BC})e^{-q_{BC}} \quad (6)$$

Figure 1 shows this U_{ABC} in q -space for $D_{eAB} = 2D_{eBC}$ with contours of constant energy at zero and multiples of $-1/2D_{eBC}$. The minimum of this very reasonable looking potential falls at $q_{AB} = q_{BC} = 0$ where $U_{ABC} = -D_{eAB} - D_{eBC}$, in accord with additivity of bond energies.

The values of D_e and r_e in diatoms and in ABC will always differ somewhat. One reason may be that a standard valence formula with ideal, localized single, double, and triple bonds may not be satisfactory. Another reason may be that B has a limited number of stable bonding orbitals. If D_e and r_e in (6) refer to diatoms rather than to bond energies and internuclear distances in ABC, then ABC and each diatom will generally be describable in terms of localized pairs of electrons in each bond. Another assumption in (6) is that ABC and the diatoms dissociate to atoms in the same electronic states.

The potential energy U_{ABC} in terms of atomic amplitude factors (4) is the real part of

$$W_{ABC} = -(u_A^* + u_C^*)u_B = -u_B^*(u_A + u_C) \quad (7)$$

If atom B were to form several bonds to atoms j , (7) is readily extended to give U about B as the real part of

$$W_B = -\left(\sum_j u_j^*\right)u_B = -u_B^*\left(\sum_j u_j\right) \quad (8)$$

Displaced Rydberg Function

The very simple bimolecular reaction $AB + C \rightarrow ABC^\pm \rightarrow A + BC$ does not stop at the activated complex ABC^\pm because B cannot form strong bonds to both A and C at once. That is, ABC^\pm is a forced compromise and (6) is no longer adequate because the A-B and B-C interactions are obviously interdependent.

In the limit $AB + C$, the strong bond in AB can be described by (1) with its minimum energy at $q = 0$. The long-range interaction $B \cdots C$ can also be de-

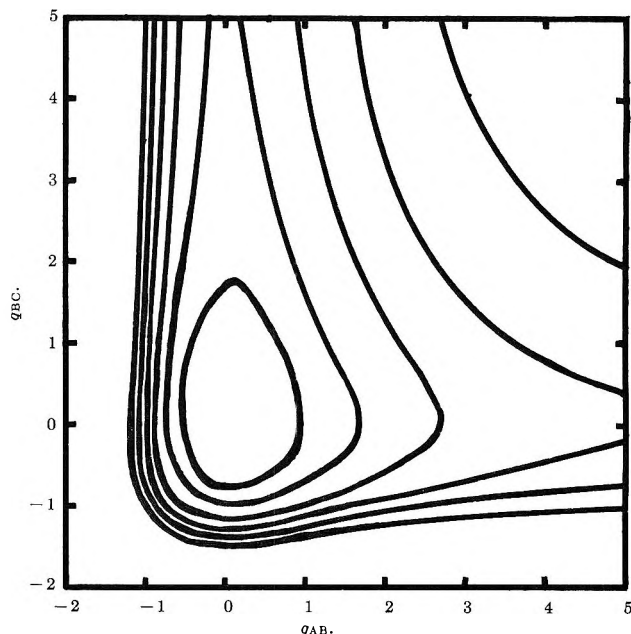


Figure 1. U_{ABC} with $D_{eAB} = 2D_{eBC}$.

scribed by a Rydberg function $U(q)$ that has its minimum at $q = \zeta$ instead of at $q = 0$.

$$U_\zeta(q) = -D_\zeta[1 + (q - \zeta)]e^{-(q-\zeta)} \quad (9)$$

In general, ζ and D_ζ remain as adjustable parameters. However, the special form for $\zeta = 2$ is appealing here because $U_2(q)$ is easily manipulated and is the real part of

$$W_2(q) = -u_B u_C = -u_B^* u_C^* \quad (10)$$

[Of course, $U_2(q)$ also has real factors of the form $e\sqrt{D^2}(1 \pm \sqrt{q})e^{-q/2}$.] Like (7), (10) is easily extended to species with many atoms.

Figure 2 shows $U_0(q)$ when $D_e = 1$ and

$$U_2(q) = D_2 e^2 (1 - q)e^{-q} = D_r (1 - q)e^{-q} \quad (11)$$

when $D_r = D_2 e^2 = 1$. The minimum energy of $U_2(q)$ is $-D_2$ at $q = 2$ and $r = r_{e2}$. The position of the minimum of $U_2(q)$ is related to the equilibrium distance r_{e0} of $U_0(q)$ by $2 = b(r_{e2} - r_{e0})$ or

$$r_{e2} = r_{e0} + 2/b \quad (12)$$

Typically, b is about 1 \AA^{-1} for alkali metals and about 2 \AA^{-1} for transition elements. It increases to about 2.5 \AA^{-1} for groups V and VI and is about 2.7 \AA^{-1} for I, Br, Cl, and H, while for N, O, and F b is about 4 \AA^{-1} . Thus, the size of the term $2b^{-1}$ in (12) corresponds roughly to the size of the atomic orbitals of the valence shell.

The interpretation of D_r varies with the size of q . At large q , $U_2(q)$ can describe stabilization of a pair

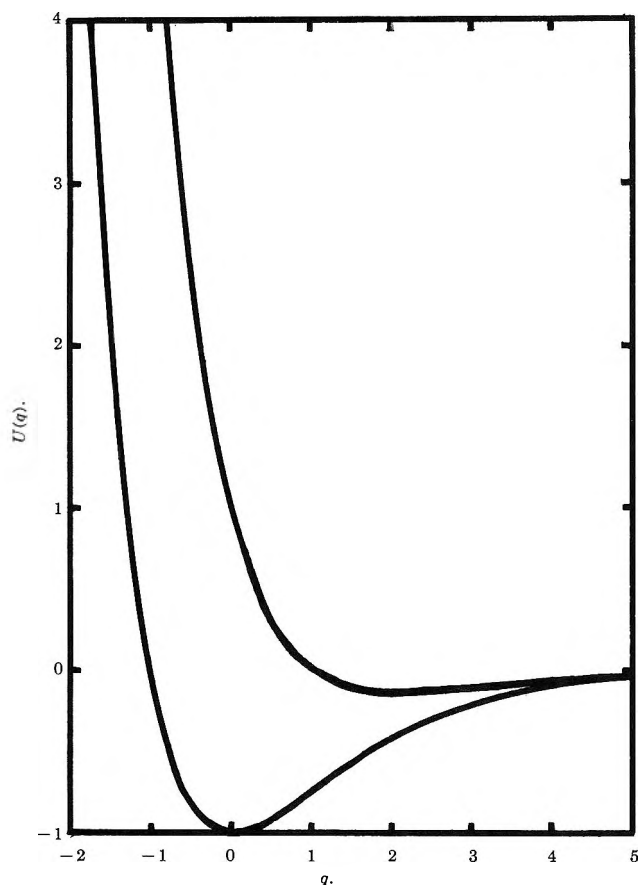


Figure 2. Ordinary and displaced Rydberg functions.

of atoms due to dispersion forces, for a van der Waals radius is often about 0.8 \AA , greater than a single-bond radius. A value of $D_2 = D_e e^{-2}$ would then be an energy of vaporization divided by half the number of neighbors in the liquid. Since e^{-2} is 0.135, D_r is then approximately a molar energy of vaporization, with larger values indicating long-range binding of a more specific character than dispersion. For q less than about unity, D_r is best considered to be an energy of repulsion.

Factors for ABC^\ddagger

A Rydberg-like potential energy function for ABC^\ddagger should reduce, in the limit of $AB + C$, to

$$U_{AB,C} = -D_{eAB}(1 + q_{AB})e^{-q_{AB}} + D_{rBC}(1 - q_{BC})e^{-q_{BC}} \quad (13)$$

and, in the other limit of $A + BC$, to

$$U_{A,BC} = -D_{eBC}(1 + q_{BC})e^{-q_{BC}} + D_{rAB}(1 - q_{AB})e^{-q_{AB}} \quad (14)$$

In two-dimensional q -space like Figure 1, each U in (13) and (14) has at $q_{ij} = 0$ and $q_{jk} = 2$ a minimum of

a kind seldom mentioned explicitly in studies of activated complexes. In factored form, both U 's are the real part of

$$W_{ij,k} = -u_j(u_i^* + u_k) = -u_j^*(u_i + u_k^*) \quad (15)$$

where like factors yield the term containing $(1 - q)$ as in (10) while a product of complex conjugates, as in (7), yields the strongly attractive term with $(1 + q)$. Equation 15 is easily generalized to describe more bonds.

Joining U 's

When A and C are alike, $U_{AB,C}$ is easily joined to $U_{A,BC}$ along the line $q_{AB} = q_{BC}$. If q^\ddagger is the distance from the origin along this line, the joined potential function along $q_{AB} = q_{BC}$ is

$$U^\ddagger_{ABA} = -D_e \left(1 + \frac{q^\ddagger}{\sqrt{2}}\right) e^{-q^\ddagger/\sqrt{2}} + D_r \left(1 - \frac{q^\ddagger}{\sqrt{2}}\right) e^{-q^\ddagger/\sqrt{2}} \quad (16)$$

where $D_e = D_{eAB} = D_{eBC}$ and $D_r = D_{rAB} = D_{rBC}$. The configuration of ABA^\ddagger lies at the minimum of U^\ddagger_{ABA} at

$$\frac{q^\ddagger_e}{\sqrt{2}} = q^\ddagger_{AB} = q^\ddagger_{BC} = q^\ddagger_{BA} = \frac{2D_r}{D_e + D_r} \quad (17)$$

The energy of activation of the forward (or reverse) process, with neglect of zero-point energy, is

$$\Delta E_e = D_e + U^\ddagger_{ABA}(q^\ddagger_e) = D_e - (D_e + D_r) \exp\left(-\frac{2D_r}{D_e + D_r}\right) \quad (18)$$

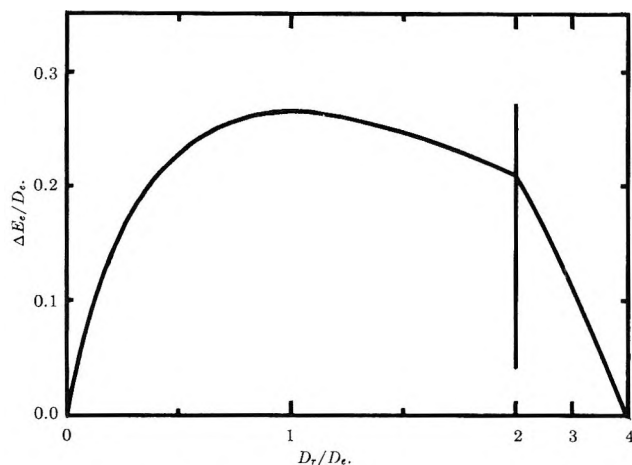
Requiring ΔE_e to exceed zero imposes the restrictions $0 \leq D_r \leq 3.92D_e$. Table I lists numerical values for (17) and (18), and Figure 3 shows how $\Delta E_e/D_e$ varies with D_r/D_e .

As D_r increases, the minimum of $U_{AB,A}$ near $q_{AB} = 0$ and $q_{BA} = 2$ deepens and eventually reduces U^\ddagger_{ABA} to the level that prevails at the atom-diatom limit at $q_{BA} = \infty$. Then ΔE_e is zero, as it also is when D_r is zero with minima matched at $q^\ddagger_e = 0$. The maximum in $\Delta E_e/D_e$ lies at $D_r = D_e$ where $\Delta E_e = 0.264D_e$.

When C differs from A, $U_{AB,C}$ is to be joined to $U_{A,BC}$ along a curve that reduces to the line $q_{BC} = q_{AB}$ when C becomes A. It is not possible to join U 's satisfactorily along a line $q_{BC} = mq_{AB}$ of adjustable slope m . If U 's and their first derivatives with respect to q^\ddagger are matched at the origin, the conditions

$$D_{eAB} + D_{rAB} = D_{eBC} + D_{rBC} \quad (19)$$

$$b_{AB}D_{rAB} = b_{BC}D_{rBC} \quad (20)$$

Figure 3. Energy of minimum of U^{\ddagger}_{ABA} relative to AB.**Table I:** Energies of Activation ΔE_e for the Symmetrical Activated Complex ABA^{\ddagger}

$\left(\frac{D_r}{D_e}\right)$	$\left(\frac{\Delta E_e}{D_e}\right)$	$\left(\frac{q^{\ddagger}_e}{\sqrt{2}}\right)$
0.00	0.000	0.000
0.05	0.045	0.095
0.10	0.083	0.182
0.20	0.140	0.333
0.40	0.209	0.572
0.60	0.244	0.750
0.80	0.260	0.889
1.00	0.264	1.000
1.20	0.261	1.091
1.40	0.252	1.167
1.60	0.241	1.231
1.80	0.226	1.286
2.00	0.209	1.333
3.00	0.108	1.500
3.92	0.000	1.593

result. If the D_e 's differ much in size, at least one D_r is large and its interpretation as a London energy or energy of vaporization becomes unrealistic. Moreover, near q^{\ddagger}_e there occur intolerable energy discontinuities between joined regions of the order of $0.2D_e$ for typical values of D_e and b . If, instead, U 's and their first derivatives are matched at q^{\ddagger}_e (which can be found by a clumsy expression in terms of given b 's and D_e 's), then unrealistically large values of D_r or q^{\ddagger}_e may result. Even for the reaction $H_2 + Cl \rightarrow H + HCl$, where the D_e 's differ by only 3%, D_r is about 50 kcal., $q^{\ddagger}_{eHH} = 0.638$, $q^{\ddagger}_{eHCl} = 0.613$, and U^{\ddagger}_{HCl} assumes the very high value of -84.0 kcal. The observed activation energy suggests a value of U^{\ddagger}_{HCl} lower by about 20 kcal. For the reaction $H_2 + I \rightarrow H + HI$, where D_e 's differ by 30%, one finds the

extraordinary values $D_r = ca. 450$ kcal., $q^{\ddagger}_{eHH} = 1.750$, $q^{\ddagger}_{eHI} = 1.578$, and $U^{\ddagger}_{HHI} = -102.6$ kcal., which is below the limit at $-D_{eHI} = -73.8$ kcal. Simple valence theory suggests that q^{\ddagger}_{eAB} is about $0.2b_{AB}$, which for $H_2 + I$ is only about 0.6. Equally unsatisfactory are results obtained by matching U 's and derivatives at the origin and letting the curve separating the $AB + C$ region from the $A + BC$ region fall where it may. It is thus impossible to avoid minima at $q_{ij} = 2$ and $q_{jk} = 0$ that are too deep and activated complexes that are too loose and of wrong energy when matching is done along a straight line through the origin.

The most satisfactory way to join $U_{AB,C}$ to $U_{A,BC}$ seems to be to determine an effective average value of D_r from the observed values of D_e and activation energy ΔE_e by use of Figure 3. If D_e 's and b 's are nearly equal, the curve separating regions is approximately a straight line, as required when A is like C or as the previous results for $H_2 + Cl \rightarrow H + HCl$ would suggest by their near acceptability. The reactions of Table II satisfy these conditions on D_e and b . In correcting the observed activation energies ΔE_a to ΔE_e , the zero-point energy of each activated complex was assumed to be the average of the zero-point energies of isolated diatoms AB and BC.

Table II: Effective Values of D_r from Observed Activation Energies

	Reaction		
	$H_2 + H \rightarrow H + H_2$	$H_2 + Cl \rightarrow H + HCl$	$Cl_2 + Br \rightarrow Cl + ClBr$
D_{eAB} , kcal.	109.5	109.5	57.9
D_{eBC} , kcal.	109.5	106.5	52.7
b_{AB} , \AA^{-1}	2.75	2.75	2.86
b_{BC} , \AA^{-1}	2.75	2.64	2.70
ΔE_a (obsd.), kcal.	7.7 ^a	5.5 ^b	6.9 ^c
ΔE_e , kcal.	7.7	6.5	7.0
D_r , kcal.	9.0	7.6	9.3
$q^{\ddagger}_{eij} = q^{\ddagger}_e/\sqrt{2}$	0.152	0.132	0.288
$r^{\ddagger}_e - r_e$, \AA .	0.055	0.049	0.104

^a G. Boato, G. Careri, A. Cimino, E. Molinari, and G. G. Volpi, *J. Chem. Phys.*, **24**, 783 (1956). ^b P. G. Ashmore and J. Chanmugam, *Trans. Faraday Soc.*, **49**, 254 (1953). ^c M. I. Christie, R. S. Roy, and B. A. Thrush, *ibid.*, **55**, 1139 (1959).

The values of D_r in Table II are of the size of dispersion energies, although they may reasonably be attributed to long-range valence forces because of the change in bonding during reaction. The minima at $q_{ij} = 0$ and $q_{jk} = 2$ have energies of $-D_e - D_r e^{-2}$. Even if D_r rises to D_e (as in Figure 2) and even if $\Delta E_a = ca.$

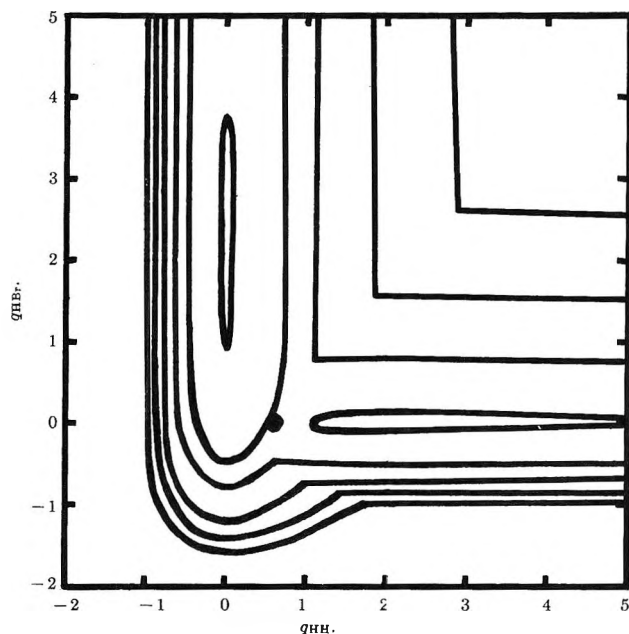


Figure 4. U_{ABC} for $H_2 + Br \rightarrow H + HBr$ with contours at 0, -25, -50, -75, -90, and -110 kcal.

$0.25D_e$ (as in Figure 3), these minima do not become unreasonably low due to attraction between non-bonded atoms. With effective values of D_e and D_r known, effective values of q_e^\ddagger and $r_e^\ddagger - r_e$ follow from (17) and the definition $q = b(r - r_e)$.

Calculation of Activation Energy

The calculations that led to D_r can be reversed for reactions having greatly different D_e 's provided the long-range energy D_r is constant at about 8 kcal., or at least at about an energy of vaporization. This has been done for H_2 reacting with Br and I. Figures 4 and 5 show U_{ABC} when $D_r = 8.0$ kcal. and when $U_{AB,C}$ is joined to $U_{A,BC}$ along whatever curve is demanded. For $H_2 + Br$, U_{HHBr}^\ddagger is -88.6 kcal. at $q_{eHH}^\ddagger = 0.59$ and $q_{eHBr}^\ddagger = 0.01$. These values of energy and configuration agree in general with the more sophisticated results of others.³ The value of ΔE_a calculated from U_{HHBr}^\ddagger , with the approximate correction for zero-point energy mentioned above, is 19.6 kcal., in good agreement with the observed activation energy of about 18 kcal.⁴ The distances in $HHBr^\ddagger$ are $r_{eHH}^\ddagger = 0.742 + 0.215 = 0.957$ Å. and $r_{eHBr}^\ddagger = 1.414 + 0.004 = 1.418$ Å. Similarly, for $H_2 + I$, U_{HHI}^\ddagger is -73.7 kcal. at $q_{eHH}^\ddagger = 0.98$ ($r_e^\ddagger = 1.098$ Å.) and $q_{eHI}^\ddagger = 0.02$ ($r_e^\ddagger = 1.612$ Å.). The calculated ΔE_a is 34.3 kcal., also in agreement with the observed⁵ value of 32.8 kcal.

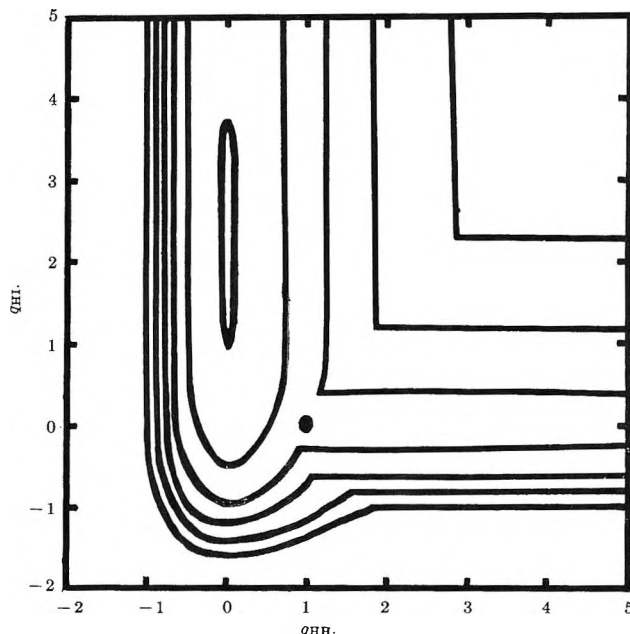


Figure 5. U_{ABC} for $H_2 + I \rightarrow H + HI$ with contours at 0, -25, -50, -70, -90, and -110 kcal.

Critique

This method of generating U_{ABC} clearly glosses over the fact that the union of $U_{AB,C}$ and $U_{A,BC}$ is not smooth and that the real nature of any triatomic configuration is not just $AB + C$ or $A + BC$, especially along the curve that joins U 's as they would cross. That is, resonance stabilization is neglected along the curve between regions. There is also no correction for proton tunneling. However, the apparent constancy of D_r as a dispersion energy and the ease of using the Rydberg functions may compensate for these empirically justified oversights.

One last remark concerns Figure 3, which predicts that ΔE_a is expected to be less than about $0.3D_e$, if the D_e 's do not differ greatly. This maximum on ΔE_a is in accord with general experience.

Acknowledgment. Acknowledgment is made to the donors of The Petroleum Research Fund, administered by the American Chemical Society, for support of this research.

(3) E. A. Moelwyn-Hughes, *Ann. Rept.*, **32**, 89 (1935); **33**, 86 (1936); A. Wheeler, B. Topley, and H. Eyring, *J. Chem. Phys.*, **4**, 178 (1936).

(4) F. Bach, K. F. Bonhoeffer, and E. A. Moelwyn-Hughes, *Z. physik. Chem.*, **B27**, 71 (1934).

(5) J. H. Sullivan, *J. Chem. Phys.*, **36**, 1925 (1962).

Acidity and Autocatalysis of Esterification of Acetylenic and Fluoro Acids

by Jack Radell,¹ B. W. Brodman,

Pitman-Dunn Institute for Research, Frankford Arsenal, Philadelphia, Pennsylvania 19137

Amiram Hirshfeld, and E. D. Bergmann

The Hebrew University of Jerusalem, Jerusalem, Israel (Received September 26, 1964)

The acetylenedicarboxylic acid and perfluoro acids, unlike propiolic acid, were found to be autocatalytic in esterification reactions with unfluorinated alcohols. Only the diester could be isolated from the diacid. A determination of pK_a values showed the acidity to decrease in the following order: perfluoro acids > acetylenedicarboxylic acid > propiolic acid. The acidity of the acetylenedicarboxylic acid was compared with that of fumaric, maleic, and succinic acids. The enhanced acidity of the acetylenedicarboxylic acid was discussed. A simplified, self-consistent method was employed to determine the effect of added salt on the pK_a and the thermodynamic pK_a . The measured and thermodynamic pK_a values were found to be insignificantly different in each case studied.

Introduction

In order to obtain compounds containing acetylenic ester groups several prototype compounds were prepared. To determine the feasibility of obtaining esters of acetylenic acids without added acid catalysts, the pK_a values of propiolic, acetylenedicarboxylic, and some perfluoro acids were measured. The latter acids were included since several cases are known² where these acids are autocatalytic in esterification reactions with nonfluorinated alcohols. For comparison, some perfluoro acids were autocatalytically esterified. The pK_a of acids were measured in order to determine which are sufficiently strong to autocatalyze their own esterification.

Discussion

Titration curves for the acetylenedicarboxylic acid and the hydrated samples of $n\text{-C}_7\text{F}_{15}\text{CO}_2\text{H}$, $n\text{-C}_3\text{F}_7\text{CO}_2\text{H}$, and $\text{HC}\equiv\text{CCO}_2\text{H}$ are listed in Table I. All the curves had a single strong inflection (Figure 1) including acetylenedicarboxylic acid for the titration of both carboxyl groups. Two pK_a values were obtained by Dondon³ and Ashton and Partington⁴ for the dihydrate of acetylenedicarboxylic acid using an approximately 50% aqueous ethanol solution ($pK_{a_1} = 2.2$; $pK_{a_2} = 4.0$). Charton⁵ reporting on the work of Ashton and Partington⁴ gave a single pK_a value.

Our measurements which resulted in a single pK_a value for acetylenedicarboxylic acid differed primarily in that we started with anhydrous material as noted by the neutralization equivalent in Table I. Dondon³ did note that a single pK_a value was obtained for the diacid when 20% ethanol in water was used as a solvent.

If we compare the pK_{a_1} and pK_{a_2} values of succinic, fumaric, and maleic acids with the single value we obtained for acetylenedicarboxylic acid, we note the values in Table II.

The succinic acid has the highest pK_a of those listed

(1) Holder of a U. S. Secretary of the Army Research and Study Fellowship at The Hebrew University of Jerusalem, 1962-1963.

(2) (a) M. Hudlicky, "Chemistry of Organic Fluorine Compounds," The Macmillan Co., New York, N. Y., 1962, p. 197; (b) J. Radell and J. W. Connolly, *Chem. Eng. Data*, **6**, 282 (1961); (c) E. E. Burgoyne and F. E. Condon, *J. Am. Chem. Soc.*, **72**, 3276 (1950).

(3) M. L. Dondon, *J. chim. phys.*, **54**, 304 (1957).

(4) H. W. Ashton and J. R. Partington, *Trans. Faraday Soc.*, **30**, 598 (1934).

(5) M. Charton, *J. Org. Chem.*, **26**, 735 (1961), erroneously reported "It should be noted that Ashton and Partington have reported values of 1.85×10^{-2} for the first and for the second ionization constant of acetylenedicarboxylic acid." In Ashton and Partington's paper⁴ there are two sets of K_a values measured with different titrant and sample concentrations giving no indication of the solvent presumed to be largely or completely aqueous. The respective values they⁴ reported for the molality of acetylenedicarboxylic acid, normality of titrant, $K_{a_1} \times 10^{-2}$, and $K_{a_2} \times 10^{-5}$ are 0.0101, 0.0314, 1.82, 4.20, and 0.00202, 0.00720, 1.88, 3.85.

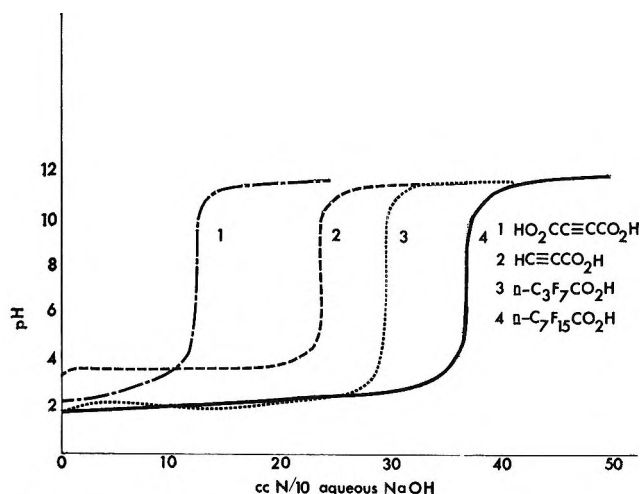
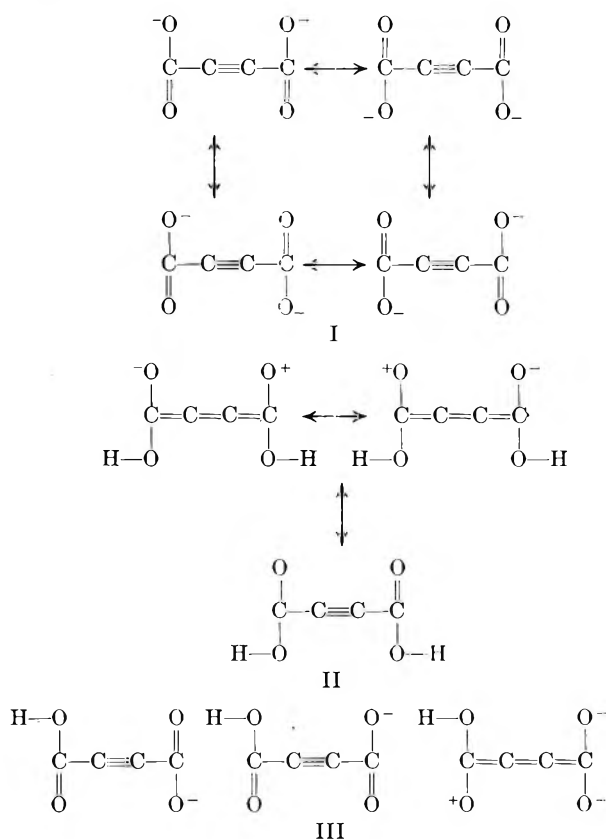


Figure 1.

above owing to the fact that the first ionization is not enhanced by any unsaturation on the centrally located carbon atoms. Furthermore, the preferred, lower energy, planar, zigzag conformation of succinic acid prevents any enhancement of the first ionization owing to the spatial proximity of the carboxyls to each other. Correspondingly, the reduction in the acidity of the second carboxyl (compared to the other diacids) resulting from the closeness of the carboxylate ion to the intact carboxyl group is also minimized resulting in a ΔpK_a of 1.47. Similarly, fumaric acid is arranged in a more rigidly controlled planar, zigzag conformation. However, the presence of the centrally located double bond enhances the acidity of both the first and second pK_a values. At the same time the spatial influence of one carboxyl on the other is minimized as in succinic acid, and the ΔpK_a is approximately the same as that for succinic acid. In maleic acid we have both the centrally located double bond and the close proximity of one carboxyl to the other causing a significant decrease of the pK_{a1} value compared to succinic and fumaric acids. The closeness of the carboxylate ion in the half-neutralized acid to the remaining carboxyl, on the other hand, causes an increase in the resulting pK_{a2} and a ΔpK_a which is approximately threefold that of succinic and fumaric acids. In extending this comparison to acetylenedicarboxylic acid, it should be noted that the two carboxyl groups are part of a linear array of four carbon atoms. Consequently, the influence of one carboxyl upon another through space must be minimized. Furthermore, the presence of a centrally located triple bond would be expected to enhance the acidity of both carboxyl groups to a greater extent than the saturated single bond in succinic or the olefinic function in fumaric and maleic.

In addition, if we now consider the effect of resonance on the completely neutralized acid (I), the free acid (II), and the half-neutralized acid (III), it is apparent that the contribution made by resonance to the stabilization of I, II, and III is much greater for I with its four highly equivalent forms in spite of the presence of the double negative charge.

In summary: (1) the presence of the triple bond in acetylenedicarboxylic acid enhances the acidity (lowers pK_a) of both carboxyl groups; (2) the absence of a spatial effect in the linear molecule minimizes any difference between pK_{a1} and pK_{a2} ; (3) the resonance structures contribute considerably greater stabilization to the dianion of acetylenedicarboxylic acid than to the half-neutralized or free diacid. This effect would enhance the acidity (lower pK_a) of the second carboxyl group. Furthermore, there is no reasonable way in which electronic influences of one carboxyl or carboxylate ion can be transmitted by resonance to the other carboxyl or carboxylate ion. This is consistent with the previously observed⁵ reduced transmission power of a triple bond compared to a *trans* double bond.



These factors account for both the single inflection in the titration curve of acetylenedicarboxylic acid and its acidity, which is greater than that of the diacids

Table I

Compounds	Mol. wt. ^a	Neut. equiv. ^b	pK _a	Number of determinations
<i>n</i> -C ₃ F ₇ CO ₂ H	214	240 ± 10	2.00 ± 0.00	7
<i>n</i> -C ₇ F ₁₅ CO ₂ H	414	427 ± 2	2.14 ± 0.06	5
HC≡CCO ₂ H	70	80 ± 2	3.40 ± 0.00	4
HO ₂ CC≡CCO ₂ H	114	59 ± 1	2.65 ± 0.05 ^c	4

^a Calculated molecular weight. ^b Neutralization equivalent determined. ^c The pK_a for acetylenedicarboxylic acid was obtained from the half-neutralization point on the titration curve after neutralization of both carboxyl groups.

Table II

Acids	pK _{a1}	pK _{a2}	ΔpK _a
Succinic	4.17	5.64	1.47 ^a
Fumaric	3.03	4.47	1.44 ^b
Maleic	2.00	6.26	4.26 ^c

^a L. F. Fieser and M. Fieser, "Advanced Organic Chemistry," Reinhold Publishing Corp., New York, N. Y., 1961, p. 565.

^b "Lange's Handbook of Chemistry," Handbook Publishers, Inc., Sandusky, Ohio, 1946, p. 1378. ^c See ref. b, p. 1379.

listed. The single inflection in the titration curve for acetylenedicarboxylic acid (Figure 1) requires that the acidity of the second carboxyl, after neutralization of the first in any one molecule, is approximately equal to or greater than the acidity of the first carboxyl in an unneutralized acid. This would result in the random or preferential (respectively) neutralization of the second carboxyl in a molecule before an unneutralized molecule reacts with the titrant. This explanation is consistent with the behavior of the acetylenedicarboxylic acid.

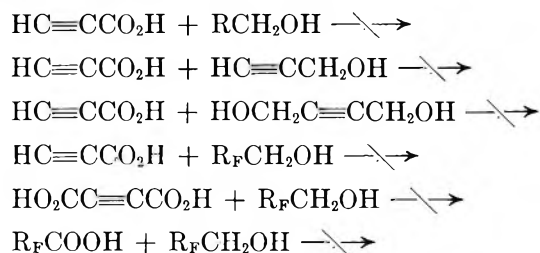
The pK_a values were determined from the titration curves (Figure 1). The half-neutralization points were obtained from these curves. In order to determine the effect of added salts and the thermodynamic pK_a, a sample was half-neutralized to the predetermined pH, successive weighed amounts of salt were added, and the pH was measured after each addition. These results were plotted and extrapolated to zero salt concentration to obtain the thermodynamic pK_a. Using this self-consistent procedure the added salts caused the pK_a to change less than 0.02 of a pK_a unit. In preliminary studies where a complete titration was made for each separate salt concentration the effect of salts fell within the error of the method. Using this self-consistent procedure in the specified range it was found that the addition of salt causes a systematic decrease

in the pK_a (increase in acidity) in the case of acetylene dicarboxylic acid and perfluorooctanoic acid. The determined thermodynamic pK_a at zero salt concentration was found by half-neutralizing a sample to a predetermined pH and then adding successive weighed amounts of salt and measuring the pH after each addition. These results were plotted, falling on a straight line, and extrapolated to zero salt concentration. The value of the pH at half-neutralization was 2.00 for the acetylenedicarboxylic acid at a total salt concentration (half-neutralized acid and sodium chloride) of 1.977 *M*. For perfluorooctanoic acid the respective values are 2.00 (pH) at 13.271 *M*. No compensation⁶ was made in these studies (Table I) for the ionization of any of the acids or for the fact that a 95% ethanol-water (1:1 by volume) was used.

The first point on the curve closest to the pK_a axis is the concentration of neutralized acid resulting from the addition of enough sodium hydroxide to half-neutralize the acid. For a mole each of perfluorooctanoic and acetylenedicarboxylic acids, 0.5 and 1 mole, respectively, are required to half-neutralize each of the acids.

The diacid had a measured pK_a of 2.63 (Table I) and a thermodynamic pK_a of 2.66. The perfluorooctanoic acid had a measured pK_a of 2.14 (Table I) and a thermodynamic pK_a of 2.16.

One of the objectives of this research was to relate the pK_a value of each acid to its autocatalytic activity in esterification reactions. The following reactions failed without catalysts.



where R_F = C_{*n*}F_{2*n*+1}.

(6) The compensation for ionization of the acid is made by the equation.

$$\text{pK}_a = \text{pH} - \log \frac{[\text{salt}] + [\text{H}^+]}{[\text{acid}] - [\text{H}^+]}$$

The pK_a values reported in Table I are in fact numerically equal to the pH in the above equation. The measured pK_a (Table I) may be compared to the pK_a in parentheses obtained from the above equation for the following compounds: *n*-C₃F₇CO₂H, 1.74 (2.00); *n*-C₇F₁₅CO₂H, 1.92 (2.14); HC≡CCO₂H, 3.39 (3.40); HO₂CC≡CCO₂H, 2.30 (2.48). As would be expected, the correction is proportional to the strength of the acid (inversely proportional to the pK_a). For the acetylenedicarboxylic acid, the pK_{a2} reported by Dondon³ rises from 3.0 at 20% ethanol to 4.0 at 50% and 6.8 at 100%. Consequently, the values in Table I have relative rather than absolute significance since no correction is made for solvent or for the ionization of strong acids.

Only the acetylenedicarboxylic and perfluoro acids showed autocatalytic activity in esterification reactions with alkanols. The autocatalytic polyesterification of acetylenedicarboxylic acid with 2-butyne-1,4-diol was reported⁷ while our research was in progress. In no case was a half-ester obtained from the autocatalytic esterification of acetylenedicarboxylic acid and an alkanol. Only diester was isolated. This is also attributable to the fact that the second carboxyl in esterification compared to the first has approximately the same or greater acidity after half-esterification.

In all esterifications benzene was used to entrain water. From the fact that propiolic acid and alkenoic and alkanolic acids are not autocatalytic and acetylenedicarboxylic and perfluoroalkanoic acids are, it would be expected that those acids having a pK_a of 2.6 or less would be autocatalytic in esterification reactions,⁸ and those having a pK_a of 3.4 or more would not. This does not preclude the possibility that acids not complying with these acidity requirements could also be autocatalytic if the esterification could be run at higher temperatures in a choice of appropriate solvent or neat to obtain the requisite activation energy. The above measures could be taken when the alcohol hydroxyl is

A possibility which was not tested is to add a salt, such as lithium chloride, to the benzene used in the esterification reaction to enhance the acidity of some acid not quite strong enough to be autocatalytic in esterification as indicated by the reported salt effect.

Experimental

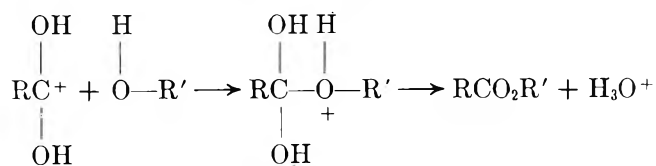
Esterification. The reactants in every case were added to a 250-ml., three-necked, round-bottom flask fitted with a mechanical stirrer, a modified Dean and Stark⁹ distilling receiver, and a water-cooled, jacketed sleeve-type or a precision-bored, plain sleeve-type stirrer with a lubricating well. Efficient stirring is especially required when the reactants are immiscible. The reaction mixture was stirred rapidly until water stopped collecting in the Dean and Stark distilling receiver. The contents of the reaction flask, if all liquid, was poured into a barostatic separatory funnel containing 10 ml. of water and 100 ml. of ether and was washed with water until the washings were neutral to litmus paper. The organic layer was then dried, concentrated, and distilled.¹⁰ When the reaction product was a solid, it was filtered and recrystallized from an appropriate solvent. See Table III.

Table III: Summary of Data on Esters

Ester	% yield	B.p., °C. (mm.)	M.p., °C. (solvent) ^b	Hours reflux	Catalyst	% C		% H		% other	
						Calcd.	Found	Calcd.	Found	Calcd.	Found
$n\text{-C}_7\text{H}_{15}\text{CO}_2\text{CH}_2\text{C}\equiv\text{CH}$	52	50-59 (2.2-3.0)		11	None	29.2	29.0	0.67	0.69	63.0	63.1(F)
$(n\text{-C}_7\text{H}_{15}\text{CO}_2\text{CH}_2)_2(\text{C}\equiv\text{C})$	51	140-144 (1.0-1.5)		13	None	27.4	27.5	0.46	0.35	64.9	64.9(F)
$(\text{CF}_2\text{CO}_2\text{CH}_2\text{C}\equiv\text{CH})_2$	6	74-76 (0.3)		10	None	45.2	45.2	2.3	2.2	28.5	28.6(F)
$(\text{CF}_2)_2(\text{CF}_2\text{CO}_2\text{CH}_2\text{C}\equiv\text{CH})_2$	25	87-90 (0.5)		7	None	41.7	41.4	2.5	1.9		
$\text{HC}\equiv\text{CCO}_2(\text{CH}_2)_2\text{C}(\text{CH}_3)_3$	78	35 (0.6)		10	H_2SO_4	70.1	70.2	9.2	9.1		
$\text{CH}_3\text{C}(\text{NO}_2)[(\text{CH}_2)_2\text{CC}\equiv\text{CH}]_2^a$	70		92-93 (benzene)	13	H_2SO_4	50.2	50.0	3.8	3.9	5.8	5.2(N)
$\text{C}(\text{CH}_2\text{O}_2\text{CC}\equiv\text{CH})_4^a$	81		110 (CH_2NO_2)	15	H_2SO_4	59.4	59.6	3.5	3.5		
$\text{H}(\text{CF}_2)_{10}\text{CH}_2\text{O}_2\text{CC}\equiv\text{CH}$	86		59-60 (CH_2NO_2)	19	H_2SO_4	28.8	28.8	0.69	0.85	65.1	65.0(F)
$(\text{CF}_2)_3(\text{CH}_2\text{O}_2\text{CC}\equiv\text{CH})_2$	6	102 (0.8)			H_2SO_4	41.8	41.3	1.9	2.3		
$(\text{C}\equiv\text{C})[\text{CO}_2(\text{CH}_2)_2\text{C}(\text{CH}_3)_3]_2$	57	132-138 (0.9)		10	None	68.1	67.8	9.3	9.2		
$(\text{C}\equiv\text{C})[\text{CO}_2(\text{CH}_2)_2\text{C}(\text{CH}_3)_3]_2$	82	147-148 (0.6)		13	None	71.0	71.2	10.1	10.2		
$(\text{C}\equiv\text{C})[\text{CO}_2\text{CH}_2(\text{CF}_2)_{10}\text{H}]_2$	5	150-168 (2.5)		18	H_2SO_4	27.3	27.9	0.53	1.1		
$(\text{C}\equiv\text{C})(\text{CO}_2\text{CH}_2\text{C}\equiv\text{CH})_2$	4	86-92 (0.3)		20	None	63.2	61.9	3.2	3.3		

^a Attempts to distil resulted in a violent explosion. ^b Solvent used to recrystallize ester.

deactivated by electronegative substituents, as in fluorinated alcohols, which decrease the availability of electrons on the oxygen of the alcohol needed to form the activated complex with the dihydroxycarbonium ion of the acid for ester formation, thus



where R' equals $-\text{CH}_2\text{R}_F$.

Autocatalytic Polyester Formation. Glycerol (0.2 mole) and acetylenedicarboxylic acid (0.3 mole) were heated together for 19 hr. in benzene to give an almost

(7) A. Zilkha, The Hebrew University, in a private communication.

(8) The comparison between pK_a and autocatalytic activity is made although the mediums in which the pK_a is measured and in which the esterification is run are not the same.

(9) J. Radell, U. S. Patent Application Serial No. 214,148 (filed Aug. 1, 1962). This is used to extract any of the reactants continuously and efficiently from the Dean and Stark collection head for return to the reaction flask.

(10) J. Radell, *Chemist-Analyst*, **46**, 73 (1957).

quantitative yield of a hygroscopic orange solid that could be pulled into threads from benzene. When pentaerythritol (0.1 mole) was substituted for glycerol, a 20% yield of a granular insoluble, infusible, light tan solid was obtained. The polyester obtained by Zilkha⁷ from acetylenedicarboxylic acid was reportedly prepared without a solvent.

pK_a Measurements. The pK_a measurements were carried out by titrating 0.15–0.20 g. of the acid dissolved in a mixture of 25 ml. of water added to 25 ml. of 95% neutralized ethanol. The dissolved acid was then titrated with 0.1 *N* aqueous sodium hydroxide, and the pH measurements were plotted against the volume. The pH at the half-neutralization point obtained from the plot (Figure 1) was taken as the pK_a , since the ratio of salt to acid at this concentration is 1.

The thermodynamic pK_a was determined for per-

fluorooctanoic and acetylenedicarboxylic acids only by dissolving the acid, using a magnetic stirrer, in a mixture of 25 ml. of water and 25 ml. of neutralized 95% ethanol in which was immersed a glass and calomel electrode. The acid was then half-neutralized by 0.1 *N* aqueous sodium hydroxide. This was based upon a previous titration from which the neutralization equivalent and the pH at half-neutralization were measured. A series of previously weighed samples of sodium chloride was added to the half-neutralized acid (waiting until the stirred salt, after each addition, was completely dissolved and until the pH meter reading was stabilized before adding the next salt sample). The thermodynamic pK_a was obtained by extrapolating to zero salt concentration. The first point on each plot is the amount of salt of the titrated acid produced by its half-neutralization.

Solvent Vapor Pressures in Dilute Solutions of Gallium in Cadmium^{1,2}

by Guy R. B. Elliott, Joe Fred Lemons, and Harold S. Swofford, Jr.

University of California Los Alamos Scientific Laboratory, Los Alamos, New Mexico
(Received September 28, 1964)

Cadmium solvent vapor pressures over solutions at 775°K. and containing 0.008 to 0.25 mole fraction gallium obey the pressure relationship

$$P_{\text{Cd alloyed}}/P_{\text{Cd pure}} = 1 - 0.856N_{\text{Ga}} + 0.943N_{\text{Ga}}^2$$

The mathematical form of this relationship was deduced by analogy with Henry's law assuming that solutions are a random mixture of molecules or atoms which interact through short-range forces. The first coefficient, 0.856, was evaluated experimentally from precise and reproducible isopiestic balance measurements. It is presumed to measure the interaction of the gallium solute atoms upon neighboring cadmium solvent atoms. The second coefficient, 0.943 as fitted to the isopiestic measurements of Predel, is included to describe the effect when solvent atoms have two solute neighbors. The data cannot be fitted to the usually accepted modified Raoult's law expression

$$P_{\text{Cd alloyed}}/P_{\text{Cd pure}} = 1 - N_{\text{Ga}} + bN_{\text{Ga}}^2$$

Also a vapor pressure estimate using the Duhem pressure relationship and Kleppa's calorimetric heats of solution of gallium in cadmium fails to predict the observed cadmium behavior.

There have been surprisingly few adequate experimental tests of the fundamental assumptions of thermodynamics relative to solvent activity. Of interest to this research is Raoult's law and its modification with a solute-solute interaction term,³ *i.e.*

$$P_A/P_A^0 = 1 - N_B + bN_B^2 \quad (1)$$

in which P_A^0 is the vapor pressure of pure solvent; P_A is the solvent partial pressure over a solution; N_B is the solute mole fraction; b is a constant which measures the effect on the solvent vapor pressure created by the interaction when two solute molecules approach each other sufficiently closely.

Using a different approach from that leading to eq. 1 one can arrive at a predicted equation for the solvent vapor pressure.³

$$P_A/P_A^0 = 1 - k_A N_B + b' N_B^2 \quad (2)$$

The constant, k_A , is designed to measure the effect on the solvent vapor pressure resulting from the interactions of the solute molecules upon their neighboring solvent molecules, and b' is introduced to treat the

solvent molecules having two solute neighbors. The development of eq. 2 is presented elsewhere in this paper. Equations 1 and 2 both assume solution randomness and would have to be modified for the amount of order in the solution.

Usual experimental practice has been to determine vapor pressures from the midregion of composition out to perhaps 0.9 mole fraction of solvent. Then a b for eq. 1 is evaluated to fit the higher solvent concentration data taken. Such measurements usually do not distinguish adequately between eq. 1 and 2. LA-2997² contains an evaluation of the cases which we found that

(1) Work done under the auspices of the U. S. Atomic Energy Commission.

(2) Taken in part from Los Alamos Scientific Laboratory Report LA-2997, "An Alternative Treatment of Solvent Activity in the Raoult's Law Region. The Gallium-Cadmium System," by G. R. B. Elliott, J. F. Lemons, and H. S. Swofford, Jr. Available for \$1.00 from the Office of Technical Services, U. S. Department of Commerce, Washington 25, D. C.

(3) Correction for lack of thermodynamic ideality in the vapor phase is here neglected, and it is recognized that a single interaction term is inadequate for an exact representation of the solvent vapor pressure behavior.

in our opinion test the two relationships; however, the treatment was limited to regions where the bN_B^2 term was not important. The weight of evidence seemed to us to favor eq. 2 rather strongly, but new experimental evidence was clearly needed.

With the development of the isopiestic balance^{4,5} it became possible to measure solvent activities with high precision and apparent high accuracy at compositions as great as 0.99 mole fraction.

Cadmium is convenient as the solvent in the isopiestic balance. The gallium chosen as the solute has several advantages: (1) It is enough unlike cadmium so that the two liquid elements have a broad range of immiscibility⁶ at temperatures sufficiently high so as to eliminate other unusual bonding effects. Thus, a choice between eq. 1 and 2 would not be obscured by an approximation to a perfect solution. (2) The heat of mixing up to 15 atom % gallium with a cadmium solvent is known to be consistent with Henry's law modified by a solute-solute interaction term.⁷ Therefore the corresponding derived solvent vapor pressure curve has the form of eq. 1 and its constant should be closely predictable through the Duhem pressure relationship coupled with known enthalpies and estimated entropies. (3) Because of the large amounts of solute which must be removed to concentrate a dilute solution, it is impractical to use a single loading of the isopiestic balance to cover a large range of composition. Therefore, the measurements by Predel⁸ could serve both as a check on the isopiestic balance method and as a source of data more useful in evaluating the curvature away from the limiting slope.

Experimental

Equipment. The isopiestic balance (Figure 1) provides the means to measure composition and thermodynamic activity simultaneously. In this case measurements were made using volatile cadmium and effectively nonvolatile gallium. A reservoir of pure cadmium at some temperature was allowed to vaporize or condense cadmium so that a gallium-cadmium alloy at slightly higher temperature could alter its composition and reach pressure equilibrium with the reservoir cadmium. From published data the vapor pressure is known as a function of temperature. The temperature difference between the alloy and the reservoir when pressure-composition equilibrium has been achieved is thus a measure of the vapor activity over an alloy at that composition and temperature.

The isopiestic balance has been described in detail elsewhere.^{4,5} Its construction and operation will be outlined briefly and further discussion will be limited to details pertinent to this series of experiments. The legs

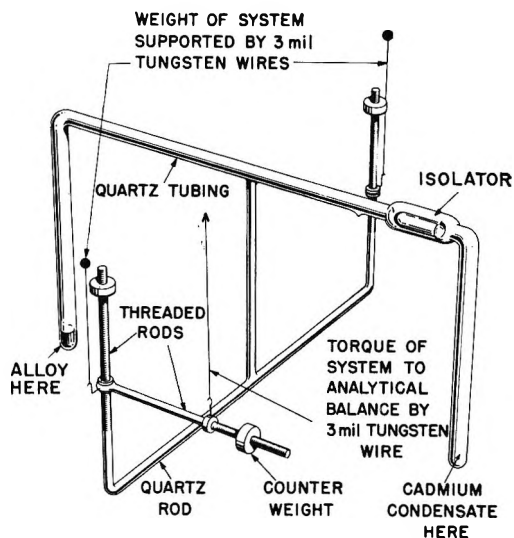


Figure 1. The isopiestic balance (schematic).

of an inverted U-tube of quartz which has been evacuated and sealed provide vapor-connected containers for both the alloy and the cadmium reservoir. This tube is mounted on a quartz frame which is suspended from fine tungsten wires so as to pivot around its approximate center of gravity. When cadmium has transferred between the alloy and the reservoir, the center of gravity has changed. A side arm on the frame is connected by another fine tungsten wire to an analytical balance. Weight at the balance is adjusted to counteract the shift in the center of gravity and thus the change in observed weight is proportional to composition change in the alloy.

The balanced quartz tube is surrounded by a furnace consisting of suitable heaters, shields, and insulating brick. The arrangement is such that hotter temperature regions are always positioned higher in the furnace. The layers of insulating bricks are separated by asbestos sheeting, and the outside of the furnace is plastered; thus there is no observable convection problem.

Temperature controllers regulate a small fraction of the current flowing to heaters. The heat is applied outside nesting copper cylinders (nickel-plated) which provide both a massive temperature ballast and a means to provide a very uniform temperature around each

(4) G. R. B. Elliott and J. F. Lemons, *J. Phys. Chem.*, **64**, 137 (1960).

(5) G. R. B. Elliott and J. F. Lemons, "Order and Microphases in CeCd_{1-x} Solid Solutions," *Advances in Chemistry Series*, No. 39, R. F. Gould, Ed., American Chemical Society, Washington, D. C., 1963, p. 153.

(6) T. Heumann and B. Predel, *Z. Metallk.*, **49**, 90 (1958).

(7) O. J. Kleppa, *Acta Met.*, **6**, 233 (1958).

(8) B. Predel, *Z. Metallk.*, **49**, 226 (1958).

leg of the inverted U-tube: the heat flows around each cylinder much faster than across the air gap so that temperatures within successive cylinders each become more uniform.

Temperatures are measured with Pt—Pt—10% Rh thermocouples positioned about 0.5 in. from the bottoms of the two tube legs. These junctions, hot and cold, are made by cutting both types of wire and forming the two junctions at the cuts. This technique assures that the junctions are of essentially identical composition. The outer copper cylinders are grounded and a grounded stainless steel screen isolates the remainder of the thermocouple leads from any external voltage. Either or neither thermocouple lead may be grounded without changing the e.m.f. Three leads out from this couple (center and ends) allow measurement of the temperature difference between the two regions or of the absolute temperature of either region. Temperature differences are measured to hundredths of a degree (0.1 μ volt) and absolute temperature to tenths of a degree.

Sample Purity. Cadmium of claimed ultrahigh purity was melted and skimmed to remove oxide, filed to remove surface material, examined with a microscope for traces of iron filings, and finally vaporized into position to leave any oxide or iron traces behind.

Analytical grade gallium was melted and splashed into droplets. Shiny droplets were selected for alloying.

To prevent later oxidation of gallium by moisture adsorbed on the quartz, the tube was repeatedly flamed at a temperature near the softening point while being evacuated. The tube was then filled with argon, the metals were introduced, and the tube was re-evacuated. Any remaining moisture would presumably ultimately precipitate gallium out of the alloy as Ga_2O_3 . It seems very unlikely that as much as 5% of the gallium was lost in this way. For reasons of caution we accept this 5% uncertainty, however.

The quartz container is not wet by either cadmium or the dilute gallium-in-cadmium alloy. Wetting and direct attack by even unalloyed gallium upon clean quartz under vacuum does not take place unless the temperature is several hundred degrees hotter than the temperatures used for these measurements. The quartz isopiestic balance containers showed no evidence of etching or other attack; by using hydrochloric acid both gallium and cadmium were readily and completely removed from the containers after the run; the alloy was heated several weeks in the isopiestic balance before measurements were started to assure that any reaction which could take place had done so.

Surface Energies. To evaluate the possibility that surface energies could cause noticeable effects,⁹ the

bottoms of the tube legs in the second run were made conical while those in the first run were hemispherical cups at the bottom of more narrow tubing.

The Measurements. The temperatures for equilibrium between a particular alloy and the reservoir were determined by slowly shifting the reservoir temperature until cadmium stopped transferring into or out of the alloy. The rate of temperature change approaching the balance reversal point was in most cases kept to less than 0.02°K./min. , and this reversal point was approached from both too large and too small temperatures of the cadmium condensate. Because of the small sample sizes (about 1 g. of alloy initially) and the fact that the system was close to the equilibrium point for hours, it is felt that this constitutes, as far as is experimentally practicable, an essentially equilibrium approach to the point of reversal.

Uncertainties. Aside from experimental uncertainty in literature values for the vapor pressure of pure cadmium, the principal uncertainties lie in the starting composition (purity, trace oxidation, weight) and in an essentially constant small bias in the temperature difference (ΔT) between the alloy and the pure cadmium reservoir. The bias is created because the cross arm of the reactor tube must be superheated a few degrees to prevent condensation. Some heat from the superheated region flows down the quartz tube legs. Most but not all of this heat is then drawn off by heat sinks near the tube legs. It is this temperature difference which creates an experimentally unavoidable small bias.

In the first run the balance factor, *i.e.*, the relationship of balance shift to composition shift, was established unequivocally and precisely. When the reservoir was slightly hotter than the alloy, all the cadmium was in the alloy and the balance reading was noted. This value was constant, was essentially independent of small changes in temperature, and was reproducible after data points had been measured. When the run was finished and the system was close to temperature-composition equilibrium so that the weight changed very slowly, the furnace was partly opened and the cross arm was quickly collapsed (at the isolator, Figure 1) using an oxyacetylene flame: Material transfer was stopped before significant cadmium transfer could occur. The system was then cooled and analyzed for how much cadmium was in the reservoir. In this case the relationship between balance reading and composition was determined well enough so that uncertainty in the *changes* of composition was trivial.

In the second run the reservoir temperature control

(9) At the suggestion of Cyril Stanley Smith.

Table I: The Activity of Cadmium Alloyed with Gallium

Point no.	Balance shift	Cd mole fraction ^a	Temperature, 0° K.				ΔT^c	Cadmium activity ^d
			Alloy ^b	Cadmium ^b	Alloy cross arm ^b	Cadmium cross arm ^b		
1	0.0400	0.99191	769.89	769.56	785.9	785.8	0.33 ± 0.01 ^e	0.99317 ± 0.00021
2	0.3254	0.99154	769.27	768.92	785.6	786.3	0.35 ± 0.01	0.99274 ± 0.00021
3	1.2095	0.99012	771.07	770.67	786.4	787.6	0.40 ± 0.01 ^f	0.99154 ^f
4	2.3715	0.98733	770.48	769.95	785.9	786.4	0.53 ± 0.015	0.98907 ± 0.00032
5	3.0667	0.98475	770.70	770.07	785.7	786.0	0.63 ± 0.01	0.98703 ± 0.00021
6	0.0924	0.99106	774.93	774.61	790.0	790.1	0.38 ± 0.01	0.99225 ± 0.00021
7	1.0144	0.98941	775.20	774.79	790.4	789.0	0.44 ± 0.005	0.99102 ± 0.00011
8	1.6345	0.98791	775.23	774.75	790.2	789.3	0.51 ± 0.01	0.98961 ± 0.00021
9	3.3660	0.98002	775.23	774.48	790.4	789.0	0.82 ± 0.015	0.98335 ± 0.00032
10	3.9775	0.97403	775.16	774.19	789.7	787.8	1.04 ± 0.01	0.97875 ± 0.00021
11	4.4969	0.96516	774.75	773.50	789.4	788.5	1.33 ± 0.02	0.97307 ± 0.00042

^a Points 1-5: Initial cadmium 1.04028-g.; gallium 0.00523 g.; 6.18569-g. balance shift = 1.00000-g. cadmium shift. Points 6-11: Initial cadmium 0.95829 g.; gallium 0.00528-g.; 6.2246-g. balance shift = 1.0000-g. cadmium shift. Points 6-11 have less certain balance factor than points 1-5. This leads to some uncertainty at large cadmium removal from alloy, *i.e.*, points 10 and 11. ^b Measured with Pt-Pt-10% Rh thermocouple against ice junction to nearest 0.1°K. The greater precision is retained for consistency with ΔT . ^c Measured with Pt-Pt-10% Rh thermocouple to 0.01°K. temperature difference between alloy and pure cadmium using thermocouple junctions from abutting pieces of thermocouple supply wire so that junction compositions are essentially identical. ΔT calculated from millivolts using the equation of Roeser and Wenzel after subtracting a constant millivolt correction (see Uncertainties) for each run. Points 1-5 reduced by 0.0011 mvolt; points 6-11 reduced by 0.0006 mvolt. For a discussion of usage of the Roeser-Wenzel equation, see ref. 5. ^d Vapor activity relative to that over pure liquid cadmium assuming that Kelley's equation describes the cadmium vapor pressure exactly (see ref. 5). ^e Uncertainty is one-half the magnitude of the difference between the reversal points approached from cadmium-rich and cadmium-lean alloy compositions. ^f Value approached from only cadmium-rich composition. Activity calculated assuming $\Delta T = 0.41$.

system broke down and caused both uncertainty in one measurement ($N_{Cd} = 0.96516$) and an unsuccessful direct analysis of the balance factor. For this reason the balance factor had to be determined by secondary means. First, the various lower arms were measured and a balance factor calculated. Second, a tube of the same dimensions was loaded with only cadmium and a balance factor was determined by the balance readings with the cadmium all on one side or all on the other. The first and second evaluations agreed within experimental error. Finally, this balance factor gave results which agree with the earlier run.

There is uncertainty due to the balance factor in this run as is indicated Figure 2. It is significant only where it applies to large removals of cadmium from the known original alloy composition.

Results

The data for the observed composition of the solution as a function of cadmium pressure are shown in Table I and plotted in Figure 2.

Certain comments are pertinent to an evaluation of the data: (1) The total dissolved gallium in each run is constant but, as discussed under Sample Purity, may be uncertain by perhaps 5%. (2) In run 1 each variation in the cadmium content is known to about 1 part in

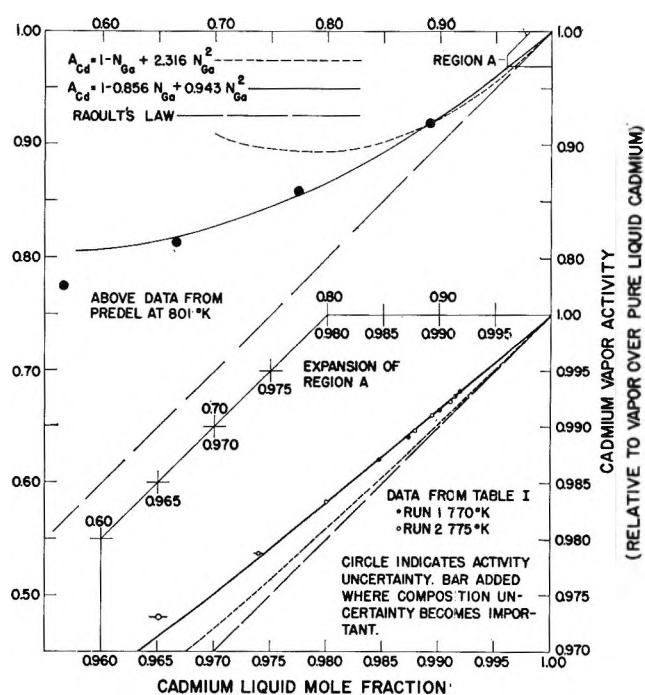


Figure 2. Vapor activities over gallium-cadmium solutions.

30,000; for run 2 the uncertainties are indicated in the figure. (3) A temperature bias correction (see Uncer-

tainties) has been applied to each of the measurements of the temperature difference, ΔT ; in run 1 the correction is 0.12°K.; in run 2, 0.07°K. The larger correction corresponds to about 1 part in 500 in the absolute vapor pressure or 3 cal. in the cadmium partial molal free energy. (4) The comparative temperature difference between the alloy and the pure cadmium, $\Delta(\Delta T)$, is reproducible to 0.01°K. or to 1 part in 5000 in the vapor pressure.

The first and third uncertainties displace the intercept but not the slope of the line describing the relationship between the cadmium activity and composition; only the second and fourth uncertainties are involved in the test of Raoult's law—the law predicts the *slope* of this activity–composition relationship while the intercept is set by the definition of activity.

Discussion of Results

Figure 2, expansion A, shows our data at about 773°K. and those of Predel⁸ at 801°K. In addition the solid curve

$$a_{\text{Cd}} = 1 - 0.856N_{\text{Ga}} + 0.943N_{\text{Ga}}^2 \quad (3)$$

and the dashed curve

$$a_{\text{Cd}} = 1 - N_{\text{Ga}} + 2.316N_{\text{Ga}}^2 \quad (4)$$

are plotted in both sections of the figure. The coefficient, 0.856, was established from our data in the range 0.008 to 0.026 mole fraction cadmium, but a slope close to that value is also required if the Predel data are to be fitted with an additional $b'N_{\text{B}}^2$ term.

Similarly with the b' term, 0.943, the value was established from the data of Predel, but it fits our data also. (An exception is made for the left-hand point in which the temperature controller had been functioning badly.) There appears to be a slightly greater curvature for our 775°K. data than for the curve tied to Predel's 801°K. measurements. The sharper curvature is consistent with the change of activity with temperature; each group of Predel's measurements shows the same general form, but at successively lower temperatures the departure from Raoult's law becomes slightly greater.

It may be noted that the coefficient, 2.316, fitted to Predel's data at 0.892 mole fraction cadmium fits only that single point. Normally it is expected that the b coefficient will lead to a fit of the data to perhaps 0.15 to 0.20 mole fraction of solute. No other Raoult's law based b can be made to fit our data, either. This statement includes an equation for the cadmium free energy partial which can be derived approximately from Kleppa's equation (in kjoules)

$$\Delta H^{\text{M}} = 14.8N_{\text{Ga}} - 25N_{\text{Ga}}^2 \quad (5)$$

for the mixing of gallium and cadmium at the cadmium-rich end. The discrepancy cannot be resolved by invoking gas nonideality because the effects of gas imperfection are almost totally cancelled¹⁰ in the activity calculation for the nearly pure solvent's vapor pressure.

Since Raoult's law has generally been considered to be a limiting law we must determine whether the gallium–cadmium data presented are in a concentration range which will effectively test the eq. 2 relationship. The data fitted by the equation cover a concentration range from about 0.75 to 0.992 mole fraction cadmium. Thus the average number of cadmium atoms separating gallium atoms ranges from about one in the more concentrated solutions to about five for the more dilute solution range. It would seem significant that eq. 2 describes the data in this region in which the degree of interaction could be expected to undergo the greatest change. It would seem most unlikely that a significant deviation could occur at a still greater dilution.

However, to evaluate effects at great dilution let us assume that the gallium activity coefficient for some unspecified cause should change even a millionfold on going from 0.00001 mole fraction to infinite dilution. Following the usual Duhem prediction, the cadmium activity would change by $\Delta \log \gamma_{\text{Cd}} \approx \frac{1}{2}(10^{-5})(6) = 0.00003$ or γ_{Cd} would shift from 1 to 1.00001. Then in the region where Henry's law was followed closely, the activity predicted for the solvent would follow a line almost paralleling Raoult's law but headed toward the point of zero cadmium activity and mole fraction. Thus the huge change assumed for the gallium behavior would cause only an experimentally indistinguishable deviation from the simple Raoult's law prediction! To correspond thermodynamically with eq. 2 behavior, the solute behavior would have to change violently and chemically unreasonably *in the region of composition measured*.

Reliability of These Results. The agreement of our data with those of Predel is excellent and both groups of workers have used isopiestic techniques which can establish thermodynamic partial molal free energies very accurately. For example, the isopiestic balance

(10) The Berthelot expression relating gas fugacity to actual and critical temperature and actual and critical pressures is

$$f \approx P + (9T_c P^2 / 128 T P_c) [1 - 6(T_c^2 T^2)]$$

For mercury¹¹ $T_c = 1733^\circ\text{K.}$ and $P_c = 1587 \text{ atm.}$ Using this equation and the mercury constants as an approximation to the cadmium behavior in our system at 0.974 mole fraction cadmium

$$f_{\text{Cd alloyed}} / f_{\text{Cd pure}} = 1.000001 (P_{\text{Cd alloyed}} / P_{\text{Cd pure}})$$

This correction is very small and is in the wrong direction to explain the experimental deviation from prediction.

(11) F. Birch, *Phys. Rev.*, **41**, 641 (1952).

measures vapor activities to 1 part in 5000 or the free energy partial to about ± 0.3 cal. The precision is comparable with that of the very finest e.m.f. work, and the vapor pressures are unequivocally and reproducibly related to the values for pure cadmium.^{11a}

The Activity Relationships in Dilute Solutions

It is possible to understand and, indeed, to anticipate the forms of the experimentally observed partial pressure relationships for solute and solvent in a dilute solution from the generally accepted view that such systems are composed of discrete molecules (or atoms) mixed essentially randomly and interacting with each other through short-range¹² forces. We will explore these relationships briefly. Special considerations peculiar to solutions of electrolytes will not be treated here.

The Solute. The partial pressures above a solution of B in A result, of course, from an equilibrium condition in which each component of the solution has an evaporation rate at the surface which is equal to its condensation rate. The evaporation rate may be looked on as depending on two primary factors: the concentration of the constituents at the surface and the various interactions between molecules of the constituents. The second factor, in simplified form, results from A-A, A-B, and B-B interactions which may be in the nature of bonding tendencies, repulsions, etc. The condensation rate depends on gas kinetics and on a gas condensation efficiency which approximates constancy in dilute solutions because the surface layer is composed predominantly of solvent (A) molecules.

The familiar Henry's law³

$$P_B/P_B^0 = k_B N_B \quad (6a)$$

relates the partial pressure and mole fraction of B, P_B and N_B , to the pure component vapor pressure, P_B^0 , by a unique constant, k_B , characteristic of the system under consideration. This law has experimental justification¹³ and has logical significance¹⁴ when it is realized that in sufficiently dilute solution each B molecule is surrounded by A molecules and is isolated from other B molecules essentially all of the time. Because all B molecules which evaporate must break from similar environments (*i.e.*, only A-B type interactions are involved), the rate of escape from the surface is a linear function of concentration. Since the rate of condensation is closely proportional to the vapor concentration, the pressure of B is correctly represented.

When the concentration of B is large enough to allow significant interaction between B molecules, a single constant, k_B , can no longer reflect the activity-mole fraction ratio. The probability that a given molecule

of B will have another B molecule as a near neighbor, and thus have its tendency to escape altered, may be described by κN_B where κ is the number of molecules in the shell around the B molecule where the interactions become significant. The fraction of the total molecules thus changed will be $(\kappa N_B)(N_B)$ and the fraction unchanged will be $(1 - \kappa N_B)(N_B)$. Therefore the Henry's law proportionality can now logically be expressed as the sum of two terms, one describing evaporation from a local environment comprised wholly of A molecules and the second involving the influence of another B molecule.

$$P_B/P_B^0 = k_B[(1 - \kappa N_B)(N_B)] + k_B''[(\kappa N_B)(N_B)] \quad (6b)$$

$$P_B/P_B^0 = k_B N_B + k_B' N_B^2 \quad (6c)$$

The Solvent. A suitable expression for a solution of B in A which relates the partial pressure of the solvent to concentration factors can be deduced in a manner entirely analogous to that described above for the solute. However, even in the most dilute solution, we must consider both A-A and A-B types of interaction. That A-A interactions are involved is obvious, and since

(11a) NOTE ADDED IN PROOF. A gross error in the ΔH of cadmium vaporization could also appear to be a deviation from Raoult's law. The equation from Kelley which we use is derived from $\Delta H_{v,298} = 26,754$ cal./mole. A value of 26,770 cal./mole is selected by R. Hultgren, R. L. Orr, P. D. Anderson, and K. K. Kelley in "Selected Values of Thermodynamic Properties of Metals and Alloys," John Wiley and Sons, Inc., New York, N. Y., 1963. A 150 cal./mole uncertainty corresponds to less than 3% of the deviation from Raoult's law which we find. Recent work by Conant, Elliott, and Lemons with solutions of cadmium containing small amounts of nickel shows a distinctly different slope for the activity vs. mole fraction curve from that obtained for gallium-cadmium solutions. An apparent deviation from Raoult's law due only to an error in ΔH would be expected to result in the same slope for the two systems in the Raoult's law region.

We are indebted to Paul C. Nordine for pointing out that the $\bar{V}dp$ terms for the effect of the different cadmium pressures upon the liquid were not discussed. These $\bar{V}dp$ corrections would be very small and in the wrong direction to explain the deviation.

(12) Short-range forces, as used here, means forces which are not significant at more than a few atoms distance. The argument is not altered, however, if longer range forces are considered so long as the forces attenuate to insignificance in some region. A dilute solution occurs when the force fields no longer overlap significantly. If thermodynamics is to have the extensive properties it requires for constant bulk properties, then the forces must be of shorter range than the smallest size specimen exhibiting the constant bulk property.

(13) Most vapor pressure measurements have been made on concentrations great enough so that a second term, as in eq. 6c, must be included to describe accurate work. In studies of the distribution of radioactive trace elements between two phases, the activity form of the relationship has received extensive justification. For example, separation plants for multigram amounts of plutonium were designed from studies at concentrations sometimes only 10^{-10} as large, plus the assumption of Henry's law.

(14) See, for example, the discussion in G. N. Lewis, M. Randall, K. S. Pitzer, and L. Brewer, "Thermodynamics," McGraw-Hill Book Co., Inc., New York, N. Y., 1961, p. 239. This reference reaches different conclusions from those which will be reached here, however.

every B molecule added has an influence on the A molecules surrounding it, this type of interaction must always be considered, too. Furthermore, it is obvious that if the solution is sufficiently dilute so that B-B interactions can be neglected, then each B molecule will influence an equal number of A molecules and the effect of the A-B type of interaction on the vapor pressure of A will be a linear function of the concentration of B. Similarly, if the sizes of B and A molecules are different, the volume fraction of A at the evaporating surface will be altered by an amount which in dilute solutions is a linear function of the concentration of B. In a very dilute solution the bulk of the A molecules are outside the sphere of influence of B molecules; consequently, their tendency to evaporate from solution will not differ from that in pure solvent. Therefore for a solution, the unit activity of the pure solvent, A, must be altered by the sum of a number of factors, *e.g.*, concentration, relative volume, and various A-B interactions, all of which are proportional to the concentration of B. These proportionality constants may be added to give a single constant k_A so that

$$P_A/P_A^0 = 1 - k_A N_B \quad (7)$$

The probability that a molecule of A already having a single molecule of B in its environment will have a second molecule of B as a near neighbor is again proportional to the concentration of B. The treatment is similar to, but more complex than, that described for the solute. Therefore when the concentration of B is sufficiently large a second term must be included which sums all of these possible effects due to two molecules of B influencing the environment of a single A molecule. The resulting equation can be reduced to eq. 2.

Although eq. 6c and 2 show an obvious similarity in form, the respective constants are different and would not be expected to bear a simple relationship to each other. They reflect related interactions, but the effect of the interactions on the evaporation processes is complex.

Raoult's Law. If the partial pressure of the solvent is to be predicted from the partial pressure of the solute, then the function relating them must take into account all types of interaction which affect the pressure, *i.e.*, A-A and A-B types of interaction for very dilute solutions. For the dilute solution region in which Henry's

law is observed to hold it is conventional to make use of the Gibbs-Duhem relationship in conjunction with Henry's law to arrive at the Raoult's law relationship¹⁵

$$P_A/P_A^0 = N_A \equiv 1 - N_B \quad (8)$$

In those concentration ranges in which B-B type interactions must be considered this equation can be modified in a manner already described to give eq. 1.¹⁵

However, the partial molal free energy as conventionally formulated and employed to arrive at eq. 7 suffers because it is unable to make use of the A-B type of interaction contained in Henry's law. This difficulty is most apparent when it is seen that for the usual derivation it is necessary to use the derivative of the partial molal free energy and that this derivative as formulated is independent of the Henry's law constant, which disappears from the relationship. Since this Henry's law constant is our only measure of A-B interaction and since A-B interactions are an essential factor in determining the partial pressure of A, we have lost a vital element in the relationship. This difficulty is further emphasized when the relationship is put in activity form¹⁵

$$(d \ln \gamma_A/dN_A) = -(N_B/N_A)(d \ln \gamma_B/dN_A) \quad (9)$$

Since in the Henry's law concentration region k_B is constant and equivalent to γ_B , eq. 9 requires that γ_A be invariant over the same concentration range. Thus eq. 8 and 9 require that the vapor pressure of the solvent be a function of concentration alone for every solution regardless of the size or chemical character of the actual chemical species present in the solution. Although the fact that the type of solvent molecule clearly influences the partial pressure of the solute as shown by Henry's law, these equations assert that these same A-B interactions are without effect on the partial pressure of the solvent. This has been shown to be contrary to fact for the gallium-cadmium system.

Acknowledgment. We wish to acknowledge contributions by Dr. Donald R. Conant to the views expressed in this paper. A more thorough presentation of these views will be given in a paper to be published shortly.¹⁶

(15) L. S. Darken and R. W. Gurry, "Physical Chemistry of Metals," McGraw-Hill Book Co., New York, N. Y., 1953, pp. 259-261 (also numerous other textbooks.)

(16) D. R. Conant, Los Alamos Scientific Laboratory Report, in preparation.

Two Phosphorescences and Electron Transfer in Dye-Disulfhydryl

Compound Complex

by Eiji Fujimori

Photobiology Section, Energetics Branch, Space Physics Laboratory, Air Force Cambridge Research Laboratories, Bedford, Massachusetts (Received October 1, 1964)

Mercaptoethanol and dimercaptopropanol form a complex with a cationic dye. Two dyes interacting with two SH groups in the complex with dimercaptopropanol exhibit two different absorptions and two different phosphorescences. Each one of them, present at a shorter wave length, corresponds to an absorption and a phosphorescence of the complex with mercaptoethanol. The dye-dimercaptopropanol complex is more photosensitive than the dye-mercaptoethanol complex. A phototropism observed in the former complex is based on an electron transfer.

Introduction

In previous studies,¹⁻³ phototropic behavior of various dye-sulfhydryl compound complexes was investigated. This phototropism was due to a photochemical reduction of the dye by sulfhydryl compounds in these complexes. Triplet formation of the conjugated dye molecule was shown to be enhanced and this enhancement of triplet state was considered to be induced by a charge-transfer process with the sulfur.

Considering characteristics of absorption, fluorescence, and phosphorescence of these complexes, the sulfhydryl compounds studied so far could be divided into two classes. The first one shows an absorption peak at 520 $m\mu$ with a considerable quenching of fluorescence. Proteins containing sulfhydryl group, sodium hydrosulfide, and glutathione belong to this class.² The second not only absorbs in a shorter wave length region than 520 $m\mu$ (showing two maxima in some cases), but also fluoresces. A phosphorescence also shifts to a shorter wave length. Thioglycolic acid and cysteine are assigned to the second group.³

A further investigation has been extended to a disulfhydryl compound and has led to a new complex which has characteristics of both the first and second type: two different phosphorescences and two different absorptions. A light-induced electron transfer related to the phototropism of this complex has also been studied.

Materials and Methods

The yellow dye (Figure 1), a derivative of 3',6'-dichlorofluoran, was prepared in the same method as reported previously.² Mercaptoethanol and dimercaptopropanol (California Corp. for Biochemical Research) were used without further purification.

All absorption spectra were determined on a Cary Model 14 spectrophotometer. In order to prevent the further oxidation of sulfhydryl compounds by air in an alkaline medium, a cell was filled with a solution immediately after mixing and closed with a stopper. Fluorescence, phosphorescence, and their action spectra were measured by means of an Aminco-Keirs spectrofluorimeter. For the determination of phosphorescence and its action spectra, solutions containing 50% glycerol were used at liquid nitrogen temperature. Photovoltaic changes were measured by a Kintel digital voltmeter, Model 456B, with readout Model 473A. The cell consisted of a platinum electrode with a saturated calomel electrode as reference. Nitrogen gas was passed through the solution. Electron spin resonance absorption was determined by a Varian V-4502 equipped with 100-kc. field modulation. Ir-

(1) E. Fujimori, *Bull. Chem. Soc. Japan*, **28**, 334 (1955).

(2) E. Fujimori, *Nature*, **201**, 1183 (1964).

(3) E. Fujimori, to be published.

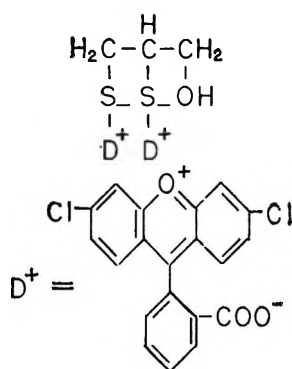
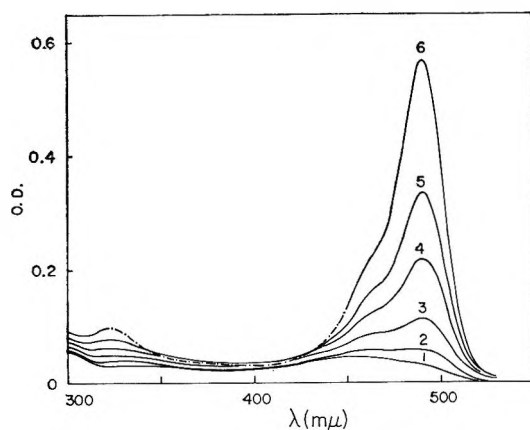


Figure 1. Dye-dimercaptopropanol complex.

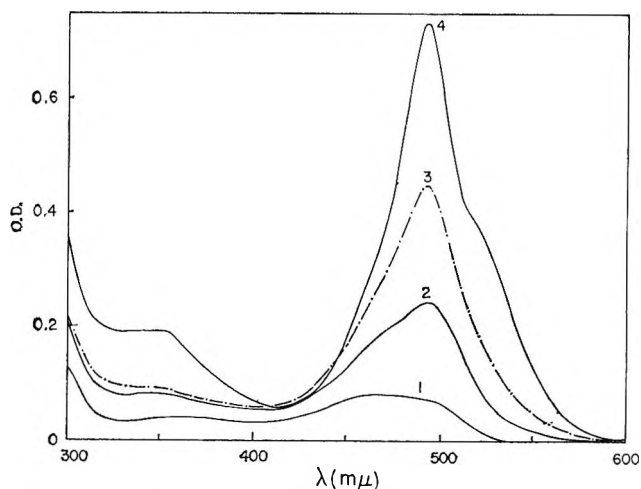
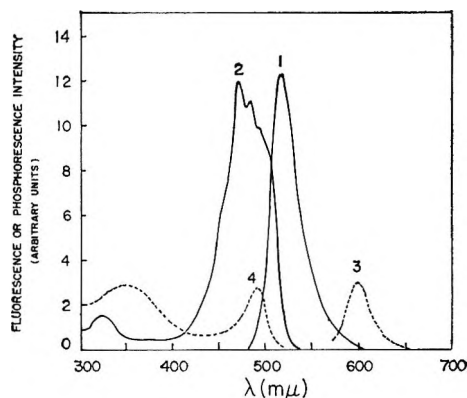
Figure 2. Formation of dye-mercaptoethanol complex followed by the change of absorption spectra; 0.1 *M* mercaptoethanol, 3.1×10^{-5} *M* dye, and 1 *N* NaOH: (1) 2 min. after mixing; (2) 1 hr.; (3) 2 hr.; (4) 4 hr.; (5) 6 hr.; (6) 24 hr.

radiation was made at a distance of 10 cm. by a 1-kw. tungsten projection lamp.

Results

The reaction of mercaptoethanol with the dye was followed by the change of absorption spectra with time. As illustrated in Figure 2, the complex between the dye and mercaptoethanol, $\text{CH}_2(\text{SD})-\text{CH}_2\text{OH}$, showed an absorption peak at $490 \text{ m}\mu$ with a shoulder at $465 \text{ m}\mu$. The complex between dimercaptopropanol and the dye, $\text{CH}_2(\text{SD})-\text{CH}(\text{SD})-\text{CH}_2\text{OH}$ (Figure 1) resulted in another shoulder at $520 \text{ m}\mu$ in addition to the absorption bands produced by the dye-mercaptoethanol complex (Figure 3).

Both complexes exhibit the same green fluorescence. Fluorescence spectra and action spectra for this fluorescence are shown in Figures 4 and 5. In the complex with mercaptoethanol, an excitation at $490 \text{ m}\mu$ caused the fluorescence band to appear at $515 \text{ m}\mu$ and a phosphorescence band at $600 \text{ m}\mu$ (1 and 3 in Figure 4). The same excitation at $490 \text{ m}\mu$ of the dimercapto-

Figure 3. Formation of dye-dimercaptopropanol complex followed by the change of absorption spectra; 0.1 *M* dimercaptopropanol, 2.5×10^{-4} *M* dye, and 1 *N* NaOH: (1) 20 min. after mixing; (2) 2 hr.; (3) 5 hr.; (4) 24 hr.Figure 4. Fluorescence, phosphorescence, and their action spectra of dye-mercaptoethanol complex; 0.1 *M* mercaptoethanol, 6.25×10^{-5} *M* dye, and 1 *N* NaOH: (1) fluorescence spectrum (excitation at $470 \text{ m}\mu$); (2) action spectrum (fluorescence at $515 \text{ m}\mu$); (3) phosphorescence spectrum (excitation at $490 \text{ m}\mu$); (4) action spectrum (phosphorescence at $600 \text{ m}\mu$).

propanol complex brought forth a new phosphorescence at $645 \text{ m}\mu$ as a shoulder, as well as the same fluorescence at $515 \text{ m}\mu$ and the phosphorescence at $600 \text{ m}\mu$ (1 and 3 in Figure 5). Exciting this complex at $520 \text{ m}\mu$ did give rise only to the phosphorescence at $645 \text{ m}\mu$ (5 in Figure 5). As is obvious from 4 and 6 in Figure 5, action spectra for these two phosphorescences at 600 and $650 \text{ m}\mu$ are clearly different, showing a peak at $490 \text{ m}\mu$ for the $600 \text{ m}\mu$ phosphorescence and a peak at $520 \text{ m}\mu$ for the $650 \text{ m}\mu$ phosphorescence. These peaks correspond to the main peak and its shoulder of the absorption spectrum (4 in Figure 3). These results

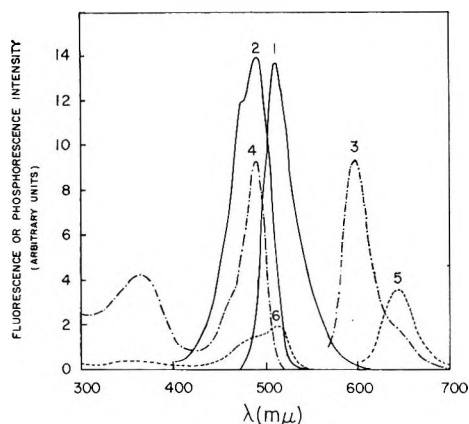


Figure 5. Fluorescence, phosphorescence, and their action spectra of dye-dimercaptopropanol complex: $0.1 M$ dimercaptopropanol, $2.5 \times 10^{-6} M$ dye and $1 N$ NaOH: (1) fluorescence spectrum (excitation at $490 m\mu$); (2) action spectrum (fluorescence at $510 m\mu$); (3) phosphorescence spectrum (excitation at $490 m\mu$); (4) action spectrum (phosphorescence at $600 m\mu$); (5) phosphorescence spectrum (excitation at $520 m\mu$); (6) action spectrum (phosphorescence at $650 m\mu$).

prove the existence of two separate species which can absorb and phosphoresce at two different wave lengths.

The dye-mercaptoethanol complex showed no noticeable photobleaching when irradiated with light, while the dye-dimercaptopropanol complex bleached in light and regenerated rapidly within a few minutes in darkness. The regeneration reaction after 10 min. of irradiation is apparent in the change of optical density at $490 m\mu$ (see Figure 6). A photo-induced electron spin resonance absorption similar to that found in complexes with other sulfhydryl compounds^{2,3} was also detected. The decay of this light-induced electron spin resonance signal in darkness can also be seen in Figure 6. A negative change of the oxidation-reduction potential was greater in the dimercaptopropanol complex than in the mercaptoethanol complex (Figure 7). This could be expected since the former complex was noticeably photobleached, thus producing the electron spin resonance signal. A recovery of the oxidation-reduction potential in darkness was as quick as the regeneration of a photobleached state and the decay of the electron spin resonance.

Discussion

The complex of the dye with mercaptoethanol containing hydroxy group as a substituent absorbs, fluoresces, and phosphoresces at the shortest wave length among complexes studied so far. Other sulfhydryl compounds, containing carboxyl group or amino group, form complexes which have a main absorption in the range $495\text{--}505 m\mu$, fluorescence in the

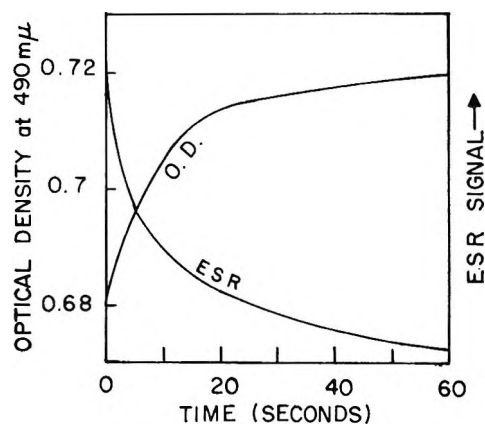


Figure 6. Change of optical density and electron spin resonance in darkness of irradiated dye-dimercaptopropanol complex; $0.1 M$ dimercaptopropanol, $2.5 \times 10^{-6} M$ dye, and $1 N$ NaOH.

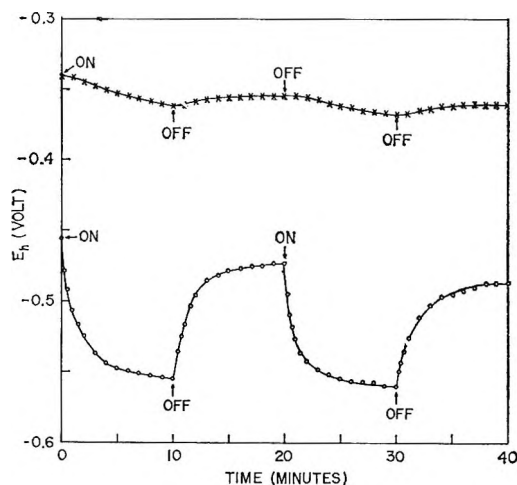


Figure 7. Photovoltaic change of the complexes: \times , $0.1 M$ mercaptoethanol, $5 \times 10^{-6} M$ dye, and $1 N$ NaOH; \circ , $0.1 M$ dimercaptopropanol, $10^{-4} M$ dye, and $1 N$ NaOH.

range $530\text{--}535 m\mu$, and phosphorescence at $615\text{--}620 m\mu$. A complex with sulfhydryl proteins absorbs at $520 m\mu$ and phosphoresces at $650 m\mu$. Such a variety of spectral characteristics is known in charge-transfer complexes between the same electron acceptor and a number of electron donors. This charge-transfer interaction possibly induces the formation of triplet state, which gives a triplet emission, phosphorescence. The complex with dimercaptopropanol exhibits not only the same absorption, fluorescence, and phosphorescence as in the one with mercaptoethanol, but also another series of absorption and phosphorescence which is similar to those found in the complex with proteins and sodium hydrosulfide. These two different absorptions and phosphorescences possibly originate from two separate dye molecules: one interacting with a sulfur at a middle carbon and

the other associating with another sulfur at a terminal carbon. It should be pointed out that energy transfer would be possible from the middle dye molecule fluorescing at 510 $m\mu$ to the terminal dye molecule absorbing at 520 $m\mu$.

Less photosensitivity is found in the mercapto-ethanol complex than in the dimercaptopropanol complex. The phototropism is related to a light-induced electron transfer which is evidenced by the change of photovoltaic effect and electron spin resonance absorption. This indicates that the two sulfurs

interacting with the same dye molecules differ in the capability of charge transfer. The fact that the same conjugated molecules associating with sulfhydryl groups in a different environment show different spectral and photochemical characteristics would be significant for the function of SH groups in energetics of biological systems.

Acknowledgments. The author wishes to thank Miss Maria Tavla and Mrs. Frances Pearlmutter for their valuable assistance.

The Photochemistry of Methyl Isopropyl Ketone^{1a}

by A. Zahra and W. Albert Noyes, Jr.^{1b}

Department of Chemistry, The University of Rochester, Rochester, New York (Received October 2, 1964)

The photochemistry of methyl isopropyl ketone (3-methyl-2-butanone) is contrasted with that of 2-pentanone since the former, as distinguished from the latter, may not undergo a Norrish Type II reaction. The main reactions are those one would expect from photochemical dissociation into radicals but there is also almost certainly some direct dissociation into acetaldehyde and propylene by a process designated by Norrish as Type III. By the addition of oxygen and of biacetyl it is possible to show that a triplet state as well as a singlet state must be considered in any detailed mechanism of the photochemistry of this ketone. Some suggestions are made as to the role each one plays. Analyses were performed for carbon monoxide, methane, ethane, propylene, and propane. The propylene always exceeds the propane so that these two gases are not formed solely by disproportionation of isopropyl radicals.

The photochemistry of simple ketones leads to a dissociation into radicals² and the over-all yields may be discussed in terms of the reactions of the radicals formed in primary and in secondary processes. However when one of the groups attached to the carbonyl group has γ carbon atoms with attached hydrogen atoms there may be another type of reaction which is nonfree-radical in character and which leads directly to the formation of a methyl ketone and an olefin. This type of reaction was first discovered by Norrish and Appleyard³ and it has become known as a Norrish Type II reaction. It was suggested⁴ that a six-membered ring formed by internal hydrogen bonding might permit the parent molecule to dissociate directly into acetone and the olefin. Strong evidence that this is

bered ring formed by internal hydrogen bonding might permit the parent molecule to dissociate directly into acetone and the olefin. Strong evidence that this is

(1) (a) This work was supported in part by a grant from the Office of Aerospace Research, Office of Scientific Research, U. S. Air Force. A. Z. is also indebted to the American Friends of the Middle East, Inc., and to the Mission Department, United Arab Republic, through the U.A.R. Education Bureau in Washington, D. C. for fellowships. (b) To whom inquiries should be addressed at: Department of Chemistry, University of Texas, Austin, Texas.

(2) For a review, see W. A. Noyes, Jr., G. B. Porter, and J. E. Jolley, *Chem. Rev.*, **56**, 49 (1956).

(3) R. G. W. Norrish and M. E. S. Appleyard, *J. Chem. Soc.*, 874 (1934).

indeed the mechanism has been obtained.^{5,6} The enol form of acetone may exchange with water adsorbed on the walls so that care must be used in interpreting results with deuterium-labeled 2-pentanone or 2-hexanone.⁵

The present work was undertaken because 3-methyl-2-butanone, which is isomeric with 2-pentanone, does not have a γ carbon atom and hence can not give a Norrish Type II reaction if the above hypothesis is correct. On the other hand a Norrish Type III reaction to give acetaldehyde and propylene is possible. This may occur *via* a four-membered ring formed by hydrogen bonding between the carbonyl carbon and the β -carbon.

Experimental

The 3-methyl-2-butanone was obtained from Matheson Coleman and Bell. It was fractionated on a spinning band column, further purified by vapor phase chromatography, and collected over Drierite. Final distillation into the apparatus completed the purification. Mass spectrographs showed less than 0.3% impurity.

Purification of other chemicals used has been often described in publications from this laboratory.

An Osram HBO 500 lamp was used at 3130 and at 4358 Å. A Hanovia s-100 lamp was used for 2537 Å. For 3130 Å. the filter described by Kasha⁷ was used. For 2537 Å. the beam passed through a nickel sulfate-cobalt sulfate filter, 11.5 cm. of chlorine gas at 1 atm. pressure, and a Corning 9863 filter. This combination passed 2654- as well as 2537-Å. radiation. For 4358 Å. a combination of Corning filters No. 3391 and 5113 was used.

The light transmitted by the cell was measured by a RCA 935 phototube. Emitted light either from the ketone or from biacetyl when the latter was present was measured by a 1P21 photomultiplier tube. A Corning No. 7380 filter which transmits only wave lengths longer than 3400 Å. was placed between the cell and the 1P21 tube when emission from 3-methyl-2-butanone was to be studied. This filter transmitted light emitted by this ketone but did not transmit scattered incident radiation. Emission from biacetyl was also measured by the 1P21 tube protected by a Corning No. 3384 filter which transmits only radiation of wave length greater than 5000 Å. Triplet state emission from biacetyl lies only in this part of the spectrum.

The products were fractionated by procedures which have been described in earlier articles. Solid nitrogen (about -210°) permitted only methane and carbon monoxide to pass. Carbon monoxide was converted

to carbon dioxide over copper oxide and the carbon dioxide was condensed and separated from the methane.

A second fraction was distilled at -160° and contained ethane along with traces of propane and of propylene. A third fraction was distilled off at -130° and contained the propane and propylene. These two fractions were examined by the mass spectrograph and a Perkin-Elmer vapor fractometer. A 4-m. column packed with tetraisobutylene on Chromosorb W was used. This column separated the propylene from the propane and the other products.

The remaining products, including acetaldehyde, acetone, 2,3-dimethylbutane, biacetyl, and the parent compound were analyzed by the vapor fractometer using a 4-m. column packed with diisodecyl phthalate on an inert support.

Results

Tests of Beer's law for the 3-methyl-2-butanone were made both at 3130 and at 2537 Å. Since in neither case was the incident radiation monochromatic according to a rigorous definition of that term, one would expect the apparent extinction coefficient to decrease as the pressure (or concentration) of the ketone increases. This is indeed the case at both wave lengths and at 27 as well as at 62° . Since the values will vary from lamp to lamp and from one filter combination to another, they have no permanent value and will not be reproduced in detail. At 3130 Å. at 27° the molar extinction coefficient (l. mole⁻¹ cm.⁻¹) decreased from 9.8 at 2 mm. to a more or less constant value of 3.35 ± 0.06 at pressures of 20 mm. or more. At 3130 Å. at 62° the change was from about 16 to a more or less constant value of 5.1 ± 0.1 l. mole⁻¹ cm.⁻¹. At 2537 Å., as would be expected, the change with pressure is less marked; at low pressures the value is about 12 and at pressures over 20 mm. it is 9.5 ± 0.2 l. mole⁻¹ cm.⁻¹.

The methods of determining absolute emission yields from pure 3-methyl-2-butanone and the sensitized biacetyl emission from mixtures of biacetyl with the ketone have already been described.⁸ They are based on 0.15 ± 0.03 as the absolute emission yield from biacetyl when excited at 4358 Å. as reported by Almy and Gillette.⁹ Absorption by biacetyl is small at 3130 but may not be neglected at 2537 Å.

(4) W. Davis, Jr., and W. A. Noyes, Jr., *J. Am. Chem. Soc.*, **69**, 2158 (1947).

(5) R. Srinivasan, *ibid.*, **81**, 5061 (1959).

(6) G. R. McMillan, J. G. Calvert, and J. N. Pitts, Jr., *ibid.*, **86**, 3602 (1964).

(7) M. Kasha, *J. Opt. Soc. Am.*, **38**, 929 (1948).

(8) H. Ishikawa and W. A. Noyes, Jr., *J. Chem. Phys.*, **37**, 583 (1962).

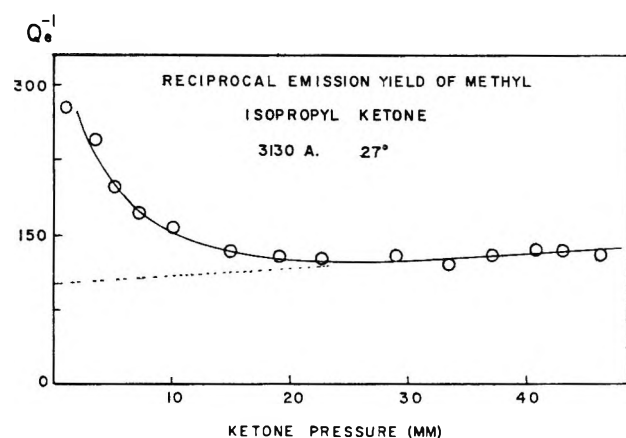


Figure 1. Inverse of the efficiency of emission of 3-methyl-2-butanone as a function of pressure at 27°.

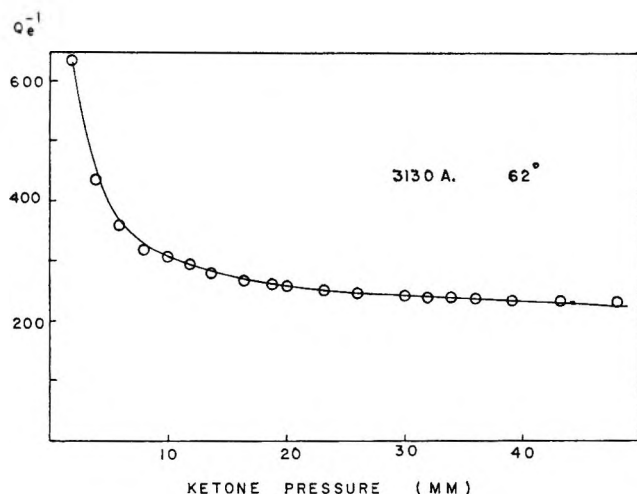


Figure 2. Inverse of efficiency of emission of 3-methyl-2-butanone as a function of pressure at 62°

Emission from 3-methyl-2-butanone is very small and probably is zero when excited at 2537 Å. This ketone resembles other simple ketones in this respect.² Figures 1 and 2 show plots of Q_e^{-1} vs. ketone pressure for the pure ketone excited at 3130 Å. at 27° and at 62°, respectively. The decrease of Q_e^{-1} (where Q_e is the absolute emission efficiency from the pure ketone) with increase in pressure is similar to that found in biacetyl at 3650^{9,10} and in acetone at 3130 Å.^{11,12} The accepted explanation is that sufficiently excited molecules may dissociate but that if they lose vibrational energy by collision they may be "saved" for emission. 3-Methyl-2-pentanone probably follows the same pattern. The presence of a minimum in Figure 1 indicates some self-quenching for those molecules whose vibrational energy has become equilibrated with the surroundings.

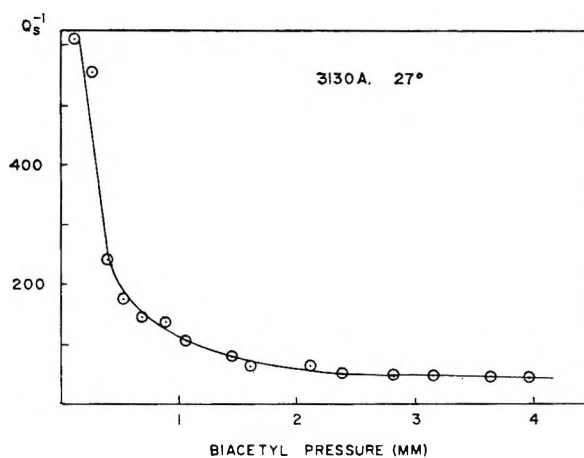


Figure 3. Inverse of efficiency of sensitized biacetyl emission in mixtures of biacetyl and 3-methyl-2-butanone at 27°.

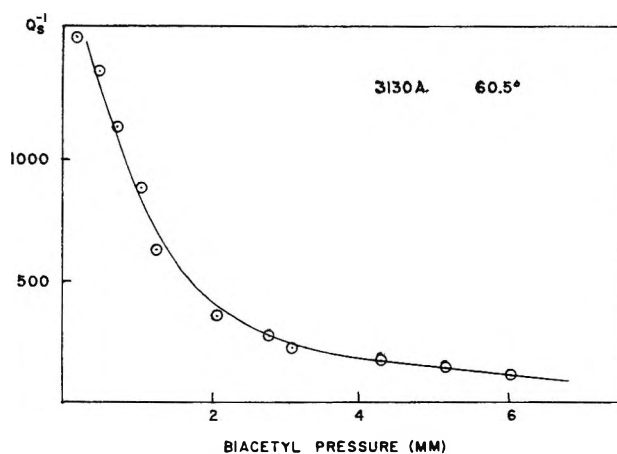


Figure 4. Inverse of the sensitized emission efficiency of biacetyl in mixtures of biacetyl and 3-methyl-2-butanone at 60.5°.

Yields of the sensitized emission of biacetyl excited by energy transfer from 3-methyl-2-pentanone are shown in Figures 3 and 4 where Q_s^{-1} is plotted against biacetyl pressure at 27° and at 60.5°, respectively. Figure 5 shows plots of $(B)/Q_s$ vs. biacetyl pressure. These plots will be discussed in the appropriate section. (Q_s is the sensitized emission yield and (B) is the concentration of biacetyl, replaced in this case by the pressure in millimeters.)

Yields of the various products per quantum absorbed are shown in Tables I and II.¹³

(9) G. M. Almy and P. R. Gillette, *J. Chem. Phys.*, **11**, 188 (1943).

(10) F. C. Henriques, Jr., and W. A. Noyes, Jr., *J. Am. Chem. Soc.*, **62**, 1038 (1940).

(11) J. Hecklen and W. A. Noyes, Jr., *ibid.*, **81**, 3858 (1959).

(12) J. Hecklen, *ibid.*, **81**, 3863 (1959).

(13) For more complete data the Ph.D. Dissertation of A. Zahra University of Rochester, 1964, should be consulted.

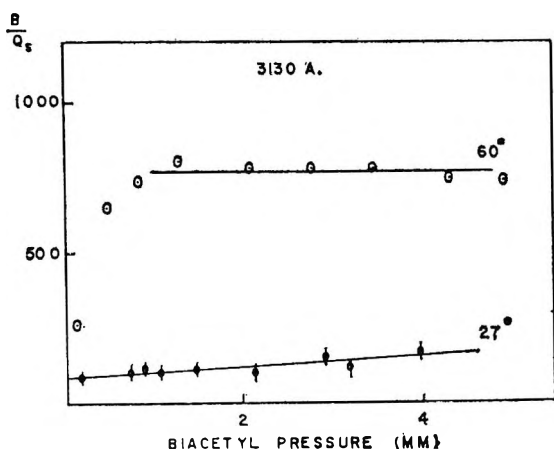


Figure 5. Plots of ratio of biacetyl pressure (mm.) divided by sensitized efficiency of emission of biacetyl as a function of biacetyl pressure.

Table I: Quantum Yields of Products from 3-Methyl-2-butanone^a

	3130 Å., at 27°					
	Pressure (mm.)					
	5.5	11.0	13.0	22.5	30.0	41.8
	Quanta (ml. ⁻¹ sec. ⁻¹ × 10 ⁻¹²)					
	3.6	4.7	5.2	7.8	10.2	13.6
	Quantum yields					
CO	0.045	0.039	0.027	0.030	0.031	0.037
CH ₄	0.009	0.004	0.005	0.002	0.001	0.001
C ₂ H ₆	0.072	0.058	0.02	0.011	0.011	b
C ₃ H ₈	0.153	0.14	0.13	0.10	0.10	0.11
C ₃ H ₈	0.11	0.10	0.076	0.069	0.069	0.074
<i>i</i> -C ₄ H ₁₀	0.076	0.027	0.018	0.012	0.012	b
C ₆ H ₁₄	0.10	0.09	0.06	0.048	0.047	0.059
(CH ₃) ₂ CO	0.041	0.028	0.016	0.018	0.013	0.016
(CH ₃ CO) ₂	0.052	b	0.065	0.052	0.053	0.064
CH ₃ CHO	b	0.01	0.01	0.005	b	0.01

	3130 Å., at 60–62°				
	Pressure (mm.)				
	5.5	10.9	15.5	26.5	51.5
	Quanta (ml. ⁻¹ sec. ⁻¹ × 10 ⁻¹²)				
	4.0	6.0	7.7	11.8	21
	Quantum yields				
CO	0.25	0.23	0.22	0.23	0.22
CH ₄	0.03	0.040	0.049	0.020	0.014
C ₂ H ₆	0.11	0.035	0.034	0.025	0.020
C ₃ H ₈	0.35	0.22	0.23	0.22	0.22
C ₃ H ₈	0.32	0.20	0.20	0.21	b
<i>i</i> -C ₄ H ₁₀	b	0.23	0.24	0.26	b
C ₆ H ₁₄	0.63	0.50	0.25	0.26	b
(CH ₃) ₂ CO	0.021	0.019	0.018	0.026	b
(CH ₃ CO) ₂	0.018	0.017	0.017	0.017	b
CH ₃ CHO	0.020	0.018	b	b	b

^a The acetaldehyde yields are the least accurate of those measured. C₆H₁₄ is 2,3-dimethylbutane. ^b Not measured.

Table II: Quantum Yields of Products from 3-Methyl-2-butanone^a

Product	2537 Å.		
	Temp., °C.		
	27	60	127
CO	0.1180	0.345	0.780
CH ₄	0.0180	0.091	0.210
C ₂ H ₆	0.0197	0.050	0.070
C ₃ H ₈	0.1100	0.467	0.560
C ₃ H ₈	0.0920	0.386	0.480
(C ₃ H ₈ + C ₃ H ₈)	0.2000	0.853	1.050
<i>i</i> -C ₄ H ₁₀	0.0570	0.067	0.190
C ₆ H ₁₄	0.2250	0.243	
CH ₃ CHO	b	0.390	0.330
CH ₃ COCH ₃	0.0140	0.0157	
(CH ₃ CO) ₂	0.0220	Trace	None

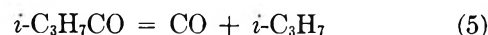
^a Ketone pressure of 22 ± 0.5 mm. ^b Not measured.

Discussion

The following primary dissociations may be visualized. Reaction 3 is the Norrish Type III process;



i-C₃H₇ is the isopropyl group or radical. The activation energy for the dissociation of COCH₃ is a matter of some debate but undoubtedly it is higher than that for the radical *i*-C₃H₇CO. Processes 1 and 2 would be followed by 4 and 5.



By analogy with 2-butanone (methyl ethyl ketone), reaction 1 should predominate over 2^{2,14,15} and the disparity should be most evident at 3130 Å. At high intensities radical-radical reactions may compete with 4 and 5. It should be noted that the quantum yield of carbon monoxide formation from 3-pentanone at 3130 Å. is much higher than either from acetone or from 2-butanone at room temperature.^{2,16} The present work shows 3-methyl-2-butanone to be more like acetone and 2-butanone than it is like 3-pentanone. Thus reaction 1 seems to be more important than 2 at all wave lengths. As the temperature is raised the

(14) V. R. Ells and W. A. Noyes, Jr., *J. Am. Chem. Soc.*, **60**, 2031 (1938).

(15) J. N. Pitts and F. E. Blacet, *ibid.*, **72**, 2810 (1950).

(16) D. S. Weir, *ibid.*, **83**, 2629 (1961).

number of C_3H_7 's in products per photon absorbed exceeds unity. Chains must be important even at low temperatures. Material balance is only fair as shown in Table III.

Table III: Number of Groups in Products

Group	Pressure, mm.		
	5.5	20-40	26
	Wave length, Å.		
	3130	3130	2537
$i-C_3H_7$	0.5 ^a	0.3 ^a	0.7 ^a
CH_3	0.6 ^a	0.2 ^a	0.6 ^a
$i-C_3H_7$	2.2 ^b	1.2 ^b	1.4 ^b
CH_3	0.6 ^b	0.5 ^b	0.8 ^b
$i-C_3H_7$			1.7 ^b
CH_3			1.3 ^b

^a At 27°. ^b At 60°.

Table IV: Effect of Oxygen on the Emission Yield of 3-Methyl-2-butanone^a

Oxygen pressure (mm.)	Emission yield ($Q_e \times 10^2$) ^b	$1/Q_e$ ^b
0.000	0.885	112.7
0.030	0.778	128.5
0.046	0.756	132.2
0.081	0.734	136.2
0.100	0.721	138.7
0.140	0.700	142.8

^a Incident wave length 3130 Å., 27°, and 3-methyl-2-butanone pressure of 26 ± 0.5 mm. ^b Q_e is the absolute emission yield of 3-methyl-2-butanone.

It has been observed empirically by Trotman-Dickenson¹⁷ that when two radicals R_1 and R_2 react to give R_1R_1 , R_2R_2 , and R_1R_2 , respectively, the relationship of eq. 6 is closely obeyed. This relationship is

$$\frac{(R_1R_2)^2}{(R_1R_1)(R_2R_2)} = 4 \quad (6)$$

not even approximately obeyed for C_2H_6 , C_6H_{14} , and C_4H_{10} by the data in Tables I and II. On the other hand, if one assumes an error in the determination of C_6H_{14} (which is logical from the nature of the methods used) and calculates C_6H_{14} from eq. 6, the material balances for CH_3 and C_3H_7 agree quite satisfactorily at room temperature. This is not true at higher temperatures. Products other than those determined must be formed and these increase in importance as the temperature increases.

The primary yield should not be less than the carbon monoxide yield. If carbon monoxide is formed in a chain step or if RCO radicals combine with other radicals either to give the parent ketone or other products, the calculation of the primary yield could only be based on unproved assumptions. The primary yield at 3130 Å. at 27° probably is about 0.5 at room temperature. Chains are apparently negligible at room temperature and become more important as the temperature is increased. The primary yield at 2537 Å. is higher than at 3130 Å. but is somewhat below unity. Little more can be said about the magnitude of the primary yield.

A few remarks may be made about the Norrish Type III process. Hydrogen abstraction by CH_3CO does not compete with dissociation but disproportionation reactions might give some acetaldehyde. That such reactions are negligible is indicated by the low acetaldehyde yield at 3130 Å.

The quantum yield of acetaldehyde is probably a rough measure of the extent of the Norrish Type III reaction. This type of reaction must be of negligible importance at 3130 Å. but has a yield of about 0.3, subject to considerable experimental error, at 2537 Å. This trend with wave length is found in other connections.^{18,19}

A few remarks about the natures of the excited states may be made. The simple ketones either do not form triplet states after absorption at 2537 Å. or the triplet states once formed dissociate with extreme rapidity. Emission by 3-methyl-2-pentanone when excited at 2537 Å. is negligible, thus indicating that molecules excited at this wave length do not emit either from the singlet or from the triplet state.

It has been shown by Michael²⁰ for 2-pentanone that the state which transfers energy to biacetyl to cause sensitized emission is the same as the one which leads to the Norrish Type II reaction. There is no emission from 3-methyl-2-butanone at 2537 Å. and there is no Norrish Type III reaction at 3130 Å. Thus a similar comparison may not be made between slope/intercept for Figure 5 and slope/intercept for a plot of $1/\Phi$ vs. P .²⁰

At 3130 Å. at room temperature the estimated primary quantum yield decreases as pressure increases

(17) A. F. Trotman-Dickenson, *Ann. Rept. Progr. Chem.* (Chem. Soc. London), **55**, 36 (1958).

(18) R. Srinivasan, *J. Am. Chem. Soc.*, **81**, 1546 (1959); **83**, 4344, 4348 (1961).

(19) P. Ausloos and R. E. Rebert [ibid., **83**, 4897 (1961)] give evidence that increase in incident frequency causes an increase in yields of somewhat similar type processes.

(20) J. L. Michael and W. A. Noyes, Jr., *ibid.*, **85**, 1027 (1963).

to a pressure of about 20 mm. and may then only slowly increase. At the same time the emission yield increases and passes through a maximum at about 20 mm. Thereafter a plot of Q_e^{-1} vs. P shows a reasonably straight line with a small slope. Thus loss of vibration energy not only decreases the dissociation yield but increases the emission yield. This same phenomenon is observed for several other ketones.²

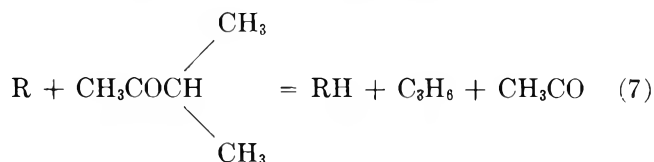
For many complex molecules, including ketones and aldehydes, the sum of the primary dissociation yield and the emission yield is well below unity. The mechanism of energy dissipation may in some instances be through the formation of unstable isomers. Such a step was suggested for biacetyl by Yang²¹ and there is some evidence for such a proposal.²² For 3-methyl-2-butanone intermediates which could lead to the Norrish Type III reaction or perhaps to an unsaturated alcohol might provide a way of ultimate degradation of energy without assuming conversion of electronic energy to large amounts of vibration energy.

A plot of Q_e^{-1} vs. oxygen pressure (Table IV) does not give a straight line, thus indicating that more than one excited state exists.

From the high pressure straight line in Figure 1 and by assuming the decay constant for fluorescent emission to be about 10^6 sec.^{-1} (as it should be for a singlet state) one can show the effective cross section for quenching to be about 10 \AA.^{1b} . This is unreasonably large. On the other hand if a mean life of about 10^{-4} sec. is assumed, as it should be for a triplet state, the effective cross section for quenching would have the reasonable value of 0.1 \AA.^{1b} .

Thus from the effect of oxygen and from other considerations it is concluded that both singlet and triplet states participate in the primary process. A detailed description of mechanism may not be given.

A few remarks may be made about secondary reactions. Chain steps become of importance at relatively low temperatures. Since propylene always exceeds propane in the products, these gases are not formed solely by disproportionation of isopropyl radicals. Propylene could be formed by a reaction similar to one previously suggested for isopropyl iodide.²³ Other steps could also be suggested but no



proof for them can be offered. The relatively low yield of carbon monoxide indicates that RCO radicals in this system react relatively rapidly with the substrate and that carbon monoxide is not a principal product of chain-propagating steps.

Since secondary reactions lead to products other than those determined, particularly as the temperature is raised, further speculation about secondary steps is not warranted.

Acknowledgment. The authors wish to express their appreciation to Professor G. R. McMillan of Western Reserve University and to Professor R. K. Brinton of the University of California, Davis, for helpful suggestions. A. Z. also wishes to thank Dr. Paul Sigal and Dr. J. A. Poole for very helpful discussions during this work.

(21) See W. A. Noyes, Jr., W. A. Mulac, and M. S. Matheson, *J. Chem. Phys.*, **36**, 880 (1962).

(22) D. S. Weir, *ibid.*, **36**, 1113 (1962).

(23) G. R. McMillan and W. A. Noyes, Jr., *J. Am. Chem. Soc.*, **80**, 2108 (1958).

Nuclear Quadrupole Resonance of Bi^{209} in BiBr_3 ¹

by Elizabeth D. Swiger,² Paul J. Green, Gary L. McKown, and Jack D. Graybeal

Department of Chemistry, West Virginia University, Morgantown, West Virginia (Received October 2, 1964)

An investigation of the nuclear quadrupole coupling of the Bi^{209} nucleus in solid BiBr_3 was undertaken in order to determine if the crystal structure was related to that of either BiCl_3 or BiI_3 . A 50-g. sample of anhydrous BiBr_3 , prepared by the direct reaction of Bi and Br_2 , was investigated between 20 and 40 Mc./sec. using a super-regenerative spectrometer. Three of the four allowed transitions of the Bi^{209} nucleus were measured. By plotting calculated frequency ratios *vs.* asymmetry parameters and by plotting relative frequency factors *vs.* asymmetry parameters, the experimental values for the asymmetry parameter and the nuclear quadrupole coupling constant of the Bi^{209} nucleus were determined to be 0.553 and 340.5 Mc./sec., respectively. The large value of the asymmetry parameter indicates considerable cross bonding among the BiBr_3 molecules in the solid.

Introduction

Since the crystal structure of BiBr_3 has not been determined, nuclear quadrupole resonance spectroscopy is being used to determine if the structure of solid BiBr_3 is more closely related to that of BiCl_3 ,³ which is also undetermined, or to that of BiI_3 ,⁴ known to crystallize with the I atoms in a hexagonal close-packed arrangement and the Bi atoms in the octahedral holes. This work presents an interpretation based only on the Bi^{209} nuclear quadrupole coupling constant. Further discussions of the structure can follow the determination of the Br nuclear quadrupole coupling constants.

Experimental

Anhydrous BiBr_3 was prepared by a modification of the method of Pattison-Muir.⁵ Bismuth metal, 110 g., screened to a size of 1–3 mm., was placed in a single-necked round-bottomed flask fitted with a reflux condenser. A stoichiometric amount, 120 g., of Br_2 was added and the reaction mixture refluxed for 72 hr. During the refluxing a deposit of yellow crystals of BiBr_3 accumulated in the upper parts of the system. The unreacted Br_2 was removed by treating the reaction mixture with CCl_4 and decanting. The BiBr_3 was separated from unreacted Bi by stirring the mixture into suspension in CCl_4 and rapidly decanting, leaving the heavy Bi metal behind. After drying *in vacuo*, 110 g. of BiBr_3 was obtained. Duplicate analyses gave 53.52 and 53.55% Br (theory, 53.44% Br). A 50-g. sample was sealed in a glass vial for studies.

An externally-quenched super-regenerative spectrometer, similar to one described in the literature,⁶ was used to observe the resonance absorption lines. A 90-cycle on-off square-wave Zeeman-modulation magnetic field and phase-sensitive detection were used for searching. Measurements were made at room temperature. The identification of the side-band or main frequency component being absorbed and the measurement of frequencies followed the method given by Graybeal and Cornwell⁶ except that a Hewlett-Packard 524C frequency counter was used.

Results

Three transitions were observed with a fourth expected to fall above the operating range of the spectrometer. All of the transitions were broad, of the order of 30–40 kc./sec. The appearance of the spectrum was that of a single resonance, indicating that all Bi sites in the unit cell are equivalent.

The identification of³ transitions and the calculation of the asymmetry parameter, η , for the Bi^{209} nucleus

(1) This research was supported by Research Grant G-21048 from the National Science Foundation.

(2) National Science Foundation Predoctoral Fellow. 1963–1964.

(3) H. G. Robinson, *Phys. Rev.*, **100**, 1731 (1955).

(4) R. W. G. Wyckoff, "Crystal Structures," Vol. II, Interscience Publishers, Inc., New York, N. Y., 1960, Chapter V, p. 12.

(5) M. M. Pattison-Muir, *J. Chem. Soc.*, **29**, 144 (1876).

(6) J. D. Graybeal and C. D. Cornwell, *J. Phys. Chem.*, **62**, 483 (1958).

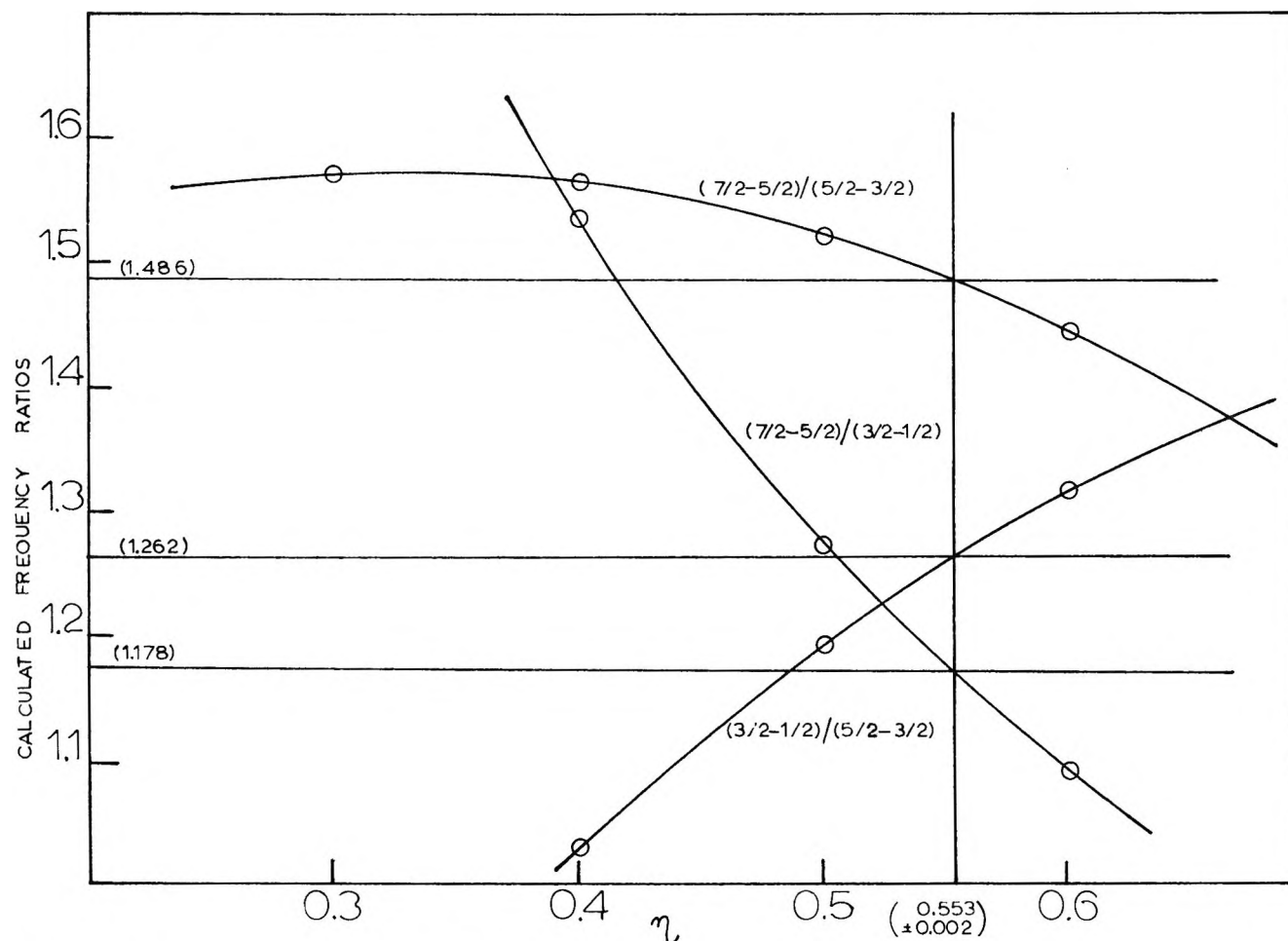


Figure 1. Determination of η and line assignments.

were made by using frequency ratios and relative frequency factors calculated from the energies as functions of the asymmetry parameter. For the Bi^{209} nucleus, having a nuclear spin $I = 9/2$, the secular equation from which the energy levels, as a function of η , can be found is

$$E^5 - 11(3 - \eta^2)E^3 - 44(1 - \eta^2)E^2 + \frac{44}{3}(3 + \eta^2)^2E + 48(3 + \eta^2)(1 - \eta^2) = 0$$

where E is in units of $6e^2Qq/4I(2I - 1)$. By using the solutions of this equation, for values of η from 0 to 1 in intervals of 0.1,⁷ one can plot the calculated frequency ratios, for the allowed $\Delta m = 1$ transitions, as a function of η and, from the intercepts of these curves with the values for the observed frequency ratios, calculate the value of η . Since a single value of η gives rise to a unique set of frequency ratios the measured frequency ratios should intercept the calculated curves in a vertical line corresponding to the experimental value of η . Figure 1 shows an enlarged

section of such a plot. The accuracy of the determination of η is limited by this graphical solution.

While perturbation methods have also been applied for direct solution of the secular equation,⁸ such methods are limited to small values of η and this is not the case for BiBr_3 . The nonapplicability of such methods is further demonstrated by the strong observed dependency of the calculated frequency ratios on η .

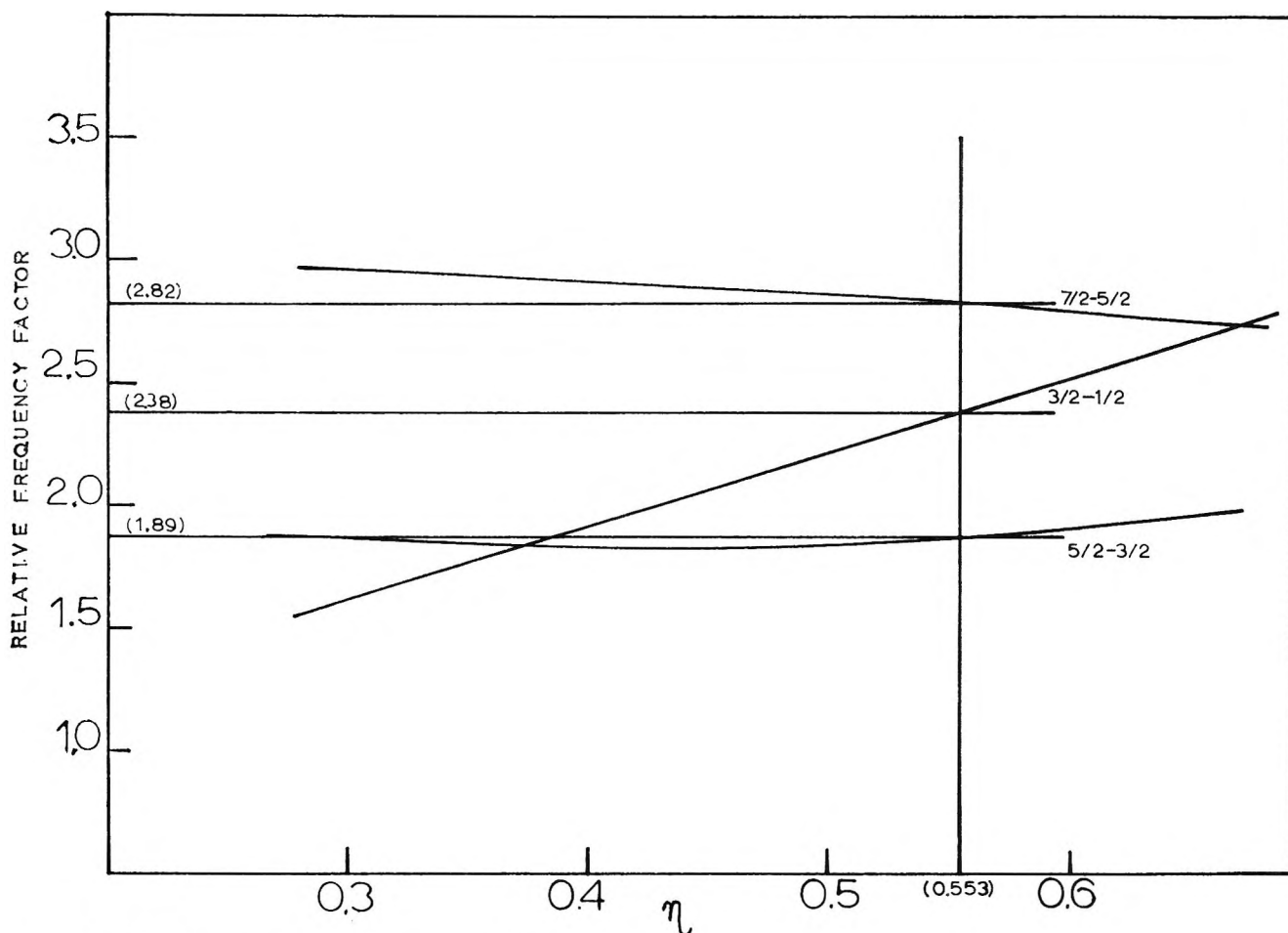
The nuclear quadrupole coupling constant, e^2Qq , can be found by plotting the calculated relative frequency factor, r_i , vs. η and determining the experimental relative factors from the intercepts of these curves with the vertical corresponding to the experimental value of η . The relative frequency factor, r_i , is given by

$$\nu_i = r_i |e^2Qq| / 24$$

This procedure is shown in Figure 2. The results of

(7) M. H. Cohen, *Phys. Rev.*, **96**, 1278 (1954).

(8) R. Berson, *J. Chem. Phys.*, **20**, 1505 (1952).


 Figure 2. Determination of the relative frequency factors, τ_1 .

the previously discussed methods as applied to the Bi^{209} nucleus in BiBr_3 are given in Table I.

Table I: Measured Transitions of Bi^{209} in BiBr_3 (300°K.)

Obad. frequencies, Mc./sec.	Obad. frequency ratios	Calcd. frequency ratios	Calcd. relative frequency factors	Assignment	e^2Qq/h , Mc./sec.
26.756 ± 0.002	1.262	1.263	1.39	$5/2 \rightarrow 3/2$	340.7
33.865 ± 0.002	1.178	1.179	2.38	$5/2 \rightarrow 1/2$	341.5
39.884 ± 0.002	1.486	1.487	2.52	$7/2 \rightarrow 5/2$	339.4
26.756 ± 0.002				Av.	340.5 ± 0.8

Discussion

The fact that a nuclear quadrupole resonance spectrum was observed precludes BiBr_3 from having a crystal structure analogous to BiI_3 .⁴ The observation of the resonance frequencies in the same region as those

observed for BiCl_3 ³ indicates that BiBr_3 has a crystal structure similar to BiCl_3 ; however, crystal structure data for neither compound are available. The melting point of BiBr_3 , 218°, is in the range expected for molecular crystals having comparable molecular weights; hence, solid BiBr_3 is viewed as a molecular crystal in which the individual BiBr_3 units retain their identity. Although d-electrons undoubtedly contribute to the bonding in solid BiBr_3 , the contribution will be predominantly in the form of cross bonding between BiBr_3 units and they will contribute little compared to p-electrons to the Bi-Br bonding within a single BiBr_3 molecule. The contribution of d-electrons to the bonding will be to affect the value of η more than that of e^2Qq .

The observed value of the coupling constant for Bi^{209} in BiBr_3 is not related to that in BiCl_3 (318.8 Mc./sec.)³ in the manner expected from consideration of electronegativity values alone. The relationship between the fraction ionic character, β , and fraction s-character, α , in an A-X bond and the quadrupole

coupling constant, $(e^2Qq_{zz})_A$, where A is the positive species, is given by⁹

$$(e^2Qq_{zz})_A = -3\alpha(1 + 2\beta)(e^2Qq_0)_A$$

where (e^2Qq_0) is the value for a single p-electron in the state $m_l = 0$ in an A atom. This relation shows that a decrease in fraction ionic character, as electronegativity values indicate, in going from a Bi-Cl to a Bi-Br bond, will produce a decrease in the coupling constant, assuming no change in s-hybridization. It is also evident from this relation that the observation of a coupling constant signifies the presence of some s-hybridization and that an increase in this factor will increase the coupling constant. Using the conventional Pauling electronegativity differences, $\Delta x = 0.9 \pm 0.1$, and $(e^2Qq_0)_{Bi} = 1500$ Mc./sec.,¹⁰ the per cent s-character and subsequently the Br-Bi-Br bond angle are calculated to be $5.6 \pm 0.3\%$ and $93.4 \pm 0.2^\circ$, respectively. The bond angle in gaseous BiBr₃ as measured by electron diffraction¹¹ is $100 \pm 4^\circ$, which is consistent with a per cent s-character of 14.8%. In the solid state the increased value of $(e^2Qq)_{Bi}$ of BiBr₃ over BiCl₃ can then be accounted for by a larger bond angle than in solid BiCl₃³ caused by an increase in s-hybridization, as indicated in the above calculations, by an increase in cross bonding, since this effect would produce the same change in the coupling constant as increasing s-hybridization, or a combination of the two.

There is little structural data available for solid group VA halides but available values for gaseous SbCl₃ ($\angle = 99.5 \pm 1.5^\circ$)¹² and solid SbCl₃ ($\angle = 95.2 \pm 0.2^\circ$)¹³ indicate that there is a decrease in the bond angle in going from the gas to the solid. The change for SbCl₃, 4.2° , is not as large as that predicted for BiBr₃, 6.6° , assuming the magnitude of the coupling constant is determined primarily by the amount of s-hybridization. While there is an uncertainty associated with comparing the behavior of antimony and bismuth compounds, the values for SbCl₃, coupled with the existence of appreciable cross bonding, involving d-orbitals, as indicated by the large asymmetry parameter, leads to the conclusion that the increase in $(e^2Qq)_{Bi}$ between BiCl₃ and BiBr₃ is due to a combination of an increase of s-hybridization and an increase of cross bonding compared to the BiCl₃ case. A study of the bromine coupling constants and asymmetry parameters could give further information regarding the extent of cross bonding.

(9) W. Gordy, W. V. Smith, and R. Trambarulo, "Microwave Spectroscopy," John Wiley and Sons, Inc., New York, N. Y., p. 281.

(10) H. G. Robinson, H. G. Dehmelt, and W. Gordy, *Phys. Rev.*, **89**, 1305 (1953).

(11) H. H. Skinner and L. E. Sutton, *Trans. Faraday Soc.*, **36**, 681 (1940).

(12) P. Kisliuk, *J. Chem. Phys.*, **22**, 680 (1954).

(13) I. Lindquist and A. Niggli, *J. Inorg. Nucl. Chem.*, **2**, 345 (1956)

Electron Spin Resonance Line Shape of Triplet Triphenylene in Rigid Solution¹

by J. B. Farmer, C. L. Gardner, and C. A. McDowell

Department of Chemistry, University of British Columbia, Vancouver, British Columbia, Canada
(Received October 3, 1964)

The electron spin resonance spectrum of the photoexcited triplet state of triphenylene in rigid solution at 77°K. has been recorded. A theoretical line-shape function for the $\Delta M = 1$ spectrum has been derived by considering the perturbation of the Zeeman energy levels by the electron spin-spin interaction. First-order perturbation theory is found to yield a line shape that correlates well with the experimental spectrum. A second-order correction improves the correlation.

1. Introduction

The detection of $\Delta M = 1$ transitions in the electron spin resonance spectra of aromatic triplet-state molecules was first reported for crystals by Hutchison and Mangum.² Similar spectra for triplet-state molecules and ions in rigid solution have recently been reported by Yager, Wasserman, and Cramer,^{3a} by de Groot and van der Waals,^{3b} and by Jesse, *et al.*⁴ It is now well established that $\Delta M = 1$ spectral peaks can be observed for glassy solutions, despite the large anisotropy, owing to a sharp change in the number of absorbing molecules at certain values of the static magnetic field. Peaks occur only for those molecules with a molecular axis approximately parallel to the field. It is the purpose of the present paper to demonstrate that the $\Delta M = 1$ spectrum of triphenylene can be represented by a line-shape function based on a perturbation treatment.

2. Experimental

Triphenylene, purchased from K and K Laboratories, Inc., Jamaica, N. Y., was dissolved in EPA (a mixture of ethyl ether, isopentane, and ethyl alcohol in the ratio of 8:3:5 by volume), the concentration being about $10^{-2} M$. The solution was sealed in a 4-mm., thin-walled, silica tube after thorough degassing. The sample was irradiated at the temperature of liquid nitrogen in a Varian No. V-4531 e.s.r. cavity. Light from a General Electric No. A-H6 mercury lamp was focused through a silica optical system. Spectra were obtained with an e.s.r. spectrometer having a modulation frequency of 100 kc. The magnetic field was calibrated with an n.m.r. magnetometer.

3. Results and Discussion

For molecules, such as triphenylene, having a three-fold or higher symmetry axis, it has been shown^{5,6a} that the triplet e.s.r. spectrum can be explained in terms of the spin-Hamiltonian

$$\mathcal{H} = g\beta\mathbf{H}\cdot\mathbf{S} + D(S_z^2 - \frac{1}{3}S^2) \quad (1)$$

written in the molecular coordinate system. For aromatic hydrocarbons, where the electronic spin-spin interaction is usually less than the Zeeman interaction, it is convenient to consider the Zeeman levels as zeroth-order levels with the spin-spin interaction as a perturbation. In an $|M_S\rangle$ basis with respect to the laboratory coordinates the matrix of $\mathcal{H}' = D(S_z^2 - \frac{1}{3}S^2)$ is

$$\mathcal{H}' = D \begin{vmatrix} \frac{1}{6}(3 \cos^2 \theta - 1), & 1/\sqrt{2} \cos \theta \sin \theta e^{-i\phi}, & \\ & \frac{1}{2} \sin^2 \theta e^{-2i\phi} & \\ 1/\sqrt{2} \cos \theta \sin \theta e^{i\phi}, & -\frac{1}{3}(3 \cos^2 \theta - 1), & \\ & 1/\sqrt{2} \cos \theta \sin \theta e^{-i\phi} & \\ \frac{1}{2} \sin^2 \theta e^{2i\phi}, & 1/\sqrt{2} \cos \theta \sin \theta e^{i\phi}, & \\ & \frac{1}{6}(3 \cos^2 \theta - 1) & \end{vmatrix} \quad (2)$$

(1) A preliminary account of this work was given at the spring meeting of the Société de Chimie Physique de France, in May 1964, at Bordeaux, France.

(2) C. A. Hutchison and B. W. Mangum, *J. Chem. Phys.*, **29**, 952 (1958).

(3) (a) W. A. Yager, E. Wasserman, and R. M. R. Cramer, *ibid.*, **37**, 1148 (1962); (b) M. S. de Groot and J. H. van der Waals, *Mol. Phys.*, **6**, 545 (1963).

(4) R. E. Jesse, P. Biloen, R. Prins, J. D. W. van Voorst, and G. J. Hooijink, *ibid.*, **6**, 633 (1963).

(5) J. H. van der Waals and M. S. de Groot, *ibid.*, **2**, 333 (1959).

The energy of the perturbed Zeeman level that is labeled by M in the limit of zero perturbation is given by

$$E_M = E_M^{(0)} + E_M^{(1)} + E_M^{(2)} + \dots + E_M^{(i)} + \dots \quad (3)$$

The expressions for $E_M^{(i)}$, which are found by standard perturbation theory, are

$$\begin{aligned} E_M^{(0)} &= g\beta HM \\ E_M^{(1)} &= 3C'_{MM} \\ E_M^{(2)} &= \sum_i' |3C'_{Mi}|^2 / (E_M^{(0)} - E_i^{(0)}) \end{aligned} \quad (4)$$

These lead to the following values for the energy levels correct to first order.

$$E_0 = \frac{-D}{3} (3 \cos^2 \theta - 1) \quad (5)$$

$$E_{\pm 1} = \pm g\beta H + \frac{D}{6} (3 \cos^2 \theta - 1)$$

For a polycrystalline sample, all orientations are equally probable, and the absorption line shape must be obtained by averaging. If the approximations (a) that the transition probability is constant for all orientations and (b) that the absorption line width is zero for a given orientation are made, then the composite line shape can be written as

$$I(H) \propto \left| \frac{d \cos \theta}{dH} \right| \quad (6)$$

From the first-order energies it is seen that, for resonance to occur, the condition $h\nu_0 = g\beta H \pm \frac{1}{2}D(3 \cos^2 \theta - 1)$ must be satisfied. Hence, the line-shape function is found to be

$$\frac{d \cos \theta}{dh'} = \frac{2}{\sqrt{3}D'} \left(\frac{\pm 2h'}{D'} + 1 \right)^{-1/2} \quad (7)$$

where $h' = H_0 - H$, $H_0 = h\nu_0/g\beta$, and $D' = D/g\beta$. This type of treatment is well known in connection with line-shape problems in n.m.r. spectrometry⁷ and has been applied by Burns⁸ to the e.s.r. powder spectrum of the Cr^{3+} ($S = \frac{3}{2}$) ion in an axial crystalline field, a system that is adequately represented by the spin-Hamiltonian of eq. 1.

Figure 1 (a) shows the first-derivative e.s.r. spectrum obtained when triphenylene in rigid solution was irradiated. The lines numbered 1 through 4 originate from $\Delta M = 1$ transitions of the triplet state. The low-field line at 1416 gauss originates from $\Delta M = 2$ transitions of the triplet state. The strong resonance in the center of the $\Delta M = 1$ spectrum is caused by

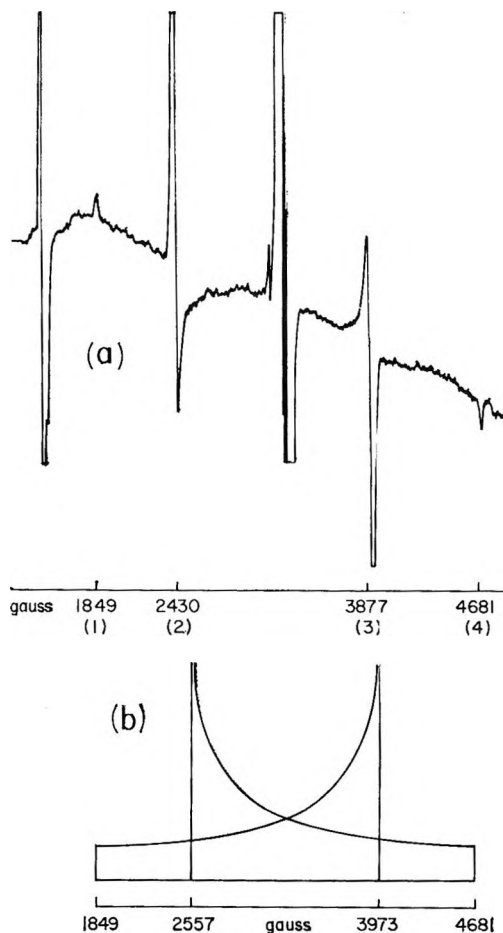


Figure 1. (a) Electron spin resonance spectrum of triplet state of triphenylene in EPA at 77°K.; (b) theoretical e.s.r. line shape for triplet state of triphenylene calculated from eq. 7.

free radicals generated from the EPA solvent. The weak line at 3137 gauss, on the low-field side of the free-radical resonance, is believed to be due to a double-quantum absorption. Such an effect has been invoked by de Groot and van der Waals⁹ in order to interpret the spectrum of deuteriophenanthrene. All the lines assigned to triplet triphenylene disappeared when irradiation ceased, and the free-radical resonance remained.

Figure 1 (b) shows the theoretical line shape given by eq. 7. The innermost singularities, corresponding to

(6) M. S. de Groot and J. H. van der Waals, *Mol. Phys.*, **3**, 190 (1960).

(6a) NOTE ADDED IN PROOF. Since this paper was submitted, a similar treatment of triplet states of randomly oriented molecules has appeared in *J. Chem. Phys.*, **41**, 1763 (1964).

(7) E. R. Andrews, "Nuclear Magnetic Resonance," Cambridge University Press, London, 1955, p. 152.

(8) G. Burns, *J. Appl. Phys.*, **32**, 2048 (1961).

(9) M. S. de Groot and J. H. van der Waals, *Physica*, **29**, 1128 (1963).

$\theta = 90^\circ$, are associated with the zero-slope points of lines 2 and 3 of the experimental spectrum, while the outermost ones, corresponding to $\theta = 0^\circ$, are associated with the inner edges of lines 1 and 4. In the plotting of the line shape, D was chosen such that lines 1 and 4 and their theoretical counterparts were coincident. With this condition, $D = 0.132 \text{ cm.}^{-1}$. The result compares well with that of $D = 0.134 \text{ cm.}^{-1}$ deduced by de Groot and van der Waals⁶ from the low-field $\Delta M = 2$ spectrum.

Although there is substantial agreement between the theoretical and experimental spectra, it is noticeable that the interval between lines 1 and 2 of the experimental spectrum is not equal to that between lines 3 and 4, as is predicted by the first-order model, but is appreciably less. Closer agreement is achieved by including second-order terms in the calculation of the energy levels, namely

$$E_0^{(2)} = 0$$

$$E_{\pm}^{(2)} = \pm \frac{D^2 \cos^2 \theta \sin^2 \theta}{2g\beta H} \pm \frac{D^2 \sin^4 \theta}{8g\beta H} \quad (8)$$

It is easily verified that singularities again occur at 0 and 90° . From the resonance condition based on the second-order energies, one obtains an expression of the form $\cos^2 \theta = f(H)$, and this yields the equation for the line shape

$$\frac{d \cos \theta}{dH} = \frac{1}{2 \cos \theta} f'(H) \quad (9)$$

The second-order correction affects the positions of the singularities of the theoretical spectrum in the following way. At $\theta = 0^\circ$ the correction vanishes. At $\theta = 90^\circ$ the correction adds $D^2/8g\beta H$ to both transition energies. Experimentally, this should be observed as a shift in lines 2 and 3 toward lower magnetic field. The shift should be 100 gauss for line 2 and 68 gauss for line 3. The actual shifts are 127 gauss for line 2 and 96 gauss for line 3. The third-order correction does not contribute a further shift. To obtain greater accuracy, it would probably be necessary to allow for finite line widths, etc., as has been done in Kottis and Lefebvre's¹⁰ treatment using a computer.

Acknowledgment. The authors wish to express their gratitude to the National Research Council of Canada and the Defence Research Board of Canada for generous grants in support of this work. C. L. G. acknowledges the award of a National Research Council Studentship during the years 1960–1963. C. A. McD. is indebted to the same body for the award of a Senior Research Fellowship during the 1963–1964 academic year. Thanks are also due to our colleague, Dr. J. A. R. Coope, for several helpful discussions. We also wish to thank Dr. J. H. van der Waals and Dr. M. S. de Groot for reading the manuscript.

(10) P. Kottis and R. Lefebvre, *J. Chem. Phys.*, **39**, 393 (1963); **41**, 379 (1964).

The Nucleation of Long-Chain Molecules in Monomolecular Layers¹

by L. Mandelkern, J. G. Fatou, and C. Howard

*Department of Chemistry and Institute of Molecular Biophysics, Florida State University, Tallahassee, Florida
(Received October 5, 1964)*

The effect of finite chain length on the nucleation of long-chain molecules whose sequences are deposited in monomolecular layers has been considered. As in the case of three-dimensional nucleation significant differences in the critical requirements for nucleus formation are found between the infinite chain and chains having less than about 10^4 bonds. In particular it is observed that the free energy of forming a critical nucleus does not become infinite at the melting temperature of the finite chain. These results have been applied to previously published data on the lineal growth rate of spherulites into molecular weight fractions of polyethylene. It is shown that, irrespective of molecular weight, the data can be described by the same interfacial energies and pre-exponential factor over the range $M = 3.9 \times 10^3$ to 8.7×10^4 where data are available.

Introduction

In a previous paper² an analysis was presented of the effect of finite molecular weight on the characteristics of three-dimensional nucleation processes which involve long-chain molecules. Significant differences were obtained for the critical conditions for nucleus formation between a chain of finite length and one of infinite molecular weight. The results for the latter model, which also correspond exactly to those for a collection of monomeric molecules arranged in a similar geometric array, have been the ones usually employed, irrespective of molecular weight. These theoretical differences are particularly accentuated when undercoolings and nucleation rates are calculated using the melting temperature of the finite chain as a reference point. In the present paper we extend these concepts to nucleation of the type described by Gibbs,³ which involves the unimolecular deposition of chain sequences. We find certain unique results which are not apparent in the infinite molecular weight approximation that has also been employed for this case.

Results and Discussion

By using the concepts and notation of the previous paper,² the change in free energy that accompanies the formation of a monomolecular nucleus, ζ units long and ρ sequences in breadth, from a collection of molten chains each of which is x units long can be expressed as

$$\Delta F = 2\zeta\sigma_u + 2\rho\sigma_e - \zeta\rho\Delta f_u + \frac{RT}{x} \zeta\rho - \rho RT \ln \frac{(x - \zeta + 1)}{x} \quad (1)$$

It is assumed in the above that the nucleus is deposited upon a crystal face already present in the system. In eq. 1, σ_u is the lateral interfacial energy per chain unit, σ_e is the excess free energy per chain unit as it emerges from an ordered sequence, and Δf_u is the free energy of fusion per repeating unit characteristic of the infinite chain. The first three terms in the above expression represent the infinite chain (or monomer) case while the last two terms represent the contributions of the finite chain as has been previously discussed.² The surface described by eq. 1 possesses neither a maximum nor a minimum but does contain a saddle point. By appropriate differentiation and substitution the coordinates of the saddle point are found to be

$$\rho^* = \frac{2\sigma_u}{\Delta f_u - \frac{RT}{x} - \frac{RT}{x - \zeta + 1}} \quad (2)$$

(1) This work was supported by a grant from the U. S. Army Research Office (Durham) and a contract with the Division of Biology and Medicine, Atomic Energy Commission.

(2) L. Mandelkern, J. G. Fatou, and C. Howard, *J. Phys. Chem.*, **68**, 3386 (1964).

(3) J. W. Gibbs, "Collected Works," Longmans Green and Co., New York, N. Y., 1928, p. 325.

$$\zeta^* = \frac{2\sigma_e - RT \ln \left(\frac{x - \zeta^* + 1}{x} \right)}{\Delta f_u - \frac{RT}{x}} \quad (3)$$

and

$$\Delta F^* = \frac{2\sigma_u \left[2\sigma_e - RT \ln \left(\frac{x - \zeta^* + 1}{x} \right) \right]}{\Delta f_u - \frac{RT}{x}} = 2\sigma_u \zeta^* \quad (4)$$

As x approaches infinity these reduce to the classical results

$$\Delta F^* = \frac{4\sigma_e \sigma_u}{\Delta f_u} \quad \zeta^* = \frac{2\sigma_e}{\Delta f_u} \quad \rho^* = \frac{2\sigma_u}{\Delta f_u} \quad (5)$$

At the melting temperature of the infinite molecular weight chain ΔF^* , ζ^* , and ρ^* all become infinite since Δf_u is zero, this conclusion being the same as that obtained for monomeric systems. However, at the equilibrium melting temperature of a finite chain, in accord with the results for three-dimensional nucleation, ζ^* does not become infinite while ρ^* does. For the three-dimensional case, we have noted previously that since $\Delta F^* = \pi^{1/2} \zeta^* \rho^{*1/2} \sigma_u$, the critical free energy becomes infinite at the melting temperature because of the infinity that develops in ρ^* . However, according to eq. 4, ΔF^* depends only on ζ^* for monomolecular nucleation, and hence it will not become infinite at the melting temperature of the finite chain. This conclusion is contrary to the results for the infinite chain. The possibility thus exists for nucleus formation at the melting temperature of the finite chain. At least, the thermodynamic barrier to nucleus formation is not infinite. The physical significance of this conclusion, from the point of view of experimental observation, resides in the fact that from both theory⁴ and experiment⁵ the melting temperature depends on chain length over the molecular weight ranges of usual interest. A numerical analysis of eq. 3, similar to that previously given for three-dimensional nucleation, indicates that the classical result is only obeyed for values of x approximately equal to or greater than 10^4 . The above conclusions should be valid, irrespective of the molecular model chosen to represent the equilibrium crystalline state, as long as the complete chain molecule does not participate in the nucleation act.

It has been postulated by various investigators⁶⁻⁸ that the lineal growth rate of spherulites in polymers is controlled by monomolecular nucleation on an

already formed crystal face. Specifically, the relationship

$$G = G_0 \exp \frac{-\Delta F^*}{RT} \quad (6)$$

has been utilized in analyzing spherulite growth rate in a wide variety of polymer systems.⁹ Recently, Lindenmeyer and Holland¹⁰ have investigated the lineal growth rate of spherulites in molecular weight fractions of linear polyethylene as a function of temperature in the vicinity of the melting temperature. Molecular weight fractions, ranging from $M = 3.9 \times 10^3$ to 8.7×10^4 , were studied. Their data were analyzed by invoking eq. 6, identifying ΔF^* with $4\sigma_e \sigma_u / \Delta f_u$, and approximating Δf_u by $(T_m - T)\Delta H_u / T_m$. Here ΔH_u is the heat of fusion per repeating unit and T_m is the equilibrium melting temperature of the finite chain. These analyses, therefore, involve the *a priori* knowledge of the equilibrium melting temperature of the finite chain. It is also tacitly being assumed that ΔF^* becomes infinite at this temperature. Melting temperatures initially used for this purpose were taken from values extrapolated from the melting temperatures of the *n*-paraffins.¹¹ Hence it was assumed that molecular crystals were formed with the chain ends being paired. However, the contribution of the entropy of end pairing to the crystallization process and consequently to the melting temperature⁴ was neglected in this analysis. Utilizing the melting temperatures thus calculated for each molecular weight, a family of straight lines resulted when $\ln G$ was plotted against $1/(T_m - T)$. The slopes of these straight lines increased with increasing molecular weight. A literal interpretation of these results would mean that the product of the interfacial energies $\sigma_u \sigma_e$ increases with increasing molecular weight. It was also found¹⁰ that the data could be made to yield a family of parallel straight lines when arbitrary equilibrium melting temperatures were selected for each molecular weight fraction. In this calculation the curves were so displaced that when compared at the same undercooling the highest molecular weight fraction had the greatest growth rate.

(4) P. J. Flory and A. Vrij, *J. Am. Chem. Soc.*, **85**, 3548 (1963).

(5) J. G. Fatou and L. Mandelkern, *J. Phys. Chem.*, **69**, 417 (1965).

(6) B. B. Burnet and W. F. McDevit, *J. Appl. Phys.*, **28**, 1101 (1957).

(7) F. P. Price, *Ann. N. Y. Acad. Sci.*, **83**, 20 (1959).

(8) J. D. Hoffman and J. I. Lauritzen, *J. Res. Natl. Bur. Std.*, **65A**, 297 (1961).

(9) L. Mandelkern, "Crystallization of Polymers," McGraw-Hill Book Co., New York, N. Y., 1964, p. 253.

(10) P. H. Lindenmeyer and V. F. Holland, *J. Appl. Phys.*, **35**, 55 (1964).

(11) M. Broadhurst, *J. Chem. Phys.*, **36**, 2578 (1962).

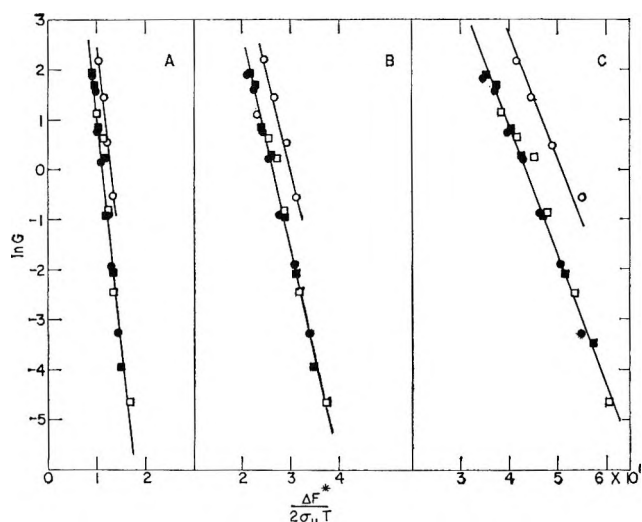


Figure 1. Plot of $\ln G$ against $\Delta F^*/2\sigma_u T$ for spherulite growth rate. ΔF^* was calculated according to eq. 4. $\sigma_e = 1200$ cal./mole, A; $\sigma_e = 2800$ cal./mole, B; $\sigma_e = 4600$ cal./mole, C; $M = 3900$, O; $M = 7950$, □; $M = 15,900$, ■; $M = 87,000$, ●.

The molecular weight range encompassed in these experiments is one in which significant departures from classical nucleation theory are expected on the basis of the analysis given above. We have, therefore, reanalyzed these experimental results in accordance with the dictates of eq. 3 and 4. It is assumed for this purpose that eq. 6 is valid in describing the spherulite growth rate.¹² We calculate the quantity $\Delta F^*/2\sigma_u$ for various values of σ_e . Besides the interfacial energy, we need only to specify the melting temperature of the infinite molecular weight chain to accomplish the calculation. Our method, therefore, avoids the necessity and attendant uncertainty in the results of having to specify the melting temperature of each molecular weight fraction. Following the analyses of Flory and Vrij⁴ we have taken 145.5° as the melting temperature of the infinite molecular weight polyethylene chain.

The results of this calculation are plotted in Figure 1 as $\ln G$ against $\Delta F^*/2\sigma_u T$ for the arbitrarily selected values of σ_e of 1200, 2800, and 4600 cal./mole, respectively. We note that for any given value assigned to σ_e , the data are well represented by a single straight line except for the lowest molecular weight sample, ($M = 3900$, $x = 279$). Over the molecular weight range studied there is no displacement or dispersion with increasing molecular weight. Hence, the pre-exponential factor G_0 can be taken to be independent of molecular weight. This result, therefore, stands in contradiction to the analyses previously given.¹⁰ The data for the lowest molecular weight, although displaced slightly, yield a straight line in each instance which is parallel to the composite straight line of the

other molecular weights. We can conclude, therefore, that for a given value of σ_u , the value assigned to σ_e will be independent of molecular weight, at least in the range over which experimental data are presently available.

If strict obedience to eq. 6 is demanded, then quite obviously from each of the straight lines (characterized by a given σ_e) a value of σ_u can be obtained. It is obvious from the onset that σ_e and σ_u cannot be independently determined. From the slopes of the straight lines in Figure 1 it is found that for $\sigma_e = 1200$ cal./mole, $\sigma_u = 100$ cal./mole; for $\sigma_e = 2200$ cal./mole, $\sigma_u = 40$ cal./mole; for $\sigma_e = 4600$ cal./mole, $\sigma_u = 30$ cal./mole. The range of values of σ_u is comparable with the value deduced by Turnbull and Cormia¹³ for the interfacial energy of low molecular weight *n*-paraffins from crystal nucleation kinetic studies involving isolated droplets. A value of $\sigma_e = 4600$ has been deduced for polyethylene, from studies of the crystallization of droplets,¹⁴ the fusion of copolymers,¹⁵ and low angle X-ray diffraction studies.¹⁶ Hence if eq. 6 does properly describe the spherulite growth rate, the products of the interfacial energies that are found are in satisfactory agreement with the values deduced from other sources. The main conclusion to be drawn in the present context, however, is that over the molecular weight range studied the data are well-represented by a single straight line. We should also note that as with all other results for the lineal growth rate of spherulites in long-chain molecules⁹ the data for the molecular weight fractions of polyethylene also adhere to the functional dependence demanded by three-dimensional nucleation processes. From this point of view, therefore, no discrimination can be made between the different nucleation processes. In the latter case also, all the molecular weight data fall on a single straight line.

Over the molecular weight range studied the size of the crystallites relative to the extended length of the molecules varies considerably. According to Anderson's¹⁷ electron microscope observation of replicas of fracture surfaces, for molecular weights less than about 15,000 the crystallite sizes are comparable to

(12) We wish to thank Drs. Lindenmeyer and Holland for so kindly making their original data available to us.

(13) D. Turnbull and R. L. Cormia, *J. Chem. Phys.*, **34**, 820 (1961).

(14) R. L. Cormia, F. P. Price, and D. Turnbull, *ibid.*, **37**, 1333 (1962).

(15) M. J. Richardson, P. J. Flory, and J. B. Jackson, *Polymer*, **4**, 221 (1963).

(16) L. Mandelkern, A. S. Posner, A. F. Diorio, and D. E. Roberts, *J. Appl. Phys.*, **32**, 1509 (1961).

(17) F. R. Anderson, *J. Polymer Sci.*, **3C**, 123 (1963); *J. Appl. Phys.*, **35**, 64 (1964).

the extended lengths of the molecules. At higher molecular weights this ratio will become severely reduced with the concomitant re-entry of chains into the crystallite from which they emerge. However, spherulites are formed over this complete molecular weight range irrespective of the relative size of the crystallites.¹⁰ Obviously, therefore, chain re-entry or folding is not a requirement for spherulite formation in long-chain molecules. Moreover, from the analysis of the data in Figure 1 the products of interfacial

energies are independent of molecular weight over the range studied (irrespective of the value of σ_e that is chosen). Hence, we must conclude that it is highly unlikely that the values of the interfacial energy or the nature of the nucleation acts themselves determine whether many sequences from the same molecule participate in the development of a given crystallite.¹⁸

(18) P. J. Flory, *J. Am. Chem. Soc.*, **84**, 2857 (1962).

Equilibrium Ultracentrifugation of Hydrolyzed Lead(II)

Perchlorate Solutions^{1a,b}

by O. E. Esva^{1c} and James S. Johnson, Jr.

Oak Ridge National Laboratory, Oak Ridge, Tennessee (Received October 5, 1964)

The degrees of polymerization (N_w) of 0.025–0.1 *M* lead(II) perchlorate solutes were investigated by equilibrium ultracentrifugation from 0 to 1.33 hydroxyls bound per lead. The distribution of hydrolyzed species was polydisperse in all cases studied. Average values of N_w were *ca.* 4 at hydroxyl number 1 and increased further in more basic solutions. The results are in agreement with light-scattering measurements carried out elsewhere and are consistent with a scheme in the literature based on e.m.f. studies. Apparent molal volumes and refractive index increments for hydrolyzed Pb(II) solutes are reported.

Some years ago, a study by equilibrium ultracentrifugation of the hydrolysis of Pb(II) and Sn(IV) in basic solution, carried out in this laboratory, indicated that monomeric species were predominant.² We report here an extension of the study of Pb(II) hydrolysis to solutions on the acidic side of the precipitation point.

There have been fewer studies made of the hydrolysis of divalent lead than of many other elements, and perhaps, as a result, there is less controversy over the species formed though agreement between various investigators is not altogether complete. Since others³ have reviewed the literature recently, we shall restrict our attention to a few authors who have covered a wide

enough range of conditions (or have examined their results closely enough) to require species higher than dimeric for interpretation.

Pederson,⁴ from acidity measurements of lead nitrate

(1) (a) Research sponsored by the U. S. Atomic Energy Commission under contract with the Union Carbide Corp.; (b) from a thesis submitted by O. E. Esva to the Graduate School of the University of North Carolina in partial fulfillment of the requirements for the Ph.D. degree, 1962; (c) Oak Ridge Institute of Nuclear Studies Graduate Fellow.

(2) J. S. Johnson and K. A. Kraus, *J. Am. Chem. Soc.*, **81**, 1569 (1959).

(3) F. C. Hentz and S. Y. Tyree, *Inorg. Chem.*, **3**, 844 (1964).

(4) K. J. Pederson, *Kgl. Danske Videnskab. Selskab Mat. Fys. Medd.*, **22**, No. 10 (1945).

as a function of concentration and added acid and base, concluded that the hydrolyzed species $\text{Pb}_2(\text{OH})^{3+}$, PbOH^+ , and $\text{Pb}_4(\text{OH})_4^{4+}$ were formed. Faucherre,⁵ from a variety of measurements, listed $\text{Pb}_4(\text{OH})_4^{4+}$ and suggested that a higher species, perhaps $\text{Pb}_9(\text{OH})_{12}^{6+}$, was formed under some conditions. Olin,⁶ in an extensive electromotive force study with both acid-sensitive and lead amalgam cells, listed PbOH^+ , $\text{Pb}_3(\text{OH})_4^{2+}$, $\text{Pb}_4(\text{OH})_4^{4+}$, and $\text{Pb}_6(\text{OH})_8^{4+}$. Later, from studies in concentrated solutions,⁷ he added $\text{Pb}_2(\text{OH})^{3+}$ and, from calorimetric measurements of acid-base titrations,⁸ estimated enthalpies for the reactions forming $\text{Pb}_4(\text{OH})_4^{4+}$, $\text{Pb}_3(\text{OH})_4^{2+}$, and $\text{Pb}_6(\text{OH})_8^{4+}$. Hugel⁹ measured the acidities of hydrolyzed lead perchlorate solutions as a function of dilution and listed formation quotients for the species PbOH^+ and $\text{Pb}_4(\text{OH})_4^{4+}$ which agree well with those of Olin. The more hydrolyzed species listed by Olin would not have been important in the range of Hugel's measurements, and he did not exclude them.

The agreement between these laboratories on the presence and the importance of the $\text{Pb}_4(\text{OH})_4^{4+}$ species is remarkable for the hydrolysis field. From experience with other solutes, however, it seemed that confirmation of the main conclusions by methods sensitive primarily to the weights of the species would be useful. The present paper describes a study by equilibrium ultracentrifugation. Hentz and Tyree carried out a light-scattering study of the same system concurrently.³ The conclusions from these weight-average studies are in general agreement with each other and with those made on the basis of the other techniques.

Experimental

1. *Ultracentrifugation.* Procedures are similar to those outlined in earlier studies.^{10,11} Centrifugations were carried out with a Spinco Model E ultracentrifuge. Solutions were contained in 12-mm. cells, which were placed in a five-cell Analytical G rotor. Sedimentation was followed by interference optics. The temperature of centrifugation was 25°. Speeds of rotation were between 11,250 and 24,630 r.p.m.; the speed was selected to give an adequate interference pattern for the degree of polymerization and Pb(II) concentration involved.

Computations were carried out on an IBM 7090 computer with a program¹² somewhat revised from that used previously.¹⁰ The equation used for computation of degree of polymerization, N_w , is

$$N_w = \frac{d \ln c_2'/d(x^2)}{A_2' - (z'/2)d \ln [(1 + \eta)/(1 - \eta)]/d(x^2)} \quad (1)$$

where subscript 2 indicates the Pb(II) component;

3, the supporting electrolyte; primes, quantities expressed in terms of monomer units; c , concentration in moles l.⁻¹; x , radius; z' , charge per monomer unit of the lead polymer (which, because of perchlorate complexing, may not be the maximum possible); $\eta = z'c_2'/2c_3$; $A_2' = M_2'(1 - \bar{v}_2\rho)\omega^2/2RT$; M , molecular weight; \bar{v} , partial specific volume; ρ , solution density; ω , angular velocity; R , gas constant; and T , absolute temperature. The definition of the (primed) polymeric component 2, $\text{Pb}(\text{OH})_n(\text{ClO}_4)_{2-n} - (z'/2)\text{NaClO}_4$, is that proposed by Scatchard¹³ and reflects the charge. The symbol n indicates hydroxyl number, the average number of moles of hydroxide bound per mole of lead(II).

The reported values of N_w were evaluated for the radius at which the initial concentration of Pb(II) occurs at centrifugation equilibrium. The procedure for obtaining c_2' from interference patterns is complicated by the effect of charge and the consequent use of the Scatchard definition of components; it is described in detail elsewhere.^{1b,10}

2. *Materials.* Stock solutions, prepared from reagent grade PbO and perchloric acid, are listed in Table I along with their hydroxyl numbers. For hydrolyzed

Table I: Stock Pb(II) Solutions

Soln. no.	mmoles of Pb(II)/g. of soln.	Dev., p.p.t.	mmoles of perchlorate/g. of soln.	Dev., p.p.t.	n
1	1.297	0.5	2.776	3.6	0 ^a
2	2.032	1.5	2.169	2.3	0.933
3	0.8243	4.7	0.5560	2.5	1.326

^a Excess HClO_4 present.

solutions 2 and 3, n is given by the stoichiometry (2 times moles of Pb(II) minus moles of perchlorate) since the free acid is negligible.⁶ A brownish color-

(5) J. Faucherre, *Bull. soc. chim. France*, 21, 128 (1954).

(6) A. Olin, *Acta Chem. Scand.*, 14, 126 (1960); *Svensk Kem. Tidskr.*, 73, 482 (1961).

(7) A. Olin, *Acta Chem. Scand.*, 14, 814 (1960).

(8) B. Carell and A. Olin, *ibid.*, 16, 2350 (1962).

(9) R. Hugel, *Bull. soc. chim. France*, 1462 (1964).

(10) J. S. Johnson, G. Scatchard, and K. A. Kraus, *J. Phys. Chem.*, 63, 787 (1959).

(11) R. M. Rush, J. S. Johnson, and K. A. Kraus, *Inorg. Chem.*, 1, 378 (1962).

(12) The program is described more fully in ref. 1b. A few modifications and corrections, which (except for centrifugations with short columns in the radial direction) affect results trivially in most cases, have since been incorporated; the revised program and a source deck (Fortran) are available from ORNL.

(13) G. Scatchard, *J. Am. Chem. Soc.*, 68, 2315 (1946).

tion of the solutions appeared which, on the basis of a benzidine spot test,¹⁴ apparently stemmed from Pb(IV). The coloration was eliminated by filtration through an ultrafine filter under nitrogen. Solution 2 was prepared at 100°. Solution 3 was prepared from a basic salt of the appropriate hydroxyl number, which in turn was prepared by the method of Willard and Kassner.¹⁵ Solutions prepared from the solid were slightly turbid, presumably owing to lead carbonate contamination, but filtration gave clear solutions.

The stock solutions were analyzed in triplicate for lead by precipitation of PbMoO₄¹⁶; perchlorate was determined as ammonium perchlorate by evaporation of the filtrate from an ammonium carbonate precipitation of lead, followed by heating at 110° to decompose excess ammonium carbonate. The analyses and mean deviations are given in Table I. A concentrated NaClO₄ stock, prepared by neutralization of HClO₄ with NaOH pellets to pH 4 while bubbling N₂ through, was analyzed by evaporation at 120°.

Fifteen solutions were used in the centrifugations with Pb(II) concentrations being *ca.* 0.025, 0.05, and 0.1 *M* at hydroxyl numbers of *ca.* 0, 0.16, 0.73, 0.93, and 1.33. They were prepared by weight from the appropriate stock solutions of Pb(II) and NaClO₄. The solutions of *n* = 0.16 were prepared from stock 1 by addition of NaOH; the solutions of *n* = 0.73 were prepared by addition of HClO₄ to stock 2. The unhydrolyzed solutions, *n* = 0, had at least 0.003 *M* HClO₄ present in excess of Pb(ClO₄)₂. All solutions except for the unhydrolyzed became slightly cloudy on standing. Since a solution filtered under nitrogen and sealed against the atmosphere remained clear for months, we presume the turbidity arose from lead carbonate. In the most turbid solution, the amount of precipitate was found to be negligible for present purposes (0.004%) and was, therefore, ignored.

Densities were measured with a ~24-ml. pycnometer, and refractive indices were measured with a Brice-Phoenix differential refractometer.

Results and Discussion

1. *Volumes and Refractive Index Increments.* Partial specific volumes of the solutes are needed in the equations for degree of polymerization, N_w , and refractive index increments are required for interpretation of equilibrium interference fringe patterns in terms of concentration distributions. The apparent molal volumes of hydrolyzed lead perchlorate solutes

$$\phi_2 = \frac{V - V_s}{m_2'} \quad (2)$$

are summarized in Figure 1a. Here V is the volume of

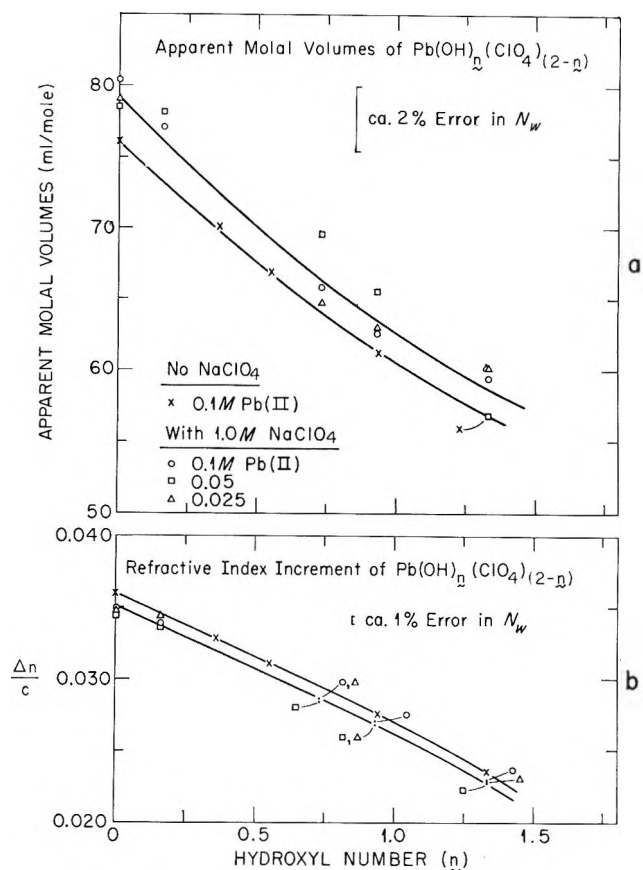


Figure 1. Apparent volumes and refractive index increments (546 μ) of hydrolyzed lead perchlorate solutions.

solution containing 1 kg. of water, V_s is the volume of "solvent" (*i.e.*, the volume of a solution of the same molality of supporting electrolyte as the solution of interest) containing 1 kg. of water, and m_2' is the molality of Pb(II). The precision of the measurements in supporting electrolyte was not sufficient to justify estimation of the dependence of volume on Pb(II) concentration; therefore, apparent molal volumes were used for partial volumes in computation of N_w . Some measurements were also made in absence of supporting electrolyte; the precision of these is better since slight percentage errors in supporting electrolyte concentration have a large effect on apparent volumes of the lead component computed from solution densities. The values, as expected, are lower in absence of excess NaClO₄. For interpretation of centrifugation results, we have used the line drawn through the values in

(14) F. Feigl, "Spot Tests," Vol. 1, Elsevier Publishing Co., New York, N. Y., 1954, p. 68.

(15) H. H. Willard and J. L. Kassner, *J. Am. Chem. Soc.*, **52**, 2391 (1930).

(16) H. B. Weiser, *J. Phys. Chem.*, **20**, 640 (1916).

1 *M* NaClO₄ media parallel to the line for solutions without supporting electrolyte (Figure 1a).

Supporting electrolyte partial volumes for computer input and for use in eq. 2 were obtained from literature data. In computation of ϕ_2 for $n = 0$ (in which case HClO₄ was present in appreciable quantities), volumes for the "solvent" were computed by the mixing rule of Young and Smith¹⁷; the data of Wirth and Collier¹⁸ were used for supporting electrolyte volumes.

Refractive index increments $\Delta n_{546}/c$ are given in Figure 1b. The symbol Δn_{546} denotes the difference in refractive index at 546 m μ between solution and background both having the same molarity of supporting electrolyte and c , the Pb(II) concentration in moles/l. Again, there was no significant dependence on Pb(II) concentration. Values for computational inputs were taken from the line drawn through the values obtained in the presence of supporting electrolyte parallel to the points without supporting electrolyte. Literature values were used for NaClO₄¹⁹ refractive index increments, and measurements were made in this laboratory²⁰ for perchloric acid.

The effect of changes of input ϕ_2 and $\Delta n/c$ on computed N_w are indicated in Figure 1. It can be seen that uncertainties in these quantities are not important in comparison with those stemming from assumptions made in analysis of data.

2. *Ultracentrifugation.* Fifteen solutions, which were ca. 1 *M* in NaClO₄ supporting electrolyte, were centrifuged. Hydroxyl numbers investigated were $n \cong 0, 0.16, 0.73, 0.93,$ and 1.33 , and at each hydroxyl number Pb(II) concentrations were ca. 0.025, 0.05, and 0.1 *M*. All were ca. 1 *M* in NaClO₄ supporting electrolyte.

Comparison of the equilibrium interference patterns for the hydrolyzed solutions with those of the unhydrolyzed indicates immediately that polymers are formed. The next question of interest is whether the Pb(II) solute is found in species all having the same molecular weight or in a polydisperse distribution. In Figure 2, we have plotted the deviation for each centrifugation of $\ln n^*$ from a linear variation with x^2 , obtained by a least-squares fit to a straight line of $\ln n^*$ values at all fringe positions. The symbol n^* indicates difference between refractive index of the solution at radius x and the background solution. An ideal (constant activity coefficients) uncharged monodisperse solute should give a straight line; an ideal charged monodisperse solute in supporting electrolyte should produce a curve which is concave downward, and a polydisperse solute, a curve which is concave upward. Figure 2 indicates that all solutions, except the unhydrolyzed, are polydisperse.

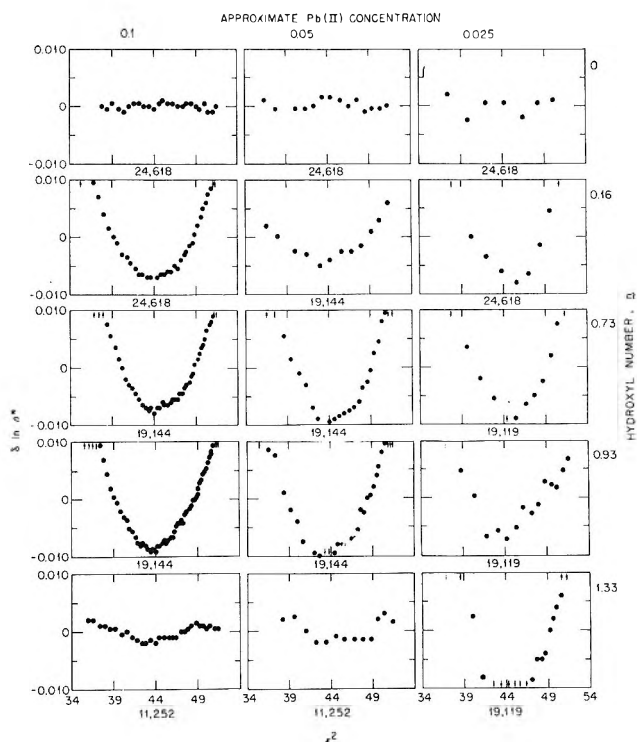


Figure 2. Deviations of $\ln n^*$ from linearity in x^2 . Points are at fringe positions. Arrows indicate points off scale. Numbers under boxes are speed of rotation in r.p.m.

Polydispersity makes determination of the degrees of polymerization by present methods of data analysis somewhat approximate. With ionic polymers, even in the presence of relatively high concentrations of slightly sedimenting supporting electrolyte, sedimentation is a function of charge, as well as of molecular weight. With monodisperse solutes or with a fixed polydisperse distribution, an estimate of charge can be made from the concentration dependence of sedimentation, *i.e.*, by selecting that charge and molecular weight best satisfying all results. In this study, different Pb(II) concentrations are compared at the same value of n . If no two species present have the same hydroxyl number, the reaction to form one from another will involve hydrogen or hydroxyl ions and will, therefore, be dependent on acidity, as well as on total lead concentration. The various species will in such a case be present in approximately (though not exactly) the same concentration ratios, and, consequently, the average degree of polymerization will be relatively

(17) T. F. Young and M. B. Smith, *J. Phys. Chem.*, **58**, 716 (1954).

(18) H. E. Wirth and F. N. Collier, *J. Am. Chem. Soc.*, **72**, 5292 (1950).

(19) H. Kohner, *Z. physik. Chem.*, **B1**, 427 (1928).

(20) R. M. Rush, unpublished results.

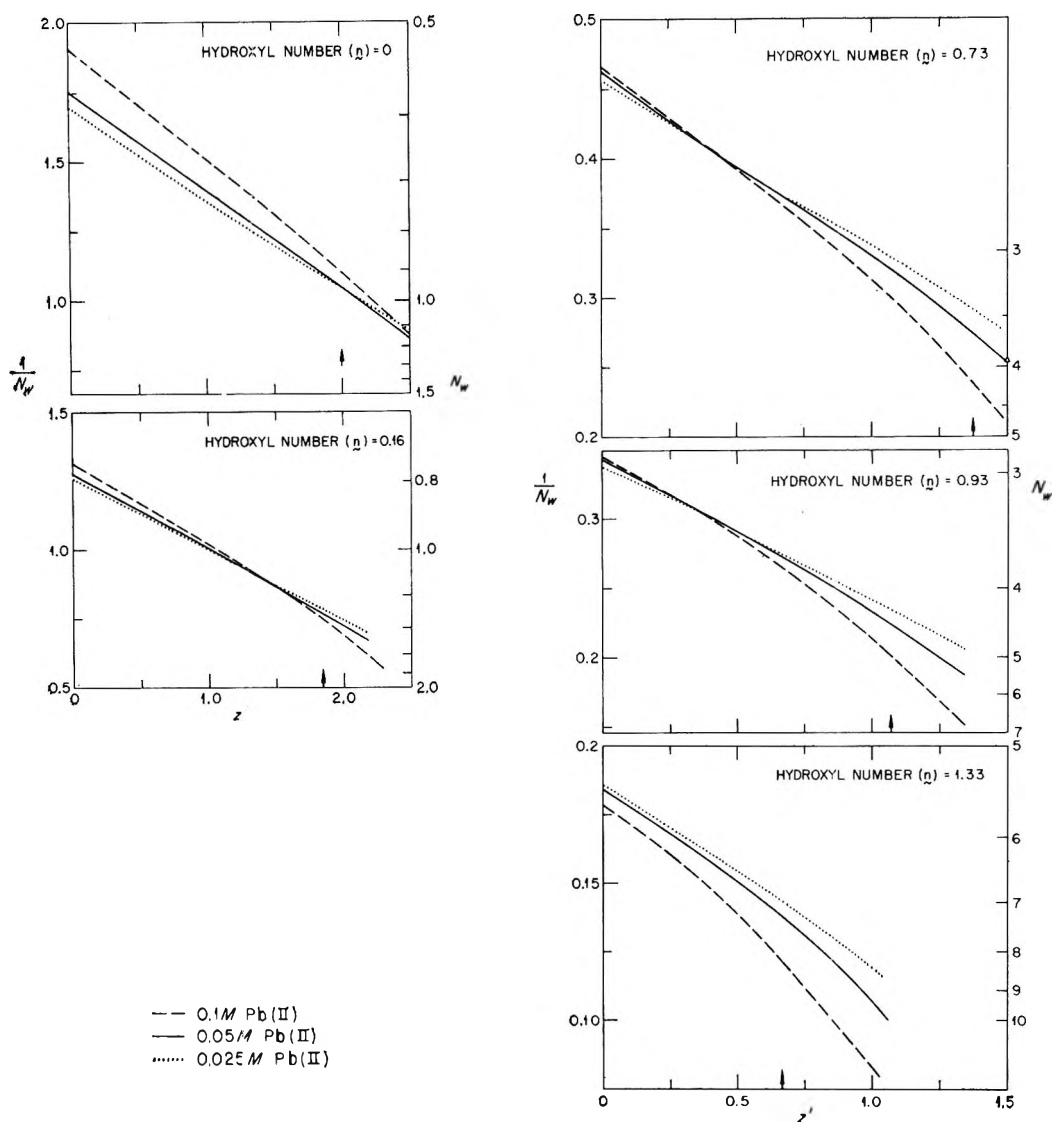


Figure 3. Degrees of polymerization of $\text{Pb}(\text{OH})_n(\text{ClO}_4)_{2-n}$ solutions, computed as a function of assumed charge. All solutions ca. 1 M in NaClO_4 . \uparrow indicates maximum feasible charge ($2 - n$).

independent of $\text{Pb}(\text{II})$ concentration. It will be seen that, of the solutions containing hydrolyzed solute, only at $n = 1.33$ do species having the same hydroxyl number appear to be present in important quantities. Estimate of charge may therefore have some significance. A serious handicap in interpretation of results here, however, is the fact that one deals with a mixture of species having different charges, z' , and different values of refractive index increments and volumes (Figure 1).

Although the values of N_w obtained must, therefore, be viewed with some reservation, similarly handicapped studies in the past, *e.g.*, of $\text{U}(\text{VI})^{11}$ and $\text{Mo}(\text{VI})^{21}$ hydrolysis, have indicated that information gained by the technique can be valuable.²² Similar difficulties

are encountered, and benefits are realized, with light scattering.

The values of degree of polymerization computed as a function of assumed charge per monomer unit (eq. 1) are given for the various degrees of hydrolysis studied

(21) J. Aveston, E. W. Anacker, and J. S. Johnson, *Inorg. Chem.*, **3**, 735 (1964).

(22) It is possible that a more detailed analysis, involving comparison of experimental interference patterns with those computed for postulated hydrolysis schemes, may yield more definitive information. Experimental accuracy is frequently sufficient for such a procedure. We have achieved some success with this approach in a test case ($\text{Bi}(\text{III})$ hydrolysis: D. F. Keeley, J. S. Johnson, Jr., and K. A. Kraus, Abstracts, 141st Meeting of the American Chemical Society, Washington, D. C., March 1962, p. 3-I), but whether assumptions concerning activity coefficients of species can be made with sufficient confidence to make the complex analysis which is necessary worthwhile is at present uncertain.

in Figure 3. The values for maximum charge and for zero charge (0.1 M Pb(II) only) are summarized in Figure 4. It is clear that the average degree of polymerization increases with hydroxyl number, whatever assumption is made concerning perchlorate complexing. For all hydroxyl numbers except 1.33, N_w computed for z' assumed 0 decreases with increasing concentration, a trend indicating that the Pb(II) species are charged. The curves for the various concentrations at each hydroxyl number in Figure 3 are so closely spaced that crossovers should be viewed with caution (especially in view of the assumptions and approximations involved), but the intersections for $n = 0.16, 0.73,$ and 0.93 all occur at values of z' less than the maximum charge, $2 - n$. The polymeric species thus appear to complex with perchlorates to some extent; consequently, the correct value of N_w should be somewhere between that computed on the assumption of zero and maximum charge.

There are no data on which to base estimates of the activity coefficient variations in the hydrolyzed solutions. The values of N_w obtained for unhydrolyzed solutions for $z' = 2$, which may be taken as a rough guide to departures from constancy, are 0.91 for 0.1 M Pb(II), 0.95 for 0.05 M Pb(II), and 0.96 for 0.025 M Pb(II). The degree of polymerization obtained from light scattering³ for $n = 0$ deviates from unity (*ca.* 0.9) by a comparable amount in the same direction.

3. *Discussion.* In Figure 4, we have plotted the degrees of polymerization obtained from light scattering³ by Hentz and Tyree. Their values fall between those computed from ultracentrifugation for $z' = 0$ and for maximum charge. Since the charges inferred by them from turbidities are also less than maximum, the conclusions drawn from the two weight-sensitive methods are in good agreement.

The curve for N_w consistent with Olin's scheme⁶ is also shown in Figure 4. Again, there is agreement within uncertainty between the different methods. Olin postulates two species, $Pb_3(OH)_4^{2+}$ and $Pb_6(OH)_8^{4+}$, having hydroxyl number 1.33, and, consequently, the equilibrium relating them does not depend on acidity. This is consistent with the observation by ultracentrifugation that N_w for $n = 1.33$ computed for zero charge increased with increasing Pb(II) concentration (Figure 3). The changes in Olin's formation quotients between 0.3 and 3 M total perchlorate are in a direction indicating perchlorate complexing by the polymeric Pb(II) species, again in agreement with our ultracentrifuge results.

At the time Olin published his results, computers were apparently not available to him. We have checked his conclusions by a least-squares fit of his

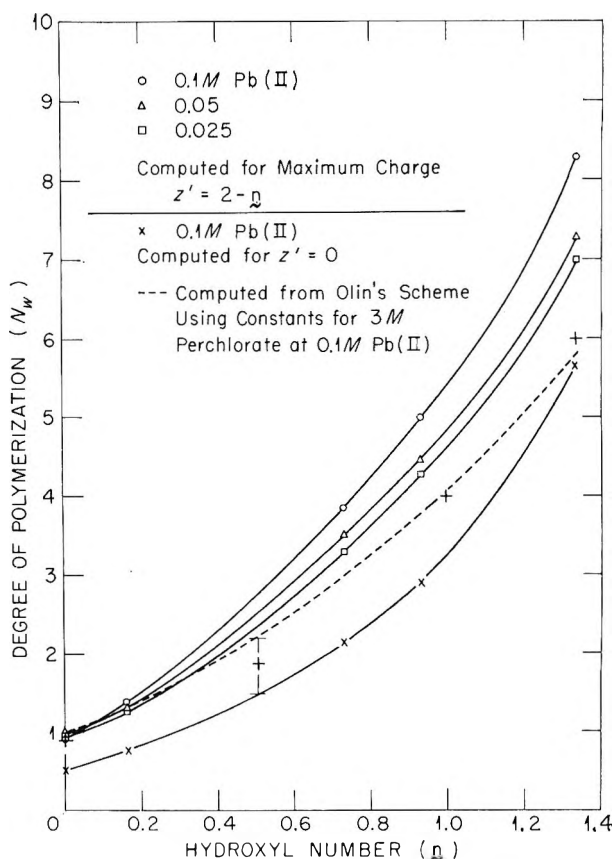


Figure 4. Degree of polymerization of $Pb(OH)_n(ClO_4)_{2-n}$ by equilibrium ultracentrifugation; +, light scattering, ref. 3.

data carried out with programs described elsewhere.²³ With the species he postulated for low Pb(II) concentration (*i.e.*, $Pb_2(OH)^{3+}$ not included) a very satisfactory fit to his data was obtained (<0.005 standard error in n), and the refined values for the formation equilibrium quotients were but little different from the values he gave. Leaving out either of the minor species ($PbOH^+$ or $Pb_3(OH)_4^{2+}$) or both gave appreciably worse agreement. With Faucherre's scheme⁵ convergence was not attained.

Further details of the least-squares analysis, including treatment of the data at high Pb(II) concentrations, may be found in ref. 1b. For present purposes, it is sufficient to say that the hydrolysis of Pb(II) is one of the relatively few cases for which most recent workers seem to agree with respect to the major species. The monomeric and tetrameric $n = 1$ species are postulated by Pederson, Faucherre, Olin, and Hugel, and the tetramer is supported by the weight-sensitive methods. Some doubt concerning the monomeric

(23) R. M. Rush, J. S. Johnson, and K. A. Kraus, U. S. Atomic Energy Commission, ORNL-3278, 1963. General least-squares program: W. R. Busing and H. A. Levy, ORNL-TM-271, 1962.

species is cast by the fact that, on the basis of measurements in concentrated Pb(II) solutions, Olin also postulates $(\text{Pb}_2\text{OH})^{3+}$. In attempts at least-squares analysis, we were unable to obtain convergence with Olin's dilute Pb(II) data⁶ if $\text{Pb}_2\text{OH}^{3+}$ was substituted for PbOH^+ , nor with his concentrated Pb(II) data⁷ with PbOH^+ substituted for $\text{Pb}_2\text{OH}^{3+}$. The tetramer, however, has received strong support from an X-ray diffraction study^{1b} of concentrated Pb(II) solutions of

n ca. 1. Beyond $n = 1$, there is obviously a species of higher molecular weight; Olin's postulated $\text{Pb}_3(\text{OH})_4^{2+}$ and $\text{Pb}_6(\text{OH})_8^{4+}$ are consistent with our results.

Acknowledgment. The authors are indebted to Prof. S. Y. Tyree for many helpful discussions. O. E. Esval is appreciative of support received through an Oak Ridge Graduate Fellowship, administered by the Oak Ridge Institute of Nuclear Studies.

Entropy and Volume Changes on Ionization of Aqueous Acids

by Loren G. Hepler¹

Division of Physical Chemistry, Australian Commonwealth Scientific and Industrial Research Organization, Fishermen's Bend, Melbourne, Australia (Received October 5, 1964)

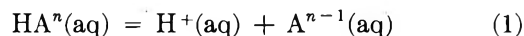
A general linear relation has been observed for changes in entropy and volume ($\Delta\bar{S}_i^\circ$ and $\Delta\bar{V}_i^\circ$) on ionization of aqueous acids. The slope, $(d\Delta\bar{S}_i^\circ/d\Delta\bar{V}_i^\circ) = 1.05 \text{ cal. deg.}^{-1} \text{ cm.}^{-3}$, has been explained in terms of a high pressure value of $(\partial P/\partial T)_V$ for water. The intercept, $\Delta\bar{S}_i^\circ \cong -7 \text{ cal. deg.}^{-1} \text{ mole}^{-1}$ at $\Delta\bar{V}_i^\circ = 0$, has been explained in terms of the usual choice of standard states and the hydration of the proton in aqueous solution.

Several recent studies²⁻⁴ of aqueous acids have shown that consideration of entropies of ionization can yield useful information about the interactions of solute species with solvent and thence also about charge distribution and bonding in the solute species. The solute-solvent interactions that largely account for various acids having different entropies of ionization ($\Delta\bar{S}_i^\circ$) should be expected to cause these acids to have different volume changes on ionization ($\Delta\bar{V}_i^\circ$). One reason for gathering the data summarized later in this paper was to test this expectation. Comparison of $\Delta\bar{V}_i^\circ$ values for several acids (for instance, *m*-nitrophenol and *p*-nitrophenol) shows that for some acids one can at least confirm conclusions already reached from consideration of $\Delta\bar{S}_i^\circ$ values.³ In the process of making detailed comparisons of $\Delta\bar{S}_i^\circ$ and $\Delta\bar{V}_i^\circ$ for various aqueous acids, the more general observations were made that constitute the subject of this paper.

Entropies of ionization ($\Delta\bar{S}_i^\circ$) of aqueous acids

have been calculated from the free energy of ionization and the temperature derivative of the free energy and also from combination of calorimetrically determined enthalpies with free energies. Volume changes ($\Delta\bar{V}_i^\circ$) have been calculated from the effect of pressure on ionization constants and also from results of density measurements. Data for 53 acids are summarized in Figure 1 in the form of a graph of $\Delta\bar{S}_i^\circ$ vs. $\Delta\bar{V}_i^\circ$.

The ionization processes under consideration may be represented by the general equation



(1) U. S. National Science Foundation Senior Postdoctoral Fellow, on leave from Carnegie Institute of Technology, Pittsburgh, Pa.

(2) E. J. King, *J. Am. Chem. Soc.*, **82**, 3575 (1960).

(3) L. P. Fernandez and L. G. Hepler, *ibid.*, **81**, 1783 (1959).

(4) F. J. Millero, J. C. Ahluwalia, and L. G. Hepler, *J. Phys. Chem.*, **68**, 3435 (1964).

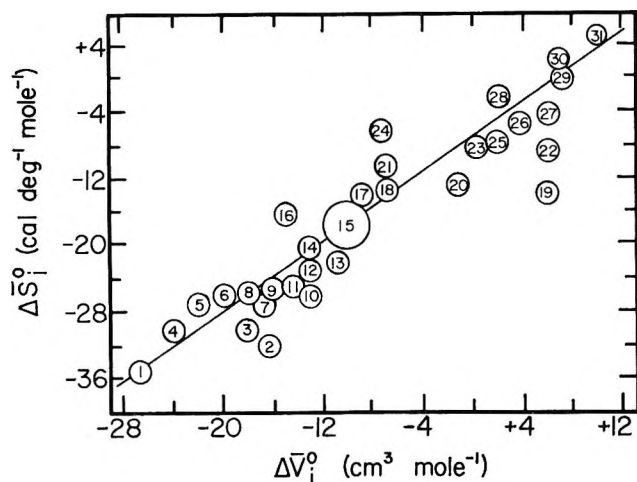
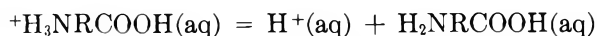
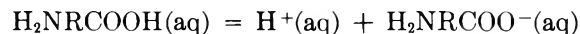


Figure 1. Graph of $\Delta\bar{S}_i^0$ vs. $\Delta\bar{V}_i^0$ for aqueous acids at 25°. Numbered circles correspond to data for ionization of various acids as follows (note that points for several acids fall within some circles): 1, HCO_3^- ; 2, third citric; 3, second malonic; 4, H_2PO_4^- ; 5, H_2O (1 *m*); 6, HSO_4^- ; 7, phenol; 8, trimethylacetic; 9, second oxalic; 10, second succinic; 11, butyric and isobutyric; 12, propionic; 13, acetic; 14, second ϵ -aminocaproic; 15, formic, benzoic, *m*-methoxybenzoic, *p*-methoxybenzoic, *p*-nitrophenol, first succinic, chloroacetic, bromoacetic, lactic, glycolic, and second citric; 16, first phosphoric; 17, *m*-nitrobenzoic and *p*-nitrobenzoic; 18, cyanoacetic; 19, $(\text{CH}_3)_3\text{NH}^+$; 20, second hydroxyproline and second proline; 21, first salicylic and first citric; 22, $(\text{CH}_3)_2\text{NH}_2^+$; 23, second glycine and second alanine; 24, first glycine, first alanine, first hydroxyproline, and first proline; 25, diethylammonium ion and piperidinium ion; 26, $\text{H}_2\text{N}(\text{CH}_2)_2\text{NH}_2^+$; 27, CH_3NH_3^+ and pyridinium ion; 28, ethylammonium ion, propylammonium ion, and first ϵ -aminocaproic acid; 29, NH_4^+ ; 30, anilinium ion; 31, $^+\text{H}_3\text{N}(\text{CH}_2)_2\text{NH}_3^+$. Data are taken from the following: (a) S. D. Hamann, Chapter 7 in "High Pressure Physics and Chemistry," Vol. 2, R. S. Bradley, Ed., Academic Press, New York, N. Y., 1963; (b) W. Kauzmann, A. Bodansky, and J. Rasper, *J. Am. Chem. Soc.*, **84**, 1777 (1962); (c) A. Distèche, *J. Electrochem. Soc.*, **109**, 1084 (1962), and personal communication to S. D. Hamann; (d) H. S. Harned and B. B. Owen, "The Physical Chemistry of Electrolytic Solutions," 3rd Ed., Reinhold Publishing Corp., New York, N. Y., 1958; (e) R. A. Robinson and R. H. Stokes, "Electrolyte Solutions," Butterworth and Co., Ltd., London, 1959; (f) L. P. Fernandez and L. G. Hepler, *J. Phys. Chem.*, **63**, 110 (1959); (g) J. T. Edsall and J. Wyman, "Biophysical Chemistry," Vol. 1, Academic Press, New York, N. Y., 1958; (h) Z. L. Ernst, R. J. Irving, and J. Menashi, *Trans. Faraday Soc.*, **60**, 56 (1964); (i) R. G. Bates and H. B. Hetzer, *J. Phys. Chem.*, **65**, 671 (1961); (j) Ref. 2 and 3 of main text.

where n is zero or an integer indicating the charge on the acid. In the case of amino acids, the first ionization refers to



and the second ionization to



Although several systematic deviations (for instance, the methylamines) from the straight line in Figure 1 are obvious and worthy of detailed consideration, there is a remarkable general correlation of $\Delta\bar{S}_i^0$ with $\Delta\bar{V}_i^0$ for a large number of quite diverse acids. The slope of the straight line in Figure 1 is $1.05 \text{ cal. deg.}^{-1} \text{ cm.}^{-3}$ and the intercept is $\Delta\bar{S}_i^0 \cong -7 \text{ cal. deg.}^{-1} \text{ mole}^{-1}$ at $\Delta\bar{V}_i^0 = 0$. These quantities are interpreted as follows.

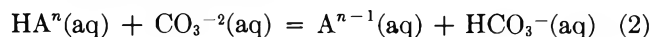
The Maxwell relation

$$(\partial S/\partial V)_T = (\partial P/\partial T)_V$$

suggests that the slope $(\partial\Delta\bar{S}_i^0/\partial\Delta\bar{V}_i^0)_T$ is related to an appropriately chosen $(\partial P/\partial T)_V$. Except for a factor related to standard states that is discussed below, entropies of ionization are chiefly determined by effects of the various solute species on the orderliness of arrangement of nearby water molecules, and $\Delta\bar{V}_i^0$ values are similarly determined by the related space occupied by the water molecules near the various solute species. Since a variety of evidence indicates that the effective pressure near ions or polar solute molecules in water is quite high (of the order of 10^4 atm.), we might expect the slope of the line in Figure 1 to be approximately equal to $(\partial P/\partial T)_V$ for H_2O at a suitable high pressure.

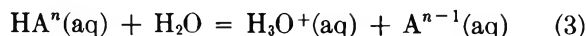
Some values of $(\partial P/\partial T)_V$ of water, taken from Dorsey's compilation,⁵ are shown in Figure 2. A value of $(\partial P/\partial T)_V$ appropriate to the high effective pressures near solute species is apparently about 40–45 atm. deg.^{-1} . Exact agreement between $(\partial\Delta\bar{S}_i^0/\partial\Delta\bar{V}_i^0)_T$ and $(\partial P/\partial T)_V$ may be obtained by taking the effective $(\partial P/\partial T)_V = 43 \text{ atm. deg.}^{-1} = 1.05 \text{ cal. deg.}^{-1} \text{ cm.}^{-3}$.

Now consider the intercept, $\Delta\bar{S}_i^0 \cong -7 \text{ cal. deg.}^{-1} \text{ mole}^{-1}$ at $\Delta\bar{V}_i^0 = 0$. Instead of comparing $\text{HA}^n(\text{aq})$ with water as in reaction 1, we might choose another reference system and consider



or some other reaction series. The best straight line through the resulting $53 - 1 = 52$ points has the same slope as the line in Figure 1 and passes through the origin where $\Delta\bar{S}_i^0 = 0 = \Delta\bar{V}_i^0$. Since both $\Delta\bar{S}_i^0$ and $\Delta\bar{V}_i^0$ for symmetrical reactions like (2) are determined almost entirely by solute-solvent interactions, it is expected that the graph of $\Delta\bar{S}_i^0$ vs. $\Delta\bar{V}_i^0$ should go through the origin, as it does.

Reaction 1 might be rewritten as



(5) N. E. Dorsey, "Water-substance," Reinhold Publishing Corp., New York, N. Y., 1940.

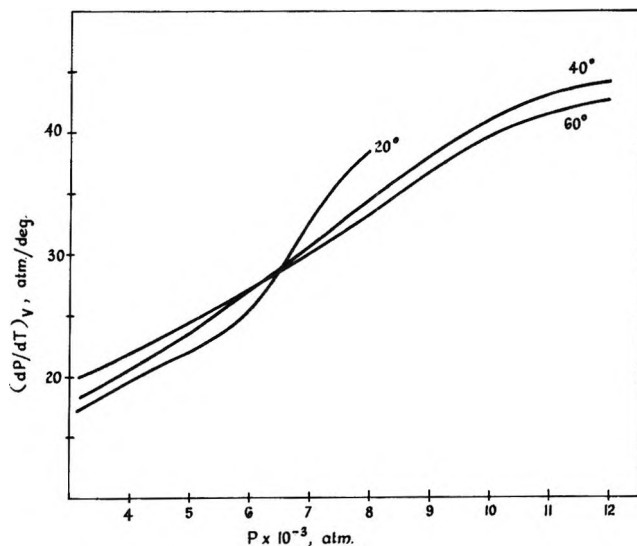


Figure 2. Graph of $(\partial P/\partial T)_v$ for liquid water vs. pressure.

to make it more explicitly symmetrical. Standard states for the species in (3) are ordinarily taken to be the hypothetical 1 *m* solution for $\text{H}_3\text{O}^+(\text{aq})$, $\text{A}^{n-1}(\text{aq})$, and $\text{HA}^n(\text{aq})$ and the pure liquid for H_2O . If we should take the standard state of H_2O to be 1 *m*, then all conventional $\Delta\bar{S}_i^\circ$ values (such as those in Figure 1) must be increased by $R \ln 55.5 = 8.0 \text{ cal. deg.}^{-1} \text{ mole}^{-1}$. Thus the intercept value of $\Delta\bar{S}_i^\circ \cong -7$ at $\Delta\bar{V}_i^\circ = 0$

in Figure 1 is seen to arise from the conventional choice of the pure liquid as solvent standard state.

It is also of interest to consider the intercept in relation to the state of the proton in aqueous solution. The above simple interpretation of the intercept in terms of $\text{H}_3\text{O}^+(\text{aq})$ may be taken as evidence that protons in aqueous solution are best described as hydrated H_3O^+ ions, with the implication that the hydrations of a H_3O^+ ion and a water molecule in liquid water are about the same. This latter implication is supported by the accumulation of evidence that absolute values of the standard partial molal entropy and also molal volume of $\text{H}^+(\text{aq})$ are both only slightly negative.

We might also consider the proton as being hydrated by *x* water molecules, as represented by $\text{H}(\text{H}_2\text{O})_x^+(\text{aq})$. Then, taking the principal species in liquid water to be *x*-mers, we could write (3) as



On this basis, the effect on $\Delta\bar{S}_i^\circ$ of changing the standard state of water from the pure liquid to a 1 *m* solution of $(\text{H}_2\text{O})_x$ is $R \ln (1000/18x)$, from which we calculate shifts of 8.0, 6.7, and 5.2 $\text{cal. deg.}^{-1} \text{ mole}^{-1}$ when *x* = 1, 2, and 4, respectively.

Acknowledgments. The author thanks Dr. S. D. Hamann and Dr. J. A. Barker for their hospitality and many helpful discussions.

Micelle Formation in Concentrated Sulfuric Acid as Solvent

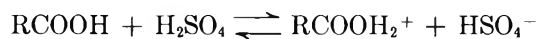
by Joseph Steigman and Norman Shane

Department of Chemistry, Polytechnic Institute of Brooklyn, Brooklyn, New York (Received October 10, 1964)

Micelle formation in concentrated sulfuric acid solutions by long-chain fatty acids (which form cationic bisulfates) was studied by means of surface tension and light scattering measurements. It was found that micelle formation in 95% sulfuric acid took place at a higher concentration than in water, that 5 *M* potassium bisulfate had a small or negligible effect, and that water (presumably present as hydronium bisulfate) had a very marked effect, lowering the c.m.c. It was concluded that electrical repulsion as a factor in micelle formation was less important in sulfuric acid than the organization of the structure of the solvent, and that water (as hydronium bisulfate) was an order-destroying substance in that medium. It was suggested that the organization of the solvent structure might also be involved in micelle formation by soaps in water, and that the effect of added electrolytes in lowering the c.m.c. of soaps might be partly electrical and partly order-destroying. If so, order-forming salts like quaternary ammonium compounds should raise c.m.c. values of cationic soaps in water.

At present, there is no theory of micelle formation which is sufficiently comprehensive to include all the varieties of molecular structure for which micelle formation has been reported in water.¹ For the particular case of straight-chain paraffin compounds carrying a single charged head, Debye formulated a theoretical basis for micelle formation in water.² The onset of micelles was ascribed to the interplay between the long-range repulsive electrostatic forces of the charged heads and the short-range attractive van der Waals forces exerted by the hydrocarbon tails for each other. The electrical work performed in assembling the micelle was calculated on the assumption that the effective dielectric constant would lie between that of the solvent and that of a hydrocarbon. The work gained by bringing together the hydrocarbon portions was assumed to vary linearly with the number of methylene groups in the hydrocarbon tail. The role of the solvent was considered to be solely electrical, in that it modified the work done against electrostatic repulsion between like charges when the micelle was formed. In a solvent with a higher dielectric constant than water, the critical micelle concentration of a simple soap should be lower than in water, since the electrical work performed against repulsion should be decreased, and (presumably) the van der Waals exchange forces should not be affected. The new solvent must be in-

organic and should resemble water in its general solvent properties. Concentrated sulfuric acid is such a solvent. The present work was undertaken in order to study micelle formation in concentrated sulfuric acid solution for a number of straight-chain carboxylic acids. The very high acidity of concentrated sulfuric acid causes weak carboxylic acids to behave like bases³



McCulloch⁴ found that higher fatty acids in cold concentrated sulfuric acid gave soap-like solutions with persistent foams. In this respect sulfuric acid appears to resemble water, that is, there is apparently an acidophobic tail and an acidophilic head in the soap molecule, corresponding to the hydrophobic and hydrophilic portions encountered in water.

Micelle formation was detected by measuring the surface tension of sulfuric acid solutions of fatty acids at different solute concentrations. These data were supplemented by observations of light scattering by several of the systems studied.

- (1) W. Philippoff, *Discussions Faraday Soc.*, **11**, 96 (1951).
- (2) P. Debye, *J. Phys. Colloid Chem.*, **53**, 1 (1949).
- (3) A. Hantzsch, *Z. physik. Chem.*, **65**, 41 (1909).
- (4) L. McCulloch, *J. Am. Chem. Soc.*, **68**, 2735 (1946).

Experimental

Materials. Sulfuric acid was pure Merck reagent grade, ACS specification for microanalysis. Acidimetric analysis showed that it was 95.01 (± 0.05)% by weight in H_2SO_4 . It was recrystallized twice and reanalyzed. It was found that surface tension measurements of lauric acid and stearic acid solutions in the unpurified acid were virtually identical with those of the corresponding solutions prepared from the recrystallized acid. Accordingly, the Merck acid was used without further purification for most of the experiments. Dilutions with distilled water produced 85.00 (± 0.05)% acid, and 82.00 (± 0.05)% acid.

Fuming sulfuric acid was obtained from the J. T. Baker Chemical Co. It was added to the Merck acid to prepare sulfuric acid solutions of acid content greater than 95%. Analysis showed that the more acid solutions were 95.51 (± 0.05)% by weight, 96.20 (± 0.05)% by weight, and 97.31 (± 0.05)% by weight. These acids were used without further purification, since two recrystallizations of the 97.3% acid did not affect the surface tension of solutions of lauric and stearic acids.

Caprylic and capric acids were chemically pure, purest grade, obtained from Eastman Organic Chemicals, Distillation Products Industries. Lauric, myristic, palmitic, and stearic acids were chemically pure products of the Fisher Scientific Co. The boiling points of the caprylic and capric acids and the melting points of the other acids agreed closely with those reported in the "International Critical Tables."

Other chemicals were of reagent grade and were used without further purification.

Stability and Preparation of Sulfuric Acid Solutions of Fatty Acids. Fatty acid solutions in sulfuric acid of concentration higher than 97.3% by weight turned brown quickly, indicating decomposition. Accordingly, 97.3% sulfuric acid was the most concentrated sulfuric acid which was used. The surface tension measurements were made less than 1 day after the preparation of the solution, in order to minimize possible decomposition. Fatty acid solutions in more dilute acid remained colorless for at least 2 days. The solid fatty acids were recoverable without change in the melting point on dilution of their sulfuric acid solutions with water after 2 days.

Each solution whose surface tension was measured was prepared individually in glass-stoppered bottles. The various solutions were made up on a molar basis.

Apparatus. Surface tension measurements were made at room temperature (27°) with a Cenco Du Nouy tensiometer equipped with a 4-cm. ring. After each measurement the ring was cleaned with cleaning

solution and distilled water, and was then heated until it was cherry red. The experimental precautions suggested for this instrument by Harkins⁵ were consistently observed in this work. Frequent measurements of the surface tension of distilled water were made, and always showed readings of 72.2 dynes/cm.

A petri dish was used to hold the different solutions during the measurements. After each determination, it was cleaned with cleaning solution, then with distilled water, and was dried at 150°. A larger inverted dish with a small hole bored in the bottom served to cover the test solution, limiting the access of moisture to the sample. Control tests showed that if measurements were made within 15 sec. of solution exposure to air, the readings could be reproduced on successive samples. If the samples were exposed to air for some minutes, the surface tension decreased noticeably.

If samples were quickly measured, placed in a desiccator, and measured again, the readings were constant. A so-called dry beaker was constructed according to Kunzler's recommendation⁶ and a series of measurements was carried out in an atmosphere of dried nitrogen gas. However, these were discontinued, since measurements made in the dry beaker were not significantly different from those made within 15 sec. of sample exposure to air.

Light scattering measurements were made with a Brice-Phoenix light scattering photometer, using a special turbidity cell which consisted of a closed container with Teflon grease surrounding its penny-head stopper. Measurements were made at 4360 Å. on solutions of lauric and stearic acids in 95% sulfuric acid, as well as on the solvent itself. The solutions and solvent prior to measurement were suction-filtered in a dry nitrogen atmosphere through glass wool laid over a sintered glass filter.

Estimation of the Critical Micelle Concentration. Surface Tension. For each fatty acid a series of solutions of different concentrations was prepared, and the surface tension was measured. Additional solutions were prepared if they were needed. For stearic acid, a total of six series, each series with six solutions, was run. The critical micelle concentration was determined by an *ad hoc* procedure. Preliminary graphical plots of the surface tension (in dynes/cm.) against the log of the fatty acid concentration (expressed initially as grams of fatty acid per 100 ml. of 95% sulfuric acid) showed that there was an approximately linear decrease followed by readings which were independent of

(5) W. D. Harkins and H. F. Jordan, *J. Am. Chem. Soc.*, **52**, 1751 (1930).

(6) J. E. Kunzler, *Anal. Chem.*, **25**, 93 (1953).

the soap concentration. The curves resembled those found in water⁷ except that there was no minimum. It was assumed that the critical micelle concentration was to be found at the intercept of two straight lines—the first of negative slope, before the c.m.c., and the second of zero (or almost zero) slope, after the c.m.c. This intercept was determined by formulating the equation for the first straight line by least squares, averaging the approximately constant surface tension values after the c.m.c., and from the equation for the first straight line determining the soap concentration corresponding to the averaged limiting value. This procedure was followed for all solutions except those in sulfuric acid more dilute than 95% and those in 95% H₂SO₄ containing 5 M KHSO₄, for which the intercepts were determined graphically. Table I shows some typical values for stearic acid in 95.0% H₂SO₄.

Table I: Surface Tension of Stearic Acid Solutions in 95% Sulfuric Acid at 27°, Series C

Concn. of stearic acid; g./100 ml. of H ₂ SO ₄	Surface tension, dynes/cm.
0.0006	57.02
0.0030	50.89
0.0060	44.76
0.0090	44.15
0.0120	41.25
0.0150	41.25

Light Scattering. The experimental terms of the absolute turbidity equation of Debye² were used for the determination of the c.m.c. These are found in the difference

$$F \frac{G_{90^\circ}}{G_{0^\circ}} - F^0 \frac{G_{90^\circ}^0}{G_{0^\circ}^0}$$

Here G_{90° refers to the galvanometer reading of the beam at 90° for the sample, G_{0° gives the galvanometer reading for the undeviated beam (plus neutral filters), F is the product of transmittances of the neutral filters used in the determination of the ratio, and the same terms with the zero superscripts refer to the same measurements for the pure solvent. It was assumed that the c.m.c. was to be found in the region of abrupt change of turbidity with concentration. Table II gives the experimental values for lauric acid in 95.0% H₂SO₄, and Table III shows the agreement between results obtained from surface tension measurements and from light scattering. It can be seen that there is a fair measure of agreement between the two methods.

Table II: Light Scattering at 4360 Å. by Lauric Acid in 95% Sulfuric Acid

Lauric acid, g./100 ml. of H ₂ SO ₄	$\left(F \frac{G_{90^\circ}}{G_{0^\circ}} - F^0 \frac{G_{90^\circ}^0}{G_{0^\circ}^0} \right) \times 10^{-1}$
1.0012	0.026
1.0755	0.033
1.1802	0.049
1.2125	0.112
1.2725	0.292
1.2775	0.301
1.2825	0.309
1.2925	0.327
1.3002	0.354
1.3487	0.382

Table III: C.m.c. for Lauric Acid and for Stearic Acid in 95% Sulfuric Acid

Method	Lauric acid c.m.c., g./100 ml.	Stearic acid c.m.c., g./100 ml.
Surface tension	1.11	0.013
Light scattering	1.18–1.21	0.0089–0.0093

Results and Discussion

Table IV shows the results of the surface tension determinations of the c.m.c. for the various fatty acids in a number of sulfuric acid–water solutions. The values in water for the potassium salts of the same carboxylic acids are listed for comparison. This comparison is assumed to be a valid one since (in water) the number of carbon atoms in the hydrocarbon portion of a group of related surface-active agents has been shown to be the most important factor in determining the c.m.c., and the nature of the charged head is much less important.

It is evident that micelle formation in 95% sulfuric acid takes place at a higher molar concentration than in water (except for stearic acid), and that the c.m.c. increases as the sulfuric acid content increases. If the dielectric constant of the solvent is an important factor in determining the formation of micelles,² then micelle formation in sulfuric acid should occur at a lower concentration than in water. Undoubtedly, there is a markedly decreased electrostatic repulsion between like ions in sulfuric acid. However, this factor, which would lower the c.m.c., must be less important than some other factors which raise the c.m.c. values.

One such factor would be a change in the van der Waals or exchange forces between paraffin chains be-

(7) J. Powney and C. C. Addison, *Trans. Faraday Soc.*, **33**, 1243 (1937).

Table IV: C.m.c. of Soaps in Water and of Fatty Acids in Various Sulfuric Acid Solutions (the latter at 27°) (moles/l.)

No. of C atoms	C.m.c. in H ₂ O at 25° ^a	C.m.c. in 82% H ₂ SO ₄	C.m.c. in 85% H ₂ SO ₄	C.m.c. in 95% H ₂ SO ₄	C.m.c. in 5 M KHSO ₄ in 95% H ₂ SO ₄	C.m.c. in 95.5% H ₂ SO ₄	C.m.c. in 96.2% H ₂ SO ₄	C.m.c. in 97.3% H ₂ SO ₄
8	0.39		~0.14	None to 3.4 M				
10	0.098		~0.024	None to 1.2 M				
12	0.0255	<0.002		0.057	0.055			None to 0.126 M
14	0.0066			0.013				
16	0.0018 (35°)			0.0028				
18	0.00045 (45°) ^b			0.00045	0.00028	0.00063	0.0011	0.0019

^a H. B. Klevens, *J. Phys. Colloid Chem.*, **52**, 130 (1948). ^b H. B. Klevens, *J. Am. Oil Chemists' Soc.*, **30**, 74 (1953).

cause of interaction between them and sulfuric acid. However, Gillespie and White⁸ concluded from a proton magnetic resonance study of acetone in sulfuric acid solution that any direct interaction of the methyl group with the solvent was small.

Micelle formation in water results at least in part from the shrinkage of the paraffin-water interface, with a loss in surface free energy. The latter is given by the product of the paraffin chain area and the interfacial tension between the hydrocarbon and water. The interfacial tension between *n*-octane and water at room temperature is 50.58 dynes/cm.⁹ The values for several other paraffin compounds are not very different. In general for nonpolar liquids which are quite insoluble in water, such as the paraffin hydrocarbons and carbon tetrachloride, the interfacial tension can be taken approximately as the difference between the surface tensions of the pure liquids in air. For more polar organic liquids, the difference in surface tensions of the saturated solutions (water in organic liquid and organic liquid in water) must be taken. The interfacial tension between paraffin hydrocarbons and sulfuric acid has not been reported. The assumption is made here that the paraffin hydrocarbons are quite insoluble in concentrated sulfuric acid, and behave at the acid-hydrocarbon interface much as they do in water. With this hypothesis, the interfacial tension of hydrocarbon-95% sulfuric acid will be equal to the difference in their air surface tensions—approximately 57 dynes/cm. less 22 dynes/cm.,⁹ or about 35 dynes/cm. This is less than the value for water, and on this basis it is possible to conclude that c.m.c. values should be higher in sulfuric acid than in water. However, when the concentration of sulfuric acid is increased from 95.0% to 97.2%, there is a decrease in surface tension of about 4%,⁹ yet the c.m.c. of stearic acid increases by more than 400%. It is thus unreasonable to ascribe the c.m.c. differences between

water and sulfuric acid to the interfacial tension differences alone.

There is an additional factor which may account for some of the difference between the two solvents. Aqueous solutions of the lower paraffins have negative enthalpies and entropies of solution.¹⁰ These unusual thermodynamic properties are explicable in terms of the hypothesis advanced by Frank and Evans¹¹ regarding the ability of liquid water to organize ordered structures around nonpolarizable solutes. In the solid state highly organized water structures have been found in clathrates of hydrocarbons and of rare gases,¹² as well as in the hydrates of quaternary ammonium salts.¹³ Some question has been raised about whether long paraffin chains show the same behavior in water as the short ones.¹⁴ If they do, that is, if the entropy of solution is still negative for a long chain, then there would be an increase in entropy accompanying the formation of micelles and this would constitute a driving force for aggregation. It can be safely assumed that liquid sulfuric acid is much more highly organized than water. It certainly possesses a very large amount of structure, maintained by very strong hydrogen bonds.¹⁵ As a consequence, highly ordered solvent structures would form around the paraffin chains of

(8) R. J. Gillespie and R. F. M. White, *Can. J. Chem.*, **38**, 1371 (1960).

(9) T. F. Young and W. D. Harkins in "International Critical Tables of Numerical Data, Physics, Chemistry, and Technology," Vol. IV, McGraw-Hill Book Co., Inc., New York, N. Y., 1928, p. 263.

(10) W. F. Claussen and M. F. Polglase, *J. Am. Chem. Soc.*, **74**, 4817 (1952).

(11) H. S. Frank and M. W. Evans, *J. Chem. Phys.*, **13**, 507 (1945).

(12) M. V. Stackelberg, *Naturwiss.*, **36**, 327 (1949).

(13) R. McMullan and G. A. Jeffrey, *J. Chem. Phys.*, **31**, 1231 (1959).

(14) W. Kauzmann, *Advan. Protein Chem.*, **14**, 43 (1959).

(15) R. J. Gillespie, E. D. Hughes, and C. K. Ingold, *J. Chem. Soc.*, 2473 (1950).

fatty acids with greater ease in sulfuric acid than in water, and the gain in entropy on micelle formation would tend to be smaller in sulfuric acid than in water, with higher c.m.c. values than in water. This is a qualitative picture, which does not account for all the differences in micelle formation between the two solvents. Thus, in water the ratio of c.m.c. values is constant for two successive members of a homologous series. In 95% sulfuric acid the ratio increases from lauric acid to stearic acid, but it also increases from lauric acid to caprylic and capric acids. It is possible that capric and caprylic acids salt themselves in; that is, micelle formation would occur at a rather high solute concentration (if it did at all), and the degree of organization of the sulfuric acid would be enhanced by the solute, making micellization even more difficult. It is also possible that the solvent cannot organize itself as successfully around very long chains.

Table IV shows that 5 *M* potassium bisulfate in 95% sulfuric acid has virtually no effect on the c.m.c. of lauric acid, and decreases that of stearic acid by one-third. This is in marked contrast to micelle formation in water, where the c.m.c. is reduced by almost one order of magnitude by salt solutions which are much less concentrated than 5 *M*.¹⁶ It is also in marked contrast to the effect of water added to concentrated sulfuric acid. In 95% sulfuric acid the water concentration is approximately 5.1 *M*, and in 97.3% it is about 2.8 *M*. The c.m.c. of stearic acid increases from 0.00045 to 0.0019 *M* in this interval of water concentration, and that of lauric is more than doubled (the actual value was not determined). An increase in the water concentration to 17.5 *M* (82% acid) decreased the c.m.c. of lauric acid from 0.057 *M* in 95% acid to less than 0.002 *M* in 82% acid. In 14.8 *M* water (85% acid), both capric and caprylic acid formed micelles, unlike their behavior in 95% sulfuric acid.

This marked difference in behavior between potassium bisulfate and water cannot be explained by electrostatic interionic effects, since there should be very little difference between potassium and hydronium ions in a medium with a high dielectric constant. It is possible that the difference is due to water itself. In sulfuric acid it is largely converted to hydronium bisulfate, but it is a surprisingly weak base in this respect. Gillespie has estimated that the formation constant of hydronium bisulfate from water is 1.2 moles/kg. at room temperature.¹⁷ It is a weaker base in sulfuric acid than either acetone or acetic acid. Its weak basicity is ascribed to its ability to substitute for a sulfuric acid molecule in the hydrogen-bonded structure of the liquid acid without disrupting that structure. This implies that the hydronium ion does not

fit into the solvent structure as well as the water molecule. The cryoscopic behavior of hydronium bisulfate in sulfuric acid tends to bear this out. It is quite different from that of the alkali bisulfates.¹⁸ The osmotic coefficients (ϕ) of all bisulfates are described by the equation

$$\phi = 1 + \phi_{e1} + b\sum m_i$$

in which ϕ_{e1} is the coefficient calculated from the Debye-Hückel theory, b is an empirical constant, and m_i is the molality of the i th species. The last term, $b\sum m_i$, is interpreted as an indication of ion-solvent interaction. For most bisulfates the osmotic coefficient decreases slightly and then increases with increasing ionic strength. This has been interpreted as a strengthening of the solvent structure. For hydronium bisulfate, the coefficient decreases steadily with increasing ionic strength. Gillespie and his co-workers concluded that it was either an incompletely dissociated compound in sulfuric acid, or else that the cation was breaking up the solvent structure. Conductance studies did not support the hypothesis of incomplete dissociation,¹⁹ but these workers argued that a small ion like the hydronium ion was incapable of breaking solvent structures. They therefore decided that cryoscopic measurements do not yield the same kind of information about these solutions as conductivity measurements, or else that the incomplete dissociation of hydronium bisulfate may involve the formation of a strongly hydrogen-bonded ion pair whose solutions may have a very high conductance.

The results which are reported in the present paper suggest very strongly that the hydronium ion is an order-destroying ion in sulfuric acid, and that potassium bisulfate has a small effect on the sulfuric acid structure. The potassium ion might tend to disrupt the hydrogen-bonded structure, but the bisulfate ion can fit into the structure quite easily, and may well increase the over-all hydrogen bonding, like the hydroxyl ion in water.²⁰ There would be only a small net effect on micelle formation. On the other hand, if the hydronium ion strongly disrupted the sulfuric acid structure, an increase in the water concentration would result in lower c.m.c. values. The entropy associated with organizing the solvent structure around the paraffin chains would become more negative, and the entropy

(16) See footnote *a* in Table IV.

(17) R. J. Gillespie, *J. Chem. Soc.*, 2493 (1950).

(18) S. J. Boss, R. J. Gillespie, and J. V. Oubridge, *ibid.*, 837 (1960).

(19) R. H. Flowers, R. J. Gillespie, E. A. Robinson, and C. Solomons, *ibid.*, 4327 (1960).

(20) R. W. Gurney, "Ionic Processes in Solution," McGraw-Hill Book Co., Inc., New York, N. Y., 1953.

change resulting from micelle formation would be more positive.

At present these conclusions can be applied only qualitatively to the formation of micelles. It is to be expected that electrostatic factors will be more important in water than in sulfuric acid, and that order-disorder effects will be less important. In this connection, the lowering of c.m.c. values in water by added electrolyte has been analyzed theoretically in terms of the action of the gegenions and simi-ions on the electrical potential of the micelle surface.²¹ It is probable that the effect of the added electrolyte is only partly electrostatic. Thus, it has been reported²² that the c.m.c. of sodium dodecyl sulfate in water is lowered to different extents by alkali chlorides, cesium being the most effective, and lithium the least. Lange²³ has found that the c.m.c. of dodecyl pyridinium chloride is lowered to different extents by sodium halides, the effect decreasing in the order iodide, bromide, chloride (the familiar Hofmeister series). With both alkali cations and halide anions the order of increasing

efficiency in micellization is the order of increasing disruption of the solvent structure.^{11,20} This suggests that an order-forming ion like a quaternary ammonium ion would have a smaller effect on micelle formation than the order-destroying ions and might even raise the c.m.c. value above that found in water. The surfactant and the order-forming ion would have to bear the same charge, since quaternary ammonium ions have been found to interact strongly with a negatively charged soap,²² probably because of coulombic attraction coupled with exchange forces. That is, a cationic surfactant in the presence of a lower quaternary ammonium halide should show a higher c.m.c. value than in water. Similarly, an anionic soap in a solution of a lower alkyl sulfonate should form micelles with more difficulty than in water.

(21) K. Shinoda, T. Nakagawa, B.-I. Iamamushi, and T. Isemura, "Colloidal Surfactants," Academic Press, New York, N. Y., 1963.

(22) E. D. Goddard, O. Harva, and T. G. Jones, *Trans. Faraday Soc.*, **49**, 980 (1953).

(23) H. Lange, *Kolloid-Z.*, **121**, 66 (1951).

The Reactivity of Metal Ions and Some Oxy Anions toward Hydrated Electrons¹

by M. Anbar² and Edwin J. Hart

Chemistry Division, Argonne National Laboratory, Argonne, Illinois (Received October 12, 1964)

The reactivity of metal ions and their complexes with hydrated electrons has been investigated by pulse radiolysis. Ligands have a profound effect on the reactivity of complex ions. The sequence of efficacy of ligands to interact with e_{aq}^- and transport the electron to the central atom is: $OH^- < CN^- < NH_3 < H_2O < F < Cl < I$. This sequence parallels their ability to channel an electron in outer-sphere oxidation-reduction processes.

Introduction

Hydrated electrons, e_{aq}^- , interact with various inorganic species³⁻⁶ at rates ranging up to $10^{11} M^{-1} \text{sec.}^{-1}$. These inorganic reactants include not only the well-known oxidizing agents such as Co(III), MnO_4^- , or H_2O_2 , but Zn(II), Cd(II), and Ni(II) as well. In addition, all of the rare earth ions react with e_{aq}^- at rates $> 10^8 M^{-1} \text{sec.}^{-1}$. Recently the

reactivity of the hydrated electrons toward different organic reactants has been correlated with their electro-

(1) Based on work performed under the auspices of the U. S. Atomic Energy Commission.

(2) On sabbatical leave from the Weizmann Institute of Science, Rehovoth, Israel.

(3) S. Gordon, E. J. Hart, M. S. Matheson, J. Rabani, and J. K. Thomas, *J. Am. Chem. Soc.*, **85**, 1375 (1963).

philic properties.^{7,8} In contrast to the simple electron-transfer processes possible in electrophilic organic reactions, the reduction of inorganic species requires, in many cases, extensive rearrangements in the outer coordination sphere. This factor, as well as the availability of an electrophilic center on the molecule, must affect the rate of the e_{aq}^- reactions with inorganic species. A study of the rate of reaction of inorganic species with e_{aq}^- is expected to contribute to the quantitative evaluation of these factors, which determine the reactivity of the ion in many oxidation-reduction processes.

Experimental

The rates of e_{aq}^- reactions were determined by the pulse radiolysis technique. The experimental details and methods of estimating errors have been described.⁵⁻⁷ Chromous ions were produced by electrolytic reduction of $Cr(ClO_4)_3$, and its oxygen-free solutions were stored at 5° in syringes. All other reagents were of analytical grade and they were used without further purification: $AgClO_4$, $Al(ClO_4)_3$, $Cr(ClO_4)_3$, $Pb(ClO_4)_2$ —G. F. Smith; $ZnSO_4$, $SnCl_2$, $KBrO_3$, KIO_3 , $NaIO_4$, $CdSO_4$ —Baker Analyzed; KF —Baker and Adamson; KCN —Mallinckrodt; K_2PdCl_4 , $K_2Pd(CN)_4$, $K_2Pt(CN)_4$ —Fluka Puriss; K_2PtCl_4 —Fluka Purum; $K_3Co(CN)_6$, $KAsF_6$ —Alpha Inorganics, Inc. All irradiated solutions contained 0.001 *M* methanol in order to scavenge the OH radicals which might compete for e_{aq}^- . pH values were determined with a Radiometer Type 4 pH meter. The complexes of the halide and cyanide ions were examined in 0.1–1.0 *M* solutions of these ions. At these concentrations, the “spontaneous” rate of disappearance of e_{aq}^- was faster than in dilute solutions. The rate constants were, however, corrected for this factor.

Results

The reactivity of e_{aq}^- with metal ions containing several ligands has been studied in the pH range from 7 to >14. No attempt has been made to measure rate constants in the acid range because of the competition of H^+ for e_{aq}^- . In Table I, the pH dependence of the reactivity of Al(III), Cr(III), Zn(II), Cu(II), Sn(II), and Pb(II) values is given for neutral and alkaline pH values. Table I shows that the effect of pH on this series of ions differs significantly from case to case. Whereas there is a very slight change in the reactivity of Sn(II) and Pb(II) and a relatively small change in the case of Cu(II), a loss in reactivity of over two orders of magnitude takes place in the case of Cr(III), Al(III), and Zn(II) at pH values of 14 and higher.

These decreases in rate constants are not due to an

Table I: The Effect of pH on the Rates of Reaction of Metal Ions with e_{aq}^-

Central atom	Anion or cation present	pH	Concn., <i>mM</i>	<i>k</i> , $M^{-1} \text{sec}^{-1}$
Al(III)	ClO_4^-	6.8	0.5	$2.0 \pm 0.3 \times 10^9$
	Na^+	11.2	0.5	$4.0 \pm 1.0 \times 10^8$
	Na^+	14 ^a	50	$5.5 \pm 1.2 \times 10^6$
Cr(III)	ClO_4^-	7.1	0.05	$6.0 \pm 0.5 \times 10^{10}$
	Na^+	10.9	0.05	$4.6 \pm 0.5 \times 10^{10}$
	Na^+	14 ^a	1.0	$2.0 \pm 0.2 \times 10^8$
	Na^+	3 <i>M</i> OH ⁻	1.0	$2.2 \pm 0.2 \times 10^8$
Cr(II)	ClO_4^-	6.9	0.05	$4.2 \pm 0.8 \times 10^{10}$
	Na^+	11.2	0.05	$1.9 \pm 0.5 \times 10^{10}$
Zn(II)	SO_4^{2-}	6.8	0.1	$1.0 \pm 0.3 \times 10^9$
	Na^+	9.7	0.5	$5.6 \pm 0.7 \times 10^8$
	Na^+	12	0.5	$2.0 \pm 0.3 \times 10^8$
	Na^+	14 ^a	4.0	$1.6 \pm 0.3 \times 10^7$
	Na^+	3 <i>M</i> OH ⁻	40.0	$7.5 \pm 1.5 \times 10^6$
Cu(II)	ClO_4^-	7	...	$3.0 \pm 0.3 \times 10^{10}$
	Na^+	14 ^a	0.05	$5.8 \pm 0.6 \times 10^9$
	Na^+	3 <i>M</i> OH ⁻	0.05	$4.5 \pm 0.5 \times 10^9$
	Na^+	5 <i>M</i> OH ⁻	0.1	$3.4 \pm 0.5 \times 10^9$
Sn(II)	Cl^-	11	0.1	$3.4 \pm 0.3 \times 10^9$
	Na^+	14 ^a	0.1	$6.2 \pm 0.5 \times 10^9$
Pb(II)	ClO_4^-	Neutral	...	$3.9 \pm 0.5 \times 10^{10}$
	Na^+	11.2	0.05	$1.3 \pm 0.1 \times 10^{10}$
	Na^+	14 ^a	0.05	$1.0 \pm 0.1 \times 10^{10}$
	Na^+	3 <i>M</i> OH ⁻	0.05	$9.2 \pm 0.1 \times 10^9$

^a 1 *M* NaOH.

effect of pH on the reactivity of e_{aq}^- as can be seen in Table II, from the relatively small changes in rate of reactions of the oxy anions. From this table, it is evident that the rate of reaction of e_{aq}^- with bromate, iodate, and periodate ions increases only moderately with pH from 7 to 14. In part, this increase may be attributed to a salt effect for the reaction of two negatively charged species. But the change in the case of IO_3^- is smaller than for BrO_3^- and may be due to a difference in the reactivity of the several species prevailing in iodate solutions over this pH range.⁹ Benzoate ions show a much smaller salt effect than the oxy anions, probably owing to a much smaller change in solvation when changed from BzO^- to BzO^{2-} in the

(4) J. H. Baxendale, E. M. Fielden, and J. P. Keene, *Proc. Chem. Soc.*, 242 (1963); J. H. Baxendale, E. M. Fielden, C. Capellos, J. M. Francis, J. V. Davies, M. Ebert, C. W. Gilbert, J. P. Keene, E. J. Land, A. J. Swallow, and J. M. Nosworthy, *Nature*, **201**, 468 (1964).

(5) J. K. Thomas, S. Gordon, and E. J. Hart, *J. Phys. Chem.*, **68**, 1524 (1964).

(6) A. Szutka, J. K. Thomas, S. Gordon, and E. J. Hart, *ibid.*, **69**, 289 (1965).

(7) M. Anbar and E. J. Hart, *J. Am. Chem. Soc.*, **86**, 5633 (1964).

(8) M. Anbar and E. J. Hart, *J. Phys. Chem.*, **68**, 271 (1965).

(9) M. Anbar and S. Guttmann, *J. Am. Chem. Soc.*, **83**, 781 (1961).

transition state. *p*-Nitrophenyl acetate and acetone follow a similar behavior. The slight decrease in the rate of reaction of e_{aq}^- observed above pH 14 for the 3 M OH⁻ solutions is probably due to a decrease in the reactivity of e_{aq}^- , a property demonstrated in concentrated electrolyte solutions.¹⁰ However, these changes in rate of reactions are very small in comparison to those observed with metal ions.

Table II: The Effect of pH on the Rate of Reactions of Cxy Anions^a

Compd.	pH 7	pH 11	pH 14	3 M OH ⁻
KBrO ₃	2.1 ± 0.3	3.8 ± 0.5	5.8 ± 0.7	5.3 ± 0.6
KIO ₃	7.7 ± 0.9	8.3 ± 1.0	9.6 ± 1.2	8.1 ± 0.8
NaIO ₄	11.0 ± 1.5	19.0 ± 2.1	21.5 ± 2.5	16.3 ± 2.0
F ₂ OH	3.5 ± 0.4	3.1 ± 0.3	2.9 ± 0.3	2.4 ± 0.3
Acetone	5.9 ± 0.2	5.6 ± 0.6	5.2 ± 0.6	4.2 ± 0.5
<i>p</i> -O ₂ NC ₆ H ₄ CH ₂ COO ⁻	18.0 ± 2	19 ± 2	21 ± 3	17 ± 2

^a Rate constants in $M^{-1} \text{ sec.}^{-1} \times 10^9$.

The effect of other ligands on the reactivity of metal ions toward e_{aq}^- has also been studied in neutral and alkaline solutions. The results appear in Table III. Amino complexes show a slightly lower reactivity than the aquo complexes. Neutral complexes like Cr(EDTA) or Co(EDTA) have a reactivity which is lower by a factor of 2 than the positive triply charged aquo complex. In contrast, the cyano complexes of Cu(II), Co(III), Cd(II), and Ag(I) are about two orders of magnitude lower in reactivity than the aquo complexes. However, those of Cr(III) and Zn(II) are lower by only a factor 4 to 5.

Discussion

It has been suggested that the rate of reaction of e_{aq}^- with different transition metal ions is diffusion controlled, being determined according to Debye's equation only by their rates of diffusion, their effective diameter, and their charge.¹¹ According to this hypothesis two ions of comparable size and equal charge should react at the same rate. In addition, the rate of reaction should increase with increasing positive charge and decrease with increasing negative charge. While these parameters unquestionably play a role, structural properties of the oxidized and reduced forms of the ions are of major importance. For example, the difference between the reactivities of Cr(H₂O)₆⁺³ and Cr(en)Cl₂⁺ is very small, with the latter compound somewhat more reactive. According to the Debye equation, the difference in reactivity between Ag(NH₃)₂⁺ and Ag(CN)₂⁻ should be less than a factor of 4, the difference found between Cr(H₂O)₆⁺³

Table III: The Effect of Ligands on the Reactivity of the Central Atom toward e_{aq}^-

Central atom	Complex	Matrix soln.	pH	<i>k</i> , $M^{-1} \text{ sec.}^{-1}$
Cr(III)	Cr(H ₂ O) ₆ ⁺³	H ₂ O	7	6.0 ± 0.5 × 10 ¹⁰
	Cr(en) ₃ ⁺³	H ₂ O	6.83	5.3 ± 0.5 × 10 ¹⁰
	Cr(en) ₂ Cl ₂ ⁺	H ₂ O	5.55	7.1 ± 0.7 × 10 ¹⁰
	Cr(EDTA) ⁻	H ₂ O	4.95	2.6 ± 0.4 × 10 ¹⁰
	CrF ₆ ⁻³	0.2 M F ⁻	10	1.4 ± 0.2 × 10 ¹⁰
	Cr(CN) ₆ ⁻³	0.1 M CN ⁻	10	1.5 ± 0.2 × 10 ¹⁰
Cu(II)	CrO ₂ (H ₂ O) _n ⁻	1.0 M NaOH	14 ^b	2.0 ± 0.2 × 10 ⁸
	Cu(H ₂ O) ₄ ⁺²	H ₂ O	6.8	3.0 ± 0.3 × 10 ¹⁰
	Cu(NH ₃) ₄ ⁺²	0.2 M NH ₃	11.1	1.8 ± 0.3 × 10 ¹⁰
	Cu(CN) ₄ ⁻²	0.1 M CN ⁻	10	3.0 ± 0.3 × 10 ⁸
Zn(II)	Cu(OH) ₄ ⁻²	1.0 M NaOH	14 ^b	5.8 ± 0.6 × 10 ⁹
	Zn(H ₂ O) ₄ ⁺²	H ₂ O	7.1	1.0 ± 0.3 × 10 ⁹
	Zn(NH ₃) ₄ ⁺²	0.2 M NH ₃	11.1	6.5 ± 0.6 × 10 ⁸
Co(III)	Zn(CN) ₄ ⁻²	0.1 M CN ⁻	10	1.8 ± 0.2 × 10 ⁸
	Zn(OH) ₄ ⁻²	1.0 M NaOH	14 ^b	1.6 ± 0.3 × 10 ⁷
	Co(NH ₃) ₆ ⁺³	0.2 M NH ₃	11.1	9.0 ± 1.3 × 10 ¹⁰
	Co(CN) ₆ ⁻³	0.1 M CN ⁻	10	3.6 ± 0.4 × 10 ⁹
Cd(II)	Cd(H ₂ O) ₄ ⁺²	H ₂ O	6.5	4.8 ± 0.6 × 10 ¹⁰
	Cd(NH ₃) ₄ ⁺²	0.2 M NH ₃	6.5	3.1 ± 0.3 × 10 ¹⁰
	CdCl(H ₂ O) ₃ ⁺	1.0 M Cl ⁻	6.8	1.1 ± 0.1 × 10 ¹⁰
	CdI(H ₂ O) ₃ ⁺	0.2 M I ⁻	7.2	1.6 ± 0.2 × 10 ¹⁰
	Cd(CN) ₄ ⁻²	0.1 M CN ⁻	10	1.4 ± 0.2 × 10 ⁸
Pt(II)	PtCl ₄ ⁻²	0.1 M Cl ⁻	6.8	1.2 ± 0.15 × 10 ¹⁰
	Pt(CN) ₄ ⁻²	0.1 M CN ⁻	10	3.2 ± 0.4 × 10 ⁹
Pd(II)	PdCl ₄ ⁻²	0.1 M Cl ⁻	7.1	1.2 ± 0.15 × 10 ¹⁰
	Pd(CN) ₄ ⁻²	0.1 M CN ⁻	10	2.0 ± 0.3 × 10 ⁹
Ag(I)	Ag(NH ₃) ₂ ⁺	0.2 M NH ₃	11.1	8.0 ± 1.5 × 10 ¹⁰
	Ag(CN) ₂ ⁻	0.1 M CN ⁻	10	1.5 ± 0.2 × 10 ⁹
As(V)	HAsO ₄ ⁻²	H ₂ C	7.2	2.1 ± 0.3 × 10 ⁸
	AsF ₆ ⁻	H ₂ C	7.0	9.0 ± 0.9 × 10 ⁹

^a Taken from ref. 6 for comparison. ^b pH 14 by definition.

and Cr(CN)₆⁻³. However, Ag(NH₃)₂⁺ reacts with e_{aq}^- 50 times faster than Ag(CN)₂⁻. Finally PtCl₄⁻² and Pt(CN)₄⁻², which are expected to show comparable reactivity according to this theory, differ by a factor of 6, as do Co(ox)₃⁻³ and Co(CN)₆⁻³. From these comparisons it is clear that the difference in reactivity of transition metal ions with e_{aq}^- is affected by their ligands far more than would be predicted from the change in the charge or size of the complex ion. Moreover, as many negatively charged ions react much faster than predicted by the Debye equation, it has limited application to e_{aq}^- reactions.

An inverse relationship has been found between the reactivity of the central ions toward e_{aq}^- and their oxidation-reduction potentials. This has been reported for a series of trivalent rare earth ions.⁵ This log *k* vs. *E*^o correlation, which is far from being linear, can be extended to other trivalent cations including Cr⁺³ (*E*^o = 0.41 v.; *k*_{*e*_{aq}⁻} = 6.0 × 10¹⁰ M⁻¹ sec.⁻¹) and Co⁺³ (*E*^o = -1.82 v.; *k*_{*e*_{aq}⁻} > 10¹¹ M⁻¹ sec.⁻¹). In the case of divalent cations even a qualitative corre-

(10) M. Anbar and E. J. Hart, to be published.

(11) H. A. Schwarz, *Radiation Res. Suppl.*, **4**, 89 (1964).

lation between E° and $k_{e_{aq}^-}$ cannot be found. Pb^{+2} and Cd^{+2} , for instance, with $k_{e_{aq}^-} = 3.9$ and $4.8 \times 10^{10} M^{-1} \text{sec.}^{-1}$ respectively, were shown to be more reactive than Cu^{+2} ($k_{e_{aq}^-} = 3.0 \times 10^{10} M^{-1} \text{sec.}^{-1}$; $E^\circ = -0.153 \text{ v.}$). Further, Cu^{+2} is expected to be more reactive than Tl^{+1} ($E^\circ = 0.336 \text{ v.}$; $k_{e_{aq}^-} = 7 \times 10^{10} M^{-1} \text{sec.}^{-1}$) both because of its electrostatic attraction and its oxidation-reduction potential. Considering the effects of ligands on the reactivity of complexes one finds that ammonia and amino derivatives like ethylenediamine or ethylenediaminetetraacetate have little effect on the reactivity of the complex compared with the aquo complex, in spite of their pronounced effect on the oxidation-reduction potential.

It may be concluded that the reactivity of a given species with e_{aq}^- is not solely determined by the free energy change in the process. A linear correlation between ΔE of activation and ΔF in a series of reactions is expected if the entropy changes in the processes are comparable. This may be true only in a few instances in inorganic reactions such as reduction of the rare earth ions. In other words, the free-energy change due to the incorporation of an additional electron may contribute to the reactivity of the oxidizing species toward e_{aq}^- , but it is not the only factor involved.

The reactivity of an organic compound with e_{aq}^- was postulated to depend on the availability of vacant electron orbitals and on the charge distribution and polarizability of the molecule, into which the diffuse charge of the hydrated electron may be localized on encounter.^{7,8} Taking a given series of the periodic table the availability of a vacant orbital increases with the atomic number. This generalization is shown by increased reactivity of Cd^{+2} compared with Zn^{+2} , of Ag^{+1} compared with Cu^{+2} , of Pt^{+2} compared with Ni^{+2} , or of Pb^{+2} compared with Sn^{+2} .

When considering the reactivity of complexes of the same metal with different ligands there are two groups of parameters which determine the reactivity. One is the case of channeling of an electron through the ligand to the central atom whereas the other is the free energy change taking place in the central atom-ligand system in order to achieve a stable configuration in the reduced form. In view of the limited information available on the chemistry and configuration of metal ions at their lower valence states, it is hard to analyze each system and to determine the contribution of these factors.

Comparing the aquo and hydroxy complexes ($Al(III)$, $Zn(II)$, and $Cr(III)$) one finds that a great change in reactivity takes place when going from the aquo to the hydroxy complex. In the case of $Al(III)$ this has been shown to be accompanied by a change in coordination

number and in configuration.¹² It was suggested that both aluminum and zinc ions form hydroxy complexes, namely, $Al(OH)_4^-$ and $Zn(OH)_4^-$.¹² The relatively low reactivity of these ions may be attributed to the fact that OH^- groups are less efficient bridges for electron transfer than H_2O . This is in accord with the observation that the rate of outer-sphere reductions of $Co(NH_3)_5OH^{+2}$ by $Ru(NH_3)_6^{+2}$ is one-hundredth as fast as that of $Co(NH_3)_5H_2O^{+3}$.¹³ Another case where a ligand is a bridge for electron transfer is in a comparison of $Cr(en)_2Cl^{+2}$ with $Cr(en)_3^{+3}$. Here the chloride ion, acting as a bridge, enhances the rate of reaction in spite of the decrease in charge. $CdI(H_2O)_3^+$ also reacts faster with e_{aq}^- than $CdCl(H_2O)_3^+$, in agreement with the effect of these anions on the $Co(NH_3)_5X$ outer-sphere reactions.¹³ Comparing the rate of reduction of $Co(NH_3)_5H_2O^{+3}$ with $Co(NH_3)_5F^{+2}$ by V^{+2} , one finds the latter compound more reactive by a factor of five.¹⁴ Consequently one is not surprised at the difference in the reactivity of $HAsO_4^{-2}$ compared with AsF_6^- , when one considers that most of the water in the coordination shell of $As(V)$ has been replaced by O^{-2} and OH^- .

The behavior of the hydroxy complexes of tin and lead, which were found to be as reactive as the aquo complexes, may be explained by the fact that these species remain six-coordinated even in alkaline solution and there are enough water molecules in their inner sphere of coordination to facilitate a fast electron transport. The effect of hydration on the reactivity of oxy anions may be demonstrated again when comparing the reactivity of arsenate(V) ion with that of antimonate(V) ion ($K = 1.2 \pm 0.2 \times 10^{10}$ at pH 11 compared with $2.1 \times 10^8 M^{-1} \text{sec.}^{-1}$ at pH 7). Copper(II) ions provide an intermediate case in the behavior of their hydroxy complex, the reactivity of which is decreased by the loss of protons, but two water molecules may still be loosely bound to the central atom even in alkaline solution.

It is interesting to note, on the other hand, that amino complexes and their derivatives show a reactivity toward e_{aq}^- comparable to that of their aquo complexes. This is in discord with the behavior of amines as ligands in outer-sphere reductions.¹³⁻¹⁵ One possible explanation to this fact is that the interaction between an amino group and the hydrated electron is more

(12) E. R. Lippincott, J. A. Psellos, and M. C. Tobin, *J. Chem. Phys.*, **20**, 536 (1952).

(13) J. F. Endicott and H. Taube, *J. Am. Chem. Soc.*, **86**, 1686 (1964).

(14) J. P. Candlin, J. Halpern and D. L. Trimm, *ibid.*, **86**, 1019 (1964).

(15) A. Zwickel and H. Taube, *ibid.*, **83**, 793 (1961).

intimate than that with any other reducing agent. Another explanation would imply that the amino complexes tend to stabilize the lower states of oxidation and thus compensate for their poorer bridging capacity. As the amino complexes of Cr(III), Cu(II), Zn(II), Co(III), Cd(II), and Ag(I) behave alike and seem to have a reactivity very close to that of the aquo complexes, the first interpretation seems more plausible.

The cyano complexes as a group are less reactive than the aquo complexes. There is no information available on the effect of CN^- as a bridge in outer-sphere reductions. The only analogy that can be drawn is from the behavior of CNS^- as a bridge in pentaamminecobalt(III) complexes. $\text{Co}(\text{NH}_3)_5\text{NCS}^{2+}$ reacts with $\text{Cr}(\text{bipy})_3^{3+}$ at one-fifth the rate of $\text{Co}(\text{NH}_3)_5\text{H}_2\text{O}^{+3}$.¹⁴ In the reduction by V^{+2} , CNS^- is again less reactive than H_2O as a bridge in these complexes for electron transport.¹⁴ The cyano group has little tendency to incorporate an electron and act as a "bridge," owing to its low electron affinity and relatively low polarizability. Cyanoacetate, for instance, has been shown to be of relatively low reactivity toward e_{aq}^- ($k = 4 \times 10^7$ compared with $1.2 \times 10^9 M^{-1} \text{sec.}^{-1}$ for chloroacetate). On the other hand, the high accumulation of electrons in the complex, taking into account the π -electrons of the cyano groups, makes the availability of a vacant orbital less likely. Thus the probability of finding an electrophilic reaction center on a cyano complex is rather low. The only exceptions to this behavior are $\text{Cr}(\text{CN})_6^{-3}$, which is comparable in its reactivity to $\text{Cr}(\text{EDTA})$, and $\text{Zn}(\text{CN})_4^{-2}$, which has one-fifth the reactivity of the aquo complex. It may be concluded that more than one parameter is involved in the case of cyano complexes and perhaps in these cases the effect of cyanide ligands on the

stability of the transition state outweighs their inertness as electron bridges.

The bridging capacity of given ligands for transport of an electron seems to parallel the reactivity of the same groups when bound to carbon in alkyl compounds,⁸ $\text{NH}_2 < \text{CN} < \text{F} < \text{Cl} < \text{Br} < \text{I}$. In the case of organic compounds this sequence was correlated with the polarizability of these groups. In the case of alkyl compounds the interaction of e_{aq}^- with these groups results in the dissociation of the C-X bond to $\text{C} + \text{X}^-$, whereas in the metal complexes the electron is rapidly conveyed to the central atom.

It has been demonstrated that the reactivity of complexes toward e_{aq}^- parallels their reactivity in outer-sphere oxidation-reduction processes. The hydrated electron is, therefore, not unique in its mode of reactivity and it shares the behavior of electrons bound to other chemical species. However, its reactivity is many orders of magnitude higher than most chemical reducing agents.

Unlike the case of organic substrates,^{7,8} it is not possible to deduce any quantitative relationships on the reactivity of e_{aq}^- toward inorganic species at this time. More experimental data need to be accumulated before a quantitative interpretation of these reactions can be offered. The number of cases in chemistry in which an electron transfer to an oxidant may be demonstrated is limited. The hydrated electron is, however, an ideal electron-transfer reducing agent for reactions in water since it is free from all restraints except those of the polarized water molecules surrounding it.

Consequently an understanding of the detailed mechanism of the e_{aq}^- reduction process may add important information on the chemical behavior of the oxidizing species.

The $n-\pi^*$ Cotton Effect of the Peptide Linkage

by Burton J. Litman and John A. Schellman

Chemistry Department, University of Oregon, Eugene, Oregon (Received October 17, 1964)

Investigations of the rotatory dispersion of the lactam of 2,4-diaminobutyric acid are reported down to 220 $m\mu$. Cyclic amides of this kind have fixed conformations and serve as useful models for the peptide bond in rigid conformations such as the α -helix. In nonpolar solvents (acetonitrile and dioxane) this compound develops an $n-\pi^*$ Cotton effect at 231 $m\mu$. The relationship of this Cotton effect with the 225- $m\mu$ Cotton effect of helical polypeptides is discussed. It is pointed out that structural situations other than helix formation can produce Cotton effects of this kind and thus lead to errors in the determination of helical content by current optical rotatory techniques.

Recent investigations of the rotatory properties of helical polypeptides and proteins, both by the measurement of optical rotatory dispersion^{1,2} and of circular dichroism,^{3,4} have revealed two Cotton effects within the broad absorption band of the peptide bond. The first is negative and centered near 225 $m\mu$, the second is positive and in the region of maximum absorption near 190 $m\mu$. Recent unpublished results of Holzwarth and Doty,⁵ of Carver, Shechter, and Blout,⁶ and of Beychok⁷ have revealed the presence of a third, negative Cotton effect, intermediate between these two, which required more refined instrumentation for its resolution from the 225- $m\mu$ Cotton effect. These Cotton effects were discovered in the wake of a considerable amount of theoretical work on the origins of the characteristic rotatory dispersion of helices and a rather vast literature on the empirical application of optical rotatory dispersion to problems of the structure of proteins and polypeptides.⁸ Since the two Cotton effects at the lower wave lengths correspond fairly well with the positions of the two peaks of the split $\pi-\pi^*$ absorption band of the peptide group,^{9,10} they have been so assigned by Holzwarth and Doty.⁵ The nearest Cotton effect presents a little more difficulty. Owing to its position, it has been assigned to the $n-\pi^*$ transition of the amide group.¹¹ This is an electron jump from the nonbonding orbital of the oxygen atom to an antibonding π^* level and thus bears a very close relationship to the 290- $m\mu$ carbonyl band, whose propensity for developing large Cotton effects in asymmetric molecules has now been demonstrated in hundreds of examples. As with the carbonyl

group, the proposed mechanism is based on the Condon, Altar, and Eyring mechanism for optical activity.¹² Though theoretically plausible, this interpretation rests on a minimum of experimental evidence. The weak $n-\pi^*$ transition is buried within the strong peptide absorption band and has never been observed directly. Its existence was initially inferred from analogies with the $n-\pi^*$ transition of the carboxyl group which can be observed directly.¹³ In addition, an $n-\pi^*$ Cotton effect of the amide group has never been reported for substances simpler than polypeptides and proteins. The purpose of the present work is to provide experimental support for this mechanism and to try to establish some of the conformational and environmental

- (1) N. S. Simmons and E. R. Blout, *Biophys. J.*, **1**, 55 (1960).
- (2) E. R. Blout, I. Schmier, and N. S. Simmons, *J. Am. Chem. Soc.*, **84**, 3193 (1962).
- (3) G. M. Holzwarth, W. B. Gratzer, and P. Doty, *ibid.*, **84**, 3194 (1962).
- (4) J. Brahm and G. Spach, *Nature*, **200**, 73 (1963).
- (5) G. M. Holzwarth and P. Doty, to be published.
- (6) J. P. Carver, E. Shechter, and E. R. Blout, preprint received from E. R. Blout.
- (7) S. Beychok, private communication.
- (8) P. J. Urnes and P. Doty, *Advan. Protein Chem.*, **16**, 401 (1961).
- (9) W. B. Gratzer, G. M. Holzwarth, and P. Doty, *Proc. Natl. Acad. Sci. U. S.*, **47**, 1785 (1961).
- (10) I. Tinoco, Jr., A. Halpern, and W. T. Simpson in "Polyamino Acids, Polypeptides, and Proteins," M. A. Stahman, Ed., University of Wisconsin Press, Madison, Wis., 1962, p. 157.
- (11) J. A. Schellman and P. Oriel, *J. Chem. Phys.*, **37**, 2114 (1962).
- (12) E. U. Condon, W. Altar, and H. Eyring, *ibid.*, **5**, 753 (1937).
- (13) J. S. Ham and J. R. Platt, *ibid.*, **20**, 335 (1952).

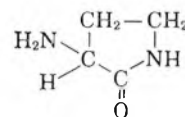
factors which contribute to the amide $n-\pi^*$ Cotton effect.

At present there are considered to be two principal mechanisms for the production of rotatory strength in an absorption band. The first is the dynamic coupling model of Kuhn and Kirkwood.¹⁴ It arises only in rather strong absorption bands and because of its dynamical nature it is relatively independent of such static conditions as dielectric constant. The application of this model to helical polymers requires special considerations (in particular band splitting, with different rules for optical rotation and absorption) which were introduced by Moffitt^{15,16} and recently brought to fruition by Tinoco¹⁷⁻¹⁹ and co-workers. The other mechanism is a modernized version of the one-electron mechanism of Condon, Altar, and Eyring.^{11,20} This mechanism depends on static interactions with the chromophore. It is potentially operative in all absorption bands, but finds special application to weak absorption bands such as the $n-\pi^*$ transition, where it is the only known mechanism which can contribute. In a helical polypeptide, these mechanisms are quite difficult to disentangle. The $n-\pi^*$ band overlaps and is obscured by the exciton band of the $\pi-\pi^*$ absorption. There is no control over environmental effects since the massive nature of the helical structure provides a local environment which is essentially invariant unless the helix is disrupted, in which case the characteristic negative Cotton effect at $225\text{ m}\mu$ disappears.

By contrast, the situation should be relatively simple in a small molecule containing a single amide or peptide group. Band splitting of the $\pi-\pi^*$ transition cannot arise because there is no degeneracy. Provided one can avoid conformational changes with change in solvent, environmental effects on rotatory strengths can be studied directly. In addition, one can make use of the well-established but opposite shifts in wave length of the $\pi-\pi^*$ and $n-\pi^*$ transitions with change in solvent polarity.²¹⁻²³

The Model Compound. There are probably at least three factors which have contributed to the circumstance that the $n-\pi^*$ transition of amides (in contrast with ketones) has so far eluded observation. These are the overlap with the strong $\pi-\pi^*$ band already mentioned, the use of strongly polar solvents normally required for the solution of amides, and the freedom of internal rotation about the bonds linking the amide group with its asymmetric environment. The latter two factors tend to diminish the size of the Cotton effect. We wished to select a compound which would optimize our chances of observing such a Cotton effect. Desirable properties of a model compound are: (1)

rigidity of structure, both to increase the inherent size of the Cotton effect in accordance with the considerations of Kauzmann and Eyring²⁴ and to permit solvent variation without change of conformation, and (2) simplicity of asymmetry to provide a favorable situation for theoretical interpretation. The theoretical aspects of this model will be discussed more fully at a later date. These considerations led us to select a five-membered ring containing the amide link (γ -lactam) and the initial compound chosen for study was the lactam of 2,4-diaminobutyric acid.



I. L-3-aminopyrrolid-2-one

The ring is presumably planar or close to it. As a result, the only groups which can contribute to the asymmetry are the hydrogen atoms and the NH₂ group attached to carbon 3, since these are the only groups in the molecule which do not have a plane of symmetry. The amide link in this compound is *cis* rather than *trans* and this could produce small differences in the energy and intensity of the $n-\pi^*$ transition. These changes should have little effect on the conclusions to be drawn since they do not affect the basic symmetry properties of the n or π^* orbitals. Moreover, at the present stage of development of the theory of the electronic structure of the amide link, no terms arise which would predict differences between the spectra of *trans* and *cis* conformations.

Experimental

Materials and Methods. The procedure for the preparation of L-3-aminopyrrolid-2-one has been given by Wilkinson²⁵ and we are indebted to him for a sample

- (14) W. Kauzmann in "Quantum Chemistry," Academic Press, New York, N. Y., 1957, Chapter 15.
- (15) W. Moffitt, *J. Chem. Phys.*, **25**, 467 (1956).
- (16) W. Moffitt, D. D. Fitz, and J. G. Kirkwood, *Proc. Natl. Acad. Sci. U. S.*, **43**, 723 (1957).
- (17) I. Tinoco, Jr., *Radiation Res.*, **20**, 133 (1963).
- (18) I. Tinoco, Jr., R. W. Woody, and D. F. Bradley, *J. Chem. Phys.*, **38**, 1317 (1963).
- (19) I. Tinoco, Jr., *J. Am. Chem. Soc.*, **86**, 297 (1964).
- (20) R. W. Woody, Ph.D. Thesis, University of California, Berkeley, Calif., 1962.
- (21) N. S. Bayliss, *J. Chem. Phys.*, **18**, 292 (1950).
- (22) N. S. Bayliss, *J. Phys. Chem.*, **58**, 1002, 1006 (1954).
- (23) M. Kasha in "Light and Life," W. D. McElroy and B. Glass, Ed., Johns Hopkins Press, Baltimore, Md., 1961, p. 31.
- (24) W. Kauzmann and H. Eyring, *J. Chem. Phys.*, **9**, 41 (1941).
- (25) S. Wilkinson, *J. Chem. Soc.*, 104 (1951).

of the original preparation sufficient for these experiments. With time, the preparation had developed a small amount of impurity, which was removed by recrystallization from acetonitrile followed by sublimation at 90° and 5×10^{-2} mm. pressure. After this procedure, the melting point and the specific rotation at the sodium D-line agreed with those originally reported by Wilkinson for this compound.

Ultraviolet absorption spectra were recorded on both a Cary Model 14 and a Cary Model 15 recording spectrophotometer. Ground glass stoppered cells, ranging from 0.1 to 1 cm. in path length and made of fused silica, were used in these spectral studies. The concentration range studied was from 5×10^{-3} to $1.5 \times 10^{-2} M$.

Optical rotation measurements were obtained with a Rudolph photoelectric polarimeter, Model 200, with rocking polarizing unit. The maximum absorbance was kept below unity in all experiments. The widest slit width employed was 0.8 mm.; additional settings were symmetric angle, 5° , and aperture, 3 mm. The source was an Osram XBO 1600-w. xenon lamp and the photomultiplier tube used was an RCA 7200. The concentration range and cells were the same as those employed in the spectral studies. Cell path lengths ranged from 10.0 to 0.1 cm.

The infrared spectra were obtained on a Beckman IR-7 infrared spectrophotometer. The measurements were made in a 0.1-mm. NaCl cell on solutions of about $6 \times 10^{-3} M$.

The investigations of Mizushima, *et al.*,²⁶ have shown that molecules with exposed amide groups associate upon solution in nonpolar solvents. It was concluded from this work that secondary amides associate to form several polymeric species, while cyclic amides form only dimers. Klemperer, *et al.*,²⁷ supported this conclusion, with respect to cyclic amides, by their work on γ -butyrolactam. They observed a splitting of the carbonyl stretching frequency in CCl_4 ; the observed values, 1716 and 1703 cm^{-1} , were assigned to the monomer and dimer, respectively. The following observations lead us to conclude that, under the conditions of our experiments, association is either absent or occurring to a negligible extent. (1) Qualitative experiments were performed to determine the infrared spectrum of the model compound in acetonitrile, dioxane, and KBr pellets. The solid L-3-aminopyrrolid-2-one spectrum exhibited a splitting of the carbonyl stretching frequency (1705 and 1694 cm^{-1}) similar to that observed by Klemperer, *et al.* Single bands were observed in acetonitrile and dioxane at 1714 and 1712 cm^{-1} , respectively. These results are taken to indicate the existence of both monomers and dimers

in the solid state, but of only monomers in the acetonitrile and dioxane solutions studied. (2) A comparison of the optical rotatory dispersion and ultraviolet spectral measurements obtained with L-3-aminopyrrolid-2-one, over a concentration range of 5×10^{-3} to $1.5 \times 10^{-2} M$, showed no correlation with concentration and all deviations were within experimental error.

The pK of the amino group of L-3-aminopyrrolid-2-one, in aqueous solution, was determined to be 7.1 by performing a spectrophotometric titration, utilizing the change in absorbance at 230 $m\mu$ as a function of pH.²⁸ Since only very small amounts of concentrated KOH and HCl solutions were required to effect pH changes, no volume correction was made for the acid or base added. The pH of all aqueous solutions was maintained at about 9.2 by dissolving the model compound in 0.1 M $NaHCO_3$ - Na_2CO_3 buffer, pH 9.2. Under these conditions the amount of charged species present is less than 1%.

Measurements in organic solvents were performed using Matheson Coleman and Bell Spectrograde solvents, with no further purification. Dioxane was stored under nitrogen to prevent oxidation and both solvents were kept at 4° .

Results

The absorption spectra of L-3-aminopyrrolid-2-one in water, acetonitrile, and dioxane are shown in Figure 1. Note first the left side of the curves. Here the absorption is dominated by the π - π^* absorption and the curves show the characteristic blue shift of such transitions as the polarity of the solvent is decreased.^{21,22} At the same time, the n - π^* transition undergoes the anticipated red shift²³ with decreasing polarity and is brought out as an easily observed shoulder in both dioxane and acetonitrile. The curve in acetonitrile is intermediate between those in water and dioxane over the whole spectrum except at the crossover region. The position and intensity of the n - π^* absorption band cannot be established with certainty, but if it is assumed that the π - π^* transition in dioxane has the same shape as the total absorption band in water (this means using the shifted water spectrum as a background for the other solvent) then the center of the n - π^* band is near 231 $m\mu$, its ϵ_{max} is 106 l./mole-cm., and its oscillator strength is 0.002. This is a higher wave length than is usually estimated for the n - π^*

(26) S. Mizushima in "Structure of Molecules and Internal Rotation," Academic Press, New York, N. Y., 1954.

(27) W. Klemperer, M. W. Cronyn, A. H. Maki, and G. C. Pimentel, *J. Am. Chem. Soc.*, **76**, 5846 (1954).

(28) J. T. Edsall and J. Wyman, "Biophysical Chemistry," Academic Press, New York, N. Y., 1958, Chapter 8.

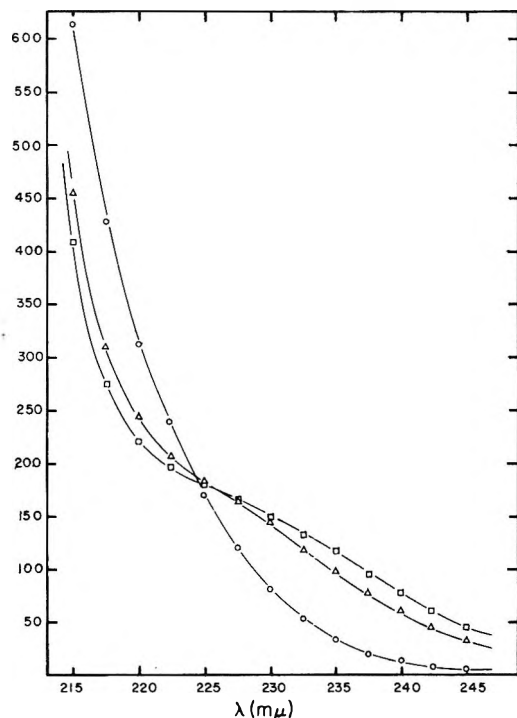


Figure 1. The ultraviolet spectrum of L-3-aminopyrrolid-2-one in 0.1 M NaHCO_3 - Na_2CO_3 buffer, pH 9.2, O; acetonitrile, Δ ; and dioxane, \square .

transition, but such estimates have usually been made for amide links in a polar environment. The oscillator strength of 0.002 obtained as a difference spectrum between aqueous and dioxane solution is to be compared with the oscillator strength of 0.004 obtained by Gratzner, *et al.*,⁹ from the difference spectrum between helical and nonhelical polyglutamic acid.

The rotatory dispersion curves of the compound are given in Figure 2, which covers the entire range of measurement, and in Figure 3, which focuses attention on the Cotton effect brought out in dioxane and in acetonitrile. The estimation of the position and magnitude of the Cotton effect can only be done approximately because it is located on the steep slope of a very much larger negative Cotton effect, presumably the $\pi-\pi^*$ Cotton effect. If we were to assign the observed maxima and minima of the curves as the peak and trough of a negative Cotton effect, the position of the responsible absorption band would be 250 $m\mu$. There is no experimental evidence of an absorption band nor any theoretical likelihood of an amide transition in this region. In addition, the minimum is too broad and shallow to resemble the trough of a Cotton effect. Consequently, the maximum of the curve is assigned as the peak of a positive Cotton effect. The trough is presumably absorbed in the trough of the much larger negative Cotton effect at lower wave

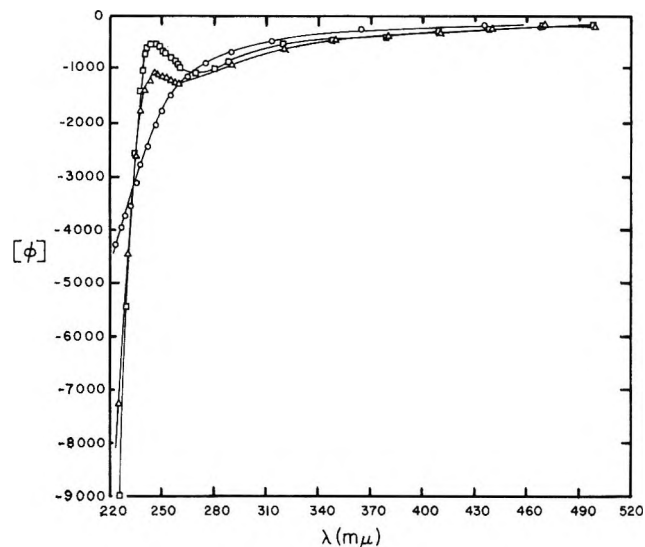


Figure 2. The rotatory dispersion of L-3-aminopyrrolid-2-one in 0.1 M NaHCO_3 - Na_2CO_3 buffer, pH 9.2, O; acetonitrile, Δ ; and dioxane, \square .

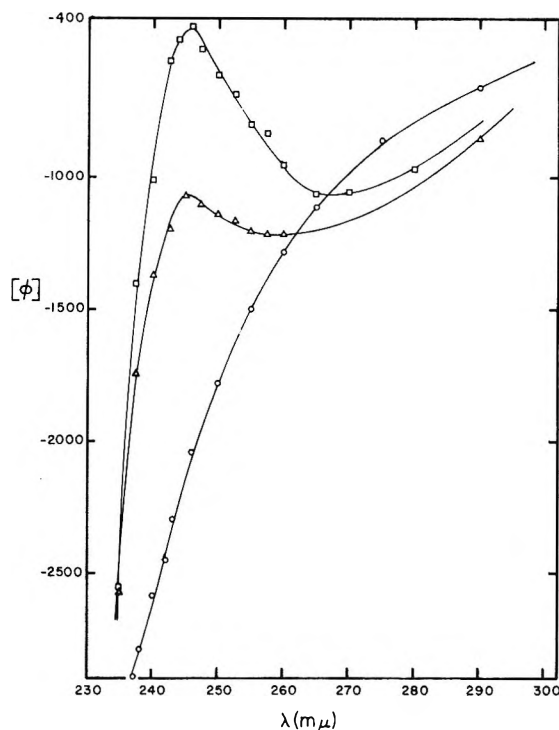


Figure 3. Details of Figure 2 in the neighborhood of the $n-\pi^*$ Cotton effect.

lengths. On this basis, the center of the Cotton effect is located somewhere approximately in the 230-235 $m\mu$ region, in satisfactory agreement with the position of the $n-\pi^*$ absorption band. It is worth noting that there is a marked enhancement of the Cotton effect

in dioxane relative to acetonitrile, whereas the absorption curves are rather close to one another.

Discussion

Even with this simple compound, the changes in the physical situation which accompany a change in solvent are rather complex. Ideally, one would like to isolate the change in rotatory properties with no change in conformation. However, with the model under consideration there are three possible positions for the $-\text{NH}_2$ group. Two of them extend a hydrogen atom toward the oxygen atom of the carbonyl group to form a rather poor, nonlinear hydrogen bond. The other extends the lone pair orbital of the $-\text{NH}_2$ group toward the oxygen atom leading to an electrostatic repulsion. The distribution among the three conformations is doubtless changed as solvent is varied, presumably with one or both of the hydrogen-bonded conformations being strongly preferred in the less polar solvents. Nevertheless, the probability of a hydrogen atom extending toward the carbonyl group is probably quite high in all three solvents so that a considerable part of the enhancement of the Cotton effect in acetonitrile and in dioxane is to be attributed to the direct influence of a decrease in dielectric constant and the concomitant increase in the strength of intramolecular electrostatic interactions.

The Cotton effect of the model compound is only 10–15% of that observed in helical polypeptides. It is also opposite in sign. Both of these characteristics are in accord with the previously published theory of the $n-\pi^*$ Cotton effect of peptides.¹¹ It is shown there that the $n-\pi^*$ peptide Cotton effect should follow a quadrant rule with the magnitude and sign of the Cotton effect being proportional to $C(\sum q_i X_i Y_i / R_i^5)$, where X_i , Y_i , and R_i are the x , y , and radial coordinates of the perturbing atoms i in the coordinate system of Figure 4, q_i is the partial charge of the i th atom,^{29,30} and the coefficient C depends on certain perturbation coefficients and transition moments of the isolated peptide group and on the effective dielectric constant of the electrostatic interactions. This coefficient is conformation-dependent only to the extent that the effective dielectric constant is conformation-dependent. Quantitative calculations have not yet been carried out for the model compound but qualitatively the quadrant rule, as illustrated in Figure 4, can be applied. The signs ascribed to the four quadrants are the signs of the Cotton effect to be anticipated for a positive source of potential in the given quadrant. The signs are reversed for a negative source of potential. Because of the R^5 term in the denominator, the

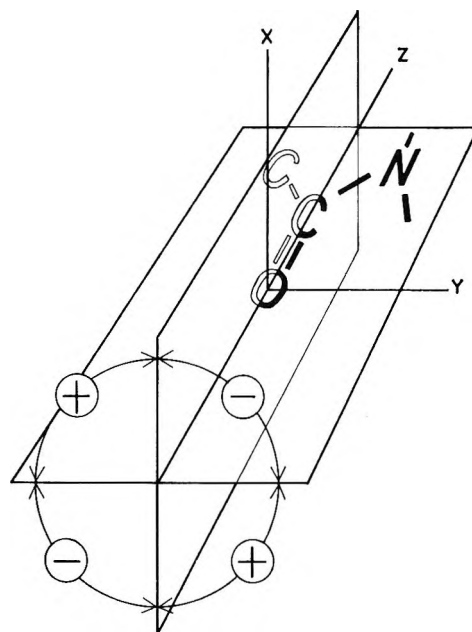


Figure 4. The quadrant rule for the peptide bond. The + and - signs refer to the sign of the Cotton effect induced by a positive source of potential in the given quadrant.

rotation is dominated by atoms which are very close. In the case of L-3-aminopyrrolid-2-one, the nearest atom should be the hydrogen atom of the amino group indicating a positive Cotton effect as can be seen by comparing the structural formula I with Figure 4. In the right-handed α -helix, the atoms are so distributed that a negative Cotton effect is predicted. The relative magnitudes of the Cotton effects in the α -helix and in the model compound are in accord with the fact that the many, close-range interactions of the former are replaced by a single interaction at a larger distance in the latter.

The final conclusions of this work are twofold. The first is that an $n-\pi^*$ Cotton effect of the peptide group is a spectral feature which is brought out by molecular rigidity, properly distributed vicinal atoms, and a low effective dielectric constant. Since all three of these features are possessed by compact helices such as the α -helix, it is apparent that this type of mechanism must play an important role in the eventual interpretation of the far-ultraviolet rotatory properties of such helices. Secondly, we are here observing a multiple

(29) This simple formula depends on the assumption that the perturbation of the peptide group arises from the electrostatic fields of polar or charged neighboring groups. In many ketone problems the perturbing atoms are not polar and a different potential is used.^{30a,b} This does not change the qualitative picture of the quadrant rule, but necessitates different quantitative treatment.

(30) (a) W. Kauzmann, J. Walter, and H. Eyring, *Chem. Rev.*, **26**, 339 (1940); (b) A. Moscowitz, *Advan. Chem. Phys.*, **4**, 67 (1962).

Cotton effect of a simple peptide. Heretofore, this has been considered to be a characteristic possessed only by helices. One is thereby brought to wonder whether or not a 225- $m\mu$ Cotton effect can be induced in the peptide links in regions of a protein which are not helical in the usual sense of the word.

A distinction must be made between a local α -helical conformation and an α -helix. A local α -helical conformation results when two consecutive peptide groups adopt the orientation characteristic of an α -helix. It is specified by the two conformational angles of the α -carbon atom connecting them. This point is discussed at length in ref. 31, section IIA. Excluded volume calculations³² and conformational energy calculations³³ indicate that the local, right-handed, α -helical conformation is particularly favored whether a real helix is formed or not. (An α -helix results from a consecutive series of local α -helical conformations.) These predictions have now been confirmed by Watson,³⁴ who has found that the local α -helical conformation occurs often in the *nonhelical* regions of the myoglobin molecule.

It is possible that such local α -helical conformations, under the appropriate circumstances, could develop an $n-\pi^*$ Cotton effect and thus contribute to the helicity as calculated from rotatory dispersion measurements or from observations of the Cotton effects of proteins.³⁵ The Cotton effect would be smaller because only a part of the array of perturbing atoms of the α -helix are present in the local α -helical conformation. Further, if the local conformation is surrounded by

water, as it is in random polypeptides and denatured proteins in aqueous solution, the Cotton effect would be greatly attenuated by the high dielectric constant of the surroundings. If, on the other hand, the local conformation is buried deep within a protein molecule in a region of low dielectric constant as it might well be in a globular protein with low helical content, then a fractional contribution to b_0 or the 225- $m\mu$ Cotton effect is a distinct possibility since the situation is analogous to the results for L-3-aminopyrrolid-2-one in nonpolar solvents.

Acknowledgment. This research was supported in part by grants from the National Science Foundation, the United States Public Health Service, PHS-Schellman-365-CA 04216-07, and the Sloan Foundation. We are grateful to Dr. S. Wilkinson of the Wellcome Research Laboratories, Langley Court, Beckenham, Kent, for a gift of the model compound and to Drs. Holzwarth, Blout, and Beychok for results prior to their publication.

(31) J. A. Schellman and C. Schellman in "The Proteins," Vol. II, H. Neurath, Ed., Academic Press, New York, N. Y., 1964.

(32) G. N. Ramachandran, V. Sasisekharan, and C. Ramakrishnan, *J. Mol. Biol.*, **7**, 95 (1963).

(33) A. M. Liquori, to be published.

(34) H. C. Watson, private communication.

(35) For convenience in exposition, we have given emphasis to the α -helical conformation. Actually, any local conformation which brings consecutive peptide groups into intimate contact with one another possesses the same possibilities; for example, the local π -helical conformation or the local 3_{10} conformation.³¹

Investigation of Fatty Acid Monolayers on Metals by Contact

Potential Measurements¹

by C. O. Timmons and W. A. Zisman

Chemistry Division, U. S. Naval Research Laboratory, Washington 25, D. C. (Received October 19, 1964)

Each of the homologous series of pure *n*-fatty acids from C₁ to C₂₆ has been studied as a condensed monomolecular layer adsorbed on Pt and NiO substrates. Both the C₁₈ and C₁₉ acids were also studied on various polished metal surfaces including Fe, Cr, Cu, Au, W, Mo, Ag, Nb, Al, Cd, Mg, Sn, Pb, Be, Zn, and Ni. The change in contact potential difference (ΔV) between the metal and an aged reference electrode was measured in air at 23° and 50% R.H. Surface packing in each monolayer was characterized by the methylene iodide contact angle (θ). Systematic and reproducible values of ΔV and θ were found for each member of the homologous series. An asymptotic maximum occurred in the ΔV vs. *N* curves when *N*, the number of carbon atoms per adsorbed molecule, was 14 or more for Pt and NiO substrates. Alternation of ΔV occurred for odd and even values of *N* on NiO and the baser metals but not on Pt and Au. Values of θ for stearic acid varied with the nature of the metal substrate, and the results were in reasonable accord with the lattice spacing of the substrate atoms. Values of ΔV for stearic acid monolayers varied from a maximum of 0.365 v. on W to -0.095 v. on Pb, and it was concluded that the perpendicular component of the dipole moment of the adsorbed acid molecule was a function of the specific interaction of metal substrate and the acid carboxylic group. Stearic acid desorbed readily from Pt but not from NiO, and it was concluded that chemisorption had occurred on the NiO. The contributions from adsorbed water, oxides, and induced polarization in determining ΔV are discussed.

Introduction

Results have been reported recently on contact potential studies of the monolayer adsorption of the homologous family of primary fatty amines.² The same methods were used to advance our knowledge of the properties of a number of autophobic liquids on platinum,^{3a} and Bewig and Zisman^{3b} have succeeded with similar techniques in demonstrating the induced polarization of *n*-alkanes, benzene, toluene, and carbon tetrachloride when adsorbed upon a variety of metals. In each of these studies the contact potential difference and the methylene iodide contact angle were found to be informative about the packing, orientation, and polarization of the molecules comprising the adsorbed monolayer.

This report presents the changes in the contact potential difference (ΔV) resulting from the adsorption of a monolayer of each of the homologous series of *n*-

fatty acids, from formic (C₁) to hexacosanoic (C₂₆), on clean polished platinum and nickel(ous) oxide. It also reports results obtained upon adsorption of stearic and nonadecanoic acids on many other metal substrates.

Experimental Procedures and Materials

Measurements of ΔV were made using the modified ionization method described by Bewig.⁴ The reference electrode, procured from the United States Radium Corp., consisted of a 6-mm. square radium-226 foil

(1) Presented at the 148th National Meeting of the American Chemical Society, Chicago, Ill., Sept. 1, 1964.

(2) K. W. Bewig and W. A. Zisman, *J. Phys. Chem.*, **67**, 130 (1963).

(3) (a) C. O. Timmons and W. A. Zisman, *ibid.*, **68**, 1137 (1964);

(b) K. W. Bewig and W. A. Zisman, *ibid.*, **68**, 1804 (1964).

(4) K. W. Bewig, *Rev. Sci. Instr.*, **35**, 1160 (1964).

sandwiched between a silver base plate and a thin gold overlayer. The electrode had an activity of $5 \mu\text{c}$.

Measurements of the slowly advancing contact angle (θ) exhibited by a sessile drop of pure methylene iodide were made on each of the monolayers studied to indicate the closeness and reproducibility of molecular packing. Contact angles were reproducible within $\pm 1^\circ$. All measurements were made in air at 23° and 50% relative humidity (R.H.)

Each of the monolayers studied was prepared as an adsorbed condensed film on the metal specimen by the retraction method from the melt and/or from nitromethane solution.⁵

The formic through valeric acids used were White Label grade products of Eastman Organic Chemicals, while the remainder were procured from Lachat Chemicals Co. The acids caproic through stearic were stated by the manufacturer to be 99.5% pure, and the nonadecanoic through hexacosanoic acids to be 99.0% pure. Melting points of those acids which were solid at room temperature were measured and all melted within 1 to 2° of the best literature values. The liquid acids were percolated through a long, narrow adsorption column of silica gel and activated alumina just before use to remove any traces of polar impurities.

The "active" electrode was always an exceptionally pure metal; the materials studied were platinum, gold, chromium, cadmium, copper, silver, beryllium, and lead, indicated to be 99.999% pure by the supplier, and nickel, magnesium, aluminum, iron, tin, niobium, molybdenum, zinc, and tungsten, which were reported 99.9% pure or better.

Each metal studied as the active electrode was a flat disk prepared by abrasion under flowing water using a graded series of carborundum metallurgical papers to a final grit size of 600-C. Next, the metal specimen was given a mirror finish on a polishing wheel covered with a Buehler Selvyt cloth using levigated alumina having an average particle size of 0.3μ . Finally, the polished surface was scrubbed on a clean Selvyt cloth under flowing distilled water and dried in an air atmosphere from which organic contamination had been removed.

The nickel oxide surface used was prepared by heating inductively a freshly polished sample of pure nickel for 3 min. at about 650° in clean air.

Experimental Results and Discussion

The contact potential change (ΔV) caused by the adsorption of a condensed monolayer of fatty acid is the result of the fact that each molecule in the monolayer contains a permanent and oriented electrostatic dipole. To this system the Helmholtz relation,

$\Delta V = 4\pi n\mu_p$, may be applied. Here n is the number of molecules adsorbed per unit area, and μ_p is the average perpendicular component of all dipole moments resulting from the adsorption process. The quantity μ_p includes the effects due directly to the electrostatic dipole moment of the adsorbate molecule, the effects due to any redistribution of charge in the vicinity of the surface of the substrate, the reorientation of any adsorbed atmospheric gases present, and the significant lateral polarization arising from neighboring dipoles.⁶⁻⁸ It is thus clear that μ_p bears no simple relation to the dipole moment of the molecule as determined in the gaseous state although it is probably approximately proportional.

Adsorption of Fatty Acids on Platinum. Figure 1 is a plot of ΔV vs. N , the number of carbon atoms per adsorbed molecule, for the homologous series of n -fatty acids adsorbed on platinum. The rectangular markers in the graph indicate the spread of the individual and independent measurements and the circles represent the arithmetical average. In general, the average deviation of any measurement from the curve is about ± 0.015 v. The curve passes through a 0.160-v. minimum for $N = 3$ (propionic acid) and then rises to an asymptotic maximum of 0.355 v. for $N \geq 14$, i.e., for myristic acid and higher homologs. Any changes in ΔV , from one member of the series to another, must reflect differences in molecular packing

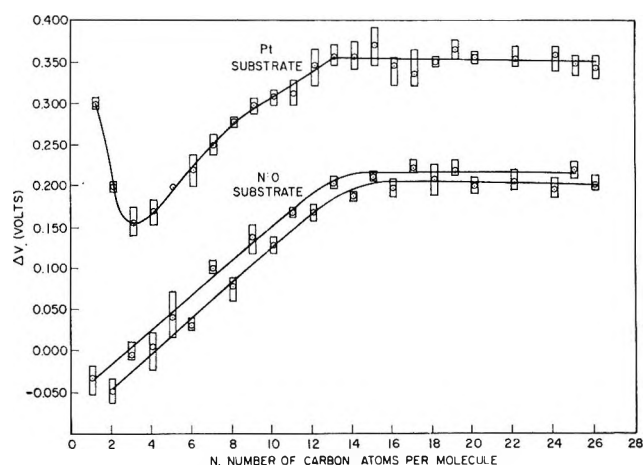


Figure 1. Contact potential difference data for the homologous series of fatty acids adsorbed on Pt and NiO.

- (5) E. G. Shafrin and W. A. Zisman, *J. Phys. Chem.*, **64**, 519 (1960).
- (6) N. K. Adam, "The Physics and Chemistry of Surfaces," 3rd Ed., Oxford University Press, London, 1941, p. 302.
- (7) J. R. Macdonald and C. A. Barlow, Jr., *J. Chem. Phys.*, **39**, 412 (1963).
- (8) M. K. Bennett, N. L. Jarvis, and W. A. Zisman, *J. Phys. Chem.*, **68**, 3520 (1964).

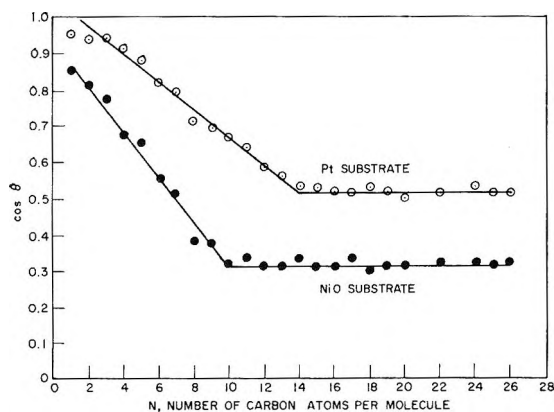


Figure 2. Methylene iodide contact angle data for the homologous series of fatty acids adsorbed on Pt and NiO.

and dipole orientation, since the dipole moments of the fatty acids are virtually the same for each member of the series.⁹

A plot of the cosine of the methylene iodide contact angle (θ) vs. N (see Figure 2) has an analogous asymptotic minimum for $N \geq 14$. The constancy of θ in this region is good evidence of constant molecular packing in these monolayers. Since there is no variation in ΔV for the higher homologs, one must conclude that the packing, as well as orientation of adsorbed molecules, is the same in all acid monolayers having $N \geq 14$. The simplest interpretation is that, when a fatty acid molecule has a paraffin chain of sufficient length, intermolecular cohesive forces between adjacent molecules become large enough to hold the monolayer in a closely packed array. Similar behavior of the primary fatty amines adsorbed on platinum has been reported by Bewig and Zisman.² Levine and Zisman came to the same conclusion from their studies of the friction and wetting properties of retracted monolayers of the fatty acids adsorbed on glass.^{10,11} In each of these investigations methylene iodide contact angles from 68 to 71° were reported on monolayers of the higher homologs. It has been shown^{5,10,11} that methylene iodide contact angles from 68 to 71° are characteristic of a surface comprised of close-packed methyl terminal groups. But it should be noted that in the present study the maximum value of θ obtained on monolayers of the fatty acids adsorbed on platinum was 58°. From this result it can be concluded that the fatty acid molecules adsorbed on platinum either are not as closely packed as on glass or are oriented at a rather large angle from the vertical, thereby exposing methylene groups of the hydrocarbon chain to the surface. The former conclusion is preferred because electron diffraction studies of Brockway and Karle¹² have established

that stearic acid molecules are oriented nearly perpendicularly to the surface of platinum.

As N decreases below 14, the progressive decrease in ΔV and the increase in $\cos \theta$ are indicative of decreased lateral attraction between the adsorbed molecules which allows looser molecular packing and increased tilting of the molecular axis away from the vertical.

The minimum occurring in the ΔV curve at propionic acid and the increase from acetic to formic acid needs explanation. Obviously, at this point a different factor enters into the mechanism determining the value of ΔV other than the trend, as N decreases, toward looser molecular packing and increased molecular tilt. There is an interesting similarity in this region of Figure 1 with the curves of Figures 3 and 4 obtained by plotting the viscosities and surface tensions of the pure, liquid fatty acids as a function of the number of carbon atoms per molecule.^{13,14} A minimum also occurs in these

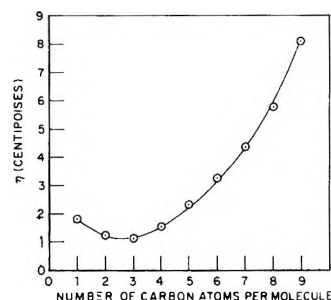


Figure 3. Viscosities of n -fatty acids at 20° as a function of chain length.

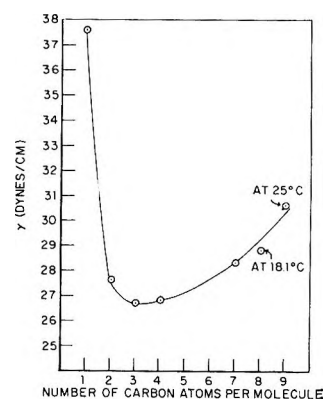


Figure 4. Surface tensions of the liquid n -fatty acids at 20° as a function of chain length.

(9) A. L. McClellan, "Tables of Experimental Dipole Moments," W. H. Freeman and Co., San Francisco, Calif., 1963, p. 580.

(10) O. Levine and W. A. Zisman, *J. Phys. Chem.*, **61**, 1068 (1957).

(11) O. Levine and W. A. Zisman, *ibid.*, **61**, 1188 (1957).

(12) L. O. Brockway and J. Karle, *J. Colloid Sci.*, **2**, 277 (1947).

curves at propionic acid. This minimum has been attributed to the greater association of the lower members of the homologous series.¹³ It is possible that the large values of ΔV obtained for formic and acetic acids are caused by the adsorption of an associated species or by the differences in the water-displacing abilities of the lowest and higher members of the fatty acid family

Adsorption of Fatty Acids on Nickel Oxide. Since the higher homologs of the fatty acids did not close pack when adsorbed on platinum, nickel oxide was chosen as a substrate on which close packing would occur. Electron diffraction patterns obtained from the oxidized nickel indicated that the surface oxide was NiO.¹⁵

In Figure 1 will also be found a plot of ΔV vs. N for the series of fatty acids adsorbed on nickel oxide. Two curves may be drawn through the experimental points, one for odd values of N , and another, about 0.020 v. lower, for even values of N . Both curves have asymptotic maxima for $N \geq 14$. This alternation of ΔV between odd and even members of the series is reminiscent of the alternation found in melting points, specific heats, etc., of these acids. That the alternation of ΔV is not caused by differences in molecular packing in the monolayers is evidenced by the single curve fitting the contact angle data in Figure 2; there is no indication of alternation whatsoever. No alternation of molecular dipole moments has been reported for these acids. Nevertheless, there existed the possibility that the odd and even members of the series adsorbed with the molecular axes at different angles of tilt from the vertical. However, electron diffraction patterns obtained from monolayers of stearic and nonadecanoic acids adsorbed on both NiO and Cu showed there was no difference, over 1 or 2°, in the tilt angle.¹⁵ Although a difference in tilt angle of 1 or 2° could contribute to the observed alternation in ΔV , it is unlikely that it is the primary cause. The major contribution of the molecular dipole moment to ΔV is the vector sum, in a vertical direction, of the group moments at opposite ends of the molecule, viz., the carboxyl group and the terminal methyl group. The addition of one more carbon atom, in going from an odd- to even-numbered acid, for example, will result in the group moment of the terminal methyl group being directed in the opposite direction from which it had been with respect to the moment of the carboxyl group; however, as the vertical component of the dipole moment is the same in each case, this cannot be the cause of the observed alternation.

The maximum methylene iodide contact angle obtained on retracted monolayers of the fatty acids ad-

sorbed on NiO was 71°, which is identical with the results for fatty acids on glass⁹ and for fatty amines on platinum.² Therefore, on NiO the long-chain fatty acids formed monolayers having close-packed methyl groups outermost. Contact angles of 71° were also obtained with methylene iodide on monolayers of capric through tridecanoic acids adsorbed on this same substrate; hence, a close-packed monolayer was formed with these compounds even though the hydrocarbon chain was not of sufficient length to cause such close packing through the action of intermolecular cohesive forces alone. For reasons that will be discussed below, it is concluded that a reaction between the fatty acid monolayer and the NiO substrate had contributed to cause the observed close packing. In other words, the monolayers of acids having $N \geq 10$ were held in a close-packed array owing to the combined effects of a chemical bond between the acid and the substrate and the forces of intermolecular attraction.

The shorter chain fatty acids adsorbed on NiO caused smaller values of ΔV and θ . Decreasing values of θ indicate looser molecular packing; this result, coupled with the possibility that the molecules below $N = 10$ can develop larger angles of tilt from the vertical, will explain the decrease in ΔV with decreasing chain length. The ΔV vs. N graphs of the fatty acids adsorbed on NiO are essentially rectilinear between formic and lauric acids, and there was no such minimum as that observed with the platinum substrate. This result is evidence of a different mechanism of adsorption on NiO than on Pt.

It will be noted that ΔV for formic, acetic, and propionic acids, when adsorbed on NiO, was negative. These values should be considered only as being less positive than the values given by the longer chain homologs. The reversal in sign in going to lower values of N is caused by the contact potential of the adsorbed monolayer becoming negative with respect to the reference electrode.

Desorption of Stearic Acid from Platinum and Nickel Oxide. In seeking to determine, at least qualitatively, whether or not the fatty acids were adsorbed more firmly, or differently, on nickel oxide than on platinum, an attempt was made to desorb a stearic acid monolayer from Pt and NiO by using two different techniques. One involved raising the temperature of the

(13) K. S. Markley, "Fatty Acids, Their Chemistry and Physical Properties," Interscience Publishers, Inc., New York, N. Y., 1947, p. 225.

(14) N. A. Lange, "Handbook of Chemistry," 9th Ed., Handbook Publishers, Inc., Sandusky, Ohio, 1956, p. 1649.

(15) R. L. Jones, private communication.

substrate to a degree sufficient to cause desorption, and the other involved the extraction of the monolayer with an appropriate pure solvent. Measurements of ΔV and θ before and after treatment of the surface were used to indicate the extent of desorption of the monolayer.

Condensed monolayers of stearic acid were adsorbed on both polished platinum and on nickel oxide, and, after ΔV and θ had been measured, each specimen was either heated or was exposed to solvent extraction using pure diethyl ether in a Soxhlet extractor. (Diethyl ether was chosen because stearic acid is soluble in ether, but nickel stearate is not.) After each specimen was treated and was allowed to equilibrate in clean air at 23°, measurements were again made of ΔV and θ . The solvent extraction treatment was repeated until no further changes in ΔV or θ were observed. It was also necessary to heat the solvent-extracted specimen to 100° to remove any adsorbed diethyl ether since our recent work^{3b} had shown that such a monolayer might remain after the solvent treatment even if the stearic acid monolayer had been removed. A temperature of 100° was not sufficient to remove any stearic acid from Pt or NiO. Equilibrium values of ΔV and θ for stearic acid monolayers, before and after desorption experiments, are given in Table I.

Table I: Results of Desorption Experiments on Stearic Acid Monolayers^a

Surface investigated	Contact potential difference, ΔV , v.	CH ₂ I ₂ contact angle, θ , deg.
Bare Pt	0.000	23
Stearic acid monolayer on Pt	0.355	58
Stearic acid monolayer on Pt after heating to 130°	0.005	22
Stearic acid monolayer on Pt after 1-hr. ether extraction and heating to 100°	-0.015	25
Bare NiO	0.000	Spread
Stearic acid monolayer on NiO	0.210	71
Stearic acid monolayer on NiO after heating to 150°	0.180	61
Stearic acid monolayer on NiO after 4-hr. ether extraction and heating to 100°	0.165	51

^a All measurements in air at 23° and 50% R.H.

A monolayer of stearic acid on Pt caused ΔV to be 0.355 v. and θ to be 58°. When the temperature of the Pt covered by stearic acid was raised, at the rate of about 1°/min., in clean air to 130° and then cooled to room temperature, values of ΔV and θ each returned to

the respective values obtained on bare Pt. However, it can be seen from the values of ΔV and θ in Table I that raising the temperature of the stearic acid coated NiO surface to 150° (at the same heating rate) removed little of the monolayer. Similarly, a 1-hr. ether extraction of a stearic acid monolayer on Pt, followed by subsequent heating to 100°, removed all the monolayer, whereas a 4-hr. ether extraction and subsequent heating removed little of the monolayer from the NiO substrate. Thus, it is clear that stearic acid is adsorbed on NiO much more strongly than on Pt, presumably by chemisorption on the former substrate and by physical adsorption on the latter.

Adsorption of Stearic and Nonadecanoic Acids on Various Metals. Condensed monolayers of stearic and nonadecanoic acids were also adsorbed on a variety of polished, clean metals, and the resulting contact potential difference (ΔV) and the methylene iodide contact angle (θ) obtained on the monolayer were measured. These results will be found in Table II.

Table II: Contact Potential Difference and CH₂I₂ Contact Angle Data for Monolayers of Stearic and Nonadecanoic Acids Adsorbed on Various Metals^a

Adsorbent metal	Stearic acid monolayer		Nonadecanoic acid monolayer	
	ΔV , v.	θ , deg.	ΔV , v.	θ , deg.
Tungsten	0.365	59	0.415	59
Platinum	0.355	58	0.360	58
Molybdenum	0.350	65	0.380	64
Aluminum	0.300	68
Nickel	0.275	63	0.315	63
Chromium	0.260	61	0.305	62
Iron	0.240	71
Silver	0.235	61
Niobium	0.220	64	0.330	63
Gold	0.140	45	0.140	47
Cadmium	0.115	64	0.130	65
Tin	0.110	66	0.130	65
Copper	0.095	66	0.170	66
Magnesium	-0.070	68
Lead	-0.095	62
Beryllium	...	68
Zinc	...	68

^a All measurements at 23° and 50% R.H.

Values of ΔV for stearic acid monolayers varied between the extremes of 0.365 v. on tungsten and -0.095 v. on lead; nonadecanoic acid caused values of ΔV between 0.415 v. on tungsten and 0.130 v. on both cadmium and tin. With the exception of the values of ΔV caused by nonadecanoic acid on niobium and copper, there is the same progression from high to low values of

ΔV for both stearic and nonadecanoic acid monolayers on the various metals. Nonadecanoic acid monolayers gave higher values of ΔV than did stearic acid monolayers on the same metal, except when adsorbed on gold and platinum; on these metals the same ΔV was obtained for each acid. This difference is not a result of differences in molecular packing in the monolayer because θ was the same for both monolayers on the same metal. These facts indicate that the alternation in ΔV between acids having an odd and even number of carbon atoms is observed on all but the noble metals. They also indicate that the phenomenon of alternating ΔV is dependent upon the ability of the monolayer to react with the substrate or otherwise adsorb more strongly than through physical adsorption alone.

It will be seen that there were also considerable variations among the metals in the values of θ ; the extremes were 71° for iron and 45° for gold. Such a range in θ indicates either a variation in the packing of the adsorbed acid molecules or in β , the angle of departure from the normal of the principal molecular axis. Since ΔV will be proportional both to the number of adsorbed molecules per unit area and to $\cos \beta$, ΔV should increase with decreasing β if no other factor is altered. Nevertheless, the variation in ΔV does not appear related to that in θ . The orientation of adsorbed, retracted monolayers of the even members of the family of fatty acids has been studied with electron diffraction techniques by many able investigators,^{12,16-19} and all have agreed that the higher members (above 8 or 10 carbon atoms per molecule) are oriented on Pt, Fe, Ag, Zn, Cd, Cu, Ni, and Al within a few degrees of the vertical; *i.e.*, $\beta \cong 0^\circ$. Hence, the variation in θ reported in Table II cannot be due to a variation in β and must be caused by variation in the surface density of packing of the acid molecules.

Any analysis of adsorption sites, whether on bare metal or metal oxide surfaces, must take into account the atomic dimensions of the outermost layer of metal atoms. The structure and orientation of a thin oxide film in its early stages of development, such as we have on the freshly polished metals studied here, is directly related to the structure and orientation of the underlying metal.²⁰ As an approximate method of analysis, we ignored the effects of crystallinity of the substrate and the fact that the metals studied, besides being oxide coated, probably were covered with adsorbed atmospheric gases, and plotted θ for methylene iodide on the various metals coated with stearic acid against the covalent radius of the metal in question (Figure 5).²¹ It was necessary to use the metallic atomic radii, assuming a coordination number of 12, for the transition metals. It will be seen that the data fall on two

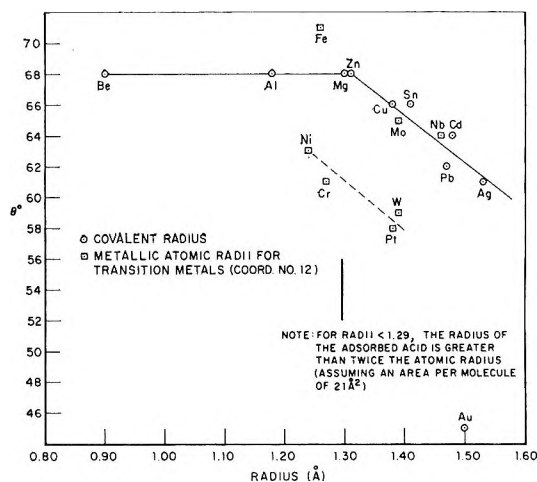


Figure 5. Methylene iodide contact angles (θ) on stearic acid monolayers on various metals *vs.* covalent radius (r_0).

curves; the lower curve involves only the transition metals and the upper curve the other metals, with the exception of the transition metals Nb and Mo. The points for Au and Fe do not fit the curve well. The upper curve reaches a maximum of $\theta = 68^\circ$ at an atomic radius of 1.31 \AA . If one assumes that the metallic atoms of the substrate are arranged in a hexagonal, close-packed array and that a stearic acid molecule will always adsorb directly over one of the metal atoms when possible, it can be seen that, because of the relatively large dimensions of the acid molecule with respect to the substrate atoms, the acid molecules will not completely close pack as long as the cross-sectional radius of the acid is less than twice the atomic radius of the substrate metal. Using this model for the adsorption process, it is an evident inference that the closest packing of adsorbed molecules will occur when the cross-sectional radius of the acid molecule is exactly twice the atomic radius. Assuming the cross-sectional area of stearic acid to be 21 \AA^2 , the cross-sectional radius is 2.59 \AA . The radius of substrate atom, then, which will create closest packing (and therefore the maximum contact angle) is 1.29 \AA , which is almost exactly the value at which the maximum contact angle is reached in Figure 5. This interesting observation indicates the possibility of

(16) J. M. Cowley, *Trans. Faraday Soc.*, **44**, 60 (1948).

(17) J. W. Menter, *Proc. Roy. Soc. (London)*, **A204**, 514 (1951).

(18) J. A. Chapman and D. Tabor, *ibid.*, **A242**, 96 (1957).

(19) R. T. Mathieson, *Nature*, **186**, 301 (1960).

(20) O. Kubaschewski and E. E. Hopkins, "Oxidation of Metals and Alloys," Butterworth and Co. Ltd., London, 1962, Chapter 1.

(21) R. T. Sanderson, "Chemical Periodicity," Reinhold Publishing Corp., New York, N. Y., 1960, pp. 26-28.

selecting the dimensions of both metal adsorbent and adsorbate in such a way as to obtain the maximum contact angle.

All of the evidence presented has led to the conclusion that a condensed, retracted monolayer of stearic acid, for example, adsorbs on a metal in a vertical orientation and with a surface-packing density determined by the spacing of adsorption sites on the metal (or oxidized metal) surface. The spacings deduced from the distances between nearest neighbors in the surface of the metal are in reasonable accord with the minimum possible spacing between adsorbed stearic acid molecules. It should now be obvious that, for a fair comparison of the values of the contact potential change (ΔV) owing to the adsorption of the acids on the various metals of Table II, it will be necessary to allow for the variation in the number of adsorbed molecules per unit area (n). We are attempting the measurement of n by using C^{14} -labeled stearic acid. It should then be possible to use n and ΔV from Table II with the Helmholtz equation to compute the value of μ_p , the perpendicular component of the dipole moment per adsorbed stearic acid molecule. Any variation in μ_p

would then reflect any differences in the adsorption mechanism between the acid group and the different metals and oxides. It should be apparent from Table II, because of the much larger range of values of ΔV than of θ , that stearic acid has an interaction with each metal which varies remarkably with the nature of the metal (or oxide).

Any chemical reaction of the carboxyl group of a fatty acid with the oxidized surface of a metal would be expected to change the original dipole moment of the molecule, and the extent of such a reaction may be different at higher temperatures. However, adsorbed water on the metal could also participate in the mechanism, and excess water may be displaced by the adsorbing organic film; if so, then the value of μ_p would be altered because of contributions from dipole moments of water molecules. Apart from any chemical reaction occurring which would alter μ_p , there would be changes in the induced polarization of the adsorbed carboxyl group caused by the highly localized electrostatic fields of the various metals.^{3b} Of course, it would be interesting to separate these three effects on ΔV , but further research is needed to do so.

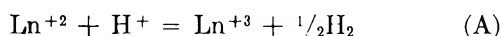
The Heats of Formation of Anhydrous Europium(II) Chloride and of the Aqueous Europium(II) Ion^{1a}

by C. T. Stubblefield, J. L. Rutledge, and R. Phillips^{1b}

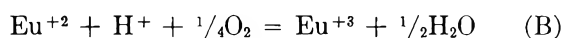
*Department of Chemistry, Prairie View Agricultural and Mechanical College, Prairie View, Texas
(Received October 20, 1964)*

The heats of reaction of metallic Eu and of EuCl₂(s) in hydrogen-saturated 6.00 M HCl were found to be -141.0 and -21.7 kcal./mole, respectively, by adiabatic calorimetry. The reactions followed virtually oxygen-free paths and were catalyzed by platinum black. Calculations for the heats of formation of EuCl₂(s) and Eu(II)(aq) yielded the values of -195.8 and -120.9 kcal./mole, respectively.

All 14 of the lanthanon metals can exist in the trivalent state in solution, but only three of them, namely, Sm, Eu, and Yb, have been definitely proved to be capable of possessing the divalent state in solution. Sm(II), Eu(II), and Yb(II) are easily oxidized to the trivalent state in acid solution according to path A

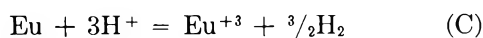


A second path is also available for the oxidation of Eu(II)^{2,3}



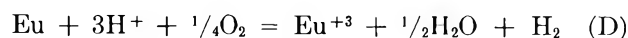
Previous attempts to measure the heats of solution and oxidation of EuCl₂ in which the reaction proceeded by only one path, A or B, gave inconsistent results.^{2,3} When emphasis was placed on path A, the EuCl₂ was oxidized in hydrogen-saturated 6.00 M HCl yielding -27 to -36 kcal./mole. Similarly, the range of results for which the reaction proceeded predominantly by path B in oxygen-saturated 0.015 M HCl was -51 to -60 kcal./mole. Since the oxidation of Eu(II) by path B liberates more heat and proceeds more rapidly than by path A, the very low hydrogen ion concentration in the latter case would favor path B.

Likewise, it is to be expected that the oxidation of metallic europium in acid solution is dependent on the availability of oxygen. If oxygen is absent, the oxidation of the metal follows path C



Burnett and Cunningham⁴ reported the heat of re-

action of Eu metal in oxygen-saturated 0.1 M HCl to be -164.57 kcal./mole at 298.2°. The reaction followed path D



In this paper the techniques which have been devised to measure the heats of solution of EuCl₂ and Eu metal in 6.00 M HCl are presented, and the results are tabulated. The calorimetric data thus obtained are combined with other published data to obtain the standard heats of formation of solid EuCl₂ and of the aqueous Eu(II) ion.

The Adiabatic Calorimeter

This 200-ml. solution calorimeter was designed for these experiments and was operated near room temperature and at atmospheric pressure. The assembly had many of the features which were described previously.² The major differences are given below.

Tantalum Calorimeter: (1) spherical bottom; (2) four tubes—two to accommodate the thermocouple junctions at the calorimeter end of the main thermel, and the other two to contain the two calibration heaters; (3) a platinized platinum stirring propeller (the

(1) (a) This research was supported by a Robert A. Welch Foundation grant; (b) National Science Foundation Graduate Research Participant, 1964.

(2) G. R. Machlan, C. T. Stubblefield, and L. Eyring, *J. Am. Chem. Soc.*, **77**, 2975 (1955).

(3) C. T. Stubblefield and L. Eyring, *ibid.*, **77**, 3004 (1955).

(4) J. L. Burnett and B. B. Cunningham, paper presented at the Fourth Rare Earth Research Conference, Phoenix, Ariz., April 22, 1964.

deposited platinum catalyzes the oxidation of Eu metal or Eu(II) by hydrogen ions).

Copper Adiabatic Shield: (1) spherical bottom; (2) a new type thermocouple support made of nickel-plated copper extending three-eighths of the distance around the circumference of the adiabatic shield, permanently attached to the top, but removable from the main part of the shield, and having 164 holes (No. 61 drill) to accommodate all the junctions of those ends of the two B. and S. 36 chromel-alumel thermels which serve the shield; (3) a platinum resistance thermometer noninductively wound with high grade, hand-drawn B. and S. 36 wire on a thin strip of mica, adjusted for 25.5 ohms at 0°, and connected to a Leeds and Northrup Model G1 Mueller bridge; (4) an automatically controlled heater wound on the outside of the adiabatic shield to supplement the other manually controlled heater; (5) a similar such arrangement operated independently on the top.

Brass Isothermal Shield: (1) spherical bottom; (2) a 0.64-cm. o.d. copper tube welded into the housing of the stirrer mechanism for attachment of a gas line to control the atmosphere above the contents of the calorimeter.

Energy-Input Circuit: (1) the Leeds and Northrup Type K3 potentiometer used to monitor the current through the two calibration heaters, as well as to measure the potential across them; (2) an American Time Products, Inc., Type 2001-2L frequency standard (60 c.p.s. ± 1 p.p.m.) to activate the relays in the push-button system so that accurate intervals of 0.2 min. of calibration heat to the calorimeter could be supplied; (3) a Kepco Model CK 40-0.8M d.c. power supply to furnish the current to the heaters.

Characteristics: (1) 76.53 cal./min. of heat supplied by the energy-input circuit; (2) a heat capacity of 48.6 cal./deg.; (3) thermometer sensitivity of 10^{-4} deg.; (4) a thermal leakage modulus of 10^{-3} min.⁻¹.

Preparation and Analysis of Samples

Anhydrous EuCl₂. Eu₂O₃, obtained from Research Chemicals and labeled 99.9% pure, was first ignited in a platinum crucible at 900° for 1 hr. in an electric furnace to rid it of any oxalate which might have been present. After cooling, the oxide was transferred to a Pyrex crucible and suspended in a chlorinating apparatus which was similar to, but larger than, the one described previously.² The oxide was completely chlorinated to anhydrous EuCl₃ within 24 to 48 hr. by cycling CCl₄ vapor over it at 450°. After this period of time, the electric power to the furnace tube was removed, and the cycling of CCl₄ was continued until the temperature of the sample was low enough to

allow some condensation of liquid over the sample. This liquid, together with the dense vapor of CCl₄, served to protect the bright yellow EuCl₃ from exposure to the atmosphere during its transfer to a simple hydrogen reduction apparatus which had been filled previously with dry nitrogen gas. The reduction apparatus was immediately attached to a vacuum line, and the CCl₄ was pumped into a trap which was cooled by liquid nitrogen, care being taken to prevent the sample from being pulled out of the crucible during the process. In order to eliminate the possibility of carbon formation during the reduction of EuCl₃, the sample was then heated for about 30 min. at 250° *in vacuo* to sublime any hexachloroethane which occurred upon pyrolysis of CCl₄. Next, it was allowed to cool to room temperature, and atmospheric pressure was restored with dry nitrogen. Pure hydrogen was then passed over the EuCl₃, and the temperature was slowly increased to 450° where reduction to EuCl₂ was completed within 6 to 8 hr. The pure white EuCl₂ was then cooled to room temperature; the stopcocks were closed, and the reduction apparatus was immediately taken to the drybox. In an argon atmosphere, the EuCl₂ was removed from the reduction apparatus, ground to a fine powder in an agate mortar, and stored in a glass-stoppered bottle until ready for use.

Qualitatively, the anhydrous EuCl₃ was shown to be free of oxide or oxychloride when a test portion produced a clear yellow solution in water. Subsequently, the solution became turbid white owing to oxidation and hydrolysis. Addition of HCl until acidic resulted in a water-clear solution. Powder X-ray patterns showed the same *d*-spacings reported in the ASTM data file.

Gravimetric quantitative determinations were made on each preparation for Cl and Eu. A weighed portion of the sample was dissolved in 0.1 *M* HNO₃ and precipitated as AgCl. After all excess Ag was removed from the filtrate with 6.00 *M* HCl, Eu was precipitated with either oxalic or tricarballic acid,⁵ and the residue was ignited to Eu₂O₃ in a platinum crucible. The analyses for three different preparations are given in Table I. The theoretical yields are 68.19% Eu and 31.81% Cl.

Eu Metal. The metal obtained from Research Chemicals was shipped under oil and labeled 99.9% pure. A thick piece was taken from the stock bottle in the argon atmosphere of the drybox and washed with anhydrous benzene. The yellowish coating on the metal was removed with an abrasive wheel, leaving the characteristic metallic appearance. The

(5) A. K. Gupta and J. E. Powell, paper presented at the Fourth Rare Earth Research Conference, Phoenix, Ariz., April 1964.

Table I: Analyses of EuCl_2

Wt., g.	% Eu	% Cl	% total
4.4	67.82	31.33	99.15
5.8	68.17	31.71	99.88
5.0	68.18	31.74	99.92

metal was then cut into pieces of suitable size for the calorimeter.

Experimental Methods

The procedure for assembling the calorimeter preparatory to carrying out a measurement on EuCl_2 is presented in detail because of the extreme importance of the elimination of oxygen from the system.

When it was deemed necessary, the platinum black deposit on the stirring propeller was dissolved in aqua regia, and a fresh coating was restored by electrolysis. It was difficult to determine when best to renew the deposit because sometimes the older job served to catalyze better the oxidation of Eu^0 or Eu^{+2} by hydrogen ions. The conditions under which the poisoning of the catalyst occurred were never clearly understood; however, the usual precautions concerning deposition and protection of platinum black were observed.

Fragile calorimeter bulbs similar in shape to those described by Westrum and Eyring⁶ were blown from flint glass, and a glass bead was fitted to each tapered neck. The bulbs were cleaned with dichromate solution and thoroughly rinsed with water. Their approximate volumes were measured by buret for later weight corrections. The bulbs were then dried in an oven at 110° and cooled in a desiccator containing Drierite.

Bulbs having volumes of 1–3 ml. were selected for the EuCl_2 runs. Each was weighed together with its glass bead and a globule of Apiezon W wax on the Mettler B6 semimicro balance (0.05 mg./div.). They were taken into the drybox, filled with EuCl_2 , sealed with a hot-wire heater, and finally returned to the same balance and reweighed.

The cleaned Eu metal samples were weighed directly on the Cahn gram electrobalance (precision: 0.05 mg. on 500-mg. range), which was set up in the drybox, and these were then sealed into bulbs having volumes 0.3 to 0.4 ml.

A bulb containing the sample to be run was firmly sealed below the platinized stirrer with additional Apiezon W wax. The calorimeter was almost filled with 215 g. of 6.00 *M* HCl. To increase the solubility of hydrogen, the acid was cooled to 15° in an ice bath

while being saturated with hydrogen by means of a fritted glass dispersion tube inside a fume hood. This hydrogen had previously been passed through a Deoxo to remove oxygen and also through a gas-washing bottle having a fritted glass disk, containing 6.00 *M* HCl to saturate it. After 5 min. the dispersion tube was removed from the calorimeter, and the calorimeter was loosely bolted to its top, leaving a small gap. Dry hydrogen was passed through the gas inlet of the stirrer housing, and Apiezon Q putty was packed over the opening at the top of the housing to force the hydrogen stream downward into the space above the acid and out through the gap. At the end of 10 min. it was assumed that all the air above the acid had been flushed out. The top was then tightened against the O-ring gasket of the calorimeter, and the putty was removed from the stirrer housing. The hydrogen then flowed upward through the stirrer mechanism and prevented the entrance of air to the calorimeter. This flow was not interrupted for the duration of the run.

The cooled calorimeter was wiped fairly free of dew; the adiabatic shield was attached and cooled to about 23.5° . After mounting the isothermal shield, the assembly was taken from the hood to the isothermal bath where the rest of the connections were made. A portable exhaust hood was mounted just above the stirrer housing to remove hydrogen from the room.

It required about 1 hr. to evacuate the space between the calorimeter and the isothermal shield owing to the dew accumulated on the cold calorimeter. This time was utilized to warm the adiabatic shield to the desired starting temperature of 24.2 or 24.3° . The rise in temperature of the calorimeter, together with the stirring of the acid, caused a further slight flushing of the acid as the solubility of the hydrogen decreased.

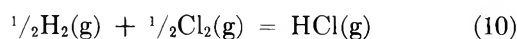
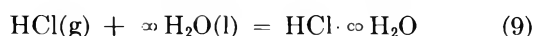
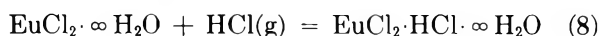
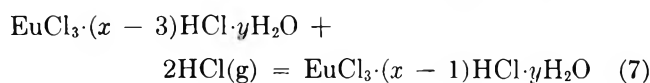
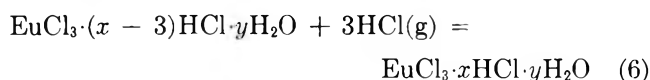
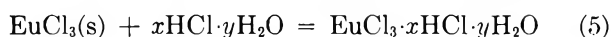
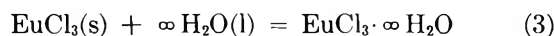
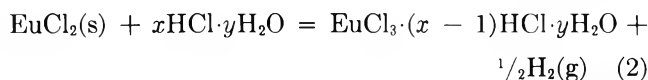
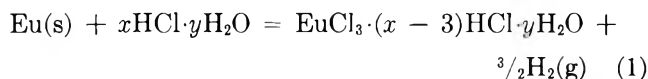
Throughout the run, the temperature of the adiabatic shield was kept as near as possible to that of the calorimeter, using both the manual and the automatic heater controls. While observing the natural drift in temperature of the calorimeter, the precision of control was about 10^{-5}° , but during the two 2-min. period when calibration heat was supplied or during the initial few minutes of the sample reaction, the precision of control was sometimes not better than 0.1° . A run consisted of (1) plotting a 20- to 40-min. temperature drift at the initial temperature, (2) supplying exactly 2 min. of calibration heat to the calorimeter by means of the heat-input circuit, which raised the temperature to about 25° , (3) plotting a second temperature drift for 40 to 100 min., (4) initiating the

(6) E. F. Westrum, Jr., and L. Eyring, *J. Am. Chem. Soc.*, **74**, 2045 (1952).

reaction by depressing the stirring shaft to break the bulb (the time required for completion of the reaction depended upon the nature and weight of the sample, and also upon the condition of the platinum catalyst on the propeller), (5) plotting a third temperature drift of the calorimeter for about 1 hr., (6) supplying another calibration heat for exactly 2 min. to the calorimeter, and (7) plotting a final temperature drift. Steps 6 and 7 were optional.

Results

The results of five runs to determine the heat of reaction of Eu metal with 6.00 *M* HCl are shown in Table II, and those for 11 runs on EuCl₂ in 6.00 *M* HCl are shown in Table III. These data were combined with other published thermodynamic quantities to obtain the standard heats of formation of EuCl₂(s) and of aqueous Eu(II). The proper combinations of the following thermochemical equations yielded the desired values



Reactions 1 and 2 occurred in these experiments, the results of which are given in Tables II and III. The mole ratio y/x was 8.131 when calculated for 6.00 *M* HCl, using data from density tables. The values of ΔH_1 and ΔH_2 were -141.0 ± 0.8 and -21.7 ± 0.7 kcal./mole, respectively.

Reaction 3 represents the heat of solution of EuCl₃ in an infinite amount of water. The liberated heat should differ little from that in a very large quantity of 0.015 *M* HCl for which ΔH_3 is -40.2 ± 0.3 kcal./mole.²

Reaction 4 is the oxidation of Eu(II) to Eu(III).

Table II: Heat of Reaction of Eu Metal in 6.00 *M* HCl

Wt., g.	Time, min. ^a	ΔH , kcal./mole ^b
0.09620	180	-141.1
0.2777	180	-140.7
0.2314	30	-141.9
0.2523	100	-139.9
0.1993	110	-141.5
Av.		-141.0 ± 0.8^c kcal./mole

^a Estimated time for completion of reaction. ^b Includes -0.45 kcal./mole for evaporation of water by the liberated hydrogen. ^c Standard deviation.

Table III: Heat of Reaction of EuCl₂ in 6.00 *M* HCl

Wt., g.	Time, min. ^a	ΔH , kcal./mole ^b
0.09805	75	-22.7
0.79189	40	-21.4
0.55963	30	-22.8
2.98691	45	-21.3
1.07343	45	-21.0
0.63925	20	-22.2
0.73342	20	-22.2
0.64129	20	-21.4
1.48597	15	-20.8
0.43040	10	-22.2
3.93607	15	-21.2
Av.		-21.7 ± 0.7^c kcal./mole

^a Estimated time for completion of reaction. ^b Includes -0.15 kcal./mole for evaporation of water by the liberated hydrogen. ^c Standard deviation.

The heat of oxidation was calculated from the oxidation-reduction potential of McCoy⁷ ($E = 0.43$ v.), and the entropies of the aqueous ions as determined from the Powell-Latimer equation.⁸ The ionic radii needed for this equation were those tabulated by Brewer, *et al.*⁹ $\Delta S_{298}^\circ[\text{Eu(II)} - \text{Eu(III)}]$ became -32.4 e.u., and ΔH_4 was -19.6 kcal./mole.

Reaction 5 is the heat of solution of EuCl₃(s) in 6.00 *M* HCl, and ΔH_5 is -30.9 ± 0.2 kcal./mole.²

Reactions 6 and 7 concern the solutions of a few moles of HCl(g) in large quantities of nearly 6.00 *M* (6.83 *m*) HCl. In calculations of the heat of formation of EuCl₂(s) and of Eu(II)(aq), cancellations resulted in the differences in the heats of formation of two nearly 6.00 *M*

(7) H. N. McCoy, *J. Am. Chem. Soc.*, **58**, 1579 (1936).

(8) W. M. Latimer, "Oxidation Potentials." Prentice-Hall, Inc., New York, N. Y., 1952, p. 365.

(9) L. Brewer, L. A. Bromley, P. W. Gilles, and N. L. Lofgren, "Chemistry and Metallurgy of Miscellaneous Materials. Thermodynamics," National Nuclear Energy Series IV, Vol. 19B, Paper 6.

HCl solutions for which differential heats of formation were employed. Successive values of published data¹⁰ for ΔH_f° of $\text{HCl} \cdot n_1\text{H}_2\text{O}$ were converted into the form $\Delta[m(\Delta H_f^\circ)_{n_2=1}]/\Delta m$, and a chord-area graph of these slopes was plotted against molality as abscissa. The desired value of the slope was taken from the graph and multiplied by the number of moles of $\text{HCl}(\text{g})$ involved in the change in concentrations of the acid solutions. The slope thus determined was -36.78 kcal./mole. The presence of small amounts of EuCl_3 in reactions 6 and 7 was ignored.

Reactions 8 and 9 each correspond to the heat of solution of $\text{HCl}(\text{g})$ at infinite dilution. The presence of EuCl_2 in reaction 8 was ignored. Since the $\text{HCl}(\text{g})$ was cancelled out when these reactions were involved in the calculations, only $\Delta H_f^\circ[\text{HCl} \cdot \infty \text{H}_2\text{O}]$ was left, and its value was found in the literature to be -40.023 kcal./mole.¹⁰

Reaction 10 is the heat of formation of $\text{HCl}(\text{g})$, which cancels out in the calculations.

The heat of formation of $\text{EuCl}_2(\text{s})$ is represented by



and

$$\begin{aligned} \Delta H_{11} &= \Delta H_1 - \Delta H_2 + \Delta H_7 + 2\Delta H_{10} \\ &= \Delta H_1 - \Delta H_2 + \{ \Delta H_f^\circ[(x-1)\text{HCl} \cdot y\text{H}_2\text{O}] - \\ &\quad \Delta H_f^\circ[(x-3)\text{HCl} \cdot y\text{H}_2\text{O}] \} \\ &= -192.8 \text{ kcal./mole} \end{aligned}$$

The heat of formation of $\text{Eu}(\text{II})(\text{aq})$ is given by

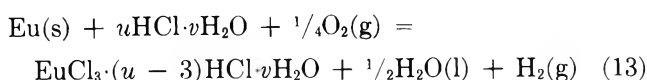


and

$$\begin{aligned} \Delta H_{12} &= \Delta H_1 + \Delta H_3 - \Delta H_4 - \Delta H_5 + \\ &\quad \Delta H_6 - \Delta H_8 - 2\Delta H_9 \\ &= \Delta H_1 + \Delta H_3 - \Delta H_4 - \Delta H_5 - 3\Delta H_f^\circ \\ &\quad [\text{HCl} \cdot \infty \text{H}_2\text{O}] + \{ \Delta H_f^\circ[x\text{HCl} \cdot y\text{H}_2\text{O}] - \\ &\quad \Delta H_f^\circ[(x-3)\text{HCl} \cdot y\text{H}_2\text{O}] \} \\ &= -120.9 \text{ kcal./mole} \end{aligned}$$

Discussion

It was desirable to correlate the results obtained in our experiments with those of Burnett and Cunningham.⁴ Their reaction of metallic europium with oxygen-saturated 0.1 M HCl may be represented by



where the mole ratio v/u is 552.6. When four selected

equations concerning dilution and solution of HCl were properly combined with reaction 13 and the equation involving the formation of 0.5 mole of $\text{H}_2\text{O}(\text{l})$ was subtracted, reaction 1 was obtained. After appropriate cancellations, the expression for the heat evolved was reduced to

$$\begin{aligned} \Delta H_1 &= \Delta H_{13} - 1/2\Delta H_f^\circ[\text{H}_2\text{O}(\text{l})] + \\ &\quad \{ \Delta H_f^\circ[u\text{HCl} \cdot v\text{H}_2\text{O}] - \\ &\quad \Delta H_f^\circ[(u-3)\text{HCl} \cdot v\text{H}_2\text{O}] \} - \\ &\quad \{ \Delta H_f^\circ[x\text{HCl} \cdot y\text{H}_2\text{O}] - \\ &\quad \Delta H_f^\circ[(x-3)\text{HCl} \cdot y\text{H}_2\text{O}] \} \end{aligned}$$

ΔH_{13} and $\Delta H_f^\circ[\text{H}_2\text{O}(\text{l})]$ are -164.57 and -68.3174 kcal./mole, respectively. Each of the terms enclosed in braces was evaluated in the same manner as were the corresponding terms in reactions 6 and 7. Within the braces, we obtained $3(-39.82)$ and $3(-36.78)$ kcal./mole, respectively. ΔH_1 was therefore calculated to be -139.53 kcal./mole, as compared to our experimental value of -141.02 kcal./mole. It should be noted here that Burnett and Cunningham rejected europium metal which was obtainable from commercial sources as being unsuitable for their calorimetry. As previously mentioned, oil and a hard yellow substance, assumed to be some form of oxide, were cleaned away from the surface of our Eu metal samples.

Burnett and Cunningham⁴ estimate the heat of formation of $\text{Eu}(\text{II})(\text{aq})$ to be -115.7 kcal./mole, as compared to our value of -120.9 kcal./mole. The main difference apparently lies in the method of obtaining the uncertain $\Delta S^\circ_{298}[\text{Eu}(\text{II}) - \text{Eu}(\text{III})]$ in reaction 4, as well as in the previous anomaly.

As shown in Tables II and III, the sizes of the samples had little to do with the reaction rates. The condition of the platinum catalyst, which was deposited on the stirring propeller of the calorimeter, apparently was the predominant factor. Also, the reaction rates may have been sensitive to slight changes in the procedures of preparation of the samples and to the time lapse between their preparation and their use.

Acknowledgments. We are indebted to Dr. Leroy Eyring (Department of Chemistry, Arizona State University) for his advice on the methods of eliminating oxygen from the calorimeter, to Dr. Charles Urby and his students (Prairie View) for the X-ray analyses of our EuCl_2 preparations, and to Mr. James Crowe (Prairie View) for the preparation and chemical analyses of some of the EuCl_2 samples.

(10) "Selected Values of Chemical Thermodynamic Properties," National Bureau of Standards Circular 500, U. S. Government Printing Office, Washington, D. C.

Ethanol Hydrate^{1a}

by A. D. Potts^{1b} and D. W. Davidson

Division of Applied Chemistry, National Research Council, Ottawa, Canada (Received October 22, 1964)

The existence of a solid ethanol hydrate below -73.5° is shown by low-frequency dielectric studies and thermal analysis. Its composition is near $C_2H_5OH \cdot 17H_2O$. This hydrate differs from the usual structure II type of water clathrate of similar composition in the absence of a contribution to the limiting high-frequency dielectric constant from rotation of the guest molecules and in the breadth of its dielectric dispersion curve. If ethanol hydrate is a structure II clathrate, the ethanol molecule must be strongly hydrogen-bonded to its water cage. A phase diagram of the ethanol-water system is presented.

The formation of a solid different from ordinary ice in concentrated solutions of ethanol in water has been reported several times.^{2,3} As early as 1896, Barendrecht^{2a} considered the question of whether the cubic crystals formed at low temperatures in solutions containing more than 50% ethanol were an alcohol hydrate. Largely from the observation that similar crystals were formed from solutions of other alcohols and acetaldehyde, he inferred that they corresponded to a cubic form of ice. More recently, Rau⁴ reported that after repeated freezing and thawing, water droplets could be induced to freeze consistently at -72° as cubic crystals, but his results could be repeated by Cwilong⁵ only when some contamination such as ether or acetone vapor was introduced into the chamber containing the sample. Brewer and Palmer³ were also unable to reproduce Rau's results with pure water, but pointed out that all of Rau's results could be explained in detail by the gradual accumulation of ethanol (probably from the cooling bath). The crystals formed at -72° from solutions of ca. 70% ethanol were apparently identical with those of Rau, and it was suggested that these possibly consisted of ethanol monohydrate.

The cubic solid formed from solutions of acetone and water under rather similar conditions has recently been identified by X-ray⁶ and dielectric⁷ studies as acetone hydrate, a structure II type⁸ of water clathrate with a composition near $CH_3COCH_3 \cdot 17H_2O$. Glew has proposed⁹ the existence in the liquid ethanol-water system of water cages of the structure II hydrate type to account for an anomaly in the partial molar volume of ethanol at an ethanol mole fraction of ~ 0.06 .

We present here the results of a study of the low-frequency dielectric properties at low temperatures of the ethanol-water system.

Experimental Methods

Solutions were prepared from conductivity water and anhydrous grade ethanol (Commercial Alcohols Ltd.) containing not more than 0.05 vol. % water and 0.01 mole % organic impurities. At room temperature, the conductivities of the solutions in the dielectric cell were in the range 1 to 2×10^{-6} ohm⁻¹ cm.⁻¹ and the dielectric constants agreed well with those of Wyman.¹⁰

Generally, electrical measurements were made with a General Radio Model 1615-A capacitance bridge at frequencies between 0.050 and 50 kc. sec.⁻¹ and with a General Radio Model 716-C bridge and guard circuit at frequencies to 500 kc. sec.⁻¹. Some measurements were also made to as high as 1 Mc. sec.⁻¹ with a capacitance-conductance bridge of the type designed by Cole.¹¹ The latter, especially for high frequencies and

(1) (a) Issued as N.R.C. No. 8354; (b) summer student.

(2) (a) H. P. Barendrecht, *Z. physik. Chem.*, **20**, 234 (1896); (b) F. F. A. Wallerant, *Bull. soc. franc. Minéral.*, **31**, 217 (1908).

(3) A. W. Brewer and H. P. Palmer, *Proc. Phys. Soc. (London)* **B64**, 765 (1951).

(4) W. Rau, *Schr. Deut. Akad. Luftfahrforsch.*, **8**, 65 (1944).

(5) B. M. Cwilong, *J. Glaciology*, **1**, 53 (1947).

(6) A. S. Quist and H. S. Frank, *J. Phys. Chem.*, **65**, 560 (1961).

(7) G. J. Wilson and D. W. Davidson, *Can. J. Chem.*, **41**, 264 (1963).

(8) M. von Stackelberg and H. R. Müller, *Z. Elektrochem.*, **58**, 25 (1954).

(9) D. N. Glew, *Nature*, **195**, 698 (1962).

(10) J. Wyman, *J. Am. Chem. Soc.*, **53**, 3292 (1931).

low conductances, gave considerably more accurate results than the 716-C bridge. Generators and detectors were of the conventional type.

The stainless steel cell was of a three-terminal, coaxial cylinder type.¹² Since hydrate commonly coexisted with either liquid or ice, depending on the composition of the solution, the measured capacitances and conductances depended on the relative proportion and distribution of the phases present, but for the same sample were commonly reproducible to a few per cent even after large and lengthy thermal excursions. Exceptions were provided by samples in which hydrate was slowly forming or in which liquid was slowly disappearing below the eutectic temperature. Air gaps undoubtedly occurred in samples in which there was little or no liquid phase present.

Temperature was controlled to a few tenths of a degree by an intermittent heater wound on an aluminum block containing the cell and actuated by the difference between the e.m.f. produced by a thermocouple in the block and that provided by a potentiometer. The block was mounted in a can lined with polyurethane foam and placed in a dewar flask containing liquid nitrogen to an automatically controlled level. Sample temperatures were measured to 0.1° by a calibrated copper-constantan thermocouple inserted into the cell.

Results and Discussion

Hydrate Dispersion Region. A characteristic region of dielectric absorption and dispersion was found at low temperatures for all ten solutions examined. These ranged in composition from 11.55 to 64.8 wt. % ethanol. Examples of ϵ'' vs. ϵ' plots are given in Figures 1 and 2. Although the amplitude and limiting high frequency dielectric constant of this dispersion region varied greatly with concentration, the shape and dependence on frequency varied only to a minor extent.

At temperatures near -80° the absorption showed a broad maximum and closely resembled a Cole-Cole arc, with values of α in the range 0.26 to 0.28. It was invariably complicated, however, by overlap on its low-frequency side by an additional absorption which increased monotonically with decreasing frequency. Prolonged application of a d.c. deionizing field of 1600 v. cm.⁻¹ reduced this low-frequency absorption to some extent but did not produce the pronounced effects noted in some other hydrate systems.^{7,13}

The most probable relaxation times τ_0 (Figure 3) of the Cole-Cole representation were estimated to an accuracy limited by the extent of the overlap. With decreasing temperature the overlap became rapidly more pronounced (see Figure 1). Even in the most

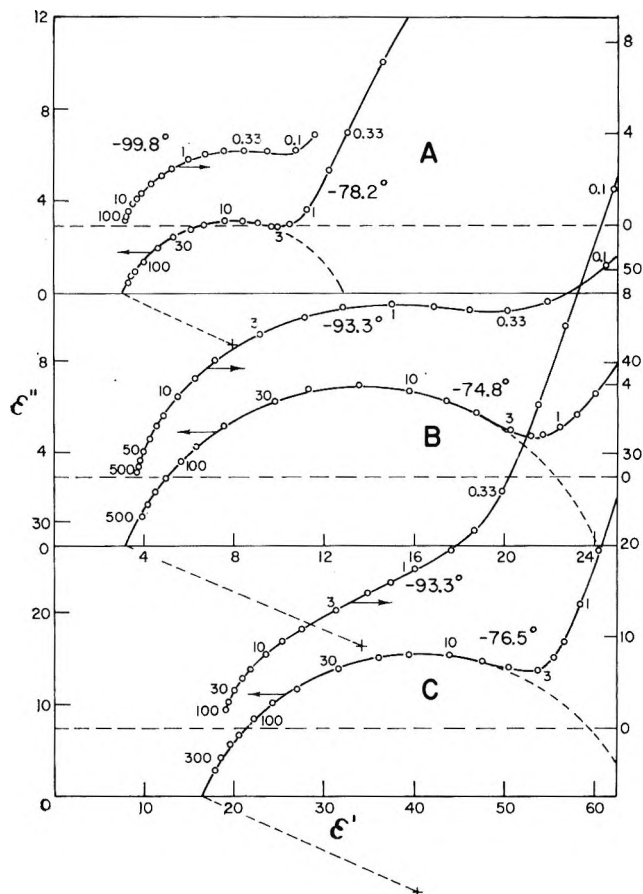


Figure 1. Ethanol hydrate dispersion region in samples containing: A, 11.55% ethanol; B, 13.37% ethanol; and C, 55.9% ethanol. Numbers refer to frequencies of measurement in kc. sec.⁻¹.

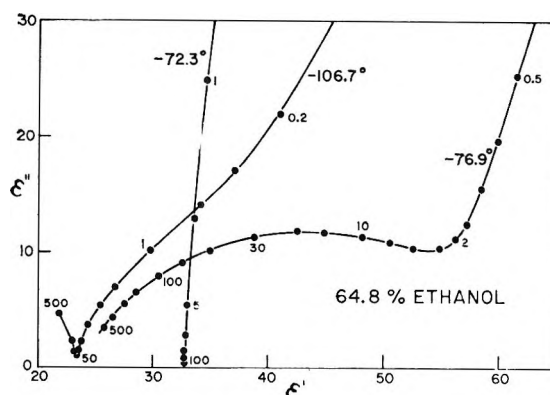


Figure 2. Dielectric behavior below and above the hydrate decomposition temperature.

(11) R. H. Cole, Annual Report, Conference on Electrical Insulation, National Academy of Sciences-National Research Council Publication 650, Washington, D. C., 1958.

(12) P. M. Gross, Jr., and R. C. Taylor, *J. Am. Chem. Soc.*, **72**, 2075 (1950).

(13) D. W. Davidson and G. J. Wilson, *Can. J. Chem.*, **41**, 1424 (1963).

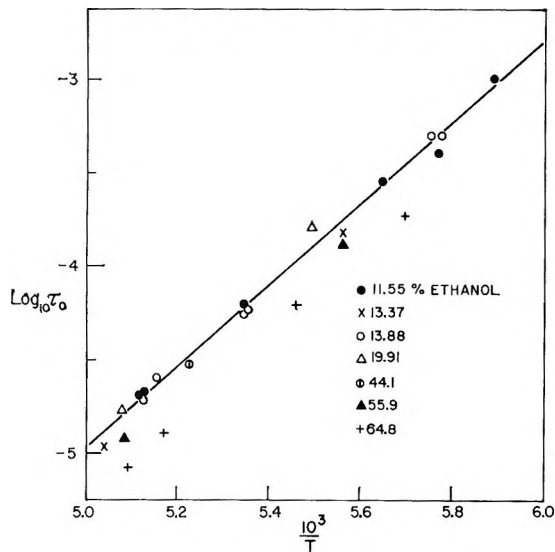


Figure 3. Apparent relaxation times τ_0 for hydrate in samples of different ethanol content.

favorable cases (in general, samples of least ethanol content), it was impossible to estimate relaxation times much below -100° to any accuracy from the shapes of the dispersion curves, although these continued to resemble arcs at relatively high frequencies.

At higher temperatures, the increasingly well-defined arcs disappeared abruptly at about -73.5° . Figure 2 illustrates the pronounced difference in the dielectric behavior below and above this hydrate decomposition temperature.

The relaxation times of Figure 3 are therefore confined to temperatures between -73.5 and -100° . Except for the two solutions of highest concentration, they depart from the straight line drawn by amounts which lie within the errors of their evaluation. The corresponding activation energy is $10.2 \text{ kcal. mole}^{-1}$. A shift toward smaller relaxation times is to be expected from the presence of liquid ethanol. Since a shift in the same direction results from air gaps, the true relaxation times may be somewhat larger than those of Figure 3. However, the temperature dependence would be relatively unaffected.

Liquid Dispersion Region. For samples relatively rich in ethanol, the limiting high-frequency dielectric constants associated with the hydrate dispersion region discussed above are relatively large and increase with increasing ethanol content. These effects arise from the presence of liquid in the sample, as is shown by the occurrence at lower temperatures of a well-defined liquid dispersion region (Figure 4). The frequencies of maximum absorption are close to those reported at comparable temperatures by Hassion and

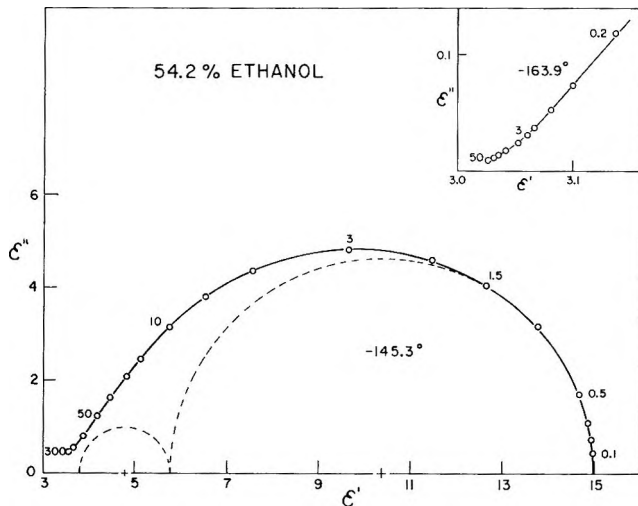


Figure 4. Dispersion region of ethanol-rich liquid phase.

Cole¹⁴ for liquid 95% ethanol solutions, with the shapes somewhat distorted by the presence in the sample of solid hydrate of relatively small dielectric constant (see next section). As was found by Hassion and Cole, it is possible to resolve this liquid dispersion into two or three separate dispersion regions.

At sufficiently low temperatures the liquid dispersion region slowly disappears, only to reappear when the sample is heated through the eutectic temperature region (*ca.* -122°). Several days were required for all liquid to disappear at temperatures below the eutectic.

The Proper Limiting High-Frequency Dielectric Constant of the Hydrate. For samples containing excess liquid, the dielectric constant approached a value of about 3 on the high-frequency side of the liquid dispersion region (see, for example, Figure 4), which was also the limiting value eventually reached below the eutectic temperature and for samples (for example, A, Figure 1) not containing excess liquid. It is evident that since this is the ϵ_∞ value for ice,¹⁵ liquid ethanol,¹⁴ and very likely for solid ethanol as well, it must also be about the proper value of ϵ_∞ for isolated single-phase ethanol hydrate. This result is in contrast to the higher values obtained under similar conditions for such gas hydrates as those formed by ethylene oxide,¹³ acetone,⁷ and tetrahydrofuran¹⁶ in which the relatively rapid orientation of the molecules engaged in the hydrate structure contributes to the dielectric constants at radiofrequencies even at liquid nitrogen

(14) F. X. Hassion and R. H. Cole, *J. Chem. Phys.*, **23**, 1756 (1955).

(15) R. P. Auty and R. H. Cole, *ibid.*, **20**, 1309 (1952).

(16) D. W. Davidson, M. M. Davies, and K. Williams, *ibid.*, **40**, 3449 (1964).

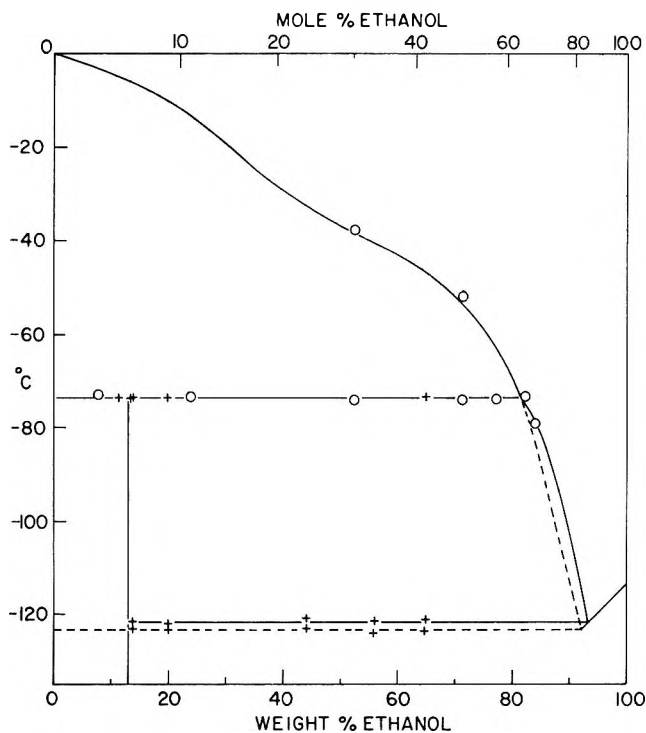


Figure 5. Phase diagram of the ethanol-water system: +, from dielectric; O, from rate of heating measurements.

temperature. In particular, the corresponding dielectric constant of the hydrate of tetrahydrofuran, a molecule with the same dipole moment as ethanol (1.7 D.), is almost 5 at 200°K. Thus ethanol hydrate is not a typical gas hydrate, despite its composition (see below).

The static dielectric constant of the isolated hydrate cannot be adequately estimated from our data, which, except for samples containing liquid in great excess, include the effects of air gaps which resulted from contraction of the samples away from the electrodes. The presence of ice in dilute solutions likewise lowers the measured values of ϵ' and ϵ'' .

We note that a static dielectric constant of 70 (comparable to the ϵ_0 -values of other hydrates^{7,13,16}) will be reduced to a measured ϵ_0 of 20 if the sample is separated from the electrodes by a uniform air gap of a thickness only 0.036 of the interelectrode distance. On the other hand, such a gap will merely reduce a high-frequency dielectric constant of 3.2 to 3.0.

The Composition of Ethanol Hydrate. It is possible to determine the composition of ethanol hydrate by finding the solution of highest ethanol content which does not give rise to a liquid dispersion region. Experimentally, the slowness with which hydrate is formed (unless the ethanol is in great excess) requires that this method be used with some care. A sample of

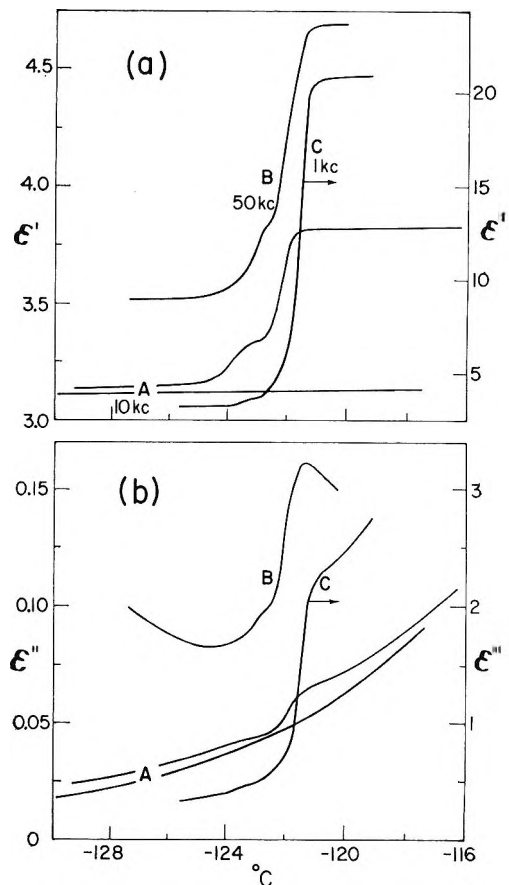


Figure 6. Changes of dielectric constant (a) and loss (b) on heating through the eutectic region. Concentrations are as in Figure 1.

composition $C_2H_5OH \cdot 16.6H_2O$ still showed a small but definite liquid dispersion region at -140° after having been kept at about -90° for 1 week. After this period of time, liquid was not disappearing at a measurable rate. On the other hand, a sample of composition $C_2H_5OH \cdot 19.6H_2O$ showed no trace of liquid dispersion after a week, nor was there any discernible break in the plots of ϵ' and ϵ'' vs. temperature in the eutectic region (cf. curves A, Figure 5). The hydrate composition thus appears to lie between the above two compositions. From an examination of the relative amplitudes of the liquid dispersion regions of samples containing varying quantities of excess ethanol, a composition of about $C_2H_5OH \cdot 17H_2O$ is suggested, and is so indicated in the phase diagram (Figure 5). Although these results seem to exclude the possibility of 16 moles of water to 1 mole of ethanol, they do not rule out mole ratios somewhat larger than 17.

The Phase Diagram of the Ethanol-Water System. Combination of freezing point data of other workers

with the results of the present study suggests the phase diagram given in Figure 5.

There is wide variation between the freezing point-concentration curves of different authors. We have based the liquidus curve of Figure 5 mainly on the data of Pickering¹⁷ as being the most complete and self-consistent. However, at high concentrations we have chosen Benjamin's data¹⁸ where they differ appreciably from those of Pickering. Pickering's liquid-solid ethanol line lies about 3° above Benjamin's, which agrees closely with Lalande's.¹⁹ None of the freezing point data is sufficiently accurate in the high concentration range to show the necessary (small) change of slope of the liquidus curve at the hydrate decomposition temperature.

To determine the hydrate decomposition temperature, measurements of ϵ' and ϵ'' at a fixed frequency (usually 10 kc. sec.⁻¹) were made on a number of solutions as a function of temperature. Heating rates were between 0.10 and 0.16°/min. The decomposition temperature was taken as that of the onset of the abrupt change in dielectric properties, since, as for other solid-solid transitions, the conversion of hydrate into ice and liquid is somewhat sluggish, although far less sluggish than the reverse transformation. Essentially the same decomposition temperature was derived from the well-defined break in the rate of heating of samples allowed to warm from *ca.* -100°. These samples were contained in a glass tube enclosed in an evacuated jacket. A further thermal lag occurred at higher temperatures as the ice gradually melted, except for concentrations greater than 72% ethanol.

Changes in ϵ' and ϵ'' were also followed for a number of samples heated through the eutectic region. Figure 6 reproduces some of these curves, for the same concentrations as Figure 1. Heating rates were between 0.08 (C) and 0.2°/min. (A). The upper of the two curves labeled A refers to a sample (11.55% ethanol) which was kept at -130° for 1 day; the lower curve refers to the same sample conditioned at *ca.* -90° for an additional 6 days. All trace of liquid had by then disappeared. Some liquid was present in the other samples of Figure 6 even below the eutectic temperature, probably because of the slow formation of solid ethanol.

As illustrated in Figure 6, both ϵ' and ϵ'' tended to increase in two steps. The relative size of the step at lower temperature decreased slowly with the length of time the sample had been kept below the hydrate decomposition temperature. There appeared to be two eutectic temperatures: one (near -123.0°) associated with the metastable ice-solid ethanol-liquid equilibrium, the other (near -121.5°) associated with the true hydrate-solid ethanol-liquid equilibrium. The broken curve (Figure 5) between the hydrate decomposition temperature and the lower eutectic point represents schematically the extension of the ice melting curve into the region of hydrate stability. The freezing point data of Lalande¹⁸ lie along this line. This, however, may only be accidental.

Conclusions

We conclude that a hydrate of ethanol exists below about -73.5° and that it has a composition similar to the structure II gas hydrates, as well as apparently the cubic symmetry required for such a structure. However, the ethanol molecules do not possess the orientational freedom shown by the encaged molecules of other gas hydrates which have been examined so far. It is possible that the hydroxyl group hydrogen bonds sufficiently strongly to the water molecules of the cage that the ethanol molecule is capable of reorientating at a rate not much different from that of the water molecules. Its orientational polarization would then contribute to the "hydrate dispersion region," the principal contribution to which, however, must arise from the rotation of water molecules. This dispersion is much broader in the case of ethanol hydrate than in the other hydrates we have studied, and the activation energy is somewhat greater.

Acknowledgment. We are indebted to R. E. Hawkins for assistance with the apparatus and the measurements.

(17) S. U. Pickering, *J. Chem. Soc.*, **63**, 998 (1893); **67**, 665 (1895).

(18) R. Benjamin, Thesis, Brussels, 1932.

(19) A. Lalande, *Bull. soc. chim. France*, **1**, 236 (1934).

Photochemistry of the Fluoroketones. Heptafluoropropyl Ethyl Ketone¹

by G. O. Pritchard and R. L. Thommarson

Department of Chemistry, University of California, Santa Barbara, California 93106
(Received October 23, 1964)

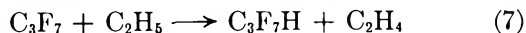
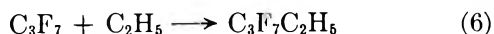
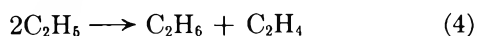
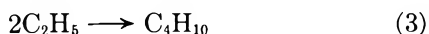
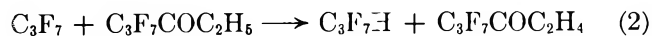
$C_3F_7COC_2H_5$ has been photolyzed in the gas phase at 3130 Å. between 353 and 635°K. Over this temperature range Φ_{CO} is close to unity, indicating the absence of any chain-carrying steps, which were previously found in the photolysis of CF_3COCH_3 . Rate constant data are presented for the H-abstraction reaction of C_3F_7 and C_2H_5 radicals from the parent ketone, and radical-radical interactions in the system are discussed.

Introduction

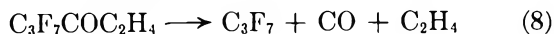
This investigation was undertaken primarily to extend our knowledge of radical-radical interactions for radicals containing F atoms. Above about 100° the primary decomposition process is



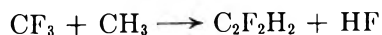
followed by the following radical reactions



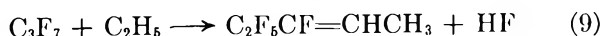
At higher temperatures decomposition of the radical formed in reactions 1 and 2 may occur



Recently, pseudo-disproportionation reactions of the type



have been observed,^{2a,b} so that we must consider the possible occurrence of the reaction



Experimental

The apparatus and procedure have been described previously.^{2a} The ketone was obtained from Columbia Organic Chemicals Corp. and purified by v.p.c. Its extinction coefficient ($\log I_0/I = \epsilon cl$) at 3130 Å. is 20.8 l. mole⁻¹ cm.⁻¹. The incident intensity (in a particular run) was either 1.04×10^{14} or 1.33×10^{14} quanta/cc./sec., as two different sets of filters were employed to facilitate renewal of the biphthalate.³

The mass spectrum of the ketone is recorded in Table I. The spectrum resembles that of CF_3COCH_3 ⁴ in that ion peaks containing fluorine are of small significance.⁵ However, the base peak is due to $C_2H_5^+$ rather than $C_2H_5CO^+$; in the CF_3COCH_3 spectrum, the base peak is due to the acetyl ion.

CO was collected at -210° and measured. The next fraction at -170° consisted of C_2H_6 and C_2H_4 and it was analyzed on the mass spectrometer. A following cut was taken at -120°; this consisted of C_3F_7H and C_4H_{10} . Analysis was effected by using ion peaks at m/e 51 (CF_2H^+) and 43 ($C_3H_7^+$). The last fraction was collected at -80°; it consisted of C_6F_{14} and $C_3F_7C_2H_5$; it was analyzed using the ion peak at m/e 79 ($C_3F_7H_5^+$), which is the major peak in the spectrum of the pentane.⁶ This peak was also used to

(1) This work was supported by a grant from the National Science Foundation.

(2) (a) G. O. Pritchard, M. Venugopalan, and T. F. Graham, *J. Phys. Chem.*, **68**, 1786 (1964); (b) E. Whittle, private communication.

(3) M. Venugopalan, G. O. Pritchard, and G. H. Miller, *Nature*, **200**, 568 (1963).

(4) J. R. Majer, *Advan. Fluorine Chem.*, **2**, 55 (1961).

(5) m/e 197 ($C_3F_7CO^+$) is less than 0.2% of the base peak, and no parent peak was detected.

Table I: Mass Spectrum of $C_3F_7COC_2H_5^a$

<i>m/e</i>	Ion	Relative abundance
15	CH_3^+	15
26	$C_2H_2^+$	42
27	$C_2H_3^+$	370
28	$C_2H_4^+$	50
29	$C_2H_5^+$	1000
31	CF^+	21
41	C_2HO^+	12
42	$C_2H_2O^+$	16
51	CF_2H^+	10
55	$C_3H_3O^+$	12
57	$C_2H_5O^+$	345
65	$C_2F_2H_3^+$	15
69	CF_3^+	99
95	$C_3F_3H_2^+$	11
100	$C_2F_4^+$	18
109	$C_3F_3O^+$	16
119	$C_2F_6^+$	13
169	$C_3F_7^+$	32
178	$C_4F_6O^+$	19

^a *m/e* less than 1% of the 29 ion peak have been omitted; no isotope corrections have been made, and isotope peaks have been omitted.

correct for some of the $C_3F_7C_2H_5$ which was present in the -120° fraction. There was some carry-over of the ketone into the -80° cut; this was analyzed for by using *m/e* 57 ($C_2H_5CO^+$), but in most of the experiments the ketone was removed completely with phenylhydrazine before analysis.⁷

Pure samples of all the compounds involved in the analysis were available for mass spectrometric calibration. The pentane was prepared from the reduction of heptafluoro-1-pentene, obtained from Peninsular ChemResearch.

The filtering system^{2a} was not employed when quantum yield determinations were not being made. The increased intensity thus obtained resulted in larger C_6F_{14} yields which facilitated more accurate analysis.

Results and Discussion

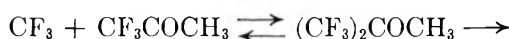
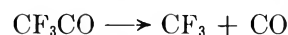
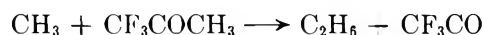
The data obtained from 15 experiments carried out in the temperature range 353 to 635°K. are recorded in Table II. The subscripts refer to the particular reactions in which the products were formed and are based on the assumed value of 0.14 for the disproportionation/recombination ratio for two ethyl radicals.⁸

Quantum Yields. An average of eight experiments in the temperature range 353 to 514°K. gave $\Phi_{CO} = 0.98 \pm 0.10$. At higher temperature values increased slightly to 1.14 at 550°K. and 1.20 at 586°K. This may well be due to the onset of reaction 8 at elevated temperatures. It is also apparent that there is no

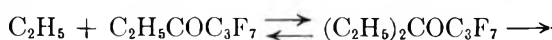
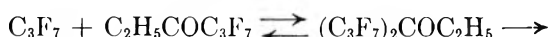
need to consider the effective participation of C_3F_7CO and/or C_2H_5CO radicals in the photolysis mechanism above 353°K.

$\Phi_{C_2H_6}$ varied approximately linearly from 0.05 to 0.5, and $\Phi_{C_3F_7H}$ from 0.05 to 0.75 over the range 353 to 586°K. In this temperature range $\Phi_{C_2H_4}$ rose from 0.05 to 0.15 and $\Phi_{C_4H_{10}}$ fell from 0.18 to 0.02. $\Phi_{C_3F_7C_2H_5}$ was about 0.15 over the entire temperature range, but the results were scattered, and $\Phi_{C_6F_{14}}$ was approximately 0.02 at all temperatures.

We may compare these data with those obtained by Sieger and Calvert,⁹ who found that CO and CH_3 -containing products were formed by chain processes at high temperatures in the photolysis of CF_3COCH_3 . In contrast to our results they found that Φ_{CO} varied from 0.15 at 353°K. to ~ 2.0 above 600°K. To explain these results at high temperatures they suggest the following reactions



Radical addition at carbonyl double bonds certainly occurs, and the first reaction presumably may occur *via* such an intermediate. Although these reactions may have low activation energies, they also have low steric factors ($\sim 10^{-5}$),¹⁰ and the probability of similar reactions occurring in the present system is presumably further reduced due to the bulkier $C_3F_7COC_2H_5$ molecule and the larger radicals involved. However, if the exchange reactions



do occur, our quantum yield data do not indicate that one is preferential to the others, or that any butane elimination occurs.

(6) G. Giacometti and E. W. R. Steacie, *Can. J. Chem.*, **36**, 1493 (1958).

(7) G. O. Pritchard, G. H. Miller, and J. K. Foote, *ibid.*, **40**, 1830 (1962).

(8) J. A. Kerr and A. F. Trotman-Dickenson, *Progr. Reaction Kinetics*, **1**, 107 (1961).

(9) R. A. Sieger and J. G. Calvert, *J. Am. Chem. Soc.*, **76**, 5197 (1954).

(10) G. O. Pritchard and E. W. R. Steacie, *Can. J. Chem.*, **35**, 1216 (1957).

Table II: Products^a in Moles $\times 10^6$

Temp., °K.	Time, sec.	Ketone concn., ^b mole cc. ⁻¹	CO	(C ₂ H ₆) ₁	(C ₂ H ₆) ₂ (C ₂ H ₄) ₂	(C ₂ H ₆) ₃ (C ₃ F ₇ H) ₂	(C ₃ F ₇ H) ₂	C ₄ H ₁₀	C ₃ F ₇ C ₂ H ₅	C ₆ F ₁₄
353	1200	1.37	12.2	0.634	0.326	0.349	0.532	2.33	0.951	0.149
369	1200	1.33	3.96	0.632	0.238	0.495	0.133	1.70	1.04	0.350
380	1500	1.53	11.1	1.25	0.294	0.662	1.31	2.10	4.08	1.58
411	1200	1.10	3.22	1.18	0.160	0.453	0.629	1.14	1.68	0.402
431	1200	1.15	7.76	1.84	0.126	0.553	1.23	0.901	1.65	0.527
454	1200	1.26	9.22	2.89	0.114	0.812	2.77	0.816	2.96	1.28
468	600	0.808	4.03	1.57	0.057	0.354	0.908	0.407	1.41	0.373
486	300	1.06	2.37	0.751	0.026	0.670	0.409	0.187
488	900	0.789	33.3	5.79	0.498	0.808	5.79	3.55	4.00	2.83
499	600	0.772	3.41	1.08	0.017	0.595	0.959	0.122
507	1800	0.421	...	5.99	0.694	2.92	12.7	4.95	16.7	3.30
514	180	0.584	0.891	0.409	0.012	0.147	0.270	0.086
529	900	0.940	39.7	10.2	0.365	1.18	10.3	2.61	6.99	3.93
586	900	0.827	4.85	2.43	0.009	0.722	2.48	0.065	0.406	0.028
635	600	0.614	23.4	8.44	0.067	2.17	11.0	0.480	2.84	1.46

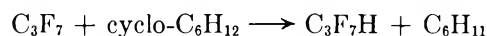
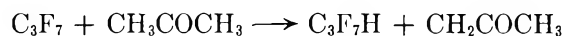
^a Subscripts refer to reaction in which product is formed. ^b Volume of reaction cell (illuminated) = 152.6 ml.

H-Abstraction Data. The customary Arrhenius plots for $k_1/k_3^{1/2}$ and $k_2/k_5^{1/2}$, both in mole^{-1/2} cc.^{1/2} sec.^{-1/2}, are shown in Figure 1. A least-squares treatment of the data leads to the expressions

$$k_1/k_3^{1/2} = 1.55 \times 10^4 \exp(-7200/RT) \text{ mole}^{-1/2} \text{ cc.}^{1/2} \text{ sec.}^{-1/2}$$

$$k_2/k_5^{1/2} = (5.9 \pm 2.3) \times 10^4 \exp(-8400 \pm 300/RT) \text{ mole}^{-1/2} \text{ cc.}^{1/2} \text{ sec.}^{-1/2}$$

The activation energy for reaction 1 is very similar to that found for the reaction of ethyl radicals with diethyl ketone, for which values of 7.4 and 7.6 kcal. mole⁻¹ have been obtained.¹¹ The correlation of the activation energy obtained for reaction 2 with similar systems is not so precise, and it appears to be high. Values of 7.2 ± 0.4 and ~ 6 kcal. mole⁻¹ for the respective reactions



have been determined.^{12a,b} Our present data indicate attack at the primary, rather than the secondary, hydrogen atom, which seems to be very unlikely. However, data on the H-atom abstraction reaction of perfluoralkyl radicals are not extensive, and some of it is contradictory,¹³ so that the value is not necessarily incorrect.

The pre-exponential factor ratios indicate normal steric factors for the two abstraction reactions.

Radical-Radical Interactions. The Arrhenius plots

for the disproportionation/combination ratio = $\bar{R}_{(\text{C}_2\text{H}_6)_7}/\bar{R}_{\text{C}_3\text{F}_7\text{C}_2\text{H}_5} = k_7/k_6$ and the cross (combination + disproportionation) ratio = $(\bar{R}_{\text{C}_3\text{F}_7\text{C}_2\text{H}_5} + \bar{R}_{(\text{C}_2\text{H}_6)_7})/(\bar{R}_{\text{C}_6\text{F}_{14}})^{1/2}(\bar{R}_{\text{C}_4\text{H}_{10}} + \bar{R}_{(\text{C}_2\text{H}_6)_4})^{1/2}$ are given in Figure 2. Both functions show a surprisingly strong temperature dependence.

A least-squares determination yields $k_7/k_6 = 0.021 \exp(2200 \pm 200/RT)$. Of the 12 experiments recorded in Table I for which data on C₃F₇C₂H₅ analysis are given, only 9 of them were used in this calculation. The experiment at 380°K. gave a very low result, and the two runs at the highest temperatures were neglected because of ethylene formation in reaction 8. While the present values of k_7/k_6 vary from 0.38 at 353°K. to 0.16 at 529°K., Giacometti and Steacie⁶ obtained a virtually constant value of 0.40 over the temperature range 360 to 469°K. Over this range our results yield an average value of $k_7/k_6 = 0.33$ with a large scatter.

Recent studies of alkyl radical interactions^{14a,b} at low temperatures indicate that $E_{\text{disp}} - E_{\text{comb}} = -350$ cal. mole⁻¹. It appears that this is a general phenomenon, suggesting that radical disproportionation and combination reactions do not proceed through a

(11) K. O. Kutschke, M. H. J. Wijnen, and E. W. R. Steacie, *J. Am. Chem. Soc.*, **74**, 714 (1952); P. Ausloos and E. W. R. Steacie, *Can. J. Chem.*, **32**, 593 (1954).

(12) (a) G. O. Pritchard, Y. P. Hsia, and G. H. Miller, *J. Am. Chem. Soc.*, **85**, 1568 (1963); (b) G. O. Pritchard and G. H. Miller, *J. Phys. Chem.*, **63**, 2074 (1959).

(13) G. O. Pritchard and F. L. Thommarson, *ibid.*, **68**, 568 (1964).

(14) (a) P. S. Dixon, A. P. Stefani, and M. Szwarc, *J. Am. Chem. Soc.*, **85**, 2551, 3344 (1963); (b) R. Klein, M. D. Scheer, and R. Kelley, *J. Phys. Chem.*, **68**, 598 (1964).

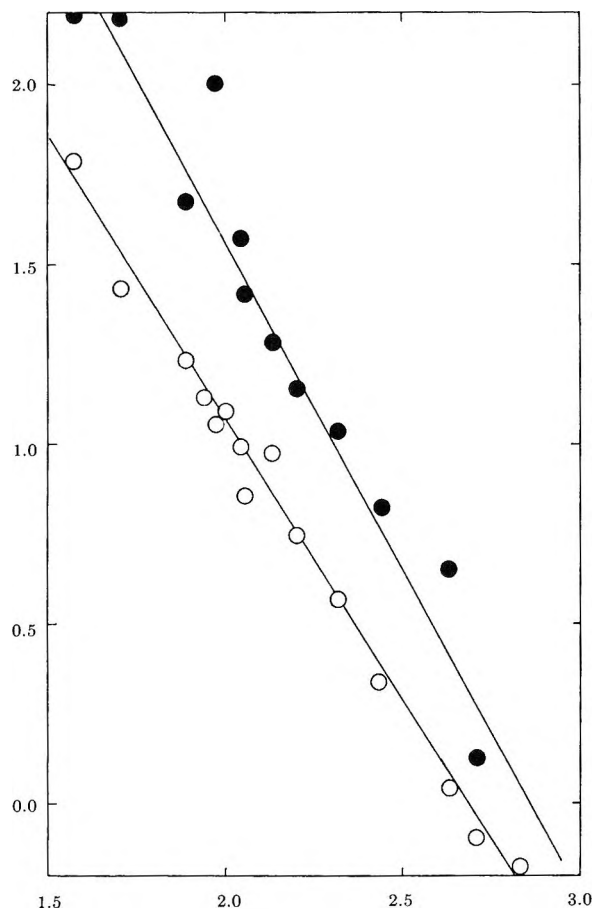


Figure 1. ●, $\log k_2/k_3^{1/2} + 0.5$ vs. $10^3/T^\circ\text{K}$.; ○, $\log k_1/k_3^{1/2}$ vs. $10^3/T^\circ\text{K}$.; units of k in $\text{mole}^{-1} \text{cc. sec.}^{-1}$.

common transition state.^{14b} The present value $E_7 - E_6 = -2200 \text{ cal. mole}^{-1}$, while considerably greater, is in agreement with this conclusion.

A least-squares treatment of the Arrhenius plot of the cross (combination + disproportionation) ratio leads to an expression equal to $28 \exp(-1900 \pm 100/RT)$. The two runs at the highest temperature, although included in Figure 2, were again not used in the calculation.¹⁵ Slopes of lesser magnitude but opposite sign have previously been obtained in the $\text{CF}_3 + \text{CH}_3^{12a}$ and $\text{C}_3\text{F}_7 + \text{CH}_3^{12a}$ systems.

The above results are not altered significantly by using a varying disproportionation/combination ratio for two ethyl radicals, which may be obtained from an extrapolation of Szwarc's^{14a} low-temperature data. This extrapolation gives $k_4/k_3 = 0.10$ at 529°K ., and we may compute $k_7/k_6 = 0.18$, and the cross (combination + disproportionation) ratio = 3.5 at this temperature. Based upon the value of $k_4/k_3 = 0.14$ which we have used, these ratios are 0.16 and 3.9,

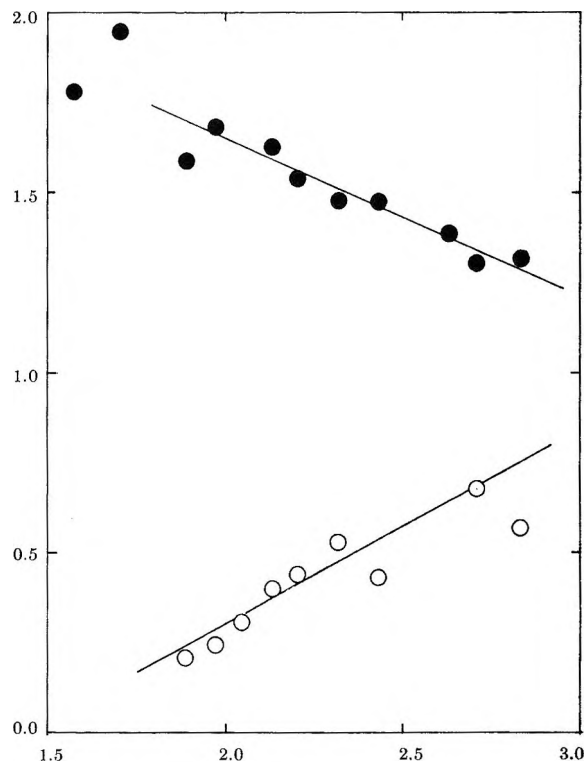
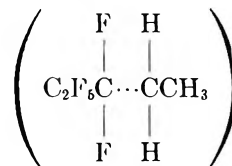


Figure 2. ●, \log cross (combination + disproportionation) ratio + 1.0 vs. $10^3/T^\circ\text{K}$.; ○, $\log k_7/k_6 + 1.0$ vs. $10^3/T^\circ\text{K}$.

respectively, at 529°K . Any deviations are reduced with decreasing temperature.

A careful search for SiF_4 was made, and none was found. This effectively rules out the occurrence of reaction 9, at least under our conditions. The formation of SiF_4 has definitely been established in systems where such pseudo-disproportionations occur, namely from interactions between two CF_2H^{2a} and two CF_2H^{17} radicals.

Both the ethylene (reaction 7) and the HF (reaction 9) eliminations are strongly exothermic (~ 60 – $70 \text{ kcal. mole}^{-1}$). If HF elimination, along with combination (reaction 6), occurs through a "head to head" intermediate one would anticipate a greatly



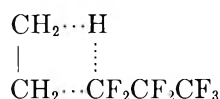
reduced possibility of the elimination than with the

(15) An Arrhenius plot of the simple cross combination ratio $k_6/k_3^{1/2}k_7^{1/2}$ produces a very similar slope, but with somewhat more scatter.

(16) G. O. Pritchard and J. R. Dacey. *Can. J. Chem.*, **38**, 182 (1960).

(17) G. O. Pritchard and J. T. Bryant, to be published.

($\text{FH}_2\text{C}\cdots\text{CFH}_2$)* intermediate, due to the many more available degrees of freedom. It is possible that reaction 9 will occur at low enough pressures; we have suppressed HF elimination from $\text{C}_2\text{F}_2\text{H}_4^*$ by the addition of inert gases.¹⁸ This picture also implies that reaction 7 occurs *via* a "head to tail" intermediate. Alternatively both combination and disproportionation (to ethylene) may occur through a four-center intermediate, but the activation energy difference obtained for $E_7 - E_6$ suggests that this is not the case.



We are currently seeking corroboration of this unexpected difference with C_2F_5 and C_2H_5 radicals, produced from the photolysis of $\text{C}_2\text{F}_5\text{COC}_2\text{H}_5$.

The data presented here, and previously,^{12a,16} by us have consistently indicated a temperature dependence for cross combination ratios involving alkyl and perfluoroalkyl radicals. This is attributed, in part, to the polar nature of the perfluoroalkyl radical. The work of Ayscough¹⁹ and Szwarc and his co-workers²⁰ on CF_3 radical recombination may be taken as substantiation of this viewpoint.²¹ Johnston and Goldfinger²² also have suggested a potential barrier to CCl_3 radical recombination due to the polar nature of the radicals.

In very few cases have investigators attempted to measure temperature coefficients carefully for simple alkyl radical recombination reactions in the gas phase. The value of 0 ± 700 cal. mole⁻¹ for CH_3 radicals is widely accepted,²³ but the data of Shepp and Kutschke²⁴ indicate a value of 2 ± 1 kcal. mole⁻¹ for C_2H_5 radicals. Over the limited temperature range 81–115° the results of Metcalfe²⁵ indicate an activation energy of 1 kcal. mole⁻¹ for *t*-butyl radical recombination.

It may well be the case that for all radicals larger than CH_3 , especially polar radicals, small potential barriers to reaction of 1–3 kcal. mole⁻¹ exist.

Acknowledgments. We are very indebted to Dr. E. Whittle for communication of his results prior to publication, and to Dr. A. S. Gordon for the mass spectrum of the ketone.

(18) G. O. Pritchard and P. Baine, unpublished data.

(19) P. B. Ayscough, *J. Chem. Phys.*, **24**, 944 (1956).

(20) L. Herk, M. Feld, and M. Szwarc, *J. Am. Chem. Soc.*, **83**, 2998 (1961); A. P. Stefani, L. Herk, and M. Szwarc, *ibid.*, **83**, 4732 (1961).

(21) Admittedly, Ayscough's data may also be interpreted as $E = 0$ for CF_3 recombination, and Szwarc's data may not be as conclusive as they were thought to be; see G. E. Owen, Jr., J. M. Pearson, and M. Szwarc, *Trans. Faraday Soc.*, **60**, 564 (1964).

(22) H. S. Johnston and P. Goldfinger, *J. Chem. Phys.*, **37**, 700 (1962).

(23) R. Gomer and G. B. Kistiakowsky, *ibid.*, **19**, 85 (1951).

(24) A. Shepp and K. O. Kutschke, *ibid.*, **26**, 1020 (1957).

(25) E. L. Metcalfe, *J. Chem. Soc.*, 3560 (1963).

Microwave Absorption and Molecular Structure in Liquids. LXI. The Dielectric Relaxation Mechanism for Molecules Similar in Structure to Diphenyl Ether^{1a,b}

by Ralph D. Nelson, Jr.,^{1c} and Charles P. Smyth

Frick Chemical Laboratory, Princeton University, Princeton, New Jersey (Received October 24, 1964)

The complex dielectric constants of benzene solutions of several organic compounds were measured at 0.5 and 600 Mc. and 1.2, 3.0, 9.3, and 24 kMc. The resulting relaxation times at 20° of bis(*p*-nitrophenyl) ether, *n*-butyl phenyl ether, diphenyl disulfide, di-*n*-decyl ether, and bis(diphenylmethyl) ether are 12.5, 25, 13, 39, and 130×10^{-12} sec., respectively. Several mechanisms for the rapid relaxation process in diphenyl ether and related compounds are examined and compared with the experimental results. The mesomeric shift, inversion, atomic dipole, and phenoxy group rotation mechanisms are concluded to be improbable or impossible. Double internal rotation seems to be the most probable mechanism for the rapid relaxation.

The time required for a system of simple, rigid, polar molecules to achieve orientation equilibrium in the presence of an applied electric field is characteristically 5 to 100 psec. (1 psec. = 10^{-12} sec.) in benzene solution at 20°. Chlorobenzene has a relaxation time of 8.3 psec. in benzene solution at 20°² and has a somewhat smaller molecular volume than diphenyl ether. The relaxation time of 4.0 psec. for diphenyl ether in benzene solution⁴ indicates that some rapid relaxation mechanism is occurring in addition to over-all molecular rotation. Several mechanisms have been discussed seriously or dismissed as improbable: (1) an in-plane inversion of the C-O-C bond,⁵ (2) a shift in atomic dipole direction,⁶ (3) double or coupled internal rotations, resembling a rowing motion with one oar feathered,^{7,8} (4) rotation of a phenoxy group with respect to the other phenyl ring,⁹ and (5) mesomeric shift of charge due to changes in the interaction between π -electrons in the phenyl rings and the unshared pairs on the oxygen as a function of ring twisting with respect to the C-O-C plane.¹⁰ Molecular models and the original papers are required for the best understanding of the details of these mechanisms. It is the purpose of this paper to examine the above mechanisms in the light of the experimental results and

to eliminate those mechanisms which seem improbable in the light of theoretical considerations or experimental data.

Experimental

Measurement. Methods of measurement and calculation have been reported in previous papers.¹¹⁻¹⁵

(1) (a) This research was supported by a National Science Foundation research grant. Reproduction, translation, use, or disposal, in whole or in part, by or for the United States Government is permitted. (b) This paper represents part of the work submitted by R. D. Nelson, Jr., to the Graduate School of Princeton University in partial fulfillment of the requirements for the degree of Doctor of Philosophy. (c) National Science Foundation Graduate Fellow, 1960-1963.

(2) C. P. Smyth, "Dielectric Behavior and Structure," McGraw-Hill Book Co., Inc., New York, N. Y., 1955, Chapter II.

(3) D. H. Whiffen, *Trans. Faraday Soc.*, **46**, 130 (1950).

(4) F. Hufnagel, G. Klages, and P. Knoblock, *Z. Naturforsch.*, **17a**, 96 (1962).

(5) E. Fischer, *ibid.*, **4a**, 707 (1949).

(6) E. Fischer, *Naturwissenschaften*, **43**, 153 (1956).

(7) W. Maier, *Arch. Sci. (Geneva)*, **12**, 20 (1959).

(8) F. K. Fong, *J. Chem. Phys.*, **40**, 132 (1964).

(9) D. M. Roberti, O. F. Kalman, and C. P. Smyth, *J. Am. Chem. Soc.*, **82**, 3523 (1960).

(10) K. Higasi and C. P. Smyth, *ibid.*, **82**, 4759 (1960).

(11) W. M. Heston, Jr., E. J. Hennelly, and C. P. Smyth, *ibid.*, **70**, 4093 (1948).

Table I: Slopes of Dielectric Constant and Loss, Squares of Refractive Index for Sodium D-Line, and Densities against Concentration for Benzene Solutions

Compd.	Temp., °C.	Wave length, cm.	a'	a''
<i>n</i> -Butyl phenyl ether (to 6 mole %)	20	57,700	2.38	..
		50.0	2.40	0.19
		25.0	2.35	0.36
		10.0	2.00	0.61
		3.22	1.20	0.76
	1.25	0.60	0.43	
n_D^2 slope = -0.02 Density slope = 0.056 g./cc. mole fraction ⁻¹				
Bis(<i>p</i> -nitrophenyl) ether (to 0.6 mole %)	20	57,700	11.0	..
		25.0	10.7	1.1
		9.9	10.3	1.8
		3.22	7.2	3.6
		1.25	5.0	3.3
n_D^2 slope = 0.80 Density slope = 1.16 g./cc. mole fraction ⁻¹				
Diphenyl disulfide (to 8 mole %)	20	57,700	5.60	..
		3.11	3.04	1.54
		1.33	2.28	1.68
n_D^2 slope = 0.98 Density slope = 0.77 g./cc. mole fraction ⁻¹				
Diphenyl disulfide (to 8 mole %)	40	57,700	5.20	..
		3.11	3.35	1.54
		1.33	2.28	1.58
Density slope = 0.75 g./cc. mole fraction ⁻¹				
<i>n</i> -Decyl ether (to 5 mole %)	20	57,700	1.48	..
		50.0	1.41	0.27
		25.0	1.07	0.45
		10.0	0.60	0.66
		3.22	0.07	0.57
	1.25	-0.18	0.36	
n_D^2 slope = -0.69 Density slope = -0.22 g./cc. mole fraction ⁻¹				
Bis(diphenylmethyl) ether (to 5 mole %)	20	57,700	3.38	..
		50.0	2.92	0.61
		25.0	2.60	0.66
		10.0	1.64	0.41
		3.11	1.53	0.16
	1.29	1.46	0.09	
n_D^2 slope = 1.14 Density slope = 1.0 g./cc. mole fraction ⁻¹				
Bis(diphenylmethyl) ether (to 5 mole %)	40	57,700	3.12	..
		50.0	2.88	0.50
		25.0	2.48	0.66
		10.0	1.76	0.47
		3.11	1.63	0.19
	1.25	1.60	0.07	
n_D^2 slope = 1.23 Density slope = 0.9 g./cc. mole fraction ⁻¹				

Some of the calculations were carried out with the aid of the Princeton University Computer Center IBM 7090 computer.

Reagents. Benzene of ACS reagent grade was used, n_D^{20} 1.5007, d_4^{20} 0.8843 g./cc.

n-Butyl phenyl ether from Eastman Kodak Co. showed only a very slight impurity in a vapor phase chromatogram (less than 0.1%) and was used as received, n_D^{20} 1.4971 (lit.¹⁶ 1.4971).

Bis(*p*-nitrophenyl) ether from Eastman Kodak Co. was purified by Dr. W. P. Purcell as previously reported.¹⁷

Diphenyl disulfide from Eastman Kodak Co. was recrystallized twice from ethanol solution to give a melting point of 60° (lit.¹⁸ m.p. 60°).

n-Decyl ether from the Connecticut Hard Rubber Co., New Haven, Conn., was fractionally crystallized from the commercial material and then fractionally distilled at 15 mm. to give a clear liquid, n_D^{20} 1.4406 (lit.¹⁹ 1.4418).

Bis(diphenylmethyl) ether from Eastman Kodak Co. was recrystallized from methanol and dried under vacuum for 3 hr. at 80° over phosphorus pentoxide to give a melting point of 109–110° (lit.²⁰ m.p. 108–109°).

Data. The experimental data are given in Tables I and II, and the calculated results are in Table III. The data are for benzene solutions unless otherwise noted, the concentration of the most concentrated solution being given in parentheses. Experimental errors are $\pm 0.2^\circ$ in temperature; $\pm 5\%$ in a' , the slope of dielectric constant against mole fraction, and a'' , the corresponding slope for loss; $\pm 0.1\%$ in wave length; ± 0.0005 in static dielectric constant; ± 0.005 in microwave dielectric constant, $\pm 2\%$ in loss, and ± 0.0002 g./cc. in density. Abbreviations used are τ for relaxation time in picoseconds, μ for dipole moment in debyes, ϵ_∞ for the optical dielectric constant, and α for the Cole-Cole distribution parameter.²¹ Values of τ for the individual points varied up to 20% from the average value reported.

(12) H. L. Laquer and C. P. Smyth, *J. Am. Chem. Soc.*, **70**, 4097 (1948).

(13) L. M. Kushner and C. P. Smyth, *ibid.*, **71**, 1401 (1949).

(14) W. M. Heston, Jr., A. D. Franklin, E. J. Hennelly, and C. P. Smyth, *ibid.*, **72**, 3443 (1950).

(15) D. A. Pitt and C. P. Smyth, *J. Phys. Chem.*, **63**, 582 (1959).

(16) A. I. Vogel, *J. Chem. Soc.*, 616 (1948).

(17) W. P. Purcell and C. P. Smyth, *J. Am. Chem. Soc.*, **83**, 1063 (1961).

(18) E. N. Guryanova, *Zh. Fiz. Khim.*, **24**, 479 (1950).

(19) G. Komppa and Y. Talvite, *J. Prakt. Chem.*, **135**, 193 (1932).

(20) F. R. Atherton, H. T. Howard, and A. R. Todd, *J. Chem. Soc.*, 1106 (1948).

(21) K. S. Cole and R. H. Cole, *J. Chem. Phys.*, **9**, 341 (1941).

Table II: Dielectric Constant and Loss, Squares of Refractive Index for Sodium D-Line, and Densities for Pure *n*-Butyl Phenyl Ether

Temp., °C.	Wave length, cm.	Dielectric constant	Loss
20	57,700	3.734	...
	3.26	2.783	0.465
	1.22	2.547	0.153
	$n_D^2 = 2.2414$		
Density = 0.9351 g./cc.			
40	57,700	3.584	...
	3.26	2.880	0.490
	1.22	2.572	0.178
	$n_D^2 = 2.2136$		
Density = 0.9184 g./cc.			
60	57,700	3.444	...
	3.26	2.951	0.452
	1.22	2.599	0.200
	$n_D^2 = 2.1852$		
Density = 0.9016 g./cc.			

Table III: Slopes (a_∞) for Optical Dielectric Constants, Distribution Parameters, Most Probable Relaxation Times, and Dipole Moments in Benzene Solution

Compd.	Temp., °C.	a_∞	α	τ , psec.	μ , D.
<i>n</i> -Butyl phenyl ether	20	0.40	0.1	25	1.19
Bis(<i>p</i> -nitrophenyl) ether	20	2.4	0.1	12.5	2.22
Diphenyl disulfide	20	0.20	0.3	13	1.90
	40	0.20	0.3	10	1.96
<i>n</i> -Decyl ether	20	-0.42	0.2	39	1.34
Bis(diphenylmethyl) ether	20	1.40	0.2	130	1.23
	40	1.57	0.1	120	1.15
<i>n</i> -Butyl phenyl ether (pure)	20	2.511	0.1	46	1.11
	40	2.534	0	32	1.13
	60	2.562	0	23	1.15

Discussion

The relaxation time of 25 psec. for *n*-butyl phenyl ether in benzene solution at 20° is much higher than the recently measured value⁴ for diphenyl ether (4 psec.) and that for *n*-butyl ether⁵ (5 psec.). It appears, therefore, that it is not merely the presence of an aromatic ring which gives rise to rapid relaxation for the diphenyl ethers. If mesomeric shift were the principal mechanism for rapid relaxation, there should be some decrease in relaxation time below the approximately 20 psec. expected for *n*-butyl phenyl ether as a rigid rotator, even though there is only one ring which can interact with the oxygen.

The bis(*p*-nitrophenyl) ether data were taken as a check against previous results.²² The relaxation time

of 12.5 psec. in Table III agrees with the previous value of 13.7 psec.²² within the limits of error involved. The relaxation time is longer than that of diphenyl ether because of the increase in molecular size, but still only about half that expected for over-all rotation, indicating a large contribution from the rapid mechanism, as discussed in detail by Fong.⁸ It would appear from the results on these two substances that the mesomeric mechanism is not a necessary postulate in the explanation of dielectric relaxation for diphenyl ether type molecules.

The relaxation time of 13 psec. for diphenyl disulfide contrasts with Hufnagel's result of 18.6 psec. obtained by using only loss values at lower frequencies.²³ Either value indicates a contribution from one or more rapid mechanisms. A larger apparent relaxation time might be expected from the lower frequency measurements, to which the rapid relaxation mechanism would make a relatively small contribution. The dipole moment of 1.90 D. agrees with previously determined values of 1.90¹⁸ and 1.86 D.²⁴ Rotation around the S-S bond provides an alternative mechanism which, in combination⁸ with the over-all molecular rotation, might lower the observed time to as little as half of that for molecular rotation alone. This would be close to the observed value of 13, which is slightly higher than the value of 10 psec. for the somewhat smaller molecule of diphenyl sulfide.²⁵

The relaxation time of 39 psec. for *n*-decyl ether in benzene solution at 20° (Table III) is long in comparison with the approximate value 32 reported²⁶ for the pure liquid, which has a viscosity of 6.3 cp., almost ten times that of benzene. This may be explained by the large experimental error which the earlier workers discussed in their paper.²⁶ The presence of internal rotation in the alkyl chains also decreases the dependence of the relaxation time on the viscosity.

The Stuart-Briegleb model of the bis(diphenylmethyl) ether molecule shows such strong steric hindrance between the four rings that no internal rotation should occur. This rigidity is confirmed by the relaxation time of 130 psec. in benzene solution at 20°, which is so high as to give no indication of intramolecular orientation.

There has been no recent attempt to interpret relaxa-

(22) W. P. Purcell and C. P. Smyth, *J. Am. Chem. Soc.*, **83**, 1063 (1961).

(23) F. Hufnagel, *Z. Naturforsch.*, **15a**, 723 (1960).

(24) M. T. Rogers and T. W. Campbell, *J. Am. Chem. Soc.*, **74**, 4742 (1952).

(25) E. N. DiCarlo and C. P. Smyth, *ibid.*, **84**, 3638 (1962).

(26) G. B. Rathmann, A. J. Curtis, P. L. McGeer, and C. P. Smyth, *J. Chem. Phys.*, **25**, 413 (1956).

tion times using the atomic dipole mechanism except as it could be construed to be mesomeric shift. It would predict small relaxation times for all ethers, contrary to experimental evidence, if a simple model not involving mesomerism were used. Since it would appear that the atomic dipole mechanism should lead to electronic resonance absorption rather than to typical dielectric relaxation absorption, there seems to be little justification for considering this mechanism further.

In-plane inversion has never been observed, even for the simplest oxygen system, H_2O .²⁷ Out-of-plane inversion for diphenyl ether is simply molecular rotation. Since it would require a large change in coordinates for many carbon atoms and since the force constant for the ether linkage is not low, in-plane inversion must be judged to be highly improbable for the diphenyl ether series. Out-of-plane inversion apparently occurs in phenoxathin^{4,28} and may be responsible for the short relaxation time of triphenylamine.²⁵

In order to conserve angular momentum the rotation of a phenoxy group with respect to the other phenyl ring would require a comparable displacement for each ring unless one ring were held in place by external forces. If angular momentum is conserved by allowing both rings to move, double internal rotation^{7,8} is developed. According to the Stuart-Briegleb models for diphenyl ether and analogous molecules, double internal rotation can occur freely and would not produce much disturbance of the surrounding medium. In strongly hindered systems this internal rotation would be impossible. In asymmetric molecules the motion would be unbalanced, leading to a greater disturbance of the environment and hence to a longer relaxation time than for the corresponding balanced molecules. In the final analysis, the experimental results seem to be best explained by the double internal rotation mechanism.

(27) For a discussion of inversion, see W. Gordy, "Handbuch der Physik," Vol. XXVIII, Springer-Verlag, Berlin, 1957, pp. 8, 9.

(28) J. E. Anderson and C. P. Smyth, to be published.

Heats of Reaction of Boron Trifluoride with $\text{HF}\cdot 3.75\text{H}_2\text{O}$ and of Diborane with Trimethylamine. Correlation of Thermochemical Data for Some Boron Compounds¹

by Stuart R. Gunn

Lawrence Radiation Laboratory, University of California, Livermore, California (Received October 24, 1964)

The standard heats of the reactions $\text{BF}_3(\text{g}) + 15.67\text{HF}\cdot 58.72\text{H}_2\text{O} \rightarrow \text{HBF}_4\cdot 14.67\text{HF}\cdot 58.72\text{H}_2\text{O}$ and $\text{Me}_3\text{N}(\text{g}) + 0.5\text{B}_2\text{H}_6(\text{g}) \rightarrow \text{Me}_3\text{N}:\text{BH}_3(\text{c})$ have been measured to be -28.29 ± 0.07 and -32.33 ± 0.06 kcal. mole⁻¹, respectively. These data are combined with others to derive the following recommended values for standard heats of formation: $\text{B}_2\text{H}_6(\text{g})$, +8.6; $\text{B}(\text{am})$, +0.8; $\text{BCl}_3(\text{l})$, -102.3; $\text{BF}_3(\text{g})$, -269.7; and $\text{H}_3\text{BO}_3(\text{c})$, -261.7 kcal. mole⁻¹.

Because of the unsatisfactory history of oxygen-combustion calorimetry of boron, the heats of formation of boron compounds have for some time been referred to the amorphous form of boron, through measurements of the heat of decomposition of diborane² and the heat of chlorination of amorphous boron.³ Recently, however, measurements have been made with crystalline boron: Wise, Margrave, Feder, and Hubbard^{4,5} and Gross, Hayman, Levi, and Stuart⁶ have measured the heat of fluorination of crystalline boron, and Good, Månsson, and McCullough⁷ have measured the heat of combustion of crystalline boron in a rotating-bomb oxygen-combustion calorimeter to produce $\text{HBF}_4\cdot 14.67\text{HF}\cdot 58.72\text{H}_2\text{O}$. Good also measured the heat of combustion of trimethylamine-borane and the heat of solution of crystalline boric acid to give the same final solution.

In the present work the heat of solution of boron trifluoride in $\text{HF}\cdot 3.75\text{H}_2\text{O}$ and the heat of reaction of diborane with trimethylamine have been measured (this last reaction was performed earlier calorimetrically by McCoy and Bauer⁸). These values can be combined with the other recent data to develop additional thermochemical cycles in the set of heats of formation of key boron compounds; the increased degree of overdetermination of the set then permits improved evaluation of the reliability of the data.

Experimental

Materials. Boron trifluoride was obtained from the Matheson Co., Inc.; it was specified as 99% minimum purity, maximum contents of SO_2 and SiF_4 0.1% and 0.03%, respectively. It was condensed in a vacuum line and subjected to a single bulb-to-bulb distillation, 10% being discarded at each end. Infrared analysis indicated SiF_4 content to be <0.1%.

Reagent hydrofluoric acid was diluted, standardized acidimetrically on a weight basis, and stored in a polyethylene bottle.

Trimethylamine was obtained from Matheson, purity

(1) Work done under the auspices of the U. S. Atomic Energy Commission.

(2) E. J. Prosen, W. H. Johnson, and F. Y. Pergiel, *J. Res. Natl. Bur. Std.*, **61**, 247 (1958).

(3) W. H. Johnson, R. G. Miller, and E. J. Prosen, *J. Res. Natl. Bur. Std.*, **62**, 213 (1959).

(4) S. S. Wise, J. L. Margrave, H. M. Feder, and W. N. Hubbard, *J. Phys. Chem.*, **65**, 2157 (1961).

(5) W. N. Hubbard, H. M. Feder, E. Greenberg, J. L. Margrave, E. Rudzitis, and S. S. Wise, Symposium on Thermodynamics and Thermochemistry, Lund, Sweden, 1963.

(6) P. Gross, C. Hayman, P. L. Levi, and M. C. Stuart, Fulmer Research Institute Report R. 146/4/23, Nov. 1960.

(7) W. D. Good, M. Månsson, and J. P. McCullough, Symposium on Thermodynamics and Thermochemistry, Lund, Sweden, 1963.

(8) R. E. McCoy and S. H. Bauer, *J. Am. Chem. Soc.*, **78**, 2061 (1956).

specified as 98% minimum. Principal contaminants were ammonia and mono- and dimethylamine. Melting-curve analysis⁹ of this material after drying by passage over calcium chloride and storage over a fresh sodium surface indicated a purity of 99.79%; probably solid solubility perturbs the result.

A batch of the same trimethylamine was then dried by passage over calcium chloride and zone-refined. A column about 15 cm. long was condensed and frozen in a Pyrex tube 11 mm. in o.d. This was positioned axially in another tube 26 mm. in i.d. immersed in liquid nitrogen. The space between the tubes was filled with nitrogen gas; a slow flow of dry nitrogen was maintained through a stopper at the top to prevent inward diffusion and condensation of moisture and air. The heater was a manganin coil wrapped in a narrow band on a short length of glass tube fitting closely around the inner tube. The leads passed upward through the stopper to a winch. The heater current was adjusted to give a molten zone roughly 1.5 cm. long; a helical rheostat coupled to the winch decreased the current slightly during the passage to minimize probability of breakage of the tube by a lengthened molten zone resulting from accumulation of impurities. Eleven downward passes were performed at 2 cm. hr.⁻¹. The top 2 cm. of material was then discarded and the next 6 cm. was recovered; melting curve analysis indicated 99.99% purity. Similar results were later obtained in an apparatus with all linear dimensions increased by a factor of two.

Diborane was obtained from Callery Chemical Co. After several bulb-to-bulb distillations, approximately 0.4% each of carbon dioxide and ethane were present. Melting-curve analysis indicated 99.85% purity; again, solid solubility may be responsible. Zone purification was performed as with trimethylamine, except that helium was used instead of nitrogen to improve heat transfer; melting-curve analysis indicated 99.99% purity.

Calorimeter. Calorimeter XXIX,¹⁰ a copper-block aneroid with vacuum jacket, was used. A copper resistance thermometer on the surface of the block was used with a G-2 Mueller bridge, Liston-Becker amplifier, and recorder to measure temperature with a precision of about 5×10^{-5} deg. The water-filled thermostat was stable to $\pm 0.001^\circ$; the thermal leakage modulus was 0.0016 min.⁻¹. Reactions were initiated at $25.00 \pm 0.05^\circ$. Temperature rises were about 0.5° for BF_3 hydrolysis and 0.7° for $\text{B}_2\text{H}_6\text{-Me}_3\text{N}$ reaction; following each run the calorimeter was cooled and calibrated electrically over the same temperature interval.

BF₃ Hydrolysis. The reaction vessel was a Teflon-

lined aluminum cup located at the bottom of the calorimeter well. Its inside dimensions were 2.10 cm. in diameter and 2.79 cm. in height; it was usually filled about 90% full. The cylindrical outer surface was covered with a 290-ohm manganin wire heater. A polyethylene tube 1 mm. in i.d. extended from the Teflon lid 55 cm. to a gas buret. The section of this tube inside the calorimeter above the reaction vessel was pressed against the wall by means of a thin phosphoro bronze sleeve. The vessel and tube were vacuum-tight within limits capable of affecting the measurements. A Teflon-covered stirring bar was included in the vessel; it was actuated by a magnetic drive located below the thermostat. Since this introduced great noise into the thermometer circuit, it was operated for 5-sec. periods at 1-min. intervals throughout the run by a sequence timer.

HF solution was weighed into the reaction vessel. BF_3 was weighed in a glass bulb equipped with greaseless valve, and then transferred in a submanifold of the vacuum line to a gas buret from which it could subsequently be displaced with mercury into the polyethylene tube of the calorimeter reaction vessel. The weighing bulb, manifold, and buret were always pretreated with BF_3 to eliminate surface moisture; a fluorocarbon stopcock grease was used. Tests by returning weighed BF_3 from the buret to the weighing bulb and reweighing showed losses during the transfer operations to be negligible.

The polyethylene tube and space above the solution in the reaction vessel were initially filled with air at atmospheric pressure. After recording the foredrift of the calorimeter, the BF_3 was forced in during a period of about 2 min. This compressed the air in the vessel to about 1.5 atm. The mercury was forced down the polyethylene tube to about 2 cm. above the reaction vessel. After the run, the mercury was brought back to the top of the buret and found to balance there at 1 atm., indicating that all the BF_3 had dissolved and no gas had leaked out of the reaction vessel.

About 40 min. was required after initiation of the reaction for attainment of constant afterdrift rate. This was probably due largely to the poor thermal conductivity of the Teflon liner. However, the time-temperature curves from reactions and electrical calibrations were very similar, and integration of the two for determination of the corrected temperature rise was performed in the same manner. The heater was so located that similar temperature gradients would be produced in the calorimeter block. The energy equivalents determined agreed within an average deviation from the

(9) S. R. Gunn, *Anal. Chem.*, **34**, 1292 (1962).

(10) S. R. Gunn, *Rev. Sci. Instr.*, **35**, 183 (1964).

mean of about 0.04%, after correction for differences in the amount of solution. Thus it appears that little loss of accuracy resulted from the slow equilibration.

After the runs, a small amount of the solution was found as droplets hanging near the center of the lid. This presumably was distilled from the solution below when the latter was warmed by reaction with the entering BF_3 . It probably was less concentrated in HF than the body of the solution, but calculation indicates the consequent thermal effect to be negligible.

B₂H₆-Me₃N Reaction. Pyrex reaction cells 2.8 cm. in o.d. and 18 cm. high were used. A Pyrex filling tube, 3.5 mm. i.d., led upward 32 cm. from the top of the cell to a stopcock. A break-seal for later recovery of the product was also located at the top of the cell. Mercury (20 ml.) was added to the calorimeter; this covered the cell to about 1 cm. above its upper end. The primary purpose of the mercury was to improve heat transfer from the small reaction zone at the lower end of the filling tube and hence reduce heating and pyrolysis of the product; it also increased the speed of temperature equilibration following reactions and calibrations. The heaters were manganin wire, about 200 ohms resistance, wound in a band 2.5 cm. wide near the top of the cell.

Diborane samples were measured in a gas buret¹¹ and condensed in the reaction cell, which was then placed in the calorimeter. A short manifold of 2-mm. i.d. tubing, having a volume of 1.5 ml., connected the reaction cell to a vacuum pump, a 5.2-ml. helium bulb, and a 320-ml. trimethylamine bulb. These bulbs were filled to about 2.1 and 1.5 atm., respectively, the trimethylamine bulb being weighed and attached to the manifold, which was then evacuated. A very fine capillary connected the trimethylamine bulb to the manifold.

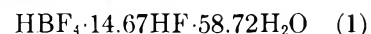
After the calorimeter foredrift was recorded, the helium was admitted to the manifold and to the cell to sweep out the filling tube. The trimethylamine was then admitted; the rate of temperature rise was nearly constant throughout the duration of the reaction. A few minutes after completion of the reaction the trimethylamine bulb was closed and it was later reweighed; the excess trimethylamine introduced to the reaction cell ranged from 1 to 2 mmoles. The product was formed in a band concentrated in the top of the reaction cell, heaviest at the lower end of the filling tube. It was pure white, with no evidence of melting. Earlier experiments without mercury in the calorimeter showed some yellowing and evidence of a little melting.

After the run, the cell was held at -78° and the excess trimethylamine pumped off. A sample of the non-condensable gas was taken for subsequent determina-

tion of the H_2 :He ratio. The amount of helium introduced into the cell being calculable, the amount of hydrogen produced by side reactions was thus determined. The filling tube was then sealed off, a trap line was sealed on above the break-seal, and the product was sublimed into a trap and weighed. Slight traces of non-volatile residues were usually visible.

Results

Results are given in Table I for reaction 1. The con-



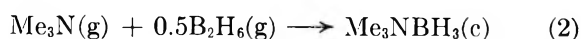
centration of the HF solution in column 4 of Table I is given as a percentage of that specified by eq. 1; that of run 6 was deliberately made more dilute to check the effect upon the heat of the reaction, and the result of this

Table I: Heat of Hydrolysis of BF_3

Run	BF_3 , mmoles	HF soln., g.	HF, % theor.	Soln./ BF_3 , % theor.	q , cal.	$-\Delta H$, kcal./mole
1	5.005	6.832	101.6	99.6	142.00	28.40
2	5.675	7.789	101.6	100.1	159.51	28.14
3	5.672	7.792	101.6	100.2	160.10	28.26
4	5.110	6.989	101.6	99.7	144.58	28.32
5	5.820	7.954	101.6	99.7	164.28	28.26
6	5.482	7.493	89.4	99.7	154.83	(28.27)
7	5.561	7.609	100.0	99.7	156.86	28.24
8	5.774	7.905	100.0	99.8	164.01	28.43
9	5.654	7.700	100.0	99.6	159.75	28.28

run is not included in the average. The ratio of mass of solution to mass of BF_3 in column 5 is also given as a percentage of that specified by eq. 1. The values of q in column 6 include the small corrections for PV work of compressing air in the polyethylene tube (0.01 cal.) and for heating the BF_3 and 2.3 g. of mercury (the amount assumed to be in thermal contact with the calorimeter) from room temperature to 25.00° . Room temperature ranged from 23.5 to 24.5° . ΔH is calculated on the basis of 99.9% of the weighed BF_3 sample, allowing for a possible 0.1% loss in grease and elsewhere. The mean value for ΔH_1 is -28.29 kcal. mole⁻¹; the uncertainty interval is taken as 0.07, twice the standard deviation of the mean.

Results are given in Table II for reaction 2. All runs



in Table II were performed under similar conditions,

(11) S. R. Gunn and L. G. Green, *J. Phys. Chem.*, **64**, 61 (1960).

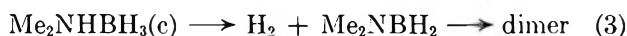
except that a larger capillary was used to control the trimethylamine flow in run 3, giving a reaction duration of 6 min., compared with 9 to 11 min. for the other runs, and twice the usual amount of helium was used in run 4.

Table II: Heat of Reaction of Me_3N with B_2H_6

Run	B_2H_6 , mmoles	Me_3NBH_3 , % yield	H_2 , mole % Me_3NBH_3	q, cal.	$-\Delta E$, kcal./mole
1	3.017	99.60	0.35	188.86	31.36
2	3.126	99.76	0.32	196.90	31.53
3	3.080	99.53	0.49	193.35	31.46
4	3.127	99.95	0.19	195.93	31.34
5	3.130	99.74	0.29	196.69	31.46
6	3.282	99.66	0.27	206.25	31.47

The observed heat values were corrected by subtraction of 4.4–5.2 cal. to allow for the PV work of the entering gas, addition of 0.08–0.02 cal. to allow for the fact that the gas entered at a room temperature ranging from 24.5 to 24.9°, and addition of 0.06 cal. to correct for the slight volatility of Me_3NBH_3 ^{12,13}; these corrected values are given in column 5.

The weight of Me_3NBH_3 found is given in column 3 as a percentage of the theoretical from the measured diborane sample, and the hydrogen found is given in column 4 as a mole percentage of the Me_3NBH_3 ; the two percentages sum to roughly 100. McCoy and Bauer⁸ noted that mono- and dimethylamine boranes decompose slowly even at 0° according to eq. 3 with an



estimated ΔH of +10 kcal. mole⁻¹, but that $\text{Me}_3\text{N}-\text{BH}_3$ is stable. It is possible that some of the hydrogen is produced by decomposition of lower methylamine boranes produced from small amounts of lower methylamines in the trimethylamine not detected by the melting-curve analysis. It seems more likely, however, that it is produced either by pyrolysis of the Me_3NBH_3 or the reactants at the time of reaction; this is supported by the observed greater amount of hydrogen in run 3 and by observation of about 4% H_2 in a preliminary run without mercury in the calorimeter, which showed slight melting of the product.

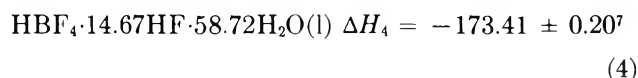
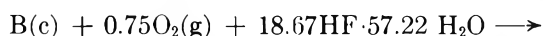
ΔE is calculated from q and the average of the B_2H_6 sample and Me_3NBH_3 product. This gives about the same result as calculating from the B_2H_6 sample only and correcting for the amount of hydrogen found on the assumption of reaction 3 at +10 kcal. mole⁻¹. The average for ΔE is -31.44 ± 0.05 (uncertainty interval twice the standard deviation of the mean) and ΔH_2 is then -32.33 kcal. mole⁻¹.

Discussion

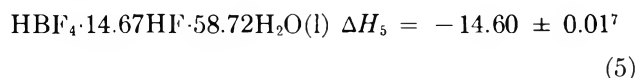
The heat of hydrolysis of boron trifluoride has been measured previously^{14–16} but not in strong HF solution at all comparable with the present conditions. The principal question is whether the solution reaches a state during the main period thermochemically equal to that produced during the main period of the three reactions of Good, *et al.*⁷; it seems probable that this is indeed the case at this high HF concentration. It is not necessary that this state be an equilibrium one. The observations of Wamser^{17,18} suggest that equilibrium should be closely approached in the time intervals involved.

McCoy and Bauer⁸ reported a value of -31.27 ± 0.15 for ΔH_2 at 0°; corrected to 25°, this becomes -31.40 .^{7,19} They give no information on purity of reactants or analysis of products. In the present work, values about 1 kcal. low were observed both with the reactants before zone-refining and with the zone-refined reactants but using no mercury to promote cooling of the reaction zone.

The interrelationships of certain thermochemical determinations on boron compounds may be illustrated by means of a pseudo energy level diagram, Figure 1. In the figure, step A is the combustion of crystalline boron (eq. 4). Step B is the heat of solution of crystal-



line orthoboric acid in $\text{HF} \cdot 2.984\text{H}_2\text{O}$ (eq. 5). Using



the heat of dilution of hydrofluoric acid (eq. 6),²⁰ and

(12) A. B. Burg and H. I. Schlesinger, *J. Am. Chem. Soc.*, **59**, 780 (1937).

(13) E. R. Alton, R. D. Brown, J. C. Carter, and R. C. Taylor, *ibid.*, **81**, 3550 (1959).

(14) H. Hammerl, *Compt. rend.*, **90**, 312 (1880).

(15) A. W. Laubengayer and G. R. Finlay, *J. Am. Chem. Soc.*, **65**, 884 (1943).

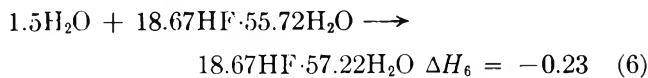
(16) D. A. Scarpiello and W. J. Cooper, *J. Chem. Eng. Data*, **9**, 364 (1964).

(17) C. A. Wamser, *J. Am. Chem. Soc.*, **70**, 1209 (1948).

(18) C. A. Wamser, *ibid.*, **73**, 409 (1951).

(19) Heat capacity data for Me_3NBH_3 are from unpublished work, Low-Temperature Thermodynamics Group, U. S. Bureau of Mines, Bartlesville Petroleum Research Center.

(20) W. H. Evans, National Bureau of Standards, private communication, 1963.



$$-68.317 \text{ for } \Delta H_f^\circ(\text{H}_2\text{O}, \text{l})^{21}$$

$$\Delta H_f^\circ(\text{H}_3\text{BO}_3, \text{c}) = \Delta H_4 - \Delta H_5 + \Delta H_6 +$$

$$1.5\Delta H_f^\circ(\text{H}_2\text{O}, \text{l}) = -261.52 \pm 0.20$$

Good, *et al.*,⁷ give -261.47 , probably by use of slightly different data for hydrofluoric acid.

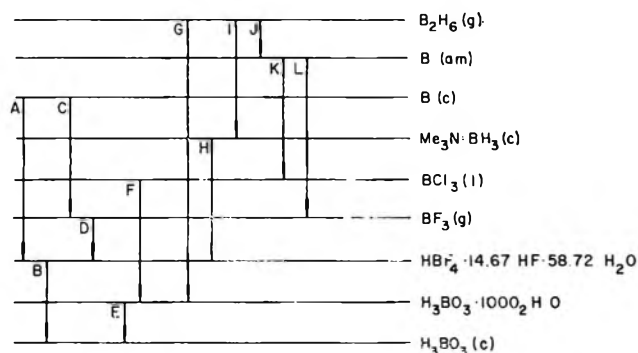
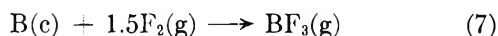
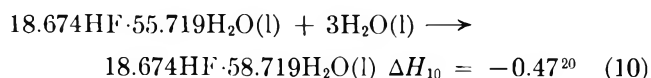
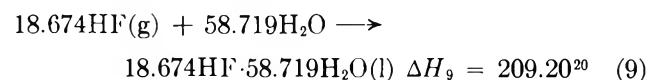
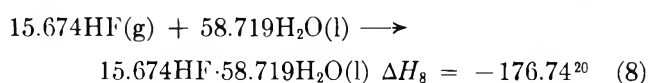


Figure 1. Thermochemical relationships of boron compounds.

Step C is the heat of fluorination of crystalline boron (eq. 7). Two values exist for $\Delta H_f^\circ(\text{BF}_3)$: Hubbard's



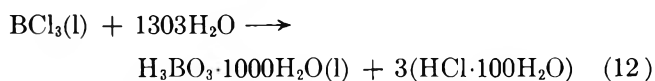
group reported -269.5 ± 0.5^5 (revised from an earlier value of -269.88 ± 0.29^4) and Gross gives $-270.57^{6,22}$. Tentatively, -270.0 will be used, combined with -28.29 ± 0.07 for ΔH_1 (step D) and auxiliary data, to obtain $\Delta H_f^\circ(\text{H}_3\text{BO}_3, \text{c})$ by steps C, D, and B.



using -64.8 for $\Delta H_f^\circ(\text{HF}, \text{g})^{20}$, $\Delta H_f^\circ(\text{H}_3\text{BO}_3, \text{c}) = \Delta H_f^\circ(\text{BF}_3, \text{g}) + \Delta H_1 - \Delta H_5 + \Delta H_8 - 3\Delta H_f^\circ(\text{HF}, \text{g}) - \Delta H_9 + \Delta H_{10} + 3\Delta H_f^\circ(\text{H}_2\text{O}, \text{l}) = -262.25$. This value derived from steps C, D, and B is much more uncertain than that derived from steps A and B; the major uncertainties are in the heat of formation of BF_3 and the heats of formation and solution of HF. A weighted value of -261.7 will be chosen for $\Delta H_f^\circ(\text{H}_3\text{BO}_3, \text{c})$. An alternative use of the data is to calculate $\Delta H_f^\circ(\text{BF}_3)$ from steps A and D; this gives -269.27 . A weighted average of this and the direct value of step C will be chosen: -269.70 .

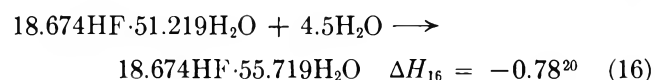
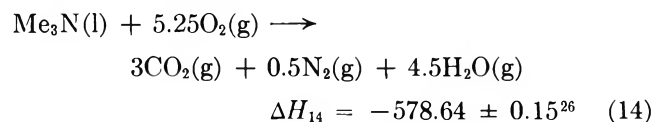
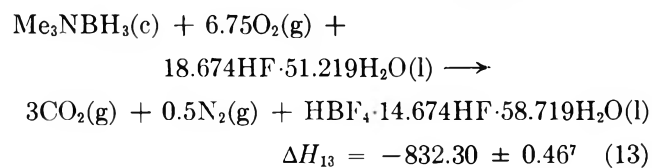
Step E, the heat of solution of crystalline boric acid in water, has been measured by many workers. Evans, Wagman, and Prosen²³ evaluated the data and gave a value of $+5.24$ kcal. mole⁻¹ for ΔH_{11} . The uncertainty is apparently about 0.05. $\Delta H_f^\circ(\text{H}_3\text{BO}_3 \cdot 1000 \text{H}_2\text{O})$ is then -256.46 .

Boron trichloride is related to boric acid through the heat of hydrolysis, step E. Converted to reaction 12



the data of Gunn and Green¹¹ and Skinner and Smith²⁴ give -67.97 ± 0.09^{25} and -68.6 , respectively, for ΔH_{12} . Using a weighted average of -68.20 for ΔH_{12} and -39.713 for $\Delta H_f^\circ(\text{HCl} \cdot 100\text{H}_2\text{O})^{21}$, $\Delta H_f^\circ(\text{BCl}_3, \text{l})$ is -102.45 .

Two routes relate diborane to boric acid: steps I, H, and B, and steps G and E. For the first route



$$\Delta H_f^\circ(\text{B}_2\text{H}_6) = 2(\Delta H_f^\circ(\text{H}_3\text{BO}_3) - \Delta H_2 - \Delta H_{13} +$$

$$\Delta H_5 + \Delta H_{14} - \Delta H_{15} + \Delta H_{16}) = +7.40 \pm 0.98$$

For ΔH_2 , the value from the present work, $-32.33 \pm$

(21) F. D. Rossini, *et al.*, National Bureau of Standards Circular 500 (1952).

(22) This value is converted to the 1961 scale of atomic weights, $B = 10.811 \pm 0.003$.

(23) W. H. Evans, D. D. Wagman, and E. J. Prosen, National Bureau of Standards Report 4943 (1956).

(24) H. A. Skinner and N. B. Smith, *Trans. Faraday Soc.*, **49**, 601 (1953).

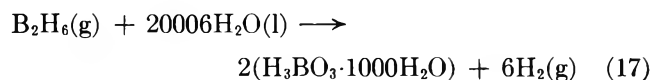
(25) These values are reduced by $0.25 \pm 0.1\%$ from those given in ref. 11; see University of California, Lawrence Radiation Laboratory, unpublished report UCRL-7992.

(26) I. Jaffe, unpublished work, National Bureau of Standards, 1958.

(27) J. G. Aston, M. L. Sagenkahn, G. J. Szasz, G. W. Moessen, and H. F. Zuhre, *J. Am. Chem. Soc.*, **66**, 1171 (1944).

(28) "Methylamines: Physical Properties and Analytical Methods," Rohm and Haas Co., Philadelphia, Pa.

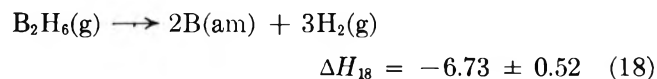
0.06, is used. In route G, E two values are available for the heat of hydrolysis of diborane (eq. 17). Prosen,



Johnson, and Pergiel²⁹ gave -111.46 ± 0.54 ; Gunn and Green¹¹ gave -111.94 ± 0.15 .²⁵ Using a weighted average of -111.80 , $\Delta H_f^\circ(\text{B}_2\text{H}_6) = 2\Delta H_f^\circ(\text{H}_3\text{BO}_3 \cdot 1000\text{H}_2\text{O}) - 6\Delta H_f^\circ(\text{H}_2\text{O}, \text{l}) - \Delta H_r = +8.78$.

The hydrolysis route G, E is considerably more direct and involves smaller experimental errors than the route I, H, B through trimethylamine-borane; accordingly a value of $+8.60$ will be tentatively adopted for $\Delta H_f^\circ(\text{B}_2\text{H}_6)$.

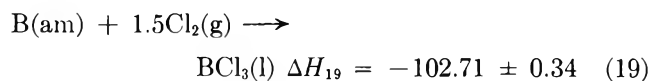
Three separate investigations, steps J, K, and L, involve a form of amorphous boron prepared by thermal decomposition of diborane. Prosen, Johnson, and Pergiel² measured step J (eq. 18), the decomposition of diborane.



$$\Delta H_f^\circ(\text{B}, \text{am}) = 0.5(\Delta H_{18} + \Delta H_r^\circ(\text{B}_2\text{H}_6, \text{g})) = +0.94$$

Gross, *et al.*,⁶ measured step L, the heat of fluorination of amorphous boron, as well as step C, the heat of fluorination of crystalline boron, and found the former to be 0.8 kcal. more exothermic, which implies

$\Delta H_f^\circ(\text{B}, \text{am}) = +0.8$. Johnson, Miller, and Prosen³ measured step K, the heat of chlorination of amorphous boron (eq. 19).



$$\Delta H_f^\circ(\text{B}, \text{am}) = \Delta H_f^\circ(\text{BCl}_3, \text{l}) - \Delta H_{19} = +0.26$$

A slightly less negative value of $\Delta H_f^\circ(\text{BCl}_3, \text{l})$, -102.3 , will be selected to bring this value of $\Delta H_f^\circ(\text{B}, \text{am})$ somewhat nearer the other two.

While discrepancies somewhat outside of the attributed experimental errors exist in many cases, none of these is gross, and the basic thermochemistry of boron compounds may be said to be in reasonably satisfactory condition. Some recommended values are given in Table III.

Table III: Recommended Values of ΔH_f°

$\text{B}_2\text{H}_6(\text{g})$	+8.6
$\text{B}(\text{am})$	+0.8
$\text{BCl}_3(\text{l})$	-102.3
$\text{BF}_3(\text{g})$	-269.7
$\text{H}_3\text{BO}_3(\text{c})$	-261.7

(29) E. J. Prosen, W. H. Johnson, and F. Y. Pergiel, *J. Res. Natl. Bur. Std.*, **62**, 43 (1959).

Thermal Diffusion Measurements by Wave-Front-Shearing Interferometry

by Silas E. Gustafsson,¹ Julius G. Becsey, and James A. Bierlein

*Aerospace Research Laboratories, Office of Aerospace Research, Wright-Patterson Air Force Base, Ohio
(Received October 28, 1964)*

The application of wave-front-shearing interferometry to the study of thermal diffusion is analyzed mathematically, and it is shown that an optimum shear exists which maximizes the sensitivity of the method. Experimental measurements on electrolyte solutions, using a form of interferometer described by Bryngdahl, give results which are comparable in precision to the best previous determinations made by other techniques. The present method has worthwhile advantages of simplicity and convenience.

Introduction

The thermal diffusion of binary liquid systems is usually studied as an unsteady-state process, in which the experimenter aims to create a convection-free one-dimensional environment of vertical heat and mass transfer in a suitably designed sample cell. The progress of the diffusion can be measured *in situ* by a variety of optical methods—image displacement,²⁻⁵ Gouy diffractometry,^{6,7} and Rayleigh interferometry⁸—all of which derive ultimately from the distortion of a transmitted wave front by the gradients of refractive index attending the diffusion process. High sensitivity is a goal of primary importance in the development of measuring techniques, so that small temperature gradients (which necessarily produce correspondingly small concentration gradients) may be used in the diffusion cell. The Soret coefficient is often strongly temperature dependent, and one wishes to identify the measured coefficient with a definite temperature; furthermore, the use of the smallest practicable temperature difference across the sample cell minimizes convective disturbances, which give rise to serious errors if not adequately suppressed.

Bryngdahl and co-workers^{9,10} have recently devised a new kind of interferometer which is particularly convenient for the study of diffusion, electrophoresis, sedimentation, heat transfer, and similar phenomena. In the present paper, we demonstrate its application to the problem of measuring Soret coefficients and establish the conditions of operation which maximize its sensitivity for this purpose.

The apparatus is shown schematically in Figure 1. A detailed analysis of the principles of its operation is

available in Bryngdahl's papers; we give here only a sufficient description to make intelligible our subsequent theoretical development and experimental results. Collimated monochromatic light illuminates the whole height a of the diffusion cell C , in which a refractive index profile is shown. L_1 and L_2 are lenses which demagnify the shaped wave front emerging from C . The beam is then plane-polarized horizontally by passage through the polarizer P . The first Savart plate S_1 is positioned normal to the optic axis and oriented so that the angle between its principal planes is bisected by the plane of polarization of P_1 ; it produces a vertical shearing of the wave front. The resultant wave fronts are polarized at right angles to one another, are of equal intensity, and are displaced by a vertical distance

$$b = \sqrt{2} \epsilon (N_o^2 - N_e^2) / (N_o^2 + N_e^2)$$

(1) Visiting Research Associate from Department of Physics, Chalmers University of Technology, Gothenburg, Sweden. Supported in part by a grant from Stiftelsen Blanceflor Boncompagni-Ludovisi, född Bildt.

(2) (a) C. C. Tanner, *Trans. Faraday Soc.*, **49**, 611 (1953); (b) H. Korsching, *Z. Naturforsch.*, **10a**, 242 (1955).

(3) J. A. Bierlein, C. R. Finch, and H. E. Bowers, *J. chim. phys.*, **54**, 872 (1957).

(4) J. Chanu and J. Lenoble, *ibid.*, **53**, 309 (1956); **55**, 743 (1958).

(5) H. J. V. Tyrrell, J. G. Firth, and M. Kennedy, *J. Chem. Soc.*, 3432 (1961).

(6) J. A. Bierlein, *J. Chem. Phys.*, **36**, 2793 (1962).

(7) J. G. Becsey and J. A. Bierlein, *ibid.*, **41**, 1853 (1964).

(8) L. G. Longworth in "The Structure of Electrolytic Solutions," W. J. Hamer, Ed., John Wiley and Sons, Inc., New York, N. Y., 1959.

(9) O. Bryngdahl and S. Ljunggren, *J. Phys. Chem.*, **64**, 1264 (1960).

(10) O. Bryngdahl, *J. Opt. Soc. Am.*, **53**, 571 (1963).

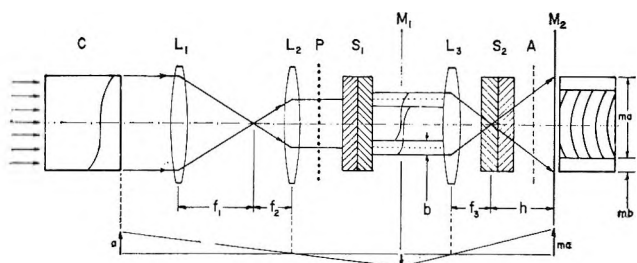


Figure 1. Optical arrangement of interferometer.

where N_o and N_e are the principal refractive indices of the birefringent crystals (each of thickness ϵ) comprising the Savart plate. A second plate S_2 , turned 90° with respect to S_1 , is placed in the converging rays of the lens L_3 . This plate produces (apart from an identical vertical displacement of both wave fronts, which is of no consequence) a horizontal displacement of each incident ray, proportional to its angle of incidence and opposite in direction for opposite polarizations. The net effect is to introduce a small angle, as viewed from above, between the sheared wave fronts. An analyzer A , crossed with P , makes visible the interference fringes in the image plane M_2 . The lens L_2 forms an image of the exit window of C in the plane M_1 , whence it is transferred to M_2 by L_3 . The interferogram at M_2 consists of two sharply focused and overlapping images of C , with the fringes superimposed in the area of overlap. The extent of overlap (best expressed as the relative shear, $s = b/a$) is determined by the telescopic power f_2/f_1 of the lens combination L_1L_2 and can be varied by selecting appropriate focal lengths. The over-all vertical magnification m of the interferometer is of course determined by the focal lengths of all three lenses and by the distance h which depends on their disposition; the horizontal magnification is influenced by the same parameters and in addition by the characteristics of the plate S_2 . An explicit examination of these relations need not concern us here.

In the case that the test zone contains only linear gradients in refractive index (an optically homogeneous medium being included as the special case of a null gradient), the interference pattern consists of uniformly spaced linear fringes, oriented vertically; the distance between fringes in the image plane corresponds to a path difference of one wave length. If nonlinear gradients exist, then the fringes take a form which approximates to the derivative curve of the refractive index, this approximation becoming exact in the limit of vanishing shear. It is the special case of vanishing shear which Bryngdahl has specially emphasized in his theoretical and experimental work. This procedure has the advantage of requiring no mathematical description of a

refractive index distribution in order to effect a direct experimental determination of its form, but this advantage is secured at the expense of a low sensitivity. When dealing with a process of known phenomenology, it is possible—as we shall show for the case of thermal diffusion—to optimize the shear for highest sensitivity. The resulting interferograms, although they are finite-difference curves rather than true derivatives, can be readily interpreted to derive Soret coefficients.

Theory

The Diffusion Process. The refractive index μ in a binary mixture during thermodiffusional unmixing develops in time and space according to the equation³

$$\mu(v, t) = \mu_0 + K_2v/a + \sigma\tau K_1 \left[\frac{v}{a} - \frac{4}{\pi^2} e^{-t/\theta} \sin \frac{\pi v}{a} \right] \quad (1)$$

Here μ_0 is the initial uniform refractive index; v is the vertical coordinate, measured upward from the mid-plane of the cell; a is the cell height; σ is the Soret coefficient; τ is the temperature difference across the cell; t is the time since the start; $\theta = a^2/\pi^2D$, where D is the isothermal diffusivity; $K_2 = \tau\partial\mu/\partial T$, where T means temperature; and $K_1 = n_0(1 - n_0)\partial\mu/\partial n$, where n is the mole fraction of the component of lesser molecular weight and n_0 denotes the initial composition. After prolonged separation, a linear gradient in μ is established. If the temperature gradient is then removed and the mixture is thermostated at the mean temperature, the ensuing isothermal remixing proceeds according to¹¹

$$\mu(v, t) = \mu_0 + \frac{4}{\pi^2} \sigma\tau K_1 e^{-t/\theta} \sin \frac{\pi v}{a} \quad (2)$$

where we now understand t to be measured from the instant that remixing begins.

Since the shearing interferometer does not record any linear gradients, we see that the essential difference between eq. 1 and 2 is only in the sign of their transient terms. From this we expect that the interferograms of the unmixing and remixing processes will be identical mirror images at equal lapsed times.

Optical Analysis. Since we postulate the interferometer to be focused on the exit window of the sample cell, we need to define the optical path length $R(v)$ of any ray leaving the cell in the horizontal plane v , assuming that all rays enter the sample at normal incidence. The general problem of formulating path length as a function of focal plane has been studied by Svensson,¹² and

(11) G. Meyerhof and K. Nachtigall, *J. Polymer Sci.*, **57**, 227 (1962).

(12) H. Svensson, *Opt. Acta*, **1**, 25 (1954); see his eq. 30.

the particular expression we require follows directly from specialization of his equations

$$R(v) = L\mu(v) - \frac{L^3[\mu'(v)]^2}{6\mu(v)} + \dots \cong L\mu(v) - \frac{L^3[\mu'(v)]^2}{6\mu_0} \quad (3)$$

The prime stands for differentiation with respect to v . Since $\mu'(v)$ is everywhere small, we neglect terms higher than the second in the series expansion; to the same order of approximation, we ignore any variability of μ in the denominator of the second term.

We have now to consider the problem of evaluating the path difference $\Delta R(v)$ between pairs of rays—one from each of the two sheared wave fronts—which lie in the same horizontal plane v after emergence from the first Savart plate. The incremental retardation $\Delta_1 R(v)$ resulting purely from the shearing is clearly equal to

$$\Delta_1 R(v) = R_+ - R_- \quad (4)$$

where the positive and negative subscripts mean that the associated function of v is to be evaluated for $v + \frac{1}{2}b$ and $v - \frac{1}{2}b$, respectively. An additional path difference $\Delta_2 R(v)$ is introduced right in the Savart plate itself. To formulate $\Delta_2 R(v)$, we note first that the path differences between two sheared rays, originating from the splitting of a single ray which falls on the plate at an angle of incidence i , is given by Bryngdahl¹³ as $b \sin i$, or more simply as bi if i is small. Figure 2 shows

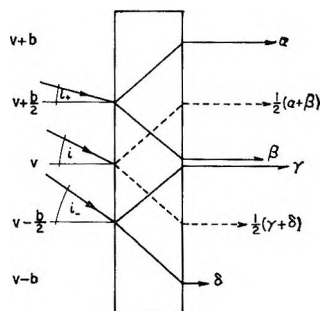


Figure 2. Differential retardation of rays entering a Savart plate at differing angles.

two rays incident at angles i_+ and i_- at levels $\pm b/2$ distant from the plane v , each split into two emergent rays of differing retardation. We seek to find the difference $\gamma - \beta \equiv \Delta_2 R(v)$. Since $\alpha - \beta = bi_+$ and $\gamma - \delta = bi_-$, it follows that $\Delta_2 R(v) + \alpha - \delta = b(i_+ + i_-)$. The term $\alpha - \delta$ may be eliminated if we recognize that $\frac{1}{2}(\alpha + \beta) - \frac{1}{2}(\gamma + \delta) = bi = \frac{1}{2}(\alpha - \delta) - \Delta_2 R(v)$, where i is the angle of incidence of the ray

striking in the plane v . Comparison of the last two equations gives

$$\Delta_2 R(v) = \frac{1}{2}b(i_+ + i_-) - bi = \frac{1}{2}b(R'_+ + R'_-) - bR' \quad (5)$$

in which we use the fact that $i \equiv dR/dv \equiv R'$. The total path difference $\Delta R(v)$ is the sum of eq. 4 and 5, and with the aid of eq. 2 we can write it in the explicit form

$$\Delta R(v) = \frac{8}{\pi^2} \sigma \tau K_1 L e^{-t/\theta} \left[\sin \frac{\pi s}{2} + \frac{\pi s}{2} \cos \frac{\pi s}{2} - \frac{\pi s}{2} \right] \cos \frac{\pi v}{a} + \frac{8L^3}{3\mu_0} \left[\frac{\sigma \tau K_1 e^{-t/\theta}}{\pi a} \right]^2 [\sin \pi s + \pi s \cos \pi s - \pi s] \sin \frac{2\pi v}{a} \quad (6)$$

where s is the constant b/a . Except for the equation of a scale factor to be considered presently, this expression defines the shape of each one of the identical fringes which appear in the final image plane M_2 of the interferometer. In the limit $s \rightarrow 0$, $\Delta R(v) = sLd\mu/dv$, and the interferogram faithfully duplicates the derivative curve of the refractive index. However, in the general case of appreciable shear, this is not true. Whereas the first term of eq. 6 is always a symmetrical (even) function of v , the second term is an odd function which does not vanish if s is finite. The presence of the odd term leads us to expect a skewness or tilt in the interferogram, which should decay away as time passes. This prediction is well fulfilled experimentally, as we shall see later on.

We consider now the practical problem of evaluating an interferogram. The fringe shape can be characterized experimentally by a series of distances $y(v)$ which define the displacement, measured perpendicular to the v axis, between points at arbitrary v values and the minimum point at $v = 0$. To relate these data to the optical path lengths defined in eq. 6, we recall that the distance between any two of the parallel fringes (call it r) corresponds to a path difference of one wave length λ . Since r can be measured directly on the interferogram and λ is known, the horizontal scale factor r/λ is readily established. It follows that the desired relation is $y(v) = (r/\lambda)[\Delta R(v) - \Delta R(0)]$. This expression is somewhat awkward when written out explicitly, as it retains the skew character inherent in eq. 6. We can arrive at a neater solution and considerably simplify the subsequent problems of curve fitting by a judicious choice of experimental procedure. Let us

(13) O. Bryngdahl, *Arkiv Fysik*, **21**, 289 (1962); see pp. 331-333.

measure the deviations of pairs of conjugate points symmetrically disposed around $v = 0$, and then deal with the mean values $y^*(v) = 1/2[y(v) + y(-v)]$. In terms of this parameter, eq. 6 transforms to

$$y^*(v) = \frac{8r}{\pi^2\lambda} \sigma\tau K_1 L e^{-t/\theta} \left[\sin \frac{\pi s}{2} + \frac{\pi s}{2} \cos \frac{\pi s}{2} - \frac{\pi s}{2} \right] \left[1 - \cos \frac{\pi v}{a} \right] \quad (7)$$

To cast (7) into the most general possible form, we must remember that the fringes in the interferogram exist only in the region of overlap of the two vertically displaced cell images. Hence the coordinate v in the interferogram never extends to the maximum values $\pm a/2$ which obtain in the cell, but is limited between closer bounds $\pm(1-s)a/2$ because of the shearing. It is therefore convenient to introduce a new vertical coordinate $\eta = 2v/(1-s)a$; the range of this parameter is always $-1 \leq \eta \leq 1$, independent of s . Rewriting eq. 7 with this generalized coordinate gives

$$y^*(\eta) = \frac{8r}{\pi^2\lambda} \sigma\tau K_1 L e^{-t/\theta} \left[\sin \frac{\pi s}{2} + \frac{\pi s}{2} \cos \frac{\pi s}{2} - \frac{\pi s}{2} \right] \left[1 - \cos \frac{\pi}{2} (1-s)\eta \right] \quad (8)$$

This expression forms the basis for determining the Soret coefficient.

Since s can be calculated right from the cell-image overlap (see Figure 1) and all the other constants can be measured beforehand, σ follows from the regression of $y^*(\eta)$ upon $\exp(-t/\theta)$ at any fixed η . A multiplicity of estimates for σ may be obtained by repeating the regression analysis for several fixed values of η ; this affords a safeguard against gross mistakes in measurement or calculation and improves the precision of the final estimate by averaging out unavoidable experimental errors. The ultimate extension of this procedure is to use all possible values of η . In this connection, consider the area $A^*(\eta)$, included between the convex side of a fringe and the tangent at $\eta = 0$ and further bounded at $\pm\eta$. The analytical expression is

$$A^*(\eta) = \frac{1}{\eta} \int_0^\eta y^*(\eta) d\eta \quad (9)$$

in which the unit value of $A^*(\eta)$ corresponds to one-half the area between two undeviated fringes. In practice, it is more convenient to work with the area on the convex side of the fringe, closed by the chord through the points $\pm\eta$. This area is given by

$$\bar{A}^*(\eta) = y^*(\eta) - A^*(\eta) = \frac{8r}{\pi^2\lambda} \sigma\tau K_1 L e^{-t/\theta} \left[\sin \frac{\pi s}{2} + \frac{\pi s}{2} \cos \frac{\pi s}{2} - \frac{\pi s}{2} \right] \times \left[\frac{\sin \frac{\pi}{2} (1-s)\eta}{\frac{\pi}{2} (1-s)\eta} - \cos \frac{\pi}{2} (1-s)\eta \right] \quad (10)$$

The area being determined on the interferograms by numerical integration, the Soret coefficient follows directly from analysis of its temporal regression.

The Optimum Shear. It is important to the experimenter to know what value of s to use in order to attain a maximum sensitivity. To answer this question, it is necessary to investigate the null values of $\partial y/\partial s$ and $\partial \bar{A}^*/\partial s$. The algebra involved is tedious but straight-

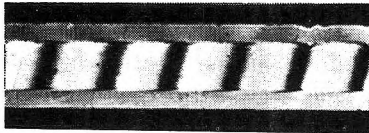
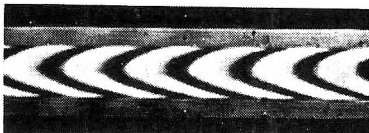
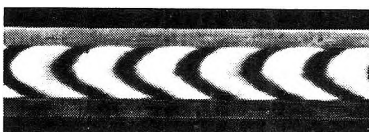
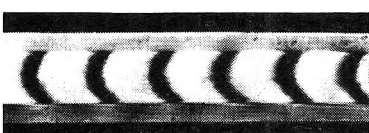

	t, min.	t/θ
	0.0	0.00
	24.1	0.40
	57.9	0.96
	106.7	1.77
	176.1	2.92

Figure 3. Experimental interferograms. Isothermal remixing of 0.5 M aqueous cadmium sulfate from the thermodiffusional steady state, under conditions specified in the first column of Table I.

forward and we do not reproduce it here. Some typical numerical results summarize the situation.

η	s for optimum	
	y^*	\bar{A}^*
0.5	0.2833	0.2864
1.0	0.2727	0.2734

It is clear that a shear of about 0.28 optimizes both cases over the range of η which is of practical interest. Further, we find by numerical analysis that the sensitivity changes slowly with the shear in the neighborhood of the maximum. For example, if s is allowed to vary $\pm 20\%$ around 0.2833, the value of $y^*(1)$ will change less than 5%. In general, any shear in the range $0.20 < s < 0.35$ will do nicely for thermal diffusion measurements; outside these limits, however, the sensitivity begins to drop off rapidly.

Experimental Tests

Apparatus. The cell used in our experiments consists of a rectangular glass frame of optical quality glass, clamped between horizontal plates of silver-coated copper; a thin film of silicone grease provides a seal against leakage at the contact surfaces of glass and metal. A number of frames of different heights are available to permit selection of a convenient relaxation time for the solution to be examined; each frame measures about 6×8 cm. in plan view, the longer dimension lying along the optic axis. The metal-glass interfaces at the top and bottom plates of the assembled cell are not sharply defined or of good optical quality, owing to unavoidable extrusion of the sealant; for this

reason, we mask off these regions with a large slit (height H), mounted on the exit window and centered on the midplane. Three circulating water baths, regulated to a maximum ripple of $\pm 0.003^\circ$, permit the cell to be operated under a steady temperature gradient or to be thermostated at an intermediate temperature. Multijunction thermocouples, inserted into wells in the plates, are used to measure temperatures at the upper and lower boundaries of the cell during operation.

In our optical system we use a 500-watt mercury arc lamp to illuminate the slit of a collimator with a focal length of about 1 m. The light is filtered to isolate λ 5461 Å. Our Savart plates are made of quartz, $e = 10$ mm. and $b = 84.2 \mu$; they were supplied by Crystal Optics, Chicago, Ill. Two different systems have been used to perform the shear-determining demagnification in front of the first Savart plate (L_1L_2 in Figure 1). One is a combination of a 914-mm. lens and a three-power microscope objective; another more flexible arrangement utilizes a compact telescope (Questar) of adjustable focal length. A 40-mm. lens between the Savart plates completes the optical train. Photographic registration of the interference fringes is accomplished on Kodak Tri-X 35-mm. film with an exposure of about 1 sec.

Results

To test the adequacy of our theory, as well as the utility of the instrument, we have measured the Soret coefficients of a number of aqueous electrolytes for which reliable data already exist. Figure 3 is a typical

Table I: Experimental Data; Mean Temperature 25°

Kind of experiment	0.5 M CdSO ₄		1.0 M AgNO ₃		4.0 M KCl	
	Remixing	Remixing	Remixing	Remixing	Unmixing	Remixing
a , cm.	0.404		0.402	0.805	0.798	
H , cm.	0.284		0.284	0.571	0.738	
K_t	-0.0127			-0.0160	-0.0254	
L , cm.	7.86			7.86	7.88	
τ , deg.	2.143	2.004	1.987	2.121	2.213	2.213
D , cm. ² /sec. [†]	0.456×10^{-5}		1.277×10^{-5}		2.165×10^{-5}	
θ , min.	60.3		21.4	76.1	49.7	
s	0.202	0.196	0.204	0.191	0.256	
η	0.562	0.568	0.507	0.587	0.720	
$\sigma \times 10^3$, sec. ⁻¹ , from						
$y^*(\eta)$	4.96 ± 0.03	5.07 ± 0.09	4.38 ± 0.05	4.46 ± 0.04	1.37 ± 0.01	1.36 ± 0.01
$\bar{A}^*(\eta)$	5.02 ± 0.02		4.46 ± 0.06		1.38 ± 0.01	
$\sigma \times 10^3$, sec. ⁻¹ , from literature	4.92 ^a		4.27 ^a		1.33 ^a	
	5.08 ± 0.02^b		4.37 ± 0.01^c		1.26 ± 0.04^d	
	4.92 ± 0.07^e		4.46 ± 0.06^e		1.31 ± 0.01^e	

^a See ref. 8. ^b See ref. 6. ^c See ref. 5. ^d See ref. 4. ^e See ref. 7.

set of interferograms from one of our experiments; the skewness predicted by theory in the early stages is clearly evident.

Table I summarizes the results quantitatively. The Soret coefficient is computed from $y^*(\eta)$ in every run, and from $\bar{A}^*(\eta)$ in some runs to demonstrate the substantial agreement which exists. In the two silver nitrate measurements, different cell heights were used; the two potassium chloride runs show the consonance between an unmixing and a remixing experiment. The precisions indicated for σ are the probable errors computed from the scatter of points about the best-fitting regression curve.

It can be seen that our data have good internal consistency and agree well with previous determinations reported in the literature. To the extent that small differences do occur, our values tend to be higher. The reason for this is very likely connected with the fact

that the high sensitivity of the instrument enables us to use lower temperature differences across the cell than was customary in most of the older work. As a consequence, parasitic remixing effects are much reduced.

In summary, the shearing interferometer yields a precision which equals or exceeds that of any other optical instrument thus far described in the literature for measuring Soret coefficients. Moreover, it has appealing advantages from the standpoint of convenience. It is very easy to set up and adjust, and since there is no need to provide an external reference beam, as in Rayleigh interferometry, the exacting problems of constructing and using a twin cell are eliminated. Further, the labor involved in analyzing an interferogram, while not insignificant, is much less arduous and time consuming than that required to read out information presented in the form of diffraction patterns, as in Gouy-fringe or image-displacement techniques.

The Formation and Decomposition Reactions of the Acetyl Radical and the Heat of Formation of the Acetyl Radical

by J. Alistair Kerr and Jack G. Calvert

Evans Chemical Laboratory, The Ohio State University, Columbus, Ohio 43210 (Received November 2, 1964)

The 3660-Å. photolyses of azomethane in the presence of either carbon monoxide or acetaldehyde have been investigated, and the formation and decomposition reactions of the acetyl radical have been shown to be dependent on the over-all pressure in the system. The activation energies obtained for the decomposition and formation reactions of the acetyl radical are consistent with recent results of O'Neal and Benson. A combination of the present results and recent independent estimates gives $\Delta H_f^\circ(\text{CH}_3\text{CO}) = -4 \pm 2$ kcal./mole. Results on the reaction (8) $\text{CH}_3 + \text{CH}_3\text{CHO} \rightarrow \text{CH}_4 + \text{CH}_3\text{CO}$ have been obtained from the azomethane-acetaldehyde system and together with three other determinations yield the Arrhenius equation: $k_8 = 10^{11.5} e^{-6.8/RT}$ cc./mole-sec. The approximate rate constant for the reaction (10) $\text{CH}_3 + (\text{CH}_3)_2\text{N}_2 \rightarrow (\text{CH}_3)_2\text{NNCH}_3$ was derived from the data: $k_{10} = 10^{11.7} e^{-7.1/RT}$ cc./mole-sec.

Much discussion has taken place concerning the thermodynamic properties of the acetyl radical determined from kinetic studies. Most recently O'Neal and Benson¹ (O and B) have published results from the 3130-Å. photolysis of acetone in the presence of hydrogen iodide which strongly support the "low" values (11–15 kcal./mole) for the activation energy of the decomposition of the acetyl radical, as opposed to the "high" values (17–20 kcal./mole). In most respects the findings of O and B were in accord with the results of Calvert and Gruver² (C and G) who also directly measured the rate of the radical decomposition from the azomethane-sensitized decomposition of acetaldehyde. One major difference appeared in these studies: O and B observed a pressure dependence of the rate constant for the acetyl decomposition; C and G did not. C and G's data, however, provided no extensive test of the pressure effect on the acetyl radical decomposition.

The heat of formation of the acetyl radical derived by O and B (–6.4 kcal./mole) ultimately depends on the activation energy of the reverse reaction ($\text{CH}_3 + \text{CO} \rightarrow \text{CH}_3\text{CO}$) as determined by C and G. The rate constant for acetyl formation showed no significant variation with a twofold change in the azomethane pressure and a fivefold change in the carbon monoxide

pressure. The limited accuracy of the C and G data, however, leaves uncertain the possible presence of a small pressure effect. Of course, if the findings of O and B are correct, then one would expect a detectable pressure effect for both the acetyl formation and decomposition reactions in the same pressure and temperature region since the same transition state for the two reactions seems probable. Therefore, before the value of the heat of formation of the acetyl radical derived by O and B from their data for the decomposition reaction and C and G data for the formation reaction can be accepted, the effect of pressure on the acetyl formation reaction requires clarification. Also the effect of pressure on the rate of the decomposition of the acetyl radical in the system of C and G requires further investigation. New data which bear on both of these points are given here; also the first direct determination of the rate constant for radical addition to the N=N bond in azomethane has been made.

Experimental

Apparatus and Materials. The photolysis system was similar to that used by C and G which has been

- (1) H. E. O'Neal and S. W. Benson, *J. Chem. Phys.*, **36**, 2196 (1962).
- (2) J. G. Calvert and J. T. Gruver, *J. Am. Chem. Soc.*, **80**, 1313 (1958).

Table I: The Effect of Pressure (M) on the Acetyl Formation Reaction, $\text{CH}_3 + \text{CO} \rightarrow \text{CH}_3\text{CO}$

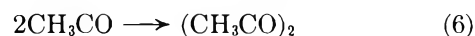
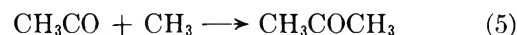
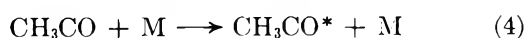
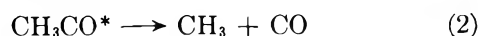
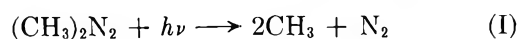
Run no.	Temp., °C.	μmoles/cc.			Rates of formation, moles/cc.-sec. × 10 ¹²					$\frac{R_1^2 \times 10^2}{R_{\text{C}_2\text{H}_6}^{1/2}[\text{CO}]}$
		[Me ₂ N ₂]	[CO]	[Me ₄ C]	R _{C₂H₆}	R _{Me₂CO}	R ₂	R _A	R ₁ '	
M = CO										
12	24.4	1.30	2.64		17.8	0.834	0.051	0.009	0.902	0.081
11	24.4	1.38	4.43		16.2	1.42	0.093	0.027	1.57	0.088
10	23.5	1.27	7.27		14.1	2.36	0.146	0.086	2.68	0.098
36	25.6	1.38	12.4		10.7	3.40	0.286	0.234	4.15	0.103
M = Me ₂ N ₂										
11	24.4	1.38	4.43		16.2	1.42	0.093	0.027	1.57	0.088
37	24.0	3.01	4.88		26.4	1.93	0.090	0.031	2.08	0.083
10	23.5	1.27	7.27		14.1	2.36	0.146	0.086	2.68	0.098
38	27.3	3.09	7.64		22.9	2.92	0.228	0.080	3.31	0.091
M = Me ₄ C										
10	23.5	1.27	7.27		14.1	2.36	0.146	0.086	2.68	0.098
42	26.9	1.44	6.42	1.63	10.8	1.77	0.156	0.063	2.05	0.097
40	23.2	1.31	6.47	3.04	10.0	1.92	0.138	0.080	2.22	0.108
41	26.9	1.35	6.25	4.50	8.56	2.21	0.218	0.123	2.67	0.146

described previously.^{2,3} Azomethane was prepared and purified as described by Renaud and Leitch.⁴ Other materials were obtained as before.²

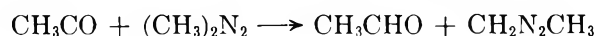
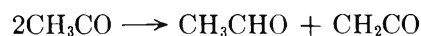
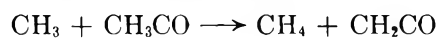
Product Analysis. With the azomethane-acetaldehyde system the products were separated by low-temperature distillation, in the usual way, into two fractions. The first fraction, noncondensable at -150° , consisted of CH_4 , CO , N_2 , and C_2H_6 and was analyzed by gas chromatography³ on a 3.3-m. column (0.63 cm. diameter) packed with 30-60 mesh molecular sieves maintained at 75° . Previously C and G had partially separated this fraction and analyzed by mass spectrometry. The technique employed here is certainly more convenient and undoubtedly more accurate. The second fraction, consisting of $(\text{CH}_3)_2\text{CO}$ plus minor products and unreacted starting materials, was also analyzed by gas chromatography on a column similar to that described before.² The azomethane-carbon monoxide system was analyzed in a similar fashion.

Discussion

The Formation of the Acetyl Radical. When azomethane is photolyzed in a large excess of carbon monoxide, the reactions I and 1-7⁵ are important with regard to the formation of the acetyl radical.



This is essentially the mechanism proposed by C and G, with the addition of reactions 3 and 4 to allow for pressure effects on the radical decomposition. Other possible reactions of the acetyl radicals such as those given below were considered by C and G, who con-



cluded that they were negligible in this system.

Disregarding the pressure effect on the acetyl decomposition reaction for the moment, it can be shown that $k_1/k_7^{1/2} = (R_{(\text{CH}_3)_2\text{CO}} + 2R_{(\text{CH}_3\text{CO})_2} + R_2)/R_{\text{C}_2\text{H}_6}^{1/2}[\text{CO}] = R'/R_{\text{C}_2\text{H}_6}^{1/2}[\text{CO}] = F_1$, where R_x = rate of formation of X and where $R_2 = [R_{(\text{CH}_3)_2\text{CO}}/R_{\text{C}_2\text{H}_6}^{1/2}]k_2k_7^{1/2}/k_5$. Table I lists the various terms in this expression, calculated as before,² and the final rate constant ratios of a series of runs at about the same temperature but with varying pressures of carbon monoxide, azomethane, and added neopentane.⁶ The

(3) J. A. Kerr and J. G. Calvert, *J. Am. Chem. Soc.*, **83**, 3391 (1961).

(4) R. Renaud and L. C. Leitch, *Can. J. Chem.*, **32**, 545 (1954).

(5) M = carbon monoxide, azomethane, or neopentane.

(6) In calculating the values of R_2 , the pressure dependence of $k_2k_7^{1/2}/k_5$ was not taken into account. To simplify the calculations, the experimentally determined value (see later), $2.9 \times 10^{21} \text{e}^{13.78T}$ (mole/cc.-sec.)^{1/2}, was used; since this is a correction within a correction term, the error introduced is not large at the lower temperatures. The result of making the correction is a small increase (a few per cent at most) in the magnitude of the observed pressure effect.

rate function F_1 increases with increasing carbon monoxide or neopentane concentration, but is surprisingly insensitive to changes in azomethane pressure; compare runs 11 and 37, and 10 and 38 in Table I. This observation is in agreement with that found by C and G; it led to their erroneous conclusion that the acetyl formation reaction was in the second-order region, and hence the acetyl decomposition reaction was assumed to be in the first-order region. The reason for the effect seen with azomethane is not clear. It would be extremely surprising if the k_3 for $M = \text{azomethane}$ is significantly lower than that for $M = \text{carbon monoxide or neopentane}$. Possibly the result is related to the addition of acetyl radicals to the azomethane double bond which may begin to contribute measurably at the higher azomethane pressures.⁷ Toby and Weiss⁸ have shown that at temperatures above 50° and pressures above 50 mm. the accepted mechanism of the photolysis of azomethane breaks down and requires an additional source of ethane. It is possible that we are observing a similar effect in this case, which might explain the lack of a pressure trend with increasing azomethane concentration. The other results, however, which were obtained at constant azomethane pressure and varied carbon monoxide and neopentane pressure clearly indicate that the rate constant of the acetyl formation reaction is pressure dependent, as one would expect from O and B's results of the reverse decomposition reaction. It was not possible to extend the pressure studies over a range of temperatures owing to the analytical difficulties of measuring the small amounts of products at the extremes of the temperature range. A more quantitative test of the suggested mechanism for the pressure effect can be made for the acetyl formation reaction using data of Table I. A steady-state treatment of the above complete mechanism leads to the following Hinshelwood-Lindemann type equation

$$\frac{R_{C_2H_6}^{1/2} k_1 [CO]}{k_7^{1/2}} = R_{(CH_3)_2CO} + 2R_{(CH_3CO)_2} + \frac{k_2 k_4 k_7^{1/2} R_{(CH_3)_2CO}}{k_3 k_5 R_{C_2H_6}^{1/2}} + \frac{k_2 [R_{(CH_3)_2CO} + 2R_{(CH_3CO)_2}]}{k_3 [M]}$$

For the data at 25° it can be shown that the fourth term of this expression amounts to only a few per cent of the rates of acetone formation for our conditions, so that the following approximate relation can be used

$$\frac{R_{C_2H_6}^{1/2} [CO]}{[R_{(CH_3)_2CO} + 2R_{(CH_3CO)_2}]} \cong \frac{k_7^{1/2}}{k_1} + \frac{k_2 k_7^{1/2}}{k_1 k_3 [M]} = F_2$$

In Figure 1, function F_2 has been plotted vs. $1/[M]$ for the data at fixed azomethane pressure and varied carbon

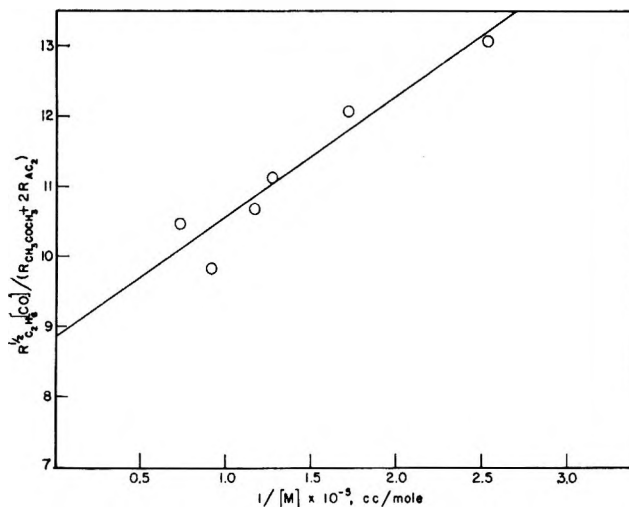


Figure 1. Hinshelwood-Lindemann plot for the formation reaction of the acetyl radical at about 25°.

monoxide and neopentane pressures. In this treatment we have assumed that all of the gaseous molecules act with equal efficiency as M . From the intercept and slope of this plot we obtain estimates of $k_7^{1/2}/k_1 \cong 8.83$ and $k_2 k_7^{1/2}/k_1 k_3 \cong 1.72 \times 10^{-5}$; these values lead to $k_2/k_3 \cong 2.0 \times 10^{-6}$ mole/cc.⁹ We can cross-check this value with a similar estimate derived from the data of the reverse reaction, acetyl decomposition. If one accepts the temperature dependence of $k_4 k_2/k_3$ derived by O and B (15 kcal./mole) and $E_4 = 12$ kcal./mole, then extrapolation of our 65° data (see below) from the reverse reaction to 25° gives $k_2/k_3 \cong 6 \times 10^{-6}$ mole/cc. The agreement is reasonable considering the inaccuracies in the data and the methods of their treatment. It is clear, however, that the data for the acetyl formation reaction are internally consistent and confirm the pressure effects observed for the decomposition reaction by O and B.

(7) In view of the rate constant for the addition of methyl radicals to azomethane derived in this work, one would expect the addition of acetyl radicals to azomethane to be relatively unimportant at 25° and at the usual pressures of azomethane used in this study. If one assumes that the rate constant for acetyl radical addition to azomethane is equal to that found here for methyl addition, the rates of addition for the conditions of runs 11 and 37 of Table I (at $[\text{Me}_2\text{N}_2] = 1.38$ and 3.01 mmoles/cc., respectively) are 0.12×10^{-12} and 0.27×10^{-12} mole/cc.-sec., respectively. It is not likely that the rates are this large, but it is possible that the observed effect is related to the occurrence of this reaction; that is, the increased rate of the formation reaction with increased $[\text{Me}_2\text{N}_2]$ might be obscured by the increase in rate of addition of acetyl to the azomethane at the higher concentration of azomethane

(8) S. Toby and B. H. Weiss, *J. Phys. Chem.*, **66**, 2681 (1962).

(9) The data for the highest pressure of neopentane were omitted in the treatment given here as they were considered less accurate than the other data. If one includes this point, the conclusions are not altered but the estimate of k_2/k_3 is raised from 2.0×10^{-6} to 3.3×10^{-6} mole/cc.

Table II: Temperature Coefficient for the Acetyl Formation Reaction at Constant Pressure

Run no.	Temp., °C.	μmoles/cc.		Rates of formation, moles/cc.-sec. × 10 ¹²				$R_1' \times 10^3$	
		[Me ₂ N ₂]	[CO]	R _{C₂H₆}	R _{Me₂CO}	R ₂	R _{Ac₂}	R _{1'}	R _{C₂H₆} ^{1/2} [CO]
53	0.0	1.19	7.07	12.3	1.45	0.019	0.037	1.54	0.062
54	0.0	1.22	6.93	10.6	1.29	0.019	0.034	1.38	0.061
55	0.0	1.13	7.34	13.4	1.60	0.019	0.042	1.70	0.063
10	23.5	1.27	7.27	14.1	2.36	0.244	0.086	2.78	0.102
50	23.8	1.47	6.94	12.8	1.94	0.211	0.064	2.28	0.092
48	33.3	1.39	6.92	9.93	1.77	0.480	0.086	2.39	0.110
46	34.1	1.40	7.59	10.3	2.17	0.616	0.099	2.99	0.123
43	37.4	1.32	5.19	10.7	1.52	0.535	0.046	2.15	0.126
47	48.0	1.35	7.45	8.31	1.77	1.44	0.082	2.37	0.157
49	55.1	1.34	6.58	8.26	1.60	2.17	0.067	3.90	0.207
45	58.1	1.26	6.45	8.27	1.50	2.45	0.059	4.07	0.220
63	62.0	1.30	6.41	9.34	1.67	3.29	0.065	5.07	0.259

To compare the results with those of C and G, the temperature coefficient of the formation reaction was measured at nearly constant pressure. The results are listed in Table II and shown in an Arrhenius plot in Figure 2. The rate constants obtained here at constant pressure are about three times as high as those obtained by C and G over a range of pressures. There is no apparent explanation of this difference, but our results are to be preferred since the analytical techniques were more refined and the data more reproducible. A least-squares calculation of the results in Table II yields the equation

$$k_1/k_7^{1/2} \cong 81.3e^{-3.9/RT} \text{ (cc./mole-sec.)}^{1/2}$$

The activation energy is in good agreement with that of C and G (3.8 kcal./mole). However, these values of E_1 do not correspond to the limiting pressure value which is required for thermochemical calculations. To make allowance for this, about 1 kcal./mole should be added to these estimates, so that $E_{1\infty} \cong 5$ kcal./mole.

The Decomposition of the Acetyl Radical. The mechanism of the selective photolysis of azomethane in a mixture with acetaldehyde was studied by C and G.² In our considerations here we will accept their mechanism again with the addition of reactions 3 and 4 to allow for pressure effects on the radical decomposition and formation reactions. If one neglects the effect

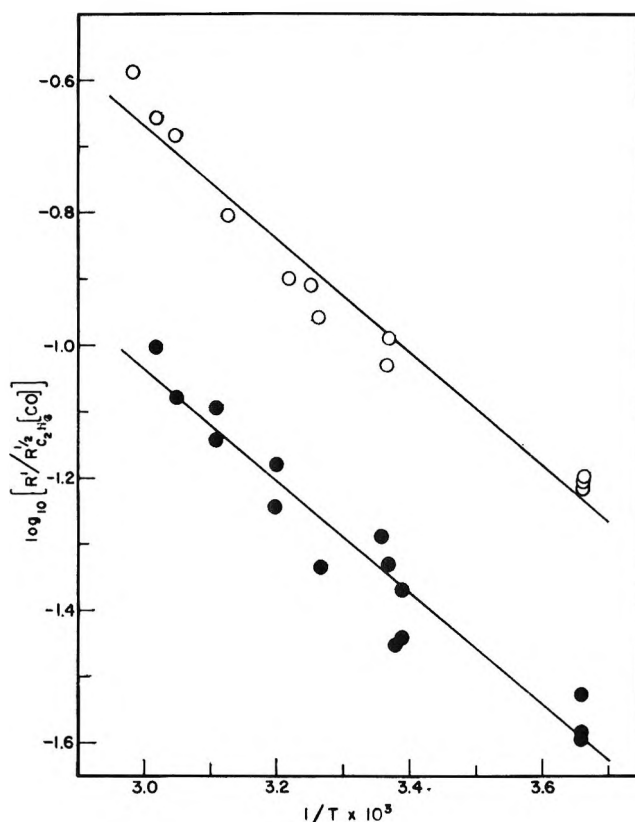
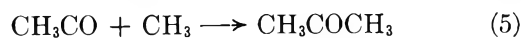
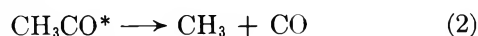
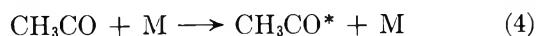
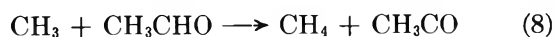


Figure 2. Arrhenius plot of the rate function $F_1 = k_1/k_7^{1/2}$; data were obtained from the photolysis of azomethane in the presence of carbon monoxide; open circles, this work, $[M] \cong 8.2$ μmoles/cc.; darkened circles, data of C and G,² $[M] \cong 2.6$ – 16.8 μmoles/cc.

of pressure for the moment, a rate expression (F_3) involving the rate constant for the acetyl radical decomposition is readily obtained. To study the effect of

$$\frac{k_2 k_7^{1/2}}{k_5} = \frac{R_{\text{CO}} R_{\text{C}_2\text{H}_6}^{1/2}}{R_{(\text{CH}_3)\text{CO}}} = F_3$$

Table III: The Effect of Pressure (M) on the Decomposition of the Acetyl Radical

Run no.	Temp., °C.	μmoles/cc.			Rates of formation, moles/cc.-sec. × 10 ¹²						$R_{CO}R_{C_2H_6}^{1/2} \times 10^6$
		[Me ₂ N ₂]	[AcH]	[Me ₄ C]	R_{N_2}	R_{CH_4}	R_{CO}	$R_{C_2H_6}$	R_{MeCO}	$R_{Me_2N_2HMe}$	R_{Me_2CO}
M = Me ₂ N ₂ and AcH											
23	63.9	1.09	1.05		9.16	7.08	1.52	4.52	0.910		0.355
22	63.2	1.97	1.47		15.8	12.6	2.29	7.31	1.18	4.63	0.525
24	66.6	2.93	1.82		22.2	18.9	3.09	8.53	1.29	6.49	0.700
M = Me ₄ C											
23	63.9	1.09	1.05		9.16	7.08	1.52	4.52	0.910		0.355
25	67.0	1.03	1.03	1.44	9.57	6.79	1.35	5.20	0.598		0.513
27	63.4	1.05	1.11	3.17	9.00	6.01	1.43	5.23	0.483		0.677

pressure on this function a series of runs was carried out at approximately 65° with varying reactant pressures and added neopentane. The results are shown in Table III. It is obvious that F_3 increases with pressure, and it is likely that this reflects the effect of M on reactions 3 and 4. From a steady-state treatment of the above total reaction scheme the following relation is found where [M] = total concentration in the

$$\frac{R_{(CH_3)_2CO}}{R_{CO}R_{C_2H_6}^{1/2}} = \frac{k_3k_5}{k_4k_2k_7^{1/2}} + \frac{k_5}{k_4k_7^{1/2}} \frac{1}{[M]}$$

system. Thus when $R_{(CH_3)_2CO}/R_{CO}R_{C_2H_6}^{1/2}$ is plotted against $1/[M]$, as in Figure 3, there is a linear relationship with the intercept equal to $k_3k_5/k_4k_2k_7^{1/2}$ and slope equal to $k_5/k_4k_7^{1/2}$. The high-pressure limiting rate constant, $k_4k_2/k_3 = k_\infty$ can be obtained from the intercept and the low-pressure limiting rate constant, $k_4 = k_0$, from the slope assuming that $k_5 = k_7 = 2.2 \times 10^{13}$ cc./mole-sec.¹⁰ The values calculated from Figure 3 for data at about 65° are $k_\infty \cong 94$ sec.⁻¹ and $k_0 \cong 9.4 \times 10^6$ cc./mole-sec. These estimates may be compared with data of the previous workers by extrapolation of the O and B data¹ obtained at higher temperatures and that calculated by O and B from the 25° acetone photolysis data of Herr and Noyes,¹¹ and Howland and Noyes,¹² extrapolated to 65° using the temperature coefficients of O and B. The values derived from the respective previous studies are: $k_\infty = 4, 50,$ and 260 sec.⁻¹; $k_0 = 4.5 \times 10^6, 8.5 \times 10^6,$ and 6.2×10^6 cc./mole-sec. The agreement of our estimates with those derived from other systems is satisfactory, considering the approximate nature of the data and the theory and the very limited range of pressure available in our experiments. Certainly the pressure effect on the acetyl radical decomposition reaction as observed by O and B is confirmed by these results. The sensitivity of the rate constant function F_3 to pressure change is much greater in these data for 65° experiments than that found for the acetyl forma-

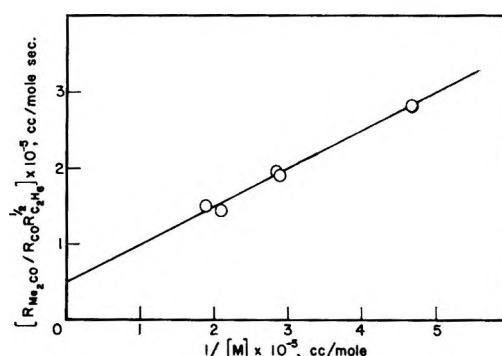


Figure 3. Hinshelwood-Lindemann plot for the decomposition of the acetyl radical at about 65°.

tion function F_1 at the lower temperatures. This is expected in theory since the middle of the pressure falloff region for the acetyl decomposition and formation reactions is expected to be only ~7 mm. at 25°.¹

A series of runs, summarized in Table IV, was made at approximately constant pressure over a range of temperatures to check the activation energy obtained by C and G. An Arrhenius plot is shown in Figure 4, where our results are compared with those of C and G and with the results from the 3130-Å. photolysis of acetone derived by Heicklen¹³ and Ausloos and Borkowski.¹⁴ Unfortunately, the results of O and B cannot be compared in this way. The rate constants from the different systems are in general agreement but the

(10) A. Shepp, *J. Chem. Phys.*, **24**, 939 (1956).

(11) D. S. Herr and W. A. Noyes, Jr., *J. Am. Chem. Soc.*, **62**, 2052 (1940).

(12) J. J. Howland and W. A. Noyes, Jr., *ibid.*, **66**, 974 (1944); **63**, 3404 (1941).

(13) J. Heicklen, Ph.D. Thesis, University of Rochester, Rochester, N. Y., 1959.

(14) Private communication from P. Ausloos, National Bureau of Standards; the dotted line represents the least-square line of many runs utilizing both CH₃COCH₃ and CD₃COCD₃ photolyses; these results are only preliminary ones which were given to the authors before completion of the detailed study which is continuing.

Table IV: Temperature Coefficient for the Acetyl Decomposition Reaction at Constant Pressure

Run no.	Temp., °C.	μmoles/cc.		Rates of formation, moles/cc.-sec. × 10 ¹²						R _{CO} R _{C₂H₆} ^{1/2} × 10 ⁵	
		[Me ₂ N ₂]	[AcH]	R _{N₂}	R _{CH₄}	R _{CO}	R _{C₂H₆}	R _{Me₂CO}	R _{Me₂N₂HMe}	R _{Me₂CO}	
31	42.0	2.05	1.30	15.0	7.38	0.433	10.9	1.12		0.161	
32	56.9	1.90	1.30	15.4	9.21	1.07	8.97	0.959		0.334	
22	63.2	1.97	1.47	15.8	12.6	2.29	7.31	1.18		0.525	
21	81.6	2.01	1.30	16.6	16.4	5.00	5.52	1.09	7.80	1.08	
29	100.8	1.96	1.40	17.1	20.7	7.92	4.03	0.516	11.4	3.08	
28	116.7	1.98	1.36	17.4	26.1	11.6	3.25	0.492	13.3	4.29	
33	121.4	2.07	1.42	17.6	26.1	15.6	3.28	0.457		6.18	

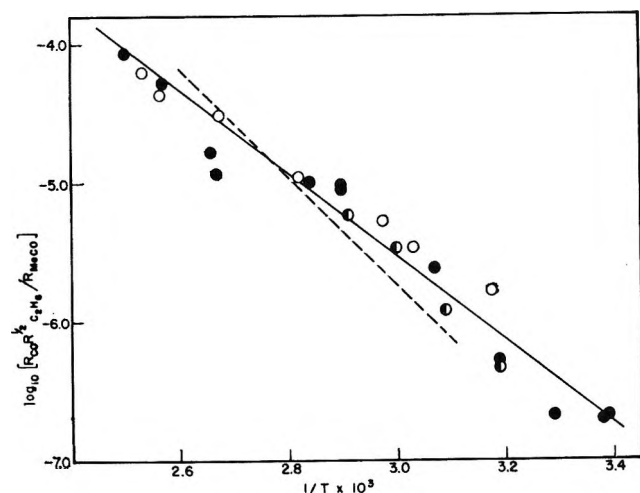


Figure 4. Arrhenius plot of the rate function $F_2 = k_2k_7^{1/2}/k_5$, obtained from the photolysis of azomethane in the presence of acetaldehyde, and compared with other results: open circles, our data; darkened circles, data of C and G²; half-darkened circles, data of Heicklen¹³; these three studies were carried out with $[M] \cong 3.4$ μmoles/cc.; the dotted line represents an average of data obtaining from a continuing study by Ausloos and Borkowski¹⁴; $[M] \cong 1.4$ μmoles/cc.

individual activation energies are not. The best line through all the points yields the Arrhenius equation $k_2k_7^{1/2}/k_5 = 2.9 \times 10^3 e^{-13.5/RT}$ (moles/cc.-sec.)^{1/2}. This is also compatible with the results of O and B. Under the circumstances the Arrhenius parameters of O and B are to be preferred since they have made the only comprehensive study of the pressure effect on the rate constant for the acetyl decomposition. Hence the high-pressure limiting activation energy of the decomposition is taken as 15 kcal./mole in subsequent thermochemical calculations in this paper.

The Heat of Formation of the Acetyl Radical. The heat of dissociation of the acetyl radical, $D_{\text{CH}_3-\text{CO}}$, is readily calculated from the high pressure activation energies of the acetyl decomposition reaction (15 kcal./mole, O and B) and the acetyl formation reaction (revised value 5 kcal./mole, estimated in this work).

Thus, allowing for difference in standard states, $D_{\text{CH}_3-\text{CO}} \cong 10.6$ kcal./mole, and taking $\Delta H_f^\circ(\text{CO}) = 26.4$ and $\Delta H_f^\circ(\text{CH}_3) = 33.9$ kcal./mole,¹⁵ we deduce $\Delta H_f^\circ(\text{CH}_3\text{CO}) = -3.1$ kcal./mole. O and B favored a lower value of $\Delta H_f^\circ(\text{CH}_3)$ of 32.0 kcal./mole, which in conjunction with the previous value of E_1 derived by C and G led to the result $\Delta H_f^\circ(\text{CH}_3\text{CO}) = -6.3$ kcal./mole. Our value $\Delta H_f^\circ(\text{CH}_3\text{CO}) = -3.1$ kcal./mole is in satisfactory agreement with two other recent determinations. O'Neal and Benson¹⁶ have also determined $\Delta H_f^\circ(\text{CH}_3\text{CO}) = -6.4$ kcal./mole from a kinetic study of the reactions of acetyl iodide with hydrogen iodide. Murad and Inghram¹⁷ have found $\Delta H_f^\circ(\text{CH}_3\text{CO}) = -6.5$ kcal./mole from photoionization mass spectrometric studies of acetyl compounds. In view of the evidence at hand, we favor a value of $\Delta H_f^\circ(\text{CH}_3\text{CO}) = -4 \pm 2$ kcal./mole. Using this estimate, $D_{\text{CH}_3\text{CO}-\text{CH}_3} \cong 79$ kcal./mole. Pyrolyses of acetone by the toluene-carrier technique^{18,19} have yielded much lower values (about 72 kcal./mole). It should be noted, however, that many of the early results by the technique have recently been shown to be inaccurate when repeated by an aniline-carrier technique.²⁰ Furthermore, pyrolyses of diethyl, di-*n*-propyl, and diisopropyl ketones by the toluene-carrier technique have been found to be extremely complex processes from which $D_{\text{C}-\text{CO}}$ values could not be obtained.²¹ A redetermination of the decomposition of acetone by the aniline-carrier technique might help to resolve this difficulty.

(15) G. C. Fettis and A. F. Trotman-Dickenson, *J. Chem. Soc.*, 3037 (1961).

(16) H. E. O'Neal and S. W. Benson, *J. Chem. Phys.*, **37**, 540 (1962).

(17) E. Murad and M. G. Inghram, *ibid.*, **41**, 404 (1964); the authors are grateful to Dr. Murad for a copy of the manuscript prior to publication.

(18) D. Clark and H. O. Pritchard, *J. Chem. Soc.*, 2136 (1956).

(19) M. Szwarc and J. W. Taylor, *J. Chem. Phys.*, **23**, 2310 (1955).

(20) G. Esteban, J. A. Kerr, and A. F. Trotman-Dickenson, *J. Chem. Soc.*, 3873 (1963).

(21) G. Esteban, J. A. Kerr, and A. F. Trotman-Dickenson, unpublished results.

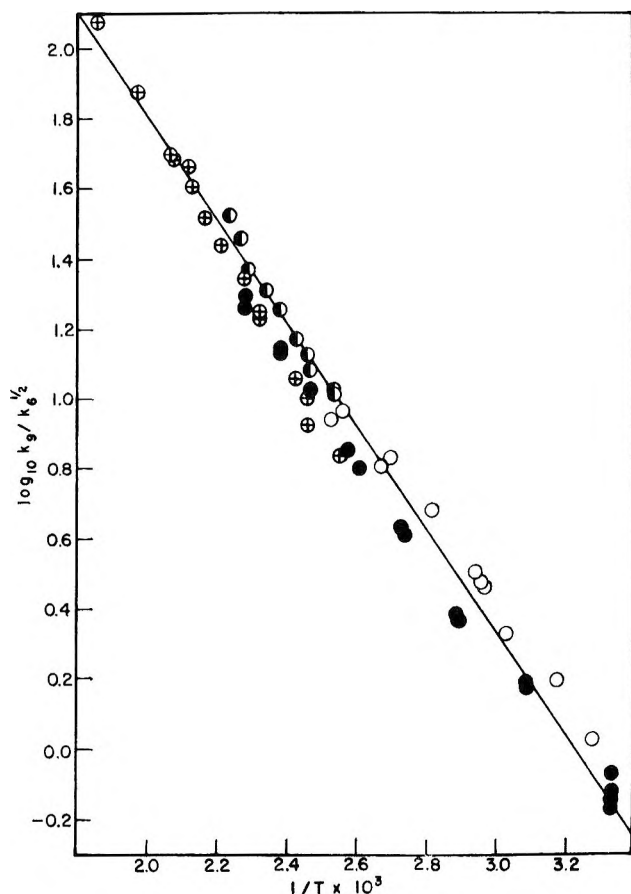
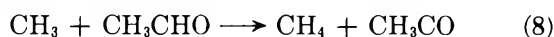


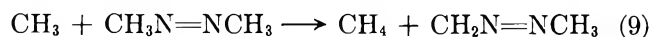
Figure 5. Arrhenius plot of the rate function $k_8/k_7^{1/2}$; data from the photolysis of azomethane in the presence of acetaldehyde in this work, open circles; Ausloos and Steacie,²³ darkened circles; Dodd,²⁴ circles with plus sign; Birrell and Trotman-Dickenson,²⁴ half-darkened circles.

The consistency of the ratio of the A factors for the acetyl decomposition and formation reactions with that expected theoretically from the calculated entropy change for the reaction, and the low absolute values of these A factors have been adequately discussed by previous workers.^{1,2} The results presented here do not alter what has already been said in this regard.

The Reactions of Methyl Radicals with Acetaldehyde. From the results in Tables III and IV, rate constants can be derived for reaction 8. Allowance must be



made for the attack of methyl radicals on azomethane (reaction 9). From the photolysis of azomethane



alone,²² $k_9/k_7^{1/2} \cong 6.6 \times 10^3 e^{-7.3/RT}$ (cc./mole-sec.)^{1/2}, and hence values of $k_8/k_7^{1/2}$ were calculated from $R_{\text{CH}_4(8)}/R_{\text{C}_2\text{H}_6}^{1/2}[\text{CH}_3\text{CHO}]$ where $R_{\text{CH}_4(8)}$ equals

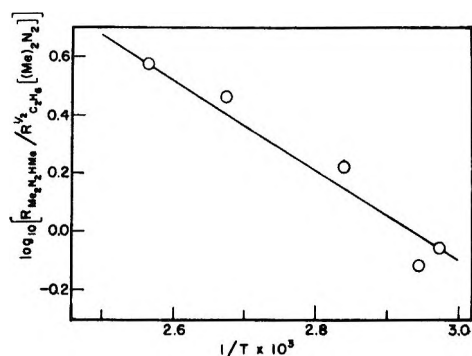
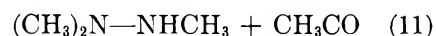
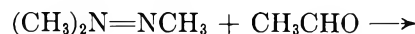
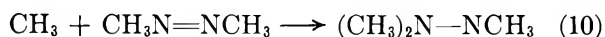


Figure 6. Arrhenius plot of the rate function $k_{10}/k_7^{1/2}$; data obtained from the photolysis of azomethane in the presence of acetaldehyde.

the rate of formation of methane from reaction 8. Previous results²³⁻²⁵ and our values for this rate ratio are plotted in Figure 5. The general agreement with our results lends support to the validity of the other results presented here. The best line through all the points in Figure 5 corresponds to the equation $k_8/k_7^{1/2} \cong 6.31 \times 10^4 e^{-6.8/RT}$ (cc./mole-sec.)^{1/2} and, assuming $k_7 = 2.2 \times 10^{13}$ cc./mole-sec., this gives $k_8 \cong 3.16 \times 10^{11} e^{-6.8/RT}$ cc./mole-sec.

The Addition of Methyl Radicals to Azomethane. In a few of the runs with the acetaldehyde-azomethane system it was possible to determine the trimethylhydrazine product, presumably formed in reactions 10 and 11. Trimethylhydrazine appeared as a very



broad peak after the elution of the acetone in the analysis of the second fraction and therefore could not be measured with great precision. There were also traces of tetramethylhydrazine which could not be measured at all.²⁶ The rates of formation of trimethylhydrazine (see Tables III and IV) can be used to obtain approximate rate constants for the addition of methyl radicals to azomethane (reaction 10) on the assumption that most of the $(\text{CH}_3)_3\text{N}_2$ radicals react to form trimethylhydrazine by reaction 11. The small amounts of tetramethylhydrazine produced

(22) P. Ausloos and E. W. R. Steacie, *Can. J. Chem.*, **32**, 593 (1954).

(23) P. Ausloos and E. W. R. Steacie, *ibid.*, **33**, 31 (1955).

(24) R. E. Dodd, *ibid.*, **33**, 699 (1955).

(25) R. N. Birrell and A. F. Trotman-Dickenson, *J. Chem. Soc.*, 2059 (1960).

(26) The authors are indebted to Dr. Trudy Enzer Smith (Connecticut College, New London, Conn.), who supplied samples of trimethyl- and tetramethylhydrazine which were used as standards in this work.

support this assumption; it is also consistent with the finding of Kerr and Trotman-Dickenson,²⁷ who have shown that alkyl radicals produced by the photolysis of an aldehyde in the presence of olefins yield predominantly alkanes from the addition of the initial radical to the olefin followed by abstraction of a hydrogen atom from the aldehyde by the ensuing radical. Values of $k_{10}/k_7^{1/2}$ were calculated from the expression, $k_{10}/k_7^{1/2} \cong R_{\text{Me}_2\text{N}_2\text{HMe}}/R_{\text{C}_7\text{H}_6}^{1/2}[(\text{CH}_3)_2\text{N}_2]$, and are shown in the Arrhenius plot in Figure 6; these data give $k_{10}/k_7^{1/2} \cong 3.6 \times 10^4 e^{-7.1/RT}$ (cc./mole-sec.)^{1/2}. Taking $k_7 = 2.2 \times 10^{13}$ cc./mole-sec., this yields $k_{10} \cong 1.8 \times 10^{11} e^{-7.1/RT}$ cc./mole-sec. The activation energy here determined directly for reaction 10, $E_{10} \cong 7.1$ kcal./mole, checks reasonably well with that estimated by

Jones and Steacie²⁸ using a mass balance technique without direct analysis; they estimate $E_{10} \cong 6.4$ kcal./mole. Apparently methyl radicals add to the N=N bond in azomethane at about the same rate as they add to a C=C bond in olefins.²⁹

Acknowledgment. The authors are grateful for the support given to this work by a grant from the Division of Air Pollution, Bureau of State Services, U. S. Public Health Service.

(27) J. A. Kerr and A. F. Trotman-Dickenson, *Trans. Faraday Soc.*, **55**, 572 (1960).

(28) M. H. Jones and E. W. R. Steacie, *J. Chem. Phys.*, **21**, 1018 (1953).

(29) J. A. Kerr and A. F. Trotman-Dickenson, *Progr. Reaction Kinetics*, **119** (1961).

C^{13} Magnetic Resonance Study of the Protonation of Acetic and Benzoic Acids and Their Ethyl Esters in Concentrated Sulfuric Acid

by Gary E. Maciel and Daniel D. Traficante

The Department of Chemistry, University of California, Davis, California, and the Frank J. Seiler Research Laboratory, O.A.R., U. S. Air Force Academy, Colorado (Received November 7, 1964)

C^{13} magnetic resonance spectra were obtained for solutions of acetic and benzoic acids and their ethyl esters in 97% sulfuric acid and in fuming (101%) sulfuric acid before and after a 5-hr. heating period at 50°. Comparison of the shifts obtained for the carbonyl group in these solvents with those obtained when phenol, acetone, and acetophenone are dissolved in sulfuric acid leads to the conclusion that the $R-\overset{+}{C}OH-OH$ ion is formed when the carboxylic acids are placed in 97% or fuming sulfuric acid or when their ethyl esters are heated in fuming sulfuric acid for 5 hr. at 50°, and that the $R-\overset{+}{C}OH-OC_2H_5$ species are formed when the esters are placed in 97% sulfuric acid at room temperature.

Several studies have been concerned with the protonation of carboxylic acids and their derivatives in strongly acidic media.¹⁻⁸ In such solutions a carboxylic acid or its derivative, both represented by $R-CO-X$ (I) where X may be OH, OR', NR'R'', etc., may exist as any one or more of the following species: the carbonyl protonated cation $R-\overset{+}{C}OH-X$ (II), the X-protonated cation $R-CO-\overset{+}{X}H$ (III), the "acylium ion" $R\overset{+}{C}O$ (IV), or possibly some other species. Several experimental methods including cryoscopy, the most commonly employed, and proton magnetic resonance spectroscopy have been applied to this problem, and the evidence seems to favor structures II and IV, depending on the nature of the carboxylic acid and the medium. In view of recent results on the effect of hydrogen-bonding and/or proton-donating solvents in the C^{13} chemical shift of the carbonyl carbon in acetone⁹ and other ketones and esters,¹⁰ we have attempted to apply C^{13} magnetic resonance spectroscopy to this question of the nature of carboxylic species in strongly acid media. Our results on acetic and benzoic acids and their ethyl esters are in accord with previous interpretations in terms of carbonyl protonation and provide another example of the usefulness of C^{13} methods in studying chemical problems.

Experimental


Materials. The 97% sulfuric acid was reagent grade from DuPont; its density at 21° was 1.8360. The fuming sulfuric acid (101.1%) was a mixture of the 97% material and Baker reagent grade 30-33% fuming sulfuric acid. The phenol, glacial acetic acid, and ethyl acetate were Baker reagent grade materials and the benzoic acid, ethyl benzoate, and acetophenone were Eastman White Label reagents. The acetone was Eastman Spectrograde.

C^{13} Magnetic Resonance Measurements. The carbon-13 n.m.r. spectra were obtained at a frequency of 15.085 Mc./sec. by measuring C^{13} resonances in natural

- (1) N. C. Deno, C. V. Pittman, and M. J. Wisotsky, *J. Am. Chem. Soc.*, **86**, 4370 (1964).
- (2) R. Stewart and K. Yates, *ibid.*, **82**, 4059 (1960).
- (3) A. Bradley and M. E. Hill, *ibid.*, **77**, 1575 (1955).
- (4) M. S. Newman, R. A. Craig, and A. B. Garrett, *ibid.*, **71**, 869 (1949).
- (5) M. S. Newman, *ibid.*, **63**, 2431 (1941).
- (6) M. S. Newman, H. G. Kuivila, and A. B. Garrett, *ibid.*, **67**, 704 (1945).
- (7) H. P. Treffers and L. P. Hammett, *ibid.*, **59**, 1709 (1937).
- (8) G. Fraenkel, *J. Chem. Phys.*, **39**, 1466 (1961).
- (9) G. E. Maciel and G. C. Ruben, *J. Am. Chem. Soc.*, **85**, 3903 (1963).
- (10) G. E. Maciel and J. J. Natterstad, *J. Chem. Phys.*, in press.

abundance, using dispersion mode and rapid passage conditions as described previously by Lauterbur.¹¹ The sample container was similar to that described by Spiesscke and Schneider¹² except that no provision was made for spinning the sample. It consisted of two concentric, thin-walled spherical bulbs about 0.1 and 1.6 ml. in volume, a geometry which eliminates the need for bulk susceptibility corrections in these results. The small inner bulb contained a reference consisting of a mixture of equal parts of $C^{13}H_3CO_2H$ and $CH_3C^{13}O_2H$, with C^{13} enrichment of about 56%. In a calibration spectrum of benzene in this cell, the carbonyl resonance was found to be -48.8 p.p.m. with respect to the benzene doublet center, and the separation between the former and the center of the methyl quartet was determined to be 156.3 p.p.m. The latter separation was used to calibrate the charts, and the former shift was used to convert the raw data to shifts with respect to benzene. Each shift is the result of at least five field scans in both increasing and decreasing senses and the data of Table I may be considered reliable to about ± 0.4 p.p.m.

Table I: Carbon-13 Chemical Shifts, p.p.m. w.r.t. Benzene

Compd.	State			
	Neat	Solution ^a in 97% H ₂ SO ₄	Solution ^a in fuming H ₂ SO ₄	Solution ^a in fuming H ₂ SO ₄ after 5 hr. at 50°
$CH_3C^{13}O_2H$	-49.3^b	-64.3	-64.9	-65.0
$CH_3C^{13}O_2C_2H_5$	-41.8^c	-62.3	$-62.4 \rightarrow -64.7^d$	-65.0
$C_6H_5C^{13}O_2H$	-44.7^b	-52.7	-53.3	-53.3
$C_6H_5C^{13}O_2C_2H_5$	-36.1^b	-51.1	-53.0	-53.1
 $C^{13}-OH$	-27.0^e	-31.1		
$CH_3C^{13}OCH_3$	-76.6^c	-115.8	-116.8	
$CH_3C^{13}OC_2H_5$	-68.1^b	-91.0	-91.5	

^a 1:6 mole ratio of solute-H₂SO₄. ^b See ref. 14. ^c See ref. 10. ^d Spectrum changed with time; the indicated change occurred over about 2 hr. ^e Estimated from data of ref. 15.

Results and Discussion

Table I contains the pertinent C^{13} chemical shifts obtained in this study and from previous reports. In none of the solutions studied was more than one peak reliably observed which could be traced to a carbonyl origin. Thus, as far as the technique is capable of discerning, only one carbonyl species was present in each solution. Table I shows that dissolving the carboxylic acids in concentrated sulfuric acid causes downfield shifts of the "carbonyl" resonances about 9 p.p.m. in the case of benzoic acid and about 16 p.p.m. in the case of acetic acid, neglecting, temporarily,

the small differences observed between shifts in the two sulfuric acid concentrations. These downfield shifts represent the effect of changing the nature of the "carbonyl group" to that in sulfuric acid solution from that in a hydrogen-bonded complex, not from that of an isolated carboxyl group. Thus, the shifts reported in the first row of Table I for acetic and benzoic acid already include a downfield shift of about 7 p.p.m.^{9,10,13,14} due to hydrogen bonding, based on analogy with hydrogen-bonding studies of similarly constituted ketones and esters. If we wish to consider the effect of sulfuric acid on the individual carboxylic acid molecules, the sulfuric acid effects should be calculated with respect to the chemical shifts one would estimate for the non-hydrogen-bonded acid molecules, about -42 and -38 p.p.m., respectively, for acetic and benzoic acids. Thus, the sulfuric acid effects can be considered more appropriately to be about -23 and -16 p.p.m., about the same effects observed upon dissolving the corresponding esters, ethyl acetate and ethyl benzoate, in concentrated sulfuric acid.

In order to understand the origin of these downfield shifts, particularly with regard to elucidating the particular species in solution, it is useful to consider some model systems. As an indication of the magnitude of the downfield shift to be expected to accompany protonation of the carbonyl group to form II, we take the 39 and 23 p.p.m. shifts to lower field observed when acetone and acetophenone, respectively, are dissolved in concentrated sulfuric acid. Short of complicating condensations and enol formation this can only lead to species of the type II. To estimate the effect on the position of the carbonyl carbon resonance line expected with protonation of the hydroxy or ethoxy oxygen atoms to form III, we consider the effect of a sulfuric acid medium on the C^{13} shift of the substituted carbon atom of phenol. This atom is also hybridized in the sp^2 manner and is attached to a hydroxyl oxygen atom which most likely becomes protonated in sulfuric acid solution, forming a cation of the type $\text{>C}-\overset{+}{O}H_2$ which is formally similar to III. Table I shows that this effect results in a downfield displacement of the C^{13} resonance of only 4 p.p.m.; a nearly negligible effect has been observed on the C^{13} spectra of aliphatic ethers.¹⁵ These "sulfuric acid shifts"

(11) P. C. Lauterbur, *J. Am. Chem. Soc.*, **83**, 1838 (1961).

(12) H. Spiesscke and W. G. Schneider, *J. Chem. Phys.*, **35**, 722 (1961).

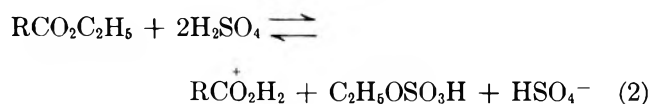
(13) G. E. Maciel and G. B. Savitsky, *J. Phys. Chem.*, **68**, 437 (1964).

(14) J. B. Stothers and P. C. Lauterbur, *Can. J. Chem.*, **42**, 1563 (1964).

are much smaller than the 16 to 23 p.p.m. shifts to lower field which are observed when the carboxylic compounds of this study are dissolved in concentrated sulfuric acid. Thus, we can conclude from C^{13} magnetic resonance data that species represented by formula III are not significantly important in the solutions used in this study and that species II are indicated. This is in agreement with the very recent results of Deno and co-workers,¹ who concluded from proton n.m.r. and ultraviolet measurements that $CH_3CO_2H_2^+$ is the principal species present in sulfuric acid solutions over a concentration range of about 90 to 110% H_2SO_4 (10% H_2O to 10% SO_3).

Closer inspection of Table I reveals small but significant differences between the C^{13} shifts obtained in 97% sulfuric acid and in fuming (101%) sulfuric acid. For ethyl acetate and ethyl benzoate these differences are 2.7 and 2.0 p.p.m., respectively. On the basis of previous chemical evidence we interpret them as the differences between the C^{13} chemical shifts of $RCO_2^+H_2$

(II with $X = OH$) and $RCOH-OC_2H_5$ (II with $X = OC_2H_5$), the carbonyl-protonated acids and esters. Newman and co-workers⁴ and Bradley and Hill³ have reported different cryoscopic properties for ethyl acetate and benzoate in 100% sulfuric acid solutions at different temperatures. Thus, at 25° the Van't Hoff i factor¹⁶ for ethyl benzoate changes from an initial value of 1.9 to a final value of 3.0 after one day, whereas at 50° this steady value is reached in only 3 hr. Similarly, the i factor of ethyl acetate was reported to change from an initial value of 1.9 to a value of 2.7 after 7 hr. at 25°, while at 50° this value was attained after only 1 hr.³ These observations were interpreted as indicating that at 25° the main process of interest is the simple protonation represented by eq. 1, while at 50° the equilibrium of eq. 2 becomes



sufficiently rapid to come into play. This interpretation was further indicated by the facts that no benzoic acid could be obtained by pouring into water a solution of ethyl benzoate in 100% sulfuric acid maintained at 25° for 1 hr.,³ whereas a 29% yield could be obtained after only 20 min. at 50°, and a 75% yield after 5 hr. at 50°. Similar results were found by Newman, Craig, and Garrett for methyl benzoate at 45°.⁴

Thus, we attribute the -51.1 p.p.m. chemical shift observed in a freshly prepared, room-temperature solu-

tion of ethyl benzoate in 97% sulfuric acid to the protonated carbonyl species II with $X = OC_2H_5$. The protonation shift is -15 compared with -23 p.p.m. in the case of acetophenone. Its smaller magnitude is consistent with the relatively greater sensitivity of ketones than esters to hydrogen-bond shifts of the carbonyl carbon resonance¹⁰ and is probably associated with the greater basicity of the ketones and the inductive effect of the ethoxy group to reduce the polarity of the carbonyl bond even more in sulfuric acid solution than in the unprotonated state.

The remaining shifts in Table I for the case of $R = C_6H_5$ are the same within experimental error. This

indicates that $C_6H_5CO_2H_2$ (II with $X = OH$) is the principal species present in a freshly prepared, room-temperature solution of ethyl benzoate in fuming (101%) sulfuric acid before as well as after the 5-hr. heating period, and in each of the three sulfuric acid solutions of benzoic acid studied. The 0.6 p.p.m. difference in chemical shift between the benzoic acid solutions in 97% and fuming (101%) sulfuric acid is outside the experimental uncertainties, and is ascribed to a medium effect on the chemical shift of the C_6H_5-

$COH-OH$ ion. In 97% sulfuric acid, the high concentration of bisulfate ions in solution and the absence of excess SO_3 may lead to differences in specific solvation of the $RCOH-OH$ ions compared to the $H_2SO_4-SO_3$ environment in 101% H_2SO_4 , leading to differences in solvent perturbation of the electronic configuration of the ion large enough to cause a detectable medium effect. As a crude check on the magnitude of such an effect we determined the C^{13} shifts of acetone and acetophenone in both sulfuric acid solvents and found differences of 1.0 and 0.5 p.p.m., respectively.

The data for acetic acid and its ethyl ester appear to be in direct correspondence with that for benzoic acid and ethyl benzoate. Thus, the C^{13} chemical shifts for acetic acid in each of the three solutions and of ethyl acetate in the fuming sulfuric acid solution resulting after a 5-hr. heating period at 50° are the same within experimental error, 64.7 ± 0.4 p.p.m. The species indicated in all these solutions is $CH_3COH-OH$.

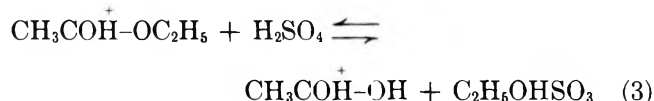
The "carbonyl" shift of ethyl acetate in 97% sulfuric acid at room temperature differs from this by 2.4 p.p.m. and is assigned to $CH_3COH-OC_2H_5$. Again, an apparent medium effect of 0.6 p.p.m. on the assumed

(15) G. E. Maciel and R. V. James, *J. Am. Chem. Soc.*, **86**, 3893 (1964), and unpublished results.

(16) The ratio of the number of solute particles to the number which would be present if no ionization occurred.

shift of $\text{CH}_3\text{CO}_2\text{H}_2^+$ is observed in the solutions of acetic acid in sulfuric acid.

One distinction is apparent between the behaviors of the two esters in 101% sulfuric acid at room temperature: the C^{13} resonance spectrum of ethyl benzoate appeared to be characteristic of the corresponding RCO_2H_2^+ ion; but the spectrum of ethyl acetate under the same conditions was difficult to obtain, and showed an obvious time dependence. In the freshly prepared solution the spectrum appeared to resemble closely that obtained in the 97% sulfuric acid, characteristic of $\text{CH}_3\text{COHOC}_2\text{H}_5^+$. About 2 hr. later the C^{13} shift more closely resembled that of the $\text{CH}_3\text{COH}^+\text{-OH}$ ion obtained after heating 5 hr. at 50° . At intermediate stages, the spectra were not reliably reproducible, indicating reaction underway which we interpret as the transformation given by eq. 3.

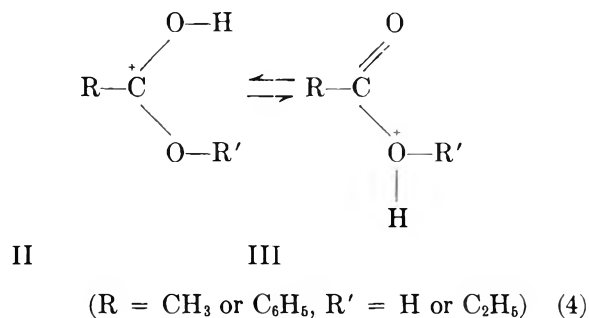


Bradley and Hill³ have stated that SO_3 is a powerful catalyst in this conversion, which is consistent with our data showing its occurrence at an observable rate in 101% H_2SO_4 but not in 97% sulfuric acid.

Conclusions

The C^{13} magnetic resonance data indicate that the principal organic species present in the three solutions of acetic or benzoic acid in the present study is the carbonyl-protonated cation $\text{R-COH}^+\text{-OH}$. This is in agreement with previous conclusions based on other types of evidence.^{2,8} The 0.6 p.p.m. difference in shift observed between the 97% and 101% sulfuric acid solutions of the acids is attributed to a medium effect on the C^{13} chemical shift of $\text{R-COH}^+\text{-OH}$. For the esters, ethyl acetate and benzoate, the present data indicate that the principal species present in a freshly

prepared solution in 97% sulfuric acid is the carbonyl-protonated ion $\text{RCOH}^+\text{-OC}_2\text{H}_5$, whereas the species $\text{R-COH}^+\text{-OH}$ is predominant in fuming (101%) sulfuric acid. In the case of ethyl acetate in fuming sulfuric acid the transformation represented by eq. 3 requires either heating at 50° or a waiting period of a few hours, while the analogous transformation of ethyl benzoate seems rapid in fuming sulfuric acid (101%) even at 25° . Of course, the possibility remains that appreciable concentrations of more than one species may exist in the solutions studied. The low natural abundance of C^{13} permits observation of only the most concentrated species. Furthermore, the existence of rapid equilibria between species protonated at different positions, as represented in eq. 4, would give rise to a single,



weighted-average peak if the transformation is rapid enough.¹⁷ In the present case we can state that the concentration of species III must be considerably lower than of species II, since the observed shifts in sulfuric acid are much closer to the values to be expected for carbonyl protonation than for protonation of the hydroxy or ethoxy oxygen positions.

Acknowledgment. The authors are grateful to the Research Corporation which supported this investigation in the form of a Frederick Gardner Cottrell Grant.

(17) J. A. Pople, W. G. Schneider, and H. J. Bernstein, "High-Resolution Nuclear Magnetic Resonance," McGraw-Hill Book Co., Inc., New York, N. Y., 1959, Chapter 10.

Electronic Commutator Determination of E° of Formation and Related Thermodynamic Quantities for Molten Lead Chloride¹

by Theodore B. Warner and Ralph L. Seifert

Department of Chemistry, Indiana University, Bloomington, Indiana (Received November 16, 1963)

The electronic commutator method for determining E° of formation of molten halides has been improved and applied to obtain the following equations for E° , ΔG° , ΔH° , ΔS° , and ΔC_p° of formation of liquid lead chloride in the temperature range 493–866°. The equation for E° reproduces the data within the experimental precision of 0.2 mv. The larger error limits in brackets are based on consideration of maximum probable temperature inhomogeneity in the melt and other possible systematic errors. The figures in brackets are average standard errors calculated for $t = 493$ – 750 and 750 – 866° , respectively; $X = (t - 700)/100$.

$$E^\circ \text{ (mv.)} = 1158.90 - 54.11X + 0.833X^2 + 0.062X^3 + 0.116X^4 [\pm 0.8 \text{ mv.}, \pm 1.2 \text{ mv.}]$$

$$\Delta G^\circ \text{ (kcal./mole)} = -53.451 + 2.496X - 0.038X^2 - 0.0029X^3 - 0.0054X^4$$

$$[\pm 0.035 \text{ kcal.}, \pm 0.053 \text{ kcal.}]$$

$$\Delta H^\circ \text{ (kcal./mole)} = -77.737 + 0.748X + 0.122X^2 + 0.2140X^3 + 0.0160X^4$$

$$[\pm 0.12 \text{ kcal.}, \pm 0.24 \text{ kcal.}]$$

$$\Delta S^\circ \text{ (e.u.)} = -24.957 + 0.768X + 0.086X^2 + 0.2140X^3 [\pm 0.14 \text{ e.u.}, \pm 0.19 \text{ e.u.}]$$

$$\Delta C_p^\circ \text{ (cal./mole deg.)} = 10.41 + 0.34X - 0.075X^2 [\pm 0.47 \text{ cal.}, \pm 0.76 \text{ cal.}]$$

Introduction

Most previous determinations of the E° of formation of molten binary halides have been made using the equilibrium cell method, which, although simple in principle, has produced widely varying results. For example, E° values obtained for the equilibrium cell $\text{Pb(l)}|\text{PbCl}_2(\text{l})|\text{Cl}_2(\text{g})$ by a number of investigators^{2–13} vary by as much as 70 mv. In general the precision has been 1 or 2 mv. (0.5 mv. in one case⁷), and most studies were restricted to temperatures below 700°, where experimental difficulties were minimized. The value of dE°/dT has usually been reported to be constant, within experimental error; although the wide range of reported values (–0.54 to –0.74 mv./°C.) produces large uncertainty in the derived values of ΔH_f° and ΔS_f° of lead chloride. Since the precision of measurement has never permitted evaluation of d^2E°/dT^2 , $(\Delta C_p^\circ)_f$ could not be calculated.

The electronic commutator method¹⁴ developed in this laboratory was used in the present study of lead chloride to test the method further, increase its pre-

cision, and determine whether it might give more reproducible results and be applicable over a wider temperature range than the equilibrium cell method. In

(1) This work was supported in part by the Directorate of Chemical Sciences, Air Force Office of Scientific Research, and by the U. S. Atomic Energy Commission.

(2) V. Czepinski, *Z. anorg. Chem.*, **19**, 208 (1899).

(3) O. H. Weber, *ibid.*, **21**, 305 (1899).

(4) R. Lorenz and M. G. Fox, *Z. physik. Chem.*, **63**, 109 (1908).

(5) J. H. Hildebrand and G. C. Ruhle, *J. Am. Chem. Soc.*, **49**, 722 (1927).

(6) R. Lorenz and H. Velde, *Z. anorg. allgem. Chem.*, **183**, 81 (1929).

(7) A. Wachter and J. H. Hildebrand, *J. Am. Chem. Soc.*, **52**, 4655 (1930).

(8) L. Holub, F. Neubert, and F. Sauerwald, *Z. physik. Chem.*, **174**, 161 (1935).

(9) S. A. Pletenev and V. N. Rozov, *Acta Physicochim. URSS*, **7**, 339 (1937).

(10) B. P. Artamonov, "Collected Works on the Electrochemistry of Fused Salts," P. F. Antipina, Ed., State Scientific-Technical Publishing House for Chemical Literature, Leningrad, 1940, pp. 31–39.

(11) S. I. Rempel and I. N. Ozeryanaya, *Zh. Fiz. Khim.*, **25**, 1181 (1951).

(12) M. F. Lantratov and A. F. Alabyshv, *J. Appl. Chem. USSR*, **26**, 235 (1953).

the commutator method, square current pulses are passed through the molten salt to form the constituents of a reversible cell periodically at inert electrodes. Measurement of cell e.m.f. as a function of time between pulses permits correction for overvoltage and determination of the reversible e.m.f.

Experimental

Details of the apparatus and procedure are given elsewhere¹⁵; they differed in many respects from those used in the earlier work with silver chloride.¹⁴

(1) *Apparatus.* The electrolysis cell, which was enclosed in a fused quartz housing, could be evacuated or filled with prepurified chlorine, hydrogen chloride, or nitrogen, either directly or by bubbling through the melt. The positions of electrodes in the cell could be adjusted and the electrodes were introduced and removed through close-fitting tubes flushed by an outward flowing stream of purified nitrogen. The melt (30 mm. deep) was contained in a high purity alumina crucible. Gas pressure in the cell was adjustable and maintained at 760 torr. The cell housing was held in a massive iron cylinder serving as temperature ballast in a crucible furnace. Furnace temperature was controlled ($\pm 0.2^\circ$) with a proportioning controller and cell temperature was measured with chromel-alumel thermocouples calibrated as before.¹⁴

(2) *Electrodes.* Electrodes were spectroscopically pure graphite rods with platinum wire leads. Quartz tube sheaths were collapsed tightly onto the graphite about 1 cm. from the bottom of the rod. The cathode¹⁶ sheath was sealed off below the graphite to form a compartment where lead generated during electrolysis could collect. A small hole at the top of the compartment admitted melt. The anode sheath extended below the end of the electrode and was open at the lower end. A small hole in the side of the sheath permitted melt to cover the end of the anode while chlorine could collect about the electrode above the melt. Apparent anode areas varied from 0.1 to 0.4 cm.²; cathode areas were much larger. The graphite rods were pretreated by heating to 1000° under vacuum for 12 hr. and then strongly igniting the electrode end in an oxy-hydrogen flame.¹⁷ After fabrication, electrodes were held under vacuum for 24 hr. at 500°, cycled ten times for approximately 20-min. periods between vacuum and gas at 1 atm. (Cl₂ for anodes, N₂ for cathodes), then cooled and stored under gas until used.

(3) *Commutator and Associated Circuitry.* The current pulsing and e.m.f. measuring circuit differed from that previously used¹⁴ by providing greater stability and a wider range of adjustable pulse length and total cycle time and by utilizing a more satisfactory

method to determine cell e.m.f. at a selected time following a current pulse. Instead of entering a gated amplifier, the difference signal from cell and K-2 potentiometer in series was amplified with a d.c. amplifier (gain of 100; current drawn 10⁻⁸ amp.; drift $\ll 1$ μ v. during the time of an observation, and noise with grounded input 30 μ v., both referred to input) and displayed on an oscilloscope. Once each cycle, at a known time after the current pulse, the oscilloscope sweep was triggered and a section of the e.m.f. decay curve was observed in relation to the reference line obtained by occasionally connecting the d.c. amplifier to ground.

(4) *Procedure.* Fisher certified reagent grade lead chloride (99.9%) was purified by first holding it under a pressure of 0.003 torr in the experimental cell for 3 days at 25°, followed by 2 days at temperatures increasing slowly to 200°. Then, under flowing dry hydrogen chloride, the salt was heated to 525° over the following 30 hr. After purified HCl, Cl₂, and N₂ were bubbled successively through the melt, it was pre-electrolyzed with auxiliary graphite electrodes at 1.2 v. (525°). New electrodes were inserted, care being taken to avoid thermoelectric e.m.f., and purity was tested with voltage-current curves.¹⁸ The curves showed no hump and residual currents fell to 0.2 ma./cm.² of apparent anode area.

Current was pulsed between the electrodes until the decay curves reached a steady state. Currents ranged from 10 to 100 ma., larger currents being necessary at higher temperatures. The reversible e.m.f. of the cell was determined by extrapolating the linear portion of the e.m.f. decay curve back to the time current was interrupted.^{14,15} Figure 1a shows a typical signal where the total e.m.f. fluctuation during ten consecutive decay curves is less than 0.2 mv. and the slope of the linear portion is less than 0.1 mv./265 msec. Observation over periods of several minutes established that this fluctuation was random within the limits shown by Figure 1. Oscilloscope sensitivity corresponding to 0.2 mv. difference potential per cm., as in Figure 1b, was generally used. In spite of the 60-cycle noise

(13) B. F. Markov, I. U. K. Delimarskii, and I. D. Panchenko, *Zh. Fiz. Khim.*, **28**, 1987 (1954).

(14) A. F. Wilde and R. L. Seifert, *J. Electrochem. Soc.*, **108**, 1059 (1961).

(15) T. B. Warner, Ph.D. Thesis, Indiana University, 1963; available from University Microfilms, Ann Arbor, Mich.

(16) When the terms "cathode" and "anode" are used, they refer to the cell functioning as an electrolytic cell.

(17) R. A. Prokop, "Electrode Processes in Molten Silver Chloride," Ph.D. Thesis, Indiana University, 1963.

(18) D. Inman, G. J. Hills, L. Young, and J. O'M. Bockris, *Ann. N. Y. Acad. Sci.*, **79**, 803 (1960).

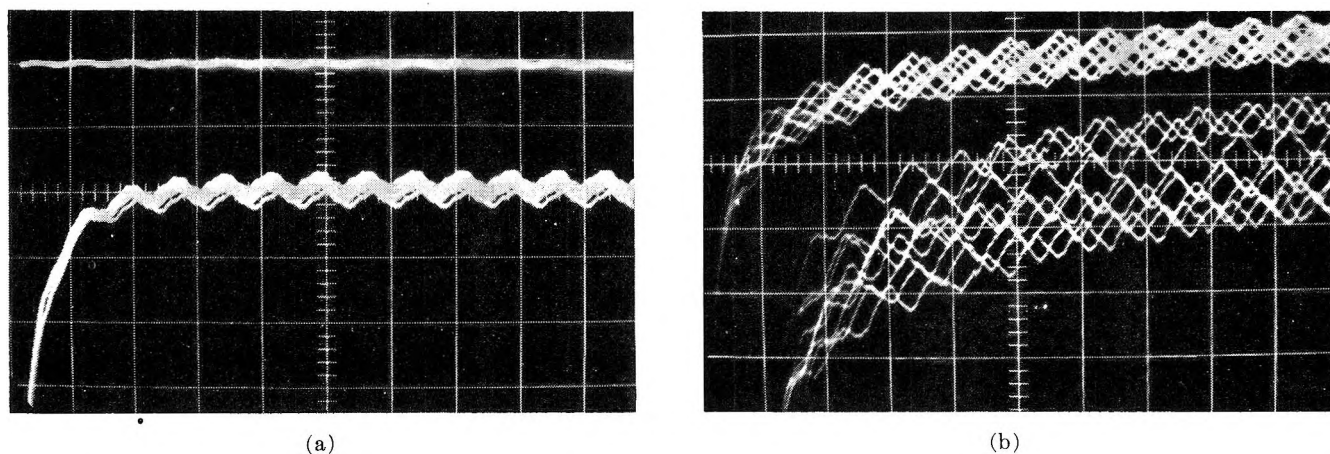


Figure 1. Representative voltage-time oscilloscope traces. Trace rises as cell e.m.f. decays. Each oscillogram shows ten consecutive cycles, each sweep being triggered 1.6 msec. following the current pulse. Sweep rates were 26.5 msec./cm. Sine waves were 60-cycle noise. (a) Typical decay curves at 600°: top trace is zero reference line; bottom is amplified e.m.f. difference signal; sensitivity 0.5 mv./cm. (b) High temperature decay curves obtained in run 11: top traces at 847°; bottom at 866°; sensitivity 0.2 mv./cm.

shown in Figure 1, extrapolated e.m.f. values could be estimated within ± 0.05 to ± 0.1 mv. from 500 to 850°, and within about ± 0.2 mv. up to 866°. Maximum activity of electrolysis products was assumed to have been obtained if 10% larger pulsing currents did not affect extrapolated e.m.f.

Most data were taken while the melt was cooled or heated about 1°/min. A slight hysteresis due to temperature lag at the somewhat isolated anode was observed and corrected for. Cell reversibility was checked frequently at stabilized temperatures by changing the pressure at the anode surface. Resulting changes in e.m.f. agreed with Nernst equation predictions, within experimental error. For example, in run 9 at 552°, pressure was reduced 14 torr; ΔE predicted was -0.64 mv., ΔE observed was -0.62 ± 0.05 mv.

That the pulsing technique provided chlorine at maximum activity at the anode was verified at low temperatures by replacing the nitrogen above the melt by chlorine at 1 atm. and taking additional data. No difference in extrapolated e.m.f. was observed below 600°; at higher temperatures the latter data were significantly greater, the difference gradually increasing to about 1 mv. at 700°. Since the anodes also developed large, slowly decaying overvoltages above 730° with nitrogen over the melt, the best high temperature data were obtained with a chlorine atmosphere. (Lowered chlorine activity at the anode resulted from increased rate of diffusion due to increasing temperature and from increased concentration gradient of chlorine in the melt resulting from increased transport of lead, by diffusion and possibly convection, from the cathode toward the anode. Work reported elsewhere¹⁵

indicated that the graphite anodes were poisoned by lead resulting from slight thermal decomposition of the melt or transport from the cathode.)

Eight series of e.m.f. measurements (runs 1–8) were made with nitrogen over the melt, three (runs 9–11) with chlorine. A number of different melts, cathodes, anodes, and calibrated thermocouples were used. Whenever possible with a given anode, measurements were made with both ascending and descending temperatures.

Results

(1) *Stability of Cell E.m.f.* In a typical test at 640°, cell pulsing current was varied from 9 to 28 ma. during a 24-min. period. The average of eleven extrapolated e.m.f. values was 1.19149 v., with a standard deviation of 5.4×10^{-5} v. Similar reproducibility was routinely obtained at the lower temperatures. At high temperatures the cell was frequently less stable, as shown by Figure 1b. E.m.f. values are given in later sections to as many figures as are significant with regard to the precision of the given measurement. Total uncertainty resulting from possible systematic errors is discussed in a later section.

(2) *Effect of Temperature Gradient.* With a given cell, highly self-consistent data were obtained. On plots of e.m.f. vs. temperature, deviations from a smooth curve were 0.1 to 0.4 mv. Data from different cells, however, differed by 0.1 to as much as 2.4 mv. Typical results are shown in Figure 2, replotted to conform to the limitations of a small plot. (For random sampling, every fifth point on the original experimental plot is plotted relative to an arbitrary reference line defined by E (mv.) = $1575.0 - 0.6t$.) All plots were

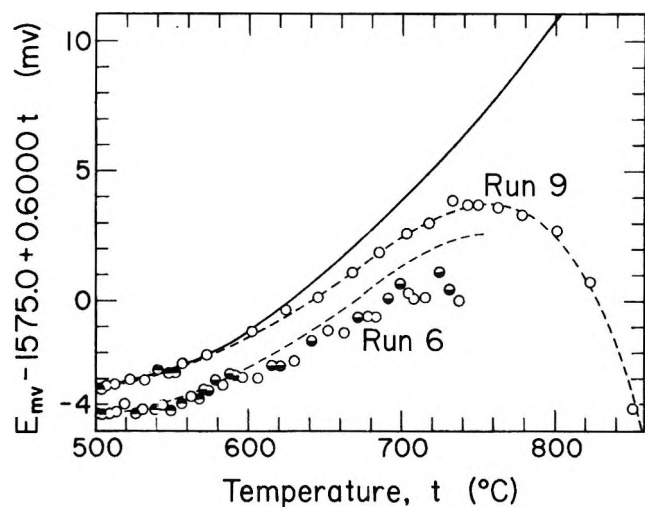


Figure 2. Representative e.m.f. data plotted on expanded scale as deviation from arbitrary reference line. Run 6: data taken from 575 to 501° (●), then from 501 to 737° (○), followed by 737 to 566° (◐). Run 9: data from 552 to 504° (●), then from 504 to 851° (○). Upper dashed curve based on eq. 1; solid curve on eq. 2. Lower dashed curve is displaced by 1.1 mv. from curve based on eq. 1.

similar, forming a family of almost parallel curves separated by small but experimentally real differences.¹⁹ This systematic bias was found to be caused by differences in electrode temperatures due to the temperature gradients in the melt created by heat leaks at the top and bottom of the cell. The relative temperatures of the two electrodes were a function of electrode positions in the melt. In an 80-mm. deep quiescent melt used to study this effect, the surface and bottom temperatures were 4.5 and 1.5° lower than the 30 mm. essentially constant temperature region ($\pm 0.5^\circ$). Stirring with chlorine produced reasonable temperature homogeneity. Measurements made at five stabilized temperatures from 541 to 855° with electrodes at different depths in stirred and quiescent melts indicated that the electrodes in run 9 were those most nearly at the same temperature and differed in temperature by no more than 1°. When the chlorine electrode is cooler than the lead electrode, the observed e.m.f. increases about 0.5 mv./deg. difference in temperature.

(3) *Selection of Data.* By all criteria¹⁵ the data obtained from 504 to 851° in run 9 and from 605 to 866° in run 11 seemed most reliable and the reported equations are based on these, though all data were used to help establish limits of possible systematic errors. In run 9, 25 e.m.f. values were obtained while cooling from 552 to 504° and 15 while again heating to 552°. These data were reproducible within 0.2 mv., and their stand-

ard deviation from the calculated curve for the entire run was 0.11 mv.

(4) *Treatment of Data.* Data from runs 9 and 11 for temperatures from 504 to 866° (136 experimental points) were treated as one set of data by the method of least squares. An IBM 709 computer evaluated the constants for the best representation of the data by linear, quadratic, cubic, and quartic equations. Analysis of variance showed that terms through the quartic were significant, so that the data are best expressed by the following equation, where $X = (t - 700)/100$.

$$E \text{ (mv.)} = 1157.46 - 56.33X - 1.54X^2 - 1.75X^3 - 0.40X^4 \quad (1)$$

The standard deviation of experimental points from this equation is 0.19 mv.

To obtain E° values the experimental values of E at 1 atm. total pressure must be corrected for the presence of lead chloride vapor in the chlorine formed at the anode. Vapor pressure data have been reported for lead chloride by various workers.²⁰ The values by Barton and Bloom were used to calculate the corrections, which ranged from 0.1 mv. at 552° to 24.1 mv. at 866°. The difference between uncorrected and corrected e.m.f. values is shown by the two upper curves in Figure 2. The resulting E° values from 504 to 866° are best represented by the equation

$$E^\circ \text{ (mv.)} = 1158.90 - 54.11X + 0.833X^2 + 0.062X^3 + 0.116X^4 \quad (2)$$

The standard deviation is 0.24 mv. The last 22 determinations of E° made in run 4 were at temperatures from 503.2 to 493.2° and are randomly scattered about the curve defined by eq. 2, with summation of deviations equal to 0.046 mv. and standard deviation of 0.099 mv. Therefore, these equations can be used with confidence down to the melting point of lead chloride and for supercooled melt.

Discussion

(1) *Comparison with Previous Work.* Previous e.m.f. measurements of the lead chloride cell by the equilibrium cell method have usually been reported as a linear function of temperature and no mention has been made of corrections for the effect of lead chloride vapor pressure. Most of the previous work was done

(19) Tabulated data are given in ref. 15.

(20) L. Brewer, Paper 7 in "The Chemistry and Metallurgy of Miscellaneous Materials," L. L. Quill, Ed., McGraw-Hill Book Co., Inc., New York, N. Y., 1950, pp. 206, 248; D. R. Stull, *Ind. Eng. Chem.*, **39**, 540 (1947); G. I. Novikov and O. G. Polyachenok, *Zh. Neorgan. Khim.*, **6**, 1951 (1961); J. L. Barton and H. Bloom, *J. Phys. Chem.*, **60**, 1413 (1956).

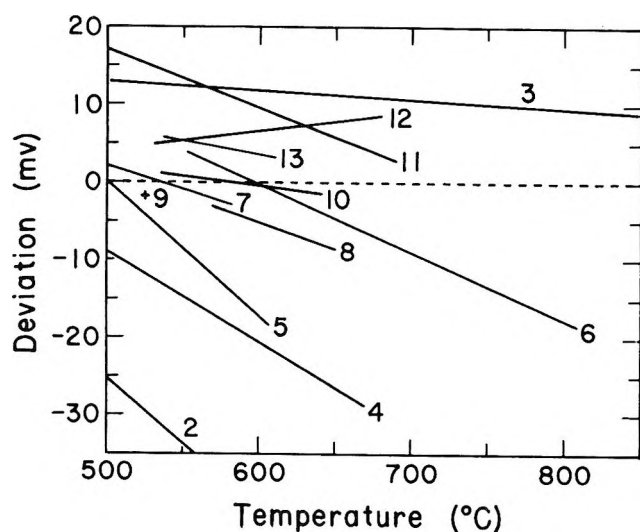


Figure 3. Deviation of e.m.f. measurements by the equilibrium cell method²⁻¹³ from those obtained in this study. The lines are numbered to correspond with the reference numbers. Pletenev and Rozov⁹ report only one measurement, the single point at 525°.

below 700°. Therefore, the linear equation best representing the uncorrected e.m.f. measurements in run 9 from 500 to 700° has been used for the comparison in Figure 3 with the earlier work.

The larger negative temperature coefficient reported for most of the equilibrium cell work is believed due to depolarization and insufficient saturation of the chlorine electrodes at higher temperatures. In using the equilibrium cell method, many workers interrupted the flow of chlorine at the time of measurement to reduce instability in the cell signal. Particularly at higher temperatures, where rates of diffusion and of convective stirring are large, this leads to low e.m.f. values.

Only the e.m.f. values reported by Lantratov and Alabyshev¹² have a smaller negative temperature coefficient than that obtained in this study, and their e.m.f. values are higher by 5 to 9 mv. This must be due to temperature inhomogeneity in their experimental arrangement. They used a large cell with a pool of lead at the bottom and a graphite electrode near the surface with chlorine flowing over it. No pre-heating of the chlorine or other precautions to provide isothermal conditions in the melt were reported. The anode was undoubtedly cool relative to the cathode, which has here been shown to produce high cell e.m.f. Since the temperature difference between electrodes would tend to increase with increasing cell temperature, $-dE/dT$ would be low.

The data reported by Artamonov¹⁰ are within 1.2 mv. of those found in this study. His primary purpose was to evaluate the suitability of the chlorine electrode

as a reference electrode. Therefore, he controlled experimental conditions very carefully. The entire cell was immersed in a stirred bath of molten lead to maintain a uniform temperature. Delimarskii²¹ considers Artamonov's measurements the most reliable of those previously reported for lead chloride.

(2) *Estimation of Errors.* In the discussion of each of the following possible sources of error, the resulting maximum possible error in E° is given in parentheses.

The maximum error of the potentiometer and the calibrated standard cell was estimated as $\pm 0.01\%$ (± 0.1 mv.). Since cell current during measurement was about 10^{-8} amp. and there was no observable change in e.m.f. when cell current was purposely increased to 10^{-7} amp., no significant systematic error resulted from polarization by cell current between current pulses.

Pressure at the anode-chlorine interface was maintained at 1 atm. within ± 4 torr (equivalent to 0.2 mv.). Published values of the vapor pressure of $PbCl_2$ agreed well up to 780°. Corrections of E calculated from the values given by Brewer²⁰ and by Barton and Bloom²⁰ differed by 0.1 to 0.2 mv. below 780° and by 0.2 to 0.5 mv. from 780 to 852°. The saturation concentration of lead in lead chloride²² at the cathode is insufficient over the entire temperature range to influence E by as much as 0.1 mv., due to reduced activity of lead chloride.

Instrumental and thermocouple calibration errors were estimated to result in an uncertainty of $\pm 0.5^\circ$ (± 0.3 mv.) in the measured temperature. Below 750° the measured temperature was estimated to be within 1.0 to 1.5° of the average temperature of the cathode (± 0.6 to 0.9 mv.) and the cathode temperature to be within 1° of the average effective anode temperature (± 0.5 mv.). Above 750° these estimates were doubled. The resulting uncertainty in cell temperature was therefore considered to be $\pm 2^\circ$ (1.1 mv.) from 500 to 750° and $\pm 4^\circ$ (2.1 mv.) from 750 to 866°. Since a difference between anode and cathode temperatures influences E° by about 0.5 mv./deg., a linear variation in this difference from 0° at 500° to 4° at 866° (the estimated probable maximum) would change dE°/dT by about 1%.

The maximum error in E° , considering temperature as known and assigning all error to e.m.f., was estimated as ± 2 mv. from 500 to 750° and ± 3 mv. from 750 to 866°.

(21) I. U. K. Delimarskii and B. F. Markov, "Electrochemistry of Fused Salts," The Sigma Press, Washington, D. C., 1961, p. 80.

(22) J. D. Corbett and S. VonWinbush, *J. Am. Chem. Soc.*, **77**, 3964 (1955).

(3) ΔG° , ΔS° , and ΔH° of Formation of $PbCl_2$. Equations for the molar free energy, entropy, and enthalpy of formation of $PbCl_2$, derived from eq. 2, have been given in the abstract. The estimated maximum possible systematic errors were treated as 99% confidence limits when combined with the standard errors of the coefficients in eq. 2 to obtain the standard errors given in brackets following the equations in the abstract. Values calculated from these equations at selected temperatures are given in Table I with corresponding values reported in the JANAF tables,²³ which incorporate data obtained from thermochemical sources.

Table I: Molar Thermodynamic Quantities for the Reaction $Pb(l) + Cl_2(g) = PbCl_2(l)$

	800°K.	900°K.	1000°K.	1100°K.
ΔG° (kcal./mole), this study	-57.920	-55.298	-52.784	-50.366
Standard error	0.035	0.035	0.035	0.053
ΔG° (kcal./mole), JANAF	-58.104	-55.501	-52.999	-50.586
ΔS° (cal./deg. mole)	-27.14	-25.56	-24.74	-23.41
Standard error	0.19	0.10	0.10	0.19
ΔS° (cal./deg. mole), JANAF	-26.549	-25.507	-24.568	-23.715
ΔH° (kcal./mole), this study	-79.63	-78.30	-77.52	-76.11
Standard error	0.16	0.10	0.11	0.24
ΔH° (kcal./mole), JANAF	-79.343	-78.457	-77.567	-76.673
ΔC_p° (cal./deg. mole)	9.6	10.1	10.5	10.7
Standard error	1.0	1.0	1.0	1.0
ΔC_p° (cal./deg. mole), JANAF	8.848	8.880	8.918	8.962

(4) ΔC_p° of Formation of $PbCl_2$. If eq. 2 is used to calculate an equation for ΔC_p° , the standard error for the coefficient of X^4 , which has little effect on the accuracy of E° and dE°/dT , dominates the error expression and gives very large limits of error. Therefore, the best cubic equation for E° was used to determine ΔC_p° . From 774 to 1139°K.

$$E^\circ (v.) = 1.15878 - 0.05397X + 0.001160X^2 - 0.00002716X^3 \quad (3)$$

where $X = (T - 973.15)/100$ and $T =$ temperature in °K. This equation gives

$$\Delta C_p^\circ = 10.41 + 0.34X - 0.075X^2 \quad (4)$$

or

$$\Delta C_p^\circ = (1.801 \pm 0.621) \times 10^{-2}T - (7.52 \pm 6.39) \times 10^{-6}T^2 \quad (5)$$

where the standard errors of the coefficients are de-

rived from those obtained for eq. 3. Standard errors in ΔC_p° calculated from these coefficient errors range from 0.18 to 0.90 cal./deg. mole. To include possible systematic errors, these values have been increased to those given in Table I.

(5) C_p° of Liquid $PbCl_2$. For the three substances involved in the formation reaction for liquid $PbCl_2$, the heat capacity of $PbCl_2$ is known with least certainty. Temperature-independent values ranging from 22.53 to 33.6 cal./deg. mole have been reported²⁴ for temperatures from 774°K up to temperatures ranging from 813 to 1073°K. Kelley²⁵ has selected Ehrhardt's value of 27.20 cal./deg. mole as the most reliable value reported prior to 1960. Bizouard and Pauty's²⁴ value of 24.9 cal./deg. mole was selected for the JANAF tables.

Equation 5, combined with heat capacity equations given by Kelley²⁶ for lead and chlorine, gives the following equation for liquid $PbCl_2$ from 774 to 1139°K.

$$C_p^\circ = 16.6 + 17.4 \times 10^{-3}T - 0.68 \times 10^5 T^{-2} - 7.5 \times 10^{-6}T^2 \quad (6)$$

Calculated values of C_p° at 800, 900, 1000, and 1100°K. are, respectively, 25.7, 26.2, 26.5, and 26.7 cal./deg. mole.

(6) *Conclusions.* Measurement of E° of formation of a molten binary halide can be made by the electronic commutator method with sufficient precision to provide thermodynamically significant results. Since variation of temperature within the cell was shown to limit the accuracy of the above results, the commutator method should be capable of even greater accuracy than achieved here. With thermally stable salts, measurements of comparable accuracy should be possible under an inert atmosphere.

Acknowledgment. We are indebted to Sigmund Schuldiner and to a referee for helpful comments. We wish to express our appreciation to the National Science Foundation and the Graduate School of Indiana University for fellowships granted to T. B. W.

(23) "JANAF Interim Thermochemical Tables," D. R. Stull, Ed., The Dow Chemical Co., Midland, Mich., March 31, 1962.

(24) O. Ehrhardt, *Wied. Ann.*, **24**, 241 (1885); H. M. Goodwin and T. H. Kalmus, *Phys. Rev.*, **28**, 1 (1909); A. N. Krestovnikov and G. A. Karetnikov, *J. Gen. Chem. USSR*, **6**, 955 (1936); M. Bizouard and F. Pauty, *Compt. rend.*, **252**, 514 (1961).

(25) K. K. Kelley, U. S. Bureau of Mines Bulletin 584, 1960, p. 103.

(26) K. K. Kelley, *ibid.*, pp. 56, 101.

Reaction of Tritium Atoms with Films of Solid Ethylene.

Disproportionation and Combination of Ethyl Radicals at 63°K.¹

by K. W. Watkins and H. C. Moser

Department of Chemistry, Kansas State University, Manhattan, Kansas (Received October 1, 1964)

Films of solid ethylene at 63°K. were bombarded with tritium atoms. Products (ethylene, ethane, and butane) of disproportionation and combination reactions of ethyl radicals were observed. Conditions were selected under which the only apparent reactions of ethyl radicals were disproportionation and combination. Under these conditions, no contribution from tritium atom addition to ethyl or product ethylene was evident. A disproportionation to combination ratio (k_d/k_c) of 0.77 ± 0.03 was observed for $C_2H_4T + C_2H_4T$, and a ratio of 0.83 ± 0.04 was observed for $C_2H_4T + C_2H_6$. Two methods of calculating the tritium isotope effect in the disproportionation of ethyl radicals gave $k_H/k_T = 1.7 \pm 0.7$ and $k_H/k_T = 2.3 \pm 0.5$. These small primary kinetic isotope effects are consistent with the mechanism discussed by Bradley and Rabinovitch that involves a "loose" transition state for disproportionation in which little or no binding occurs.

Introduction

Hydrogen atoms produced by the atomization of molecular hydrogen at a hot tungsten filament react with films of solid olefins. Reactions with solid propene^{2,3} and solid *cis*-2-butene⁴ are among those that have been studied. When the hydrogen atoms reacted before reaching thermal equilibrium with the solid, hydrogen atom abstraction and nonterminal addition occurred along with terminal addition.³ When the hydrogen atoms were thermalized to the temperature of the olefin film (77 or 90°K.), hydrogen atom addition to the terminal carbon atom of the olefin appeared to be the only initial reaction. Under conditions of rapid olefin diffusion all of the products in the propene and *cis*-2-butene systems were explained by disproportionation and combination reactions of isopropyl² and *sec*-butyl⁴ radicals, respectively.

In the present paper, the results of hydrogen and tritium atom reactions with films of solid ethylene are reported. Here, as in the above cases, the products of reaction can be explained best by the existence of alkyl radical intermediates, *i.e.*, ethyl radicals. We have measured disproportionation to combination ratios (k_d/k_c) for two types of ethyl radicals, C_2H_4T and C_2D_4T , at 63°K. Ratios at other temperatures for ethyl⁵ and isopropyl⁴ radicals have been reported in the litera-

ture. In both cases k_d/k_c increased with decreasing temperature.

By labeling with deuterium, it was shown that disproportionation of ethyl radicals involves a transfer of a hydrogen atom from the CH_3 group of one radical to the CH_2 group of the other radical.^{6,7} A transition state which involves a "loose" association of radicals has been proposed^{8,9} as being more consistent with the large A factor for disproportionation than the rigid transition state of a "head to tail" mechanism analogous to hydrogen abstraction reactions. The magnitudes of

(1) Presented in part at the 148th National Meeting of the American Chemical Society, Chicago, Ill., Sept. 1964. Work performed under Contract AT(11-1)584 with the U. S. Atomic Energy Commission. From the Ph.D. Thesis of K. W. Watkins to be submitted to the Graduate School, Kansas State University.

(2) R. Klein, M. D. Scheer, and J. G. Waller, *J. Phys. Chem.*, **64**, 1247 (1960).

(3) H. B. Yun and H. C. Moser, *ibid.*, **67**, 2806 (1963).

(4) R. Klein, M. D. Scheer, and R. Kelley, *ibid.*, **68**, 598 (1964).

(5) P. S. Dixon, A. P. Stefani, and M. Szwarc, *J. Am. Chem. Soc.*, **85**, 2551 (1963).

(6) M. H. Wijnen and E. W. R. Steacie, *Can. J. Chem.*, **29**, 1092 (1951).

(7) J. R. McNesby, C. M. Drew, and A. S. Gordon, *J. Phys. Chem.*, **59**, 988 (1955).

(8) J. N. Bradley, *J. Chem. Phys.*, **35**, 748 (1961).

(9) J. N. Bradley and B. S. Rabinovitch, *ibid.*, **36**, 3498 (1962).

the hydrogen-tritium (for C_2H_4T) and the deuterium-tritium (for C_2D_4T) primary kinetic isotope effects in the disproportionation of two ethyl radicals should serve as a further test of the mechanism. The kinetic isotope effects k_H/k_T and k_D/k_T are reported here for ethyl radical disproportionation at 63°K.

Experimental

Ethylene (99.97%, Phillips research grade) and ethylene- d_4 (99%, Stohler Isotope Co.) were used without further purification. The reaction flask consisted of a cold finger and a tungsten filament ($2.5 \times 10^{-3} \times 1.5$ cm.) placed vertically so that its center was 4 cm. from the bottom of the cold finger. The filament was supported by tungsten leads sealed in glass. Three to five μ moles of ethylene was introduced into the vacuum system and was frozen with liquid nitrogen as a film on the bottom of the cold finger. More liquid nitrogen was then added. By pumping the liquid nitrogen, either with a vacuum pump or with an aspirator, its temperature was reduced to 63°K. (*i.e.*, its freezing point). At this temperature the vapor pressure of solid ethylene is about 10^{-6} torr. Hydrogen containing tritium or carrier-free tritium was introduced into the vacuum system through heated palladium thimbles. The specific activity of the hydrogen was approximately 1 and 58 c./mmole (carrier free). The hydrogen was atomized by the tungsten filament at pressures from 1×10^{-3} to 9×10^{-3} torr. The pressure was measured with a Pirani gauge which was calibrated with a McLeod gauge.

The filament was placed perpendicular to the ethylene film in order to minimize heat transfer from the filament to the ethylene film. Also, most of the hydrogen atoms struck the glass wall before encountering the ethylene film. This allowed the H atoms to lose most of their kinetic energy; thus hydrogen atom abstraction from ethylene to form vinyl radicals was not an important reaction. This was verified by the absence of 1-butene as a product. Only in a very few reactions was a trace of 1-butene observed.

The tungsten filament temperature was measured with an optical pyrometer, and corrections were made for emissivity. The reaction products were separated by gas chromatography and counted by an ionization chamber placed in the effluent stream.¹⁰ The ionization chamber was calibrated by noting the response (peak area) from tritium-labeled 2,3-dimethylbutane as it flowed through the chamber. The 2,3-dimethylbutane was then trapped in toluene scintillator solution and counted in a liquid scintillation spectrometer.

Products were separated by a gas chromatography column of $AgNO_3$ in ethylene glycol in series with a di-

methylsulfolane column and were identified by comparison with retention volumes of known compounds.

Results

The reaction of tritium atoms with films of frozen ethylene at 63°K. yields under proper conditions only three products which contain tritium, ethylene, ethane, and butane.

Table I shows how the product distribution changed

Table I: Tritium Atom Reactions with C_2H_4 at 63°K.^a

Reaction time, ^b min.	Tritium dist., %			Rel. ³ H act.
	C=C	C-C	C-C-C-C	
	(A)			
1	11.8 ± 0.7	31.7 ± 2.2	56.4 ± 1.8	(1.0)
2	9.0 ± 0.5	32.3 ± 1.8	58.7 ± 1.3	1.5
3	7.2 ± 0.2	34.9 ± 2.8	57.9 ± 2.8	1.7
5	5.0	37.9	57.1	2.7
9	2.9	46.2	50.9	3.0
	(B)			
1	11.8 ± 0.7	31.7 ± 2.2	56.4 ± 1.8	(1.0)
4	8.5 ± 0.6	37.4 ± 2.3	54.1 ± 1.7	1.5
9	6.3	42.0	51.7	2.2

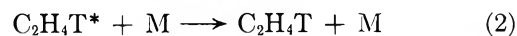
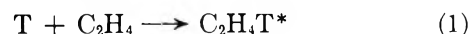
^a Filament temperature 1830°K. ^b Constant $H_2 + HT$ pressure of 10^{-3} torr. ^c Constant reaction time of 1 min.

with increasing reaction time and increasing hydrogen pressure for a tungsten filament temperature of 1830°K. Table II shows that when the filament temperature is reduced to 1400°K. the product distribution is constant in time and also that changing the tritium pressure makes little difference.

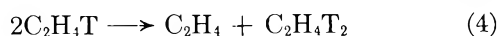
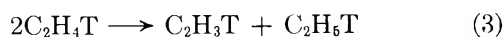
Table III shows the average product distributions, with standard deviations, obtained from the reactions of H and T with C_2H_4 , T with C_2H_4 , and T with C_2D_4 carried out under the conditions given in Table II.

Discussion

Reactions of Atoms and Radicals. The three products observed from reactions of tritium atoms with solid ethylene are considered to result from reactions 1-5. Hydrogen addition to the olefin and subsequent



(10) D. C. Nelson, P. C. Ressler, Jr., and R. C. Hawes, *Anal. Chem.*, **35**, 1575 (1963).



disproportionation or combination of the alkyl radicals have been proposed previously.²⁻⁴ The excited ethyl radical which results from tritium atom addition to ethylene (1) should be easily deactivated (2) either on the surface or in the bulk of the solid. All further reactions (3-5) are assumed to occur between thermalized radicals since they must diffuse to each other before they react, and time is thus available for deactivation by transfer of energy to the surrounding molecules.

Table II: Tritium Atom Reactions with C_2H_4 at 63°K .^a

Reaction time, ^b min.	Tritium dist., %			Rel. ³ H act.
	C=C	C-C	C-C-C-C	
(A)				
1	17.8 ± 0.8	26.5 ± 1.5	55.7 ± 1.5	(1.0)
2	17.5 ± 0.6	26.0 ± 0.9	56.5 ± 1.3	2.0
3	17.6 ± 0.6	24.8 ± 1.2	57.6 ± 1.1	3.4
5	17.6 ± 0.5	25.9 ± 2.0	56.5 ± 1.6	4.9
10	18.2	24.1	57.7	9.9
T ₂ pressure, ^c torr × 10 ³				
(B)				
1	17.8 ± 0.8	26.5 ± 1.5	55.7 ± 1.5	(1.0)
4	18.8 ± 0.4	24.7 ± 0.1	56.5 ± 0.2	1.9

^a Filament temperature 1400°K . ^b Constant T₂ pressure of 10^{-3} torr. ^c Constant reaction time of 1 min.

Table III: Tritium Atom Reactions with C_2H_4 and C_2D_4 at 63°K .^a

Reactants		Tritium dist., %		
		C=C	C-C	n-C ₄
C_2H_4	$\text{H}_2 + \text{HT}$	17.4 ± 0.8	27.9 ± 1.4	54.7 ± 1.5
C_2H_4	T ₂	17.9 ± 0.7	25.7 ± 1.4	56.4 ± 1.3
C_2D_4	T ₂	16.0 ± 0.5	26.7 ± 0.9	57.3 ± 0.7

^a Filament temperature 1400°K .; hydrogen pressure 10^{-3} torr.

Table I (A) shows that the per cent ethylene yield decreased and the per cent ethane yield increased when the reaction time was increased at a filament temperature of 1830°K . The butane remained nearly constant. This trend is also shown in Table I (B) for an increase in the hydrogen pressure. This effect is believed to be due to consecutive reactions of tritium atoms with

product ethylene molecules which results in the formation of more ethane and butane. As the reaction time was increased, the total yield of tritium-labeled ethylene remained about the same, but the total yields of labeled ethane and butane increased. Hydrogen and tritium atom combination with ethyl radicals is ruled out as a possible explanation of the effect because an appreciable contribution from this reaction would diminish the percentage of tritium in butane. The nearly constant butane percentage is evidence for the predominant addition of tritium atoms to ethylene.

If consecutive reactions occur with product ethylene molecules, then all the reactions must occur on the surface of the film since the concentration of product ethylene molecules would be too small for consecutive reactions to be important in the bulk of the film. Only if the product ethylene molecules were on the surface of the film could their concentration be high enough for consecutive reactions to be important.¹¹ The occurrence of surface reactions has been suggested previously.¹² The fact that the tritium activity does not increase linearly with time or with hydrogen pressure¹³ (Table I) suggests that the products remain on the surface. Since both ethane and butane react more slowly with hydrogen atoms than does ethylene, the over-all rate of incorporation of tritium into products is decreased.

By lowering the tungsten filament temperature to 1400°K ., the rate of hydrogen atomization is decreased about 90-fold.¹³ Also, by using carrier-free tritium, a much smaller amount of products could be observed. Under these conditions consecutive reactions were not apparent (Table II). As the reaction time was increased, the tritium activity increased linearly and no change in the product distribution was observed. When the T₂ pressure was increased fourfold, the tritium activity in the products increased twofold as would be expected from the pressure dependence of the atomization rate.¹³ These observations under conditions of low tritium atomization rate indicate that consecutive reactions with product ethylene molecules were negligible. Thus under these conditions the yields of C₂ and C₄ products could be used to evaluate disproportionation to combination ratios of tritium-labeled ethyl radicals.

(11) We estimate that there are 10^{15} surface ethylene molecules and 10^{18} bulk molecules. Assuming the specific activity of the products to be the same as that of the hydrogen (1 c./mmole), we calculate 10^{16} product molecules. Thus consecutive reactions appear to be likely only on the surface.

(12) R. Klein and M. D. Scheer, *J. Phys. Chem.*, **66**, 2677 (1962).

(13) At 1830°K . the rate of atomization of hydrogen is proportional to P_{H_2} , and at 1400°K . the rate is proportional to $P_{\text{H}_2}^{1/2}$: D. Brennan and P. C. Fletcher, *Proc. Roy. Soc. (London)*, **A250**, 389 (1959).

That the radical reactions occurred before warm-up was shown by experiments in which oxygen was introduced within 1 sec. after turning off the tungsten filament. The ethylene was allowed to warm up in the presence of oxygen (pressure, 1 torr), and neither the product distribution nor the total tritium activity of the products was changed.

Disproportionation to Combination Ratio. Under conditions where consecutive reactions were not apparent, the ratio of the tritium in the C_2 products to that in butane, $C_2(T)/C_4(T)$, was taken as the ratio k_d/k_c . The k_d/k_c ratios for ethyl radicals at -210° given in Table IV follow the trend of increasing k_d/k_c with decreasing temperature reported by Dixon, Stefani, and Szwarc.⁵ However, extrapolation of their values (0.284 at -128° and 0.346 at -191° in iso-octane) to -210° leads to a value of 0.4, which is significantly less than our value of 0.8 at this temperature. We believe that the difference is due to environmental effects, some of which are more significant than the effect of temperature alone. Radical reactions in our system appear to occur on the surface, but the reactions studied by Dixon, Stefani, and Szwarc were with radicals generated homogeneously throughout the bulk. The influence of environment other than temperature was emphasized by these authors. For example, they reported the following values of k_d/k_c for ethyl radicals: 0.327 in glycol at -195° , 0.304 in toluene at -194° , 0.187 in solid azoethane at -195° , and 0.352 in liquid methane at -184° .

Table IV: Reactions of Ethyl Radicals at $63^\circ K$.

Radicals	k_d/k_c	k_H/k_T or k_D/k_T	
		From C-C/C=C	From k_d/k_c
$C_3H_5 + C_2H_4T$	0.83 ± 0.04	5.0 ± 5.1	1.7 ± 0.7
$C_2H_4T + C_2H_4T$	0.77 ± 0.03	2.3 ± 0.5	
$C_2D_4T + C_2D_4T$	0.75 ± 0.02	1.5 ± 0.2	

Large values of the k_d/k_c ratio seem to be characteristic of reactions of radicals produced by the bombardment of condensed olefins with H atoms. Reactions of both ethyl and isopropyl radicals can be cited as examples. By the use of H atom reactions with films of propene (using tritium as a tracer), a value of 5.5 at $90^\circ K$. for the k_d/k_c ratio for isopropyl radicals was found in our laboratory.¹⁴ A k_d/k_c ratio of approximately 8 for isopropyl radicals at $90^\circ K$. was reported by Klein, Scheer, and Kelley.⁴ In contrast, the same authors report a ratio of 1.6 for isopropyl radicals at $90^\circ K$. produced by the photolysis of azoisopropane.

They have suggested that intramolecular elimination of N_2 to produce more dimer may have occurred in the photolysis experiments. If this process produced the change, then the amount of dimer from elimination of N_2 relative to that from combination was 8/1.6 or 5.5/1.6, and the practicality of the use of the photolysis experiments to measure the k_d/k_c ratio is questionable. In the photolysis of azoethane, the differences in C_2 and C_4 yields when the solvent is changed do not seem to be explained best by the environmental influence on the intramolecular elimination of N_2 . Rather, a definite change in the k_d/k_c ratio is indicated.

The environmental influence on the k_d/k_c ratio emphasizes the small but significant difference in the transition states for disproportionation and combination.

Primary Kinetic Isotope Effects. If in the disproportionation of CTH_2CH_2 radicals the tritium atom is never transferred, the ratio ethane-T/ethylene-T in the tritiated products should be 1:1. If, on the other hand, the tritium atom is randomly transferred, the ethane-T/ethylene-T ratio should be 2:1. A ratio of 1.44:1 is obtained from the data in Table III. This indicates that the tritium atom is transferred sometimes but not randomly. This ratio was used to calculate the kinetic isotope effect (k_H/k_T) in the disproportionation reaction. The expression used was

$$\frac{\text{ethane-T}}{\text{ethylene-T}} = \frac{2k_H + k_T(2)}{2k_H} = 1 + \frac{k_T}{k_H} \quad (6)$$

This expression was derived by considering labeled ethane and ethylene to result from the transfer of a hydrogen or a tritium atom from the methyl group of one CTH_2CH_2 radical to the methylene group of the other radical. For ethane-T/ethylene-T = 1.44 ± 0.10 , we calculated $k_H/k_T = 2.3 \pm 0.5$. From a similar expression with k_D substituted for k_H , we obtained $k_D/k_T = 1.5 \pm 0.2$.

For the system of mixed radicals ($C_2H_5 + C_2H_4T$) a slightly different expression was used to calculate k_H/k_T .

$$\frac{\text{ethane-T}}{\text{ethylene-T}} = \frac{3k_H + k_T}{2k_H} = \frac{3 + k_T/k_H}{2} \quad (7)$$

For an ethane-T/ethylene-T ratio of 1.60 ± 0.11 , $k_H/k_T = 5.0 \pm 5.1$. In this case with such a large standard deviation we present the data only as an indication of the magnitude of the isotope effect.

The kinetic isotope effect (k_H/k_T) was also calculated from the difference in the disproportionation to combination ratios for $C_2H_5 + C_2H_4T$ and $C_2H_4T + C_2H_4T$.

(14) H. B. Yun and H. C. Moser, *J. Phys. Chem.*, **69**, 1059 (1965).

The rate of combination was assumed to be the same in both systems. The expression used was

$$\frac{k_d \text{ for } C_2H_5 + C_2H_4T}{k_d \text{ for } C_2H_4T + C_2H_4T} = \frac{5k_H + k_T}{4k_H + 2k_T} =$$

$$\frac{5 + k_T/k_H}{4 + 2k_T/k_H} = \frac{0.83 \pm 0.04}{0.77 \pm 0.03}$$

This leads to $k_H/k_T = 1.7 \pm 0.7$.

In all three cases of ethyl radical disproportionation listed in Table IV, only small kinetic isotope effects were observed. We believe the one value of 5 is least reliable due to its large standard deviation. Boddy and Steacie¹⁵ also reported a small kinetic isotope effect in the disproportionation of ethyl radicals. They reported $k_H/k_D = 1.4$ independent of temperature in comparing the rate of disproportionation of C_2D_6 radicals to that of C_2H_6 from 50 to 300°.

Several workers^{8,9,16} have suggested, on the basis of large pre-exponential factors for disproportionation reactions of alkyl radicals, that radicals in the transition state for disproportionation have freedom of motion comparable to radicals in the transition state for combination. The above authors state that this free-

dom of motion is not consistent with the head-to-tail transition state which was proposed earlier.⁶

The small primary kinetic isotope effects reported here are consistent with the proposed "loose" transition state for disproportionation in which little or no binding occurs.^{8,9} In contrast, a very large kinetic isotope effect ($k_H/k_T \sim 10^6$) could be expected at 63°K. for a symmetric "head-to-tail" transition state.

From arguments presented by Westheimer¹⁷ to explain small kinetic isotope effects, we suggest that in the transition state for disproportionation the C-H bond length is essentially the same as in the undisturbed ethyl radical. This implies that the reaction has little or no activation energy since energy is not required to extend the C-H bond in forming the transition state.

Acknowledgment. The authors wish to acknowledge helpful conversations concerning this paper with Dr. D. W. Setser.

(15) P. J. Boddy and E. W. R. Steacie, *Can. J. Chem.*, **38**, 1576 (1960).

(16) J. A. Kerr and A. F. Trotman-Dickenson, "Progress in Reaction Kinetics," Vol. I, Pergamon Press, New York, N. Y., 1961, p. 107.

(17) F. H. Westheimer, *Chem. Rev.*, **61**, 265 (1961).

Effect of Density on the Radiolysis of Ethane

by Catherine M. Wodetzki, P. A. McCusker, and D. B. Peterson^{1a}

Department of Chemistry and the Radiation Laboratory,^{1b} University of Notre Dame, Notre Dame, Indiana 46556 (Received October 26, 1964)

Hydrogen and butane are the products of ⁶⁰Co γ -radiolysis of ethane most significantly affected by variation of density in the range 0.001 (atmospheric pressure) to 0.30 g. cc.⁻¹. $G(\text{H}_2)$ decreases from 8.3 at the low end of this density range to a plateau value of 6.6 at about 0.25 g. cc.⁻¹. $G(n\text{-C}_4\text{H}_{10})$ increases comparatively rapidly from 2.5 at 0.001 g. cc.⁻¹ to a plateau value of 3.8 at 0.075 g. cc.⁻¹. From studies of the effect of density on γ -radiolysis of ethane and of a 1:1 mixture of ethane and ethane-*d*₆ in the absence and in the presence of ethylene, it is concluded that there are at least three modes of hydrogen formation. Two of these, abstraction by thermal hydrogen atoms and molecular detachment, decrease in importance with increasing density; the third, a bimolecular reaction uninhibited by ethylene, increases with increasing density. The bimolecular reaction may be either an ion-molecule reaction or an abstraction by a hot hydrogen atom. Increase in $G(n\text{-C}_4\text{H}_{10})$ with increasing density is attributed to increased production of ethyl radicals, combination of which is almost exclusively responsible for butane production at all densities. It is concluded that these effects are primarily a consequence of decreased ion fragmentation and increased parent-ion recapture at high gas densities.

The radiolysis of ethane at atmospheric pressure and below has been studied rather extensively by a number of investigators²⁻⁴ and is relatively well-understood. Some preliminary results on the radiolysis of ethane at higher pressures have been reported by Von Bünau and Burton⁵ from this laboratory and Carmichael and Ausloos⁶ have reported some results on the effects of pressure on the radiolysis of ethane in the presence of nitric oxide.

The present investigation was undertaken to provide further information as to density effects in ethane radiolysis particularly on the yields of products at very low conversions. The pressure dependence of parent-ion recapture of electrons has been considered theoretically by ElKomoss and Magee⁷ and Stevenson⁸ has treated the effects of pressure on parent-ion fragmentation and on ion-molecule reactions.

Experimental

Materials. Phillips research grade ethane was purified by passage through a column of brominated charcoal followed by three bulb-to-bulb distillations. The purified ethane contained less than 0.0002% each of methane and ethylene. Hexadeuterioethane, ob-

tained from Volk Radiochemical Co., contained approximately 7% C₂D₆H and less than 0.0002% ethylene and was used without purification. Hexadeuterioethane from Merck contained 5.5% C₂D₆H and approximately 1% ethylene. The ethylene content was reduced to less than 0.0002% by the purification procedure described above. Phillips research grade propylene, ethylene, and NO were purified by bulb-to-bulb distillation. Gas chromatographic analysis showed that the purified olefins contained less than 0.01%

(1) (a) The authors acknowledge with thanks helpful discussions with Professor Milton Burton. (b) The Radiation Laboratory of the University of Notre Dame is operated under contract with the U. S. Atomic Energy Commission. This is A.E.C. Document No. COO-38-362.

(2) L. M. Dorfman, *J. Phys. Chem.*, **62**, 29 (1958).

(3) R. A. Back, *ibid.*, **64**, 124 (1960).

(4) K. Yang and P. Gant, *ibid.*, **65**, 1861 (1961).

(5) G. Von Bünau and M. Burton, Abstracts, 137th National Meeting of the American Chemical Society, Cleveland, Ohio, April 1960, p. 46R.

(6) H. H. Carmichael and P. Ausloos, Abstracts, 146th National Meeting of the American Chemical Society, Denver, Colo., Jan. 1964, p. 3D.

(7) S. G. ElKomoss and J. L. Magee, *J. Chem. Phys.*, **36**, 256 (1962).

(8) D. P. Stevenson, *Radiation Res.*, **10**, 610 (1959).

hydrocarbon impurity; mass spectral analysis showed that the purified NO was free of detectable amounts of N_2O and NO_2 .

Sample Preparation. Irradiations at atmospheric pressure were carried out in a 230-ml. Pyrex bulb fitted with a break-seal. Irradiations in which the gas pressure exceeded 1 atm. were carried out in a stainless steel autoclave with a volume of 10.0 ± 0.1 ml. and an inner diameter of 1.15 cm. Measured volumes of purified ethane were condensed into the cell by means of liquid nitrogen. To prepare mixtures of gases, the individual components were measured consecutively and condensed into the cell.

Irradiation and Dosimetry. Two ^{60}Co γ -sources were used; a Ghormley-Hochanadel type source of approximately 800 c. and the Notre Dame 10,000-c. ^{60}Co facility. During irradiation of samples in the autoclave, the temperature was controlled within $\pm 1^\circ$ by circulating water from a constant temperature bath through a metal jacket surrounding the autoclave.

At densities above 0.075 g. cc^{-1} the absorbed dose was calculated by Fricke dosimetry. For samples irradiated in the autoclave at densities below 0.075 g. cc^{-1} , the doses calculated by Fricke dosimetry were corrected for wall effects using correction factors determined as described previously.⁹ Ethylene dosimetry was used to calculate the dose absorbed by samples irradiated in the glass cell at atmospheric pressure. $G(H_2)$ for ethylene was taken as 1.28.

Analysis. Hydrogen and methane were collected with a modified Saunders-Taylor apparatus and analyzed on a Consolidated 21-103A mass spectrometer. The fraction condensable at -196° was analyzed using an F and M Model 609 chromatograph with a flame ionization detector. Before gas chromatographic analysis, a measured quantity of methane ($\sim 0.02\%$) was added to each sample as an internal standard. Prepared standards of composition similar to that of the irradiated samples were run with each group of analyses for control purposes. Ethylene was analyzed on an activated charcoal column at 125° . Propane, propylene, and *n*-butane were analyzed on a silica gel column at 90° . Higher molecular weight hydrocarbons were analyzed on three columns: silica gel at 125° , silicone grease at 50° , and β,β -oxydipropionitrile at room temperature. Helium carrier gas was used in all cases.

Results

Dose Effects. Yields in μ moles of hydrogen, *n*-butane, and ethylene from γ -radiolysis of ethane at a density of 0.075 g. cc^{-1} are plotted in Figure 1 as a

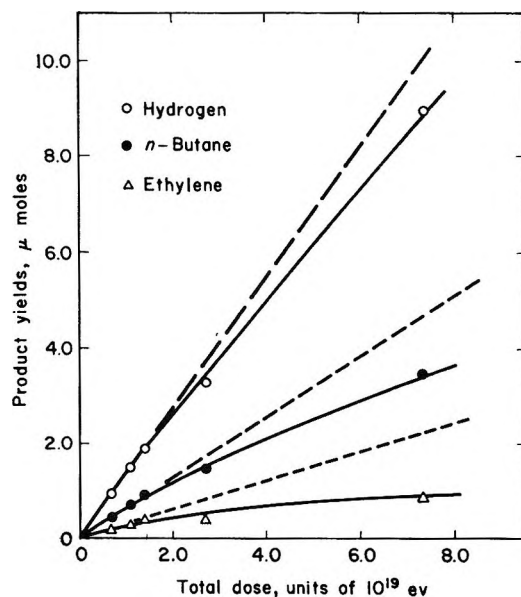


Figure 1. Product yields as a function of absorbed dose for the ^{60}Co γ -radiolysis of ethane; density, 0.075 g. cc^{-1} .

function of absorbed dose. Similar results were obtained at 0.001 and 0.240 g. cc^{-1} . At all densities; yields of hydrogen and *n*-butane are linear functions of absorbed dose only for conversions below about 0.01% . The ethylene yield decreases so sharply with dose that it is difficult to obtain a true initial yield.

For all runs at densities greater than 0.001 g. cc^{-1} , the temperature was $40 \pm 1^\circ$; at 0.001 g. cc^{-1} , the temperature was 25° . Irradiations of ethane at densities of 0.02 , 0.05 , and 0.075 g. cc^{-1} gave the same yields of products at 25 and 40° indicating that this small temperature difference is of no consequence.

Hydrogen Yields. Figure 2 shows the variation with gas density of $G(H_2)$ from γ -radiolysis of ethane in absence and in presence of ethylene; these data are also summarized in Table I. In the absence of ethylene conversion was kept below 0.01% so that $G(H_2)$ -values are initial yields in molecules/100 e.v.

Table II gives the distribution at various densities of isotopic hydrogens from radiolysis of 1:1 mixtures of ethane and ethane- d_6 in the presence of 2.8 mole % of ethylene. No correction has been made for the small amount of ethane- d_5 impurity in the ethane- d_6 .

Other Products. Variations with density of G -values of ethylene and *n*-butane from radiolysis of ethane are shown in Figure 3. $G(n-C_4H_{10})$ -values are initial yields but, because of the marked dose effect in the case of ethylene, $G(C_2H_4)$ -values are probably lower than the true initial yields. Yields of butane

(9) Y. Toi, D. B. Peterson, and M. Burton, *Radiation Res.*, **17**, 399 (1962).

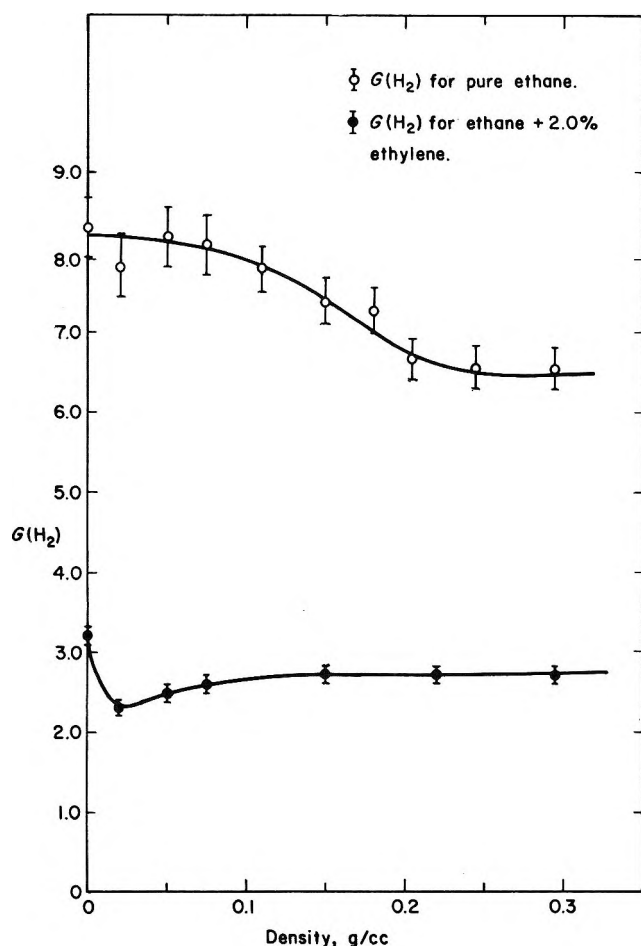


Figure 2. Variation in $G(\text{H}_2)$ with density for ^{60}Co γ -radiolysis of ethane in the absence and presence of ethylene.

Table I: Variation of $G(\text{H}_2)$ for Radiolysis of Ethane in Absence and in Presence of Ethylene

Density, g. cc. ⁻¹	$G(\text{H}_2)$, molecules/100 e.v.		G_{H}
	Pure ethane	Ethane and ethylene ^a	
0.001	8.3	3.2	5.1
0.020	7.8	2.3	5.5
0.050	8.2	2.5	5.7
0.075	8.1	2.6	5.5
0.150	7.4	2.7	4.7
0.240	6.6	2.7	3.9
0.292	6.6	2.7	3.9

^a 2 mole % of ethylene.

and ethylene from radiolysis of ethane in the presence of 3 mole % of NO are summarized in Table III.

Methane and propane yields were also determined. $G(\text{CH}_4)$ increases slowly with increasing density from about 0.50 at a density of 0.001 g. cc.⁻¹ to about 0.8

Table II: Distribution of Isotopic Hydrogens from Radiolysis of 1:1 Ethane-Ethane- d_6 in the Presence of Ethylene^a

Density, g. cc. ⁻¹	%			HD/D:
	H ₂	HD	D ₂	
0.001	52.5	10.2	37.4	0.27
0.020	54.4	10.7	34.8	0.31
0.075	54.2	15.0	30.8	0.49
0.240	54.8	20.2	25.0	0.81
0.293	54.3	20.8	24.8	0.84

^a 2.8 mole % of ethylene.

Table III: Butane and Ethane Yields from Radiolysis of Ethane in the Presence of NO^a

Density, g. cc. ⁻¹	$G(n\text{-C}_4\text{H}_{10})$	$G(\text{C}_2\text{H}_6)$
0.001	0.40	2.0
0.075	0.39	1.7
0.240	0.25	1.2

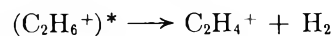
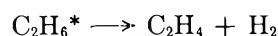
^a 3.0 mole % of nitric oxide.

at 0.240 g. cc.⁻¹. $G(\text{C}_3\text{H}_8)$ is essentially constant at 0.75 over the entire density range. The carbon to hydrogen ratios calculated from product yields is 1:3.49 at 0.001 g. cc.⁻¹, 1:3.25 at 0.075 g. cc.⁻¹, and 1:3.07 at 0.240 g. cc.⁻¹.

Discussion

Hydrogen Formation. $G(\text{H}_2)$ from γ -radiolysis of pure ethane decreases with increasing density as shown by the upper curve in Figure 2.

From previous studies with additives such as ethylene and nitric oxide,²⁻⁴ it has been concluded that about 60% of the total hydrogen yield at atmospheric pressure (0.001 g. cc.⁻¹) is the result of thermal hydrogen atoms. Presumably, in the absence of a scavenger, these thermal hydrogen atoms produce H_2 by abstraction from ethane. The remaining 40% of the H_2 yield is attributed to simple molecular detachment processes, *e.g.*



Application of this technique to radiolysis of ethane at higher densities¹⁰ shows that thermal hydrogen atoms contribute significantly to $G(\text{H}_2)$ up to the highest density studied, 0.3 g. cc.⁻¹ (Table I or Figure 2).

(10) C. M. Wodetzki, P. A. McCusker, and D. B. Peterson, *J. Phys. Chem.*, **69**, 1056 (1965).

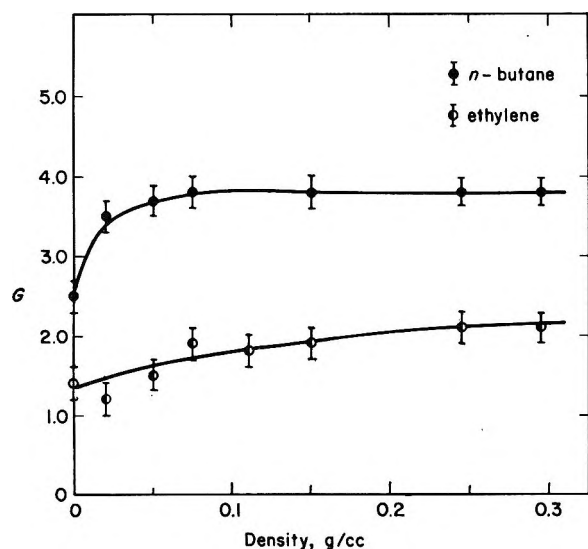


Figure 3. Variation of G -values of products with density in the ^{60}Co γ -radiolysis of ethane.

However, G_{H} , the yield of thermal hydrogen atoms, decreases at high densities. The observation that the nonradical (*i.e.*, unscavenged) yield of H_2 is nearly independent of density shows that the decrease in $G(\text{H}_2)$ with density in radiolysis of pure ethane is equal to the decrease in G_{H} . The apparent corollary that simple molecular detachment is little influenced by density, however, does not hold as shown by results in Table II. The relatively high yield of HD from radiolysis at high densities of 1:1 mixtures of C_2D_6 and C_2H_6 in the presence of ethylene demonstrates clearly that hydrogen is produced by a bimolecular process (uninhibited by ethylene) as well as by molecular detachment; the increase in HD/ D_2 with density shows that the importance of this bimolecular process increases with density. Apparently this increase is nearly balanced by a decrease in molecular detachment because the total yield of hydrogen from radiolysis of ethane in the presence of ethylene is nearly independent of density.

Thus, the over-all decrease with density of $G(\text{H}_2)$ from γ -radiolysis of pure ethane reflects a combination of decreases in simple molecular detachment and production of thermal hydrogen atoms and an increase in an unspecified bimolecular process which is uninhibited by ethylene.

These effects are, in turn, reasonably attributed to decreased importance of ion-fragmentation processes at high densities. From the theory of unimolecular dissociation of ions Stevenson⁸ has calculated that f_p , the fraction of ethane parent ions remaining undissociated, is 0.38 at 10^{-10} sec. This calculation indicates that, at a density of 0.001 g. cc.⁻¹ where the collision

time is about 10^{-10} sec., fragmentation competes very effectively with ion-molecule reactions. However, at 10^{-12} sec., which corresponds to the collision time at densities of about 0.10 g. cc.⁻¹, f_p is nearly 1 and fragmentation competes much less effectively. Fragmentation and the subsequent neutralization of fragment ions are expected to be important sources of thermal hydrogen atoms and molecular hydrogen.

The previously unspecified bimolecular process which contributes to the yield of hydrogen in presence of ethylene may be an ion-molecule reaction which permits mixing of hydrogens such as shown in (1) followed by reaction 2. Reaction 1 has been observed



recently in the mass spectrometer at a pressure of 0.08 mm.¹¹ Ausloos and Carmichael have suggested that it is important in radiolysis of ethane at high pressures.⁶ The increasing importance of the bimolecular process with increasing density, indicated by data in Table II, is readily accounted for by reaction 1 if ion fragmentation decreases with increasing density as proposed.

At high densities parent-ion recapture of electrons may also compete with fragmentation and thus contribute to the observed effects of density. Magee and ElKomoss⁷ have found, from a theoretical treatment of this problem, that the probability of parent-ion recapture increases rapidly at pressure in the region of 100–200 atm. (ideal gas pressure) for O_2 , N_2 , and H_2 . Calculations have not been made for ethane but it can be reasonably assumed that the probability of parent-ion recapture in ethane increases significantly as the density approaches the upper end of the range covered in this study. Recapture will produce highly excited ethane molecules in singlet and in triplet states. Little is known about dissociation of such states except that the low-lying singlet excited states of ethane preferentially dissociate by molecular detachment of hydrogen.¹² The observation that G of ethyl radicals increases with increasing density suggests that, if parent-ion recapture is important, the excited state of ethane so produced dissociates preferentially to ethyl radicals and hydrogen atoms. If some of these hydrogen atoms are hot, the observed increase with density of production of hydrogen by a bimolecular process uninhibited by ethylene is also explained. However, on the basis of existing data, it is impossible to choose between a hot atom

(11) G. A. Derwish, A. Galli, A. Guardini, and G. G. Volpi, *J. Chem. Phys.*, **40**, 5 (1964).

(12) R. F. Hampson, Jr., J. R. McNesby, H. Akemito, and Y. Tanaka, *ibid.*, **40**, 1099 (1964).

process and the ion-molecule process discussed earlier. It is quite possible that both contribute to $G(\text{H}_2)$.

Butane Formation. The second most important product of γ -radiolysis of ethane at all densities is *n*-butane. Figure 3 shows that $G(n\text{-C}_4\text{H}_{10})$ increases from 2.4 to 3.8 as the density is increased from 0.001 to 0.075 g. cc.⁻¹ and then remains essentially constant up to the highest density studied. Addition of NO reduces $G(n\text{-C}_4\text{H}_{10})$ to 0.4 or lower at all densities, indicating that butane is formed almost exclusively by combination of ethyl radicals at all densities.

Thus, the observed increase in $G(n\text{-C}_4\text{H}_{10})$ with increasing density can be attributed to increased production of ethyl radicals. Further evidence that the production of ethyl radicals increases with density has been obtained from studies of the radiolysis of ethane in the presence of propylene.¹⁰

The increase in $G(\text{ethyl})$ is consistent with the proposed interpretation of the effect of density on $G(\text{H}_2)$. Decreased ion fragmentation should increase the probability of ethyl formation directly, as well as indirectly, through its effect on reactions such as 1 or its equivalent. Ion fragmentation, also, is expected to produce unsaturated free radicals which may react with ethyl and thus reduce $G(n\text{-C}_4\text{H}_{10})$. Presumably, a variety of unsaturated products would be formed in such low yields as to be undetectable. Evidence that this may be of some importance is provided by a comparison of

the material balance at various densities. At 0.001 g. cc.⁻¹, C/H is 1:3.49, in good agreement with the value reported by Yang and Gant.⁴ As the density is increased, the material balance is improved and, at 0.240 g. cc.⁻¹, the balance is excellent.

Ethylene Formation. Initial values of $G(\text{C}_2\text{H}_4)$ are difficult to determine because of dose effects which are important even at very low conversion and, for that reason, $G(\text{C}_2\text{H}_4)$ values in Figure 3 are probably all lower than the true initial yields. Nonetheless, the slight increase in $G(\text{C}_2\text{H}_4)$ with density is considered experimentally significant. An increase in $G(\text{C}_2\text{H}_4)$ of the order of 0.2 would be expected on the basis of the observed increase in $G(n\text{-C}_4\text{H}_{10})$ because of increased ethyl-ethyl disproportionation. The observed increase is somewhat larger but, because of the experimental uncertainties in $G(\text{C}_2\text{H}_4)$, this difference may not be significant.

From studies of radiolysis of ethane in the presence of NO, it has been concluded that, at 0.001 g. cc.⁻¹, most of the ethylene is the result of nonradical processes.⁴ Attempts to use NO to determine the nonradical yield of ethylene at higher gas densities were unsuccessful because NO participates in a chain reaction which generates nitrogen and NO₂.¹¹ The NO₂ attacks olefins so that $G(\text{C}_2\text{H}_4)$ -values obtained under such conditions are low and not a good measure of the yield of nonradical ethylene.

Sedimentation Equilibria in Polydisperse Pseudo-Ideal Solutions and at Low Centrifugal Fields

by H. W. Osterhoudt and J. W. Williams

Laboratory of Physical Chemistry, University of Wisconsin, Madison, Wisconsin (Received November 13, 1964)

Equations which provide an accurate description of the concentration gradients for a polydisperse component at sedimentation equilibrium under pseudo-ideal conditions are presented in part I. Consideration of the centrifugal field as a quantity to be varied from experiment to experiment suggests a new method for measuring the "weight," " z ," and " $z + 1$ " average molecular weights. The quantities M_w and M_z now appear as the slopes of linear plots of experimentally measurable quantities *vs.* the magnitude of the field. The utility of these equations was tested experimentally by the performance of two series of sedimentation equilibrium experiments at several low rotor speeds with two different polystyrenes in solution at the Flory temperature. The data confirm the predictions as to the shapes and intercepts of the several plots. The application of the Schulz function to describe the actual differential molecular weight distribution of the two polystyrenes is also considered. In part II, an examination of the equations which describe the sedimentation equilibrium of a polydisperse polymer in a "good solvent" indicates that series of experiments performed at several low centrifugal fields and at several low concentrations ought to permit the evaluation of the light scattering second virial coefficient.

Introduction

The essential working equations for the sedimentation equilibrium experiment derive from classical thermodynamics. As they pertain to the ultracentrifuge, contributions of Svedberg,^{1,2} Rinde,³ and Lansing and Kraemer⁴ provide a substantial introduction to the subject. The equations of Rinde for the sedimentation equilibrium of a polydisperse solute were given in a form similar to the ones used today. Furthermore, it is evident from these equations that a description of the molecular weight distribution may be drawn from them. Lansing and Kraemer demonstrated how the results of an experiment could be interpreted to provide several average molecular weights which they had defined.

Although there was at once considerable interest in this experiment with the advent of the ultracentrifuge there had been little concern with regard to the effect of nonideal solution behavior on the establishment of equilibrium. In independent endeavors and with but slightly different assumptions Schulz⁵ and Wales, Bender, Williams, and Ewart⁶ extended sedimentation equilibrium theory by allowing for the effects of the ap-

parent gradients of osmotic pressure in the ultracentrifuge cell. With this beginning Wales and associates went on to describe several systems in considerable detail, indeed to the extent that it might be said their equations are the precursors of the more elegant relationships which are to be found in the Fujita monograph,⁷ ones which we shall adopt.

The report is divided into two main parts. The first has to do with the determination of molecular weight distributions in an organic high polymer system by the construction of a curve which fits the observed moments M_w , M_z , and M_{z+1} . This method, an extension

- (1) T. Svedberg, *Kolloid Z. Erg. Bd.*, **36**, 53 (1925).
- (2) T. Svedberg, *Z. physik. Chem.*, **121**, 65 (1926).
- (3) H. Rinde, Dissertation, Uppsala, 1928.
- (4) W. D. Lansing and E. O. Kraemer, *J. Am. Chem. Soc.*, **57**, 1369 (1935).
- (5) G. V. Schulz, *Z. physik. Chem.*, **A193**, 168 (1944).
- (6) M. Wales, M. M. Bender, J. W. Williams, and R. H. Ewart, *J. Chem. Phys.*, **14**, 353 (1946); *cf.* also M. Wales, *et al.*, *J. Phys. Chem.*, **52**, 235, 983 (1948).
- (7) H. Fujita, "Mathematical Theory of Sedimentation Analysis," Academic Press, Inc., New York and London, 1962, Chapter V.

of the Lansing-Kraemer treatment, is based upon the assumption that an exponential distribution which contains these moments as parameters is a good approximation to the true distribution curve. In arriving at the several moments we present a new approach which makes use of a series of experiments performed at several low centrifugal fields.

In the second part we indicate that a conclusion of Mandelkern, Williams, and Weissberg⁸ to the effect that interpretable measurements on high polymers can be made only at the Flory temperature is probably incorrect. An examination of the equations which describe the sedimentation equilibrium in a "good" solvent indicates that series of experiments performed at several low centrifugal fields and several low concentrations ought to allow the evaluation of the light scattering second virial coefficient.

Part I. Pseudo-Ideal, Incompressible Solutions

Theory. A component of a solution is at sedimentation equilibrium when its total potential is constant from phase to phase as distance in the cell varies from the center of rotation. If the polymeric solute components and the medium are adjusted to the Flory temperature, if the initial solute concentration is low, and if the solution is incompressible, one finds

$$\frac{-dc_t}{d\xi} = \lambda M_t c_t \quad (1)$$

Here

$$\xi = \frac{b^2 - r^2}{b^2 - a^2}$$

The quantities a , b , and r are the radial distances of the top, the bottom, and any arbitrary intermediate cell position. The quantity λ , to which frequent reference will be made, is defined as

$$\lambda = \frac{(1 - \bar{v}\rho_0)\omega^2(b^2 - a^2)}{2RT}$$

in which the several quantities have their usual significance. It has the units moles per gram.

Making use of this basic statement it can be shown that

$$c(\xi) = c_0 \int_0^\infty \frac{\lambda M f(M) e^{-\lambda M \xi}}{1 - e^{-\lambda M}} dM \quad (2)$$

and by differentiation with respect to ξ

$$\frac{-dc}{d\xi} = c_0 \int_0^\infty \frac{\lambda^2 M^2 f(M) e^{-\lambda M \xi}}{1 - e^{-\lambda M}} dM \quad (3)$$

Integration of eq. 3 yields

$$\frac{\Delta c}{c_0} = \lambda M_w \quad (4)$$

Here Δc is the difference in equilibrium concentration at the top and bottom of the cell, and c_0 is the original solute concentration in grams per ml.

Equations 2, 3, and 4 are important for us in that they provide a means by which several average molecular weights for a given polymer sample may be computed. The first two of them appear in the Fujita book as eq. 5.171 and 5.172, where the assumptions under which they have been derived are clearly delineated. The quantity $f(M)dM$ is the weight fraction of the total sample which lies between molecular weights M and $M + dM$.

In terms of the continuous distribution function, the weight, "z," and "z + 1" average molecular weights are defined as

$$M_w = \int_0^\infty M f(M) dM \quad (5)$$

$$M_z = \frac{\int_0^\infty M^2 f(M) dM}{\int_0^\infty M f(M) dM} \quad (6)$$

$$M_{z+1} = \frac{\int_0^\infty M^3 f(M) dM}{\int_0^\infty M^2 f(M) dM} \quad (7)$$

For their evaluations we describe three quantities

$$P(\lambda) = \frac{-1}{\lambda c_0} \left(\frac{dc}{d\xi} \right)_{\xi=0} = M_w + \frac{\lambda}{2} M_w M_z + \frac{\lambda^2}{12} M_w M_z M_{z+1} - \frac{\lambda^4}{720} M_w M_z M_{z+1} M_{z+2} M_{z+3} + \dots \quad (8)$$

$$Q(\lambda) = \frac{-1}{\lambda c_0} \left(\frac{dc}{d\xi} \right)_{\xi=1/2} = M_w - \frac{\lambda^2}{24} M_w M_z M_{z+1} + \frac{7}{5760} \lambda^4 M_w M_z M_{z+1} M_{z+2} M_{z+3} + \dots \quad (9)$$

$$R(\lambda) = \frac{-1}{\lambda c_0} \left(\frac{dc}{d\xi} \right)_{\xi=1} = M_w - \frac{\lambda}{2} M_w M_z + \frac{\lambda^2}{12} M_w M_z M_{z+1} - \frac{\lambda^4}{720} M_w M_z M_{z+1} M_{z+2} M_{z+3} + \dots \quad (10)$$

These equations should be adequate descriptions of the respective gradients if $\lambda \leq 1/M_w$. It will be noted that

(8) L. Mandelkern, L. C. Williams, and S. G. Weissberg, *J. Phys. Chem.*, **61**, 271 (1957).

the quantities $P(\lambda)$, $Q(\lambda)$, and $R(\lambda)$ have the units grams per mole.

The expression which involves the concentration gradient at the cell meniscus, $R(\lambda)$, may be subtracted from or added to the corresponding equation descriptive of the condition at the bottom of the cell, $P(\lambda)$, to give

$$P(\lambda) - R(\lambda) = \lambda M_w M_z \quad (11)$$

$$P(\lambda) + R(\lambda) = 2M_w + \frac{\lambda^2}{6} M_w M_z M_{z+1} - \frac{\lambda^4}{360} M_w M_z M_{z+1} M_{z+2} M_{z+3} + \dots \quad (12)$$

So, if the solution is subjected to relatively low centrifugal fields, the quantity λ can be kept within the range $0 < \lambda \leq 1/M_w$. Equations 4 and 8-12 then should furnish methods for obtaining M_w , M_z , and M_{z+1} . The average, M_w , is evaluated from the slope of the plot $\Delta c/c_0$ vs. λ . The product of M_w and M_z is obtained by way of the slope of a $P(\lambda) - R(\lambda)$ vs. λ graph, while the curves of $Q(\lambda)$ vs. λ^2 and $P(\lambda) + R(\lambda)$ vs. λ^2 yield $M_w M_z M_{z+1}$ values as limiting slopes.

Experimental. A Spinco Model E ultracentrifuge was employed in the performance of the sedimentation equilibrium experiments. For them rotor speeds of 4500 r.p.m. or less were required, so that it was necessary to use the 22-pound rotor to reduce effects of precession and fluctuations in speed. Cells were of the double sector type, with solvent in one of the compartments to provide the reference experiment. The location of the bottom of the solution column was achieved by way of the "false bottom" technique with an immiscible heavy liquid, in these experiments anhydrous glycerol. The schlieren optical system measured the concentration gradients directly.

The experiments were carried out with the system polystyrene-cyclohexane at the Flory temperature, 35.0°. The solvent, a Baker reagent grade chemical, was distilled from lithium aluminum hydride to remove traces of water just prior to use. Polymer and solvent were weighed into glass-stoppered flasks for the dissolution process, which required warming at 45° for 72 hr. Loading of the centrifuge cell was achieved in the usual way; the temperature control circuit of the instrument maintained the proper temperature. The camera was loaded with Kodak Type II-G spectroscopic plates. A Kodak 77A filter was placed between the light source and the rotor chamber.

The value of the quantity λ was fixed for each experiment but the height of the solution column was arbitrarily varied. With 2-mm. columns the equilibrium time was generally less than 1 day. After the schlieren

image appeared to be unchanged with time for some 12 hr. a series of photographs was taken in which different orientations of the schlieren phase plate were used. After the image had been recorded the rotor speed was adjusted to a new (higher) λ value and a new equilibrium established. Thus, as many as four experiments, each involving a different λ value, were performed in a single series.

Two different polystyrenes were involved. One of these, designated as 19F, originally distributed by the Dow Chemical Co., has been the subject of several physical chemical characterizations.⁹ The second sample, PS-706, was provided by the U. S. National Bureau of Standards, also with certain molecular characteristic constants.

Data and Results. The concentration of any given solution was computed by making use of the relationship $\rho = \rho_0 + (1 - \bar{v}\rho_0)c$. In it, ρ is the solution density in g./ml., ρ_0 is the solvent density as taken from the International Critical Tables, \bar{v} is the partial specific volume of the polystyrene, taken to be 0.930 ml./g., and c is the solute concentration in grams per ml. The density calculated from this relationship by using a concentration based upon the original solvent and solute weights permitted an estimate of the total volume of the solution and therefore a revised concentration. By successive approximation a final value of the concentration was made available.

The schlieren patterns, two photographs for each sedimentation equilibrium experiment, were analyzed by means of a Gaertner plate reader. Displacements, Δz , were plotted against comparator readings, R , as measures of distances from the center of rotation. Then, a smooth curve was drawn and extrapolated to the meniscus and cell bottom positions.

The area under this curve is related to the concentration change over the cell. Thus

$$\Delta c = c(b) - c(a) = \int_a^b \frac{dc}{dr} dr = \frac{10^{-2}}{F \frac{dn}{dc} GAB \tan \theta} \int_a^b \Delta z dR \quad (13)$$

where dR is the differential radial distance as read from the photographic plate, the factors F , G , A , B , and $\tan \theta$ are the constants of the schlieren optical system, and 10^{-2} is the transformation constant for the conversion of mm. to cm. The refractive index increment, dn/dc , for polystyrene in cyclohexane was taken to be 0.1705

(9) J. E. Blair and J. W. Williams, *J. Phys. Chem.*, **68**, 161 (1964).

ml./g., the datum reported by McIntyre and co-workers.¹⁰

Calculations for the quantities $P(\lambda)$, $Q(\lambda)$, and $R(\lambda)$ require the transformation

$$\frac{dc}{d\xi} = -\frac{(b^2 - a^2)}{2r} \frac{dc}{dr} \quad (14)$$

The slopes of the linear plots of $\Delta c/c_0$ vs. λ and $P(\lambda) - R(\lambda)$ vs. λ were determined by least-squares analysis. In each case the intercept was taken to be the origin, as required by eq. 4 and 11. The nonlinear plots, such as $Q(\lambda)$ vs. λ^2 , were fitted where possible so that the sum of the deviations of the individual points was approximately zero. They were extrapolated to an intercept which had been previously determined by a least-squares analysis of a linear plot. For example, M_w , the intercept of the $Q(\lambda)$ vs. λ^2 curve, was accurately known from the slope of the $\Delta c/c_0$ vs. λ plot.

For the polystyrene PS-706 there are presented in Figures 1-5 plots of the several functions of λ vs. λ or

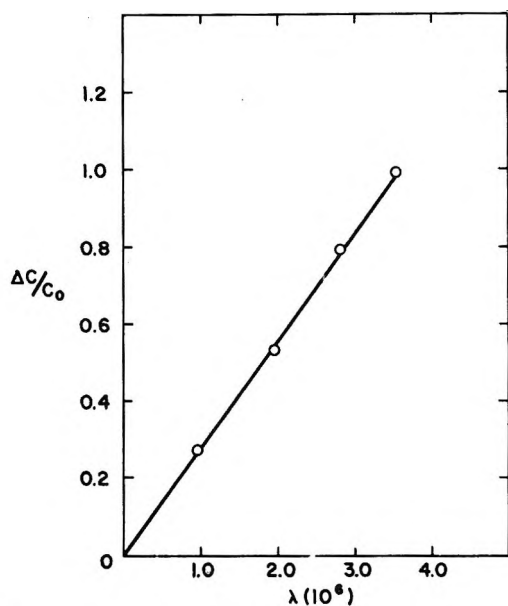


Figure 1. $\Delta c/c_0$ vs. λ for PS-706.

λ^2 . From their intercepts and limiting slopes and based on eq. 4 and 8-12, values of M_w , $M_w M_z$, and $M_w M_2 M_{z+1}$ were obtained. In this way, the successive moments of the molecular weight distribution curve are supplied. Entirely analogous graphs for the polystyrene 19F lead to similar data.

This information has been utilized in connection with the well-known Schulz distribution function¹¹ to describe the heterogeneity of the two polymers. The differential weight distribution may be expressed as

$$(M) = \frac{1}{\Gamma(b+2)} \left(\frac{b+2}{M_w} \right)^{b+2} M^{b+1} \times \exp -(b+2)M/M_w \quad (15)$$

It contains two adjustable parameters, b and M_w .

For the polystyrene PS-706 and 19F we have made use of the equations

$$f(M) = 1.82 \times 10^{-13} M^{1.5} \exp[-8.99 \times 10^{-6} M] \\ b = 0.5; M_w = 2.78 \times 10^5$$

and

$$f(M) = 6.89 \times 10^{-9} M^{0.5} \exp[-3.34 \times 10^{-6} M] \\ b = -0.5; M_w = 4.49 \times 10^6$$

There have been assembled in Table I the several moments for the two samples. Compared are the

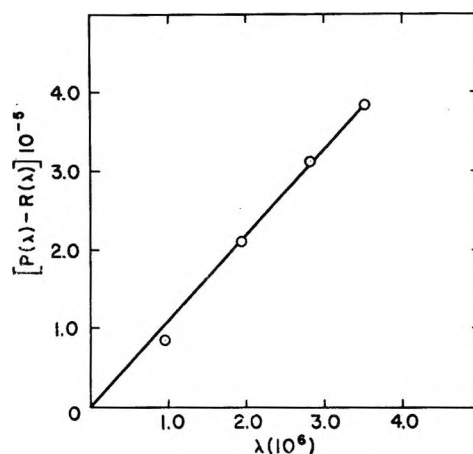


Figure 2. $[P(\lambda) - R(\lambda)]$ vs. λ for PS-706.

moments which were obtained from the sedimentation equilibrium experiments performed at different values of λ and those computed from the Schulz function with the parameters indicated. Also included in this table are the two number-average molecular weights, M_n , both obtained by osmometry, in one case at the National Bureau of Standards and in the other at the University of Wisconsin.¹² It is seen that observed and calculated values of M_n do not show good agreement.

Discussion. There have been presented equations which provide an accurate description of the concentration gradients of a polydisperse solute at sedimentation equilibrium under pseudo-ideal conditions and when low centrifugal fields are employed. Consideration of the

(10) D. McIntyre, A. Wims, L. C. Williams, and L. Mandelkern, *J. Phys. Chem.*, **66**, 1932 (1962).

(11) G. V. Schulz, *Z. physik. Chem.*, **B43**, 25 (1939).

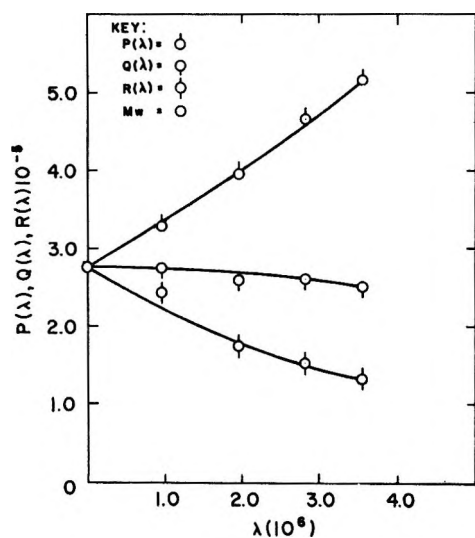
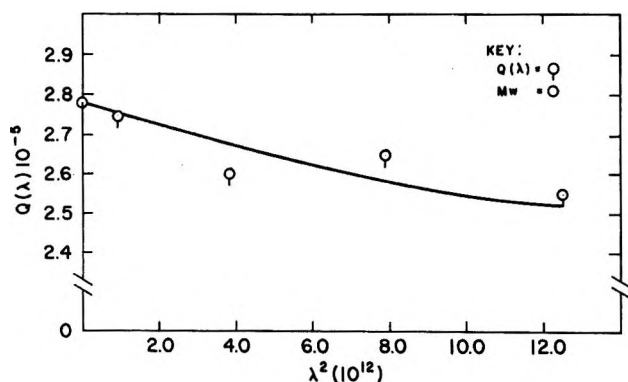
(12) L. D. Grandine, Jr., Dissertation, 1952.

Table I: Moments for Polystyrene PS-706 and 19F

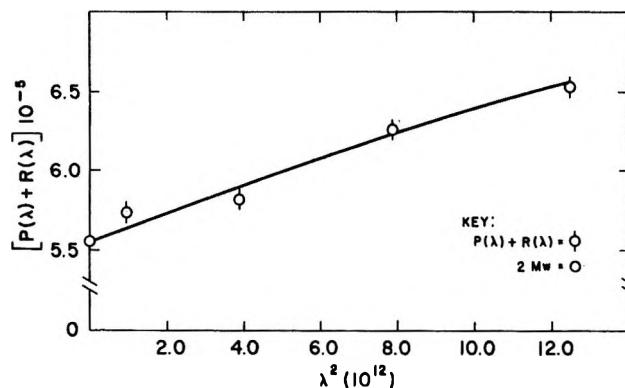
	PS-706		19F		
	Experimental	Schulz distribution	Experimental this research	A.M.L. ^a	Schulz distribution
M_w	$(2.78 \pm 0.05) \times 10^5$	2.78×10^5	$(4.49 \pm 0.08) \times 10^5$	4.56×10^5	4.49×10^5
$M_w M_z$	$(1.09 \pm 0.02) \times 10^{11}$	1.08×10^{11}	$(3.25 \pm 0.07) \times 10^{11}$	3.47×10^{11}	3.37×10^{11}
$M_w M_z M_{z+1}^b$	$(5.32 \pm 0.39) \times 10^{16}$	5.42×10^{16}	$(3.77 \pm 0.41) \times 10^{17}$	3.40×10^{17}	3.53×10^{17}
M_n	1.365×10^5	1.67×10^5	$(1.97 \pm 0.10) \times 10^5$		1.5×10^5

^a Results of Mrs. A. M. Linklater, Communicated in Progress Report, Aug. 1, 1957–Oct. 31, 1958 to Department of the Navy, Bureau of Ordnance, Contract N 123-60530S-1979A. Sedimentation equilibrium experiments at a single rotor speed in cyclohexane at 34.2°.

^b For each polystyrene the figure presented for the moment $M_w M_z M_{z+1}$ is an average of the values obtained from the limiting slopes of eq. 9 and 12 and the value obtained by using eq. 5.175 of Fujita.⁷ Data from the experiments in which $\lambda \cong 1/M_w$ were used.

Figure 3. $P(\lambda)$, $Q(\lambda)$, and $R(\lambda)$ vs. λ for PS-706.Figure 4. $Q(\lambda)$ vs. λ^2 for PS-706.

field as a quantity to be varied from experiment to experiment has suggested a new method for measuring M_w , M_z , and M_{z+1} in which the first two now appear as the slopes of linear plots, while the third one is obtained from the limiting slopes of certain quantities plotted

Figure 5. $[P(\lambda) + R(\lambda)]$ vs. λ^2 for PS-706.

against the square of the field strength. The utility of the plots and the equations upon which they are based have been amply tested. The Schulz function to describe the actual molecular weight distribution seems to provide a useful specification.

However, for the polystyrene 19F, a distribution somewhat different from the one previously reported⁹ from sedimentation velocity data was provided by this analysis. It is believed that this inconsistency arises from uncertainties in the several constants employed in the equilibrium and in the transport equations. As regards the latter, the doubt lies in the quantities which are used in the equation which relates sedimentation coefficient to molecular weight, namely $s = KM^a$. Thus, the reports of Cantow¹³ and McCormick¹⁴ give for a the values 0.48 and 0.51; but Blair and Williams adopted the theoretical value 0.50 for the pseudo-ideal system. Had the latter taken $a = 0.49$ for their computations the two distribution curves would have been in quite good agreement.

(13) H. J. Cantow, *Makromol. Chem.*, **30**, 169 (1959).(14) H. W. McCormick, *J. Polymer Sci.*, **36**, 341 (1959).

The value of M_w for polystyrene PS-706 obtained by sedimentation equilibrium at the National Bureau of Standards is $M_w = 2.88 \times 10^5$, as compared to our value $M_w = 2.78 \times 10^5$. Fractionation of the sample at NBS has provided the ratio $M_z/M_w = 1.4$. The ratio from this investigation is 1.41.

As ordinarily performed only a single value of λ is used in a sedimentation equilibrium experiment; on occasion this datum is missing from a published article. It would appear that the selection of a value for λ should be dictated by the kind of data sought in the experiment. If the quantities M_w , M_z , and the light scattering second virial coefficient are desired, λ should be ideally $0.5/M_w$. This condition (1) allows M_z to be readily computed from the concentration gradient at the top and at the bottom of the cell, and (2) provides insurance that a small correction only is to be applied to the sedimentation equilibrium second virial coefficient to obtain the corresponding light scattering quantity (*cf.* part II). If the experiment is to be performed at the Flory temperature and the quantities M_w , M_z , and M_{z+1} are sought, λ should be approximately $1/M_w$ because the calculation of M_{z+1} requires an appreciable difference between the slopes of the $dc/d\xi$ vs. ξ curve at the two ends of the cell.

Part II. Nonideal Systems

Theory and Discussion. With relatively few exceptions the polydisperse polymer-solvent systems encountered in practical laboratory work are nonideal in behavior. For them the equations are more cumbersome because the distribution of the several species at each radial distance will differ from that of the original solute, and the correction for the nonidealities depends both on the total concentration and on the molecular weight distribution at any given distance from the center of rotation. While there may be doubt on the part of some investigators whether the experiment being considered may be used to study solute-solvent interactions, the problem has attracted attention in this laboratory. Thus, by way of improving the situation as it stood in 1957,⁸ Fujita has derived expressions for the intercept and the limiting slope of a plot of $1/(M_w)_{app}$ vs. c_0 for systems not too far removed from the Flory temperature and as c_0 becomes very small. It was shown⁷ that this intercept permits evaluation of the weight-average molecular weight of the solute and the limiting slope can be correlated with the second virial coefficient obtained from light scattering measurements, B_{LS} . The quantity $(M_w)_{app}$ is given experimentally by the use of the equation

$$(M_w)_{app} = [(c)_{\xi=0} - (c)_{\xi=1}]/\lambda c_0$$

or its equivalent. For the low concentrations the resulting equation of Fujita is

$$\frac{1}{(M_w)_{app}} = \frac{1}{M_w} + B''c_0 \quad (16)$$

where

$$B'' = \left[1 + \frac{\lambda^2 M_z^2}{12} \right] B_{LS}$$

$$B_{LS} = \left(\frac{1}{M_w^2} \right) \sum_{i=1}^q \sum_{k=1}^q f_i f_k M_i M_k (B_{ik} + \bar{v}/M_k)$$

$$f_i = c_i^0/c_0; B_{ik} = \frac{1}{M_i} \left(\frac{\partial \ln y_i}{\partial c_k} \right)_{T,P,c_j \neq k}$$

The term $\lambda^2 M_z^2/12$ is a correction term, the magnitude of which may be controlled by adjustments of the quantity λ , or its equivalent, the rotor speed, ω .

We shall prefer to write eq. 16 in the form

$$\frac{\Delta c}{c_0} = \lambda(M_w - B_{LS}'c_0) + \dots \quad (17)$$

Here, B_{LS}' is the product of M_w^2 and B_{LS} . The higher terms which are neglected involve both λ and c_0 .

This equation can be derived by considering the expression which describes the concentration gradient of a simple polymer species at sedimentation equilibrium.¹⁵ It is

$$-\lambda M_i c_i = \frac{dc_i}{d\xi} + M_i c_i \sum_{k=1}^q B_{ik} \frac{dc_k}{d\xi} - \lambda M_i c_i \bar{v} \sum_{k=1}^q c_k \quad (18)$$

In order now to simplify the derivation we assume that we consider very dilute solutions at low centrifugal fields. Then, two approximations may be made

$$\frac{dc_k}{d\xi} \cong -\lambda M_k c_k$$

$$c_k(\xi) \cong \frac{c_k^0 \lambda M_k e^{-\lambda M_k \xi}}{1 - e^{-\lambda M_k}}$$

The results upon insertion of these into the expression for the concentration gradient is

$$-\lambda M_i c_i = \frac{dc_i}{d\xi} - \lambda^2 M_i c_i \times \sum_{k=1}^q \frac{c_k^0 M_k e^{-\lambda M_k \xi}}{1 - e^{-\lambda M_k}} (B_{ik} M_k + \bar{v}) \quad (19)$$

(15) This expression, except for a single substitution, is equation 5.103 of the Fujita monograph.

If the exponents in this equation are expressed as a series expansion it is seen that

$$-\lambda M_i c_i = \frac{dc_i}{d\xi} - \lambda M_i c_i \sum_{k=1}^q c_k^0 M_k (B_{ik} + \bar{v}/M_k) + O(\lambda^2) \quad (20)$$

Integration over the entire cell, remembering that $f_i = c_i^0/c_0$, yields

$$-\lambda M_i f_i c_0 = c_i(1) - c_i(0) - \lambda M_i f_i c_0^2 \sum_{k=1}^q f_k M_k (B_{ik} + \bar{v}/M_k) + \dots \quad (21)$$

Equation 17 is obtained from eq. 21 by summation over all components and rearrangement.

Thus, an examination of the equations which describe the sedimentation equilibrium of a polydisperse solute in a better than "poor" solvent indicates that series of

experiments performed at several low concentrations and at several low centrifugal fields ought to permit the evaluation of the light scattering second virial coefficient. The approximations made in the derivation become better as c_0 and λ decrease. The double plot which is indicated is quite analogous to the Zimm plot of the light scattering experiment in which a quantity related to the intensity of the scattered light is plotted in terms of both the initial polymer concentration and the angle to the incident beam at which the scattered light is observed.

Acknowledgments. The authors are indebted to Drs. E. T. Adams, Jr., and V. J. MacCosham for many fruitful discussions. The work itself was supported in part by the U. S. Army Research Office, under Contract DA-ORD-11, and in part by the University Research Committee, with funds supplied by the Wisconsin Alumni Research Foundation.

NOTES

Effect of Additives in Radiolysis of Ethane at High Densities

by Catherine M. Wodetzki, P. A. McCusker, and D. B. Peterson^{1a}

Department of Chemistry and the Radiation Laboratory,^{1b} University of Notre Dame, Notre Dame, Indiana 46556 (Received October 26, 1964)

In the course of an investigation² of the effect of density on the γ -radiolysis of gaseous ethane, the thermal hydrogen atom scavengers ethylene, propylene, and nitric oxide were employed as additives. In order to interpret results of such studies properly, it was necessary to examine critically the role of these additives in radiolysis and how this role depends upon density in the range 0.001 (atmospheric pressure) to 0.30 g. cc.⁻¹.

The three additives under consideration have frequently been employed as thermal hydrogen atom scavengers in studies of the mechanism of hydrogen formation in the radiolysis of gaseous hydrocarbons at

pressures near or below 1 atm.³⁻⁶ For a given hydrocarbon, $G(\text{H}_2)$ is reduced to the same plateau value by all three additives and it is generally assumed that this reduction is solely the result of scavenging of thermal hydrogen atoms. However, evidence supporting this assumption is rather limited and there is very little information concerning the use of these additives at high gas densities.

Experimental

Experimental details are described in an accompanying paper.²

(1) (a) The authors acknowledge with thanks helpful discussions with Professor Milton Burton. (b) The Radiation Laboratory of the University of Notre Dame is operated under contract with the U. S. Atomic Energy Commission. This is A.E.C. Document No. COO-38-361.

(2) C. M. Wodetzki, P. A. McCusker, and D. B. Peterson, *J. Phys. Chem.*, **69**, 1045 (1965).

(3) L. Dorfman, *ibid.*, **60**, 826 (1956).

(4) K. Yang and P. J. Manno, *J. Am. Chem. Soc.*, **81**, 3507 (1959).

(5) R. A. Back, *J. Phys. Chem.*, **64**, 124 (1960).

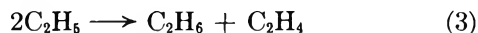
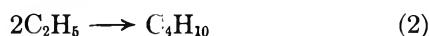
(6) K. Yang and P. Gant, *ibid.*, **65**, 1861 (1961).

Results and Discussion

Ethylene. Dorfman⁷ has shown that addition of ethylene to mixtures of C₂D₆ and C₂H₆ preferentially reduces HD production. This result is consistent with the assumption that ethylene inhibits production of hydrogen by scavenging thermal hydrogen atoms. More recently, Yang⁸ has studied the effect of ethylene and propylene on $G(\text{H}_2)$ from propane and found that the relative rates of reactions and the temperature dependence of these rates are also consistent with a simple mechanism involving hydrogen atom addition to the olefins.

In the present study, we have attempted to examine further the role of ethylene by measuring the yields of products of the scavenging reactions as well as the decrease in hydrogen. In these studies, the concentration of ethylene was high enough to reduce $G(\text{H}_2)$ from ethane to its plateau value.

If only hydrogen atom scavenging is involved, the significant reactions in the presence of ethylene are reactions 1-3. In the absence of ethylene, reaction 1



is replaced by hydrogen abstraction from ethane to give H₂ and C₂H₅, and, hence, addition of ethylene should reduce $G(\text{H}_2)$ but not $G(\text{C}_2\text{H}_6)$.

Because butane is formed almost exclusively by reaction 3,² $G(\text{butane})$ is a good measure of $G(\text{C}_2\text{H}_6)$. At low concentrations of ethylene, where the important reactions of ethyl radicals are 2 and 3 ($k_3/k_2 \sim 0.14$),⁹ a constant value of $G(\text{C}_2\text{H}_6)$ will result in a constant value of $G(\text{butane})$. If addition of ethyl radicals to ethylene becomes important, higher molecular weight products, particularly *n*-hexane, will be produced and the simple correlation between $G(\text{ethyl})$ and $G(\text{butane})$ will no longer hold.

Results in Table I show that at a density of 0.001 g. cc.⁻¹ addition of 2% ethylene reduces $G(\text{H}_2)$ from 8.1 to 3.2 without significantly affecting $G(\text{butane})$. At this density, products higher than C₄ are not detected in significant yield either in the absence or in the presence of ethylene, indicating that radical addition to ethylene is not important. Thus, we conclude that, at this density, ethylene functions solely as a hydrogen atom scavenger.

At a density of 0.075 g. cc.⁻¹, addition of ethylene again reduces $G(\text{H}_2)$ but $G(\text{butane})$ is also decreased. However, *n*-hexane, which is not detected in the absence of ethylene, is produced in relatively high yield clearly demonstrating that addition of ethyl

Table I: ⁶⁰Co γ -Radiolysis of Ethane. Effect of Ethylene^a

Density, g. cc. ⁻¹	[Ethylene], mole %	$G(\text{H}_2)$	$G(n\text{-C}_4\text{H}_{10})$	$G(n\text{-C}_6\text{H}_{14})$	$G(\text{C}_4\text{H}_8)$
0.001 ^b	0	8.3	2.4	0	~0.1
0.001 ^b	2	3.2	2.3	0	~0.1
0.075	0	8.1	3.8	0	~0.1
0.075	2	2.6	2.4	1.5	~0.1

^a Only products important to the discussion are included in Table I. ^b Irradiations at this density were carried out in glass vessels at ambient temperature ($\sim 25^\circ$). At 0.075 g. cc.⁻¹, irradiations were carried out in a stainless steel autoclave at $40 \pm 1^\circ$.

radicals to ethylene is important. This is not surprising because, although the mole percentage of ethylene is the same as at 0.001 g./cc., the molar concentration is much higher. Also, the temperature was higher at the higher density (see footnote b of Table I). Thus, at 0.075 g. cc.⁻¹ the prediction is that the sum of $G(\text{butane})$ and $G(\text{hexane})$ for radiolysis in the presence of ethylene should equal $G(\text{butane})$ for radiolysis in the absence of ethylene. This prediction is borne out by results in Table I and the conclusion is that ethylene continues to function simply as a radical scavenger at this density.

As a further test of the role of ethylene in radiolysis of ethane, the distribution of isotopic hydrogens from radiolysis of 3 mole % of C₂D₄ in C₂H₆ was determined at a density of 0.075 g. cc.⁻¹. The difference between the observed value of H₂:HD:D₂, 95:2.5:2.5, and that calculated on the assumption that ethylene functions solely as a thermal hydrogen atom scavenger, 98:0:2, is not considered experimentally significant.

Also, there was no evidence at any density that the presence of ethylene leads to production of butene,¹⁰ although butene would be expected to result from sensitized decomposition of ethylene.

These results indicate that energy transfer from ethane to ethylene does not occur to a significant extent under these conditions and, thus, further support the conclusion that ethylene functions simply as a radical scavenger in the density range 0.001 to 0.075 g. cc.⁻¹.

Propylene. Attempts to establish the role of propylene as an additive in radiolysis of ethane by complete

(7) L. Dorfman, *J. Phys. Chem.*, **62**, 29 (1958).

(8) K. Yang, *J. Am. Chem. Soc.*, **84**, 720 (1962).

(9) J. A. Kerr and A. F. Trotman-Dickenson, *Progr. Reaction Kinetics*, **1**, 111 (1961).

(10) A very small yield, $G \sim 0.2$, of butene is observed in radiolysis of pure ethane. This is unaffected by addition of C₂H₄.

product analysis were rather inconclusive because of the greater complexity of radical reactions. However, it was possible to obtain yields of 2,3-dimethylbutane, 2-methylbutane, and butane, which are the products of radical combination reactions involving isopropyl and ethyl radicals. (About 94% of the propyl radicals formed by addition of hydrogen atoms to propylene should be isopropyl.)¹¹ From these yields and values of ratios of disproportionation to combination, k_d/k_c , a value of $G(\text{propyl})$ can be calculated.

Calculated values of $G(\text{propyl})$ should equal the decrease in $G(\text{H}_2)$ produced by addition of propylene, $\Delta G(\text{H}_2)$. However, values of $G(\text{propyl})$ calculated in this way are 15–20% lower than $\Delta G(\text{H}_2)$ at all densities (Table II). This agreement is about as good as can be expected considering the uncertainties in ratios of disproportionation to combination but it is unsatisfactory for a quantitative evaluation of the role of propylene.

Table II: ⁶⁰Co γ -Radiolysis of Ethane. Effect of Propylene^a

Density, g. cc. ⁻¹	$\Delta G(\text{H}_2)^b$	$G(n\text{-C}_4\text{H}_{10})$	$G(\text{C}_2\text{H}_6)^c$	$G(\text{C}_3\text{H}_8)^d$	$G(\text{C}_2\text{H}_5)^e$	$G(\text{C}_2\text{H}_4)^e$
0.001	5.0	0.1	0.65	1.0	4.3	1.0
0.050	5.8	/	0.85	1.1	5.0	1.3
0.075 ^d	5.3	0.6	1.0	0.85	4.3	1.6
0.075	5.5	0.2	/	/	/	/

^a 2.0 mole % of propylene added. ^b $\Delta G(\text{H}_2)$ is the decrease in $G(\text{H}_2)$ produced by addition of propylene. ^c 2-Methylbutane. ^d 2,3-Dimethylbutane. ^e These values were calculated from product yields using k_d/k_c values of 0.64, 0.15, and 0.62 for isopropyl with isopropyl, ethyl with ethyl, and isopropyl with ethyl, respectively. ^f Yields not determined. ^g 0.2 mole % of propylene added.

We include Table II because the results clearly demonstrate that $G(\text{propyl})$ exceeds $G(\text{ethyl})$, and hence that thermal hydrogen atoms are produced in greater yield than ethyl radicals¹² in γ -radiolysis of ethane. The quantitative significance of values of $G(\text{C}_2\text{H}_6):G(\text{C}_3\text{H}_8)$ in Table II is somewhat limited because of uncertainties in values of k_d/k_c , but there can be little doubt of the order of the inequality.

This result is not surprising because several processes expected in radiolysis of ethane produce hydrogen atoms without producing ethyl radicals, *e.g.*, neutralization of fragment ions and dissociation of excited ethane to two hydrogen atoms and C_2H_4 . The variation with density of $G(\text{propyl}):G(\text{ethyl})$ is real and is

probably a consequence of decreased ion fragmentation at high gas densities.²

Nitric Oxide. We were interested in the possibility of using NO to determine the importance of free radical processes in the formation of organic products of the radiolysis of ethane. Ethylene and propylene are less satisfactory for this purpose because the scavenging reactions themselves produce some of these organic products. Yang and Gant⁶ have used NO for this purpose in a study of radiolysis of ethane at atmospheric pressure.

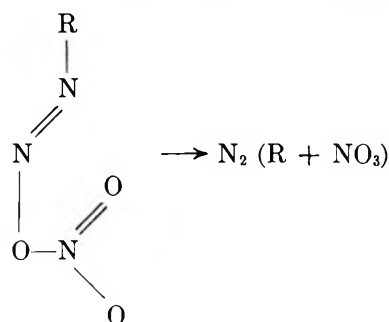
Table III: ⁶⁰Co γ -Radiolysis of Ethane. Effect of NO^a

Density, g. cc. ⁻¹	$G(n\text{-C}_4\text{H}_{10})$	$G(\text{C}_2\text{H}_6)$	$G(\text{N}_2)$
0.001	0.40	2.0	3.3
0.075	0.39	1.7	45
0.240	0.25	1.2	50

^a 3.0% NO.

In Table III results are summarized for irradiations of ethane in the presence of NO at three gas densities. Results at 0.001 g. cc.⁻¹ are in good agreement with those obtained by Yang and Gant except that they did not report a yield of nitrogen. The most significant observation is that nitrogen is produced in very large yields at high densities, suggesting that a chain reaction may be involved. Nitrogen dioxide is also produced in radiolysis at the higher densities as evidenced by its characteristic colors as a solid at -196° (blue) and as a gas (brown).

The results with NO at high gas densities are similar to results reported by Milhaud and Durup¹³ and by Burrell¹⁴ in the radiolysis of liquid cyclohexane in the presence of NO. They suggest that RNO, produced by scavenging of R radicals, reacts further with NO to give an intermediate which dissociates to give N_2 .



(11) R. J. Cventanović, *Advan. Photochem.*, 1, 155 (1963).

(12) Reference here is to ethyl radicals initially generated in radiolysis. They are to be distinguished from ethyl radicals produced by $\text{H} + \text{C}_2\text{H}_6$.

Parentheses indicate that, in their systems, R and NO₃ are produced in the same solvent cage. R and NO₃ may either escape the cage or react with each other to generate RONO₂ (by combination) or RO and NO₂ (by disproportionation). R radicals escaping the solvent cage react with NO to propagate the chain and NO₃ presumably reacts with NO to produce NO₂.

It is reasonable to assume that these reactions also occur in the radiolysis of ethane in the presence of NO. Although a chain reaction does not occur at 0.001 g. cc.⁻¹ (atmospheric pressure), the $G(N_2)$ of 3.3 indicates that these reactions are of some importance even at low density.

Because the NO₂ produced by these reactions is known to add rapidly to olefins, there was considerable doubt about the validity of $G(C_2H_4)$ values measured in the presence of NO, particularly at high densities. As a test, several irradiations were carried out with ethane containing 3% NO and various low concentrations of propylene. The results which are summarized in Table IV show that the propylene is consumed during radiolysis, supporting the assumption that NO₂ generated in these systems attacks olefins. This almost certainly accounts for the apparent decrease in $G(C_2H_4)$ with density in Table IV.

Table IV: Radiolysis of Ethane Containing Propylene. Effect of NO^a

Density, g. cc. ⁻¹	Dose, e. v. × 10 ⁻²⁰	Mole % C ₃ H ₆		$G(N_2)$
		Initial	Final	
0.001	0.26	0.014	0.011	2.0
0.240	1.60	0.015	<0.0002	70
0.240	0.80	0.50	0.042	~500

^a 3 mole % of NO.

(13) J. Milhaud and J. Durup, *J. chim. phys.*, **59**, 309 (1962).

(14) E. J. Burrell, Jr., *J. Phys. Chem.*, **66**, 401 (1962).

Disproportionation and Combination of Tritium-Labeled Isopropyl Radicals¹

by Han Bo Yun and H. C. Moser

Department of Chemistry, Kansas State University, Manhattan, Kansas (Received October 1, 1964)

There has been considerable recent interest in comparing the nature of the transition states for disproportionation and combination of alkyl free radicals.²⁻⁴

Additional experimental information is needed to determine if there is any essential difference between the two transition states.

We have previously studied the reactions of hydrogen atoms with solid propene using tritium as a tracer.⁵ The products which contained tritium from reactions run with a mixture of hydrogen and tritium atoms moderated to 77°K. appeared to result essentially from the disproportionation or combination of isopropyl free radicals. The present work was undertaken to determine the effect of bath temperature and the effect of using pure tritium (instead of a mixture of H and T) on the product distribution.

Experimental

Most of the experimental features have been described. Films of propene (Matheson C.P. grade) were allowed to react with hydrogen atoms (H + T or T) which were produced by the atomization of hydrogen gas at a hot tungsten filament. All reactions reported here were performed with helium (Airco assayed reagent grade) present to serve as moderator of the hydrogen atoms emanating from the filament. Tritium-containing products were counted with a proportional counter or ionization chamber placed in the effluent stream from a gas chromatograph.

The reaction flask had a diameter of 4.2 cm. A tungsten filament (0.008 × 3.1 cm.) was suspended with glass-covered tungsten leads to the center of the flask. Propene was introduced into the reaction vessel through an 8-mm. glass tube that extended to the top of the reaction flask.

Bath temperatures of 90, 77, and 63°K. were obtained with the use of liquid oxygen, liquid nitrogen, and a slush of liquid and solid nitrogen, respectively.

Results

The results are shown in Tables I and II. In each case 7.6×10^{-6} mole of propene was deposited for reaction, although the amount that reacted was only a small fraction of this. In Table I each of the values represents an average of the results of four to eight reactions, and in Table II each of the values represents an average of the results of nine to eleven reactions. Standard deviations are indicated in both tables.

(1) Work performed under Contract AT(11-1)-584 with the U. S. Atomic Energy Commission; from the Ph.D. Thesis of H. B. Yun to be submitted to the Graduate School, Kansas State University.

(2) J. N. Bradley, *J. Chem. Phys.*, **35**, 748 (1961).

(3) J. N. Bradley and B. S. Rabinovitch, *ibid.*, **36**, 3498 (1962).

(4) P. S. Dixon, A. P. Stefani, and M. Szwarc, *J. Am. Chem. Soc.*, **85**, 2551 (1963).

(5) H. B. Yun and H. C. Moser, *J. Phys. Chem.*, **67**, 2806 (1963).

Table I: Products of Reactions of Moderated Hydrogen and Tritium Atoms with Solid Propene at 77°K.

H ₂ pressure, torr × 10 ³	He pressure, torr × 10 ³	Tritium distribution, %			Ratio, C—C—C/C ₃	Ratio; C ₃ /C ₂
		C—C=C	C—C—C	$\begin{array}{c} \text{C—C—C—C} \\ \quad \\ \text{C} \quad \text{C} \end{array}$		
1.0	50	38.0 ± 1.3	47.0 ± 1.3	15.0 ± 0.8	3.1 ± 0.5	5.7 ± 0.4
1.5	50	38.0 ± 1.3	48.0 ± 1.3	14.0 ± 1.0	3.4 ± 0.5	6.1 ± 0.4
2.0	50	38.0 ± 0.7	46.6 ± 0.7	15.4 ± 0.4	3.0 ± 0.3	5.5 ± 0.9
4	50	39.0 ± 0.8	48.5 ± 0.9	12.5 ± 1.0	3.7 ± 0.3	6.7 ± 0.6
10	50	39.0 ± 1.3	47.0 ± 1.8	14.0 ± 1.0	3.3 ± 0.1	6.0 ± 0.6
34	60	28.7 ± 1.0	58.0 ± 2.0	13.3 ± 0.5	4.4 ± 0.2	6.5 ± 0.2
67	80	24.0 ± 0.5	63.0 ± 0.7	13.0 ± 0.3	4.8 ± 0.2	6.5 ± 0.1
120	150	20.0 ± 1.6	65.5 ± 2.0	14.5 ± 1.0	4.5 ± 0.4	5.9 ± 0.8
160	200	16.8 ± 0.7	70.0 ± 0.3	13.2 ± 0.4	5.3 ± 0.4	6.6 ± 1.0
0.5 (pure T ₂)	80	37.0 ± 0.6	45.7 ± 0.6	17.3 ± 0.5	2.7 ± 0.2	4.9 ± 0.3

Table II: Effect of Bath Temperature on Products of Reactions of Moderated Hydrogen and Tritium Atoms with Propene

Bath temp., °K.	Tritium distribution, %			Ratio, C ₃ /C ₂
	C—C=C	C—C—C	$\begin{array}{c} \text{C—C—C—C} \\ \quad \\ \text{C} \quad \text{C} \end{array}$	
63	37.5 ± 0.5	48.0 ± 0.6	14.5 ± 0.5	5.9 ± 0.3
77	38.0 ± 0.7	46.6 ± 0.7	15.4 ± 0.4	5.5 ± 0.9
90	38.0 ± 0.6	46.5 ± 0.5	15.5 ± 0.8	5.5 ± 0.3

Discussion

Mechanism of Product Formation. In contrast to reactions with hot hydrogen atoms, only three products (propene, propane, and 2,3-dimethylbutane) are obtained when hydrogen atoms moderated with helium react with solid propene. Under a limited range of hydrogen pressure (see Table I) the product distribution remains essentially constant and independent of pressure. In this range, the products are considered to result solely from (a) hydrogen atom addition to propene to form isopropyl radicals followed by (b) disproportionation and combination of isopropyl free radicals. Addition of hydrogen atoms to isopropyl radicals is ruled out because of the pressure independence of the product distribution. Hydrogen atom-isopropyl radical disproportionation is ruled out for the same reason.

At higher hydrogen pressures, the product distribution shifts in favor of propane at the expense of propene and 2,3-dimethylbutane. The latter is affected only slightly. The shift in product distribution might be due to (1) hydrogen atom addition to isopropyl radicals to form propane and/or (2) consecutive reactions of product, surface propene molecules to produce more isopropyl radicals which then react by disproportionation and combination. We prefer explana-

tion (2) as the predominant reason for the shift because an appreciable contribution from (1) would diminish the percentage of dimer. We did not observe this. Only the relative yields of the C₃ products were appreciably affected.

Tritium Isotope Effects. The primary tritium isotope effect can be calculated from the propane-T/propene-T ratio. This can be done providing the tritium-containing propene and propane result exclusively from disproportionation (without consecutive reactions with product propene) and providing that secondary isotope effects can be ignored.

For the disproportionation of two tritium-labeled isopropyl radicals the following expression can be used to calculate $k_{\text{H}}/k_{\text{T}}$

$$\frac{\text{propane-T}}{\text{propene-T}} = 1 + 0.4 \frac{k_{\text{T}}}{k_{\text{H}}}$$

Thus the C—C—C(T)/C—C=C(T) ratio could vary from 1.0 for a very large isotope effect to 1.4 for no isotope effect. Experimentally, an activity ratio of 1.24 ± 0.02 was observed which leads to a $k_{\text{H}}/k_{\text{T}}$ ratio of 1.7 ± 0.2 .

For the disproportionation of mixed isopropyl radicals (one containing tritium and the other one not) the ratio $k_{\text{H}}/k_{\text{T}}$ can be calculated from

$$\frac{\text{propane-T}}{\text{propene-T}} = 1.2 + 0.2 \frac{k_{\text{T}}}{k_{\text{H}}}$$

In this case a ratio of 1.2–1.4 is possible. In the hydrogen pressure range of 10^{-3} to 10^{-2} torr, values of C—C—C(T)/C—C=C(T) ranged from 1.21 to 1.26. If an average of 1.24 ± 0.02 is used, this leads to a $k_{\text{H}}/k_{\text{T}}$ ratio of 5 ± 2.5 . We believe this value is high and the other value of $k_{\text{H}}/k_{\text{T}}$ is more reliable. Similar measurements of the tritium isotope effect in the dis-

proportionation of ethyl radicals gave small values⁶ ($k_H/k_T = 1.7, 2.3$). Also, the k_d/k_c ratio was not greatly affected by changing from two tritium-labeled isopropyl radicals to mixed radicals where only one contained tritium.

Activation Energy. Three different bath temperatures were used to measure any difference in the activation energies of disproportionation and combination. The product distribution was practically the same at all three temperatures. The propene (m.p. 88°K.) was a liquid at 90°K. but was solidified at the other two temperatures. On the basis of our experiments, an activation energy difference as large as 100 cal./mole is unlikely. This is in contrast to a value of 260 cal./mole reported by Klein, Scheer, and Kelley.⁷

Both the small primary isotope effect in disproportionation and negligibly small temperature effect on k_d/k_c support the proposition that the transition states for disproportionation and combination are loose and similar. However, the k_d/k_c ratio is different for different phases (gas and solid), and a distinct difference between the two transition states is therefore indicated.

(6) K. W. Watkins and H. C. Moser, *J. Phys. Chem.*, **69**, 1040 (1965).

(7) R. Klein, M. D. Scheer, and R. Kelley, *ibid.*, **68**, 598 (1964).

Remarks on Förster's Theory of Transfer of Excitation Energy¹

by Mira Leibowitz

Department of Physics, The Hebrew University,
Jerusalem, Israel (Received October 8, 1964)

In a well-known paper by Förster,² a law is derived for the dependence of the fluorescence decay of donor molecules on the concentration of acceptor molecules in solution. A dipole-dipole interaction between donor and acceptor is assumed. The probability $\rho(t)$ for an individual donor molecule to be in an excited state at time t after excitation is subject to the equation

$$\frac{d\rho(t)}{dt} = -\left\{\frac{1}{\tau_0} + \frac{1}{\tau_0} \sum_{k=1}^N \left(\frac{R_0}{R_k}\right)^6\right\} \rho(t) \quad (1)$$

where τ_0 is the lifetime of the excited donor molecule in the absence of acceptor molecules, R_k is the distance of the donor molecule from the k th molecule of the acceptor, R_0 is a constant depending on the nature of the molecule, and N is the number of acceptor molecules around the donor molecule.

It then follows, as is explicitly stated by Förster, that an individual donor molecule decays exponentially, *i.e.*

$$\rho(t) = \rho_0 e^{-\left\{1 + \sum_{k=1}^N (R_0/R_k)^6\right\} (t/\tau_0)} \quad (2)$$

It is however, not the decay of a single molecule which is observed, but that of the whole ensemble of molecules with varying distributions of distances R_k . Accordingly, Förster averages over all possible values of R_k and obtains

$$\overline{\rho(t)} = e^{-t/\tau_0} \prod_{k=1}^N \int_0^{R_g} e^{-(R_0/R_k)^6 (t/\tau_0)} \omega(R_k) dR_k \quad (3)$$

where $\omega(R_k) dR_k$ is the probability of finding an acceptor molecule at a distance between R_k and $R_k + dR_k$ from the excited donor molecule. From this expression, the final approximated result is derived.

Sveshnikov³ rightly criticizes this approach. He remarks that the above averaging procedure does not account for the different distributions of acceptor molecules around different donor molecules. The proper procedure, according to Sveshnikov, is described by the relation

$$\overline{\rho(t)} = \frac{1}{n_0} e^{-t/\tau_0} \sum_{i=1}^{n_0} \prod_{k=1}^N e^{-(R_0/R_{ki})^6 (t/\tau_0)} \quad (4)$$

where n_0 is the number of excited donors and R_{ki} is the distance between the k th acceptor and the i th donor. Sveshnikov treated the problem in a subsequent article⁴ and arrived by an approximated method at results similar to those of Förster.

In reply to Sveshnikov's criticism, Galanin⁵ remarks that Förster's method is justified by the following argument: since a great number of molecules is assumed, one is allowed to convert the sum in eq. 4 into an integral by weighing the integrand by $\omega(R_k) dR_k$ (the distribution function of R_k). Then, by changing the order of multiplication and integration, eq. 3 is obtained.

Galanin is right in that one may convert the sum in eq. 4 into an integral, but then one must apply the distribution function of the *product* in (4) (which may be rather complicated) and not that of the individual R_k 's. If one were to follow Galanin's suggestion, one would average over the donor molecules with the dis-

(1) Supported by the U. S. Atomic Energy Commission, Division of Biology and Medicine.

(2) T. Förster, *Z. Naturforsch.*, **4a**, 321 (1949).

(3) B. Ia. Sveshnikov, *Dokl. Akad. Nauk SSSR*, **111**, 78 (1956).

(4) B. Ia. Sveshnikov, *ibid.*, **115**, 274 (1957).

(5) V. V. Antonov-Romanovsky and M. D. Galanin, *Opl. i Spektroskopiya*, **3**, 389 (1957).

tribution function of the acceptor molecules, which is not a plausible procedure.

Rozman⁶ indeed applies the proper method, which involves some extended calculations. Remarkably enough, he arrives at Förster's final results.

Galanin himself^{5,7} treats the problem by a different approach, averaging already in the differential equation (1). The resulting formula is identical with that of Förster.

The question now arises: how is it that Förster's method, which is open to the above criticism, still yields the correct result? It is the purpose of this communication to clarify this question.

Following Galanin's approach,⁵ the decay with time of the number of excited donor molecules $n(t)$ is given by

$$\frac{dn(t)}{dt} = - \left\{ \frac{1}{\tau_0} + \int_0^\infty N(R,t) f(R) \omega(R) dR \right\} n(t) \quad (5)$$

where $f(R) \equiv 1/\tau_0(R_0/R)^6$ and $N(R,t)$ is the number of acceptor molecules whose distance from an excited donor molecule at time t is R . It is assumed that an acceptor molecule, once excited, can exert no further quenching effect on a donor molecule. Therefore, $N(R,t)$ decays exponentially with time with a rate determined by $f(R)$.

$$\begin{aligned} \frac{dN(R,t)}{dt} &= -f(R)N(R,t) \\ N(R,t) &= N_0 e^{-f(R)t} \end{aligned} \quad (6)$$

Substituting (6) in (5) he obtains

$$\frac{dn(t)}{dt} = - \left\{ \frac{1}{\tau_0} + N_0 \int_0^\infty e^{-f(R)t} f(R) \omega(R) dR \right\} n(t) \quad (7)$$

In integrating this equation, one may change the order of integration with respect to the variables R and t . The result is

$$n(t) = n_0 e^{-t/\tau_0 - N_0 \int_0^\infty (1 - e^{-f(R)t}) \omega(R) dR} \quad (8)$$

This relation developed by Galanin, however, contains an integral which is identical with that of Förster (eq. 3), and which, after proper approximations, leads to an identical result.

The fact that Galanin's correct approach coincides mathematically with Förster's incorrect approach is a "coincidence," due to the assumption that the acceptor molecules decay exponentially with the coefficient $f(R)$. This causes $f(R)$ to appear in eq. 7 both as a factor and as an exponent, and this again causes the result upon integration to be equal to that of Förster. Had we assumed $N(R,t)$ to decrease at a different rate,

(say, by some additional mechanism) the integration of the corresponding new equation (7) would have yielded an integral, not necessarily equal to that obtained by Förster's approach. It thus seems, that the proper result obtained by Förster nevertheless does not justify his statistical reasoning.

Acknowledgment. The author wishes to thank Dr. A. Weinreb for helpful discussions.

(6) I. M. Rozman, *Opt. i Spektroskopiya*, **4**, 536 (1958).

(7) M. D. Galanin, *Zh. Eksperim. i Teor. Fiz.*, **28**, 485 (1955).

The Temperature Dependence of the *cis-trans* Photoisomerization of Azo Compounds: Theoretical Considerations

by David R. Kearns

Department of Chemistry, University of California, Riverside, California (Received January 18, 1964)

Recent studies¹⁻⁴ of the temperature and wave length sensitivity of the *cis* \rightleftharpoons *trans* photoisomerization of aromatic azo compounds have revealed that (i) the quantum yields, ϕ_c , for the *cis* \rightarrow *trans*, and, ϕ_t , for the *trans* \rightarrow *cis* photoisomerizations decrease with decreasing temperature, indicating that an activation energy is required for photoisomerization; (ii) the activation energy for the *cis* \rightarrow *trans* transformation is smaller than for the *trans* \rightarrow *cis* transformation; (iii) the sum of ϕ_c and ϕ_t is less than unity at all temperatures studied; and (iv) excitation of an azo molecule to its lowest ($n-\pi^*$) singlet state results in a greater photoisomerization quantum yield than does excitation to the higher lying ($\pi-\pi^*$) state.

In an attempt to understand some of these observations we have applied molecular orbital theory (with overlap included) to a calculation of the dependence of the ground state and of the excited ($n-\pi^*$) and ($\pi-\pi^*$) state energies of simple aliphatic azo compounds on the angle of rotation about the N-N bond axis. In this note we present the results of these calculations and show how they offer a possible theoretical explanation.

(1) P. B. Birnbaum and D. W. G. Syles, *Trans. Faraday Soc.*, **50**, 1192 (1954).

(2) G. Zimmerman, L. Chow, and E. Paik, *J. Am. Chem. Soc.*, **80**, 3528 (1958).

(3) E. Fischer, *ibid.*, **82**, 3249 (1960).

(4) J. Malkin and E. Fischer, *J. Phys. Chem.*, **66**, 2482 (1962).

tion of the experimental observations on aromatic azo compounds.

According to MO theory, the two nitrogen $2P_z$ atomic orbitals p_{z_a} and p_{z_b} of a planar aliphatic azo molecule can be combined to form a set of molecular orbitals $\pi_{\pm} = (P_{z_a} \pm P_{z_b})/\sqrt{2(1 \pm S_{pp}^0)}$ with corresponding energies $\epsilon_{\pm}^{\pi} = (\alpha_p \pm \beta_{pp}^0)/(1 \pm S_{pp}^0)$ where $S_{pp}^0 = \langle P_{z_a}(i) | P_{z_b}(i) \rangle = 0.22$, $\alpha_p = \langle P_{z_a}(i) | \mathcal{H}(i) | P_{z_a}(i) \rangle \equiv 0$, $\beta_{pp}^0 = \langle P_{z_a}(i) | \mathcal{H}(i) | P_{z_b}(i) \rangle = -20$ kK., and $\mathcal{H}(i)$ is some effective one-electron Hamiltonian. Values for these integrals, as well as those given below, were obtained previously from spectral studies.⁵⁻⁷ In a similar fashion, the nitrogen sp^2 hybridized lone-pair atomic orbitals, n_a and n_b , may be combined to form molecular orbitals $N_{\pm} = (n_a \pm n_b)/\sqrt{(1 \pm S_{nn}^0)2}$ with corresponding energies $\epsilon_{\pm}^n = \alpha_n \pm \beta_{nn}^0/(1 \pm S_{nn}^0)$, where $S_{nn}^0 = \langle n_a(i) | n_b(i) \rangle = 0.11$, $\alpha_n = \langle n_a(i) | \mathcal{H}(i) | n_a(i) \rangle = -8$ kK., and $\beta_{nn}^0 = \langle n_a(i) | \mathcal{H}(i) | n_b(i) \rangle = -6$ kK. For the planar isomers the n and p_z and the N_{\pm} and π_{\pm} orbitals are orthogonal. For nonplanar isomers, however, the n and p orbitals on adjacent centers are not orthogonal, and consequently the N_{+}' and π_{-}' orbitals and the N_{-}' and π_{+}' orbitals will overlap, although N_{+}' and N_{-}' remain orthogonal to π_{+}' and π_{-}' , respectively. (Primes are used here to indicate that the n and p orbitals on one center have been rotated by some angle θ about the N-N axis.)

If the normalized molecular orbitals N_{+}' , N_{-}' , π_{+}' , and π_{-}' are chosen as the basis functions for the calculation, the problem of determining orbital energies is reduced to one of solving the following two 2×2 secular determinants

$$\begin{vmatrix} \frac{\alpha_p + \beta_{pp}^0 \cos \theta}{1 + S_{pp}^0 \cos \theta} - \epsilon & \\ -\frac{(\beta_{np}^0 - S_{np}^0 \epsilon) \sin \theta}{\sqrt{(1 + S_{pp}^0 \cos \theta)(1 - S_{nn}^0 \cos \theta)}} & \end{vmatrix}$$

and

$$\begin{vmatrix} \frac{\alpha_p - \beta_{pp}^0 \cos \theta}{1 - S_{pp}^0 \cos \theta} - \epsilon & \\ +\frac{(\beta_{np}^0 - S_{np}^0 \epsilon) \sin \theta}{\sqrt{(1 - S_{pp}^0 \cos \theta)(1 + S_{nn}^0 \cos \theta)}} & \end{vmatrix}$$

where $\beta_{np}^0 = \langle n_a(i) | \mathcal{H}(i) | P_{y_b}(i) \rangle = -10$ kK., and $S_{np}^0 = \langle n_a(i) | P_{y_b}(i) \rangle = 0.18$. In writing these expressions we made use of the fact that the overlap between n orbitals on adjacent centers, and naturally between n and p orbitals, is primarily of the π -type, the σ contributions to the overlap cancelling one

another. A value of -10 kK. was assigned to β_{np}^0 on the basis of overlap considerations. Orbital energies, ϵ_i , were obtained by solving the secular determinants for various angles θ and these results are shown in Figure 1a. The angular dependence of the energies of the ground state and the excited ($n-\pi^*$) and ($\pi-\pi^*$) states were obtained by summing the appropriate orbital energies, and these results are presented in Figure 1b. As the calculations were based on a one-electron approximation, excited singlet and triplet states of the same configuration are not distinguished. This can easily be rectified for the ($n-\pi^*$) states by introducing the singlet-triplet splitting factor, which according to ASMO theory will be determined primarily by one-center exchange integrals involving n and the p orbitals on the same center.⁷ By the use of the wave functions which we obtain from our calculations for the planar and perpendicular isomers and by evaluation of the appropriate integrals, the singlet-triplet splitting was found to change from 5 to 16.6 kK. in going from a planar to the perpendicular isomer. Inclusion of this factor in the calculation of the state energies leads to the results given by the dotted curves in Figure 1b.

Since we would like to use the above results to discuss the photoisomerization of the aromatic azo compounds, it is necessary to consider how the aromatic substituents will modify our initial results. In the first place, as a result of the greater electron delocalization in the aromatic than in the aliphatic azo compounds, aromatic substituents will reduce the antibonding character of the π^* orbital involved in the $n \rightarrow \pi^*$ transition, without a corresponding reduction in the ground-

$$\begin{vmatrix} -\frac{(\beta_{np}^0 - S_{np}^0 \epsilon) \sin \theta}{\sqrt{(1 + S_{pp}^0 \cos \theta)(1 - S_{nn}^0 \cos \theta)}} & \\ \frac{\alpha_n - \beta_{nn}^0 \cos \theta}{1 - S_{nn}^0 \cos \theta} - \epsilon & \end{vmatrix} = 0,$$

$$\begin{vmatrix} +\frac{(\beta_{np}^0 - S_{np}^0 \epsilon) \sin \theta}{\sqrt{(1 - S_{pp}^0 \cos \theta)(1 + S_{nn}^0 \cos \theta)}} & \\ \frac{\alpha_n + \beta_{nn}^0 \cos \theta}{1 + S_{nn}^0 \cos \theta} - \epsilon & \end{vmatrix} = 0$$

state bond order. This alone would increase the energies of all the excited states of the perpendicular

(5) S. F. Mason, *J. Chem. Soc.*, 1246 (1957); 493 (1962).

(6) D. R. Kearns and M. A. El Bayoumi, *J. Chem. Phys.*, **38**, 1508 (1963).

(7) L. Goodman and R. W. Harrell, *ibid.*, **30**, 1131 (1959).

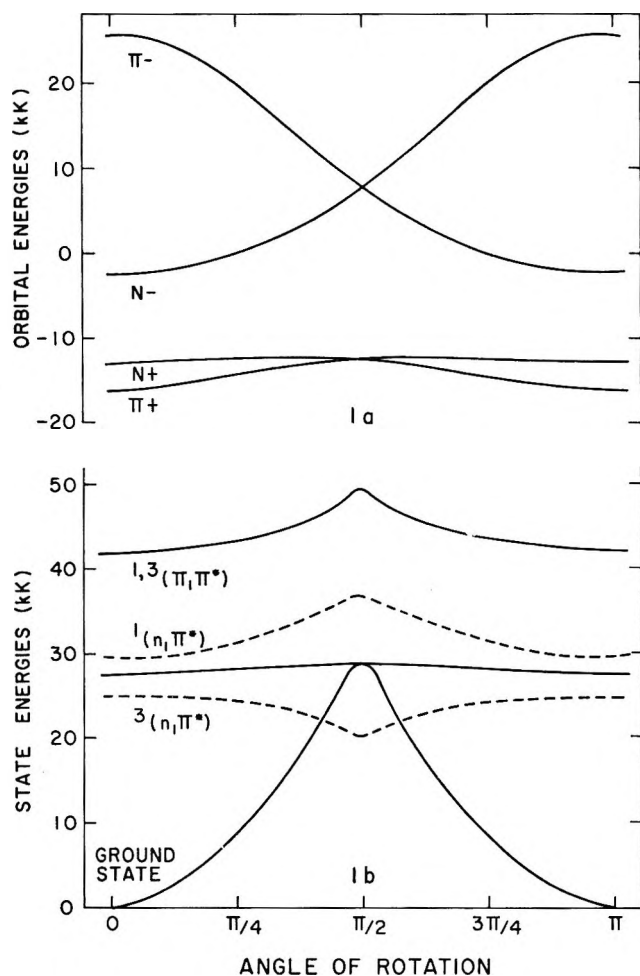


Figure 1. (a) The variation of the orbital energies with angle of rotation about the N-N bond for a simple, aliphatic azo molecule. The N_{\pm} and π_{\pm} designations are appropriate only for the planar isomers. (b) The angular dependence of the ground state and the lowest ($n-\pi^*$) and ($\pi-\pi^*$) states of a simple aliphatic azo molecule: solid line, one-electron approximation; dashed line, one-electron results corrected for the effect of the singlet-triplet splitting.

isomer relative to those for the planar isomers. Secondly, as a result of steric interactions between the aromatic groups, *trans* isomers will in general be more stable than *cis* isomers. This effect is easily incorporated into our results by raising the energy of all of the electronic states of the *cis* isomer by some amount ΔE_{steric} with respect to the *trans* isomer. If we incorporate these two modifications into the results obtained for the aliphatic azo compounds, then they should be at least qualitatively useful for discussion of the photoisomerization of the aromatic azo compounds.

Examination of the dotted curves of Figure 1b indicates that for a molecule in its lowest ($n-\pi^*$) singlet

state there will be an energy barrier to rotation from the planar to the perpendicular configuration. This barrier is due partly to the angular dependence of the orbital energies and primarily to the angular dependence of the singlet-triplet splitting. If a planar isomer undergoes intersystem crossing from the lowest ($n-\pi^*$) singlet state to the lowest ($n-\pi^*$) triplet state, which is also predicted to be the lowest excited state, we observe that no barrier to rotation from the planar to the perpendicular configuration is expected.

As the curves in Figure 1b for the ($\pi-\pi^*$) states indicate, a rather large activation energy is required for a molecule to be converted from a planar to the perpendicular configuration. Since the singlet-triplet splitting of the ($\pi-\pi^*$) states is large for both the planar and the perpendicular isomers, inclusion of this factor in the calculations would not qualitatively alter the orbital results.

On the basis of the above considerations we conclude that when an azo molecule is in its lowest ($\pi-\pi^*$) singlet or triplet state or lowest ($n-\pi^*$) singlet state, an activation energy will be required for isomerization. No activation energy should be required when the molecule is in its lowest ($n-\pi^*$) triplet state. These results would appear to offer an explanation for the fact that the photoisomerization of the aromatic azo compounds is temperature dependent.

If the effect of steric interaction is included in our results, we note that there will necessarily be a lowering of the ($n-\pi^*$) excited state barrier for the *cis* \rightarrow perpendicular conversion without any effect on the reverse transitions. In qualitative agreement with this expectation it is found that the quantum yield for the *cis* \rightarrow *trans* photoisomerization of azobenzene is almost constant from room temperature to -180° , whereas the quantum yield for the *trans* \rightarrow *cis* photoisomerization decreases by a factor of 2 over this same temperature range. Similar results were obtained with other azo compounds.⁴

Continuing with the assumption that our calculations are qualitatively applicable to aromatic azo compounds, we predict that the excitation process which is most efficient in populating the ($n-\pi^*$) triplet state will be the most efficient one for promoting isomerization. Excitation directly to the ($n-\pi^*$) singlet state should be more efficient in this respect than excitation to the lowest ($\pi-\pi^*$) singlet state, which would allow more opportunity for radiationless transitions to occur which are competitive with formation of the ($n-\pi^*$) triplet state. Experimentally, excitation in the $n \rightarrow \pi^*$ band does result in higher quantum yields for the photoisomerization than does excitation in the $\pi \rightarrow \pi^*$ band.⁴ This would not necessarily

have been the case if isomerization could occur in the ($\pi-\pi^*$) singlet state.

We conclude that the results of our MO calculation provide a possible explanation for a number of the features of the photoisomerization of azo aromatics including the origin of the excited state barrier to rotation about the N-N bond and the wave length sensitivity.

Finally, by way of justification of our use of an MO method we note that (i) when an MO calculation, including overlap, is carried out for ethylene the results are qualitatively quite similar to those obtained by including the effects of electron-electron interaction explicitly⁸; and (ii) recent MC calculations, including overlap, on the ground-state energies of a number of aliphatic and olefinic systems have been found to be quite reliable for predicting the stability of various isomeric configurations.⁹ While these successes with other systems do not guarantee the success of our calculations on azo molecules, they are certainly encouraging.

Acknowledgment. The support of the U. S. Public Health Service (Grant No. GM-10499) is most gratefully acknowledged.

(8) R. G. Parr and B. L. Crawford, *J. Chem. Phys.*, **16**, 526 (1948).

(9) R. Hoffman, *ibid.*, **39**, 1397 (1963).

Note on the Thermodynamics of Formation of Dolomite

by F. Halla

Martinstrasse 28, Vienna 110, Austria (Received July 2, 1964)

For the free energy of formation of dolomite (D) from its solid components calcite (C) and magnesite (M) Stout and Robie¹ recently gave the value $\Delta G^\circ = -2700$ cal., starting from the dissociation pressures of D and M, as determined by Graf and Goldsmith² and Marc and Simek,³ and from their own entropy values. This ΔG° value differs considerably from earlier values between -500 and -1000 cal. obtained in the solubility measurements of Halla.⁴

Stout and Robie saw the reason for the divergence in the lack of reversibility in the solubility experiments involving two solid residues and in the erroneous use of the first power of the mean activity coefficient instead of the third. However, these well-founded objections

have already been considered in a recent paper of Halla⁵ (and Van Tassel) which has been overlooked by Stout and Robie and which gave $\Delta G^\circ = -1720 \pm 280$ cal.

Stout and Robie also made a correctional recalculation of Halla's data using the solubilities $m_D = 3.25 \times 10^{-3}$ and $m_M = 13.6 \times 10^{-3}$ of Yanat'eva⁶ and found $\Delta G^\circ = -2700$ cal., in agreement with their first value. Between their data and Halla's -1720 cal. a considerable difference still exists. It is explained by the fact that the m_D value employed by Stout and Robie is too low compared with $m_D = 4.5 \times 10^{-3}$ given in ref. 5 and repeatedly confirmed.

It has to be mentioned here that -1720 ± 280 cal. already represents an average including Kramer's⁷ value. That it coincides fairly well with the value derived directly from the pH determination is no independent confirmation but shows only the correctness of the formula employed in the evaluation of the latter.

Another reason for backing our value lies in the fact that, for the enthalpy derived with the aid of Stout and Robie's entropy value, $\Delta S^\circ_{298} = 0.81 \pm 0.29$, one obtains $\Delta H^\circ_{298} = -1720 - 240 = -1960 \pm 370$ cal., which agrees with the value -1600 given by Roth and Müller-Mangold⁸ within the error limits. This would seem to plead for our value,⁹ but, on the other hand, no serious reason may be found which would invalidate Stout and Robie's result. The only explanation for the divergence may be sought, at the moment, in a difference of the dispersity and, consequently, of the surface energy of the different samples of magnesite employed in the investigations. Irregularities which may be connected with the problem in question have already been observed.¹⁰

A redetermination of the enthalpies of the substances involved had to include those of the magnesite gel of Kraubath, Styria, and those of the well-crystallized magnesite of high purity, obtained by hydrothermal decomposition of solutions of $Mg(HCO_3)_2$.

(1) J. W. Stout and R. A. Fobie, *J. Phys. Chem.*, **67**, 2248 (1963).

(2) D. L. Graf and J. R. Goldsmith, *Geochim. Cosmochim. Acta*, **7**, 109 (1955).

(3) R. Marc and A. Simek, *Z. anorg. Chem.*, **82**, 17 (1913).

(4) F. Halla, *Z. physik. Chem. (Frankfurt)*, **17**, 368 (1958); **21**, 349 (1959); **25**, 267 (1960).

(5) F. Halla, *Sedimentology*, **1**, 191 (1962).

(6) O. K. Yanat'eva, *Zh. Neorgan. Khim.*, **1**, 1475 (1956).

(7) J. R. Kramer, *J. Sediment. Petrol.*, **29**, 465 (1959).

(8) W. A. Roth and D. Müller-Mangold, "Landolt-Börnsteins physikalisch-chemische Tabellen," 5th Ed., Vol. IIIc, p. 2762.

(9) The attempt made in ref. 5 to calculate ΔG° on the same lines as Stout and Robie proved to be fallacious because the mixing energy was not considered.

(10) F. Halla and R. Van Tassel, *Radex Rundschau*, **42** (1964).

Relation of Ring Size to Ultraviolet Extinction Coefficient in Cyclosiloxanes Containing Phenyl Substituents on Silicon

by C. R. Sporck and A. E. Coleman

General Electric Company, Silicone Products Department, Waterford, New York (Received September 21, 1964)

In the course of investigations of the ultraviolet spectra of a large number of cyclosiloxanes containing alkyl and phenyl groups bonded to silicon, we have noted that the intensity at the absorption maximum per mole of phenyl of the ${}^1L_b \leftarrow {}^1A$ transition appears to be a function of the siloxane ring size. This result has been confirmed by the measurement of oscillator strength and published as a portion of a paper¹ dealing chiefly with monophenylsilanes and -siloxanes. We are making available here our data on a large number of cyclics.

Experimental

The methods for preparation of the cyclosiloxanes examined here have been published.² A more detailed description of the synthetic methods will be provided in later publications of this laboratory.

The structures, melting points, and intensities are tabulated in Table I. Typical spectra appear in Figure 1. All spectra were recorded with a Beckman DK-2

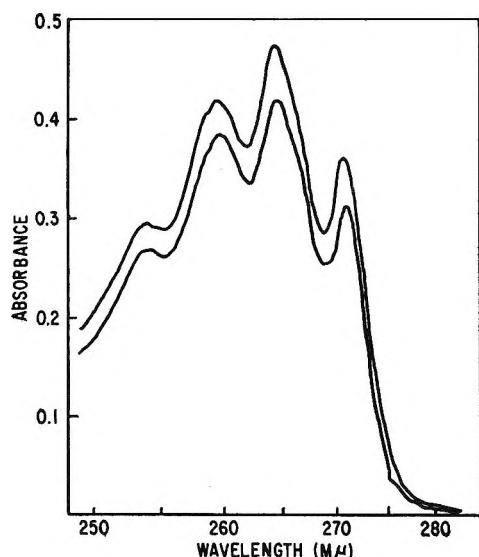


Figure 1. Ultraviolet absorption spectra of 1,1,3,3-tetramethyl-5,5-diphenylcyclotrisiloxane (top) and 1,1,3,3,5,5-hexamethyl-7,7-diphenylcyclotetrasiloxane (bottom) in chloroform; 1.1×10^{-3} mole of $C_6H_5^-/l$.

spectrophotometer using chloroform as solvent. The intensity is ϵ_{max} measured at 265 $m\mu$ and calculated in units of 1000 cm^2 (moles of C_6H_5)⁻¹. Each ϵ_{max} is the average of two independent determinations.

Table I: Ultraviolet Absorption Coefficients of Cyclosiloxanes

Compd. ^a	M.p., °C.	ϵ_{max} [10^3 cm^2 (C_6H_5) ⁻¹]
Cyclotrisiloxanes		
I $P_2SiOP_2SiOP_2SiO$	190-191	417
II $P_2SiOP_2SiOMe_2SiO$	87-88	412
III $P_2SiOMe_2SiOMe_2SiO$	64-64.5	412
IV $P_2SiOP_2SiOMeVSiO$	83.5-84	414
V $P_2SiOP_2SiOMeEtSiO$	73.5-74.5	413
VI $P_2SiOP_2SiOMePrSiO$	68-69	412
	Average =	413
	S =	2.0
Cyclotetrasiloxanes		
VII $P_2SiOP_2SiOP_2SiOP_2SiO$	199-200	366
VIII $P_2SiOMe_2SiOP_2SiOMe_2SiO$	130-131.5	364
IX $P_2SiOP_2SiOMe_2SiOMe_2SiO$	71-73	360
X $P_2SiOP_2SiOP_2SiOMe_2SiO$	87-89	368
XI $P_2SiOP_2SiOP_2SiOMeVSiO$	92-94.5	370
XII $P_2SiOMe_2SiOMe_2SiOMe_2SiO^b$		365
XIII $P_2SiOP_2SiOP_2SiOMeEtSiO$	90-91	368
XIV $P_2SiOP_2SiOP_2SiOMePrSiO$	86-88	366
	Average =	366
	S =	3.0
Cyclopentasiloxanes		
XV $P_2SiOP_2SiOP_2SiOMe_2SiOMe_2SiO$	87-89	355
XVI $P_2SiOP_2SiOMe_2SiOMe_2SiOMe_2SiO$	67-68.5	346
Cyclohexasiloxanes		
XVII $P_2SiOP_2SiOMe_2SiOP_2SiOP_2SiOM_2SiO$	179.5-182	355
XVIII $P_2SiOMe_2SiOMe_2SiOP_2SiOMe_2SiOMe_2SiO$	124-124.5	342

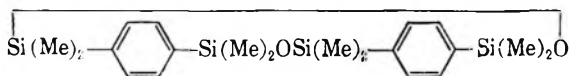
^a In this table P = phenyl, Me = methyl, Pr = *n*-propyl, Et = ethyl, and V = vinyl. ^b This compound is a liquid at room temperature; $n_{D}^{25} 1.4817$.

- (1) J. F. Brown and P. I. Prescott, *J. Am. Chem. Soc.*, **86**, 1402 (1964).
 (2) C. R. Sporck, Belgian Patents 635,643-635,649 (1963).

Discussion

The data of Table I clearly show that the average absorption intensity differences between the cyclotrisiloxanes, cyclotetrasiloxanes, and higher cyclics are much larger than the standard deviations for each group of cyclics. The differences between the cyclopentasiloxanes and the cyclhexasiloxanes do not appear to be significant.

If we consider the geometric configurations of these cyclics in order of increasing ring size, we find that the average angle between the substituents on successive silicon atoms and consequently the average distance between these substituents will decrease as the ring size increases. These changes in intergroup distance as the ring size changes from cyclotetrasiloxane to cyclopentasiloxane to cyclohexasiloxane could be less important as opportunity for ring puckering increases in the larger rings. Cases of rigidly enforced proximity and orientation of phenylene groups are found in the paracyclophanes and 1,4-polymethylenebenzene cyclics studied by Cram³ and in the siloxane analog of the paracyclophanes studied by MacKay.⁴ MacKay's compound is



In these compounds the benzene rings of the smaller cyclics are distorted from planarity and bathochromic and hypochromic effects are observed in the ultraviolet. In our compounds the distortion would be smaller, and we do not detect a bathochromic shift but do observe a hypochromic effect, weaker than Cram's, upon going from the cyclotrisiloxane to the cyclotetrasiloxane. A still weaker hypochromic effect is observed upon going from cyclotetrasiloxane to groups of cyclopentasiloxanes and cyclohexasiloxanes, which are undifferentiated. It would appear that methyl, ethyl, vinyl, and propyl groups on adjacent silicons have as large an effect on the transition probability as does the phenyl group.

Brown and Prescott¹ stress calculation of oscillator strengths and analyze them into vibrational and substituent components following the method of Petruska.⁵ However, in the case of our compounds, the substituents on silicon are similar so that intensity maxima are sufficient. The spectra of all the compounds are superposable with vertical shifts.

Lastly, the development of Tinoco⁶ used by Brown and Prescott¹ to estimate hypochromism in mono-phenylsiloxane structures cannot explain the results presented here as these authors have themselves observed. Induced dipole-dipole interaction between

phenyl groups has nothing to do with the virtual identity of ϵ_{\max} for, say, compounds I and III of Table I among the trisiloxanes and for compounds VII and XII among the tetrasiloxanes.

(3) D. J. Cram, N. L. Allinger, and H. Steinberg, *J. Am. Chem. Soc.*, **76**, 6132 (1954).

(4) F. P. MacKay, Thesis, The Pennsylvania State University Graduate School, 1956.

(5) J. Petruska, *J. Chem. Phys.*, **34**, 1111, 1120 (1961).

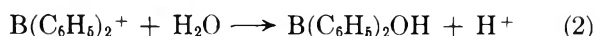
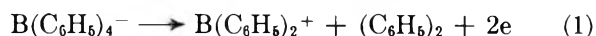
(6) I. Tinoco, *J. Am. Chem. Soc.*, **82**, 4785 (1960).

Electrooxidation of the Tetraphenylborate Ion in Aqueous Solution at the Platinum Disk Electrode

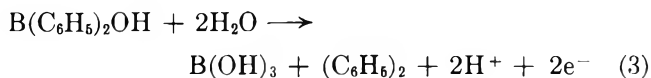
by W. Richard Turner and Philip J. Elving

University of Michigan, Ann Arbor, Michigan
(Received October 5, 1964)

The tetraphenylborate ion will undergo electrochemical oxidation at the wax-impregnated graphite electrode in aqueous solution,^{1,2} although Geske³ has reported being unable to obtain voltammetric waves for this ion in aqueous solution at the rotating platinum wire electrode. He was able to obtain a single wave in acetonitrile which was ascribed to the reactions



During the course of an investigation of the electrooxidation of tetraphenylborate in aqueous solution at the pyrolytic graphite electrode,⁴ the oxidation at a platinum disk electrode was attempted. Waves were obtained at both the stationary and rotated platinum disk electrodes which were comparable to those obtained at the pyrolytic graphite electrode (Figure 1A). In addition to the wave observed by Geske, a second wave has been characterized at the pyrolytic graphite electrode⁴



(1) P. J. Elving and D. L. Smith, *Anal. Chem.*, **32**, 1849 (1960).

(2) D. L. Smith, D. R. Jamieson, and P. J. Elving, *ibid.*, **32**, 1253 (1960).

(3) D. H. Geske, *J. Phys. Chem.*, **63**, 1062 (1959).

(4) W. R. Turner and P. J. Elving, *Anal. Chem.*, **37**, 207 (1965).

Two waves were obtained at the stationary platinum disk electrode in acid solution (pH 2.0 and 4.6); however, half-peak potentials ($E_{p/2}$) and peak currents (i_p) were not too reproducible due to the lack of an adequate method for renewing the surface of the platinum electrode. It has been amply demonstrated that the previous use of platinum electrodes can profoundly affect the results⁵ obtained with them and that there is no satisfactory method of guaranteeing a reproducible behavior for this electrode. The following procedure was adopted in the present study. Prior to running the voltammogram, the electrode was maintained at 0.0 v. vs. s.c.e. until the current was negligible; *i.e.*, less than 0.2 μa . However, larger background currents were frequently observed at higher potentials. The electrode was wiped clean between runs with a clean tissue wetted with acetone to remove any organic films which may have formed. When not in use, the electrode was stored in 0.1 M perchloric acid. Care was taken that the electrode was not held at positive potentials. At no time was the electrode used beyond +1.0 v. and, when the background electrolyte discharge occurred at less positive potentials than +1.0 v., the circuit was broken when the current reached about 30 μa .

A typical voltammogram at pH 4.6 had a well-formed wave with an $E_{p/2}$ of 0.34 v. and an i_p of 9.9 μa , and a second less well-formed wave with an E_p of 0.83 v. When the electrode was rotated at 200 r.p.m., a single large rounded wave resulted (Figure 1B). At pH 2, $E_{p/2}$ for the first wave was 0.33 v. and i_p was 15 μa .

An interesting phenomenon was observed at pH 12. In acid solution, the evolution of oxygen occurs at potentials beyond 1.0 v. However, at pH 12, the evolution is shifted to about 0.6 v. Figure 1C shows three successive voltammograms recorded at pH 12. A waxy film was observed on the electrode surface which was probably a mixture of biphenyl and diphenylborinic acid. This film was soluble in acetone; cleaning the electrode with an acetone-soaked tissue removed it and restored the bright platinum surface. Although the electrode was cleaned between runs in this manner, the wave was successively shifted into the region of background discharge. This would indicate that the electrolytic discharge of the background electrolyte in basic solution alters the surface of the platinum electrode to such an extent that the half-peak potential for the oxidation of tetraphenylborate ion is shifted to a potential greater than that required for the background discharge process. A similar effect has been observed by Lingane for the oxidation of oxalate ion at the platinum electrode.⁶ Successive chrono-

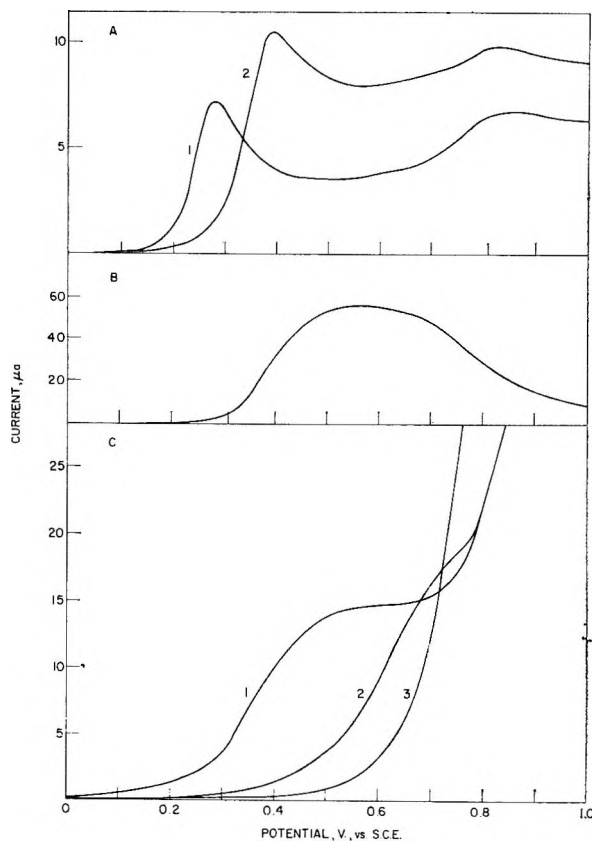


Figure 1. Voltammograms of tetraphenylborate. A: (1) At the stationary graphite electrode (area: 0.126 cm^2); (2) at the stationary platinum disk electrode (area: 0.283 cm^2). Solution composition: 1.0 mM sodium tetraphenylborate, 0.5 M acetate buffer (pH 4.6). B: At the rotating platinum disk electrode (rate of rotation: 200 r.p.m.). Solution composition as in A. C: Successive voltammograms of 1 mM tetraphenylborate in 0.01 M NaOH-0.5 M NaCl solution at the stationary platinum disk electrode. Numbers refer to the order in which the voltammograms were recorded.

potentiograms showed a marked decrease in the transition time and a shift to more positive potentials. This was shown to be due to the formation of platinum oxides which apparently decrease the rate of the electron-transfer process.

It should be noted that, in the present investigation, the potential scan was stopped at +1.0 v., which is insufficient to produce background discharge or oxygen evolution in acid or neutral solution. However, in basic solutions a discharge current was observed.

If the electrode used by Geske³ had been inadvertently held at a sufficiently positive potential to produce a platinum oxide film on the electrode, then

(5) See, for example, F. C. Anson and J. J. Lingane, *J. Am. Chem. Soc.*, **79**, 1015 (1957).

(6) J. J. Lingane, *J. Electroanal. Chem.*, **1**, 379 (1960).

negative results would be expected; this seems to be a likely possibility.⁷

Experimental

The platinum disk electrode was prepared by sealing a disk (6-mm. diameter) to the base of a piece of 6-mm. soft glass tubing using Epon 815 epoxy resin. Electrical contact was made by placing a small quantity of mercury in the tube and inserting a piece of copper wire into the mercury.

Voltammograms were recorded using a Sargent Model XV polarograph and a jacketed H-cell maintained at $25.0 \pm 0.1^\circ$. Potentials were measured *vs.* the saturated sodium chloride calomel electrode whose potential is within a few millivolts of that of the saturated potassium chloride calomel electrode. The polarization rate was 1.66 mv./sec.

A Holtzer-Cabot 300 r.p.m. synchronous motor was used to rotate the electrode. The rate of rotation was varied by means of belt-driven pulleys.

Sodium tetraphenylborate (Fisher Scientific) was used without further purification. All solutions were 1.0 mM in sodium tetraphenylborate and 0.5 M in total ionic strength.

Acknowledgment. The authors wish to thank the U. S. Atomic Energy Commission for partial support of this work. W. R. T. thanks the Institute of Science and Technology of The University of Michigan for a postdoctorate fellowship.

(7) D. H. Geske, private communication.

The Thermodynamic and Physical Properties of Beryllium Compounds. VII. Enthalpy and Entropy of Sublimation of Beryllium Fluoride

by Jay A. Blauer, Michael A. Greenbaum, and Milton Farber

Maremont Corporation, Research Division, Pasadena, California
(Received October 8, 1964)

The limited amount of data concerning the sublimation of $\text{BeF}_2(\text{c})$ which are available is of a controversial nature. Efimenko¹ has recently reported a value of 55.35 ± 0.53 kcal./mole for the heat of sublimation of $\text{BeF}_2(\text{c})$ at 755°K . based upon data obtained by means of mass spectroscopy. A value of 63.0 kcal./mole at an

average temperature of 794°K . and based upon data obtained by means of transpiration was reported by Novoselova, *et al.*²

In an effort to obtain a reliable value for the heat of sublimation of $\text{BeF}_2(\text{c})$, it was decided to undertake an experimental program to determine a definitive value for this thermodynamic property which could then be combined with the value for the heat of vaporization previously reported from these laboratories³ to yield a value for the heat of fusion. This was accomplished by direct measurement of the vapor pressure of crystalline BeF_2 .

The vapor pressure data for $\text{BeF}_2(\text{c})$ were obtained in the temperature range of $713\text{--}795^\circ\text{K}$. by means of the torsion effusion technique. The present experimental technique differs from the one previously described³ only in the following details. A radiation shield was placed around the graphite effusion cell and reference block within the vacuum chamber. With the furnace in a fixed position, it was found that the temperature difference between the positions occupied by the effusion cell and reference block was less than 1° at all temperatures within the experimental range.

Crystalline BeF_2 of 99.8% purity was obtained commercially (Brush Beryllium Co.). The loaded cell was outgassed at 500° and 10^{-6} mm. pressure for 24 hr. before actual measurements were made. It was found that samples treated in this manner gave no further shift in measured equilibrium pressures when pressures were measured on successive days.

The possible presence of an accommodation coefficient of significant magnitude was investigated by duplicating the data in two cells having different orifice areas.

Results and Discussion

The experimental data obtained in this study are tabulated in Table I and are shown plotted in Figure 1 in the manner prescribed by the van't Hoff equation. The geometrical constants of the two cells are listed in Table II.

An examination of the data plotted in Figure 1 reveals that there is, within experimental error, no evidence that the accommodation coefficient differs significantly from unity. Owing to the small temperature range within which data could be taken, it was not possible to vary the total cross-sectional area of the orifices by more than a factor of 4.

(1) J. Efimenko, NBS Report 8033, July 1963.

(2) A. V. Novoselova, F. Sh. Muratov, L. P. Reshetnikova, and I. V. Gordeev, *Vestn. Mosk. Univ. Ser. Mat. Mekhan. Astron. Fiz. i Khim.*, **13**, No. 6, 181 (1958).

(3) M. A. Greenbaum, J. N. Foster, M. L. Arin, and M. Farber; *J. Phys. Chem.*, **67**, 36 (1963).

Table I: Experimental Sublimation Data

No.	Temp., °K.	Cell	Pressure, atm. × 10 ⁷	No.	Temp., °K.	Cell	Pressure, atm. × 10 ⁷
44	713	A	0.32	66	773	A	6.48
45	724	A	0.55	67	785	A	10.87
46	735	A	0.94	68	779	A	8.17
47	745	A	1.45	80	714	A	0.30
48	755	A	2.66	81	723	A	0.48
49	765	A	4.26	82	735	A	0.94
50	776	A	6.63	83	746	A	1.60
53	717	A	0.42	84	755	A	2.56
54	727	A	0.67	85	762	A	3.99
55	738	A	1.15	86	773	A	6.68
56	748	A	2.05	87	785	A	11.51
57	758	A	3.27	12	755	B	2.15
58	768	A	5.23	13	763	B	3.72
60	714	A	0.27	14	774	B	6.86
61	725	A	0.52	19	755	B	2.13
62	734	A	0.80	20	764	B	3.95
63	744	A	1.62	21	773	B	6.43
64	755	A	2.69	22	784	B	11.15
65	764	A	4.34	23	795	B	18.82

Table II: Geometrical Factors of Effusion Cells

Cell	Description	l/a^2	Total orifice area × 10 ² cm. ²
A	4 hole × 1-mm. diam.	0.49	3.35
B	4 hole × 2-mm. diam.	0.98	13.0

^a The length of the orifice is l and a is its radius.

The data listed in Table I were fitted to the van't Hoff equation by the method of least squares. The resultant enthalpy and entropy changes for the sublimation process at an average temperature of 750°K. were found to be 56.6 ± 0.7 kcal./mole and 44.9 ± 0.9 cal./ (°K. mole), respectively. Interpolation within the estimated heat capacity data⁴ gives values for the enthalpy and entropy of sublimation at 298°K. of 58.1 ± 0.7 kcal./mole and 47.8 ± 0.9 cal./ (°K. mole), respectively.

Values of 53.3 ± 0.3 kcal./mole and 38.7 ± 0.6 cal./ (°K. mole) for the enthalpy and entropy of vaporization at an average temperature of 1023°K. were reported previously from this laboratory.³ The corresponding values at 298°K. as found by interpolation within the estimated heat capacity data⁴ are 57.1 kcal./mole and 44.2 cal./ (°K. mole), respectively. Accordingly, the corresponding enthalpy and entropy changes of fusion at the melting point (815°K.)³ are 1.6 ± 0.8 kcal./mole and 4.2 ± 1.1 cal./ (°K. mole), respectively.

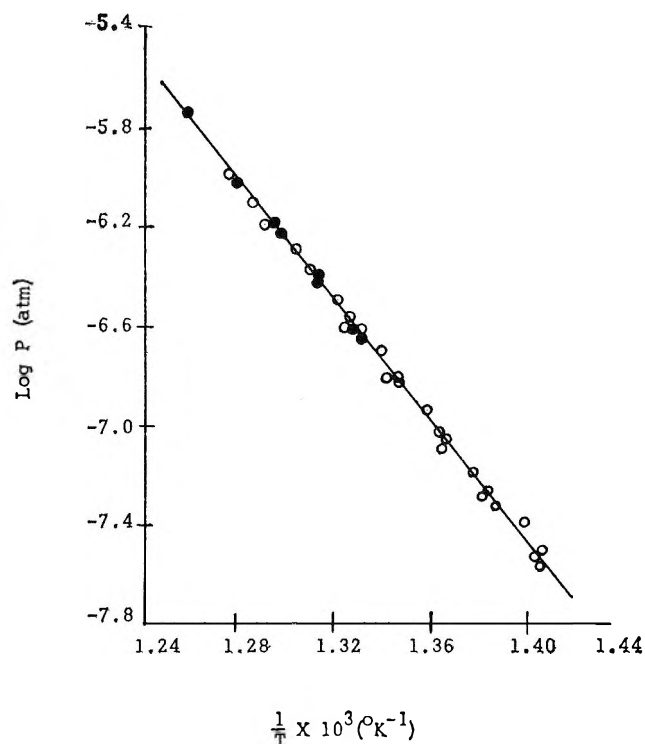


Figure 1. Sublimation pressure of BeF₂ as a function of temperature: O, cell A; ●, cell B.

It should be pointed out that the absolute vapor pressure values obtained from the solid BeF₂ employed in this investigation and those previously reported for liquid BeF₂ show a high degree of consistency. This lends considerable support to the validity of the thermodynamic values for sublimation and fusion of BeF₂ reported here.

(4) "JANAF Thermochemical Tables," USAF Contract AF 33(616)-6149, Advanced Research Projects Agency, Washington 25, D. C.

Reactivities of Perfluoroalkynitriles toward Butadiene¹

by Alan R. Monahan² and George J. Janz

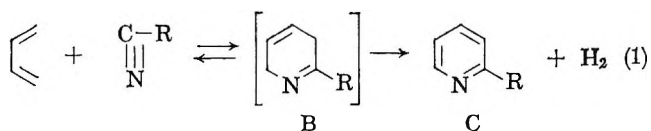
Department of Chemistry, Rensselaer Polytechnic Institute, Troy, New York (Received October 19, 1964)

The formation of pyridines from nitriles and 1,3-dienes was first noted³ with cyanogen and butadiene.

(1) Abstracted in part from a thesis submitted by A. R. Monahan in partial fulfillment of the requirements for the Ph.D. degree, Aug. 1964.

(2) Union Carbide Fellow in chemistry, 1963-1964.

More recent studies^{4a,b} have shown that the perfluoroalkylnitriles, similarly, have pronounced dienophilic properties. Kinetic studies of the thermally initiated reaction of $(\text{CN})_2$ and CF_3CN with 1,3-butadiene in the temperature range 350–450° have been reported^{5,6}; the reactions may be classed as examples of a high-temperature Diels–Alder type synthesis, *i.e.*, eq. 1, but



differ in that the product found in each case is the fully aromatized pyridinic product C, rather than the cyclic adduct B. A quantitative measure of the "diene" affinities in this series of dienophiles in the homogeneous gas phase and at moderately high temperatures (350–450°) would be of interest relative to current viewpoints on gas-phase diene reactions. Use of the kinetics of the CF_3CN –butadiene cyclization as a reference standard suggests a possible approach. The present note reports a competitive rate technique for this purpose, and the results for studies with CF_3CN , $\text{CF}_3\text{CF}_2\text{CN}$, and $\text{CF}_3(\text{CF}_2)_2\text{CN}$ with 1,3-butadiene in this synthesis.

Experimental

Chemicals. Butadiene, 99.0% purity, b.p. -3.0° (Matheson Co., C.P. grade), was vacuum degassed three times (-195°) prior to use. The nitriles (CF_3CN , b.p. -60° ; $\text{CF}_3\text{CF}_2\text{CN}$, b.p. -35° ; and $\text{CF}_3(\text{CF}_2)_2\text{CN}$, b.p. -5°), each obtained in 98% purity (Peninsular ChemResearch Inc., Columbia Organic Chemicals Co.), were similarly treated.

Apparatus and Procedure. The continuous flow assembly previously described^{4,7} was adapted to take a 15-mm. diameter, 70-cm. length Pyrex spiral reactor (vol. 124 ml.). Errors due to the possibility of reaction occurring in the inlet and exit of the reactor were minimized by using capillary tubing (2-mm. i.d.; vol. 1.3 ml.). The temperature profile along the depth of the reactor (28 cm.) was maintained at $\pm 1.0^\circ$ and the temperature variation throughout the course of a run was $\pm 1.0^\circ$.

Quantitative analysis of the two pyridinic products from each run was with vapor phase chromatography [Beckman GC-2A gas chromatograph, with a 6-ft. di-*n*-decyl phthalate column (30% on C-22 firebrick; 130–160°)]. Calibrations (mmoles/cm.²) were made with the three 2-perfluoroalkylpyridines.

The experimental conditions and results for three competitive series, each with butadiene, *i.e.*, CF_3CN and $\text{C}_2\text{F}_5\text{CN}$, CF_3CN and $\text{C}_3\text{F}_7\text{CN}$, and $\text{C}_2\text{F}_5\text{CN}$ and $\text{C}_3\text{F}_7\text{CN}$, are in Table I. The rate data for the standard

Table I: Competitive Reactions of Perfluoroalkylnitriles for 1,3-Butadiene

Temp., °C.	Contact time, sec.	X_1 (mole ratio)	X_2 (mole ratio)	$k_2\text{CF}_3\text{CN}$ (cc. mole ⁻¹ sec. ⁻¹)	k_2'
Series I $\left[X_1 = \frac{\text{C}_2\text{F}_5\text{CN}}{\text{CF}_3\text{CN}} \right];$					
$X_2 = \frac{\text{C}_3\text{F}_7\text{CN}}{\text{C}_2\text{F}_5\text{CN}}; k_2 = k_2' \text{C}_2\text{F}_5\text{CN}$					
347.9	1380	0.896	1.68	55.02	26.68
350.5	28.83	0.983	1.34	59.84	45.49
366.9	1169	0.838	1.47	92.43	75.02
381.4	1184	0.788	1.56	135.4	115.9
394.9	1207	0.922	1.20	188.4	170.0
412.5	32.96	1.05	0.983	286.4	276.7
462.2	31.32	1.15	0.997	829.9	950.6
Series II $\left[X_1 = \frac{\text{CF}_3(\text{CF}_2)_2\text{CN}}{\text{CF}_3\text{CN}} \right];$					
$X_2 = \frac{\text{C}_3\text{F}_7\text{CN}}{\text{CF}_3\text{CN}}; k_2 = k_2' \text{C}_3\text{F}_7\text{CN}$					
363.9	33.97	0.771	2.16	85.90	51.61
394.9	26.42	1.25	1.12	191.0	136.4
Series III ^a $\left[X_1 = \frac{\text{CF}_3(\text{CF}_2)_2\text{CN}}{\text{CF}_3\text{CF}_2\text{CN}} \right];$					
$X_2 = \frac{\text{C}_3\text{F}_7\text{CN}}{\text{C}_2\text{F}_5\text{CN}}; k_2 = k_2' \text{C}_3\text{F}_7\text{CN}$					
344.2	35.75	0.917	1.58	36.56	25.26
377.0	33.43	1.05	1.57	102.1	62.22
419.4	40.25	0.981	1.30	329.6	257.9
488.6	39.28	1.03	1.22	869.0	694.1

^a In Series III it is to be noted that k_2 is no longer equal to $k_2\text{CF}_3\text{CN}$ but rather $k_2\text{C}_3\text{F}_7\text{CN}$.

(3) G. J. Janz, R. G. Asch, and A. G. Keenan, *Can. J. Res.*, **B25**, 272 (1947).

(4) (a) G. J. Janz and A. R. Monahan, *J. Org. Chem.*, **29**, 569 (1964); (b) *ibid.*, in press.

(5) P. J. Hawkins and G. J. Janz, *J. Chem. Soc.*, **76**, 1479 (1949).

(6) G. J. Janz and J. M. S. Jarvie, *J. Phys. Chem.*, **60**, 1430 (1956).

(7) G. J. Janz and M. A. De Crescente, *J. Org. Chem.*, **23**, 765 (1958).

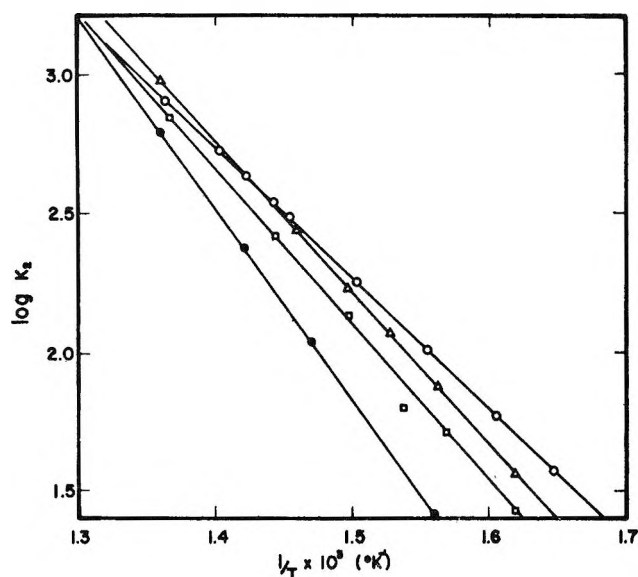


Figure 1. Comparison of the temperature dependence of the reaction rates in the synthesis of pyridines from butadiene with $(\text{CN})_2$ (\bullet), CF_3CN (\circ), $\text{CF}_3\text{CF}_2\text{CN}$ (Δ), and $\text{CF}_3(\text{CF}_2)_2\text{CN}$ (\square) in the range 350–460°.

reaction (CF_3CN and C_4H_6) are those previously reported,⁶ but were checked by several independent experiments in the present study. The agreement in new check experiments with the previous results was within the limits of experimental study (accuracy $\pm 4\%$). The rate constants k_2' were gained by the expression $k_2' = k_2^{\text{CF}_3\text{CN}}(R_2/R_1)([\text{CF}_3\text{CN}]/[\text{RCN}])$ where $k_2^{\text{CF}_3\text{CN}}$ and the rate, R_1 , are known for the "standard" reaction (*i.e.*, CF_3CN and C_4H_6), and k_2' and R_2 are the rate constant and velocity for the competitive cyclization process. The ratio of the two reaction rates (R_2/R_1) was gained from the relative amounts of two pyridinic products in each experiment and the concentration of the two nitriles is known from the flow rates and temperature.

A graphical analysis ($\log k_2$ vs. $1/T$ ($^\circ\text{K}.$)) of the temperature dependence of these rates was made and is summarized in Figure 1 with the results for two related high-temperature Diels–Alder processes: $(\text{CN})_2$ and C_4H_6 , and CF_3CN and C_4H_6 . The derived kinetic parameters are in Table II. Owing to rather limited series of experiments in this study, the parameters for $\text{CF}_3\text{CF}_2\text{CN}-\text{C}_4\text{H}_6$ and for $\text{CF}_3(\text{CF}_2)_2\text{CN}-\text{C}_4\text{H}_6$ reactions must be viewed as less certain than the results for the more rigorous kinetic studies with $(\text{CN})_2$ and CF_3CN . Nevertheless, from the straight line plots (Figure 1) it can be concluded that the comparisons are intrinsically valid. The dienophilic reactivity of the simplest monoolefin, $\text{CH}_2=\text{CH}_2$, with butadiene has been investigated by Rowley and Steiner,⁸ under rather comparable re-

action conditions (480–650°, homogeneous gas phase, normal pressures); these results are also in Table II for comparison.

Table II: Kinetic Parameters for the Reactions of Ethylene, Cyanogen, and Cyanogen-Like Molecules with Butadiene

Diene	Dienophile	Temp. range, $^\circ\text{C}.$	A factor	ΔE^* , kcal./mole	ΔS^* , e.u.
Butadiene	$\text{CH}_2=\text{CH}_2^a$	485–650	3.0×10^{10}	27.5	-14.5
Butadiene	$(\text{CN})_2^b$	325–450	1.6×10^{12}	31.6	-11.8
Butadiene	CF_3CN^b	350–525	2.1×10^9	21.5	-19.4
Butadiene	$\text{CF}_3\text{CF}_2\text{CN}$	340–460	2.6×10^{10}	25.0	-14.5
Butadiene	$\text{CF}_3(\text{CF}_2)_2\text{CN}$	340–460	3.2×10^{10}	25.8	-14.2

^a See ref. 8. ^b See ref. 5, 6.

Discussion

For the present series of perfluoroalkylnitriles, inspection shows no very marked differences in the reaction rates (Table I) and in the kinetic parameters (Table II) relative to CF_3CN . It is clear that the first observation supports the intuitive conclusion that the butadiene affinities of CF_3CN , $\text{CF}_3\text{CF}_2\text{CN}$, and $\text{CF}_3(\text{CF}_2)_2\text{CN}$ are closely similar in this gas phase synthesis (350–450°). From current viewpoints, based largely on data from condensed state studies, it follows that the electrophilicity in this series of dienophiles decreases in the order $\text{CF}_3\text{CN} \gg \text{CF}_3\text{CF}_2\text{CN} > \text{CF}_3(\text{CF}_2)_2\text{CN} > (\text{CN})_2$. A measure of the magnitudes in this trend is given in the kinetic parameters summarized in Table II. When CF_3 is substituted for F on the α -carbon of CF_3CN , ΔE^* increases from 21.5 to 25.0 kcal./mole and ΔS^* increases from -19.4 to -14.5 e.u. Substitution of CF_3 for F on the β -carbon of $\text{CF}_3\text{CF}_2\text{CN}$ increases ΔE^* only 800 cal. and ΔS^* by 0.3 e.u. The relatively large decrease in reactivity of $(\text{CN})_2$, compared to the perfluoroalkylnitriles, relates, without doubt, to the lowered electrophilic properties of this compound and in part to the resonance stabilization in this molecular system. It is clear that this synthesis lends itself favorably to "diene affinity" studies with cyanogen-like compounds in the high-temperature Diels–Alder reaction; the prospect of quantitative measurements of diene reactivities relative to a common cyanogen-like dienophile appears equally possible and bears attention.

Acknowledgment. This work has been possible, in large part, by grants-in-aid from the American Chemical Society, Petroleum Research Fund, and the Union Carbide Chemicals Co.

(8) D. Rowley and H. Steiner, *Discussions Faraday Soc.*, **10**, 198 (1951).

The Thermal Isomerization of Cyclobutene^{1a}

by Robert W. Carr, Jr.,^{1b} and W. D. Walters

Department of Chemistry, The University of Rochester,
Rochester, New York (Received October 22, 1964)

Cyclobutene has been observed to isomerize to 1,3-butadiene by a homogeneous, unimolecular process, uncomplicated by side reactions, at 130–175°. The first-order rate constants decrease significantly with decreasing initial pressure at pressures below about 5 mm., but no experiments were done at pressures greater than 50 mm. This work was undertaken in order to obtain data over a greater portion of the first-order region of cyclobutene isomerization and to determine values for the Arrhenius parameters at pressures considerably higher than those where the falloff becomes important. It was felt that the results of the investigation would allow a comparison of the experimentally observed values of k , A , and E at pressures near 1500 mm. with the high pressure values obtained earlier by extrapolation methods.³ Also, in the event that either a marked increase or decrease in the first-order rate constant resulted from an increase in the initial pressure above 50 mm., additional consideration of either the reaction mechanism or the intramolecular energy-transfer process would have to be made.^{4,5}

Experimental

Cyclobutene from two sources was used in this study. One sample has been prepared in this laboratory by Dr. W. Cooper,² and the other was kindly supplied by Prof. W. R. Moore of the Massachusetts Institute of Technology. The first sample was purified by gas chromatography, and subsequent gas chromatographic analysis with a 3-m. column containing tetraisobutylene upon 60–80 mesh firebrick at room temperature indicated the purity to be 99.9% or greater. The second sample, which contained a small amount of 1,3-butadiene, was treated with maleic anhydride in chlorobenzene at 60° for 24 hr. in a sealed tube. Analysis by gas chromatography and by absorption spectrophotometry in a Cary Model 11 spectrophotometer revealed that a small amount of butadiene remained in the sample. Quantitative analysis with a Beckman DU instrument, as described below, showed the amount to be 0.42%, and appropriate corrections were applied in experiments where this sample was used. Matheson Instrument Grade 1,3-butadiene was used after trap-to-trap distillation. Gas chromatographic analysis showed that it was better than 99.9% pure.

Kinetic experiments were performed in the apparatus described in a previous publication,⁴ using similar techniques, with the exception of five higher pressure experiments which were carried out near 131° in sealed tubes immersed in an oil bath controlled to $\pm 0.1^\circ$. In the usual experiment the reaction mixture was removed rapidly from the reaction vessel by condensation at -196° and then was transferred to an analytical section. Analysis of the butadiene content was done by means of a Beckman DU spectrophotometer equipped with a photomultiplier tube. Precautions were taken to keep the drift to a negligible amount. The 10-mm. quartz cell was connected to a mixing bulb and a McLeod gauge. Since the instrument was balanced against the evacuated cell for each analysis and calibrated periodically with pure 1,3-butadiene at 209.5, 214.5, and 221 $m\mu$, the results should not be affected appreciably by any change in the condition of the instrument or absorption cell. Tests showed that the results obtained for the percentage of reaction from data at two or three wave lengths were in reasonable agreement. (The deviations from the mean averaged 1.2 p.p.h.)

Results

Products. That 1,3-butadiene is the sole reaction product of importance in this study at higher pressures was shown by the fact that 1,3-butadiene and cyclobutene were the only substances found in excess of 0.1% by gas chromatographic and mass spectrometric analysis of the reaction mixtures from two 1520-mm. experiments, one at 150° and the other at 175°, carried to about 25% conversion. In an exploratory experiment it had been found that 1,3-butadiene (under conditions more severe with respect to butadiene pressure and time of reaction than those encountered in most of the cyclobutene experiments) does not dimerize to an appreciable extent. Likewise, a calculation based on data of Kistiakowsky and Ransom⁶ showed that the dimerization of 1,3-butadiene should not be of significance under any of the experimental conditions encountered in the present work.

(1) (a) This work was supported by a grant from the National Science Foundation to the University of Rochester. (b) Union Carbide Predoctoral Fellow, 1961–1962; Shell Postdoctoral Fellow during the last quarter of 1962.

(2) W. Cooper and W. D. Walters, *J. Am. Chem. Soc.*, **80**, 4220 (1958).

(3) W. P. Hauser and W. D. Walters, *J. Phys. Chem.*, **67**, 1328 (1963).

(4) R. W. Carr, Jr., and W. D. Walters, *ibid.*, **67**, 1370 (1963).

(5) D. J. Wilson, *ibid.*, **64**, 323 (1960).

(6) G. B. Kistiakowsky and W. W. Ransom, *J. Chem. Phys.*, **7**, 725 (1939).

Kinetics. In Table I are listed first-order rate constants for the isomerization of cyclobutene at three different temperatures. For purposes of comparison they have been corrected to 175.0, 150.0, and 131.0° using corrections in the range 0.8 to 1% for 0.1°. For some experiments near 131° where the differences were greater than 0.5° the correction factors were in an exponential form containing the observed activation energy. The data indicate that the rate constants are essentially invariant with pressure as expected for a unimolecular reaction close to its high pressure limit.⁷

Table I: Effect of Initial Pressure upon the First-Order Rate Constant for the Isomerization of Cyclobutene

150°		175°		131°	
P_0 , mm.	$10^4 k$, sec. ⁻¹	P_0 , mm.	$10^4 k$, sec. ⁻¹	P_0 , mm.	$10^4 k$, sec. ⁻¹
48.5	2.49	50 ^a	21.6 ± 0.5 ^a	101 ^b	0.372
102 ^b	2.41	109 ^a	22.4 ± 0.1 ^a	102	0.466
106 ^a	2.53 ± 0.03 ^a	194	21.9	125 ^c	0.434
113	2.44	414	23.9 ^d	1,381 ^c	0.447
155	2.55	421 ^b	22.0	1,488	0.406
294	2.50	689 ^b	21.6	1,497	0.381 ^d
638	2.47	743	23.8 ^d	3,310 ^c	0.445
1160 ^b	2.55 ± 0.03 ^a	807	24.6 ^d	6,600 ^c	0.416
1396	2.63 ^c	1485 ^b	22.3	12,250 ^c	0.451
1519 ^b	2.50	1520	25.6 ^d		
1521	2.45 ^e				

^a Average of two to four experiments. ^b Experiment in a packed vessel. ^c Experiment in a sealed tube. ^d Comments in footnote 7 apply to these experiments. ^e In earlier work³ k_{∞} (by extrapolation) was 2.52×10^{-4} at 150.4° and 21.3×10^{-4} sec.⁻¹ at 175.4°.

The experiments in the packed vessel afford some information concerning whether heterogeneous reactions occur to a measurable extent and whether temperature gradients exist in the reaction vessel during the isomerization. Approximate calculations,⁸ taking into account only conduction of heat, indicated that at 175° and 2 atm. the temperature at the center of the 27-ml. vessel might be several degrees different from that at the walls, and lesser gradients could exist at less severe conditions. The fact that the rate in the packed vessel (with ninefold greater S/V) usually did not change significantly from that in a similar unpacked vessel is an indication either that any effects caused by temperature gradients and heterogeneous reactions were not large in the present work or that they just cancel. It seems somewhat unlikely that such fortuitous compensation would occur at the various pressures and temperatures.

The temperature dependence of the isomerization was studied at pressures near 100 and 1500 mm. for temperatures usually in the neighborhood of 130°, 140°, 150°, 160°, and 175°. The experimental data from both series of experiments, plotted as $\log k$ vs. $1/T$, are shown in Figure 1. The results from experiments in the packed and unpacked vessels have been included in the same plot. The activation energy from the 100-mm. experiments was determined graphically and by the method of least squares, the latter calculations being done on an IBM 650 computer. A value of 32.2 ± 0.4 kcal./mole was obtained from the 100-mm. experiments. The pre-exponential factor was calculated from the experimental rate constants by the use of the expression $k = A \exp(-E_a/RT)$ where E_a was taken as 32.2 kcal./mole. The resultant values of the pre-exponential factor were averaged, giving $A = 1.1 \pm 0.1 \times 10^{13}$ sec.⁻¹.

To evaluate the activation energy from the experiments near 1500 mm., least-squares calculations were made on the data from packed and unpacked bulb experiments taken together and then from packed vessel experiments considered separately. Also, graphical evaluations were done from Arrhenius plots. A value of $E_a = 32.9 \pm 0.7$ kcal./mole will encompass all values plus their standard deviations which were obtained by various treatments (with or without the experiments mentioned in footnote 7). Using 32.9 kcal./mole for E_a , values of A were calculated from the values of k for all the experiments near 1500 mm., from which an average A , $2.5 \pm 0.1 \times 10^{13}$ sec.⁻¹, was determined.

Discussion

The first-order rate constants for cyclobutene have been found to be independent of pressure from about 50 to 1500 mm. at 150 and 175°, and from 100 to 12,000 mm. at 131°. This is the behavior generally predicted for a quasi-unimolecular reaction near the high pressure limit. Over the pressure range studied the present findings do not indicate any decrease in the rate constants with increasing pressure, an observation which might have certain implications concerning intramolec-

(7) In one series in an unpacked bulb (see Table I), k at 175° for 414, 743, 807, and 1520 mm. averaged $24.5 \pm 0.7 \times 10^{-4}$ sec.⁻¹. These values (~10% higher than the other results) could not be duplicated, but they confirmed the absence of a significant change in the rate constant from 400 to 1500 mm. The reliability of five other experiments at lower temperatures in the same series is somewhat in doubt although the agreement with comparable experiments sometimes was more satisfactory.

(8) Similar to those of S. W. Benson ["The Foundations of Chemical Kinetics," McGraw-Hill Book Co., Inc., New York, N. Y., 1960, pp. 426-431]. Since no value for the heat of formation of cyclobutene could be found in the literature, these calculations were based on an estimated heat of reaction. Transfer of heat by any process in addition to conduction will tend to lower any gradient.

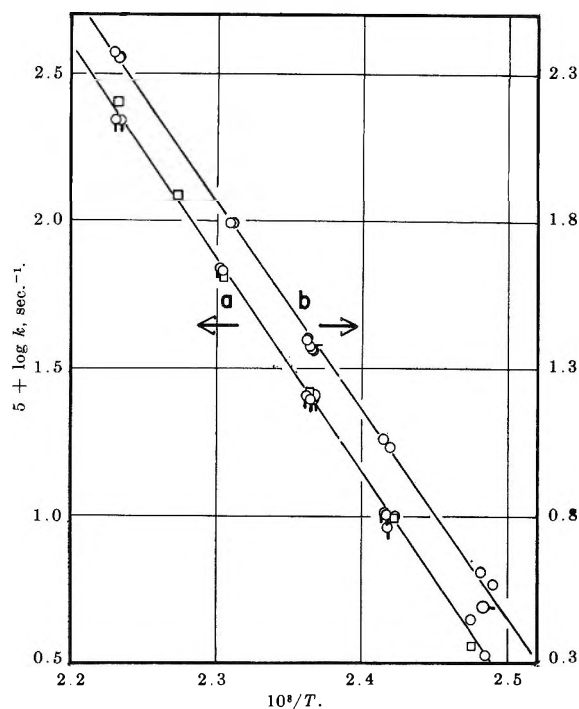


Figure 1. Temperature dependence of the first-order rate constant: a (left-hand scale), experiments near 1500 mm.; b (right-hand scale), experiments near 100 mm.; O-, packed vessel, 100 mm.; □, packed vessel, 1500 mm.; □, experiments referred to in footnote 7.

ular energy transfer in activated molecules. The possibility of a decrease in rate at higher pressures has been pointed out by Wilson⁵ and has been discussed elsewhere.⁹ In this connection it has also been found that the first-order rate constants observed for the thermal decomposition of cyclobutane up to 1500 mm. appear to show a "conventional" high pressure limit.⁴ Flowers and Frey¹⁰ have reported that a change in rate constant does not occur with 1,1-dimethylcyclopropane over the pressure range 16 to 1596 mm.

From the presently available information the value of the activation energy obtained from the 1500-mm. experiments ($E_a = 32.9 \pm 0.7$ kcal./mole) may be regarded as approximating the activation energy for the isomerization of cyclobutene at the high pressure limit. This value is in good accord with that previously determined by extrapolation methods ($E_a = 32.7 \pm 0.8$ kcal./mole).³ The difference between the values of the activation energy from the 100-mm. and the 1500-mm. data probably represents an experimental variation and not the decrease in activation energy expected when a quasi-unimolecular reaction is well into the falloff region.

The isomerization of cyclobutene has an activation energy markedly lower than the values obtained for the decomposition of cyclobutane and its alkyl derivatives

(61–63 kcal./mole) and proceeds in a much lower temperature range. Various factors which might contribute to decreasing the stability of the ring in the case of cyclobutene have been discussed earlier,^{2,11} and there are several indications of considerable strain in the cyclobutene ring.¹² According to Nangia and Benson¹³ the difference in the strain energy between cyclobutene and cyclobutane needed to account for the lower E_a for cyclobutene is rather unreasonable. A suggestion has been made recently that the low activation energy is due to the ionic character of the transition state.¹⁴ The activation energies for the isomerizations of several substituted cyclobutenes (31.5–36.0 kcal./mole) are in the same low range as that observed for cyclobutene and the differences in the rates have been explained in terms of changes in (a) the strain energy, (b) steric repulsion, and (c) resonance stabilization of the activated complex.¹⁵

The entropy of activation at 150° calculated for the 1500-mm. experiments from the expression $A = \kappa e(k_B T/h) \exp(\Delta S^*/R)$ is +0.1 e.u. for $\kappa = 1$ and +1.5 e.u. for $\kappa = 0.5$ compared to an over-all entropy change of +4.5 e.u. for the isomerization at 127° (which is indicated from the entropy values for cyclobutene¹⁶ and 1,3-butadiene¹⁷).

Acknowledgment. The authors wish to thank Mr. Carl Whiteman for his assistance and Professor W. R. Moore of the Massachusetts Institute of Technology for a sample of cyclobutene.

- (9) R. W. Carr, Jr., Ph.D. Thesis, University of Rochester, 1962.
 (10) M. C. Flowers and H. M. Frey, *J. Phys. Chem.*, **65**, 373 (1961).
 (11) E. Vogel, *Angew. Chem.*, **66**, 640 (1954); **68**, 189 (1956).
 (12) E. Goldish, K. Hedberg, and V. Schomaker, *J. Am. Chem. Soc.*, **78**, 2714 (1956); R. C. Lord and D. G. Rea, *ibid.*, **79**, 2401 (1957).
 (13) P. Nangia and S. W. Benson, *ibid.*, **84**, 3411 (1962).
 (14) S. W. Benson, "Advances in Photochemistry," Vol. 2, W. A. Noyes, Jr., G. S. Hammond, and J. N. Pitts, Jr., Ed., Interscience Publishers, Inc., New York, N. Y., 1964, p. 14.
 (15) H. M. Frey, *Trans. Faraday Soc.*, **60**, 83 (1964); E. Gil-Av and J. Shabtai, *J. Org. Chem.*, **29**, 257 (1964).
 (16) A. Danti, *J. Chem. Phys.*, **27**, 1227 (1957).
 (17) J. G. Aston, G. Szasz, H. W. Woolley, and F. G. Brickwedde, *ibid.*, **14**, 67 (1946).

The C-C Bond Dissociation Energy in C_2F_6 ¹

by E. Tschuikow-Roux

Jet Propulsion Laboratory, California Institute of Technology, Pasadena, California (Received November 2, 1964)

Recently, Bibby and Carter² reported a mass spectrometric study of the dissociation and ion production

in C_2F_6 and other fluorocarbon gases. From their measured appearance potentials and a quoted value of $I(CF_3) = 9.35$ e.v., which in turn was deduced from measured $A(CF_3^+)$ in CF_3Br^{3a} and $D(CF_3-Br)^{3b}$ and represents an upper limit, Bibby and Carter obtain a surprisingly high C-C bond energy in C_2F_6 , $D(CF_3-CF_3) = 139.5$ kcal./mole. This value is to be compared with earlier mass spectrometric studies as well as other data obtained by various indirect methods. Thus Dibeler, *et al.*,⁴ deduced $D(CF_3-CF_3) = 124$ kcal./mole from appearance potential measurements in CF_3CH_3 and C_2F_6 using a derived value of the ionization potential, $I(CF_3) = 8.9$ e.v. based on their $A(CF_3^+)$ and $A(CH_3^+)$, and the known $I(CH_3)$. This value of the ionization potential for CF_3 is much lower than the measured value of Farmer, *et al.*,⁵ who determined $I(CF_3) = 10.10$ e.v. and also the appearance potentials for CF_3^+ from CF_4 and CF_3H which lead to $D(CF_3-F)$ and $D(CF_3-H)$ values consistent with the heats of formation of these compounds. From these data they obtained $\Delta H_f(CF_3) = -117 \pm 2$ kcal./mole. Using $I(CF_3) = 10.10$ e.v. together with the $A(CF_3^+)$ from C_2F_6 reported by Dibeler, *et al.*, leads to $D(CF_3-CF_3) = 97$ kcal./mole, while Bibby and Carter's value of $A(CF_3^+) = 15.4$ e.v. gives a bond energy of 122 kcal./mole. On the other hand a value of 69 kcal./mole is obtained if the above $\Delta H_f(CF_3)$ is used with $\Delta H_f(C_2F_6) = -303$ kcal./mole.⁶ Farmer, *et al.*, believed this bond energy to be too low and suggested that $\Delta H_f(C_2F_6)$ may be in error, however subsequent work showed the value to be indeed lower.

Thus, $D(CF_3-CF_3)$ values calculated from kinetic plus thermochemical data tend to be lower. Pritchard, *et al.*,⁷ determined the C-H bond energy in fluoroform from a study of the reversible reaction between CF_3 radicals and methane, and the known value for $D(CH_3-H)$. Based on this work they deduced the values: $\Delta H_f(CF_3) = -119$ and $D(CF_3-CF_3) = 65$ kcal./mole. At the time of their work the heat of formation of fluoroform was not yet known and they used an estimated value of -169 kcal./mole together with $\Delta H_f(C_2F_6) = -303$ kcal./mole. Using the calorimetric value for $\Delta H_f(CF_3H) = -162.6$ kcal./mole⁸ leads to a revision of the above quantities: $\Delta H_f(CF_3) = -112.7$ and $D(CF_3-CF_3) = 77.6$ kcal./mole. A higher value for the bond dissociation energy in C_2F_6 is supported by the recent work of Corbett, Tarr, and Whittle⁹ on the vapor phase bromination of fluoroform. These authors determined $D(CF_3-H) = 109.5$ kcal./mole (a rather high value) which leads to $\Delta H_f(CF_3) = -105$ and $D(CF_3-CF_3) = 93$ kcal./mole. However, Pritchard and Thommarson¹⁰ redetermined the C-H bond energy in fluoroform by the classical kinetic method used

previously⁷ and their result of $D(CF_3-H) = 102$ kcal./mole corroborates earlier work. Rabinovitch and Reed^{11,12} used the diffusion flame method to study the reaction between sodium atoms and the series of compounds: CH_3Cl , CH_2FCl , CHF_2Cl , and CF_3Cl . From the activation energies of the primary step in the series they evaluated the C-Cl bond energies in these compounds which in turn enabled them to calculate $\Delta H_f(CF_3) = -119.5$ and $D(CF_3-CF_3) = 64$ kcal./mole.

The above divergency of results of the C-C bond dissociation energy in C_2F_6 and the heat of formation of the CF_3 radical clearly indicates that further work is necessary to resolve this question. Especially desirable would be a direct pyrolytic value for the dissociation energy. Mercer and Pritchard¹³ have made an attempt to obtain this quantity by pyrolyzing C_2F_6 in a flow system with toluene as carrier and found the rate constant for the decomposition (eq. 1) to be: $k_1 \approx$



$10^8 \exp(-50,000/RT)$ sec.⁻¹. In view of the abnormally low frequency factor the authors do not regard the observed activation energy as a measure of the dissociation energy and suggest that the reaction was probably heterogeneous. Thus no significance can be attached to this pyrolysis work.

We have studied the kinetics of the thermal decomposition of C_2F_6 in the presence of hydrogen in a single pulse shock tube under homogeneous reaction conditions in the temperature range 1300 to 1600°K. and de-

(1) This paper presents results of one phase of research carried out at the Jet Propulsion Laboratory, California Institute of Technology, under Contract No. NSA 7-100, sponsored by the National Aeronautics and Space Administration.

(2) M. M. Bibby and G. Carter, *Trans. Faraday Soc.*, **59**, 2455 (1963).

(3) (a) J. Marriott and J. D. Craggs, *J. Electron.*, **1**, 405 (1955); (b) A. H. Sehon and M. Szwarc, *Proc. Roy. Soc. (London)*, **A209**, 110 (1951).

(4) V. H. Dibeler, R. M. Reese, and F. L. Mohler, *J. Chem. Phys.*, **20**, 761 (1952).

(5) J. B. Farmer, I. H. S. Henderson, F. P. Lossing, and D. G. H. Marsden, *ibid.*, **24**, 348 (1956).

(6) F. W. Kirkbride and F. G. Davidson, *Nature*, **174**, 79 (1954).

(7) G. O. Pritchard, H. O. Pritchard, H. I. Schiff, and A. F. Trotman-Dickenson, *Chem. Ind. (London)*, 896 (1955); *Trans. Faraday Soc.*, **52**, 849 (1956).

(8) C. A. Neugebauer and J. L. Margrave, *J. Phys. Chem.*, **62**, 1043 (1958).

(9) P. Corbett, A. M. Tarr, and E. Whittle, *Trans. Faraday Soc.*, **59**, 1609 (1963).

(10) G. O. Pritchard and R. L. Thommarson, *J. Phys. Chem.*, **68**, 568 (1964).

(11) B. S. Rabinovitch and J. F. Reed, *J. Chem. Phys.*, **22**, 2092 (1954).

(12) J. F. Reed and B. S. Rabinovitch, *J. Phys. Chem.*, **61**, 598 (1957).

(13) P. D. Mercer and H. O. Pritchard, *J. Chem. Soc.*, 2843 (1957).

duced the rate constant for the unimolecular decomposition (eq. 1) to be: $k_1 = 1.7 \times 10^{18} \exp(-94,400/RT)$ sec.⁻¹ with an estimated uncertainty of ± 4 kcal./mole.¹⁴ If we accept an activation energy of 1 to 2 kcal./mole for the recombination of CF₃ radicals,^{15,16} then $D(\text{CF}_3\text{-CF}_3) \approx 93 \pm 4$ kcal./mole and with $\Delta H_f(\text{C}_2\text{F}_6) = -303$ kcal./mole we find $\Delta H_f(\text{CF}_3) = -105 \pm 2$ kcal./mole. These results, together with all previous investigations, are summarized in Table I. Our results are in agreement with the value deduced by Corbett, Tarr, and Whittle, which was based, however, on their unusually high C-H bond energy in CF₃H. The above value for the heat of formation of CF₃, when used with the now relatively well established $D(\text{CF}_3\text{-H}) = 102$ kcal./mole, leads to $\Delta H_f(\text{CF}_3\text{H}) = -155$ kcal./mole, which is in disagreement with the experimental value of -162.6 kcal./mole reported by Neugebauer and Margrave. It is obvious that the results could be reconciled if either $\Delta H_f(\text{CF}_3\text{H})$ were indeed higher as indicated above, or if $\Delta H_f(\text{C}_2\text{F}_6)$ were correspondingly lower (-318 kcal./mole) then Kirkbride and Davidson reported. Thus a redetermination of these quantities may be desirable.

Table I: Bond Dissociation Energies and Heats of Formation^a

$D(\text{CF}_3\text{-CF}_3)^b$	$D(\text{CF}_3\text{-H})^b$	$\Delta H_f(\text{CF}_3)^b$	Method	Ref.
139.5	...	-82	Electron impact	c
122 ^d	...	-90.5		
124	...	-89.5	Electron impact	e
97 ^f	Electron impact	g
69	102 ± 2	-117 ± 2		
65	102 ± 2	-119 ^h	H abstraction	i
77.6	...	-112.7		
93	109.5 ± 1.5	-105 ± 2	Bromination of CF ₃ H	j
79	102.6	-112.1	Calculated ^k	j, l
64	...	-119.5	Na diffusion flame	m
93 ± 4	...	-105 ± 2	Pyrolysis	n

^a Unless otherwise stated the following heats of formation were used in these calculations: $\Delta H_f(\text{C}_2\text{F}_6) = -303$ kcal./mole and $\Delta H_f(\text{CF}_3\text{H}) = -162.6$ kcal./mole. ^b Values are in kcal./mole. ^c Ref. 1. ^d Based on $I(\text{CF}_3) = 10.10$ e.v. from ref. 5. ^e Ref. 4. ^f Based on $A(\text{CF}_3^+) = 14.3$ e.v. from ref. 4. ^g Ref. 5. ^h Based on $\Delta H_f(\text{CF}_3\text{H}) = -169$ kcal./mole. ⁱ Ref. 7. ^j Ref. 9. ^k Calculated from $D(\text{CF}_3\text{-Br}) = 64.5^3$ and $\Delta H_f(\text{CF}_3\text{Br}) = -149.8$ kcal./mole.⁹ ^l Ref. 3b. ^m Ref. 11. ⁿ This work.

In conclusion it may be stated that the result of Bibby and Carter for the C-C bond energy in C₂F₆ is much too high, which is also true of most of the other appearance potential studies and is probably due to excess kinetic

or excitation energy of the ion. However, the value of Farmer, *et al.*, although still high, is in fair agreement with our result.

(14) E. Tschuikow-Roux, to be published.

(15) P. B. Ayscough, *J. Chem. Phys.*, **24**, 944 (1956).

(16) G. O. Pritchard and J. R. Dacey, *Can. J. Chem.*, **38**, 182 (1960).

Radiation Yields of Carbon Monoxide and Dioxide for Some Aromatic Carbonyl Compounds

by A. A. Miller

General Electric Research Laboratory, Schenectady, New York
(Received October 29, 1964)

An aromatic group in an organic molecule can produce opposing effects on its radiation chemistry: (a) increased stability, and (b) activation of specific bonds. These effects are illustrated in this paper by measurements of carbon monoxide and dioxide yields and ratios in the radiolysis of selected carbonyl compounds.

Experimental

Unless specified otherwise, Eastman White Label materials were used. Samples were outgassed and irradiated in a gas-measurement cell¹ with 1.5-Mev. electrons from a G.E. resonant transformer unit at an intensity of 20 Mr./min. and near room temperature. The evolved gas was analyzed in a mass spectrometer for H₂, CO, CO₂, and CH₄. The dosimetry was by an air-ionization chamber¹ and the radiation yields, $G(\text{molecules})/100$ e.v., are based on an energy absorption of 1 Mr. = 6×10^{19} e.v./g.

Results and Discussion

In Table I, the first eight esters are grouped as follows: methyl, phenyl, and benzyl acetates (1-3), benzoates (4-6), and phenylacetates (7, 8). The total gas yield, $G(\text{gas})$, was predominantly CO and CO₂, except for the acetates, where appreciable yields of H₂ and CH₄ were also produced. $G'(\text{CO} + \text{CO}_2)$ represents the combined yields of carbon monoxide and dioxide, divided by the weight fraction of carboxyl, $-\text{OC}=\text{O}$, in the original molecule. Thus, G' measures the sensi-

(1) A. A. Miller, *J. Am. Chem. Soc.*, **82**, 3519 (1960).

Table I: Gas Yields for Carbonyl Compounds

No.	Compd.	G(gas)	CO	CO ₂	G'(CO + CO ₂)	CO/CO ₂
1	$\text{CH}_3\text{OC}(=\text{O})\text{CH}_3^a$	3.4	1.2	0.40	2.7	3.0
2	$\text{PhOC}(=\text{O})\text{CH}_3$	2.4	1.86	0.15	6.2	13.0
3	$\text{PhCH}_2\text{OC}(=\text{O})\text{CH}_3^a$	2.7	0.15	1.6	5.9	0.09
4	$\text{CH}_3\text{OC}(=\text{O})\text{Ph}$	0.48	0.23	0.14	1.1	1.65
5	$\text{PhOC}(=\text{O})\text{Ph}$	0.30	0.27	0.026	1.3	10.4
6	$\text{PhCH}_2\text{OC}(=\text{O})\text{Ph}$	0.74	0.068	0.62	3.3	0.11
7	$\text{PhOC}(=\text{O})\text{CH}_2\text{Ph}^b$	5.4	5.2	0.13	25.6	40
8	$\text{PhCH}_2\text{-}p\text{-Ph-CH}_2\text{OC}(=\text{O})\text{CH}_2\text{Ph}^b$	3.9	0.34	3.5	27.5	0.09
9	$\text{PhCH}_2\text{CH}_2\text{OC}(=\text{O})\text{Ph}$	0.39	0.12	0.18	1.6	0.7
10	$\beta\text{-C}_{10}\text{H}_7\text{-OC}(=\text{O})\text{Ph}$	0.057	0.027	0.01	0.21	2.7
11	$\text{PhOC}(=\text{O})\text{OPh}$	2.0	1.53	0.48	7.2	3.2
12	$\text{PhC}(=\text{O})\text{Ph}$	0.02	0.008	(<0.003)	0.053	...

^a Data from E. M. Kinderman, WADC, TR 57-465 (1957). ^b These esters were synthesized by J. R. Ladd and M. J. Smith.

tivity of the molecule toward radiation-induced decarboxylation, and the CO/CO₂ ratio indicates the mode of radiolysis of the carboxyl group.

In both the acetate and the benzoate series, the phenyl and the benzyl esters give higher *G'* values than the methyl esters. This effect can be attributed to the labilization of the adjacent bond by the phenoxy (C₆H₅O-) and the benzyl (C₆H₅CH₂-) structures. Scission of the phenoxy group as a unit is evidenced by the high CO/CO₂ ratio in all of the phenyl esters.

When the carbonyl group is adjacent to and conjugated with the aromatic ring, the stability against decarboxylation is increased, as shown by a comparison of the *G'* values for the benzoates (4-6) with the corresponding acetates (1-3). On the other hand, when both groups adjacent to the carbonyl are phenoxy and/or benzyl (7 and 8), extremely high values of *G'* result. It may be noted that 2 is isomeric with 4, and 6 is isomeric

with 7. In each pair, the positions of the aliphatic and aromatic groups with respect to the carbonyl are merely interchanged.

In β -phenylethyl benzoate (9), the benzyl group is separated from the carboxyl by an additional methylene unit, producing an increased stability compared with benzyl benzoate (6). For the benzoates, the change from phenyl (5) to β -naphthyl (10) increases the stability about sevenfold. The lower CO/CO₂ ratio for the latter suggests also an increase in the amount of aryl, as opposed to aryloxy, scission.

In the change from phenyl benzoate (5) to diphenyl carbonate (11), the carbonyl group is no longer conjugated with either aromatic ring, resulting in a fivefold increase in *G'*. Conversely, conjugation of the carbonyl group with both aromatic rings greatly stabilizes the benzophenone molecule (12) against the loss of carbon monoxide.

Acknowledgments. J. R. Ladd and M. J. Smith prepared the two phenylacetate esters. Mass spectral gas analyses were done by P. C. Noble.

Molar Extinction Coefficients of O_4F_2 in the Visible Range and a Comparison with Other Oxygen Fluorides¹

by A. G. Streng and L. V. Streng

The Research Institute of Temple University, Philadelphia, Pennsylvania (Received October 23, 1964)

Tetraoxygen difluoride, O_4F_2 , has been synthesized recently^{2,3} and its properties are being studied at the present time. In these studies, the molar extinction coefficients of liquid O_4F_2 have been determined. The data obtained are presented herewith.

Four oxygen fluorides, OF_2 , O_2F_2 , O_3F_2 , and O_4F_2 , are known to date. The molar extinction coefficients of O_2F_2 and O_3F_2 have been reported earlier.⁴ A literature search showed that there are no quantitative data available on the visible absorption spectrum of liquid OF_2 , in spite of the fact that this oxygen fluoride has been known since 1927.⁵ The only known data for OF_2 are the qualitative data for gaseous OF_2 .⁶ Therefore, the molar extinction coefficients of liquid OF_2 have been measured by us and are being reported here.

Experimental

Oxygen Fluorides Used. The O_4F_2 used in this study was prepared in our laboratories directly from the elements by the method described elsewhere.³ The OF_2 was a commercial product obtained from the Baton Rouge Development Laboratory, General Chemical Division, Allied Chemical Corp. It originally contained 97.7% by weight OF_2 , 1.75% O_2 , and 0.55% CO_2 and was purified by fractional distillation.

Pure undiluted liquid OF_2 and a 0.05 ± 0.01 mole/l. solution of O_4F_2 in liquid $CF_4 + 3\%$ O_2 (by volume; liquid) have been investigated at 77°K. Liquid oxygen was added to carbon tetrafluoride to avoid the solidification of CF_4 (m.p. of CF_4 is 89.2°K.).

Solvent. Carbon tetrafluoride (Freon 14) used as the solvent was a commercial product manufactured by E. I. du Pont de Nemours and Co., Inc., Wilmington, Del. It originally contained 99.74 mole % CF_4 ,

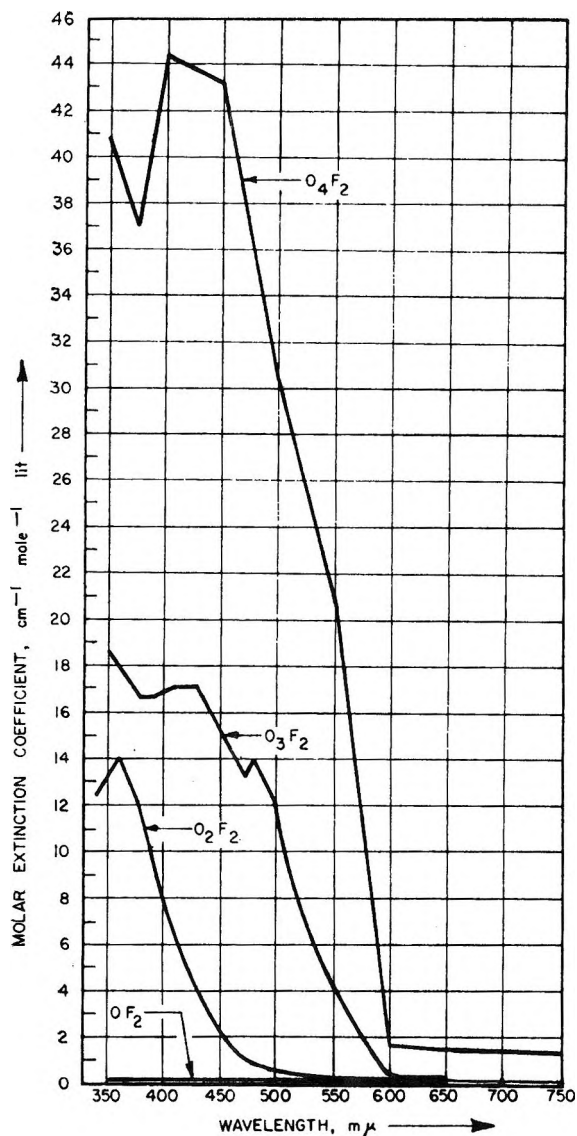


Figure 1. Visible absorption spectra of oxygen fluorides.

0.02% $CClF_3$, 0.24% air, traces of CO_2 , and 10 p.p.m. of H_2O . Before use it was treated with fluorine gas at room temperature and purified by fractional distillation.

(1) This paper describes a part of work performed for the Office of Naval Research, Contract Nonr 3085(01).

(2) A. V. Grosse, A. G. Streng, and A. D. Kirshenbaum, *J. Am. Chem. Soc.*, **83**, 1004 (1961).

(3) A. G. Streng and A. V. Grosse, First Annual Progress Report for the Office of Naval Research, Contract Nonr 3085(01), Research Institute of Temple University, Philadelphia, Pa., Jan. 3, 1961.

(4) A. D. Kirshenbaum and A. G. Streng, *J. Chem. Phys.*, **35**, 1440 (1961).

(5) P. Lebean and A. Damiens, *Compt. rend.*, **185**, 652 (1927).

(6) A. Glissman and N. J. Schumacher, *Z. physik. Chem.*, **B24**, 328 (1934).

Apparatus. A Beckman spectrophotometer, Model DU, was used for measurements. The apparatus was fitted with a special cell compartment to permit measurements at 77°K. Liquid nitrogen was used as a coolant. The cell with samples was immersed into a dewar flask containing liquid nitrogen and having two unsilvered strips for the passage of the light beam. Corrections were made for absorption by the solvent and refrigerant.

Results

The molar extinction coefficient was calculated using the equation

$$D = A_m C d$$

where D is the absorbance, A_m = molar extinction coefficient, in $l. cm^{-1} mole^{-1}$, c = concentration, in mole/l., and d = cell thickness, 1 cm.

The numerical results obtained are presented in Table I. In Figure 1, the molar extinction coefficient

Table I: Molar Extinction Coefficients of OF_2 and O_4F_2 in the Visible Range

Wave length, $m\mu$	—Molar extinction coefficient, $l. cm^{-1} mole^{-1}$ —	
	OF_2	O_4F_2
350	0.070	40.8
360	...	37.4
375	0.073	..
380	...	36.5
400	0.061	44.3
425	0.050	..
450	0.039	43.1
475	0.029	..
500	0.021	30.3
520	0.015	..
550	0.010	20.5
600	0.007	1.6
650	0.006	1.4
675	0.006	..
700	0.005	1.3
750	0.005	1.3

data for O_4F_2 and OF_2 are compared with the earlier reported data for O_2F_2 and O_3F_2 .⁶ As can be seen, the absorbance of visible light by OF_2 is negligible compared to the other oxygen fluorides. Tetraoxygen difluoride, as expected, has the highest absorbance.

Acknowledgment. The authors wish to thank Dr. A. V. Grosse for his helpful suggestions.

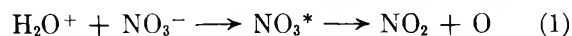
Radiolysis of Frozen Solutions. II.

Sodium Nitrite Ices

by Larry Kevan

Department of Chemistry and Enrico Fermi Institute for Nuclear Studies, University of Chicago, Chicago, Illinois
(Received November 13, 1964)

In a recent study¹ it was found that the NO_2 and NO_3 radicals were produced in the radiolysis of sodium nitrate ices at 77°K. From the concentration dependence and from scavenging data it was postulated that H_2O^+ was reacting with nitrate ions as in reaction 1. To examine such a mechanism further, we



have studied the radiolysis of sodium nitrite ices under similar conditions.

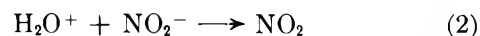
Cylindrical ice samples were irradiated at 77°K. by cobalt-60 γ -rays and were subsequently examined by electron spin resonance. The experimental details have been described.¹

Results and Discussion

The initial e.s.r. spectrum at 77°K. is a composite of the hydroxyl radical spectrum and that due to NO_2 . The ice sample is then warmed to 145°K. over a 3-min. period and re-examined at 77°K. After this treatment the hydroxyl radical spectrum has decayed while the NO_2 spectrum remains unchanged. A comparison of the spectra observed in this fashion in sodium nitrite and sodium nitrate ices is shown in Figures 1 and 2. In Figure 2 the identification of the NO_2 anisotropic triplet and NO_3 singlet (unresolved triplet) in sodium nitrate ices has been thoroughly discussed.¹ Figure 1 clearly shows that NO_2 is also formed in sodium nitrite ice and that NO_3 is *not* formed.

The NO_2 yield is proportional to $[NaNO_2]^{1/2}$; this is identical with the previous results found with sodium nitrate. Such a concentration dependence has been explained in terms of a diffusion kinetic model.¹ Furthermore, the NO_2 yield is unaffected by added acetone, which has been shown to be a good electron scavenger in irradiated ice.²

All of these results are in accord with reaction of H_2O^+ as in reaction 2; this is a direct analogy of reaction 1. It would seem that most of the NO_2 was stabilized as formed. No evidence for NO was seen in irradiated



(1) L. Kevan, *J. Phys. Chem.*, **68**, 2590 (1964).

(2) L. Kevan, P. N. Moorthy, and J. J. Weiss, *J. Am. Chem. Soc.*, **86**, 771 (1964).

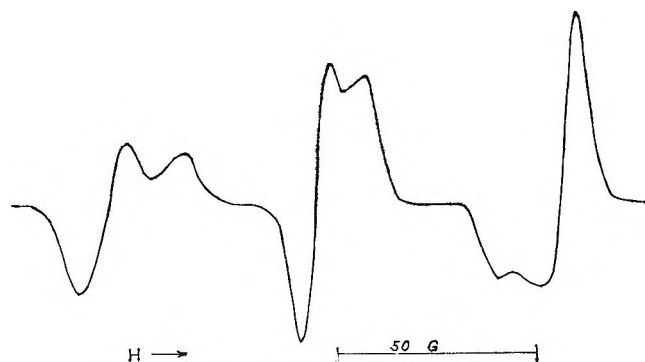


Figure 1. E.s.r. spectrum of NO_2 in irradiated $0.2 M \text{NaNO}_2$ at 77°K .

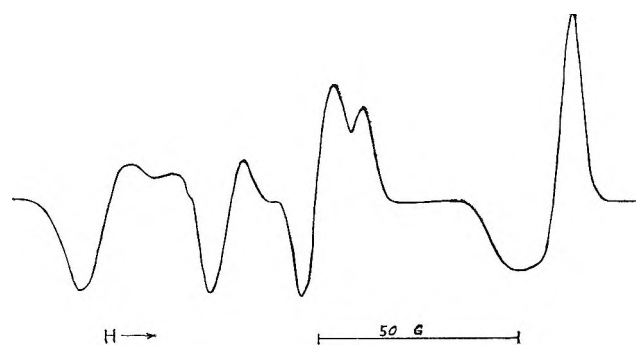


Figure 2. E.s.r. spectrum of NO_2 and NO_3 in irradiated $0.2 M \text{NaNO}_2$ at 77°K .

sodium nitrite ice but due to overlapping spectra the formation of a small amount cannot be excluded. The NO_2 yields in sodium nitrite ice and in sodium nitrate ice are about the same. Since the contribution from NO_3 in sodium nitrate ice is small, this implies that H_2O^+ has about the same reactivity toward nitrate and nitrite anions in ice.

Acknowledgment. We thank the U. S. Atomic Energy Commission for support under Contract No. At(11-1)-1365.

On Electron Trapping in Polycrystalline and in Glassy Alkaline Ices¹

by Larry Kevan

Department of Chemistry and Enrico Fermi Institute for Nuclear Studies, University of Chicago, Chicago, Illinois
(Received November 10, 1964)

Recently, there has been much interest in the detection of trapped electrons in γ -irradiated frozen solu-

tions. Schulte-Frohlinde and Eiben² first detected trapped electrons in irradiated, glassy, highly alkaline ices by electron spin resonance. Hamill and co-workers³ have identified trapped or solvated electrons in a variety of irradiated frozen organic glasses such as tetrahydro-2-methylfuran, ethanol, and 3-methylpentane by ultraviolet spectroscopy.

The above-mentioned systems are optically transparent glasses when rapidly frozen at 77°K . The question arises as to the role of the glassy state in "trapping" the electrons. Is the polycrystalline state equally effective?

Other work has shown that irradiation of glassy and polycrystalline matrices often gives quite different radical yields; the yields in the glassy state are usually higher than those in the polycrystalline state. This has been observed in both organic media⁴ and inorganic media.^{5,6} In the present note, the effect of glassy and polycrystalline solid phases on the trapped electron yield in alkaline ices is examined.

Experimental

All solutions were made with triply distilled water and reagent grade chemicals. Frozen samples were prepared in the form of cylinders 3 mm. in diameter as previously described⁷ or in spherical form by dropping the solution into liquid nitrogen.

Irradiations were carried out with Co^{60} γ -rays at a dose rate of 0.70 Mrad/hr. at 77°K . The total dose was 0.30 Mrad . Measurements of the trapped electron concentrations were made with a Varian-4500 spectrometer at 0.1-mw. power, at which power level saturation effects were negligible. Irradiated samples were warmed at an approximately linear rate from 77 to 140°K . over a 3-min. period. This treatment caused the hydroxyl and other background radicals to decay but left the electron spectrum unchanged.

To obtain the yield of trapped electrons, a comparison of the doubly integrated first derivative spectrum of the trapped electron in $2.0 M \text{KOH}$ and that of the hydrogen atoms in $1.0 M \text{NaH}_2\text{PO}_4$ was made for iden-

- (1) This is part III of a series on the radiolysis of frozen solutions.
- (2) D. Schulte-Frohlinde and K. Eiben, *Z. Naturforsch.*, **17a**, 445 (1962); **18a**, 199 (1963); these authors have reversed their original assignment: e^- appears at $g = 2.002$ and O^- at $g = 2.06$.
- (3) M. R. Ronayne, J. P. Guarino, and W. H. Hamill, *J. Am. Chem. Soc.*, **84**, 4230 (1962); J. P. Guarino and W. H. Hamill, *ibid.*, **86**, 777 (1964); E. P. Bertin and W. H. Hamill, *ibid.*, **86**, 1301 (1964).
- (4) H. W. Fenrick, S. V. Filseth, A. L. Hanson, and J. E. Willard, *ibid.*, **85**, 3731 (1963).
- (5) R. Livingston and A. Weinberger, *J. Chem. Phys.*, **33**, 499 (1960).
- (6) F. S. Dainton and F. T. Jones, *Radiation Res.*, **17**, 388 (1962).
- (7) L. Kevan, P. N. Moorthy, and J. J. Weiss, *J. Am. Chem. Soc.*, **86**, 771 (1964).

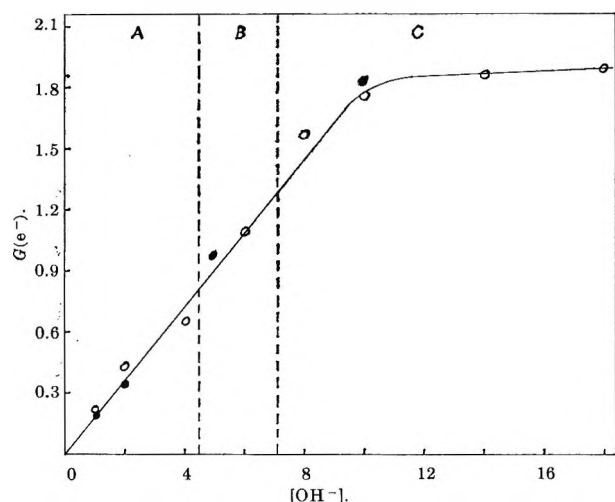


Figure 1. Trapped electron yields in KOH (O) and in NaOH (●) irradiated frozen solutions at 77°K. In region A both solutions are polycrystalline; in region B NaOH solutions are glassy while KOH solutions remain polycrystalline; and in region C both solutions are glassy.

tical cylindrical samples. A power saturation correction was necessary for the hydrogen atom yield. $G(H)$ for 1.0 M NaH_2PO_4 was taken as 0.27.⁵

Results and Discussion

The trapped electron yields in alkaline ices irradiated at 77°K. were determined by electron spin resonance as a function of hydroxide in NaOH and KOH ices. The trapped electron appears at $g = 2.002$. The results are shown in Figure 1. In NaOH solutions of less than 4.5 M, rapid freezing in liquid nitrogen gives an opaque (polycrystalline) solid. Above 5.0 M, rapid freezing gives a clear transparent (glassy) solid. A gradual transition from polycrystalline to glassy appearance occurs over a range of about 0.5 M. In KOH the median transition concentration is 7.1 M. As can be seen in Figure 1 the trapped electron yield increases linearly with hydroxide concentration independently of whether NaOH or KOH is used and, most importantly, it shows no discontinuities in either of the polycrystalline-glassy transition regions. Samples at identical concentrations within the phase transition regions can be prepared which appear transparent, opaque, or translucent. These samples all show the same trapped electron yield within experimental error. Such results would seem to indicate that the efficiency of electron trapping in irradiated alkaline ices is independent of the nature of the frozen solution.

It must be remembered that all samples are prepared by rapid (1-3 sec.) freezing and are thought to be representative of a frozen solution (*i.e.*, solvated ions). A frozen solution is necessary for the formation of an efficient electron trap; pure ice and pure

KOH do not trap electrons at 77°K. If the samples are annealed at temperatures around -50° before irradiation, apparent recrystallization is observed and transparent samples become opaque. Subsequent irradiation of annealed samples gives reduced yields of trapped electrons. It is likely that some phase segregation takes place in the annealing process and that it results in reduced electron yields.⁸

The maximum value of $G(e^-)$ in alkaline ices (1.9) is comparable to the values found by the use of scavengers in frozen organic media (1.1 to 3.2)³ and in sulfuric acid ices (2.1).⁶ Irradiation of pure NaOH or KOH pellets produces no trapped electrons at 77°K.

Acknowledgment. The author wishes to thank Carol Fine for her careful experimental assistance and the U. S. Atomic Energy Commission for support of this research under Contract AT(11-1)-1365.

(8) As this work was completed, Henrikson (*Radiation Res.*, 23, 63 (1964)) reported that trapped electron yields were lower in polycrystalline than in glassy alkaline ices. His conclusion was based on results from *annealed* polycrystalline samples.

The Effect of Oxygen on the Electron Spin Resonance Spectra of Anthracene and Perylene Adsorbed on Silica-Alumina

by Haruo Imai, Yoshio Ono, and Tominaga Keii

Department of Chemical Engineering, Tokyo Institute of Technology, Meguro, Tokyo, Japan (Received November 14, 1964)

Electron spin resonance spectra of polynuclear aromatic hydrocarbons adsorbed on silica-alumina catalyst have been observed by many workers. Contradictory observations concerning the effect of oxygen on the e.s.r. spectra of anthracene and perylene adsorbed on silica-alumina catalyst were reported. Fogo¹ found a large absorption spectrum only when air was admitted, whereas Brouwer² reported that the positive ion was almost completely destroyed within a few hours upon contact with air. Moreover, Rooney and Pink³ recently observed that the peak height of the spectra of both adsorbed perylene and anthracene decreased with increasing oxygen pressure. The purpose of the pres-

(1) J. K. Fogo, *J. Phys. Chem.*, 65, 1919 (1961).

(2) D. M. Brouwer, *Chem. Ind. (London)*, 77 (1961).

(3) J. J. Rooney and R. C. Pink, *Trans. Faraday Soc.*, 58, 1632 (1962).

ent work is to examine the effect of oxygen on the spectra of these adsorbed hydrocarbons.

Silica-alumina (17% alumina) was prepared by the method of gel mixing and activated by heating in air at 550° for 2 hr. Silica and alumina gel were obtained by the hydrolysis of ethyl orthosilicate and aluminum isopropoxide, respectively. The specific surface area of the catalyst, measured by the nitrogen adsorption method, is 280 m.²/g.

The e.s.r. measurements were carried out at room temperature with spectrometer JES 3110-X with 100 kc./sec. field modulation.

The cell used is a Pyrex tube (4 mm. in diameter), which contains ca. 40 mg. of the catalyst, joined with a 10-mm. tube at the upper part. Two glass bulbs containing ca. 200 mg. of a 0.05 M anthracene in benzene solution were placed at the 10-mm. part of the cell.

After the catalyst had been heated in air at 400° for 30 min. *in situ*, and evacuated for 1 hr. at the same temperature, the bulbs were broken to mix the catalyst with the solution. After 5 min. of contact, the system was pumped out for 30 min. to remove the solvent.

The catalyst developed a green color and a weak e.s.r. absorption with slightly resolved hyperfine structure. Then, admitting oxygen into the cell, the e.s.r. measurement was carried out. As oxygen pressure increased, the relative peak height of the spectrum increased to its maximum value and then decreased, as shown by curve a in Figure 1. After this run, the measurements were repeated while reducing the oxygen pressure. The results are shown by curve a' in Figure 1. It seems that the effect of oxygen on the spectrum is reversible. The disagreement between the two curves (a and a') may be attributed to the slow desorption of oxygen.

The color changed from green to brown when the system was kept 1 week under a 200-mm. oxygen atmosphere. The peak height vs. oxygen pressure curve of this system is similar to that found with fresh catalyst, except that its height is about three times that of the latter (curve b). It has been further observed that the height is increased considerably by heating the system in an oxygen atmosphere at 180° for 30 min.

In the case of perylene, a similar effect of oxygen on the peak height has been found. The well-resolved hyperfine structure observed in the absence of oxygen was removed by the admission of oxygen above 7 mm. The hyperfine structure was restored when the system was pumped out.

By carrying out the measurements with different amounts of the adsorbates, it has been found that the oxygen pressure at which the maximum peak height appears decreases as the adsorbed amounts decrease.

Using a silica-alumina catalyst which had been preliminarily base-exchanged with sodium acetate by the method of Webb,⁴ it has been observed that the peak height reduced to one-third in the case of anthracene (curve c) and to one-sixth in the case of perylene, respectively. Here, the specific surface area of the catalyst remains unchanged by base exchange. This strongly suggests that the Brønsted acid site plays an important role in cation radical formation, as reported by Hirschler and Hudson.⁵

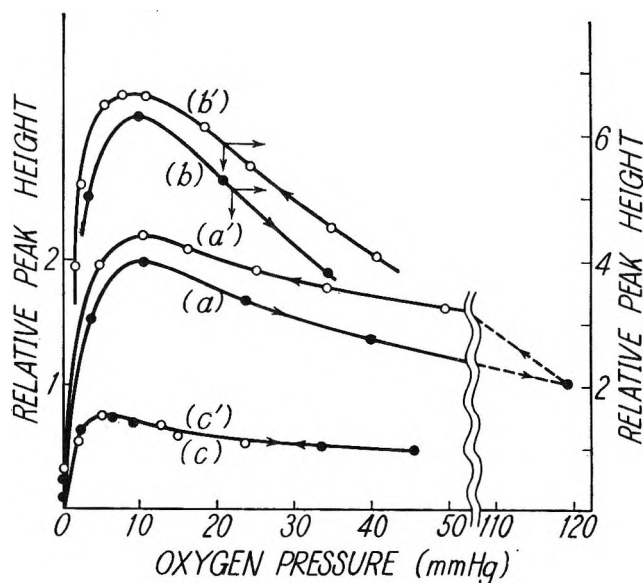


Figure 1. Effect of oxygen pressure on the peak height: a and a', with fresh catalyst; b and b', with the catalyst kept 1 week under 200 mm. of oxygen pressure; c and c', with base-exchange catalyst; ●, increasing oxygen pressure; ○, decreasing oxygen pressure.

The increase of the e.s.r. absorption thus obtained at low pressure (below 10 mm.) may be explained by cation radical formation with electron transfer to oxygen from a hydrocarbon-proton complex.⁶ In order to explain the whole behavior of the spectra, further experiments must be performed.

(4) A. N. Webb, *Actes congr. intern. catalyse, 2^e Paris*, 1, 1289 (1960).

(5) A. E. Hirschler and J. O. Hudson, *J. Catalysis*, 3, 239 (1964).

(6) W. I. Aalbersberg, J. Gaaf, and E. L. Macmor, *J. Chem. Soc.*, 905 (1961).

COMMUNICATIONS TO THE EDITOR

Surface Free Energy of Polymers

Sir: It has been reported in wettability experiments that the interfacial free energies at the solid-liquid interface (γ_{SL}) of "low energy" solids are essentially zero.¹ Experiments dealing with the kinetics of homogeneous nucleation of polymers² have demonstrated that at the crystal-melt interface, $50 < \gamma_{SL} < 100$ ergs/cm.². In this communication, we shall attempt to resolve the apparent contradiction in the above interfacial free energies.

Fowkes³ has shown that

$$\gamma_{SL} = \gamma_S + \gamma_{LV} - 2(\gamma_S^d \gamma_{LV}^d)^{1/2} \quad (1)$$

Good, *et al.*,⁴ have developed a similar expression. The Young equation

$$\gamma_S = \gamma_{SL} + \gamma_{LV} \cos \theta + \pi_e \quad (2)$$

where $\pi_e = (\gamma_S - \gamma_{SV})$ has been used in conjunction with eq. 1 to calculate γ_S .⁴ However, *no* distinction was made in the above studies to account for the relative degree of crystallinity of the polymers. Consequently, the combination of eq. 1 and 2 has led some authors^{1,4} to the conclusion that $\gamma_S \cong \gamma_C$, where γ_C is the critical surface tension of wetting (c.s.t.).⁵

Wettability studies^{1,5} have not attempted to distinguish between the relative degrees of crystallinity in a polymer species. Lacking any evidence to the contrary, we propose that

$$(\gamma_S^a - \gamma_{SL}^a) \cong (\gamma_S^{ac} - \gamma_{SL}^{ac}) \cong (\gamma_S^c - \gamma_{SL}^c) \quad (3)$$

where the superscripts a, ac, and c refer to amorphous, partially crystalline and crystalline, respectively. For amorphous polymers, eq. 1 becomes

$$\gamma_S^a - \gamma_{SL}^a = 2(\gamma_S^{ad} \gamma_{LV}^d)^{1/2} - \gamma_{LV} \quad (4)$$

Schonhorn⁶ has shown that at the crystal-melt interface of polymers

$$\gamma_{SL} = (1 - x_2)k_S \frac{V_S^{1/3}}{N^{1/3}} \left(\frac{\Delta H_m}{\Delta V_m} \right) \quad (5)$$

where x_2 is the mole fraction of amorphous polymer, k_S is a binding constant, V_S is the molar volume of the solid phase in equilibrium with the melt, ΔH_m is the molar heat of fusion, and ΔV_m is the molar volume change on melting. When $x_2 = 1$, $\gamma_{SL} = \gamma_{SL}^a = 0$ and for $x_2 = 0$, $\gamma_{SL} = \gamma_{SL}^c$.

To illustrate the utility of eq. 4, we shall deal exclusively with polyethylene although the development has general applicability. For polyethylene, where only dispersion forces are operative, $\gamma_{LV} = \gamma_{LV}^d$. In

the limit when $x_2 = 1$ and $\gamma_{SL}^a = 0$, there is no discontinuity in the surface free energy of the polymer. Then we conclude that $\gamma_S^{ad} = \gamma_{LV}^d$ and

$$\gamma_{LV} = \gamma_S^{ad} = \gamma_S^a \quad (6)$$

This is an important conclusion. If we extrapolate the surface tension data of Schonhorn and Sharpe⁷ for molten polyethylene to 20°, $\gamma_{LV} = 35$ ergs/cm.². A similar extrapolation for polypropylene⁸ yields $\gamma_{LV} = 28$ ergs/cm.². We conclude that for amorphous solids, $\gamma_S^a = \gamma_C$. This is consistent with wettability experiments. Since the temperature dependence of γ_S^a is known from γ_{LV} , we automatically know the temperature dependence of γ_C .

From eq. 3 and 4 we obtain for crystalline polymers

$$\gamma_S^c - \gamma_{SL}^c = 2(\gamma_S^{ad} \gamma_{LV}^d)^{1/2} - \gamma_{LV} \quad (7)$$

For an ordered polymer, $\gamma_S^c \neq \gamma_S^{ad}$. This distinction has not been made previously. From eq. 5, when $x_2 = 0$, $\Delta H_m = 960$ cal./mole of CH₂,⁹ $\Delta V_m = 3.08$ cm.³/mole of CH₂,¹⁰ $V_S^{1/3} = 2.44$ cm.³/mole of CH₂,¹⁰ and $k_S = 0.312$,⁶ we obtain $\gamma_{SL}^c = 117$ ergs/cm.². Therefore, we conclude that depending upon the degree of crystallinity and the melting point of polyethylene ($\sim 141^\circ$),¹¹ $0 \leq \gamma_{SL} \leq 117$ ergs/cm.². Since $\gamma_S^{ad} = \gamma_{LV}$, we have from eq. 7

$$\gamma_{SL}^c = \gamma_S^c - \gamma_{LV} \quad (8)$$

which is a statement of Antonow's rule.¹² When

(1) E. Wolfram, *Kolloid-Z.*, **182**, 75 (1962); K. L. Wolf, *Z. physik. Chem.* (Leipzig), **225**, 1 (1964); V. R. Gray, *Forest Prod. J.*, **12**, 452 (1962); A. V. Neumann and P. J. Sell, *Z. physik. Chem.* (Frankfurt), **41**, 183, 191 (1964); J. L. Gardon, *J. Phys. Chem.*, **67**, 1935 (1963).

(2) J. I. Lauritzen, Jr., and J. D. Hoffman, *J. Res. Natl. Bur. Std.*, **64A**, 73 (1960); F. P. Price, *J. Polymer Sci.*, **42**, 49 (1960).

(3) F. M. Fowkes, *J. Phys. Chem.*, **66**, 1863 (1962); **67**, 2538 (1963); 66th ASTM Meeting, Atlantic City, N. J., June 1963; *Advances in Chemistry Series*, No. 43, American Chemical Society, Washington, D. C., 1964, p. 99.

(4) R. J. Good, *et al.*, *J. Phys. Chem.*, **62**, 1418 (1958); **61**, 904 (1957); **64**, 561 (1960); *Advances in Chemistry Series*, No. 43, American Chemical Society, Washington, D. C., 1964, p. 74.

(5) W. A. Zisman, *Advances in Chemistry Series*, No. 43, American Chemical Society, Washington, D. C., 1964, p. 1.

(6) H. Schonhorn, to be published.

(7) H. Schonhorn and L. H. Sharpe, *J. Polymer Sci.*, in press.

(8) H. Schonhorn and L. H. Sharpe, *ibid.*, to be published.

(9) L. Mandelkern, "Crystallization of Polymers," McGraw-Hill Book Co., Inc., New York, N. Y., 1964.

(10) S. Matsuoka, *J. Polymer Sci.*, **57**, 569 (1962).

(11) M. Broadhurst, *J. Chem. Phys.*, **36**, 2578 (1962).

(12) G. Antonow, *J. chim. phys.*, **5**, 372 (1907); *J. Phys. Colloid Chem.*, **52**, 969 (1948).

interactions other than dispersion forces are operative, $\gamma_s^{\text{ad}} \neq \gamma_{\text{LV}}$ and Antonow's rule may be violated.

If $d\gamma_s/dT = d\gamma_{\text{LV}}/dT$ as was demonstrated by Greenhill and McDonald¹³ for a partially crystalline wax, then $\gamma_s^c = 152$ ergs/cm.² at 20°. We fully realize that this value of γ_s does not take into account defects, mechanical stresses, and other possible deviation from equilibrium. From eq. 4 and 7, it is apparent that S_p , the spreading coefficient, and W_A , the work of adhesion, are independent of bulk properties. This is entirely consistent with wettability experiments.

(13) E. B. Greenhill and S. R. McDonald, *Nature*, 171, 37 (1953).

BELL TELEPHONE LABORATORIES, INC. HAROLD SCHONHORN
MURRAY HILL, NEW JERSEY

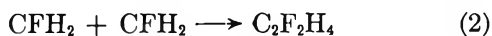
RECEIVED DECEMBER 28, 1964

An Anomaly in the Interaction of CF₂H Radicals

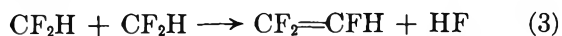
Sir: We have recently found¹ that the gas-phase interaction of CFH₂ radicals leads to an important elimination reaction



as well as to recombination



The radicals were produced by photolysis of (CFH₂)₂CO. At 5 cm. ketone pressure, $k_1/k_2 = 0.6$ at room temperature, rising to a value of 3.5 at 304°. At lower ketone pressures, reaction 1 is even more favored at any particular temperature, and values of k_1/k_2 as high as 6.0 were obtained.¹ We have now extended our investigations to the photolysis of (CF₂H)₂CO, and it was expected that



would compete significantly with recombination

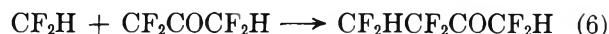
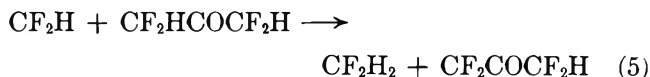


as it appears that the probability of HF elimination is statistically identical for either the configuration (F₂HC-CF₂H)* or (FH₂C-CF₂H)*. However, our experiments show that reaction 3 is of very little importance, and we have been unable to obtain any trifluoroethylene in the system.

Employing ketone pressures in the range 3.5–6.5 cm., the following mass balances (m.b. = $(\frac{1}{2}\text{CF}_2\text{H}_2 + \text{C}_2\text{F}_4\text{H}_2)/\text{CO}$) were obtained

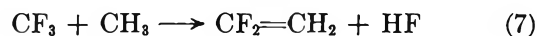
Temp., °C.	20.5	111	153	204	277	305
M.b.	0.92	0.88	0.89	0.80	0.73	0.73

The decrease in the radical balance with rising temperature is to be expected unless analysis is conducted for the methyl ethyl ketone formed in reaction 6.



Reaction 3 cannot be ruled out entirely, as trace amounts (0–1% of CO formed) of SiF₄ were obtained, of which HF is the precursor. Any small amounts of C₂F₃H formed are presumably rapidly removed by radical addition. We have shown this by dosing the system with C₂F₃H, which greatly reduces the values of the mass balances. This also served as a check on our analytical procedure for C₂F₃H. Radical balance indicated that the addition of CFH₂ radicals to C₂FH₃ was not significant under the conditions used.¹

Our previous observation¹ that



does not occur is invalid, as this reaction has now been found by Whittle,² who obtained ratios of k_7/k_8 similar in



magnitude to those that we obtained for k_1/k_2 , dependent upon both the temperature and the pressure. Also, the rapid addition of CF₃ to C₂F₂H₂ occurs.^{2a} In these experiments the radicals were produced by the cophotolysis^{2a} of (CH₃)₂CO and (CF₃)₂CO or in the system^{2b} CF₃ + CH₃I → CF₃I + CH₃. It is therefore surprising that in a recent reinvestigation of the photolysis of CF₃COCH₃ by Dawidowicz and Patrick³ no mention of reaction 7 is made; complete conditions for individual runs are unfortunately not specifically stated, but we may estimate k_7/k_8 to be ~0.1–0.3 in some of the experiments (Whittle^{2a} found smaller k_7/k_8 ratios in the two-ketone system than in the methyl iodide experiments^{2b}). It would seem that the criticism made by these authors concerning (CF₃CH₃)/(C₂F₆·C₂H₆)^{1/2} ratios determined previously⁴ is also applicable to their own experiments⁵ and that the more correct function (CF₃CH₃ + CF₂CH₂)/(C₂F₆·C₂H₆)^{1/2} must

(1) G. O. Pritchard, M. Venugopalan, and T. F. Graham, *J. Phys. Chem.*, 68, 1786 (1964).

(2) (a) E. Whittle, private communication; (b) W. G. Alcock and E. Whittle, *Trans. Faraday Soc.*, in press.

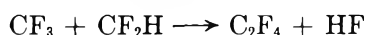
(3) E. A. Dawidowicz and C. R. Patrick, *J. Chem. Soc.*, 4250 (1964).

(4) G. O. Pritchard and J. R. Dacey, *Can. J. Chem.*, 38, 182 (1960).

(5) In both investigations,^{3,4} analysis was effected by mass spectrometry, which is not a sensitive way of detecting CF₂CH₂ in the presence of CF₃CH₃, CF₃H, C₂H₆, and C₂F₆.

be used in any case.⁶ The unexplained formation of difluoropropane and a polymer in the system³ is more readily understood if reaction 7 occurs.

Some further support for the anomalously small occurrence of reaction 3 arises from recent work on the mercury-photosensitized decomposition of chlorodifluoromethane.⁷ CF_2H radicals are formed in the primary process and $\text{C}_2\text{F}_4\text{H}_2$ is produced; $\text{C}_2\text{F}_3\text{H}$ was not reported as a reaction product. Also, Whittle^{2a} is currently investigating the system $\text{CF}_3 + \text{CF}_2\text{H}_2 \rightarrow \text{CF}_3\text{H} + \text{CF}_2\text{H}$. Trace amounts of $\text{C}_2\text{F}_3\text{H}$ are formed, indicating that reaction 3 does occur to a small extent (in agreement with our results), but analysis shows that C_2F_4 is absent, suggesting that the possible reaction



occurs even less. We may thus make the generalization that increased fluorination of *both* the interacting radicals appears to reduce the possibility of HF elimination. We are conducting additional experiments on these and related systems.

Acknowledgments. We are very indebted to Drs. O. P. Strausz and E. Whittle for communication of their results prior to publication, and to the National Science Foundation for a grant-in-aid.

(6) A. R. Blake, J. F. Henderson, and K. O. Kutschke, *Can. J. Chem.*, **39**, 1920 (1961).

(7) M. G. Bellas, O. P. Strausz, and H. E. Gunning, *ibid.*, in press.

DEPARTMENT OF CHEMISTRY
UNIVERSITY OF CALIFORNIA
SANTA BARBARA, CALIFORNIA

G. O. PRITCHARD
J. T. BRYANT

RECEIVED JANUARY 27, 1965

Note on Molecular Diffusion and Heat Conductivity in Liquids

Sir: The concept of a static diffusion constant which defines the kinetic behavior of a gas highly diluted in another has been useful to predict the dynamic diffusion of a small gas packet in a moving gas stream in a conduit. When the conduit is round with an inner radius r , Taylor has shown that the dynamic diffusion proceeds as if the gas were not flowing, and its effective diffusion were given by the expression

$$D_e = D + \frac{r^2 v^2}{12D}$$

where D and v are the static diffusion constant and the average gas velocity, respectively.

When D_e/v is plotted as a function of v , we should obtain a hyperbola, as has been verified for gases within the limits of experimental errors.

On the other hand, in the case of liquids all experimental curves obtained so far by S. Norem (private communication) have exhibited, to the right of the minimum, an inflection point, beyond which the slope of the curve decreases markedly for increasing values of v .

Turbulent flow cannot be invoked to explain this trend, because Poiseuille's law has been verified to govern the liquid's behavior for the range of v for which the observations were made. Therefore, only one possible explanation remains, namely, that the concept of the static diffusion constant, adequate to account for molecular diffusion in still and moving gases and in still liquids, is no longer valid in moving liquids. Instead, diffusivity in moving liquids appears to increase with increasing curls of the liquid velocity, even in laminar flow.

If, then, one adopts the existence of this increased diffusivity with increasing velocity curls, and attempts to explain it physically, one is led to the assumption of agglomerates or micelles of higher viscosity than the remaining liquid, which rotate with the liquid's velocity curls, thereby increasing the transfer of molecules from points of high concentration to points of low concentration.

This is admittedly a surprising behavior on the part of such liquids as water in which a small amount of acetone is diffusing, and crucial experiments are required to test this view. Since heat transfer also should be increased in the same circumstances which cause an increased diffusivity, one such crucial experiment could consist in rotating a cylinder in which a given electrical power is dissipated, in another cylinder, the space between the two cylinders being filled by a liquid, and in verifying whether the temperature difference between the two cylinders decreases with increased rate of rotation.

THE PERKIN-ELMER CORPORATION
NORWALK, CONNECTICUT

MARCEL J. E. GOLAY

RECEIVED FEBRUARY 2, 1965